

PET and SPECT of Neurobiological Systems

Rudi A.J.O. Dierckx
Andreas Otte
Erik F.J. de Vries
Aren van Waarde
Editors

Paul G.M. Luiten
Guest Editor

 Springer

PET and SPECT of Neurobiological Systems

Rudi A.J.O. Dierckx • Andreas Otte
Erik F.J. de Vries • Aren van Waarde
Editors

Paul G.M. Luiten
Guest Editor

PET and SPECT of Neurobiological Systems

 Springer

Editors

Rudi A.J.O. Dierckx
Department of Nuclear Medicine
and Molecular Imaging
University Medical Center Groningen
University of Groningen
Groningen
The Netherlands

Erik F.J. de Vries
Department of Nuclear Medicine
and Molecular Imaging
University Medical Center Groningen
University of Groningen
Groningen
The Netherlands

Department of Nuclear Medicine
University Hospital Gent
University of Gent
Gent
Belgium

Aren van Waarde
Department of Nuclear Medicine
and Molecular Imaging
University Medical Center Groningen
University of Groningen
Groningen
The Netherlands

Andreas Otte
Faculty of Electrical Engineering
and Information Technology
University of Applied Sciences Offenburg
Offenburg
Germany

Guest Editor
Paul G.M. Luiten
Department of Molecular Neurobiology
University of Groningen
Groningen
The Netherlands

ISBN 978-3-642-42013-9

ISBN 978-3-642-42014-6 (eBook)

DOI 10.1007/978-3-642-42014-6

Springer Heidelberg New York Dordrecht London

Library of Congress Control Number: 2014931856

© Springer-Verlag Berlin Heidelberg 2014

This work is subject to copyright. All rights are reserved by the Publisher, whether the whole or part of the material is concerned, specifically the rights of translation, reprinting, reuse of illustrations, recitation, broadcasting, reproduction on microfilms or in any other physical way, and transmission or information storage and retrieval, electronic adaptation, computer software, or by similar or dissimilar methodology now known or hereafter developed. Exempted from this legal reservation are brief excerpts in connection with reviews or scholarly analysis or material supplied specifically for the purpose of being entered and executed on a computer system, for exclusive use by the purchaser of the work. Duplication of this publication or parts thereof is permitted only under the provisions of the Copyright Law of the Publisher's location, in its current version, and permission for use must always be obtained from Springer. Permissions for use may be obtained through RightsLink at the Copyright Clearance Center. Violations are liable to prosecution under the respective Copyright Law.

The use of general descriptive names, registered names, trademarks, service marks, etc. in this publication does not imply, even in the absence of a specific statement, that such names are exempt from the relevant protective laws and regulations and therefore free for general use.

While the advice and information in this book are believed to be true and accurate at the date of publication, neither the authors nor the editors nor the publisher can accept any legal responsibility for any errors or omissions that may be made. The publisher makes no warranty, express or implied, with respect to the material contained herein.

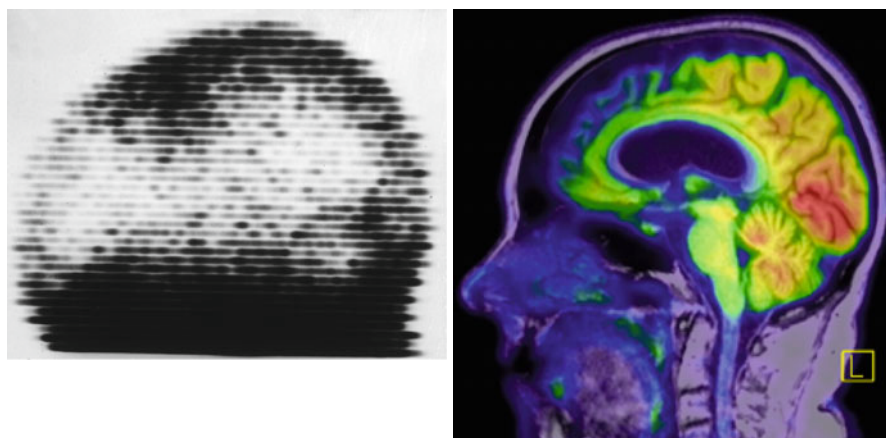
Printed on acid-free paper

Springer is part of Springer Science+Business Media (www.springer.com)

Foreword

In this ambitious undertaking, the Editors have assembled the most comprehensive and updated compilation of material, describing the use of single photon and positron emission tomography in the neurosciences. Three volumes address the use of SPECT and PET in Psychiatry, in Neurology, and in Neurobiological Systems. A large international team of experts have come together to accomplish this task.

The progress achieved in this area has been staggering. The two images below, obtained half a century apart, speak a thousand words.



On the *left*, a 1969 blood–brain barrier scan in cerebral lymphoma and on the *right* a PETMR study in frontotemporal dementia. Institute of Nuclear Medicine 2012

In this context, this volume triad is needed and timely. Novel instrumentation and probes, and significant advances in the understanding of the pathophysiology of the various pathological entities described in these texts, have led to clear clinical benefit. This is apparent in movement disorders, in the identification of nonlesional MR focal epilepsies, and now, in a rapidly emerging field, in the diagnosis of fibrillar amyloid plaque deposition, in mild cognitive impaired individuals. The next few years will see a rapid expansion of this already fast progressing field.

The Editors are to be congratulated in bringing together and to print this significant volume of expertise and experience.

Professor Peter J. Ell, FMedSci, DR HC
Emeritus University College London
Institute of Nuclear Medicine

Preface

The neuroscientist of today disposes of a powerful instrumentarium for functional imaging that has never made more impressive advances before, helping to better understand the mechanisms of diseases and to develop and design drug treatment options with a superior efficacy and safety profile. Among this instrumentarium, positron emission tomography (PET) and single photon emission computed tomography (SPECT) have become forerunners in the functional imaging arena, much more than functional magnetic resonance imaging, and for this reason, this book is dedicated to PET and SPECT.

Although there have been some textbooks on PET or SPECT in the neurosciences, e.g., De Deyn et al. 1997 or Otte et al. 2004, the number of these books is limited, and – to the best of our knowledge – there is no recent comprehensive publication on PET and SPECT in the neurosciences, especially a compilation by a large number of international experts, as it is undertaken in the project at hand.

When the idea to edit a book on PET and SPECT in neurosciences came up, it was soon realized that all the new data would never fit into one single volume. Hence it was decided to write a trilogy. *PET and SPECT in Psychiatry* is the first volume of this trilogy: volume 2 (*PET and SPECT in Neurology*) and volume 3 (*PET and SPECT in Neurobiological Systems*) complete the series.

In all volumes, we have tried to assemble the combined expertise of renowned authors whose dedication to the investigation of psychiatric and neurological disorders or of neurobiological systems through nuclear medicine technology has achieved international recognition. Prior to writing the trilogy, Rudi Dierckx organized an International Symposium on PET and SPECT in Neurology and Psychiatry in Groningen, the Netherlands (April 23–25, 2012). At this symposium, many of the authors included in this trilogy were invited to present a state-of-the-art review of their specific field of research. The editors, who are nuclear medicine specialists, radiochemists, and biologists with a strong exposure to neurosciences, have also invited experts from the psychiatry, neurology, and molecular neurobiology fields to enhance the editorial board as guest editors for each volume of the trilogy. For volumes 1, 2, and 3 these were, respectively, Johan A (Hans) den Boer, professor in biological psychiatry; Klaus L (Nico) Leenders, professor in neurology; and Paul Luiten, professor in neurobiology. Furthermore, we tried to increase the quality of our books by introducing an external peer-review system with experts

in the field in addition to review by the editors. The external peer reviewers are listed in the corresponding [Appendix](#).

We are very happy that our book is produced by one of the premier publishers in the field. This guarantees a high quality of reproduction and allows for the inclusion of many color figures, which is essential in the field of functional neuroimaging.

We are intrigued by the enthusiastic response from contributors from all over the world who made this endeavor successful. We also would like to thank all external peer reviewers who have done an excellent work for ensuring the quality of this compilation. Finally we would like to thank Dr. Ute Heilmann and Dr. Sylvana Freyberg from Springer Verlag for their continuous help and support during the development of this book.

We sincerely hope that this book will become a key tool not only for all physicians in nuclear medicine, psychiatry, neurology, or geriatrics, but also for all professionals working to understand or treat brain disorders. In addition, the trilogy may be interesting and important for industry, as PET and SPECT imaging of the brain is becoming more and more important in today's aging population.

May this book serve as a guide towards the present use of PET and SPECT in brain disorders and as a catalyst for future research. There is much to be explored, and the engine has been started already.

Groningen, The Netherlands
 Offenburg, Germany
 Groningen, The Netherlands
 Groningen, The Netherlands
 Groningen, The Netherlands

Rudi A.J.O. Dierckx
 Andreas Otte
 Erik F.J. de Vries
 Aren van Waarde
 Paul G.M. Luiten

References

- De Deyn PP, Dierckx RA, Alavi, Pickut BA (eds) (1997) A textbook of SPECT in neurology and psychiatry. John Libbey, London/Paris/Rome/Sydney
- Otte A, Audenaert K, Peremans K, Van Heering C, Dierckx RA (eds) (2004) Nuclear medicine in psychiatry. Springer, Berlin/Heidelberg/New York/Hong Kong/London/Milan/Paris/Tokyo

Contents

Part I Basics

1 Animal Models for Brain Research	3
Debby Van Dam and Peter Paul De Deyn	
2 Small Animal Molecular Imaging Through μPET and μSPECT	47
Steven Staelens, Tine Wyckhuys, Steven Deleeye, Jeroen Verhaeghe, Leonie Wyffels, and Sigrid Stroobants	
3 Cerebral Glucose Metabolism	85
Wolf-Dieter Heiss	
4 Cerebral Blood Flow Measurement with Oxygen-15 Water Positron Emission Tomography	103
Vilia Zeisig, Marianne Patt, Georg Becker, Johannes Boltze, Osama Sabri, and Henryk Barthel	
5 Principles of Brain Perfusion SPECT	125
Shana Elman and David H. Lewis	
6 The Impact of Genetic Polymorphisms on Neuroreceptor Imaging	149
Matthäus Willeit, Siegfried Kasper, and Nicole Praschak-Rieder	

Part II Systems

7 Imaging of Adenosine Receptors	181
David Elmenhorst, Dirk Bier, Marcus Holschbach, and Andreas Bauer	
8 PET Tracers for Beta-Amyloid and Other Proteinopathies	199
Agneta Nordberg	
9 Imaging of Central Benzodiazepine Receptors in Chronic Cerebral Ischemia	213
Hiroschi Yamauchi	

10	PET and SPECT Imaging of the Central Dopamine System in Humans	229
	Jan Booij, Jan-Peter van Wieringen, Elsmarieke van de Giessen, Remco J.J. Knol, and Sjoerd J. Finnema	
11	PET Imaging of Endocannabinoid System	249
	Andrew G. Horti, Vanessa Raymond, and Garth E. Terry	
12	Imaging Type 1 Glycine Transporters in the CNS Using Positron Emission Tomography	321
	Jan Passchier, Roger N. Gunn, and Aren van Waarde	
13	Imaging Histamine Receptors Using PET and SPECT	331
	Uta Funke, Danielle J. Vugts, Bieneke Janssen, Arnold Spaans, Perry S. Kruijer, Adriaan A. Lammertsma, Lars R. Perk, and Albert D. Windhorst	
14	PET and SPECT Imaging of Steroid Hormone Receptors	377
	Mohammed A. Khayum, Janine Doorduin, Andor W.J.M. Glaudemans, Rudi A.J.O. Dierckx, and Erik F.J. de Vries	
15	Current Radioligands for the PET Imaging of Metabotropic Glutamate Receptors	409
	Linjing Mu and Simon M. Ametamey	
16	PET Imaging of Muscarinic Receptors	445
	Hideo Tsukada	
17	Preclinical Aspects of Nicotinic Acetylcholine Receptor Imaging	465
	Peter Brust, Winnie Deuther-Conrad, Cornelius K. Donat, Henryk Barthel, Patrick Riss, Louise Paterson, Alexander Höpping, Osama Sabri, and Paul Cumming	
18	Development of Radioligands for In Vivo Imaging of NMDA Receptors	513
	Takeshi Fuchigami, Morio Nakayama, and Yasuhiro Magata	
19	Progress in PET Imaging of the Norepinephrine Transporter System	561
	Yu-Shin Ding	
20	Positron Emission Tomography (PET) Imaging of Opioid Receptors	585
	Aren van Waarde, Anthony R. Absalom, Anniek K.D. Visser, and Rudi A.J.O. Dierckx	

21	PET Imaging of ABC Transporters in the BBB.	625
	Marcel Benadiba, Heli Savolainen, Nicola A. Colabufo, Albert D. Windhorst, Aren van Waarde, and Gert Luurtsema	
22	PET Imaging of Translocator Protein Expression in Neurological Disorders.	653
	David J. Brooks	
23	Imaging of the Serotonin System: Radiotracers and Applications in Memory Disorders	669
	Gitte Moos Knudsen and Steen G. Hasselbalch	
24	Serotonin Synthesis Studied with Positron Emission Tomography (PET).	687
	Per Hartvig Honoré and Pinelopi Lundquist	
25	Monoamine Oxidase A and Serotonin Transporter Imaging with Positron Emission Tomography	711
	Jeffrey H. Meyer	
26	PET Imaging of Sigma₁ Receptors	741
	Jun Toyohara, Muneyuki Sakata, and Kiichi Ishiwata	
27	Radioligands for Imaging Vesicular Monoamine Transporters.	765
	Michael R. Kilbourn	
	The Editors	791
	Guest Editor	793
	Reviewers	795
	Anthology of Apologies.	799
	Index.	801

Contributors

Anthony R. Absalom Department of Anaesthesiology, University Medical Center Groningen, University of Groningen, Groningen, The Netherlands

Simon M. Ametamey Department of Chemistry and Applied Biosciences, Center for Radiopharmaceutical Sciences of ETH, PSI and USZ, ETH Zürich, Zürich, Switzerland

Henryk Barthel Department of Nuclear Medicine, University Hospital Leipzig, University of Leipzig, Leipzig, Germany

Andreas Bauer INM-2, Institute of Neuroscience and Medicine, Forschungszentrum Jülich, Jülich, Germany

Department of Neurology, Heinrich-Heine University Düsseldorf, Düsseldorf, Germany

Georg Becker Department of Nuclear Medicine, University Hospital Leipzig, University of Leipzig, Leipzig, Germany

Marcel Benadiba Department of Nuclear Medicine and Molecular Imaging, University Medical Center Groningen, University of Groningen, Groningen, The Netherlands

Dirk Bier INM-5, Institute of Neuroscience and Medicine, Forschungszentrum Jülich, Jülich, Germany

Johannes Boltze Department of Cell Therapy, Ischemia Research Unit, Fraunhofer Institute for Cell Therapy and Immunology, Leipzig, Germany

Translational Centre for Regenerative Medicine, University of Leipzig, Leipzig, Germany

Jan Booij Department of Nuclear Medicine, F2N, Academic Medical Center, University of Amsterdam, Amsterdam, The Netherlands

David J. Brooks Department of Medicine, Imperial College London, London, UK

Department of Nuclear Medicine, Aarhus University, Aarhus, Denmark

Peter Brust Department of Neuroradiopharmaceuticals,
Institute of Radiopharmaceutical Cancer Research, Helmholtz-Zentrum
Dresden – Rossendorf, Research Site Leipzig, Leipzig, Germany

Nicola A. Colabufo Department of Pharmacochemistry, University of Bari,
Bari, Italy

Paul Cumming ABX Pharmaceuticals, Radeberg, Germany

Peter Paul De Deyn Department of Neurology and Memory Clinic,
Hospital Network Antwerp (ZNA), Middelheim and Hoge Beuken,
Antwerp, Belgium

Department of Neurology and Alzheimer Research Center, University Medical
Center Groningen (UMCG), Groningen, Netherlands

Erik F.J. de Vries Department of Nuclear Medicine and Molecular Imaging,
University Medical Center Groningen, University of Groningen, Groningen,
The Netherlands

Steven Deleye Molecular Imaging Center Antwerp (MICA), University
of Antwerp, Antwerp (Wilrijk), Belgium

Winnie Deuther-Conrad Department of Neuroradiopharmaceuticals,
Institute of Radiopharmaceutical Cancer Research, Helmholtz-Zentrum
Dresden – Rossendorf, Research Site Leipzig, Leipzig, Germany

Rudi A.J.O. Dierckx Department of Nuclear Medicine and Molecular Imaging,
University Medical Center Groningen, University of Groningen, Groningen,
The Netherlands

Department of Nuclear Medicine, University Hospital Gent, University of Gent,
Gent, Belgium

Yu-Shin Ding Departments of Radiology, Psychiatry and Chemistry, New York
University School of Medicine, New York, NY, USA

Cornelius Donat Department of Neuroradiopharmaceuticals, Institute of
Radiopharmaceutical Cancer Research, Helmholtz-Zentrum Dresden –
Rossendorf, Research Site Leipzig, Leipzig, Germany

Janine Doorduyn Department of Nuclear Medicine and Molecular Imaging,
University Medical Center Groningen, University of Groningen, Groningen,
The Netherlands

Shana Elman Division of Nuclear Medicine, Department of Radiology,
University of Washington Medical Center, Seattle, WA, USA

David Elmenhorst INM-2, Institute of Neuroscience and Medicine,
Forschungszentrum Jülich, Jülich, Germany

Sjoerd J. Finnema Department of Clinical Neuroscience, Center for Psychiatry
Research and Education, Karolinska Institutet, Stockholm, Sweden

Takeshi Fuchigami Pharmaceutical Sciences, Graduate School of Biomedical Sciences, Nagasaki University, Nagasaki, Japan

Uta Funke Research and Development, BV Cyclotron VU, Amsterdam, The Netherlands

Department of Radiology and Nuclear Medicine, VU University Medical Center, Amsterdam, The Netherlands

Andor W.J.M. Glaudemans Department of Nuclear Medicine and Molecular Imaging, University Medical Center Groningen, University of Groningen, Groningen, The Netherlands

Roger N. Gunn Imanova Limited, Burlington Danes Building, Imperial College London, Hammersmith Hospital, London, UK

Steen G. Hasselbalch Neurobiology Research Unit, Center for Integrated Molecular Brain Imaging, Rigshospitalet, University of Copenhagen, Copenhagen, Denmark

Memory Disorders Research Group, Department of Neurology, Neuroscience Center, Danish Dementia Research Center, Copenhagen University Hospital, Rigshospitalet, University of Copenhagen, Copenhagen, Denmark

Wolf-Dieter Heiss Department of General Neurology, Max Planck Institute for Neurological Research, Köln, Germany

Marcus Holschbach INM-5, Institute of Neuroscience and Medicine, Forschungszentrum Jülich, Jülich, Germany

Per Hartvig Honoré Department of Drug design and Pharmacology, SUND, University of Copenhagen, Copenhagen, Denmark

Department of Drug Design and Pharmacology, Faculty of Health Sciences and Medicine, Farma, University of Copenhagen, Copenhagen, Denmark

Alexander Höpping ABX Pharmaceuticals, Radeberg, Germany

Andrew G. Horti Division of Nuclear Medicine, Department of Radiology, Johns Hopkins School of Medicine, Baltimore, MD, USA

Kiichi Ishiwata Research Team for Neuroimaging, Tokyo Metropolitan Institute of Gerontology, Tokyo, Japan

Bieneke Janssen Department of Radiology and Nuclear Medicine, VU University Medical Center, Amsterdam, The Netherlands

Siegfried Kasper Division of Biological Psychiatry, Department of Psychiatry and Psychotherapy, Medical University Vienna, Vienna, Austria

Mohammed A. Khayum Department of Nuclear Medicine and Molecular Imaging, University Medical Center Groningen, University of Groningen, Groningen, The Netherlands

Michael R. Kilbourn Division of Nuclear Medicine, Department of Radiology, University of Michigan Medical School, Ann Arbor, MI, USA

Remco J.J. Knol Department of Nuclear Medicine, Medical Center Alkmaar, Alkmaar, The Netherlands

Gitte Moos Knudsen Neurobiology Research Unit, Center for Integrated Molecular Brain Imaging, Rigshospitalet, University of Copenhagen, Copenhagen, Denmark

Perry S. Kruijer Research and Development, BV Cyclotron VU, Amsterdam, The Netherlands

Adriaan A. Lammertsma Department of Radiology and Nuclear Medicine, VU University Medical Center, Amsterdam, The Netherlands

David H. Lewis Division of Nuclear Medicine, Department of Radiology, University of Washington Medical Center, Seattle, WA, USA

Pinelopi Lundquist Uppsala University PET Centre, Uppsala University Hospital, Uppsala, Sweden

National Board of Health and Welfare, Stockholm, Sweden

Gert Luurtsema Department of Nuclear Medicine and Molecular Imaging, University Medical Center Groningen, University of Groningen, Groningen, The Netherlands

Yasuhiro Magata Medical Photonics Research Center, Hamamatsu University School of Medicine, Hamamatsu, Japan

Jeffrey H. Meyer Department of Psychiatry, Center for Addiction and Mental Health, University of Toronto, Toronto, ON, Canada

Linjing Mu Department of Nuclear Medicine, Center for Radiopharmaceutical Sciences of ETH, PSI and USZ, University Hospital Zürich, Zürich, Switzerland

Morio Nakayama Pharmaceutical Sciences, Graduate School of Biomedical Sciences, Nagasaki University, Nagasaki, Japan

Agneta Nordberg Alzheimer Neurobiology Center, Karolinska Institutet, Department of Geriatric Medicine, Karolinska University Hospital Huddinge, Stockholm, Sweden

Jan Passchier Imanova Limited, Burlington Danes Building, Imperial College London, Hammersmith Hospital, London, United Kingdom

Louise Paterson Division of Experimental Medicine, Imperial College London, London, UK

Marianne Patt Department of Nuclear Medicine, University Hospital Leipzig, University of Leipzig, Leipzig, Germany

Lars R. Perk Research and Development, BV Cyclotron VU, Amsterdam, The Netherlands

Nicole Praschak-Rieder Division of Biological Psychiatry, Department of Psychiatry and Psychotherapy, Medical University Vienna, Vienna, Austria

Vanessa Raymont Division of Nuclear Medicine, Department of Radiology, Johns Hopkins School of Medicine, Baltimore, MD, USA

Department of Medicine, Center for Mental Health, Imperial College London, London, UK

Patrick Riss Department of Clinical Neurosciences, Wolfson Brain Imaging Centre, Cambridge University, Manchester, UK

Osama Sabri Department of Nuclear Medicine, University Hospital Leipzig, University of Leipzig, Leipzig, Germany

Muneyuki Sakata Research Team for Neuroimaging, Tokyo Metropolitan Institute of Gerontology, Tokyo, Japan

Heli Savolainen Department of Nuclear Medicine and Molecular Imaging, University Medical Center Groningen, University of Groningen, Groningen, The Netherlands

Arnold Spaans Research and Development, BV Cyclotron VU, Amsterdam, The Netherlands

Department of Radiology and Nuclear Medicine, VU University Medical Center, Amsterdam, The Netherlands

Steven Staelens Molecular Imaging Center Antwerp (MICA), University of Antwerp, Antwerp (Wilrijk), Belgium

Sigrid Stroobants Molecular Imaging Center Antwerp (MICA), University of Antwerp, Antwerp (Wilrijk), Belgium

Nuclear Medicine Department, University Hospital Antwerp, Antwerp (Edegem), Belgium

Garth E. Terry Department of Psychiatry, Resnick Neuropsychiatric Hospital, University of California, Los Angeles, Los Angeles, CA, USA

Jun Toyohara Research Team for Neuroimaging, Tokyo Metropolitan Institute of Gerontology, Tokyo, Japan

Hideo Tsukada Central Research Laboratory, Hamamatsu Photonics K.K., Hamamatsu, Shizuoka, Japan

Debby Van Dam Laboratory of Neurochemistry and Behaviour, Institute Born-Bunge, University of Antwerp, Wilrijk, Belgium

Aren van Waarde Department of Nuclear Medicine and Molecular Imaging, University Medical Center Groningen, University of Groningen, Groningen, The Netherlands

Jan-Peter van Wieringen Department of Nuclear Medicine, F2N, Academic Medical Center, University of Amsterdam, Amsterdam, The Netherlands

Elsmarieke van de Giessen Department of Nuclear Medicine, F2N, Academic Medical Center, University of Amsterdam, Amsterdam, The Netherlands

Jeroen Verhaeghe Molecular Imaging Center Antwerp (MICA), University of Antwerp, Antwerp (Wilrijk), Belgium

Anniek K.D. Visser Department of Nuclear Medicine and Molecular Imaging, University Medical Center Groningen, University of Groningen, Groningen, The Netherlands

Danielle J. Vugts Department of Radiology and Nuclear Medicine, VU University Medical Center, Amsterdam, The Netherlands

Matthäus Willeit Division of Biological Psychiatry, Department of Psychiatry and Psychotherapy, Medical University Vienna, Vienna, Austria

Albert D. Windhorst Nuclear Medicine and PET Research, Free University, Amsterdam, The Netherlands

Department of Radiology and Nuclear Medicine, VU University Medical Center, Amsterdam, The Netherlands

Tine Wyckhuys Molecular Imaging Center Antwerp (MICA), University of Antwerp, Antwerp (Wilrijk), Belgium

Leonie Wyffels Molecular Imaging Center Antwerp (MICA), University of Antwerp, Antwerp (Wilrijk), Belgium

Cyclotron Radiopharmacy, University Hospital Antwerp, Antwerp (Edegem), Belgium

Hiroshi Yamauchi Division of PET Imaging, Shiga Medical Center Research Institute, Moriyama-City, Shiga, Japan

Vilia Zeisig Department of Nuclear Medicine, University Hospital Leipzig, University of Leipzig, Leipzig, Germany

Part I
Basics

Debby Van Dam and Peter Paul De Deyn

Contents

1.1 Introduction to Animal Modelling for Human Brain Disease.....	5
1.1.1 Relevance of Animal Models.....	6
1.1.2 Validity of Animal Models	7
1.1.3 Homology, Analogy and Isomorphism.....	8
1.1.4 Generalisation and Extrapolation.....	9
1.2 Animal Models of Psychiatric Disorders	9
1.2.1 The Endophenotype Concept in Psychiatry.....	10
1.2.2 Approaches to Modelling Psychiatric Disease	11
1.2.3 Animal Models of Schizophrenia	12
1.3 Animal Models of Neurological Disorders	20
1.3.1 Approaches to Modelling Neurological Disorders.....	21
1.3.2 Animal Models of Alzheimer's Disease	21
1.4 Imaging in Rodent Models of Brain Disease	29
1.4.1 Imaging in Schizophrenia	30
1.4.2 Imaging in AD	32
Conclusion	34
References.....	35

D. Van Dam (✉)

Laboratory of Neurochemistry and Behaviour, Institute Born-Bunge,
University of Antwerp, Universiteitsplein 1, Wilrijk 2610, Belgium
e-mail: debby.vandam@ua.ac.be

P.P. De Deyn

Department of Neurology and Memory Clinic, Hospital Network Antwerp (ZNA),
Middelheim and Hoge Beuken, Lindendreef 1, Antwerp 2020, Belgium

Department of Neurology and Alzheimer Research Center, University Medical Center
Groningen (UMCG), Hanzeplein 1, Groningen 9713 GZ, The Netherlands
e-mail: dedeyn@skynet.be

Abstract

Animal models are important experimental tools in neuroscience research since they allow appraisal of selected and specific brain pathogenesis-related questions – often not easily accessible in human patients – in a temporal and spatial pattern. Translational research based on valid animal models may aid in alleviating some of the unmet needs in the current pharmaceutical market. Of primary concern to a neuroscience researcher is the selection of the most relevant animal model to achieve pursued research goals. Researchers are challenged to develop models that recapitulate the disorder in question, but are quite often confronted with the choice between models that reproduce cardinal pathological features of the disorders caused by mechanisms that may not necessarily occur in the patients versus models that are based on known aetiological mechanisms that may not reproduce all clinical features. Besides offering some general concepts concerning the relevance, validity and generalisation of animal models for brain disorders, this chapter focuses in detail on animal models of brain disease, in particular schizophrenia models as examples of animal models of psychiatric disorders and Alzheimer's disease models as examples of animal models of neurological/neurodegenerative disorders.

Abbreviations

AChE	Acetylcholinesterase
AD	Alzheimer's disease
APP	Amyloid precursor protein
A β	Amyloid β
BPSD	Behavioural and psychological signs and symptoms of dementia
ChAT	Choline O-acetyltransferase
<i>DISC1</i>	Disrupted in schizophrenia-1 gene
DSM-IVTR	Diagnostic and Statistical Manual of Mental Disorders 4th edition
<i>DTNBP1</i>	Dysbindin gene
<i>ERBB4</i>	Neuregulin 1 receptor gene
FRL	Flinders resistant line
FSL	Flinders sensitive line
HAB	High-anxiety-related behaviour Wistar rat line
LAB	Low-anxiety-related behaviour Wistar rat line
LI	Latent inhibition
NFT	Neurofibrillary tangle
NGF	Nerve growth factor
NMDA	N-methyl-D-aspartate
<i>NRG1</i>	Neuregulin 1 gene
PCP	Phencyclidine
PDAPP	Platelet-derived growth factor promoter-driven APP
PPI	Prepulse inhibition
PSEN	Presenilin

RELN	Reelin gene
SAM	Senescence-accelerated mouse
SAMP	SAM-prone substrain
SNP	Single nucleotide polymorphism
TDP-43	TAR DNA-binding protein 43

1.1 Introduction to Animal Modelling for Human Brain Disease

Animal models aiming at studying human disorders emerged in the 1800s and experienced a major boost over the last decades. The value of animal experimentation in the advances of human health is exemplified by the list of Nobel Prizes awarded for Physiology or Medicine. Since the beginning of the twentieth century, these prizes have chronicled the world's greatest medical advances. Of the 102 Nobel Prizes awarded for Physiology or Medicine up to 2011, 82 were directly dependent on animal-based research or the discovery relied on crucial data obtained from animal studies by other research groups.

Basic neuroscience research on animal models is essential to understand the nature of brain disorders that afflict humans and develop purposeful therapies. In the mid-1960s, the neural circuits containing and utilising the neurotransmitters dopamine and norepinephrine were visualised for the first time in rodent brain (Glowinski et al. 1966; Glowinski and Iversen 1966a, b; Iversen and Glowinski 1966). Further development of other (antibody-based) methods allowed neuroscientists to link synaptic molecules to neural circuits in rodent and nonhuman primate brains, thereby coordinating neuroanatomy, neuropharmacology and neurophysiology into a cohesive view of biochemically coded brain circuitry. Application of these techniques in human brain aided in elucidating the neurotransmitter-based nature of specific brain circuits affected in disease, e.g. the degeneration of cholinergic neurons in the basal forebrain of Alzheimer's disease (AD) patients (Whitehouse et al. 1982). The concept of synaptic communication between nerve cells as the key level of interaction in the brain further culminated with the work of E. Kandel and colleagues, who were awarded the Nobel Prize in 2000. The synapse has become a key target for pharmaceutical intervention in many brain disorders that are now understood at the level of synaptic circuitry and functional brain organisation, including multiple psychiatric disorders (e.g. schizophrenia, depression), as well as neurodegenerative disorders (e.g. AD, amyotrophic lateral sclerosis, Parkinson's disease).

The starting point for the development of a new animal model for a specific brain disease is mostly the current dominant theory about the disorder. Although a logical first approach, it is essential to broaden the focus of animal models under development based on the increasing knowledge of underlying disease mechanisms.

Animal models of human disease can be classified into spontaneous, induced, negative and orphan models, of which the two latter types are in general not relevant for psychiatric and neurological disorders. Negative models after all are models in which

a specific human disorder does not develop, while orphan models display a condition which has never been described in man or other target species. Spontaneous models are presumed to develop their condition without experimental manipulation, but selective breeding is often compulsory to establish and maintain the desired line. Especially for psychiatric and neurological conditions, few spontaneous models exist, and experimentally induced pathology is often required. Such artificial manipulations include surgical procedures, administration or withdrawal of biologically active substances, application of physical or physicochemical stimuli and genetic manipulations.

1.1.1 Relevance of Animal Models

Relevance reflects the meaningfulness and usefulness of results obtained with an animal model for a particular scientific and/or clinical purpose (van der Staay 2006). The two most important clinically inspired applications of animal models in neuroscience research are (1) the development and evaluation of mechanistic hypotheses about neurological and psychiatric disorders in general and their neural substrates in particular (i.e. brain–behaviour relation) and (2) the identification and screening of novel therapeutic approaches, most frequently drugs.

Opponents of animal research often question the relevance of animal models to understanding diseases and disease processes in humans. The disputed similarities between human and other species at the structural and functional level of the CNS are often considered a major hurdle for the use of animal models in studies of human neurological and psychiatric conditions.

Neuroscientists are far from reaching consensus about the level of similarity between the brains and ‘minds’ of humans and other species. Comparative neuroscience can provide essential information for the adequate comparison of both structural and functional aspects of human and nonhuman brain and thereby identify research areas in which animal models are likely to be useful, as well as the appropriate species for such studies. Specifically when considering models of psychiatric disease, the issue of similarities between the mental lives of animals and humans is fundamental. Animal consciousness or unconsciousness is difficult, if not impossible, to corroborate. On the other hand, one could argue whether it is necessary for the animal mind to be as complex as the human mind. Behavioural responses and brain mechanisms associated with anxiety, fear, aggression and coping serve such a crucial adaptive function that they must have evolved very early in the development of mammalian species and are probably highly conserved (Steimer 2011). Other classes of vertebrates and even lower invertebrates may display some form of anxiety and have the capacity to detect danger and react to threat, i.e. display a fight-or-flight response. Components of emotional processes, as well as the biological and neuronal logistic systems essential for their realisation, gain in complexity higher up in the phylum. Species located higher in the phylogenetic tree gain additional capabilities (e.g. autothetic consciousness in humans, orang-utans, chimpanzees and bonobos) but never lose the more primitive abilities shared with lower invertebrates (Belzung and Philippot 2007), thereby opening perspectives for the

use of lower species like zebrafish (Gerlai 2010) or even fruit flies (Iliadi 2009) in the studies of emotional responses and specific psychiatric disorders. The further focus of this chapter will be, however, on rodent models given their widespread use and applicability of microimaging techniques in these species.

Although some attributes still appear to be rather unique to the human brain, other aspects seem to be shared with more species than originally believed. Also at the neuroanatomical level, major species differences should be taken into consideration. The complex pattern of human cortical sulci and gyri, as well the extent of the prefrontal cortex, the neural substrate of many higher functions, is beyond compare in the rest of the animal kingdom (Fuster 1980). The prefrontal cortex may be present, however, in more species than initially thought, and the prefrontal to nonprefrontal cortical surface ratio in itself may not be an optimal index of evolution. Improved knowledge of rat prefrontal cortex anatomy has modified strategies to manipulate specific cortical areas to model prefrontal involvement, although reports delineating boundaries between prefrontal cortical subareas of the rat in comparison with the primate homologues show some dissimilarities. Nevertheless, current anatomical and functional data indicate that rats do have a prefrontal cortex, although not as differentiated as the primate prefrontal cortex. Rats have a functionally divided prefrontal cortex that includes not only features of the medial and orbital areas in primates, but also some features of the primate dorsolateral prefrontal cortex (Uylings et al. 2003).

1.1.2 Validity of Animal Models

The conclusions drawn from animal models largely depend on the validity of the model in representing the human condition. The more levels of validity a model satisfies, the greater its value, utility and relevance to the human condition. The validity of a model can only be determined in a multidisciplinary approach. A ‘perfect’ model would account for aetiology, symptomatology, treatment response and physiological basis, as originally proposed by McKinney and Bunney in 1969. Animal models in general do not meet all of these criteria. Moreover, in developing and assessing an animal model, it is critical to consider the explicit purpose intended for the model, because the intended purpose determines the criteria that the model must satisfy to establish its validity. The following perspectives are commonly used in the characterisation of a model’s validity (Van Dam and De Deyn 2006, 2011b).

1.1.2.1 Face Validity

Face validity refers to the resemblance between the animal model and the situation or process being modelled. It refers to the phenomenological similarity between the model and the human condition. Similarity of symptoms is most commonly used to assess face validity in animal models of behavioural dysfunction. Throughout this chapter, several behavioural paradigms will be mentioned. Writing a complete ‘how-to manual’ for the behavioural phenotyping of a new brain disease model would go beyond the scope of this chapter. For further reading, we would like to

refer the readers to excellent manuals on behavioural neuroscience as, e.g. ‘What’s wrong with my mouse?’ (Crawley 2000) and ‘Methods of Behavior Analysis in Neuroscience’ (Buccafusco 2008).

1.1.2.2 Construct Validity

Construct validity refers to the theoretical clarification of what a test measures or a model is supposed to mimic. Because a given condition may manifest itself in different ways in different species, the behaviour used in the animal model may not match that of humans, yet the test or model may still be valid. Construct validation is useful in the incessant process of further developing and refining an animal model.

1.1.2.3 Aetiological Validity

Aetiological validity is closely related to construct validity and refers to identical aetiologies or phenomena in the model and the human condition. Models with high aetiological validity are most valuable in drug development and discovery.

1.1.2.4 Predictive Validity

Predictive validity represents the extent to which the performance of the animal model in a test predicts the performance in the condition being modelled. This level of validation necessitates parallel development of clinical measures for meaningful comparisons between model and man. In a more narrow sense, this term is sometimes used to indicate pharmacological isomorphism, i.e. the model’s ability to identify compounds with potential therapeutic effects in the human condition.

1.1.3 Homology, Analogy and Isomorphism

As a consequence of the different validation levels, validity is highest in the so-called homologous models, where the symptoms displayed and the cause of the condition in the animal are identical to those of the human condition. Especially in neurosciences, homologous models are very rare and mostly limited to well-defined lesion syndromes. Analogous or isomorphic models are more common, but, although they display similar symptoms, the condition is not provoked by the same events as the human condition. In reality, most animal models are partial models, focusing only on restricted aspects of a disease, and modelling the complete condition is often not pursued. Of primary concern to neuroscientists is the selection of the most relevant animal model to achieve his/her research goals. Researchers are challenged to develop models that recapitulate the disorder in question, which is often not as straightforward as it may seem. Quite often they are confronted with the choice between models that reproduce cardinal pathological features of the disorders caused by mechanisms that may not necessarily occur in the patients versus models that are based on known etiological mechanisms that may not reproduce all clinical features. Although animal models cannot replicate human pathophysiology or psychopathology in every detail, we should envisage them as experimental systems in which selected and specific CNS pathogenesis-related questions – often not

easily accessible in human patients – can be studied in a temporal and spatial pattern. Partial models may be of substantial value in the gradual process of building a more complete image of the disease and underlying pathophysiological mechanisms, whereas more complete and complex models are only possible in case of better understood diseases (De Deyn and Van Dam 2011).

1.1.4 Generalisation and Extrapolation

The ultimate goal of animal modelling is the generalisation of results and insights to the target species, which in most occasions of course is man. The term extrapolation is also often used to describe how data obtained from animal studies can be reliably used to apply to the human condition. Extrapolation is therefore not performed in its mathematical sense, in which data fit a certain function that may be described graphically and the graph extends beyond the highest or lowest sets of data to describe a situation outside the window of observation. Generalisation across species is intrinsically based on the Darwinian evolutionary concept. Phylogenetic similarity in morphology and physiology between different species allows observations made in animals to be translated to the human condition based on homology. Related to animal models for psychiatric and neurological disorders, this cross-species comparison may focus or be based on the biological, genetic or environmental basis of personality traits (Gosling 2001) or neuroanatomical structures and their function (Striedter 1998). Uncritical generalisation or extrapolation of animal findings to the human condition may lead to unreliable or even dangerous conclusions. As a general rule, extrapolation tends to be most reliable when a plurispecies approach is taken and the condition is studied in a variety of relatively unrelated laboratory animals. Differences in metabolic patterns and speed, as well as several other confounding variables (e.g. age, sex, distress, diet, housing condition, route of administration, rhythmic variations), need to be taken into account, particularly when quantitative extrapolation is intended (De Deyn and Van Dam 2011).

Generalisation may be advanced by the development of translatable preclinical biomarkers, including small animal imaging (Kaimal and McConville 2009; Sakoğlu et al. 2011), and biochemical assays on biological fluids such as plasma and cerebrospinal fluid (Liu and Duff 2008). These biomarkers could be used to characterise the translatability of animal models, determine the translatability of a novel therapeutic intervention if the same biomarker can be used in a clinical trial, assess target engagement of investigational treatments and monitor biological responses to treatment in real time.

1.2 Animal Models of Psychiatric Disorders

Psychiatric disorders represent a diverse set of conditions, variously affecting all domains of mental function and affecting the most fundamental human attributes, namely, language, thought, perception, mood and sense of self. Many psychiatric

symptoms, e.g. hallucinations, delusions, sadness, guilt and suicidal thoughts, are probably uniquely human and cannot be convincingly ascertained in animals. Researchers should also refrain from uncritical anthropomorphising of emotional behaviour in general. Feeling anxious or depressed are subjective emotional experiences that may require a certain minimal level of consciousness that may well be uniquely human.

The evaluation of animal models of neuropsychiatric disorders is further challenged by the use of the Diagnostic and Statistical Manual of Mental Disorders, 4th edition (DSM-IVTR) criteria in the clinical diagnosis, combined with the lack of knowledge of pathophysiological mechanisms and objective diagnostic tests. DSM-IVTR diagnosis is based on phenomenology (i.e. signs, symptoms, course of illness), and mostly, a minimal number of symptoms should be present for at least a specified period of time. In the case of schizophrenia, two (or more) of the following symptoms should be present for a significant portion of time during a 1-month period (or less if successfully treated): delusions, hallucinations, disorganised speech, grossly disorganised or catatonic behaviour and negative symptoms, i.e. affective flattening, avolition, or avolition, in addition to social/occupational dysfunction (4th ed., text rev.; *DSM-IV-TR*; American Psychiatric Association 2000). Two individuals with the same DSM-IVTR diagnosis of schizophrenia may therefore present with extremely heterogeneous symptom combinations. Similar problems exist for most DSM-IVTR-based diagnoses, thereby further complicating the evaluation and validation process of newly developed mouse models for psychiatric illnesses (Nestler and Hyman 2010).

1.2.1 The Endophenotype Concept in Psychiatry

The concept of endophenotypes appears to be unique to the broad field of psychiatry. An endophenotype is a biomarker associated with genetic components, as well as the clinical symptoms of neuropsychiatric disorders. It plays an important role to bridge the gap between the microscopic and macroscopic level of neuropsychiatric disorders. It is per definition any hereditary characteristic that is normally associated with some condition but is not a direct symptom of that condition. Criteria useful for the identification of endophenotypes of diseases that display complex inheritance patterns have been suggested (Gottesman and Gould 2003):

1. The endophenotype is associated with illness in the population.
2. The endophenotype is heritable.
3. The endophenotype is primarily state-independent (manifests in an individual whether or not illness is active).
4. Within families, endophenotypes and illness co-segregate.
5. The endophenotype found in affected family members is found in nonaffected family members at a higher rate than in the general population.

Endophenotype analysis can be based on neuroanatomical, neurophysiological, biochemical, endocrinological, cognitive and neuropsychological/behavioural measures (Leboyer et al. 1998). Advanced neuroimaging techniques, including PET and SPECT, have left little doubt that specific structural CNS anomalies can be linked

to particular neurological and psychiatric diseases. Neuroimaging endophenotypes are vitally important to the identification of genetic determinants of complex brain-related disorders (Glahn et al. 2007).

The study of endophenotypes is particularly useful to understanding underlying disease mechanisms in neuropsychiatric disorders, essential for the accurate diagnosis, classification, early detection purposes, the development and evaluation of valid animal models and accelerating the drug discovery pipeline concerned.

1.2.2 Approaches to Modelling Psychiatric Disease

1.2.2.1 Behavioural Approach

In the absence of knowledge of underlying genetic causes, the first attempts to model psychiatric disturbances in animals consisted of the behavioural approach that defined behavioural assays thought to mimic particular psychiatric symptoms. Animals with specific behavioural deficits were generated through pharmacological, surgical or genetic (e.g. comparison of inbred strains) procedures. Well-known examples are the learned helplessness model of depression, spontaneous alternation indexing working memory in schizophrenia, decreased social interaction linked to autism spectrum disorder and approach–avoidance conflict behaviours associated with anxiety disorders (Crawley 2000; Mitchell et al. 2011). The development of valid behavioural models and paradigms is currently still ongoing, but with more attention for the neurobiological and clinical relevance (Baker 2011). A rodent behavioural paradigm has neurobiological construct validity if it isolates and measures a behavioural process with similar environmental regulators and neural mediators as the human process of interest. However, many behavioural assays lack sufficient construct validity, and their use in the development of rodent models for psychiatric disorder is mainly based on face validity (Moore 2010).

Although brain–behaviour relationships are assumed to be conserved across evolution for many aspects of normal motor and sensory functions, this may not be translated as easily to abnormal behaviour, let alone psychiatric disease. Animal brain circuitry and neurochemical systems involved may differ from the complex human (disease) system. A mental disorder is not characterised by an aberration in one single feature, but is a syndrome with a myriad of deviations in behaviour, cognition and/or emotion. Behavioural models of psychiatric disease, like the learned helplessness model of depression, are of course partial models that mimic only one single isolated feature of the human condition (Insel 2007).

1.2.2.2 Pharmacological Models

The administration of certain chemicals may induce behavioural changes reminiscent of specific psychiatric symptoms based on interference with central neurotransmission pathways. Understanding the mechanisms of these actions might contribute to our fundamental understanding of the illness. Drug-based models include the reserpine model of depression (Hendley and Welch 1975) and N-methyl-D-aspartate (NMDA) receptor antagonist-based models of psychosis (Andiné et al. 1999).

1.2.2.3 Genetic Models

Genetic models of psychiatric disorders were initially dominated by inbred strains, often after selection for a relevant psychiatric-like phenotype. Examples include the selectively bred Flinders Sensitive Line and the Flinders Resistant Line of rats (FSL versus FRL), a genetic animal model of depression (Overstreet et al. 1989); selectively bred Wistar rat lines with high- versus low-anxiety-related behaviour (HAB versus LAB) (Liebsch et al. 1998); and the continuous distribution of PPI (see section “[Sensory Discrimination](#)”) response amongst mouse inbred strains, which indicates PPI to be a polygenetic trait (Willott et al. 1994; Bullock et al. 1997; Paylor and Crawley 1997). The success of inbred and selectively bred strains was closely followed by single-gene models developed through homologous recombination in embryonic stem cells, as illustrated by neurokinin-1 receptor knockout mice that display significantly reduced anxiety and stress-related responses (Santarelli et al. 2001) and the glutathione S-transferase M1-knockout mouse model for autism (Yochum et al. 2010). Based on information obtained from genome-wide association studies, single-gene knockout or mutation models will undoubtedly maintain a stable position in the field of psychiatry models. They aid in assessing the putative link between gene and disorder using increasingly powerful and sophisticated tools to elucidate underlying neurobiology and disease mechanisms from the level of synapses over brain circuitry to behavioural outcome (Mitchell et al. 2011). With the advancement of genetic engineering techniques, the number of genetic mouse – and even rat – models is strongly increasing. The development of genetic rat models is of specific value for the study of psychiatric disorders, since they display more complex and sociable behaviour compared to mice. Genetic possibilities in rodents include full knockouts, spatial and/or temporal knockouts, knock-in of human alleles, and precisely engineered chromosomal rearrangements (e.g. inversions, deletions, translocations or duplications) into syntenic animal genes (van der Weyden and Bradley 2006). The theory that genes and environment combine to confer susceptibility to the development of diseases surfaced in the early half of the last century, but the use of such a framework for exploring the aetiology of psychiatric disorders is more recent. Given the fact that many – if not all – psychiatric disorders are multifactorial, sophisticated genetically engineered animal models can of course also be used to disentangle complex aetiological mechanisms with the appraisal of gene–environment interactions. Laviola et al. (2009), for example, studied the effect of repeated maternal separation or exposure to pesticides early in ontogeny on the reelin-deficient mouse, i.e. the reeler model that has been linked to autism and schizophrenia.

1.2.3 Animal Models of Schizophrenia

1.2.3.1 Aetiology and Symptomatology of Schizophrenia

Schizophrenia is a devastating and common psychiatric disorder that is associated with a high degree of medical morbidity and reduced life span. Both incidence and prevalence estimates vary across the world, and even within countries, and at the

local and neighbourhood level. The median lifetime prevalence was estimated at 4/1,000 and the lifetime morbid risk at 7.2/1,000, while the median incidence was estimated at 15.2/100,000 individuals. Incidence rates differ between sexes with a male to female ratio of 1.4:1 (for review, see McGrath et al. 2008). These variations are supportive of the assumption that schizophrenia is a clinical syndrome, perhaps comprising several disease entities.

Symptoms cluster into three categories: positive symptoms (including hallucinations, delusions, thought disorder and conceptual disorganisation), negative symptoms (including emotional blunting, social withdrawal, anhedonia, avolition, poverty of thought and content of speech) and cognitive dysfunction (including impaired executive functioning, working memory and attention) (Andreasen 1995). The onset of some aspects of the disease may be observed from birth onward, but psychotic symptoms generally become manifest in late adolescence and early adulthood in males, with an extended onset period in females (Carpenter and Koenig 2008; McGrath et al. 2008).

The dopamine hypothesis of schizophrenia proposes that dysfunction in dopaminergic neurotransmission, specifically hyperactivity of dopaminergic neurons in the limbic system and striatum, produces the positive symptoms, while underactive mesocortical dopaminergic neurons cause the negative, cognitive and affective symptoms of schizophrenia (Seeman 1987). Besides the dopaminergic hypothesis, dysfunction of the glutamatergic system has been implicated in schizophrenia (Olney and Farber 1995; Tsai and Coyle 2002). Glutamate is the major excitatory neurotransmitter in the CNS. The glutamate hypothesis posits that the function of the NMDA receptor is compromised in this disease. NMDA receptors mediate slow excitatory postsynaptic potentials, which are considered critical for the proper expression of complex behaviours, such as associative learning, working memory, behavioural flexibility and attention, many of which are impaired in schizophrenia.

1.2.3.2 Validating Animal Models of Schizophrenia

When validating animal models of schizophrenia, behavioural and electrophysiological endophenotypes are most commonly employed. Currently, still less commonly used endophenotypes focus on neurochemical alterations, e.g. brain dopamine levels (Winter et al. 2009; Ayhan et al. 2011), or on neuroanatomical changes, e.g. reduction of brain (region) volume (Ayhan et al. 2011; Drew et al. 2011), ventricular enlargement (Li et al. 2009; Ayhan et al. 2011) and dendritic spine density (Ayhan et al. 2011; Berlanga et al. 2011).

Electrophysiological Endophenotypes

Electroencephalography recordings have been widely used to assess sensory processing deficits in schizophrenia. Analogous human and rodent auditory-evoked event-related potentials that are similarly affected by pharmacological interventions and stimulus manipulations were described. The human auditory-evoked potential waveform shows characteristic positive deflections 50, 200 and 300 ms poststimulus (respectively, P50, P200 and P300) and a negative deflection 100 ms poststimulus (N100). The rodent analogues are P20, N40, P80 and P120 in order of occurrence.

When exposed to a paired-click paradigm (S1 – 500 ms interval – S2), the waveform amplitudes are lower after S2 than after S1. Schizophrenia patients display a gating deficit based on a decreased response to S1 and/or a failure to inhibit S2 that results in similar amplitudes after S1 and S2. Useful endophenotypes with acknowledged heritability include decreased P50 (P20), N100 (N40) and P200 (P80) amplitude and gating, as well as decreased P300 (P120) amplitude. Schizophrenia patients also show a reduced ability to detect changes in the auditory environment, which is measured with a mismatch negativity paradigm, an exaggerated negative voltage deflection following N100 (N40), elicited when the qualitative features of a novel tone fail to match the pattern of a previous series of repetitive tones (for review, see Amann et al. 2010).

Cognitive Endophenotypes

The cognitive phenotype can be evaluated using various protocols and paradigms (Crawley 2000), including a wide range of dry land (e.g. radial arm maze) and water mazes (e.g. Morris water maze) to specifically assess working memory. Contextual and fear conditioning are based on learning the association of a nonaversive context or cue with an aversive stimulus and the evaluation of freezing responses. The novel object recognition task is based on the rodents' tendency to focus attention on novel objects in their surroundings and the evaluation of exploration of a familiar versus a new object. Impairments in different forms of behavioural flexibility are commonly associated with schizophrenia. A number of behavioural paradigms using different sensory modalities and classes of stimuli have been developed to assess behavioural flexibility, in particular reversal learning, in rodents (Floresco et al. 2009).

Locomotor Activity

The majority of early tests for schizophrenia-related behaviours in rodents were based on the antipsychotic activity of dopamine D2 receptor antagonists (Ellenbroek and Cools 1990), with behavioural outcome parameters including locomotor hyperactivity and stereotyped sniffing and/or grooming. Locomotor activity can be scored in an open-field arena equipped with a video tracking system or infrared sensors to detect spontaneous exploration and ambulatory horizontal locomotion over a specific time frame (Crawley 2000). Motor stereotypy is mostly scored in rodents employing the Creese–Iversen stereotypy scale ranging from 0 (mouse either sleeping or inactive) to 6 (mouse engaged in continuous and nonstop route-tracing stereotypic behaviours) (Creese and Iversen 1973). Repeated administration of psychostimulants, including amphetamine, causes sensitisation to the motor-activating properties, as exemplified by enhanced hyperlocomotion and increased neuronal release of dopamine after the second or third administration. Behavioural sensitisation is quantified by repeatedly testing spontaneous ambulatory locomotion in an open-field arena (Crawley 2000).

Sensory Discrimination

Abnormalities in the automatic processes of sensory discrimination, orienting and reorienting of attention are evident in the early phases of schizophrenia. Two

attentional tasks were developed to be used both in humans and rodents: latent inhibition (LI) and PPI of the startle reflex. LI is the retarded conditioning to a stimulus that is repeatedly presented without reinforcement. In other words, the prior experience that a stimulus does not have a consequence makes it less likely that the brain will form an association with that stimulus later. LI is widely considered to relate to the cognitive abnormalities that characterise schizophrenia because it reflects an organism's ability to ignore irrelevant stimuli. One major strength of the LI task is that it can be applied across (mammalian) species (Lubow and Gewirtz 1995; for review, see Amann et al. 2010).

PPI of the startle reflex is a neurophysiological and behavioural measure of sensorimotor gating. One of its primary advantages is its ability to translate between mice and humans, as it is one of the few tests that is largely conserved across all vertebrate species. In rodents, the startle response is typically evoked using either acoustic or tactile stimuli and is characterised by contractions of the major muscles of the body, generally leading to extension of the forepaws and hind paws followed by muscle flexion into a hunched position. PPI is evoked when a weak stimulus (e.g. a 70- to 80-dB tone or a puff of air) inhibits the subsequent startle response to a strong stimulus (e.g. a 120-dB tone or a second puff of air) if presented within 100 ms. The whole-body startle from the rodent, restrained in a cylindrical holder, is quantified with piezoelectric motion sensors. Abnormal sensory inhibition may reflect a deficit in processing and prioritising incoming sensory information (Crawley 2000; for review, see Amann et al. 2010). A genetic component underlying PPI was suggested based on inbred mouse strain differences (Paylor and Crawley 1997).

Negative Symptoms

Certain negative symptoms, like poverty of speech, may be uniquely human, but other negative symptoms can be assessed in rodents using relatively simple behavioural paradigms. Anhedonia is studied with the sucrose preference test, which measures reduction in reward function in rodents (Crawley 2000). Deficits in social functioning is best scrutinised in rodents using a range of behavioural protocols, which may include a social choice paradigm for spontaneous affiliative behaviour, assessments of social recognition–discrimination, play-soliciting behaviour, social grooming, dominance, aggression and social defeat. Other negative symptoms, including avolition and blunted affect, have been studied in rodents using respectively behavioural despair tests (forced swim test and tail suspension test) and general anxiety tests, but interpretation is rather controversial (O'Tuathaigh et al. 2010).

1.2.3.3 Neurodevelopmental Schizophrenia Models

Epidemiological evidence indicates gestational or perinatal exposure to adverse environmental events, like maternal stress, malnutrition and infection, and obstetric complication (e.g. hypoxia) increases the risk of developing schizophrenia (Lewis and Levitt 2002). Exposure to early-life adverse events combined with genetic predisposition is hypothesised to trigger deviating neuronal development and connectivity leading to the development of schizophrenia. When developing animal models

based on this neurodevelopmental hypothesis, the timing of the exposure to a certain adverse event during the sensitive perinatal period is critical. Various adverse events have been applied, including postweaning social isolation (Fone and Porkess 2008), gestational exposure to the DNA-alkylating agent methylazoxymethanol acetate (Lodge and Grace 2008), exposure to bacterial or viral infection of pregnant rats (Gayle et al. 2004; Buka et al. 2008) or maternal exposure to stress (Martínez-Téllez et al. 2009; Markham et al. 2010). Depending on the chosen procedure and timing, these models may display, amongst others, disrupted sensory gating, decreased social interaction, cognitive deficits and enhanced drug-induced locomotion.

1.2.3.4 Drug-Induced Schizophrenia Models

The development of an animal model is often based on the observation that certain drugs produce abnormal behaviour in healthy people. Usually the following steps are included in the process of developing an animal model based on pharmacological compounds: (1) the drug in question induces behavioural effects in healthy people that resemble human psychiatric pathology; (2) the drug induces specific biochemical alterations in animals; (3) the drug produces similar behavioural effects in animals, allowing for any species differences in behaviour; (4) the biochemical observations in animals provide insight into the behavioural effects of the drug in humans; and (5) if the behavioural effect of the drug in humans has the same characteristics as pathological behaviour, then the biochemical changes produced by the drug in animals may also provide data relevant for the understanding of the abnormal human behaviour. The vast majority of schizophrenia-related models have been based on the induction of abnormal behaviour by psychotomimetics, including both psychostimulants and hallucinogens. These drug-induced states, however, resemble the early stages of a range of psychotic disorders, and not necessarily the diagnostic syndrome of schizophrenia.

Psychostimulant Models

The most widely studied class of drug-induced animal models of schizophrenia is based on behavioural effects of psychostimulant drugs, such as amphetamine. Amphetamine-induced psychosis has been used as a model to support the dopaminergic hypothesis of schizophrenia (Seeman 1987). A hypodopaminergic state in the frontal-cortical terminal fields of mesocortical dopaminergic neurons has also been proposed to be the basis of negative symptoms (Dworkin and Opler 1992), but these are relatively rare in amphetamine-induced psychosis, due to the hyperdopaminergic nature of this model. One of the primary consequences of amphetamine treatment is the release of catecholamines from nerve terminals. In addition to its effects on release, amphetamine also blocks the reuptake of catecholamines from the synaptic cleft, and in high dosages, it is a potent monoamine oxidase inhibitor (Kokkinidis and Anisman 1981).

In rodents, chronic amphetamine administration induces a persistent sensitisation that, both behaviourally and neurochemically, mirrors several features linked to the positive symptoms of schizophrenia. Behavioural alterations include locomotor

hyperactive and/or stereotypy or perseverative behaviours, reduced PPI and disrupted LI (for review, see Featherstone et al. 2007). While amphetamine sensitisation does not produce memory impairments similar to those seen in schizophrenia, it does produce strong impairments in set-shifting, suggesting schizophrenia-like changes in prefrontal functioning (Featherstone et al. 2007, 2008). Interestingly, rhesus monkeys displayed behavioural alterations reminiscent of schizophrenia-like hallucination, including tracking, grasping ‘at thin air’, manipulating nonapparent stimuli (e.g. picking at imaginary parasites) and hypervigilance after amphetamine administration (Castner and Goldman-Rakic 1999, 2003).

Hallucinogen Models

NMDA receptor antagonists, such as phencyclidine (PCP, ‘angel dust’) and ketamine, produce psychotic symptoms and cognitive disturbances reminiscent of schizophrenia (Cohen et al. 1962; Krystal et al. 1994), findings that have contributed to the hypoglutamatergic hypothesis of schizophrenia. As opposed to amphetamine-induced psychosis, hallucinogen-induced psychosis encompasses negative symptoms (e.g. emotional withdrawal) as well. Positive schizophrenia-like symptoms induced in laboratory animals include hyperlocomotion, stereotyped movements, circling and ataxia, while deficits in social behaviour are reminiscent of negative symptoms typical for schizophrenia. PCP and PCP-like drugs impair sensorimotor discrimination (LI and PPI) and affect performance in several cognitive paradigms, both in rats and monkeys (Javitt and Zukin 1991; Jentsch and Roth 1999).

1.2.3.5 Lesion-Induced Schizophrenia Models

To address some of the issues surrounding progressive neurodevelopmental or neurodegenerative changes in schizophrenia, a number of targeted lesion animal models have been developed. Besides electrolytic and aspiration lesions, the majority of models is based on the application of excitotoxic agents (Marcotte et al. 2001). Three major sites of actions were chosen based on their presumed involvement in schizophrenia, i.e. the prefrontal cortex, hippocampus and thalamus. The prefrontal cortex is involved in higher cognitive functions, including attention, working memory, emotional expression and social interaction. Executive function allows us to interact with the world in a purposive, goal-directed manner. It relies on several cognitive control operations that are mediated by different regions of the prefrontal cortex. The hippocampus modulates activity of the prefrontal cortex and thus exerts direct control over the schizophrenia-linked mesolimbic dopaminergic system. The thalamus is the brain’s relay station that filters and gates sensory information and is therefore involved in PPI. Despite reasonable claims of predictive and face validity for many adult lesion models, the required size and temporal nature of these lesions limits their construct validity as animal models of schizophrenia. The neonatal ventral hippocampus lesion model is the best characterised model to test neurodevelopmental hypotheses of schizophrenia. This excitotoxicity model leads to dopamine-related behavioural alterations in adolescence or early adulthood, which include hyperlocomotion in response to stress, sensory gating deficits (PPI and LI),

disturbed working memory and reduced social contacts, as well as psychotomimetic-induced hyperactivity, apomorphine-induced stereotypies and reduced catalepsy in response to haloperidol. Aberrant development of the prefrontal cortex, illustrated by molecular changes in this region, in response to neonatal hippocampal damage may be a critical factor in the onset of symptoms (for review, see Lipska and Weinberger 2000). The neonatal rat excitotoxic brain lesion model was also adapted to the ventral thalamus (Wolf et al. 2010) and the prefrontal cortex (Klein et al. 2008; Lazar et al. 2008).

1.2.3.6 Genetic Schizophrenia Models

As exemplified by twin studies, schizophrenia has a substantial genetic component (Cardno et al. 1999). An important shift can be observed in the way animal models are being used for the genetic dissection of psychiatric disease. Initially, inbred strains, often selectively bred for a disease-specific trait, dominated the literature, followed by single-gene knockout or mutation models developed with homologous recombination in embryonic stem cells. Whole-genome association studies are presently expected to provide strong evidence for the involvement of susceptibility genes that will lead to attempts to model multiple susceptibility genes. In addition, the development of microarray and proteomic technology has enabled global description of gene expression in schizophrenia, although it may be difficult to distinguish between primary aetiology and secondary pathology, confounding influences or compensatory mechanisms. Changes in gene expression with a primary etiopathological role may arise from sequence variants in regulatory regions of genomic DNA, epigenetic/stochastic variation or environmental influences, while secondary changes may reflect points of convergence in the action of individual susceptibility genes (for review, see Bray 2008). Given the complex aetiological nature of schizophrenia, genetic models expressing risk genes may form the basis to study the effect of environmental manipulation on such mutant phenotypes at specific developmental stages and may help in defining the trajectory, relative contribution of and interaction between genes and environmental factors in the emergence of the schizophrenia phenotype (Desbonnet et al. 2009).

Inbred and Selectively Bred Rodent Strains

Remarkable variability in outcome of specific cognitive and behavioural tasks is evident in different rodent strains (van der Staay and Blokland 1996; Crawley et al. 1997; Crawley 2000). Genetic factors determine sensory and sensorimotor gating in rodents, and consequently, strain differences in baseline startle response and PPI have been described (Paylor and Crawley 1997; Palmer et al. 2000; Willott et al. 2003; Pietropaolo and Crusio 2009). Moreover, strain and substrain differences for pharmacological (e.g. amphetamine-based) disruption of sensorimotor gating were observed (Kinney et al. 1999; Swerdlow et al. 2000, 2012; Varty et al. 2001). Interestingly, strain-dependent changes across adolescence have been observed, indicating that genetic factors and the early adolescent phase are critically important considerations in the design of animal models of neuropsychiatric disturbances (Pietropaolo and Crusio 2009). Variations between strains and substrains, whether

or not accomplished through selective breeding, form a good basis to study the underlying biological mechanisms and hence, therapeutic strategies in schizophrenia (Swerdlow et al. 2005, 2012; Dieckmann et al. 2007; Gogos et al. 2008; Flood et al. 2011).

Genetically Modified Models

Promising candidate genes for schizophrenia are dysbindin (*DTNBP1*, for review, see Williams et al. 2005); neuregulin 1 (*NRG1*) and its receptor *ERBB4* (for review, see Banerjee et al. 2010); *DISC1* (i.e. disrupted in schizophrenia-1; for review, see Muir et al. 2008); reelin (*RELN*; for review, see Grayson et al. 2006); components of the Akt-GSK3 β signalling pathway, including AKT1 (Freyberg et al. 2010); and genes located in chromosomal region $\Delta 22q11.2$, which has been implicated in schizophrenia based on the 22q11.2 deletion syndrome (for review, see Paylor and Lindsay 2006). For an updated list of published genetic association, studies for schizophrenia readers are referred to the SzGene database (Allen et al. 2008).

Several spontaneous mutant rodent models have been studied as presumed phenocopies of schizophrenia. The *sandy* mouse has a deletion of two of the exons of the dysbindin gene and is therefore a naturally occurring dysbindin-knockout model. *Sandy* mice display some behavioural phenotypes with relevance to schizophrenia, including increased anxiety and deficits in social interaction (Hattori et al. 2008). After the discovery of *DISC1* as a potential schizophrenia candidate gene, some of the earliest animal studies on its potential role included the detection of natural mutations in different mouse strains. All 129 mouse substrains carry a 25-bp deletion in the *mDISC1*, which modulates working memory (Clapcote and Roder 2006; Koike et al. 2006). Reeler is an autosomal recessive mutant mouse with reduced cerebellar size, disruption of the laminar organisation in several brain regions and inversion of neocortical cellular layers (Falconer 1951; Caviness 1976). The reelin-haploinsufficient heterozygous reeler mouse has been used as an animal model for schizophrenia based on several neuropathological and behavioural abnormalities homologous to schizophrenia. Heterozygous reeler mice exhibit alterations in sensorimotor gating (Barr et al. 2008), deficits in working memory (Brigman et al. 2006) and impaired social interaction (Podhorna and Didriksen 2004).

DNA variation that affects expression of candidate disease genes can take various forms, including single nucleotide polymorphisms (SNPs), deletions, insertions, variable repeat sequences, rearrangements or duplications (copy number variations). Downregulation of individual susceptibility genes can be mimicked via gene knockout or via RNA interference, while upregulation can be achieved with gene knock-in techniques or RNA activation.

Multiple genes (perhaps thousands) of small effect are thought to exist for the illness, given its status as a complex genetic illness (Gejman et al. 2011). Nonetheless, tissue effects in animals with risk mutations are presumed to be associated in some way with schizophrenia pathophysiology. The biological characterisation of animals with risk genes is highly relevant to ultimately discovering disease pathophysiology, even though every aspect of the biology may not be critical. For the currently most promising risk genes, few transgenic mouse models will be briefly discussed.

Many mouse models with manipulated expression levels of the different NRG1 isoforms have been created. Mutants with heterozygous deletion of the transmembrane domain exhibit hyperactivity, a deficit in PPI, selective impairment in social novelty preference and altered patterns of social interaction. Studies focusing on deletion of specific NRG1 isoforms have shown that type III NRG1 mutant mice display even more pronounced PPI deficits in addition to working memory dysfunction (for review, see Desbonnet et al. 2009). Homozygous knockout of *NRG1* is developmentally lethal in mice, but viable heterozygous, hypomorphic/conditional knockouts that can modulate neuregulin–ErbB4 signalling have been developed, all with distinct ‘schizophrenia-like’ alterations, including – depending on the genetic models studied – hyperactivity, PPI, LI and social interaction deficits, impairment in contextual fear conditioning and mismatch negativity (Harrison and Law 2006; Mei and Xiong 2008; for review, see Jones et al. 2011). Seven different strains of transgenic mice containing inducible and/or partial *DISC1* gene mutations resulting in a (partial) loss of DISC-1 function have been created (for review, see Jaaro-Peled 2009). These mice exhibit enlarged lateral ventricles and reduced cortical thickness and brain volume, mimicking some characteristics of schizophrenia. Some mutants display reductions in hippocampal dendritic complexity, structure and density. Some *DISC1* mice display PPI deficits that are attenuated with antipsychotics, while hyperactivity, reduced sociability, working memory and executive function impairments have been described as well.

Discussing all currently developed genetic models of schizophrenia would go beyond the scope of this chapter. Readers are referred to some of the recent review papers referred to in the preceding paragraphs or the Schizophrenia Research Forum website for more in-depth information (<http://www.schizophreniaforum.org/>).

1.3 Animal Models of Neurological Disorders

The discovery of new therapies for neurological disorders is predicated on the use of animal models both to identify new therapeutic targets and to perform preclinical trials of drugs prior to clinical application. In both cases, the challenge is to develop models that recapitulate the disorder. The starting point for the development of a new animal model for a specific neurological condition is often the current dominant theory about the disease. Although a logical first approach, it is essential to broaden the focus of animal models under development based on the increasing knowledge of underlying disease mechanisms. The development of animal models for Alzheimer’s disease (AD) serves an excellent example of such a strategy.

Advances in biochemical pathology and human genetics have yielded striking progress in our understanding of molecular mechanisms underlying nervous system diseases such as AD, Parkinson’s and Huntington’s disease. Of great importance is the pivotal concept that certain normally soluble neuronal proteins can misfold and aggregate into oligomers and fibrils, which can confer profound cytotoxicity. Perhaps the foremost example, both in terms of its societal impact and how far knowledge has moved toward the clinic, is that of AD, hence the focus of the following paragraphs.

1.3.1 Approaches to Modelling Neurological Disorders

In contrast with psychiatric disorders, approaches to model neurological conditions are not easily categorised. The approach largely depends on the aetiology of the human neurological condition, which may be acquired or degenerative. Specific approaches when developing new animal models should be applied depending on the aetiology, which may be amongst others infectious (e.g. Creutzfeldt–Jakob disease, HIV dementia), immune-related (e.g. multiple sclerosis), genetic (e.g. Charcot–Marie–Tooth disease; leukodystrophies), lesion-based (e.g. head trauma), and environmental/toxicity-related (e.g. alcohol-related dementia, toxic-metabolic encephalopathy).

1.3.2 Animal Models of Alzheimer’s Disease

1.3.2.1 Aetiology and Symptomatology of Alzheimer’s Disease

As the prototype of cortical dementias, AD is characterised by prominent cognitive deficits. Patients initially exhibit limited forgetfulness with disturbance of memory imprinting, which further evolves to short-term memory disruption and, ultimately, to long-term memory deficits. At more advanced stages, patients display executive dysfunctioning leading to advanced helplessness (Selkoe 2000). Besides cognitive deterioration, patients demonstrate behavioural and psychological signs and symptoms of dementia (BPSD), including paranoid and delusional ideation, hallucinations, activity disturbances, aggressiveness, diurnal rhythm disturbances, affective disturbances, anxieties and phobias (Reisberg et al. 1987). The histopathological hallmarks of AD brain are extracellular amyloid- β (A β) plaques and intracellular neurofibrillary tangles (NFT), accompanied by decreased synaptic density, which eventually leads to widespread neurodegeneration and failure of neurotransmitter pathways, particularly those of the basal forebrain cholinergic system (Selkoe 2001). The number of affected individuals is likely to grow in the decades to come as a result of demographic changes and rising life expectancy. It is forecast that the worldwide number of elderly people suffering from dementia will rise to 63 million in 2030 and to 114 million in 2050 (Wimo et al. 2003).

1.3.2.2 Validating Animal Models of Alzheimer’s Disease Cognitive Symptoms

A variety of paradigms and protocols has been developed to assess cognitive functions in rodents (for review, see Crawley 2000 and Buccafusco 2008). Ideally, several paradigms requiring distinct sensory and motor abilities are chosen when phenotyping a new dementia model. Protocols distinguishing explicit versus implicit memory can be chosen, as well as designs assessing short-term versus long-term memory (Tulving 1987). The Morris water maze is presently the most widely used paradigm for the evaluation of hippocampus-dependent visual-spatial learning and memory skills in rodents, which represents the highest cognitive level appreciable in rodents (for review, see; D’Hooge and De Deyn 2001). Besides the Morris

water maze, several other mazes could be employed, which are all based on the same principle; successfully passing through the maze is rewarded by escaping from the water in wet mazes or by food as a positive reinforcer in dry-land mazes. Examples include the plus-shaped water maze, radial arm mazes, multiple Y mazes and the Barnes maze. Complex nonspatial hippocampus-dependent tasks like the odour paired-associates task (Bunsey and Eichenbaum 1996) are analogous to the verbal paired-association task for humans, but the long duration of the protocol, which requires several months, makes it unsuitable for the assessment for memory in progressing phenotypes (Van Dijck et al. 2008). The same disadvantage may arise when using schedule-induced operant tasks employing operant conditioning or Skinner boxes. Both active and passive avoidance learning protocols are widely used to assess cognitive function in a short time frame. However, procedural components of the task are not easily distinguishable from declarative memory components as is the case in the Morris water maze or in cued and contextual learning (Crawley 2000). Associative learning (cued and contextual conditioning) requires a different set of sensory and motor functions, so that the procedural components of associative tasks do not overlap. Other potentially useful learning and memory tasks include novel object recognition, conditioned taste aversion, social recognition and discrimination learning.

BPSD-Related Symptoms

In accordance with the increased clinical focus on BPSD, major efforts have been made to mimic specific behavioural alterations in animal models and to develop useful tools (for review, see Crawley 2000 and Buccafusco 2008) to evaluate new psychopharmacological strategies to replace atypical antipsychotics or classic neuroleptics, which display only modest effect size and are frequently associated with significant side effects (De Deyn et al. 2005).

Activity and circadian rhythm disturbances can be easily screened using infrared sensors surrounding the animal's home cage. The number of beam interruptions over a specific time interval is recorded as a measure of activity comparable to actigraphic measurements in the clinical setting (Vloeberghs et al. 2004). Aggressive behaviour in male rodents can be provoked using a variety of behavioural protocols based on dominance hierarchy, as is the case in the commonly used isolation-induced resident-intruder protocol (Valzelli 1973). Anxiety and fear-related behaviours can be assessed using both conditioned (i.e. conflict tests like the Vogel's lick-suppression test) and unconditioned response tests, which are based on the quantification of fear-related responses like freezing, defecation and thigmotaxis, and the conflict between the innate trait of nocturnal animal like mice and rats to prefer narrow, dark enclosures and the tendency to explore new environments (Crawley 2000). Appraisal of depression-related symptoms in rodents is based on learned helplessness and behavioural despair phenomena, in which animals are exposed to uncontrollable and inescapable stress, e.g. the Porsolt forced swim test, the tail suspension test and inescapable shock paradigms. Failure to try to escape from this type of aversive stimulus in rodents is considered to model a depression-like state (Chourbaji et al. 2005). Anhedonia, a core symptom of clinical depression, which is defined as the

loss of sensitivity to reward, can be assessed in rodents with a sucrose preference test during which the consumption of a 0.8 % sucrose solution is compared to the simultaneous consumption of tap water (Sanchis-Segura et al. 2005). Phenotyping can also focus on ingestive behaviour. The intake of food and water can be screened using metabolic cages. More detailed analysis of food intake is possible in operant conditioning boxes equipped with pellet dispensers and optical lick-o-meters that allow appraisal of the circadian rhythm of ingestive behaviour (Vloeberghs et al. 2008).

Pathological Alterations

Amyloid structure is most commonly stained using congo red, thioflavin S or A β -specific antibodies (for review, see Castellani et al. 2007; Vidal and Ghetti 2011). Amyloid plaque burden can be evaluated by employing stereological methods, which allow a three-dimensional geometrical interpretation of structures based on observations made on two-dimensional sections. Levels of A β peptides and other APP-derived molecules can be quantified using ELISA or Western blotting techniques. While ELISA is a very sensitive method to detect and quantify total A β levels, commercially available kits provide no or very little information on the possible aggregation state and structure of A β . Western blotting, on the other hand, is less suited for quantification but makes it possible to detect aggregates and roughly estimate their size. However, it still only provides very limited information about the structure and composition of the aggregates. Researchers more interested in the molecular structure, composition and formation of the oligomers turned to mass spectrometry techniques, which allow very accurate determination of protein identity, amino acid sequence and presence of modifications, or even – when using non-denaturing approaches – the macromolecular structure (Ashcroft 2010; Bleiholder et al. 2011). Tau pathology can be assessed at various levels, including a quantitative assessment using Western blot, biochemical and immunohistochemical determination of different phosphorylation states and sites, as well as the immunohistochemical assessment (e.g. with the ALZ-50 monoclonal antibody) of the spatiotemporal progression of tau pathology (Rankin and Gamblin 2008). Monitoring inflammatory processes can be based on the use of histopathological and immunohistochemical markers of astrocyte and microglia activation, as well as on various biochemical assays of inflammatory markers in body fluids (McGeer and McGeer 2003). Potential biomarkers of oxidative stress, including an imbalance between free radicals (reactive oxygen and nitrogen species) and the antioxidant response (free radical scavengers and antioxidant enzymes), as well as the subsequent damage to macromolecules (lipids, proteins, nucleic acids and sugars), can be determined in body fluids or brain using a wide range of biochemical techniques, including spectrophotometric, fluorometric, chromatographic and immunohistochemical assays (Migliore et al. 2005). Degenerative processes (e.g. neuritic spheroids) can be visualised by silver impregnation, neurofilament or ubiquitin immunostaining (Castellani et al. 2007).

Neurochemical Alterations

The cholinergic hypothesis of AD is based on the fact that degeneration of cholinergic neurons in the nucleus basalis of Meynert, situated in the basal forebrain and

primarily projecting to the neocortex, occurs early in the course of the disease and leads to a marked decline in the activities of choline O-acetyltransferase (ChAT) and acetylcholinesterase (AChE) (for review, see Contestabile 2011). In rodent models, the presence of cholinergic deficits can be scrutinised with the determination of ChAT or AChE enzyme activities based on, respectively, a radiochemical (Fonnum 1975) and a spectrophotometric (Ellman et al. 1961) protocol. Microdialysis extraneuronal sampling coupled with a high-sensitivity HPLC detection and quantification method has been often used for assessing the cholinergic impairment and its recovery in many AD models (Pepeu and Giovannini 2007). Moreover, immunohistochemical visualisation and quantification of ChAT- or AChE-positive neurons and fibres has been employed, as well as determination of high-affinity choline uptake, considered a biochemical marker of the localisation and integrity of the cholinergic nerve endings and a measure of the activity of the cholinergic neurons (for review, see Pepeu and Rosi 2011).

Neurochemical alterations observed in AD brain, however, are not confined to the cholinergic system. Moreover, many data indicate that the neurochemical alterations underlying cognitive deterioration and related disturbances in cortical processing implicate more widespread neurodegeneration that cannot be attributed solely to the cholinergic system (for review, see Dringenberg 2000). Neuronal loss and, inherently, alterations in the concentration of neurotransmitters and metabolites of the noradrenergic, adrenergic, dopaminergic and serotonergic system, as well as neurotransmitter amino acids, have been described in AD (for review, see Gsell et al. 2004). In rodent models, chromatography-based determination of neurotransmitter (and metabolite) levels in microdialysis samples or brain (region) homogenates can be employed to assess neurotransmitter alterations. Deficits in peptidergic neurotransmission (or co-transmission) have been implicated in AD. Classically, neuropeptides are mainly studied by radioimmunoassay and immunohistochemistry, but recently researchers have shifted to mass spectrometry-based methodologies (for review, see Van Dam et al. Accepted for publication *Current Alzheimer Research* 2013).

1.3.2.3 Spontaneous and Selectively Bred Alzheimer's Disease Models

Some species, including dogs (Cummings et al. 1993, 1996; Rofina et al. 2006), cats (Head et al. 2005; Gunn-Moore et al. 2006), bears (Cork et al. 1988; Tekirian et al. 1996; Uchida et al. 1995), goats and sheep (Braak et al. 1994), wolverine (Roertgen et al. 1996), as well as several nonhuman primate species (Bons et al. 1994; Gearing et al. 1994, 1997; Lane 2000; Geula et al. 2002; Kimura et al. 2003; Sani et al. 2003; Lemere et al. 2004, 2008), spontaneously develop plaque pathology and some species even display tauopathies. These histopathological changes can be accompanied by cognitive decline (Cummings et al. 1996; Voytko and Tinkler 2004; Rofina et al. 2006; Gunn-Moore et al. 2006). The use of these species for experimental research is however limited by availability, economical (based on long lifespan) and/or ethical reasons.

Ageing rodents do not spontaneously develop histopathological AD-like hallmarks, but do display senescence-related cognitive decline and behavioural alterations associated with neurochemical and morphological alterations (Erickson and

Barnes 2003), including age-associated cholinergic hypofunction (Sherman and Friedman 1990). In addition, they aid in uncovering the boundary between normal and pathological ageing, allowing in-depth investigation of basic neural mechanisms underlying brain ageing.

Selective breeding from a genetic pool of AKR/J mice has led to the development of the senescence-accelerated mouse (SAM) model, which includes nine major SAM-prone (SAMP) substrains and three major SAM-resistant substrains. The SAMP8 substrain is of particular interest given the development of age-associated learning and memory deficits in association with A β deposition (Butterfield and Poon 2005; for review, see Ren \tilde{a} and Butterfield 2011).

Pharmacological, Chemical and Lesion-Induced Rodent Models of Alzheimer's Disease

Disruption of multiple neurotransmitter systems underlies the cognitive and behavioural disturbances associated with AD. The majority of animal models that fall within this category are based on the cholinergic hypothesis of AD, which states that degeneration of cholinergic neurons in the nucleus basalis of Meynert, located in the basal forebrain and projecting to the neocortex, occurs early in the course of the disease (Davies and Maloney 1976; Whitehouse et al. 1982). The most widely used pharmacological model is scopolamine-induced amnesia (Sunderland et al. 1986; Ebert and Kirch 1998). The application of this muscarinic antagonist has increased our knowledge of the role of the cholinergic system in cognition and allows preclinical evaluation of symptomatic efficacy of cholinomimetics. The applicability of this model is however limited by the fact that cholinergic hypofunction is not associated with the development of AD-typical pathology, and the lack of disease progression both at the cholinergic and cognitive level. Blockade of nicotinic receptors by mecamylamine also induces learning impairment (Moran 1993; Estap \acute{e} and Steckler 2002). Since AD brain shows both reduced muscarinic and nicotinic acetylcholine receptor densities (Whitehouse and Au 1986; Nordberg et al. 1989), blockade of both receptors may offer a better animal model for AD-related amnesia (Levin et al. 1990; Riekkinen et al. 1990).

In addition to scopolamine-induced amnesia, cortical cholinergic involution has been replicated in lesion models that focus on specific cholinergic centres of the basal forebrain, as well as more general lesions of all basal forebrain cholinergic neurons. Focal lesions are most often directed at the nucleus basalis magnocellularis (Lescaudron and Stein 1999; Vale-Mart \acute{i} nez et al. 2002), the rodent analogue of the nucleus basalis of Meynert, the septal area (Mulder et al. 2005), or include fimbria/fornix transection leading to septo-hippocampal cholinergic denervation (He et al. 1992; Alonso et al. 1996). Lesions can be induced by mechanical, i.e. knife cut, or electrolytic procedures and intraparenchymal or intracerebroventricular microinjections of neurotoxic substances, such as quinolic, kainic, ibotenic and quisqualic acids, NMDA, the cholinotoxin AF64, and the immunotoxin 192 IgG-saporin (for review, see Toledana and Alvarez 2011). Such lesion models increase our understanding of the role of cholinergic innervations in the aetiology and treatment of cognitive disorders.

AD-related memory deficits can also be (partially) reproduced by lesioning brain structures or pathways essential for different aspects of learning and memory, such as the hippocampus, striatal or cortical regions (Gray and McNaughton 1983; Glenn et al. 2003; Sloan et al. 2006; Castañé et al. 2010). These models increase our knowledge of the neural mechanisms underlying memory dysfunction, but of course lack disease progression and do not develop AD-like pathological hallmarks. Moreover, selected lesions are compared with the more global disease process of AD.

Certain chemically induced models focus on one specific pathophysiological pathway thought to underlie AD, such as neuroinflammation or glucose/energy metabolism impairment, and their effects on neurodegeneration. Neuroinflammation develops upon the infusion of endotoxins, like lipopolysaccharide (Hauss-Wegrzyniak et al. 1998), or proinflammatory cytokines (Wenk et al. 2003). Brain metabolism can be disrupted through interference with mitochondrial metabolic pathways (Szabados et al. 2004) or neuronal insulin signal transduction (Ishrat et al. 2009).

1.3.2.4 Amyloid- β Infusion Rodent Models of Alzheimer's Disease

The amyloid cascade hypothesis states that cerebral accumulation and aggregation of A β peptides into amyloid plaques is the primary culprit in AD (Selkoe 2000; Hardy and Selkoe 2002). More recently, a key role was assigned to soluble A β oligomers (Gong et al. 2003; Lacor et al. 2004; Walsh and Selkoe 2007; Selkoe 2008) (Fig. 1.1).

Aspects of AD can be modelled by acute or repetitive intracerebral or intracerebroventricular infusion of A β peptides in rodent brain (for review, see Lawlor and Young 2011). To better mimic the progressive nature of AD, chronic and continuous administration is accomplished by connecting an implanted cannula to an osmotic mini-pump (Nakamura et al. 2001; Olariu et al. 2002) or a micro-infusion pump (Nag et al. 1999), or with microdialysis (Harkany et al. 2000). In addition to measurable adverse effects on memory and behaviour (Harkany et al. 1998; Yamada et al. 2005; Sipos et al. 2007), exogenous administration of A β peptides can lead to AD-like neuropathological alterations (Frautschy et al. 1996; Sipos et al. 2007), although the full complexity of the human pathology is not reproduced and pathology is not widespread as in patients. Accumulation of A β deposits can be associated with, e.g. inflammation and microglial activation, oxidative stress and local cell loss (Weldon et al. 1998). More specifically, disruption of cholinergic function was reported (Harkany et al. 1998; Yamada et al. 2005).

CNS A β infusion animal models provide insight into the mechanisms and secondary effects of A β toxicity and allow preclinical evaluation of drugs targeting A β , as well as evaluation of protective efficacy of pharmacological modulation of microglial signalling. Rodent infusion models have some advantages over transgenic amyloid-related models. Infusion models can deliver the desired (pathological) outcome within a time frame of a few weeks (Frautschy et al. 1996) versus several months in transgenic models. Moreover, they allow researchers to administer defined amounts of a specific A β species of known sequence and length or to introduce controlled cofactors related to plaque development, while transgenic overexpression of APP results not only in increased production of A β 1-40 and/or A β 1-42, but in elevated

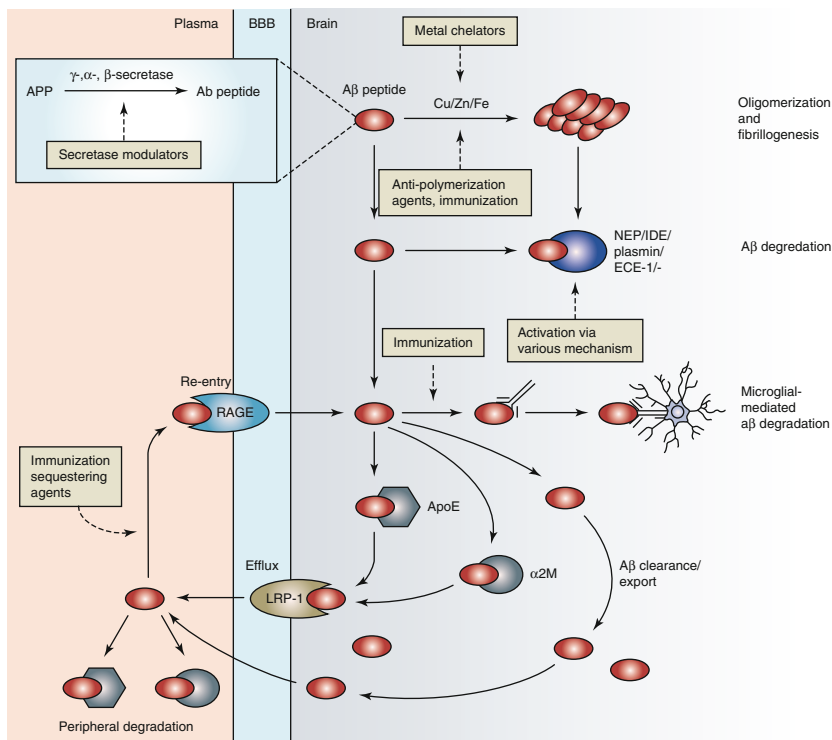


Fig. 1.1 This figure represents the major processing pathways of amyloid precursor protein (APP) and amyloid β ($A\beta$) peptides, including the potential therapeutic targets and therapeutic interventions. *APP* amyloid precursor protein, *CTF* C-terminal fragment, *NTF* N-terminal fragment, *A β* amyloid β peptide, *ApoE* apolipoprotein E, *BBB* blood–brain barrier, *CSF* cerebrospinal fluid, *ECE-1* endothelin-converting enzyme-1, *IDE* insulin-degrading enzyme, *LRP-1* low-density lipoprotein receptor-related protein-1, *NEP* neprilysin, *RAGE* receptor for advanced glycation end products, *$\alpha 2M$* α -2-macroglobulin

levels of other APP fragments, which can have neuroprotective, neurotoxic or signaling functions and influence learning and memory. On the other hand, major caveats of infusion models are the fact that administered $A\beta$ concentrations are much higher than $A\beta$ levels found in the brain or cerebrospinal fluid of AD patients (Vickers et al. 2000) and that effects of ageing on AD progression are lacking. Moreover, the invasive nature of $A\beta$ infusion inevitably brings about brain injury, which – in addition to the potential neurotoxic effects of vehicles used – may contribute to the induction of inflammation observed in these models. These potentially confounding effects should be controlled for by including proper sham and/or scrambled peptide groups.

1.3.2.5 Genetically Modified Alzheimer’s Disease Mouse Models

Modelling of AD in transgenic mouse models became reality in the mid-1990s with the development of the platelet-derived growth factor promoter-driven APP (PDAPP) model (Games et al. 1995; for review, see Basak and Holtzman 2011), followed in

subsequent years by the Tg2576 (Hsiao et al. 1996; for review, see Deacon 2011) and the APP23 mouse model (Sturchler-Pierrat et al. 1997; for review, see Van Dam and De Deyn 2011a), currently the most widely used amyloidosis models in AD-related research. The choice of *APP* as the incorporated transgene was based on two lines of evidence: *APP* is the precursor of $A\beta$ and it is the target of the first described early-onset AD mutations. The PDAPP model expresses human *APP* carrying the Indiana familial AD mutation driven by the platelet-derived growth factor- β promoter, whereas both the Tg2576 and APP23 model express human *APP* with the Swedish mutation driven by the hamster prion protein and murine Thy-1 promoter, respectively. The discovery of familial AD mutations in the presenilin (*PSEN*) genes, which influence *APP* processing, opened the path for *PSEN1* and *PSEN2* transgenic mouse models and double-cross *APP/PSEN* models. Although early-onset AD accounts for only a small proportion of AD cases, models expressing pathogenic mutations of human genes have become crucial tools in unravelling disease processes and have boosted drug discovery and development.

Apolipoprotein E (ApoE) has been identified as a major genetic risk factor for developing late-onset AD. Mice expressing a human ApoE isoform, such as Apo ϵ 4 (Huber et al. 2000), have been developed to study the pathophysiological link between ApoE and AD.

Genetically modified mouse models based on other aetiological hypotheses that are considered relevant to the preclinical AD field include, e.g. mutated human α -synuclein models (Freichel et al. 2007), TAR DNA-binding protein 43 (TDP-43)-related models (Wu et al. 2010; Wils et al. 2012), mutated human cyclooxygenase-2 overexpression models (Andreasson et al. 2001), anti-nerve growth factor (NGF) mice (in which NGF activity is neutralised using antibodies) (Capsoni et al. 2000), neprilysin (Iwata et al. 2001), insulin-degrading enzyme knockout mice (Farris et al. 2003) and recent crosses between mutated human *APP* overexpression strains and nitric oxide synthase 2 knockouts (Colton et al. 2008). For more in-depth information and latest updates, readers are referred to the Alzheimer Research Forum website (<http://www.alzforum.org>), which includes an online compendium of relevant mouse models for AD and related disorders. Most of these models robustly mimic a subset of AD features, including $A\beta$ deposition, plaque formation and cerebral amyloid angiopathy, as well as neurodegeneration, synaptic dysfunction and inflammation, in addition to cognitive decline.

The major limitation of the above-mentioned models, i.e. the lack of NFT formation, was partially counterbalanced with the development of several (mutated) tau models, and the crossing of tau and amyloidosis models, which featured enhanced amyloid deposition accompanied by tau phosphorylation, NFT-like formation and overt neuronal loss (Götz et al. 2004; Ribé et al. 2005). It has proven challenging to develop mice in which both histopathological hallmarks occur in AD-relevant brain regions, such as the hippocampus and cortex. However, the development of triple transgenic (3 \times Tg) mice seems to have overcome this hurdle (Oddo et al. 2003; for review, see Sy et al. 2011). Rather than crossing independent mutant mouse lines, two transgenes (mutant *APP* and tau) were microinjected into single-cell embryos from homozygous mutant *PSEN1* mice. The major advantages of this approach are

the integration of APP and tau at the same genetic locus (which prevents segregation in subsequent generations), more cost-effective breeding requirements and the fact that there is no mixing or altering of the genetic background. In accordance with the amyloid cascade theory, these 3×Tg mice develop A β plaques prior to NFT pathology with a temporal and spatial profile equivalent to AD. Studies using the 3×Tg-AD mice have revealed a strong interaction between A β and tau, which synergistically drive the pathogenesis in the brain. The first signs of cognitive decline manifest at age 4 months as a deficit in long-term retention and correlate with accumulation of intraneuronal A β in the hippocampus and amygdala (Billings et al. 2005).

For an updated list of genetically modified AD-related models, readers are referred to the website of the Alzheimer Research Forum (<http://www.alzforum.org/res/com/tra/default.asp>).

More recently, the use of viral vector gene transfer technology has allowed the development of ‘somatic transgenic’ models, whereby genes putatively involved in AD pathogenesis can be selectively overexpressed in specific brain regions involved in AD (for review, see Jaworski et al. 2010; Lawlor and Young 2011). Although this promising strategy has been shown to result in the development of both cognitive deficits and A β deposits, these genetic models require further characterisation to show reproducible development of behavioural deficits and neuropathology prior to their widespread adoption as a reliable and useful model of AD.

1.4 Imaging in Rodent Models of Brain Disease

This chapter does not aim at giving an overview of neuroimaging involving PET and SPECT in models of brain disease, but rather serves as an introduction to models of brain disorders with a selected overview of modelling approaches and methodological aspects with regard to phenotyping. We will briefly describe some relevant imaging techniques and show a couple of examples related to schizophrenia and AD.

With the development of more sophisticated techniques, neuroimaging has become an essential component of studying brain structure and function in the diseased state. In drug development research, utilising methodology and results that can easily be translated from preclinical to clinical platforms will facilitate the identification and the assessment of efficacy of neuroprotective therapeutic compounds to treat CNS diseases. Translational neuroimaging can provide quantitative information on brain morphology and function in preclinical models of CNS diseases, healthy human subjects and patients. Amongst the variety of imaging methods used for understanding and treating brain diseases are PET, SPECT, X-ray/computed tomography, near-infrared optical imaging and magnetic resonance imaging.

Normal laboratory rodents may be used for *in vivo* biodistribution experiments focussing on CNS penetration and washout of radiotracers, while (transgenic) disease models may form the basis for *ex vivo* autoradiography to assess binding of probes to the targeted molecule on brain slices, or of course the *in vivo* evaluation of tracer retention in brain.

1.4.1 Imaging in Schizophrenia

Recent advances in the development and applications of neurochemical brain imaging have improved the ability to study the neurochemistry of the living brain in psychiatric disorders. In particular, PET and SPECT have been used to determine neurochemical substrates of schizophrenia and to uncover the mechanism of action of antipsychotic medications. The growing availability of radiotracers for monoaminergic neurotransmitter synthesis, transporters and receptors has enabled the evaluation of hypotheses regarding neurotransmitter function in schizophrenia derived from preclinical and clinical observations. Ongoing clinical schizophrenia PET-/SPECT-based trials study (1) abnormalities in indices of neurotransmitter systems with an established role in schizophrenia in patients versus controls, (2) new tools to study other neurotransmitter systems or potential biomarkers (e.g. inflammation markers) (Doorduyn et al. 2009) (Figs. 1.2 and 1.3) and (3) characterisation of target occupancy by antipsychotic drugs, as well as its relationship to efficacy and side effects (for review, see Urban and Abi-Dargham 2010; <http://www.clinicaltrials.gov>).

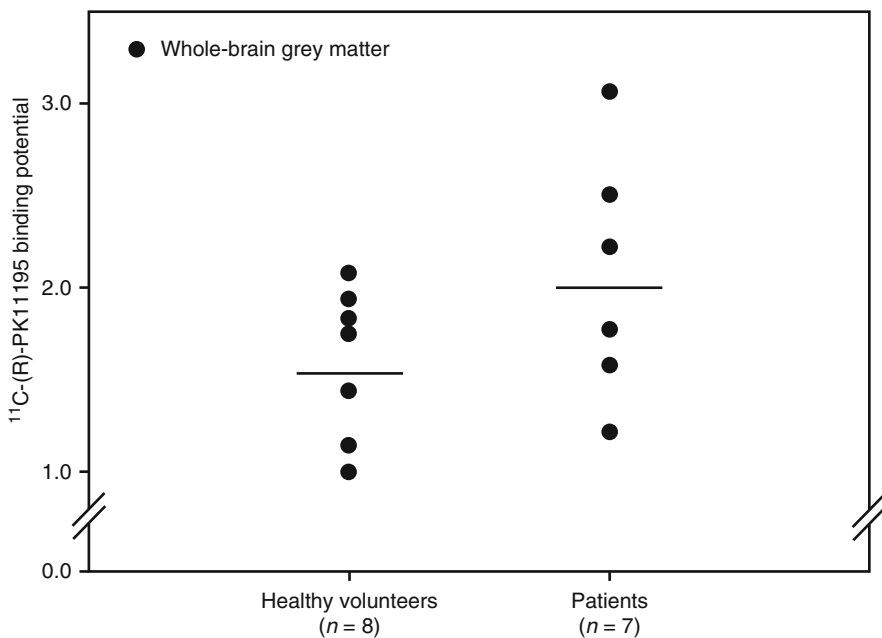


Fig. 1.2 Binding potential of the PET marker [^{11}C]-PK11195 that binds to translocator protein (TSPO), a biomarker to study activated microglia cells, in healthy volunteers and schizophrenia patients. All schizophrenia patients met the DSM-IV criteria of schizophrenia spectrum disorders. Each dot represents an individual subject, and *horizontal lines* represent mean values. Whole-brain grey matter binding potential was 30 % higher in patients versus healthy controls, although this difference did not reach statistical significance (Reprinted from Doorduyn et al. (2009) with permission. Copyright©2009 Society of Nuclear Medicine and Molecular Imaging)

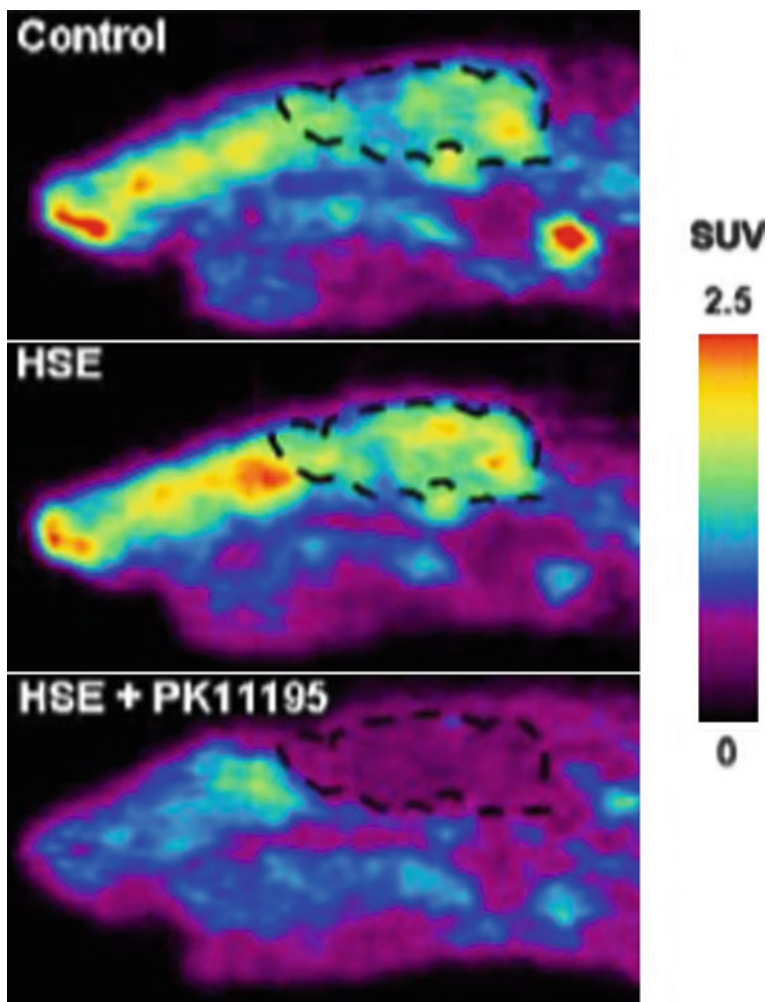


Fig. 1.3 Many neurological and psychiatric disorders are associated with neuroinflammation, which can be studied using PET markers like [^{11}C]-PK11195 that binds to translocator protein (TSPO), a biomarker to study activated microglia cells. The sensitivity of [^{11}C]-PK11195 may however be insufficient to visualise mild neuroinflammation. [^{11}C]-N-(2,5-dimethoxybenzyl)-N-(4-fluoro-2-phenoxyphenyl)-acetamide, [^{11}C]-DAA1106, proposed as a potentially more sensitive neuroinflammation tracer, was evaluated in a rat model of herpes encephalitis (*HSE*). Sagittal view of the head of a control rat (*control*), a rat with *HSE* and a *HSE* rat pretreated with 5 mg/kg of unlabeled PK11195 (*HSE + PK11195*), in which the brain is delineated by a *dashed line*. The images represent tracer uptake between 30 and 60 min after injection of [^{11}C]-DAA1106 (44 ± 14 MBq). Images show a high uptake of [^{11}C]-DAA1106 in the brainstem. Pretreatment with unlabeled PK11195 resulted in effective blocking of [^{11}C]-DAA1106 uptake. In vivo uptake, however, did not significantly differ between control and *HSE* rats. [^{11}C]-DAA1106 may not be an ideal tracer to perform longitudinal PET studies in small animals to study the role of neuroinflammation in neurological and psychiatric disorders (Reprinted from Doorduyn et al. (2010) with permission. Copyright©2010 Elsevier)

A variety of PET tracers, including ^{11}C , ^{15}O -water, ^{18}F -fallypride and L-3, 4-dihydroxy-6- ^{18}F -fluorophenylalanine (^{18}F -FDOPA), has been used to identify brain abnormalities in schizophrenia based on kinetic modelling. The most consistent findings show a difference in the dopamine content in the prefrontal cortex, anterior cingulate gyrus and hippocampus between healthy controls and schizophrenia patients. In addition, a higher density of D2 receptors in the striatum and neural brain dysconnectivity was observed (for review, see Patel et al. 2010), while [^{11}C]PET to map D1/D2 receptors identified reduced D1R densities in the prefrontal cortex (Okubo et al 1997).

There have been some PET studies of the behavioural sensitisation to psychostimulant drugs in dogs (Nakamura et al. 1997), rhesus monkeys (Castner et al. 2000) and rats (Kilbourn and Domino 2011). Given the presumed contribution of excitatory NMDA-linked neurotransmission to schizophrenia, PET/SPECT has scarcely been used for investigations of NMDA perturbations in experimental animals, including rats (Reith et al. 1998), cats (Vollenweider et al. 2000) and monkeys (Tsukada et al. 2000; van Berckel et al. 2006). Albeit the application of microPET/SPECT in schizophrenia is currently still limited, it will most probably advance with the further development of valid genetically modified mouse models.

1.4.2 Imaging in AD

A β plaque-bearing mice are obviously a potentially interesting tool for the development of PET/SPECT tracers aiming at the visualisation of amyloid plaques and/or other AD-typical pathological alterations. With the development of a specific tracer that reliably visualises AD pathology in an amyloidosis mouse model, small animal imaging techniques may be used to assess treatment efficacy of anti-A β leads in the AD drug discovery pipeline. More in general, the impact of PET/SPECT imaging on drug discovery can also be situated at various levels, including validation of mechanisms of drug localisation, establishing transport efficiency of a drug to the target, establishing drug occupancy of saturable receptor sites and determining half-time of occupancy of the drug (Eckelman 2003).

2-Deoxy-2-(^{18}F)fluoro-D-glucose-based PET, [^{18}F]FDG-PET, is a sensitive surrogate marker for AD diagnosis. A typical activity pattern shows decreased metabolism in the posterior cingulate and temporoparietal and prefrontal association cortex, while metabolism is maintained in the primary sensorimotor cortex and basal ganglia. Changes in [^{18}F]FDG-PET are evident prior to the onset of cognitive symptoms in AD-related mutation carriers. Moreover, [^{18}F]FDG-PET has predictive power for conversion of MCI to AD (for review, see Zhang et al. 2012). However, given the lack of specificity of [^{18}F]FDG-PET for AD, much efforts are directed at the development of A β -specific radioligands. [N-methyl- ^{11}C]2-(4'-methylaminophenyl)-6-hydroxybenzothiazole, a fluorescent analogue of thioflavin T better known as Pittsburgh compound B, [^{11}C]PiB-PET, emerged as the lead A β -specific PET ligand to proceed to clinical development. [^{11}C]PiB-PET studies have demonstrated significant regional retention of radioactive signal in CNS areas with extensive plaque burden in AD brain, including the frontal, parietal and lateral temporal cortex and

the striatum (Klunk et al. 2004; Price et al. 2005). [^{18}F]FDDNP (2-(1-{6-[(2-[fluorine-18]fluoroethyl)(methyl)amino]-2-naphthyl]-ethylidene)malononitrile) is the only currently available PET radiotracer to image neurofibrillary tangles, besides A β aggregates, and it is also the only radiotracer to visualise AD pathology in the hippocampal region of living humans (for review, see Shin et al. 2011).

The search for other A β -binding radiopharmaceuticals is still ongoing, and also several [^{18}F]-labelled tracers have been developed that are currently undergoing extensive phase II and III clinical trials, e.g. 3'-[^{18}F]F-PiB (Flutemetamol), [^{18}F]AV-45 (Florbetapir) and [^{18}F]AV-1 (Florbetaben) (for review, see Vallabhajosula 2011). By mid-2012, [^{18}F]AV-45 (AmyvidTM) has become the first FDA-approved PET ligand available however only in select US markets. More information concerning current clinical trials in AD with PET and/or SPECT imaging can be obtained at <http://www.clinicaltrials.gov>.

Based on often disappointing PET imaging results in AD mouse models (Klunk et al. 2005; Toyama et al. 2005; Kuntner et al. 2009; Luo et al. 2012), the usefulness of currently available transgenic mouse models for the identification and optimisation imaging tracers is somewhat controversial. The spatial resolution of PET is often insufficient to allow reliable estimation of A β -specific tracer binding. Repeated PET imaging in the same mouse, however, may be applied to study the evolution of plaque burden and may be useful to complement *ex vivo* autoradiographic radionuclide imaging of brain slices, which provides sufficient spatial resolution for assessment of specific tracer binding but of course lacks the possibility of time-linked observations (Wirths et al. 2009; Teipel et al. 2011). Substantial differences in pharmacokinetics and pharmacodynamics are often observed between animals and humans for CNS targeted molecules (Carpenter et al. 2009). Moreover, the detection of amyloid plaques often depends on the presence of one specific A β subtype that may not be present in the same proportion in mouse versus man, or in different transgenic amyloidosis mouse models, as is the case for A β N3-pyroglutamate recognised by [^{11}C]PiB (Maeda et al. 2007). In addition, the presence of high-affinity binding sites may differ between species, as well as between the sources of A β even within the same species (Klunk et al. 2005; Rabinovici and Jagust 2009; Rosen et al. 2011). Latter hurdle may be overcome, however, by increasing the specific activity of [^{11}C]PiB to afford an A β -specific binding signal in transgenic mouse brain that could be quantified with small animal PET (Maeda et al. 2007; Fig. 1.4).

Despite differences between humans and animals, the development of new radioligands for AD brain lesions still strongly relies on preclinical tests in transgenic amyloidosis mice. For example, the recently developed [^{18}F]AV-45 ligand, which is expected to become a good substitute to [^{11}C]PiB in the coming years, has first been successfully tested in transgenic amyloidosis mice (Choi et al. 2009).

The most important advantage of (micro)PET imaging over (micro)SPECT is that of exhibiting a much higher sensitivity, while (micro)SPECT offers the possibility to widen the observational time window (based on the longer half-life of single-photon emitters) thus allowing the observation of biological processes *in vivo* several hours or days after administration of the labelled compound. By using different energy radioisotopes conjugated to different molecular targets, (micro)

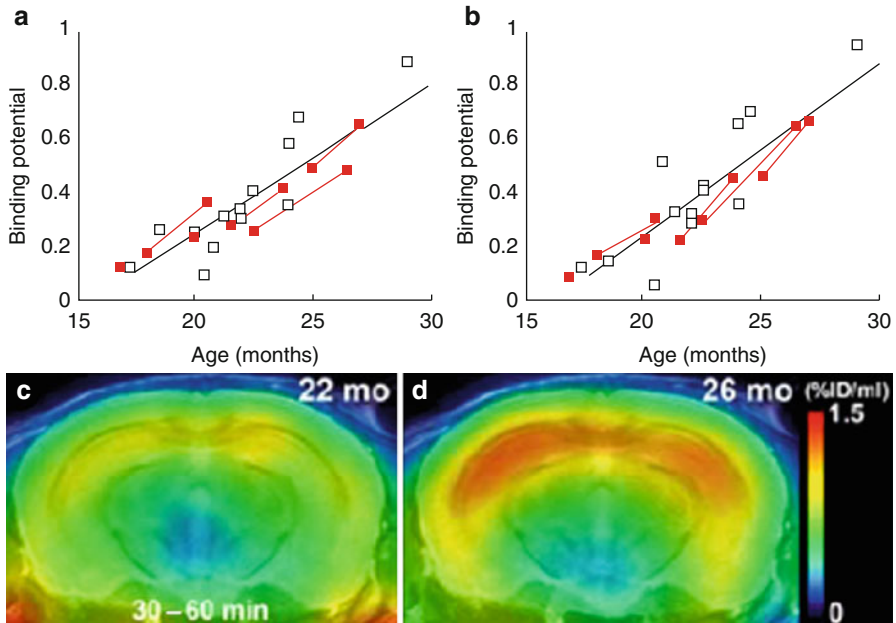


Fig. 1.4 Ability of mouse PET to capture age-dependent evolution of brain amyloidosis. (a, b) Represent scatter plots of binding potential of N-[^{11}C]methyl-2-(4-methylaminophenyl)-6-hydroxybenzothiazole (or [^{11}C]PIB for ‘Pittsburgh compound B’) versus age in the hippocampus (a) and neocortex (b) of Tg2576 mice, with the correlation of the two parameters being statistically significant in both regions. *Black lines* represent regression, and *red elements* indicate longitudinal analysis of the same individuals ($n=5$). (c, d) Represent PET images to illustrate [^{11}C]PIB’s substantial increase in tracer binding in the hippocampal formations of the same animal at the age of 22 (c) and 26 months (d), indicating progression of amyloid accumulation. Images were generated by averaging dynamic scan data at 30–60 min after tracer injection and were merged onto an MRI template. *mo* month (Reprinted from Maeda et al. (2007) with permission. Copyright©2007 Society for Neuroscience)

SPECT has the advantage over (micro)PET in being able to image several molecular events simultaneously. Few examples on the application of SPECT in amyloidosis models can be found. Most studies evaluate newly developed SPECT tracers, biodistribution in normal mice and A β -specific binding on brain slices of plaque-bearing mice (Cui et al. 2011; Cheng et al. 2012). However, Opazo et al. (2006) assessed radioiodinated clioquinol as an amyloid biomarker in Tg2576 mice, which exhibited higher brain retention of tracer compared to nontransgenic mice.

Conclusion

Patho(physio)logical alterations in rodent models of human disease are usually studied using invasive techniques, requiring sacrificing the animals. This approach implies, amongst other, the use of a large number of animals to reach statistical significance, high associated (labour) costs and follow-up or longitudinal studies is impossible in the same animal. Recent improvements in molecular

imaging technologies employed to image small animal models, at least partially, overcome these limitations. Small animal imaging is increasingly recognised as an important facet of preclinical and translational (neuroscience) research. Perhaps most significant amongst the clear advantages of imaging experimental animals is that physiology, pathology and novel phenotypes can be understood in the most relevant milieu – in an intact, living system. Moreover, longitudinal imaging studies will allow researchers to gain more insight into the (developmental) time course of the modelled endophenotypes. The nuclear imaging modalities PET and SPECT can provide the sensitivities required to obtain the same physiological imaging acuity in small animals as can be obtained in humans, which will greatly facilitate the translation of preclinical studies to applications in the clinic.

Acknowledgements This work was supported by the Research Foundation Flanders (FWO), Interuniversity Poles of Attraction (IAP Network P7/16) of the Belgian Federal Science Policy Office, Methusalem excellence grant of the Flemish Government, agreement between the Institute Born-Bunge and the University of Antwerp, the Medical Research Foundation Antwerp, the Thomas Riellaerts research fund and Neurosearch Antwerp. DVD is a postdoctoral fellow of the FWO.

References

- Allen NC, Bagade S, McQueen MB et al (2008) Systematic meta-analyses and field synopsis of genetic association studies in schizophrenia: the SzGene database. *Nat Genet* 40:827–834
- Alonso JR, HS U, Amaral DG (1996) Cholinergic innervation of the primate hippocampal formation: II. Effects of fimbria/fornix transection. *J Comp Neurol* 375:527–551
- Amann LC, Gandal MJ, Halene TB et al (2010) Mouse behavioral endophenotypes for schizophrenia. *Brain Res Bull* 83:147–161
- American Psychiatric Association (2000) Diagnostic and statistical manual of mental health disorders, 4th edn. American Psychiatric Publishing, Washington, DC. doi:10.1176/appi.books.9780890423349
- Andiné P, Widermark N, Axelsson R et al (1999) Characterization of MK-801-induced behavior as a putative rat model of psychosis. *J Pharmacol Exp Ther* 290:1393–1408
- Andreasen NC (1995) Symptoms, signs, and diagnosis of schizophrenia. *Lancet* 346:477–481
- Andreasson KI, Savonenko A, Vidensky S et al (2001) Age-dependent cognitive deficits and neuronal apoptosis in cyclooxygenase-2 transgenic mice. *J Neurosci* 21:8198–8209
- Ashcroft AE (2010) Mass spectrometry and the amyloid problem—how far can we go in the gas phase? *J Am Soc Mass Spectrom* 21:1087–1096
- Ayhan Y, Abazyan B, Nomura J, Kim R et al (2011) Differential effects of prenatal and postnatal expressions of mutant human DISC1 on neurobehavioral phenotypes in transgenic mice: evidence for neurodevelopmental origin of major psychiatric disorders. *Mol Psychiatry* 16:293–306
- Baker M (2011) Animal models: inside the minds of mice and men. *Nature* 475:123–128
- Banerjee A, Macdonald ML, Borgmann-Winter KE et al (2010) Neuregulin 1-erbB4 pathway in schizophrenia: from genes to an interactome. *Brain Res Bull* 83:132–139
- Barr AM, Fish KN, Markou A et al (2008) Heterozygous reeler mice exhibit alterations in sensorimotor gating but not presynaptic proteins. *Eur J Neurosci* 27:2568–2574
- Basak JM, Holtzman DM (2011) APP-based transgenic models: the PDAPP model. In: De Deyn PP, Van Dam D (eds) *Animal models of dementia*, 1st edn. Springer Science + Business Media, New York

- Belzung C, Philpott P (2007) Anxiety from a phylogenetic perspective: is there a qualitative difference between human and animal anxiety? *Neural Plast* 2007:59676
- Berlanga ML, Price DL, Phung BS et al (2011) Multiscale imaging characterization of dopamine transporter knockout mice reveals regional alterations in spine density of medium spiny neurons. *Brain Res* 1390:41–49
- Billings LM, Oddo S, Green KN et al (2005) Intraneuronal abeta causes the onset of early Alzheimer's disease-related cognitive deficits in transgenic mice. *Neuron* 45:675–688
- Bleiholder C, Dupuis NF, Wytenbach T et al (2011) Ion mobility-mass spectrometry reveals a conformational conversion from random assembly to β -sheet in amyloid fibril formation. *Nat Chem* 3:172–177
- Bons N, Mestre N, Ritchie K et al (1994) Identification of amyloid beta protein in the brain of the small, short-lived lemurian primate *microcebus murinus*. *Neurobiol Aging* 15:215–220
- Braak H, Braak E, Strothjohann M (1994) Abnormally phosphorylated tau protein related to the formation of neurofibrillary tangles and neuropil threads in the cerebral cortex of sheep and goat. *Neurosci Lett* 171:1–4
- Bray NJ (2008) Gene expression in the etiology of schizophrenia. *Schizophr Bull* 34:412–418
- Brigman JL, Padukiewicz KE, Sutherland ML et al (2006) Executive functions in the heterozygous reeler mouse model of schizophrenia. *Behav Neurosci* 120:984–988
- Buccafusco JJ (2008) *Methods of behavior analysis in neuroscience*. CRC Press/Taylor & Francis Group, Boca Raton
- Buka SL, Cannon TD, Torrey EF et al, Collaborative Study Group on the Perinatal Origins of Severe Psychiatric Disorders (2008) Maternal exposure to herpes simplex virus and risk of psychosis among adult offspring. *Biol Psychiatry* 63:809–815
- Bullock AE, Slobe BS, Vazquez V et al (1997) Inbred mouse strains differ in the regulation of startle and prepulse inhibition of the startle response. *Behav Neurosci* 111:1353–1360
- Bunsey M, Eichenbaum H (1996) Conservation of hippocampal memory function in rats and humans. *Nature* 379:255–257
- Butterfield DA, Poon HF (2005) The senescence-accelerated prone mouse (SAMP8): a model of age-related cognitive decline with relevance to alterations of the gene expression and protein abnormalities in Alzheimer's disease. *Exp Gerontol* 40:774–783
- Capsoni S, Ugolini G, Comparini A et al (2000) Alzheimer-like neurodegeneration in aged anti-nerve growth factor transgenic mice. *Proc Natl Acad Sci U S A* 97:6826–6831
- Cardno AG, Marshall EJ, Coid B et al (1999) Heritability estimates for psychotic disorders: the Maudsley twin psychosis series. *Arch Gen Psychiatry* 56:162–168
- Carpenter WT, Koenig JI (2008) The evolution of drug development in schizophrenia: past issues and future opportunities. *Neuropsychopharmacology* 33:2061–2079
- Carpenter AP Jr, Pontecorvo MJ, Hefti FF et al (2009) The use of the exploratory IND in the evaluation and development of 18F-PET radiopharmaceuticals for amyloid imaging in the brain: a review of one company's experience. *Q J Nucl Med Mol Imaging* 53:387–393
- Castañe A, Theobald DE, Robbins TW (2010) Selective lesions of the dorsomedial striatum impair serial spatial reversal learning in rats. *Behav Brain Res* 210:74–83
- Castellani RJ, Alexiev BA, Phillips D et al (2007) Microscopic investigations in neurodegenerative diseases. In: Méndez-Vilas A, Díaz J (eds) *Modern research and educational topics in microscopy*. Formatex, Badajoz
- Castner SA, Goldman-Rakic PS (1999) Long-lasting psychotomimetic consequences of repeated low-dose amphetamine exposure in rhesus monkeys. *Neuropsychopharmacology* 20:10–28
- Castner SA, Goldman-Rakic PS (2003) Amphetamine sensitization of hallucinatory-like behaviors is dependent on prefrontal cortex in nonhuman primates. *Biol Psychiatry* 54:105–110
- Castner SA, al-Tikriti MS, Baldwin RM et al (2000) Behavioral changes and [123I]IBZM equilibrium SPECT measurement of amphetamine-induced dopamine release in rhesus monkeys exposed to subchronic amphetamine. *Neuropsychopharmacology* 22:4–13
- Caviness VS Jr (1976) Patterns of cell and fiber distribution in the neocortex of the reeler mutant mouse. *J Comp Neurol* 170:435–447

- Cheng Y, Ono M, Kimura H et al (2012) Technetium-99m labeled pyridyl benzofuran derivatives as single photon emission computed tomography imaging probes for β -amyloid plaques in Alzheimer's brains. *J Med Chem* 55:2279–2286
- Choi SR, Golding G, Zhuang Z et al (2009) Preclinical properties of 18F-AV-45: a PET agent for Abeta plaques in the brain. *J Nucl Med* 50:1887–1894
- Chourbaji S, Zacher C, Sanchis-Segura C et al (2005) Learned helplessness: validity and reliability of depressive-like states in mice. *Brain Res Brain Res Protoc* 16:70–78
- Clapcote SJ, Roder JC (2006) Deletion polymorphism of *Disc1* is common to all 129 mouse substrains: implications for gene-targeting studies of brain function. *Genetics* 173:2407–2410
- Cohen BD, Rosenbaum G, Luby ED et al (1962) Comparison of phencyclidine hydrochloride (Sernyl) with other drugs. Simulation of schizophrenic performance with phencyclidine hydrochloride (Sernyl), lysergic acid diethylamide (LSD-25), and amobarbital (Amytal) sodium; II. Symbolic and sequential thinking. *Arch Gen Psychiatry* 6:395–401
- Colton CA, Wilcock DM, Wink DA et al (2008) The effects of *NOS2* gene deletion on mice expressing mutated human AbetaPP. *J Alzheimers Dis* 15:571–587
- Contestabile A (2011) The history of the cholinergic hypothesis. *Behav Brain Res* 221:334–340
- Cork LC, Powers RE, Selkoe DJ et al (1988) Neurofibrillary tangles and senile plaques in aged bears. *J Neuropathol Exp Neurol* 47:629–641
- Crawley J (2000) What's wrong with my mouse? Behavioral phenotyping of transgenic and knockout mice. Wiley-Liss, Wilmington
- Crawley JN, Belknap JK, Collins A et al (1997) Behavioral phenotypes of inbred mouse strains: implications and recommendations for molecular studies. *Psychopharmacology (Berl)* 132:107–124
- Creese I, Iversen SD (1973) Blockage of amphetamine induced motor stimulation and stereotypy in the adult rat following neonatal treatment with 6-hydroxydopamine. *Brain Res* 55:369–382
- Cui M, Ono M, Kimura H et al (2011) Radioiodinated benzimidazole derivatives as single photon emission computed tomography probes for imaging of β -amyloid plaques in Alzheimer's disease. *Nucl Med Biol* 38:313–320
- Cummings BJ, Su JH, Cotman CW et al (1993) Beta-amyloid accumulation in aged canine brain: a model of early plaque formation in Alzheimer's disease. *Neurobiol Aging* 14:547–560
- Cummings BJ, Head E, Ruehl W et al (1996) The canine as an animal model of human aging and dementia. *Neurobiol Aging* 17:259–268
- D'Hooge R, De Deyn PP (2001) Applications of the Morris water maze in the study of learning and memory. *Brain Res Brain Res Rev* 36:60–90
- Davies P, Maloney AJ (1976) Selective loss of central cholinergic neurons in Alzheimer's disease. *Lancet* 2:1403
- De Deyn PP, Van Dam D (2011) General introduction to animal models of human conditions. In: De Deyn PP, Van Dam D (eds) *Animal models of dementia*, 1st edn. Springer Science + Business Media, New York
- De Deyn PP, Katz IR, Brodathy H et al (2005) Management of agitation, aggression, and psychosis associated with dementia: a pooled analysis including three randomized, placebo-controlled double-blind trials in nursing home residents treated with risperidone. *Clin Neurol Neurosurg* 107:497–508
- Deacon R (2011) APP-based transgenic models: the Tg2576 model. In: De Deyn PP, Van Dam D (eds) *Animal models of dementia*, 1st edn. Springer Science + Business Media, New York
- Desbonnet L, Waddington JL, O'Tuathaigh CM (2009) Mutant models for genes associated with schizophrenia. *Biochem Soc Trans* 37:308–312
- Dieckmann M, Freudenberg F, Klein S et al (2007) Disturbed social behavior and motivation in rats selectively bred for deficient sensorimotor gating. *Schizophr Res* 97:250–253
- Doorduyn J, de Vries EF, Willemsen AT et al (2009) Neuroinflammation in schizophrenia-related psychosis: a PET study. *J Nucl Med* 50:1801–1807
- Doorduyn J, Klein HC, de Jong JR et al (2010) Evaluation of [11C]-DAA1106 for imaging and quantification of neuroinflammation in a rat model of herpes encephalitis. *Nucl Med Biol* 37:9–15

- Drew LJ, Stark KL, Fénelon K et al (2011) Evidence for altered hippocampal function in a mouse model of the human 22q11.2 microdeletion. *Mol Cell Neurosci* 47:293–305
- Dringenberg HC (2000) Alzheimer's disease: more than a 'cholinergic disorder' – evidence that cholinergic–monoaminergic interactions contribute to EEG slowing and dementia. *Behav Brain Res* 115:235–249
- Dworkin RH, Opler LA (1992) Simple schizophrenia, negative symptoms, and prefrontal hypodopaminergia. *Am J Psychiatry* 149:1284–1285
- Ebert U, Kirch W (1998) Scopolamine model of dementia: electroencephalogram findings and cognitive performance. *Eur J Clin Invest* 28:944–949
- Eckelman WC (2003) The use of PET and knockout mice in the drug discovery process. *Drug Discov Today* 8:404–410
- Ellenbroek BA, Cools AR (1990) Animal models with construct validity for schizophrenia. *Behav Pharmacol* 1:469–490
- Ellman GL, Courtney KD, Andres J Jr et al (1961) A new and rapid colorimetric determination of acetylcholinesterase activity. *Biochem Pharmacol* 7:88–95
- Erickson CA, Barnes CA (2003) The neurobiology of memory changes in normal aging. *Exp Gerontol* 38:61–69
- Estapé N, Steckler T (2002) Cholinergic blockade impairs performance in operant DNMT1 in two inbred strains of mice. *Pharmacol Biochem Behav* 72:319–334
- Falconer DS (1951) Two new mutants, Trembler and 'Reeler', with neurological actions in the house mouse. *J Genetics* 50:182–201
- Farris W, Mansourian S, Chang Y et al (2003) Insulin-degrading enzyme regulates the levels of insulin, amyloid beta-protein, and the beta-amyloid precursor protein intracellular domain in vivo. *Proc Natl Acad Sci U S A* 100:4162–4167
- Featherstone RE, Kapur S, Fletcher PJ (2007) The amphetamine-induced sensitized state as a model of schizophrenia. *Prog Neuropsychopharmacol Biol Psychiatry* 31:1556–1571
- Featherstone RE, Rizos Z, Kapur S et al (2008) A sensitizing regimen of amphetamine that disrupts attentional set-shifting does not disrupt working or long-term memory. *Behav Brain Res* 189:170–179
- Flood DG, Zuvich E, Marino MJ et al (2011) Prepulse inhibition of the startle reflex and response to antipsychotic treatments in two outbred mouse strains in comparison to the inbred DBA/2 mouse. *Psychopharmacology (Berl)* 215:441–454
- Floresco SB, Zhang Y, Enomoto T (2009) Neural circuits subserving behavioral flexibility and their relevance to schizophrenia. *Behav Brain Res* 204:396–409
- Fone KC, Porkess MV (2008) Behavioural and neurochemical effects of post-weaning social isolation in rodents—relevance to developmental neuropsychiatric disorders. *Neurosci Biobehav Rev* 32:1087–1102
- Fonnum F (1975) A rapid radiochemical method for the determination of choline acetyltransferase. *J Neurochem* 24:407–409
- Frautschy SA, Yang F, Calderón L et al (1996) Rodent models of Alzheimer's disease: rat A beta infusion approaches to amyloid deposits. *Neurobiol Aging* 17:311–321
- Freichel C, Neumann M, Ballard T et al (2007) Age-dependent cognitive decline and amygdala pathology in alpha-synuclein transgenic mice. *Neurobiol Aging* 28:1421–1435
- Freyberg Z, Ferrando SJ, Javitch JA (2010) Roles of the Akt/GSK-3 and Wnt signaling pathways in schizophrenia and antipsychotic drug action. *Am J Psychiatry* 167:388–396
- Fuster JM (1980) The prefrontal cortex. Anatomy, physiology, and neuropsychology of the frontal lobe. Raven Press, New York
- Games D, Adams D, Alessandrini R et al (1995) Alzheimer-type neuropathology in transgenic mice overexpressing V717F beta-amyloid precursor protein. *Nature* 373:523–527
- Gayle DA, Beloosesky R, Desai M et al (2004) Maternal LPS induces cytokines in the amniotic fluid and corticotropin releasing hormone in the fetal rat brain. *Am J Physiol Regul Integr Comp Physiol* 286:R1024–R1029
- Gearing M, Rebeck GW, Hyman BT et al (1994) Neuropathology and apolipoprotein E profile of aged chimpanzees: implications for Alzheimer's disease. *Proc Natl Acad Sci U S A* 91:9382–9386

- Gearing M, Tigges J, Mori H et al (1997) β -amyloid (A β) deposition in the brains of aged orangutans. *Neurobiol Aging* 18:139–146
- Gejman PV, Sanders AR, Kendler KS (2011) Genetics of schizophrenia: new findings and challenges. *Annu Rev Genomics Hum Genet* 12:121–144
- Gerlai R (2010) Zebrafish antipredatory responses: a future for translational research? *Behav Brain Res* 207:223–231
- Geula C, Nagykerly N, Wu CK (2002) Amyloid-beta deposits in the cerebral cortex of the aged common marmoset (*Callithrix jacchus*): incidence and chemical composition. *Acta Neuropathol* 103:48–58
- Glahn DC, Thompson PM, Blangero J (2007) Neuroimaging endophenotypes: strategies for finding genes influencing brain structure and function. *Hum Brain Mapp* 28:488–501
- Glenn MJ, Nesbitt C, Mumby DG (2003) Perirhinal cortex lesions produce variable patterns of retrograde amnesia in rats. *Behav Brain Res* 141:183–193
- Glowinski J, Iversen L (1966a) Regional studies of catecholamines in the rat brain. 3. Subcellular distribution of endogenous and exogenous catecholamines in various brain regions. *Biochem Pharmacol* 15:977–987
- Glowinski J, Iversen LL (1966b) Regional studies of catecholamines in the rat brain. I. The disposition of [3H]norepinephrine, [3H]dopamine and [3H]dopa in various regions of the brain. *J Neurochem* 13:655–669
- Glowinski J, Axelrod J, Iversen LL (1966) Regional studies of catecholamines in the rat brain. IV. Effects of drugs on the disposition and metabolism of H3-norepinephrine and H3-dopamine. *J Pharmacol Exp Ther* 153:30–41
- Gogos A, Bogeski M, van den Buuse M (2008) Role of serotonin-1A receptors in the action of antipsychotic drugs: comparison of prepulse inhibition studies in mice and rats and relevance for human pharmacology. *Behav Pharmacol* 19:548–561
- Gong Y, Chang L, Viola KL et al (2003) Alzheimer's disease-affected brain: presence of oligomeric A beta ligands (ADDLs) suggests a molecular basis for reversible memory loss. *Proc Natl Acad Sci U S A* 100:10417–10422
- Gosling SD (2001) From mice to men: what can we learn about personality from animal research? *Psychol Bull* 127:45–86
- Gottesman II, Gould TD (2003) The endophenotype concept in psychiatry: etymology and strategic intentions. *Am J Psychiatry* 160:636–645
- Götz J, Schild A, Hoerndli F et al (2004) Amyloid-induced neurofibrillary tangle formation in Alzheimer's disease: insight from transgenic mouse and tissue-culture models. *Int J Dev Neurosci* 22:453–465
- Gray JA, McNaughton N (1983) Comparison between the behavioural effects of septal and hippocampal lesions: a review. *Neurosci Biobehav Rev* 7:119–188
- Grayson DR, Chen Y, Costa E et al (2006) The human reelin gene: transcription factors (+), repressors (-) and the methylation switch (+/-) in schizophrenia. *Pharmacol Ther* 111:272–286
- Gsell W, Jungkunz G, Riederer P (2004) Functional neurochemistry of Alzheimer's disease. *Curr Pharm Des* 10:265–293
- Gunn-Moore DA, McVee J, Bradshaw JM et al (2006) Ageing changes in cat brains demonstrated by beta-amyloid and AT8-immunoreactive phosphorylated tau deposits. *J Feline Med Surg* 8:234–242
- Hardy J, Selkoe DJ (2002) The amyloid hypothesis of Alzheimer's disease: progress and problems on the road to therapeutics. *Science* 297:353–356
- Harkany T, O'Mahony S, Kelly JP et al (1998) Beta-amyloid(Phe(SO₃H)₂₄)₂₅₋₃₅ in rat nucleus basalis induces behavioral dysfunctions, impairs learning and memory and disrupts cortical cholinergic innervation. *Behav Brain Res* 90:133–145
- Harkany T, Penke B, Luiten PG (2000) beta-Amyloid excitotoxicity in rat magnocellular nucleus basalis. Effect of cortical deafferentation on cerebral blood flow regulation and implications for Alzheimer's disease. *Ann N Y Acad Sci* 903:374–386
- Harrison P, Law A (2006) Neuregulin 1 and schizophrenia: genetics, gene expression, and neurobiology. *Biol Psychiatry* 60:132–140

- Hattori S, Murotani T, Matsuzaki S et al (2008) Behavioral abnormalities and dopamine reductions in *sdyl* mutant mice with a deletion in *Dtnbp1*, a susceptibility gene for schizophrenia. *Biochem Biophys Res Commun* 373:298–302
- Hauss-Wegrzyniak B, Dobrzanski P, Stoehr JD et al (1998) Chronic neuroinflammation in rats reproduces components of the neurobiology of Alzheimer's disease. *Brain Res* 780:294–303
- He Y, Yao Z, Gu Y et al (1992) Nerve growth factor promotes collateral sprouting of cholinergic fibers in the septohippocampal cholinergic system of aged rats with fimbria transection. *Brain Res* 586:27–35
- Head E, Moffat K, Das P et al (2005) β -amyloid deposition and tau phosphorylation in clinically characterized aged cats. *Neurobiol Aging* 26:749–763
- Hendley ED, Welch BL (1975) Electroconvulsive shock: sustained decrease in norepinephrine uptake affinity in a reserpine model of depression. *Life Sci* 16:45–54
- Hsiao K, Chapman P, Nilson S et al (1996) Correlative memory deficits, A β elevation, and amyloid plaques in transgenic mice. *Science* 274:99–102
- Huber G, März W, Martin JR et al (2000) Characterization of transgenic mice expressing apolipoprotein E4(C112R) and apolipoprotein E4(L28P; C112R). *Neuroscience* 101:211–218
- Iliadi KG (2009) The genetic basis of emotional behavior: has the time come for a *Drosophila* model? *J Neurogenet* 23:136–146
- Insel TR (2007) From animal model to model animals. *Biol Psychiatry* 62:1337–1339
- Ishrat T, Parveen K, Khan MM et al (2009) Selenium prevents cognitive decline and oxidative damage in rat model of streptozotocin-induced experimental dementia of Alzheimer's type. *Brain Res* 1281:117–127
- Iversen LL, Glowinski J (1966) Regional studies of catecholamines in the rat brain. II. Rate of turnover of catecholamines in various brain regions. *J Neurochem* 13:671–682
- Iwata N, Tsubuki S, Takaki Y et al (2001) Metabolic regulation of brain A β by neprilysin. *Science* 292:1550–1552
- Jaaro-Peled H (2009) Gene models of schizophrenia: DISC1 mouse models. *Prog Brain Res* 179:75–86
- Javitt DC, Zukin SR (1991) Recent advances in the phencyclidine model of schizophrenia. *Am J Psychiatry* 148:1301–1308
- Jaworski T, Dewachter I, Seymour CM et al (2010) Alzheimer's disease: old problem, new views from transgenic and viral models. *Biochim Biophys Acta* 1802:808–818
- Jentsch JD, Roth RH (1999) The neuropsychopharmacology of phencyclidine: from NMDA receptor hypofunction to the dopamine hypothesis of schizophrenia. *Neuropsychopharmacology* 20:201–225
- Jones CA, Watson DJ, Fone KC (2011) Animal models of schizophrenia. *Br J Pharmacol* 164:1162–1194
- Kaimal V, McConville P (2009) Importance of preclinical imaging in drug discovery. Charles River. http://www.criver.com/SiteCollectionDocuments/DIS_I_Imaging.pdf. Accessed 20 Apr 2012
- Kilbourn MR, Domino EF (2011) Increased in vivo [11 C]raclopride binding to brain dopamine receptors in amphetamine-treated rats. *Eur J Pharmacol* 654:254–257
- Kimura N, Tanemura K, Nakamura S et al (2003) Age-related changes of Alzheimer's disease-associated proteins in cynomolgus monkey brains. *Biochem Biophys Res Commun* 310:303–311
- Kinney GG, Wilkinson LO, Saywell KL et al (1999) Rat strain differences in the ability to disrupt sensorimotor gating are limited to the dopaminergic system, specific to prepulse inhibition, and unrelated to changes in startle amplitude or nucleus accumbens dopamine receptor sensitivity. *J Neurosci* 19:5644–5653
- Klein S, Koch M, Schwabe K (2008) Neuroanatomical changes in the adult rat brain after neonatal lesion of the medial prefrontal cortex. *Exp Neurol* 209:199–212
- Klunk WE, Engler H, Nordberg A et al (2004) Imaging brain amyloid in Alzheimer's disease with Pittsburgh Compound-B. *Ann Neurol* 55:306–319
- Klunk WE, Lopresti BJ, Ikonovic MD et al (2005) Binding of the positron emission tomography tracer Pittsburgh compound-B reflects the amount of amyloid-beta in Alzheimer's disease brain but not in transgenic mouse brain. *J Neurosci* 25:10598–10606

- Koike H, Arguello PA, Kvajo M et al (2006) *Disc1* is mutated in the 129S6/SvEv strain and modulates working memory in mice. *Proc Natl Acad Sci U S A* 103:3693–3697
- Kokkinidis L, Anisman H (1981) Amphetamine psychosis and schizophrenia: a dual model. *Neurosci Biobehav Rev* 5:449–461
- Krystal JH, Karper LP, Seibyl JP et al (1994) Subanesthetic effects of the noncompetitive NMDA antagonist, ketamine, in humans. Psychotomimetic, perceptual, cognitive, and neuroendocrine responses. *Arch Gen Psychiatry* 51:199–214
- Kuntner C, Kesner AL, Bauer M et al (2009) Limitations of small animal PET imaging with [¹⁸F]FDDNP and FDG for quantitative studies in a transgenic mouse model of Alzheimer's disease. *Mol Imaging Biol* 11:236–240
- Lacor PN, Buniel MC, Chang L et al (2004) Synaptic targeting by Alzheimer's-related amyloid beta oligomers. *J Neurosci* 24:10191–10200
- Lane MA (2000) Nonhuman primate models in biogerontology. *Exp Gerontol* 35:533–541
- Laviola G, Ognibene E, Romano E et al (2009) Gene-environment interaction during early development in the heterozygous reeler mouse: clues for modelling of major neurobehavioral syndromes. *Neurosci Biobehav Rev* 33:560–572
- Lawlor PA, Young D (2011) A β infusion and related models of Alzheimer dementia. In: De Deyn PP, Van Dam D (eds) *Animal models of dementia*, 1st edn. Springer Science + Business Media, New York
- Lazar NL, Rajakumar N, Cain DP (2008) Injections of NGF into neonatal frontal cortex decrease social interaction as adults: a rat model of schizophrenia. *Schizophr Bull* 34:127–136
- Leboyer M, Bellivier F, Nosten-Bertrand M et al (1998) Psychiatric genetics: search for phenotypes. *Trends Neurosci* 21:102–105
- Lemere CA, Beierschmitt A, Iglesias M et al (2004) Alzheimer's disease abeta vaccine reduces central nervous system abeta levels in a non-human primate, the Caribbean vervet. *Am J Pathol* 165:283–297
- Lemere CA, Oh J, Stanish HA et al (2008) Cerebral amyloid-beta protein accumulation with aging in cotton-top tamarins: a model of early Alzheimer's disease? *Rejuvenation Res* 11:321–332
- Lescaudron L, Stein DG (1999) Differences in memory impairment and response to GM1 ganglioside treatment following electrolytic or ibotenic acid lesions of the nucleus basalis magnocellularis. *Restor Neurol Neurosci* 15:25–37
- Levin ED, Rose JE, McGurk SR et al (1990) Characterization of the cognitive effects of combined muscarinic and nicotinic blockade. *Behav Neural Biol* 53:103–112
- Lewis DA, Levitt P (2002) Schizophrenia as a disorder of neurodevelopment. *Annu Rev Neurosci* 25:409–432
- Li Q, Cheung C, Wei R et al (2009) Prenatal immune challenge is an environmental risk factor for brain and behavior change relevant to schizophrenia: evidence from MRI in a mouse model. *PLoS One* 4:e6354
- Liesch G, Linthorst AC, Neumann ID et al (1998) Behavioral, physiological, and neuroendocrine stress responses and differential sensitivity to diazepam in two Wistar rat lines selectively bred for high- and low-anxiety-related behavior. *Neuropsychopharmacology* 19:381–396
- Lipska BK, Weinberger DR (2000) To model a psychiatric disorder in animals: schizophrenia as a reality test. *Neuropsychopharmacology* 23:223–239
- Liu L, Duff K (2008) A technique for serial collection of cerebrospinal fluid from the cisterna magna in mouse. *J Vis Exp* (21):e960
- Lodge DJ, Grace AA (2008) Hippocampal dysfunction and disruption of dopamine system regulation in an animal model of schizophrenia. *Neurotox Res* 14:97–104
- Lubow RE, Gewirtz JC (1995) Latent inhibition in humans: data, theory, and implications for schizophrenia. *Psychol Bull* 117:87–103
- Luo F, Rustay NR, Ebert U et al (2012) Characterization of 7- and 19-month-old Tg2576 mice using multimodal in vivo imaging: limitations as a translatable model of Alzheimer's disease. *Neurobiol Aging* 33:933–944
- Maeda J, Ji B, Irie T et al (2007) Longitudinal, quantitative assessment of amyloid, neuroinflammation, and anti-amyloid treatment in a living mouse model of Alzheimer's disease enabled by positron emission tomography. *J Neurosci* 27:10957–10968

- Marcotte ER, Pearson DM, Srivastava LK (2001) Animal models of schizophrenia: a critical review. *J Psychiatry Neurosci* 26:395–410
- Markham JA, Taylor AR, Taylor SB et al (2010) Characterization of the cognitive impairments induced by prenatal exposure to stress in the rat. *Front Behav Neurosci* 4:173
- Martínez-Téllez RI, Hernández-Torres E, Gamboa C et al (2009) Prenatal stress alters spine density and dendritic length of nucleus accumbens and hippocampus neurons in rat offspring. *Synapse* 63:794–804
- McGeer EG, McGeer PL (2003) Inflammatory processes in Alzheimer's disease. *Prog Neuropsychopharmacol Biol Psychiatry* 27:741–749
- McGrath J, Saha S, Chant D et al (2008) Schizophrenia: a concise overview of incidence, prevalence, and mortality. *Epidemiol Rev* 30:67–76
- McKinney WT Jr, Bunney WE Jr (1969) Animal model of depression. I. Review of evidence: implications for research. *Arch Gen Psychiatry* 21:240–248
- Mei L, Xiong W (2008) Neuregulin 1 in neural development, synaptic plasticity and schizophrenia. *Nat Rev Neurosci* 9:437–452
- Migliore L, Fontana I, Colognato R et al (2005) Searching for the role and the most suitable biomarkers of oxidative stress in Alzheimer's disease and in other neurodegenerative diseases. *Neurobiol Aging* 26:587–595
- Mitchell KJ, Huang ZJ, Moghaddam B et al (2011) Following the genes: a framework for animal modelling of psychiatric disorders. *BMC Biol* 9:76
- Moore H (2010) The role of rodent models in the discovery of new treatments for schizophrenia: updating our strategy. *Schizophr Bull* 36:1066–1072
- Moran PM (1993) Differential effects of scopolamine and mecamylamine on working and reference memory in the rat. *Pharmacol Biochem Behav* 45:533–538
- Muir WJ, Pickard BS, Blackwood DH (2008) Disrupted-in-schizophrenia-1. *Curr Psychiatry Rep* 10:140–147
- Mulder J, Harkany T, Czolner K et al (2005) Galantamine-induced behavioral recovery after sublethal excitotoxic lesions to the rat medial septum. *Behav Brain Res* 163:33–41
- Nag S, Yee BK, Tang F (1999) Chronic intracerebroventricular infusion of beta-amyloid (1-40) results in a selective loss of neuropeptides in addition to a reduction in choline acetyltransferase activity in the cortical mantle and hippocampus in the rat. *Ann N Y Acad Sci* 897:420–422
- Nakamura H, Hishinuma T, Tomioka Y et al (1997) Effects of haloperidol and cocaine pretreatments on brain distribution and kinetics of [¹¹C]methamphetamine in methamphetamine sensitized dog: application of PET to drug pharmacokinetic study. *Nucl Med Biol* 24:165–169
- Nakamura S, Murayama N, Noshita T et al (2001) Progressive brain dysfunction following intracerebroventricular infusion of beta(1-42)-amyloid peptide. *Brain Res* 912:128–136
- Nestler EJ, Hyman SE (2010) Animal models of neuropsychiatric disorders. *Nat Neurosci* 13:1161–1169
- Nordberg A, Nilsson-Håkansson L, Adem A et al (1989) Multiple actions of THA on cholinergic neurotransmission in Alzheimer brains. *Prog Clin Biol Res* 317:1169–1178
- O'Tuathaigh CM, Kirby BP, Moran PM et al (2010) Mutant mouse models: genotype-phenotype relationships to negative symptoms in schizophrenia. *Schizophr Bull* 36:271–288
- Oddo S, Caccamo A, Kitazawa M et al (2003) Amyloid deposition precedes tangle formation in a triple transgenic model of Alzheimer's disease. *Neurobiol Aging* 24:1063–1070
- Okubo Y, Suhara T, Suzuki K et al (1997) Decreased prefrontal dopamine D1 receptors in schizophrenia revealed by PET. *Nature* 385:634–636
- Olariu A, Yamada K, Mamiya T et al (2002) Memory impairment induced by chronic intracerebroventricular infusion of beta-amyloid (1-40) involves downregulation of protein kinase C. *Brain Res* 957:278–286
- Olney JW, Farber NB (1995) Glutamate receptor dysfunction and schizophrenia. *Arch Gen Psychiatry* 52:998–1007
- Opazo C, Luza S, Villemagne VL et al (2006) Radioiodinated clioquinol as a biomarker for beta-amyloid: Zn complexes in Alzheimer's disease. *Aging Cell* 5:69–79

- Overstreet DH, Double K, Schiller GD (1989) Antidepressant effects of rolipram in a genetic animal model of depression: cholinergic supersensitivity and weight gain. *Pharmacol Biochem Behav* 34:691–696
- Palmer AA, Dulawa SC, Mottiwala AA et al (2000) Prepulse startle deficit in the Brown Norway rat: a potential genetic model. *Behav Neurosci* 114:374–388
- Patel NH, Vyas NS, Puri BK et al (2010) Positron emission tomography in schizophrenia: a new perspective. *J Nucl Med* 51:511–520
- Paylor R, Crawley JN (1997) Inbred strain differences in prepulse inhibition of the mouse startle response. *Psychopharmacology (Berl)* 132:169–180
- Paylor R, Lindsay E (2006) Mouse models of 22q11 deletion syndrome. *Biol Psychiatry* 59:1172–1179
- Pepeu G, Giovannini MG (2007) Changes in acetylcholine extracellular levels during cognitive processes. In: Westerink BH, Cremers TI (eds) *Handbook of microdialysis. Methods, applications and perspectives*. Elsevier, Amsterdam
- Pepeu G, Rosi MC (2011) Validation of animal models of dementia: neurochemical aspects. In: De Deyn PP, Van Dam D (eds) *Animal models of dementia*, 1st edn. Springer Science + Business Media, New York
- Pietro Paolo S, Crusio WE (2009) Strain-dependent changes in acoustic startle response and its plasticity across adolescence in mice. *Behav Genet* 39:623–631
- Podhorna J, Didriksen M (2004) The heterozygous reeler mouse: behavioural phenotype. *Behav Brain Res* 153:43–54
- Price JC, Klunk WE, Lopresti BJ et al (2005) Kinetic modeling of amyloid binding in humans using PET imaging and Pittsburgh Compound-B. *J Cereb Blood Flow Metab* 25:1528–1547
- Rabinovici GD, Jagust WJ (2009) Amyloid imaging in aging and dementia: testing the amyloid hypothesis in vivo. *Behav Neurol* 21:117–128
- Rankin CA, Gamblin TC (2008) Assessing the toxicity of tau aggregation. *J Alzheimers Dis* 14:411–416
- Reisberg B, Borenstein J, Salob SP et al (1987) Behavioral symptoms in Alzheimer's disease: phenomenology and treatment. *J Clin Psychiatry* 48:9–15
- Reith J, Cumming P, Gjedde A (1998) Enhanced [3H]DOPA and [3H]dopamine turnover in striatum and frontal cortex in vivo linked to glutamate receptor antagonism. *J Neurochem* 70:1979–1985
- Renā AS, Butterfield DA (2011) Spontaneous vertebrate models of Alzheimer dementia: selectively bred strains (SAM strains). In: De Deyn PP, Van Dam D (eds) *Animal models of dementia*, 1st edn. Springer Science + Business Media, New York
- Ribé EM, Pérez M, Puig B et al (2005) Accelerated amyloid deposition, neurofibrillary degeneration and neuronal loss in double mutant APP/tau transgenic mice. *Neurobiol Dis* 20:814–822
- Riekkinen P Jr, Sirviö J, Aaltonen M et al (1990) Effects of concurrent manipulations of nicotinic and muscarinic receptors on spatial and passive avoidance learning. *Pharmacol Biochem Behav* 37:405–410
- Roertgen KE, Parisi JE, Clark HB et al (1996) A beta-associated cerebral angiopathy and senile plaques with neurofibrillary tangles and cerebral hemorrhage in an aged wolverine (*Gulo gulo*). *Neurobiol Aging* 17:243–247
- Rofina JE, van Ederen AM, Toussaint MJ et al (2006) Cognitive disturbances in old dogs suffering from the canine counterpart of Alzheimer's disease. *Brain Res* 1069:216–226
- Rosen RF, Walker LC, Levine H 3rd (2011) PIB binding in aged primate brain: enrichment of high-affinity sites in humans with Alzheimer's disease. *Neurobiol Aging* 32:223–234
- Sakoğlu U, Upadhyay J, Chin CL et al (2011) Paradigm shift in translational neuroimaging of CNS disorders. *Biochem Pharmacol* 81:1374–1387
- Sanchis-Segura C, Spanagel R, Henn FA et al (2005) Reduced sensitivity to sucrose in rats bred for helplessness: a study using the matching law. *Behav Pharmacol* 16:267–270
- Sani S, Traul D, Klink A et al (2003) Distribution, progression and chemical composition of cortical amyloid- β deposits in aged rhesus monkeys: similarities to the human. *Acta Neuropathol* 105:145–156

- Santarelli L, Gobbi G, Debs PC et al (2001) Genetic and pharmacological disruption of neurokinin 1 receptor function decreases anxiety-related behaviors and increases serotonergic function. *Proc Natl Acad Sci U S A* 98:1912–1917
- Seeman P (1987) Dopamine receptors and the dopamine hypothesis of schizophrenia. *Synapse* 1:133–152
- Selkoe DJ (2000) Toward a comprehensive theory for Alzheimer's disease. Hypothesis: Alzheimer's disease is caused by the cerebral accumulation and cytotoxicity of amyloid beta-protein. *Ann N Y Acad Sci* 924:17–25
- Selkoe DJ (2001) Alzheimer's disease: genes, proteins, and therapy. *Physiol Rev* 81:741–766
- Selkoe DJ (2008) Soluble oligomers of the amyloid beta-protein impair synaptic plasticity and behavior. *Behav Brain Res* 192:106–113
- Sherman KA, Friedman E (1990) Pre- and post-synaptic cholinergic dysfunction in aged rodent brain regions: new findings and an interpretive review. *Int J Dev Neurosci* 8:689–708
- Shin J, Kepe V, Barrio JR et al (2011) The merits of FDDNP-PET imaging in Alzheimer's disease. *J Alzheimers Dis* 26:135–145
- Sipos E, Kurunzi A, Kasza A et al (2007) Beta-amyloid pathology in the entorhinal cortex of rats induces memory deficits: implications for Alzheimer's disease. *Neuroscience* 147:28–36
- Sloan HL, Good M, Dunnett SB (2006) Double dissociation between hippocampal and prefrontal lesions on an operant delayed matching task and a water maze reference memory task. *Behav Brain Res* 171:116–126
- Steimer T (2011) Animal models of anxiety disorders in rats and mice: some conceptual issues. *Dialogues Clin Neurosci* 13:495–506
- Striedter GF (1998) Progress in the study of brain evolution: from speculative theories to testable hypotheses. *Anat Rec* 253:105–112
- Sturchler-Pierrat C, Abramowski D, Duke M et al (1997) Two amyloid precursor protein transgenic mouse models with Alzheimer disease-like pathology. *Proc Natl Acad Sci U S A* 94:13287–13292
- Sunderland T, Tariot PN, Weingartner H et al (1986) Pharmacologic modelling of Alzheimer's disease. *Prog Neuropsychopharmacol Biol Psychiatry* 10:599–610
- Swerdlow NR, Martinez ZA, Hanlon FM et al (2000) Toward understanding the biology of a complex phenotype: rat strain and substrain differences in the sensorimotor gating-disruptive effects of dopamine agonists. *J Neurosci* 20:4325–4336
- Swerdlow NR, Kuczenski R, Goins JC et al (2005) Neurochemical analysis of rat strain differences in the startle gating-disruptive effects of dopamine agonists. *Pharmacol Biochem Behav* 80:203–211
- Swerdlow NR, Shilling PD, Breier M et al (2012) Fronto-temporal-mesolimbic gene expression and heritable differences in amphetamine-disrupted sensorimotor gating in rats. *Psychopharmacology (Berl)* 224:349–362
- Sy M, Kitazawa M, LaFerla F (2011) The 3xTg-AD mouse model: reproducing and modulating plaque and tangle pathology. In: De Deyn PP, Van Dam D (eds) *Animal models of dementia*, 1st edn. Springer Science + Business Media, New York
- Szabados T, Dul C, Majtényi K et al (2004) A chronic Alzheimer's model evoked by mitochondrial poison sodium azide for pharmacological investigations. *Behav Brain Res* 154:31–40
- Teipel SJ, Buchert R, Thome J et al (2011) Development of Alzheimer-disease neuroimaging-biomarkers using mouse models with amyloid-precursor protein-transgene expression. *Prog Neurobiol* 95:547–556
- Tekirian TL, Cole GM, Russell MJ et al (1996) Carboxy terminal of beta-amyloid deposits in aged human, canine, and polar bear brains. *Neurobiol Aging* 17:249–257
- Toledana A, Alvarez MI (2011) Lesion-induced vertebrate models of Alzheimer dementia. In: De Deyn PP, Van Dam D (eds) *Animal models of dementia*, 1st edn. Springer Science + Business Media, New York
- Toyama H, Ye D, Ichise M et al (2005) PET imaging of brain with the beta-amyloid probe, [11C]6-OH-BTA-1, in a transgenic mouse model of Alzheimer's disease. *Eur J Nucl Med Mol Imaging* 32:593–600

- Tsai G, Coyle JT (2002) Glutamatergic mechanisms in schizophrenia. *Annu Rev Pharmacol Toxicol* 42:165–179
- Tsukada H, Harada N, Nishiyama S et al (2000) Ketamine decreased striatal [(11)C]raclopride binding with no alterations in static dopamine concentrations in the striatal extracellular fluid in the monkey brain: multiparametric PET studies combined with microdialysis analysis. *Synapse* 37:95–103
- Tulving E (1987) Multiple memory systems and consciousness. *Hum Neurobiol* 6:67–80
- Uchida K, Yoshino T, Yamaguchi R et al (1995) Senile plaques and other senile changes in the brain of an American black bear. *Vet Pathol* 32:412–414
- Urban N, Abi-Dargham A (2010) Neurochemical imaging in schizophrenia. *Curr Top Behav Neurosci* 4:215–242
- Uylings HB, Groenewegen HJ, Kolb B (2003) Do rats have a prefrontal cortex? *Behav Brain Res* 146:3–17
- Vale-Martínez A, Guillazo-Blanch G, Martí-Nicolovius M et al (2002) Electrolytic and ibotenic acid lesions of the nucleus basalis magnocellularis interrupt long-term retention, but not acquisition of two-way active avoidance, in rats. *Exp Brain Res* 142:52–66
- Vallabhajosula S (2011) Positron emission tomography radiopharmaceuticals for imaging brain Beta-amyloid. *Semin Nucl Med* 41:283–299
- Valzelli L (1973) The “isolation syndrome” in mice. *Psychopharmacologia* 31:305–320
- van Berckel BN, Kegeles LS, Waterhouse R et al (2006) Modulation of amphetamine-induced dopamine release by group II metabotropic glutamate receptor agonist LY354740 in non-human primates studied with positron emission tomography. *Neuropsychopharmacology* 31:967–977
- Van Dam D, De Deyn PP (2006) Drug discovery in dementia: the role of rodent models. *Nat Rev Drug Discov* 5:956–970
- Van Dam D, De Deyn PP (2011a) APP-based transgenic models: the APP23 model. In: De Deyn PP, Van Dam D (eds) *Animal models of dementia*, 1st edn. Springer Science + Business Media, New York
- Van Dam D, De Deyn PP (2011b) The role of rodent models in the drug discovery pipeline for dementia. In: De Deyn PP, Van Dam D (eds) *Animal models of dementia*, 1st edn, *NeuroMethods* series. Springer Science + Business Media, New York
- Van Dam D, Van Dijk A, Janssen L et al (2013) Neuropeptides in Alzheimer’s disease: from pathophysiological mechanisms to therapeutic opportunities. *Curr Alzheimer Res* 10(5):449–68
- van der Staay FJ (2006) Animal models of behavioral dysfunctions: basic concepts and classifications, and an evaluation strategy. *Brain Res Rev* 52:131–159
- van der Staay FJ, Blokland A (1996) Behavioral differences between outbred Wistar, inbred Fischer 344, brown Norway, and hybrid Fischer 344 x brown Norway rats. *Physiol Behav* 60:97–109
- van der Weyden L, Bradley A (2006) Mouse chromosome engineering for modeling human disease. *Annu Rev Genomics Hum Genet* 7:247–276
- Van Dijk A, Vloeberghs E, Van Dam D et al (2008) Evaluation of the APP23-model for Alzheimer’s disease in the odour paired-associate test for hippocampus-dependent memory. *Behav Brain Res* 190:147–151
- Varty GB, Walters N, Cohen-Williams M et al (2001) Comparison of apomorphine, amphetamine and dizocilpine disruptions of prepulse inhibition in inbred and outbred mice strains. *Eur J Pharmacol* 424:27–36
- Vickers JC, Dickson TC, Adlard PA et al (2000) The cause of neuronal degeneration in Alzheimer’s disease. *Prog Neurobiol* 60:139–165
- Vidal R, Ghetti B (2011) Characterization of amyloid deposits in neurodegenerative diseases. In: Manfredi G, Kawamata H (eds) *Neurodegeneration: methods and protocols*, 1st edn. Springer Science + Business Media, New York
- Vloeberghs E, Van Dam D, Engelborghs S et al (2004) Altered circadian locomotor activity in APP23 mice: a model for BPSD disturbances. *Eur J Neurosci* 20:2757–2766

- Vloeberghs E, Van Dam D, Franck F et al (2008) Altered ingestive behavior, weight changes, and intact olfactory sense in an APP overexpression model. *Behav Neurosci* 122:491–497
- Vollenweider FX, Vontobel P, Oye I et al (2000) Effects of (S)-ketamine on striatal dopamine: a [¹¹C]raclopride PET study of a model psychosis in humans. *J Psychiatr Res* 34:35–43
- Voytko ML, Tinkler GP (2004) Cognitive function and its neural mechanisms in nonhuman primate models of aging, Alzheimer disease, and menopause. *Front Biosci* 9:1899–1914
- Walsh DM, Selkoe DJ (2007) A beta oligomers – a decade of discovery. *J Neurochem* 101:1172–1184
- Weldon DT, Rogers SD, Ghilardi JR et al (1998) Fibrillar beta-amyloid induces microglial phagocytosis, expression of inducible nitric oxide synthase, and loss of a select population of neurons in the rat CNS in vivo. *J Neurosci* 18:2161–2173
- Wenk GL, McGann K, Hauss-Wegrzyniak B et al (2003) The toxicity of tumor necrosis factor- α upon cholinergic neurons within the nucleus basalis and the role of norepinephrine in the regulation of inflammation: implications for Alzheimer's disease. *Neuroscience* 121:719–729
- Whitehouse PJ, Au KS (1986) Cholinergic receptors in aging and Alzheimer's disease. *Prog Neuropsychopharmacol Biol Psychiatry* 10:665–676
- Whitehouse PJ, Price DL, Struble RG et al (1982) Alzheimer's disease and senile dementia: loss of neurons in the basal forebrain. *Science* 215:1237–1239
- Williams NM, O'Donovan MC, Owen MJ (2005) Is the dysbindin gene (DTNBP1) a susceptibility gene for schizophrenia? *Schizophr Bull* 31:800–805
- Willott JF, Carlson S, Chen H (1994) Prepulse inhibition of the startle response in mice: relationship to hearing loss and auditory system plasticity. *Behav Neurosci* 108:703–713
- Willott JF, Tanner L, O'Steen J et al (2003) Acoustic startle and prepulse inhibition in 40 inbred strains of mice. *Behav Neurosci* 117:716–727
- Wils H, Kleinberger G, Pereson S et al (2012) Cellular ageing, increased mortality and FTLD-TDP-associated neuropathology in progranulin knockout mice. *J Pathol* 228:67–76
- Wimo A, Winblad B, Aguero-Torres H et al (2003) The magnitude of dementia occurrence in the world. *Alzheimer Dis Assoc Disord* 17:63–67
- Winter C, Djodari-Irani A, Sohr R et al (2009) Prenatal immune activation leads to multiple changes in basal neurotransmitter levels in the adult brain: implications for brain disorders of neurodevelopmental origin such as schizophrenia. *Int J Neuropsychopharmacol* 12:513–524
- Wirhns O, Breyhan H, Cynis H et al (2009) Intraneuronal pyroglutamate-A β 3-42 triggers neurodegeneration and lethal neurological deficits in a transgenic mouse model. *Acta Neuropathol* 118(4):487–496
- Wolf R, Matzke K, Paelchen K et al (2010) Reduction of Prepulse Inhibition (PPI) after neonatal excitotoxic lesion of the ventral thalamus in pubertal and adult rats. *Pharmacopsychiatry* 43:99–109
- Wu LS, Cheng WC, Hou SC et al (2010) TDP-43, a neuro-pathosignature factor, is essential for early mouse embryogenesis. *Genesis* 48:56–62
- Yamada M, Chiba T, Sasabe J et al (2005) Implanted cannula-mediated repetitive administration of A β 25-35 into the mouse cerebral ventricle effectively impairs spatial working memory. *Behav Brain Res* 164:139–146
- Yochum CL, Bhattacharya P, Patti L et al (2010) Animal model of autism using GSTM1 knockout mice and early post-natal sodium valproate treatment. *Behav Brain Res* 210:202–210
- Zhang S, Han D, Tan X et al (2012) Diagnostic accuracy of 18F-FDG and 11 C-PIB-PET for prediction of short-term conversion to Alzheimer's disease in subjects with mild cognitive impairment. *Int J Clin Pract* 66:185–198

Small Animal Molecular Imaging Through μ PET and μ SPECT

2

Steven Staelens, Tine Wyckhuys, Steven Deleeye, Jeroen Verhaeghe, Leonie Wyffels, and Sigrid Stroobants

Contents

2.1	Introduction	48
2.2	μ SPECT	48
2.2.1	System Characterization	50
2.2.2	Application in Neuromodulation	54
2.3	μ PET	65
2.3.1	Standardization: Factors Influencing [18F]-FDG Uptake in the Brain.....	67
2.3.2	Evaluation of Different Quantification Methods	73
2.3.3	Recommendations for Preclinical Protocol Optimization	75
2.3.4	Drug Testing	76
	Conclusion	81
	References.....	81

Abstract

Compared to techniques such as autoradiography and microscopy, the possibility to longitudinally study small animals in vivo justifies the need for preclinical

S. Staelens, MScEng, PhD (✉) • T. Wyckhuys • S. Deleeye • J. Verhaeghe
Molecular Imaging Center Antwerp (MICA), University of Antwerp,
Universiteitsplein 1, Antwerp (Wilrijk), Belgium
e-mail: steven.staelens@uantwerpen.be

L. Wyffels
Cyclotron Radiopharmacy, University Hospital Antwerp,
Wilrijkstraat 10, Antwerp (Edegem), Belgium

Molecular Imaging Center Antwerp (MICA), University of Antwerp,
Universiteitsplein 1, Antwerp (Wilrijk), Belgium

S. Stroobants
Molecular Imaging Center Antwerp (MICA), University of Antwerp,
Universiteitsplein 1, Antwerp (Wilrijk), Belgium

Nuclear Medicine Department, University Hospital Antwerp,
Wilrijkstraat 10, Antwerp (Edegem), Belgium

molecular imaging: μ SPECT and μ PET. In the first part of this chapter, we describe a performance evaluation to compare the three most widespread state-of-the-art μ SPECT systems. Once the optimal system is chosen, we use it to study neuromodulation in rats as an application of high-resolution μ SPECT imaging. Both the neurobiological effects of deep brain stimulation and transcranial magnetic stimulation are visualized *in vivo* in healthy animals. In the second part of this chapter, μ PET is discussed. We first describe how a preclinical acquisition protocol can be standardized and how the resulting reconstructed images can be accurately quantified. Next, we apply this standardized protocol to a typical application of μ PET in drug design, where we study the potency of a mGluR2/3 agonist in an animal model of schizophrenia.

2.1 Introduction

Molecular imaging is the visualization, characterization, and measurement of biological processes at the molecular and cellular level in humans and animals. Molecular imaging instrumentation consists of a variety of modalities that are nowadays often combined in multimodal imaging systems: SPECT (single photon emission computed tomography), PET (positron emission tomography), optical imaging, MRI (magnetic resonance imaging), MRS (magnetic resonance spectroscopy), and US (ultrasound). Functional molecular imaging studies such as PET and SPECT usually assess the spatial distribution of administered exogenous molecules and expression levels of their target (mostly enzymes and receptors). These imaging biomarkers can provide a certain degree of contrast by specifically binding to a target at an exquisite sensitivity in the picomolar range. Compared to techniques such as autoradiography and microscopy, the possibility to longitudinally study small animals *in vivo* justifies the need for preclinical molecular imaging.

2.2 μ SPECT

The use of extrinsic collimation to derive the photon's direction is the main limitation in SPECT overall sensitivity compared to PET, which is based on electronic coincidence counting to gather spatial information. Therefore, in SPECT, one needs to find an optimum between imaging time, injected dose, image resolution, and image noise. On the other hand, the theoretical spatial resolution of μ SPECT can be much higher than that of μ PET since there is no physical lower limit caused by positron range (which can be reasonably high for some positron emitters, e.g., mean 0.6 mm for ^{18}F in water) and photon acolinearity as is the case in μ PET. Also, parallax (depth-of-interaction effects) in the detector, which is the most dominant factor in the resolution loss of PET, is much smaller in SPECT due to its lower photon energy. Moreover in μ SPECT, these depth-of-interaction effects are usually reduced by pinhole magnification (typically a factor 3–12). While PET is able to follow the distribution of radiolabeled synthetic molecules with exquisite sensitivity, the

relatively short half-lives of the common positron emitters ^{11}C (20 min) and ^{18}F (109 min) make them less suited to radiolabeling biomolecules. Due to their relatively large size, peptides and antibodies diffuse slowly into tissue, particularly if obstacles such as the blood–brain barrier reduce the delivery rate, and have relatively slow clearance from blood. In imaging studies, this may require hours or days for localization and washout from blood to achieve acceptable target to background levels. The time required for localization and blood clearance of these molecules favors isotopes with longer half-lives such as the single photon emitters $^{99\text{m}}\text{Tc}$ (6.02 h), ^{123}I (13.2 h), and ^{111}In (2.8 days). Technetium, indium, and iodine also have good chemical properties in binding biological compounds and do not require a nearby or in-house cyclotron, which reduces costs. Although in the clinical world PET imaging nowadays outperforms SPECT image quality, the contrary is true for the preclinical arena where the higher resolution (in a smaller FOV) of μ SPECT compared to μ PET is, in many cases, essential when imaging small animals.

Small animal SPECT systems are not merely scaled-down versions of their clinical counterparts, but make use of dedicated multipinhole collimators. As a consequence of the pinhole magnification, measuring with a pinhole collimator can yield a reconstructed spatial resolution that is better than the detector's intrinsic spatial resolution. However, working with a small pinhole reduces the sensitivity, which has to be counteracted to avoid high injected activities or excessive acquisition times. While the first-generation systems were still manufactured with a single pinhole in combination with a conventional gamma camera requiring long scan times (even up to 1 h) and high doses (>1 mCi), recent systems are now built with multiple pinhole collimators. These systems either rotate the detectors combined with axial bed translation or have stationary detectors and translate the bed in XYZ directions to extend the FOV up to the entire animal's body. Examples of such designs are, amongst others, the A-SPECT (McElroy et al. 2002), the HiSPECT (Schramm et al. 2003), the T-SPECT (Lackas et al. 2005), the SemiSPECT (Kim et al. 2006), the U-SPECT-II, the NanoSPECT, and the X-SPECT. A more extensive overview of pinhole imaging can be found in (Beekman and Have 2006).

To provide multimodality imaging, recent SPECT systems are often combined with an integrated CT, which is placed behind or within the gantry of the SPECT imager. The most important application is to localize activity in the anatomical framework provided by CT. The CT information can also be used to perform partial volume, scatter, and attenuation correction for improved tracer quantification. SPECT can be used for a broad spectrum of applications such as cardiovascular imaging, imaging gene expression, neuroimaging, and oncology, bone metabolism, and inflammation tests.

Recently, there is a growing demand to apply imaging techniques to challenging questions that relate to multiple molecular pathways in the body. Thus, the ability of SPECT to simultaneously acquire separate images of different molecules, enabling to resolve the temporal relationship between different biological processes, becomes more important. This cannot be assured with sequential studies when there is a rapidly changing pathophysiology. Imaging multiple molecular pathways at the same time can be solved by multi-isotope imaging in SPECT or the use of another collimator for simultaneous μ PET and μ SPECT (Goorden and Beekman 2010).

2.2.1 System Characterization

A performance evaluation comparing three of the most widespread state-of-the-art μ SPECT systems for small animal imaging such as the U-SPECT-II (MILabs), the NanoSPECT (Bioscan), and the X-SPECT (GE) was performed. The evaluation criteria used in our comparison are reconstructed spatial resolution, sensitivity, contrast recovery, and image uniformity for different isotopes (^{99m}Tc , ^{125}I , and ^{111}In). These evaluations are performed for high-resolution (HR) and general purpose (GP) collimators and involved small animal-sized phantoms.

2.2.1.1 Description

The U-SPECT-II system shown in Fig. 2.1a has three detectors similar to a clinical triple-headed SPECT system, resulting in a triangular shape. Before reaching the detectors the photons first need to pass the 75-pinhole collimator in a configuration of five rings with fifteen pinholes per ring. This provides sufficient sampling in a small region so there is no need for rotation of either the object or the detector. However, the small field of view requires the animal bed to be translated in three dimensions in order to image the whole animal; this acquisition mode is called the scanning focus method (SFM). Around the pinholes of the mouse collimators, there is a tungsten tube with 75 rectangular holes to prevent the overlap of the projections. Here we use the 0.35, 0.6, and 1 mm aperture size collimator tubes. A more detailed description of the system can be found in (van der Have et al. 2009).

The X-SPECT (Fig. 2.1b) as part of the Triumph (SPECT/PET/CT) in its most complete configuration has four rotating gamma camera heads and is mounted on the same axial location of the gantry as the CT tube and X-ray detector. The camera consists of 5-by-5 CZT (CdZnTe) modules and each gamma camera head can be equipped with interchangeable single, multi(5)-pinhole (Mok et al. 2011), or parallel hole collimators. In this study, we only make use of the 0.5 and 1.0 mm multi-pinhole collimators.

The NanoSPECT (Fig. 2.1c) consists in its most complete form of 4 rotating heads. These detectors feature multipinhole collimation with 9 and up to 16

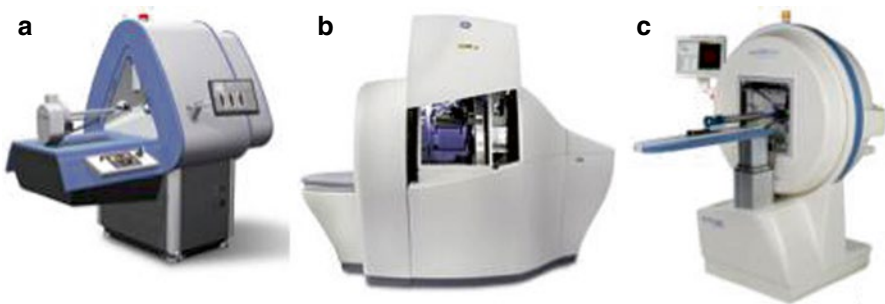


Fig. 2.1 Commercially available small animal SPECT systems evaluated: (a) U-SPECT-II, (b) X-SPECT, (c) NanoSPECT

(optional) pinholes per detector. Here, we use the 0.6 and 1mm pinhole collimators. More information can be found in (Schramm et al. 2006).

The main difference for the systems under evaluation is that one camera (U-SPECT-II) has stationary detectors, while the others (NanoSPECT and X-SPECT) make use of a gantry rotation around the object. A stationary system does not need rotation of heavy detectors and the only moving part is a XYZ stage that is also used for accurate system matrix measurement alleviating the need to perform a geometric parameter calibration. Second, the X-SPECT and the NanoSPECT have an adjustable radius of rotation (ROR) to alter the magnification and an FOV for each specific imaging task. The U-SPECT-II on the other hand uses cylindrical collimators with different sizes and imaging FOV for rats and mice in order to maximize the sensitivity for the task at hand. Furthermore, there is also a difference in the overlap of the projections. The U-SPECT-II makes use of detectors where the projections do not overlap. The NanoSPECT and the X-SPECT on the other hand make use of projections that can overlap. This technique is called multiplexing. While multiplexing increases the sensitivity, it also creates ambiguity during image reconstruction (Benabid et al. 2009). It has been reported that artifacts leading to, e.g., image nonuniformities and “ghost activity,” can be attributed to this ambiguity (Benabid et al. 2009). The effects of multiplexing will depend on the activity distribution but also on the pinhole design, detector size, and imaging distance.

2.2.1.2 Resolution

The collimators used are the respective vendor’s highest resolution option, being the 0.35 mm UHR whole body (WB)/focused mouse (75 pinholes) for the U-SPECT-II, the 0.5 mm low-energy (LE) mouse (5 pinholes/plate) for the X-SPECT, and the 0.6 mm UHR/focused mouse (9 pinholes/plate) for the NanoSPECT.

To have a qualitative measure of the resolution over the entire transaxial FOV, we scanned a mouse-sized phantom containing three Derenzo inserts (outer diameter of one insert is 1 cm, length 0.85 cm) with diameter sizes of the capillaries ranging from 0.35 to 0.75 mm (Fig. 2.2) for 1 h on all systems. The mouse-sized Derenzo phantoms were filled with a ^{99m}Tc solution in a relatively high concentration of 500 MBq/ml to avoid noise as a confounding factor in this high-resolution experiment. Ordered subset expectation maximization (OSEM) image reconstruction was used for all systems and the software recommended settings were used for the number of iterations and subsets with the lowest image voxel sizes possible, for U-SPECT-II, X-SPECT, and NanoSPECT-NSO 0.125, 0.25, and 0.13 mm, respectively. An energy window of 20 % was set around 140 keV for all three systems.

As shown in Fig. 2.2, the U-SPECT-II could resolve rods up to 0.4mm, and with the X-SPECT, the 0.75 mm rods were visible. The NanoSPECT could distinguish rods up to 0.6 mm, but the transaxial FOV is only 20 mm, leaving one Derenzo phantom truncated. These measurements indicate that the U-SPECT-II obtains the highest resolution over the entire FOV, which is attributed to the smaller diameter of the pinholes combined with a larger number of pinholes, the higher pinhole magnification factor, and the fact that the pinholes are closer to the object.

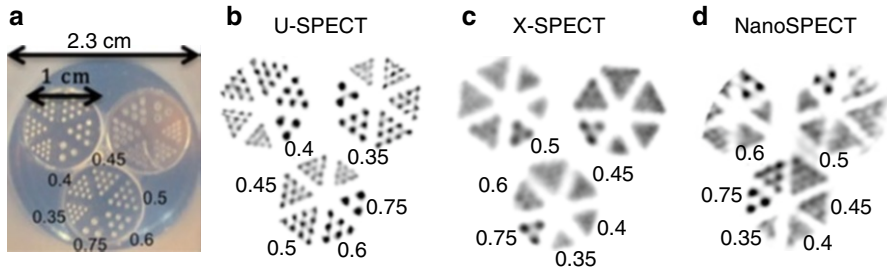


Fig. 2.2 Small animal-sized phantom with three Derenzo inserts (0.35–0.4–0.45–0.5–0.6–0.75 mm) as measured with the three systems using their HR collimators: (**a**) illustration of the phantom, (**b**) U-SPECT-II with 0.35 mm collimator, (**c**) X-SPECT with 0.5 mm collimator, and (**d**) NanoSPECT with 0.6 mm collimator

2.2.1.3 Contrast to Noise

The evaluation of the resolution as described in Sect. 2.2.1.2 measures the basic characteristics of these systems. However, sensitivity and size of the FOV (spiral pitch, number of bed positions needed) is an equally important aspect when using these μ SPECT systems for molecular imaging in daily preclinical routine since those will determine injected dose and scan time and may put the sensitivity versus resolution trade-off in another daylight. Our custom-made contrast phantom (Fig. 2.3) has a warm background, 20-mm-long capillaries with 0.2–0.4-mm-thin walls so that we can measure contrast/resolution over more slices and in a more realistic FOV size. This serves also as an indirect measure for the sensitivity over a larger FOV. Also the capillary diameters are optimized to evaluate the different scanners equipped with their high-sensitivity 1 mm collimators for mice (rods ranging from 0.6 to 2.0 mm). This phantom may also be used to characterize different collimators, acquisition and reconstruction parameters, and effect of scatter and attenuation correction.

We measured this mouse-sized phantom (Fig.2.3) for 20 min with 1 mm pinhole apertures on all three systems. The background (5 MBq/ml) and the four smallest capillaries (20 MBq/ml) were filled with a ^{99m}Tc solution to result in a capillary to background ratio of 4–1. The 2mm capillary was left unfilled to create a cold region in a hot background. Capillary and background volumes of interest (VOIs) were delineated on the corresponding CT images. The VOIs were repeated in seven 1-mm-thick transaxial slices, 1.5 mm apart to obtain seven samples. The contrast recovery coefficient (CRC) was then calculated as

$$\text{CRC} = \frac{m_{\text{hot}} - m_{\text{BG}}}{C_{\text{true}} - 1} \quad (2.1)$$

where m_{hot} and m_{BG} are the mean concentrations measured in capillary and back - ground VOIs averaged over the seven samples and C_{true} is the real capillary to

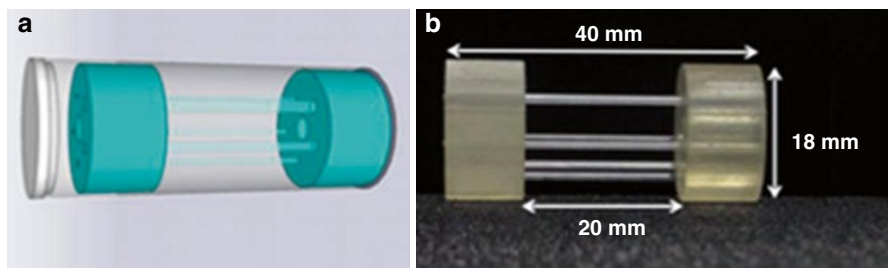


Fig. 2.3 (a) Schematic drawing of the contrast phantom with five capillaries inside surrounded by a hot background. (b) Photograph of the capillaries and the rings

background ratio. The cold-to-background ratio (CBR_{cold}) is defined as the activity measured in the cold region (m_{cold}) divided by the mean of the background concentration (m_{BG}) as

$$CRC_{\text{cold}} = 1 - CBR_{\text{air}} = \frac{m_{\text{cold}}}{m_{\text{BG}}} \quad (2.2)$$

The images were repeatedly smoothed with a 0.3 mm Gaussian filter to reach different levels of background standard deviation and to obtain the contrast recovery and the cold-to-background ratio at those noise levels. This noise coefficient (NC) was calculated as follows in (Eq. 2.3):

$$NC(\%) = 100 \times \frac{1}{P} \sum_p \frac{\sigma_p}{m_p} \quad (2.3)$$

where P is the total number of pixels in the background VOI and σ_p is the standard deviation and m_p the mean of a single background pixel calculated from the seven slices.

The average object-to-collimator distance for the U-SPECT-II was 22mm, while the ROR for the X-SPECT and the NanoSPECT was 35 and 30 mm, respectively. The same number of iterations and subsets was used as in the HR measurements, and software-selected voxel sizes for the 1 mm collimators for U-SPECT-II, X-SPECT, and NanoSPECT were, respectively, 0.2, 0.5, and 0.2 mm.

As can be seen in Fig. 2.4, the U-SPECT-II maintains its higher resolution for a full-size FOV when acquiring this contrast recovery μ SPECT image quality phantom, especially for the 1.5 and the 1.0 mm capillaries. For the 0.8 mm hot rods, the performance of the U-SPECT-II and NanoSPECT is comparable and the 0.6 mm capillaries are not distinguishable for any of the systems evaluated here. In terms of the CRC_{cold} , the U-SPECT-II clearly outperforms the other two systems. The better CRC_{cold} and CRC values for the U-SPECT-II may be attributed to the lack of multiplexing and/or higher resolution obtainable over the entire phantom with the scanning focusing method.

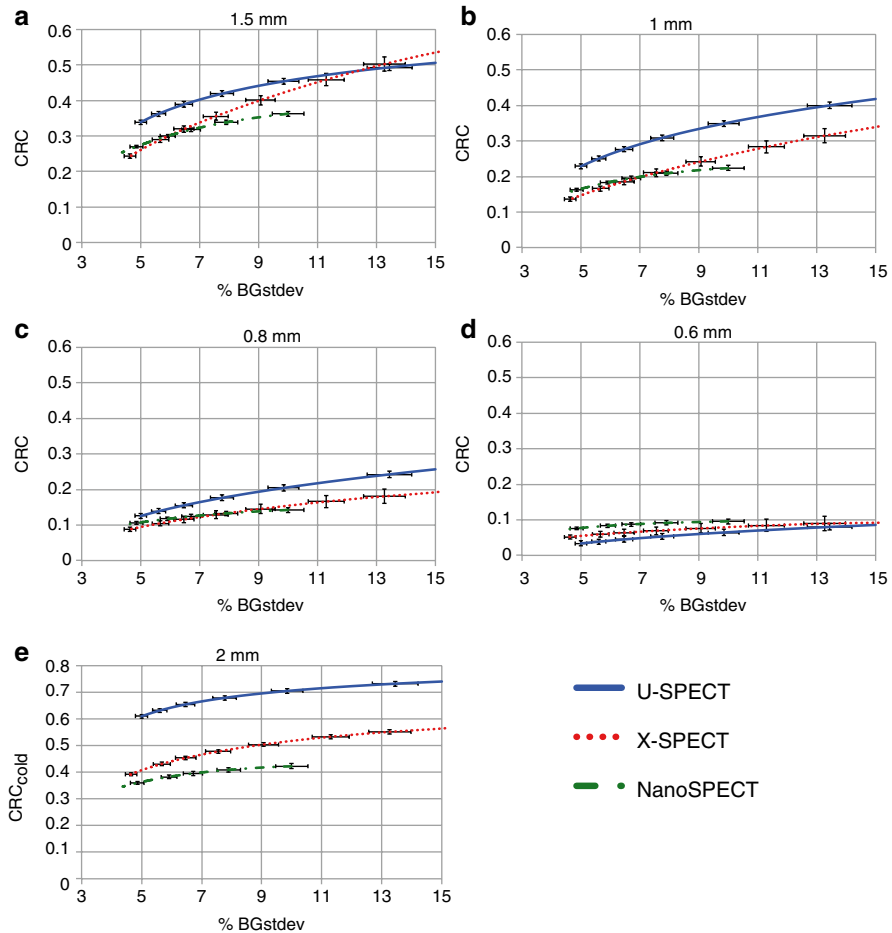


Fig. 2.4 (a–d) CRC curves for the different capillary diameters as a function of the standard deviation of the background. (e) CRC_{cold} curves for the 2 mm cold capillary (only air) as a function of the standard deviation of the background

In summary, we believe our evaluation realistically reflects the potential of each system to acquire small animal-sized objects with sub-mm resolution. All three scanners have made significant progress compared to the early human SPECT cameras that were modified for small animal imaging by using single or multipinhole collimator plates. We will use the U-SPECT-II here to study neuromodulation in rats by rCBF μ SPECT.

2.2.2 Application in Neuromodulation

Deep brain stimulation (DBS) is a therapeutic approach that involves the intracranial implantation of one or more electrodes in a specific brain region. By means of

an implantable battery and a subcutaneous lead, electrical pulses are sent to the target site to interfere with the neural activity. DBS is a promising treatment for a variety of neurological disorders, such as movement disorders (Benabid et al. 2009), chronic pain, obsessive–compulsive disorder, and refractory epilepsy. Temporal lobe epilepsy (TLE) is the most refractory form of epilepsy (Kwan and Brodie 2000). Because there is considerable evidence that the hippocampal formation is involved in seizure initiation in TLE patients (Spencer 2002), electrical stimulation of the limbic system has been successfully applied to treat refractory TLE. Despite promising results, the precise mechanism of action of DBS and the pathways affected due to hippocampal depth stimulation are unknown. Furthermore, the optimal stimulation parameters are undetermined, hampering its therapeutic potential.

Repetitive transcranial magnetic stimulation (rTMS) is an emerging method for the noninvasive stimulation of the human cortex through the intact skull. A rapidly changing perpendicular magnetic field (B-field) is generated by the currents in an rTMS coil, which induces an electrical field in the conducting brain that triggers depolarization or hyperpolarization of neuronal ensembles, by forcing the shift of free charges in the intra- and extracellular space of neuronal tissue (Barker et al. 1985). rTMS is a promising treatment for a variety of neurological and psychiatric disorders, such as depression, phantom pain and noise, ischemic stroke, neuropathic pain, migraine, and Parkinson's disease (Ridding and Rothwell 2007). Despite these promising results, the precise mechanism of action of rTMS and the pathways affected due to it are also still largely unknown. Furthermore, the optimal stimulation parameters and coil design are still undetermined, hampering its therapeutic potential. There are an innumerate number of degrees of freedom in terms of possible combinations of stimulation frequency, duration, intensity, coil design, stimulation pattern, brain target, etc. emphasizing the need for a fast research, development, and screening tool in the evaluation of rTMS' neurophysiological effect of each of these parameters. Human studies are restricted due to ethical considerations, the difficulty in gathering large and homogeneous patient groups, and the high costs. Therefore, to explore rTMS in a systematic, flexible, and reliable manner, miniaturization of rTMS for rodent brain studies is an indispensable and complementary addition to the human studies.

Neuroimaging by means of (μ)SPECT is such a noninvasive technique to evaluate regional cerebral blood flow (rCBF) changes, which are assumed to reflect changes in neural activity (Matsuda et al. 1993). Intravenously injected [^{99m}Tc]-hexamethylpropyleneamine oxime ([^{99m}Tc]-HMPAO) distributes rapidly (<2 min) within the brain, representing perfusion at the time of injection and is assumed to reflect neuronal and interneuronal activity downstream from cell bodies and in distant input pathways. Consequently, μ SPECT is a useful tool to indicate alterations in the local (inter)neuronal activity that is provoked by DBS or rTMS and can be used to evaluate changes induced by different paradigms as well as stimulator and coil designs. As described in Sect. 2.2.1, (μ)SPECT scanners allow for a high enough spatial resolution with an acceptable sensitivity in rats and mice.

2.2.2.1 DBS

We compared four hippocampal DBS paradigms with stimulation off (sham stimulation) in the rat by means of μ SPECT subtraction analysis. Additionally, stimulation amplitudes were varied and effect on location, spatial extent, and intensity of rCBF changes were evaluated.

Stimulation Paradigms

A multi-contact DBS electrode was custom-made by gluing together four polyimide-coated stainless steel wires (125 μ m diameter, Bilaney, Germany). Each of the wires was straight-cut at a different length resulting in a quadripolar electrode with 1 mm distance between each of the four tips. This DBS electrode was inserted stereotactically in the right hippocampus of 13 healthy Wistar rats. The electrodes were led to a connector, which was fixed to the screws and the skull with acrylic dental cement. After recovery from surgery, rats were handled for more than a week and afterwards all rats underwent five μ SPECT/ μ CT scans at least 48 h apart. Every such μ SPECT/ μ CT scan was preceded by either 75 min of continuous DBS or 75 min of sham stimulation. After one hour of DBS or sham stimulation, rats were, while awake, intravenously injected with 370 MBq [99m Tc]-HMPAO. Stimulation was not interrupted during injection and continued until 15 min following injection. After termination of all μ SPECT scans, rats were deeply anesthetized, electrodes (and connector) were removed, and rats then underwent a final MR scan.

Rats were subjected to one sham stimulation and four DBS paradigms: bipolar high-frequency stimulation (HFS2), quadripolar HFS (HFS4), bipolar Poisson distributed stimulation (PDS2), and quadripolar PDS (PDS4). All stimulation paradigms consisted of a series of biphasic, charge-balanced square-wave pulses with a pulse width of 100 μ s and an average frequency of 130 Hz. In the quadripolar paradigms all 4 contact points are used to deliver pulses, while there are only 2 used in the bipolar paradigms. High-frequency stimulation is at a fixed frequency of 130 Hz, and in the PDS protocol, the interstimulus intervals were drawn from a Poisson distribution with a mean frequency of 130 Hz also so that on average, the same number of stimulus pulses was delivered in both PDS and HFS protocols. Seven animals were subject to one sham stimulation and four DBS paradigms, while stimulation amplitude was fixed for all four paradigms at 100 μ A. Six out of 13 rats were subjected to one sham stimulation and four stimulation amplitudes of bipolar PDS: 25, 50, 100 and 200 μ A. For each rat, the five stimulation paradigms were presented in a randomized order.

μ SPECT Imaging and Analysis

Static scanning in 18 frames of 5 min was performed using the MILabs U-SPECT-II (MILabs, Utrecht, the Netherlands) as described in Sect. 2.2.1.1. This μ SPECT scanner is equipped with the rat collimator consisting of a tungsten cylinder with 5 rings of 15 pinhole apertures of 1.0 mm diameter. The data were reconstructed on 0.75 mm³ voxels by 3 iterations of 16 pixel-based OSEM subsets. Afterwards the animals were sacrificed, their electrode was removed, and an MRI scan was

performed using a dedicated rat brain coil (Rapid Biomedical, Rimpar, Germany) on a Siemens Trio 3T (Siemens, Erlangen, Germany). A MPRAGE sequence resulting in $0.281 \times 0.281 \times 0.3$ mm resolution was applied with the rats placed head first and prone. Statistical parametric mapping (SPM) analysis was not preferred in this study as the interindividual variation in DBS-electrode positioning might mask the results around the tip of the electrode. Therefore, subtraction analysis was preferred in this study: both stimulation-off (sham) and stimulation-on μ SPECT scans are normalized within this MRI brain mask and subtracted from each other. The Z -score, representing the activation map, is achieved through dividing by the standard deviation of the stimulus-off (sham) μ SPECT. Accordingly, the magnitude of the Z -score can thus be determined for each voxel, indicating the significance of differences in rCBF for stimulation on/off. For each resulting standardized image, we determined the location, the maximal and minimal Z -score, and the total number of significant voxels (assuming uncorrected $p < 0.05$ to indicate significant differences; i.e., $Z\text{-score} > 1.96$ or $Z\text{-score} < -1.96$). Data are expressed as mean and standard error of the mean (SEM). Statistical evaluation of the maximal and minimal Z -score and total number of significant voxels was performed using repeated measures ANOVA.

Neurophysiological Findings

Predominantly decreases in rCBF were visualized when the different DBS scans were subtracted from sham stimulation scans. Hyperperfusion was occasionally seen, but these changes were never consistent between different rats and/or different scans.

The hyperperfusion was restricted to the different structures of the hippocampal formation in an intensity and stimulation paradigm-dependent manner. These decreases in rCBF were both in the ipsilateral (at the side of DBS) and the contralateral hippocampus as shown in Fig. 2.5.

Subtraction analysis in the rats ($n=7$) subjected to the four different stimulation paradigms revealed that during PDS2, more significantly hypoperfused voxels were counted in the hippocampal formation than during the three other stimulation paradigms as shown in Fig. 2.6. For all stimulation paradigms at equal amplitude, there was no statistical difference between the volume of hypoperfused brain in the ipsilateral hippocampal formation and the one in the contralateral hippocampal formation.

However, subtraction analysis in the other rats ($n=6$) subjected to one paradigm (PDS2) at four different stimulation amplitudes (25–200 μ A) revealed a linear increase in number of significant voxels at the contralateral hippocampal formation with increasing stimulation intensities and simultaneously a linear decrease at the ipsilateral hippocampal formation as shown in Fig. 2.7. For the entire hippocampal structure, however, the total number of significant voxels was not different between all stimulation amplitudes.

Several human studies are also available. Recent subtraction SPECT analysis of on-DBS versus off-DBS in patients with dystonia confirms decreased cerebral blood flow in the frontal lobes, the premotor and supplementary motor cortex due to

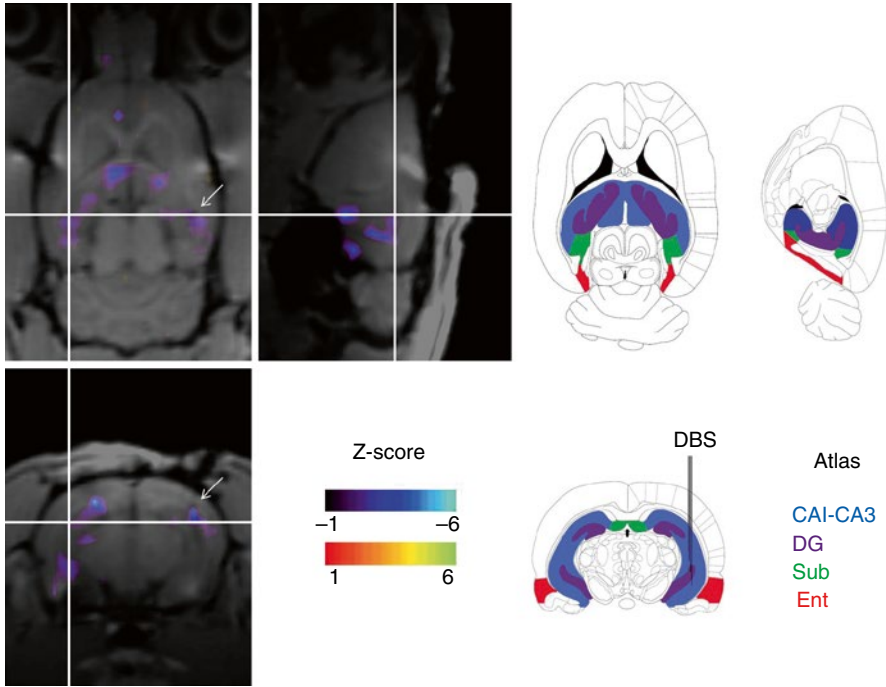
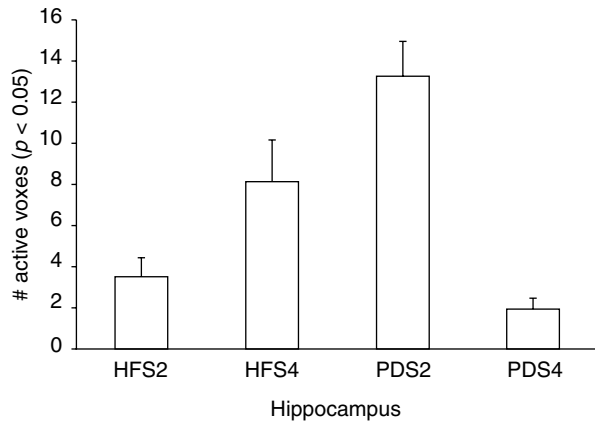


Fig. 2.5 Coronal, sagittal, and transverse anatomical scans coregistered with the colored subtraction SPECT data illustrating the rCBF changes induced by DBS (in this example PDS2, 100 μ A). Colored bars indicate Z-scores for increases (*warm colors*) and decreases (*cold colors*) induced by DBS in comparison with sham stimulation. The *white arrows* indicate the hippocampal DBS electrode artifact

Fig. 2.6 Mean (\pm SEM) number of significantly ($p < 0.05$; Z-score < -1.96) active voxels (volume of hypoperfused brain) during four different stimulation paradigms for the whole hippocampal formation



DBS, suggesting the reduction of the hyperactivity causing the clinical symptoms (Katsakiori et al. 2009). In a case study with pallidal DBS for tardive dyskinesia, a decrease in rCBF was also reported during on-DBS versus off-DBS (Kefalopoulou

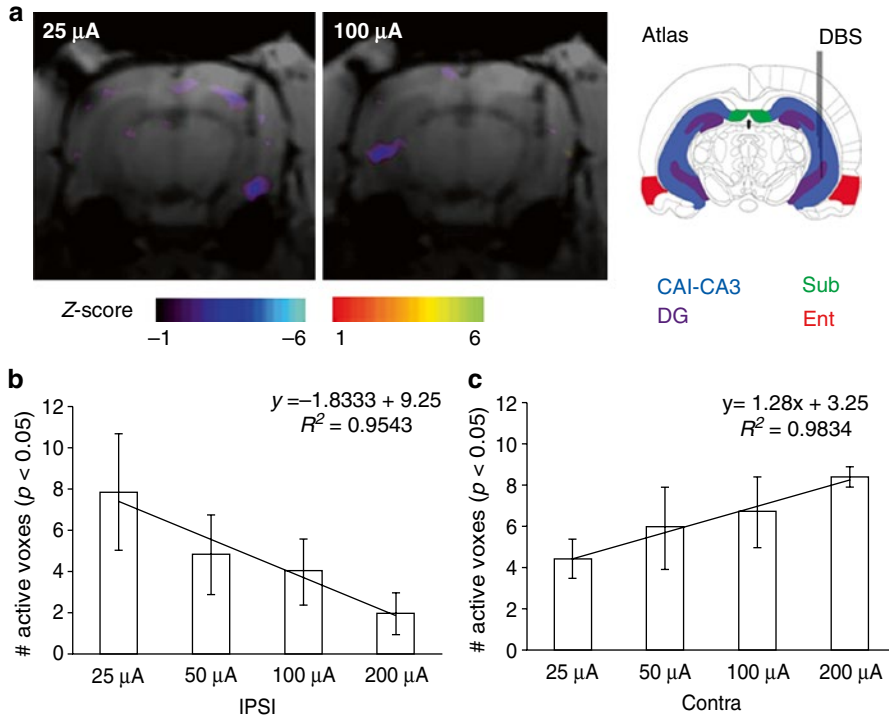


Fig. 2.7 (a) Difference in spatial extent of hypoperfusion within the hippocampal formation during PDS2 with different stimulation intensities: 25 μ A reveals mainly ipsilateral hypoperfusion; 100 μ A reveals more contralateral. (b, c) Number of significantly (Z -score < -1.96) active voxels (volume of hypoperfused brain) during PDS2 with four different stimulation amplitudes for both the ipsilateral (b) and contralateral hippocampus (c)

et al. 2009). Clinical improvement of this patient with bilateral pallidal DBS implies a possible correlation between brain functional imaging findings and the clinical response to DBS. Further, STN-DBS in Parkinson's disease (PD) patients revealed bilateral rCBF decrements in motor cortical areas and prefrontal cortex bilaterally compared to presurgical condition as well as compared to PD controls (Cilia et al. 2008).

In conclusion, during application of DBS in the hippocampus, significant hypoperfusion is seen in all hippocampal structures, both at the ipsilateral and at the contralateral side. We found that bipolar PDS induced the most intense and widespread hypoperfusion. In a previous animal study, bipolar PDS were delivered in kainate-treated animals with spontaneous seizures. Hippocampal bipolar PDS was found to suppress epileptic seizures more effectively than bipolar HFS (Wyckhuys et al. 2010). These findings may possibly indicate a correlation between the potential of a stimulation paradigm to induce hypoperfusion and its seizure suppressive potential. The effect of DBS on the contralateral side is probably mediated

by commissural fibers. These fibers are activated either directly or via activation of the corresponding neurons.

All these findings may provide important mechanistic insights into the mechanism of action of DBS and promote further research on stimulation parameters for DBS using μ SPECT in rats.

2.2.2.2 TMS

A volume-of-interest (VOI)-based and statistical parametric mapping (SPM) analysis of stimulation-on versus stimulation-off (sham stimulation) μ SPECT images was performed. Stimulation parameters were varied and effect on location, spatial extent, and intensity of rCBF changes were evaluated, in relation to the electrical field induced by the rTMS coil.

Experimental Procedures

Transcranial magnetic stimulation was delivered to healthy male Wistar rats ($n=6$) with a MagStim Rapid² stimulator (MagStim, UK) using the smallest commercially available TMS coil, a figure-of-eight 20 mm coil (MagStim, UK). The stimulation parameters being delivered were (1) trains of high-frequency 10Hz, 50 % of device power, 6 s duration, and 54 s intervals and (2) continuous low-frequency 1Hz, 50 % of device power. The average number of pulses delivered was accordingly the same (60 pulses per minute) in both stimulation paradigms. Sham stimulation was performed with the coil positioned perpendicular and a few centimeters away from the skull. As no muscle twitches could be evoked in the rat during rTMS with the current setup and overheating of the coil limited the maximal intensity of stimulation, we chose to set the intensity at 50 % device power. This correlates with a peak amplitude of 1430A in each wing of the figure-of-eight coil. Fixed position of the TMS coil in relation to the rat brain was ensured by using a custom-made silicone mold (Belosil, Equator, Belgium). The center of the TMS coil was positioned ± 0.5 cm to the left, ± 0.5 cm anterior to bregma with the coil in proximity of the rat's head (± 0.5 cm above the head).

After 1 week of behavioral training, all rats underwent three μ SPECT scans. Each μ SPECT scan was separated in time by at least 48 h for sufficient radioactive decay between scans. For each rat, the three stimulation paradigms (i.e., sham, 1 and 10 Hz) were presented in a randomized order. After 2 min of rTMS or sham stimulation, awake rats were intravenously injected with 370 MBq [^{99m}Tc]-HMPAO (Ceretek, GE Healthcare, UK). Stimulation was not interrupted during injection and was continued during the entire uptake of the [^{99m}Tc]-HMPAO tracer (for at least 2 min) following injection. After discontinuation of stimulation (or sham), rats were removed from the silicone mold and anesthetized to be scanned.

Multimodality Imaging with Electrical Field Calculations

Dynamic multi-frame scanning in 18 frames of 5 min was performed using the MILabs U-SPECT-II (MILabs, Utrecht, the Netherlands) as described in

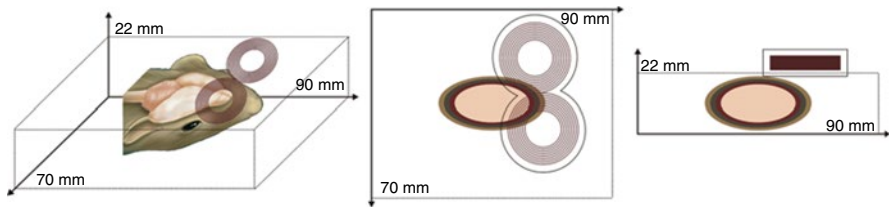


Fig. 2.8 Position of the figure-of-eight coil and the rat in the field of interest. Axial and sagittal views of the modeled coil with coating and modeled rat head (ellipsoids)

Sect. 2.2.1.1. This μ SPECT scanner was equipped with the rat collimator consisting of a tungsten cylinder with five rings of 15 pinhole apertures of 1.0 mm diameter. Similarly as in section “ [\$\mu\$ SPECT imaging and analysis](#)”, all pinholes focused on a single volume in the center of the tube. For imaging the rat’s brain, the animal bed was translated in three dimensions using an XYZ stage into eight different bed positions. A 20% main photopeak was centered at 140keV to reconstruct the Tc^{99m} images. The data were reconstructed on 0.75 mm^3 voxels by three iterations of 16 OSEM subsets as in section “ [\$\mu\$ SPECT imaging and analysis](#)”. In one rat, MRI (3D T2 weighted) was performed on a 9.4 T MR system (BioSpec 94/20 USR, Bruker Biospin, Germany). This image was used as a template for anatomical localization of perfusion maps.

The electric field, induced by the varying magnetic field generated by the coil current, is calculated using the recently developed independent impedance method (De Geeter et al. 2011). Both the magnetic field and electric field distributions, generated by the currently used 20mm figure-of-eight coil (MagStim, UK), modeled as a coil with two wings with nine loops each, consisting of a rectangular copper wire ($0.80 \times 5.50 \text{ mm}$) and inner and outer radii of the loops being 4.35 and 13.15 mm, respectively, are calculated for a volume of interest of $30 \times 50 \times 22 \text{ mm}$ under the coil with a resolution of 0.4 mm as illustrated in Fig. 2.8. The rat head is modeled as four concentric ellipsoids representing the tissues scalp, bone, cerebrospinal fluid (CSF), and brain. The exact positioning of the TMS coil in relation to the rat head was determined based on the microCT image containing the rat’s head in the silicone mold with the imprint of the coil position. To coregister the calculated induced electrical field distributions with the rat brain, the microCT image of the rat in the silicone mold is used to manually coregister the 9.4 T MRI image of the rat brain using Amide (freeware; <http://amide.sourceforge.net>). This is straightforward and was performed by rotating the MRI image exactly within the boundaries of the skull, clearly visible at the microCT. The rat head model (four concentric ellipsoids) was manually coregistered with the microCT image and MR of the rat in the silicone mold (Amide). As a result of previous coregistration steps, the rat brain areas (on MRI) were exactly located with respect to the induced electric field distribution map under the TMS coil (Wyckhuys et al. 2013).

To enable group comparisons between the stimulation paradigms, all data for all animals were spatially normalized into a common stereotactic atlas space

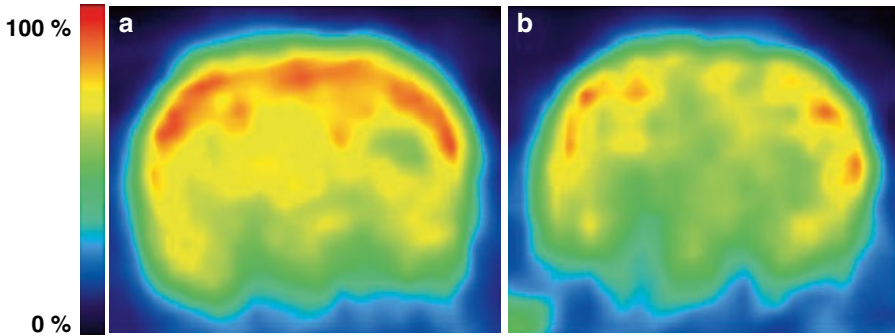


Fig. 2.9 Coronal section of one representative rat during (a) sham stimulation and (b) 10 Hz TMS. Color bar represents relative intensity for [^{99m}Tc]-HMPAO. Note the lower uptake during 10 Hz stimulation in comparison with SPECT taken during sham stimulation

– according to the Paxinos atlas for rat brain (PMOD v3.2, PMOD Technologies, Switzerland). Then, SPECT images were count normalized versus the cerebellum, which is the brain structure most remote from the TMS coil and was presumed to experience the least influence from stimulation.

Unlike the DBS study, SPM analysis was preferred in comparison with (the less powerful) subtraction analysis as the position of the rTMS coil in relation to the rat's head is fixed within subjects. For SPM analysis, images were smoothed (FWHM 3 times voxel size), and the hyper- and hypoperfusion T-map was achieved after paired analysis (stimulation vs. sham) for both 1 and 10 Hz (for each paradigm 6 pairs of data) using SPM8 (SPM8, Wellcome Department of Cognitive Neurology, London, UK). These T-maps were overlaid on the 9.4T MR rat brain image (PMOD v3.2) and VOIs were calculated delineated by discretized iso-values of electric field strength, generated by the rTMS coil.

For each T-map, we determined the location, the maximal and minimal T -value, and the total number of significant voxels (assuming uncorrected $p < 0.05$ to indicate significant differences; i.e., $T\text{-value} > 2.015$ or $T\text{-value} < -2.015$; degrees of freedom = 5) and correlated with the electric field strength using VOI-based analysis on the SPM parametric images. The percentage of significant hypoperfused volume per electric field-VOI was calculated as follows: volume (mm^3) of significant hypoperfusion per such VOI/total volume of VOI (mm^3).

rCBF Changes

We demonstrate in Fig. 2.9 that repetitive TMS in rats, using the smallest commercially available human coil, caused a significant and widespread decrease in rCBF relative to sham stimulation. Two different stimulation paradigms, i.e., low-frequency (1 Hz) and high-frequency (10 Hz) stimulation, were evaluated and revealed a clear distinction in spatial extent and intensity of hypoperfusion between the stimulation paradigms. Low-frequency (1 Hz) stimulation induced an overall significant

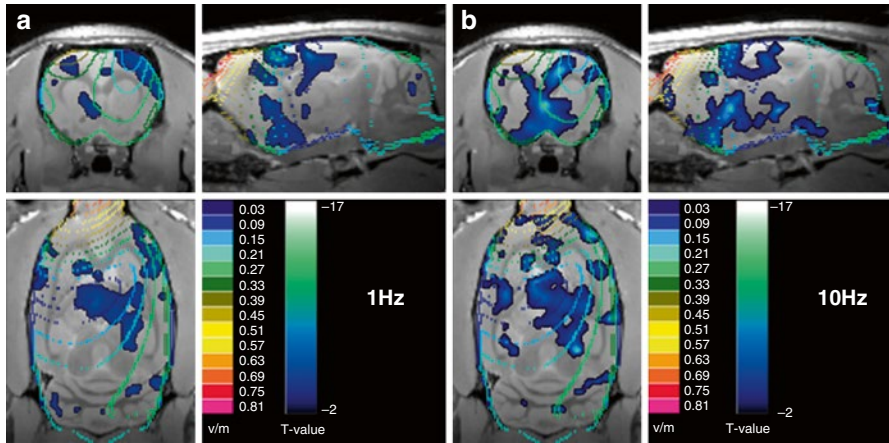


Fig. 2.10 9.4 T MR rat brain with overlay of hypoperfusion T-map (*blue*) and VOI-map of the electric field strengths (multicolored) for 1 Hz (**a**) and 10 Hz (**b**) illustrating the difference in spatial extent of the effect induced by both stimulation paradigms of rTMS

hypoperfusion of 11.9 % (i.e., 65 mm³, total rat brain volume=600 mm³) of the total rat brain, while high-frequency (10 Hz) stimulation induced an overall significant hypoperfusion of 23.5 % (i.e., 131 mm³), which is 197 % more than due to 1 Hz rTMS, as Fig. 2.10 illustrates. Low-frequency stimulation induced, however, more intense (with a minimal *T*-value of -24.77) hypoperfusion than 10 Hz stimulation (minimal *T*-value -17.98) as shown on Fig. 2.11. Differences in location of induced hypoperfusion were observed for both paradigms: both 1 and 10Hz affected the most widespread and most intense brain tissue at low electric field strengths of 0.03–0.15 V/m, but 10 Hz induced a second maximum of hypoperfusion at tissue affected by electric field strengths of 0.27–0.39 V/m. This suggests that the intensity of the electric field at the tissue is crucial: the location of the maximal neurophysiological response following rTMS will be different depending on the choice of the stimulation paradigm and/or the choice of the stimulation intensity.

For human experiments, the intensity of the induced electric field under the coil is typically around 100 V/m (Roth et al. 1991) and has been described to be optimally around 150–180 V/m to trigger slow waves over the sensorimotor cortex. Additionally, in previous monkey experiments, electrical field strengths of 70 V/m were observed to induce significant changes in brain metabolism (Hayashi et al. 2004). Despite the relatively low-induced electrical fields (0.03–0.81 V/m) in our experiment, we nevertheless observe widespread significant changes in rCBF in the rat brain. This indicates that the currently used rTMS coil, which was the smallest commercially available coil (figure of eight, 20 mm), was not focal and/or not powerful enough to pinpoint one specific brain area in the rat. This is consistent with the notion that rTMS in small animals, even with miniaturized coils, is restricted due to spatial selectivity of stimulation (Funke and Benali 2011).

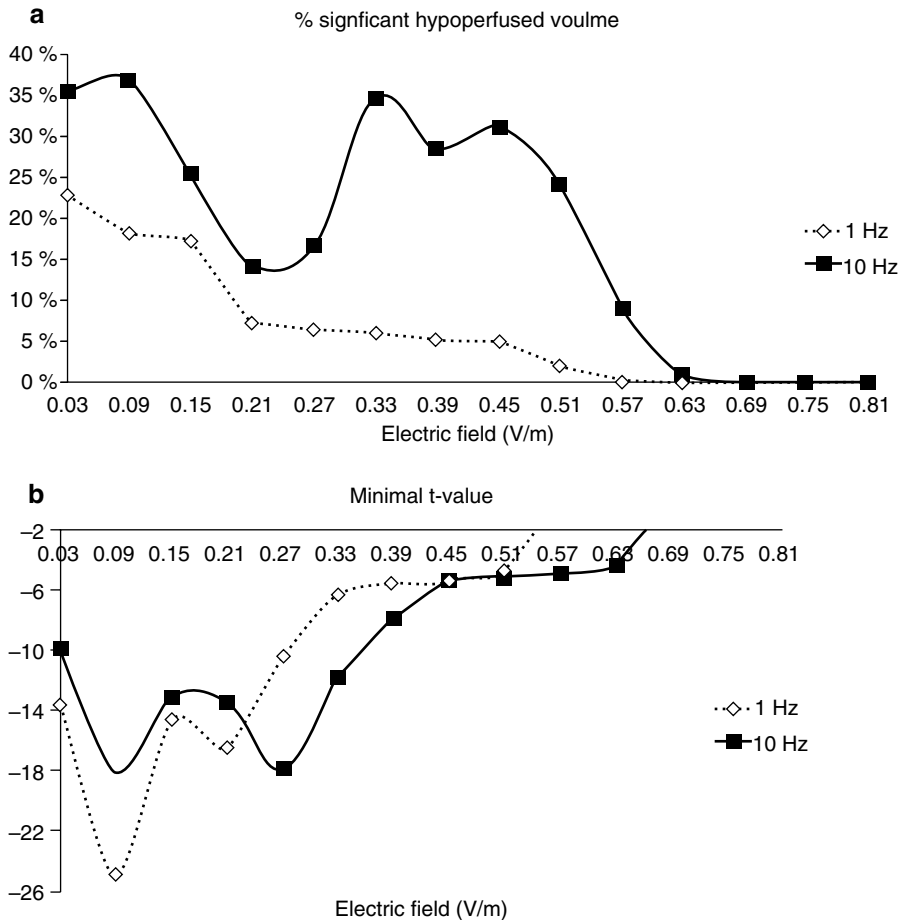


Fig. 2.11 Graphs illustrating (a) percentage tissue volume being significantly hypoperfused in relation to the electric field strength generated at the tissue due to 1 Hz (dotted line) or 10 Hz (full line); (b) the minimal intensity of hypoperfusion induced by 1 and 10 Hz, in relation to the electric field strength

Currently, no dedicated small animal TMS coils are commercially available. We developed an experimental small animal TMS coils and stimulators that might provide more flexibility for future animal research and that strive to deliver field strengths up to 120 V/m as in human applications, although the current study indicates significant effects already at 0.03–0.09 V/m. Extensive numerical modeling studies, however, are required to explore the optimal combination of coil geometry, size, and orientation in relation to the animal's head to achieve focal stimulation in small animals especially due to the different ratio of coil size/head size between animal and human. Here again, molecular imaging can be of help in validating the numerical models and quantifying the neurophysiological effect induced by these experimental rTMS coils.

2.3 μ PET

Although preclinical PET studies have been used for a long time, most of these studies were performed on human PET scanners using larger animal models such as the nonhuman primate for neuroscience research (Cherry 2006). The development of high-resolution, dedicated small animal μ PET scanners during the 1990s allowed the use of smaller, cheaper rodent models and allowed PET technology to be exploited by a wider base of users, including the pharmaceutical industry. The availability of μ PET scanners has positioned PET as a leading translational tool in the study of molecular interactions and in pharmacokinetic and pharmacodynamic studies for drug discovery and development of pharmaceuticals.

The positron emitters required for PET imaging are in general accelerator-produced. Although longer living PET isotopes like ^{124}I (4.2 days) and ^{89}Zr (78.4 h) produced by large accelerator facilities are gaining in popularity for antibody-based imaging, PET imaging is still mainly based on the use of short-living radioisotopes, produced by lower energy, commercial cyclotrons. The most widely used PET isotopes are ^{15}O (2 min), ^{13}N (10 min), ^{11}C (20 min), and ^{18}F (109 min). The very short half-life of ^{13}N and ^{15}O precludes extensive radiochemistry and, therefore, limits the use of ^{13}N and ^{15}O to a few simple procedures such as [^{13}N]ammonia for measurement of myocardial blood flow (Inubushi et al. 2004) and [^{15}O]H₂O for regional cerebral blood flow (rCBF) measurement (Ose et al. 2012) or oxygen metabolism. The most widely used isotopes for the radiochemical synthesis of positron-emitter radiotracers are ^{11}C and ^{18}F . ^{11}C is the isotope of choice for on-site short labeling procedures and limited imaging protocols. As carbon is a natural constituent of most molecules, it allows for the production of radiotracers indistinguishable from their non-labeled counterparts. Well-known examples of ^{11}C in neuroimaging are [^{11}C]raclopride for D2 receptor imaging (Patel et al. 2008) and [^{11}C]PIB for amyloid imaging (Manook et al. 2012). The low positron emission energy (max 635 keV) and short positron range make ^{18}F the isotope of choice for high-resolution brain imaging. Its half-life is long enough to allow for more extended imaging protocols and gives access to high-quality metabolite analysis compared to ^{11}C . It is therefore used not only to radiolabel small molecules, but also peptides and even proteins through ^{18}F -labeled prosthetic groups (Li and Conti 2010). The best known example is the ^{18}F -labeled glucose analogue, 2- ^{18}F -fluoro-2-deoxy-D-glucose ([^{18}F]FDG), which brought PET imaging to general clinical practice.

Small animal [^{18}F]FDG PET allows us to study glucose metabolism longitudinally in vivo in animals. The uptake of [^{18}F]FDG allows to quantify tumor metabolism, inflammation, or brain activation. In neuroimaging, [^{18}F]FDG that neurons utilize for energy instead of glucose becomes phosphorylated and trapped once transported into cells. The concentration of [^{18}F]FDG within cells of specific brain regions is considered an indirect measure of neural activity.

Many quantitative measures can be derived from [^{18}F]FDG PET studies, but the application of a pharmacokinetic model or a graphical evaluation of the data

derived from dynamic PET studies may be considered the gold standard. However, pharmacokinetic modeling requires invasive catheterization procedures to obtain a plasma blood input function. Therefore, alternatives use a population-based input function or an image-derived input function by a dynamic scan of the heart or a reference tissue model that does not require an input function. Nevertheless, to obtain an accurate measure from the kinetic modeling scan durations of 60 up to 90 min need to be considered, greatly reducing scan throughput. Moreover, animals need to be anesthetized during the whole scan duration including the initial period following bolus injection when most of the tracer is accumulated in the cells. These practical considerations have led to the development of simplified quantitative measures that can be obtained from a shorter static scan after an awake uptake period.

Currently the most widely used quantification index in [^{18}F]FDG PET studies is the semiquantitative SUV (standard uptake value) measure. The SUV is the ratio of the activity concentration within a certain region of interest (ROI) obtained during a static scan and the injected dose divided by the weight of the subject. Despite the incorporation of scatter and attenuation correction in image reconstruction to improve quantitative accuracy, SUV will only account for gross changes and significant variability remains within and between subjects in pre-clinical molecular imaging studies. Various factors affecting SUV quantification in humans are also applicable to small animals. Factors that have been studied in rodents include the effects of various anesthetics (Lee et al. 2005; Fueger et al. 2006), fasting duration (Lee et al. 2005; Fueger et al. 2006; Wong et al. 2011), the route of [^{18}F]FDG administration (Wong et al. 2011; Schiffer et al. 2007), and the influence of the body temperature of animals during the experiment in various organs (Fueger et al. 2006). Other factors include circadian cycles and stress resulting from animal handling procedures such as restraint and injection (Meijer et al. 2005). Each of these factors has been shown to be able to affect [^{18}F]FDG biodistribution, either by directly influencing blood glucose levels or by changing the glucose needs and thus also [^{18}F]FDG uptake in certain organs. All these findings highlight the importance of a standardized preparation of animals for [^{18}F]FDG PET imaging studies.

The variability in [^{18}F]FDG uptake has already been assessed in mice (Jan et al. 2004; Dandekar et al. 2007), while others have looked at the impact of animal handling (Fueger et al. 2006), administration route, dietary condition, blood glucose level (Wong et al. 2011; Schiffer et al. 2007), and quantification method (Schiffer et al. 2007) in rats.

In particular we additionally investigated the influence of repeated scanning, the interval between scans and fasting duration on inter- and intra-animal variation, and reproducibility of semiquantitative [^{18}F]FDG uptake measures. Different SUV quantification methods and their influence on inter- and intra-animal variation and reproducibility of brain [^{18}F]FDG uptake were also explored, in an attempt to establish a reliable and reproducible quantification technique. Finally, we tested and validated a small animal [^{18}F]FDG PET brain imaging protocol for its potential use in a high-throughput preclinical setting.

2.3.1 Standardization: Factors Influencing [^{18}F]-FDG Uptake in the Brain

2.3.1.1 Glucose Levels

It is well established that blood glucose levels influence [^{18}F]FDG uptake in organs. Both human PET studies and studies in rats that employed tissue sampling to assess [^{18}F]FDG uptake (Wahl et al. 1992) have shown that hyperglycemia decreases [^{18}F]FDG uptake in tumor cells as a result of the competition between [^{18}F]FDG and glucose for transport into the cells. A more recent small animal PET study by Fueger et al. (2006) confirmed these findings, but also revealed that [^{18}F]FDG uptake in various organs was not influenced in the same manner by different glucose levels. The Fueger study found that cerebral [^{18}F]FDG uptake in non-fasted mice was higher than in fasted mice, while in contrast myocardial uptake was higher in non-fasted mice. Similarly, a dynamic [^{18}F]FDG PET study by Wong et al. (2011) in mice found that brain [^{18}F]FDG uptake was significantly higher in fasted mice compared to non-fasted mice, while the opposite was observed with respect to myocardial uptake.

Glucose levels can be influenced by several factors. Of these factors we investigated fasting time and inter-scan duration in particular.

2.3.1.2 Fasting Time

Fasting is used as an effective means to ascertain uniformity in the results of [^{18}F]FDG PET studies, where it is used to lower glycemia (Hildebrandt et al. 2008). In a clinical setting patients are required to fast 4–6 h before a [^{18}F]FDG scan. In rodents a fasting duration of around 6 h should clear all contents from the stomach. Besides decreasing glucose levels, longer fasting durations may result in alterations in water consumption, lowered fatty acid levels, a loss of body mass, and increased stress levels. Based on these findings we conducted an elaborate fasting experiment to investigate the effect various fasting durations have on glucose levels and subsequent [^{18}F]FDG brain uptake in rats.

To this end 20 male Sprague–Dawley rats were allowed to acclimatize to laboratory conditions for at least a 7-day period before the start of the experiment. Animals were subjected to a 12 h light/dark cycle (8 a.m. to 8 p.m.) across the whole duration of the study. The rats were divided into five groups with each group containing four animals. The first group did not fast (i.e., control group), while the second group fasted for 6 h, the third group for 12 h, the fourth group for 18 h, and the final group for 24 h. Animals were subjected to a 12 h light/dark cycle (8 a.m. to 8 p.m.) and the scans of all groups were performed between 9:00 a.m. and 11:30 a.m. To ensure that all animals of the same group had exactly the same fasting duration, food was removed depending on the time at which the tracer injection had been planned (during the night by an attending animal handler) to account for the nocturnality of the animals.

The experimental protocol is illustrated in Fig. 2.12. Animals were weighed and then put in individual cages before the beginning of the experiment and then placed on an electrically heated animal pad. Animals were anesthetized with isoflurane (5% for induction and 2% for maintenance) 25 min later to and received an i.v. bolus

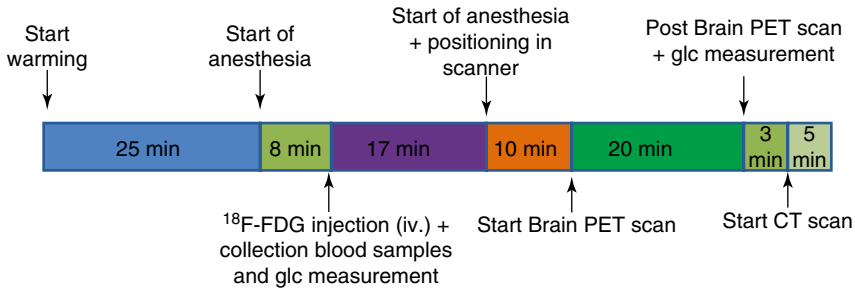


Fig. 2.12 Experimental protocol of fasting experiment

injection of [^{18}F]FDG in the left lateral tail vein after 5 min of anesthesia. Two blood samples were taken within 3 min after [^{18}F]FDG injection. These samples were then used to determine pre-scan serum glucose which was subsequently used (i.e., incorporated in an SUV) to evaluate various quantification techniques and to assess their effects on inter-animal and intergroup variation of cerebral [^{18}F]FDG uptake. The blood samples were always collected from the right lateral tail vein, the opposite tail vein in which [^{18}F]FDG was injected, by means of inserting a needle (BD Microlance; 0.6×25 mm). Serum glucose samples consisted of 10 drops of blood and were collected in a test PP tube (Novolab). Double measurement of the whole blood glucose levels using the One Touch Ultra 2 strips was first performed. Blood samples were then stored at 4 °C until the end of the last PET scan that particular experimental day. Samples were then allowed to coagulate for at least one hour before centrifugation for 15 min at 3,300 rpm and 20 °C (Eppendorf Centrifuge 5430R; Rotor 35–6–30). Subsequently 100 μL serum samples were obtained for accurate serum glucose determination at the hematology department on a Vista Dimension (Siemens).

Eight minutes after the start of anesthesia, when all blood samples and blood glucose concentrations were collected, anesthesia was stopped and the animal was allowed a 17 min conscious uptake period. After this conscious uptake period, animals were anesthetized again with isoflurane (5 % for induction and 2 % for maintenance) for a 10 min unconscious uptake period. During this period the animals were placed in prone position on the scanner and further preparations for the start of the PET scan were carried out. After a total uptake period of 30 min, the PET scan was started. Whole blood glucose concentrations were again measured twice after the PET scan, followed by a 5 min CT scan for attenuation and scatter correction. In Table 2.1, we put the necessary definitions forward for quantification throughout the analysis of the study.

The results of this fasting experiment as shown in Fig. 2.13 indicate that a fasting period of 6 h in naïve rats does not result in significantly lower glucose levels compared to non-fasting levels. Furthermore, cerebral [^{18}F]FDG uptake (all measures) in the 6 h fasting group was not significantly affected by the slight decrease in glucose levels after 6 h fasting compared to the non-fasting group as shown in Fig. 2.14a, b. Longer fasting durations than 6 h did result in a significant reduction of glycemia in the naïve rats at 12 h fasting time, but glucose levels did not decrease further in the 18 and 24 h fasting groups compared to those in the 12 h group as shown in Fig. 2.13. In addition, [^{18}F]FDG brain uptake in the 12, 18 and 24 h fasting groups

Table 2.1 Overview of all the quantification methods that were used to quantify the data in the various experiments and the formulas used to calculate them

Quantification method	Formula	Unit
ACR	/	kBq/cc
$SUV_{(ID/BW)}$	$ACR/(ID/BW)$	g/cc
SUV_{Glc1}	$[ACR/(ID/BW)] \times \text{whole blood pre-scan [Glc]}$	$(g/cc) \times (mg/dL)$
SUV_{Glc2}	$[ACR/(ID/BW)] \times \text{serum pre-scan [Glc]}$	$(g/cc) \times (mg/dL)$

Abbreviations: ACR average activity concentration in an ROI, SUV standard uptake value, ID injected dose, BW body weight, Glc1 pre-scan whole blood glucose concentration (One Touch Ultra 2 blood glucose meter), Glc2 pre-scan serum glucose concentration

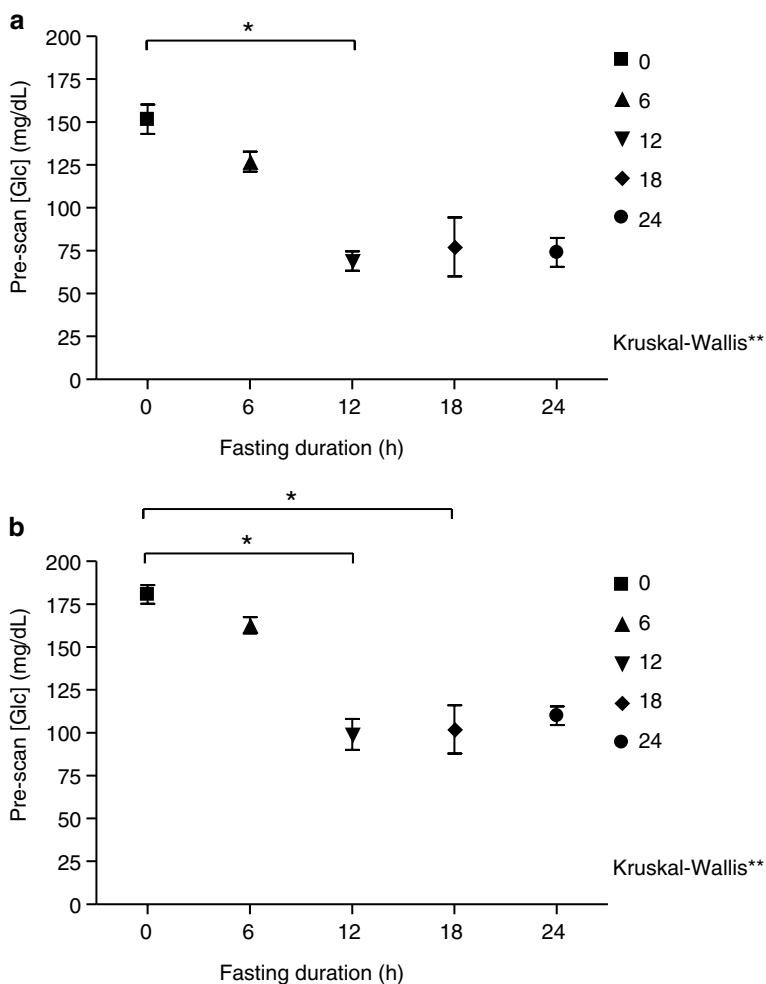


Fig. 2.13 Overview of pre-scan glucose levels of the different fasting durations. (a) Whole blood pre-scan glucose levels measured with the One Touch Ultra glucose meter (LifeScan, France). (b) Serum pre-scan glucose levels. Data is represented as mean \pm SEM. *Abbreviation:* [Glc] concentration of glucose. Asterisks represent a significant difference between pre-scan glucose levels (* $p < 0.05$, ** $p < 0.01$)

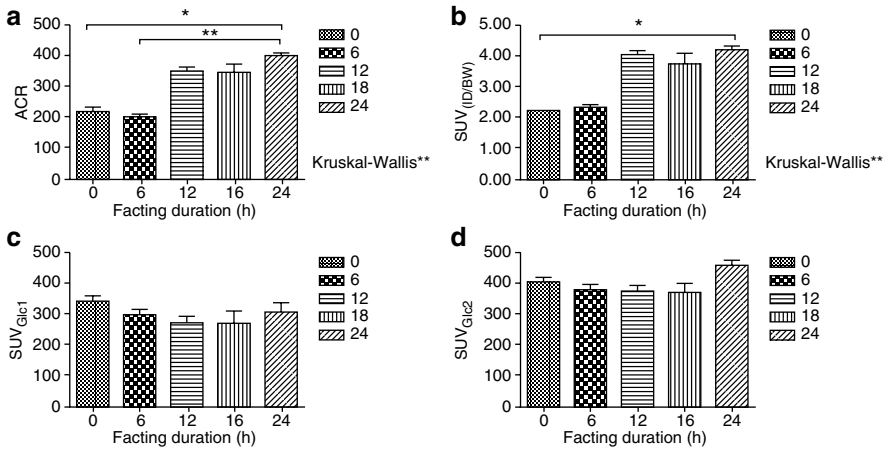


Fig. 2.14 Overview of the whole brain $[^{18}\text{F}]\text{FDG}$ uptake of the different fasting groups. (a) ACR quantification. (b) $\text{SUV}_{\text{ID/BW}}$ quantification. (c) SUV_{Glc1} quantification. (d) SUV_{Glc2} quantification. For an overview of the different quantification methods, see Table 2.1. Data is represented as mean \pm SEM. Asterisks represent significant differences between groups connected by the bridge ($*p < 0.05$, $**p < 0.01$)

was also found to not be significantly different, while the $[^{18}\text{F}]\text{FDG}$ signal in these three fasting groups was increased compared to those of the 0 and 6 h fasting groups as shown in Fig. 2.14a, b. In Sect. 2.3.2, we will address the influence of correcting for glucose levels on absolute quantification.

A study by Nowland et al. (2011) has investigated the effect of 24 h fasting period on various physiological markers (e.g., serum glucose and corticosterone) in Sprague–Dawley rats. In that experiment, animals were divided in seven different groups each subjected to a different fasting duration. Serum glucose levels were determined at the 0, 6 and 16 h time points, while corticosterone levels were measured throughout the entire 24 h fasting period. The results of Nowland et al. (2011) showed glucose levels at the 16 h time point were significantly lower in the fasted rats than in non-fasted rats at the same time point. Although this is not exactly the same time point as in the fasting experiment conducted in this study, it remains comparable to 12 and 18 h fasting duration time points used here. Both these fasting periods showed a significant reduction of serum glucose levels compared to the 0 h fasting duration in our fasting experiment.

In addition, Nowland et al. (2011) found significantly higher serum corticosterone levels in rats that had been fasted for 24 h, whereas this increase was not detected at 16 h or earlier time points. This suggests that at some point between 16 and 24 h of fasting, a significant corticosterone response occurred in the rats. Corticosterone, as stress hormone, is measured to evaluate stress in laboratory animals and has been shown to elevate plasma glucose levels also known as stress hyperglycemia. This stress effect on glycemia might offer an explanation for the observation that glucose levels in the fasting experiment conducted in this current study did not significantly differ between the 12, 18 and 24 h fasting groups as increased corticosterone levels might counter a further decrease of glucose levels.

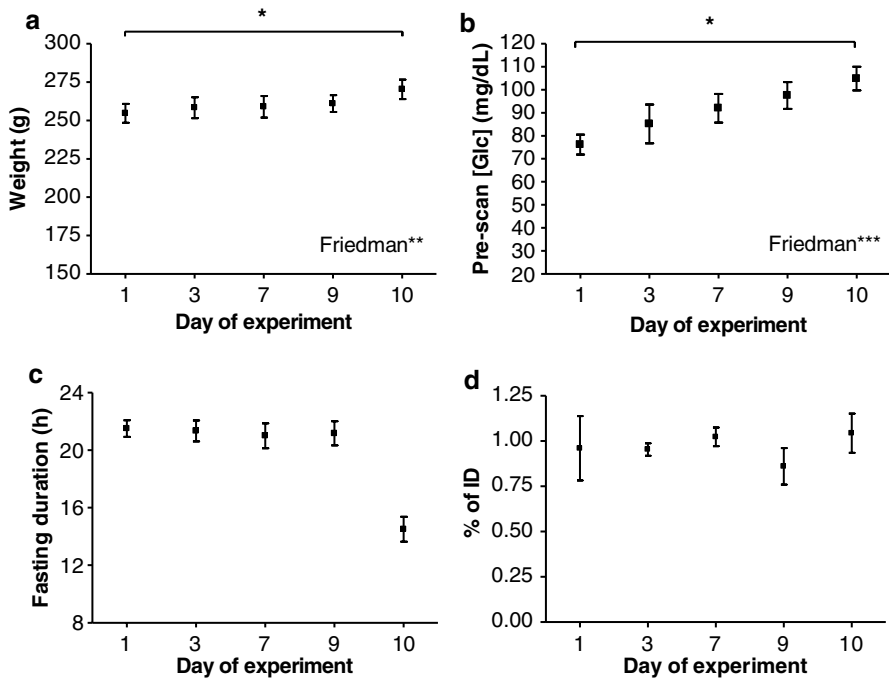


Fig. 2.15 Overview of the variables that possibly affected cerebral [^{18}F]FDG uptake during the longitudinal experiment. (a) Evolution of body weight during experiment. (b) Pre-scan glucose levels. (c) Pre-scan fasting durations. (d) Activity remaining in the tail after [^{18}F]FDG injection, as a percentage of the ID. All data is presented as mean \pm SEM. Abbreviation: [Glc] concentration of glucose. Asterisks represent a significant difference between different days of the experiment (* $p < 0.05$, ** $p < 0.01$, *** $p < 0.001$)

2.3.1.3 Inter-scan Time Duration and Repeated Scanning

In order to establish whether an experimental protocol for small animal [^{18}F]FDG PET imaging could be used in longitudinal studies to achieve reproducible cerebral tracer uptake, male Wistar rats ($n = 3$) were subjected to a longitudinal test–retest paradigm. The experiment was spread over 10 days and animals were scanned on days 1, 3, 7, 9, and 10. Hence, the effect of different inter-scan periods on the reproducibility of the resulting small animal PET data was tested. The experimental protocol is similar to that of Fig. 2.12.

In this study a short inter-scan duration (i.e., two PET scans conducted within a 24 h period – Fig. 2.15c) resulted in significantly decreased cerebral [^{18}F]FDG uptake (Fig. 2.16a, b) and significantly higher glycemia in the animals during the second scan (Fig. 2.15b). For the experiment performed on two consecutive days, animals were subjected to a longer fasting duration prior to the first scan than to the second scan (Fig. 2.15c). Therefore, the possibility that the observed difference in pre-scan glucose levels was a consequence of the variation in pre-scan fasting duration could not be excluded. However, pre-scan glucose levels and cerebral [^{18}F]FDG uptake in the fasting experiment (Figs. 2.13 and 2.14) did not change significantly between the 12, 18 and 24h fasting groups. These results and the fact that almost all

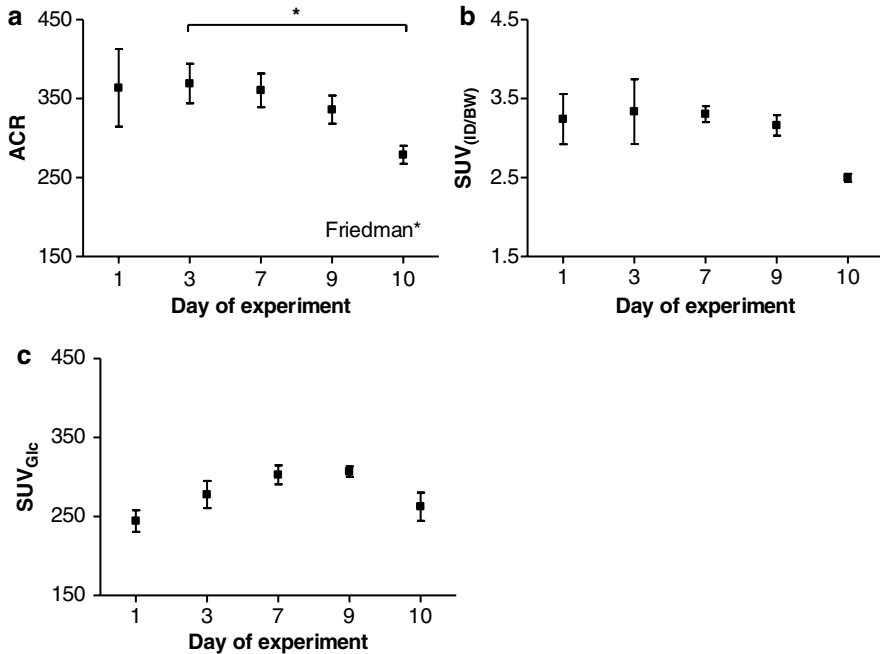


Fig. 2.16 Whole brain [^{18}F]FDG uptake values across different scanning sessions of the longitudinal experiment. (a) ACR quantification. (b) $\text{SUV}_{(\text{ID}/\text{BW})}$ quantification. (c) SUV_{Glc} quantification. All data is presented as mean \pm SEM. Asterisks represent a significant difference between different days of the experiment ($*p < 0.05$)

animals subjected to the repeated scans were consistently fasted within this range suggest that the elevated glucose levels during the second scanning sessions cannot be solely explained by intra-animal variation in pre-scan fasting duration.

One must also take into account that animals in the fasting experiment (Figs 2.13 and 2.14) were only fasted once in contrast to animals in the longitudinal experiment that were fasted, anesthetized, and scanned repeatedly (Figs. 2.15 and 2.16). In addition, the animals in the longitudinal experiment did show increasing glucose levels during the first four scanning sessions of this experiment (Fig. 2.15b), while fasting durations of the animals were almost identical and the time between two scan sessions was longer than 24 h (Fig. 2.15c). This could suggest longer-term effects of repeated fasting or isoflurane anesthesia or cumulative stress. It has been shown that repeated fasting affects energy metabolism-regulating hormones such as leptin (i.e., adipocyte-derived hormone) in rats (Kim and Scarpace 2003). Isoflurane on the other hand has been shown to be cleared (to a negligible amount) from the brain within 24 h (Saab et al. 2010).

In contrast to our findings, a study by Dandekar et al. (2007) found a significant reduction in glucose levels and no significant change in FDG uptake in tumors between two repeated scans with a short inter-scan time. In this study nude female mice with tumor xenografts were subjected to two [^{18}F]FDG injections and two PET

scans within an 8 h period. Similar to the protocol used in our experiments, glucose levels were obtained around the injection of [^{18}F]FDG. This difference in animal response to repeated scanning might be a consequence of differences in sex and type of rodents used or the type of tumor that was investigated. Furthermore, since [^{18}F]FDG uptake in tumors has been shown to be influenced by glucose levels, it seems contradictory that uptake in the tumors during the Dandekar et al. study was not influenced by the significant changes in glucose levels during this experiment.

2.3.1.4 Injection Route

The effects of different injection methods on the results of [^{18}F]FDG small animal PET studies have been investigated by previous studies. A study by Schiffer et al. (2007) compared measurements of cerebral [^{18}F]FDG uptake obtained after intraperitoneal (i.p.) injection with those obtained after intravenous (i.v.) injection. They found the two routes of administrations delivered almost identical quantitative values. However, this was dependent on the time point at which brain uptake was measured which is due to differences in rate of [^{18}F]FDG delivery to the brain with i.p. injection having a slower absorption of [^{18}F]FDG into the blood stream and subsequently slower distribution of [^{18}F]FDG throughout the body compared to i.v. injection, for which [^{18}F]FDG is immediately available in the blood stream.

Our goal was to evaluate whether repeated intravenous tail vein [^{18}F]FDG injections contributed to variation of [^{18}F]FDG uptake in the brain. The results of tail scans indicate this was not the case as residual activity levels in the tails did not vary significantly across the longitudinal reproducibility experiment and were only around 1 % of the injected dose as shown in Fig. 2.15d.

2.3.1.5 Anesthesia

Anesthetics used in small animal imaging studies (e.g., xylazine, ketamine, and isoflurane) have been shown to influence insulin secretion and to affect blood glucose levels (Lee et al. 2005). This is consistent with our results. In the longitudinal experiment post-scan glucose levels were consistently elevated compared to pre-scan levels.

It is possible that isoflurane could have a longitudinal effect on glucose levels when animals are repeatedly scanned, as glucose levels increased in the longitudinal experiment with each scanning session (Fig. 2.15b). However, a study by Saab et al. (2010) found only residual concentrations of isoflurane in the brains of mice 24 h after 1 h anesthetization with isoflurane and no detectable concentration of isoflurane in expired gas within 7 min after termination of anesthesia. Furthermore, isoflurane is only minimally metabolized by the liver (less than 0.2 %). This would argue against any long-term carry-over effects of isoflurane on glucose levels.

2.3.2 Evaluation of Different Quantification Methods

To allow the use of [^{18}F]FDG small animal PET scanning in longitudinal pharmacological studies aiming at the assessment of therapy response and drug efficacy, the reproducibility of such scans needs to be investigated as explained in the

introduction of Sect. 2.3.1. The variation in these scans must be determined in order to establish whether changes in uptake during different time points of longitudinal experiments are reflecting effects of the administered treatments or are rather a consequence of changes in animal physiology or methodological variability.

We tested the use of various SUVs (Table 2.1), which each incorporated different parameters (ID, body weight, and glucose levels), to establish whether their use in uptake quantification could possibly decrease intra- and inter-animal variation. Decreased intra- and inter-animal variation during a longitudinal study increases the statistical power to detect therapeutic effects over time within the same animal or between treatment groups. Increased statistical power decreases the amount of animals needed to detect significant therapeutic effects or allows to detect smaller changes with the same number of animals.

Inter-animal variation of brain uptake using the different quantification methods ranged between 3.49 and 25.86 % across the various experiments of our study. These results are comparable to those obtained by others. A study by Martic-Kehl et al. (2012) which investigated test–retest variability of [^{18}F]FDG uptake in two groups of Sprague–Dawley rats found inter-animal COVs of 8 ± 2 % ($\pm\text{SD}$) and 14 ± 7 % ($\pm\text{SD}$) using SUV quantification with normalization to injected dose and body weight. A [^{18}F]FDG PET study by Marsteller et al. (2006) found inter-animal COVs of 18 % for normalization of ACR values to injected dose, 36 % for normalization to plasma [^{18}F]FDG levels, and 15 % for normalization to injected dose, body weight, and glucose levels.

Incorporation of glucose levels in the SUV did not seem to increase the variability of SUV measurements (Figs. 2.14c, d and 2.16c), suggesting that correcting [^{18}F]FDG brain uptake for significant differences in glucose levels might be possible without the introduction of extra variability due to biological and analytical variation, as has also been suggested by previous studies (Hadi et al. 2008).

It is important to take into account that the SUV normalized to injected dose and body weight is a semiquantitative index of the [^{18}F]FDG uptake rate, and it is not a quantitative measure of glucose metabolism (i.e., glucose metabolic rate or GMR). A dynamic [^{18}F]FDG PET study by Wong et al. (2011) showed that the measured cerebral GMR did not correlate with blood glucose level or dietary condition, while the [^{18}F]FDG uptake constant varied inversely with blood glucose levels. Since GMR is proportional to the product of [^{18}F]FDG uptake rate and glucose concentration, it can be expected that the glucose-corrected SUV can be a more robust measure of GMR than SUV normalized to injected dose and body weight alone. This is in correspondence with our findings as SUV normalized to injected dose and body weight significantly decreased for an increasing glucose level, while the glucose-corrected SUV did not show any significant changes as clearly shown in Fig. 2.14c, d and by Fig. 2.16c.

Quantification with plasma activity levels results in higher inter-animal variation as described in the Marsteller study. This increased inter-animal variation using normalization to plasma [^{18}F]FDG levels may partly be explained by variation in time duration between [^{18}F]FDG injection and the collection of the plasma activity blood samples. As the plasma samples are often taken shortly after injection, a time where the plasma concentration changes quickly, small variations in the time points can result in large variation in measured plasma concentration.

2.3.3 Recommendations for Preclinical Protocol Optimization

The results of our longitudinal reproducibility experiment (Sect. 2.3.1) demonstrate that raw data expressed as activity concentration in ROIs (ACR) or the use of $SUV_{ID/BW}$ quantification together with a well-controlled experimental protocol could be used to achieve reproducible measurements of $[^{18}F]FDG$ brain uptake in repeatedly scanned control animals. However, a well-controlled protocol is required as several external factors exist that lead to significant differences of blood glucose levels within (inter and intra) animals over time, which will result in significant variations of $[^{18}F]FDG$ uptake thus reducing the reproducibility of $[^{18}F]FDG$ uptake quantification. In addition these variations in $[^{18}F]FDG$ uptake also reflect the effect of competition with glucose (Figs. 2.14a, b and 2.15a, b) and do not necessarily reflect changes in brain glucose metabolism induced by, for example, a pharmacological treatment.

In the experiments conducted here, fasting time and a short time span between subsequent scans were identified as factors with a significant effect on $[^{18}F]FDG$ uptake likely through their effect on blood glucose levels. These factors can also disguise the effects of a pharmacological treatment (e.g., memantine), if blood glucose levels were not taken into account during data quantification. However, an SUV that corrects for pre-scan glucose levels was shown to provide a measure of $[^{18}F]FDG$ uptake in the brain that is not significantly influenced by potential confounding differences in the scan protocol (Figs. 2.14c, d and 2.16c). An alternative for the use of glucose correction in the SUV calculation could be a well-controlled experimental protocol, designed in such a manner that animals are scanned at a similar blood glucose level. The fasting experiment using naïve animals showed considerable reduction of pre-scan glucose levels as in the animals of the 12 h fasting group, compared to glucose levels in the animals of the 0 and 6h fasting groups. For longer fasting times pre-scan glucose levels did not further decrease as a function of fasting time. As a result, animals that were scanned after a fasting period of at least 12h exhibited comparable ACR or $SUV_{ID/BW}$ brain uptake values (Fig. 2.14a, b). Thus, scanning naïve animals after a fasting time ranging between 12 and 24h h seems to be a practically feasible procedure to ensure optimal $[^{18}F]FDG$ brain uptake. However, this relationship was only established in naïve animals and fasting duration was not the sole determining factor with regard to varying blood glucose levels in the longitudinal experiment. A short inter-scan duration (i.e., two subsequent scans within 24 h) was also shown to be able to cause significant variations in $[^{18}F]FDG$ brain uptake potentially due to changes in blood glucose levels (Fig. 2.16). Also a clear trend of rising glucose levels was shown over time in a longitudinal study (Fig. 2.15b). Therefore, the measurement and correction for pre-scan glucose levels seems advisable over solely relying on the diligent control of fasting duration and inter-scan times in case a particular experimental protocol does not seem to lead to reproducible glucose levels. Especially in longitudinal experiments with different pharmacological challenges that may have unknown effects on glucose levels, measurement and potentially correction for aberrant blood glucose levels seems advisable.

A possible disadvantage of the use of glucose-corrected SUV values is that they could lead to increased inter-animal variability (COV). This can be expected as

systemic errors in the glucose measurements add to the SUV variability. However, the latter effect can be reduced by using a more accurate glucose measure such as repeatedly using the glucose strip at one time point for whole blood or determining the serum glucose levels analytically. A feasible alternative to the use of a glucose correction is the establishment of a glucose level range within which animals can be scanned without a significant effect of glucose levels on cerebral [^{18}F]FDG uptake. This however also requires glucose measurements with their corresponding variability.

2.3.4 Drug Testing

In developing new and innovative drugs in neurosciences, the use of fast preclinical screening methods using animal models is indispensable. In the search for suitable models, focus is on the similarities of the animal model with the clinical behavioral symptoms and for instance the increased activation in discrete brain areas associated with the disease. Additionally, validity of these animal models is confirmed by determination of the effects of known drugs on the reversal of the pathological behavior. Molecular imaging with PET in the rat, using a VOI-based approach, has a major advantage for screening of novel drugs in comparison with other preclinical screening techniques such as autoradiography, microdialysis, and ex vivo tissue analysis, being its noninvasiveness, allowing longitudinal studies and intra-animal comparisons with significantly lower numbers of animals (Lancelot and Zimmer 2010).

2.3.4.1 Exemplified in Schizophrenia

Schizophrenia is a mental disorder characterized by disintegration of thought and emotional responsiveness, with a global lifetime prevalence of about 0.3–0.7 %. *N*-methyl-D-aspartate (NMDA) receptor hypofunction has been hypothesized to play a crucial role in the pathophysiology of the disease (Tsai and Coyle 2001). These findings have been strengthened by the fact that administration of NMDA antagonists in healthy patients induces behavioral and perceptual symptoms similar to those associated with schizophrenia or profoundly exacerbates preexisting symptoms in schizophrenic patients (Krystal et al. 1994). Paradoxically, NMDA-receptor antagonism produces increased activation in discrete brain areas in both humans and animals. This can be explained by the fact that NMDA receptors preferentially drive the activity of cortical inhibitory interneurons, causing cortical excitation by disinhibition of pyramidal neurons (Homayoun and Moghaddam 2007).

Acute administration of subanesthetic doses of ketamine has been used as an on-demand animal model of schizophrenia as both the behavior resembles the clinical pathology and the increased activation in distinct brain areas such as the prefrontal and cingulate cortices and hippocampus. Reversal of these ketamine-induced effects was evaluated using both the typical antipsychotic haloperidol and the atypical antipsychotic clozapine and confirmed the model's validity (Duncan et al. 1998). Besides the ketamine model, administration of the nonselective NMDA-receptor antagonist memantine has also been suggested as an appropriate on-demand model of schizophrenia (Dedeurwaerdere et al. 2010).

However, much controversy exists on which of both NMDA antagonists is best suited as an animal model for fast screening of potential antipsychotics. The criteria for a suitable animal model are a pronounced increase in [^{18}F]FDG signal in delineated brain structures with a broad dynamic range and the complete reversal following administration of known antipsychotics. Therefore, in the present study, we compare both memantine and ketamine (1) on their potential to induce increases in activation in discrete brain regions and (2) on the reversal effects in these models induced by a known antipsychotic, i.e., the mGlu2/3 agonist LY404039 (Patil et al. 2007).

2.3.4.2 Study Protocol

The study protocol is schematically illustrated in Fig. 2.17: 12 Sprague–Dawley rats (Charles River Laboratories, Lyon, France) weighing 275–350 g undergo six experimental conditions once, each time followed by a microPET scan, i.e., rats are subjected to injection (sc.) of LY404039 (10 mg/kg) or vehicle, 30 min prior to challenge with the NMDA-receptor antagonist. Saline, ketamine (30 mg/kg, i.p.), or memantine (20 mg/kg, i.p.) injection is performed 15 min prior to [^{18}F]FDG injection (1 mCi, i.v. under short anesthesia). [^{18}F]FDG injection is followed by a 25 min awake uptake period. Anesthesia with isoflurane is started 25 min following tracer injection; the animal is positioned onto the μ PET scan bed and scanned (PET) during 20 min, followed by a μ CT scan. Imaging was performed on the Siemens Inveon PET–CT scanner, and during the entire procedure, we followed the SUV standardization guidelines as denoted in Sect. 2.3.1. However, no glucose measurements were determined in this experiment.

For quantitative analysis, μ PET images are reconstructed using the 2D filtered back projection (FBP). Data are corrected for scatter and attenuation. Each individual PET image is transformed into the space of a PET template using brain normalization in PMOD v3.2 (PMOD Technologies, Switzerland). The normalized images are thus coregistered with the rat brain VOI template available in the same software package. Averaged activity concentrations ACR (kBq/cc) for the different VOIs were extracted and SUV (g/ml) for these VOIs were calculated as described in Sect. 2.3.1 – Table 2.1. The SUV values for eight clearly identifiable and relevant brain areas (caudate putamen, cingulate cortex, frontal cortex, medial prefrontal cortex, motor cortex, parietal cortex, anterodorsal hippocampus, and thalamus) were determined for the six experimental conditions, for all animals.

Data were expressed as mean values, \pm standard error of the mean. For statistical comparisons within data sets, to determine the difference between the six experimental conditions, we performed the nonparametric Friedman test with post hoc analysis using the Wilcoxon signed-rank test, taking into account a Bonferroni adjustment (SPSS20, Chicago, USA). Significance is reached at $p < 0.05$.

2.3.4.3 Evaluation by SUV

The Effect of Memantine/Ketamine

The results of this μ PET experiment as shown in Fig. 2.18 clearly indicates that both memantine and ketamine induce increases in rat brain [^{18}F]FDG uptake. Memantine pretreatment induces between 31.0 and 50.1 % of [^{18}F]FDG SUV increase in

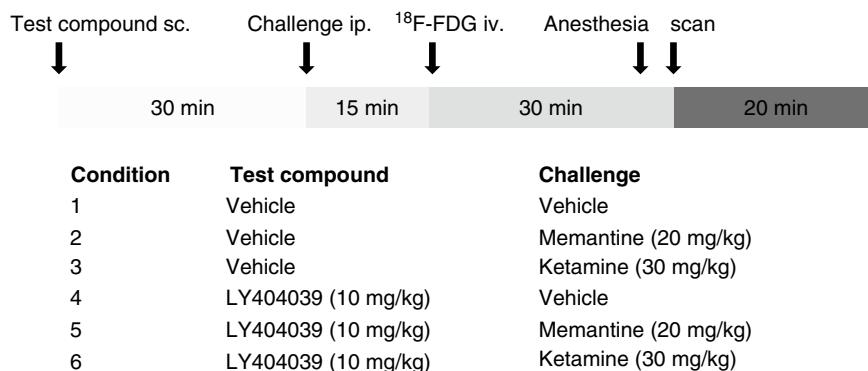


Fig. 2.17 Schematic illustration of the study design

relevant brain areas, while ketamine induces between 13.2 and 22.4 % of SUV increase with respect to saline pretreatment. This increase is located at delineated brain areas such as the anterodorsal part of the hippocampus; cortical areas such as the cingulate cortex, frontal cortex, medial prefrontal cortex, motor cortex, parietal cortex; and other areas such as the striatum (caudate putamen) and thalamus.

Our study also reveals that memantine is more potent at inducing statistically significant regional increases in SUV [^{18}F]FDG in the rat brain than ketamine. Memantine induces between 16.6 and 25.0% more [^{18}F]FDG uptake than ketamine. The increase by memantine over vehicle was significant in six out of eight relevant brain areas, while this was never significant for ketamine (Fig. 2.18). This finding strengthens the hypothesis that both memantine and ketamine animal models are suitable models of pharmacologically induced psychosis but that the memantine-pretreated model necessitates lower numbers of animals to reach statistically significant results in comparison with ketamine-pretreated animals. It has been previously shown that ketamine and memantine have equipotent binding affinities at the NMDA receptor (Gilling et al. 2009). However, the pronounced differences in pharmacokinetics between memantine and ketamine and their difference in specificity for the NMDA receptor (Gilling et al. 2009) might explain the difference in resulting increase in [^{18}F]FDG SUV. The overall degree of memantine-induced [^{18}F]FDG increases correlates with the literature on memantine activation or NMDA-receptor density distributions in rat brain (Dedeurwaerdere et al. 2010; Knol et al. 2009), and the overall degree of ketamine-induced [^{18}F]FDG increases correlates with the literature on ketamine activation using 2-DG autoradiography.

The Effect of LY404039 Challenge

Additionally, subsequent pharmacological reversal testing in both the memantine and ketamine model showed that the mGlu2/3 receptor agonist LY404039 significantly attenuated the memantine-induced [^{18}F]FDG uptake (all 8 relevant brain areas), while this was less pronounced for the ketamine-induced [^{18}F]FDG uptake (3 out of 8 relevant brain areas). LY404039 almost fully reversed (-0.3 to -10.9 %

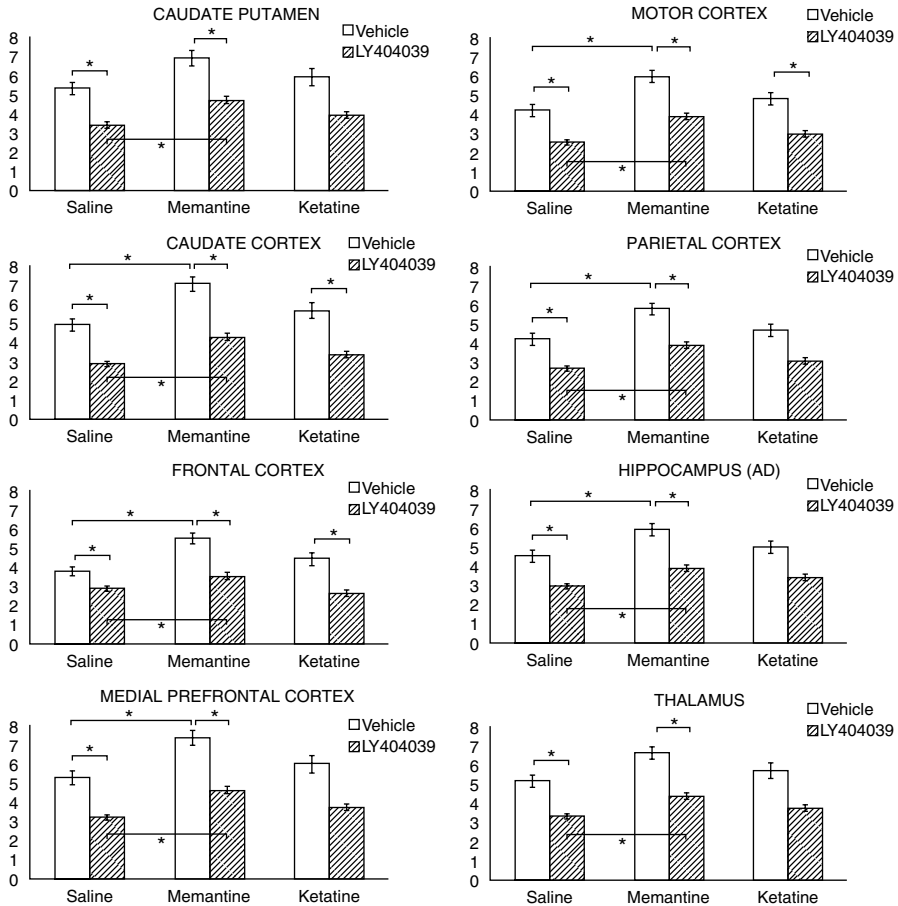


Fig. 2.18 SUV for $[^{18}\text{F}]\text{FDG}$ for eight relevant brain areas, for saline, for memantine, and for ketamine with vehicle (white) or LY404039 (shaded) pretreatment; $*p < 0.05$

compared to vehicle + saline) the memantine-induced $[^{18}\text{F}]\text{FDG}$ increase, while for the ketamine-induced increase, there was an overshoot in the reversal (-20.7 to -27.1% compared to vehicle + saline) as shown in Fig. 2.19. These findings again illustrate the superiority of the memantine model, which was already highlighted in a previous 2DG autoradiography study with mice (Dedeurwaerdere et al. 2010).

These findings implicate that memantine pretreatment serves as a more suitable on-demand animal model for schizophrenia compared to ketamine-pretreated animals. Further, we present a robust and translational method for antipsychotic compound screening, allowing longitudinal studies, intra-animal comparisons, and low(er) numbers of animals. The use of predefined and standardized VOI templates enables very fast and automated analysis of large regions of interest, which are a major advantage for the high-throughput screening of pharmacological compounds and radiotracers using in vivo functional imaging with μ PET.

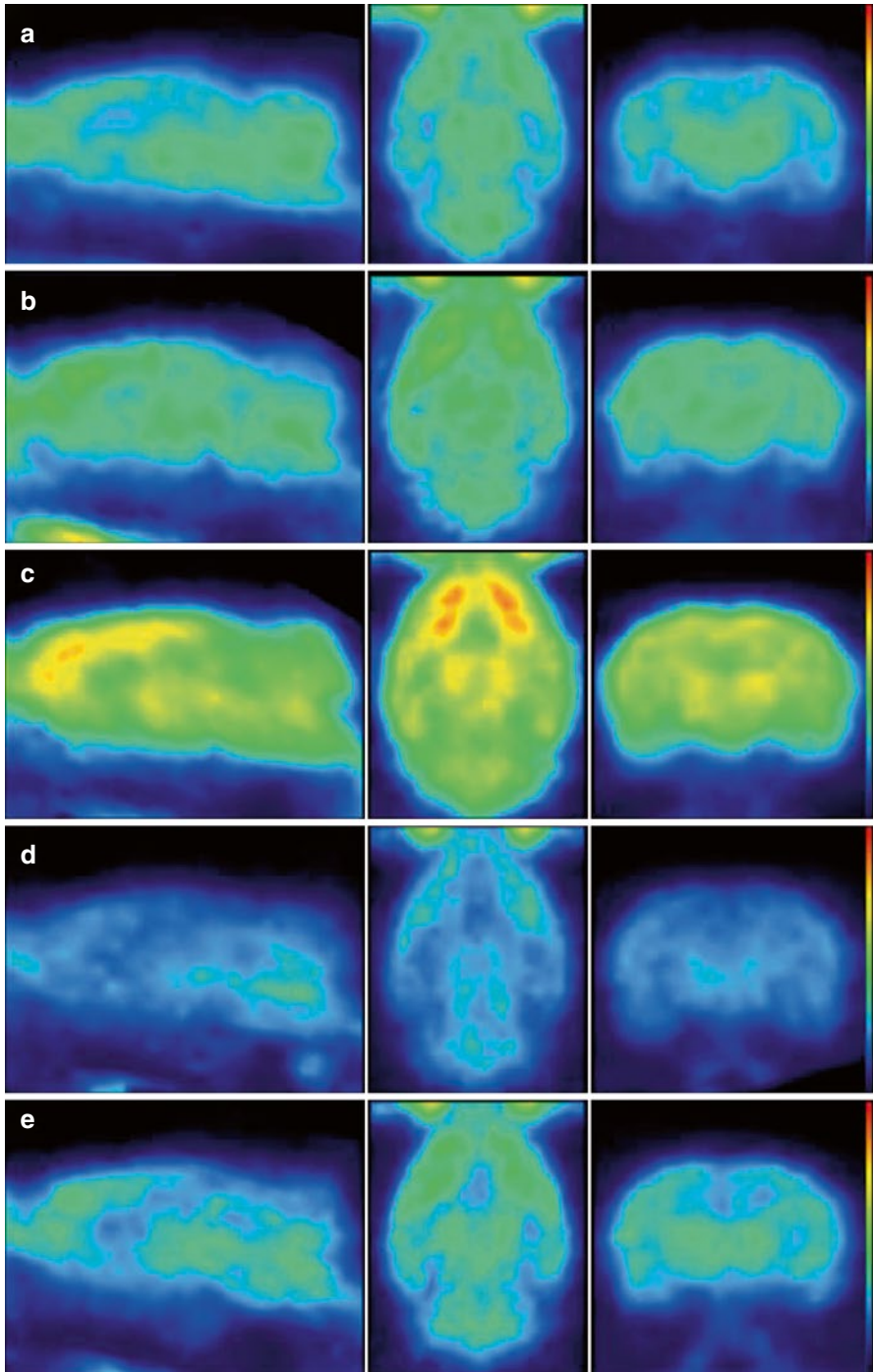


Fig. 2.19 Illustration of (a) vehicle+saline, (b) vehicle +ketamine (30 mg/kg), (c) vehicle+memantine (20 mg/kg), (d) LY404039 (2.5 mg/kg)+ketamine (30 mg/kg), and (e) LY404039 (2.5 mg/kg)+memantine (20 mg/kg) pretreated $[^{18}\text{F}]$ FDG scan from the rat brain

Conclusion

In this chapter, we describe a performance evaluation to compare the three most widespread state-of-the-art μ SPECT systems, and we have accordingly used the optimal system to study neuromodulation in rats as an application of high-resolution μ SPECT imaging to visualize the neurobiological effects of therapy in vivo in healthy animals. For drug testing, we describe how a preclinical μ PET acquisition protocol can be standardized and how the resulting reconstructed images can be accurately quantified. Next, we showed how to use such a standardized protocol for longitudinal evaluation in an animal disease model to test the potency of a receptor agonist as an example of how preclinical molecular imaging can be applied to assist in pharmaceutical development.

Acknowledgements We would like to thank our other colleagues from the Molecular Imaging Center Antwerp of Antwerp University, the Cyclotron Radiopharmacy and the Nuclear Medicine Department of the University Hospital Antwerp as well as our partners at Neuroscience Janssen Pharmaceutical companies of Johnson & Johnson and our former colleagues of UGent-Medisip-Infinity.

References

- Barker AT, Jalinous R, Freeston IL (1985) Non-invasive magnetic stimulation of human motor cortex. *The Lancet* 1(8437):1106–1107
- Beekman F, Have F (2006) The pinhole: gateway to ultra-high-resolution three-dimensional radio-nuclide imaging. *Eur J Nucl Med Mol Imaging* 34(2):151–161
- Benabid AL, Chabardes S, Mitrofanis J, Pollak P (2009) Deep brain stimulation of the subthalamic nucleus for the treatment of Parkinson's disease. *Lancet neurology* 8(1):67–81
- Cherry SR (2006) The 2006 Henry N. Wagner Lecture: of mice and men (and Positrons)—advances in PET imaging technology. *J Nucl Med* 47(11):1735–1745
- Cilia R, Marotta G, Landi A, Isaia IU, Mariani CB, Vergani F, Benti R, Sganzerla E, Pezzoli G, Antonini A (2008) Clinical and cerebral activity changes induced by subthalamic nucleus stimulation in advanced Parkinson's disease: a prospective case-control study. *Clin Neurol Neurosurg* 111(2):140–146
- Dandekar M, Tseng JR, Gambhir SS (2007) Reproducibility of 18F-FDG microPET studies in mouse tumor xenografts. *J Nucl Med* 48(4):602–607
- De Geeter N, Crevecoeur G, Dupre L (2011) An efficient 3-D eddy-current solver using an independent impedance method for transcranial magnetic stimulation. *IEEE Trans Biomed Eng* 58(2):310–320
- Dedeurwaerdere S, Wintmolders C, Straetmans R, Pemberton D, Langlois X (2010) Memantine-induced brain activation as a model for the rapid screening of potential novel anti-psychotic compounds: exemplified by activity of an mGlu2/3 receptor agonist. *Psychopharmacology (Berl)* 214(2):505–514
- Duncan GE, Leipzig JN, Mailman RB, Lieberman JA (1998) Differential effects of clozapine and haloperidol on ketamine-induced brain metabolic activation. *Brain Res* 812(1):65–75
- Fueger BJ, Czernin J, Hildebrandt I, Tran C, Halpern BS, Stout D, Phelps ME, Weber WA (2006) Impact of animal handling on the results of 18F-FDG PET studies in mice. *J Nucl Med* 47(6):999–1006
- Funke K, Benali A (2011) Modulation of cortical inhibition by rTMS—findings obtained from animal models. *J Physiol* 589(18):4423–4435
- Gilling KE, Jatzke C, Hechenberger M, Parsons CG (2009) Potency, voltage-dependency, agonist concentration-dependency, blocking kinetics and partial untrapping of the uncompetitive N-methyl-D-aspartate (NMDA) channel blocker memantine at human NMDA (GluN1/GluN2A) receptors. *Neuropharmacology* 56(5):866–875

- Goorden MC, Beekman FJ (2010) High-resolution tomography of positron emitters with clustered pinhole SPECT. *Phys Med Biol* 55(5):1265–1277
- Hadi M, Bacharach SL, Whatley M, Libutti SK, Straus SE, Rao VK, Wesley R, Carrasquillo JA (2008) Glucose and insulin variations in patients during the time course of a FDG-PET study and implications for the ‘glucose-corrected’ SUV. *Nucl Med Biol* 35(4):441–445
- Hayashi T, Ohnishi T, Okabe S, Teramoto N, Nonaka Y, Watabe H, Imabayashi E, Ohta Y, Jino H, Ejima N, Sawada T, Iida H, Matsuda H, Ugawa Y (2004) Long-term effect of motor cortical repetitive transcranial magnetic stimulation [correction]. *Ann Neurol* 56(1):77–85
- Hildebrandt IJ, Su H, Weber WA (2008) Anesthesia and other considerations for in vivo imaging of small animals. *ILAR J* 49(1):17–26
- Homayoun H, Moghaddam B (2007) NMDA receptor hypofunction produces opposite effects on prefrontal cortex interneurons and pyramidal neurons. *J Neurosci* 27(43):11496–11500
- Inubushi M, Jordan MC, Roos KP, Ross RS, Chatziioannou AF, Stout DB, Dahlbom M, Schelbert HR (2004) Nitrogen-13 ammonia cardiac positron emission tomography in mice: effects of clonidine-induced changes in cardiac work on myocardial perfusion. *Eur J Nucl Med Mol Imaging* 31(1):110–116
- Jan S, Boisgard R, Fontyn Y, Eroukhanoff C, Comtat C, Trebossen R (2004) Accuracy and variability of quantitative values obtained for mouse imaging using the microPET FOCUS. Presented at the nuclear science symposium conference record, 2004 IEEE, Rome, Italy, vol 5
- Katsakiori PF, Kefalopoulou Z, Markaki E, Paschali A, Ellul J, Kagadis GC, Chroni E, Constantoyannis C (2009) Deep brain stimulation for secondary dystonia: results in 8 patients. *Acta Neurochir* 151(5):473–478, discussion 478
- Kefalopoulou Z, Paschali A, Markaki E, Vassilakos P, Ellul J, Constantoyannis C (2009) A double-blind study on a patient with tardive dyskinesia treated with pallidal deep brain stimulation. *Acta neurologica Scandinavica* 119(4):269–273
- Kim Y-W, Scarpace PJ (2003) Repeated fasting/refeeding elevates plasma leptin without increasing fat mass in rats. *Physiol Behav* 78(3):459–464
- Kim H, Furenlid LR, Crawford MJ, Wilson DW, Barber HB, Peterson TE, Hunter WCJ, Liu Z, Woolfenden JM, Barrett HH (2006) SemiSPECT: a small-animal single-photon emission computed tomography (SPECT) imager based on eight cadmium zinc telluride (CZT) detector arrays. *Med Phys* 33(2):465
- Knol RJS, De Bruin K, Van Eck-Smit BLF, Pimlott S, Wyper DJ, Booij J (2009) In vivo [(123)I] CNS-1261 binding to D-serine-activated and MK801-blocked NMDA receptors: a storage phosphor imaging study in rats. *Synapse* 63(7):557–564
- Krystal JH, Karper LP, Seibyl JP, Freeman GK, Delaney R, Bremner JD, Heninger GR, Bowers MB, Charney DS (1994) Subanesthetic effects of the noncompetitive NMDA antagonist, ketamine, in humans. Psychotomimetic, perceptual, cognitive, and neuroendocrine responses. *Arch Gen Psychiatry* 51(3):199–214
- Kwan P, Brodie MJ (2000) Early identification of refractory epilepsy. *N Engl J Med* 342(5):314–319
- Lackas C, Schramm NU, Hoppin JW, Engeland U, Wirrwar A, Halling H (2005) T-SPECT: a novel imaging technique for small animal research. *IEEE Trans Nucl Sci* 52(1):181–187
- Lancelot S, Zimmer L (2010) Small-animal positron emission tomography as a tool for neuropharmacology. *Trends Pharmacol Sci* 31(9):411–417
- Lee K-H, Ko B-H, Paik J-Y, Jung K-H, Choe YS, Choi Y, Kim B-T (2005) Effects of anesthetic agents and fasting duration on 18F-FDG biodistribution and insulin levels in tumor-bearing mice. *J Nucl Med* 46(9):1531–1536
- Li Z, Conti PS (2010) Radiopharmaceutical chemistry for positron emission tomography. *Adv Drug Deliv Rev* 62(11):1031–1051
- Manook A, Yousefi BH, Willuweit A, Platzer S, Reder S, Voss A, Huisman M, Settles M, Neff F, Velden J, Schoor M, von der Kammer H, Wester H-J, Schwaiger M, Henriksen G, Drzezga A (2012) Small-animal PET imaging of amyloid-beta plaques with [11C]PiB and its multi-modal validation in an APP/PS1 mouse model of Alzheimer’s disease. *PLoS ONE* 7(3):e31310
- Marsteller DA, Barbarich-Marsteller NC, Fowler JS, Schiffer WK, Alexoff DL, Rubins DJ, Dewey SL (2006) Reproducibility of intraperitoneal 2-deoxy-2-[18F]-fluoro-d-glucose cerebral uptake in rodents through time. *Nucl Med Biol* 33(1):71–79

- Martik-Kehl MI, Ametamey SM, Alf MF, Schubiger PA, Honer M (2012) Impact of inherent variability and experimental parameters on the reliability of small animal PET data. *EJNMMI Research* 2(1):26
- Matsuda H, Tsuji S, Shuke N, Sumiya H, Tonami N, Hisada K (1993) Noninvasive measurements of regional cerebral blood flow using technetium-99m hexamethylpropylene amine oxime. *Eur J Nucl Med* 20(5):391–401
- McElroy DP, MacDonald LR, Beekman FJ, Wang YC, Patt BE, Iwanczyk JS, Tsui BMW, Hoffman EJ (2002) Performance evaluation of A-SPECT: A high resolution desktop pinhole SPECT system for imaging small animals. *IEEE Transactions on Nuclear Science* 49(5):2139–2147. doi:10.1109/TNS.2002.803801
- Meijer MK, Lemmens AG, Van Zutphen BFM, Baumans V (2005) Urinary corticosterone levels in mice in response to intraperitoneal injections with saline. *J Appl Anim Welf Sci* 8(4):279–283
- Mok GSP, Yu J, Du Y, Wang Y, Tsui BMW (2011) Evaluation of a multi-pinhole collimator for imaging small animals with different sizes. *Mol Imaging Biol* 14(1):60–69
- Nowland MH, Hugunin KMS, Rogers KL (2011) Effects of short-term fasting in male Sprague–Dawley rats. *Comp Med* 61(2):138–144
- Ose T, Watabe H, Hayashi T, Kudomi N, Hikake M, Fukuda H, Teramoto N, Watanabe Y, Onoe H, Iida H (2012) Quantification of regional cerebral blood flow in rats using an arteriovenous shunt and micro-PET. *Nucl Med Biol* 39(5):730–741
- Patel VD, Lee DE, Alexoff DL, Dewey SL, Schiffer WK (2008) Imaging dopamine release with Positron Emission Tomography (PET) and 11C-raclopride in freely moving animals. *Neuroimage* 41(3):1051–1066
- Patil ST, Zhang L, Martenyi F, Lowe SL, Jackson KA, Andreev BV, Avedisova AS, Bardenstein LM, Gurovich IY, Morozova MA, Mosolov SN, Neznanov NG, Reznik AM, Smulevich AB, Tochilov VA, Johnson BG, Monn JA, Schoepp DD (2007) Activation of mGlu2/3 receptors as a new approach to treat schizophrenia: a randomized Phase 2 clinical trial. *Nature medicine* 13(9):1102–1107
- Ridding M, Rothwell J (2007) Is there a future for therapeutic use of transcranial magnetic stimulation? *Nat Rev Neurosci* 8(7):559–567
- Roth B, Saypol J, Hallett M, Cohen L (1991) A theoretical calculation of the electric field induced in the cortex during magnetic stimulation. *Electroencephalogr Clin Neurophysiol* 81(1):47–56
- Saab BJ, Maclean AJB, Kanisek M, Zurek AA, Martin LJ, Roder JC, Orser BA (2010) Short-term memory impairment after isoflurane in mice is prevented by the $\alpha 5$ γ -aminobutyric acid type A receptor inverse agonist L-655,708. *Anesthesiology* 113(5):1061–1071
- Schiffer WK, Mirrione MM, Dewey SL (2007) Optimizing experimental protocols for quantitative behavioral imaging with 18F-FDG in rodents. *J Nucl Med* 48(2):277–287
- Schramm NU, Ebel G, Engeland U, Schurrat T, Behe M, Behr TM (2003) High-resolution SPECT using multipinhole collimation. *IEEE Trans Nucl Sci* 50(3):315–320
- Schramm NU, Lackas C, Hoppin JW, Forrer F, de Jong M (2006) The nanoSPECT/CT: a high-sensitivity small-animal SPECT/CT with submillimeter spatial resolution. *Eur J Nucl Med Mol Imaging* 33:S117
- Spencer SS (2002) Neural networks in human epilepsy: evidence of and implications for treatment. *Epilepsia* 43(3):219–227
- Tsai GG, Coyle JTJ (2001) Glutamatergic mechanisms in schizophrenia. *Pharmacology and Toxicology* 42:165–179
- van der Have F, Vastenhouw B, Ramakers RM, Branderhorst W, Kraaij G, Ji C, Staelens SG, Beekman FJ (2009) U-SPECT-II: an ultra-high-resolution device for molecular small-animal imaging. *J Nucl Med* 50(4):599–605
- Wahl RL, Henry CA, Ethier SP (1992) Serum glucose: effects on tumor and normal tissue accumulation of 2-[F-18]-fluoro-2-deoxy-D-glucose in rodents with mammary carcinoma. *Radiology* 183(3):643–647
- Wong KP, Sha W, Zhang X, Huang SC (2011) Effects of administration route, dietary condition, and blood glucose level on kinetics and uptake of 18F-FDG in mice. *J Nucl Med* 52(5):800–807

-
- Wyckhuys T, Boon P, Raedt R, Van Nieuwenhuyse B, Vonck K, Wadman W (2010) Suppression of hippocampal epileptic seizures in the kainate rat by Poisson distributed stimulation. *Epilepsia* 51(11):2297–2304
- Wyckhuys T, De Geeter N, Crevecoeur G, Stroobants S, Staelens S (2013) Quantifying the effect of repetitive transcranial magnetic stimulation in the rat brain by μ SPECT CBF scans. *Brain Stimul* 6:554–562

Wolf-Dieter Heiss

Contents

3.1	Energy Requirements of Brain Tissue.....	86
3.2	Brain Energy Metabolism	86
3.2.1	Glycolysis and Oxidative Phosphorylation	88
3.2.2	Determination of the Regional Cerebral Metabolic Rate for Glucose (rCMRGl).....	88
3.2.3	Normal Glucose Consumption of the Brain.....	91
3.2.4	Coupling of Neuronal Activity to Metabolism and Flow	95
3.2.5	Clinical Applications of FDG-PET.....	95
	References.....	99

Abstract

Glucose is the main substrate for energy metabolism of the brain, and the regional cerebral metabolic rate is directly related to regional brain activity. Therefore, the measurement of regional glucose metabolism is of great importance for the assessment of regional normal function and of pathological changes. Quantitation of glucose metabolism by PET is based on the 2-deoxyglucose method developed by Sokoloff and colleagues: F18-labelled deoxyglucose (FDG) is transported into the brain and phosphorylated, but cannot be further metabolised and therefore is accumulated intracellularly. The concentration of the tracer can be measured three dimensionally by PET, and together with the arterial tracer concentration, the kinetics of glucose uptake can be assessed and the regional cerebral metabolic rate of glucose (rCMRGl) can be calculated.

rCMRGl is high in cortex and grey matter structures and low in white matter, but there are significant differences among various regions. Metabolic rate is

Wolf-Dieter Heiss was supported by the WDH Foundation.

W.-D. Heiss

Department of General Neurology, Max Planck Institute for Neurological Research,
Gleueler Str. 50, Köln 50931, Germany

e-mail: wdh@nf.mpg.de

slightly reduced with ageing and changed by sleep, dream, and functional activation. CMRGluc is significantly affected in pathological states and the regional and global changes are important for assessing severity of disorders and for differential diagnosis of diseases of the brain. Therefore, FDG-PET has still great importance in brain research and many applications in clinical neurology.

3.1 Energy Requirements of Brain Tissue

The energy demand of the nervous tissue is very high and therefore sufficient blood supply to the brain must be maintained consistently. A normal adult male's brain containing approximately 130 billion neurons (21.5 billion in the neocortex) (Pakkenberg and Gundersen 1997) comprises only 2 % of total body mass, yet consumes at rest approximately 20 % of the body's total basal oxygen consumption supplied by 16 % of the cardiac blood output. The brain's oxygen consumption is almost entirely for the oxidative metabolism of glucose, which in normal physiological conditions is the almost exclusive substrate for the brain's energy metabolism (Clarke and Sokoloff 1999). It must be kept in mind that the glucose metabolised in neuronal cell bodies is mainly to support cellular vegetative and house-keeping functions, e.g. axonal transport, biosynthesis of nucleic acids, proteins, lipids as well as other energy-consuming processes not related directly to action potentials. Therefore the rate of glucose consumption of neuronal cell bodies is essentially unaffected by neuronal functional activation. Increases in glucose consumption (and regional blood flow) evoked by functional activation are confined to synapse-rich regions, i.e. neuropil which contains axonal terminals, dendritic processes and also the astrocytic processes that envelope the synapses. The magnitudes of these increases are linearly related to the frequency of action potentials in the afferent pathways, and increases in the projection zones occur regardless of whether the pathway is excitatory or inhibitory. Only at the next downstream projection zones glucose utilisation (and, as a consequence, blood supply) is depressed in inhibited neurons and increased in excited neurons. Energy metabolism by functional activation is due mostly to stimulation of the Na^+K^+ -ATPase activity to restore the ionic gradients across the cell membrane and the membrane potentials that were degraded by the spike activity and is rather high compared to the demand of neuronal cell bodies (Sokoloff 1999). Overall, 87 % of the total energy consumed is required by signalling, mainly action potential propagation and postsynaptic ion fluxes, and only 13 % is expended in maintaining membrane resting potential (Laughlin and Attwell 2001).

3.2 Brain Energy Metabolism

Glucose is the obligatory energy substrate for brain and it is almost entirely oxidised to CO_2 and H_2O . Although the brain represents only 2 % of the body weight, it receives 15 % of the cardiac output, 20 % of total body oxygen consumption and 25 % of total body glucose utilisation. With a global blood flow of 57 ml/100 g·min, the brain extracts approximately 50 % of oxygen and 10 % of glucose from the

arterial blood. Hence, the glucose utilisation of the brain, as assessed by measuring the arterial–venous difference (Kety and Schmidt 1948), is 31 mmol/100 g·min. Oxygen consumption is 160 mmol/100 g·min; because CO₂ production is almost identical, the respiratory quotient (RQ) of the brain is nearly 1, indicating that carbohydrates are the substrates for oxidative metabolism (Sokoloff 1989). Given a theoretical stoichiometry of 6 mmol of oxygen consumed for each mmole of glucose, glucose utilisation by the brain should in theory be 26.6 mmol/100 g·min. As indicated earlier, the measured glucose utilisation is 31 mmol/100 g·min, indicating that an excess of 4.4 mmol/100 g·min of glucose follows other metabolic fates. Glucose can produce metabolic intermediates, such as lactate and pyruvate, which do not enter necessarily in the tricarboxylic acid cycle, but rather can be released and removed by the circulation. Glucose can be incorporated into lipids, proteins and glycogen, and it is also the precursor of certain neurotransmitters such as gamma-aminobutyric acid (GABA), glutamate and acetylcholine (Sokoloff 1989).

Of molecules that could substitute for glucose as an alternative substrate for brain energy metabolism, mannose is the only one that can sustain normal brain function in the absence of glucose. Lactate and pyruvate can sustain synaptic activity *in vitro*. Because of their limited permeability across the blood–brain barrier, they cannot substitute for plasma glucose to maintain brain function (Pardridge and Oldendorf 1977). However, if formed inside the brain parenchyma, they are useful metabolic substrates for neural cells (review in Magistretti et al. (1995)).

Whole-organ studies, which allowed the determination of the substrate requirements for the brain, failed to provide the appropriate level of resolution to appreciate two major features of brain energy metabolism: (a) its regional heterogeneity and (b) its tight relationship with the functional activation of specific pathways. The autoradiographic 2-deoxyglucose method (2-DG) developed by Sokoloff and colleagues afforded a sensitive means to measure local rates of glucose utilisation (LCMRglu) with a spatial resolution of approximately 50–100 μ (Sokoloff et al. 1977). The method is based on the fact that tracer amounts of radioactive 2-DG are taken up by glucose transporters and phosphorylated by hexokinase with kinetics that are similar to those for glucose; however, unlike glucose-6-phosphate, 2-deoxyglucose-6-phosphate cannot be metabolised further and therefore accumulates intracellularly, thus providing, after appropriate corrections (Sokoloff et al. 1977), an accurate measurement of the amount of glucose utilised. Using this method, LCRMglu have been determined in virtually all morphologically and functionally defined brain structures in various physiological and pathological states including sleep, seizures and dehydration and following a variety of pharmacological treatments. Furthermore, the increase in glucose utilisation following activation of pathways subserving specific modalities, such as visual, auditory, olfactory or somatosensory stimulations, as well as during motor activity, has been revealed in the pertinent brain structures.

Basal glucose utilisation of the grey matter as determined by the 2-DG technique varies, depending on the brain structure, between 50 and 150 μ mol/100 g wet weight·min in the rat (Sokoloff et al. 1977). Physiological activation of specific pathways results in a 1.5–3-fold increase in LCRMglu as determined by the 2-DG technique.

With the advent of PET and the use of positron-emitting isotopes such as ¹⁸F, local glucose utilisation has been studied in humans with 2-(¹⁸F)fluoro-2-deoxyglucose

(Reivich et al. 1979). Changes in local brain energy metabolism can now be studied in humans with PET by monitoring alterations in glucose utilisation, oxygen consumption and blood flow during activation of specific areas. Recent studies in which these three parameters have been analysed during activation of a given modality have yielded an uncoupling between glucose uptake and oxygen consumption during activation, since the increase in blood flow and in glucose utilisation in the activated cortical area was not matched by an equivalent increase in oxygen consumption (Fox et al. 1988). This observation raises the puzzling possibility that, at least during the early stages of activation, the increased energy demand is met by glycolysis rather than by oxidative phosphorylation (Vaishnavi et al. 2010).

3.2.1 Glycolysis and Oxidative Phosphorylation

Glycolysis (Embden–Meyerhof pathway) is the metabolism of glucose to pyruvate and lactate. It results in the net production of only 2 mol of adenosine triphosphate (ATP)/mol of glucose as well as in the regeneration of reducing equivalents (the oxidised form of nicotinamide adenine dinucleotide, NAD⁺) through the conversion of pyruvate into lactate. Alternatively, pyruvate can enter the tricarboxylic acid (TCA) cycle (or the Krebs cycle) and produce 30 mol of ATP/mol of glucose via the mitochondrial oxidative phosphorylation cascade. The energetic value of oxidative phosphorylation over glycolysis is thus obvious. The respiratory quotient of the brain is virtually 1; PET studies indicate an uncoupling between glucose uptake and oxygen consumption during activation (Fox et al. 1988) and rises in lactate have been monitored. During activation, lactate may normally be taken up by neurons as an energy fuel. It should be remembered that, after conversion to pyruvate, lactate can enter the TCA cycle with the potential to generate a total of 36 mol of ATP/mol of glucose. Activation-induced glycolysis may provide ATP to fuel energy-dependent ion transport, in particular the Na⁺/K⁺-ATPase, which represents the main energy-consuming process in neural cells (Siesjö 1978).

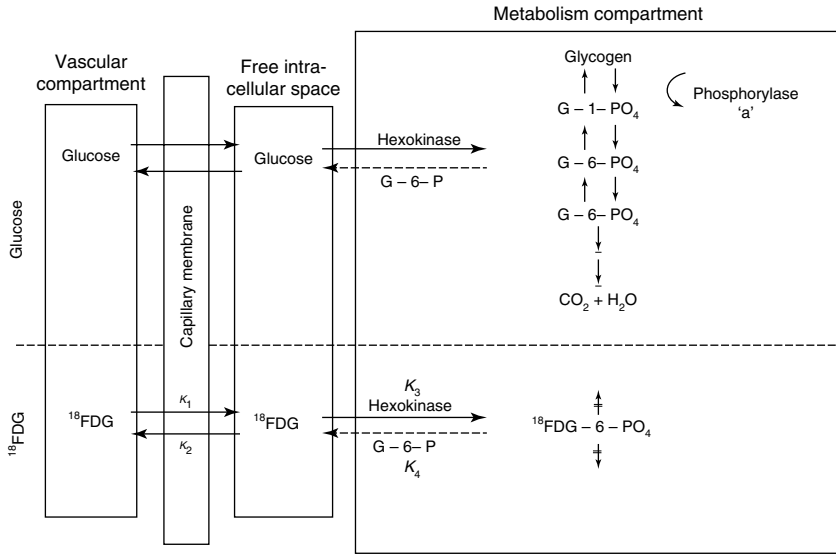
3.2.2 Determination of the Regional Cerebral Metabolic Rate for Glucose (rCMRGI)

The study of glucose metabolism with ¹⁸FDG is a direct application of the autoradiographic technique of Sokoloff et al. (1977) with [¹⁴C]deoxyglucose. The model developed by Sokoloff et al. can be applied directly because the fluorodeoxyglucose labelled at point 2 behaves in the same way as deoxyglucose. It is transported into the cell in the same way as glucose and, with the aid of hexokinase, is phosphorylated to [¹⁸F]deoxyglucose-6-phosphate. Deoxyglucose-6-phosphate, however, cannot be further converted to fructose-6-phosphate and degraded to CO₂ and H₂O, but accumulates in the cell. The kinetics of the back reaction (phosphatase) to deoxyglucose is much slower, and the deoxyglucose-6-phosphate can penetrate through the cell membrane only in small amounts. The kinetics of the accumulation of deoxyglucose-6-phosphate can be described with the transport and enzyme

constants of a three-compartment model. The corresponding complex formula (Reivich et al. 1979) for calculating the regional cerebral metabolic rate of glucose (rCMRGl) can be simplified to the following form (Phelps et al. 1979):

$$rCMRGl = \frac{(Gl)}{LC} \cdot \frac{C(^{18}F) - C(FDG)}{A_b}$$

where $C(^{18}F)$ is the total fluorine activity measured in the tissue, which is determined directly in the PET; $C(FDG)$ is the concentration of free FDG in the tissue, calculated



Labeled metabolic product
formed in interval of time 0 to T

Total activity in tissue Non-phosphorylated substrate in tissue

Plasma conc. glucose

$$rCMRGl = \frac{C_p \left[C_i(T) - K_i e^{-(k_2 + k_3)T} \int_0^T C_p(t) e^{(k_2 + k_3)t} dt \right]}{LC \left[\int_0^T C_p(t) dt - e^{-(k_2 + k_3)T} \int_0^T C_p(t) e^{(k_2 + k_3)t} dt \right]}$$

Correction factor for isotope

Integral of the spec. plasma activity Correction for delay in equilibration of the tissue with plasma

Integral of the spec. activity of the substrate

Operational equation for calculation of rCMRGl

from the plasma concentration up to time point T with the aid of the constants of the model. The difference between these two values gives the local tissue concentration of FDG-6-phosphate; A_b is the total quantity of FDG released into the tissue and is calculated from the plasma FDG concentration curve up to time point T , decreased by the delay in the tissue equilibration using the corresponding model constants. The quotient therefore gives the proportional phosphorylation rate of FDG. Multiplication by the plasma concentration of glucose (Gl) would yield the rate of glucose phosphorylation if it behaved in the same way as FDG. Since the arterial–venous extraction of glucose is not identical with that of FDG, the value must be corrected with an experimentally determined constant (LC = lumped constant). For the measurement of the regional glucose consumption in the brain, therefore, after i.v. administration of 3–6 mCi ^{18}F FDG, the plasma curve of ^{18}F FDG from the injection to the measurement time point (usually determined in arterialised venous blood), the glucose value in plasma and the regional ^{18}F activity in the brain must be determined.

Errors resulting with this model from widely diverging kinetic constants in pathological tissue (Hawkins et al. 1981) can be reduced by dynamic PET. For this purpose the tissue activity is determined at short time intervals from the time point of injection. By variation of the values for the kinetic constants, the curve deriving from the model equation is adapted to the measured regional activity–time curve. The kinetic constants thus determined correspond best to the activity uptake in the corresponding tissue segment. They allow the regional metabolic rate for glucose to be directly calculated (Wienhard et al. 1985). It is now only necessary to assume a known value for the LC.

There remains some uncertainty as to the exact value of the normal “lumped constant” (LC) for FDG. The initial value empirically derived by Phelps et al. (1979) was 0.42. It has been directly measured by Reivich et al. (1985), who found a value of 0.52, assuming $k_4=0$. But LC could be even as high as 0.65 (Wu et al. 2003). However, regional changes in LC are small. For the sake of uniformity, the actual value used should be quoted in all publications. This will allow direct comparison of numerical values because the LC is a linear scaling factor in the operational equations.

With rate constants measured by dynamic curve fitting or by integration techniques, the equation for calculation of CMR_{glc} is:

$$\text{CMR}_{\text{glc}} = C_a / \text{LC} \times (k_1 k_3 / (k_2 + k_3))$$

The term $k_1 k_3 / (k_2 + k_3)$, representing the metabolic rate of FDG, can be substituted by the influx rate constant k_i determined with the linear approximation of Patlak et al. (1983). There have also been modifications that avoid the assumption of a fixed LC and refer instead to the Michaelis–Menten equation to account for the relations between enzyme affinities for FDG and glucose (Kuwabara et al. 1990).

Determination of individual rate constants is not very practical in many clinical applications, and methods are preferred that can be done with a single scan, a situation similar to the original development of the method for autoradiography. Then the deviation from population average CMR_{glc} (given by the average rate constants) is estimated from a single scan. Actual measured FDG activity is compared with the

activity that would have been expected at the time of the scan with the individual's blood activity-time course and average rate constants (Wienhard et al. 1985).

To avoid the conversion factor needed with the analogue tracer FDG, native glucose labelled with ^{11}C in the 1-position (1- ^{11}C -D-glucose) has also been used for quantitation of CMRglc (Raichle et al. 1975). Modelling is based on the same two-tissue-compartment model as with FDG, but an additional term is necessary to account for labelled metabolites (mainly lactate and other monocarboxylic acids and CO_2). Metabolites occur in plasma and in brain, and loss of labelled CO_2 from the brain is dependent on CBF. Data indicate that there is a rapid loss of labelled lactate from the brain, suggesting that it represents a significant nonoxidative part of glucose metabolism in brain (approx. 10 % of total CMRglc) (Blomqvist et al. 1990).

3.2.3 Normal Glucose Consumption of the Brain

In healthy volunteers, a mean glucose consumption of 29–32 $\mu\text{mol}/100\text{ g}/\text{min}$ was found by means of FDG and PET (Reivich et al. 1979; Heiss et al. 1984), which corresponds well to whole brain metabolic rates provided by the Kety–Schmidt method. Under controlled conditions (darkened laboratory and steady noise from fans of equipment cooling systems), the functional anatomy of the brain is reflected in the metabolic activity of the individual regions. However, reliable regional values for cerebral metabolic rate of glucose (rCMRGlC) can only be obtained by equipment permitting high 3D resolution of tracer concentration in the brain tissue (Heiss et al. 2004). This progressively improved spatial resolution of PET is documented in Fig. 3.1 showing FDG images of the brain in the same volunteer assessed with different tomographs over the years (Heiss 2009a, b). Typical resting state grey matter CMRGl values are in the range of 40–60 $\mu\text{mol}/100\text{ g}/\text{min}$, and the corresponding level in the white matter is about 15 $\mu\text{mol}/100\text{ g}/\text{min}$. There are significant differences among regions with highest values in basal ganglia, primary visual cortex, cingulate and frontal cortex (42–50 $\mu\text{mol}/100\text{ g}/\text{min}$), lower values in other cortical and subcortical areas (35–42 $\mu\text{mol}/100\text{ g}/\text{min}$) and in the structures of the brainstem (25–30 $\mu\text{mol}/100\text{ g}/\text{min}$) and the cerebellum (33 $\mu\text{mol}/100\text{ g}/\text{min}$). There exist also significant asymmetries with largely right hemispheric predominance ((Pawlik and Heiss 1989), review in Silverman and Melega (2003)). The resting regional metabolism and its asymmetry are highly dependent on the state of resting wakefulness (e.g. apprehensive or relaxed) and background conditions (e.g. laboratory noise).

Local CMRGlC measured with PET is influenced by age: glucose metabolism of various grey matter structures was low at birth (13–25 $\mu\text{mol}/100\text{ g}/\text{min}$), reached a level of 19–33 $\mu\text{mol}/100\text{ g}/\text{min}$ by 2 years and continued to rise until age 3–4 years and was maintained at a high level (49–55 $\mu\text{mol}/100\text{ g}/\text{min}$) until age of 10 years (Chugani et al. 1987). At about 10 years CMRGlC began to decline with a rather uniform decrease by 26 % in all investigated brain regions of 40 healthy resting subjects between the ages of 18 and 78 years (Kuhl et al. 1982). However, these age-dependent changes were not observed in all studies (Duara et al. 1984). In our own study on 42 normal subjects aged 15–85 years, a small (0.65 $\mu\text{mol}/100\text{ g}/\text{min}$ per decade/ $p < 0.05$)

age-dependent decrease in global CMRGlc was found (Fig. 3.2). However, as demonstrated in Fig. 3.2, the various regions contributed differently to this overall effect: decreases of 16.6–11.3 % in cingulate, frontal, parietal, insular, temporal and sensorimotor cortex, virtually no change in primary visual cortex and cerebellum (Pawlik and Heiss 1989). Similar age-dependent changes of rCMRGI were described in further studies (Kalpouzos et al. 2009; Hsieh et al. 2012; Chetelat et al. 2013).

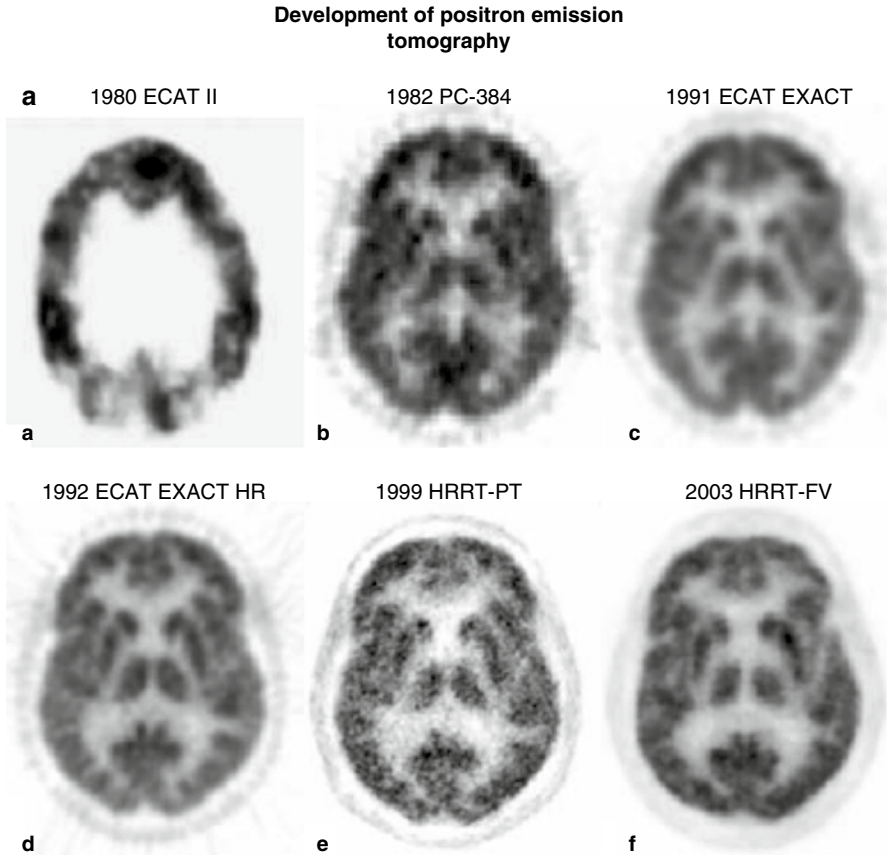


Fig. 3.1 (a) Development of PET: a horizontal slice. Various PET systems over the years demonstrate improvement in image quality and spatial resolution. *a* ECAT II, spatial resolution 15 mm. *b* PC-384, FWHM 8.4 mm. *c* ECAT EXACT, FWHM 6.5–7 mm. *d* ECAT EXACT HR, FWHM 3.6–4.5 mm. *e, f* HRRT PET: *e* prototype; *f* final version (HRRT-FV), FWHM 2.3–3.2 mm. Images of glucose metabolism were acquired for 20 min of steady state starting 30 min after tracer administration. (b) Coronal views of glucose consumption of the brain in a volunteer acquired with various PET systems over the years demonstrate improvement in axial resolution due to decreased slice thickness and advances in image reconstruction. *a* ECAT II (1980) was a single-ring camera; axial reconstruction was therefore not feasible. *b* PC-384, slice thickness 12 mm. *c* ECAT EXACT, axial FWHM 5–8 mm. *d* ECAT EXACT HR, axial FWHM 4.0–6.7 mm. *e, f* HRRT PET: *e* prototype; *f* final version (HRRT-FV), axial FWHM 2.5–3.4 mm

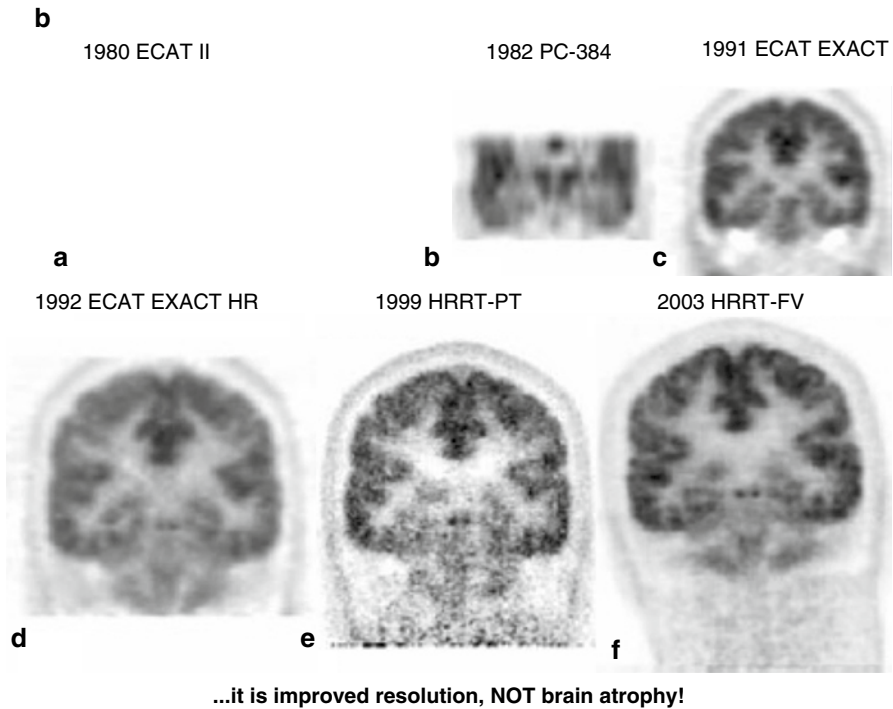


Fig. 3.1 (continued)

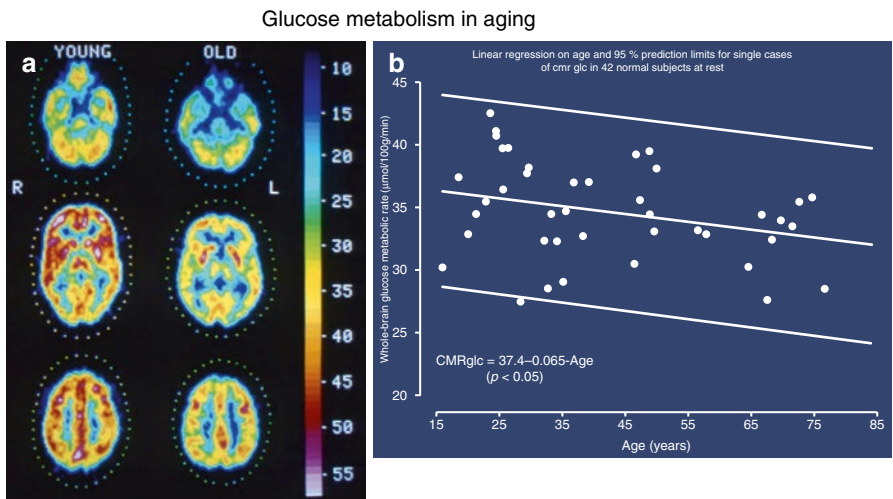


Fig. 3.2 (a) PET scans of glucose metabolism ($\mu\text{mol}/100\text{g}/\text{min}$ according to scale) in cerebral sections at the level of cerebellum, basal ganglia, thalamus and semioval centre in young (23 years) and old (67 years) healthy subjects. The individual brain structures can be differentiated according to different metabolic rates; metabolism decreases slightly in all regions in older patients. (b) Decrease of mean global glucose metabolic rate in 42 healthy subjects with increasing age. The regression line shows a significant relationship despite the large range of variation

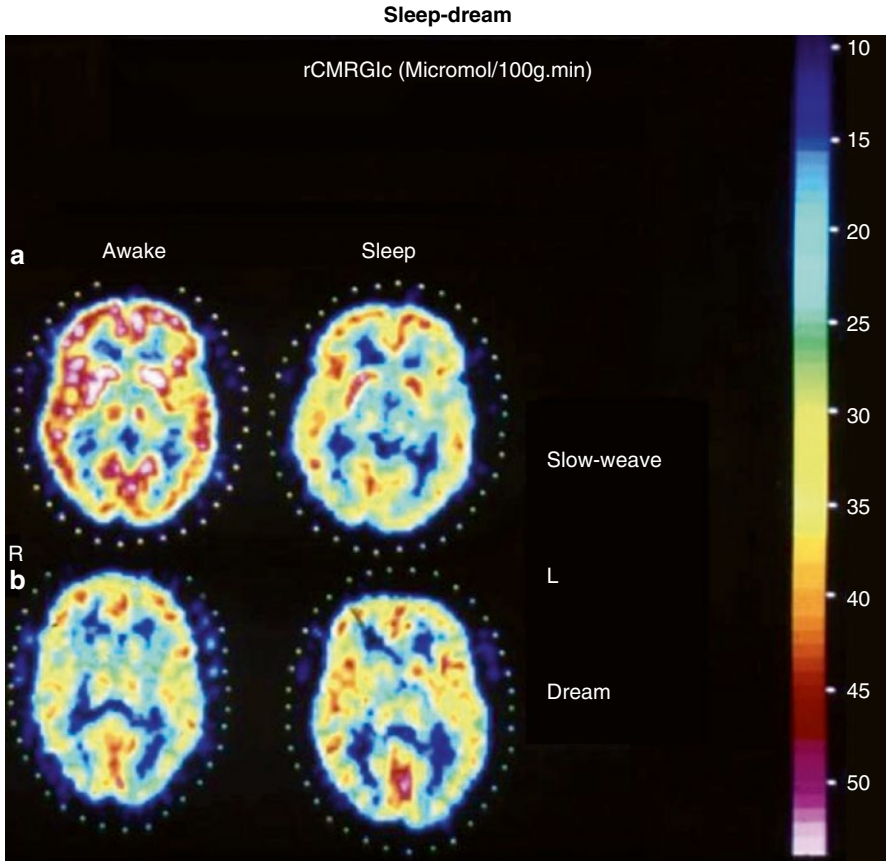


Fig. 3.3 (a) Corresponding images of the local cerebral metabolic rate for glucose determined by FDG-PET in a characteristic horizontal brain slice across the basal ganglia of a healthy 37-year-old male subject representative of the non-dreamers group, showing non-selective decrease in glucose utilisation from wakefulness (W) to sleep (S). Frontal poles are on top, occipital poles at bottom, sides as marked (R, L). Values on reference scale are in $\mu\text{mol}/100\text{ g}\cdot\text{min}$. (b) Corresponding metabolic maps of a 28-year-old normal volunteer's brain slice recorded by FDG-PET while the subject was awake (W) and asleep dreaming (S). A generalised activation, most marked in the insular regions, visual cortex and hippocampal formations, is clearly demonstrated during sleep with dreaming

Hardly any normal functional state is as regularly associated with as dramatic changes of general behaviour and shifting of attention as is sleep. The conclusion of no effect of sleep on human cerebral hemodynamics and metabolism, derived from early Kety–Schmidt studies (Mangold et al. 1955), could be disproved with PET (Heiss et al. 1985). As shown in Fig. 3.3, during stages II–IV sleep, a significant ($P < 0.001$) global decrease of brain functional activity was observed, with the largest declines in orbitofrontal cortex and in thalamus. In dream sleep, by contrast, both a general metabolic increase and conspicuous regional activations of superior frontal, insular, inferior parietal, hippocampal and visual association cortex (Heiss

et al. 1985) were found. Increased CMRGlc during REM sleep has also been observed in limbic and paralimbic regions including hypothalamus, amygdala, orbitofrontal cingulate, entorhinal and insular cortices (Nofzinger et al. 1997).

3.2.4 Coupling of Neuronal Activity to Metabolism and Flow

The activation of Na^+, K^+ -ATPase represents the coupling mechanism between the increase in glucose utilisation and functional activity of the nervous tissue. The activation-induced increase in glucose uptake is visualised in the neuropil, that is, where synapses ensheathed by astrocytes are present, and not at the level of the neuronal perikarya. Glucose, taken up by astrocytic processes, is metabolised glycolytically to lactate and pyruvate, which are then released as substrates for oxidative phosphorylation in neurons (Wyss et al. 2011). Mapping of neuronal activity in the brain can be primarily achieved by quantitation of the regional cerebral metabolic rate for glucose (rCMRGlc), as introduced for autoradiographic experimental studies by Sokoloff (1999) and adapted for positron emission tomography (PET) in humans (Reivich et al. 1979). Functional mapping, as it is widely used now, relies primarily on the hemodynamic response assuming a close association between energy metabolism and blood flow. While it is well documented that increases in blood flow and glucose consumption are closely coupled during neuronal activation, the increase in oxygen consumption is considerably delayed leading to a decreased oxygen extraction fraction (OEF) during activation (Mintun et al. 2001). PET detects and, if required, can quantify changes in CBF and CMRGlc accompanying different activation states of the brain tissue. The regional values of CBF or CMRGlc represent the brain activity due to a specific state, task or stimulus, in comparison to the resting condition, and colour-coded maps can be analysed or coregistered to morphologic images. Due to the radioactivity of the necessary tracers, activation studies with PET are limited to a maximum of 12 doses of ^{15}O -labelled tracers, e.g. 12 flow scans, or two doses of ^{18}F -labelled tracers, e.g. two metabolic scans. Especially for studies of glucose consumption, the time to metabolic equilibrium (20–40 min) as well as the time interval between measurements required for isotope decay (HT for ^{18}F 108 min, for ^{15}O 2 min) must be taken into consideration. FDG-PET was the leading method to investigate functional activation in humans in the 1980s (Phelps et al. 1981; Pawlik and Heiss 1989). FDG activation studies can also be applied in patients with functional disorders due to localised brain damage, e.g. by stroke and tumour, and has found broad application to patients with aphasia (Heiss 2009a, b). An example is given in Fig. 3.4 showing different activation patterns in poststroke aphasia which are related to prognosis and recovery of language function.

3.2.5 Clinical Applications of FDG-PET

Since its introduction FDG-PET has been applied for studying the pathophysiology and for differential diagnosis of several neurological and psychiatric disorders

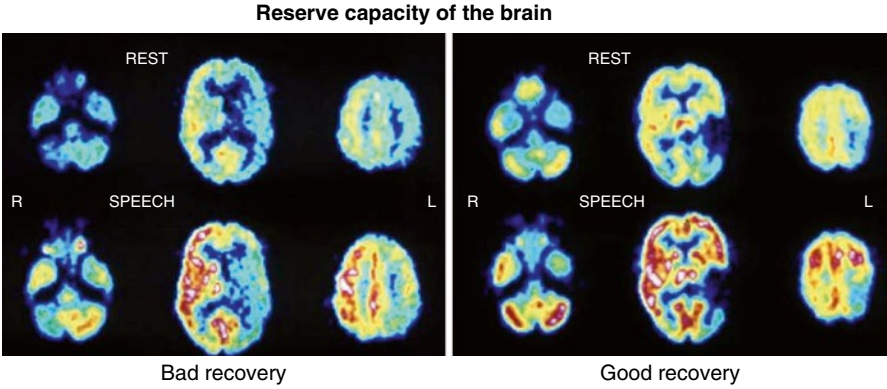


Fig. 3.4 Resting and speech-activated regional glucose metabolism in two patients with aphasia after ischemic stroke: if only contralateral regions are activated by speech, the prognosis is poor. If activation takes also place in homolateral peri-infarct regions, prognosis is better and speech performance shows satisfactory recovery

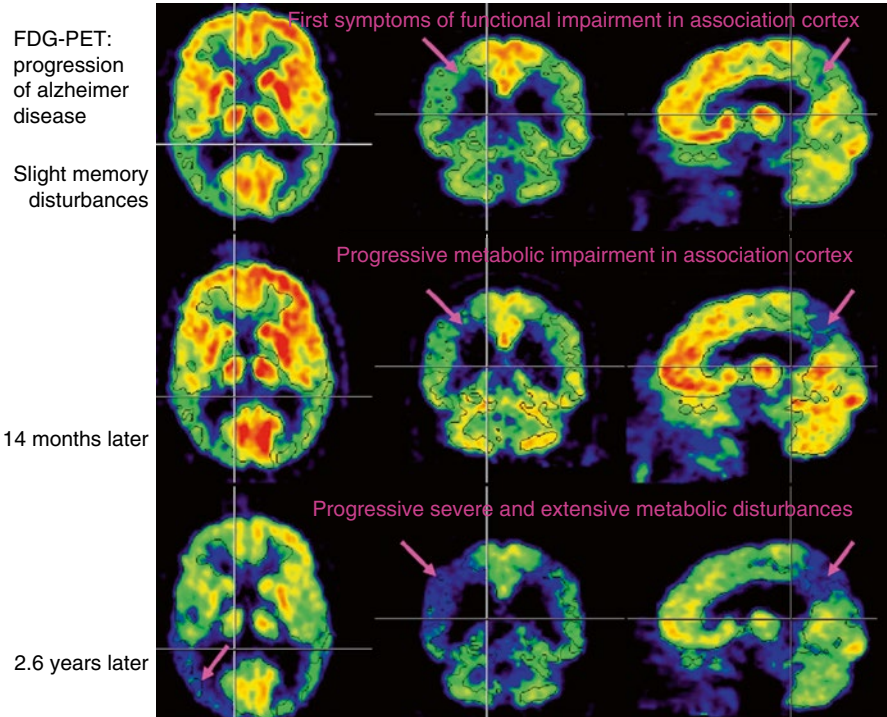


Fig. 3.5 Decline of cerebral metabolic rate (glucose) (CMRGlc) in association areas with progression of AD from the clinical stage of mild cognitive impairment (MCI) to mild dementia (three follow-up FDG-PET scans, each showing same orthogonal slices at position marked by crosshairs)

Differential diagnosis of dementias by FDG-PET

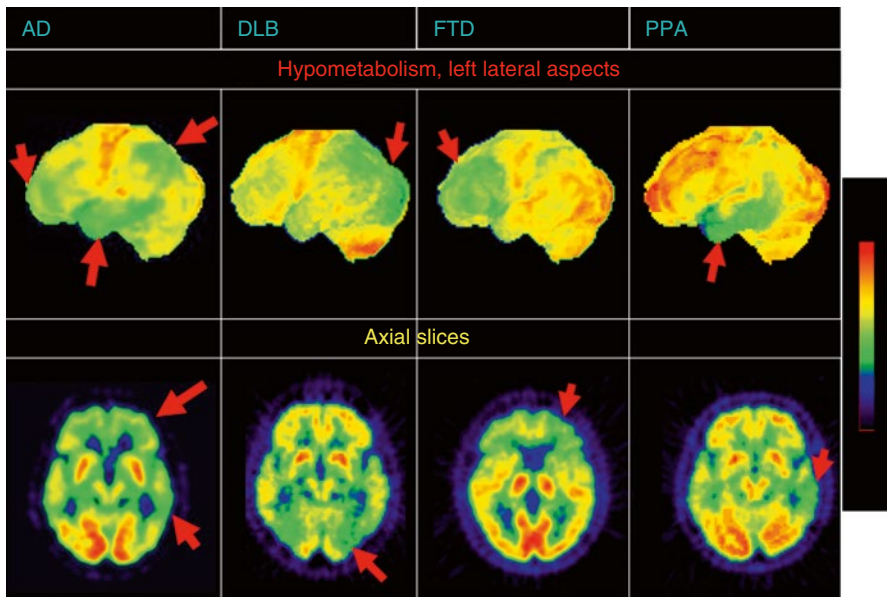


Fig. 3.6 FDG-PET in the differential diagnosis of various degenerative dementias. *Upper row*: typical transaxial slices. *Lower row*: reconstructed surface view. *AD* Alzheimer dementia is characterised by the decreases in temporoparietal and temporal association and in cingulate cortex, *FTD* in frontotemporal dementia the metabolic decrease is most severe in the anterior frontal and temporal regions, *DLB* in dementia with Lewy body (Parkinson's disease) the metabolic disturbance also affects the visual cortex, *PPA* in primary progressive aphasia the disturbance is most accentuated in the temporal (Wernicke) area. *Arrows* indicate most prominent changes

(Herholz et al. 2004; Jones et al. 2012). These applications will be described in the special clinical chapters of this book series. A few examples where FDG-PET has gained special importance are shown here.

In dementias, FDG-PET has attained a special role to detect progression of regional functional disturbance related to severity of cognitive and memory impairment (Fig. 3.5), for differential diagnosis to other degenerative disorders (Fig. 3.6) and to vascular dementia (Fig. 3.7) (Drzezga 2009; Bohnen et al. 2012; Heiss and Zimmermann-Meinzingen 2012; Choo et al. 2013). In brain tumours, FDG-PET has been successful in differentiating between necrosis and recurrent tumour (Fig. 3.8) and has value for grading of gliomas and for assessing effect of chemotherapy (Heiss et al. 2011; Chierichetti and Pizzolato 2012; Herholz et al. 2012). The impact of PET might be increased in the future by the advent of integrated MRI-PET facilities (Catana et al. 2012; Portnow et al. 2013).

**Metabolic pattern in dementia:
VaD vs AD**

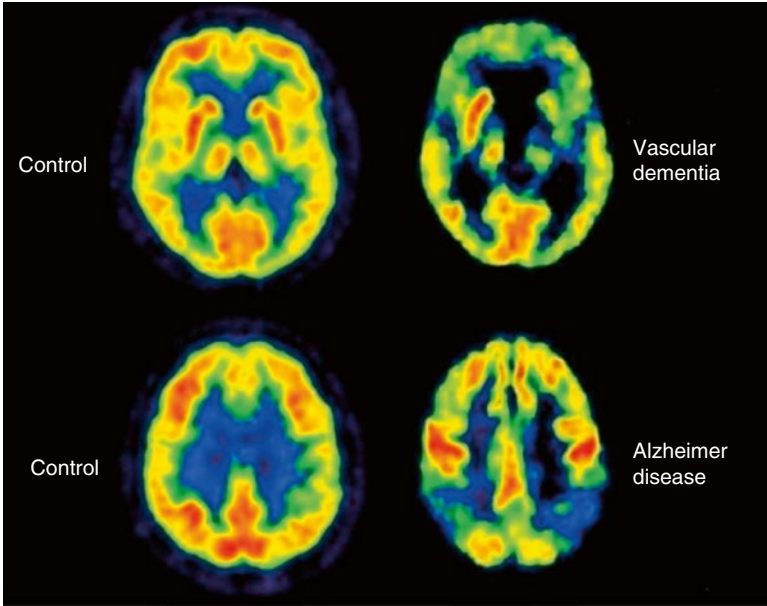


Fig. 3.7 Glucose metabolism in a normal control, in a patient with vascular dementia and a patient with Alzheimer's disease. The severity of dementia was comparable; the pattern of pathological changes differentiated these two cases: patchy metabolic defects in VaD in the frontal lobe, basal ganglia and thalamus; hypometabolism in AD bilateral in parieto-temporal cortex and to a lesser degree in the frontal association areas, whereas primary cortical regions are spared

Necrosis or recurrent tumor

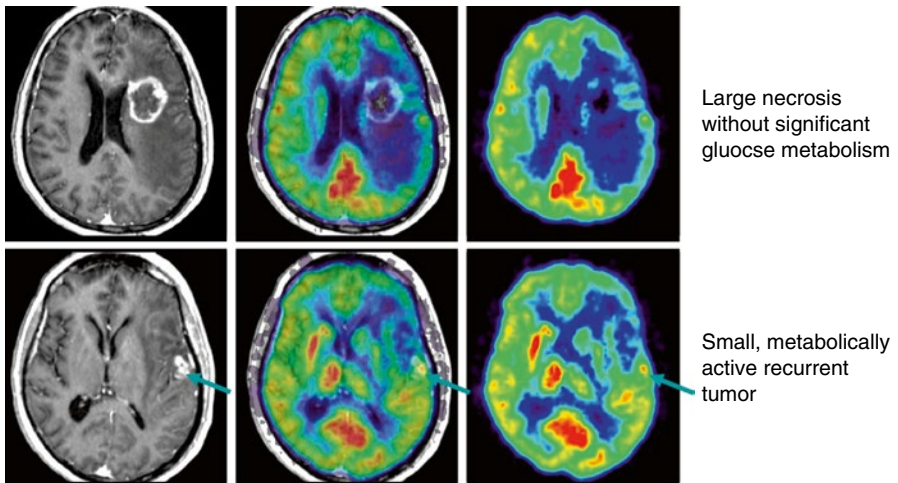


Fig. 3.8 FDG-PET and coregistered MRI in a patient with a large contrast enhancing radiation necrosis (*top row*) and a small recurrent active carcinoma metastasis (*bottom row*)

References

- Blomqvist G, Stone-Elander S, Halldin C, Roland PE, Widen L, Lindqvist M, Swahn CG, Langström B, Wiesel FA (1990) Positron emission tomographic measurements of cerebral glucose utilization using [1–11 C]D-glucose. *J Cereb Blood Flow Metab* 10(4):467–483
- Bohnen NI, Djang DS, Herholz K, Anzai Y, Minoshima S (2012) Effectiveness and safety of ¹⁸F-FDG PET in the evaluation of dementia: a review of the recent literature. *J Nucl Med* 53(1):59–71
- Catana C, Drzezga A, Heiss WD, Rosen BR (2012) PET/MRI for neurologic applications. *J Nucl Med* 53:1916–1925
- Chetelat G, Landeau B, Salmon E, Yakushev I, Bahri MA, Mezenge F, Perrotin A, Bastin C, Manrique A, Scheurich A, Scheckenberger M, Desgranges B, Eustache F, Fellgiebel A (2013) Relationships between brain metabolism decrease in normal aging and changes in structural and functional connectivity. *Neuroimage* 76:167–177
- Chierichetti F, Pizzolato G (2012) F-18-Fdg-Pet/Ct. *Q J Nucl Med Mol Imaging* 56(2):138–150
- Choo IH, Ni RQ, Scholl M, Wall A, Almkvist O, Nordberg A (2013) Combination of F-18-FDG PET and cerebrospinal fluid biomarkers as a better predictor of the progression to Alzheimer's disease in mild cognitive impairment patients. *J Alzheimers Dis* 33(4):929–939
- Chugani HT, Phelps ME, Mazziotta JC (1987) Positron emission tomography study of human brain functional development. *Ann Neurol* 22:487–497
- Clarke DD, Sokoloff L (1999) Circulation and energy metabolism of the brain. In: Siegel G, Agranoff B, Albers RW, Fisher S (eds) *Basic neurochemistry: molecular, cellular, and medical aspects*, 6th edn. Lippincott-Raven, Philadelphia, pp 637–669
- Drzezga A (2009) Diagnosis of Alzheimer's disease with [¹⁸F]PET in mild and asymptomatic stages. *Behav Neurol* 21(1–2):101–115
- Duara R, Grady C, Haxby J, Ingvar D, Sokoloff L, Margolin RA, Manning RG, Cutler NR, Rapoport SI (1984) Human brain glucose utilization and cognitive function in relation to age. *Ann Neurol* 16:702–713
- Fox PT, Raichle ME, Mintun MA, Dence C (1988) Nonoxidative glucose consumption during focal physiologic neural activity. *Science* 241:462–464
- Hawkins RA, Phelps ME, Huang SC, Kuhl DE (1981) Effect of ischemia on quantification of local cerebral glucose metabolic rate in man. *J Cereb Blood Flow Metab* 1:37–51
- Heiss W-D (2009a) The potential of PET/MR for brain imaging. *Eur J Nucl Med Mol Imaging* 36:105–112
- Heiss W-D, Raab P, Lanfermann H (2011) Multimodality assessment of brain tumors and tumor recurrence. *J Nucl Med* 52(10):1585–1600
- Heiss WD (2009b) WSO Leadership in Stroke Medicine Award Lecture Vienna, September 26, 2008: functional imaging correlates to disturbance and recovery of language function. *Int J Stroke* 4(2):129–136
- Heiss WD, Habedank B, Klein JC, Herholz K, Wienhard K, Lenox M, Nutt R (2004) Metabolic rates in small brain nuclei determined by high-resolution PET. *J Nucl Med* 45(11):1811–1815
- Heiss WD, Pawlik G, Herholz K, Wagner R, Göldner H, Wienhard K (1984) Regional kinetic constants and CMR glucose in normal human volunteers determined by dynamic positron emission tomography of [¹⁸F]-2-fluoro-2-deoxy-D-glucose. *J Cereb Blood Flow Metab* 4(2):212–223
- Heiss WD, Pawlik G, Herholz K, Wagner R, Wienhard K (1985) Regional cerebral glucose metabolism in man during wakefulness, sleep, and dreaming. *Brain Res* 327(1–2):362–366
- Heiss WD, Zimmermann-Meinzingen S (2012) PET imaging in the differential diagnosis of vascular dementia. *J Neurol Sci* 322(1–2):268–273
- Herholz K, Herscovitch P, Heiss WD (2004) *NeuroPET – positron emission tomography in neuroscience and clinical neurology*. Springer, Berlin
- Herholz K, Langen KJ, Schiepers C, Mountz JM (2012) Brain tumors. *Semin Nucl Med* 42(6):356–370
- Hsieh TC, Lin WY, Ding HJ, Sun SS, Wu YC, Yen KY, Kao CH (2012) Sex- and age-related differences in brain FDG metabolism of healthy adults: an SPM analysis. *J Neuroimaging* 22(1):21–27

- Jones T, Rabiner EA, PET Research Advisory Company (2012) The development, past achievements, and future directions of brain PET. *J Cereb Blood Flow Metab* 32(7):1426–1454
- Kalpourzou G, Chetelat G, Baron JC, Landeau B, Mevel K, Godeau C, Barre L, Constans JM, Viader F, Eustache F, Desgranges B (2009) Voxel-based mapping of brain gray matter volume and glucose metabolism profiles in normal aging. *Neurobiol Aging* 30(1):112–124
- Kety SS, Schmidt CF (1948) The nitrous oxide method for the quantitative determination of cerebral blood flow in man: theory, procedure and normal values. *J Clin Invest* 27(4):476–483
- Kuhl DE, Metter EJ, Riege WH, Phelps ME (1982) Effects of human aging on patterns of local cerebral glucose utilization determined by the (¹⁸F)fluorodeoxyglucose method. *J Cereb Blood Flow Metab* 2:163–171
- Kuwabara H, Evans AC, Gjedde A (1990) Michaelis-Menten constraints improved cerebral glucose metabolism and regional lumped constant measurement with (18) fluorodeoxyglucose. *J Cereb Blood Flow Metab* 10:180–189
- Laughlin SB, Attwell D (2001) The metabolic cost of neural information: from fly eye to mammalian cortex. In: Frackowiak RSJ, Magistretti PJ, Shulman RG, Altman JS, Adams M (eds) *Neuroenergetics: relevance for functional brain imaging*. HFSP – Workshop XI, Strasbourg, pp 54–64
- Magistretti PJ, Pellerin L, Martin J-L (1995) Brain energy metabolism: an integrated cellular perspective. In: Bloom FE, Kupfer DJ (eds) *Psychopharmacology: the fourth generation of progress*. Raven, New York, pp 657–670
- Mangold R, Sokoloff L, Conner E, Kleinerman J, Therman PO, Kety SS (1955) The effects of sleep and lack of sleep on the cerebral circulation and metabolism of normal young men. *J Clin Invest* 34(7, Part 1):1092–1100
- Mintun MA, Lundstrom BN, Snyder AZ, Vlassenko AG, Shulman GL, Raichle ME (2001) Blood flow and oxygen delivery to human brain during functional activity: theoretical modeling and experimental data. *Proc Natl Acad Sci U S A* 98(12):6859–6864
- Nofzinger EA, Mintun MA, Wiseman M, Kupfer DJ, Moore RY (1997) Forebrain activation in REM sleep: an FDG PET study. *Brain Res* 770(1–2):192–201
- Pakkenberg B, Gundersen HJ (1997) Neocortical neuron number in humans: effect of sex and age. *J Comp Neurol* 384(2):312–320
- Pardridge WM, Oldendorf WH (1977) Transport of metabolic substrates through the blood–brain barrier. *J Neurochem* 28(1):5–12
- Patlak CS, Blasberg RG, Fenstermacher JD (1983) Graphical evaluation of blood-to-brain transfer constants from multiple-time uptake data. *J Cereb Blood Flow Metab* 3(1):1–7
- Pawlik G, Heiss WD (1989) Positron emission tomography and neuropsychological function. In: Bigler ED, Yeo RA, Turkheimer E (eds) *Neuropsychological function and brain imaging*. Plenum Publ. Corp, New York, pp 65–138
- Phelps ME, Huang SC, Hoffman EJ, Selin C, Sokoloff L, Kuhl DE (1979) Tomographic measurement of local cerebral glucose metabolic rate in humans with (F-18)2-fluoro-2-deoxy-D-glucose: validation of method. *Ann Neurol* 6:371–388
- Phelps ME, Mazziotta JC, Kuhl DE (1981) Metabolic response of the brain to visual and auditory stimulation: studies in man. *Stroke* 12:122–122
- Portnow LH, Vaillancourt DE, Okun MS (2013) The history of cerebral PET scanning from physiology to cutting-edge technology. *Neurology* 80(10):952–956
- Raichle ME, Larson KB, Phelps ME, Grubb RL, Welch MJ, Ter-Pogossian MM (1975) In vivo measurement of brain glucose transport and metabolism employing glucose – 11 C. *Am J Physiol* 228:1936–1948
- Reivich M, Alavi A, Wolf A, Fowler J, Russell J, Arnett C, Macgregor RR, Shiue CY, Atkins H, Anand A, Dann R, Greenberg JH (1985) Glucose metabolic rate kinetic model parameter determination in humans: the lumped constants and rate constants for (18F) fluorodeoxyglucose and (11 C)deoxyglucose. *J Cereb Blood Flow Metab* 5:179–192
- Reivich M, Kuhl D, Wolf A, Greenberg J, Phelps M, Ido T, Casella V, Fowler J, Hoffman E, Alavi A, Som P, Sokoloff L (1979) The (¹⁸F)fluorodeoxyglucose method for the measurement of local cerebral glucose utilization in man. *Circ Res* 44:127–137

- Siesjö BK (1978) Brain energy metabolism. Wiley, New York
- Silverman DHS, Melega WP (2003) Molecular imaging of biologic processes with PET: evaluation biologic bases of cerebral function. In: Phelps ME (ed) PET. Molecular imaging and its biological applications. Springer, New York, pp 509–583
- Sokoloff L (1989) Circulation and energy metabolism of the brain. In: Siegel G, Agranoff B, Albers RW, Molinoff P (eds) Basic neurochemistry: molecular, cellular, and medical aspects. Raven Press, New York
- Sokoloff L (1999) Energetics of functional activation in neural tissues. *Neurochem Res* 24(2):321–329
- Sokoloff L, Reivich M, Kennedy C, Des Rosiers MH, Patlak CS, Pettigrew KD, Sakurada O, Shinohara M (1977) The (14 C)-deoxyglucose method for the measurement of local cerebral glucose utilization: theory, procedure, and normal values in the conscious and anesthetized albino rat. *J Neurochem* 28:897–916
- Vaishnavi SN, Vlassenko AG, Rundle MM, Snyder AZ, Mintun MA, Raichle ME (2010) Regional aerobic glycolysis in the human brain. *Proc Natl Acad Sci U S A* 107(41):17757–17762
- Wienhard K, Pawlik G, Herholz K, Wagner R, Heiss WD (1985) Estimation of local cerebral glucose utilization by positron emission tomography of [¹⁸F]2-fluoro-2-deoxy-D-glucose: a critical appraisal of optimization procedures. *J Cereb Blood Flow Metab* 5(1):115–125
- Wu HM, Bergsneider M, Glenn TC, Yeh E, Hovda DA, Phelps ME, Huang SC (2003) Measurement of the global lumped constant for 2-deoxy-2-[¹⁸F]fluoro-D-glucose in normal human brain using [¹⁵O]water and 2-deoxy-2-[¹⁸F]fluoro-D-glucose positron emission tomography imaging. A method with validation based on multiple methodologies. *Mol Imaging Biol* 5(1):32–41
- Wyss MT, Jolivet R, Buck A, Magistretti PJ, Weber B (2011) In vivo evidence for lactate as a neuronal energy source. *J Neurosci* 31(20):7477–7485

Cerebral Blood Flow Measurement with Oxygen-15 Water Positron Emission Tomography

Vilia Zeisig, Marianne Patt, Georg Becker, Johannes Boltze,
Osama Sabri, and Henryk Barthel

Contents

4.1	Introduction.....	105
4.2	Radiochemistry of [¹⁵ O]H ₂ O.....	106
4.3	[¹⁵ O]H ₂ O Brain PET Data Generation.....	107
4.4	Kinetic Modeling of CBF.....	108
4.5	Role of PET for CBF Measurements.....	111
4.5.1	General Principles for CBF Measurements.....	111
4.5.2	Advantages and Disadvantages of Perfusion Imaging Methods.....	112
4.6	Applications for CBF PET.....	114
4.6.1	Cerebral Ischemia.....	114
4.6.2	Activation Studies.....	119
4.6.3	Other Applications for CBF PET.....	119
4.7	Summary and Conclusions.....	120
	References.....	120

Abstract

The human brain receives approximately 15 % of the cardiac output and therefore is the most demanding organ in respect to blood flow supply. This fact emphasizes the importance of perfusion as a key factor in a variety of cerebrovascular

V. Zeisig (✉) • M. Patt, PhD • G. Becker, PhD • O. Sabri, MD, PhD • H. Barthel, MD, PhD
Department of Nuclear Medicine, University Hospital Leipzig, University of Leipzig,
Liebigstrasse 18, Leipzig 04103, Germany
e-mail: vilia.zeisig@medizin.uni-leipzig.de; marianne.patt@medizin.uni-leipzig.de;
georg.becker@medizin.uni-leipzig.de; osama.sabri@medizin.uni-leipzig.de;
henryk.barthel@medizin.uni-leipzig.de

J. Boltze, MD, PhD
Department of Cell Therapy, Ischemia Research Unit, Fraunhofer Institute for Cell Therapy
and Immunology, Perlickstraße 1, Leipzig 04103, Germany

Translational Centre for Regenerative Medicine, University of Leipzig, Philipp-Rosenthal-Str. 55,
04103 Leipzig, Germany
e-mail: johannes.boltze@izi.fraunhofer.de

and other diseases including stroke, migraine, and brain tumors. Today, numerous imaging techniques are able to visualize brain perfusion, but only few of them provide quantitative information. In the field of modern in vivo imaging techniques, positron emission tomography (PET) is considered to be the gold standard to give reliable results about major aspects of cerebral physiology. [^{15}O]H $_2$ O allows for quantitative cerebral blood flow (CBF) measurement within a few minutes, and subsequent ^{15}O imaging can provide precise information on oxygen metabolism like cerebral oxygen metabolism and oxygen extraction fraction. As a result, PET has become an extremely useful research tool for defining cerebral blood flow and physiology. However, complex methodological logistics and a limited availability of the imaging system hamper the widespread use of CBF PET in clinical routine. The chapter aims at summarizing the radiosynthesis, data acquisition, and analysis, as well as major preclinical and clinical applications of [^{15}O]H $_2$ O PET.

Abbreviations

$c_a(t)$	Arterial input function (arterial activity concentration over time)
CBF	Cerebral blood flow
CBV	Cerebral blood volume
CMRO $_2$	Cerebral metabolic rate of oxygen
CT	Computed tomography
$c_v(t)$	Activity concentration in venous blood over time
f_a	Arterial blood flow
GBq	Gigabecquerel
GM	Gray matter
IAP	Iodoantipyrine
iNO	Inhaled nitric oxide
k	Washout-constant
kBq	Kilobecquerel
MBq	Megabecquerel
MRI	Magnetic resonance imaging
NO	Nitric oxide
OEF	Oxygen extraction fraction
PET	Positron emission tomography
rCBF	Regional cerebral blood flow
ROI	Region of interest
S/N	Signal-to-noise
SPECT	Single-photon emission computed tomography
TSE	Turbo spin echo
V_d	Partition coefficient
V_{tissue}	Tissue volume
WM	White matter
Xe	Xenon

4.1 Introduction

Although the adult human brain assumes only about 2 % of the total body weight, it receives nearly 15 % of the resting cardiac output and 20 % of the total body oxygen consumption. This high metabolic rate reveals the need to ensure a constant delivery of oxygen and energy-providing substrates at the capillary level and to remove the waste products of metabolism. Owing to a complex autoregulatory mechanism, the cerebral perfusion is maintained relatively constant over a wider range of mean arterial pressures. A complete interruption of brain–blood supply, however, leads immediately to neuronal impairments because of the limited availability of nutrition and energy reserves in the brain. Hence, perfusion parameters are important key factors involved in major cerebrovascular and other brain diseases. Important information about cerebral characteristics is given by measurement of the cerebral blood flow (CBF) which describes the rate of blood delivery to the brain parenchyma. Traditionally, the respective literature reports CBF units in ml blood/100 g of tissue per minute. Other authors use ml instead of gram tissue to describe the volumetric character especially with imaging techniques. Due to the fact that 1 g of brain tissue nearly corresponds to 1 ml, both values can be more or less used interchangeably.

Global average CBF values in middle-aged healthy human subjects are around 55 ml/100 g/min (Kety and Schmidt 1945). However, CBF values vary regionally: In cortical gray matter, the CBF is 60–100 ml/100 g/min (Slosman et al. 2001; Sokoloff et al. 1957) and around 20 ml/100 g/min for white matter (Law et al. 2000). It has been demonstrated that neuronal activity as well as CBF is closely coupled to brain metabolism (Pantano et al. 1984; Roy and Sherrington 1890). This may explain the generally higher blood flow in younger subjects which is typically exceeding values that are 50–85 % higher than those of adults (age: 6–7 years, Chiron et al. 1992). This age dependency of CBF is probably caused, at least in parts, by an age effect on the gray-to-white matter ratio. Additionally, a decline of CBF with age is described (Brody 1955).

Kety and Schmidt (1945) were the first who introduced a method for quantitative CBF measurement in the unanesthetized human. This method is based on the Fick principle. During the inhalation of the freely diffusible nitrous oxide, the brain perfusion was calculated by measuring the amount of gas removed from the blood by the brain per minute and dividing this by the arteriovenous difference of N₂O. This method was an important step to study brain function in humans and has contributed fundamentally to our understanding of physiological and pathological cerebral processes. However, this first technique lacked the possibility to measure CBF in different brain subregions. This limitation has led to further developments in perfusion imaging techniques. As important examples, radioactive agents such as ¹³³Xe and ⁸⁵Kr were later used to measure their washout with external radiation detectors (Lassen and Ingvar 1961; Veall and Mallett 1967; Bruce et al. 1973; Obrist et al. 1975). Today, a wide variety of brain perfusion imaging techniques is available for preclinical and clinical research settings as well as clinical routine applications. CBF measurement using positron emission tomography (PET) became available in the 1970s, followed by other *in vivo* imaging techniques, like single-photon

emission computed tomography (SPECT), magnetic resonance imaging (MRI), and transmission computed tomography (CT), to obtain CBF readouts (Hoeffner 2005). This chapter will focus on CBF PET with [^{15}O]H $_2$ O as this represents the gold standard technique for in vivo CBF measurements (Carroll et al. 2002; Hoeffner 2005). One possible application for its usage is studying CBF in brain activation studies to localize brain segments involved in processing certain tasks. More important today, however, is the diagnostic potential of CBF PET imaging mainly in cerebrovascular disorders and oncology. Hence alterations of cerebral perfusion can theoretically be detected by quantitative CBF measurement leading to optimal therapy and providing estimates of the potentially salvable part of the affected brain.

4.2 Radiochemistry of [^{15}O]H $_2$ O

Oxygen-15 can be produced by different nuclear reactions using both high- and low-energy protons as well as deuterons as projectiles. The $^{14}\text{N}(\text{d}, \text{n})^{15}\text{O}$ nuclear reaction is the most efficient and economic production pathway and is therefore applied most frequently. For cyclotrons that do not have the possibility of accelerating deuterons, either the $^{15}\text{N}(\text{p}, \text{n})^{15}\text{O}$ (Powell and O'Neil 2006) for low-energy protons (>3.7 MeV) or the $^{16}\text{O}(\text{p}, \text{pn})^{15}\text{O}$ (Beaver et al. 1976; Krohn et al. 1986) for high-energy protons (>16.6 MeV) nuclear reactions can be used as an alternative.

Two methods are available for conversion of the ^{15}O to [^{15}O]H $_2$ O, the in-target production method and the out-of-target external conversion method. In case of the in-target production method, [^{15}O]H $_2$ O is produced by either addition of small amounts of hydrogen to the target gas or direct irradiation of H $_2$ ^{16}O . For the first approach, the $^{15}\text{N}(\text{p}, \text{n})^{15}\text{O}$ nuclear reaction is used (Powell and O'Neil 2006), and the trace amounts of H $_2$ in the target lead to the formation of [^{15}O]H $_2$ O by radiolytic reactions which can be trapped in a cooled stainless steel loop. The possible radioactive impurities such as $^{11}\text{CH}_4$ and $^{13}\text{NH}_3$ (resulting from trace amounts of N-14 and O-16 in the target gas) are directed to the exhaust. By heating the loop, [^{15}O]H $_2$ O vapor is released and can be trapped again in a sterile water or saline solution. The major drawbacks are the high costs for enriched $^{15}\text{N}_2$ which is used as target material. An alternative approach for [^{15}O]H $_2$ O in-target production is the direct irradiation of H $_2$ ^{16}O in a liquid target (Mulholland et al. 1990; van Naemen et al. 1996). As mentioned above this method is feasible only with high-energy protons, a restriction that excludes this approach for commonly used cyclotrons in a clinical setting.

As an alternative to the in-target production of [^{15}O]H $_2$ O, external out-of-target tracer production by catalytic conversion of a mixture of H $_2$ and [^{15}O]O $_2$ has been demonstrated for all abovementioned nuclear reactions, i.e., $^{16}\text{O}(\text{p}, \text{pn})^{15}\text{O}$ (Krohn et al. 1986), $^{15}\text{N}(\text{p}, \text{n})^{15}\text{O}$ (Explora $^{\text{®}}$ H $_2$ O module, Siemens Healthcare, Erlangen, Germany), and $^{14}\text{N}(\text{d}, \text{n})^{15}\text{O}$ (Clark et al. 1987; Clark and Tochon-Danguy 1991; Sajjad et al. 2000). For the $^{14}\text{N}(\text{d}, \text{n})^{15}\text{O}$ nuclear reaction, N $_2$ with up to 4 % O $_2$ is irradiated with deuterons (≈ 7 MeV). In most cases, Pd is used as the catalyst; however, if the same target is used as well for production of C ^{15}O , it might be necessary

to reduce the amount of O_2 in order to minimize the production of toxic carrier CO. Under these conditions it has been shown that Pt as catalyst is superior (Berridge et al. 1990). The most simple production and application approach consists of an H_2 supply that is connected to the target line via a T connector. The target gas/ H_2 mixture (2–10 %, Berridge et al. 1990; Sajjad et al. 2000) is then directed over the heated catalyst (≈ 170 °C, temperatures up to 450 °C have been reported as well (Berridge et al. 1990)), and the resulting $[^{15}O]H_2O$ vapor is bubbled into a sterile reservoir containing water, saline, or preferably buffer since the catalyst might as well generate trace amounts of ammonia which un-buffered may lead to elevated pH values. The $[^{15}O]H_2O$ -containing solution is then drawn up into a syringe and manually applied to the investigated subject. However, due to the relatively high radiation exposure of the medical personnel, it might be worth to automate the injection procedure. In a relatively simple setup, the injection is performed by means of two infusion pumps and a 4-port valve (Sajjad et al. 2000). A more sophisticated method uses a dialysis membrane to enable exchange of $[^{15}O]H_2O$ with sterile water (Clark and Tochon-Danguy 1991) together with an infusion pump and several valves to enable automatic injection. This system is commercially available (Veenstra Instruments, Joure, Netherlands).

4.3 $[^{15}O]H_2O$ Brain PET Data Generation

After a transmission scan for attenuation correction, the emission scan is acquired preferentially in 3D mode and initiated immediately before tracer administration. The tracer is injected as a fast bolus followed by a flush of inert saline solution. The amount of injected tracer in humans typically ranges between 550 and 1,000 MBq for an adult subject, but studies using up to 2.2 GBq were also found in the literature (Heiss et al. 2000).

For the bolus injection method, Kanno et al. (1991) investigated an optimal scan time for $[^{15}O]H_2O$ to improve image quality and signal-to-noise ratios. A minimum scan duration of 90 s was recommended. For most applications, however, scan durations of 2–5 min are chosen. A typical protocol for a 5-min dynamic data acquisition is shown in Table 4.1.

The advantageous short half-life of the tracer (122 s) enables the performance of multiple image acquisition scans in rapid sequence. Inter-scan intervals should, however, not be shorter than 15 min to allow isotope decay. Due to the fast radioactive decay, an on-site cyclotron or linear accelerator for isotope production becomes necessary. Further data analyses generally include the absolute quantification of CBF. For this purpose, the experimental setting implies arterial blood sampling in parallel to the PET acquisition. This is preferentially performed using an automated

Table 4.1 Acquisition protocol for a 5-min PET scan with $[^{15}O]H_2O$

Frame duration[s]	5	10	30
Number of frames	24	12	2

sampling system (e.g., ALLOGG AB blood sampler; Allogg Mariefred, Sweden) with a peripheral artery, e.g., the radial artery. Using such a device, arterial blood samples are continuously drawn at a constant speed with activity measurements for every 0.5 or 1 s. The blood sampler needs to be cross-calibrated to the PET scanner, allowing the decay-corrected blood data to be used as input function for kinetic modeling.

Obtaining arterial blood samples via the placement of an arterial catheter is accepted as the gold standard method for CBF quantification. However, there are some limitations, like invasiveness, complications for the patient, and sensitivity to errors (Hall 1971; Machleder et al. 1972). Aiming to replace the arterial canalization and corresponding input function, alternatives were suggested, like image-derived input functions (Zanotti-Fregonara et al. 2011) and methods without the need of any input function (Lammertsma 1994; Watabe et al. 1996). Another possibility to avoid arterial canalization is the use of arterialized venous blood, which is an often used method also with other PET tracers. With this technique, the hand of the patient or volunteer is heated well above 37 °C to achieve a shunting of arterial blood to the venous system (Wakita et al. 2000). Nevertheless, all alternative techniques have their drawbacks, and the CBF values obtained by them need to be handled with caution.

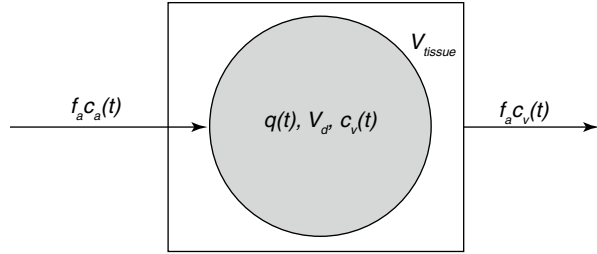
As for all brain PET tracers, the resulting PET data require a correlation with structural information from MRI (preferably 3D-T1 data). In this regard, the use of combined PET/MRI scanners might improve this situation in the future. Combined PET/MR imaging gives the opportunity for accurate registration and exact correlation of PET functional aspects with anatomical information from MRI. This will result in better image quality because of the comparably lower spatial resolution of PET in contrast to MRI and also shortens imaging times for the patients/anesthetized research animals.

4.4 Kinetic Modeling of CBF

The first method to measure CBF in humans was proposed by Kety and Schmidt in 1945 who utilized nitrous oxide for CBF detection. Later, other tracers like $^{133}\text{Xenon}$ (Veall and Mallett 1967) were applied within this concept which was based on the Fick principle and a single-tissue compartment model. It states that the amount of a metabolically inert and freely diffusible gas that is taken up by a tissue per unit of time is equal to the product of the blood flow through that tissue and the difference between the amount of gas entering it via the arterial blood and the gas leaving in the venous blood.

The single-tissue compartment model describes the behavior of a freely diffusible tracer like $^{15}\text{O}]\text{H}_2\text{O}$ in tissue as shown in Fig. 4.1 and can be used to determine the local arterial blood flow in the brain (on a region of interest (ROI) or voxel basis). The model consists of two parameters that have to be estimated from the data of a dynamic PET scan ($q(t)$) and from the measured arterial input function $c_a(t)$.

Fig. 4.1 Schematic description of a single-tissue compartment. V_{tissue} is the anatomical tissue volume (1 cm^3), and V_d is the volume of the tissue compartment accessible to the tracer. The products of flow and concentration describe the amount of tracer which enters or leaves the tissue compartment per time unit. Please refer to the main text for further explanation of the other symbols



Assuming that the transport of tracer from the vessel into the tissue compartment is fast (high permeability surface area product) compared to the delivery by the arterial blood flow, the tracer dynamics can be described by a one-tissue compartment model with one input function. The mass balance for the tracer (Fick principle) yields the differential equation

$$\frac{dq(t)}{dt} = f_a c_a(t) - f_a c_v(t) \quad (4.1)$$

where $q(t)$ is the quantity of tracer per unit volume of tissue (kBq cm^{-3}), f_a is the local arterial blood flow per unit volume ($\text{ml min}^{-1} \text{cm}^{-3}$), and $c_a(t)$ and $c_v(t)$ are the tracer concentrations in arterial and venous blood (kBq ml^{-3}).

The tracer concentration in the venous blood ($c_v(t)$) is related to the tracer concentration in the tissue space ($q(t)$) through the relative volume of distribution (V_d (ml cm^{-3})) by the Kety–Schmidt assumption:

$$q(t) = V_d c_v(t) \quad (4.2)$$

reflecting the assumption that the concentrations in the water spaces of venous blood and tissue are always equilibrated (this assumption is not generally valid, because a diffusion limitation exists for $^{15}\text{O}]\text{H}_2\text{O}$ at low CBF rates).

From Eqs. (4.1) and (4.2), the differential equation

$$\frac{dq(t)}{dt} = f_a c_a(t) - kq(t) \quad (4.3)$$

is obtained with the washout constant k (min^{-1}) defined to be

$$k = \frac{f_a}{V_d}. \quad (4.4)$$

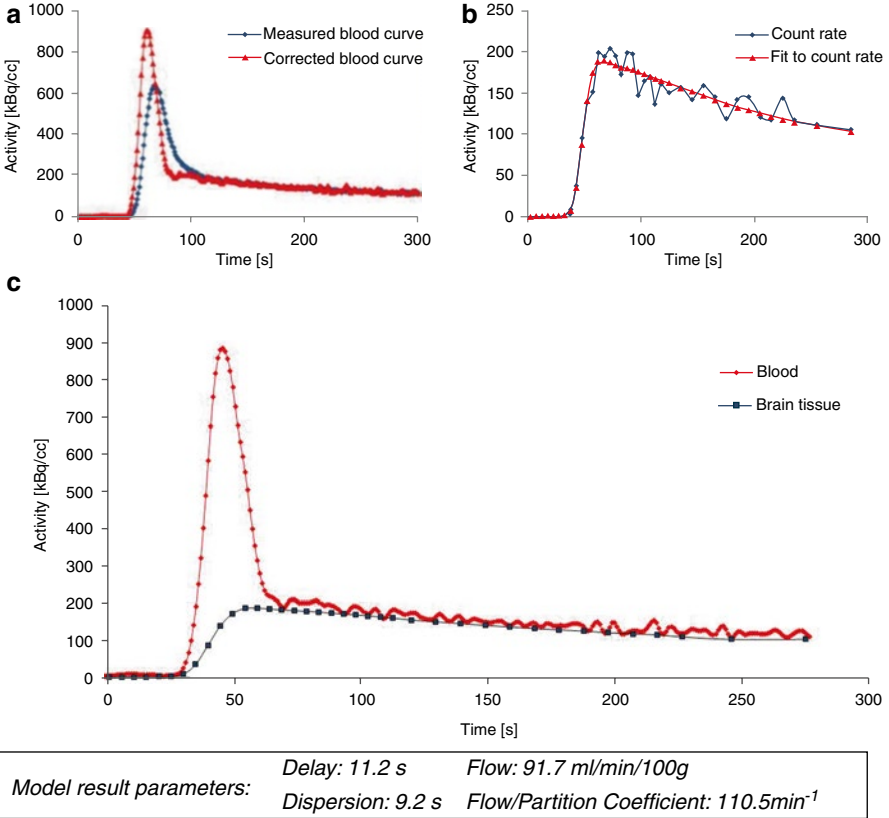


Fig. 4.2 Model parameter estimation. The arterial input function (a) and corresponding tissue response in a cortical ROI (b) after bolus injection of $[^{15}\text{O}]\text{H}_2\text{O}$ are shown. Blood activity data were determined by taking arterial blood samples with a dedicated sampling device. The input function and tissue response are corrected for tracer arrival times and bolus dispersion. Further kinetic modeling is based on the resulting corrected curves (c)

By estimating values of f_a and k , the partition coefficient of the tracer can be calculated for every tissue voxel. An example of parameter estimation for a cortical region of interest based on the arterial input function is shown in Fig. 4.2.

Equation (4.3) has the solution

$$q(t) = f_a e^{-kt} \otimes c_a(t) \quad (4.5)$$

where \otimes describes the convolution of an exponential function with the arterial input function $c_a(t)$:

$$e^{-kt} \otimes c_a(t) = \int_0^t t e^{-kt} c_a(t - \hat{o}) d\hat{o}. \quad (4.6)$$

The experimental design is further specified in a way that the tissue response, $q(t)$, as well as the arterial, $c_a(t)$, input is measured and thus known for the duration of the experiment. Additionally, $q(0) = 0$.

[¹⁵O]H₂O is the most commonly used tracer for brain perfusion imaging and CBF quantification with PET. However, there are some notable restrictions concerning the diffusion limitation of [¹⁵O]H₂O. A study of Eichling et al. investigated the cerebral behavior of [¹⁵O]H₂O after administration to rhesus monkeys. They found that only about 90 % of the injected tracer freely exchanges with the brain tissue, with even lower rates at higher flow rates. This incomplete first-pass extraction (80–90 % in gray matter structures) resulted in a slightly underestimation of CBF especially in high-flow regions (Eichling et al. 1974; Bolwig and Lassen 1975; Raichle et al. 1983).

In this respect, lipophilic gaseous tracers (like nitrous oxide and xenon) behave superior for CBF measurements as compared with [¹⁵O]H₂O.

Further consideration should be done concerning partial volume effect that among others derive from relatively low spatial resolution of typically 6–10 mm in PET. The resulting spread out of signal is a phenomenon that introduces distortion effects in the targeted region and adjacent tissue (Links et al. 1996). The partial volume effect primarily leads to an increased bias for small anatomical structures (like vessels) in the brain (Rousset et al. 1998).

Since the early 1980s, several methods have been described to calculate CBF from PET measurements with [¹⁵O]H₂O, including simplified techniques that include parameter fixation, e.g., fixation of the partition coefficient (Watabe et al. 1996). The partition coefficient of [¹⁵O]H₂O is a parameter that has been investigated in many studies and varies from 0.77 to 1.05 ml/ml (Herscovitch and Raichle 1985; Iida et al. 1993; Kanno et al. 1991). A good approximation for the whole brain was considered by Herscovitch and Raichle to be 0.9 ml/ml (Herscovitch and Raichle 1985). However, CBF calculation methods with fixed values for V_d are only applicable to identify global blood flow changes. In presence of regional blood flow deficits, CBF calculation results in incorrect values.

4.5 Role of PET for CBF Measurements

4.5.1 General Principles for CBF Measurements

A general distinction must be made between the behaviors of different CBF tracers. One class of techniques utilizes agents which are restricted to the intravascular space and do not interact with the nonvascular space. These can be, in cases of an intact blood–brain barrier, referred to as nondiffusible CBF tracers. Many brain imaging techniques, such as contrast-enhanced MR and CT, use these intravascular tracers to calculate CBF on the basis of the indicator dilution theory (Meier and Zierler 1954; Zierler 1962). In contrast, a direct tracer exchange from the arterial vascularity to the parenchyma occurs in case of freely diffusible CBF tracers and enables to give a direct measurement of parenchymal blood flow, as originally described by Kety (1951). This concept is utilized, for example, with [¹⁵O]H₂O PET, Xenon–CT, and Xenon SPECT. Some basic characteristics appear to be necessary for a useful CBF measurement method: Ideally, the incorporated indicator should be early and completely mixed with blood and must stay identifiable for position and concentration in time of image acquisition. Further, the indicator should be metabolically inert and rapidly eliminated.

4.5.2 Advantages and Disadvantages of Perfusion Imaging Methods

Various modalities have been developed to obtain hemodynamic parameters in research and clinical settings. These include the older ^{133}Xe inhalation method, PET, SPECT, X-ray computed tomography methods, and several MRI techniques. However, each technique has its own advantages and drawbacks. It depends on the study subject and the targeted question which method to choose appropriately. A review from Wintermark et al. (2005) gives a comparative overview about current brain perfusion measurement techniques and their clinical relevance. At this point, a brief overview is given on the role of ^{15}O] H_2O PET in this context.

4.5.2.1 Nuclear Medicine Methods

CBF can be measured after incorporation of radioactive agents which are detected outside the investigated subject with dedicated scintillation detectors. Based on this principle, tracers like $^{99\text{m}}\text{Tc}$]HMPAO or $^{99\text{m}}\text{Tc}$]ECD and ^{133}Xe were commonly used for CBF measurements with SPECT (Barthel et al. 2001; Lass et al. 1998; Sakai et al. 1987). In comparison to the coincidence method in PET imaging, the detection of single photons is less sensitive. SPECT imaging with $^{99\text{m}}\text{Tc}$]HMPAO or $^{99\text{m}}\text{Tc}$]ECD only allows for semiquantitative CBF estimation (Markus 2004). In contrast, the ^{133}Xe SPECT method relies on the Kety–Schmidt model (Kety and Schmidt 1945) and is considered to give quantitative measures of CBF (Wintermark et al. 2005). In several studies, however, a systematic CBF overestimation was reported in low-flow areas, as well as an underestimation of cortical CBF (Matsuda et al. 1996; Skyhøj Olsen et al. 1981).

However, the coincidence PET technique is commonly accepted to be the reference standard for CBF imaging. With PET, the tissue perfusion can be directly measured by using the diffusible radiotracer ^{15}O] H_2O . This method is well validated and combines several favorable properties. The tracer is easy to produce, and the fast acquisition time permits repetitive measurements with whole brain coverage. Additionally, the major advantage of CBF measurement with PET is the high accuracy for assessing quantitative parameter maps as well as a high reproducibility (Carroll et al. 2002; Matthew et al. 1993).

Additionally, PET imaging with ^{15}O -labeled compounds is of special interest for studying cerebrovascular diseases and if a comprehensive view on brain hemodynamic is demanded. In addition to the determination of CBF with ^{15}O] H_2O , a successive ^{15}O inhalation allows for quantitative determination of essential parameters of hemodynamics and energy metabolism like oxygen consumption (cerebral metabolic rate of oxygen; CMRO_2) and oxygen extraction fraction (OEF) (Frackowiak et al. 1980; Ibaraki et al. 2004). Further, because of its binding to hemoglobin in red blood cells (Martin et al. 1987), radiolabeled CO is used as an intravascular tracer to measure the cerebral blood volume (CBV). Compared to other modalities, PET is the only technique which is able to gain all of these different functional parameters noninvasively and in 3D for the entire brain, a fact which allowed PET imaging to become the gold standard method in the field of brain circulation physiology and pathophysiology imaging (Hoeffner 2005).

In comparison to SPECT, which is widely accessible and a routine perfusion imaging tool, PET imaging is technically more demanding and its availability is limited by complex logistics. Not only a PET scanner, but also the constant access to a cyclotron producing the radiopharmaceutical online is required, a fact limiting the application of the method especially in emergency settings. A further restriction occurs in patients who will receive a thrombolytic therapy. Because quantitative PET preferentially requires invasive arterial blood sampling in order to obtain an input function for kinetic CBF modeling, this procedure is not applicable in these patients. As a consequence, [^{15}O]H $_2$ O PET did not manage to become a clinical routine imaging tool in the acute stroke situation. Clinical applications instead mainly refer to chronic cerebrovascular disorders, brain tumors, and brain activation studies. Moreover, due to the wide acceptance of PET as standard for CBF visualization and quantification, the method is used as the reference to validate other brain perfusion imaging techniques, like perfusion-weighted or arterial spin labeling MRI (Zaro-Weber et al. 2010a, b; Chen et al. 2008)

Apart from [^{15}O]H $_2$ O PET, CBF measurements with [^{11}C]butanol have been suggested to be an alternative tracer for detection with PET. In comparison to radiolabeled water, butanol has the advantage of being permeable through the blood–brain barrier to 100 %. However, this tracer is not used in routine practice because of its complex and radiochemical synthesis (Herscovitch et al. 1987).

[^{14}C]iodoantipyrine (IAP) autoradiography is another nuclear medicine perfusion imaging method used in preclinical research (Hatakeyama et al. 1992; Jay et al. 1988). As with butanol and H $_2$ O, IAP is also able to freely cross the blood–brain barrier. It is not metabolized and as such accumulates in the brain tissue depending on the regional CBF. After tracer application, the animals need to be sacrificed to prevent tracer diffusion and to autoradiographically determine the CBF at the time-point of tracer injection. Sequential arterial blood samples can be used for absolute CBF quantification. This autoradiographic *ex vivo* method provides accurate and high-resolution quantitative CBF values for a specific time-point and is therefore mainly used in small animal studies.

4.5.2.2 Computed Tomography Methods

The physical principle that underlies the CT technique is based on tissue-specific attenuation of X-rays that are directed to the body. The image contrast then resulted from variations in attenuation depending on tissue density. Due to similar densities in white and gray matter structures, this technique is not the ideal tool to image anatomical brain structures (Griffiths et al. 2001). However, with a bolus injection of a contrast agent, such as iodine, most prerequisites of the abovementioned indicator dilution theory are satisfied to measure blood flow in the brain. However, due to different acquisition hardware, acquisition protocols, varying post-processing protocols, and differences in the interpretation of perfusion CT data, a reliable CBF quantification remains challenging and varies widely between centers (Kudo et al. 2010). A further approach for CBF measurement uses inhaled Xenon to detect concentration changes of the substance (Pindzola and Yonas 1998). The lipophilic gas is soluble in water, and its X-ray attenuation is similar to that of iodine. As in ^{133}Xe SPECT, the Xe–CT technique also utilizes the Kety–Schmidt method to calculate

quantitative CBF maps with sufficient accuracy (Wintermark et al. 2005). Although newer CT scanners are able to achieve whole brain coverage, a main limitation of commonly used CT scanners derives from the limited anatomical coverage, which is restricted to few brain slices.

4.5.2.3 Magnetic Resonance Methods

Several methods for CBF estimation by means of MR had been developed. The most commonly used method for neuroimaging studies is the dynamic susceptibility contrast (DSC) MRI method. It relies on changes in relaxation time on T2*-weighted images. With the bolus of a paramagnetic contrast agent agents (e.g., gadolinium-DTPA) passing through the vascular system, a detectable signal loss occurs in T2*-weighted sequences. Mathematical conclusions were then drawn from the signal reductions to further calculate several perfusion or perfusion-related parameters including mean transit time (MTT), time to peak (TTP), relative cerebral blood volume (rCBV), and relative CBF (Ostergaard et al. 1996a, b). Contrast agents for MR imaging are not radioactive and relatively inexpensive as compared with PET and SPECT tracers. A further advantage of this method is the short acquisition time that enables to visualize perfusion-weighted measurements within a few minutes. However, the absolute quantification of CBF remains unsolved (Wintermark et al. 2005). The use of a local internal input function (Calamante et al. 2004) is necessary to receive parametric maps. As such, the detection of a plausible AIF which is influenced by numerous factors, such as partial volume effects, is important for reproducible and reliable perfusion values (van Osch et al. 2001). Another respective challenge is the localization of the intracranial region of interest for the AIF calculation (Zaro-Weber et al. 2012). Thus, most of the calculated parameter maps in perfusion MR are named as “relative” (Griffiths et al. 2001; Jezzard 1998). Nevertheless, perfusion MRI is employed for diagnostic purposes, for instance in acute stroke, and in clinical settings regarding the combination of the various read-out parameters. In comparison to gadolinium-based MRI, the arterial spinlabeling approach is another promising MR perfusion technique. Here, magnetically labeled water protons are used as endogenous tracer. However, problems with image interpretation may occur due to a limited signal-to-noise ratio and in the presence of prolonged blood transit times, like in patients with stroke or atherosclerosis (Petersen et al. 2006). In latter cases (e.g., stroke patients), the labeled water spins did not reach the target brain tissue within a given time, with the consequence of underestimating the real blood flow values (Jezzard 1998; Kimura et al. 2005).

4.6 Applications for CBF PET

4.6.1 Cerebral Ischemia

The increasing incidence for vascular diseases, like atherosclerosis, is associated with a worldwide increasing number of ischemic attacks (Feigin et al. 2009). Interruptions in brain–blood supply rapidly leads to ischemic cell damage that

results in necrotic tissue if no sufficient therapy or spontaneous reperfusion becomes available. Current therapies aim to restore perfusion in the ischemic, salvageable brain tissue. In order to determine this hypoperfused yet viable tissue – the so-called ischemic penumbra (Astrup et al. 1981) – in acute stroke patients, perfusion imaging techniques were developed to identify this “tissue at risk” and to separate it from the already necrotic infarction core. The transition from reversible to irreversible damage is a function of ischemia duration as well as of CBF. A hemodynamic determination of the ischemic penumbra is used for many research studies in laboratory animals and humans, and CBF thresholds to characterize different tissue states were proposed: While normal human CBF is in the range of 50–80 ml/100 g/min, reversible ischemia (“ischemic penumbra”) is evident when CBF drops below values around 22 ml/100 g/min, and neuronal cell death occurs below a CBF of 8 ml/100 g/min (Baron 2001). However, penumbra detection, based on CBF thresholds, is highly dependent on a reliable and accurate quantitative imaging method in an acute stroke diagnostic setting.

The opportunity to investigate different parameters of brain function, like CBF, CBV, OEF, and CMRO₂, within one PET imaging session is a further advantage in the investigation of cerebrovascular diseases such as ischemic stroke. Here, it is essential to reliably separate primary perfusion deficits from events of decreased metabolic demand. This is as CBF decreases may not only appear in the surrounding tissue of the stenotic vessel, but sometimes also distant from the obviously damaged part of the brain. This well-recognized phenomenon is called “diaschisis.” One example is the so-called crossed cerebellar diaschisis in which a CBF reduction in the cerebellum contralateral to the stroke-affected brain hemisphere occurs as a result of crossed functional deafferentiation (Baron et al. 1981; Feeney and Baron 1986).

4.6.1.1 PET Perfusion Imaging in Preclinical Stroke Research

This paragraph will handle the employment of [¹⁵O]H₂O PET in translational research studies of experimental stroke.

In 2008, our group proposed a new large animal model that is applicable for acute and chronic stroke induction (Boltze et al. 2008) and is highly suitable to reflect the human brain pathophysiology. Due to a similar cerebral anatomy and the favorable ovine brain size, brain imaging protocols, scanners, and data analysis techniques as used in clinical routine become feasible. This enables us to perform studies while meeting main conditions for translational research. Like in humans, in sheep, the middle cerebral artery (MCA) usually gives rise to three arterial branches. Different stroke sizes can be induced by permanent transcranial occlusion of one, two, or all three MCA branches, with the latter being referred to as permanent MCA occlusion (pMCAO). Fig. 4.3 shows examples of different occlusion types for experimental pMCAO in sheep. One-, two-, and three-branch (total) occlusions of the MCA could clearly be visualized by magnetic resonance angiography (MRA), together with the resulting CBF defects in [¹⁵O]H₂O PET. In addition, slight CBF decreases, probably due to the transcranial surgery, were also detected in the sham-operated animals. Further, it was possible to demonstrate that the ischemic strokes

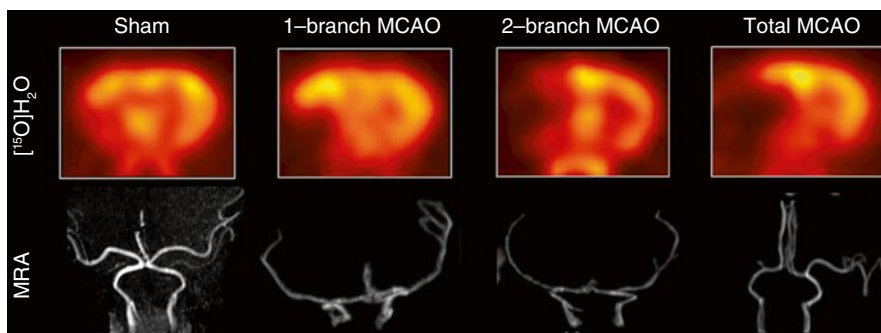
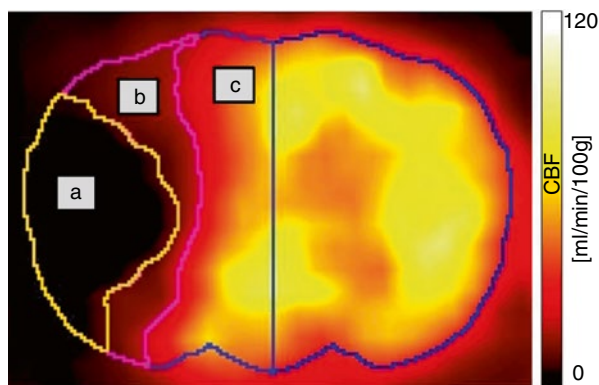


Fig. 4.3 Differential CBF deficits dependent on extent of experimental permanent middle cerebral artery occlusion in sheep. The extent of the post-pMCAO CBF deficit is clearly visualized with $[^{15}\text{O}]\text{H}_2\text{O}$ PET. Corresponding to angiographic MRI findings, the CBF deficit increases in the order sham > 1-branch pMCAO > 2-branch pMCAO > total pMCAO. *MCAO* middle cerebral artery occlusion, *MRA* magnetic resonance angiography (Modified from Boltze et al. (2008))

Fig. 4.4 Parametric CBF map as obtained by $[^{15}\text{O}]\text{H}_2\text{O}$ PET in the Leipzig permanent middle cerebral artery occlusion sheep stroke model. For volume of interest analysis, the stroke-related regions were defined as follows: infarction core (a): <8 ml/100 g/min, ischemic penumbra: (b) 8–22 ml/100 g/min, normal brain tissue (c): >22 ml/100 g/min



induced by the transcranial pMCAO lead to reproducible CBF deficits, which remain stable over time and eventually leading to necrotic brain tissue.

The major advantage of $[^{15}\text{O}]\text{H}_2\text{O}$ PET is the option to perform serial scans in a short time period due to the short half-life of the ^{15}O (122 s). As an example, CBF PET measurements were applied for a controlled preclinical study that aimed to test inhaled nitrous oxide (iNO) for its potential to protect the ischemic tissue in the penumbra in acute ischemic stroke. All animals were subjected to repeated PET scans at 110, 150, 175, and 210 min following pMCAO (a total of four PET scans within 100 min). In the treatment group, 50 ppm iNO were applied from 120 to 180 min after pMCAO. By using kinetic modeling, parametric CBF maps were created. Based on the abovementioned commonly accepted CBF thresholds (Baron 2001), operator-independent brain volumes of interest were defined for penumbra, infarction core, and remaining normal brain tissue (Fig. 4.4). Our experiments

showed that iNO selectively restores CBF in the ischemic penumbra. While the volume of the necrotic core was not affected, the volume of the penumbra decreased by up to 50 % turning into normally perfused tissue (>22 ml/100 g/min) under iNO application, but remained unchanged in the untreated control animals ($p < 0.05$ vs. baseline and vs. control; Figs. 4.5 and 4.6; Terpolilli et al. 2012).

To give an outlook for further projects on CBF PET imaging in the Leipzig sheep pMCAO stroke model, Fig. 4.7 shows first images acquired by a simultaneous PET/3T-MRI system (Biograph mMR, Siemens). Comparative PET and MR imaging studies in acute stroke setting will greatly benefit from the new possibility to acquire data of both modalities simultaneously. This will significantly improve the investigation of the very fast pathophysiological processes in early ischemia. The first experience with this new simultaneous imaging approach, however, triggers great enthusiasm to employ this new technique for further preclinical and clinical research in the acute stroke situation.

With regard to the abovementioned possibility of PET imaging to provide multi-parameter readouts (CBF, OEF, CMRO₂, CBV), in experimental ischemic stroke, so far mainly the brains of monkeys (Kuge et al. 2001; Pappata et al. 1993), pigs (Sakoh et al. 2000a) and felines (Heiss et al. 1994) were investigated by using [¹⁵O] H₂O for CBF measurements. With examinations of different time points after stroke, the studies by Heiss et al. aimed at monitoring important parameters of the temporal transversion of penumbral tissue to the final infarct core. The ischemic penumbra is characterized by an initial increase of OEF and CBV and preserved values of CMRO₂. In progress of the infarct and decreasing blood flow supply, CMRO₂ declines to values of 25 % of baseline within the first hour after stroke, while the initially increase of OEF becomes less prominent. In the final stage, the lack of CBF

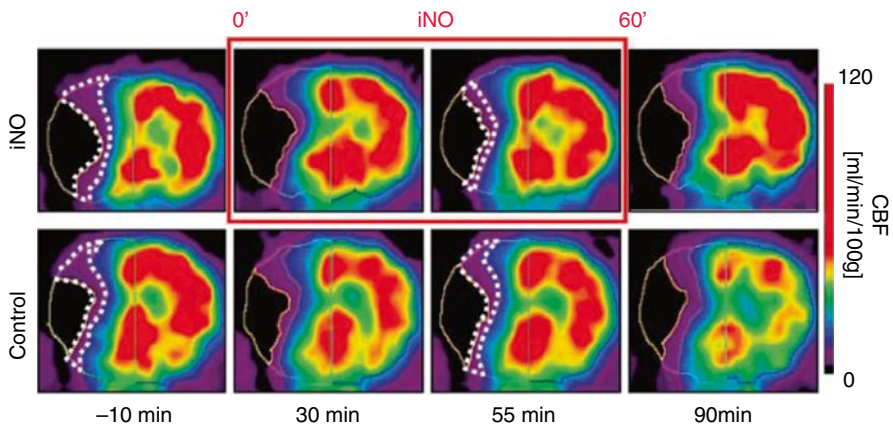


Fig. 4.5 Serial [¹⁵O]H₂O PET scans show therapeutic effect of iNO in the Leipzig permanent middle cerebral artery occlusion sheep stroke model. Stroke-related tissue regions were defined on the basis of quantitative CBF maps. Volumetric analysis showed a significant decrease of the penumbra volume under iNO therapy in favor of the normal brain tissue compartment. This beneficial effect was not detected in control animals (Terpolilli et al. 2012)

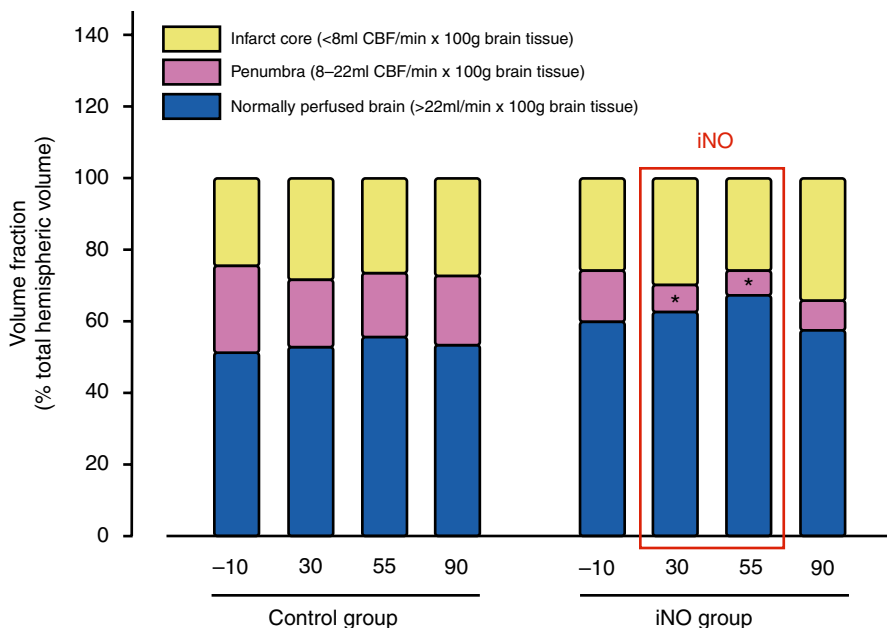


Fig. 4.6 iNO improves penumbral blood flow after permanent middle cerebral artery occlusion in sheep. Quantification of normally perfused, ischemic, and penumbral tissue volumes revealed that penumbral volume decreased significantly during NO inhalation ($n=3$ per group; $*p<0.05$ vs. control and vs. baseline PET at t-10 min) in favor of the normally perfused brain tissue (Terpolilli et al. 2012)

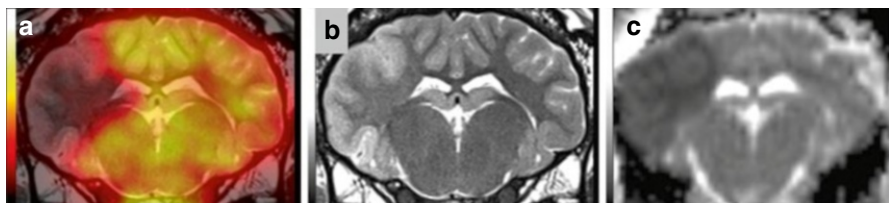


Fig. 4.7 Multimodal PET-MRI imaging in the Leipzig sheep stroke model. Four hours after permanent middle cerebral artery occlusion, (a) CBF was determined by [^{15}O]H $_2$ O PET (shown here in overlay with anatomical T2-MRI) demonstrating the typical poststroke deficit. (b) T2-MRI acquired to exclude hemorrhage. (c) Diffusion-weighted MRI with deficit similar to the CBF abnormality. The image data were acquired simultaneously using a PET/3T-MR (Siemens mMR) system

is associated with a decrease in OEF and the occurrence of brain tissue necrosis. This progress from still viable to necrotic tissue was defined as a function of duration and severity of stroke (Heiss et al. 1994, 1997; Heiss and Rosner 1983). In further experiments from the Cologne group, postischemic hemodynamic and metabolic processes were investigated after temporary MCAO (from 30 to 120 min of duration) in anesthetized cats (Heiss et al. 1997). CBF PET was performed

immediately after MCAO and was repeated at 30-min intervals. After reopening the vessel, a distinct hyperperfusion was found in all animals, depending on the duration of the MCAO. After 30 min of ischemia, the reactive CBF increase was found to be transient with a fast normalization to pre-occlusion CBF values and without major tissue necrosis. By comparison, the reperfusion period after 60 or 120 min of ischemia was associated with severe hyperperfusion (CBF increase up to 300 % compared to basal levels) and irreversible tissue damage, depending on the severity of prior ischemia. Approximately 50 % of animals died after the prolonged ischemic period and suffered from higher CBF than the surviving animals from the same group. One explanation might be the hyperperfusion processes with massive cerebral edema that resulted in malignant brain swelling. These observations let to assume a relatively high tolerance against moderate hyperemia, whereas extensive hyperperfusion leads to an increased mortality (Heiss et al. 1997).

Other large animal experiments utilized [^{15}O]H $_2\text{O}$ (Sakoh et al. 2000a, b) in combination with [^{15}O]CO PET to study regional correlations of CBF and CBV after acute stroke and in cases of reperfusion (Sakoh et al. 2000a). For that purpose, 13 pigs underwent PET, and the results were compared to MRI measurements of the same parameters. A good agreement was found between the values of both modalities in the ischemic tissue. After MCAO, a significant correlation between CBF reduction and CBV increase was observed. However, the decrease of CBF below 60 % of the contralateral side was found to induce a reduction in CBV. In contrast, both parameters were less correlated in cases of reperfusion (Sakoh et al. 2000a).

4.6.2 Activation Studies

Perfusion parameters are closely coupled with changes in neuronal activity (Roy and Sherrington 1890; Fox et al. 1988; Villringer and Dirnagl 1995). In the last decades, numerous neuronal activation studies have reported this effect, which, nevertheless, is not completely understood (Peterson et al. 2011). The possibility to perform sequential measurements within a certain time window made CBF PET an attractive tool to study perfusion during cognitive, motor, or sensomotor tasks in humans. During local brain activation, cerebral areas that are involved in task performance were identified by CBF changes (Feng et al. 2004; Worsley et al. 1992).

4.6.3 Other Applications for CBF PET

In general, PET is a useful tool to study perfusion and oxygen metabolism in any cerebral disease, such as dementia (Yao et al. 1990; Cohen et al. 1997), schizophrenia (Ragland et al. 2001), and migraine. Latter approaches addressed hemodynamic changes and oxygen metabolism during and between acute attacks. An increase in CBF was found in cortical areas and in the brainstem which appeared to be pain related (Andersson et al. 1997; Cutrer et al. 2000). Similar to these migraine studies, other preclinical and clinical investigations focus on epilepsy to determine

perfusion changes during and between epileptic seizures (Szabo et al. 2007; Kahane 1999; Gaillard et al. 1995). A few studies also used CBF PET (mostly in combination with other PET readouts, like oxygen metabolism from ^{15}O inhalation) for detailed characterization of brain tumors (Leenders 1994; Hino et al. 1990; Tomura et al. 1993). Due to the neo-formed vessels which often appear in the tumor parenchyma or its surrounding, a regional CBF increase could be detected and may provide additionally useful information about the progression of the brain tumors.

4.7 Summary and Conclusions

PET imaging with ^{15}O H₂O represents the gold standard to visualize and quantify CBF in vivo. As such, this method plays a relevant role mainly for the investigation of cerebrovascular diseases. Despite advantageous characteristics of the tracer, like the possibility to monitor CBF changes over time in sequential scans, ^{15}O H₂O PET imaging remains a technological and infrastructural challenge, preventing it from gaining a wider acceptance in a clinical routine setting. In contrast to clinical routine, ^{15}O H₂O PET plays an important role in preclinical and clinical research, for instance, in (1) clarifying the pathophysiology of ischemic stroke and other cerebrovascular disorders, (2) cross-evaluation of alternative imaging methods to estimate CBF, and (3) the testing of new stroke treatment concepts.

Acknowledgments The authors are grateful to the cyclotron, radiochemistry, and PET crews of the Department of Nuclear Medicine of the Leipzig University Hospital for their excellent support in acquiring the PET data. Further, we would like to thank the stroke sheep model group of the Leipzig Fraunhofer Institute for Cell Therapy and Immunology for providing the research animals, and to our collaborators at the Department of Neuroradiology of the Leipzig University Hospital for providing the sheep MRI data.

References

- Andersson JL, Muhr C, Lilja A et al (1997) Regional cerebral blood flow and oxygen metabolism during migraine with and without aura. *Cephalalgia* 17(5):570–579
- Astrup J, Siesjö BK, Symon L (1981) Thresholds in cerebral ischemia – the ischemic penumbra. *Stroke* 12(6):723–725
- Baron JC (2001) Perfusion thresholds in human cerebral ischemia: historical perspective and therapeutic implications. *Cerebrovasc Dis* 11 Suppl 1:2–8
- Baron JC, Bousser MG, Comar D et al (1981) “Crossed cerebellar diaschisis” in human supratentorial brain infarction. *Trans Am Neurol Assoc* 105:459–461
- Barthel H, Hesse S, Dannenberg C et al (2001) Prospective value of perfusion and X-ray attenuation imaging with single-photon emission and transmission computed tomography in acute cerebral ischemia. *Stroke* 32(7):1588–1597
- Beaver J, Finn RD, Hupf HB et al (1976) A new method for the production of high concentration oxygen-15 labeled carbon dioxide with protons. *Appl Radiat Isot* 27:195–197
- Berridge MS, Terries AH, Cassidy EH et al (1990) Low-carrier production of ^{15}O oxygen, water and carbon monoxide. *Appl Radiat Isot* 41:1173–1175
- Boltze J, Forschler A, Nitzsche B et al (2008) Permanent middle cerebral artery occlusion in sheep: a novel large animal model of focal cerebral ischemia. *J Cereb Blood Flow Metab* 28(12):1951–1964

- Bolwig TG, Lassen NA (1975) The diffusion permeability to water of the rat blood-brain barrier. *Acta Physiol Scand* 93(3):415–422
- Brody H (1955) Organization of the cerebral cortex. III. A study of aging in the human cerebral cortex. *J Comp Neurol* 102(2):511–516
- Bruce DA, Langfitt TW, Miller JD et al (1973) Regional cerebral blood flow, intracranial pressure, and brain metabolism in comatose patients. *J Neurosurg* 38(2):131–144
- Calamante F, Morup M, Hansen LK (2004) Defining a local arterial input function for perfusion MRI using independent component analysis. *Magn Reson Med* 52(4):789–797
- Carroll TJ, Teneggi V, Jobin M et al (2002) Absolute quantification of cerebral blood flow with magnetic resonance, reproducibility of the method, and comparison with H215O positron emission tomography. *J Cereb Blood Flow Metab* 22:1149–1156
- Chen JJ, Wieckowska M, Meyer E et al (2008) Cerebral blood flow measurement using fMRI and PET: a cross-validation study. *Int J Biomed Imaging* 2008:516359
- Chiron C, Raynaud C, Maziere B et al (1992) Changes in regional cerebral blood flow during brain maturation in children and adolescents. *J Nucl Med* 33(5):696–703
- Clark JC, Crouzel C, Meyer GJ et al (1987) Current methodology for oxygen-15 production for clinical use. *Int J Rad Appl Instrum A* 38(8):597–600
- Clark JC, Tochon-Danguy H (1991) R2D2, - a bedside [oxygen-15]water infuser. *PSI Proceedings* 92-01, pp 234–235. ISSN 1019-6447. Proc. IV. Int. Workshop on Targetry and Target Chemistry; Sept 9-12th; Villigen, Switzerland, 1991. (Abstract)
- Cohen RM, Andreason PJ, Doudet DJ et al (1997) Opiate receptor avidity and cerebral blood flow in Alzheimer's disease. *J Neurol Sci* 148(2):171–180
- Cutrer FM, O'Donnell A, Sanchez del Rio M (2000) Functional neuroimaging: enhanced understanding of migraine pathophysiology. *Neurology* 55(9 Suppl 2):S36–S45
- Eichling JO, Raichle ME, Grubb RL et al (1974) Evidence of the limitations of water as a freely diffusible tracer in brain of the rhesus monkey. *Circ Res* 35(3):358–364
- Feeney DM, Baron JC (1986) Diaschisis. *Stroke* 17(5):817–830
- Feigin VL, Lawes CMM, Bennett DA et al (2009) Worldwide stroke incidence and early case fatality reported in 56 population-based studies: a systematic review. *Lancet Neurol* 8(4):355–369
- Feng C, Narayana S, Lancaster JL et al (2004) CBF changes during brain activation: fMRI vs. PET. *Neuroimage* 22(1):443–446
- Fox PT, Mintun MA, Reiman EM et al (1988) Enhanced detection of focal brain responses using intersubject averaging and change-distribution analysis of subtracted PET images. *J Cereb Blood Flow Metab* 8(5):642–653
- Frackowiak RS, Lenzi GL, Jones T et al (1980) Quantitative measurement of regional cerebral blood flow and oxygen metabolism in man using 15O and positron emission tomography: theory, procedure, and normal values. *J Comput Assist Tomogr* 4(6):727–736
- Gaillard WD, Fazilat S, White S et al (1995) Interictal metabolism and blood flow are uncoupled in temporal lobe cortex of patients with complex partial epilepsy. *Neurology* 45(10):1841–1847
- Griffiths PD, Hoggard N, Dannels WR et al (2001) In vivo measurement of cerebral blood flow: a review of methods and applications. *Vasc Med* 6(1):51–60
- Hall R (1971) Vascular injuries resulting from arterial puncture of catheterization. *Br J Surg* 58(7):513–516
- Hatakeyama T, Sakaki S, Nakamura K et al (1992) Improvement in local cerebral blood flow measurement in gerbil brains by prevention of postmortem diffusion of 14Ciodoantipyrine. *J Cereb Blood Flow Metab* 12(2):296–300
- Heiss WD, Rosner G (1983) Functional recovery of cortical neurons as related to degree and duration of ischemia. *Ann Neurol* 14(3):294–301
- Heiss WD, Graf R, Wienhard K et al (1994) Dynamic penumbra demonstrated by sequential multitracer PET after middle cerebral artery occlusion in cats. *J Cereb Blood Flow Metab* 14(6):892–902
- Heiss WD, Graf R, Lottgen J et al (1997) Repeat positron emission tomographic studies in transient middle cerebral artery occlusion in cats: residual perfusion and efficacy of postischemic reperfusion. *J Cereb Blood Flow Metab* 17(4):388–400

- Heiss W, Kracht L, Grond M et al (2000) Early [¹¹C]flumazenil/H₂O positron emission tomography predicts irreversible ischemic cortical damage in stroke patients receiving acute thrombolytic therapy. *Stroke* 31(2):366–369
- Herscovitch P, Raichle ME (1985) What is the correct value for the brain–blood partition coefficient for water? *J Cereb Blood Flow Metab* 5(1):65–69
- Herscovitch P, Raichle ME, Kilbourn MR et al (1987) Positron emission tomographic measurement of cerebral blood flow and permeability-surface area product of water using ¹⁵Owater and ¹¹Cbutanol. *J Cereb Blood Flow Metab* 7(5):527–542
- Hino A, Imahori Y, Tenjin H et al (1990) Metabolic and hemodynamic aspects of peritumoral low-density areas in human brain tumor. *Neurosurgery* 26(4):615–621
- Hoeffner EG (2005) Cerebral perfusion imaging. *J Neuroophthalmol* 25(4):313–320
- Ibaraki M, Shimosegawa E, Miura S et al (2004) PET measurements of CBF, OEF, and CMRO₂ without arterial sampling in hyperacute ischemic stroke: method and error analysis. *Ann Nucl Med* 18(1):35–44
- Iida H, Jones T, Miura S (1993) Modeling approach to eliminate the need to separate arterial plasma in oxygen-15 inhalation positron emission tomography. *J Nucl Med* 34(8):1333–1340
- Jay TM, Lucignani G, Crane AM et al (1988) Measurement of local cerebral blood flow with [¹⁴C]iodoantipyrine in the mouse. *J Cereb Blood Flow Metab* 8(1):121–129
- Jeppard P (1998) Advances in perfusion MR imaging. *Radiology* 208(2):296–299
- Kahane P (1999) An H₂¹⁵O-PET study of cerebral blood flow changes during focal epileptic discharges induced by intracerebral electrical stimulation. *Brain* 122(10):1851–1865
- Kanno I, Iida H, Miura S et al (1991) Optimal scan time of oxygen-15-labeled water injection method for measurement of cerebral blood flow. *J Nucl Med* 32(10):1931–1934
- Kety SS, Schmidt CF (1945) The determination of cerebral blood flow in man by use of nitrous oxide in low concentrations. *Am J Physiol* 143:53–66
- Kety SS (1951) The theory and applications of the exchange of inert gas at the lungs and tissues. *Pharmacol Rev* 3:1–41
- Kimura H, Kado H, Koshimoto Y et al (2005) Multislice continuous arterial spin-labeled perfusion MRI in patients with chronic occlusive cerebrovascular disease: a correlative study with CO₂ PET validation. *J Magn Reson Imaging* 22(2):189–198
- Krohn K, Link JM, Lewellen TK et al (1986) The use of 50 MeV protons to produce C-11 and O-15. *J Labelled Compd Radiopharm* 23:1190–1192
- Kudo K, Sasaki M, Yamada K et al (2010) Differences in CT perfusion maps generated by different commercial software: quantitative analysis by using identical source data of acute stroke patients. *Radiology* 254(1):200–209
- Kuge Y, Yokota C, Tagaya M et al (2001) Serial changes in cerebral blood flow and flow-metabolism uncoupling in primates with acute thromboembolic stroke. *J Cereb Blood Flow Metab* 21(3):202–210
- Lammertsma AA (1994) Noninvasive estimation of cerebral blood flow. *J Nucl Med* 35(11):1878–1879
- Lass P, Koseda M, Romanowicz G et al (1998) Cerebral blood flow assessed by brain SPECT with ^{99m}Tc-HMPAO utilising the acetazolamide test in systemic lupus erythematosus. *Nucl Med Rev Cent East Eur* 1(1):20–24
- Lassen NA, Ingvar DH (1961) The blood flow of the cerebral cortex determined by radioactive krypton. *Experientia* 17:42–43
- Law I, Iida H, Holm S et al (2000) Quantitation of regional cerebral blood flow corrected for partial volume effect using O-15 water and PET: II. Normal values and gray matter blood flow response to visual activation. *J Cereb Blood Flow Metab* 20(8):1252–1263
- Leenders KL (1994) PET: blood flow and oxygen consumption in brain tumors. *J Neurooncol* 22(3):269–273
- Links JM, Zubieta JK, Meltzer CC et al (1996) Influence of spatially heterogeneous background activity on “hot object” quantitation in brain emission computed tomography. *J Comput Assist Tomogr* 20(4):680–687
- Machleder HI, Sweeney JP, Barker WF (1972) Pulseless arm after brachial-artery catheterisation. *Lancet* 1(7747):407–409

- Markus HS (2004) Cerebral perfusion and stroke. *J Neurol Neurosurg Psychiatry* 75(3):353–361
- Martin WR, Powers WJ, Raichle ME (1987) Cerebral blood volume measured with inhaled C15O and positron emission tomography. *J Cereb Blood Flow Metab* 7(4):421–426
- Matsuda M, Lee H, Kuribayashi K et al (1996) Comparative study of regional cerebral blood flow values measured by Xe CT and Xe SPECT. *Acta Neurol Scand Suppl* 166:13–16
- Matthew E, Andreason P, Carson RE et al (1993) Reproducibility of resting cerebral blood flow measurements with H2(15)O positron emission tomography in humans. *J Cereb Blood Flow Metab* 13(5):748–754
- Meier P, Zierler KL (1954) On the theory of the indicator-dilution method for measurement of blood flow and volume. *J Appl Physiol* 6(12):731–744
- Mulholland GK, Kilbourn MR, Moskwa JJ (1990) Direct simultaneous production of 15Owater and 13Nammonia or 18Ffluoride ion by 26 MeV proton irradiation of a double chamber water target. *Int J Rad Appl Instrum A* 41(12):1193–1199
- Obrist WD, Thompson HK JR, Wang HS et al (1975) Regional cerebral blood flow estimated by 133-xenon inhalation. *Stroke* 6(3):245–256
- Ostergaard L, Weisskoff RM, Chesler DA et al (1996a) High resolution measurement of cerebral blood flow using intravascular tracer bolus passages. Part I: mathematical approach and statistical analysis. *Magn Reson Med* 36(5):715–725
- Ostergaard L, Sorensen AG, Kwong KK et al (1996b) High resolution measurement of cerebral blood flow using intravascular tracer bolus passages. Part II: experimental comparison and preliminary results. *Magn Reson Med* 36(5):726–736
- Pantano P, Baron JC, Lebrun-Grandie P et al (1984) Regional cerebral blood flow and oxygen consumption in human aging. *Stroke* 15(4):635–641
- Pappata S, Fiorelli M, Rommel T et al (1993) PET study of changes in local brain hemodynamics and oxygen metabolism after unilateral middle cerebral artery occlusion in baboons. *J Cereb Blood Flow Metab* 13(3):416–424
- Petersen ET, Zimine I, Ho YL et al (2006) Non-invasive measurement of perfusion: a critical review of arterial spin labelling techniques. *Br J Radiol* 79(944):688–701
- Peterson EC, Wang Z, Britz G (2011) Regulation of cerebral blood flow. *Int J Vasc Med* 2011:1–8
- Pinzola RR, Yonas H (1998) The xenon-enhanced computed tomography cerebral blood flow method. *Neurosurgery* 43(6):1488–1492
- Powell J, O'Neil JP (2006) Production of 15Owater at low-energy proton cyclotrons. *Appl Radiat Isot* 64(7):755–759
- Ragland JD, Gur RC, Raz J, et al (2001) Effect of schizophrenia on frontotemporal activity during word encoding and recognition: a PET cerebral blood flow study. *Am J Psychiatry* 158(7):1114–1125
- Raichle ME, Martin WR, Herscovitch P et al (1983) Brain blood flow measured with intravenous H2(15)O. II. Implementation and validation. *J Nucl Med* 24(9):790–798
- Rousset OG, Ma Y, Evans AC (1998) Correction for partial volume effects in PET: principle and validation. *J Nucl Med* 39(5):904–911
- Roy CS, Sherrington CS (1890) On the regulation of the blood-supply of the brain. *J Physiol* 11(1–2):85–158
- Sajjad M, Liow JS, Moreno-Cantu J (2000) A system for continuous production and infusion of 15OH2O for PET activation studies. *Appl Radiat Isot* 52(2):205–210
- Sakoh M, Rohl L, Gyldensted C et al (2000a) Cerebral blood flow and blood volume measured by magnetic resonance imaging bolus tracking after acute stroke in pigs: comparison with [15O] H2O positron emission tomography. *Stroke* 31(8):1958–1964
- Sakoh M, Ostergaard L, Røhl L et al (2000b) Relationship between residual cerebral blood flow and oxygen metabolism as predictive of ischemic tissue viability: sequential multitracer positron emission tomography scanning of middle cerebral artery occlusion during the critical first 6 hours after stroke in pigs. *J Neurosurg* 93(4):647–657
- Sakai Y, Kasuga T, Nakanishi F et al (1987) Cerebral blood flow study by 133Xe inhalation and single photon emission CT in occlusive cerebrovascular diseases. *Kaku Igaku* 24(1):47–54

- Skyhøj Olsen T, Larsen B, Bech Skriver E et al (1981) Focal cerebral ischemia measured by the intra-arterial ^{133}Xe method. Limitations of 2-dimensional blood flow measurements. *Stroke* 12(6):736–744
- Slosman DO, Chicherio C, Ludwig C et al (2001) ^{133}Xe SPECT cerebral blood flow study in a healthy population: determination of T-scores. *J Nucl Med* 42(6):864–870
- Sokoloff L, Perlín S, Kornetsky C et al (1957) The effects of D-lysergic acid diethylamide on cerebral circulation and overall metabolism. *Ann N Y Acad Sci* 66(3):468–477
- Szabo CA, Narayana S, Kochunov PV et al (2007) PET imaging in the photosensitive baboon: case-controlled study. *Epilepsia* 48(2):245–253
- Tomura N, Kato T, Kanno I et al (1993) Increased blood flow in human brain tumor after administration of angiotensin II: demonstration by PET. *Comput Med Imaging Graph* 17(6):443–449
- Terpolilli NA, Kim S, Thal SC et al (2012) Inhalation of nitric oxide prevents ischemic brain damage in experimental stroke by selective dilatation of collateral arterioles. *Circ Res* 110(5):727–738
- van Naemen J, Monclus M, Damhaut P et al (1996) Production, automatic delivery and bolus injection of ^{15}O water for positron emission tomography studies. *Nucl Med Biol* 23(4):413–416
- van Osch MJ, Voncken EJ, Bakker CJ et al (2001) Correcting partial volume artifacts of the arterial input function in quantitative cerebral perfusion MRI. *Magn Reson Med* 45(3):477–485
- Veall N, Mallett BL (1967) The ^{133}Xe inhalation technique for regional cerebral blood flow studies. *Strahlentherapie Sonderb* 65:166–173
- Villringer A, Dirnagl U (1995) Coupling of brain activity and cerebral blood flow: basis of functional neuroimaging. *Cerebrovasc Brain Metab Rev* 7(3):240–276
- Wakita K, Imahori Y, Ido T et al (2000) Simplification for measuring input function of FDG PET: investigation of 1-point blood sampling method. *J Nucl Med* 41(9):1484–1490
- Watabe H, Itoh M, Cunningham V et al (1996) Noninvasive quantification of rCBF using positron emission tomography. *J Cereb Blood Flow Metab* 16:311–319
- Wintermark M, Sesay M, Barbier E et al (2005) Comparative overview of brain perfusion imaging techniques. *J Neuroradiol* 32(5):294–314
- Worsley KJ, Evans AC, Marrett S et al (1992) A three-dimensional statistical analysis for CBF activation studies in human brain. *J Cereb Blood Flow Metab* 12(6):900–918
- Yao H, Sadoshima S, Kuwabara Y et al (1990) Cerebral blood flow and oxygen metabolism in patients with vascular dementia of the Binswanger type. *Stroke* 21(12):1694–1699
- Zanotti-Fregonara P, Chen K, Liow J et al (2011) Image-derived input function for brain PET studies: many challenges and few opportunities. *J Cereb Blood Flow Metab* 31(10):1986–1998
- Zaro-Weber O, Moeller-Hartmann W, Heiss W et al (2010a) Maps of time to maximum and time to peak for mismatch definition in clinical stroke studies validated with positron emission tomography. *Stroke* 41(12):2817–2821
- Zaro-Weber O, Moeller-Hartmann W, Heiss W et al (2010b) MRI perfusion maps in acute stroke validated with ^{15}O -water positron emission tomography. *Stroke* 41(3):443–449
- Zaro-Weber O, Moeller-Hartmann W, Heiss W et al (2012) Influence of the arterial input function on absolute and relative perfusion-weighted imaging penumbral flow detection: a validation with ^{15}O -water positron emission tomography. *Stroke* 43(2):378–385
- Zierler K (1962) Theoretical basis of indicator-dilution methods for measuring flow and volume. *Circ Res* 10:393–407

Shana Elman and David H. Lewis

Contents

5.1	Indications	126
5.2	Radiopharmaceuticals.....	131
5.2.1	¹³³ Xenon (¹³³ Xe).....	132
5.2.2	¹²³ I-Isopropylidoamphetamine (¹²³ I-IMP).....	132
5.2.3	^{99m} Tc-Hexamethyl Propylene Amine Oxime (HMPAO) and ^{99m} Tc-Ethyl Cysteinate Dimer (ECD)	132
5.3	Patient Preparation.....	134
5.4	Imaging Technique	135
5.4.1	Camera Requirements and Image Acquisition.....	135
5.4.2	Interventional Studies.....	136
5.4.3	Image Reconstruction and Post-Processing	140
5.5	Interpretation and Reporting.....	143
	References.....	145

Abstract

Brain perfusion SPECT (single-photon emission computed tomography) is a noninvasive molecular imaging technique in which gamma photons emitted from an injected radioactive tracer allow three-dimensional estimation of regional cerebral blood flow (rCBF). The technique is similar to that of a CT scan, except that the radiation source that is imaged is internal to the patient, thereby allowing for acquisition of functional data. This allows identification of regional hypoperfusion to aid in diagnosis of cerebrovascular disorders and neurologic and neurodegenerative disorders. This chapter describes the technical aspects of performing brain perfusion SPECT, as well as a brief overview of the established clinical and investigational indications for brain perfusion SPECT.

S. Elman, MD (✉) • D.H. Lewis, MD
 Division of Nuclear Medicine, Department of Radiology, University of Washington
 Medical Center, 1959 NE Pacific Street, Box 357115, Seattle, WA 98195-7115, USA
 e-mail: shana01@uw.edu; lewis@uw.edu

Brain perfusion SPECT (single-photon emission computed tomography) is a noninvasive molecular imaging technique in which gamma photons emitted from an injected radioactive tracer allow three-dimensional estimation of regional cerebral blood flow (rCBF). This allows identification of regional hypoperfusion due to vascular etiologies (e.g., stroke, subarachnoid hemorrhage-associated vasospasm, moyamoya disease, trauma). In addition, cerebral perfusion and metabolism are coupled in most physiologic and pathologic conditions, with a few exceptions (e.g., subacute stroke and some brain tumors due to disruption of the blood-brain-barrier). Therefore, rCBF can be utilized to identify abnormalities in brain metabolism and neuronal activity (Miller and Bell 1987). Accordingly, interpretation of relative perfusion differences allows characterization of abnormal brain function in the gray matter of cerebral cortical and subcortical structures, brainstem, and cerebellum (Catafau 2001). With the emergence of radiotracers targeted specifically to neurotransmitters, functional imaging of neurodegenerative diseases for which specific neurotransmitter abnormalities have been identified has also become possible (e.g., targeting of the dopamine transporter in Parkinson's disease and parkinsonism). However, this topic of neurotransmission SPECT is beyond the scope of this chapter and will be covered elsewhere in this text.

The information provided by brain perfusion SPECT is often complementary to the anatomic detail provided by structural neuroimaging techniques such as computed tomography (CT), magnetic resonance imaging (MRI), and ultrasound, particularly when the findings of these imaging modalities are equivocal. Furthermore, brain perfusion SPECT may identify abnormalities even before structural neuroimaging because functional impairment in cerebral diseases often precedes or, in some cases, may be independent of structural changes imaged by other modalities. Compared to the alternative nuclear medicine functional imaging modality, ^{18}F -fluorodeoxyglucose (FDG) positron emission tomography (PET) imaging, brain SPECT has inferior intrinsic spatial resolution. However, the temporal resolution of brain perfusion SPECT is superior to ^{18}F -FDG PET, enabling the characterization of brief neurologic events, like seizures. In addition, perfusion SPECT is relatively simple to perform, is widely available, and tends to be less expensive than PET. Therefore, brain SPECT maintains an important role in the diagnosis, therapeutic management, and follow-up of patients. Finally, SPECT is a useful tool for research in diseases involving the brain, because it is widely available and provides noninvasive in vivo assessment of human brain function.

5.1 Indications

Brain perfusion SPECT is helpful in the diagnosis of neurodegenerative (e.g., dementia), neurologic (e.g., epilepsy), cerebrovascular disorders, and traumatic brain injury (Table 5.1). In particular, SPECT imaging is often useful in confirming the underlying diagnosis when neurologic or neuropsychiatric symptoms cannot be definitively explained by structural neuroimaging findings. Brain SPECT has also been used in the research setting to characterize a number of brain disorders,

Table 5.1 Indications for brain perfusion SPECT

Clinical indication	Typical brain perfusion SPECT findings
Differential diagnosis in dementia (Borghesani et al. 2010)	
Alzheimer's disease (AD)	Hypoperfusion of bilateral temporoparietal association cortices (often asymmetric) with characteristic sparing of the primary sensorimotor cortex, primary visual cortex, and basal ganglia. Early changes also include hypoperfusion of the posterior cingulate (Bradley et al. 2002; Devous 2002; Bonte et al. 2004) (Fig. 5.1). In later stages, the frontal cortex may also show hypoperfusion (Brown et al. 1996; Bradley et al. 2002)
Dementia with Lewy bodies (DLB)	Main differentiating feature from AD is occipital hypoperfusion (Lobotesis et al. 2001). Similar to AD, may have mild perfusion deficit in temporoparietal and frontal regions, but, unlike AD, DLB usually spares medial temporal lobes (Fig. 5.2). Additional findings of hyperperfusion in the thalamus and bilateral striatum may strengthen the accuracy of the diagnosis of DLB (Shimizu et al. 2008) Because of the loss of dopaminergic neurons in the nigrostriatal pathway, DaTSCAN SPECT imaging can also be performed to enhance diagnostic accuracy of DLB and differentiate this parkinsonian syndrome from AD (Papathanasiou et al. 2012)
Multi-infarct dementia	Multiple, randomly distributed focal areas of hypoperfusion. Hypoperfusion of motor and sensory cortices, although not always involved, can help to differentiate multi-infarct dementia from AD. Correlation with anatomic images, e.g., CT or MRI, is extremely important, as cortical or subcortical infarcts may be seen increasing the confidence in diagnosis. Subcortical infarcts alone, without cortical lesions on CT, can explain nearby cortical perfusion defects by disconnection between cortical and subcortical neurons. The Binswanger type of dementia, a rare variant of vascular dementia, is a gradually progressive syndrome caused by diffuse or patchy ischemic events to the deep white matter. The magnitude of cortical hypoperfusion has been shown to correlate with the severity of the disease (Tohgi et al. 1991)
Frontotemporal dementia (FTD)	Perfusion deficits in orbitofrontal area and temporal lobes, often asymmetric (Fig. 5.5). Basal ganglia may also be hypoperfused. When the right temporal lobe is involved, behavioral disturbances are usually a prominent clinical feature; aphasia is more frequent when the left temporal lobe is involved. In Pick's disease, the frontal lobe is more affected than temporal lobe, with relatively symmetric hypoperfusion of the frontal lobes often extending to the cingulate gyrus (Miller et al. 1991)
Parkinson's disease (PD) and other parkinsonian disorders	There is no consensus on a specific brain perfusion SPECT pattern in Parkinson's disease or other parkinsonian disorders. However, generalized hypoperfusion of the cortex has been described. Brain perfusion SPECT is most useful to differentiate PD from the causes of dementia listed above. Demented PD patients and AD patients may share a common pattern of marked posterior hypoperfusion. However, the defects are more prominent and extensive in AD (Spampinato et al. 1991) As with DLB, DaTSCAN SPECT imaging is extremely helpful in confirming the diagnosis of parkinsonian disorders because of the loss of dopaminergic neurons in the nigrostriatal pathway (Fig. 5.3)

(continued)

Table 5.1 (continued)

Clinical indication	Typical brain perfusion SPECT findings
Huntington's disease (HD)	Decreased or absent tracer uptake in the bilateral caudate nucleus or basal ganglia, not necessarily symmetric. The sensitivity of brain SPECT with perfusion agents in HD has been high, even in patients with normal CT or MRI findings. Decreased caudate nuclei uptake has also been reported for several individuals at risk of HD who have undergone brain SPECT with perfusion tracers prior to onset of symptoms (Ichise et al. 1993). Brain perfusion SPECT findings may also be combined with DaTSCAN SPECT to enhance diagnostic accuracy
TIA/stroke (Masdeu and Brass 1995; Ueda and Yuh 2005)	
Detection of acute ischemia (Ueda and Yuh 2005)	Focal or regional area of absent perfusion or hypoperfusion immediately following the ischemic event. In early acute ischemia, changes can be seen on brain perfusion SPECT that are not yet visible on CT or MRI, making this a modality of choice in the first few hours following the event. The hypoperfused region on SPECT will generally be larger than the lesion that eventually becomes visible on CT or MRI. Crossed cerebellar diaschisis is frequent in cortical strokes and is caused by disconnection of the cerebellar–corticopontine fibers as a consequence of ischemia or stroke. With either ^{99m}Tc -HMPAO or ^{99m}Tc -ECD, the perfusion defect will be fixed; however, with ^{123}I -IMP, redistribution with partial reperfusion may occur. The timing of the study is important as the sensitivity for stroke localization may decrease as the stroke evolves due to the luxury perfusion phenomenon. Focal hyperperfusion of the lesion secondary to relative hyperemia can be seen at days 1–5 following the ischemia event and persist as long as 20 days. By 30 days following the initial ischemic event, the hypoperfused area should easily be detected again. Between the hyperemic and the delayed hypoperfusion phases, study findings may appear normal. Luxury perfusion may be easier to detect with ^{99m}Tc -HMPAO than with ^{99m}Tc -ECD (Miyazawa et al. 1998). False-negative brain perfusion SPECT findings can frequently occur in lacunar or small cortical infarcts
Vasospasm following SAH (Rajendran et al. 2001; Mustonen et al. 2008; Cooke et al. 2010)	Focally or regionally absent perfusion or hypoperfusion at the site of vasospasm. Findings correlate well with the severity and magnitude of neurologic deficits in the evolution of the condition. A follow-up post-interventional study should be obtained to confirm restoration of perfusion to the affected region
Candidacy for fibrinolytic therapy (Alexandrov et al. 1996)	Mild to moderate hypoperfusion in the vascular distribution of an acute stroke confers favorable outcome from fibrinolytic therapy. Complete absence of tracer uptake in the vascular distribution of the stroke suggests poor prognosis and is associated with an increased rate of hemorrhagic complication from fibrinolytic therapy. A normal brain SPECT image in a patient with CT or MRI evidence of stroke implies preexisting effective collateral circulation with favorable prognosis whether fibrinolytic therapy is used or not

Table 5.1 (continued)

Clinical indication	Typical brain perfusion SPECT findings
Epilepsy (Spencer 1994; Markand et al. 1995; Devous et al. 1998)	
Presurgical ictal detection of seizure focus (Won et al. 1996; Devous et al. 1998)	<p>Focal hyperperfusion at the epileptogenic focus may be seen, particularly in temporal lobe epilepsy (Fig. 5.4). Hyperperfusion may extend to the ipsilateral basal ganglia and thalamus and possibly also into the ipsilateral motor cortex and contralateral cerebellar cortex. Crossed cerebellar hyperperfusion of the contralateral cerebellum has been reported in up to 75 % of ictal studies for temporal lobe epilepsy, providing increased confidence in lateralization of the seizure focus. In frontal lobe seizures, the difficulty in detecting the epileptogenic focus is caused by the short duration of the seizure and the magnitude of hyperperfusion, which is frequently less than that of temporal lobe epilepsy.</p> <p>As described in the Seizure Imaging section, ictal images should always be interpreted in comparison with the interictal images, as subtle hyperperfusion relative to interictal hypoperfusion at the same site may only be appreciated when viewing the ictal and interictal images simultaneously or when using software to compare quantifiable differences in regional cerebral brain flow.</p>
Interictal detection of seizure focus (Devous et al. 1998)	<p>Interictal SPECT images may show focal or diffuse hypoperfusion of the epileptic focus. However, in approximately 50 % of patients, the interictal SPECT will be normal without any perfusion abnormalities. The sensitivity of interictal brain SPECT alone is relatively low at 44 %; therefore, interictal images should be interpreted in conjunction with ictal images whenever possible to identify foci of increased perfusion in the ictal state that were normal or hypoperfused in the interictal state.</p>
Brain death (Al-Shammri and Al-Feeli 2004)	<p>Absent cerebral and cerebellar perfusion supports the clinical diagnosis of brain death. Planar images can generally confirm the absence of intracranial perfusion; however, SPECT may be useful in equivocal cases, particularly to differentiate persistent cerebral perfusion from hyperperfusion to overlying soft tissue injuries.</p>
Traumatic brain injury (Masdeu et al. 1995; Society of Nuclear Medicine Brain Imaging Council 1996; Jacobs et al. 1996; Hattori et al. 2009)	<p>Brain perfusion SPECT is more sensitive than either CT or MRI in detection of brain abnormalities, especially in the acute (<24 h) phase following head injury. Brain SPECT will often show focal, multifocal, or regional areas of hypoperfusion that correlate well with the neurologic status of the patient.</p> <p>Focal cerebral hyperemia after head injury was associated with a lower mortality rate and better outcome than was lack of hyperemia after head injury. Also, normal brain SPECT findings were found to be a reliable tool in the exclusion of the clinical sequelae of mild head injury.</p>

including psychiatric and infectious disorders. Although interesting results have been shown in these studies, routine use of brain perfusion SPECT in these latter diagnoses is not well established and remains investigational at this time. Large, well-designed, and controlled trials on brain SPECT imaging are necessary before research results in neuropsychiatric diseases can be applied in clinical practice. Nonetheless, given the common comorbidity of psychiatric disease in the

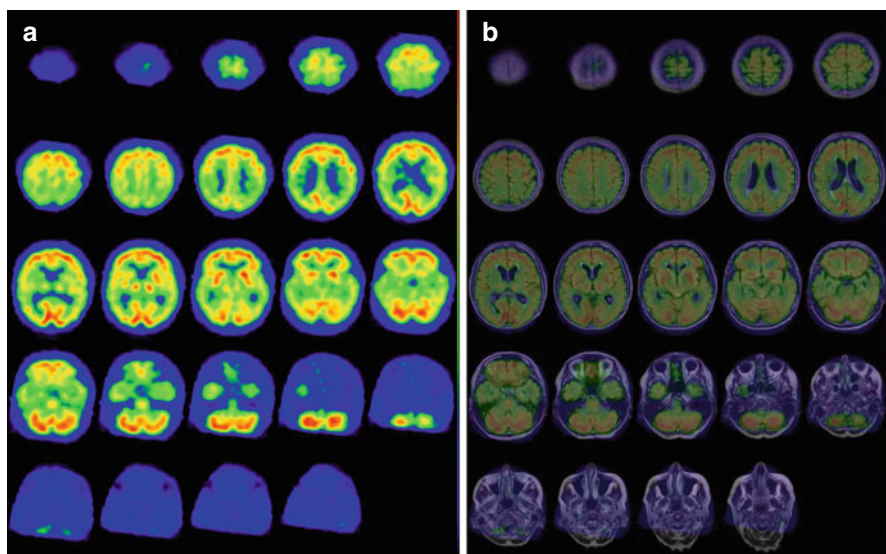


Fig. 5.1 In an 81-year-old woman with progressive cognitive decline and Mini-Mental Status Exam score=24/30, (a) transaxial ^{99m}Tc -HMPAO SPECT images show severe hypoperfusion in the temporoparietal association cortices and posterior cingulate, with sparing of the occipital cortex, sensorimotor cortex, basal ganglia, thalamus, and cerebellum, consistent with a diagnosis of Alzheimer's disease. (b) Fusion of SPECT with MRI confirms the above findings and demonstrates mild gross cerebral atrophy and white matter changes suggestive of concomitant microvascular disease, a common comorbidity in this population

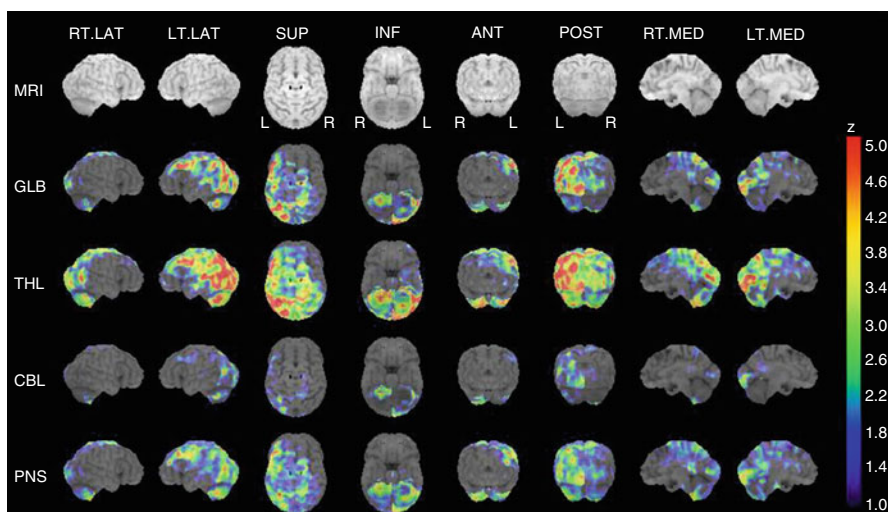


Fig. 5.2 In a 70-year-old man with dementia, 3D-SSP reconstruction of ^{99m}Tc -HMPAO brain SPECT images demonstrates generalized hypoperfusion, left greater than right, with profound hypoperfusion in bilateral parieto-occipital regions, consistent with Lewy body dementia. Involvement of the occipital cortices is often the key element differentiating this diagnosis from Alzheimer's disease

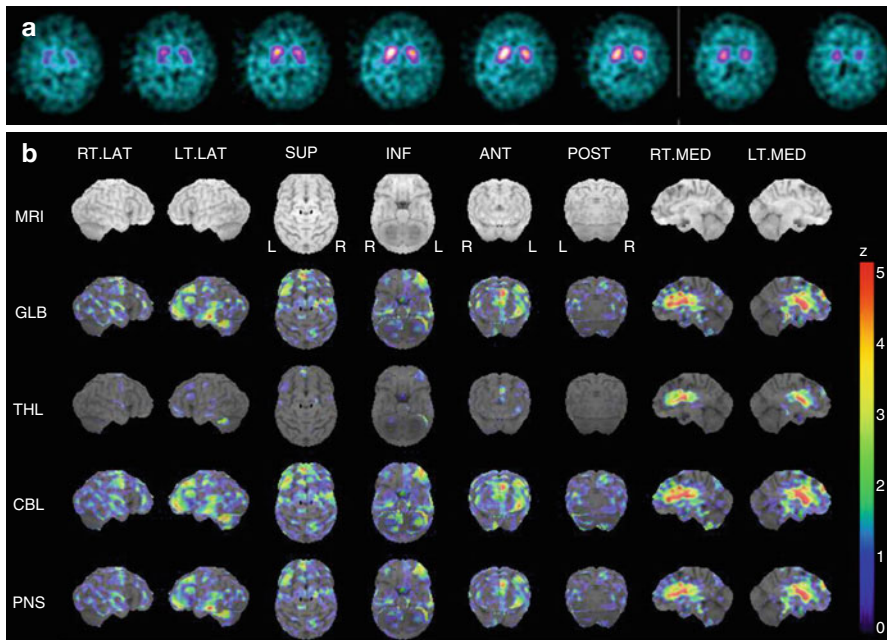


Fig. 5.3 In a 55-year-old man with rigidity, (a) transaxial DaTSCAN SPECT images show mild reduction of radiotracer uptake in the bilateral putamen, left more severe than right, confirming mild nigrostriatal degeneration typically seen in idiopathic Parkinson's disease or related parkinsonian disorders. (b) 3D-SSP reconstruction of ^{99m}Tc -HMPAO brain SPECT demonstrates hypoperfusion in the frontal and anterior temporal lobe as well as in the upper brainstem and thalamus, providing further differentiation between the subtypes of parkinsonian disorders. Involvement of the upper brainstem seen on brain perfusion SPECT, combined with the findings of nigrostriatal degeneration seen on brain DaTSCAN, leads to the diagnosis of progressive supranuclear palsy

populations undergoing functional neuroimaging, it is important to understand the typical patterns of brain SPECT imaging for various neurologic and psychiatric diseases (e.g., major depression) to appreciate the impact that comorbid disorders might have in image interpretation for the other clinically validated uses.

5.2 Radiopharmaceuticals

In order to be used for estimation of rCBF in brain perfusion SPECT imaging, a radiopharmaceutical must meet the following criteria:

1. It must cross the blood–brain barrier (BBB).
2. It must be retained within the brain long enough for images to be obtained and ideally will retain the initial distribution pattern of uptake without undergoing redistribution.
3. Extraction of the radiotracer must be equal to or proportional to actual rCBF to provide an accurate estimate of blood flow.

5.2.1 ^{133}Xe (^{133}Xe)

Historically, the gold standard radiopharmaceutical for rCBF quantification was the diffusible gas ^{133}Xe . By measuring cerebral washout of the inhaled ^{133}Xe , an absolute rCBF value can be obtained (mL/min/100 g tissue). However, this radiopharmaceutical has several limitations that have restricted its use in clinical practice. Due to the rapid clearance of ^{133}Xe , a short acquisition time (around 5 min during the inhalation of the ^{133}Xe gas) necessitates dynamic SPECT instrumentation, which provides high-sensitivity but low-resolution SPECT images. In addition, the low gamma-ray energy of ^{133}Xe results in marked attenuation of deep structures, which makes this isotope less than optimal to obtain good-quality SPECT images. Finally, because ^{133}Xe inhalation requires active cooperation, patients with respiratory or severe cognitive impairment may not be studied adequately.

Several other radiopharmaceuticals, such as ^{123}I -labeled amines and technetium-labeled compounds, can offer higher-resolution SPECT images with the use of conventional rotating gamma cameras. However, these more commonly used radiotracers require generation of arterial input functions via blood sampling and extraction techniques to estimate rCBF (Tsuchida et al. 1997) rather than providing an absolute rCBF value.

5.2.2 ^{123}I -Isopropylidoamphetamine (^{123}I -IMP)

Among the initially used ^{123}I -labeled amines, ^{123}I -IMP (IK-3; CIS Bio-International, Gif-Sur-Yvette, France) has been the most frequently used. The typical adult dose is 5 mCi, representing an effective dose of approximately 3.53 mSv. After crossing the intact blood–brain barrier, ^{123}I -IMP binds to amphetamine receptors on neurons. This radiopharmaceutical has good characteristics for brain perfusion SPECT. However, peak brain activity is reached as late as 20 min after injection. In addition, ^{123}I -IMP shows redistribution over time such that there is reuptake by the cerebral cortex that is not proportional to blood flow. These latter characteristics, in addition to the high cost and poor availability of ^{123}I -labeled compounds, have contributed to the current predominant use of technetium compounds for brain perfusion SPECT examinations.

5.2.3 $^{99\text{m}}\text{Tc}$ -Hexamethyl Propylene Amine Oxime (HMPAO) and $^{99\text{m}}\text{Tc}$ -Ethyl Cysteinate Dimer (ECD)

Two virtually interchangeable technetium-labeled compounds are primarily used for brain perfusion imaging (Table 5.2): technetium-99 m ($^{99\text{m}}\text{Tc}$) hexamethyl propylene amine oxime (HMPAO; CeretecTM; GE Healthcare, Buckinghamshire, United Kingdom) and $^{99\text{m}}\text{Tc}$ -ethyl cysteinate dimer (ECD; NeuroliteTM; Lantheus, MA, USA). The doses used in adults are typically 20 mCi (740 MBq) for $^{99\text{m}}\text{Tc}$ -HMPAO and 30 mCi (1,100 MBq) for $^{99\text{m}}\text{Tc}$ -ECD, representing effective doses of 0.0093 and 0.011 mSv/MBq, respectively. These compounds have several advantages over ^{123}I -IMP. The peak brain activity is reached faster (within 2 min

Table 5.2 ^{99m}Tc -labeled radiopharmaceuticals for brain perfusion SPECT imaging

	^{99m}Tc -HMPAO	^{99m}Tc -ECD
Radiopharmaceutical dose	740 MBq (20 mCi)	1,000 MBq (30 mCi)
Effective whole body dose	0.0093 mSv/MBq	0.011 mSv/MBq
Stability/labeling issues	Highly unstable in vitro; high radiochemical purity must be assured before injection because only a small proportion of injected dose will reach the brain. Stabilized forms of ^{99m}Tc -HMPAO using either methylene blue or cobalt chloride have recently become available and allow easier labeling and improvement of image quality by reducing background activity	Stable up to at least 4 h in vitro and freshly eluted ^{99m}Tc is not required. However, the labeling procedure is longer, taking about 30 min
Maximal tracer uptake	Cerebellum	Calcarine cortex
Response to cerebral perfusion–metabolic uncoupling	Increased uptake may occur at site of infarct, called the “luxury” perfusion phenomenon	Uptake usually remains low, more accurately reflecting hypometabolism at the site of infarct. “Luxury” perfusion is rare

Twenty milliCuries (mCi) (740 MBq) for ^{99m}Tc -HMPAO and 30 mCi (1,100 MBq) for ^{99m}Tc -ECD, representing effective doses of 0.0093 and 0.011 mSv/MBq, respectively

after injection), and there is no redistribution, so the initial tracer uptake and distribution, which are proportional to rCBF at the time of injection, remain unchanged up to at least 2 h, independent of rCBF variations occurring after the fixation time. Accordingly, the tracer can be injected while the subject is performing a specific task, when seizure activity starts, or at the moment of maximum central effect of a drug, so that SPECT images reflect the rCBF distribution at the time of injection, independent of the timing of SPECT acquisition. Thus, the tracer can be injected into the patient outside the nuclear medicine facility, and images can be acquired later providing a “snapshot” of rCBF at the time of injection. This offers an advantage over PET or MRI, because patients do not need to stay positioned in the imaging device with the head fixed while performing tasks to allow simultaneous image acquisition, as is necessary with these other modalities.

The mechanism underlying the fixation of these radiotracers within the intracellular space is due to their highly lipophilic nature which allows them to easily cross the blood–brain barrier where they undergo rapid cellular localization by diffusion. These agents are then converted into hydrophilic compounds after entering the brain, causing them to become “fixed” intracellularly. As well, the ability to obtain delayed images is beneficial in cases in which sedation must be used, as sedating agents can be administered after the injection without compromising the images. Although both ^{99m}Tc -HMPAO and ^{99m}Tc -ECD are distributed proportionally to rCBF, their retention is not completely linear with rCBF because of an initial back diffusion. Accordingly, compared to ^{133}Xe , high blood flow may be underestimated, and low blood flow may be overestimated with both tracers (Devous et al. 1993; Payne et al. 1996).

The main differences between ^{99m}Tc -HMPAO and ^{99m}Tc -ECD relate to their *in vitro* stability, dosimetry, and uptake mechanism. ^{99m}Tc -HMPAO is highly unstable *in vitro*. Moreover, high radiochemical purity must be assured before injection, because only a small proportion of the injected dose will reach the brain. This purity is not difficult to achieve if the timing of the labeling process is done properly, as follows: time since the last generator elution <24 h; time since the ^{99m}Tc dose was eluted <2 h; and time since the cold vial was labeled with fresh ^{99m}Tc <20 min. Older labeling methods advised against mixture of ^{99m}Tc -HMPAO with blood during intravenous injection because the lipophilic compound enters into red blood cells. Stabilized forms of ^{99m}Tc -HMPAO using either methylene blue or cobalt chloride have recently become available and allow easier labeling and improvement of image quality by reducing background activity. By contrast, ^{99m}Tc -ECD is stable up to at least 4 h *in vitro*, and freshly eluted ^{99m}Tc is not required. However, the labeling procedure is longer, taking about 30 min.

The dosimetry for ^{99m}Tc -ECD is more favorable compared to ^{99m}Tc -HMPAO due to rapid urinary excretion of ^{99m}Tc -ECD, allowing for higher doses of ^{99m}Tc -ECD to be administered. The dosimetry is similar to lower doses of ^{99m}Tc -HMPAO if patients are instructed to force diuresis and void after the scan procedure. The use of higher doses, together with the higher gray-matter-to-white-matter ratio, contributes to the better image quality obtained with ^{99m}Tc -ECD in comparison with ^{99m}Tc -HMPAO.

In normal brain tissue, the kinetic properties are similar for ^{99m}Tc -ECD and ^{99m}Tc -HMPAO. However, in patients with brain disease, the distribution of these compounds may differ because of the biochemistry of lipophilic-to-hydrophilic conversion. In ^{99m}Tc -ECD, the hydrophilic conversion is related to de-esterification of the compound, requiring enzymatic function in the cell. For ^{99m}Tc -HMPAO, instability of the lipophilic form with intracellular conversion to hydrophilic form via glutathione interaction has been proposed. Therefore, ^{99m}Tc -ECD would have a predominant cellular–metabolic uptake mechanism of retention, while ^{99m}Tc -HMPAO would reflect only blood flow to cerebral regions. This situation accounts for slight differences in the normal SPECT pattern (e.g., the cerebellum tends to have maximal tracer uptake with HMPAO, as opposed to the calcarine cortex with ECD), and it is one of the explanations suggested for the different behavior of these tracers in subacute stroke. For episodes of cerebral perfusion–metabolic uncoupling, increased ^{99m}Tc -HMPAO uptake may occur, thus reflecting the “luxury” perfusion phenomenon, whereas ^{99m}Tc -ECD uptake usually remains low during this period, reflecting hypometabolism at the site of infarct.

5.3 Patient Preparation

For optimal imaging, patient preparation is an important consideration, with particular attention paid to environmental conditions, patient cooperation, and patient positioning.

Because of the sensitivity of brain perfusion SPECT in detecting rCBF changes coupled with neuronal activity, sensorial and cognitive stimuli must be kept at a

minimum level during tracer injection and uptake. Injection in a quiet room and no interaction with patients at this time is desirable. For each patient, the room conditions should be consistent during tracer injection and uptake. Injection conditions should be well recorded and should be considered during image interpretation as various modifications can affect the radiotracer uptake pattern. For example, if the patient's eyes are open in a bright room during injection, increased radiotracer uptake in the calcarine cortex is an expected SPECT pattern. On the other hand, if the patient's eyes are closed in a dimly lit room during injection, the uptake will still usually be high but not as high as in a visually stimulated state.

Patient cooperation is of particular importance to minimize head movement which will limit motion artifact and ultimately result in better quality images. To avoid head movement during scanning (20–30 min), the patient should be made comfortable prior to image acquisition. Bladder voiding, a pad under the knees, and a blanket are simple measures that can greatly improve patient comfort and encourage patient cooperation. Belts at the forearm level or a sheet wrapped around the patient's arms can help to hold the patient's arms to minimize arm fatigue and reduce patient motion. Patients with severe cognitive impairment or dementia may need sedation or constant observation and reminders to not move during scan. If a technetium-99 m radiopharmaceutical (HMPAO or ECD) is used, tracer injection must precede sedation to avoid sedation-induced metabolism/blood flow changes in the SPECT images, as described above.

Patient positioning relation to the collimators also largely contributes to the final quality of SPECT images. Measures should be taken to place the collimators as close as possible to the patient's head to improve spatial resolution and sensitivity. Techniques include excluding shoulders from the field of view and keeping the head in flexion to reduce the radius of rotation to a minimum. Lowering the chin to the chest helps to include the entire cerebellum within the field of view and allows a better reorientation plane for oblique slices during reconstruction.

5.4 Imaging Technique

5.4.1 Camera Requirements and Image Acquisition

SPECT imaging is obtained using a gamma camera with rotating camera heads, which allows three-dimensional reconstruction with isotropic voxels of images in the axial, coronal, and sagittal projections, as well as three-dimensional reconstructions important for volumetric statistical analyses. The technique is similar to that of a CT scan, except that the radiation source that is imaged is internal to the patient, thereby allowing for acquisition of functional data.

Due to the small size of important anatomically and functionally independent cerebral structures, spatial resolution is the main concern in brain imaging. The typical spatial resolution of SPECT studies should be approximately 6–8 mm. Ideally, multiple detector (two headed or more) or other dedicated SPECT cameras for brain imaging should be used for the data acquisition because they afford

superior results compared with single-headed gamma cameras. However, high-resolution dedicated cameras are not widely available. Therefore, a suitable compromise is to fit a SPECT dual-head rotating camera with fan-beam collimators. Alternatively, SPECT information can be obtained using standard rotating gamma cameras fitted with parallel-hole, high-resolution collimators. The detector pan and zoom capabilities are often used to ensure that the entire brain is included in the field of view while allowing the detector to clear the patient's shoulders.

High-resolution collimators are recommended for brain SPECT, provided that enough total counts per study are guaranteed and at least a 128×128 matrix is chosen. A low counting rate would require a smoother filtering during reconstruction, which would result in loss of spatial resolution but might reduce artifacts that could be caused by sharpening filters in situations with low counting statistics. The same contradictory effect would occur if a 64×64 matrix is used with a high-resolution collimator.

The matrix and pixel size should be assessed on each specific SPECT device. The pixel size can be calculated by dividing the useful field of view of the camera by the matrix size. The matrix size chosen must provide a pixel size less than half the spatial resolution of the final image. For example, if the final resolution of brain SPECT slices is 10 mm, the matrix size should be chosen to give a pixel size of 5 mm or less.

The number of projections should be kept close to the number of pixels in the matrix. A higher number of projections will yield minimal reconstruction benefits, and a lower number of projections will cause reconstruction artifacts. For example, the best choice for a 128×128 matrix is one projection for each 3° in a 360° orbit for a total of 120 projections. On the other hand, for a 64×64 matrix, the best choice is one projection for each 6° in a 360° orbit for a total of 60 projections.

A final factor to consider is the duration of the acquisition process. Longer acquisition times will yield a higher number of total counts and better quality of the final images. However, longer acquisition times increase the possibility of motion artifact, which will degrade the image quality. So, the shortest imaging time required to obtain an adequate number of total counts is recommended.

5.4.2 Interventional Studies

Interventional SPECT is the study of rCBF changes induced by a specific change in clinical symptomatology (e.g., during a seizure or when a patient is experiencing hallucinations), a pharmacologic intervention (e.g., acetazolamide challenge to investigate vasodilatory reserve), or a neurologic activation by specific sensorial, motor, or cognitive stimuli or tasks. The central effect induced by some therapeutic or diagnostic procedures, such as electroconvulsive therapy or transcranial magnetic stimulation, has also been investigated by SPECT using this approach (Catafau 2001).

Interventional SPECT studies require the performance of at least two SPECT scans: one under baseline conditions and the other during the desired state

(e.g., clinical event, under a pharmacologic effect, or during a desired task). For proper comparison of these two studies, quantification or subtraction techniques are used on slices reconstructed identically (see Sect. 5.4.3.1 below). These two studies may be performed on separate days or on the same day using the split-dose technique. The administered dose for the first SPECT must be at least half of the second. If the patient stays positioned in the camera until the second SPECT ends, neither patient repositioning nor software realignment is required. However, other technical issues, such as corrections for decay and injected dose, need to be addressed. Moreover, the longer acquisition time increases the risk for patient motion and associated image artifacts. When the two SPECT studies are compared, obtaining the identical tomographic slices is important, and software for three-dimensional realignment may be required if movement has occurred between scans (Pavía et al. 1994).

5.4.2.1 Seizure Imaging

The most commonly utilized example of interventional SPECT to examine a specific change in clinical symptomatology is the use of SPECT during the ictal and interictal states of epilepsy. Brain perfusion SPECT plays an important role in preoperative planning for medically refractory epilepsy, serving to identify the lateralization and localization of an epileptic focus before surgery. Patients should be monitored in an epilepsy unit by video-electroencephalography (video-EEG), so that the radiotracer can be injected during seizure activity (for the ictal scan). Ideally, radiopharmaceutical should be injected within 30 s of the onset of seizure activity, as this has been shown to significantly improve the accuracy and sensitivity of seizure localization with SPECT. The technologist and/or nurse in charge of the video-EEG monitoring should be trained in handling radiopharmaceuticals. Either ^{99m}Tc -HMPAO or ^{99m}Tc -ECD can be used. If unstabilized HMPAO is used, a cold vial and the corresponding freshly eluted ^{99m}Tc dose should be provided to the video-EEG technologist or nurse in a separate syringe. The ^{99m}Tc dose should then be replaced every 2 h if no seizures have occurred. As soon as seizure activity is noted on video-EEG, the technologist labels the cold vial with the fresh ^{99m}Tc and immediately injects this into the patient through a previously placed intravenous line. Alternatively, stabilized ^{99m}Tc -HMPAO or ^{99m}Tc -ECD can be used, which must be replaced every 4–6 h, respectively, if no seizure activity occurs. Similarly, the tracer should be injected as soon as seizure activity is noted. Patients can be scanned in the nuclear medicine department after recovering from the seizure. As described above, the peak brain activity of both ^{99m}Tc -labeled radiopharmaceuticals is reached within 2 min after injection, but because of intracellular fixation of the tracer, there is no redistribution, and consequently the initial tracer uptake and distribution remain unchanged up to at least 2 h.

The sensitivity of ictal brain SPECT in localizing a unilateral epileptic focus is 96 %, with a typical finding of hyperperfusion at the epileptic focus (Devous et al. 1998). However, it is important to interpret ictal (or postictal, which is defined at 30 s to 5 min post-seizure completion) with interictal imaging. An ictal or postictal

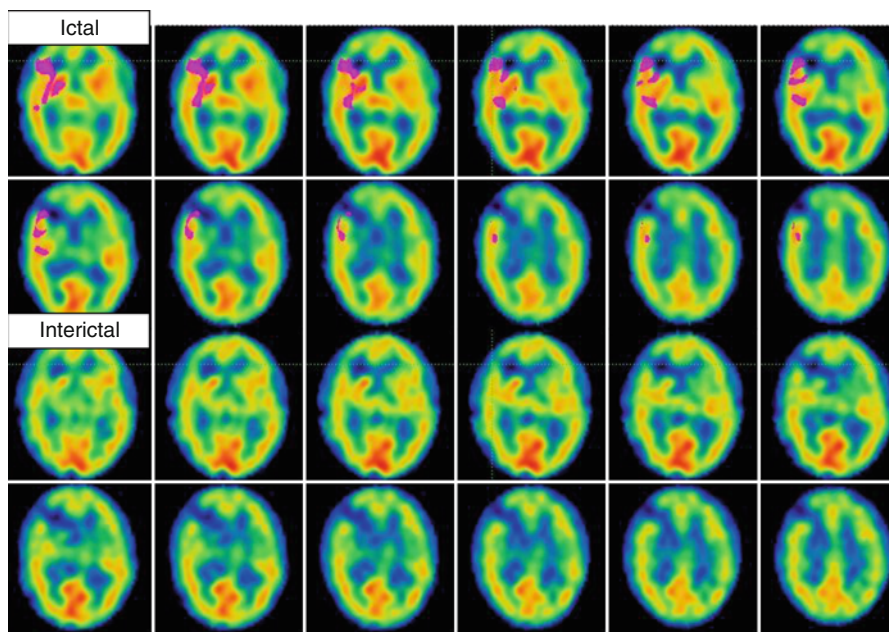


Fig. 5.4 Transaxial ictal (*top*) and interictal (*bottom*) ^{99m}Tc -ECD SPECT images show focal hyperperfusion in the right medial frontal gyrus in the ictal state, consistent with localization of the epileptic focus to right medial frontal gyrus. The *pink marking* overlying the epileptic focus is generated by the subtraction imaging technique using Hermes BRASS software which compares the rCBF between the two studies and quantifies the differences, indicating regions where large differences between the ictal and interictal states are seen

image could appear normal if read independently, but comparison with the interictal images may reflect increased perfusion at the seizure focus relative to interictal hypoperfusion at the same site. Utilization of software to compare the two studies with each other and quantify the differences in rCBF is quite helpful in confirming the site of epileptic focus (Fig. 5.4).

For the interictal scan, the conditions for tracer injection are as outlined above, but ideally continuous EEG monitoring should be performed from at least 2 h before injection until 15 min after injection to exclude the possibility that seizures have occurred shortly before and during the uptake period of the radiopharmaceuticals.

The sensitivity of interictal brain SPECT alone is relatively low at 44 % (Devous et al. 1998). Therefore, interictal ^{18}F -FDG PET can be considered to increase sensitivity of interictal functional neuroimaging if ictal SPECT is not possible (sensitivity of interictal ^{18}F -FDG PET is about 70 %). However, ^{18}F -FDG PET is difficult to obtain in the ictal state, mainly due to the inability to have radiotracer available to inject at the time of seizure activity because of the relatively short half-life of ^{18}F -FDG (110 min). Therefore, SPECT is the preferred functional neuroimaging modality in the ictal state (Devous et al. 1998).

5.4.2.2 Acetazolamide (Vasodilatory) Challenge

The most popular pharmacologic intervention in clinical use is acetazolamide challenge to assess cerebrovascular reserve with SPECT imaging (Masdeu and Brass 1995), which has both therapeutic and prognostic implications. The concept underlying this intervention is similar to the principles underlying pharmacologic coronary stress imaging, with imaging performed in the induced vasodilatory state compared to images in the rest state. As outlined in the EANM procedure guideline for brain perfusion SPECT using ^{99m}Tc -labeled radiopharmaceuticals (Kapucu et al. 2009), vasodilatory challenge is indicated in the evaluation of cerebrovascular reserve in TIA, completed stroke, carotid artery stenosis or occlusion, and vascular anomalies; evaluation of the results of carotid surgery; preoperative evaluation of need for selective carotid shunting during carotid endarterectomy; and evaluation of cerebrovascular reserve before and after cerebrovascular surgery or stent placement; and to aid in distinguishing vascular from neuronal causes of dementia. In patients with carotid artery stenosis, the finding of compromised cerebral hemodynamics on acetazolamide brain SPECT confers higher likelihood of benefit from endarterectomy (Cikrit et al. 1997). Also, a higher risk of stroke has been reported in patients presenting with compromised cerebrovascular reserve, either before endarterectomy (Kuroda et al. 1993) or after bypass surgery (Ishikawa et al. 1995). In addition, studies with and without acetazolamide may provide information on the mechanism of ischemia, for example, in moyamoya disease. Finally, in patients who are difficult to explore neurologically (i.e., patients in a coma or under sedation, such as patients in intensive care units), SPECT can help in selecting a treatment directed toward cerebral perfusion maintenance (Carter et al. 1993).

Cerebral vasodilation challenge is usually induced by slow intravenous push of 1 g of acetazolamide in adults (14 mg/kg in children) approximately 15–20 min prior to injection of radiotracer (Juni et al. 2009). Less frequently, inhaled CO_2 or intravenous injection of adenosine is used to induce cerebral vasodilation.

Various protocols have been used for the baseline and vasodilator challenge, including a 1-day, split-dose study and 2-day repeated study. The 1-day protocol using split-dose techniques (second dose at least twice the first dose) requires more sophisticated evaluation and data processing and is therefore less favored. The 2-day repeated study using a standard dose of ^{99m}Tc -ECD or ^{99m}Tc -HMPAO is simpler and therefore often preferable.

Typically, the challenge portion is performed first. If this has normal results, the baseline study may be abandoned. Under normal conditions, such pharmacologic stimuli produce global increase in cerebral blood flow. However, abnormal vessels cannot dilate, and therefore blood is shunted away from these regions, accentuating any territory with impaired vasodilatory reserve. If abnormality is identified, a baseline scan should be performed. Sufficient time must be allowed for clearance of residual activity from the vasodilator challenge scan (typically 24 h). Interpretation of these studies depends on identification of a significant area of relatively decreased perfusion (actually indicating increased perfusion in the unaffected portions of the brain) after stimulation that was not present on the baseline study, suggesting a region of ischemia that may benefit from revascularization. A “fixed” perfusion

defect present on both baseline and challenge images may indicate infarction. Alternatively, comparison with anatomic neuroimaging may reveal other reasons for fixed regional perfusion defects, such as prior surgery, edema, and space-occupying lesions. As with coronary studies, evaluation of clinical data, accurate registration of images, and comparison to a radiopharmaceutical-specific normal database are important.

Additional considerations with acetazolamide include the following: (1) known sulfa allergy is a contraindication; (2) in patients with history of migraine, acetazolamide may induce migraine; (3) acetazolamide is generally avoided within 3 days of an acute stroke; and (4) acetazolamide is a diuretic; therefore, the patient should be instructed to void immediately before the beginning of image acquisition.

5.4.2.3 Neuroactivation

Neuroactivation SPECT has been used successfully to study sensorial, motor, and cognitive functions (Catafau et al. 1998). The tracer is injected while the subject is engaged in a task, which should be continued until tracer fixation in the brain is complete (at least 3–5 min). Tasks should be carefully selected, because no other cerebral activity than the target one is desirable. Cognitive tasks represent a major difficulty to overcome. The performance of a control task would be preferable to a baseline “rest” condition. The task should involve the same parameters as the test task but without the cognitive function. For example, when using the Wisconsin Card Sorting Test as a cognitive task, an acceptable control task could be to match the cards with no criteria. Neuroactivation is a common approach in research SPECT studies; however, it is not widely used in the clinical setting, most probably because of the technical demands, although it has been reported to be useful in the differential diagnosis of dementia.

5.4.3 Image Reconstruction and Post-Processing

Transaxial reconstruction of 2D images from the projection data collected by the rotating gamma cameras is usually performed with spatial filtering. Filtering is an important step to carefully consider during SPECT reconstruction as the resulting image may vary substantially depending on the filter applied (Juni et al. 2009). The diversity in type of filters and filter parameters that can be applied cannot be covered in depth in this chapter, but further guidance can be found elsewhere (Keyes 1995). In general, application of a smoothing filter will reduce the final resolution. Accordingly, it would not be sensible to use a high-resolution SPECT device and then lose resolution by applying an inappropriately smoothing filter to the acquired images. On the contrary, a very sharp filter will result in noisy images particularly with low count data. The number of final counts in the study can be a guide for the best filter to apply. Sharp filters can be applied when a high number of total counts has been achieved, whereas low total counts require a smoother filter. An acceptable solution is to have three or four predefined filters for different ranges of total counts, which can be applied based on best fit for the individual study.

In addition, attenuation correction via software methods should be performed during reconstruction except when special devices that intrinsically correct attenuation, such as transmission-based attenuation correction systems, are used. Different algorithms have been developed to correct for photon attenuation. The most recent correction techniques are based on measured attenuation maps using transmission scans to reveal an attenuation map specific to each patient. Scattering of the photons in the body of a patient is another important source of error in quantification of activity distribution. The amount of scatter can vary between 10 and 60 % of the detected events. Different techniques, such as pulse height analysis, use of multiple energy windows, or deconvolution, allow subtraction of the scatter from the projection data before the image reconstruction. Finally, several iterative reconstruction methods such as ordered subsets expectation maximization have been proposed recently to correct images for artifacts and noise. Starting from an “initial guessed counts distribution” in the voxel grid or from an already created filtered back projection image, the ordered subset expectation maximization algorithm elaborates iteratively the image grid, the final end point being to reach a state in which each pixel contains the number of counts it was containing in the raw matrix.

Another important process performed during SPECT image reconstruction is the orientation of the slicing planes. There is no consensus on the best reference to orient slices in the transaxial plane. To be able to carefully compare SPECT images to structural images, a similar orientation to that provided by CT, which is the canthomeatal plane, is the most popular. However, brain perfusion SPECT images lack bone references, and therefore it is not possible to accurately find the canthomeatal line for orientation. Hence, a reference plane that could be identified easily in the perfusion SPECT images would be preferable to be consistent with the orientation and to reproduce the same orientation plane. A somewhat similar orientation to the canthomeatal line for oblique brain SPECT slices can be achieved by a line passing through the base of the frontal and occipital lobes (fronto-occipital plane or commissural line). Nevertheless, other orientations are also frequently used, such as the frontocerebellar plane. Apart from the classical oblique, coronal, and sagittal slices, slices parallel to the longitudinal edge of the temporal lobe can be obtained. These temporal slices are particularly useful when clear differentiation between the mesial and lateral aspects of the temporal lobe is required. The main goal is to have a “repeatable” orientation for all images done in a particular facility or institution that is standard, and if a different orientation is used, then it should be clearly noted.

5.4.3.1 Computer-Assisted Diagnosis

Perfusion SPECT images are interpreted visually but are aided greatly by analytic quantitative comparisons to normal databases (i.e., use of a computed numerical value representing local radiotracer uptake) or region of interest techniques (i.e., comparison of local radiotracer uptake with that of a relatively unaffected structure, such as cerebellum). Many software packages are widely available, which include 3D-SSP, BRASS, NeuroQ, Scenium, Cort-Ex, and MiMneuro, among others. The software packages with which we have the most experience at our institution are highlighted below.

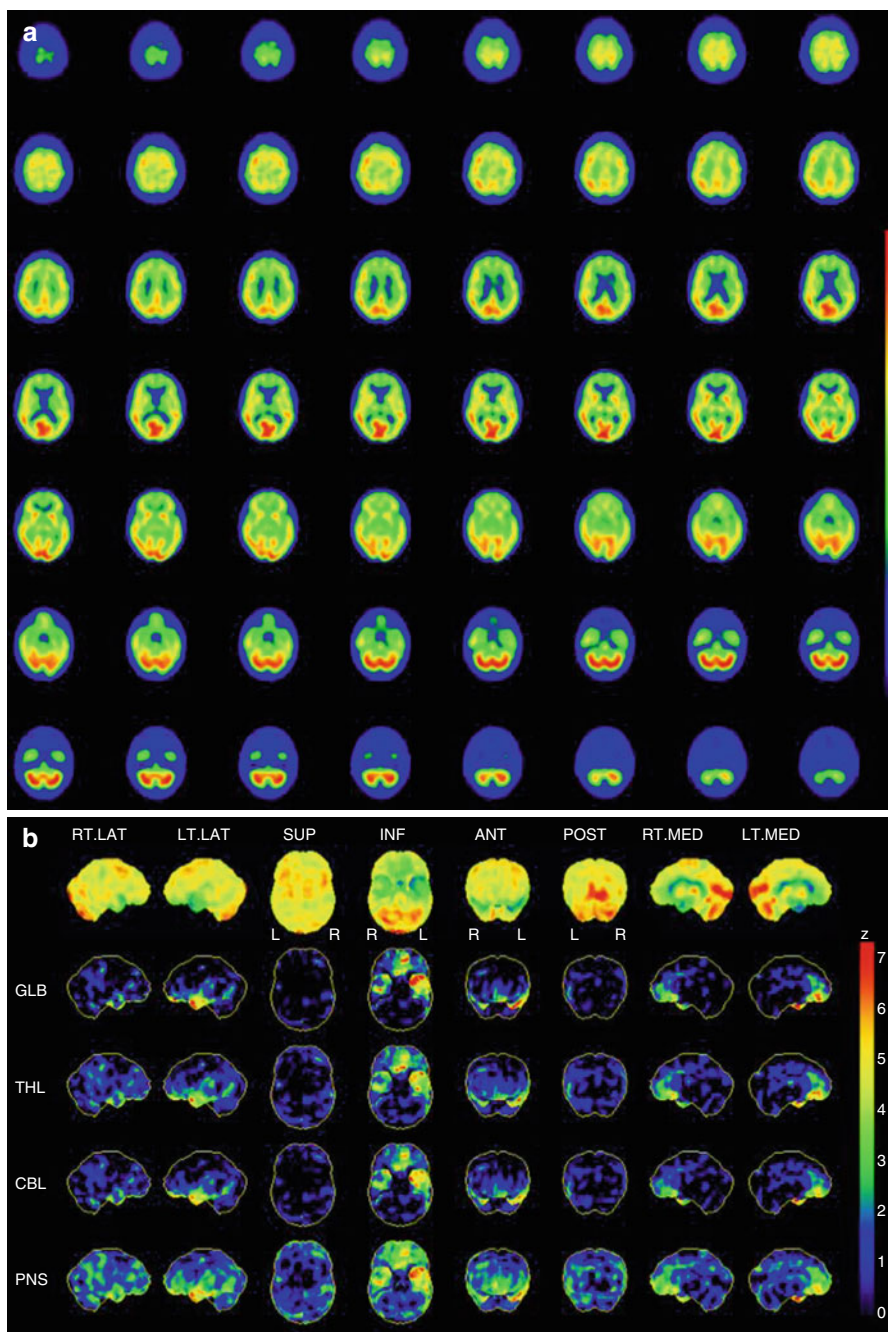


Fig. 5.5 (a) Transaxial ^{99m}Tc -ECD SPECT images show severe hypoperfusion of the frontal and temporal cortices, left slightly greater than right, with sparing of posterior parietal and occipital cortices and cerebellum. (b) Stereotactic statistical mapping analysis is performed on the SPECT dataset using 3D-SSP. The above findings are confirmed and more clearly visualized, with frontotemporal hypoperfusion again seen (z -scores > 4 SD), as well as sparing of posterior parietal and occipital cortices, basal ganglia, thalamus, and cerebellum, consistent with a diagnosis of frontotemporal dementia

3D-SSP is a software program for three-dimensional stereotactic surface projection (Neurostat, University of Washington, Seattle, WA, USA, <http://128.95.65.28/~Download/>), which stereotactically maps the patient's brain to a "standard brain" (obtained from population age-matched controls) and compared on a voxel-by-voxel basis with age- and radiopharmaceutical-matched normal databases (Fig. 5.5). This map enables a comparison of radiotracer uptake at each voxel (3D pixel) in the patient's image with the corresponding voxel in the standard brain, yielding a numerical z -score that quantifies this comparison. A map of color-coded z -scores allows subtle regional abnormalities to be appreciated. The 3D-SSP software programs can greatly enhance physician interpretation of the studies. For example, augmenting perfusion SPECT image interpretation with the use of 3D-SSP software has been shown to improve accuracy with an increase in sensitivity from 61 % without 3D-SSP to 90 % with 3D-SSP (specificity also 90 %). The largest improvement in reading accuracy was seen in cases of mild dementia, with the implication that perfusion SPECT with 3D-SSP may have a unique role in early AD detection (Uchida et al. 2006). Fully automated software is now available that examines certain regions of interest in the brain to make a diagnosis. These programs show promise in distinguishing between AD, FTD, DLB, as well as other causes of dementia (Toney et al. 2011).

Another example of available software is the BRASS software (Hermes Medical Solutions, Stockholm, Sweden), which automatically fits and quantifies brain perfusion scans. This software can either compare a study to three-dimensional reference templates, which are created from images of normal patients, with automatic masking, or it can compare two studies with each other from the same patient and quantify the differences (Fig. 5.4). The process requires the transverse slice sets of one or two studies for automatic or manual alignment with the normal template. The software performs normalization using total counts, maximum counts, or region of interest (Cooke et al. 2010).

5.4.3.2 Fusion with Anatomic Imaging

SPECT images should be interpreted in conjunction with available anatomic neuroimaging. This can be aided by fusing the two modalities, employing an overlay of anatomic and functional images with or without the use of fiducial markers. Several software programs are available for this purpose, such as MIMfusion (MIMvista Corp., Cleveland, OH), which allows alignment and easy viewing of 2D and 3D images for anatomic localization of functional imaging (Fig. 5.1). With brain perfusion SPECT, this becomes especially helpful in determining whether abnormalities in perfusion are due to anatomic abnormalities (e.g., postsurgical changes, cerebral volume loss, space-occupying lesion) or functional abnormalities (e.g., hypoperfusion within the temporoparietal cortices due to Alzheimer's disease).

5.5 Interpretation and Reporting

In interpreting and reporting brain perfusion studies, the guidelines recommended by the Society of Nuclear Medicine (Council 1996; Juni et al. 2009) and the EANM (Kapucu et al. 2009) serve as excellent resources.

When viewing brain SPECT images, it is important that a continuous color scale (or a continuous gray scale) be employed to avoid artifactual edges and that background subtraction is not excessive.

The range of normal variation should be considered, which is greatly aided by comparison to a normal database that is specific to the radiopharmaceutical employed. This can be performed via visual comparison to a normal database, such as the searchable SNM Brain Imaging Council normal SPECT brain perfusion database (available at brainscans.indd.org), or through the use of software, such as 3D-SSP described above. In general, in normal functioning brain, cortical and subcortical gray matter structures have high perfusion and therefore have the highest tracer uptake. Subcortical white matter shows low tracer uptake, and no tracer uptake is seen in areas containing cerebrospinal fluid (e.g., cerebral ventricles, fissures, and sulcus) or bone (Catafau et al. 1996). The cerebral region showing the maximum tracer uptake varies with the radiopharmaceutical used. For example, as described above, the cerebellum tends to have maximal tracer uptake with $^{99m}\text{Tc-HMPAO}$, as opposed to the calcarine cortex with $^{99m}\text{Tc-ECD}$. The patient's condition at the time of injection (e.g., influence of visual stimuli and activity) and image manipulation during reconstruction can also affect perfusion patterns.

Distribution patterns of perfusion abnormalities should be recognized, particularly in the context of the patient's clinical symptoms, making note of patterns typical for specific vascular territories and eventual diaschisis patterns, dementia patterns, temporal lobe localization of epileptic foci, or herpetic encephalitis. The extent and severity of perfusion abnormalities should be reported.

SPECT findings should be integrated with findings from anatomic neuroimaging (e.g., CT or MRI), with particular attention paid to areas of regional perfusion defects. This task can be aided by fusion imaging, as described above, but visual comparison is also very useful.

In final interpretation, provide a diagnosis based on established disease-specific patterns (Table 5.1). For patterns that are atypical for a specific diagnosis, provide a differential diagnosis stating the aspects of the SPECT findings and other corroborative information (patient's symptoms, other imaging studies, additional test results) that argue in favor of or against each differential diagnosis. Any interpretation based on disease-specific patterns still considered to be investigational (e.g., psychiatric disorders, infectious etiologies) should be explicitly reported as such.

Overall, a detailed knowledge of patient symptomatology and the associated functional brain regions expected to be involved is important for the interpretation of functional images. A close working relationship with the referring physician should be established, and the SPECT findings should be integrated with other clinical symptomatology and test results, such as neuropsychiatric tests. Interdisciplinary cooperation improves the quality of the final report and optimizes the clinical yield of the SPECT technique.

References

- Alexandrov AV, Ehrlich LE, Bladin CF, Norris JW (1996) Simple visual analysis of brain perfusion on HMPAO SPECT predicts early outcome in acute stroke. *Stroke* 27:1537–1542
- Al-Shammri S, Al-Feeli M (2004) Confirmation of brain death using brain radionuclide perfusion imaging technique. *Med Princ Pract* 13(5):267–272
- Bonte FJ, Harris TS, Roney CA, Hynan LS (2004) Differential diagnosis between Alzheimer's and frontotemporal disease by the posterior cingulate sign. *J Nucl Med* 45(5):771–774
- Borghesani PR, DeMers SM, Manchanda V, Pruthi S, Lewis DH, Borson S (2010) Neuroimaging in the clinical diagnosis of dementia: observations from a memory disorders clinic. *J Am Geriatr Soc* 58(8):1453–1458
- Bradley KM, O'Sullivan VT, Soper NDW, Nagy Z, King EM-F, Smith AD, Shepstone BJ (2002) Cerebral perfusion SPET correlated with Braak pathological stage in Alzheimer's disease. *Brain* 125:1772–1781
- Brown DR, Hunter R, Wyper DJ, Patterson J, Kelly RC, Montaldi D, McCullouch J (1996) Longitudinal changes in cognitive function and regional cerebral function in Alzheimer's disease: a SPECT blood flow study. *J Psychiatr Res* 30(2):109–126
- Carter LP, Weinand ME, Oommen KJ (1993) Cerebral blood flow (CBF) monitoring in intensive care by thermal diffusion. *Acta Neurochir Suppl (Wien)* 59:43–46
- Catafau AM (2001) Brain SPECT in clinical practice. Part I: perfusion. *J Nucl Med* 42(2):259–271
- Catafau AM, Lomena FJ, Pavia J, Parellada E, Bernardo M, Setoain J, Tolosa E (1996) Regional cerebral blood flow pattern in normal young and aged volunteers: a 99mTc-HMPAO SPET study. *Eur J Nucl Med* 23(10):1329–1337
- Catafau AM, Parellada E, Lomena F, Bernardo M, Setoain J, Catarineu S, Pavia J, Herranz R (1998) Role of the cingulate gyrus during the Wisconsin Card Sorting Test: a single photon emission computed tomography study in normal volunteers. *Psychiatry Res* 83(2):67–74
- Cikrit DF, Dalsing MC, Harting PS (1997) Cerebral vascular reactivity assessed with acetazolamide single photon emission computer tomography scans before and after carotid endarterectomy. *Am J Surg* 174:193–197
- Cooke D, Koppula B, Seiler D, Rajendran J, Hallam D, Ghodke B, Lewis D (2010) Semiquantitative software SPECT analysis in aneurysmal subarachnoid hemorrhage-related vasospasm. *Nucl Med Commun* 31(1):53–58
- Devous MD Sr (2002) Functional brain imaging in the dementias: role in early detection, differential diagnosis, and longitudinal studies. *Eur J Nucl Med Mol Imaging* 29(12):1685–1696
- Devous MD Sr, Payne JK, Lowe JL, Leroy RF (1993) Comparison of technetium-99m-ECD to Xenon-133 SPECT in normal controls and in patients with mild to moderate regional cerebral blood flow abnormalities. *J Nucl Med* 34(5):754–761
- Devous MD, Thisted RA, Morgan GF, Leroy RF, Rowe CC (1998) SPECT brain imaging in epilepsy: a meta-analysis. *J Nucl Med* 39(2):285–293
- Hattori N, Swan M, Stobbe GA, Uomoto JM, Minoshima S, Djang D, Krishnananthan R, Lewis DH (2009) Differential SPECT activation patterns associated with PASAT performance may indicate frontocerebellar functional dissociation in chronic mild traumatic brain injury. *J Nucl Med* 50(7):1054–1061
- Ichise M, Toyama H, Fornazzari L, Ballinger JR, Kirsh JC (1993) Iodine-123-IBZM dopamine D2 receptor and technetium-99m-HMPAO brain perfusion SPECT in the evaluation of patients with and subjects at risk for Huntington's disease. *J Nucl Med* 34(8):1274–1281
- Ishikawa T, Houkin K, Abe H, Isobe M, Kamiyama H (1995) Cerebral haemodynamics and long-term prognosis after extracranial-intracranial bypass surgery. *J Neurol Neurosurg Psychiatry* 59(6):625–628
- Jacobs A, Put E, Ingels M, Put T, Bossuyt A (1996) One-year follow-up of technetium-99m-HMPAO SPECT in mild head injury. *J Nucl Med* 37(10):1605–1609

- Juni JE, Waxman AD, Devous MD Sr, Tikofsky RS, Ichise M, Van Heertum RL, Carretta RF, Chen CC, Society for Nuclear Medicine (2009) Procedure guideline for brain perfusion SPECT using (99m)Tc radiopharmaceuticals 3.0. *J Nucl Med Technol* 37(3):191–195
- Kapucu OL, Nobili F, Varrone A, Booi J, Vander Borgh T, Nagren K, Darcourt J, Tatsch K, Van Laere KJ (2009) EANM procedure guideline for brain perfusion SPECT using 99mTc-labelled radiopharmaceuticals, version 2. *Eur J Nucl Med Mol Imaging* 36(12):2093–2102
- Keyes JWJ (1995) Single photon emission computed tomography (SPECT). operational guidelines. In: Wagner HNJ, Szabo Z, Buchanan JW (eds) *Principles of nuclear medicine*. Saunders, Philadelphia, pp 332–341
- Kuroda S, Kamiyama H, Abe H, Houkin K, Isobe M, Mitsumori K (1993) Acetazolamide test in detecting reduced cerebral perfusion reserve and predicting long-term prognosis in patients with internal carotid artery occlusion. *Neurosurgery* 32(6):912–918; discussion 918–919
- Lobotesis K, Fenwick JD, Phipps A, Ryman A, Swann A, Ballard C, McKeith IG, O'Brien JT (2001) Occipital hypoperfusion on SPECT in dementia with Lewy bodies but not AD. *Neurology* 56(5):643–649
- Markand ON, Spencer SS, Anderson AR (1995) SPECT in epilepsy. *J Neuroimaging* 5(Suppl 1):S23–S33
- Masdeu JC, Brass LM (1995) SPECT imaging of stroke. *J Neuroimaging* 5(Suppl 1):S14–S22
- Masdeu JC, Abdel-Dayem H, Van Heertum RL (1995) Head trauma: use of SPECT. *J Neuroimaging* 5(Suppl 1):S53–S57
- Miller JD, Bell BA (1987) Cerebral blood flow variations with perfusion pressure and metabolism. In: Wood JH (ed) *Cerebral blood flow. Physiologic and clinical aspects*. McGraw-Hill, New York, pp 19–130
- Miller BL, Cummings JL, Villanueva-Meyer J, Boone K, Mehinger CM, Lesser IM, Mena I (1991) Frontal lobe degeneration: clinical, neuropsychological, and SPECT characteristics. *Neurology* 41(9):1374–1382
- Miyazawa N, Koizumi K, Mitsuka S, Nukui H (1998) Discrepancies in brain perfusion SPECT findings between Tc-99m HMPAO and Tc-99m ECD: evaluation using dynamic SPECT in patients with hyperemia. *Clin Nucl Med* 23(10):686–690
- Mustonen T, Koivisto T, Vanninen R, Hninen T, Vapalahti M, Hernesniemi J, Kuikka JT, Vanninen E (2008) Heterogeneity of cerebral perfusion 1 week after haemorrhage is an independent predictor of clinical outcome in patients with aneurysmal subarachnoid haemorrhage. *J Neurol Neurosurg Psychiatry* 79(10):1128–1133
- Papathanasiou ND, Boutsidiadis A, Dickson J, Bomanji JB (2012) Diagnostic accuracy of (1)(2)(3) I-FP-CIT (DaTSCAN) in dementia with Lewy bodies: a meta-analysis of published studies. *Parkinsonism Relat Disord* 18(3):225–229
- Pavía J, Ros D, Catafau A, Lomençà F, Huguet M, Setoain J (1994) 3-D realignment of activation brain SPECT studies. *Eur J Nucl Med* 21:1298–1302
- Payne JK, Trivedi MH, Devous MD Sr (1996) Comparison of technetium-99m-HMPAO and xenon-133 measurements of regional cerebral blood flow by SPECT. *J Nucl Med* 37(10):1735–1740
- Rajendran JG, Lewis DH, Newell DW, Winn HR (2001) Brain SPECT used to evaluate vasospasm after subarachnoid hemorrhage: correlation with angiography and transcranial Doppler. *Clin Nucl Med* 26(2):125–130
- Shimizu S, Hanyu H, Hirao K, Sato T, Iwamoto T, Koizumi K (2008) Value of analyzing deep gray matter and occipital lobe perfusion to differentiate dementia with Lewy bodies from Alzheimer's disease. *Ann Nucl Med* 22(10):911–916
- Society of Nuclear Medicine Brain Imaging Council (1996) Ethical clinical practice of functional brain imaging. *J Nucl Med* 37(7):1256–1259
- Spampinato U, Hoabert MO, Mas JL, Bourdel MC, Ziegler M, de Recondo J, Askienazy S, Rondot P (1991) (99mTc)-HM-PAO SPECT and cognitive impairment in Parkinson's disease: a comparison with dementia of the Alzheimer type. *J Neurol Neurosurg Psychiatry* 54(9):787–792

- Spencer SS (1994) The relative contributions of MRI, SPECT, and PET imaging in epilepsy. *Epilepsia* 35(Suppl 6):S72–S89
- Tohgi H, Chiba K, Sasaki K, Hiroi S, Ishibashi Y (1991) Cerebral perfusion patterns in vascular dementia of Binswanger type compared with senile dementia of Alzheimer type: a SPECT study. *J Neurol* 238(7):365–370
- Toney LK, McCue TJ, Minoshima S, Lewis DH (2011) Nuclear medicine imaging in dementia: a practical overview for hospitalists. *Hosp Pract* 39(3):149–160
- Tsuchida T, Sadato N, Yonekura Y (1997) Quantification of regional cerebral blood flow with continuous infusion of technetium-99m-ethyl cysteinate dimer. *J Nucl Med* 1997(38):1699–1702
- Uchida Y, Minoshima S, Okada S, Kawata T, Ito H (2006) Diagnosis of dementia using perfusion SPECT imaging at the patient's initial visit to a cognitive disorder clinic. *Clin Nucl Med* 31(12):764–773
- Ueda T, Yuh WT (2005) Single-photon emission CT imaging in acute stroke. *Neuroimaging Clin N Am* 15(3):543–551, x
- Won JH, Lee JD, Chung TS, Park CY, Lee BI (1996) Increased contralateral cerebellar uptake of technetium-99m-HMPAO on ictal brain SPECT. *J Nucl Med* 37(3):426–429

The Impact of Genetic Polymorphisms on Neuroreceptor Imaging

6

Matthäus Willeit, Siegfried Kasper,
and Nicole Praschak-Rieder

Contents

6.1	Introduction	150
6.2	Serotonin	151
6.2.1	The Serotonin Transporter	151
6.2.2	Serotonin Transporter Gene-Linked Polymorphic Region (5-HTTLPR)	152
6.2.3	Effects of 5-HTTLPR on Serotonin Transporter Binding	152
6.2.4	Serotonin 2A Receptor Polymorphisms	154
6.2.5	Brain-Derived Neurotrophic Factor (BDNF) Polymorphisms (Val66Met).....	154
6.2.6	The Serotonin 1A Receptor.....	155
6.2.7	The Serotonin 4 Receptor.....	157
6.3	Dopamine	159
6.3.1	Dopamine D _{2/3} Receptors	159
6.3.2	The Dopamine Transporter	162
6.3.3	Measuring Dopamine Transporter Function	162
6.4	Other Polymorphisms	163
6.4.1	The Catechol-O-methyltransferase Val158Met Polymorphism	163
6.4.2	Monoamine Oxidase A.....	165
6.4.3	18-kD Translocator Protein.....	166
6.5	Summary and Outlook	167
	References.....	168

Abstract

Major psychiatric disorders are highly heritable. Nevertheless, more than two decades of candidate gene studies and genome-wide association studies have yielded few, if any, unambiguous and stably replicable results that would be strong enough as to direct research towards new pharmacological targets. This is in part due to the complex non-Mendelian inheritance patterns and hard-to-define

M. Willeit, MD (✉) • S. Kasper • N. Praschak-Rieder
Division of Biological Psychiatry, Department of Psychiatry and Psychotherapy, Medical
University Vienna, Waehringer Guertel 18-20, Vienna A-1090, Austria
e-mail: matthaeus.willeit@meduniwien.ac.at

phenotypes of psychiatric disorders. In addition, the relationship between genetic risk and phenotypic expression is blurred by strong contribution of environmental factors and epigenetic modification. A research strategy that has successfully been pursued over the last years with magnetic resonance-based methods is imaging of endophenotypes. However, these techniques have the drawback that their results are not easily transferable to a molecular level potentially accessible to therapeutic drugs. Imaging methods such as positron emission tomography (PET) and single photon emission computer tomography (SPECT) make it possible to explore the impact of genetic variation on certain aspects of molecules that play a central role in our understanding and treatment of psychiatric disorders. This chapter tries to cover the current state of knowledge about the impact of genetic variation on the behaviour of PET and SPECT radioligands in the living human brain.

6.1 Introduction

Since more than a century, diagnoses in psychiatry are syndrome based, that is, the diagnostic process relies on the presence (or absence) of a bundle of more or less specific symptoms that are either reported by the patient or observed by the physician. The diagnostic classification is the ground for prognosis and treatment decision. However, it is fully unrelated to the putative neurochemical alterations thought to be the pathogenic substrate of major psychiatric disorders. The high heritability of disorders such as schizophrenia or affective illness, together with enormous advances in molecular genetics made in the last decades, has incited the hope that molecular genetics might be able to contribute substantially to our knowledge on molecular alterations associated with specific disorders. Moreover, it is anticipated that these methods would help identify biomarkers that would make the diagnostic process more reliable and objective.

Until recently, case-control studies comparing frequencies of putative risk alleles in patient groups and healthy subjects were the predominant research strategy in psychiatric genetics. Candidate genes were selected a priori on grounds of hypotheses on the pathogenesis and available knowledge on genetic variation in these targets (so-called biological candidate genes). In keeping with the predominant pathogenetic hypotheses, many of the investigated polymorphisms (polymorphisms are frequent genetic variants) were in one or the other way related to brain monoamine neurotransmission. However, it is now increasingly evident that the genetic mechanisms associated with heritability of psychiatric disorders are far more complex than initially thought and that the variance introduced by single genetic variants is rarely strong enough for having relevant influence on a specific disease risk. Results of recent genome-wide association studies (GWAS) rather suggest that the genetic risk for disorders such as schizophrenia is due to a combination of common low-risk and rare high-risk variants (Purcell et al. 2009; Shi et al. 2009; Stefansson et al. 2009). One of the major advantages of the

methodology employed in GWAS is that it does not rely on a priori hypotheses. Thus, results surviving the extremely rigid statistical thresholds merit further scientific attention. Gene variants in regions derived from GWAS studies have been termed ‘positional candidate genes’. In contrast to biological candidate genes, the function and biological role of positional candidate genes is frequently unknown and needs to be determined in sometimes complicated follow-up studies. A possible way to relate the function of biological and positional candidate genes to the actual body of knowledge on pathogenesis and neuropharmacology of psychiatric disorders is certainly imaging genetics.

Imaging genetics uses magnetic resonance imaging (MRI)-based methods such as functional MRI (fMRI) or voxel-based morphometry (VBM) and radiation-based methods such as single photon emission computer tomography (SPECT) and positron emission tomography (PET) to study the effects of genetic variants in the living brain. While MRI-based methods can provide information on brain structure, regional brain metabolism and functional or anatomical connectivity between brain regions, radiation-based methods allow investigating distribution and, in part, function of selected molecules in the brain.

In this chapter, we will review the scientific evidence on the influence of genetic variation upon neuroreceptor PET and SPECT radioligand binding in the brain.

6.2 Serotonin

Serotonin is a phylogenetically ancient modulatory neurotransmitter that is synthesized in brain and periphery from the essential amino acid tryptophan. The rate-limiting step of serotonin synthesis is hydroxylation of tryptophan by the enzyme tryptophan hydroxylase (TPH). Two isoenzymes are known in humans: TPH-1 catalyzes the reaction in the periphery, whereas TPH-2 (Walther et al. 2003; Zill et al. 2004) is found in the central nervous system (CNS). The serotonin system is involved in the regulation of circadian and seasonal rhythms, mood, sleep, feeding behaviour and energy homeostasis and consequently in a number of psychiatric problems and disorders, notably depression, anxiety, obsessive-compulsive disorder, impulsivity, self-harm and suicide.

6.2.1 The Serotonin Transporter

The presynaptic serotonin transporter (5-HTT) is a key regulator of serotonin signalling and a major target for antidepressant medications and psychostimulants. The 5-HTT takes up serotonin after its release into the extracellular space, thereby controlling the magnitude and duration of serotonergic responses (Bel and Artigas 1992; Shen et al. 2004; Jennings et al. 2006). High presynaptic 5-HTT density is associated with low extracellular serotonin (Jennings et al. 2006), and raising extracellular serotonin by pharmacological blocking 5-HTT is the main mechanism of action of many antidepressant drugs.

6.2.2 Serotonin Transporter Gene-Linked Polymorphic Region (5-HTTLPR)

An insertion-deletion polymorphism in the promoter region of the 5-HTT transporter gene, the serotonin transporter-linked polymorphic region (5-HTTLPR; Heils et al. 1996) has been extensively studied in psychiatry. In human cell lines, the 5-HTTLPR long (or *l*-allele) is associated with 30–40 % higher 5-HTT expression than the short (or *s*-allele) (Heils et al. 1996; Lesch et al. 1996). Initially, 5-HTTLPR was found to be associated with anxiety-related traits: Individuals carrying the short allele had higher neuroticism scores than individuals homozygous for the long allele (Lesch et al. 1996). Several studies were able to find associations between 5-HTTLPR and neuropsychiatric illness (Collier et al. 1996; Kunugi et al. 1997; Malhotra et al. 1998; Rosenthal et al. 1998; Anguelova et al. 2003; Bondy et al. 2006; Grunblatt et al. 2006). However, there are many studies who failed to replicate earlier results (Seretti et al. 1999; Johansson et al. 2003; Willeit et al. 2003). An intensively discussed finding was the association with the 5-HTTLPR *s*-allele and risk for depression in interaction with traumatic life events (Caspi et al. 2003, 2010). Although this finding has been replicated several times (see, e.g. Zalsman et al. 2006), meta-analyses of this finding are conflicting (Risch et al. 2009; Karg et al. 2011).

In light of inconsistent and contradicting results, it is a rational research strategy to investigate biological endophenotypes associated with the 5-HTTLPR genotype, such as amygdala reactivity (Hariri et al. 2002; Hariri and Holmes 2006) or the influence of 5-HTTLPR on the interaction between brain areas relevant for psychiatric disorders (Pezawas et al. 2005). Today, the *s*-allele is not seen any more as a variant leading to deficient function of brain proteins or brain circuits. Interestingly, *s*-allele carriers were found to outperform subjects carrying the long allele in a number of cognitive and social tasks (for review, see Homberg and Lesch 2010). Hyperactivity in corticolimbic structures associated with the *s*-allele resulting in hypervigilance in the sense of increased sensitivity to both aversive and rewarding stimuli and possibly greater mood reactivity (Willeit et al. 2003) may have beneficial or negative consequences, depending on the environmental circumstances (Homberg and Lesch 2010).

6.2.3 Effects of 5-HTTLPR on Serotonin Transporter Binding

First studies in human platelets investigated the effects of 5-HTTLPR on serotonin transporter expression and function. The amount of transporter protein was not found to be altered, but an influence of 5-HTTLPR on maximal serotonin uptake velocity was described in some (Greenberg et al. 1999; Nobile et al. 1999; Patkar et al. 2004) but not all (Willeit et al. 2008) studies. Two of these studies also showed a significant effect of season on functional 5-HTT parameters (Greenberg et al. 1999; Nobile et al. 1999), and one study also found a significant interaction between 5-HTTLPR genotype and seasonal change in serotonin uptake velocity (Greenberg et al. 1999).

Studies on the effects of 5-HTTLPR on 5-HTT availability in the human brain using the radiolabelled cocaine-analog on [¹²³I]-2-β-carbomethoxy-3-b-(4-iodophenyl)

tropane ($[^{123}\text{I}]\beta\text{-CIT}$; Neumeyer et al. 1991) and SPECT (Table 6.1) found higher (Heinz et al. 2000b) or unchanged (Jacobsen et al. 2000; Willeit et al. 2001) binding in carriers of the high-expressing *l*-allele, while other studies found higher binding in subjects homozygous for the low-expressing *s*-allele (Van Dyck et al. 2004). However, rather than being selective for the 5-HTT, $[^{123}\text{I}]\beta\text{-CIT}$ is a nonspecific monoamine-transporter ligand. Moreover, $[^{123}\text{I}]\beta\text{-CIT}$ binding shows a clear age-dependent decrease (Pirker et al. 2000), and a major limitation of the van Dyck et al. study is that *s/s* homozygous subjects were significantly younger than *l/l* and *l/s*-carriers. A recent study using the $\beta\text{-CIT}$ derivative $[^{123}\text{I}]\text{nor-}\beta\text{-CIT}$ described slightly higher $[^{123}\text{I}]\text{nor-}\beta\text{-CIT}$ binding in the thalamus of *s*-allele carriers (Kauppila et al. 2013).

The effects of 5-HTTLPR or the so-called triallelic 5-HTTLPR – a functional single-nucleotide variant within the 5-HTTLPR *l*-allele termed *LA* and *LG*, with only *LA* being associated with high levels of 5-HTT mRNA, whereas *LG* is more similar to the *s*-allele (Nakamura et al. 2000; Kraft et al. 2005) – have also been studied with two PET ligands that are selective for the 5-HTT, $[^{11}\text{C}](+)\text{-6beta-(4-methylthiophenyl)-1,2,3,5,6alpha,10beta-hexahydropyrrolo[2,1-a]isoquinoline}$ ($[^{11}\text{C}]\text{McN 5652}$; Suehiro et al. 1993) and $[^{11}\text{C}]\text{-3-amino-4-(2-dimethylaminomethylphenylthio)benzonitrile}$ ($[^{11}\text{C}]\text{DASB}$; Wilson and Houle 1999; Houle et al. 2000; Wilson et al. 2000). $[^{11}\text{C}]\text{DASB}$ is currently the method of choice for PET imaging of the 5-HTT, and it has been shown to be superior to $[^{11}\text{C}]\text{McN 5652}$ in several aspects (Huang et al. 2002; Szabo et al. 2002; Frankle et al. 2004).

In contrast to studies using $[^{11}\text{C}]\text{McN 5652}$ (Shioe et al. 2003; Parsey et al. 2006a), three studies using $[^{11}\text{C}]\text{DASB}$ were able to detect higher serotonin transporter binding in *LA/LA* homozygous subjects (Praschak-Rieder et al. 2007; Reimold et al. 2007; Kalbitzer et al. 2009). The three studies disagree on the location of higher $[^{11}\text{C}]\text{DASB}$ binding in *LA/LA* homozygous subjects in the brain: Praschak-Rieder et al. found significant 5-HTTLPR effects in the putamen, Reimold et al. in midbrain and Kalbitzer et al. in the caudate nucleus. What these regions have in common is that they contain large amounts of serotonin transporter protein, and it is inherent to PET methodology that accuracy of measurements is greater in regions with high density of the target molecule than in those who express the target scarcely (Willeit and Praschak-Rieder 2010). Kalbitzer et al. also showed that light-dependent changes in serotonin transporter binding (Praschak-Rieder et al. 2008; Ruhe et al. 2009) were influenced by 5-HTTLPR genotype, with *LA/LA* carriers showing greater seasonal fluctuation in serotonin transporter binding. However, another recent study did not find any relevant effects of 5-HTTLPR on $[^{11}\text{C}]\text{DASB}$ binding in the human brain (Murthy et al. 2010).

In summary, the literature reports contradictory results on the influence of 5-HTTLPR genotype on serotonin transporter binding in the living human brain. Apart from the natural variation in individual 5-HTT density, one major factor may be the quality of the imaging methods applied. $[^{11}\text{C}]\text{DASB}$ is clearly superior to $[^{11}\text{C}]\text{McN 5652}$ or $[^{123}\text{I}]\beta\text{-CIT}$ for imaging the 5-HTT in vivo (Huang et al. 2002; Szabo et al. 2002; Frankle et al. 2004). Moreover, nongenetic aspects have been shown to influence or associate with 5-HTT binding. These include ethnicity (Praschak-Rieder et al. 2007), personality (Kalbitzer et al. 2009), biography (Miller et al. 2009) and

psychiatric diagnoses (Malison et al. 1998; Willeit et al. 2000; Meyer et al. 2004; Selvaraj et al. 2009; for review, see Stockmeier 2003; Meyer 2007) and the intensity of environmental light at the time of the year when scanning takes place (Buchert et al. 2006; Praschak-Rieder et al. 2008; Ruhe et al. 2009; Kalbitzer et al. 2010). Studies on the effects of season show that 5-HTT binding is higher in fall and winter as compared to spring and summer, and covarying for season in the Praschak-Rieder et al. sample (Praschak-Rieder et al. 2007) increased the significance of the effects of 5-HTTLPR on [¹¹C]DASB binding (Praschak-Rieder et al. 2008). Thus, three of four PET imaging studies using [¹¹C]DASB support the notion that 5-HTTLPR is indeed associated with 5-HTT binding in the living human brain. However, in contrast to restricted systems like human cell lines, where a 30–40 % difference in 5-HTT binding between high- and low-expressing genotypes has been observed, genotype effects of 5-HTTLPR, if any, were found to be quite small.

6.2.4 Serotonin 2A Receptor Polymorphisms

A relatively large study has investigated the effects of several single-nucleotide polymorphisms (SNPs) in the serotonin 2A (5-HT_{2A}) receptor gene on [¹¹C]DASB binding in the brain (Laje et al. 2010). Genetic variation in this region had previously been associated with antidepressant treatment response to citalopram (McMahon et al. 2006). An association between 5-HTT binding in thalamus and three SNPs (rs7333412, rs7997012, rs977003) was found, and results were suggestive for a gene-dose effect (rs7333412 AA < AG < GG). This study may thus help to explain differences in treatment response to SSRIs due to genetic variation in the 5-HT_{2A} receptor gene. This result is among of the few ones in the literature strong enough as to survive correction for multiple testing.

6.2.5 Brain-Derived Neurotrophic Factor (BDNF) Polymorphisms (Val66Met)

Brain-derived neurotrophic factor (BDNF) is a relatively well-characterized neurotrophic protein that supports survival, sprouting and synaptogenesis of neurons. It is encoded on chromosome 11p13-14 (Jones and Reichardt 1990; Maisonpierre et al. 1991). Polymorphisms within the BDNF gene have been shown to influence brain structure and function (Egan et al. 2003; Hariri et al. 2003; Pezawas et al. 2008; Pezawas et al. 2004) and have been associated with affective disorders, antidepressant treatment response, substance abuse, eating disorders and schizophrenia (Neves-Pereira et al. 2002; Sklar et al. 2002; Castren 2004; Gratacos et al. 2007; Brunoni et al. 2008). Experimental and clinical evidence suggests that there is a close interaction between BDNF and brain serotonin transmission (Neumeister et al. 2005; Brunoni et al. 2008).

Two PET studies have investigated a possible association of the BDNF Val66Met polymorphism and binding to brain 5-HT_{2A} receptors (Klein et al. 2010) and to 5-HT_{1A} receptors and the serotonin transporter (Henningsson et al. 2009). While there was no

effect of the BDNF Val66Met polymorphism on 5-HT_{1A} or 5-HT_{2A} receptor binding, one study (Henningsson et al. 2009) found significantly higher binding of the serotonin transporter radioligand [¹¹C]MADAM in male subjects. This finding was replicated in the same study at a trend level in second cohort using the radioligand [¹²³I]β-CIT and SPECT. However, the study by Klein et al. (2010) using the radioligand [¹¹C]DASB did not find any effect of the BDNF Val66Met polymorphism or BDNF plasma levels on brain serotonin transporter binding in a larger sample (Table 6.1).

6.2.6 The Serotonin 1A Receptor

The serotonin 1A (5-HT_{1A}) receptor is a G-protein-coupled transmembrane protein whose main signalling effect is a reduction in the formation of cyclic adenosine monophosphate (cAMP). 5-HT_{1A} receptors are abundantly expressed in the frontal and temporal cortex, hippocampus, septum, amygdala and the raphe nuclei, and lower levels are found in basal ganglia and the thalamus (Ito et al. 1999; de Almeida and Mengod 2008; Storvik et al. 2009). 5-HT_{1A} receptors are considered inhibitory as, upon activation, they reduce the probability of neuronal discharge. Cortical and subcortical 5-HT_{1A} receptors are mostly postsynaptic receptors located on glutamatergic and GABAergic neurons (Freund et al. 1990; Palchadhuri and Flugge 2005; de Almeida and Mengod 2008), while 5-HT_{1A} receptors in the raphe nuclei, the origin of brain serotonin innervation, are somatodendritic autoreceptors that reduce serotonergic output from the raphe into the respective target areas (Sprouse and Aghajanian 1988).

Reductions in brain 5-HT_{1A} receptor binding have been described in anxiety disorders (Neumeister et al. 2004; Lanzenberger et al. 2007; for review, see Akimova et al. 2009), depression (Drevets et al. 1999, 2000; Meltzer et al. 2004; Hirvonen et al. 2008, but see Parsey et al. 2006b) (for review, see Drevets et al. 2007; Savitz et al. 2009) and schizophrenia (Tauscher et al. 2002; but see Frankle et al. 2006). Results on the effects of antidepressant treatment with selective serotonin reuptake inhibitors or electroconvulsive therapy on 5-HT_{1A} binding are mixed (Moses-Kolko et al. 2007; Spindelegger et al. 2009; Saijo et al. 2010; Lanzenberger et al. 2012a). Increased 5-HT_{1A} receptor binding has been observed in anorexia nervosa (Bailer et al. 2005, 2007) and post-traumatic stress disorder (Sullivan et al. 2013).

Several polymorphisms in 5-HT_{1A} receptor gene (located on chromosome 5q11.2-q13; Fargin et al. 1989; Albert et al. 1990) have been studied for association with psychiatric disorders (for review, see Drago et al. 2008; Le Francois et al. 2008). The best studied polymorphism is a functional SNP in a palindromic region within the 5-HT_{1A} promoter region (C(-1019)G; rs6295; Wu and Comings 1999) that influences gene expression by modulating the interaction of the promoter with transcription factors. The C(-1019)G C-allele has been associated with reduced 5-HT_{1A} expression (Pernhorst et al. 2013) and was found to be associated with affective disorders in a recent meta-analysis (Kishi et al. 2012).

There is only limited evidence on the *in vivo* influence of the C(-1019)G polymorphism on brain 5-HT_{1A} receptor binding. One study did not show any effect of the C(-1019)G polymorphism on brain 5-HT_{1A} receptor binding but instead reduced 5-HT_{1A} binding in carriers of the 5-HTTLPR short allele (David et al. 2005). Another

Table 6.1 Effects of serotonin transporter-linked polymorphic region (5-HTTLPR), brain-derived neurotrophic factor (BDNF) Val66Met and 5-HT_{2A} receptor polymorphisms on serotonin transporter binding

	Polymorphism	Number of subjects ^a	Radioligand	Results	Region	Comment
Heinz et al. (2000b)	5-HTTLPR	22 (14 AD) ^b	[¹²³ I]β-CIT	<i>ll</i> > <i>s</i> -Carriers (healthy subjects)	Brainstem	Opposite genotype effects in AD ^b
Willeit et al. (2001)	5-HTTLPR	11	[¹²³ I]β-CIT	No effect	Midbrain	
Van Dyck et al. (2004)	5-HTTLPR	96	[¹²³ I]β-CIT	<i>ss</i> > <i>ll</i> > <i>ls</i>	Midbrain	<i>s/s</i> Homozygotes younger than other genotypes
Shioe et al. (2003)	5-HTTLPR	27	[¹¹ C]M ₁ CN 5652	No effect	Midbrain	
Parsey et al. (2006a)	Triallelic 5-HTTLPR	67 (25 MDD) ^c	[¹¹ C]M ₁ CN 5652	No effect	Serotonin-rich regions	
Praschak-Rieder et al. (2007)	Triallelic 5-HTTLPR	43	[¹¹ C]DASB	<i>LalLa</i> > <i>s</i> -carriers	Putamen	Results clearer when covarying for ethnicity and effects of season
Reimold et al. (2007)	Triallelic 5-HTTLPR	19	[¹¹ C]DASB	<i>LalLa</i> > <i>s</i> -carriers	Midbrain	
Kalbitzer et al. (2009)	Triallelic 5-HTTLPR	50	[¹¹ C]DASB	<i>LalLa</i> > <i>s</i> -carriers	Caudate	
Murthy et al. (2010)	Triallelic 5-HTTLPR	63	[¹¹ C]DASB	No effect	Serotonin-rich regions	Only male Caucasians, no effects of daylight
Kauppila et al. (2013)	5-HTTLPR	30	[¹²³ I]nor-β-CIT	<i>s</i> -Carriers > <i>ll</i>	Thalamus	No effect in other regions
Laje et al. (2010)	5-HT _{1A}	43	[¹¹ C]DASB	rs7333412, rs7997012, rs977003 AA < AG < GG	Thalamus	
Henningsson et al. (2009)	BDNF Val66Met	25	[¹¹ C]MADAM	Val/Val > Met+	Serotonin-rich regions	Finding significant in males only
Klein et al. (2010)	BDNF Val66Met	49	[¹¹ C]DASB	No effect	Caudate, putamen, thalamus	Also no effect of plasma BDNF levels

Adapted from Willeit and Praschak-Rieder (2010)

^aHealthy subjects if not otherwise indicated^bAD Patients with alcohol dependence^cMDD Major depressive disorder

study (Parsey et al. 2006b, c) showed increased binding of the selective 5-HT_{1A} receptor radioligand [¹¹C]WAY100635 in carriers of the C(-1019)G *G*-allele. This study also showed higher 5-HT_{1A} receptor binding in antidepressant-naïve subjects. *GG*-homozygous subjects were overrepresented in the group of depressed patients in this study; however, the majority of studies find the low-expressing *C*-allele of C(-1019)G to be overrepresented in major depression (Kishi et al. 2012). A recent study in a relatively large collective of healthy subjects (Lanzenberger et al. 2012b) did not show any effect of C(-1019)G on brain [¹¹C]WAY100635 binding.

The literature also reports some studies that investigated the influence of the 5-HTTLPR polymorphism on 5-HT_{1A} receptor binding in the brain (Table 6.2). Two studies (one of them was performed in a relatively large sample of nonhuman primates) describe lower 5-HT_{1A} receptor binding in carriers of the low-expressing 5-HTTLPR *s*-allele (David et al. 2005; Christian et al. 2013). Two further studies describe higher 5-HT_{1A} receptor binding in female carriers of the 5-HTTLPR *l*-allele (Lee et al. 2005; Borg et al. 2009), and a third study does not detect any effect 5-HTTLPR on 5-HT_{1A} receptor binding in a relatively large sample of healthy subjects (Borg et al. 2009). In sum, the evidence concerning the impact of genetic polymorphisms on 5-HT_{1A} receptor binding in the brain is, as of yet, inconclusive.

6.2.7 The Serotonin 4 Receptor

The 5-HT₄ receptor is abundant in serotonin-rich areas of the brain like the basal ganglia and hippocampus (Waeber et al. 1996; Varnas et al. 2003) and plays a role in anxiety- and depression-like behaviour. Studies in mice using autoradiography have shown that modification of 5-HTT gene expression was associated with alterations in 5-HT₄ density: 5-HTT knockout mice showed reduced 5-HT₄ density, and mice over-expressing 5-HTT showed increased 5-HT₄ density (Jennings et al. 2011). 5-HT₄ receptor expression and function seems to be influenced by extracellular serotonin levels, as increases in extracellular serotonin induced by paroxetine given for several weeks are associated with low 5-HT₄ levels (Licht et al. 2009; Vidal et al. 2009).

The PET radioligand [¹¹C]SB207145 is a newly developed selective tracer for imaging 5-HT₄ receptors in the human brain (Marnier et al. 2009, 2010; Paterson et al. 2010). Since a study in healthy volunteers suggested that acute administration of citalopram does not alter binding of [¹¹C]SB207145 (Marnier et al. 2010), it was speculated that [¹¹C]SB207145 PET could be a useful tool for indirectly measuring chronic, but not acute, changes in extracellular serotonin levels. Fisher et al. thus conducted a study on the effects of 5-HTTLPR on binding of the selective 5-HT₄ radioligand [¹¹C]SB207145 in healthy subjects (Fisher et al. 2012). 5-HT₄ receptor binding in the neocortex was 9 % lower in *s*-allele carriers compared to *l/l* homozygous subjects, providing further evidence that 5-HTTLPR genotype may influence serotonin transmission in humans. No effect of season or season-by-5-HTTLPR interaction on [¹¹C]SB207145 binding was found in this sample. Limitations of this study are that *l/l* subjects were older than *s*-allele carriers and that datasets were collected on two different PET scanners with a significant effect of scanner type.

Table 6.2 Effects of polymorphisms on serotonin 1A (5-HT1A), serotonin 2A (5-HT2A) and serotonin 4 (5-HT4) receptor binding

	Polymorphism	Number of subjects ^a	Radioligand	Results	Region	Comment
David et al. (2005)	5HT1A C(-1019)G	35	[¹ C]WAY 100635 (5-HT1A)	No effect	5HT1A receptor-rich regions	Subjects also genotyped for 5-HTTLPR (see below)
Parsey et al. (2006b)	5HT1A C(-1019)G	71 (28 MDD) ^b	[¹ C]WAY 100635 (5-HT1A)	GG>CG>CC	Raphe nuclei	
Lanzemberger et al. (2012b)	5HT1A C(-1019)G	50	[¹ C]WAY 100635 (5-HT1A)	No effect	5HT1A receptor-rich regions	
David et al. (2005)	5-HTTLPR	35	[¹ C]WAY 100635 (5-HT1A)	ll>ls/ss	Widespread	Subjects also genotyped for 5-HT1A C(-1019)G (see above)
Lee et al. (2005)	5-HTTLPR	16	[¹ C]WAY 100635 (5-HT1A)	ll<ls/ss	Anterior cingulum	All female study sample
Borg et al. (2009)	5-HTTLPR	54	[¹ C]WAY 100635 (5-HT1A)	No effect	–	5-HTTLPR effects cognitive performance
Lothe et al. (2009)	Triallelic 5-HTTLPR	38	[¹⁸ F]MPPF (5-HT1A)	La carriers <ss, females only	Widespread except raphe nuclei	No genotype effect in males (<i>n</i> =13)
Fisher et al. (2012)	Triallelic 5-HTTLPR	47	[¹ C]SB207145 (5-HT4)	ll>ls/ss	Neocortex	ll Subjects older than ls/ss
Henningsson et al. (2009)	BDNF Val66Met	53	[¹ C]WAY 100635 (5-HT1A)	No effect	Cortex and pons	
Klein et al. (2010)	BDNF Val66Met	133	[¹⁸ F]flanserin (5-HT2A)	No effect	Cortex	

Adapted from Willeit and Praschak-Rieder (2010)

^aHealthy subjects if not otherwise indicated^bMDD Major depressive disorder

6.3 Dopamine

Due to their preeminent role in addiction and psychotic disorders, brain dopamine systems have been extensively studied with PET and SPECT imaging techniques in psychiatric populations (see Cumming 2009 for in-depth review of dopamine imaging). Dopamine neurons in the brain originate almost exclusively in the brainstem substantia nigra and the more medially located ventral tegmental area. Important projection areas for dopamine neurons are the frontal cortex and subcortical structures, especially the striatum. The best studied dopaminergic region in the brain is the striatum, since it has a high density of dopamine nerve terminals and is thus a region that is particularly well suited for PET and SPECT imaging. Frequently targeted molecules are G-protein-coupled postsynaptic dopamine receptors and the dopamine transporter (DAT).

6.3.1 Dopamine $D_{2/3}$ Receptors

According to their effects on postsynaptic levels of cyclic adenosine monophosphate (cAMP), dopamine receptors are grouped into two families, the D_1 receptor family (dopamine D_1 and D_5 receptors) and the D_2 receptor family (dopamine D_2 , D_3 and D_4 receptors). As the main target of antipsychotic medication, dopamine $D_{2/3}$ receptors have been of particular interest for imaging studies in schizophrenia. Moreover, $D_{2/3}$ receptor imaging techniques have successfully been used to demonstrate alterations in brain dopamine transmission in addictive disorders (Volkow et al. 2009; Urban and Martinez 2012). While current evidence speaks against a relevant alteration in the quantity of $D_{2/3}$ receptors that are accessible to PET imaging in schizophrenia (Howes et al. 2012), several studies have shown a reduction of $D_{2/3}$ binding in addictive disorders (Volkow et al. 2009; Urban and Martinez 2012).

There are several studies on the influence of genetic variation on $D_{2/3}$ receptor binding in the literature (Table 6.4; for review, see Willeit and Praschak-Rieder 2010). To our knowledge, the only replicated finding as of yet is a reduction in binding of the $D_{2/3}$ radioligand [^{11}C]raclopride in carriers of the Taq1 A1 allele as compared to A2 homozygotes (Pohjalainen et al. 1998; Jonsson et al. 1999). However, a study of this polymorphism with SPECT and the radioligand [^{123}I]IBZM did not show differences between the genotypic groups (Laruelle et al. 1998). Other polymorphisms in the D_2 receptor gene showed in part significant effects but still warrant replication (Table 6.3). A recent study investigated a possible association between polymorphisms in the Period2 (PER2) gene and dopamine $D_{2/3}$ receptor binding as measured using [^{11}C]raclopride and PET (Shumay et al. 2012a). PER2 is part of the clock-gene family and involved in the reaction of organisms to circadian and circannual changes in lighting conditions and day length. Dopamine transmission shows circadian and seasonal changes in rodents and humans (Castaneda et al. 2004; Tsai et al. 2011; Eisenberg et al. 2010). The authors report on a newly identified VNTR polymorphism in the human PER2 gene that was associated with cocaine craving and striatal dopamine $D_{2/3}$ receptor binding. This finding is so far very

Table 6.3 Effects of dopamine D2 receptor polymorphisms on D2 receptor binding, dopamine transporter (DAT) binding and dopamine synthesis

	Polymorphism	Number of subjects ^a	Radioligand	Results	Region	Comment
Pohjalainen et al. (1998)	Taq1 A	54	[¹¹ C]raclopride (2 scans)	A1 carriers <A2/A2	Striatum	No effect on D2 affinity
Laruelle et al. (1998)	Taq1 A, Taq1 B	70 (23 SCZ) ^b	[¹²³ I]IBZM	No effect	Striatum	
Jönsson et al. (1999)	Taq1 A Taq1 B - ⁴¹ C Ins/Del	56	[¹¹ C]raclopride	A1 carriers <A2/A2 B1 carriers <B2/B2 Del carriers >Ins/Ins	Striatum	
Pohjalainen et al. (1999)	- ⁴¹ C Ins/Del	52	[¹¹ C]raclopride	No effect	Striatum	Same sample as in Pohjalainen et al. (1998)
Hirvonen et al. (2004)	C957T	45	[¹¹ C]raclopride	T/T > C/T > CC	Striatum	Same sample as in Pohjalainen et al. (1998)
Hirvonen et al. (2009)	C957T	45	[¹¹ C]raclopride (2 scans)	Effect on affinity: K_D C/C > C/T > TT	Striatum	Same sample as in Pohjalainen et al. (1998)
Bertolino et al. (2010)	D2 rs1076560 (G>T)	37	[¹²³ I]IBZM [¹²³ I]FP-CIT	No effect on B_{max} D2 binding T < G DAT binding T < G	Striatum	Effect on correlation between D2 binding and prefrontal activity
Laakso et al. (2005)	Taq1 A - ⁴¹ C Ins/Del C957T	33	[¹⁸ F]FDOPA	Higher uptake in A1 carriers; no effect of - ⁴¹ C Ins/Del, C957T	Striatum	
Laine et al. (2001)	Taq1 A	29 AD ^c	[¹²³ I] β-CIT	Higher DAT binding in A1 carriers	Striatum	
Sambataro et al. (2011)	D2 rs1076560 (G>T)	28	[¹²³ I]FP-CIT	No effect	Striatum	
Shumay et al. (2012a)	PER2 (Period2)	52	[¹¹ C]raclopride	Higher binding in 4R and 3R homozygotes	Striatum	Clock-gene family

Adapted from Willeit and Praschak-Rieder (2010)

^aHealthy subjects if not otherwise indicated^bSchizophrenia^cAlcohol dependence

Table 6.4 Effects of polymorphisms within the dopamine transporter gene SLC6A3 on in vivo dopamine transporter binding in humans

Polymorphism	Number of subjects ^a	Radioligand	Results	Region	Comment
Heinz et al. (2000a)	25 (14 AD) ^b	[¹²³ I]-β-CIT	9-repeat carriers <10/10	Putamen	Alcohol not associated with DAT binding genotype
Jacobsen et al. (2000)	44 (14 CA) ^c	[¹²³ I]-β-CIT	9-repeat carriers >10/10	Striatum	5-HTTLPR not associated with [¹²³ I]-β-CIT binding in midbrain
Martinez et al. (2001)	43 (22 SCZ) ^d	[¹²³ I]-β-CIT	No effect	Striatum	No genotype effect on amphetamine-induced dopamine release
Lynch et al. (2003)	166 (100 PD) ^e	[^{99m} Tc]TRODAT-1	No effect	Striatum	Also no effect of COMT and MAO-B polymorphisms
Van Dyck et al. (2005)	96	[¹²³ I]-β-CIT	9-repeat carriers >10/10	Striatum	
Cheon et al. (2005)	11 children with ADHD ^f	[¹²³ I] IPT	9-repeat carriers <10/10	Basal ganglia	Response to methylphenidate better in 9-repeat-allele carriers
Krause et al. (2006)	22 ADHD ^f	[^{99m} Tc]TRODAT	No effect	Striatum	
Lafuente et al. (2007)	15 SCZ ^d	[¹²³ I] FP-CIT	No effect	Striatum	
van de Giessen et al. (2009)	79	[¹²³ I]-β-CIT	9-repeat carriers >10/10	Striatum	Haplotype 5' T-A 3' 9R highest DAT binding
Drgon et al. (2006)	15 (6 ADHD) ^f (rs2652511, rs2937639)	[¹¹ C]-cocaine PET	C-G > T-A	Ventral striatum	5' C-G combination confirmed postmortem
Szobot et al. (2010)	17 ADHD ^f DRD4 48-bp VNTR	[^{99m} Tc]TRODAT	Reduced occupancy in DAT10R homozygotes/ DRD4-7R carriers	Striatum	Subjects scanned before and after 3 weeks of methylphenidate treatment

Adapted from Willeit and Praschak-Rieder (2010)

^aHealthy subjects if not otherwise indicated^bAD Alcohol dependence^cCA Cocaine abuse^dSchizophrenia^eParkinson's disease^fAttention-deficit hyperactivity disorder

exciting as it brings together several research strings on the physiology of dopamine function and its implication in addiction (see also Praschak-Rieder and Willeit 2012 for further discussion).

6.3.2 The Dopamine Transporter

Another frequently studied target is the dopamine transporter (DAT), a member of the monoamine-transporter family that transports dopamine back into the presynaptic neuron immediately after its release into the extracellular space. DAT is the main target of therapeutic drugs, for example, methylphenidate, used to treat attention-deficit hyperactivity disorder (ADHD) or the antidepressant bupropion. DAT is also the main site of action of drugs of abuse such as cocaine or amphetamines. Radiolabelled DAT blockers such as [¹¹C]methylphenidate or [¹¹C]cocaine have successfully been used to quantify DAT availability in the human brain.

Several polymorphisms within the DAT gene or in its promoter region have been identified and studied for association with psychiatric disorders, and there is extensive literature on imaging the effects of some of these polymorphisms on DAT binding in the human brain (Willeit and Praschak-Rieder 2010). The most frequently imaged polymorphism is a 40-bp (base pair) VNTR (variable number of tandem repeats) polymorphism in the 3' untranslated region of exon 15 of the DAT gene SLC6A3 (Vandenberg et al. 1992, 2000). These studies included healthy subjects as well as patients with alcohol dependence, schizophrenia, ADHD and Parkinson's disease (Heinz et al. 2000a; Jacobsen et al. 2000; Martinez et al. 2001; Lynch et al. 2003; Cheon et al. 2005; van Dyck et al. 2005; Krause et al. 2006; Lafuente et al. 2007; van de Giessen et al. 2009; Table 6.4). A recent methodologically sound meta-analysis (Costa et al. 2011) provides no evidence to support the hypothesis that the DAT 40-bp VNTR is significantly associated with interindividual differences in DAT availability in the striatum. A SPECT study investigating a cluster of polymorphisms flanking a recently described splice variant in the DAT gene (Talkowski et al. 2010) did not show significant differences in [¹²³I]-β-CIT binding (van de Giessen et al. 2012). In summary, the results of these studies give no clear picture on the effects of the DAT 40-bp VNTR polymorphism. However, the number of studies is relatively small, and there is significant heterogeneity between the studies.

6.3.3 Measuring Dopamine Transporter Function

Radiolabelled dopamine precursors able to cross the blood-brain barrier (e.g. [¹⁸F] dihydroxyphenylalanine, [¹⁸F]DOPA) are converted into the DAT substrate [¹⁸F] dopamine in dopaminergic neurons. The striatal [¹⁸F]DOPA influx constant K_i reflects presynaptic dopamine uptake, synthesis and storage capacity and is regarded as a good proxy for presynaptic dopamine metabolism in the brain (Cumming 2009). Together with so-called 'competition' paradigms, a research technique that

allows for measuring the inhibition of radioligand binding at $D_{2/3}$ receptors by endogenous dopamine, [^{18}F]DOPA studies have now clearly shown that presynaptic dopamine synthesis capacity (Reith et al. 1994; Hietala et al. 1995, 1999; Lindstrom et al. 1999; Meyer-Lindenberg et al. 2002; McGowan et al. 2004; Kumakura et al. 2007; Bose et al. 2008; Nozaki et al. 2009), baseline synaptic dopamine levels (Abi-Dargham et al. 2000, 2009; Kegeles et al. 2010) and pharmacologically induced dopamine release (Laruelle et al. 1996; Breier et al. 1997; Abi-Dargham et al. 1998, 2009) are increased in schizophrenia (for review, see Howes et al. 2012).

Imaging measures of the hyper-dopaminergic state in schizophrenia can as well be conceptualized as an endophenotype of the disorder. Indeed, there are a number of studies on the genetic background of in vivo imaging measures of presynaptic dopamine function (Table 6.5). These studies investigated the influence of polymorphisms in the DAT gene (Martinez et al. 2001; Brody et al. 2006), in D_2 and D_3 receptor-related genes (Brody et al. 2006; Pecina et al. 2012; Savitz et al. 2013), in the gene coding for oxytocin (Love et al. 2012) and in the μ -opioid receptor gene (Domino et al. 2010) on DAT function. In these studies, dopamine release was induced either by administration of d-amphetamine, by nicotine from cigarettes or by behavioural stimuli such as stress and pain. All of the above-mentioned studies describe an association with reductions in $D_{2/3}$ radioligand binding (as an indirect measure for dopamine release) and the respective candidate genes. Although there emerges no consistent picture due to the variety of polymorphisms and the different methods used, all of these studies were able to show that results of ‘competition studies’ are in part driven by genetic variation. Some of the information collected in these studies might thus be used for refining future studies in patients with schizophrenia. Perhaps even more important, these studies were able to show that several neurochemical pathways are involved in regulating dopamine release in the living human brain. Regulatory mechanisms include feedback regulation in dopamine terminal fields (see, e.g. Savitz et al. 2013, brain opioid systems (Domino et al. 2010) and the neuropeptide oxytocin (Love et al. 2012)).

6.4 Other Polymorphisms

6.4.1 The Catechol-O-methyltransferase Val158Met Polymorphism

Catechol-O-methyltransferase (COMT) is an enzyme that catalyzes degradation of catecholamines (including epinephrine, norepinephrine and dopamine) in the periphery and the brain. While regulation of extracellular dopamine levels is heavily dependent on DAT function in subcortical brain areas, COMT is believed to be a key mechanism regulating dopamine activity in cortical, especially frontal cortical brain areas (Ciliax et al. 1999; Lewis et al. 2001; Matsumoto et al. 2003).

Several SNPs have been described in the COMT gene, but without doubt, the SNP causing a valine-to-methionine substitution at position 158 (COMT Val158Met) is one of the most studied polymorphisms in psychiatry and a series of other

Table 6.5 Effects of genetic polymorphisms on dopamine-induced reductions in $D_{2/3}$ receptor binding

	Polymorphism	Number of subjects ^a	Outcome measure	Results	Region	Comment
Martinez et al. (2001)	DAT 3' VNTR	59 (28 SCZ) ^b	d-Amphetamine-induced decrease in [¹²⁵ I]IBZM binding	No effect	Striatum	Greater reductions in patients; trend for greater reductions in 9-repeat carriers
Brody et al. (2006)	DAT 3' VNTR, D2 Taq A1/A, D4 VNTR, COMT Val158Met	45	Nicotine-induced decrease in [¹¹ C] raclopride binding	DAT: 9R > 10/10R D2: no effect D4: greater in <7R Val/Val > Met	Striatum	
Pecina et al. (2012)	D2 rs4274224 (A > G)	52	Stress-induced decrease in [¹¹ C] raclopride binding	AG > AA/GG	Caudate, putamen, ventral striatum	
Savitz et al. (2013)	D3 Ser9Gly	36 (10 MDD) ^c	Reward-induced decrease in [¹¹ C] raclopride binding	Gly > Ser	Caudate, ventral striatum	No genotype effect on baseline $D_{2/3}$ binding
Love et al. (2012)	Oxytocin Rs4813625	55	Pain-stress-induced decrease in [¹¹ C] raclopride binding	GC/CC > GG	Ventromedial caudate	Significant effects in females ($n = 32$) but not males
Domino et al. (2012)	μ -Opioid 1 receptor A118G	19 males	Nicotine-induced decrease in [¹¹ C] carfentanyl binding	AG/GG > AA	Caudate, ventral putamen	Significant effect of the polymorphism also on plasma cortisol levels

^aHealthy subjects if not otherwise indicated^bSCZ Schizophrenia^cMDD Major depressive disorder

disorders. The COMT 158Val variant degrades dopamine more efficiently than the COMT 158Met variant (Lachman et al. 1996), and the polymorphism has been associated with several psychiatric and other disorders. A finding that seems to hold true is a difference in executive function mediated mainly by prefrontal cortex dopamine between carriers of the gene variants. Thus, several studies have investigated behavioural, cognitive, functional and anatomical variance associated with this gene as an endophenotype in various disorders (see, e.g. Schosser et al. 2011; Witte and Floel 2011; Ira et al. 2013).

Two studies investigated the effects of COMT Val158Met using [^{18}F]DOPA and PET. A study (Meyer-Lindenberg et al. 2005) in healthy volunteers found increased striatal [^{18}F]DOPA uptake in 158Val carriers when compared to 158Met homozygotes. Another study in patients with early Parkinson's disease (Wu et al. 2012) describes higher [^{18}F]DOPA uptake measured between 150 and 210 min after radioligand injection in 158Met homozygous patients. Besides differences between study samples (young healthy volunteers versus patients with Parkinson's disease), the difference might be due to the fact that higher [^{18}F]DOPA in 158VMet homozygous patients with Parkinson's disease was measured from 150 min after tracer injection onwards. At this time, the [^{18}F]DOPA signal is believed to reflect rates of dopamine metabolism to 3,4-dihydroxyphenylacetic acid and homovanillic acid (Ruottinen et al. 2001; Ceravolo et al. 2002).

A study in healthy volunteers investigated the effects of COMT Val158Met on dopamine $D_{2/3}$ receptor binding using PET and the radioligands [^{11}C]raclopride and [^{11}C]FLB457 for assessing striatal and cortical $D_{2/3}$ binding, respectively. Since genotype had no effect on binding of either radioligand, the authors concluded that baseline in vivo $D_{2/3}$ receptor availability does not differ between COMT Val158Met genotypic groups. In contrast, another study using the dopamine D_1 receptor radioligand [^{11}C]NNC112 (Slifstein et al. 2008) found significantly higher cortical D_1 receptor binding in Val158 homozygotes, while no difference was found in striatum. This finding is in good agreement with the functional role of COMT Val158Met, as low dopamine levels have been found to cause upregulation of dopamine D_1 receptors in the rodent brain, while dopamine transmission in the basal ganglia is less affected due to the prominent role of DAT in these brain areas (Gogos et al. 1998; Guo et al. 2003). A recent study investigating the effects of the COMT Val158Met polymorphism on brain 5-HT $_{1A}$ receptor binding found significantly higher [^{11}C]WAY100635 binding in Val158 homozygotes in orbitofrontal cortex, cingulum, insula and amygdale (Baldinger et al. 2013). Peak differences were found in the posterior cingulate cortex.

6.4.2 Monoamine Oxidase A

Monoamine oxidase is an enzyme that catalyzes the oxidative degradation of biogenic amines. There are two isoforms, MAO-A and MAO-B. MAO-A has high affinity for serotonin norepinephrine and epinephrine. MAO-B mainly degrades phenethylamine, a so-called trace amine. Dopamine is a substrate of

both isoenzymes (Kalgutkar et al. 2001). The gene for MAO-A is located on the X chromosome (Xp11.23-11.4). A rare loss-of-function mutation of the gene is associated with behavioural features such as impulsive aggression, hypersexuality and reduced intelligence (Brunner et al. 1993). A polymorphism in the promoter region of the MAO-A gene affecting transcriptional activity (Sabol et al. 1998) has been linked to aggressive or antisocial behaviour in subjects exposed to childhood maltreatment (Caspi et al. 2002; Fergusson et al. 2011) or brain injury (Pardini et al. 2011). The polymorphism consists of a 30-bp repeat sequence present in three to five copies and is termed MAO-A *high* and *low* according to the amount of MAO-A produced in cell lines. As the polymorphism is located on the X chromosome, males are hemizygous for either the MAO-A *high* or *low* allele.

Radioligands for quantifying MAO-A activity in the brain are modified MAO-A inhibitors such as [^{11}C]clorgyline (MacGregor et al. 1985) or [^{11}C]harmine (Bergstrom et al. 1997; Ginovart et al. 2006). Both radioligands have successfully been used to study the role of MAO-A in aggression (Alia-Klein et al. 2008) or affective disorders (Meyer et al. 2006; Sacher et al. 2010).

To our knowledge, there are no studies published on the effects of genetic heterogeneity on [^{11}C]harmine binding in the human brain. A study investigating the MAO-A *high/low* polymorphism in 38 healthy subjects using [^{11}C]clorgyline (Fowler et al. 2007) did not find any relationship between genotype and brain [^{11}C]clorgyline binding. Males are hemizygous for this polymorphism (the MAO-A gene is located on the X chromosome); the effects of this polymorphism, if functional *in vivo*, should therefore be clearest in a male-only sample. A possible explanation for the negative finding is epigenetic regulation: Methylation of the MAO-A promoter has indeed been shown to have a clear influence on brain [^{11}C]clorgyline distribution volumes (Shumay et al. 2012b). Another study investigating the effects of this polymorphism on binding of the 5-HT_{1A} receptor radioligand [^{11}C]WAY 100635 (Mickey et al. 2008) found higher binding in females carrying the MAO-A *high* allele. No genotype effect was found in males.

6.4.3 18-kD Translocator Protein

Immune cells express an 18-kD translocator protein (TSPO) formerly known as the peripheral benzodiazepine receptor (Anholt et al. 1986). Expression of TSPO has been studied as a marker of microglia activation and inflammation in various disorders, including Alzheimer's disease, multiple sclerosis, front-temporal dementia and schizophrenia (Debruyne et al. 2002; Cagnin et al. 2004; Edison et al. 2008; Kreisl et al. 2012) using a variety of TSPO radioligands. The TSPO radioligand [^{11}C]PBR28 was observed to bind to TSPO with high affinity in some subjects, with low affinity in others and with intermediate affinity in a third group (Fujita et al. 2008; Kreisl et al. 2009; Owen et al. 2010, 2011), an observation that has been related to a polymorphism (rs6971) affecting binding of the radioligand PBR28 to TSPO in human platelets (Owen et al. 2011).

A study using the TSPO radioligand [^{18}F]FEPPA (Wilson et al. 2008) has shown clear effects of the rs6971 polymorphism in the human brain (Mizrahi et al. 2012). Another study using the radioligand [^{11}C]PBR28 confirmed these effects and showed increased [^{11}C]PBR28 binding in patients with schizophrenia when accounting for genotype effects (Kreisl et al. 2012). This study showed that data on TSPO binding need to be stratified by genotype in order to get information on TSPO expression in various disorders.

6.5 Summary and Outlook

This review shows that combining genetic research with neuroreceptor imaging using PET and SPECT has produced a large array of findings suggesting effects of genetic variants on protein expression in the living brain. Some genetic effects, for example, those of polymorphisms in the TSPO gene, seem strong enough as to produce plausible results with large effect sizes in PET imaging studies. Other results, such as those on the effects of 5-HTTLPR on 5-HTT binding or Taq1 A on dopamine $D_{2/3}$ receptor binding in the brain, show less clear-cut effects, and despite having been replicated independently, they are contrasted by studies with differing or negative results. Many studies in the field either are not replicated at all or are replicated with slightly different imaging methods or in differing study collectives, thus creating a ‘penumbra’ of a 0.05 significance level (Kapur et al. 2012) around the original findings without being able to answer the question whether a certain genetic variant does really have an effect on protein binding in the brain.

The way genetic research in psychiatry is conducted has changed dramatically in the last years. Typical studies at the beginning of this research had sample sizes in the low three-digit number range. The picture that emerged from these studies was quite similar to what we see in PET and SPECT imaging genetics today: many significant findings, few replications and no definite answers on candidate gene loci. Researchers have thus started to combine their efforts and to implement logistics for large international consortia that are able to collect data from tens or hundreds of thousands of subjects (Sullivan 2010). Similar efforts have been made in the field of MRI-based imaging genetics (the IMAGEN consortium started in 2007 is a good example; <http://www.imagen-europe.com>).

The single most important limitation of all studies reviewed here is a lack of power. Sample sizes in PET and SPECT imaging genetic studies are maybe even a bit larger than those in other PET and SPECT studies, most probably because genotyping is sometimes used to extract some additional scientific output from already existing projects sharing a radioligand (the mean sample size in the here reported studies is 44 subjects, the range 11–166). Still, due to the relatively small effect of most genetic variants and the large number of other factors influencing availability of target receptors, much larger samples would be needed to have adequately powered studies in this field. Neuroreceptor PET is an expensive and logistically difficult research technology available in a limited number of research centres around the world. It is time for the field to follow the example of other research areas and

to start combining efforts and cooperate. This would benefit not only imaging genetics but also all other research topics addressed with PET and SPECT imaging techniques.

References

- Abi-Dargham A, Gil R, Krystal J et al (1998) Increased striatal dopamine transmission in schizophrenia: confirmation in a second cohort. *Am J Psychiatry* 155(6):761–767
- Abi-Dargham A, Rodenhiser J, Printz D et al (2000) Increased baseline occupancy of D2 receptors by dopamine in schizophrenia. *Proc Natl Acad Sci U S A* 97(14):8104–8109
- Abi-Dargham A, van de Giessen E, Slifstein M, Kegeles LS, Laruelle M (2009) Baseline and amphetamine-stimulated dopamine activity are related in drug-naive schizophrenic subjects. *Biol Psychiatry* 65(12):1091–1093
- Akimova E, Lanzenberger R, Kasper S (2009) The serotonin-1A receptor in anxiety disorders. *Biol Psychiatry* 66(7):627–635
- Albert PR, Zhou QY, Van Tol HH, Bunzow JR, Civelli O (1990) Cloning, functional expression, and mRNA tissue distribution of the rat 5-hydroxytryptamine1A receptor gene. *J Biol Chem* 265(10):5825–5832
- Alia-Klein N, Goldstein RZ, Kriplani A et al (2008) Brain monoamine oxidase A activity predicts trait aggression. *J Neurosci* 28(19):5099–5104
- Angelova M, Benkelfat C, Turecki G (2003) A systematic review of association studies investigating genes coding for serotonin receptors and the serotonin transporter: II. Suicidal behavior. *Mol Psychiatry* 8(7):646–653
- Anholt RR, Pedersen PL, De Souza EB, Snyder SH (1986) The peripheral-type benzodiazepine receptor. Localization to the mitochondrial outer membrane. *J Biol Chem* 261(2):576–583
- Bailer UF, Frank GK, Henry SE et al (2005) Altered brain serotonin 5-HT1A receptor binding after recovery from anorexia nervosa measured by positron emission tomography and [¹¹C]WAY-100635. *Arch Gen Psychiatry* 62(9):1032–1041
- Bailer UF, Frank GK, Henry SE et al (2007) Exaggerated 5-HT1A but normal 5-HT2A receptor activity in individuals ill with anorexia nervosa. *Biol Psychiatry* 61(9):1090–1099
- Baldinger P, Hahn A, Mitterhauser M et al. (2013) Impact of COMT genotype on serotonin-1A receptor binding investigated with positron emission tomography. *Brain Struct Funct* (e-pub ahead of print August 9; DOI: [10.1007/s00429-013-0621-8](https://doi.org/10.1007/s00429-013-0621-8))
- Bel N, Artigas F (1992) Fluvoxamine preferentially increases extracellular 5-hydroxytryptamine in the raphe nuclei: an in vivo microdialysis study. *Eur J Pharmacol* 229(1):101–103
- Bergstrom M, Westerberg G, Langstrom B (1997) 11C-harmine as a tracer for monoamine oxidase A (MAO-A): in vitro and in vivo studies. *Nucl Med Biol* 24(4):287–293
- Bertolino A, Taurisano P, Pisciotto NM et al (2010) Genetically determined measures of striatal D2 signaling predict prefrontal activity during working memory performance. *PLoS One* 5(2):e9348
- Bondy B, Buettner A, Zill P (2006) Genetics of suicide. *Mol Psychiatry* 11(4):336–351
- Borg J, Henningsson S, Saijo T et al (2009) Serotonin transporter genotype is associated with cognitive performance but not regional 5-HT1A receptor binding in humans. *Int J Neuropsychopharmacol* 12(6):783–792
- Bose SK, Turkheimer FE, Howes OD et al (2008) Classification of schizophrenic patients and healthy controls using [¹⁸F] fluorodopa PET imaging. *Schizophr Res* 106(2–3):148–155
- Breier A, Su TP, Saunders R et al (1997) Schizophrenia is associated with elevated amphetamine-induced synaptic dopamine concentrations: evidence from a novel positron emission tomography method. *Proc Natl Acad Sci U S A* 94(6):2569–2574
- Brody AL, Mandelkern MA, Olmstead RE et al (2006) Gene variants of brain dopamine pathways and smoking-induced dopamine release in the ventral caudate/nucleus accumbens. *Arch Gen Psychiatry* 63(7):808–816

- Brunner HG, Nelen MR, van Zandvoort P et al (1993) X-linked borderline mental retardation with prominent behavioral disturbance: phenotype, genetic localization, and evidence for disturbed monoamine metabolism. *Am J Hum Genet* 52(6):1032–1039
- Brunoni AR, Lopes M, Fregni F (2008) A systematic review and meta-analysis of clinical studies on major depression and BDNF levels: implications for the role of neuroplasticity in depression. *Int J Neuropsychopharmacol* 11(8):1169–1180
- Buchert R, Schulze O, Wilke F et al (2006) Is correction for age necessary in SPECT or PET of the central serotonin transporter in young, healthy adults? *J Nucl Med* 47(1):38–42
- Cagnin A, Rossor M, Sampson EL, Mackinnon T, Banati RB (2004) In vivo detection of microglial activation in frontotemporal dementia. *Ann Neurol* 56(6):894–897
- Caspi A, McClay J, Moffitt TE et al (2002) Role of genotype in the cycle of violence in maltreated children. *Science* 297(5582):851–854
- Caspi A, Sugden K, Moffitt TE et al (2003) Influence of life stress on depression: moderation by a polymorphism in the 5-HTT gene. *Science* 301(5631):386–389
- Caspi A, Hariri AR, Holmes A, Uher R, Moffitt TE (2010) Genetic sensitivity to the environment: the case of the serotonin transporter gene and its implications for studying complex diseases and traits. *Am J Psychiatry* 167(5):509–527
- Castaneda TR, de Prado BM, Prieto D, Mora F (2004) Circadian rhythms of dopamine, glutamate and GABA in the striatum and nucleus accumbens of the awake rat: modulation by light. *J Pineal Res* 36(3):177–185
- Castren E (2004) Neurotrophic effects of antidepressant drugs. *Curr Opin Pharmacol* 4(1):58–64
- Ceravolo R, Piccini P, Bailey DL et al (2002) 18F-dopa PET evidence that tolcapone acts as a central COMT inhibitor in Parkinson's disease. *Synapse* 43(3):201–207
- Cheon KA, Ryu YH, Kim JW, Cho DY (2005) The homozygosity for 10-repeat allele at dopamine transporter gene and dopamine transporter density in Korean children with attention deficit hyperactivity disorder: relating to treatment response to methylphenidate. *Eur Neuropsychopharmacol* 15(1):95–101
- Christian BT, Wooten DW, Hillmer AT et al (2013) Serotonin transporter genotype affects serotonin 5-HT_{1A} binding in primates. *J Neurosci* 33(6):2512–2516
- Ciliax BJ, Drash GW, Staley JK et al (1999) Immunocytochemical localization of the dopamine transporter in human brain. *J Comp Neurol* 409(1):38–56
- Collier DA, Stober G, Li T et al (1996) A novel functional polymorphism within the promoter of the serotonin transporter gene: possible role in susceptibility to affective disorders. *Mol Psychiatry* 1(6):453–460
- Costa A, Riedel M, Muller U, Moller HJ, Ettinger U (2011) Relationship between SLC6A3 genotype and striatal dopamine transporter availability: a meta-analysis of human single photon emission computed tomography studies. *Synapse* 65(10):998–1005
- Cumming P (2009) *Imaging dopamine*. Cambridge University Press, New York
- David SP, Murthy NV, Rabiner EA et al (2005) A functional genetic variation of the serotonin (5-HT) transporter affects 5-HT_{1A} receptor binding in humans. *J Neurosci* 25(10):2586–2590
- de Almeida J, Mengod G (2008) Serotonin 1A receptors in human and monkey prefrontal cortex are mainly expressed in pyramidal neurons and in a GABAergic interneuron subpopulation: implications for schizophrenia and its treatment. *J Neurochem* 107(2):488–496
- Debruyne JC, Van Laere KJ, Versijpt J et al (2002) Semiquantification of the peripheral-type benzodiazepine ligand [11C]PK11195 in normal human brain and application in multiple sclerosis patients. *Acta Neurol Belg* 102(3):127–135
- Domino EF, Evans CL, Ni L et al (2010) Tobacco smoking produces greater striatal dopamine release in G-allele carriers with mu opioid receptor A118G polymorphism. *Prog Neuropsychopharmacol Biol Psychiatry* 38(2):236–240
- Domino EF, Evans CL, Ni L et al (2012) Tobacco smoking produces greater striatal dopamine release in G-allele carriers with mu opioid receptor A118G polymorphism. *Prog Neuropsychopharmacol Biol Psychiatry* 38(2):236–240
- Drago A, Ronchi DD, Serretti A (2008) 5-HT_{1A} gene variants and psychiatric disorders: a review of current literature and selection of SNPs for future studies. *Int J Neuropsychopharmacol* 11(5):701–721

- Drevets WC, Frank E, Price JC et al (1999) PET imaging of serotonin 1A receptor binding in depression. *Biol Psychiatry* 46(10):1375–1387
- Drevets WC, Frank E, Price JC et al (2000) Serotonin type-1A receptor imaging in depression. *Nucl Med Biol* 27(5):499–507
- Drevets WC, Thase ME, Moses-Kolko EL et al (2007) Serotonin-1A receptor imaging in recurrent depression: replication and literature review. *Nucl Med Biol* 34(7):865–877
- Drgon T, Lin Z, Wang GJ et al (2006) Common human 5' dopamine transporter (SLC6A3) haplotypes yield varying expression levels in vivo. *Cell Mol Neurobiol* 26(4–6):875–889
- Edison P, Archer HA, Gerhard A et al (2008) Microglia, amyloid, and cognition in Alzheimer's disease: an [11C](R)PK11195-PET and [11C]PIB-PET study. *Neurobiol Dis* 32(3):412–419
- Egan MF, Kojima M, Callicott JH et al (2003) The BDNF val66met polymorphism affects activity-dependent secretion of BDNF and human memory and hippocampal function. *Cell* 112(2):257–269
- Eisenberg DP, Kohn PD, Baller EB et al (2010) Seasonal effects on human striatal presynaptic dopamine synthesis. *J Neurosci* 30(44):14691–14694
- Fargin A, Raymond JR, Regan JW et al (1989) Effector coupling mechanisms of the cloned 5-HT_{1A} receptor. *J Biol Chem* 264(25):14848–14852
- Fergusson DM, Boden JM, Horwood LJ, Miller AL, Kennedy MA (2011) MAOA, abuse exposure and antisocial behaviour: 30-year longitudinal study. *Br J Psychiatry* 198(6):457–463
- Fisher PM, Holst KK, Mc Mahon B et al (2012) 5-HTTLPR status predictive of neocortical 5-HT₄ binding assessed with [(11)C]SB207145 PET in humans. *Neuroimage* 62(1):130–136
- Fowler JS, Alia-Klein N, Kriplani A et al (2007) Evidence that brain MAO A activity does not correspond to MAO A genotype in healthy male subjects. *Biol Psychiatry* 62(4):355–358
- Frankle WG, Huang Y, Hwang DR et al (2004) Comparative evaluation of serotonin transporter radioligands 11C-DASB and 11C-McN 5652 in healthy humans. *J Nucl Med* 45(4):682–694
- Frankle WG, Lombardo I, Kegeles LS et al (2006) Serotonin 1A receptor availability in patients with schizophrenia and schizo-affective disorder: a positron emission tomography imaging study with [11C]WAY 100635. *Psychopharmacology (Berl)* 189(2):155–164
- Freund TF, Gulyas AI, Acsady L, Gorcs T, Toth K (1990) Serotonergic control of the hippocampus via local inhibitory interneurons. *Proc Natl Acad Sci U S A* 87(21):8501–8505
- Fujita M, Imaizumi M, Zoghbi SS et al (2008) Kinetic analysis in healthy humans of a novel positron emission tomography radioligand to image the peripheral benzodiazepine receptor, a potential biomarker for inflammation. *Neuroimage* 40(1):43–52
- Ginovart N, Meyer JH, Boovariwala A et al (2006) Positron emission tomography quantification of [11C]-harmine binding to monoamine oxidase-A in the human brain. *J Cereb Blood Flow Metab* 26(3):330–344
- Gogos JA, Morgan M, Luine V et al (1998) Catechol-O-methyltransferase-deficient mice exhibit sexually dimorphic changes in catecholamine levels and behavior. *Proc Natl Acad Sci U S A* 95(17):9991–9996
- Gratacos M, Gonzalez JR, Mercader JM et al (2007) Brain-derived neurotrophic factor Val66Met and psychiatric disorders: meta-analysis of case-control studies confirm association to substance-related disorders, eating disorders, and schizophrenia. *Biol Psychiatry* 61(7):911–922
- Greenberg BD, Tolliver TJ, Huang SJ et al (1999) Genetic variation in the serotonin transporter promoter region affects serotonin uptake in human blood platelets. *Am J Med Genet* 88(1):83–87
- Grunblatt E, Loffler C, Zehetmayer S et al (2006) Association study of the 5-HTTLPR polymorphism and depression in 75-year-old nondemented subjects from the Vienna transdanube aging (VITA) study. *J Clin Psychiatry* 67(9):1373–1378
- Guo N, Hwang DR, Lo ES et al (2003) Dopamine depletion and in vivo binding of PET D1 receptor radioligands: implications for imaging studies in schizophrenia. *Neuropsychopharmacology* 28(9):1703–1711
- Hariri AR, Holmes A (2006) Genetics of emotional regulation: the role of the serotonin transporter in neural function. *Trends Cogn Sci* 10(4):182–191
- Hariri AR, Mattay VS, Tessitore A et al (2002) Serotonin transporter genetic variation and the response of the human amygdala. *Science* 297(5580):400–403

- Hariri AR, Goldberg TE, Mattay VS et al (2003) Brain-derived neurotrophic factor val66met polymorphism affects human memory-related hippocampal activity and predicts memory performance. *J Neurosci* 23(17):6690–6694
- Heils A, Teufel A, Petri S et al (1996) Allelic variation of human serotonin transporter gene expression. *J Neurochem* 66(6):2621–2624
- Heinz A, Goldman D, Jones DW et al (2000a) Genotype influences in vivo dopamine transporter availability in human striatum. *Neuropsychopharmacology* 22(2):133–139
- Heinz A, Jones DW, Mazzanti C et al (2000b) A relationship between serotonin transporter genotype and in vivo protein expression and alcohol neurotoxicity. *Biol Psychiatry* 47(7):643–649
- Henningsson S, Borg J, Lundberg J et al (2009) Genetic variation in brain-derived neurotrophic factor is associated with serotonin transporter but not serotonin-1A receptor availability in men. *Biol Psychiatry* 66(5):477–485
- Hietala J, Syvalahti E, Vuorio K et al (1995) Presynaptic dopamine function in striatum of neuroleptic-naïve schizophrenic patients. *Lancet* 346(8983):1130–1131
- Hietala J, Syvalahti E, Vilkmann H et al (1999) Depressive symptoms and presynaptic dopamine function in neuroleptic-naïve schizophrenia. *Schizophr Res* 35(1):41–50
- Hirvonen M, Laakso A, Nagren K et al (2004) C957T polymorphism of the dopamine D2 receptor (DRD2) gene affects striatal DRD2 availability in vivo. *Mol Psychiatry* 9(12):1060–1061
- Hirvonen J, Karlsson H, Kajander J et al (2008) Decreased brain serotonin 5-HT_{1A} receptor availability in medication-naïve patients with major depressive disorder: an in-vivo imaging study using PET and [carbonyl-¹¹C]WAY-100635. *Int J Neuropsychopharmacol* 11(4):465–476
- Hirvonen MM, Laakso A, Nagren K et al (2009) C957T polymorphism of dopamine D2 receptor gene affects striatal DRD2 in vivo availability by changing the receptor affinity. *Synapse* 63(10):907–912
- Homberg JR, Lesch KP (2010) Looking on the bright side of serotonin transporter gene variation. *Biol Psychiatry* 69(6):513–519
- Houle S, Ginovart N, Hussey D, Meyer JH, Wilson AA (2000) Imaging the serotonin transporter with positron emission tomography: initial human studies with [C-11]DAPP and [C-11]DASB. *Eur J Nucl Med* 27(11):1719–1722
- Howes OD, Kambaitz J, Kim E et al (2012) The nature of dopamine dysfunction in schizophrenia and what this means for treatment. *Arch Gen Psychiatry* 69(8):776–786
- Huang TY, Hwang DR, Narendran R et al (2002) Comparative evaluation in nonhuman primates of five PET radiotracers for imaging the serotonin transporters: [C-11]McN 5652, [C-11]ADAM, [C-11]DASB, [C-11]DAPA, and [C-11]AFM. *J Cereb Blood Flow Metab* 22(11):1377–1398
- Ira E, Zanoni M, Ruggeri M, Dazzan P, Tosato S (2013) COMT, neuropsychological function and brain structure in schizophrenia: a systematic review and neurobiological interpretation. *J Psychiatry Neurosci* 38(3):120178
- Ito H, Halldin C, Farde L (1999) Localization of 5-HT_{1A} receptors in the living human brain using [carbonyl-¹¹C]WAY-100635: PET with anatomic standardization technique. *J Nucl Med* 40(1):102–109
- Jacobsen LK, Staley JK, Zoghbi S et al (2000) Prediction of dopamine transporter binding availability by genotype: a preliminary report. *Am J Psychiatry* 157(10):1700–1703
- Jennings KA, Loder MK, Sheward WJ et al (2006) Increased expression of the 5-HT transporter confers a low-anxiety phenotype linked to decreased 5-HT transmission. *J Neurosci* 26(35):8955–8964
- Jennings KA, Licht CL, Bruce A et al (2011) Genetic variation in 5-hydroxytryptamine transporter expression causes adaptive changes in 5-HT₄ receptor levels. *Int J Neuropsychopharmacol* 15(8):1099–1107
- Johansson C, Willeit M, Levitan R et al (2003) The serotonin transporter promoter repeat length polymorphism, seasonal affective disorder and seasonality. *Psychol Med* 33(5):785–792
- Jones KR, Reichardt LF (1990) Molecular cloning of a human gene that is a member of the nerve growth factor family. *Proc Natl Acad Sci U S A* 87(20):8060–8064

- Jonsson EG, Nothen MM, Grunhage F et al (1999) Polymorphisms in the dopamine D2 receptor gene and their relationships to striatal dopamine receptor density of healthy volunteers. *Mol Psychiatry* 4(3):290–296
- Kalbitzer J, Frokjaer VG, Erritzoe D et al (2009) The personality trait openness is related to cerebral 5-HTT levels. *Neuroimage* 45(2):280–285
- Kalbitzer J, Erritzoe D, Holst KK et al (2010) Seasonal changes in brain serotonin transporter binding in short serotonin transporter linked polymorphic region-allele carriers but not in long-allele homozygotes. *Biol Psychiatry* 67(11):1033–1039
- Kalgutkar AS, Dalvie DK, Castagnoli N Jr, Taylor TJ (2001) Interactions of nitrogen-containing xenobiotics with monoamine oxidase (MAO) isozymes A and B: SAR studies on MAO substrates and inhibitors. *Chem Res Toxicol* 14(9):1139–1162
- Kapur S, Phillips AG, Insel TR (2012) Why has it taken so long for biological psychiatry to develop clinical tests and what to do about it? *Mol Psychiatry* 17(12):1174–1179
- Karg K, Burmeister M, Shedden K, Sen S (2011) The serotonin transporter promoter variant (5-HTTLPR), stress, and depression meta-analysis revisited: evidence of genetic moderation. *Arch Gen Psychiatry* 68(5):444–454
- Kaupilla E, Vanninen E, Kaurijoki S et al (2013) Influence of serotonin transporter gene polymorphism (5-HTTLPR polymorphism) on the relation between brain 5-HT transporter binding and heart rate corrected cardiac repolarization interval. *PLoS One* 8(1):e50303
- Kegeles LS, Abi-Dargham A, Frankle WG et al (2010) Increased synaptic dopamine function in associative regions of the striatum in schizophrenia. *Arch Gen Psychiatry* 67(3):231–239
- Kishi T, Yoshimura R, Fukuo Y et al (2012) The serotonin 1A receptor gene confer susceptibility to mood disorders: results from an extended meta-analysis of patients with major depression and bipolar disorder. *Eur Arch Psychiatry Clin Neurosci* 263(2):105–118
- Klein AB, Trajkovska V, Erritzoe D et al (2010) Cerebral 5-HT_{2A} receptor and serotonin transporter binding in humans are not affected by the val66met BDNF polymorphism status or blood BDNF levels. *J Cereb Blood Flow Metab* 30(11):e1–e7
- Kraft JB, Slager SL, McGrath PJ, Hamilton SP (2005) Sequence analysis of the serotonin transporter and associations with antidepressant response. *Biol Psychiatry* 58(5):374–381
- Krause J, Dresel SH, Krause KH et al (2006) Striatal dopamine transporter availability and DAT-1 gene in adults with ADHD: No higher DAT availability in patients with homozygosity for the 10-repeat allele. *World J Biol Psychiatry* 7(3):152–157
- Kreisl WC, Fujita M, Fujimura Y et al (2009) Comparison of [(11)C]-(R)-PK 11195 and [(11)C]PBR28, two radioligands for translocator protein (18 kDa) in human and monkey: implications for positron emission tomographic imaging of this inflammation biomarker. *Neuroimage* 49(4):2924–2932
- Kreisl WC, Jenko KJ, Hines CS et al (2012) A genetic polymorphism for translocator protein 18 kDa affects both in vitro and in vivo radioligand binding in human brain to this putative biomarker of neuroinflammation. *J Cereb Blood Flow Metab* 33(1):53–58
- Kumakura Y, Cumming P, Vernaleken I et al (2007) Elevated [18F]fluorodopamine turnover in brain of patients with schizophrenia: an [18F]fluorodopa/positron emission tomography study. *J Neurosci* 27(30):8080–8087
- Kunugi H, Hattori M, Kato T et al (1997) Serotonin transporter gene polymorphisms: ethnic difference and possible association with bipolar affective disorder. *Mol Psychiatry* 2(6):457–462
- Laakso A, Pohjalainen T, Bergman J et al (2005) The A1 allele of the human D2 dopamine receptor gene is associated with increased activity of striatal L-amino acid decarboxylase in healthy subjects. *Pharmacogenet Genomics* 15(6):387–391
- Lachman HM, Morrow B, Shprintzen R et al (1996) Association of codon 108/158 catechol-O-methyltransferase gene polymorphism with the psychiatric manifestations of velo-cardio-facial syndrome. *Am J Med Genet* 67(5):468–472
- Lafuente A, Bernardo M, Mas S et al (2007) Dopamine transporter (DAT) genotype (VNTR) and phenotype in extrapyramidal symptoms induced by antipsychotics. *Schizophr Res* 90(1–3):115–122
- Laine TP, Ahonen A, Rasanen P et al (2001) The A1 allele of the D2 dopamine receptor gene is associated with high dopamine transporter density in detoxified alcoholics. *Alcohol Alcohol* 36(3):262–265

- Laje G, Cannon DM, Allen AS et al (2010) Genetic variation in HTR2A influences serotonin transporter binding potential as measured using PET and [¹¹C]DASB. *Int J Neuropsychopharmacol* 13(6):715–724
- Langenberger RR, Mitterhauser M, Spindelegger C et al (2007) Reduced serotonin-1A receptor binding in social anxiety disorder. *Biol Psychiatry* 61(9):1081–1089
- Langenberger R, Baldinger P, Hahn A et al (2012a) Global decrease of serotonin-1A receptor binding after electroconvulsive therapy in major depression measured by PET. *Mol Psychiatry* 18(1):93–100
- Langenberger R, Mitterhauser M, Hahn A et al (2012b) Molecular imaging genetics of the serotonin-1A receptor investigating the common rs6295 single nucleotide polymorphism. *J Cereb Blood Flow Metab* 32(Suppl 1):S85
- Laruelle M, Abi-Dargham A, van Dyck CH et al (1996) Single photon emission computerized tomography imaging of amphetamine-induced dopamine release in drug-free schizophrenic subjects. *Proc Natl Acad Sci U S A* 93(17):9235–9240
- Laruelle M, Gelernter J, Innis RB (1998) D2 receptors binding potential is not affected by Taq1 polymorphism at the D2 receptor gene. *Mol Psychiatry* 3(3):261–265
- Le Francois B, Czesak M, Steubl D, Albert PR (2008) Transcriptional regulation at a HTR1A polymorphism associated with mental illness. *Neuropharmacology* 55(6):977–985
- Lee M, Bailer UF, Frank GK et al (2005) Relationship of a 5-HT transporter functional polymorphism to 5-HT1A receptor binding in healthy women. *Mol Psychiatry* 10(8):715–716
- Lesch KP, Bengel D, Heils A et al (1996) Association of anxiety-related traits with a polymorphism in the serotonin transporter gene regulatory region. *Science* 274(5292):1527–1531
- Lewis DA, Melchitzky DS, Sesack SR et al (2001) Dopamine transporter immunoreactivity in monkey cerebral cortex: regional, laminar, and ultrastructural localization. *J Comp Neurol* 432(1):119–136
- Licht CL, Marcussen AB, Wegener G et al (2009) The brain 5-HT₄ receptor binding is down-regulated in the Flinders Sensitive Line depression model and in response to paroxetine administration. *J Neurochem* 109(5):1363–1374
- Lindstrom LH, Gefvert O, Hagberg G et al (1999) Increased dopamine synthesis rate in medial prefrontal cortex and striatum in schizophrenia indicated by L-(beta-¹¹C) DOPA and PET. *Biol Psychiatry* 46(5):681–688
- Lothe A, Boni C, Costes N et al (2009) Association between triallelic polymorphism of the serotonin transporter and [F-¹⁸] MPPF binding potential at 5-HT_{1A} receptors in healthy subjects. *Neuroimage* 47(2):482–492
- Love TM, Enoch MA, Hodgkinson CA et al (2012) Oxytocin gene polymorphisms influence human dopaminergic function in a sex-dependent manner. *Biol Psychiatry* 72(3):198–206
- Lynch DR, Mozley PD, Sokol S et al (2003) Lack of effect of polymorphisms in dopamine metabolism related genes on imaging of TRODAT-1 in striatum of asymptomatic volunteers and patients with Parkinson's disease. *Mov Disord* 18(7):804–812
- MacGregor RR, Halldin C, Fowler JS et al (1985) Selective, irreversible in vivo binding of [¹¹C] clorgyline and [¹¹C]-L-deprenyl in mice: potential for measurement of functional monoamine oxidase activity in brain using positron emission tomography. *Biochem Pharmacol* 34(17):3207–3210
- Maisonpierre PC, Le Beau MM, Espinosa R 3rd et al (1991) Human and rat brain-derived neurotrophic factor and neurotrophin-3: gene structures, distributions, and chromosomal localizations. *Genomics* 10(3):558–568
- Malhotra AK, Goldman D, Mazzanti C et al (1998) A functional serotonin transporter (5-HTT) polymorphism is associated with psychosis in neuroleptic-free schizophrenics. *Mol Psychiatry* 3(4):328–332
- Malison RT, Price LH, Berman R et al (1998) Reduced brain serotonin transporter availability in major depression as measured by [¹²³I]-2 beta-carbomethoxy-3 beta-(4-iodophenyl)tropane and single photon emission computed tomography. *Biol Psychiatry* 44(11):1090–1098
- Marner L, Gillings N, Comley RA et al (2009) Kinetic modeling of ¹¹C-SB207145 binding to 5-HT₄ receptors in the human brain in vivo. *J Nucl Med* 50(6):900–908

- Marner L, Gillings N, Madsen K et al (2010) Brain imaging of serotonin 4 receptors in humans with [¹¹C]SB207145-PET. *Neuroimage* 50(3):855–861
- Martinez D, Gelernter J, Abi-Dargham A et al (2001) The variable number of tandem repeats polymorphism of the dopamine transporter gene is not associated with significant change in dopamine transporter phenotype in humans. *Neuropsychopharmacology* 24(5):553–560
- Matsumoto M, Weickert CS, Akil M et al (2003) Catechol O-methyltransferase mRNA expression in human and rat brain: evidence for a role in cortical neuronal function. *Neuroscience* 116(1):127–137
- McGowan S, Lawrence AD, Sales T, Queded D, Grasby P (2004) Presynaptic dopaminergic dysfunction in schizophrenia: a positron emission tomographic [¹⁸F]fluorodopa study. *Arch Gen Psychiatry* 61(2):134–142
- McMahon FJ, Buervenich S, Charney D et al (2006) Variation in the gene encoding the serotonin 2A receptor is associated with outcome of antidepressant treatment. *Am J Hum Genet* 78(5):804–814
- Meltzer CC, Price JC, Mathis CA et al (2004) Serotonin 1A receptor binding and treatment response in late-life depression. *Neuropsychopharmacology* 29(12):2258–2265
- Meyer JH (2007) Imaging the serotonin transporter during major depressive disorder and antidepressant treatment. *J Psychiatry Neurosci* 32(2):86–102
- Meyer JH, Houle S, Sagrati S et al (2004) Brain serotonin transporter binding potential measured with carbon 11-labeled DASB positron emission tomography – effects of major depression episodes and severity of dysfunctional attitudes. *Arch Gen Psychiatry* 61(12):1271–1279
- Meyer JH, Ginovart N, Boovariwala A et al (2006) Elevated monoamine oxidase A levels in the brain: an explanation for the monoamine imbalance of major depression. *Arch Gen Psychiatry* 63(11):1209–1216
- Meyer-Lindenberg A, Miletich RS, Kohn PD et al (2002) Reduced prefrontal activity predicts exaggerated striatal dopaminergic function in schizophrenia. *Nat Neurosci* 5(3):267–271
- Meyer-Lindenberg A, Kohn PD, Kolachana B et al (2005) Midbrain dopamine and prefrontal function in humans: interaction and modulation by COMT genotype. *Nat Neurosci* 8(5):594–596
- Mickey BJ, Ducci F, Hodgkinson CA et al (2008) Monoamine oxidase A genotype predicts human serotonin 1A receptor availability in vivo. *J Neurosci* 28(44):11354–11359
- Miller JM, Kinnally EL, Ogden RT et al (2009) Reported childhood abuse is associated with low serotonin transporter binding in vivo in major depressive disorder. *Synapse* 63(7):565–573
- Mizrahi R, Rusjan PM, Kennedy J et al (2012) Translocator protein (18 kDa) polymorphism (rs6971) explains in-vivo brain binding affinity of the PET radioligand [(18)F]-FEPPA. *J Cereb Blood Flow Metab* 32(6):968–972
- Moses-Kolko EL, Price JC, Thase ME et al (2007) Measurement of 5-HT_{1A} receptor binding in depressed adults before and after antidepressant drug treatment using positron emission tomography and [¹¹C]WAY-100635. *Synapse* 61(7):523–530
- Murthy NV, Selvaraj S, Cowen PJ et al (2010) Serotonin transporter polymorphisms (SLC6A4 insertion/deletion and rs25531) do not affect the availability of 5-HTT to [¹¹C] DASB binding in the living human brain. *Neuroimage* 52(1):50–54
- Nakamura M, Ueno S, Sano A, Tanabe H (2000) The human serotonin transporter gene linked polymorphism (5-HTTLPR) shows ten novel allelic variants. *Mol Psychiatry* 5(1):32–38
- Neumeister A, Bain E, Nugent AC et al (2004) Reduced serotonin type 1A receptor binding in panic disorder. *J Neurosci* 24(3):589–591
- Neumeister A, Yuan P, Young TA et al (2005) Effects of tryptophan depletion on serum levels of brain-derived neurotrophic factor in unmedicated patients with remitted depression and healthy subjects. *Am J Psychiatry* 162(4):805–807
- Neumeyer JL, Wang SY, Milius RA et al (1991) [¹²³I]-2 beta-carbomethoxy-3 beta-(4-iodophenyl) tropane: high-affinity SPECT radiotracer of monoamine reuptake sites in brain. *J Med Chem* 34(10):3144–3146
- Neves-Pereira M, Mundo E, Muglia P et al (2002) The brain-derived neurotrophic factor gene confers susceptibility to bipolar disorder: evidence from a family-based association study. *Am J Hum Genet* 71(3):651–655

- Nobile M, Begni B, Giorda R et al (1999) Effects of serotonin transporter promoter genotype on platelet serotonin transporter functionality in depressed children and adolescents. *J Am Acad Child Adolesc Psychiatry* 38(11):1396–1402
- Nozaki S, Kato M, Takano H et al (2009) Regional dopamine synthesis in patients with schizophrenia using L-[beta-11C]DOPA PET. *Schizophr Res* 108(1–3):78–84
- Owen DR, Howell OW, Tang SP et al (2010) Two binding sites for [3H]PBR28 in human brain: implications for TSPO PET imaging of neuroinflammation. *J Cereb Blood Flow Metab* 30(9):1608–1618
- Owen DR, Yeo AJ, Gunn RN et al (2011) An 18-kDa translocator protein (TSPO) polymorphism explains differences in binding affinity of the PET radioligand PBR28. *J Cereb Blood Flow Metab* 32(1):1–5
- Palchoudhuri M, Flugge G (2005) 5-HT1A receptor expression in pyramidal neurons of cortical and limbic brain regions. *Cell Tissue Res* 321(2):159–172
- Pardini M, Krueger F, Hodgkinson C et al (2011) Prefrontal cortex lesions and MAO-A modulate aggression in penetrating traumatic brain injury. *Neurology* 76(12):1038–1045
- Parsey RV, Hastings RS, Oquendo MA et al (2006a) Effect of a triallelic functional polymorphism of the serotonin-transporter-linked promoter region on expression of serotonin transporter in the human brain. *Am J Psychiatry* 163(1):48–51
- Parsey RV, Olvet DM, Oquendo MA et al (2006b) Higher 5-HT1A receptor binding potential during a major depressive episode predicts poor treatment response: preliminary data from a naturalistic study. *Neuropsychopharmacology* 31(8):1745–1749
- Parsey RV, Oquendo MA, Ogden RT et al (2006c) Altered serotonin 1A binding in major depression: a [carbonyl-C-11]WAY100635 positron emission tomography study. *Biol Psychiatry* 59(2):106–113
- Paterson LM, Tyacke RJ, Nutt DJ, Knudsen GM (2010) Measuring endogenous 5-HT release by emission tomography: promises and pitfalls. *J Cereb Blood Flow Metab* 30(10):1682–1706
- Patkar AA, Berrettini WH, Mannelli P et al (2004) Relationship between serotonin transporter gene polymorphisms and platelet serotonin transporter sites among African-American cocaine-dependent individuals and healthy volunteers. *Psychiatr Genet* 14(1):25–32
- Pecina M, Mickey BJ, Love T et al (2012) DRD2 polymorphisms modulate reward and emotion processing, dopamine neurotransmission and openness to experience. *Cortex* 49(3):877–890
- Pernhorst K, van Loo KM, von Lehe M et al (2013) Rs6295 promoter variants of the serotonin type 1A receptor are differentially activated by c-Jun in vitro and correlate to transcript levels in human epileptic brain tissue. *Brain Res* 1499:136–144
- Pezawas L, Verchinski BA, Mattay VS et al (2004) The brain-derived neurotrophic factor val66met polymorphism and variation in human cortical morphology. *J Neurosci* 24(45):10099–10102
- Pezawas L, Meyer-Lindenberg A, Drabant EM et al (2005) 5-HTTLPR polymorphism impacts human cingulate-amygdala interactions: a genetic susceptibility mechanism for depression. *Nat Neurosci* 8(6):828–834
- Pezawas L, Meyer-Lindenberg A, Goldman LA et al (2008) Evidence of biologic epistasis between BDNF and SLC6A4 and implications for depression. *Mol Psychiatry* 13(7):709–716
- Pirker W, Asenbaum S, Hauk M et al (2000) Imaging serotonin and dopamine transporters with 123I-beta-CIT SPECT: binding kinetics and effects of normal aging. *J Nucl Med* 41(1):36–44
- Pohjalainen T, Rinne JO, Nagren K et al (1998) The A1 allele of the human D2 dopamine receptor gene predicts low D2 receptor availability in healthy volunteers. *Mol Psychiatry* 3(3):256–260
- Pohjalainen T, Nagren K, Syvalahti EK, Hietala J (1999) The dopamine D2 receptor 5'-flanking variant, -141C Ins/Del, is not associated with reduced dopamine D2 receptor density in vivo. *Pharmacogenetics* 9(4):505–509
- Praschak-Rieder N, Willeit M (2012) Imaging of seasonal affective disorder and seasonality effects on serotonin and dopamine function in the human brain. *Curr Top Behav Neurosci* 11:149–167
- Praschak-Rieder N, Kennedy J, Wilson AA et al (2007) Novel 5-HTTLPR allele associates with higher serotonin transporter binding in putamen: a [C-11] DASB positron emission tomography study. *Biol Psychiatry* 62(4):327–331

- Praschak-Rieder N, Willeit M, Wilson AA, Houle S, Meyer JH (2008) Seasonal variation in human brain serotonin transporter binding. *Arch Gen Psychiatry* 65(9):1072–1078
- Purcell SM, Wray NR, Stone JL et al (2009) Common polygenic variation contributes to risk of schizophrenia and bipolar disorder. *Nature* 460(7256):748–752
- Reimold M, Smolka MN, Schumann G et al (2007) Midbrain serotonin transporter binding potential measured with [11 C]-DASB is affected by serotonin transporter genotype. *J Neural Transm* 114(5):635–639
- Reith J, Benkelfat C, Sherwin A et al (1994) Elevated dopa decarboxylase activity in living brain of patients with psychosis. *Proc Natl Acad Sci U S A* 91(24):11651–11654
- Risch N, Herrell R, Lehner T et al (2009) Interaction between the serotonin transporter gene (5-HTTLPR), stressful life events, and risk of depression: a meta-analysis. *JAMA* 301(23):2462–2471
- Rosenthal NE, Mazzanti CM, Barnett RL et al (1998) Role of serotonin transporter promoter repeat length polymorphism (5-HTTLPR) in seasonality and seasonal affective disorder. *Mol Psychiatry* 3(2):175–177
- Ruhe HG, Booij J, Reitsma JB, Schene AH (2009) Serotonin transporter binding with [123 I]beta-CIT SPECT in major depressive disorder versus controls: effect of season and gender. *Eur J Nucl Med Mol Imaging* 36(5):841–849
- Ruottinen HM, Niinivirta M, Bergman J et al (2001) Detection of response to COMT inhibition in FDOPA PET in advanced Parkinson's disease requires prolonged imaging. *Synapse* 40(1):19–26
- Sabol SZ, Hu S, Hamer D (1998) A functional polymorphism in the monoamine oxidase A gene promoter. *Hum Genet* 103(3):273–279
- Sacher J, Wilson AA, Houle S et al (2010) Elevated brain monoamine oxidase A binding in the early postpartum period. *Arch Gen Psychiatry* 67(5):468–474
- Saijo T, Takano A, Suhara T et al (2010) Effect of electroconvulsive therapy on 5-HT $_{1A}$ receptor binding in patients with depression: a PET study with [11 C]WAY 100635. *Int J Neuropsychopharmacol* 13(6):785–791
- Sambataro F, Fazio L, Taurisano P et al (2011) DRD2 Genotype-based variation of default mode network activity and of its relationship with striatal DAT binding. *Schizophr Bull* 39(1):206–216
- Savitz J, Lucki I, Drevets WC (2009) 5-HT $_{1A}$ receptor function in major depressive disorder. *Prog Neurobiol* 88(1):17–31
- Savitz J, Hodgkinson CA, Martin-Soelch C et al (2013) The functional DRD3 Ser9Gly polymorphism (rs6280) is pleiotropic, affecting reward as well as movement. *PLoS One* 8(1):e54108
- Schossner A, Calati R, Serretti A et al (2011) The impact of COMT gene polymorphisms on suicidality in treatment resistant major depressive disorder—a European multicenter study. *Eur Neuropsychopharmacol* 22(4):259–266
- Selvaraj S, Murthy NV, Bhagwagar Z et al (2009) Diminished brain 5-HT transporter binding in major depression: a positron emission tomography study with [11 C]DASB. *Psychopharmacology (Berl)* 213(2–3):555–562
- Serretti A, Cusin C, Lattuada E et al (1999) Serotonin transporter gene (5-HTTLPR) is not associated with depressive symptomatology in mood disorders. *Mol Psychiatry* 4(3):280–283
- Shen HW, Hagino Y, Kobayashi H et al (2004) Regional differences in extracellular dopamine and serotonin assessed by in vivo microdialysis in mice lacking dopamine and/or serotonin transporters. *Neuropsychopharmacology* 29(10):1790–1799
- Shi J, Levinson DF, Duan J et al (2009) Common variants on chromosome 6p22.1 are associated with schizophrenia. *Nature* 460(7256):753–757
- Shioe K, Ichimya T, Suhara T et al (2003) No association between genotype of the promoter region of serotonin transporter gene and serotonin transporter binding in human brain measured by PET. *Synapse* 48(4):184–188
- Shumay E, Fowler JS, Wang GJ et al (2012a) Repeat variation in the human PER2 gene as a new genetic marker associated with cocaine addiction and brain dopamine D2 receptor availability. *Transl Psychiatry* 2:e86

- Shumay E, Logan J, Volkow ND, Fowler JS (2012b) Evidence that the methylation state of the monoamine oxidase A (MAOA) gene predicts brain activity of MAO A enzyme in healthy men. *Epigenetics* 7(10):1151–1160
- Sklar P, Gabriel SB, McInnis MG et al (2002) Family-based association study of 76 candidate genes in bipolar disorder: BDNF is a potential risk locus. *Brain-derived neurotrophic factor. Mol Psychiatry* 7(6):579–593
- Slifstein M, Kolachana B, Simpson EH et al (2008) COMT genotype predicts cortical-limbic D1 receptor availability measured with [¹¹C]NNC112 and PET. *Mol Psychiatry* 13(8):821–827
- Spindelegger C, Lanzenberger R, Wadsak W et al (2009) Influence of escitalopram treatment on 5-HT(1A) receptor binding in limbic regions in patients with anxiety disorders. *Mol Psychiatry* 14(11):1040–1050
- Sprouse JS, Aghajanian GK (1988) Responses of hippocampal pyramidal cells to putative serotonin 5-HT_{1A} and 5-HT_{1B} agonists: a comparative study with dorsal raphe neurons. *Neuropharmacology* 27(7):707–715
- Stefansson H, Ophoff RA, Steinberg S et al (2009) Common variants conferring risk of schizophrenia. *Nature* 460(7256):744–747
- Stockmeier CA (2003) Involvement of serotonin in depression: evidence from postmortem and imaging studies of serotonin receptors and the serotonin transporter. *J Psychiatr Res* 37(5):357–373
- Storvik M, Hakkinen M, Tupala E, Tiihonen J (2009) 5-HT(1A) receptors in the frontal cortical brain areas in Cloninger type 1 and 2 alcoholics measured by whole-hemisphere autoradiography. *Alcohol Alcohol* 44(1):2–7
- Suehiro M, Scheffel U, Ravert HT, Dannals RF, Wagner HN (1993) [¹¹C]-(+)-MCN5652 as a radiotracer for imaging serotonin uptake sites with PET. *Life Sci* 53(11):883–892
- Sullivan PF (2010) The psychiatric GWAS consortium: big science comes to psychiatry. *Neuron* 68(2):182–186
- Sullivan GM, Ogdan RT, Huang YY et al (2013) Higher in vivo serotonin-1a binding in posttraumatic stress disorder: a pet study with [¹¹C]way-100635. *Depress Anxiety* 30(3):197–206
- Szabo Z, McCann UD, Wilson AA et al (2002) Comparison of (+)-C-11-McN5652 and C-11-DASB as serotonin transporter radioligands under various experimental conditions. *J Nucl Med* 43(5):678–692
- Szobot CM, Roman T, Hutz MH et al (2010) Molecular imaging genetics of methylphenidate response in ADHD and substance use comorbidity. *Synapse* 65(2):154–159
- Talkowski ME, McCann KL, Chen M et al (2010) Fine-mapping reveals novel alternative splicing of the dopamine transporter. *Am J Med Genet B Neuropsychiatr Genet* 153B(8):1434–1447
- Tauscher J, Kapur S, Verhoeff NP et al (2002) Brain serotonin 5-HT(1A) receptor binding in schizophrenia measured by positron emission tomography and [¹¹C]WAY-100635. *Arch Gen Psychiatry* 59(6):514–520
- Tsai HY, Chen KC, Yang YK et al (2011) Sunshine-exposure variation of human striatal dopamine D(2)/D(3) receptor availability in healthy volunteers. *Prog Neuropsychopharmacol Biol Psychiatry* 35(1):107–110
- Urban NB, Martinez D (2012) Neurobiology of addiction: insight from neurochemical imaging. *Psychiatr Clin North Am* 35(2):521–541
- van de Giessen EM, de Win MM, Tanck MW et al (2009) Striatal dopamine transporter availability associated with polymorphisms in the dopamine transporter gene SLC6A3. *J Nucl Med* 50(1):45–52
- van de Giessen E, Nimgaonkar VL, Watson AM et al (2012) Association tests of striatal DAT availability and SNPs that impact a novel splice variant in the DAT gene. *J Nucl Med* 53(5):839
- Van Dyck CH, Malison RT, Staley JK et al (2004) Central serotonin transporter availability measured with [¹-123]beta-CIT SPECT in relation to serotonin transporter genotype. *Am J Psychiatry* 161(3):525–531
- van Dyck CH, Malison RT, Jacobsen LK et al (2005) Increased dopamine transporter availability associated with the 9-repeat allele of the SLC6A3 gene. *J Nucl Med* 46(5):745–751

- Vandenberg DJ, Persico AM, Hawkins AL et al (1992) Human dopamine transporter gene (DAT1) maps to chromosome 5p15.3 and displays a VNTR. *Genomics* 14(4):1104–1106
- Vandenberg DJ, Thompson MD, Cook EH et al (2000) Human dopamine transporter gene: coding region conservation among normal, Tourette's disorder, alcohol dependence and attention-deficit hyperactivity disorder populations. *Mol Psychiatry* 5(3):283–292
- Varnas K, Halldin C, Pike VW, Hall H (2003) Distribution of 5-HT₄ receptors in the postmortem human brain—an autoradiographic study using [¹²⁵I]SB 207710. *Eur Neuropsychopharmacol* 13(4):228–234
- Vidal R, Valdizan EM, Mostany R, Pazos A, Castro E (2009) Long-term treatment with fluoxetine induces desensitization of 5-HT₄ receptor-dependent signalling and functionality in rat brain. *J Neurochem* 110(3):1120–1127
- Volkow ND, Fowler JS, Wang GJ, Baler R, Telang F (2009) Imaging dopamine's role in drug abuse and addiction. *Neuropharmacology* 56(Suppl 1):3–8
- Waeber C, Sebben M, Bockaert J, Dumuis A (1996) Regional distribution and ontogeny of 5-HT₄ binding sites in rat brain. *Behav Brain Res* 73(1–2):259–262
- Walther DJ, Peter JU, Bashammakh S et al (2003) Synthesis of serotonin by a second tryptophan hydroxylase isoform. *Science* 299(5603):76
- Willeit M, Praschak-Rieder N (2010) Imaging the effects of genetic polymorphisms on radioligand binding in the living human brain: a review on genetic neuroreceptor imaging of monoaminergic systems in psychiatry. *Neuroimage* 53(3):878–892
- Willeit M, Praschak-Rieder N, Neumeister A et al (2000) [¹²³I]-beta-CIT SPECT imaging shows reduced brain serotonin transporter availability in drug-free depressed patients with seasonal affective disorder. *Biol Psychiatry* 47(6):482–489
- Willeit M, Stastny J, Pirker W et al (2001) No evidence for in vivo regulation of midbrain serotonin transporter availability by serotonin transporter promoter gene polymorphism. *Biol Psychiatry* 50(1):8–12
- Willeit M, Praschak-Rieder N, Neumeister A et al (2003) A polymorphism (5-HTTLPR) in the serotonin transporter promoter gene is associated with DSM-IV depression subtypes in seasonal affective disorder. *Mol Psychiatry* 8(11):942–946
- Willeit M, Sitte HH, Thierry N et al (2008) Enhanced serotonin transporter function during depression in seasonal affective disorder. *Neuropsychopharmacology* 33(7):1503–1513
- Wilson AA, Houle S (1999) Radiosynthesis of carbon-11 labelled N-methyl-2-(arylthio)benzylamines: potential radiotracers for the serotonin reuptake receptor. *J Labelled Compd Radiopharm* 42(13):1277–1288
- Wilson AA, Ginovart N, Schmidt M et al (2000) Novel radiotracers for imaging the serotonin transporter by positron emission tomography: synthesis, radiosynthesis, and in vitro and ex vivo evaluation of C-11-labeled 2-(phenylthio)araalkylamines. *J Med Chem* 43(16):3103–3110
- Wilson AA, Garcia A, Parkes J et al (2008) Radiosynthesis and initial evaluation of [¹⁸F]-FEPPA for PET imaging of peripheral benzodiazepine receptors. *Nucl Med Biol* 35(3):305–314
- Witte AV, Floel A (2011) Effects of COMT polymorphisms on brain function and behavior in health and disease. *Brain Res Bull* 88(5):418–428
- Wu S, Comings DE (1999) A common C-1018G polymorphism in the human 5-HT_{1A} receptor gene. *Psychiatr Genet* 9(2):105–106
- Wu K, O'Keefe D, Politis M et al (2012) The catechol-O-methyltransferase Val(158)Met polymorphism modulates fronto-cortical dopamine turnover in early Parkinson's disease: a PET study. *Brain* 135(Pt 8):2449–2457
- Zalsman G, Huang YY, Oquendo MA et al (2006) Association of a triallelic serotonin transporter gene promoter region (5-HTTLPR) polymorphism with stressful life events and severity of depression. *Am J Psychiatry* 163(9):1588–1593
- Zill P, Buttner A, Eisenmenger W, Bondy B, Ackenheil M (2004) Regional mRNA expression of a second tryptophan hydroxylase isoform in postmortem tissue samples of two human brains. *Eur Neuropsychopharmacol* 14(4):282–284

Part II
Systems

David Elmenhorst, Dirk Bier, Marcus Holschbach,
and Andreas Bauer

Contents

7.1 Introduction	182
7.2 A ₁ Adenosine Receptor Ligands	184
7.3 A _{2A} Adenosine Receptor Ligands	192
7.4 A _{2B} Adenosine Receptor	194
7.5 A ₃ Adenosine Receptor	194
Conclusion	194
References	194

Abstract

Adenosine is a fundamental molecule of life. It is a part of the DNA and the main degradation product of the central currency of energy metabolism in humans and animals – adenosine triphosphate (ATP). Under pathological conditions like hypoxia, the adenosine concentration can rise severalfold – up to micromolar concentrations. The net effect of adenosine on excitable tissue is inhibitory affecting the release of classical neurotransmitters like glutamate, GABA (gamma-aminobutyric acid), and dopamine. The widely used neurostimulant caffeine exerts its effects as an antagonist at adenosine receptors. Four different types of adenosine

D. Elmenhorst, MD (✉)

INM-2, Institute of Neuroscience and Medicine, Forschungszentrum Jülich,
Jülich 52425, Germany

e-mail: d.elmenhorst@fz-juelich.de

D. Bier, PhD • M. Holschbach, PhD

INM-5, Institute of Neuroscience and Medicine, Forschungszentrum Jülich,
Jülich 52425, Germany

A. Bauer, MD

INM-2, Institute of Neuroscience and Medicine, Forschungszentrum Jülich,
Jülich 52425, Germany

Department of Neurology, Heinrich-Heine-University Düsseldorf, Düsseldorf, Germany

receptors have been described in mammals: A_1 , A_{2A} , A_{2B} , and A_3 which are all G-protein-coupled receptors. Over the last 25 years, adenosine receptor ligands, agonists as well as antagonists, have emerged as a class of useful therapeutics. For the A_1 and A_{2A} subtypes several antagonist radioligands have been used successfully for PET imaging in humans and animals especially for the brain.

7.1 Introduction

Adenosine is a fundamental molecule of life. It is a part of the DNA and the main degradation product of the central currency of energy metabolism in humans and animals – adenosine triphosphate (ATP). The nucleoside adenosine is composed of the nucleobase adenine and the sugar ribose. It has a short biological half-life of about 1–2 s, and the endogenous extracellular level of adenosine is in the range of several hundred nanomolar in the heart and brain of humans (Zeitzer et al. 2006). Adenosine is formed by the breakdown of ATP to ADP to AMP and finally to adenosine by the enzyme 5'-nucleotidase. Adenosine is metabolized by adenosine deaminase to inosine and mainly by phosphorylation by adenosine kinase to AMP. Extra- and intracellular concentrations of adenosine can equilibrate quickly by equilibrative nucleoside transporters. Under pathological conditions like hypoxia, the adenosine concentration can rise severalfold – up to micromolar concentrations. Adenosine is a part of the heterogeneous group of neuromodulators. In contrast to classical neurotransmitters, it is not stored and released from vesicles. The net effect of adenosine on excitable tissue is inhibitory affecting the release of classical neurotransmitters like glutamate, GABA (gamma-aminobutyric acid), and dopamine. Adenosine, for example, reduces the contraction frequency of a tachycardic heart or reduces epileptic activity in the brain. The most prominent and most widespread used substance that interacts with adenosine in daily life is caffeine. The widely used neurostimulant caffeine exerts its effects as an antagonist at adenosine receptors. Four different types of adenosine receptors have been described in mammals: A_1 , A_{2A} , A_{2B} , and A_3 which are all G-protein-coupled receptors. The coupling of A_1 and A_3 to a G_i -protein leads to inhibition of adenylyl cyclase, whereas the coupling of A_{2A} and A_{2B} to G_s - or G_o -proteins leads to stimulation of adenylyl cyclase. In humans, the A_1 adenosine receptor (A_1AR) shows the most abundant distribution and highest concentrations (in descending order) in the brain, heart, adipose tissue, stomach, testis, spleen, kidney, aorta, liver, eye, and bladder. The A_{2A} adenosine receptor ($A_{2A}AR$) can be found in striatum, nucleus accumbens, olfactory tubercle, heart, lung, and blood vessels. A_{2B} adenosine receptors ($A_{2B}AR$) are expressed in low levels in all tissues, and A_3 adenosine receptors (A_3ARs) show low levels in the brain and high levels in the lung and liver (Jacobson and Gao 2006). The affinities of endogenous adenosine for the A_1AR and the $A_{2A}AR$ are in the nanomolar range, whereas the affinities for the $A_{2B}AR$ and the A_3AR are in the micromolar range (Dunwiddie and Masino 2001). This discrepancy in affinity in combination with normal adenosine levels in the nanomolar range suggests that $A_{2B}AR$ and A_3AR are primarily activated under pathological conditions and massively increased levels of intracellular adenosine. An important aspect is that $A_{2A}ARs$ form heterodimers with A_1ARs or dopamine D_2 receptors and A_1AR with dopamine D_1 receptors which in

Table 7.1 Requirements for a suitable radiotracer

Criterion	Requirements	Evaluation system
Affinity and reversibility	K_D or K_I in nM range	Assays with brain tissue or cell homogenates, autoradiography
Specificity	Selectivity compared to receptors of the same subfamily and to receptors mainly present in the region of interest	
Unspecific binding potential	Low	
Agonism	Antagonists	Functional assays, for instance cAMP
Penetration of BBB	>1 % ID/g @ t_{max}	Organ distribution in animals, animal PET or SPECT
Metabolism	Preferably no metabolism in the target organ (brain) or biologically inactive metabolites	
Bioavailability	Half-life of radionuclide compatible with physiological kinetic Fraction of “free” ligand should be as high as possible (>1 %)	
Mutagenicity	Very low	Specific assays for instance chromosome aberration, Ames test
Toxicity	Low \ll effects 1,000-fold of applied mass	Theoretically <i>quantitative structure-activity relationship</i> ; animal experiments LD ₅₀

turn influence the affinity of the adenosine receptors (Ciruela et al. 2006; Cristovao-Ferreira et al. 2011; Franco et al. 2007).

Over the last 25 years, adenosine receptor ligands, agonists as well as antagonists, have emerged as a class of useful therapeutics (for a comprehensive review, see Jacobson 2009; Jacobson and Gao 2006). The requirements for compounds suitable for noninvasive in vivo imaging of adenosine receptors (radiopharmaceuticals, radiotracers) with positron emission tomography (PET) are in some aspects different from those for therapeutic drugs. This difference is even more pronounced in the case of radiotracers involved in neurotransmission research. One possible process for adenosine receptor ligand development in combination with adequate evaluation methods is depicted in Table 7.1.

In contrast to therapeutically dosed drugs, the amounts of intravenously (i.v.) administered radiopharmaceuticals are extremely small. Thus, biochemical equilibria are not or only marginally disturbed, allowing quantitative receptor scintigraphy (determination of concentration of binding sites, B_{max}).

Depending on the amount of applied radioactivity and on the specific activity of the respective radiotracer, the applied mass of a PET radiopharmaceutical typically lies in the range of nano- to micrograms. Thus, even toxic drugs, which are not suitable as therapeutics, can be used as radiotracers for PET.

A brain radiotracer, in order to be suitable for imaging, has to fulfill a number of criteria with regard to its physical and physiological properties (Ding and Fowler 2005; Halldin et al. 2001; Mason and Mathis 2005). The ligand should have nanomolar to subnanomolar affinity (K_D) and sufficient selectivity for the target receptor.

Ideally, binding to the receptor should be reversible over the experimental time range because this allows the use of biomathematical equilibrium approaches for the quantification of ligand-receptor interaction. Lipophilicity ($\log P$) of the tracer should be appropriate for crossing the blood–brain barrier (BBB). For radioligands, there is an optimal, rather narrow “window” of lipophilicity in the $\log P$ range between 1 and 4 (Dishino et al. 1983; Moerlein et al. 1985). As a rule of thumb, molecules with a $\log P$ value <1 will not cross the BBB, while those with a $\log P >4$ generally tend to exhibit high unspecific binding. Other criteria for a successful radiotracer are sufficient in vivo stability in plasma and, in respect to tracer availability, low affinity for plasma proteins. With regard to image analysis, there should be no radiolabeled metabolites which are capable of crossing the BBB. Further, a suitable radiotracer should show a kinetic profile that allows adequate quantification of the obtained data.

Radiolabeled subtype-specific adenosine receptor ligands currently under development are depicted in Table 7.2.

A_1 AR and A_{2A} AR antagonists are either xanthines or non-xanthine monocyclic or fused bi- or tricyclic substituted heteroaromatic compounds, some of them containing hetero-ring atoms such as nitrogen, oxygen, and sulfur.

Three characteristics identify xanthines that are potent and selective antagonists at the A_1 AR. They possess long alkyl chains in positions 1 and 3 as well as a bulky (bi)cycloalkyl substituent at C-8, the optimum substituents at N-1 and N-3 being propyl groups. Additionally, N-7 must be unsubstituted in order to act as a hydrogen bond donor, a feature which is essential for binding to the A_1 AR. Whereas some modifications of the 1- and 3-substituents (fluorination, iodination, substitution of an aralkyl group at N-3) preserve or at least do not seriously affect activity, the criteria based on N-7 and C-8 are required for antagonist activity at the A_1 AR.

Xanthine-type A_{2A} AR antagonists with high A_{2A} AR affinity either contain a (substituted) (*E*)-styryl substituent at C-8 in combination with alkyl/alkynyl moieties at N-1 and N-3; a methyl group at N-7 reduces affinity to the A_1 AR by suppressing the formation of hydrogen bonds and can sterically interact with the styryl group by forcing the vinylic double bond into a favored conformation for binding to the A_{2A} AR.

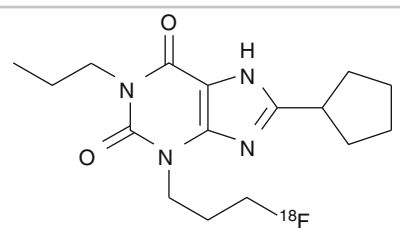
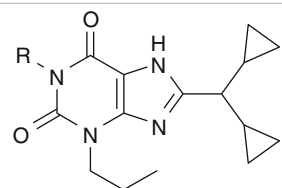
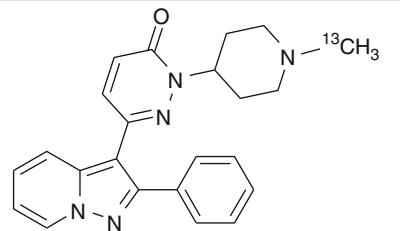
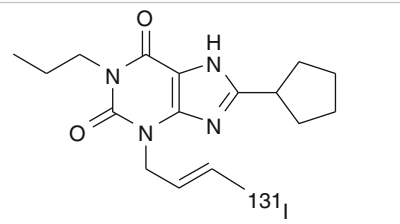
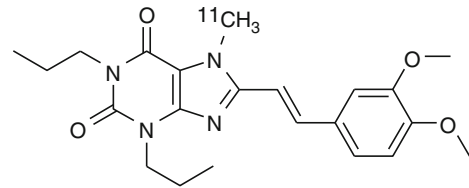
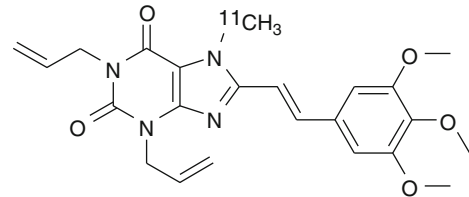
Non-xanthine A_1 AR antagonists are often structurally based on adenine, having a 6-amino group substituted with bulky cycloaliphatic moieties and variable nitrogen atoms in the heterocyclic core.

Nitrogen polyheterocyclic A_{2A} AR ligands, especially those based on a triazolopyrimidine structure, show good affinity and selectivity when they bear a furan moiety off the core aromatic scaffold, a prerequisite which is crucial for binding. Moreover, bi- and tricyclic fused nitrogen heterocyclic antagonists, in order to be active, often contain a long-chain aralkyl moiety. PET ligands for adenosine receptors of various states of development have been reviewed recently (Bauer and Ishiwata 2009).

7.2 A_1 Adenosine Receptor Ligands

So far two PET tracers have been applied and evaluated to image A_1 ARs in humans: [^{11}C]MPDX (Noguchi et al. 1997) and [^{18}F]CPFPX (Holschbach et al. 2002). Both are xanthine derivatives. Potential scientific applications for A_1 AR imaging and first findings have been reviewed recently (Paul et al. 2011).

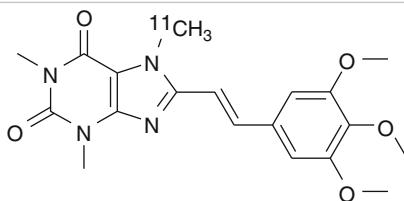
Table 7.2 Selection of PET ligands for adenosine receptors

<p>A₁ [¹⁸F]CPFPX Holschbach et al. (2002)</p>	
<p>R=CH₃CH₂¹¹CH₂, [¹¹C] KF15372 R=CH₃¹¹CH₂, [¹¹C]EDPX R=¹¹CH₃, [¹¹C]MDPX Ishiwata et al. (1995) Noguchi et al. (1997)</p>	
<p>[¹¹C]FR194921 Matsuya et al. (2005)</p>	
<p>[¹³¹I]CPIPX Sihver et al. (2003)</p>	
<p>A_{2A} [¹¹C]KF117837 Ishiwata et al. (1996)</p>	
<p>[¹¹C]KF19631 Ishiwata et al. (1996)</p>	

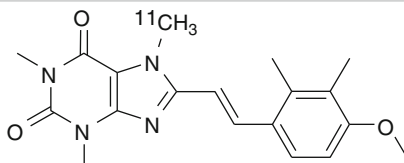
(continued)

Table 7.2 (continued)

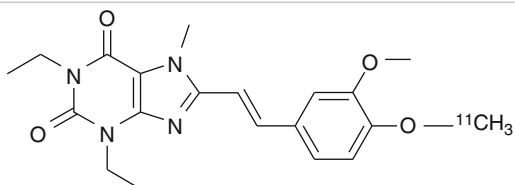
[¹¹C]KF18446([¹¹C]TMSX)
Ishiwata et al. (2000a)



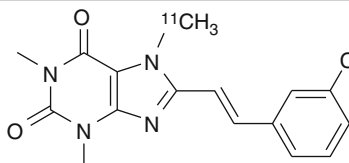
[¹¹C]KF21213
Wang et al. (2000)



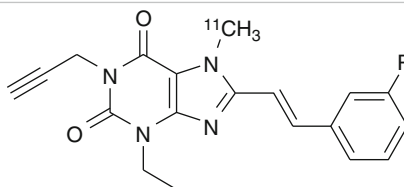
[¹¹C]KW-6002
Hirani et al. (2001)



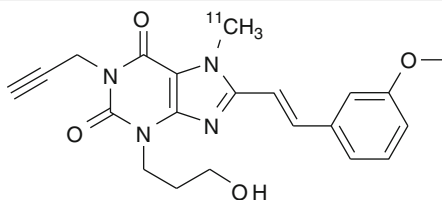
[¹¹C]CSC
Ishiwata et al. (2000a)
Marian et al. (1999)



R=Br, [¹¹C]BS-DMPX
R=I, [¹¹C]IS-DMPX
Ishiwata et al. (2000c)



[¹¹C]MSX-2
Holschbach et al. (2000)



[¹¹C]SCH442416
Todde et al. (2000)
Moresco et al. (2005)

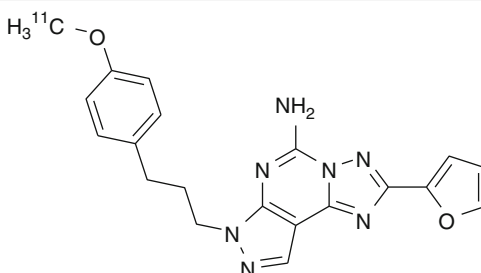
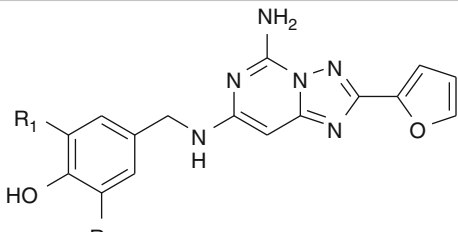
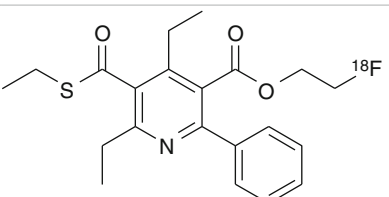


Table 7.2 (continued)

<p>R₁ = H, R₂ = ¹³¹I, [¹³¹I] iodo-ZM241385 R₁ = I, R₂ = ¹³¹I, [¹³¹I] diiodo-ZM241385 Poucher et al. (1995) Sihver et al. (2004)</p>	
<p>A_{2B} – A₃ [¹⁸F]FE@SUPPY Wadsak et al. (2008)</p>	

The antagonist [¹⁸F]CPFPX (Log *P* = 2.1) shows a high affinity (*K_D* 1.26 nM in cloned human receptors) and high selectivity (*A_{2A}*AR affinity 940 nM) for the *A₁*AR (Bauer et al. 2003; Holschbach et al. 2002). After i.v. injection, it rapidly (within 5 min) reaches a maximum brain uptake of approximately 3 % of injected dose (Bauer et al. 2003; Meyer et al. 2004) (Fig. 7.1). Free fraction of parent compound in plasma is about 1–2 % (Meyer et al. 2004). [¹⁸F]CPFPX is metabolized fast in the liver by the cytochrome isoenzyme CYP1A2 so that the fraction of parent compound is reduced to approximately 50 % after 10 min and to less than 10 % after 60 min (Matusch et al. 2006; Meyer et al. 2004). Formed metabolites are hydrophilic and do not cross the blood–brain barrier (>98 % unchanged ligand in mouse brain tissue after 60 min) (Holschbach et al. 2002). The chemical structure of seven main metabolites (Fig. 7.2) and their pathways have been described (Bier et al. 2006). The regional cortical and subcortical distribution of in vivo binding is in agreement with the human *postmortem* distribution in autoradiographic measurements (Bauer et al. 2003).

The suitability of [¹⁸F]CPFPX for clinical applications has been shown in a dosimetry study (Herzog et al. 2008) which revealed that an injected dose of 300 MBq posed a radiation burden of 5.3 mSv on a patient. This dose is comparable to other ¹⁸F-labeled PET tracers in clinical use.

[¹⁸F]CPFPX has been administered i.v. as bolus and as bolus plus subsequent infusion (Meyer et al. 2004, 2005a). Pharmacokinetic modeling of an injection of a bolus can be described significantly better with a two-compartment model than with a one-compartment model. Nevertheless, the individual rate constants were highly correlated, leading to high standard errors of the estimates and the derived outcome parameter *BP_p* denoting the specific binding (Meyer et al. 2004). The parameter total distribution volume (*V_T*) is a more valid measure as it combines the specific and unspecific binding. *V_T* can also be determined with Logan's graphical analysis

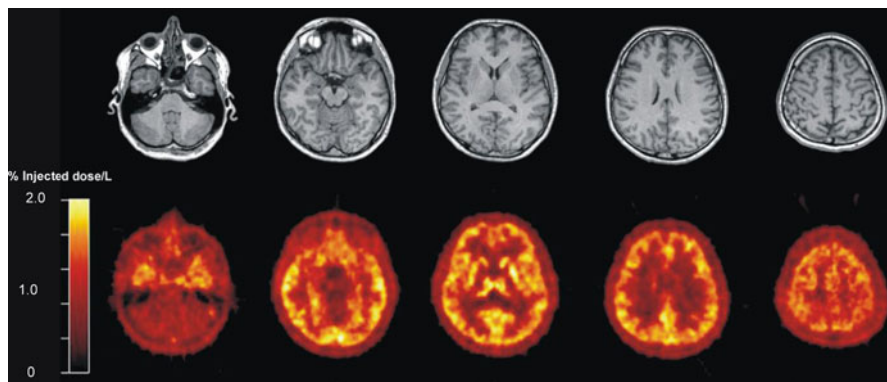


Fig. 7.1 In vivo distribution of $[^{18}\text{F}]\text{CPFPX}$: individual MRI (*top*) and summed (5–60 min postinjection) PET (*bottom*) of a representative healthy volunteer. Note the high accumulation of $[^{18}\text{F}]\text{CPFPX}$ in cerebral cortex, basal ganglia, and thalamus

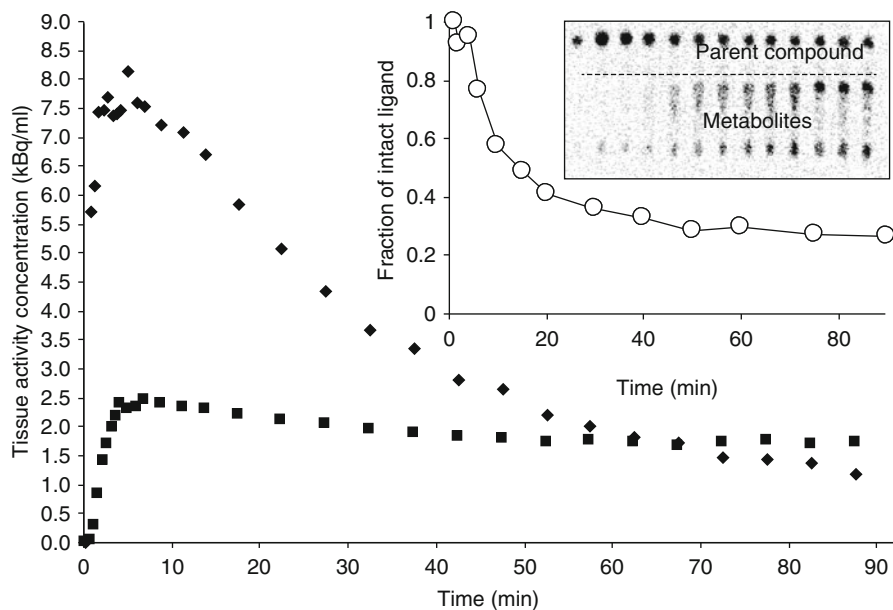


Fig. 7.2 Examples of representative bolus (*diamonds*) and bolus plus constant infusion (*boxes*) experiments in humans with $[^{18}\text{F}]\text{CPFPX}$. Depicted is the tissue time-activity of the frontal lobe. Steady state is reached after approximately 50 min. Inserted figure shows $[^{18}\text{F}]\text{CPFPX}$ metabolism, fraction of parent compound of the bolus/infusion experiment, and thin-layer chromatography radioactivity distribution

which allows voxel-wise determination and statistical parametric mapping. The noise-dependent bias in V_T parametric images can be reduced by spatial smoothing before applying the graphical analysis. A relatively short scan duration of 60 min is sufficient (Meyer et al. 2006b). Including the free fraction into the model increases variation and is therefore often omitted. Because of the high fraction of metabolites

at late time points, a blood volume correction should be applied. It had been shown that not only arterial but also venous input function for the graphical analysis allows reliable quantification of V_T (Meyer et al. 2005b).

Displacement studies with unlabeled CFPFX revealed that about one-third of cerebellar binding and at least two-thirds of cortical binding (depending on the cortical region) are specific (V_S) (Meyer et al. 2006c). [^{18}F]CFPFX is displaceable by caffeine in rats (Meyer et al. 2003) and humans (Elmenhorst et al. 2012). Therefore, it is compulsory that subjects refrain from caffeine intake at least 36 h before participating in a PET study. Due to the selective liver metabolism, special caution has to be taken in patients with liver dysfunction where the elimination half-life of caffeine is extremely prolonged (Matusch et al. 2006).

The in vitro inhibitory concentration of caffeine that displaces 50 % of the binding (IC_{50}) of [^3H]CFPFX at human brain *postmortem* $A_1\text{AR}$ s is in the range of 113–170 μM (Elmenhorst et al. 2011). Therefore, the dose of caffeine after common consumptions of coffee or tea has probably a direct impact on the in vivo quantification of $A_1\text{AR}$ s with the PET ligand [^{18}F]CFPFX.

The bolus plus subsequent infusion method allows quantifying modulations of binding (e.g., displacement) within a single scan. After establishing a steady state of ligand concentration in plasma and brain tissue, the total distribution volume V_T can be determined as the ratio of the concentrations in brain tissue and plasma. Due to the fast kinetics of [^{18}F]CFPFX, equilibrium can be achieved within approximately 60 min (Meyer et al. 2005a).

In the case of [^{18}F]CFPFX, the relatively low fraction of specific binding (about 2/3 of V_T) reduces the sensitivity for possible changes in V_T . Another shortcoming is the dependence on error-prone individual plasma input functions, which increases variability. These drawbacks can be avoided by a reference region input for BP_{ND} (specific vs. non-displaceable input) which is independent of blood sampling using (Elmenhorst et al. 2007a; Meyer et al. 2006a). The cerebellar cortex is used as reference region. Although the cerebellar cortex is the region with the lowest $A_1\text{AR}$ density in the human brain, one-third of the V_T is displaceable with unlabeled CFPFX (Meyer et al. 2006c). Therefore, changes in BP_{ND} deserve careful consideration with regard to their dependency on V_S changes in the reference region. BP_{ND} can be determined by Logan's noninvasive graphical analysis. Test-retest evaluation of the variability and reproducibility revealed that reference-based measures were superior to those based on plasma input function (Elmenhorst et al. 2007a). Exemplary values for V_T and BP_{ND} in the frontal cortex are 0.80 ml/ml and 0.92, respectively.

In an approach to determine the in vivo IC_{50} value of caffeine at the $A_1\text{AR}$ in humans, 18 subjects underwent bolus plus constant infusion PET experiments after caffeine abstinence. Caffeine in varying concentrations (0.5–4.3 mg/kg body weight) was administered during the steady-state phase of ligand delivery (Fig. 7.3). [^{18}F]CFPFX binding was displaced in a concentration-dependent manner ranging from 5 to 44 % (Fig. 7.4). No displacement (0.3 %) was found after placebo administration. IC_{50} was estimated to be 65 μM in plasma which corresponds to 460 mg in a 70 kg subject (approximately 4.5 cups of coffee). Given both the biological half-life of caffeine of about 5 h and the repeated consumption of caffeinated beverages during a day, occupancies of 50 % of the cerebral $A_1\text{AR}$ are probably common conditions in caffeine consumers.

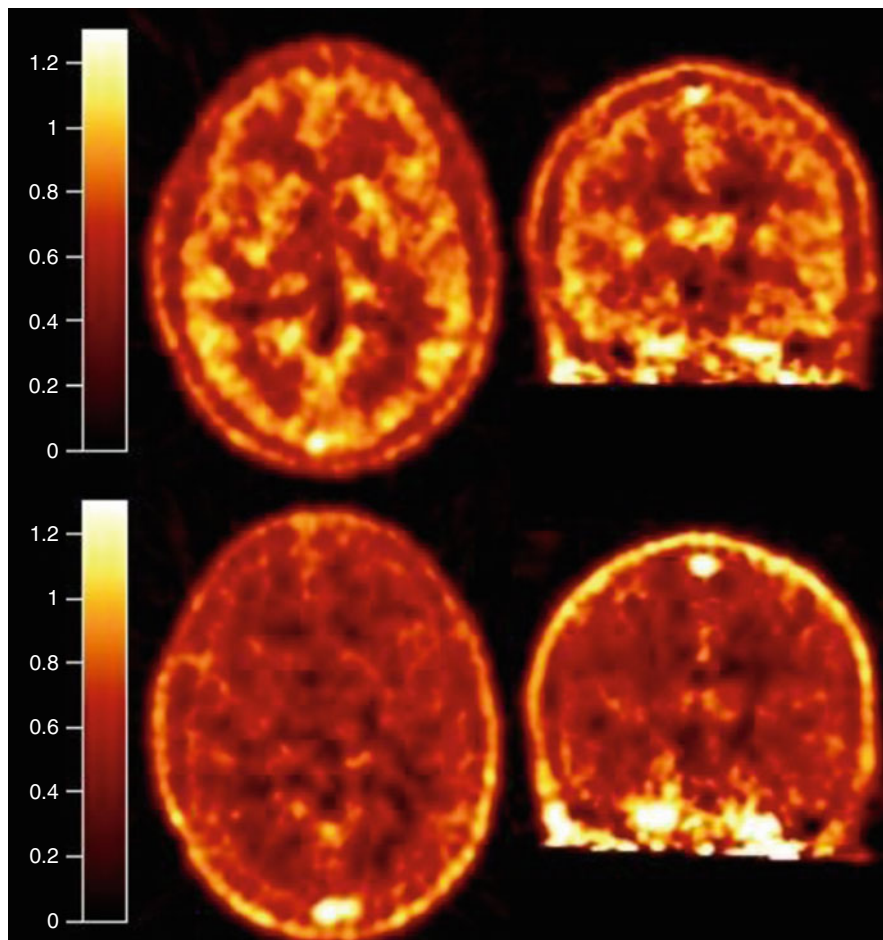


Fig. 7.3 Equilibrium imaging of caffeine action: parametric total distribution volume PET images before (50–90 min, *top*) and after caffeine infusion (100–140 min, *bottom*) of a subject receiving 4.3 mg caffeine per kg body weight

The A_1AR is supposed to be involved in numerous physiological and pathophysiological processes. Age-related changes were investigated over a time span of approximately 50 years showing a range of decline of BP_{ND} between -17% (putamen) and -34% (postcentral gyrus) (Meyer et al. 2006a). It is currently hypothesized that adenosine is involved in the induction of sleep after prolonged wakefulness. Twenty-four hours of sleep deprivation increased V_T in a region-specific pattern in the brain with a maximum increase in the orbitofrontal cortex (15.3%). The upregulation in cortical and subcortical brain regions after prolonged wakefulness is likely to indicate that A_1AR expression is contributing to the homeostatic sleep regulation (Elmenhorst et al. 2007b). In a pilot study on a patient with recurrent glioblastoma multiforme, increases in A_1AR density in the direct vicinity of the tumor confirmed corresponding results in an F98 glioma-bearing rat model (Bauer et al. 2005). In a

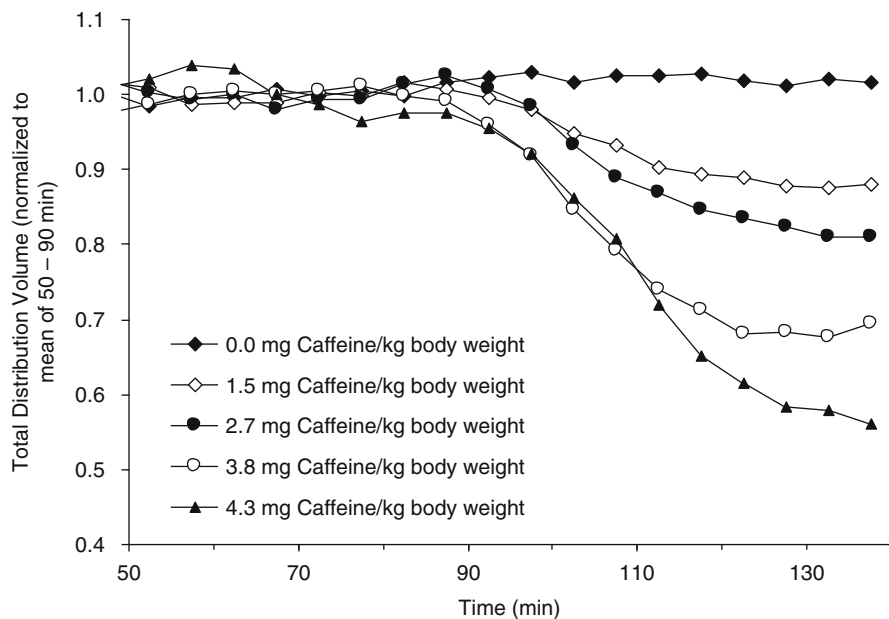


Fig. 7.4 Displacement of [^{18}F]CPFPX $A_1\text{AR}$ binding by caffeine under equilibrium conditions (bolus/infusion PET scanning): representative [^{18}F]CPFPX displacement studies employing increasing doses of caffeine. Intravenous infusion of 0.0–4.3 mg caffeine per kg body weight (equivalent to approximately 0–4 cups of coffee) between 90 and 100 min. Note the rapid and dose-dependent displacement of [^{18}F]CPFPX (x-axis: time after start of bolus/infusion study, y-axis: total volume of distribution normalized to the mean of 50–90 min)

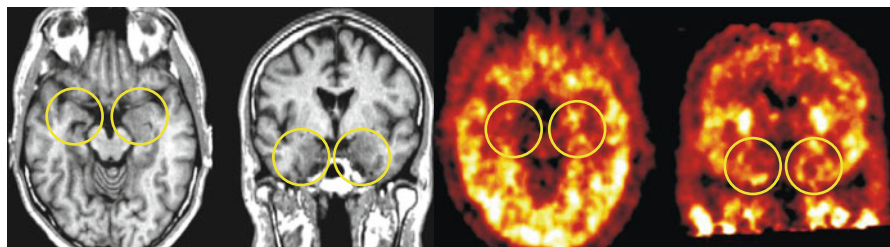


Fig. 7.5 Corresponding MRI (left) and [^{18}F]CPFPX PET (right) planes of a patient suffering from mesial temporal lobe epilepsy (focus in the right hemisphere). Note the considerably reduced $A_1\text{AR}$ binding in the left mesial temporal lobe

case of temporal lobe epilepsy, there was evidence that $A_1\text{AR}$ binding is reduced in the epileptic focus (Fig. 7.5).

The inverse antagonist [^{11}C]MPDX (Log $P < 2.2$) (Ishiwata et al. 1995) shows a slightly lower affinity (K_i 4.2 nM) (Noguchi et al. 1997) for the $A_1\text{AR}$ compared to [^{18}F]CPFPX. After i.v. injection, it rapidly (within 2.5 min) reaches a maximum brain uptake of approximately 6 % of injected dose (Kimura et al. 2004). [^{11}C]MPDX is metabolized slowly, so that the fraction of parent compound is reduced to approximately 75 % after 60 min. The relative density distribution pattern of [^{11}C]MPDX is

comparable to [^{18}F]CPFPX. Pharmacokinetic modeling of V_T was evaluated and performed with both a two-tissue-compartment model (with K_1/k_2 parameter estimates based on cerebellum as a reference region) and a graphical approach in the time span between 10 and 60 min (Logan's plot) (Fukumitsu et al. 2003). Using an arterial input function with and without metabolite correction produced only a small negative bias of 4 %. Parametric BP_{ND} images based on V_T determined by graphical analysis and cerebellum as reference region have been published (Fukumitsu et al. 2003). A blocking experiment in cats with DPCPX revealed that about 53 % of V_T was specific binding. Exemplary values for V_T and BP_{ND} in the frontal cortex are 0.82 ml/ml and 0.23, respectively (Kimura et al. 2004). Interestingly, the radioactivity concentration of [^{11}C]MPDX in whole blood was slightly higher than in plasma suggesting an uptake in or binding to red blood cells (Fukumitsu et al. 2005). A noninvasive method to determine the outcome parameters based on independent component analysis has been proposed. Plasma time-activity curves could be estimated from dynamic PET images because the slow metabolization of [^{11}C]MPDX allowed to disregard metabolite correction. The previously mentioned decline of adenosine receptor densities with increasing age measured with [^{18}F]CPFPX was replicated for the A_1 subtype with [^{11}C]MPDX (Mishina et al. 2012). Interestingly, in the same study, no effect of aging on the A_{2A} AR was observed. In patients suffering from Alzheimer's disease, a decreased binding of [^{11}C]MPDX was detected in temporal cortex and thalamus (Fukumitsu et al. 2008). As the pattern of binding differs from the widely used [^{18}F]FDG, adenosine receptor imaging might provide an additional diagnostic value.

PET imaging of A_1 ARs has been evaluated as a tool to predict the severity of ischemic cerebral insults. In 13 cats, the right middle cerebral artery was occluded transiently. [^{11}C]MPDX uptake was significantly lower in those animals with a severe ischemic damage, and the authors concluded that the binding after reperfusion was a sensitive predictor of severity (Nariai et al. 2003).

P-gp regulates the ability of endogenous and exogenous compounds to cross the BBB. Pretreatment of mice with the P-gp blocker cyclosporine A before [^{11}C]TMSX and [^{11}C]MPDX PET increased both the blood-to-brain ratio and the cerebral uptake (Ishiwata et al. 2007). [^{11}C]TMSX and [^{11}C]MPDX binding are therefore dependent on P-gp function (at least in mice).

7.3 A_{2A} Adenosine Receptor Ligands

The A_{2A} AR antagonist [^{11}C]TMSX (calculated Log $P=1.1$) (Ishiwata et al. 2000b) was the first radioligand to visualize A_{2A} ARs in humans (Ishiwata et al. 2005). The compound presents a high affinity to A_{2A} ARs ($K_i=5.9$ nM) and a high selectivity compared to the A_1 AR ($K_i=1,600$ nM) (Ishiwata et al. 2003). It was confirmed in vitro that TMSX has a very low affinity for 13 different neuroreceptors (Ishiwata et al. 2000c). After i.v. injection, it rapidly (within 1.5–2.5 min) reaches a maximum brain uptake of approximately 1–2 % of injected dose (estimated from the data provided by Naganawa et al. (2007)). In humans, [^{11}C]TMSX is very slowly metabolized (over 90 % parent compound after 60 min) (Naganawa et al. 2007). Exemplary

values for V_T and BP_{ND} in the putamen are 1.75 ml/ml and 1.26, respectively. In a single subject, Ishiwata et al. (2005) showed that [^{11}C]TMSX binding is blocked by a simultaneous and constant infusion of theophylline. V_T was reduced 8 % in caudate nucleus and 4.5 % in putamen but not in other brain areas. Theophylline infusion had an inhibiting effect on the metabolism of [^{11}C]TMSX. Quantification of A_{2A} ARs based on arterial blood samples and metabolite analyses in five healthy volunteers were described by a two-compartment model and showed highest distribution volumes in putamen and thalamus (Mishina et al. 2007). Simplified methods for the determination of BP_{ND} by Logan's graphical analysis and distribution volume ratio to the reference region (centrum semiovale) have been reported for [^{11}C]TMSX. One method is based on the generation of an estimated plasma time-activity curve by independent component analysis (EPICA), which is applicable to [^{11}C]TMSX modeling because of the negligible metabolism of the compound (Naganawa et al. 2007). The second method using an intersectional searching algorithm and clustering (called EPISA) is independent of the metabolism of a ligand. In contrast to Logan's noninvasive method EPISA based V_T calculations to obtain BP_{ND} with a reference region, circumvent k_2 parameter determinations which necessitate arterial blood sampling and metabolite correction (Naganawa et al. 2008). This is achieved by obtaining an unscaled integral of the metabolite-corrected plasma input function which is determined by clusters of distinct tissue time-activity curves.

Due to the heterodimerization between dopamine D_2 and A_{2A} ARs, adenosine antagonists were explored as therapeutics for Parkinson's disease. Using PET, it was investigated whether the disease affects basal cerebral A_{2A} AR density and whether therapeutic interventions with standard antiparkinsonian medication had an impact on A_{2A} AR binding. It was found that the binding potential in the putamen was higher in patients with additional dyskinetic symptoms compared to controls (Mishina et al. 2011). In another study with the A_{2A} AR ligand [^{11}C]SCH442416, this finding could be reproduced as patients with dyskinesia had higher binding potentials in contrast to patients without dyskinesia who showed binding potentials comparable to the control subjects (Ramlackhansingh et al. 2011).

In a preliminary analysis, the EPICA method has been used to determine the BP_{ND} of patients with Parkinson's disease. BP_{ND} was significantly lower on the more affected side of the posterior putamen in Parkinson's disease, while [^{11}C]raclopride binding to dopamine receptors was increased.

Regarding occupancy studies of drug candidates, [^{11}C]SCH442416 has been used to assess adenosine A_{2A} AR occupancy of vipadenant (BIIB014) in healthy subjects (Brooks et al. 2010) and [^{11}C]KW-6002 (istradefylline) to find optimal oral doses of the same unlabeled compound (Brooks et al. 2008).

Besides the aforementioned application of [^{11}C]TMSX in brain imaging studies, it has additionally been used to study the human A_{2A} AR in skeletal muscle and heart. An infusion of theophylline resulted in a reduction of binding suggesting specific binding of [^{11}C]TMSX in human muscles (Ishiwata et al. 2004). Increased adenosine A_{2A} AR densities were found in the muscles of endurance-trained vs. untrained men (Mizuno et al. 2005). This finding could not be confirmed in a subsequent study (Heinonen et al. 2008).

7.4 A_{2B} Adenosine Receptor

Although several A_{2B}AR agonists and antagonist have been evaluated for preclinical applications (Kalla et al. 2009), none of these compounds has so far been introduced as a preclinical or clinical PET ligand.

7.5 A₃ Adenosine Receptor

There are no reports on A₃AR in vivo imaging studies so far although some radioligands were evaluated in biodistribution studies in rodents. Distribution and metabolism experiments have been performed in rodents with the fluoroethyl ester [¹⁸F]FE@SUPPY and its fluoroethyl thioester analogue [¹⁸F]FE@SUPPY:2 (Haeusler et al. 2010; Wadsak et al. 2008). Unfortunately, both tracers are metabolized to BBB-permeating metabolites which complicate pharmacokinetic evaluation of the binding. Fifteen minutes after injection of [¹⁸F]FE@SUPPY:2, the metabolites accounted for ~40 % of brain tissue radioactivity, and this fraction increased to ~80 % after 60 min. [¹⁸F]FE@SUPPY was more favorable in this respect as no metabolites were detected in the brain tissue up to 15 min after injection. However, the concentration increased to ~80 % after 60 min (Haeusler et al. 2010). In another biodistribution study, the [⁷⁶Br]-labeled antagonist MRS5147 was evaluated in rats showing an increased uptake in A₃AR-rich testes (Kiesewetter et al. 2009). However, in a dipping study with whole brain and testes, no specific binding of [⁷⁶Br]MRS5147 was detected.

Conclusion

Adenosine and its receptors play an important role in the physiology and pathophysiology of the brain as well as in other organs, particularly the kidney, bowel, and vascular system, and in tumors. At present, only the A₁AR and the A_{2A}AR are accessible with molecular in vivo imaging. So far, these tools revealed important insights into neurologic and psychiatric disorders, sleep physiology, and cancer. The constantly increasing amount of data on adenosine and its important role in multiple organ systems as well as in the pathophysiology of frequent diseases underscores the need for further research in the field of ligand development for adenosine receptors.

References

- Bauer A, Ishiwata K (2009) Adenosine receptor ligands and PET imaging of the CNS. *Handb Exp Pharmacol* (193):617–642
- Bauer A, Holschbach MH, Meyer PT, Boy C, Herzog H, Olsson RA, Coenen HH, Zilles K (2003) In vivo imaging of adenosine A1 receptors in the human brain with [¹⁸F]CPFPX and positron emission tomography. *Neuroimage* 19:1760–1769
- Bauer A, Langen KJ, Bidmon H, Holschbach MH, Weber S, Olsson RA, Coenen HH, Zilles K (2005) 18F-CPFPX PET identifies changes in cerebral A1 adenosine receptor density caused by glioma invasion. *J Nucl Med* 46:450–454

- Bier D, Holschbach MH, Wutz W, Olsson RA, Coenen HH (2006) Metabolism of the A1 adenosine receptor positron emission tomography ligand [18F]8-cyclopentyl-3-(3-fluoropropyl)-1-propylxanthine ([18F]cpfpfx) in rodents and humans. *Drug Metab Dispos* 34:570–576
- Brooks DJ, Doder M, Osman S, Luthra SK, Hirani E, Hume S, Kase H, Kilborn J, Martindill S, Mori A (2008) Positron emission tomography analysis of [11C]KW-6002 binding to human and rat adenosine A2A receptors in the brain. *Synapse* 62:671–681
- Brooks DJ, Papapetropoulos S, Vandenhende F, Tomic D, He P, Coppell A, O'Neill G (2010) An open-label, positron emission tomography study to assess adenosine A2A brain receptor occupancy of vipadenant (BIIB014) at steady-state levels in healthy male volunteers. *Clin Neuropharmacol* 33:55–60
- Ciruela F, Casado V, Rodrigues RJ, Lujan R, Burgueno J, Canals M, Borycz J, Rebola N, Goldberg SR, Mallol J, Cortes A, Canela EI, Lopez-Gimenez JF, Milligan G, Lluís C, Cunha RA, Ferre S, Franco R (2006) Presynaptic control of striatal glutamatergic neurotransmission by adenosine A1-A2A receptor heteromers. *J Neurosci* 26:2080–2087
- Cristovao-Ferreira S, Navarro G, Brugarolas M, Perez-Capote K, Vaz SH, Fattorini G, Conti F, Lluís C, Ribeiro JA, McCormick PJ, Casado V, Franco R, Sebastiao AM (2011) Modulation of GABA transport by adenosine A1R-A2AR heteromers, which are coupled to both Gs- and G(i/o)-proteins. *J Neurosci* 31:15629–15639
- Ding YS, Fowler J (2005) New-generation radiotracers for nAChR and NET. *Nucl Med Biol* 32:707–718
- Dishino DD, Welch MJ, Kilbourn MR, Raichle ME (1983) Relationship between lipophilicity and brain extraction of C-11-labeled radiopharmaceuticals. *J Nucl Med* 24:1030–1038
- Dunwiddie TV, Masino SA (2001) The role and regulation of adenosine in the central nervous system. *Annu Rev Neurosci* 24:31–55
- Elmenhorst D, Meyer PT, Matusch A, Winz OH, Zilles K, Bauer A (2007a) Test-retest stability of cerebral A(1) adenosine receptor quantification using [(18)F]CPFPX and PET. *Eur J Nucl Med Mol Imaging* 34:1061–1070
- Elmenhorst D, Meyer PT, Winz OH, Matusch A, Ermert J, Coenen HH, Basheer R, Haas HL, Zilles K, Bauer A (2007b) Sleep deprivation increases A1 adenosine receptor binding in the human brain: a positron emission tomography study. *J Neurosci* 27:2410–2415
- Elmenhorst D, Garibotto V, Prescher A, Bauer A (2011) Adenosine A(1) receptors in human brain and transfected CHO cells: inhibition of [(3)H]CPFPX binding by adenosine and caffeine. *Neurosci Lett* 487:415–420
- Elmenhorst D, Meyer PT, Matusch A, Winz OH, Bauer A (2012) Caffeine occupancy of human cerebral A1 adenosine receptors: in vivo quantification with 18F-CPFPX and PET. *J Nucl Med* 53:1723–1729
- Franco R, Lluís C, Canela EI, Mallol J, Agnati L, Casado V, Ciruela F, Ferre S, Fuxe K (2007) Receptor-receptor interactions involving adenosine A1 or dopamine D1 receptors and accessory proteins. *J Neural Transm* 114:93–104
- Fukumitsu N, Ishii K, Kimura Y, Oda K, Sasaki T, Mori Y, Ishiwata K (2003) Imaging of adenosine A1 receptors in the human brain by positron emission tomography with [11C]MPDX. *Ann Nucl Med* 17:511–515
- Fukumitsu N, Ishii K, Kimura Y, Oda K, Sasaki T, Mori Y, Ishiwata K (2005) Adenosine A1 receptor mapping of the human brain by PET with 8-dicyclopropylmethyl-1-11C-methyl-3-propylxanthine. *J Nucl Med* 46:32–37
- Fukumitsu N, Ishii K, Kimura Y, Oda K, Hashimoto M, Suzuki M, Ishiwata K (2008) Adenosine A(1) receptors using 8-dicyclopropylmethyl-1-[(11)C]methyl-3-propylxanthine PET in Alzheimer's disease. *Ann Nucl Med* 22:841–847
- Haeusler D, Nics L, Mien LK, Ungersboeck J, Lanzenberger RR, Shanab K, Spreitzer H, Sindelar KM, Viernstein H, Wagner KH, Dudczak R, Kletter K, Wadsak W, Mitterhauser M (2010) [18F]FE@SUPPY and [18F]FE@SUPPY:2—metabolic considerations. *Nucl Med Biol* 37:421–426
- Hallidin C, Gulyas B, Langer O, Farde L (2001) Brain radioligands—state of the art and new trends. *Q J Nucl Med* 45:139–152

- Heinonen I, Nesterov SV, Liukko K, Kemppainen J, Nagren K, Luotolahti M, Virsu P, Oikonen V, Nuutila P, Kujala UM, Kainulainen H, Boushel R, Knuuti J, Kalliokoski KK (2008) Myocardial blood flow and adenosine A2A receptor density in endurance athletes and untrained men. *J Physiol* 586:5193–5202
- Herzog H, Elmenhorst D, Winz O, Bauer A (2008) Biodistribution and radiation dosimetry of the A1 adenosine receptor ligand 18F-CPFPX determined from human whole-body PET. *Eur J Nucl Med Mol Imaging* 35:1499–1506
- Hirani E, Gillies J, Karasawa A, Shimada J, Kase H, Opacka-Juffry J, Osman S, Luthra SK, Hume SP, Brooks DJ (2001) Evaluation of [4-O-methyl-(11)C]KW-6002 as a potential PET ligand for mapping central adenosine A(2A) receptors in rats. *Synapse* 42:164–176
- Holschbach M, Müller CE, Wutz W, Schüller M, Coenen HH (2000) C-11 Markierung und erste ex vivo Evaluierung des Adenosin A2A Rezeptorliganden MSX-2 an NMRI Mäusen. *Nuklearmedizin* 39:P154
- Holschbach MH, Olsson RA, Bier D, Wutz W, Sihver W, Schuller M, Palm B, Coenen HH (2002) Synthesis and evaluation of no-carrier-added 8-cyclopentyl-3-(3-[(18)F]fluoropropyl)-1-propylxanthine ([18F]CPFPX): a potent and selective A(1)-adenosine receptor antagonist for in vivo imaging. *J Med Chem* 45:5150–5156
- Ishiwata K, Furuta R, Shimada J, Ishii S, Endo K, Suzuki F, Senda M (1995) Synthesis and preliminary evaluation of [11C]KF15372, a selective adenosine A1 antagonist. *Appl Radiat Isot* 46:1009–1013
- Ishiwata K, Noguchi J, Toyama H, Sakiyama Y, Koike N, Ishii S, Oda K, Endo K, Suzuki F, Senda M (1996) Synthesis and preliminary evaluation of [11C]KF17837, a selective adenosine A2A antagonist. *Appl Radiat Isot* 47:507–511
- Ishiwata K, Noguchi J, Wakabayashi S, Shimada J, Ogi N, Nariai T, Tanaka A, Endo K, Suzuki F, Senda M (2000a) 11C-labeled KF18446: a potential central nervous system adenosine A2a receptor ligand. *J Nucl Med* 41:345–354
- Ishiwata K, Ogi N, Shimada J, Nonaka H, Tanaka A, Suzuki F, Senda M (2000b) Further characterization of a CNS adenosine A2a receptor ligand [11C]KF18446 with in vitro autoradiography and in vivo tissue uptake. *Ann Nucl Med* 14:81–89
- Ishiwata K, Ogi N, Shimada J, Wang W, Ishii K, Tanaka A, Suzuki F, Senda M (2000c) Search for PET probes for imaging the globus pallidus studied with rat brain ex vivo autoradiography. *Ann Nucl Med* 14:461–466
- Ishiwata K, Kawamura K, Kimura Y, Oda K, Ishii K (2003) Potential of an adenosine A2A receptor antagonist [11C]TMSX for myocardial imaging by positron emission tomography: a first human study. *Ann Nucl Med* 17:457–462
- Ishiwata K, Mizuno M, Kimura Y, Kawamura K, Oda K, Sasaki T, Nakamura Y, Muraoka I, Ishii K (2004) Potential of [11C]TMSX for the evaluation of adenosine A2A receptors in the skeletal muscle by positron emission tomography. *Nucl Med Biol* 31:949–956
- Ishiwata K, Mishina M, Kimura Y, Oda K, Sasaki T, Ishii K (2005) First visualization of adenosine A(2A) receptors in the human brain by positron emission tomography with [11C]TMSX. *Synapse* 55:133–136
- Ishiwata K, Kawamura K, Yanai K, Hendrikse NH (2007) In vivo evaluation of P-glycoprotein modulation of 8 PET radioligands used clinically. *J Nucl Med* 48:81–87
- Jacobson KA (2009) Introduction to adenosine receptors as therapeutic targets. *Handb Exp Pharmacol* (193):1–24
- Jacobson KA, Gao ZG (2006) Adenosine receptors as therapeutic targets. *Nat Rev Drug Discov* 5:247–264
- Kalla RV, Zablocki J, Tabrizi MA, Baraldi PG (2009) Recent developments in A2B adenosine receptor ligands. *Handb Exp Pharmacol* (193):99–122
- Kiesewetter DO, Lang L, Ma Y, Bhattacharjee AK, Gao ZG, Joshi BV, Melman A, de Castro S, Jacobson KA (2009) Synthesis and characterization of [76Br]-labeled high-affinity A3 adenosine receptor ligands for positron emission tomography. *Nucl Med Biol* 36:3–10
- Kimura Y, Ishii K, Fukumitsu N, Oda K, Sasaki T, Kawamura K, Ishiwata K (2004) Quantitative analysis of adenosine A1 receptors in human brain using positron emission tomography and

- [1-methyl-11C]8-dicyclopropylmethyl-1-methyl-3-propylxanthine. *Nucl Med Biol* 31:975–981
- Marian T, Boros I, Lengyel Z, Balkay L, Horvath G, Emri M, Sarkadi E, Szentmiklosi AJ, Fekete I, Tron L (1999) Preparation and primary evaluation of [11C]CSC as a possible tracer for mapping adenosine A2A receptors by PET. *Appl Radiat Isot* 50:887–893
- Mason NS, Mathis CA (2005) Positron emission tomography agents for central nervous system drug development applications. In: Doherty AM (ed) *Annual reports in medicinal chemistry*, vol 40. Academic, Sandwich, pp 49–51
- Matsuya T, Takamatsu H, Murakami Y, Noda A, Ichise R, Awaga Y, Nishimura S (2005) Synthesis and evaluation of [11C]FR194921 as a nonxanthine-type PET tracer for adenosine A1 receptors in the brain. *Nucl Med Biol* 32:837–844
- Matusch A, Meyer PT, Bier D, Holschbach MH, Woitalla D, Elmenhorst D, Winz OH, Zilles K, Bauer A (2006) Metabolism of the A(1) adenosine receptor PET ligand [(18F)]CPFPX by CYP1A2: implications for bolus/infusion PET studies. *Nucl Med Biol* 33:891–898
- Meyer PT, Bier D, Holschbach MH, Cremer M, Tellmann L, Bauer A (2003) Image of the month. In vivo imaging of rat brain A1 adenosine receptor occupancy by caffeine. *Eur J Nucl Med Mol Imaging* 30:1440
- Meyer PT, Bier D, Holschbach MH, Boy C, Olsson RA, Coenen HH, Zilles K, Bauer A (2004) Quantification of cerebral A1 adenosine receptors in humans using [18F]CPFPX and PET. *J Cereb Blood Flow Metab* 24:323–333
- Meyer PT, Elmenhorst D, Bier D, Holschbach MH, Matusch A, Coenen HH, Zilles K, Bauer A (2005a) Quantification of cerebral A1 adenosine receptors in humans using [18F]CPFPX and PET: an equilibrium approach. *Neuroimage* 24:1192–1204
- Meyer PT, Elmenhorst D, Zilles K, Bauer A (2005b) Simplified quantification of cerebral A1 adenosine receptors using [18F]CPFPX and PET: analyses based on venous blood sampling. *Synapse* 55:212–223
- Meyer PT, Elmenhorst D, Boy C, Winz O, Matusch A, Zilles K, Bauer A (2006a) Effect of aging on cerebral A(1) adenosine receptors: A [(18F)]CPFPX PET study in humans. *Neurobiol Aging* 28:1914–24
- Meyer PT, Elmenhorst D, Matusch A, Winz O, Zilles K, Bauer A (2006b) 18F-CPFPX PET: on the generation of parametric images and the effect of scan duration. *J Nucl Med* 47:200–207
- Meyer PT, Elmenhorst D, Matusch A, Winz O, Zilles K, Bauer A (2006c) A1 adenosine receptor PET using [18F]CPFPX: displacement studies in humans. *Neuroimage* 32:1100–1105
- Mishina M, Ishiwata K, Kimura Y, Naganawa M, Oda K, Kobayashi S, Katayama Y, Ishii K (2007) Evaluation of distribution of adenosine A(2A) receptors in normal human brain measured with [C-11]TMSX PET. *Synapse* 61:778–784
- Mishina M, Ishiwata K, Naganawa M, Kimura Y, Kitamura S, Suzuki M, Hashimoto M, Ishibashi K, Oda K, Sakata M, Hamamoto M, Kobayashi S, Katayama Y, Ishii K (2011) Adenosine A(2A) receptors measured with [C]TMSX PET in the striata of Parkinson's disease patients. *PLoS One* 6:e17338
- Mishina M, Kimura Y, Naganawa M, Ishii K, Oda K, Sakata M, Toyohara J, Kobayashi S, Katayama Y, Ishiwata K (2012) Differential effects of age on human striatal adenosine A(1) and A(2A) receptors. *Synapse* 66:832–839
- Mizuno M, Kimura Y, Tokizawa K, Ishii K, Oda K, Sasaki T, Nakamura Y, Muraoka I, Ishiwata K (2005) Greater adenosine A(2A) receptor densities in cardiac and skeletal muscle in endurance-trained men: a [11C]TMSX PET study. *Nucl Med Biol* 32:831–836
- Moerlein SM, Laufer P, Stocklin G (1985) Effect of lipophilicity on the in vivo localization of radiolabelled spiperone analogues. *Int J Nucl Med Biol* 12:353–356
- Moresco RM, Todde S, Belloli S, Simonelli P, Panzacchi A, Rigamonti M, Galli-Kienle M, Fazio F (2005) In vivo imaging of adenosine A2A receptors in rat and primate brain using [11C]SCH442416. *Eur J Nucl Med Mol Imaging* 32:405–413
- Naganawa M, Kimura Y, Mishina M, Manabe Y, Chihara K, Oda K, Ishii K, Ishiwata K (2007) Quantification of adenosine A2A receptors in the human brain using [11C]TMSX and positron emission tomography. *Eur J Nucl Med Mol Imaging* 34:679–687

- Naganawa M, Kimura Y, Yano J, Mishina M, Yanagisawa M, Ishii K, Oda K, Ishiwata K (2008) Robust estimation of the arterial input function for Logan plots using an intersectional searching algorithm and clustering in positron emission tomography for neuroreceptor imaging. *Neuroimage* 40:26–34
- Nariai T, Shimada Y, Ishiwata K, Nagaoka T, Shimada J, Kuroiwa T, Ono K, Ohno K, Hirakawa K, Senda M (2003) PET imaging of adenosine A(1) receptors with (11)C-MPDX as an indicator of severe cerebral ischemic insult. *J Nucl Med* 44:1839–1844
- Noguchi J, Ishiwata K, Furuta R, Simada J, Kiyosawa M, Ishii S, Endo K, Suzuki F, Senda M (1997) Evaluation of carbon-11 labeled KF15372 and its ethyl and methyl derivatives as a potential CNS adenosine A1 receptor ligand. *Nucl Med Biol* 24:53–59
- Paul S, Elsinga PH, Ishiwata K, Dierckx RA, van Waarde A (2011) Adenosine A(1) receptors in the central nervous system: their functions in health and disease, and possible elucidation by PET imaging. *Curr Med Chem* 18:4820–4835
- Poucher SM, Keddie JR, Singh P, Stogdall SM, Caulkett PW, Jones G, Coll MG (1995) The in vitro pharmacology of ZM 241385, a potent, non-xanthine A2a selective adenosine receptor antagonist. *Br J Pharmacol* 115:1096–1102
- Ramlackhansingh AF, Bose SK, Ahmed I, Turkheimer FE, Pavese N, Brooks DJ (2011) Adenosine 2A receptor availability in dyskinetic and nondyskinetic patients with Parkinson disease. *Neurology* 76:1811–1816
- Sihver W, Holschbach MH, Bier D, Wutz W, Schulze A, Olsson RA, Coenen HH (2003) Evaluation of radioiodinated 8-Cyclopentyl-3-[(E)-3-iodoprop-2-en-1-yl]-1-propylxanthine [¹²⁵I]CPIPX as a new potential A1 adenosine receptor antagonist for SPECT. *Nucl Med Biol* 30:661–668
- Sihver W, Bier D, Holschbach MH, Schulze A, Wutz W, Olsson RA, Coenen HH (2004) Binding of tritiated and radioiodinated ZM241,385 to brain A2A adenosine receptors. *Nucl Med Biol* 31:173–177
- Todde S, Moresco RM, Simonelli P, Baraldi PG, Cacciari B, Spalluto G, Varani K, Monopoli A, Matarrese M, Carpinelli A, Magni F, Kienle MG, Fazio F (2000) Design, radiosynthesis, and biodistribution of a new potent and selective ligand for in vivo imaging of the adenosine A(2A) receptor system using positron emission tomography. *J Med Chem* 43:4359–4362
- Wadsak W, Mien LK, Shanab K, Ettliger DE, Haeusler D, Sindelar K, Lanzenberger RR, Spreitzer H, Viernstein H, Keppler BK, Dudczak R, Kletter K, Mitterhauser M (2008) Preparation and first evaluation of [(18F)FE@SUPPY: a new PET tracer for the adenosine A(3) receptor. *Nucl Med Biol* 35:61–66
- Wang WF, Ishiwata K, Nonaka H, Ishii S, Kiyosawa M, Shimada J, Suzuki F, Senda M (2000) Carbon-11-labeled KF21213: a highly selective ligand for mapping CNS adenosine A(2A) receptors with positron emission tomography. *Nucl Med Biol* 27:541–546
- Zeitler JM, Morales-Villagran A, Maidment NT, Behnke EJ, Ackerson LC, Lopez-Rodriguez F, Fried I, Engel J, Wilson CL (2006) Extracellular adenosine in the human brain during sleep and sleep deprivation: an in vivo microdialysis study. *Sleep* 29:455–461

PET Tracers for Beta-Amyloid and Other Proteinopathies

8

Agneta Nordberg

Contents

8.1	Introduction	200
8.2	Molecular Imaging	201
8.3	Amyloid PET Tracers.....	202
8.3.1	Different Chemical Classes.....	202
8.3.2	Multiple Binding Sites	202
8.4	Amyloid Imaging in AD and MCI.....	203
8.5	Longitudinal Changes in Amyloid Deposition in AD.....	206
8.6	Correlation of Amyloid, Cerebral Glucose Metabolism, ApoE Genotype, and Cognition	206
8.7	Amyloid Deposition in Healthy Elderly	207
8.8	Amyloid Imaging in Other Conditions	207
8.9	Tau PET Imaging	207
	Conclusions.....	208
	References.....	209

Abstract

The recent rapid development of molecular imaging techniques has provided us with great possibilities to follow neurodegenerative disease processes in the brain. Molecular imaging with positron emission tomography (PET) has been important in further understanding the role of various proteinopathies in dementia disorders. For Alzheimer's disease (AD), several PET beta amyloid (A β) tracers have been developed. These include the most-investigated ^{11}C -Pittsburgh compound B (^{11}C -PIB), but also several ^{18}F -labeled tracers, such as ^{18}F -florbetapir, ^{18}F -florbetaben, ^{18}F -flutemetamol, and ^{18}F -NAV-4694, which

A. Nordberg
Alzheimer Neurobiology Center, Karolinska Institutet,
Department of Geriatric Medicine, Karolinska University Hospital Huddinge,
Novum 5th Floor, S-14186 Stockholm, Sweden
e-mail: agneta.k.nordberg@ki.se

have longer half-lives and therefore are more suitable for clinical use. Fibrillar brain A β is able to be detected by PET very early in the progression of AD, several years before the observed decline in cerebral glucose metabolism that is more closely related to cognitive impairment. PET A β imaging allows discrimination between AD and other non-A β diseases, including frontotemporal lobar dementia (FTLD). However, A β brain expression may also be observed in other dementia disorders, including dementia with Lewy bodies (DLB), Parkinson's disease with dementia (PDD), and cortical basal dementia. Most importantly, different PET tau tracers, which should provide additional important insights and understandings of the complex pathophysiology processes in various neurodegenerative diseases, are being developed.

8.1 Introduction

Modern molecular imaging has provided new exciting tools to investigate the brain and the functional disturbances and time courses of different pathological changes. Several neurodegenerative brain disorders are characterized by proteinopathies with extracellular and intracellular deposits of abnormal proteins. Some similarities seem to exist for some diseases, such as Parkinson's disease (PD), dementia with Lewy bodies (DLB), and Alzheimer's disease (AD), which show a continuum of and similarity in pathology. Beta amyloid (A β) plaques, a histopathological feature of AD, may also be detected in DLB patients and PD patients with dementia (PDD) in addition to the presence of the Lewy bodies that are characteristic of DLB and PD. Neurofibrillary tangles (NFTs) similar to those found in AD brains may also be found in DLB brains. Some similarities may also exist between frontotemporal lobar dementia (FTLD) and amyotrophic lateral sclerosis (ALS) (Sendtner 2011).

AD is the most common neurodegenerative disorder, and is characterized by a progressive loss of memory, especially of episodic memory, and of other cognitive functions, that finally leads to a loss of independence and to a need for assistance. The neuropathological hallmarks of AD include brain deposition of A β in extracellular plaques and vascular walls as well as intracellular NFTs. The current predominant hypothesis for the cause of AD has been related to dysfunction in brain of processing, deposition, and clearance of the A β protein.

A β was initially purified and sequenced by Glenner and Wong (1984). Braak and Braak (1991) described the gradual cortical deposition of A β from the basal neocortex, then to all areas of the cortex, and, at later stages, to subcortical brain regions. The distribution of A β , thus, differs from the distribution of NFTs in AD brains (Braak and Braak 1998). It is assumed that the A β pathology precedes the presence of NFTs during the progression of AD. The amyloid cascade hypothesis by Hardy and Higgins (1992) postulates the cleavage of APP by γ and β secretases, generating the soluble fragments, APP and β APP, and, from the A β monomers, oligomers, protofibrils, fibrils, and, finally, A β plaques (Fig. 8.1). The smaller forms of A β , such as the oligomers, are assumed to directly interfere with nerve cell synaptic activity. Functional studies in tissue slice preparations and animals have shown that A β oligomers can inhibit long-term potentiation (LTP) and synaptic function in mature neurons (Lambert et al. 1998; Shankar et al. 2008). A negative correlation has been observed

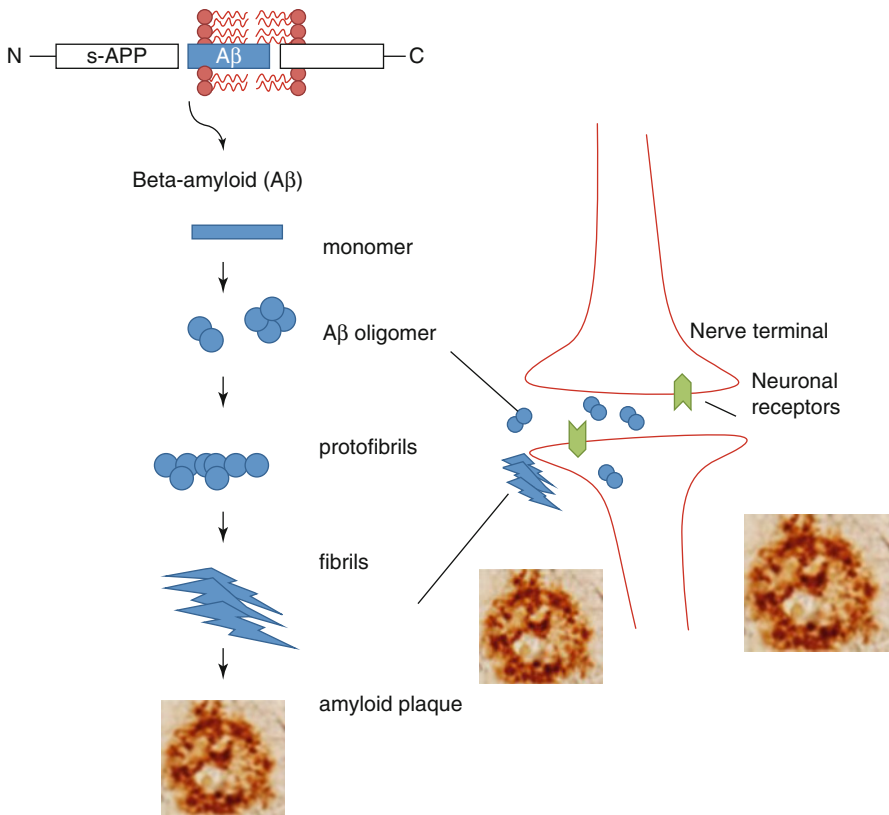


Fig. 8.1 Beta amyloid (A β) processes from soluble amyloid precursor protein (s-APP) to different forms of A β with their possible interaction with the nerve terminal (synapse)

between the number of nicotinic acetylcholine receptors and choline acetyltransferase activity with the total amount of A β oligomers in early-onset AD patients, and with the A β oligomers species decamer (45 kDa) in late-onset AD patients (Bao et al. 2012). Thus far, it has only been possible to visualize the smaller oligomeric forms of A β in vivo by imaging techniques; the fibrillar A β form has not been visualized.

8.2 Molecular Imaging

The landscape of AD research has significantly changed during recent years, moving away from studies in autopsy brain tissue and evaluation of clinical trials with quite insensitive cognitive scales, and toward the use of structural and molecular imaging and biomarkers in cerebrospinal fluid (CSF), and increasing the understanding of the pathological cascade of events in AD. The introduction of amyloid PET imaging with radiotracers such as ^{11}C -Pittsburgh compound B (PIB) (Klunk et al. 2004) has provided new and valuable insight into the dynamic processes and time course of deposition of fibrillar A β in the brain from preclinical through clinical stages of AD. Several different ^{18}F -labeled amyloid PET tracers have been

tested, and one, ^{18}F -florbetapir, has been recently approved by the US Food and Drug Administration (FDA) and the European Medicine Agency (EMA) for clinical assessment of cognitive problems. Recently also ^{18}F -flutemetamol was approved by FDA. The new molecular imaging techniques have provided opportunities to develop diagnostic biomarkers for early detection at preclinical stages as well as for monitoring effects of drug therapy. Incorporation of biomarkers into the standardized clinical diagnosis of AD is recommended (Dubois et al. 2007, 2010; Albert et al. 2011). It is now possible to recognize different stages of AD in affected populations, such as “asymptomatic AD,” “prodromal AD,” “mild cognitive impairment caused by AD (MCI/AD),” and “clinical AD” stages (Dubois et al. 2010; Albert et al. 2011; McKhann et al. 2011; Sperling et al. 2011).

8.3 Amyloid PET Tracers

8.3.1 Different Chemical Classes

After testing some radiolabeled amyloid antibodies (Friedland et al. 1994) to peptide fragments (Wengenack et al. 2000) that failed to label brain A β in vivo, the small molecule strategy emanating from amyloid dyes such as Congo red and thioflavine was more fruitful (Nordberg 2004). ^{18}F -FFDNP (Shoghi-Jadid et al. 2002) and ^{11}C -PIB (Klunk et al. 2004) were the two first PET A β tracers studied in AD patients. The compounds differ in chemical structure (Fig. 8.2) as well as in the binding patterns in the brain. Increased binding of ^{18}F -FDDNP was observed in the temporal, parietal, and frontal regions of AD brain compared with controls (Shoghi-Jadid et al. 2002). ^{11}C -PIB showed higher binding in the frontal, parietal, temporal, occipital, and striatal brain regions compared with controls (Klunk et al. 2004). The difference in binding between AD brains and control brains was significantly higher for ^{11}C -PIB compared with ^{18}F -FDDNP (Klunk et al. 2004; Shoghi-Jadid et al. 2002). On the other hand, ^{18}F -FDDNP was found to also bind to tau proteins in the brain (Small et al. 2006). ^{11}C -PIB has so far been the most explored and most used amyloid PET tracer. As illustrated in Fig. 8.2, several A β PET tracers have now been developed belonging to different chemical classes including thioflavine (^{11}C -PIB, ^{18}F -flutemetamol, ^{11}C -AZD2184), benzoxazole (^{11}C -BF227, ^{18}F -BF227), stilbene (^{18}F -FDDNP), naphthalenes (^{11}C -SB13, ^{18}F -AV-1 (florbetaben), ^{18}F -AV-45 (florbetapir)), and benzofuran (^{18}F -NAV-4694; ^{18}F -AZD-4694). ^{18}F -labeled compounds have the advantage that they do not require a cyclotron on site because of the longer half-time of ^{18}F (110 min) compared with ^{11}C (20 min). ^{18}F -labeled compounds also provide the possibility of a short scanning time of 15–20 min. Generally, ^{18}F amyloid tracers show a greater binding to white matter compared with ^{11}C -PIB.

8.3.2 Multiple Binding Sites

Two binding sites have been observed in autopsy human brain tissue for ^{11}C -PIB with a high-affinity site in the nanomolar range in addition to a low-affinity binding site (Klunk et al. 2004). High-affinity binding sites in the nanomolar range have also

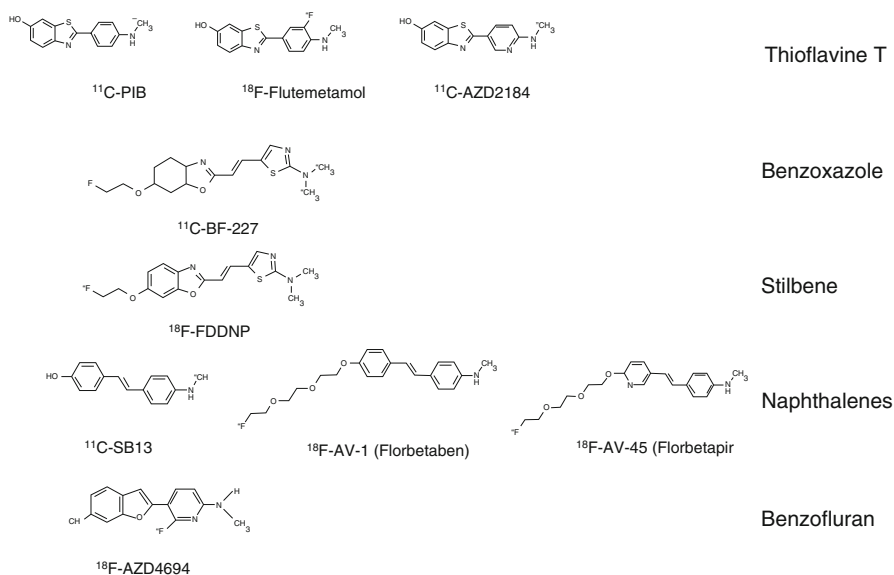


Fig. 8.2 Different PET amyloid tracers and their chemical structures

been reported in *in vitro* binding studies in human brain for AV-45 (florbetapir) (Choi et al. 2009) as well as AV-1 (florbetaben) (Fodero-Tavoletti et al. 2012). When comparing the *in vitro* binding properties of several of the PET amyloid tracers, a multitracer binding-site model could be postulated where PIB, flumetamol, and florbetaben all show nanomolar affinity for a major high-affinity site 1, whereas BF227 shows affinity mainly to binding sites 3 and FDNP, with only some binding to site 2 (Ni et al. 2013). Different chemical structures may offer binding to different parts of the A β fibrils but also to other nonfibrillar A β components. Whether the A β tracer binding properties differ in brain tissues from different familial AD (FAD) brains compared with sporadic cases has not yet been shown, nor have possible differences between the different stages of AD been investigated. Consistent comparable data have been reported between *in vivo* ^{11}C -PIB (Bacsikai et al. 2007; Ikonovic et al. 2008; Kadir et al. 2011), ^{18}F -florbetapir (Clark et al. 2012), ^{18}F -flumetamol (Wolk et al. 2011), and brain histopathology. There are, however, few studies in which different forms of A β were quantified with PCR or similar methods and additional research is needed to study the similarities/dissimilarities between *in vivo* A β scanning and *in vitro* autopsy studies.

8.4 Amyloid Imaging in AD and MCI

Representative PET images with ^{11}C -PIB overlaid on magnetic resonance imaging (MRI) images for patients with mild AD are shown in Fig. 8.3. The high retention of ^{11}C -PIB observed in the frontal cortex, parietal cortex, and temporal cortex, with sparing of the cerebellum, follows the deposition of A β as described earlier by Braak and Braak (1991) from autopsy histopathological studies. The first ^{11}C -PIB

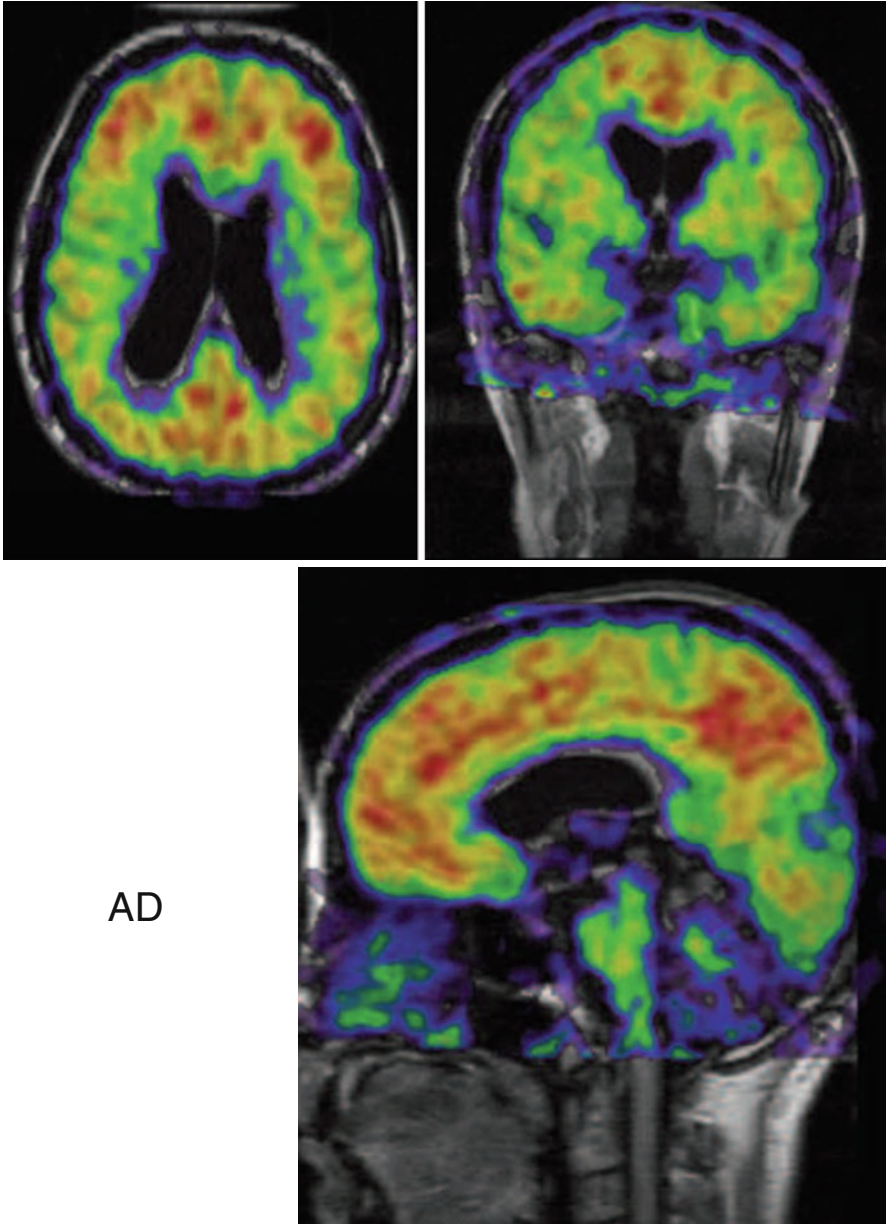


Fig. 8.3 ^{11}C -Pittsburg compound B (^{11}C -PIB) retention in brains of Alzheimer patients. Color scale: *red* high, *yellow* medium, *green* medium-low, *blue* low (Photo: A. Nordberg, Karolinska Institutet)

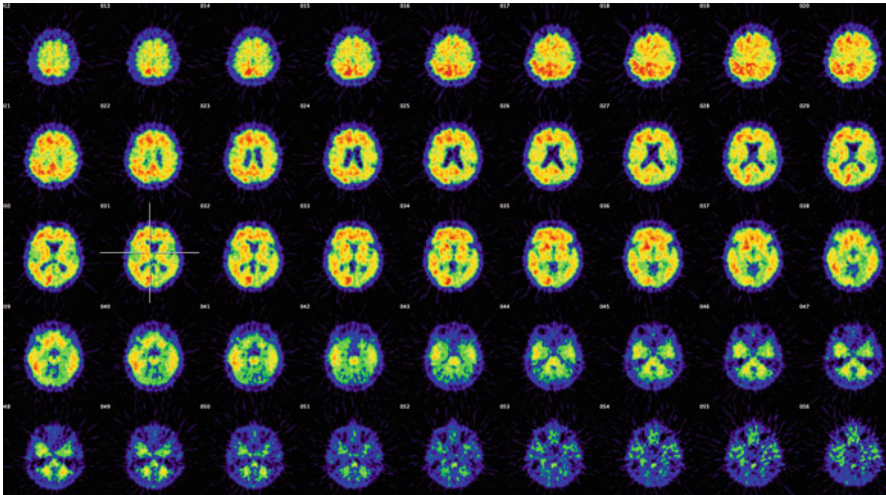


Fig. 8.4 ^{11}C -Pittsburg compound B (^{11}C -PiB) retention in 45 transverse sections of the brain of patients with mild cognitive impairment (MCI) who later converted to AD. The first section illustrates high cortical regions and the last is on the level of the cerebellum (Photo: A. Nordberg, Karolinska institutet)

scan study, in a cohort of 15 AD patients, convincingly showed a significantly higher ^{11}C -PiB retention in both cortical and subcortical brain regions in comparison with control subjects (Klunk et al. 2004), since then, numerous PET studies with ^{11}C -PiB have verified the findings (for reviews see (Nordberg et al. 2010; Cohen et al. 2012; Rowe and Villemagne 2013)). A large multicenter study on 238 subjects scanned with ^{11}C -PiB at five AD centers in Europe demonstrated the robustness of this technique in measuring A β deposition in the brain (Nordberg et al. 2013). A high correlation between ^{11}C -PiB imaging and different ^{18}F -amyloid PET tracers (florbetapir, flumetamol, florbetaben, and NAV-4694 (AZD-4694)) has been found (for review, see (Johnson et al. 2013)).

Most interestingly, patients with mild cognitive impairment (MCI) have shown either high (PiB+) or low (PiB-) ^{11}C -PiB retention (Forsberg et al. 2008; Okello et al. 2009; Wolk et al. 2009; Koivunen et al. 2011). Figure 8.4 shows ^{11}C -PiB retention in multiple brain regions of patients with MCI. It is evident from the scans that high ^{11}C -PiB retention is observed in large parts of the brain and is quite comparable to what is observed in AD patients. Because the cerebellum shows very low ^{11}C -PiB retention, the cerebellum is often used as a reference region when expressing standard uptake values (SUV). Consistent data from several follow-up studies indicate that PiB+ MCI patients have a higher risk to convert to AD than PiB- MCI patients. When 64 MCI patients were longitudinally followed clinically for a mean duration of 28 ± 15 months, 67 % of PiB+ MCI patients converted to AD, whereas none of

the PIB– MCI patients converted to AD (Nordberg et al. 2013). The observations support the possibility that, during memory assessments, the patients with MCI who are most likely to convert to AD in the future could be identified and therefore offered preventive or disease-modifying drug treatment.

8.5 Longitudinal Changes in Amyloid Deposition in AD

A 2-year follow-up study in 15 AD patients showed unchanged ^{11}C -PIB retention in the brain while declines in cerebral glucose metabolism (assessed by ^{18}F -fluorodeoxyglucose (^{18}F -FDG) uptake) and cognition (Engler et al. 2006) were observed; this study was followed by a 5-year follow-up study in the same cohort of AD patients (Kadir and Nordberg 2010). A discussion of whether there is a continuous increase in fibrillar A β with the progression of AD has been ongoing in the literature. Although imaging studies in placebo-treated AD patients in immunization trials showed increases in amyloid (Rinne et al. 2010; Ostrowitzki et al. 2012), several studies based on larger numbers of subjects suggest an A β plateau in AD (Jack et al. 2013b; Villemagne et al. 2013). Patients with mild MCI who are PIB+ show longitudinal increases in A β (Kadir et al. 2012). From data generated from 18-month follow-up PIB PET studies in healthy subjects, patients with MCI, and AD patients, Villemagne et al. (2013) estimated that it takes 19 years to reach the A β levels observed during the clinical phase of AD. Recent cross-sectional PET imaging studies in subjects from families with autosomal dominant inherited AD have shown high fibrillar A β deposition up to 15 years before the expected onset of symptoms (Batesman et al. 2012; Morris et al. 2012; Fleisher et al. 2012).

8.6 Correlation of Amyloid, Cerebral Glucose Metabolism, ApoE Genotype, and Cognition

The deposition of fibrillar A β starts earlier in the course of AD in comparison with the decline in cerebral glucose metabolism as measured by ^{18}F -FDG uptake (Nordberg et al. 2010; Jack et al. 2013a). A negative correlation has been observed between cerebral glucose metabolism and ^{11}C -PIB retention in brain regions of AD patients and control patients in the parietal and temporal cortices but not in the frontal cortex (Klunk et al. 2004; Engler et al. 2006). ^{11}C -PIB PET seems to detect prodromal AD at an earlier disease stage and better separates between MCI subtypes than ^{18}F -FDG uptake (Forsberg et al. 2008). The decline in cerebral glucose metabolism seems to be more regionally specific compared with the increased ^{11}C -PIB retention in large areas of the AD brain (Engler et al. 2006; Forsberg et al. 2010). Higher fibrillar A β deposition has been observed in brains of patients with MCI and AD who have the ApoE E4 gene carrier compared with those who have the ApoE3 gene carrier, as measured by ^{11}C -PIB and ^{18}F -florbetapir (Drzezga et al. 2009; Fleisher et al. 2013; Nordberg et al. 2013). Correlation between A β PET imaging results and cognition has been observed in patients with MCI as well as in control

subjects (Pike et al. 2007; Forsberg et al. 2008; Kawas et al. 2013; Rosenberg et al. 2013); but also in AD patients when analyzing regional A β load and episodic memory (Engler et al. 2006; Chetelat et al. 2012).

8.7 Amyloid Deposition in Healthy Elderly

An increasing A β load has been measured by PET in cognitively healthy subjects, with the measured load ranging between 10 % (Nordberg et al. 2013; Mintun et al. 2006), 22 % (Pike et al. 2007), 33 % (Rowe et al. 2010), and 55 % (Mathis et al. 2013). The increase in fibrillar A β as measured by amyloid PET tracers appears to increase with age, and it has recently been estimated that approximately 20 years is needed to reach clinical symptomatology (Villemagne et al. 2013). The presence of brain injury measured by MRI and PET FDG in cognitively healthy elderly subjects assigned for preclinical AD has been reported to be unrelated to the presence of A β (Knopman et al. 2012; Wirth et al. 2013). This lack of correlation may change the view of the role of A β in AD (Chetelat 2013).

8.8 Amyloid Imaging in Other Conditions

Amyloid imaging may help in differentiating AD from other forms of dementia. For example, in most patients with FTLN, PET A β scans are negative (Raboinvici et al. 2007; Engler et al. 2008; Drzezga et al. 2008; Laforce and Rabinovici 2011). In corticobasal syndrome, PIB-positive patients showed greater visuospatial deficits and repetition impairment than PIB-negative patients (Burrell et al. 2013). The presence of A β , as assessed by PET imaging, has not been found in brains of Parkinson patients who have no cognitive impairment (Johansson et al. 2008). Patients with Parkinson MCI and amyloid show declines in cognition compared with patients with no A β in brain observed in imaging studies (Gomperts et al. 2012). High fibrillar A β levels are often observed in the brains of patients with DLB (Rowe et al. 2007; Edison et al. 2008; Maetzler et al. 2009; Shimada et al. 2013), and it is therefore difficult to discriminate between AD and DLB by A β tracer PET imaging. High ^{11}C -PIB retention has been observed in patients with cerebral A β angiopathy, and the regional pattern is different from that observed in AD (Johnson et al. 2007).

8.9 Tau PET Imaging

Accumulation of tau is known to occur in several neurodegenerative diseases, including AD, FTLN, Down's syndrome, cortical basal degeneration, progressive nuclear palsy, FTLN with Parkinson dementia, multiple system atrophy, and prion disease. Although tau is present in several diseases, there are probably variations in the presence of the different tau isoforms. Histopathologically, the presence of tau in the brain is demonstrated as NFTs, as paired helical filaments as well as dystrophic

neurites in senile plaques. The number of NFTs in autopsy brain tissue has been reported to negatively correlate with cognitive function before death. ^{18}F -FDDNP, which was introduced as an A β PET tracer, was demonstrated to bind to NFTs (Agdeppa et al. 2001). A correlation between ^{18}F -FDDNP binding and episodic memory was reported in AD and MCI patients (Tolboom et al. 2009). Presently, other candidates for PET tracers, such as ^{18}F -THK523, ^{18}F -5105, ^{18}F -5117, and ^{18}F -T-807, have been suggested (Fodero-Tavoletti et al. 2011; Zhang et al. 2012; Harada et al. 2013; Chien et al. 2013; Chun-Fang et al. 2013; Okamura et al. 2013), and clinical studies of these compounds are in progress. Harada et al. (2013) assessed the in vitro binding profile to tau and A β fibrils and compared the binding of ^{18}F -THK523 with the A β ligands ^{18}F -BF-227, ^{18}F -FDDNP, and ^3H -PIB. They observed that ^{18}F -THK523 showed a higher affinity for binding tau fibrils compared with A β fibrils than the other three PET tracers investigated (Harada et al. 2013). Okamura et al. (2013) demonstrated a higher in vitro binding affinity for THK-5105 and THK-5117 compared with THK-523. In autoradiographical studies in autopsy AD brain tissue, they also showed that the radiotracers bound preferentially to NFTs and that the distribution was different from the ^{11}C -PIB binding (Okamura et al. 2013). ^{18}F -T-807 has also been shown to bind with high affinity to human brain tissue NFTs (Zhang et al. 2012). In vivo PET studies showed a higher retention of ^{18}F -T-807 in the temporal cortex and hippocampus of AD patients compared with controls (Chien et al. 2013). Because the number of NFTs seems to correlate with the degree of dementia, tau PET tracers might be more useful for following the progression of AD and for evaluating drug efficacy than for being a very early diagnostic biomarker.

Conclusions

Molecular imaging techniques have increased the opportunities for studying the time course of pathophysiological processes in the brain during neurodegenerative disorders. A β peptide deposition in plaques can be measured by PET with different available A β tracers. Different time courses of pathological changes have been observed when using imaging (Fig. 8.5). The accumulation of fibrillar A β in the brain starts much earlier than the decline in cerebral glucose metabolism. This seems to be similar for early astrocytosis in the brain. Changes in cognition, neurotransmitter impairment, and brain atrophy seem to be closely related temporally. The introduction of new PET tracers for visualizing different forms of A β peptides (including A β oligomers), different forms of tau (including tau oligomers), and other not-yet studied peptides, such as α -synuclein, will open up new possibilities for the further understanding of proteinopathies.

Acknowledgement Great thanks to MPharm Ruiqing Ni, Karolinska institutet for drawing Fig. 8.1. Financial support was received from the Swedish Research Council (project 05817), the Karolinska Institutet Strategic Neuroscience program, the Stockholm County Council-Karolinska Institutet regional agreement on medical training and clinical research (ALF grant), Swedish Brain Power, the Swedish Brain Foundation, Stohne's foundation, the Alzheimer Foundation in Sweden, the Foundation for Old Servants, and EU FW7 large-scale integrating project INMiND (<http://www.uni-muenster.de/InMind>).

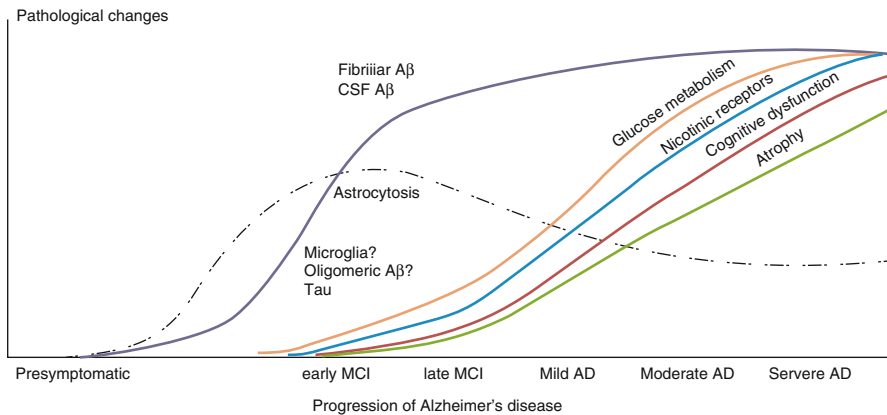


Fig. 8.5 Time course of pathological and functional imaging markers during progression of Alzheimer's disease. $A\beta$ amyloid beta, *AD* Alzheimer's disease, *CSF* cerebral spinal fluid, *MCI* mild cognitive impairment (From Nordberg 2011)

References

- Agdeppa ED, Kepe V, Liu J et al (2001) Binding characteristics of radiofluorinated 6-dialkylamino-2-naphtylen derivatives as positron emission tomography imaging probes for β -amyloid plaques in Alzheimer's disease. *J Neurosci* 21:1–5
- Albert MS, DeKosky ST, Dickson D et al (2011) The diagnosis of mild cognitive impairment due to Alzheimer's disease: recommendations from the National Institute on Aging-Alzheimer's Association workgroups on diagnostic guidelines for Alzheimer's disease. *Alzheimers Dement* 7:270–279
- Bacskaï BJ, Frosch MP, Freeman SH et al (2007) Molecular imaging with Pittsburgh compound B confirmed at autopsy: a case report. *Arch Neurol* 64:431–434
- Bao F, Wicklund L, Lacor PN et al (2012) Different β -amyloid oligomer assemblies in Alzheimer brains correlate with age of disease of onset and impaired cholinergic activity. *Neurobiol Aging* 33:825.e1–825.e13
- Batesman RJ, Xiong C, Benzinger TLS et al (2012) Clinical and biomarker changes in dominantly inherited Alzheimer's disease. *N Engl J Med* 365:795–804
- Braak H, Braak E (1991) Neuropathological staging of Alzheimer-related changes. *Acta Neuropathol* 82:239–259
- Braak H, Braak E (1998) Evolution of neuronal changes in the course of Alzheimer's disease. *J Neural Transm Suppl* 53:127–140
- Burrell JR, Hornberger M, Villemagne VL et al (2013) Clinical profile of PIB positive corticobasal syndrome. *PLoS One* 8:e61025
- Chetelat G (2013) $A\beta$ -independent processes—rethinking preclinical AD. *Nat Rev Neurol* 9:123–124
- Chetelat G, Villemagne VL, Pike KE et al (2012) Relationship between memory performance and β -amyloid deposition at different stages of Alzheimer's disease. *Neurodegener Dis* 10:141–144
- Chien DT, Bahri S, Szardenings AK et al (2013) Early clinical PET imaging results with the novel PHF-tau radioligand [18-F]-T807. *J Alzheimers Dis* 34:457–468. doi:10.3233/JAD-122059
- Choi SR, Golding G, Zhuang Z et al (2009) Preclinical properties of 18F-AV-45: a PET agent for A β plaques in the brain. *J Nucl Med* 50:1887–1894
- Chun-Fang X, Arteaga J, Chen G et al (2013) [18F]T-807, a novel tau positron emission tomography imaging agent for Alzheimer's disease. *J Alzheimers Dis* 9:1–11

- Clark CM, Pontocorvo MJ, Beach TG et al (2012) Cerebral PET with florbetapir compared with neuropathology at autopsy for detection of neuritic amyloid- β plaques : a prospective cohort study. *Lancet Neurol* 11:669–678
- Cohen AD, Rabinovici GD, Mathis CA et al (2012) Using Pittsburgh compound B for in vivo PET imaging of fibrillar amyloid beta. *Adv Pharmacol* 64:27–81
- Drzezga A, Grimmer T, Henriksen G (2008) Imaging of amyloid plaques and cerebral glucose metabolism in semantic dementia and Alzheimer's diseases. *Neuroimage* 39:619–633
- Drzezga A, Grimmer T, Henriksen G (2009) Effect of APOE genotype on amyloid plaque load and gray matter volume in Alzheimer disease. *Neurology* 72:1487–1494
- Dubois B, Feldman HH, Jacova C et al (2007) Research criteria for the diagnosis of Alzheimer's disease: revising the NINCDS-ADRDA criteria. *Lancet Neurol* 6:734–746
- Dubois B, Feldman HH, Jacova C et al (2010) Revising the definition of Alzheimer's disease: a new lexicon. *Lancet Neurol* 9:1118–1127
- Edison P, Rowe CC, Rinne JO et al (2008) Amyloid load in Parkinson's disease dementia and Lewy body dementia measured with [11 C]PIB positron emission tomography. *J Neurol Neurosurg Psychiatry* 79:1331–1338
- Engler H, Forsberg A, Almqvist O et al (2006) Two-year follow-up for amyloid deposition in patients with Alzheimer's disease. *Brain* 129:2856–2866
- Engler H, Fritzell Santillo A, Wang SX et al (2008) In vivo amyloid imaging with PET in fronto-temporal dementia. *Eur J Nucl Med Mol Imaging* 35:100–106
- Fleisher AS, Chen K, Quiroz YT et al (2012) Florbetapir PET analysis of amyloid- β deposition in the presenilin 1 E280A autosomal dominant Alzheimer's disease kindred: a cross-sectional study. *Lancet Neurol* 11:1057–1065
- Fleisher AS, Chen K, Liu X et al (2013) Apolipoprotein E ϵ 4 and age on florbetapir positron emission tomography in healthy aging and Alzheimer's disease. *Neurobiol Aging* 34:1–12
- Fodero-Tavoletti MT, Okamura N, Furumoto S et al (2011) 18F-THK523: a novel tau imaging ligand for Alzheimer's disease. *Brain* 134:1089–1100
- Fodero-Tavoletti MT, Brockschnieder D, Villemagne VL et al (2012) In vitro characterization of [(18)F]-florbetaben, an A β imaging radiotracer. *Nucl Med Biol* 39:1042–1048
- Forsberg A, Engler H, Almqvist O et al (2008) PET imaging of amyloid deposition in patients with mild cognitive impairment. *Neurobiol Aging* 29:1456–1465
- Forsberg A, Almqvist O, Engler H et al (2010) High PIB retention in Alzheimer's disease is an early event with complex relationship with CSF biomarkers and functional parameters. *Curr Alzheimer Res* 7:56–66
- Friedland RP, Majocha RE, Reno JM et al (1994) Development of an anti-A β monoclonal antibody for in vivo imaging of amyloid angiopathy in Alzheimer's disease. *Mol Neurobiol* 9:107–113
- Glenner GG, Wong CW (1984) Alzheimer's disease: initial report of the purification and characterization of a novel cerebrovascular amyloid protein. *Biochem Biophys Res Commun* 120:885–890
- Gomperts SN, Locascio JJ, Marquie M et al (2012) Brain amyloid and cognition in Lewy body diseases. *Mov Disord* 8:965–973
- Harada R, Okamura N, Furumoto S et al (2013) Comparison of the binding of [18F] THK-523 and other imaging tracers to Alzheimer's disease pathology. *Eur J Nucl Med Mol Imaging* 40:125–132
- Hardy JA, Higgins GA (1992) Alzheimer's disease: the amyloid cascade hypothesis. *Science* 256:184–185
- Ikonomic MD, Klunk WE, Abrahamson EE (2008) Post-mortem correlates of in vivo PIB-PET amyloid imaging in a typical case of Alzheimer's disease. *Brain* 131:1630–1645
- Jack CR, Knopman DS, Jagust WJ et al (2013a) Tracking pathophysiological processes in Alzheimer's disease: an updated hypothetical model of dynamic biomarkers. *Lancet Neurol* 12:207–216
- Jack CR, Wiste HJ, Lesnick TG et al (2013b) Brain β -amyloid load approaches a plateau. *Neurology* 80:1–7

- Johansson A, Savitcheva I, Forsberg A et al (2008) ^{11}C -PIB imaging in patients with Parkinson's disease. *Parkinsonism Relat Disord* 14:345–347
- Johnson KA, Gregas M, Becker JA et al (2007) Imaging of amyloid burden and distribution in cerebral amyloid angiopathy. *Ann Neurol* 62:229–234
- Johnson KA, Minoshima S, Bohnen NI et al (2013) Appropriate use criteria for amyloid PET: a report of the amyloid imaging task force, the society of nuclear medicine and molecular imaging and the Alzheimer association. *Alzheimers Dement* 9:1–16
- Kadir A, Nordberg A (2010) Target – specific PET probes for neurodegenerative disorders relegated to dementia. *J Nucl Med* 51:1418–1430
- Kadir A, Marutle A, Gonzalez D et al (2011) Positron emission tomography imaging and clinical progression in relation to pathology in the first Pittsburgh Compound B positron emission tomography patient with Alzheimer's disease. *Brain* 134:301–317
- Kadir A, Almkvist O, Forsberg A et al (2012) Dynamic changes in PET amyloid and FDG imaging at different stages of Alzheimer's disease. *Neurobiol Aging* 33:198.e1–198.e14
- Kawas CH, Greenia DE, Bullain SS et al (2013) Amyloid imaging and cognitive decline in nondemented oldest-old: The 90+ study. *Alzheimer Dement* 9:199–203
- Klunk WE, Engler H, Nordberg A et al (2004) Imaging brain amyloid in Alzheimer's disease with Pittsburgh Compound-B. *Ann Neurol* 55:306–319
- Knopman DS, Jack Jr CR, Wiste HJ et al (2012) Brain injury markers are not dependent on β amyloid in normal elderly. *Ann Neurol* 2012 Nov 23. doi:10.1002/ana.23816. [Epub ahead of print]
- Koivunen J, Scheinin N, Virta JR et al (2011) Amyloid PET imaging in patients with mild cognitive impairment: a 2 year follow-up study. *Neurology* 76:1085–1090
- Laforce R, Rabinovici GD (2011) Amyloid imaging in the differential diagnosis of dementia: review and potential clinical applications. *Alzheimers Res Ther* 3:31
- Lambert MP, Barlow AK, Chromy BA et al (1998) Diffusible, nonfibrillar ligands derived from A β 1–42 are potent central nervous system neurotoxins. *Proc Natl Acad Sci U S A* 95:6448–6453
- Maetzler W, Liespelt I, Reimold M et al (2009) Cortical PIB binding in Lewy body disease as associated with Alzheimer-like characteristics. *Neurobiol Dis* 34:107–112
- Mathis CA, Kuller LH, Klunk WE et al (2013) In vivo assessment of amyloid- β deposition in nondemented very old subjects. *Ann Neurol* 73:751–761
- McKhann GM, Knopman DS, Chertkow H et al (2011) The diagnosis of dementia due to Alzheimer's disease: recommendations from the National Institute on Aging-Alzheimer's Association workgroups on diagnostic guidelines for Alzheimer's disease. *Alzheimers Dement* 7:263–269
- Mintun MA, LaRossa GN, Sheline YI et al (2006) [^{11}C]PIB in a nondemented population: potential antecedent marker of Alzheimer disease. *Neurology* 67:446–452
- Morris JC, Aisen P, Randall J et al (2012) Developing an international network for Alzheimer's research: the Dominantly Inherited Alzheimer Network. *Clin Investig* 2:975–984
- Ni R, Gillberg P-G, Bergfors A, Marutle A, Nordberg A (2013) Amyloid tracers detect multiple binding sites in Alzheimer's disease tissue. *Brain* 136:2217–2227
- Nordberg A (2004) PET imaging of amyloid in Alzheimer's disease. *Lancet Neurol* 3:519–527
- Nordberg A (2011) Molecular imaging in Alzheimer's disease—new perspectives on biomarkers for early diagnosis and drug development. *Alzheimer Res Ther* 3:34, e.1–9
- Nordberg A, Rinne J, Kadir A, Långström B (2010) The use of PET in Alzheimer's disease. *Nature Rev Neurol* 6:68–87
- Nordberg A, Carter S, Rinne J et al (2013) A European multi-center PET study of fibrillar amyloid in Alzheimer's disease. *Eur J Nucl Med Mol Imaging* 40:104–114
- Okamura N, Furumoto S, Harada R et al (2013) Novel ^{18}F -labeled arylquinoline derivatives for noninvasive imaging of tau pathology in Alzheimer disease. *J Nucl Med* 54:1420–1427
- Okello A, Koivunen J, Edison P et al (2009) Conversion of amyloid positive and negative MCI to AD over 3 years: a ^{11}C -PIB PET study. *Neurology* 73:754–760
- Ostrowitzki S, Deptula D, Thjurfell L et al (2012) Mechanism of amyloid removal with Alzheimer disease treated with gantenerumab. *Arch Neurol* 69:198–207

- Pike KE, Savage G, Villemagne VL et al (2007) Beta-amyloid imaging and memory in non-demented individuals: evidence for preclinical Alzheimer's disease. *Brain* 130:2837–2844
- Rabinovici GD, Furst AJ, O'Neill JP et al (2007) 11C-PIB PET imaging in Alzheimer's disease and frontotemporal lobar degeneration. *Neurology* 68:1205–1212
- Rinne JO, Brooks D, Rossor MN et al (2010) 11C-PIB PET in assessment of change in fibrillar amyloid-beta load in Alzheimer's disease patients treated with babineuzumab: a phase 2 double-blind, placebo controlled, ascending dose study. *Lancet Neurol* 9:363–372
- Rosenberg PB, Edell SL, Ross JS et al (2013) Cognition and amyloid load in Alzheimer disease imaged with florbetapir F18 (AV-45) positron emission tomography. *Am J Geriatr Psychiatry* 21:272–278
- Rowe CC, Villemagne VL (2013) Brain amyloid imaging. *J Nucl Med Technol* 41:11–18
- Rowe CC, Ng S, Ackermann U et al (2007) Imaging β amyloid burden in aging and dementia. *Neurology* 68:1718–1725
- Rowe CC, Ellis KA, Rimajova M et al (2010) Amyloid imaging results from the Australian Imaging, Biomarkers and Lifestyle (AIBL) study of aging. *Neurobiol Aging* 31:1275–1283
- Sendtner M (2011) TDP-43 multiple targets, multiple disease mechanisms? *Nat Neurosci* 14:403–405
- Shankar GM, Li S, Mehta TH (2008) Amyloid-beta protein dimers isolated directly from Alzheimer's brains impair synaptic plasticity and memory. *Nat Med* 14:837–842
- Shimada H, Shinotoh H, Hirano S et al (2013) β -amyloid in Lewy body disease is related to Alzheimer's disease-like atrophy. *Mov Disord* 28:169–175
- Shoghi-Jadid K, Small GW, Agdeppa ED et al (2002) Localization of neurofibrillary tangles and betaamyloid plaques in the brains of living patients with Alzheimer disease. *Am J Geriatr Psychiatry* 10:24–35
- Small GW, Kepe V, Ercoli LM et al (2006) PET of brain amyloid and tau in mild cognitive impairment. *N Engl J Med* 355:2652–2663
- Sperling RA, Aisen PS, Beckett LA et al (2011) Toward defining the preclinical stages of Alzheimer's disease: recommendations from the National Institute of Aging-Alzheimer Association workgroups on the diagnostic guidelines for Alzheimer's disease. *Alzheimers Dement* 7:280–292
- Tolboom N, Van der Flier WM, Yaqub M et al (2009) Differential association of [11C]PIB and [18F]FDDNP binding with cognitive impairment. *Neurology* 73:2079–2085
- Villemagne VI, Burnham S, Bourgeat P et al (2013) Amyloid β deposition, neurodegeneration, and cognitive decline in sporadic Alzheimer's disease: a prospective cohort study. *Lancet Neurol* 13:357–367
- Wengenack TM, Curran GL, Poduslo JF (2000) Targeting Alzheimer amyloid plaques in vivo. *Nat Biotechnol* 18:868–872
- Wirth M, madison CM, Rabinovici GD et al (2013) Alzheimer's disease neurodegenerative biomarkers are associated with decreased cognitive function but not β -amyloid in cognitive normal older individuals. *J Neurosci* 33:5553–5563
- Wolk DA, Price JC, Saxton JA et al (2009) Amyloid imaging in mild cognitive impairment subtypes. *Ann Neurol* 65:557–658
- Wolk DA, Grachev ID, Buckley C et al (2011) Association between in vivo fluorine 18-labeled flumetamol amyloid positron emission tomography imaging and in vivo cerebral cortical histopathology. *Arch Neurol* 68:1398–1403
- Zhang W, Arteaga J, Xashion DK et al (2012) A highly selective and specific PET tracer for imaging of tau pathologies. *J Alzheimers Dis* 31:602–612

Imaging of Central Benzodiazepine Receptors in Chronic Cerebral Ischemia

9

Hiroshi Yamauchi

Contents

9.1	Introduction	214
9.1.1	Chronic Hemodynamic Compromise and a Risk for Stroke	214
9.1.2	Selective Neuronal Damage/Loss or Incomplete Infarction	215
9.2	Imaging of Central-Type Benzodiazepine Receptors	216
9.3	Pathophysiology of Selective Neuronal Damage Demonstrated as Decreased BZR	217
9.3.1	Selective Neuronal Damage and Chronic Hemodynamic Cerebral Ischemia	217
9.3.2	Selective Neuronal Damage and Low-Flow Infarction	218
9.3.3	Selective Neuronal Damage and Misery Perfusion	219
9.4	Silent Cortical Neuronal Damage in Asymptomatic Patients	222
9.5	Clinical Impact of Selective Neuronal Damage: Cognitive Impairment	222
	Conclusions	224
	References	224

Abstract

In patients with atherosclerotic internal carotid artery (ICA) or middle cerebral artery (MCA) occlusive disease, fluctuation of cerebral perfusion in the condition of chronic hemodynamic compromise may cause not only cerebral infarction but also selective neuronal damage in the cerebral cortex that is not detectable as infarction on CT or MRI. Imaging of the central-type benzodiazepine receptors (cBZR), which are expressed by most cortical neurons, has made it possible to visualize the neuronal alterations induced by ischemia in vivo in humans. Using PET and ¹¹C-Flumazenil, we showed that selective neuronal

H. Yamauchi, MD, PhD
Division of PET Imaging, Shiga Medical Center Research Institute,
5-4-30 Moriyama, Moriyama-city, Shiga 524-8524, Japan
e-mail: yamauchi@res.med.shiga-pref.jp

damage demonstrated as a decrease in cBZR in the normal-appearing cerebral cortex was associated with increased oxygen extraction fraction (OEF) (misery perfusion) in patients with atherosclerotic ICA or MCA occlusive disease in the chronic stage. Follow-up examinations of the patients without ischemic episode showed that a decrease of cBZR was associated with an increase of OEF (hemodynamic deterioration). A decrease of cBZR was also associated with executive dysfunction. Chronic hemodynamic ischemia causes selective neuronal damage demonstrated as a decrease in cBZR that has an impact on the functional outcomes.

9.1 Introduction

9.1.1 Chronic Hemodynamic Compromise and a Risk for Stroke

In patients with atherosclerotic internal carotid artery (ICA) or middle cerebral artery (MCA) occlusive disease, chronic reduction in cerebral perfusion pressure (chronic hemodynamic compromise) increases the risk of cerebral ischemic damage (Baron et al. 1981; Klijn and Kappelle 2010; Powers 1991; Yamauchi et al. 1992). Previous studies have shown that chronic hemodynamic compromise, as indicated by increased oxygen extraction fraction (OEF; misery perfusion) (Baron et al. 1981) on positron emission tomography (PET) or severely decreased vasodilatory capacity, is a risk factor for subsequent ischemic stroke in atherosclerotic ICA or MCA occlusive disease (Derdeyn et al. 1999; Grubb et al. 1998; Kuroda et al. 2001; Markus and Cullinane 2001; Ogasawara et al. 2002; Vernieri et al. 1999; Yamauchi et al. 1996b, 1999, 2012). Furthermore, follow-up examinations of the patients without ischemic episode showed that an increase of OEF (hemodynamic deterioration) was associated with an increase in the risk for subsequent stroke (Yamauchi et al. 2000b). Thus, understanding the pathophysiology of chronic hemodynamic cerebral ischemia is essential for the management of patients with atherosclerotic ICA or MCA occlusive disease.

Vascular reconstruction surgery can improve chronic hemodynamic compromise (Yamauchi et al. 1994), which may prevent subsequent ischemic stroke of hemodynamic origin (Fig. 9.1). Extracranial-to-intracranial (EC-IC) bypass surgery, which has no benefit in patients with ICA or MCA occlusive disease in general (The EC/IC Bypass Study Group 1985), may prevent recurrent strokes in select patients with hemodynamic compromise. To test this hypothesis, two randomized clinical trials have used hemodynamic criteria for patient selection (Ogawa 2012; Powers et al. 2011). One in Japan (Japanese EC-IC Bypass Trial; JET study) demonstrated a benefit of bypass surgery for preventing disabling stroke (modified Rankin scale >2) (2-year ipsilateral ischemic stroke rate including perioperative stroke: 2.9 % in the surgical group vs. 10.7 % in the medical group) (Ogawa 2012), while the other study (Carotid Occlusion Surgery Study; COSS) did not (any stroke, 21 % vs. 23 %) (Powers et al. 2011). The perioperative stroke rate in the two studies differed (disabling stroke, 0 % vs. any stroke, 15 %), which may have led to their different

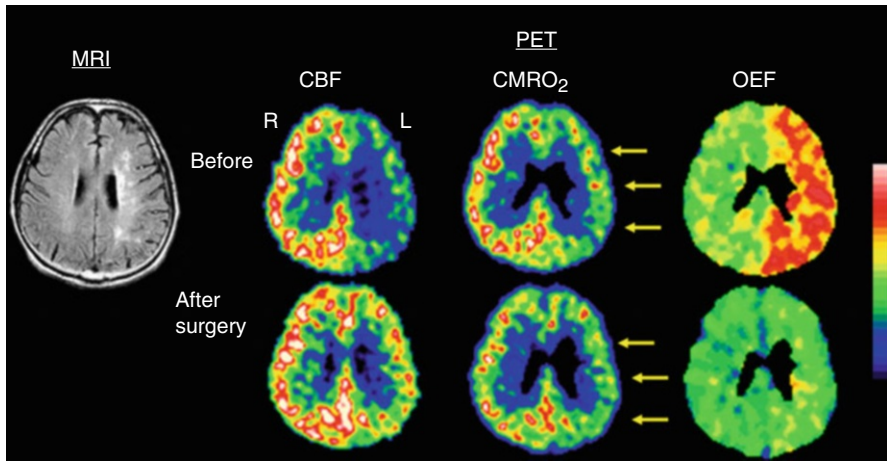


Fig. 9.1 Reduced cerebral cortical oxygen metabolism without morphological changes. A patient with occlusion of the left internal carotid artery showed decreased cerebral blood flow (*CBF*) and increased oxygen extraction fraction (*OEF*, misery perfusion) in the hemisphere with occlusion. Surgical reperfusion with bypass improved misery perfusion. However, we should note that cerebral metabolic rate of oxygen, which was decreased in the normal-appearing cerebral cortex before surgery, was unchanged after surgical reperfusion. Some irreversible damage may occur in the cerebral cortex

conclusions. Because of the high prevalence of moyamoya disease, EC-IC bypass with postoperative management has been an essential skill of neurosurgeons in Japan (Kuroda and Houkin 2008), which may have resulted in the 0 % perioperative disabling stroke rate of the Japanese EC-IC Bypass Trial (Ogawa 2012). Achieving low operative risk could lead to the benefit of bypass surgery.

Although correct evaluations of hemodynamic status are essential to determine patient prognosis, therapeutic strategies to prevent recurrent strokes, which should differ between patients with and without hemodynamic compromise, are not clearly established. We should continue to make efforts to seek strategies for selecting treatments based on hemodynamic measurements.

9.1.2 Selective Neuronal Damage/Loss or Incomplete Infarction

In atherosclerotic ICA or MCA occlusive disease, chronic hemodynamic compromise increases the risk for cerebral ischemic damage, irrespective of the development of symptoms. Hemodynamic cerebral ischemia due to ICA or MCA occlusive disease may cause not only cerebral infarction but also minor tissue damage in the cerebral cortex that is not detectable as infarction on CT or magnetic resonance imaging (MRI). Neuropathological studies have demonstrated cortical granular atrophy or watershed territory microemboli in the cerebral cortex distal to large cerebral arterial occlusion (Graham 1992). Observations in both humans and animals also suggest that selective cortical neuronal loss results from acute occlusion

of the large cerebral arteries accompanied by ischemia of moderate severity (Garcia et al. 1996; Lassen et al. 1983). However, it is unclear whether selective neuronal ischemic change develops in patients with atherosclerotic occlusion of the large cerebral arteries, because a direct demonstration of the cortical neuronal loss in the living brain is not possible.

To address the issue of neuronal loss without infarction in ICA or MCA occlusive diseases, indirect markers for neuronal damage including brain atrophy and decreased metabolism have been investigated. A decrease in glucose or oxygen metabolism in the normal-appearing cerebral cortex is one result of ischemic damage to the tissue, but it can also be caused by a decrease in neural input from distant regions with fiber connections (Feeney and Baron 1986). Atrophy of the corpus callosum may be an indirect but sensitive indicator of ischemic cortical neuronal loss. The largest fraction of neurons projecting into the corpus callosum is the large pyramidal cells in layer 3, which is one of the groups of cortical neurons most vulnerable to ischemia (Graham 1992). Therefore, callosal atrophy may result from cortical ischemic loss. Reduced cerebral cortical oxygen metabolism in the normal-appearing cerebral cortex, which surgical reperfusion cannot improve, has been demonstrated in occlusive diseases of ICA or MCA by using PET, suggesting that selective neuronal damage may occur (Powers et al. 1984; Yamauchi et al. 1990). Our studies showed that a decrease in bilateral cerebral cortical oxygen metabolism occurs in association with callosal atrophy in patients with ICA occlusive disease, suggesting that ischemic neuronal loss may contribute to the reduced cortical oxygen metabolism (Yamauchi et al. 1993, 1995, 1996a, 2000b). However, to address this issue further, a more direct marker for neuronal damage was needed.

9.2 Imaging of Central-Type Benzodiazepine Receptors

Development of imaging techniques makes it possible to visualize the distribution of central-type benzodiazepine receptors (cBZR) in humans by using ^{11}C -labeled flumazenil (FMZ) for PET or ^{123}I -labeled iomazenil (IMZ) for single-photon emission computed tomography (SPECT) (Beer et al. 1990; Persson et al. 1985; Samson et al. 1985). Central BZR is coupled with γ -aminobutyric acid receptors (GABAA/BZ receptor complex), and cBZR exists in the membrane of neuron (Olsen 1981). Central BZR is expressed by most cortical neurons. Binding of FMZ is high in the cerebral cortex and is low in the cerebellum, thalamus, and basal ganglia, while it is lacking in the white matter (Fig. 9.2). As shown in the case of crossed cerebellar diaschisis, a simple decrease of neural input may not decrease cBZR (Dong et al. 1997; Hatazawa et al. 1995a). Thus, imaging of the cBZR may detect cortical neuronal damage, which could not be evaluated directly by other neuroimaging modalities (Garcia et al. 1996; Hatazawa and Shimosegawa 1998; Sette et al. 1993). Cortical neuronal damage should lead to a decrease in cBZR.

Histopathological correlations between decreased cBZR and selective neuronal loss were confirmed recently (Ejaz et al. 2013). A rat ischemia-reperfusion model with 45-min occlusion of the distal MCA was examined with FMZ PET

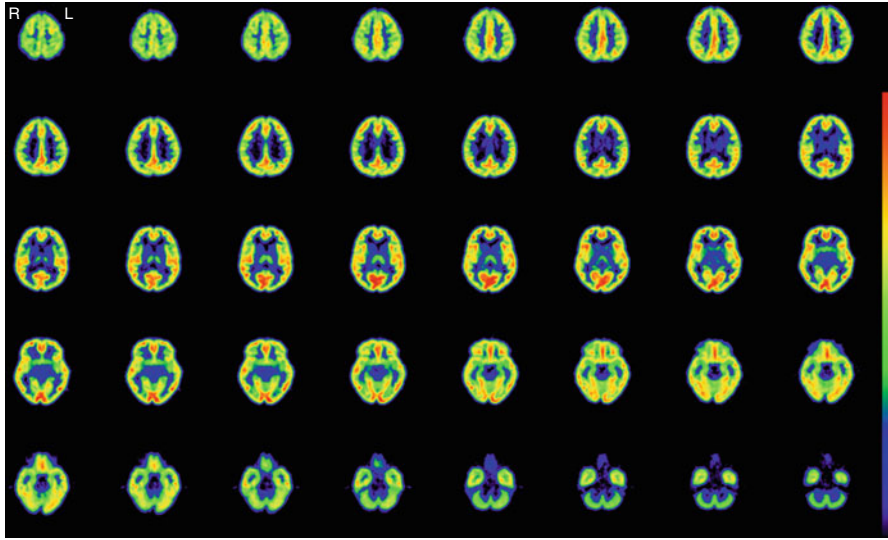


Fig. 9.2 BZR imaging with ^{11}C -Flumazenil PET. Images of a male normal volunteer of 49 years old show high binding in the cerebral cortex

and immunohistochemistry 28 days after ischemia. The study demonstrated that a decrease in FMZ binding in the normal-appearing cerebral cortex on T2-weighted MRI was associated with selective neuronal loss on stains with antibody for neurons. Imaging of cBZR by using ^{11}C -FMZ and PET can detect selective neuronal damage or loss.

9.3 Pathophysiology of Selective Neuronal Damage Demonstrated as Decreased BZR

9.3.1 Selective Neuronal Damage and Chronic Hemodynamic Cerebral Ischemia

Several small studies in patients with atherosclerotic ICA or MCA disease in the chronic stage demonstrated a reduction in cBZR in the normal-appearing cortical areas on CT or MRI, suggesting the presence of selective neuronal damage (Dong et al. 1997; Kuroda et al. 2004, 2006; Moriwaki et al. 1998; Sasaki et al. 1997; Yamauchi et al. 2000a). The IMZ uptake on SPECT was significantly but weakly correlated with the cerebral metabolic rate of oxygen, while no significant correlation was found of the IMZ uptake with the blood flow, the cerebrovascular reactivity, or the cerebral metabolic rate of glucose, which suggested that the reduction of IMZ uptake may be due to selective neuronal loss that may not be revealed by other imaging tracers (Dong et al. 1997; Moriwaki et al. 1998; Sasaki et al. 1997). These findings were also shown by using FMZ and PET (Kuroda et al. 2004, 2006).

A decrease in cortical BZR binding was correlated with corpus callosum atrophy, which supported that decreased cortical BZR binding may reflect cortical neuronal damage (Yamauchi et al. 2000a).

However, the incidence, extent, and severity of selective neuronal damage demonstrated as decreased cBZR are unclear. Furthermore, the factors responsible for the decreased cBZR are not well understood. Specifically, although a chronic hemodynamic mechanism may be responsible for the decreased cBZR, the relationship between the decreased BZR and chronic hemodynamic compromise is unknown. The clarification of this relationship is important because vascular reconstruction surgery can improve chronic hemodynamic compromise, which may prevent the development of selective neuronal damage as well as infarction.

9.3.2 Selective Neuronal Damage and Low-Flow Infarction

Borderzone infarction has been demonstrated to be associated with ICA occlusive disease and hemodynamic compromise (Momjian-Mayoy and Baron 2005; Yamauchi et al. 1990, 1991). Hemodynamic ischemia due to ICA occlusive disease may cause not only borderzone infarction but also selective neuronal damage beyond the regions of infarcts that may be detected by a decrease in cBZR in the normal-appearing cerebral cortex. To determine whether selective neuronal damage is associated with borderzone infarction in ICA occlusive disease, we measured cBZR using PET and ^{11}C -FMZ in 62 nondisabled patients with ICA steno-occlusive lesions in the chronic stage (Yamauchi et al. 2005). FMZ-binding potential (BP) was calculated using the dynamic data and Logan graphical analysis with the reference tissue, with the pons as reference region (Logan et al. 1996; Okazawa et al. 2004). The infarcts on MRI, which were categorized as territorial, borderzone (external or internal), striatocapsular, lacunar, and other white matter infarcts, were correlated with mean cerebral/cerebellar cortical BP ratio in the hemisphere with ICA occlusive disease. Patients with borderzone infarction ($n=18$) had significantly decreased FMZ-BP ratio in the hemisphere with ICA disease, compared with patients without borderzone infarction ($n=44$) and normal control subjects ($n=10$). Both external and internal borderzone infarctions were associated with the decreased FMZ-BP ratio. Multivariate analysis showed that external borderzone infarction was an independent predictor of the decreased FMZ-BP ratio. In ICA occlusive disease, selective neuronal damage demonstrated as decreased cBZR is associated with borderzone infarction. Microemboli can cause borderzone infarction, particularly in cases of ICA stenosis (Moustafa et al. 2010). However, it is less likely that borderzone infarction due to microemboli causes extensive decreases of BZR beyond the regions of the infarct, because ischemia due to microemboli is restricted to the borderzone region. Therefore, hemodynamic ischemia leading to borderzone infarction may cause selective neuronal damage beyond the regions of infarcts in the chronic stage.

Decreased cBZR was closely associated with decreased oxygen metabolism. However, the correlation of decreased cBZR with increased OEF (hemodynamic

compromise) was relatively weak. Selective neuronal damage caused by hemodynamic ischemia in turn decreases the degree of hemodynamic compromise due to ICA occlusive disease through causing reduced metabolic demand of the tissue (Kuroda et al. 2004; Yamauchi et al. 2004), which may lead to normalization of OEF after the development of selective neuronal damage. The association of decreases in cBZR with borderzone infarctions suggests that severe hemodynamic compromise, which was present in the acute stage of infarction, may have disappeared according to the decrease of the metabolic needs of the tissue between the time of infarction and the PET examination. Careful medical managements in the acute stage for patients with borderzone infarction should prevent selective neuronal damage, even when infarct size is small and symptom is mild. Then, the preserved metabolic needs of the cortical tissue in the chronic stage may permit the persistence of the hemodynamic compromise that can be improved by vascular reconstruction surgery. This strategy results in preservation of cortical metabolism that may lead to good functional outcomes. Recognition and prevention of selective neuronal damage are important for the management of patients with ICA occlusive disease.

The association between borderzone infarction (internal borderzone infarction) and a decrease in cBZR in the overlying cerebral cortex was also found in 62 non-disabled patients with atherosclerotic occlusive disease of the MCA and no cortical infarction (Yamauchi et al. 2009).

9.3.3 Selective Neuronal Damage and Misery Perfusion

9.3.3.1 A Cross-Sectional Study

The notion that normalization of OEF may occur after the development of selective neuronal damage suggests that it may be not easy to demonstrate an association of decreased cBZR with chronic hemodynamic compromise (increased OEF) in the chronic stage. To overcome this issue, we studied 105 nondisabled patients with atherosclerotic ICA or MCA occlusive disease and *no cortical infarction* on routine MRI images (T1-weighted, T2-weighted, or fluid-attenuated inversion recovery images) and measured cBZR and OEF using PET. We investigated the association of selective neuronal damage demonstrated as a decrease in cBZR in the normal-appearing cerebral cortex with increased OEF (misery perfusion) (Yamauchi et al. 2007).

A three-dimensional stereotactic surface projection (3D-SSP) technique was used to analyze FMZ-BP (Minoshima et al. 1995). After anatomical standardization, a method of data extraction is performed in which the cortical activity is projected onto the brain surface. The algorithm searches the highest pixel value in a direction inward along the vector to a six-pixel depth into the cortex on an individual's anatomically standardized PET image set and assigns the maximum value to the surface pixel. The surface projection technique minimizes the effect of cortical atrophy. Then, a comparison of the resultant cortical projections between a patient and controls is performed. To quantify a decrease of FMZ-BP, pixel-by-pixel z-scores were used; z-scores ($[(\text{mean normalized pixel value of controls}) - (\text{normalized$

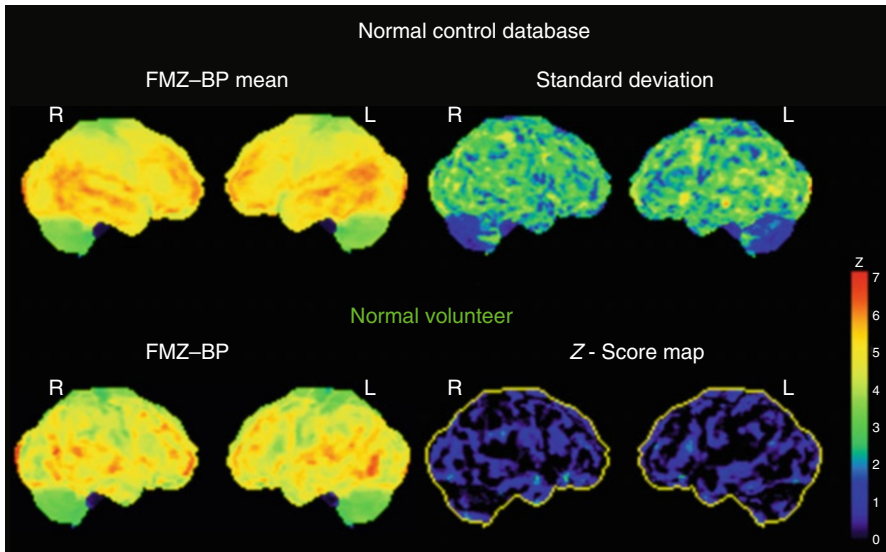


Fig. 9.3 Three-dimensional stereotactic surface projection (3D-SSP) analysis. *Upper row.* 3D-SSP images showing the value of mean and standard deviation for normal control database ($n=10$, mean age 57 years). *Lower row.* 3D-SSP images and z -score maps of a male normal volunteer of 49 years old shown in Fig. 9.2

pixel value of each patient)]/[SD of controls]) were calculated for each surface pixel (z -score map) (Fig. 9.3). A positive z -score represents a reduced FMZ-BP in patients relative to controls. To assess the degree of abnormal FMZ-BP reduction in each patient quantitatively, the BZR index [(the extent of the pixels with z -score more than 2 compared with controls) \times (average z -score in those pixels)] in the cerebral cortex of the MCA distribution with arterial disease was calculated by the stereotactic extraction estimation (SEE) method (Mizumura et al. 2003).

All patients had pixels with abnormally decreased cBZR in the cerebral cortex of the MCA distribution, with the extent varying from 0.04 to 60.91 % (Fig. 9.4). The BZR index was significantly correlated with the mean hemispheric value of OEF or CBF in the ipsilateral hemisphere. Multivariate analysis showed that the BZR index was positively correlated with the value of OEF and the history of stroke, which suggested that misery perfusion might cause selective neuronal damage. On the other hand, the BZR index was negatively correlated with the presence of statin treatment. Several studies have shown that statins have beneficial effects on the cerebral circulation and brain parenchyma during ischemic stroke and reperfusion (Vaughan and Delanty 1999). The antioxidative properties of statins might be involved in their beneficial effects against neuronal damage in cerebral ischemia (Nagotani et al. 2005). Statins might also reduce microemboli by plaque stabilization in patients with ICA or MCA stenosis. Therefore, statins may reduce the occurrence of selective neuronal damage due to ischemia in atherosclerotic ICA or MCA occlusive disease.

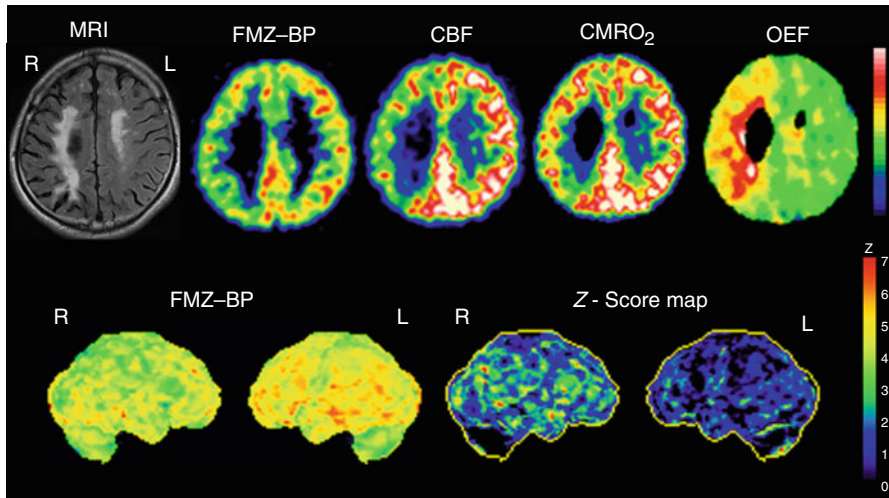


Fig. 9.4 Selective cortical neuronal damage and misery perfusion. *Upper row.* Examples of PET images showing a decrease of flumazenil-binding potential (*FMZ-BP*), cerebral blood flow (*CBF*), and cerebral metabolic rate of oxygen (*CMRO₂*) with increased oxygen extraction fraction (*OEF*) in a patient with right (*R*) internal carotid artery occlusion who showed internal borderzone infarction on the corresponding MRI images. This patient presented with left hemiparesis and spatial neglect. *Lower row.* 3D-SSP images and z -score maps showing a decrease of *FMZ-BP* in the right hemisphere. The extent of abnormally decreased benzodiazepine receptors (BZR) was 47.6 % in the right middle cerebral artery distribution; the mean z -score in those pixels was 2.92; and the BZR index was 139.2

9.3.3.2 A Follow-up Study

To demonstrate a causal relationship between misery perfusion and selective neuronal damage more directly, it is essential to show a correlation between an increase of *OEF* and progression of selective neuronal damage using a longitudinal study. Therefore, follow-up PET examinations in 17 selected patients without ischemic episode were performed to investigate the relationship between changes in cerebral hemodynamics and the decrease in *cBZR* (Yamauchi et al. 2007). The interval between the first and follow-up PET studies ranged from 2.5 to 39 (mean 18 ± 9) months. The total change of the BZR index or the *OEF* value in the cerebral cortex of the MCA distribution with arterial disease was calculated by subtracting the value obtained at the second scanning from that obtained at the first scanning. The relation between the change of the BZR index and that of the *OEF* value was analyzed. T2-weighted MRI disclosed extension of the confluent white matter lesions preexisted at the first evaluation in one stroke patient. The other 16 patients showed no apparent changes on the follow-up MRI images. The BZR index increased significantly between the first and second examinations from 25.61 ± 32.79 to 50.75 ± 76.11 . The degree of increase in the BZR index was positively correlated with that in the *OEF* value. Follow-up data indicate that hemodynamic deterioration causes selective neuronal damage demonstrated as decreased BZR without overt episode of stroke. This study confirmed the relationship between

selective neuronal damage and chronic hemodynamic compromise for the first time. In patients with chronic hemodynamic compromise, the perfusion may fall below the penumbra threshold for a matter of minutes, causing selective neuronal damage.

9.4 Silent Cortical Neuronal Damage in Asymptomatic Patients

The finding that selective neuronal damage manifested as loss of cBZR occurs in association with hemodynamic deterioration without overt episode of stroke suggests that selective neuronal damage may occur in association with hemodynamic compromise in patients whose atherosclerotic ICA or MCA disease is asymptomatic. To test this hypothesis, we measured cBZR using PET and ^{11}C -FMZ in 79 patients with asymptomatic atherosclerotic ICA or MCA disease and no cortical infarction (Yamauchi et al. 2011b). 3D-SSP was used to calculate the BZR index, a measure of abnormally decreased cBZR in the cerebral cortex within the MCA distribution. The BZR index was abnormal (>5.84) in 71 % of the asymptomatic patients compared to healthy control subjects. This abnormality was mild compared with that previously reported for symptomatic patients (the BZR index; 16.0 ± 14.5 vs. 48.2 ± 54.1). Multiple regression analysis showed the BZR index to be positively correlated with the value of OEF, with the presence of silent subcortical infarcts and with the presence of ischemic heart disease, which suggested that hemodynamic compromise is associated with selective neuronal damage in asymptomatic patients. Hemodynamic compromise may cause silent cortical neuronal damage in asymptomatic patients as well. Patients at high risk of stroke may have already suffered ischemic cerebral damage at the time their asymptomatic ICA or MCA disease is discovered. Therapeutic strategies to prevent neuronal damage, including vascular reconstruction surgery, may be called for in asymptomatic patients with chronic hemodynamic compromise. On the other hand, the BZR index was negatively correlated with the treatment of hypertension with angiotensin receptor blockers (ARBs). ARBs were associated with preservation of cortical cBZR. Several experimental studies have shown that ARBs can attenuate ischemic neuronal injury through various mechanisms, including decreased oxidative stress and improved arterial compliance (Mogi and Horiuchi 2009). ARBs might have beneficial effects against neuronal damage in atherosclerotic ICA or MCA disease.

9.5 Clinical Impact of Selective Neuronal Damage: Cognitive Impairment

In atherosclerotic ICA or MCA disease, chronic hemodynamic compromise causes selective neuronal damage which can be detected as a decrease in cBZR in the normal-appearing cerebral cortex. However, the impact of selective neuronal damage on clinical outcomes is unclear. In patients with atherosclerotic ICA or MCA disease, a few patients with reduced cBZR in the cerebral cortex overlying subcortical infarcts

were reported to show aphasia (Hatazawa et al. 1995a; Moriwaki et al. 1998), and a decrease in cortical cBZR was shown to be correlated with atrophy of the corpus callosum that is associated with global cognitive impairment (Yamauchi et al. 1996a, 2000a). However, the relationship between a decrease in cBZR and the neurological symptoms has not been systematically investigated. Clinical correlates are essential to establish the clinical significance of cBZR imaging.

In patients with subcortical hemorrhage, patients with aphasia or anopsia showed an ipsilateral/contralateral IMZ uptake ratio of ≤ 0.78 in the cortical area (Hatazawa et al. 1995b). Another SPECT study also showed that cerebral hyperperfusion after carotid endarterectomy resulted in a postoperative decrease in IMZ uptake that correlated with postoperative cognitive impairment (Chida et al. 2009). Therefore, selective neuronal damage may contribute to the development of subtle poststroke cognitive impairment, depending on the degree of neuronal damage. Executive dysfunction may be an early sign of vascular cognitive impairment and may have considerable impact on the functional outcomes of patients with stroke (Roman and Royall 1999). The Wisconsin Card Sorting Test (WCST) is a widely used clinical test for assessing executive functions (Nagahama et al. 1996; Nelson 1976).

To determine whether a decrease in the cBZRs in the non-infarcted cerebral cortex is associated with poor performance on the WCST, we measured cBZR using PET and ^{11}C -FMZ in 60 nondisabled patients with unilateral atherosclerotic ICA or MCA disease and no cortical infarction (Yamauchi et al. 2011a). Using 3D-SSP, the BZR indices in the cerebral cortex of the anterior cerebral artery (ACA) and the MCA territories were calculated and found to be correlated with the patient's score on the WCST. We used the Keio-Fukuoka-Shimane version of the WCST that can be performed on a personal computer (Kobayashi 2002). Because the WCST method used in this study needs verbal mediation during the performance, the language-related left hemisphere may contribute more than the right hemisphere to the performance of the WCST used here. The BZR index was associated with an increase in the OEF in the ACA and MCA territories of the hemisphere with ICA or MCA disease. On the basis of the WCST results, 39 patients were considered abnormal (low categories achieved) for their age. The BZR index of the ACA territory in the hemisphere affected by arterial disease was significantly higher in abnormal patients than in normal patients. The BZR index of the MCA territory differed significantly between the two groups when patients with left arterial disease ($n=28$) were analyzed separately. Among the BZR indices for the subregions of the ACA territory, those of the anterior cingulate gyrus and the medial frontal gyrus were positively correlated with the total number of errors after controlling for the effect of age by using multiple regression analysis. In patients with left arterial diseases, among the BZR indices for the subregions of the MCA territory, the BZR index of the middle frontal gyrus was also positively correlated with the total number of errors. These subregions have been reported to be essential for performance on the WCST (Buckley et al. 2009; Nagahama et al. 1996).

In atherosclerotic ICA or MCA disease, selective neuronal damage that is manifested as a decrease in cBZR in the non-infarcted cerebral cortex may contribute to the development of executive dysfunction. PET imaging of BZR may be useful as

an objective measure of cognitive impairments in atherosclerotic occlusive disease of the major cerebral artery. In this study, a decrease in cBZR was also associated with hemodynamic compromise. Interestingly, a recent IMZ SPECT study showed that improvement of hemodynamic compromise after carotid endarterectomy resulted in a postoperative increase in IMZ uptake that correlated with postoperative improvement of cognitive impairment (Chida et al. 2010). In patients with severe hemodynamic compromise, a part of the cBZR decrease may be reversible, and improvement of hemodynamic compromise may lead to the improvement of cognitive impairment with cBZR reduction.

Conclusions

1. In patients with atherosclerotic ICA or MCA occlusive disease, misery perfusion contributes selective neuronal damage demonstrated as decreased BZR in the normal-appearing cerebral cortex.
2. Hemodynamic deterioration can contribute selective neuronal damage without overt episode of stroke.
3. Selective neuronal damage appears to impact on the functional outcomes.
4. Careful medical managements and successful vascular reconstruction surgery for patients with misery perfusion may prevent selective neuronal damage.
5. Statins and angiotensin receptor blockers may reduce the occurrence of selective neuronal damage.
6. Imaging of BZR may become a tool for quantitatively evaluating the success of future therapeutic interventions for protecting neurons from ischemic damage.

References

- Baron JC, Bousser MG, Rey A, Guillard A, Comar D, Castaigne P (1981) Reversal of focal "misery-perfusion syndrome" by extra-intracranial arterial bypass in hemodynamic cerebral ischemia. A case study with ^{15}O positron emission tomography. *Stroke* 12:454–459
- Beer HF, Blauenstein PA, Hasler PH, Delaloye B, Riccabona G, Bangerl I, Hunkeler W, Bonetti EP, Pieri L, Richards JG et al (1990) In vitro and in vivo evaluation of iodine-123-Ro 16–0154: a new imaging agent for SPECT investigations of benzodiazepine receptors. *J Nucl Med* 31:1007–1014
- Buckley MJ, Mansouri FA, Hoda H, Mahboubi M, Browning PG, Kwok SC, Phillips A, Tanaka K (2009) Dissociable components of rule-guided behavior depend on distinct medial and prefrontal regions. *Science* 325:52–58
- Chida K, Ogasawara K, Suga Y, Saito H, Kobayashi M, Yoshida K, Otawara Y, Ogawa A (2009) Postoperative cortical neural loss associated with cerebral hyperperfusion and cognitive impairment after carotid endarterectomy: 123I-iomazenil SPECT study. *Stroke* 40:448–453
- Chida K, Ogasawara K, Aso K, Suga Y, Kobayashi M, Yoshida K, Terasaki K, Tsushina E, Ogawa A (2010) Postcarotid endarterectomy improvement in cognition is associated with resolution of crossed cerebellar hypoperfusion and increase in 123I-iomazenil uptake in the cerebral cortex: a SPECT study. *Cerebrovasc Dis* 29:343–351
- Derdeyn CP, Grubb RL Jr, Powers WJ (1999) Cerebral hemodynamic impairment: methods of measurement and association with stroke risk. *Neurology* 53:251–259
- Dong Y, Fukuyama H, Nabatame H, Yamauchi H, Shibasaki H, Yonekura Y (1997) Assessment of benzodiazepine receptors using iodine-123-labeled iomazenil single-photon emission computed tomography in patients with ischemic cerebrovascular disease. A comparison with PET study. *Stroke* 28:1776–1782

- Ejaz S, Williamson DJ, Ahmed T, Sitnikov S, Hong YT, Sawiak SJ, Fryer TD, Aigbirhio FI, Baron JC (2013) Characterizing infarction and selective neuronal loss following temporary focal cerebral ischemia in the rat: a multi-modality imaging study. *Neurobiol Dis* 51:120–132
- Feeney DM, Baron JC (1986) Diaschisis. *Stroke* 17:817–830
- Garcia JH, Lassen NA, Weiller C, Sperling B, Nakagawara J (1996) Ischemic stroke and incomplete infarction. *Stroke* 27:761–765
- Graham DI (1992) Hypoxia and vascular disorders. Edward Arnold, London
- Grubb RL Jr, Derdeyn CP, Fritsch SM, Carpenter DA, Yundt KD, Videen TO, Spitznagel EL, Powers WJ (1998) Importance of hemodynamic factors in the prognosis of symptomatic carotid occlusion. *JAMA* 280:1055–1060
- Hatazawa J, Shimosegawa E (1998) Imaging neurochemistry of cerebrovascular disease with PET and SPECT. *Q J Nucl Med* 42:193–198
- Hatazawa J, Satoh T, Shimosegawa E, Okudera T, Inugami A, Ogawa T, Fujita H, Noguchi K, Kanno I, Miura S, Murakami M, Iida H, Miura Y, Uemura K (1995a) Evaluation of cerebral infarction with iodine 123-iomazenil SPECT. *J Nucl Med* 36:2154–2161
- Hatazawa J, Shimosegawa E, Satoh T, Kanno I, Uemura K (1995b) Central benzodiazepine receptor distribution after subcortical hemorrhage evaluated by means of [¹²³I]iomazenil and SPECT. *Stroke* 26:2267–2271
- Klijn CJ, Kappelle LJ (2010) Haemodynamic stroke: clinical features, prognosis, and management. *Lancet Neurol* 9:1008–1017
- Kobayashi S (2002) Neuropsychological test using personal computer. *Japanese J Neuropsychol* 18:188–193
- Kuroda S, Houkin K (2008) Moyamoya disease: current concepts and future perspectives. *Lancet Neurol* 7:1056–1066
- Kuroda S, Houkin K, Kamiyama H, Mitsumori K, Iwasaki Y, Abe H (2001) Long-term prognosis of medically treated patients with internal carotid or middle cerebral artery occlusion: can acetazolamide test predict it? *Stroke* 32:2110–2116
- Kuroda S, Shiga T, Ishikawa T, Houkin K, Narita T, Katoh C, Tamaki N, Iwasaki Y (2004) Reduced blood flow and preserved vasoreactivity characterize oxygen hypometabolism due to incomplete infarction in occlusive carotid artery diseases. *J Nucl Med* 45:943–949
- Kuroda S, Shiga T, Houkin K, Ishikawa T, Katoh C, Tamaki N, Iwasaki Y (2006) Cerebral oxygen hypometabolism and neuronal integrity in patients with impaired vasoreactivity attributable to occlusive carotid artery diseases. *Stroke* 37:393–398
- Lassen NA, Losen TS, Højgaard K, Skriver E (1983) Incomplete infarction: a CT-negative irreversible ischemic brain lesion. *J Cereb Blood Flow Metab* 3(suppl 1):S602–S603
- Logan J, Fowler JS, Volkow ND, Wang GJ, Ding YS, Alexoff DL (1996) Distribution volume ratios without blood sampling from graphical analysis of PET data. *J Cereb Blood Flow Metab* 16:834–840
- Markus H, Cullinane M (2001) Severely impaired cerebrovascular reactivity predicts stroke and TIA risk in patients with carotid artery stenosis and occlusion. *Brain* 124:457–467
- Minoshima S, Frey KA, Koeppe RA, Foster NL, Kuhl DE (1995) A diagnostic approach in Alzheimer's disease using three-dimensional stereotactic surface projections of fluorine-18-FDG PET. *J Nucl Med* 36:1238–1248
- Mizumura S, Kumita S, Cho K, Ishihara M, Nakajo H, Toba M, Kumazaki T (2003) Development of quantitative analysis method for stereotactic brain image: assessment of reduced accumulation in extent and severity using anatomical segmentation. *Ann Nucl Med* 17:289–295
- Mogi M, Horiuchi M (2009) Effects of angiotensin II receptor blockers on dementia. *Hypertens Res* 32:738–740
- Momjian-Mayoy I, Baron JC (2005) The pathophysiology of watershed infarction in internal carotid artery disease. Review of cerebral perfusion studies. *Stroke* 36:567–577
- Moriwaki H, Matsumoto M, Hashikawa K, Oku N, Ishida M, Seike Y, Fukuchi K, Hori M, Nishimura T (1998) Iodine-123-iomazenil and iodine-123-iodoamphetamine SPECT in major cerebral artery occlusive disease. *J Nucl Med* 39:1348–1353
- Moustafa RR, Izquierdo-Garcia D, Jones PS, Graves MJ, Fryer TD, Gillard JH, Warburton EA, Baron JC (2010) Watershed infarcts in transient ischemic attack/minor stroke with > or = 50% carotid stenosis: hemodynamic or embolic? *Stroke* 41:1410–1416

- Nagahama Y, Fukuyama H, Yamauchi H, Matsuzaki S, Konishi J, Shibasaki H, Kimura J (1996) Cerebral activation during performance of a card sorting test. *Brain* 119(Pt 5):1667–1675
- Nagotani S, Hayashi T, Satoh K, Zhang W, Deguchi K, Nagano I, Shoji M, Abe K (2005) Reduction of cerebral infarction in stroke-prone spontaneously hypertensive rats by statins associated with amelioration of oxidative stress. *Stroke* 36:670–672
- Nelson HE (1976) A modified card sorting test sensitive to frontal lobe defects. *Cortex* 12:313–324
- Ogasawara K, Ogawa A, Yoshimoto T (2002) Cerebrovascular reactivity to acetazolamide and outcome in patients with symptomatic internal carotid or middle cerebral artery occlusion: a xenon-133 single-photon emission computed tomography study. *Stroke* 33:1857–1862
- Ogawa A, for the JET Study Group (2012) Beneficial effect of extracranial-intracranial arterial bypass for symptomatic hemodynamic cerebral ischemia due to cerebrovascular steno-occlusive disease: Japanese extracranial-intracranial bypass trial. *Cerebrovasc Dis* 34(suppl 1):7
- Okazawa H, Yamauchi H, Sugimoto K, Magata Y, Kudo T, Yonekura Y (2004) Effects of metabolic correction for arterial input function on quantitative receptor images with ¹¹C-flumazenil in clinical positron emission tomography studies. *J Comput Assist Tomogr* 28:428–435
- Olsen RW (1981) The GABA postsynaptic membrane receptor-ionophore complex. Site of action of convulsant and anticonvulsant drugs. *Mol Cell Biochem* 39:261–279
- Persson A, Ehrin E, Eriksson L, Farde L, Hedstrom CG, Litton JE, Mindus P, Sedvall G (1985) Imaging of [¹¹C]-labelled Ro 15–1788 binding to benzodiazepine receptors in the human brain by positron emission tomography. *J Psychiatr Res* 19:609–622
- Powers WJ (1991) Cerebral hemodynamics in ischemic cerebrovascular disease. *Ann Neurol* 29:231–240
- Powers WJ, Martin WRW, Herscovitch P, Raichle ME, Grubb RL (1984) Extracranial-intracranial bypass surgery: hemodynamic and metabolic effects. *Neurology* 34:1168–1174
- Powers WJ, Clarke WR, Grubb RL Jr, Videen TO, Adams HP Jr, Derdeyn CP, Investigators C (2011) Extracranial-intracranial bypass surgery for stroke prevention in hemodynamic cerebral ischemia: the Carotid Occlusion Surgery Study randomized trial. *JAMA* 306:1983–1992
- Roman GC, Royall DR (1999) Executive control function: a rational basis for the diagnosis of vascular dementia. *Alzheimer Dis Assoc Disord* 13(Suppl 3):S69–S80
- Samson Y, Hantraye P, Baron JC, Soussaline F, Comar D, Maziere M (1985) Kinetics and displacement of [¹¹C]RO 15–1788, a benzodiazepine antagonist, studied in human brain in vivo by positron tomography. *Eur J Pharmacol* 110:247–251
- Sasaki M, Ichiya Y, Kuwabara Y, Yoshida T, Fukumura T, Masuda K (1997) Benzodiazepine receptors in chronic cerebrovascular disease: comparison with blood flow and metabolism. *J Nucl Med* 38:1693–1698
- Sette G, Baron JC, Young AR, Miyazawa H, Tillet I, Barre L, Traverso JM, Derlon JM, MacKenzie ET (1993) In vivo mapping of brain benzodiazepine receptor changes by positron emission tomography after focal ischemia in the anesthetized baboon. *Stroke* 24:2046–2057
- The EC/IC Bypass Study Group (1985) Failure of extracranial-intracranial arterial bypass to reduce the risk of ischemic stroke. Results of an international randomized trial. The EC/IC Bypass Study Group. *N Engl J Med* 313:1191–1200
- Vaughan CJ, Delanty N (1999) Neuroprotective properties of statins in cerebral ischemia and stroke. *Stroke* 30:1969–1973
- Vernieri F, Pasqualetti P, Passarelli F, Rossini PM, Caltagirone C, Silvestrini M (1999) Outcome of carotid artery occlusion is predicted by cerebrovascular reactivity. *Stroke* 30:593–598
- Yamauchi H, Fukuyama H, Kimura J, Konishi J, Kameyama M (1990) Hemodynamics in internal carotid artery occlusion examined by positron emission tomography. *Stroke* 21:1400–1406
- Yamauchi H, Fukuyama H, Yamaguchi S, Miyoshi T, Kimura J, Konishi J (1991) High-intensity area in the deep white matter indicating hemodynamic compromise in internal carotid artery occlusive disorders. *Arch Neurol* 48:1067–1071
- Yamauchi H, Fukuyama H, Fujimoto N, Nabatame H, Kimura J (1992) Significance of low perfusion with increased oxygen extraction fraction in a case of internal carotid artery stenosis. *Stroke* 23:431–432

- Yamauchi H, Fukuyama H, Nabatame H, Harada K, Kimura J (1993) Callosal atrophy with reduced cortical oxygen metabolism in carotid artery disease. *Stroke* 24:88–93
- Yamauchi H, Fukuyama H, Kimura J, Ishikawa M, Kikuchi H (1994) Crossed cerebellar hypoperfusion indicates the degree of uncoupling between blood flow and metabolism in major cerebral arterial occlusion. *Stroke* 25:1945–1951
- Yamauchi H, Pagani M, Fukuyama H, Ouchi Y, Nagahama Y, Matsuzaki S, Kimura J, Yonekura Y, Konishi J (1995) Progression of atrophy of the corpus callosum with deterioration of cerebral cortical oxygen metabolism after carotid artery occlusion: a follow up study with MRI and PET. *J Neurol Neurosurg Psychiatry* 59:420–426
- Yamauchi H, Fukuyama H, Nagahama Y, Katsumi Y, Dong Y, Konishi J, Kimura J (1996a) Atrophy of the corpus callosum associated with cognitive impairment and widespread cortical hypometabolism in carotid artery occlusive disease. *Arch Neurol* 53:1103–1109
- Yamauchi H, Fukuyama H, Nagahama Y, Nabatame H, Nakamura K, Yamamoto Y, Yonekura Y, Konishi J, Kimura J (1996b) Evidence of misery perfusion and risk for recurrent stroke in major cerebral arterial occlusive diseases from PET. *J Neurol Neurosurg Psychiatry* 61:18–25
- Yamauchi H, Fukuyama H, Nagahama Y, Nabatame H, Ueno M, Nishizawa S, Konishi J, Shio H (1999) Significance of increased oxygen extraction fraction in 5-year prognosis of major cerebral arterial occlusive diseases. *J Nucl Med* 40:1992–1998
- Yamauchi H, Fukuyama H, Dong Y, Nabatame H, Nagahama Y, Nishizawa S, Konishi J, Shio H (2000a) Atrophy of the corpus callosum associated with a decrease in cortical benzodiazepine receptor in large cerebral arterial occlusive diseases. *J Neurol Neurosurg Psychiatry* 68:317–322
- Yamauchi H, Fukuyama H, Nagahama Y, Oyanagi C, Okazawa H, Ueno M, Konishi J, Shio H (2000b) Long-term changes of hemodynamics and metabolism after carotid artery occlusion. *Neurology* 54:2095–2102
- Yamauchi H, Kudoh T, Sugimoto K, Takahashi M, Kishibe Y, Okazawa H (2004) Pattern of collaterals, type of infarcts, and hemodynamic impairment in carotid artery occlusion. *J Neurol Neurosurg Psychiatry* 76:1697–1701
- Yamauchi H, Kudoh T, Kishibe Y, Iwasaki J, Kagawa S (2005) Selective neuronal damage and borderzone infarction in carotid artery occlusive disease: a ¹¹C-flumazenil PET study. *J Nucl Med* 46:1973–1979
- Yamauchi H, Kudoh T, Kishibe Y, Iwasaki J, Kagawa S (2007) Selective neuronal damage and chronic hemodynamic cerebral ischemia. *Ann Neurol* 61:454–465
- Yamauchi H, Nishii R, Higashi T, Kagawa S, Fukuyama H (2009) Hemodynamic compromise as a cause of internal border-zone infarction and cortical neuronal damage in atherosclerotic middle cerebral artery disease. *Stroke* 40:3730–3735
- Yamauchi H, Nishii R, Higashi T, Kagawa S, Fukuyama H (2011a) Selective neuronal damage and Wisconsin Card Sorting Test performance in atherosclerotic occlusive disease of the major cerebral artery. *J Neurol Neurosurg Psychiatry* 82:150–156
- Yamauchi H, Nishii R, Higashi T, Kagawa S, Fukuyama H (2011b) Silent cortical neuronal damage in atherosclerotic disease of the major cerebral arteries. *J Cereb Blood Flow Metab* 31:953–961
- Yamauchi H, Higashi T, Kagawa S, Nishii R, Kudo T, Sugimoto K, Okazawa H, Fukuyama H (2012) Is misery perfusion still a predictor of stroke in symptomatic major cerebral artery disease? *Brain* 135:2515–2526

PET and SPECT Imaging of the Central Dopamine System in Humans

10

Jan Booij, Jan-Peter van Wieringen, Elsmarieke van de Giessen, Remco J.J. Knol, and Sjoerd J. Finnema

Contents

10.1	Introduction	230
10.2	Imaging of the Presynaptic Dopamine System	231
10.2.1	[¹⁸ F]FDOPA and [¹⁸ F]FMT	231
10.2.2	Imaging of the VMAT-2	233
10.2.3	Imaging of the Dopamine Transporter	234
10.3	Imaging of the Postsynaptic Dopaminergic System	236
10.3.1	Imaging of Dopamine D ₁ Receptors	236
10.3.2	Imaging of Dopamine D ₂ -Like Receptors	237
	Conclusion	241
	References	241

Abstract

The neurotransmitter dopamine plays a role in many different functions of the human brain, ranging from psychomotor planning to cognition. This short review addresses which parts of the dopamine system can be imaged quantitatively in the living human brain using positron-emission tomography (PET) or single-photon emission computed tomography (SPECT).

Nowadays, imaging of the nigrostriatal dopaminergic pathway in humans can be performed quantitatively using radiotracers like the aromatic amino acid decarboxylase (AADC) substrate [¹⁸F]FDOPA, vesicular monoamine transporter

J. Booij (✉) • J.-P. van Wieringen • E. van de Giessen
Department of Nuclear Medicine, F2N, Academic Medical Center, University of Amsterdam,
Meibergdreef 9, Amsterdam 1105, AZ, The Netherlands
e-mail: j.booij@amc.uva.nl

R.J.J. Knol
Department of Nuclear Medicine, Medical Center Alkmaar, Alkmaar, The Netherlands

S.J. Finnema
Department of Clinical Neuroscience, Center for Psychiatry Research and Education,
Karolinska Institutet, Stockholm, Sweden

2 (VMAT-2) radioligands derived from tetrabenazine or PET/SPECT radioligands that bind to the dopamine transporter (DAT). Using PET, also several other dopaminergic projection pathways (e.g. mesocortical projections) can be assessed in humans. Several antagonist PET radioligands for the dopamine D₁ receptor have been developed successfully. In addition, well-validated antagonist PET and SPECT radioligands are available for imaging of dopamine D_{2/3} receptors in the living human brain. Recently, also agonist PET radioligands for the dopamine D_{2/3} receptors have become available, which afford the opportunity to evaluate the existence of the high-affinity state of these receptors *in vivo*. These agonist radiopharmaceuticals may also prove more sensitive to changes in dopamine concentrations (e.g. induced by the dopamine releaser amphetamine). Finally, selective antagonist PET radioligands for the dopamine D₄ receptor have recently been synthesized and evaluated successfully in small laboratory animals, although these radioligands have not yet been reported as applied in human subjects.

In conclusion, after almost three decades of research, several relevant parts of the central dopamine system can be assessed quantitatively in the living human brain using PET or SPECT. Future studies may include application of agonist radioligands and more dopamine receptor subtype selective radioligands.

10.1 Introduction

Numerous cognitive, psychomotor and emotional functions are regulated, at least in part, by dopaminergic circuits in the brain. The neurotransmitter dopamine plays, for example, an important role in movement and the experience of pleasure (hedonia). Dopaminergic neurons in the midbrain area are relevant in coding the value of neuronal signals, and indeed, these neurons are activated by a rewarding stimuli (like amphetamines, which induce dopamine release), but may also play a role in reward learning, the prediction of error signalling and the interpretation of the salience of events (Fiorillo et al. 2003; Nakahara et al. 2004; Morris et al. 2006; Zijlstra et al. 2008; Enomoto et al. 2011). In addition, neurodegeneration of the dopaminergic neurons in the midbrain can lead to severe locomotor dysfunction such as in Parkinson's disease. Given the broad spectrum of functions of dopamine in the brain, it is reasonable that imaging of the central dopamine system has been used frequently as a tool to assess different aspects of dopaminergic functioning in health and disease, particularly in a variety of neuropsychiatric disorders.

Here we will review shortly which parts of the central dopamine system can be imaged quantitatively in the living human brain using positron-emission tomography (PET) or single-photon emission computed tomography (SPECT). The findings of SPECT and PET studies of the dopamine system in different neuropsychiatric disorders will be discussed only shortly, since they will be discussed in depth in other chapters of this book.

10.2 Imaging of the Presynaptic Dopamine System

10.2.1 [^{18}F]FDOPA and [^{18}F]FMT

The majority of the cell bodies of dopaminergic neurons are located in the midbrain area, with axons predominantly projecting to the striatum (e.g. the nigrostriatal dopaminergic pathway). The scintigraphic techniques PET and SPECT offer unique means to assess the *in vivo* integrity of the nigrostriatal pathway. The biochemical integrity of presynaptic dopamine neurons can be assessed with the PET radioligands 6- ^{18}F -fluoro-*L*-DOPA ([^{18}F]FDOPA) or 6- ^{18}F -fluoro-meta-tyrosine ([^{18}F]FMT) (for reviews, see Booij et al. 1999; Kumakura and Cumming 2009).

[^{18}F]FDOPA is a widely applied PET tracer commonly radiolabelled with fluorine-18, although in some clinical studies, DOPA was applied as radiolabelled with carbon-11. After injection, the radiotracer will be taken up into dopaminergic neurons by the amino acid transporter (Fig. 10.1), decarboxylated (by aromatic amino acid decarboxylase; AADC) to [^{18}F]fluorodopamine (or [^{11}C]dopamine when [^{11}C]DOPA is used) and then temporarily stored in vesicles within the nerve terminals. Therefore, [^{18}F]FDOPA distribution in dopamine neurons reflects a regulated aspect of the synthesis of dopamine in presynaptic neurons. The trapping of [^{18}F]fluorodopamine in nigrostriatal dopamine terminals has, however, been demonstrated not to be completely irreversible (Holden et al. 1997; Cumming et al. 2001). Indeed, steady-state kinetic analyses of [^{18}F]FDOPA PET studies have shown that besides the synthesis, also the turnover of [^{18}F]FDOPA to *O*-methyl-[^{18}F]FDOPA can be assessed (Kumakura et al. 2005). Importantly, in most clinical studies, static striatal [^{18}F]FDOPA uptake was assessed relative to uptake in a reference tissue (reflecting the non-specific radioactivity concentration) and using linear graphical analysis. This approach is convenient for clinical studies in which arterial blood samples are commonly not available (Kumakura and Cumming 2009). However, the kinetic properties of [^{18}F]FDOPA are complex and include not only the washout of radiotracer but also the entry of a metabolite of [^{18}F]FDOPA into brain. Consequently, relative long acquisitions of dynamic PET images, as well as the analysis of the metabolite-corrected arterial [^{18}F]FDOPA input function, are required to yield a more physiological index of [^{18}F]FDOPA utilization, including [^{18}F]FDOPA turnover (for a review, see Kumakura and Cumming 2009).

As an alternative to [^{18}F]FDOPA, the tyrosine derivative [^{18}F]FMT has been developed. This radiotracer is similar to [^{18}F]FDOPA in that both radiotracers are substrates of AADC. However, unlike [^{18}F]FDOPA, [^{18}F]FMT is not a substrate for catechol-*O*-methyl-transferase (COMT), an enzyme essential in the breakdown of dopamine. Therefore, there are no radioactive *O*-methyl-metabolites which contribute to the non-specific radioactivity in the brain, which enables the use of simplified kinetic modelling approaches (Dejesus et al. 2001).

The enzyme AADC plays an important role in the synthesis of dopamine, in that it converts *L*-DOPA to dopamine. It is important to consider that AADC also plays a role in the synthesis of other monoamine transmitters, e.g. in the conversion of 5-hydroxytryptophan to serotonin (5-HT). Since both [^{18}F]FDOPA and [^{18}F]FMT

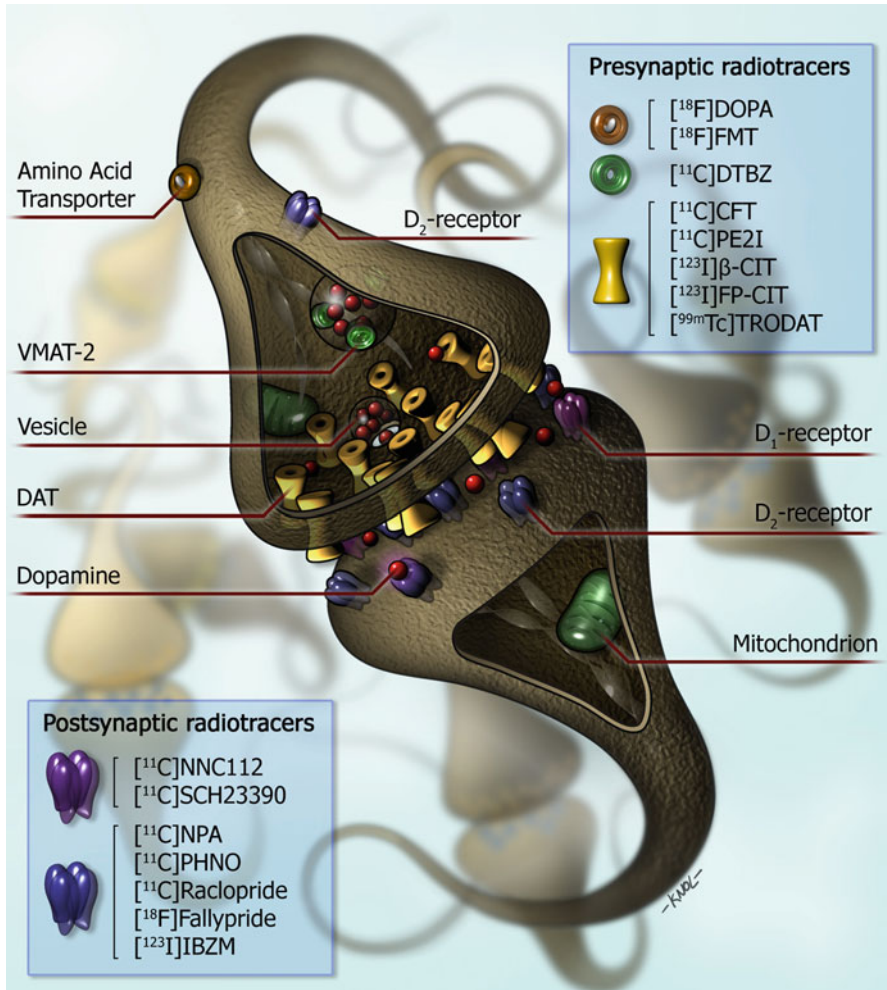


Fig. 10.1 Simplified diagram of a striatal dopaminergic synapse. On the presynaptic side, potential markers for imaging of the integrity of dopaminergic neurons in humans are shown. [¹⁸F]FDOPA and [¹⁸F]FMT PET provide measures of the structural and biochemical integrity of the dopaminergic neurons. [¹¹C]DTBZ is a commonly used radiopharmaceutical for the vesicular monoaminergic transporter. Substituted (nor)phenyltropanes ([¹¹C]CFT, [¹¹C]PE2I, [¹²³I]β-CIT, [¹²³I]FP-CIT and [^{99m}Tc]TRODAT) are frequently used PET and SPECT radioligands for imaging of the DAT in humans. On the postsynaptic sides, [¹¹C]NNC112 and [¹¹C]SCH23390 are commonly used antagonist radiopharmaceuticals for the dopamine D₁ receptor. Dopamine D₂ receptors are predominantly expressed on the postsynaptic side than on the presynaptic side of the dopaminergic synapse. [¹¹C]NPA and [¹¹C]PHNO are agonist radioligands for dopamine D_{2/3} receptors. Commonly used antagonist radioligands for D_{2/3} receptors are substituted benzamides ([¹¹C]raclopride, [¹¹C]FLB 457, [¹⁸F]fallypride and [¹²³I]IBZM). DAT dopamine transporter, VMAT-2 vesicular monoaminergic transporter 2

are substrates of AADC, these tracers are not only converted in dopaminergic neurons but also in serotonergic and noradrenergic neurons (Brown et al. 1999; Moore et al. 2003). The striatal accumulation of these tracers does however predominantly reflect conversion in nigrostriatal dopaminergic neurons (Pavese et al. 2012).

Initial PET studies applying [^{18}F]FDOPA or [^{18}F]FMT focused on evaluation of the nigrostriatal pathway, by studying the distribution of these tracers in the striatum (Antonini et al. 1995). Due to the better performance characteristics of the PET systems, as well as the improved PET data analysis methods, also extrastriatal radioactivity concentrations can nowadays be quantified (e.g. cortical areas). However, and as mentioned before, due to the expression of AADC in all monoaminergic neurons, accumulation in the raphe nuclei and locus coeruleus likely reflects predominantly serotonergic and noradrenergic activity, respectively, instead of accumulation in dopaminergic neurons (Ito et al. 2008; Lewis et al. 2012; Pavese et al. 2012). An important consideration when studying extrastriatal brain regions is that the reliability of measurements in extrastriatal regions is lower than in the striatum (Egerton et al. 2010).

Neuropsychiatric diseases like Parkinson's disease and dementia with Lewy bodies are characterized by severe loss of dopaminergic nigrostriatal neurons. Consequently, many PET studies have utilized [^{18}F]FDOPA and [^{18}F]FMT to demonstrate the ability to detect loss of dopaminergic neurons in cohorts of these patients (Brooks et al. 1990; Antonini et al. 1995; Hu et al. 2000; Pavese et al. 2012). In addition, several [^{18}F]FDOPA PET studies have been performed in patients suffering from psychosis, with the majority of them demonstrating an elevated striatal [^{18}F]FDOPA uptake, which suggests an increased synthesis as well as dopamine turnover in these patients (Kumakura et al. 2007; Howes and Kapur 2009). [^{18}F]FDOPA has also been applied to evaluate the role of dopamine in the human reward system (Dreher et al. 2008; Schlagenhauf et al. 2013). Finally, in healthy controls [^{18}F]FDOPA and [^{18}F]FMT PET have been used to assess ageing effects and cognitive functions (Braskie et al. 2008; Dreher et al. 2008; Kumakura et al. 2010).

10.2.2 Imaging of the VMAT-2

The vesicular monoamine transporter type 2 (VMAT-2; Fig. 10.1) is located in pre-synaptic dopaminergic neurons. Initially, carbon-11-labelled tetrabenazine derivatives have been developed successfully for PET imaging to visualize and quantify the VMAT-2 in humans (for a review, see Kilbourn 1997). Recently, also fluorine-18-labelled radioligands for the VMAT-2 have been developed successfully (Lin et al. 2010), which affords the opportunity to use these radioligands also in hospitals not equipped with a cyclotron.

VMAT-2 is not exclusively present in dopaminergic neurons, but also in other monoaminergic neurons, including serotonergic (Guillot and Miller 2009), although the vast majority of the striatal radioactivity concentration represents binding in dopaminergic nerve terminals (Wang et al. 2010). In this regard, it is of interest that it has been suggested that VMAT-2 radioligands can also be used to visualize loss

of pancreatic beta-cell mass in type 1 diabetes (Goland et al. 2009), since beta-cells express VMAT-2. However, the specific binding of VMAT-2 PET radioligands binding to beta-cell mass has recently been disputed (Virostko et al. 2011).

Like [^{18}F]FDOPA and [^{18}F]FMT use in PET studies, VMAT-2 studies in humans have demonstrated that VMAT-2 imaging is a sensitive technique to detect reductions of nigrostriatal dopaminergic terminals in patients suffering from Parkinson's disease or dementia with Lewy bodies (Frey et al. 1996; Okamura et al. 2010; Burke et al. 2011a; Villemagne et al. 2011). In addition, VMAT-2 binding has been evaluated in relation to natural ageing effects (Bohnen et al. 2006). Until now, SPECT radioligands have not been developed successfully for imaging of the VMAT-2.

10.2.3 Imaging of the Dopamine Transporter

The dopamine transporter (DAT) is mainly located in the membrane of terminals of presynaptic dopaminergic neurons (Fig. 10.1), but is also expressed at much lower levels in cell bodies in the substantia nigra (Ma et al. 1999). Radioligands for the DAT have been developed successfully for both PET and SPECT. Regarding SPECT radioligands, radiopharmaceuticals derived from cocaine, e.g. [$^{99\text{m}}\text{Tc}$]TRODAT-1, [^{123}I] β -CIT and [^{123}I]FP-CIT, are non-selective DAT radioligands, although binding in the striatum predominantly reflects binding to DAT (Laruelle et al. 1993; Booij et al. 1997a, 2007; Dresel et al. 1998; Ziebell et al. 2010; Koopman et al. 2012). Indeed, [^{123}I]FP-CIT SPECT studies have shown that extrastriatal binding (in the diencephalon and midbrain) can be blocked by a selective serotonin reuptake inhibitor, indicating predominantly binding to serotonin transporters in these brain areas (Booij et al. 2007; Ziebell et al. 2010). In addition, also promising and DAT-selective SPECT ligands, like [^{123}I]PE2I, have been developed and used in human subjects (Kuikka et al. 1998; Ziebell et al. 2010).

PET radioligands for imaging of the DAT have been developed numerously over the last two decades (see for reviews Varrone and Halldin 2012a, b). Initially, non-selective DAT radioligands (e.g. [$^{11}\text{C}/^{18}\text{F}$]CFT, Rinne et al. 2002; Nurmi et al. 2003; [^{18}F]FP-CIT; Oh et al. 2012) were applied in human studies, but more recently reported radioligands have an improved DAT selectivity (e.g. [^{11}C]PE2I (Hirvonen et al. 2008) (Fig. 10.2) or [^{18}F]FE-PE2I (Varrone et al. 2009; Sasaki et al. 2012)). The developed PET radioligands also afford the opportunity to assess extrastriatal DAT binding, i.e. binding in the midbrain area and the orbitofrontal area (Jucaite et al. 2005; Hirvonen et al. 2008; Yagi et al. 2010), while with SPECT only DAT binding in the striatum can be assessed accurately.

The DAT plays an important role in regulating dopaminergic neurotransmission. In this regard, appropriate regulation of the DAT expression is critical. Indeed, the DAT expression undergoes dynamic control by cellular protein kinases and phosphatases (Ramamoorthy et al. 2011). So, the DAT is not only expressed on the plasma membrane of dopaminergic neurons, as internalization of the DAT has been reported (Eriksen et al. 2009; Chen et al. 2010). Until now, it is not clear whether the abovementioned DAT radioligands label only plasma membrane-bound

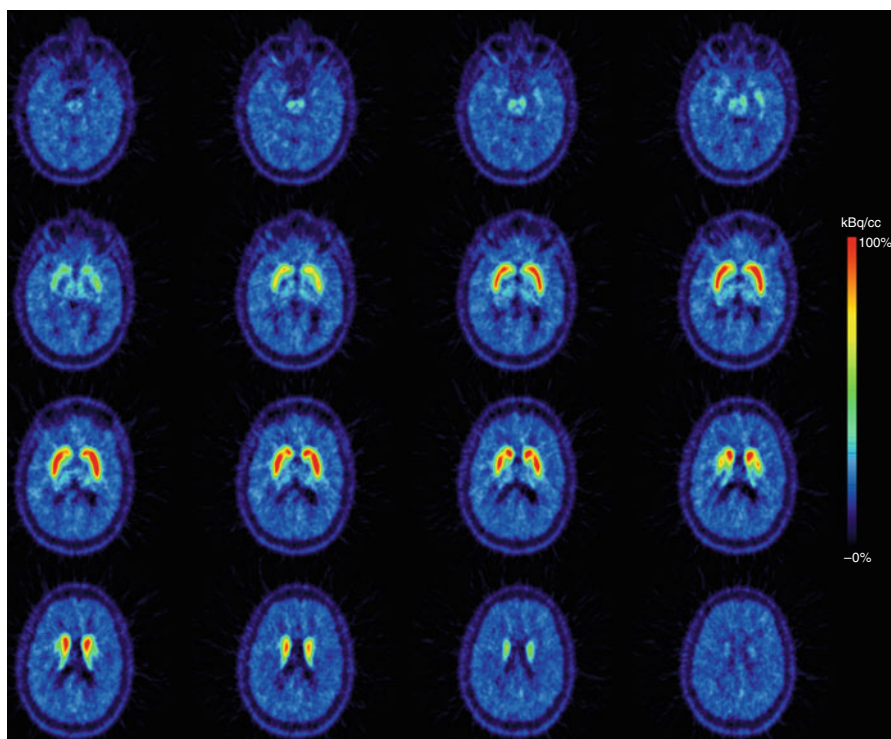


Fig. 10.2 Transversal planes of a mean PET summation image (6–93 min) obtained after i.v. injection of [^{11}C]PE2I (selective radiotracer for the dopamine transporter) into a healthy male control subject. Intense specific binding is visible in the caudate nucleus and putamen and lower specific binding in extrastriatal brain areas (thalamus/midbrain). This study has been acquired on a brain-dedicated PET system (HRRT) (Images courtesy of Dr. Andrea Varrone and Professor Christer Halldin, Karolinska Institutet)

transporters or also internalized transporters when applied in PET/SPECT studies evaluating *in vivo* conditions (Earley et al. 2011). The radioligand binding characteristics to internalized transporters may differ from those transporters that are not internalized. Interestingly, Guo and co-workers have recently demonstrated that radioligands binding the dopamine $\text{D}_{2/3}$ receptors have a lower affinity to internalized than to non-internalized receptors (Guo et al. 2010). Future studies are necessary to evaluate whether DAT internalization is a relevant consideration for *in vivo* imaging of DAT.

Numerous PET and SPECT studies evaluating DAT binding have shown the possibility to detect *in vivo* degeneration of nigrostriatal cells in disorders like Parkinson's disease and dementia with Lewy bodies (Booij et al. 1997b; Varrone et al. 2001; McKeith et al. 2007; Yagi et al. 2010; Oh et al. 2012). Also, DAT binding has been examined in relation to ageing and gender effects in healthy controls, as well as the effects of polymorphism of the DAT gene (Lavalaye et al. 2000; van Dyck et al. 2005; van de Giessen et al. 2009; Troiano et al. 2010; Burke et al. 2011b). Generally

speaking, brain SPECT imaging of neuroreceptors/transporters is cheaper than PET imaging, and consequently DAT imaging with SPECT is commonly used in routine clinical studies to exclude or detect loss of nigrostriatal neurons in individual patients (Booij et al. 2001; Løkkegaard et al. 2002; Catafau et al. 2004; Ziebell et al. 2012).

10.3 Imaging of the Postsynaptic Dopaminergic System

10.3.1 Imaging of Dopamine D₁ Receptors

Dopamine exerts its pharmacological action through G-protein-coupled receptors. These transmembrane receptors can be divided into two subfamilies based on their pharmacological properties: the D₁- (D₁, D₅) and D₂-like receptor subfamily (D₂, D₃, D₄; Stoof and Kebabian 1981; Strange 1993; Beaulieu and Gainetdinov 2011).

The dopamine D₁ receptor is a highly prevalent dopamine receptor in the striatum and neocortex and is located postsynaptically (Cortés et al. 1989; Volkow et al. 1996). The radiopharmaceuticals [¹¹C]NNC 112 and [¹¹C]SCH 23390 have successfully been developed to image dopamine D₁ receptors in the living human brain using PET (Fig. 10.3). Both radioligands are high-affinity dopamine D₁ receptor antagonists, although they also have been reported to bind to serotonin 2A (5-HT_{2A}) receptors, estimated as approximately 25 % of cortical binding being due to binding to 5-HT_{2A} receptors (Ekelund et al. 2007). To circumvent this limitation, a recent study proposed the use of the 5-HT_{2A} receptor antagonist ketanserin. After ketanserin administration, the 5-HT_{2A} receptor binding is inhibited, and cortical D₁ receptor binding can be accurately assessed using [¹¹C]NNC 112 in humans (Catafau et al. 2010).

Although [¹¹C]NNC 112 and [¹¹C]SCH 23390 bind to both dopamine D₁ and 5-HT_{2A} receptors, the affinity to dopamine D₂-like receptors is substantially lower (Andersen et al. 1992) although binding to dopamine D₅ receptors cannot be excluded (Sunahara et al. 1991; Chou et al. 2006). While dopamine D₁ receptors are expressed at high levels in the striatum and cortical areas, the expression of dopamine D₅ receptors in the brain is low (Beaulieu and Gainetdinov 2011). Consequently, *in vivo* binding to dopamine D₅ receptors, as compared to D₁ receptors, with PET radioligands like [¹¹C]NNC 112 is likely negligible.

Dopamine receptors have been demonstrated to exist in two affinity states *in vitro*. The two receptor states are convertible and consist of a state of high and low affinity for the endogenous agonist dopamine (or exogenous agonists) (Sibley et al. 1982; Chio et al. 1994). The high-affinity state represents the active form of the receptors that are coupled to G proteins (Zahniser and Molinoff 1978). Regarding dopamine D₁ receptors, results of *in vitro* experiments suggest that 20–40 % of these receptors are in the high-affinity state (Richfield et al. 1989; Mamelak et al. 1993; McCauley et al. 1995). Importantly, while antagonist radioligands label both the high- and low-affinity state of the receptors, agonist radioligands may label receptors only in its high-affinity state. So far, the available radioligands [¹¹C]NNC 112 and [¹¹C]SCH 23390 are both antagonists for the dopamine D₁ receptor. Developments of agonist radioligands for the dopamine D₁ receptor are ongoing and will enable to examine in

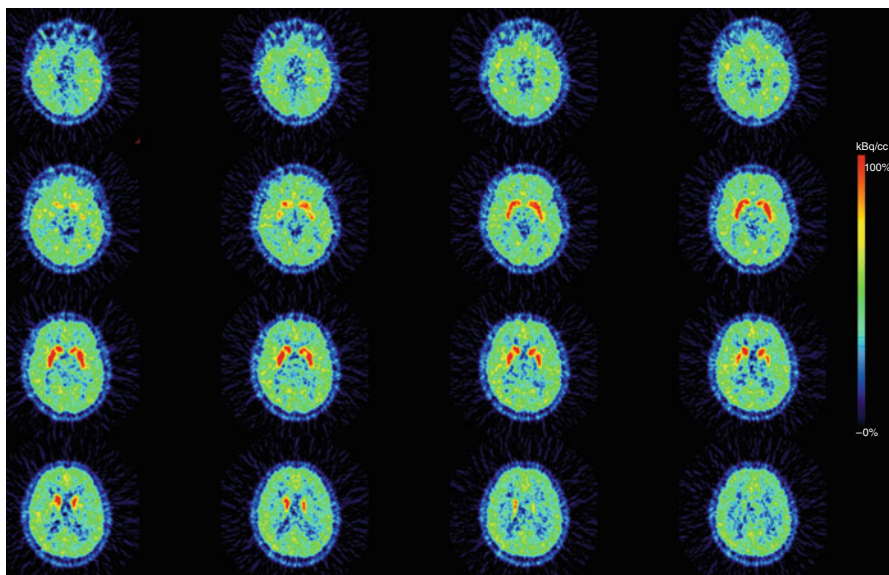


Fig. 10.3 Transversal plane of a mean PET summation image (12–63 min) obtained after i.v. injection of [^{11}C]SCH 23390 (radiotracer for the dopamine D_1 receptor) into a healthy male control subject. Intense specific binding is visible in the caudate and putamen, and lower specific binding in the extrastriatal brain areas (cortex). This study has been acquired on a brain-dedicated PET system (ECAT EXACT HR) (Images are courtesy of Per Stenkrona and Professor Christer Halldin, Karolinska Institutet)

future studies whether the high-affinity state of the dopamine D_1 receptor exists in living humans (Palner et al. 2010). Also, dopamine agonist radioligands may be more sensitive to detect changes in dopamine concentrations in the synapse, e.g. changes induced by dopamine releasers like amphetamines (see below).

Since dopamine D_1 receptors have been implicated in cognitive performance, dopamine D_1 PET studies in healthy volunteers have been used to examine changes in working memory (McNab et al. 2009), amygdala response to affective stimuli (Takahashi et al. 2010) and natural ageing (Jucaite et al. 2010) and to study the effects of genes involved in the dopaminergic tone (Slifstein et al. 2008). Dopamine D_1 receptor imaging in neuropsychiatric disorders has so far focused on schizophrenia (and the mechanism of action of antipsychotics) and cocaine addiction (Nordström et al. 1995; Karlsson et al. 2002; Hirvonen et al. 2006; Martinez et al. 2009). Until now, the development of SPECT radioligands for the dopamine D_1 receptor has not been successful.

10.3.2 Imaging of Dopamine D_2 -Like Receptors

10.3.2.1 Dopamine $\text{D}_{2/3}$ Receptor Imaging

In the past three decades, PET as well as SPECT radioligands have been developed successfully to image and quantify dopamine $\text{D}_{2/3}$ receptors in the human brain.

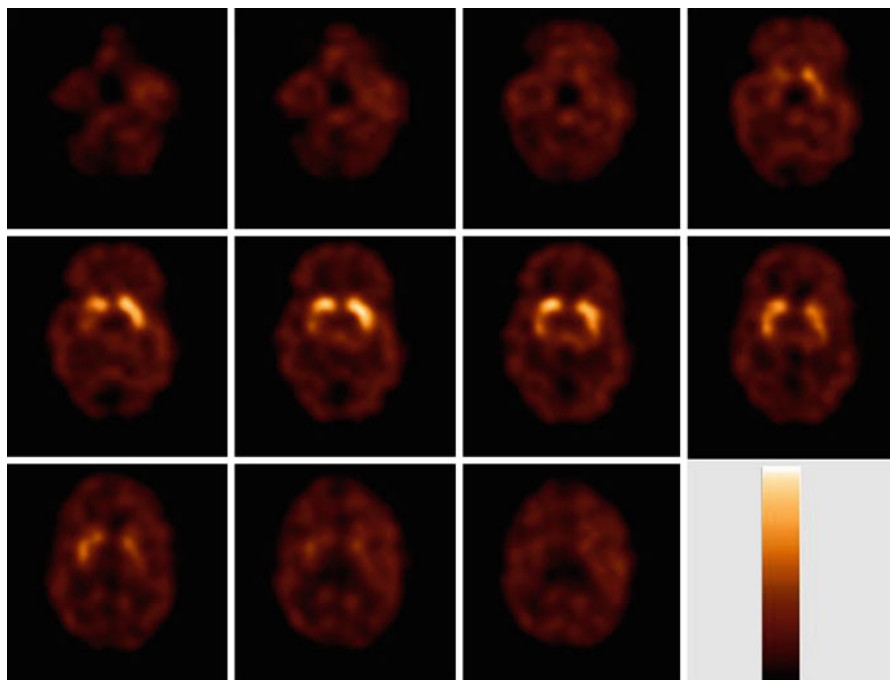


Fig. 10.4 Transversal [^{123}I]IBZM slices obtained in a healthy control, 2 h after start of bolus/constant infusion. Intense specific binding is visible in the striatum, and much lower specific binding in the extrastriatal brain areas (thalamus/midbrain). The used colour scale represents a maximum intensity scale. This study has been acquired on a brain-dedicated SPECT system (Neurofocus)

Regarding SPECT imaging, the commonly used benzamide [^{123}I]IBZM is an antagonist radioligand which binds with high affinity to dopamine $\text{D}_{2/3}$ receptors (i.e. in the low nanomolar range) (Verhoeff et al. 1993; Videbaek et al. 2000; de Haan et al. 2003; Boot et al. 2008; Visser et al. 2008). With this radioligand striatal dopamine $\text{D}_{2/3}$ receptors can be assessed accurately, and extrastriatal distribution may be visualized, particularly when using brain-dedicated SPECT systems (Fig. 10.4). The radioligand [^{123}I]epidepride is a dopamine $\text{D}_{2/3}$ receptors antagonist with an enhanced affinity (picomolar range) for the $\text{D}_{2/3}$ receptors (Kessler et al. 1991). This ultrahigh-affinity SPECT radioligand allows assessing $\text{D}_{2/3}$ receptors availability in extrastriatal brain areas, such as the midbrain, diencephalon and cortical areas (Kornhuber et al. 1995; Varrone et al. 2000; Glenhøj et al. 2006; Tuppurainen et al. 2010).

Regarding PET imaging, the benzamide [^{11}C]raclopride is an antagonist radioligand that binds with high affinity to dopamine $\text{D}_{2/3}$ receptors (in the low nanomolar range; Farde et al. 1986) and is commonly used in human studies (Ito et al. 2011; Martinez et al. 2011). The radioligand [^{11}C]N-methylspiperone binds also with high affinity to dopamine $\text{D}_{2/3}$ receptors, although binding has also been shown to be partly related to 5-HT $_{2A}$ receptors (Nyberg et al. 1999). Also antagonist PET

radioligands with ultrahigh affinity for the dopamine $D_{2/3}$ receptors have been developed successfully. For example, [^{11}C]FLB 457 (Halldin et al. 1995) and [^{18}F]fallypride (Mukherjee et al. 1995) are radioligands with a very high receptor affinity allowing for evaluation of extrastriatal dopamine $D_{2/3}$ receptors (picomolar range; Mukherjee et al. 1995; for a review see Höglberg 1993).

More recently, at least three agonist PET radioligands for dopamine $D_{2/3}$ receptors have been developed and tested successfully in humans, that is [^{11}C]PHNO, [^{11}C]NPA and [^{11}C]MNPA (Willeit et al. 2006; Laymon et al. 2009; Otsuka et al. 2009). The apomorphine derivatives NPA and MNPA bind with high affinity to both dopamine D_2 and D_3 receptors (Seeman et al. 1985; Neumeyer et al. 1990). In contrast, *in vitro* studies have shown that the affinity of PHNO is 30- to 50-fold lower for the dopamine D_2 than for the D_3 receptor (Freedman et al. 1994; van Vliet et al. 2000). Indeed, a recent study in humans demonstrated that binding of [^{11}C]PHNO in several brain regions, e.g. hypothalamus, substantia nigra, ventral pallidum and globus pallidus, is predominantly to dopamine D_3 receptors. On the other hand, in striatal subregions, *in vivo* binding is predominant to dopamine D_2 receptors (Tziortzi et al. 2011). Although the agonist [^{11}C]PHNO binds predominantly to dopamine D_3 receptors in certain brain areas, selective radioligands for dopamine D_2 or D_3 receptors are not available yet.

Regarding dopamine D_2 receptors, *in vitro* experiments on homogenized striata from rats and mice show that roughly 15–30 % of the receptors are in the high-affinity state with a range up to 80 % depending on the detection method used. In more intact tissue (brain slices), 90 % of these receptors may even be in the high-affinity state (van Wieringen et al. 2013). Initial results of *in vivo* PET measurements using amphetamine in non-human primates suggested that 60–80 % of these receptors are in the high-affinity state (Narendran et al. 2004). However, although several attempts have been made, formerly the existence of the high- and low-affinity state has until now not been confirmed or disputed *in vivo* (Finnema et al. 2009; see for reviews Finnema et al. 2010; Skinbjerg et al. 2012). The results of the recent application of agonist radioligands in human PET studies suggest that 60–65 % of dopamine D_2 receptors are in the high-affinity state *in vivo* (Narendran et al. 2010; Shotbolt et al. 2012).

As discussed earlier, dopamine agonist radioligands may be more sensitive to detect changes in dopamine concentrations in the synapse, e.g. changes induced by dopamine releasers like amphetamines (Laruelle et al. 1995) or depletion induced by AMPT (Laruelle et al. 1997; Boot et al. 2008). Indeed, recent studies have indicated that the agonist radioligands ([^{11}C]NPA and [^{11}C]PHNO) are more vulnerable to endogenous dopamine competition than the antagonist radioligand [^{11}C]raclopride in humans (Narendran et al. 2010; Shotbolt et al. 2012). It can be concluded that agonist dopamine $D_{2/3}$ receptors radioligands hold promise for studying changes in dopamine concentrations although further confirmation in human subjects is required.

The dopamine $D_{2/3}$ receptors are not only expressed on the plasma membrane of postsynaptic neurons, but also presynaptically (Fig. 10.1). There are two splice variants of dopamine D_2 receptors, the dopamine D_2 long (D_{2L}) and the short variant

(D₂S) (Chio et al. 1990). These isoforms have different localizations, with D₂S primarily located presynaptically (as an autoreceptor) (Khan et al. 1998). From a pharmacological point of view, these splice variants cannot be discriminated, and consequently, radioligands for the dopamine D_{2/3} receptors may bind to both D₂L and D₂S. However, since the striatal density of D₂L is much higher than that of D₂S (Rani and Kanungo 2006), imaging of dopamine D_{2/3} receptors is frequently referred to as imaging of postsynaptic D_{2/3} receptors. Also, imaging of the midbrain dopamine D_{2/3} receptors may predominantly visualize dopamine D_{2/3} autoreceptors (Buckholtz et al. 2010).

Dopamine D₂ receptors can internalize into the intracellular compartment after agonist stimulation, similar as for other G-protein-coupled receptors. Interestingly, Guo and co-workers recently reported that dopamine D₂ receptor radioligands have a lower affinity to internalized than to non-internalized receptors (Guo et al. 2010). A frequently used approach to assess dopamine release *in vivo* is the use of dexamphetamine (see for review Laruelle 2000). Administration of dexamphetamine intravenously or orally in doses of 0.2–0.3 mg/kg body weight induces a substantial release of endogenous dopamine, which will result in a displacement of radioligand binding to dopamine D_{2/3} receptors (i.e. decrease of, e.g. striatal [¹²³I]IBZM or [¹¹C] raclopride binding; Laruelle et al. 1995; Breier et al. 1997). Typically, administration of dexamphetamine leads to a rapid release of extracellular dopamine which is not long lasting (Breier et al. 1997). However, in imaging studies a prolonged displacement of radioligand binding has been observed, which may be caused (partly) by receptor internalization (Laruelle 2000; Cárdenas et al. 2004; Scott et al. 2007). Indeed, studies in knockout mice, which are incapable of internalizing dopamine D₂ receptors, suggest that the prolonged displacement is mainly due to internalization of D₂ receptors (Skinbjerg et al 2010). Additional studies are needed to demonstrate whether molecular imaging studies are able to assess internalization of dopamine D₂ receptors in humans, which may be relevant to study the role of a possible abnormal internalization of these receptors in neuropsychiatric disorders.

10.3.2.2 Dopamine D₄ Receptor Imaging

The dopamine D₄ receptor was cloned for the first time in 1991 (Van Tol et al. 1991) and is thought to play a role in a variety of neuropsychiatric disorders. This receptor is mainly expressed postsynaptically (Rivera et al. 2002). In contrast to dopamine D_{2/3} receptors, dopamine D₄ receptors do not internalize after agonist stimulation (Spooren et al. 2010). Interestingly, the antipsychotic clozapine, for instance, demonstrates a substantially higher affinity for the dopamine D₄ than for the D₂ receptor subtype (Van Tol et al. 1991; Eisenegger et al. 2010; Smith 2010). Very recently, progress has been reported on the development of a dopamine D₄ receptor radioligand. This has been a challenging task as the density of dopamine D₄ receptors in the human brain is much lower than that of other D₂-like receptors (Marazziti et al. 2009) (Lacivita et al. 2010; Kügler et al. 2011). Although Lacivita and co-workers reported that their radioligand mainly demonstrated high binding in the retina of non-primates (Lacivita et al. 2010), it is promising that a recent study demonstrated clear brain uptake of a dopamine D₄ receptor antagonist radioligand in mice (Kügler et al. 2011).

Conclusion

Imaging of the nigrostriatal pathway in humans can be performed quantitatively with PET and SPECT techniques, using the PET radiotracer [^{18}F]FDOPA, PET radioligands for the VMAT-2 and PET or SPECT radioligands for the DAT. With PET, also several other dopaminergic projections (e.g. mesocortical projections) can be assessed adequately in the human brain. Several antagonist PET radioligands for the dopamine D_1 receptor have been developed successfully. In addition, well-validated antagonist PET and SPECT radioligands are available to image dopamine $\text{D}_{2/3}$ receptors in the living human brain. Recently, also agonist PET radioligands for the dopamine $\text{D}_{2/3}$ receptors have been developed, which affords the opportunity to evaluate the existence of the high-affinity state of these receptors *in vivo*, and these radiopharmaceuticals may be more sensitive to detect changes in dopamine concentrations. Finally, although selective antagonist PET radioligands for the dopamine D_4 receptor have been synthesized and evaluated successfully in small laboratory animals, these radioligands have not yet been applied in human research.

References

- Andersen PH, Grønvald FC, Hohlweg R et al (1992) NNC-112, NNC-687 and NNC-756, new selective and highly potent dopamine D_1 receptor antagonists. *Eur J Pharmacol* 219:45–52
- Antonini A, Vontobel P, Psylla M et al (1995) Complementary positron emission tomographic studies of the striatal dopaminergic system in Parkinson's disease. *Arch Neurol* 52:1183–1190
- Beaulieu JM, Gainetdinov RR (2011) The physiology, signaling, and pharmacology of dopamine receptors. *Pharmacol Rev* 63:182–217
- Bohnen NI, Albin RL, Koeppe RA (2006) Positron emission tomography of monoaminergic vesicular binding in aging and Parkinson disease. *J Cereb Blood Flow Metab* 26:1198–1212
- Booij J, Andringa G, Rijks LJ et al (1997a) [^{123}I]FP-CIT binds to the dopamine transporter as assessed by biodistribution studies in rats and SPECT studies in MPTP-lesioned monkeys. *Synapse* 27:183–190
- Booij J, Tissingh G, Boer GJ (1997b) [^{123}I]FP-CIT SPECT shows a pronounced decline of striatal dopamine transporter labelling in early and advanced Parkinson's disease. *J Neurol Neurosurg Psychiatry* 62:133–140
- Booij J, Tissingh G, Winogrodzka A, van Royen EA (1999) Imaging of the dopaminergic neurotransmission system using single-photon emission tomography and positron emission tomography in patients with parkinsonism. *Eur J Nucl Med* 26:171–182
- Booij J, Speelman JD, Horstink MW, Wolters EC (2001) The clinical benefit of imaging striatal dopamine transporters with [^{123}I]FP-CIT SPET in differentiating patients with presynaptic parkinsonism from those with other forms of parkinsonism. *Eur J Nucl Med* 28:266–272
- Booij J, de Jong J, de Bruin K, Knol R, de Win MM, van Eck-Smit BL (2007) Quantification of striatal dopamine transporters with ^{123}I -FP-CIT SPECT is influenced by the selective serotonin reuptake inhibitor paroxetine: a double-blind, placebo-controlled, crossover study in healthy control subjects. *J Nucl Med* 48:359–366
- Boot E, Booij J, Hasler G et al (2008) AMPT-induced monoamine depletion in humans: evaluation of two alternative [^{123}I]IBZM SPECT procedures. *Eur J Nucl Med Mol Imaging* 35:1350–1356
- Braskie MN, Wilcox CE, Landau SM et al (2008) Relationship of striatal dopamine synthesis capacity to age and cognition. *J Neurosci* 28:14320–14328

- Breier A, Su T-P, Saunders R, Carson R et al (1997) Schizophrenia is associated with elevated amphetamine-induced synaptic dopamine concentrations: evidence from a novel positron emission tomography method. *Proc Natl Acad Sci U S A* 94:2569–2574
- Brooks DJ, Ibanez V, Sawle GV et al (1990) Differing patterns of striatal 18F-dopa uptake in Parkinson's disease, multiple system atrophy, and progressive supranuclear palsy. *Ann Neurol* 28:547–555
- Brown WD, DeJesus OT, Pyzalski RW (1999) Localization of trapping of 6-[¹⁸F]fluoro-L-m-tyrosine, an aromatic L-amino acid decarboxylase tracer for PET. *Synapse* 34:111–123
- Buckholtz JW, Treadway MT, Cowan RL et al (2010) Dopaminergic network differences in human impulsivity. *Science* 329:532
- Burke JF, Albin RL, Koeppe RA et al (2011a) Assessment of mild dementia with amyloid and dopamine terminal positron emission tomography. *Brain* 134:1647–1657
- Burke SM, van de Giessen E, de Win M et al (2011b) Serotonin and dopamine transporters in relation to neuropsychological functioning, personality traits and mood in young adult healthy subjects. *Psychol Med* 41:419–429
- Cárdenas L, Houle S, Kapur S, Busto UE (2004) Oral D-amphetamine causes prolonged displacement of [¹¹C]raclopride as measured by PET. *Synapse* 51:27–31
- Catafau AM, Tolosa E, DaTSCAN Clinically Uncertain Parkinsonian Syndromes Study Group (2004) Impact of dopamine transporter SPECT using 123I-Ioflupane on diagnosis and management of patients with clinically uncertain Parkinsonian syndromes. *Mov Disord* 19:1175–1182
- Catafau AM, Searle GE, Bullich S (2010) Imaging cortical dopamine D1 receptors using [¹¹C] NNC112 and ketanserin blockade of the 5-HT 2A receptors. *J Cereb Blood Flow Metab* 30:985–993
- Chen R, Furman CA, Gnegy ME (2010) Dopamine transporter trafficking: rapid response on demand. *Future Neurol* 5:123
- Chio CL, Hess GF, Graham RS, Huff RM (1990) A second molecular form of D2 dopamine receptor in rat and bovine caudate nucleus. *Nature* 343:266–269
- Chio CL, Lajiness ME, Huff RM (1994) Activation of heterologously expressed D3 dopamine receptors: comparison with D2 dopamine receptors. *Mol Pharmacol* 45:51–60
- Chou YH, Halldin C, Farde L (2006) Clozapine binds preferentially to cortical D1-like dopamine receptors in the primate brain: a PET study. *Psychopharmacology (Berl)* 185:29–35
- Cortés R, Gueye B, Pazos A, Probst A, Palacios JM (1989) Dopamine receptors in human brain: autoradiographic distribution of D1 sites. *Neuroscience* 28:263–273
- Cumming P, Munk OL, Doudet D (2001) Loss of metabolites from monkey striatum during PET with FDOPA. *Synapse* 41:212–218
- de Haan L, van Bruggen M, Lavalaye J, Booij J, Dingemans PM, Linszen D (2003) Subjective experience and D2 receptor occupancy in patients with recent-onset schizophrenia treated with low-dose olanzapine or haloperidol: a randomized, double-blind study. *Am J Psychiatry* 160:303–309
- DeJesus OT, Endres CJ, Shelton SE, Nickles RJ, Holden JE (2001) Noninvasive assessment of aromatic L-amino acid decarboxylase activity in aging rhesus monkey brain in vivo. *Synapse* 39:58–63
- Dreher JC, Meyer-Lindenberg A, Kohn P, Berman KF (2008) Age-related changes in midbrain dopaminergic regulation of the human reward system. *Proc Natl Acad Sci U S A* 105:15106–15111
- Dresel SH, Kung MP, Plössl K, Meegalla SK, Kung HF (1998) Pharmacological effects of dopaminergic drugs on in vivo binding of [^{99m}Tc]TRODAT-1 to the central dopamine transporters in rats. *Eur J Nucl Med* 25:31–39
- Earley CJ, Kuwabara H, Wong DF et al (2011) The dopamine transporter is decreased in the striatum of subjects with restless legs syndrome. *Sleep* 34:341–347
- Egerton A, Demjaha A, McGuire P, Mehta MA, Howes OD (2010) The test-retest reliability of 18 F-DOPA PET in assessing striatal and extrastriatal presynaptic dopaminergic function. *Neuroimage* 50:524–531

- Eisenegger C, Knoch D, Ebstein RP, Gianotti LR, Sándor PS, Fehr E (2010) Dopamine receptor D4 polymorphism predicts the effect of L-DOPA on gambling behavior. *Biol Psychiatry* 67:702–706
- Ekelund J, Slifstein M, Narendran R et al (2007) In vivo DA D1 receptor selectivity of NNC 112 and SCH 23390. *Mol Imaging Biol* 9:117–125
- Enomoto K, Matsumoto N, Nakai S et al (2011) Dopamine neurons learn to encode the long-term value of multiple future rewards. *Proc Natl Acad Sci U S A* 108:15462–15467
- Eriksen J, Rasmussen SG, Rasmussen TN et al (2009) Visualization of dopamine transporter trafficking in live neurons by use of fluorescent cocaine analogs. *J Neurosci* 29:6794–6808
- Farde L, Hall H, Ehrin E, Sedvall G (1986) Quantitative analysis of D2 dopamine receptor binding in the living human brain by PET. *Science* 231:258–261
- Finnema SJ, Halldin C, Bang-Andersen B, Gulyás B, Bundgaard C, Wikström HV, Farde L (2009) Dopamine D_{2/3} receptor occupancy of apomorphine in the nonhuman primate brain—a comparative PET study with [¹¹C]raclopride and [¹¹C]MNPA. *Synapse* 63:378–389
- Finnema SJ, Bang-Andersen B, Wikström HV, Halldin C (2010) Current state of agonist radioligands for imaging of brain dopamine D2/D3 receptors in vivo with positron emission tomography. *Curr Top Med Chem* 10:1477–1498
- Fiorillo CD, Tobler PN, Schultz W (2003) Discrete coding of reward probability and uncertainty by dopamine neurons. *Science* 299:1898–1902
- Freedman SB, Patel S, Marwood R et al (1994) Expression and pharmacological characterization of the human D3 dopamine receptor. *J Pharmacol Exp Ther* 268:417–426
- Frey KA, Koeppe RA, Kilbourn MR et al (1996) Presynaptic monoaminergic vesicles in Parkinson's disease and normal aging. *Ann Neurol* 40:873–884
- Glenthøj BY, Mackeprang T, Svarer C et al (2006) Frontal dopamine D(2/3) receptor binding in drug-naïve first-episode schizophrenic patients correlates with positive psychotic symptoms and gender. *Biol Psychiatry* 60:621–629
- Goland R, Freeby M, Parsey R et al (2009) 11C-dihydrotrabenazine PET of the pancreas in subjects with long-standing type 1 diabetes and in healthy controls. *J Nucl Med* 50:382–389
- Guillot TS, Miller GW (2009) Protective actions of the vesicular monoamine transporter 2 (VMAT2) in monoaminergic neurons. *Mol Neurobiol* 39:149–170
- Guo N, Guo W, Kralikova M et al (2010) Impact of D2 receptor internalization on binding affinity of neuroimaging radiotracers. *Neuropsychopharmacology* 35:806–817
- Halldin C, Farde L, Höglberg T et al (1995) Carbon-11-FLB 457: a radioligand for extrastriatal D2 dopamine receptors. *J Nucl Med* 36:1275–1281
- Hirvonen J, van Erp TG, Huttunen J et al (2006) Brain dopamine d1 receptors in twins discordant for schizophrenia. *Am J Psychiatry* 163:1747–1753
- Hirvonen J, Johansson J, Teräs M (2008) Measurement of striatal and extrastriatal dopamine transporter binding with high-resolution PET and [¹¹C]PE2I: quantitative modeling and test-retest reproducibility. *J Cereb Blood Flow Metab* 28:1059–1069
- Höglberg T (1993) The development of dopamine D2-receptor selective antagonists. *Drug Des Discov* 9:333–350
- Holden JE, Doudet D, Endres CJ et al (1997) Graphical analysis of 6-fluoro-L-dopa trapping: effect of inhibition of catechol-O-methyltransferase. *J Nucl Med* 38:1568–1574
- Howes OD, Kapur S (2009) The dopamine hypothesis of schizophrenia: version III—the final common pathway. *Schizophr Bull* 35:549–562
- Hu XS, Okamura N, Arai H (2000) 18F-fluorodopa PET study of striatal dopamine uptake in the diagnosis of dementia with Lewy bodies. *Neurology* 55:1575–1577
- Ito H, Takahashi H, Arakawa R, Takano H, Suhara T (2008) Normal database of dopaminergic neurotransmission system in human brain measured by positron emission tomography. *Neuroimage* 39:555–565
- Ito H, Kodaka F, Takahashi H et al (2011) Relation between presynaptic and postsynaptic dopaminergic functions measured by positron emission tomography: implication of dopaminergic tone. *J Neurosci* 31:7886–7890

- Jucaite A, Fernell E, Halldin C, Forsberg H, Farde L (2005) Reduced midbrain dopamine transporter binding in male adolescents with attention-deficit/hyperactivity disorder: association between striatal dopamine markers and motor hyperactivity. *Biol Psychiatry* 57:229–238
- Jucaite A, Forsberg H, Karlsson P, Halldin C, Farde L (2010) Age-related reduction in dopamine D1 receptors in the human brain: from late childhood to adulthood, a positron emission tomography study. *Neuroscience* 167:104–110
- Karlsson P, Farde L, Halldin C, Sedvall G (2002) PET study of D(1) dopamine receptor binding in neuroleptic-naive patients with schizophrenia. *Am J Psychiatry* 159:761–767
- Kessler RM, Ansari MS, de Paulis T et al (1991) High affinity dopamine D2 receptor radioligands. I. Regional rat brain distribution of iodinated benzamides. *J Nucl Med* 32:1593–1600
- Khan ZU, Mrzljak L, Gutierrez A, de la Calle A, Goldman-Rakic PS (1998) Prominence of the dopamine D2 short isoform in dopaminergic pathways. *Proc Natl Acad Sci U S A* 95:7731–7736
- Kilbourn MR (1997) In vivo radiotracers for vesicular neurotransmitter transporters. *Nucl Med Biol* 24:615–619
- Koopman KE, la Fleur SE, Fliers E, Serlie MJ, Booij J (2012) Assessing the optimal time-point for the measurement of extrastriatal serotonin transporter binding with ¹²³I-FP-CIT SPECT in healthy, male subjects. *J Nucl Med* 53:1087–1090
- Kornhuber J, Brücke T, Angelberger P, Asenbaum S, Podreka I (1995) SPECT imaging of dopamine receptors with [¹²³I]epidepride: characterization of uptake in the human brain. *J Neural Transm Gen Sect* 101:95–103
- Kügler F, Sihver W, Ermert J et al (2011) Evaluation of 18 F-labeled benzodioxine piperazine-based dopamine D4 receptor ligands: lipophilicity as a determinate of nonspecific binding. *J Med Chem* 54:8343–8352
- Kuikka JT, Baulieu JL, Hiltunen J et al (1998) Pharmacokinetics and dosimetry of iodine-123 labelled PE2I in humans, a radioligand for dopamine transporter imaging. *Eur J Nucl Med* 25:531–534
- Kumakura Y, Cumming P (2009) PET studies of cerebral levodopa metabolism: a review of clinical findings and modeling approaches. *Neuroscientist* 15:635–650
- Kumakura Y, Vernaleken I, Gründer G, Bartenstein P, Gjedde A, Cumming P (2005) PET studies of net blood–brain clearance of FDOPA to human brain: age-dependent decline of [¹⁸F]fluorodopamine storage capacity. *J Cereb Blood Flow Metab* 25:807–819
- Kumakura Y, Cumming P, Vernaleken I et al (2007) Elevated [¹⁸F]fluorodopamine turnover in brain of patients with schizophrenia: an [¹⁸F]fluorodopa/positron emission tomography study. *J Neurosci* 27:8080–8087
- Kumakura Y, Vernaleken I, Buchholz HG et al (2010) Age-dependent decline of steady state dopamine storage capacity of human brain: an FDOPA PET study. *Neurobiol Aging* 31:447–463
- Lacivita E, De Giorgio P, Lee IT et al (2010) Design, synthesis, radiolabeling, and in vivo evaluation of carbon-11 labeled N-[2-[4-(3-cyanopyridin-2-yl)piperazin-1-yl]ethyl]-3-methoxybenzamide, a potential positron emission tomography tracer for the dopamine D4 receptors. *J Med Chem* 53:7344–7355
- Laruelle M (2000) Imaging synaptic neurotransmission with in vivo binding competition techniques: a critical review. *J Cereb Blood Flow Metab* 20:423–451
- Laruelle M, Baldwin RM, Malison RT (1993) SPECT imaging of dopamine and serotonin transporters with [¹²³I]beta-CIT: pharmacological characterization of brain uptake in nonhuman primates. *Synapse* 13:295–309
- Laruelle M, Abi-Dargham A, van Dyck CH et al (1995) SPECT imaging of striatal dopamine release after amphetamine challenge. *J Nucl Med* 36:1182–1190
- Laruelle M, D'Souza CD, Baldwin RM et al (1997) Imaging D2 receptor occupancy by endogenous dopamine in humans. *Neuropsychopharmacology* 17:162–174
- Lavalaye J, Booij J, Reneman L, Habraken JB, van Royen EA (2000) Effect of age and gender on dopamine transporter imaging with [¹²³I]FP-CIT SPET in healthy volunteers. *Eur J Nucl Med* 27:867–869

- Laymon CM, Mason NS, Frankle WG et al (2009) Human biodistribution and dosimetry of the D_{2/3} agonist 11C-N-propylnorapomorphine (11C-NPA) determined from PET. *J Nucl Med* 50:814–817
- Lewis SJ, Pavese N, Rivero-Bosch M et al (2012) Brain monoamine systems in multiple system atrophy: a positron emission tomography study. *Neurobiol Dis* 46:130–136
- Lin KJ, Weng YH, Wey SP et al (2010) Whole-body biodistribution and radiation dosimetry of 18 F-FP-(+)-DTBZ (18 F-AV-133): a novel vesicular monoamine transporter 2 imaging agent. *J Nucl Med* 51:1480–1485
- Lökkegaard A, Werdelin LM, Friberg L (2002) Clinical impact of diagnostic SPET investigations with a dopamine re-uptake ligand. *Eur J Nucl Med Mol Imaging* 29:1623–1629
- Ma SY, Ciliax BJ, Stebbins G et al (1999) Dopamine transporter-immunoreactive neurons decrease with age in the human substantia nigra. *J Comp Neurol* 409:25–37
- Mamelak M, Chiu S, Mishra RK (1993) High- and low-affinity states of dopamine D₁ receptors in schizophrenia. *Eur J Pharmacol* 233:175–176
- Marazziti D, Baroni S, Masala I et al (2009) [(3)H]-YM-09151-2 binding sites in human brain postmortem. *Neurochem Int* 55:643–647
- Martinez D, Slifstein M, Narendran R et al (2009) Dopamine D₁ receptors in cocaine dependence measured with PET and the choice to self-administer cocaine. *Neuropsychopharmacology* 34:1774–1782
- Martinez D, Carpenter KM, Liu F (2011) Imaging dopamine transmission in cocaine dependence: link between neurochemistry and response to treatment. *Am J Psychiatry* 168:634–641
- McCauley PG, O'Boyle KM, Waddington JL (1995) Dopamine-induced reduction in the density of guanine nucleotide-sensitive D₁ receptors in human postmortem brain in the absence of apparent D₁: D₂ interactions. *Neuropharmacology* 34:777–783
- McKeith I, O'Brien J, Walker Z et al (2007) Sensitivity and specificity of dopamine transporter imaging with 123I-FP-CIT SPECT in dementia with Lewy bodies: a phase III, multicentre study. *Lancet Neurol* 6:305–313
- McNab F, Varrone A, Farde L et al (2009) Changes in cortical dopamine D₁ receptor binding associated with cognitive training. *Science* 323:800–802
- Moore RY, Whone AL, McGowan S, Brooks DJ (2003) Monoamine neuron innervation of the normal human brain: an 18 F-DOPA PET study. *Brain Res* 982:137–145
- Morris G, Nevet A, Arkadir D, Vaadia E, Bergman H (2006) Midbrain dopamine neurons encode decisions for future action. *Nat Neurosci* 9:1057–1063
- Mukherjee J, Yang ZY, Das MK, Brown T (1995) Fluorinated benzamide neuroleptics—III. Development of (S)-N-[(1-allyl-2-pyrrolidinyl)methyl]-5-(3-[18 F]fluoropropyl)-2, 3-dimethoxybenzamide as an improved dopamine D-2 receptor tracer. *Nucl Med Biol* 22:283–296
- Nakahara H, Itoh H, Kawagoe R, Takikawa Y, Hikosaka O (2004) Dopamine neurons can represent context-dependent prediction error. *Neuron* 41:269–280
- Narendran R, Hwang DR, Slifstein M et al (2004) In vivo vulnerability to competition by endogenous dopamine: comparison of the D₂ receptor agonist radiotracer (–)-N-[11C]propyl-norapomorphine ([11C]NPA) with the D₂ receptor antagonist radiotracer [11C]-raclopride. *Synapse* 52:188–208
- Narendran R, Mason NS, Laymon CM et al (2010) A comparative evaluation of the dopamine D_{2/3} agonist radiotracer [¹¹C](–)-N-propyl-norapomorphine and antagonist [¹¹C]raclopride to measure amphetamine-induced dopamine release in the human striatum. *J Pharmacol Exp Ther* 333:533–539
- Neumeyer JL, Gao YG, Kula NS, Baldessarini RJ (1990) Synthesis and dopamine receptor affinity of (R)-(–)-2-fluoro-N-n-propylnorapomorphine: a highly potent and selective dopamine D₂ agonist. *J Med Chem* 33:3122–3124
- Nordström AL, Farde L, Nyberg S, Karlsson P, Halldin C, Sedvall G (1995) D₁, D₂, and 5-HT₂ receptor occupancy in relation to clozapine serum concentration: a PET study of schizophrenic patients. *Am J Psychiatry* 152:1444–1449

- Nurmi E, Bergman J, Eskola O, Solin O, Vahlberg T, Sonninen P, Rinne JO (2003) Progression of dopaminergic hypofunction in striatal subregions in Parkinson's disease using [^{18}F]CFT PET. *Synapse* 48:109–115
- Nyberg S, Eriksson B, Oxenstierna G, Halldin C, Farde L (1999) Suggested minimal effective dose of risperidone based on PET-measured D2 and 5-HT $_2\text{A}$ receptor occupancy in schizophrenic patients. *Am J Psychiatry* 156:869–875
- Oh M, Kim JS, Kim JY et al (2012) Subregional patterns of preferential striatal dopamine transporter loss differ in Parkinson disease, progressive supranuclear palsy, and multiple-system atrophy. *J Nucl Med* 53:399–406
- Okamura N, Villemagne VL, Drago J et al (2010) In vivo measurement of vesicular monoamine transporter type 2 density in Parkinson disease with ^{18}F -AV-133. 2010. *J Nucl Med* 51:223–228
- Otsuka T, Ito H, Halldin C et al (2009) Quantitative PET analysis of the dopamine D2 receptor agonist radioligand 11C-(R)-2-CH $_3\text{O}$ -N-n-propylnorapomorphine in the human brain. *J Nucl Med* 50:703–710
- Palmer M, McCormick P, Parkes J, Knudsen GM, Wilson AA (2010) Systemic catechol-O-methyl transferase inhibition enables the D1 agonist radiotracer R-[^{11}C]SKF 82957. *Nucl Med Biol* 37:837–843
- Pavese N, Simpson BS, Metta V, Ramlackhansingh A, Chaudhuri KR, Brooks DJ (2012) [^{18}F]FDOPA uptake in the raphe nuclei complex reflects serotonin transporter availability. A combined [^{18}F]FDOPA and [^{11}C]DASB PET study in Parkinson's disease. *Neuroimage* 59:1080–1084
- Ramamoorthy S, Shippenberg TS, Jayanthi LD (2011) Regulation of monoamine transporters: role of transporter phosphorylation. *Pharmacol Ther* 129:220–238
- Rani M, Kanungo MS (2006) Expression of D2 dopamine receptor in the mouse brain. *Biochem Biophys Res Commun* 344:981–986
- Richfield EK, Penney JB, Young AB (1989) Anatomical and affinity state comparisons between dopamine D1 and D2 receptors in the rat central nervous system. *Neuroscience* 30:767–777
- Rinne JO, Laine M, Kaasinen V, Norvasuo-Heilä MK, Någren K, Helenius H (2002) Striatal dopamine transporter and extrapyramidal symptoms in frontotemporal dementia. *Neurology* 58:1489–1493
- Rivera A, Cuéllar B, Girón FJ, Grandy DK, de la Calle A, Moratalla R (2002) Dopamine D4 receptors are heterogeneously distributed in the striosomes/matrix compartments of the striatum. *J Neurochem* 80:219–229
- Sasaki T, Ito H, Kimura Y et al (2012) Quantification of dopamine transporter in human brain using PET with 18 F-FE-PE2I. *J Nucl Med* 53:1065–1073
- Schlagenhauf F, Rapp MA, Huys QJ et al (2013) Ventral striatal prediction error signaling is associated with dopamine synthesis capacity and fluid intelligence. *Hum Brain Mapp* 34:1490–1499
- Scott DJ, Stohler CS, Koeppe RA, Zubieta JK (2007) Time-course of change in [^{11}C]carfentanil and [^{11}C]raclopride binding potential after a nonpharmacological challenge. *Synapse* 61:707–714
- Seeman P, Waanabe M, Grigoriadis D et al (1985) Dopamine D2 receptor binding sites for agonists. A tetrahedral model. *Mol Pharmacol* 28:391–399
- Sholtz P, Tziortzi AC, Searle GE et al (2012) Within-subject comparison of [^{11}C]-(+)-PHNO and [^{11}C]raclopride sensitivity to acute amphetamine challenge in healthy humans. *J Cereb Blood Flow Metab* 32:127–136
- Sibley DR, De Lean A, Creese I (1982) Anterior pituitary dopamine receptors. Demonstration of interconvertible high and low affinity states of the D-2 dopamine receptor. *J Biol Chem* 257:6351–6361
- Skinbjerg M, Liow JS, Seneca N et al (2010) D2 dopamine receptor internalization prolongs the decrease of radioligand binding after amphetamine: a PET study in a receptor internalization-deficient mouse model. *Neuroimage* 50:1402–1407
- Skinbjerg M, Sibley DR, Javitch JA, Abi-Dargham A (2012) Imaging the high-affinity state of the dopamine D2 receptor in vivo: fact or fiction? *Biochem Pharmacol* 83:193–198

- Slifstein M, Kolachana B, Simpson EH et al (2008) COMT genotype predicts cortical-limbic D1 receptor availability measured with [¹¹C]NNC112 and PET. *Mol Psychiatry* 13:821–827
- Smith TF (2010) Meta-analysis of the heterogeneity in association of DRD4 7-repeat allele and AD/HD: stronger association with AD/HD combined type. *Am J Med Genet B Neuropsychiatr Genet* 153B:1189–1199
- Spooren A, Rondou P, Debowska K et al (2010) Resistance of the dopamine D4 receptor to agonist-induced internalization and degradation. *Cell Signal* 22:600–609
- Stoof JC, Keabian JW (1981) Opposing roles for D-1 and D-2 dopamine receptors in efflux of cyclic AMP from rat neostriatum. *Nature* 294:366–368
- Strange PG (1993) New insights into dopamine receptors in the central nervous system. *Neurochem Int* 22:223–236
- Sunahara RK, Guan HC, O'Dowd BF et al (1991) Cloning of the gene for a human dopamine D5 receptor with higher affinity for dopamine than D1. *Nature* 350:614–619
- Takahashi H, Takano H, Kodaka F et al (2010) Contribution of dopamine D1 and D2 receptors to amygdala activity in human. *J Neurosci* 30:3043–3047
- Troiano AR, Schulzer M, de la Fuente-Fernandez R et al (2010) Dopamine transporter PET in normal aging: dopamine transporter decline and its possible role in preservation of motor function. *Synapse* 64:146–151
- Tuppurainen H, Kuikka JT, Viinamäki H, Husso M, Tiihonen J (2010) Extrapyramidal side-effects and dopamine D_{2/3} receptor binding in substantia nigra. *Nord J Psychiatry* 64:233–238
- Tziortzi AC, Searle GE, Tzimopoulou S et al (2011) Imaging dopamine receptors in humans with [¹¹C](+)-PHNO: dissection of D3 signal and anatomy. *Neuroimage* 54:264–277
- van de Giessen E, de Win MM, Tanck MW, van den Brink W, Baas F, Booij J (2009) Striatal dopamine transporter availability associated with polymorphisms in the dopamine transporter gene SLC6A3. *J Nucl Med* 50:45–52
- van Dyck CH, Malison RT, Jacobsen LK et al (2005) Increased dopamine transporter availability associated with the 9-repeat allele of the SLC6A3 gene. *J Nucl Med* 46:745–751
- Van Tol HHM, Bunzow JR, Guan HC et al (1991) Cloning of the gene for a human D4 receptor with high affinity for the antipsychotic clozapine. *Nature* 350:610–614
- van Vliet L, Rodenhuis N, Dijkstra D et al (2000) Synthesis and pharmacological evaluation of thiopyran analogues of the dopamine D3 receptor-selective agonist (4aR,10bR)-(p)-trans-3,4,4a,10b-tetrahydro-4-n-propyl-2H,5H-[1]benzopropyno[4,3-b]-1,4-oxazin-9-ol (PD128907). *J Med Chem* 43:2871–2882
- van Wieringen J-P, Booij J, Shalgunov V et al (2013) Agonist high- and low-affinity states of dopamine D₂ receptors: methods of detection and clinical implications. *Naunyn Schmiedeberg Arch Pharmacol* 386:135–154
- Varrone A, Halldin C (2012a) New developments of dopaminergic imaging in Parkinson's disease. *Q J Nucl Med Mol Imaging* 56:68–82
- Varrone A, Halldin C (2012b) Molecular imaging of the dopamine transporter. *J Nucl Med* 51:1331–1334
- Varrone A, Fujita M, Verhoeff NP et al (2000) Test-retest reproducibility of extrastriatal dopamine D2 receptor imaging with [¹²³I]epidepride SPECT in humans. *J Nucl Med* 41:1343–1451
- Varrone A, Marek KL, Jennings D, Innis RB, Seibyl JP (2001) [¹²³I]beta-CIT SPECT imaging demonstrates reduced density of striatal dopamine transporters in Parkinson's disease and multiple system atrophy. *Mov Disord* 16:1023–1032
- Varrone A, Steiger C, Schou M et al (2009) In vitro autoradiography and in vivo evaluation in cynomolgus monkey of [¹⁸F]FE-PE2I, a new dopamine transporter PET radioligand. *Synapse* 63:871–880
- Verhoeff NP, Kapucu O, Sokole-Busemann E, van Royen EA, Janssen AG (1993) Estimation of dopamine D2 receptor binding potential in the striatum with iodine-123-IBZM SPECT: technical and interobserver variability. *J Nucl Med* 34:2076–2084
- Videbaek C, Toska K, Scheideler MA, Paulson OB, Moos Knudsen G (2000) SPECT tracer [¹²³I] IBZM has similar affinity to dopamine D2 and D3 receptors. *Synapse* 38:338–342

- Villemagne VL, Okamura N, Pejoska S et al (2011) In vivo assessment of vesicular monoamine transporter type 2 in dementia with lewy bodies and Alzheimer disease. *Arch Neurol* 68:905–912
- Virostko J, Henske J, Vinet L et al (2011) Multimodal image coregistration and inducible selective cell ablation to evaluate imaging ligands. *Proc Natl Acad Sci U S A* 108:20719–20724
- Visser I, Lavini C, Booij J et al (2008) Cerebral impairment in chronic solvent-induced encephalopathy. *Ann Neurol* 63:572–580
- Volkow ND, Fowler JS, Gatley SJ, Logan J, Wang GJ, Ding YS, Dewey S (1996) PET evaluation of the dopamine system of the human brain. *J Nucl Med* 37:1242–1256
- Wang JL, Oya S, Parhi AK et al (2010) In vivo studies of the SERT-selective [¹⁸F]FPBM and VMAT2-selective [¹⁸F]AV-133 radiotracers in a rat model of Parkinson's disease. *Nucl Med Biol* 37:479–486
- Willeit M, Ginovart N, Kapur S et al (2006) High-affinity states of human brain dopamine D2/3 receptors imaged by the agonist [¹¹C]-(+)-PHNO. *Biol Psychiatry* 59:389–394
- Yagi S, Yoshikawa E, Futatsubashi M et al (2010) Progression from unilateral to bilateral parkinsonism in early Parkinson disease: implication of mesocortical dopamine dysfunction by PET. *J Nucl Med* 51:1250–1257
- Zahniser, Molinoff (1978) Effect of guanine nucleotides on striatal dopamine receptors. *Nature* 275:453–455
- Ziebell M, Holm-Hansen S, Thomsen G et al (2010) Serotonin transporters in dopamine transporter imaging: a head-to-head comparison of dopamine transporter SPECT radioligands 123I-FP-CIT and 123I-PE2I. *J Nucl Med* 51:1885–1891
- Ziebell M, Andersen BB, Thomsen G et al (2012) Predictive value of dopamine transporter SPECT imaging with [¹²³I]PE2I in patients with subtle parkinsonian symptoms. *Eur J Nucl Med Mol Imaging* 39:242–250
- Zijlstra F, Booij J, van den Brink W, Franken IH (2008) Striatal dopamine D2 receptor binding and dopamine release during cue-elicited craving in recently abstinent opiate-dependent males. *Eur Neuropsychopharmacol* 18:262–270

Andrew G. Horti, Vanessa Raymont, and Garth E. Terry

Contents

11.1	Introduction	251
11.1.1	Endocannabinoid System	251
11.1.2	Physiology of the Endocannabinoid System	255
11.1.3	Pharmacology of Cannabinoids	256
11.1.4	Endocannabinoid System-Related Pathologies	257
11.1.5	Role of PET and SPECT in Cannabinoid Receptor Research	263
11.2	PET Radioligand Requirements	263
11.2.1	Binding Site Density and the Radioligand Binding Affinity	264
11.2.2	Molecular Descriptors of CNS Radioligands	265
11.3	Imaging of CB ₁ Receptors	267
11.3.1	Initial CB ₁ Radioligands and Imaging Studies	267
11.3.2	Current CB ₁ Receptor Radioligands for Human PET Imaging	272
11.3.3	PET Imaging of CB ₁	279
11.3.4	Current and Future Clinical Application in CB ₁ Receptor Imaging	292
11.4	Imaging of CB ₂	294
11.4.1	Development of CB ₂ Radioligands	295
11.4.2	CB ₂ Imaging Studies	298
11.4.3	Potential Clinical Application of CB ₂ Imaging	299

A.G. Horti (✉)

Division of Nuclear Medicine, Department of Radiology, Johns Hopkins School of Medicine, Baltimore, MD 21205, USA

e-mail: ahorti1@jhmi.edu

V. Raymont

Department of Medicine, Centre for Mental Health, Imperial College, London, UK

Division of Nuclear Medicine, Department of Radiology, Johns Hopkins School of Medicine, Baltimore, MD 21205, USA

G.E. Terry

Department of Psychiatry, Resnick Neuropsychiatric Hospital, University of California, Los Angeles, 740 Westwood Plaza, Room C8-193, Los Angeles, CA 90024-1759, USA

11.5 Imaging of FAAH	300
11.6 Future	303
Conclusion	303
References.....	304

Abstract

The endocannabinoid system consists of cannabinoid receptors (which mediate the actions of cannabis), their endogenous ligands (endocannabinoids), and the enzymes and proteins associated with their regulation. In brain, the endocannabinoid system functions to modulate the release of other neurotransmitters via the subtype 1 (CB₁) receptor. Abnormalities of CB₁ receptor expression or endocannabinoid transmission have been associated with several neuropsychiatric diseases. Subtype 2 (CB₂) receptors are found primarily on immune and neuroimmune cells and are overexpressed in states of inflammation and neuroinflammation. Both receptors are of particular interest for biomarker development and therapeutic targets. Growing evidence supports the regulation of endocannabinoids as involved in neuropsychiatric and neuroinflammatory diseases. However, the function of endocannabinoid system components *in vivo* remains difficult to assess. Therefore, the use of functional imaging techniques, such as positron emission tomography (PET), may be particularly useful in the assessment and quantification of the endocannabinoid system. This chapter will cover the current understanding of functional imaging that directly targets the endocannabinoid system.

Abbreviations

AAI	Aminoalkylindoles
AD	Alzheimer's disease
AChE	Acetylcholinesterase
AEA	N-arachidonylethanolamine, aka anandamide
2-AG	2-arachidonoyl glycerol
AIDS	Acquired immunodeficiency syndrome
ALS	Amyotrophic lateral sclerosis
AM404	An endocannabinoid transporter inhibitor
BBB	Blood-brain barrier
B _{max}	Binding maximum (i.e., total receptor density)
BP	Binding potential
cAMP	3'-5'-cyclic adenosine monophosphate
CB1	Cannabinoid subtype 1
CB2	Cannabinoid subtype 2
<i>CNR1</i>	Gene encoding cannabinoid subtype 1 receptor
<i>CNR2</i>	Gene encoding cannabinoid subtype 2 receptor
CNS	Central nervous system

CP-55,940	A nonclassical cannabinoid agonist
COX-2	Cyclooxygenase type 2
DAGL	Diacylglycerol lipase
D2	Dopamine subtype 2
EAE	Experimental autoimmune encephalomyelitis
ECS	Endocannabinoid system
FAAH	Fatty acid amide hydrolase
FUR	Fractional uptake ratio
GABA	Gamma-aminobutyric acid
GPCR	G protein-coupled receptor
GPR55	G protein-coupled receptor 55
GTP	Guanosine-5'-triphosphate
HD	Huntington's disease
HRRT	High-resolution research tomograph
ICC	Intraclass correlation coefficient
LTD	Long-term depression
LTP	Long-term potentiation
MAGL	Monoacylglycerol lipase
MDR1	Multidrug resistance gene 1 (encodes P-gp)
mRNA	Messenger ribonucleic acid
MS	Multiple sclerosis
NAPE-PLD	N-acyl-phosphatidylethanolamine-selective phospholipase D
PET	Positron emission tomography
P-gp	P-glycoprotein (an efflux transporter)
PSA	Polar surface area
SPECT	Single-photon emission computed tomography
SUV	Standardized uptake value
Δ^9 -THC	Δ^9 -tetrahydrocannabinol
TRPV1	Transient receptor potential vanilloid 1 (a cation channel)
TSPO	Translocator protein (18 kDa)
URB597	A FAAH inhibitor
V_T	Total distribution volume
WIN 55,212-2	An aminoalkylindole cannabinoid agonist

11.1 Introduction

11.1.1 Endocannabinoid System

Cannabis has been known to have medicinal and narcotic effects for thousands of years and is the most commonly used illegal drug in the world today (Copeland and Swift 2009).¹ However, it was not until 1964 that Δ^9 -tetrahydrocannabinol (Δ^9 -THC) was described by Gaoni and Mechoulam as the principal psychoactive

¹Except for limited legal permissions as in the Netherlands.

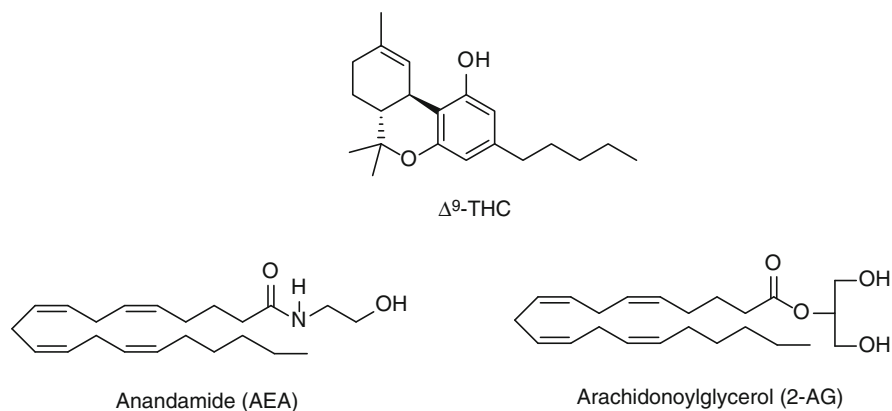


Fig. 11.1 Structure of Δ^9 -THC and the endocannabinoids, anandamide (AEA) and 2-arachidonoylglycerol (2-AG)

component of cannabis and hashish (Gaoni and Mechoulam 1964) (Fig. 11.1). Currently, tens of plant-derived cannabinoids have been discovered.

The effects of Δ^9 -THC are mediated by cannabinoid receptors. Cannabinoid receptors are seven-transmembrane domain proteins that mediate their intracellular action via guanosine-5'-triphosphate (GTP)-activated mechanisms and are thus classified as G protein-coupled receptors (GPCR). These cannabinoid receptors have subsequently been described as part of the endocannabinoid system (ECS), which also consists of endogenous ligands and their biochemical components required for synthesis, uptake, and degradation (Fig. 11.2). The endogenous cannabinoid system (ECS) is fundamental to physiology and has widespread influences on the human brain, immune system, and other organs. Abnormalities of this system have been implicated in many cognitive, neuropsychiatric, and metabolic disorders (Pacher et al. 2006). ECS is found in fish, reptiles, and all mammals, suggesting it is evolutionarily an ancient system (Elphick and Egertova 2005). It was not until the 1990s that the first of two GPCRs, the subtype 1 cannabinoid receptor (CB_1), was discovered and cloned (Devane et al. 1988; Matsuda et al. 1990) and was subsequently found to be responsible for the psychotropic effects of cannabinoids. In 1993, the discovery of a second cannabinoid receptor, the subtype 2 (CB_2), was reported (Munro et al. 1993). The cerebral CB_1 receptors are involved in inhibition of neurotransmitter release (Schlicker and Kathmann 2001), whereas CB_2 receptors participate in the regulation of cytokine release and function (Klein 2005).

CB_1 is abundantly expressed in the brain, with the highest density in the hippocampus, striatum, cerebral cortex, and the molecular layer of the cerebellum and with the lowest density in the brain stem, thalamus, and white matter (Glass et al. 1997; Herkenham et al. 1990, 1991; Howlett et al. 2002; Iversen 2003; Lynn and Herkenham 1994). CB_1 is also widely expressed in the gut, liver, and adipose tissue (Massa et al. 2005).

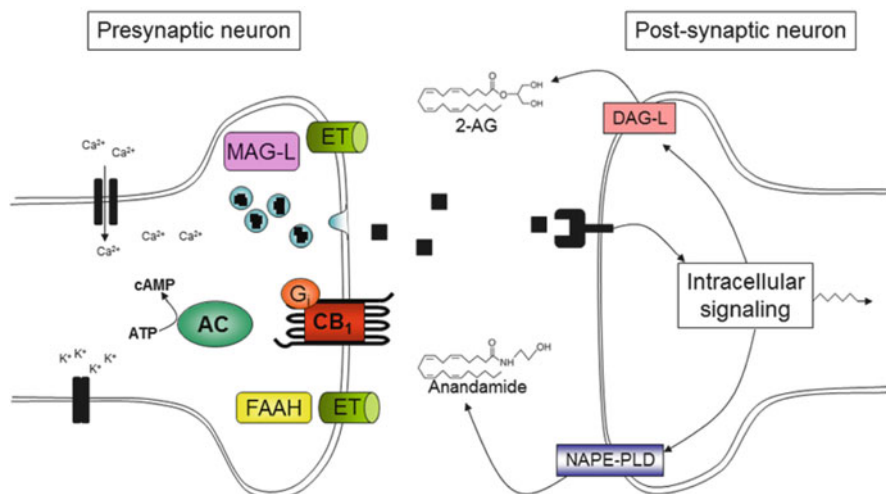


Fig. 11.2 Endocannabinoid system signaling (Reprinted from Terry (2009))

CB₂ is mostly found in the peripheral immune system (Howlett et al. 2002; Munro et al. 1993). They are typically in low density in the brain (Onaivi et al. 2006; Van Sickle et al. 2005), but are overexpressed during states of neuroinflammation on activated microglia (Howlett et al. 2002). In the periphery, they have high density in spleen and leukocytes, particularly B lymphocytes (Munro et al. 1993). Recent studies have demonstrated that cannabinoids engage with other receptors, some with no previously known endogenous ligand (known as orphan receptors), in orthosteric and allosteric interactions. These studies suggest that these receptors, such as GPR55 and transient receptor potential (TRP) vanilloid 1, are additional cannabinoid receptor subtypes (Pertwee et al. 2010).

The discovery of cannabinoid receptors prompted the search for their endogenous ligands, also called endocannabinoids, which could activate them. Endocannabinoids were discovered and are structurally a class of lipids, which include amides, esters, and ethers of long-chain polyunsaturated fatty acids. Anandamide (*N*-arachidonylethanolamine; AEA) and 2-arachidonoylglycerol (2-AG) (Fig. 11.1) are the main endogenous agonists of cannabinoid receptors and are able to mimic several pharmacological effects of Δ^9 -THC (Paradisi et al. 2006). Unlike classical neurotransmitters which are synthesized, stored in vesicles, and released upon signaling, endocannabinoids are synthesized by *N*-acyl-phosphatidylethanolamine phospholipase D (NAPE-PLD) and diacylglycerol (DAG) lipase “on demand” following Ca²⁺ elevation in the postsynaptic cell (Di Marzo et al. 2011; Marsicano et al. 2003). They subsequently diffuse across the synapse in a retrograde manner where they act on presynaptic CB₁ receptors, which in turn propagate second messenger signaling through G-stimulatory and G-inhibitory proteins, among other mechanisms. The resulting cascade of events leads to decreased cAMP production, closing of Ca²⁺ channels, and reduced

mobilization of neurotransmitter containing vesicles, and therefore an inhibition of neurotransmitter release (e.g., GABA, glutamate, dopamine). In addition to decreased calcium influx, the cell potential is further altered by opening of potassium channels (in part by G protein-coupled inward rectifying potassium channels, or GIRKs). Cellular functions may be additionally affected by activity changes of protein kinases (e.g., protein kinase A, mitogen-activated protein kinase) and enzymes involved in gene transcription. Regional differences in cannabinoid receptor effects are likely due to local endocannabinoid activity or tone and the particular protein coupling or second messenger signaling system with which a specific receptor interacts (also known as functional selectivity) (Varga et al. 2008). CB₂ receptors demonstrate somewhat less heterogeneity than CB₁ receptors and also demonstrate functional selectivity toward different endocannabinoids (Shoemaker et al. 2005).

Endocannabinoids undergo a degradation and reuptake process. Fatty acid amide hydrolase (FAAH) is primarily responsible for the breakdown of AEA, whereas the monoacylglycerol lipase (MAGL) plays a key role in the enzymatic hydrolysis of 2-AG (Dinh et al. 2002). Interestingly, cyclooxygenase 2 (COX-2) is among a number of other enzymes identified in endocannabinoid processing and forms prostacannabinoids which in turn can participate in cell signaling (Kozak et al. 2002). Indirect evidence supports the presence of an endocannabinoid transporter on postsynaptic membranes; however, no protein structure has been elucidated to confirm its existence (Felder et al. 2006; Fowler 2012). Acetaminophen (paracetamol), a widely used pain reliever which has long lacked an understood mechanism, is metabolized *in vivo* to *N*-(4-hydroxyphenyl)arachidonylethanolamide (AM404), an inhibitor of the putative endocannabinoid transporter and a compound known to reduce pain (Bertolini et al. 2006; Hogestatt et al. 2005; La Rana et al. 2006).

While this represents a rather straightforward model of the ECS, several other potential ligands and enzymes involved in cannabinoid receptor and endocannabinoid signaling have been identified, and their role in the ECS remains unclear. For example, endocannabinoids also bind to another class of receptors (transient receptor potential vanilloid type-1, TRPV1) (Di Marzo and De Petrocellis 2010), intracellular carriers of endocannabinoids (Kaczocha et al. 2009), and additional catabolic enzymes have been discovered (e.g., FAAH2) (Wei et al. 2006), and other endogenous compounds have been identified that have cannabinoid receptor antagonist qualities (Heimann et al. 2007) or have inhibitory properties for FAAH (Thors et al. 2010). As mentioned, GPCRs such as CB₁ and CB₂ receptors are associated with a variety of second messenger systems, such as G-stimulatory, G-inhibitory, IP₃, and GIRK channels. In addition, GPCRs have the ability to be in high-affinity states (protein-coupled and agonist-preferring), low-affinity states (protein uncoupled and inverse agonist preferring), and constitutively active (i.e., engaging in signal transduction without the binding of a ligand). However, due to the lipophilicity of endocannabinoids and their ability to travel within the plasma membrane, they may laterally translocate to the binding site; thus, the description of true inverse agonist activity of these receptors has been called into question in lieu of antagonist and/or partial agonist inhibition of baseline endocannabinoid activity. Finally, cannabinoid receptors are able to undergo heteromerization with other GPCRs. Thus,

the number of components in the endocannabinoid family is larger than initially thought, which adds to the complexity of this system.

11.1.2 Physiology of the Endocannabinoid System

The ECS plays an important modulating role in homeostasis, metabolism, and immunological reactions as well as motor functions, learning, and reward processing. In the brain, endocannabinoids mostly act on CB₁ receptors as retrograde messengers and modulate the neurotransmitters GABA-A, dopamine, glutamate, and opioids (Wilson and Nicoll 2002). Generally, increased or decreased endocannabinoid neurotransmission results in decreases or increases in neurotransmitter release, respectively (Iversen 2003), and additionally, changes in neurotransmitter function can modulate endocannabinoid signaling (Degroot and Nomikos 2007). By inhibiting excitatory or inhibitory signals, endocannabinoids facilitate long-term potentiation (LTP) or depression (LTD) between neurons both directly and indirectly, which enables the process of learning and memory formation (Di Marzo et al. 2004; Riedel and Davies 2005). The process of learning and memory formation likely depends on the timing and location of endocannabinoid release, which permits the extinction of previous memories (Chhatwal et al. 2005). Therefore, global stimulation of CB₁ receptors, as from cannabis, interrupts the local formation of LTP and LTD and delays learning and memory. CB₁ receptors are associated with a wide range of behaviors, including cognition, pain perception, movement, drug addiction, and memory consolidation. Stimulation of these receptors also has anti-inflammatory, antioxidant, and neuroprotective effects (Drysdale and Platt 2003), as well as a role in neuronal gene expression (Piomelli 2003) and endocrinological modulation (Cota et al. 2007). CB₁ receptor expression is affected by the estrous cycle in females (Rodriguez de Fonseca et al. 1994), suggesting its sensitivity to estrogen. As such, when examining the ECS, differences between males, females, and phases of the estrous cycle may need to be taken into consideration.

Less is known about the physiological role of CB₂ receptors. In the absence of inflammatory CNS disease, CB₂ receptors are not expressed in any significant amount in the human brain with the exception of the brain stem, where low concentrations can be found (Van Sickle et al. 2005). However, in inflammatory conditions such as cancer, atherosclerosis, peripheral inflammation, and several brain disorders, there is a marked upregulation of CB₂ receptors, which can be ten times that of basal levels (Cabral and Marciano-Cabral 2005; Maresz et al. 2005), primarily in activated microglia. Microglia are immune cells in the CNS which are activated by neuronal injury or infection. The activation of glial cells, in addition to excitotoxicity, mitochondrial failure, and oxidative stress, is a primary event in neuroinflammation, and CB₂ receptor activation has been shown to induce neuroprotective effects (Fernandez-Ruiz et al. 2007). The peripheral benzodiazepine receptor (PBR), recently renamed as translocator protein 18-kDa (TSPO) (Papadopoulos et al. 2006), is also found in activated microglia, and consequently TSPO antagonists have been proposed to prevent or attenuate disease progression (Kim et al. 2006;

Yiangou et al. 2006). Whether CB₂ receptors and TSPO are expressed by the same mechanism during inflammation is not clear; however, they may be considered as independent biomarkers of neuroinflammatory processes.

In neurodegenerative brain disorders, CB₂ receptor upregulation was noted post-mortem in microglia surrounding and coincident with the beta-amyloid plaques of patients with Alzheimer's disease (Benito et al. 2003) and related to the extent and progression of neuronal loss in Huntington's disease (Sapp et al. 2001). CB₂ agonists have been found to stimulate human macrophages to remove beta-amyloid in *in vitro* studies, thereby suggesting a potential therapeutic approach in AD treatment (Tolon et al. 2009).

Even though CB₂ receptor upregulation is most commonly linked to inflammatory conditions, the exact role of CB₂ receptors in other conditions is still unclear. In peripheral tissues, CB₂ receptors have been implicated in mediating pain transmission (i.e., nociception) and in the function and communication of immune cells (e.g., mediating cytokine release). CB₂ receptor agonists have been shown to have analgesic effects and decrease lymphocyte function (Cencioni et al. 2010; Hsieh et al. 2011). In brain cancers, CB₂ receptor expression has been found to correlate with the stage of tumor malignancy (Calatuzzolo et al. 2007; Ellert-Miklaszewska et al. 2007). The CB₂ receptor is also expressed in normal skin and skin tumors of mice and humans and involved in both the proliferation of skin tumor cells following inflammation and induction of their apoptosis (Casanova et al. 2003; Zheng et al. 2008). Treatment with CB₂ agonists has resulted in a reduction of both tumor growth and occurrence of metastasis (Qamri et al. 2009).

As FAAH is highly involved in controlling the concentration of endocannabinoids, it has a key role in determining endocannabinoid tone. In brain, FAAH expression is somewhat different from that of CB₁ with regard to distribution and density. Genetic knockout or pharmacologic blockade of FAAH has been shown to reduce anxiety and depression in animal models (Moreira et al. 2008). As mentioned with CB₂ receptors, FAAH overexpression has been associated with neuritic plaques in Alzheimer's disease. Similar to the influence of estrogen on CB₁ receptor expression, the gene encoding FAAH, *FAAH*, contains an estrogen binding site on the promoter region (Waleh et al. 2002), again suggesting sex differences in the ECS.

11.1.3 Pharmacology of Cannabinoids

Cannabis has been consumed in its natural form for 3,000 years and has been utilized as an analgesic, appetite stimulant, anti-inflammatory, and decongestant (Booth 2005). Historically, many pharmacists tried to purify the active ingredient, but its lipophilic nature made it difficult to isolate until twentieth-century techniques allowed Δ^9 -THC to be identified. The ECS is vital to learning, memory, motor behavior, and pain and weight control, as well as inflammation, gut motility, and intracellular apoptosis. Thus, cannabinoid drugs are being used or have potential for use in treating multiple pathologies, including schizophrenia, obesity, anorexia (in

AIDS and cachexia secondary to cancer), emesis, pain, inflammation, multiple sclerosis, neurodegenerative disorders, epilepsy, stroke, glaucoma, osteoporosis, cardiovascular disorders, and cancer (Di Marzo et al. 2004; Howlett 1995; Kogan and Mechoulam 2007; Pertwee 1999; Timpone et al. 1997).

Despite the potential therapeutic value of the cannabinoid agonist Δ^9 -THC and its analogs, side effects have been a problem and the potential for abuse has been a concern (Howlett 1995, 2002; Howlett et al. 2002; Murray et al. 2007), although it has become apparent that adverse effects may be reduced by developing subtype-selective drugs (Hertzog 2004). At the present time, there are only two cannabinoid agonists on the market in the United States, dronabinol (Marinol, Δ^9 -THC) and nabilone (Cesamet, a THC synthetic analog), for treatment of nausea, vomiting, and appetite stimulation in cancer and AIDS. Nabiximols (Sativex®), a Δ^9 -THC and cannabidiol mixture is available in some EU countries and Canada, for treatment of multiple sclerosis.

The first clinically useful selective CB₁ inverse agonist, rimonabant, has been used as an antiobesity medication and was investigated for use in alcohol and tobacco addiction (Cahill and Ussher 2007; Despres et al. 2009; Nissen et al. 2008; Pi-Sunyer et al. 2006; Rosenstock et al. 2008; Soyka et al. 2008; Van Gaal et al. 2005). In addition to its central mechanism by decreasing appetite, rimonabant mediated improvements in peripheral comorbidities of obesity, including increased HDL, decreased triglyceride levels, and decreased hemoglobin A1c (Van Gaal et al. 2005). Later, rimonabant was withdrawn from the market due to its central side effects of depression and anxiety. CB₁ inverse agonists that act predominantly peripherally (thus avoiding psychiatric side effects (Cluny et al. 2010)) are under preclinical investigation. An FAAH inhibitor (URB597) is also under preclinical investigation to target anxiety disorders (Piomelli et al. 2006).

11.1.4 Endocannabinoid System-Related Pathologies

11.1.4.1 Eating Disorders

There is overwhelming evidence that the ECS plays a central role in the control of food intake and in eating disorders (Cooper 2004; Di Marzo et al. 2001; Maresz et al. 2007; Morton et al. 2006). The administration of cannabinoid CB₁ receptor agonists can promote body weight gain (Cota et al. 2003; Vickers and Kennett 2005), and CB₁ receptor agonists have been used as eating stimulants in AIDS and cancer patients (Croxford 2003). Conversely, antagonists or inverse agonists are associated with long-term weight loss (Smith and Fathi 2005; Vickers and Kennett 2005). Mechanism-of-action studies have shown that the effect of inverse agonists is likely caused by a combination of central effects (e.g., reduction in food intake) (Nogueiras et al. 2008) and peripheral effects (increased resting energy expenditure and fat oxidation) (Addy et al. 2008; Jbilo et al. 2005). In addition, different alleles of the gene encoding the CB₁ receptor (*CNRI*) and FAAH (*FAAH*) have been associated with anorexia nervosa (Monteleone et al. 2009; Siegfried et al. 2004) and obesity (Benzinou et al. 2008; Sipe et al. 2005). The highly selective CB₁ inverse

agonist SR-141716 (rimonabant) was developed by Sanofi-Aventis in the European Union to treat obesity (Rinaldi-Carmona et al. 1994) and has been found to improve lipid and glucose metabolism in obese humans. However, shortly after its introduction to the market, the safety of rimonabant was called into question due to the side effects that included severe depression and suicidal thoughts (Kelly et al. 2011; Le Foll et al. 2009; Lee et al. 2009). After the collection of additional clinical data, and preclinical results with taranabant (another inverse agonist developed by Merck) showing similar side effects, rimonabant was withdrawn from the market and further development of centrally acting CB₁ inverse agonists were largely abandoned (Le Foll et al. 2009). Due to the structural dissimilarity of taranabant from rimonabant, and preclinical data from animal studies, the adverse effects are thought to be mechanism dependent and not merely compound-specific effects.

11.1.4.2 Drug Addiction

Multiple preclinical and clinical studies have suggested that CB₁ antagonists could be used as treatments for multiple types of drug dependence (Le Foll and Goldberg 2005). Cannabis itself has the highest level of abuse, after alcohol and nicotine (Compton et al. 2005). Postmortem studies have shown that the density of CB₁ mRNA-positive neurons is significantly lower in long-term cannabis users in the striatum, nucleus accumbens, and hippocampal regions (Villares 2007). Rimonabant blocks effects induced by Δ^9 -THC in humans and has been found to increase smoking cessation (Cahill and Ussher 2007; Huestis et al. 2001; Soyka et al. 2008). Although animal studies suggested rimonabant would be a useful agent for treating alcohol dependence, the results in clinical trials were thus far negative (George et al. 2010; Soyka et al. 2008). In animal models using both pharmacologic and genetic knockout methods, rimonabant decreases the reward effects of opiates and alcohol and reduces cocaine-seeking behavior (Le Foll and Goldberg 2005). The ECS is central in the brain's reward circuitry and interacts with the opioid and dopamine system circuitry and thus plays a role in other addictions (Caille et al. 2007; Economidou et al. 2006; Gonzalez et al. 2004; Hungund and Basavarajappa 2004; Moranta et al. 2006; Nowak et al. 2006). In both *CNR1* and *FAAH*, genetic polymorphism has been associated with increased risk of alcohol or drug use (Hutchison et al. 2008; Sipe et al. 2002; Zhang et al. 2004).

11.1.4.3 Schizophrenia

Cannabis has long been associated with schizophrenia, and a genetic susceptibility has been found in subjects who develop psychotic symptoms after cannabis use (Caspi et al. 2005; Ho et al. 2011). In addition, large epidemiological studies have suggested an overall increased risk for developing schizophrenia after cannabis use (Fernandez-Espejo et al. 2009; Malone et al. 2010). In schizophrenia, hyperactivity of dopamine neurotransmission in the mesencephalic projections to the nucleus accumbens appears to contribute to the psychotic (positive) symptoms and hypodopaminergic and hypoglutamatergic transmission in the prefrontal cortex to the negative symptoms (van der Stelt and Di Marzo 2003). These transmitters are under CB₁ receptor signaling control, and hyperactivity of the central ECS has been shown to

be involved in the pathogenesis of schizophrenia and its symptoms (Dean et al. 2001; Laviolette and Grace 2006; Ujike and Morita 2004; Vinod and Hungund 2006b; Zavitsanou et al. 2004). Postmortem data has shown a significant increase in CB₁ receptor binding in the frontal and cingulate cortex of subjects with schizophrenia (Dean et al. 2001) and has also been reported to be increased by up to 25 % in the posterior cingulum (Newell et al. 2006). Other studies have shown a decrease in CB₁ receptor mRNA and protein by nearly 15 and 12 %, respectively (Eggen et al. 2008). Antipsychotics have been shown to affect CB₁ receptor expression (Secher et al. 2010), and patients with significant lifetime antipsychotic exposure could confound postmortem studies, and in vivo imaging studies would be of great assistance in distinguishing the changes in receptor expression due to disease versus medication. Finally, genetic studies have reported an association between the CB₁ receptor encoding gene, *CNR1*, and schizophrenia, especially the hebephrenic type (Ujike et al. 2002); individuals with a 9-repeat allele of an AAT-repeat polymorphism of the gene have a 2.3-fold higher susceptibility to schizophrenia (Leroy et al. 2001). Since increasing evidence from the anatomical, pharmacological, and behavioral studies points to functional interactions between the cannabinoid and dopamine receptor systems (Laviolette and Grace 2006), this could be a key to the development of innovative therapy for psychotic illnesses (Ujike and Morita 2004).

11.1.4.4 Mood and Anxiety Disorders

Cannabinoid agonists demonstrate mood-altering effects (Degenhardt et al. 2003). The location of CB₁ receptors in limbic and cerebral cortex suggests that they are involved in mood dysfunction, and endocannabinoid stimulation does indeed have anxiolytic and antidepressant effects in animals (Gobbi et al. 2005). Inhibitors of FAAH are a hopeful and novel target for anxiety and depression, suggesting that enhancement of local endocannabinoid tone is preferred to exogenous cannabinoid agonists, which are potentially anxiogenic as well as anxiolytic (Moreira and Wotjak 2010). While the effect of cannabinoid agonists on depression is unclear, inverse agonists have been shown to increase depression and suicidal thoughts (as previously discussed). Several genetic polymorphisms have been identified in association with mood and anxiety disorders and likely cause alterations to endocannabinoid signaling (Hillard et al. 2011). Genetic and postmortem studies have implicated the ECS in depression and suicide, and CB₁ receptors have been found to be upregulated in suicide victims (Vinod and Hungund 2006a).

11.1.4.5 Multiple Sclerosis

In multiple sclerosis, meta-analyses have supported the beneficial effect of cannabinoid agonists as treatment for neuropathic pain (Iskedjian et al. 2007; Rog et al. 2005) and muscle spasticity (Pryce and Baker 2007). In multiple sclerosis, there is selective CB₁ receptor overexpression on various glial cells, and CB₂ receptor-positive microglia are located within active plaques and in the periphery of chronic active plaques, supporting a role for the ECS (Benito et al. 2007; Bifulco et al. 2007). Treatment of multiple sclerosis with cannabinoids appears to be based on two mechanisms: (1) reducing excitotoxicity by CB₁ receptors on glia and neurons

and (2) reducing inflammation by CB₂ receptors on microglia (Rossi et al. 2010). Nabiximols is a sublingual spray developed by GW Pharmaceuticals for the treatment of multiple sclerosis using a proprietary blend of a Δ^9 -THC and cannabidiol, which show differing affinities for CB₁ and CB₂ receptors, as well as other targets.

Experimental autoimmune encephalomyelitis (EAE) is a commonly used animal model for multiple sclerosis (MS). Ten days after EAE induction in mice, CB₂ receptor gene (*CNR2*) mRNA was tenfold higher in activated microglia compared to microglia in a resting state. In total brain, *CNR2* mRNA was upregulated 100-fold (Maresz et al. 2005). In humans, CB₂-expressing microglial cell staining was observed in spinal cord and brain sections of patients with MS and amyotrophic lateral sclerosis (Palazuelos et al. 2008; Yiangou et al. 2006). CB₂ receptor-positive microglial cells were homogeneously distributed within active MS plaques, but found only in the periphery of chronic active plaques (Benito et al. 2007). Therefore, CB₂ receptor imaging may be useful to identify MS plaques of the active type.

11.1.4.6 Pain

Cannabinoids are antinociceptive in several types of animal models, acute tissue injury and nerve-injury-induced nociception, and play a role in transmission, processing, perception, and modulation of pain (Anand et al. 2009; Hohmann and Suplita 2006). Cannabinoid agonists and endocannabinoids act on CB₁ receptors in the brain, dorsal root ganglia, and peripheral nerves (Pacher et al. 2006). Activation of CB₂ receptors has been shown to reduce inflammatory pain (see above, Multiple Sclerosis). In addition, anti-inflammatory and analgesic medications affect proteins involved in lowering endocannabinoid levels (e.g., COX-2, endocannabinoid transporter) and act synergistically with cannabinoid agonists in animal studies (Guindon et al. 2006). Interestingly, cannabidiol which behaves as a cannabinoid antagonist has shown anti-inflammatory properties as well (Booz 2011). In humans, the mechanism of cannabinoid receptor-mediated analgesia is less clear. The exact mechanism of pain suppression is unknown, but synergistic actions and interactions with the endogenous opioid system have been reported (Corchero et al. 2004), and the ECS modulates the actions of cytokines and glucocorticoids (Hill and McEwen 2009), which play important roles in inflammation. In female migraine patients, platelets have been observed to have an increased rate of endocannabinoid metabolism, suggesting a decreased endocannabinoid tone in patients suffering from migraine headaches (Cupini et al. 2006). In addition, TRPV1 receptors are directly linked to pain transmission and are affected by the ECS. Thus, the modulation of pain by the endocannabinoid system is likely a mixed interplay between central and peripheral mechanisms, CB₁, CB₂, and TRPV1 receptors, and signal propagation to other neurotransmitter systems.

11.1.4.7 Parkinson's Disease

Several studies have reported neuroprotective effects of cannabinoids in glutamatergic excitotoxicity, oxidative damage, traumatic injury, ischemia, and neurodegeneration models (Paradisi et al. 2006; Sarne and Mechoulam 2005). CB₁ receptors are densely located in the basal ganglia, and the ECS has a modulatory effect on excitation and inhibition, as evident in movement disorders. Parkinson's disease

leads to a decrease in voluntary movements, secondary to insufficient striatal dopamine, causing a subsequent increase in GABA-ergic activity (Pacher et al. 2006). Early on CB₁ receptor density is reduced, but later the density is increased to compensate for the subsequent overexcitation of GABA (Orgado et al. 2009). mRNA expression of CB₁ is changed and an increased binding capacity has been observed in postmortem tissue of subjects with Parkinson's disease (Lastres-Becker et al. 2001). It is hypothesized that alterations of endocannabinoid synthesis stimulate increased dopamine release (Giuffrida et al. 1999), and cannabinoids inhibit the excitotoxic glutamate release and counteract oxidative stress to dopaminergic neurons which is responsible for nigrostriatal damage (Levenes et al. 1998). Deficiency in endocannabinoid transmission is thought to contribute to late-stage dyskinesias. Thus, modulation of CB₁-mediated basal ganglia transmission can be used to suppress or prevent the development of these complications (Di Marzo et al. 2000; Fox et al. 2002; Segovia et al. 2003; Sevcik and Masek 2000; Sieradzan et al. 2001); however, the results to date have been mixed (Carroll et al. 2004).

11.1.4.8 Huntington's Disease

Huntington's disease (HD) is caused by a trinucleotide repeat expansion on the *HTT* gene, leading to a polyglutamine tail of the Huntington protein. Although the normal physiologic function of the protein remains unclear, this pathological variant has been shown to cause disruptions in nuclear transcription factors, presumably leading to a decrease in normal expression of certain proteins. The pathological characteristic is progressive neuronal loss, preferentially affecting the caudate nucleus, resulting in motor (choreiform movements), cognitive (early onset dementia), and psychiatric symptoms (behavioral changes, e.g., disinhibition, aggression). One of the earliest neurochemical alterations in HD is the loss of CB₁ receptors in the basal ganglia (Glass et al. 2000), which occurs before the D₁/D₂ receptor dopaminergic dysfunction and characteristic choreic motor dysfunction. In animal models, the ECS is hypofunctional (Lastres-Becker et al. 2003). A Huntington/CB₁ double-knockout mouse model demonstrated that endocannabinoid signaling was essential to the neuropathologic symptoms and that CB₁ receptor loss may sensitize cells to additional excitotoxic damage (Blazquez et al. 2011). It has been suggested that CB₁ agonists may delay development of this disease (Glass et al. 2004; Lastres-Becker et al. 2003), and at least one clinical study has shown that they improve neuropsychiatric symptoms (Curtis et al. 2009).

In HD, there is also selective loss of spinal neurons and the appearance of activated microglia in striatum, cortex, and white matter. The number of activated microglia in the striatum and cortex has been shown to correlate with the extent and progression of neuronal loss (Sapp et al. 2001), and CB₂ agonists show neuroprotective effects in an HD animal model (Paldy et al. 2008; Sagredo et al. 2009). In this way, CB₂ receptor imaging may be useful in monitoring the progression of neuronal loss in HD.

11.1.4.9 Epilepsy

In epilepsy, an uncontrolled excitatory signal causes an epileptic seizure. Endocannabinoid-mediated self-inhibition reduces excitability of neocortical

interneurons (Bacci et al. 2004). The CB₁ receptor acts as an important endogenous locus of epileptic seizure modulation (Wallace et al. 2002), and endocannabinoids block status epilepticus in hippocampal neurons (Deshpande et al. 2007). There is evidence of a compensatory upregulation of CB₁ receptors in epilepsy (Chen et al. 2003; Wallace et al. 2003). Both animal and human clinical studies have shown mixed results on the use of cannabinoid agents for seizure depending on model, pathology, and the dose of the agent. This is likely due to the complex interplay of multiple actions of cannabinoid receptors and their dual association with excitatory and inhibitory neurotransmitters.

11.1.4.10 Alzheimer's Disease

CB₁ and CB₂ receptors and FAAH have been found to be co-localized with amyloid plaques in Alzheimer's disease (AD). CB₂-selective agonists were shown to block amyloid-induced activation of cultured microglial cells (Ramirez et al. 2005) and would presumably decrease neuroinflammation in AD. In postmortem studies, [¹²⁵I]SD7015, a CB₁-selective ligand, has demonstrated an inverse correlation of CB₁ receptor density and Braak tau pathology staging (Farkas et al. 2012), suggesting a novel *in vivo* method of staging AD progression. Independent of cannabinoid receptor activation, Δ⁹-THC competitively inhibits acetylcholinesterase (AChE) and prevents AChE-induced amyloid beta-peptide aggregation (Eubanks et al. 2006). Study of CB₁ and CB₂ receptors in correlation with amyloid load could lead to new treatment options for AD.

11.1.4.11 Amyotrophic Lateral Sclerosis

Amyotrophic lateral sclerosis (ALS) is a rapidly progressing neurodegenerative disease accelerated by neuroinflammation. CB₂ receptors are dramatically upregulated in the spinal cords of mice with ALS, and CB₂ agonists have been shown to slow motor neuron degeneration (Shoemaker et al. 2007). Animal models have demonstrated that increased endocannabinoid tone delays disease progression (Kim et al. 2006), though the limited clinical data available to date has not shown cannabinoid agonists to be helpful in ongoing disease. Nevertheless, the potential for ECS to affect neuroinflammatory and glutamate-mediated processes in ALS, along with the sparse number of therapeutics available, should prompt additional investigation.

11.1.4.12 Stroke

CB₂ receptor-positive cells occur in the brain within minutes following stroke (Ashton et al. 2007), and CB₁ receptor expression is increased in the ischemic zone (Jin et al. 2000). In a CB₁ receptor knockout mouse model of stroke, mortality was increased and infarct size and ischemia were more severe compared to wild-type mice (Parmentier-Batteur et al. 2002). This suggests that endogenous cannabinoid signaling pathways may protect against additional anoxic and inflammatory injury following ischemic stroke.

11.1.4.13 Non-CNS Applications

Cannabinoid drugs have recently also become candidates for peripheral inflammatory and degenerative disorders such as atherosclerosis (Steffens et al. 2005) and in

the field of oncology (Herrera et al. 2005). For example, CB₂ receptors have been shown to be involved in the apoptotic pathway in certain tumor cell lines and have correlated with certain brain tumor grades (Ellert-Miklaszewska et al. 2007). In tissues with normally low receptor expression, there may be a >1,000-fold increase in receptor density in the presence of certain tumor types (Oesch et al. 2009). Finally, CB₁ and CB₂ receptors are upregulated in liver fibrosis as a consequence of cirrhosis (Teixeira-Clerc et al. 2008; Wasmuth and Trautwein 2007).

11.1.5 Role of PET and SPECT in Cannabinoid Receptor Research

Until recently, only *in vitro*, animal model, electrophysiological, behavioral, and postmortem data existed on the ECS. However, there is a need for direct functional measurement in human subjects given the differences between species (Howlett et al. 2002; Pertwee et al. 2010). There are several important applications of functional imaging of the central CB₁ receptor using PET and SPECT (Horti and Van Laere 2008; Van Laere 2007). They have a role in planning drug therapy using inverse agonists or antagonists. Quantitative information about the receptor occupancy can be obtained after a titration of individual doses and existing radioligands. They also allow for the investigation of CNS side effects, which are frequent problems, particularly with CB₁ receptor blockade. PET or SPECT imaging allows information from preclinical models to be tested in humans and may also lead to the development of novel diagnostic biomarkers where marked regional up- or down-regulation is present. These imaging techniques can be used to examine the interactions of the ECS with other neurotransmitter systems (e.g., GABA-A, dopamine, and opioid systems). Functional imaging could provide quantitative measurements of endocannabinoid release and allow study of its effects in pathological and cognitive states. However, more data is needed on the sensitivity of existing cannabinoid ligands to displacement by endocannabinoids.

Multiple efforts have been undertaken to probe the ECS through imaging. Methods such as [¹⁵O]H₂O or [¹⁸F]FDG PET, or fMRI do not directly probe the ECS, though they have provided information regarding the effects of cannabinoids on the brain and behavior. While the results are often intriguing, they are outside the scope of this chapter and have been described elsewhere (Martin-Santos et al. 2010).

11.2 PET Radioligand Requirements

PET radioligands for quantification of cerebral receptors must possess a variety of imaging properties such as a high specific signal that is linked to optimally high binding affinity and low nonspecific binding and high receptor selectivity. Adequate permeability of the blood-brain barrier and favorable blood-brain distribution, rapid clearance from the blood, appropriate brain kinetics, and absence of active radiometabolites are also among the crucial imaging properties of cerebral PET

radioligands. The most important physical-chemical characteristics of the cerebral radioligands are binding affinity, lipophilicity, and polar surface area, but a number of other molecular descriptors including molecular weight, number of hydrogen donors and hydrogen acceptors, molecule shape, molar volume, and the number of freely rotatable bonds must be taken into account. There is certain serendipity in development of novel PET radioligands because relationships of some physical-chemical properties with imaging properties are still not fully understood.

In addition to the abovementioned properties, the radioligands must be safe for human use. Important safety requirements are a low radiation burden and low toxicity.

The manufacturing process of a good PET radioligand must yield a sufficient dose of the final radiolabeled drug product, with high radiochemical and chemical purity with high specific radioactivity and formulated as a sterile and apyrogenic solution in saline. Because most PET radionuclides exhibit a short half-life, the radiosynthesis process must be rapid, simple, and automated.

When all the requirements for PET radioligands are considered, it becomes obvious that development of new radioligands is a challenge. Since the invention of PET in 1975 less than 40 cerebral binding sites have been successfully quantified by PET in human subjects. Development of every novel PET radioligand for study of the human brain is an exciting event in the field of nuclear medicine and neuroscience.

11.2.1 Binding Site Density and the Radioligand Binding Affinity

An advantage of PET is its quantitative ability, and one of the main quantitative measures is known as binding potential. Binding potential (BP) is proportional to the density of receptor binding sites (B_{\max}) and inversely proportional to the K_i value of the radioligand ($1/K_i$ =binding affinity). The cerebral receptors with a greater value of B_{\max} exhibit greater BP values than those of the receptors with low B_{\max} . Obviously, the binding affinity of a cerebral radioligand has to be optimally high in order to gather sufficiently quantitative data. Another quantitative measure of PET is distribution volume (V_T), which is calculated using pharmacokinetic and mathematic modeling, and is also proportional to B_{\max} . Prior to recent standardization, terms to define variables and endpoints from multi-compartment models have been varied and, often, confusing (Innis et al. 2007). Organ uptake of radioactivity is generally referred to standardized uptake value (SUV or %SUV), which corrects only for injected radioactivity and total body weight. Previous terms such as V_3 , V'' , and distribution volume ratio (DVR) have referred to estimates that were expected to represent receptor density. It is also essential to keep in mind that CNS radioligands with binding affinities that are too high can demonstrate slow or even seemingly irreversible brain kinetics that may complicate quantification of the receptor. Additionally, radioligands must demonstrate sufficient specific signal, and thus have low affinity for other nontarget

Table 11.1 Molecular descriptors of successful PET radioligands ($n=23$) for imaging of brain binding sites in humans (Horti AG, 2011, unpublished results)

Molecular property	Range	Mean \pm SD
Molecular weight (Da)	157–490	319 \pm 87
Lipophilicity, $c\log D_{7.4}$	–1.65 to 6.00	2.1 \pm 1.8
PSA (\AA^2)	23–84	47 \pm 19

receptors or proteins, and low nonspecific binding to proteins, lipids, or extracellular matrix (see Sect. 11.3.3.1 for more detailed discussion). Because the two subtypes of cannabinoid receptors, CB_1 and CB_2 , exhibit very different density and regional distribution, the binding affinity requirements for these subtypes are also different. The CB_1 receptor subtype is found in remarkably high expression in the various brain regions (Howlett et al. 2002). The CB_2 subtype is mainly found in peripheral nervous system and its expression in the brain is low, although it is substantially greater in states of neuroinflammation (see Sect. 11.4 for details).

Estimation of required binding affinities using a conventional approach (Eckelman et al. 1979) suggests that a successful CB_1 receptor PET radioligand should exhibit a moderately high binding affinity with a low nanomolar value of K_i or even lower. B_{\max} data for the CB_2 subtype in normal mammalian brain tissue and during neuroinflammation are not available yet, but expression of *CNR1* gene transcripts in the normal mouse brain stem is 100 times of the *CNR2* gene expression (Onaivi et al. 2006). These results make us to believe that a good CB_2 receptor radioligand for PET should exhibit very high binding affinities with K_i values in the picomolar range.

11.2.2 Molecular Descriptors of CNS Radioligands

A common molecular descriptor of CNS drugs that is also important for CNS radiotracers is molecular weight (MW). The classic Lipinski “rule-of-5” that proposes an upper limit of MW of 500 as acceptable for orally absorbed drugs seems to be valid for the majority of successful PET radiotracers for brain imaging that are administered intravenously in humans (Table 11.1).

Lipophilicity ($\log D_{7.4}$) and polar surface area (PSA) (Table 11.1) are linked to the vital properties of cerebral PET radioligands: passive transport through the blood-brain barrier (BBB), blood-brain partitioning, and nonspecific binding. It is conventionally agreed that most good CNS PET radioligands with reasonable BBB permeability and minimal nonspecific binding should exhibit $\log D_{7.4}=0 - 4$. Radioligands with a low value of $\log D_{7.4}$ are likely to exhibit a low BBB permeability, whereas very lipophilic compounds bind to plasma proteins and produce a low concentration of free radioligand in the blood and, correspondingly, show poor permeability through the BBB. Nonspecific binding of PET radioligands is greater for

lipophilic compounds. Lipophilicity values of PET radioligands should be minimal and within the optimal range for BBB permeability.

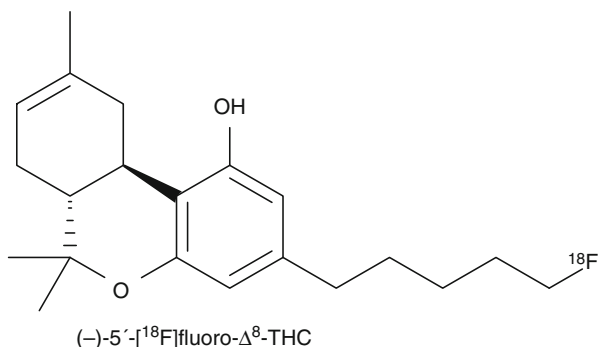
The high lipophilicity of most cannabinoids and cannabinomimetic ligands ($\log D_{7.4} \gg 4$) remains a main concern of medicinal radiochemists who are involved in the development of CB₁ and CB₂ PET radioligands. A number of high-affinity-labeled cannabinoids demonstrated poor imaging properties due to their high lipophilicity. Development of high-affinity cannabinoids with reduced lipophilicities represents a difficult undertaking (Katoch-Rouse et al. 2003). The most CB₁ and CB₂ radiotracers shown below that were developed in the last few years exhibit relatively high lipophilicity values ($c\log D_{7.4} = 3.3\text{--}6.0$).

PSA is used for characterization of the transport and partitioning properties of cerebral drugs and radiotracers. PSA embodies an optimal combination of H-bonding, molecular polarity, and solubility. A common measure of brain-blood distribution ($\log BB$) can be calculated as a simple function of lipophilicity and PSA. The great majority of CNS drugs exhibit a PSA value of $<70 \text{ \AA}^2$ (Ertl 2008). Calculation of PSA for all currently available PET radioligands for CNS receptor imaging in humans suggests a window of opportunity $PSA < 84 \text{ \AA}^2$ (Table 11.1) (Horti AG, 2011, unpublished results). It is likely that successful CB₁ and CB₂ radioligands for PET imaging should display the molecular property range that is shown in Table 11.1.

An additional component to the BBB is the presence of efflux transporters, which prevent entry and/or eject substrates from the brain (Pike 2009). In particular, permeability glycoprotein (P-gp)-mediated efflux has proven to be a burden to CNS drug and radiotracer development. Δ^9 -THC and several other cannabinoid ligands are partial substrates for this particular transporter (Bonhomme-Faivre et al. 2008). P-gp is normally expressed at the BBB and blood-testes barrier to protect these sensitive tissues from potentially harmful compounds and is sometimes overexpressed on cancer cells, causing multidrug resistance (hence, the gene name, *MDR1*) (Ambudkar et al. 2003). As a result, compounds that act as substrates for P-gp are prevented from entering and accumulating in the brain; many CNS drug and radiotracer candidates have been abandoned due to this limitation.

An ideal CNS radioligand is found only in its parent form after entering the brain. Metabolites that retain the radiolabel and either remain in or re-enter the brain will be registered as additional signal by the PET camera. Thus, unless these radiometabolites are accounted for in the pharmacokinetic modeling, they may be erroneously interpreted as parent compound in brain. Attempts to model these confounding radiometabolites are often complicated and may require additional blood measurements. It is thus preferred that a radioligand's primary radioactive metabolite is polar enough to prevent it from entering the brain. A notable exception is that of fluorinated radioligands, which if metabolized to free fluoride could cause substantial radioactive uptake in bone to the extent that its resulting image will "spill over" into neighboring brain tissue due to signal artifact. Therefore, efforts should be made to prevent or reduce the susceptibility of radioligands to defluorination.

Fig. 11.3 Structure of (-)-5'-[¹⁸F]- Δ^8 -THC, the first cannabinoid PET radioligand



11.3 Imaging of CB₁ Receptors

Radioligands that have been developed for imaging CB₁ receptors may be broadly categorized as first- and second-generation compounds. As discussed, first-generation compounds were limited by their low specific binding and poor brain uptake. Second-generation compounds achieved success largely by retaining a high binding affinity with more moderate lipophilicity. Pharmacokinetic modeling of these radioligands is challenging; however, these compounds have been used in numerous clinical investigations.

11.3.1 Initial CB₁ Radioligands and Imaging Studies

11.3.1.1 (-)-5'-[¹⁸F]- Δ^8 -THC

The starting point in the development of CB₁ receptor PET radioligands was established when a ¹⁸F-derivative of Δ^8 -THC (Fig. 11.3), one of the active constituents of marijuana, was synthesized in 1991 (Charalambous et al. 1991). The radioligand was studied in mice and baboons. The mouse study demonstrated some initial brain uptake of (-)-5'-[¹⁸F]- Δ^8 -THC (1 % ID/g tissue, 5 min) with rapid clearance. The clearance of radioactivity from the baboon brain was also rapid and no specific binding was observed. The relatively low binding affinity of the radioligand ($K_i=57$ nM) (Compton et al. 1993), its potentially P-gp-mediated efflux (Bonhomme-Faivre et al. 2008), and, most importantly, its high lipophilicity ($clogD_{7.4}=6.9$) are the likely factors behind the discouraging imaging results.

11.3.1.2 Radiolabeled CB₁ Antagonists, Derivatives of SR141716 (Rimonabant)

In 1994 the discovery of rimonabant, a highly selective and potent CB₁ receptor antagonist, by Sanofi-Aventis (Rinaldi-Carmona et al. 1994) stimulated progress in development of PET and SPECT radioligands for imaging CB₁ receptors. Several research groups synthesized many analogs of rimonabant and radiolabeled, some of them for emission tomography studies (Gatley et al. 1996; Gatley et al. 1998;

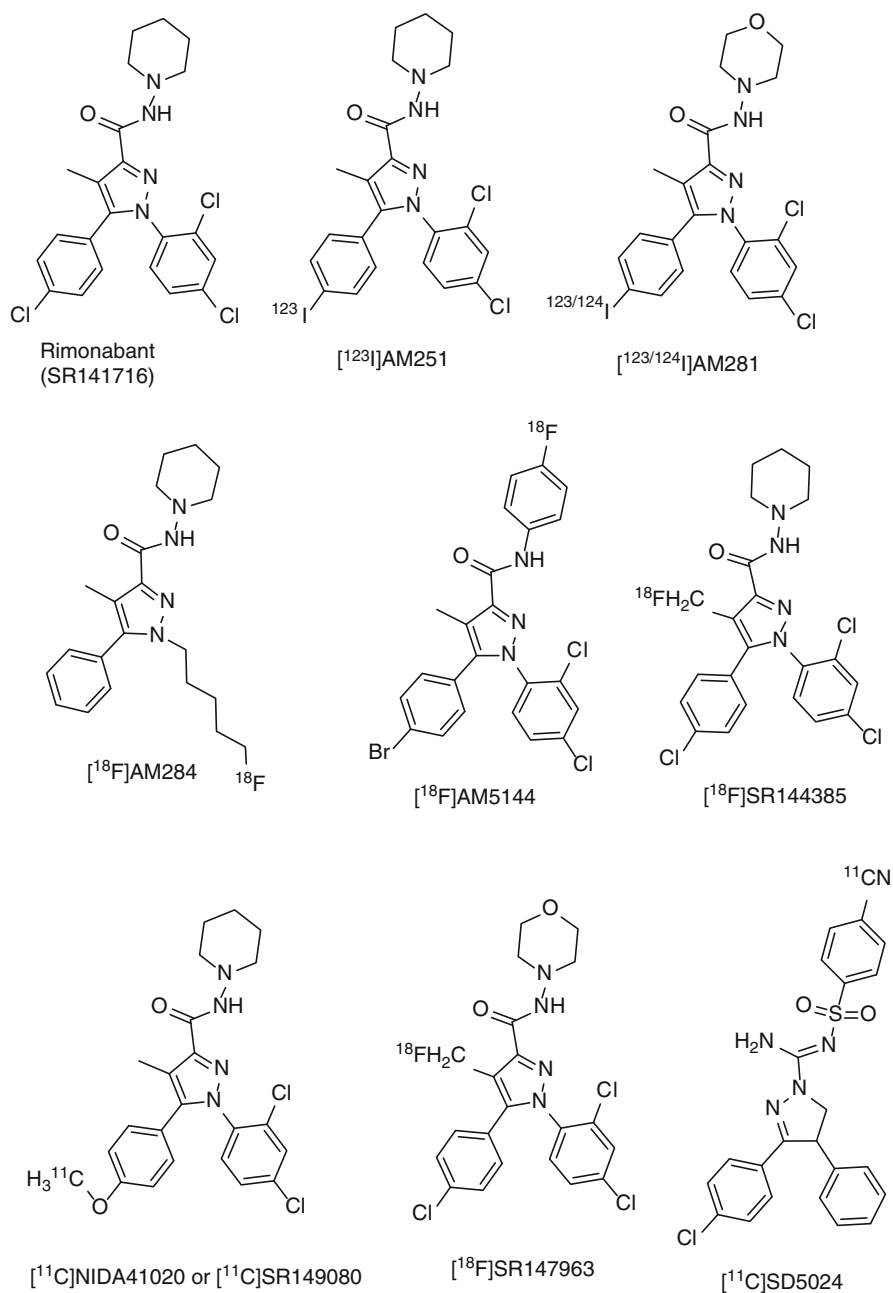


Fig. 11.4 Initial radiolabeled analogs of rimonabant and structurally related compounds

Katoch-Rouse et al. 2002, 2003; Lan et al. 1996, 1999; Mathews et al. 1999, 2000, 2002; Nojiri et al. 2008) (Fig. 11.4). While more details on the initial stage of CB₁ radioligand development can be obtained from the original literature and previous

reviews (Gatley et al. 2004; Horti and Van Laere 2008), a brief summary of the most representative initial radioprobes is given below.

Iodinated analogs of SR141716, AM251 and AM281, exhibited high and moderate CB₁ receptor binding affinity, respectively, and good CB₁/CB₂ selectivity (Lan et al. 1999) and were radiolabeled with ¹²³I for SPECT studies (Gatley et al. 1998; Lan et al. 1996) (Fig. 11.4). The molecular weights of AM251 and AM281 are rather high (>500) for passive BBB transport (Table 11.2). In mouse experiments, [¹²³I]AM251 and [¹²³I]AM281 demonstrated reasonable specific brain uptake (Table 11.2), and both radioligands were found to be suitable for further baboon SPECT studies. In baboon experiments, [¹²³I]AM251 exhibited little brain uptake, whereas [¹²³I]AM281 showed good permeation of the blood-brain barrier (Gatley et al. 1998). A likely explanation for these results is the high lipophilicity of [¹²³I]AM251 and lower lipophilicity of [¹²³I]AM281 (Table 11.2) that is within the conventional range for in vivo radioligands. Notably, both radioligands manifest PS areas that are within the range for passive blood-brain transport (Table 11.2). The highest regional accumulation of [¹²³I]AM281 in the baboon brain was in the cerebellum, cortex, and striatum and lower in the other regions. A blocking study with rimonabant demonstrated that [¹²³I]AM281 specifically bound to CB₁ receptors in baboon cerebellum, but the value of the signal-to-noise ratio was moderate (Table 11.2). Substantial nonspecific binding was observed in other brain regions. In spite of the modest imaging results in animals, [¹²³I]AM281 remained the best available CB₁ receptor radioligand for almost a decade and the only hope for in vivo CB₁ receptor imaging in humans.

The first CB₁ receptor SPECT imaging study in humans was performed with [¹²³I]AM281 in six patients suffering from Tourette's syndrome before and after Δ⁹-THC treatment (Berding et al. 2004). The radioligand displayed some brain uptake that did not change significantly after Δ⁹-THC treatment. However, V₃' declined in the only patient that showed a treatment response suggesting that specific binding of [¹²³I]AM281 in human subjects is mediated by CB₁ receptors. Because of the low specific signal and high nonspecific binding in human subjects, it was concluded that [¹²⁴I]AM281/PET could give better results than [¹²³I]AM281/SPECT because PET provides better image statistics than SPECT.

Human PET imaging with [¹²⁴I]AM281 in a single patient suffering from schizophrenia was performed by a research group from MHH (Berding et al. 2006). The radioligand manifested limited accumulation in regions enriched with CB₁ receptors: the striatum and pallidum (DVR - 1 = 0.3–0.4), cerebral cortex and cerebellum (DVR - 1 = 0.2) (Fig. 11.5). It was also stated that the high radiation burden of ¹²⁴I, a radionuclide with 4 days half-life, represents a radiation safety issue in human subjects. The low specific signal, high nonspecific binding, and safety concerns were the main reasons why [¹²⁴I]AM281/PET was never used again in clinical experiments.

In summary, initial studies with radiolabeled analogs of rimonabant (Table 11.2) demonstrated that CB₁ receptor imaging is a tough nut to crack. Structure-imaging properties of these radioligands suggests that most of them exhibit lipophilicity that is too high (logD_{7.4} > 4) and/or binding affinity that is too low (Table 11.2). As a

Table 11.2 Physical-chemical and in vivo imaging characteristics of the first generation of radioligands for PET/SPECT imaging of CB₁

Code name	M.W. ^a , Da	K_i^{CB1} , nM	K_i^{CB2} , nM	$clogD_{7.4}$ ^b	PSA ^b	Target-to-nontarget region ratio –1			References
						Mouse	Monkey	Human	
<i>Analogues of rimonabant</i>									
[¹²³ I]AM251	555	0.6–1	2,290	5.3	50	0.7 ^c	Low uptake	–	Gatley et al. (1996, 1998), Katoch-Rouse et al. (2003), Lan et al. (1999)
[¹²³ I]AM281 or [¹²⁴ I]AM281	557	4.5	4,200	3.9	59	~0.9 ^c	~0.4 ^d	0.21 ^e 0.37 ^e	Berding et al. (2004, 2006), Gatley et al. (1998), Gifford et al. (1997)
[¹⁸ F]AM284	372	30	–	5.0	50	0.4 ^f	–	–	Gatley et al. (2004), Li et al. (2005)
[¹⁸ F]AM5144	519	31	–	5.7	47	–	0.5 ^g	–	Li et al. (2005)
[¹⁸ F]SR144385	482	14 ^h	1,000 ^h	4.8	50	1.5 ⁱ	–	–	Mathews et al. (1999, 2000)
[¹⁸ F]SR147963	484	120 ^h	–	3.4	59	0.7 ⁱ	–	–	Mathews et al. (2000)
[¹¹ C]NIDA41020 or [¹¹ C]SR149080	459	4.1–16	800	4.0	59	1.2 ^g	0.5 ^g	–	Katoch-Rouse et al. (2002, 2003), Mathews et al. (2002)
[¹¹ C]SD5024	464	0.5	>5,000	2.8	120	–	0.8 ^j	–	Donohue et al. (2008c)
<i>Indole derivatives</i>									
[¹⁸ F]NIDA54	400	0.7	–	3.8 ^k	25	–	0.7	–	Willis et al. (2005)
[¹⁸ F]PipISB	492	1.5 ^l	–	5.0	80	–	0.9	–	Donohue et al. (2008a), Finnema et al. (2009)

^aMolecular weight^bLipophilicity ($clogD_{7.4}$) and polar surface area (PSA) are calculated with ACD/Structure Designer software^cCerebellum/brain stem ratio –1^dCerebellum baseline/cerebellum block with rimonabant ratio –1^eBinding potential^fWhole-brain baseline/whole brain blocked with rimonabant ratio –1^gCerebellum/thalamus ratio –1^hIC₅₀ (Mathews et al. 2000)ⁱHippocampus/thalamus ratio –1^jStriatum/pons-1 (time-uptake curves)^kExperimental data^lIn vitro functional binding activity (K_b)

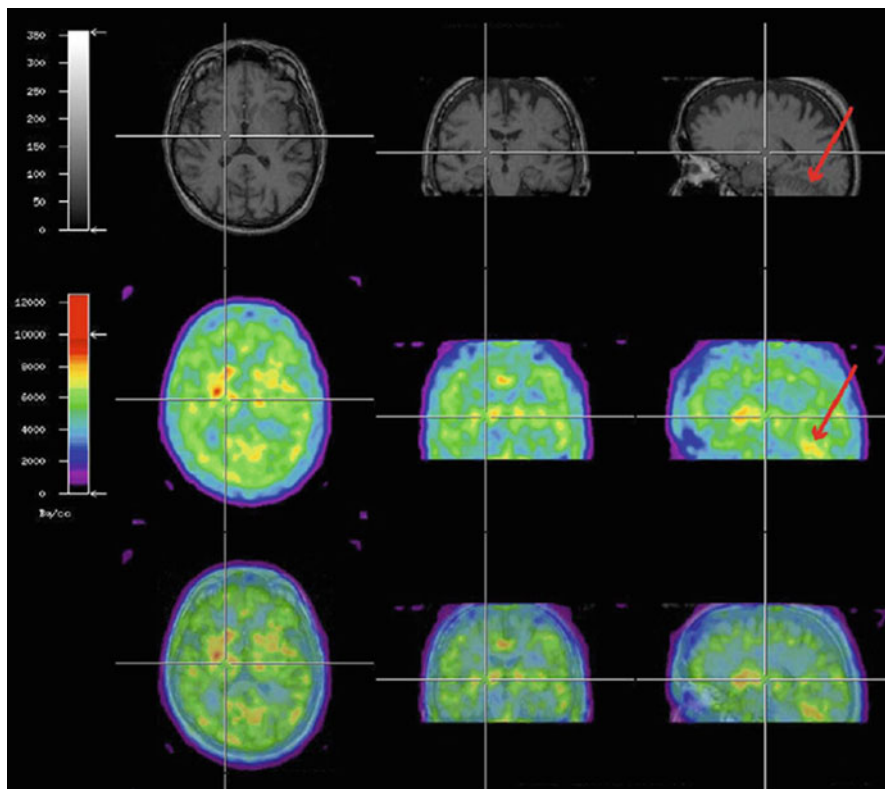


Fig. 11.5 [^{124}I]AM281 PET of central cannabinoid CB_1 receptors in a patient with schizophrenia (*second row*) coregistered to the individual's MRI (*first row*). The fusion image is shown in third row. Prominent binding of the radioligand can be seen in the basal ganglia (*white cross*) and the cerebellum (*red arrow*) (Reprinted from Berding et al. (2006) with permission of Elsevier). The high nonspecific binding and relatively low accumulation of radioactivity in the CB_1 receptor-rich brain regions suggest limited utility of [^{124}I]AM281 for PET imaging in human subjects

result, animal studies with these radioligands showed either little brain uptake or some brain uptake with high nonspecific binding and relatively low target-to-nontarget ratio – 1 value (<1). It is noteworthy that within the initial series of radioligands, the most reasonable imaging properties were exhibited by the least lipophilic radioligand [$^{123/124}\text{I}$]AM281, which also manifested a moderate CB_1 receptor binding affinity (Table 11.2). [^{123}I]AM251, an analog of AM281 with excellent binding affinity but high lipophilicity, showed little brain uptake in monkey and was clearly not suitable for PET studies.

11.3.1.3 Radiolabeled Aminoalkylindole Derivatives and Structurally Related Compounds

Aminoalkylindoles (AAI) that are exemplified by WIN-55,212-2 (Fig. 11.6) represent a large group of compounds that exhibit typical cannabinoid pharmacology.

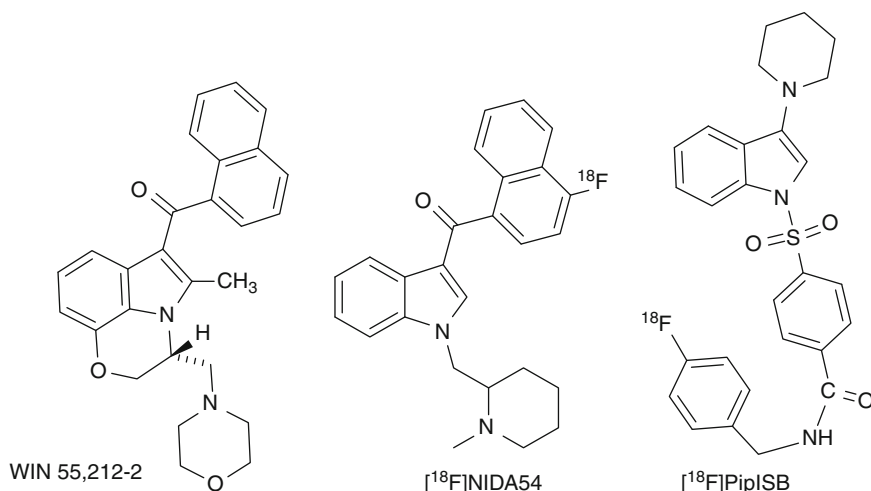


Fig. 11.6 Aminoalkylindole derivatives

Because the structure-activity relationship for AAIs is well developed (Huffman et al. 2005) and many AAI display excellent CB₁ affinity, it is not a surprise that several compounds of this class have been radiolabeled for PET or SPECT application (Deng et al. 2005; Donohue et al. 2008a; Finnema et al. 2009; Makriyannis and Deng 2007; Tamagnan et al. 1999; Willis et al. 2003; Willis et al. 2005).

The most notable PET radioligands among AAI are [¹⁸F]NIDA54 (Willis et al. 2005) and [¹⁸F]PipISB (Donohue et al. 2008a; Finnema et al. 2009). [¹⁸F]NIDA54 manifests greater binding affinity and more appropriate molecular weight, PSA, and lipophilicity for a CNS radioligand, but both radioligands exhibit comparable specific binding in monkey brain. This finding can be explained by the functional properties of the inverse agonist [¹⁸F]PipISB that should bind with a greater population of CB₁ receptors than agonist [¹⁸F]NIDA54. Neither [¹⁸F]NIDA54 nor [¹⁸F]PipISB was sufficiently good CB₁ radiotracers in animal experiments to initiate further clinical investigation.

11.3.2 Current CB₁ Receptor Radioligands for Human PET Imaging

11.3.2.1 [¹¹C]OMAR ([¹¹C]JHU75528)

[¹¹C]OMAR ([¹¹C]JHU75528) was the first CB₁-selective radioligand with adequate properties for PET imaging (Fan et al. 2006; Horti et al. 2006). Structurally [¹¹C]OMAR is an analog of rimonabant (Fig. 11.7) with comparable CB₁ receptor binding affinity and good CB₁/CB₂ selectivity. The lipophilicity of OMAR is considerably lower because the hydrophobic methyl and chlorine substituents of the rimonabant molecule are replaced with cyano- and methoxy groups that exhibit

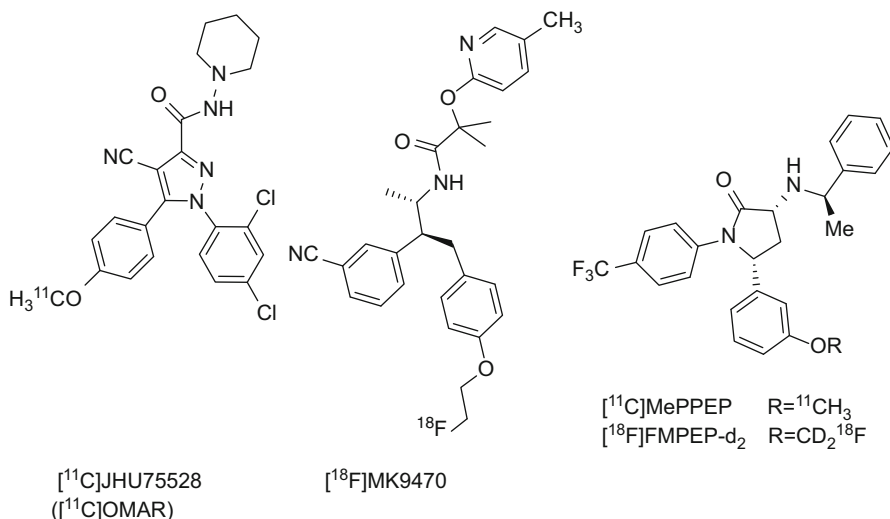


Fig. 11.7 Currently available CB₁ receptor PET radioligands for human studies

negative constants of lipophilicity ($\pi = 0.56, 0.71, -0.57,$ and -0.02 , correspondingly (Kubinyi 1995)), but the PSA value of OMAR is relatively high (Table 11.3). An *in vitro* functional assay demonstrated that OMAR is a cannabinoid antagonist (Fan et al. 2009).

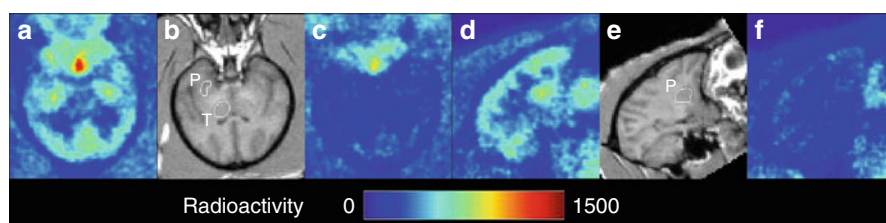
Radiosynthesis of $[^{11}\text{C}]\text{OMAR}$ is straightforward (Fan et al. 2006) and is achieved by ^{11}C -methylation of the corresponding phenol precursor that is currently commercially available.

In mice and baboon studies, $[^{11}\text{C}]\text{OMAR}$ manifested promising imaging results (Table 11.3). In comparison with the previously reported CB₁ receptor radiotracers of the first generation (Table 11.2), $[^{11}\text{C}]\text{OMAR}$ showed substantially greater signal-to-noise ratios (Table 11.3). Pharmacological evaluation of $[^{11}\text{C}]\text{OMAR}$ in mice demonstrated that the radioligand labels CB₁ receptors specifically and selectively and does not bind to various other cerebral receptors including D₁, D₂, D₅, 5-HT_{2A}, 5-HT_{1C/2C}, 5-HT_{1C/2C}, opioid, and $\alpha 4\beta 2$ -nAChR. The specific *in vivo* binding of $[^{11}\text{C}]\text{OMAR}$ in CD1 mice was blocked by selective CB₁ antagonists in a dose-dependent manner (Horti et al. 2006). MicroPET studies with $[^{11}\text{C}]\text{OMAR}$ showed a 50 % higher brain uptake in wild-type mice versus CB₁ knockout animals (Herance et al. 2011).

Baboon PET studies demonstrated that $[^{11}\text{C}]\text{OMAR}$ exhibits good values of BP in CB₁ receptor-rich brain regions (Table 11.3) and reasonable total brain uptake (%SUV = 150 %). A blockade PET study with rimonabant showed that *in vivo* binding of $[^{11}\text{C}]\text{OMAR}$ in baboon brain is mediated by CB₁ receptors (Horti et al. 2006) (Fig. 11.8). Kinetic analysis suggests that $[^{11}\text{C}]\text{OMAR}$ rapidly reaches the steady state in the baboon brain before the end of the 90-min PET scanning session, which is a logistical advantage of $[^{11}\text{C}]\text{OMAR}$ versus other available PET radioligands (see below).

Table 11.3 Physical-chemical and in vivo imaging characteristics of the clinical radioligands for PET imaging of CB₁

Code name	M.W. ^a , Da	<i>clogD</i> _{7.4} ^b	PSA	K _i ^{CB1} , K _i ^{CB2} , nM		Target-to-nontarget region ratio -1			References
				Mouse	Nonhuman primate	Human			
[¹¹ C] OMAR	470	3.3–3.6 ^c 4.3	83	11	2,700 5,250	2.4	1.4	1.0	Fan et al. (2006), Horti et al. (2006), Wong et al. (2010a)
[¹⁸ F] MK-9470	489	4.9	84	0.7	44	–	~3–4	3	Burns et al. (2007), Van Laere et al. (2008b)
[¹¹ C] MePPEP	454	6.0	42	0.5 ^d	363	2.3	~2	1.4	Terry et al. (2008), Yasuno et al. (2008)
[¹⁸ F] FMPEP- <i>d</i> ₂	474	6.0	42	0.2 ^d	669	–	~2.2	1.8 ^e	Donohue et al. (2008b), Terry et al. (2009)

^aMolecular weight^bLipophilicity (*clogD*_{7.4}) and PSA are calculated with ACD/Structure Designer software^cExperimental data^dIn vitro functional binding activity (*K*_i)^eTwo hours scanning**Fig. 11.8** Summed baboon brain HRRT PET images (10–90 min) of [¹¹C]OMAR and aligned MRI images (**b** and **e**). Transaxial images (**a**=baseline; **c**=blocking) show putamen (*P*), thalamus (*T*), and temporal and occipital cortices. Sagittal (**d**=baseline; **f**=blocking) show frontal, parietal, occipital cortices and putamen, among other structures. In the baseline scan, the radioactivity accumulated predominantly in the putamen, frontal cortex, and cerebellum and less in thalamus and pons (Courtesy of Dr. Hiroto Kuwabara, Johns Hopkins University)

[¹¹C]OMAR was used by the Johns Hopkins group under an Investigational New Drug Application, approved by the FDA, for quantification of cerebral CB₁ receptors in healthy subjects and schizophrenia patients (Wong et al. 2010a) (Fig. 11.9). Within ten control male subjects, [¹¹C]OMAR peaked at approximately 20 min postinjection (% SUV = 136–207 % in the putamen) and decreased gradually thereafter to reach an SUV between 80 and 117 % at 90 min. The globus pallidus showed

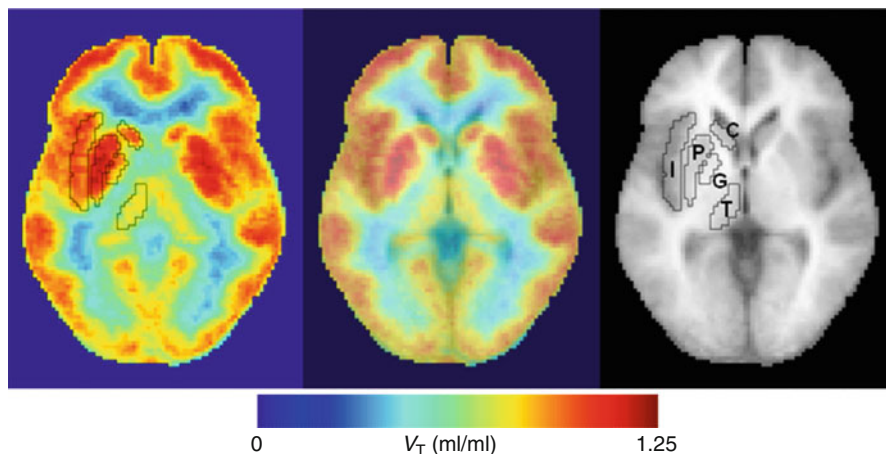


Fig. 11.9 Transaxial images of distribution volume (V_T) of [^{11}C]OMAR, mean of ten healthy subjects in a standard space (*left panel*), a standard MRI (*right*), and merged image (*middle*). Volumes of interest of selected structures in the standard space are shown on the V_T image and MRI. Regions are insula (*I*), putamen (*P*), globus pallidus (*G*), thalamus (*T*), and caudate nucleus (*C*) (Reprinted from Wong et al. (2010a) with permission of Copyright Clearance Center)

the highest V_T (1.47 ± 0.25), with a range of 0.95–1.82 in individual subjects. The cingulate cortex (mean 1.23 ± 0.16) and the putamen (mean 1.32 ± 0.20) also showed high binding. White matter, pons, and thalamus were the regions with the lowest accumulation of [^{11}C]OMAR radioactivity. The study demonstrated an increased V_T of [^{11}C]OMAR in ten subjects with schizophrenia, which is consistent with previous postmortem data. [^{11}C]OMAR binding in healthy controls appeared to decline with increasing age in the globus pallidus and putamen, the regions with the highest values of V_T .

Human PET studies with the CB_1 antagonist blocker AVE1625 demonstrated the utility of [^{11}C]OMAR for successful occupancy evaluation of cannabinoid receptors by drugs in human brain (Wong et al. 2010b). Because of the short half-life of ^{11}C ($t_{1/2} \sim 20$ min), the baseline and drug challenge scans with [^{11}C]OMAR can be done in the same subject in a single day, an advantage of [^{11}C]OMAR over [^{18}F]labeled CB_1 receptor radioligands for drug development research.

11.3.2.2 [^{18}F]MK-9470

Discovery of the selective CB_1 inverse agonist rimonabant by Sanofi-Aventis (Rinaldi-Carmona et al. 1994), available in United Kingdom and EU as antiobesity drug in 2006–2009, stimulated development of cannabinoid drugs by many pharmaceutical companies. As a result, a large number of rimonabant analogs and structurally different CB_1 inverse agonists have been developed. Merck disclosed a series of non-rimonabant-based CB_1 receptor inverse agonists (Lin et al. 2006). The best compound of the Merck series, taranabant, demonstrated a substantially higher affinity (0.4 nM) than that of rimonabant (Lin et al. 2008). Using taranabant as a lead compound Merck

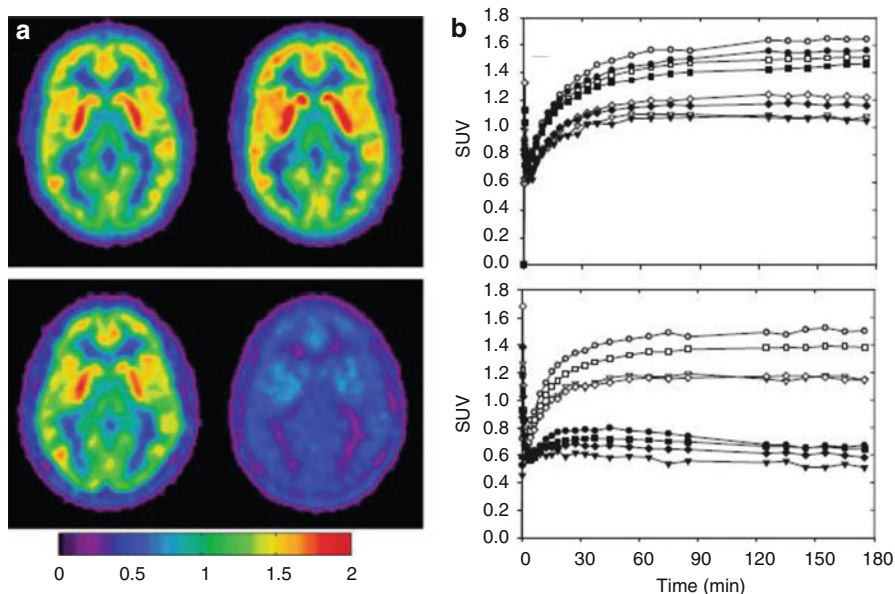


Fig. 11.10 ^{18}F -MK-9470 PET images of CB_1 receptors were acquired in normal healthy male subjects before and after treatment with MK-3640 or placebo. (a) Representative transverse parametric SUV images at the level of the basal ganglia for two human subjects, acquired before (*left*) and 24 h after (*right*) treatment with either placebo (*upper*) or a 7.5 mg dose of MK-0364 (*lower*). (b) Graphs show the corresponding TACs. The open symbols denote baseline values, and the closed symbols denote the scan after treatment (Reprinted from Burns et al. (2007) with permission of Copyright National Academy of Sciences, U.S.A., PNAS)

has developed MK-9470, a CB_1 receptor selective fluoroalkyl analog of taranabant with high CB_1 receptor binding affinity but also relatively high values of $\log D_{7.4}$ and PSA (Burns et al. 2007) (Table 11.3). Radiolabeling of $[^{18}\text{F}]\text{MK-9470}$ was performed in two steps by preparation of $[^{18}\text{F}]\text{fluoroethylbromide}$ and $[^{18}\text{F}]\text{fluoroethylation}$ of the corresponding phenol with moderate radiochemical yield.

In vitro autoradiography of $[^{18}\text{F}]\text{MK-9470}$ in rhesus monkey brain slices (Burns et al. 2007) produced images with a high signal in cerebral cortex, cerebellum, caudate/putamen, globus pallidus, substantia nigra, and hippocampus, which is consistent with the reported localization of CB_1 receptors in the brain of various mammalian species. Additional in vitro studies showed that $[^{18}\text{F}]\text{MK-9470}$ is not a P-gp substrate.

Baseline PET scans in the rhesus monkey showed gradual brain penetration and accumulation of $[^{18}\text{F}]\text{MK-9470}$ in gray matter regions of the brain as expected for binding to CB_1 receptors and consistent with autoradiography studies. The specificity of the in vivo binding was confirmed in a blockade study with MK-034, a CB_1 -selective inverse agonist.

After bolus injection of $[^{18}\text{F}]\text{MK-9470}$ in human controls, the radioactivity reached a plateau at ~ 120 min (Burns et al. 2007) (Fig. 11.10). The distribution of

radioactivity corresponded to the known CB₁ receptor distribution and regional concentrations remained nearly unchanged for 2–6 h postinjection. Despite the seemingly irreversible brain kinetics, the excellent signal-to-noise characteristics of [¹⁸F]MK-9470 (Table 11.3) made it suitable for several human PET imaging studies (Burns et al. 2007; Gerard et al. 2010, 2011; Sanabria-Bohorquez et al. 2010; Van Laere et al. 2008a, b, c, 2009) that were performed by the imaging group from K.U. Leuven in collaboration with Merck.

A methoxy analog of MK-9470, CB-119, was designed as a carbon-11 alternative for PET imaging (Hamill et al. 2009). While it showed nearly identical binding characteristics to [¹⁸F]MK-9470, it was not able to achieve equilibrium within scanning time. It was therefore abandoned for further clinical development in lieu of [¹⁸F]MK-9470.

11.3.2.3 [¹¹C]MePPEP and [¹⁸F]FMPEP-*d*₂

A collaborative group from Eli Lilly, NIH, and Karolinska University developed two structurally similar CB₁ radioligands, [¹¹C]MePPEP and [¹⁸F]FMPEP-*d*₂ (Fig. 11.7), for human PET studies (Donohue et al. 2008b; Suter et al. 2010; Terry et al. 2008; Yasuno et al. 2008). Both compounds are CB₁ receptor inverse agonists with high CB₁ receptor binding affinity and selectivity (Table 11.3). MePPEP has about ten times higher binding affinity compared to rimonabant and has >700 times greater selectivity for CB₁ than CB₂. The lipophilicity values of MePPEP and FMPEP-*d*₂ are high, but the PSAs are in the acceptable range for passive BBB transport and lower than those of OMAR and MK-9470 (Table 11.3).

Radiosynthesis of [¹¹C]MePPEP is simple and it was performed by reaction of the corresponding desmethyl precursor with [¹¹C]methyl iodide (Terry et al. 2009). In the monkey brain, [¹¹C]MePPEP showed very high uptake with a good specific signal (Table 11.3) (Yasuno et al. 2008). An IND approval for the radioligand was obtained, and [¹¹C]MePPEP was studied in 17 human control subjects (Terry et al. 2009). The radioligand exhibited high human brain uptake, slow washout from brain, and regional distribution consistent with that of CB₁ receptors. Also, [¹¹C]MePPEP provided acceptable quantification of receptor density using distribution volume as the outcome measure. However, the precision and accuracy of quantification of CB₁ receptor with [¹¹C]MePPEP in human brain may have been diminished by slow brain kinetics and a very low fraction of free radioligand in plasma (*f_p*) (Terry et al. 2009) that can be explained by the high lipophilicity of this compound (Table 11.3). Further studies determined that quantification was not limited by measurements from brain, but rather by measurements of radioligand in plasma (see Sect. 11.3.3.4).

Difficulties with the mathematical analysis of [¹¹C]MePPEP-PET data were the driving force behind the development of its derivative [¹⁸F]FMPEP-*d*₂. The radioligand manifests at least as high binding affinity as that of [¹¹C]MePPEP (Table 11.3). Two deuterium atoms were introduced into the molecule to reduce de-[¹⁸F]fluorination and diminish the relatively high uptake of [¹⁸F]fluoride in the skull bone. The same precursor was used for the preparation of [¹⁸F]FMPEP-*d*₂ and [¹¹C]MePPEP. The radiosynthesis of [¹⁸F]FMPEP-*d*₂ involves [¹⁸F]fluorination of dibromomethane-*d*₂, purification

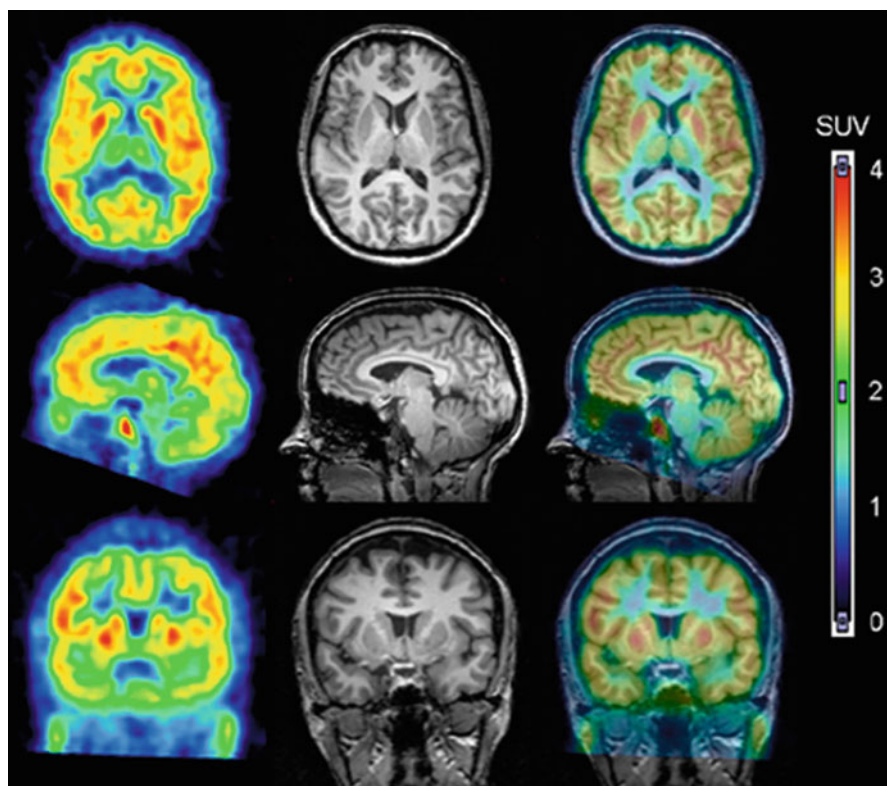


Fig. 11.11 ^{18}F -FMPEP- d_2 in human brain. PET images from 30 to 60 min after injection of ^{18}F -FMPEP- d_2 were averaged (*left column*) and coregistered to the subject's MR images (*middle column*). PET and MR images are overlaid in *right column* (Reprinted from Terry et al. (2009) with permission of Copyright Clearance Center)

of [^{18}F]fluorobromomethane- d_2 , and [^{18}F]fluoromethylation of the phenol precursor (Donohue et al. 2008b).

In a rhesus monkey study, [^{18}F]FMPEP- d_2 peaked in the brain at 20 min post bolus injection (SUV 4.5–6.5) with gradual washout thereafter. The blocking experiment revealed that specific binding in the monkey brain was 80–90 % of total tissue uptake. Radioactivity concentration in the mandible reached an SUV of approximately 2.0 by the end of the 3 h scan (Terry et al. 2009). After injection of [^{18}F]FMPEP- d_2 in human, radioactivity peaked in putamen (SUV=5) by 30 min post bolus administration followed by slow washout (Terry et al. 2010b). The regional distribution of radioactivity matched the density of CB $_1$ receptors in human brain (Fig. 11.11). The skull had substantial uptake of radioactivity that reached a peak SUV value of 4.5 by the end of 5 h of scanning. Mathematical modeling demonstrated that 60–120 min of human imaging gives the most accurate measurements of V_T , whereas a longer acquisition is likely vulnerable to contamination of the brain with radiometabolites and spillover of radioactivity from the skull, which

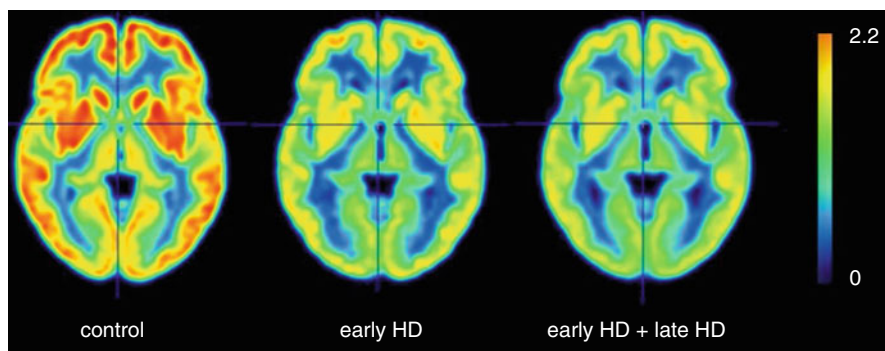


Fig. 11.12 Cross-sectional, partial-volume-corrected, modified standardized uptake value (mSUV) parametric images of [^{18}F]MK-9470, averaged for all controls ($n=14$), early-HD patients ($n=7$), and total group of HD patients ($n=19$) (Courtesy of Dr. Koen Van Laere, KU Leuven)

presumably outweighs any added accuracy from a more extended scan time. The test-retest variability of [^{18}F]FMPEP- d_2 PET was 16 %.

11.3.3 PET Imaging of CB $_1$

11.3.3.1 Considerations in Imaging CB $_1$ Receptors

An advantage of PET over other imaging modalities is its quantitative ability, and quantitative analysis is achieved in large part through pharmacokinetic modeling. Pharmacokinetic modeling of CB $_1$ receptor PET radioligands in brain poses some particular challenges compared to more established compounds. These challenges include the high concentration of receptors throughout the brain, lack of a receptor devoid region, slow pharmacokinetics of the radioligands, low plasma concentrations of parent radioligand, and high plasma protein binding. Careful consideration should be made when interpreting data from clinical PET studies, as radioligand properties and modeling methods may potentially confound results or their interpretation. To better appreciate such potential confounding variables, a brief review of modeling considerations is discussed here.

The noninvasive nature of in vivo PET imaging limits the ability to establish a “gold standard” method to validate endpoint measurements such as receptor density, as absolute measurements might require surgical excision followed by in vitro quantitation of receptors. Using a two-tissue compartment model, the radioligand can be conceptualized as being in a “non-displaceable compartment,” which represents radioligand nonspecifically bound to proteins or lipids or is free in tissue, and a “specifically bound” compartment, which represents radioligand bound to a receptor and is potentially displaceable. Both compartments are detected as radioactivity by the PET camera, and so pharmacokinetic analysis with mathematical modeling serves to separate out these two compartments as discernible and quantitative measures. In doing so, estimates of receptor density and/or receptor occupancy can be

calculated. Estimates of receptor density are approximated by distribution volume (V_T) (Innis et al. 2007), which in turn can be conceptualized as the ratio of areas under the curve of radioligand in tissue (e.g., brain) divided by radioligand in arterial plasma. Over the course of the entire study, the brain was exposed to the amount of radioligand available in plasma (i.e., the input function), and the brain responded by taking up the radioligand. Unfortunately, we cannot always measure the complete area under the curve because of the short radioactive half-life or slow pharmacokinetics of the radioligand. Using mathematical modeling, the curves can be extrapolated to infinity (or, in practice, described using rate constants) with only part of the entire curve of brain or plasma data; however, enough of the curve shape must be observed for it to be successful, in particular the tissue uptake, peak, and initial decline.

The additional steps required to perform compartment modeling and calculate distribution volume yield theoretically more accurate outcome measures than simple methods, as it avoids potentially confounding variables. At equilibrium radioligand in brain changes proportionally by the amount of radioligand in arterial plasma and is therefore susceptible to pharmacokinetic variables from the periphery that may affect the delivery of the radioligand to brain (e.g., metabolism, distribution, excretion which could change radioligand concentration) (Liow et al. 2007). Additionally, compartment models account for radioligand in brain that is both receptor bound and unbound or free. Even for radioligands that have nearly 90 % receptor specificity, not accounting for unbound radioligand may reduce the significance or obscure results.

The high density and widespread location of CB_1 receptors is likely the cause for several hurdles when performing pharmacokinetic modeling of its radioligands (Hirvonen et al. 2010). First, extremely slow washout of CB_1 inverse agonists may be due to a rapid process of reversible binding and rebinding to receptors, a phenomenon known as “synaptic barrier” (Frost and Wagner 1984). Similar kinetics suggestive of synaptic barrier has been seen with other radioligands targeting receptors found in high density (e.g., iomazenil and benzodiazepine receptors) (Laruelle et al. 1994). Second, the widespread location of CB_1 receptors in brain eliminates the use of reference tissue modeling methods, an alternative to compartment modeling using arterial plasma samples. Even areas of relatively low receptor density show up to 90 % specific binding by some radioligands, and small changes in receptor binding in these regions would lead to potentially large systemic errors in outcome measurements. A potential advantage of high receptor density is that radioligands with lower specific activity could be used while maintaining the principle of tracer dosing. Tracer doses are needed to avoid inducing pharmacological effects, such as receptor internalization, and are generally accepted at 5–10 % receptor occupancy or less; CB_1 receptor imaging studies are well below this threshold, even in rodents, and typically maintain <1 % receptor occupancy in humans.

The CB_1 receptor radioligands discussed here demonstrate slow pharmacokinetics. Slow pharmacokinetics implies that ligands take a longer time to reach steady state when equilibrium has been achieved and for reversible radioligands, after the identifiable peak in brain concentration has been achieved. This is a particular

problem in PET imaging, as data acquisition time is typically limited by the radioactive half-life of the radioligand, as measured in brain and/or plasma. Thus, there is a chance that insufficient data may be collected within the time allowed and consequently an increased likelihood that measurement errors can be introduced. Test-retest studies are particularly useful to identify potential sources of error in kinetic modeling in measurements (brain uptake, plasma) and outcome measures (brain uptake, V_T).

Additional potential causes of error are likely due to the high lipophilicity of CB_1 receptor radioligands. First, most of the ligands have a relatively rapid distribution phase following administration, followed by a very slow excretion phase (taken together as clearance). As a result, the excretion phase of plasma clearance typically has very low concentrations of parent radioligand, which are difficult to measure accurately. Second, CB_1 receptor ligands tend to exhibit very high plasma protein binding, sometimes >99 %, meaning that free ligand available to cross the BBB may be very small (e.g., <1 %). Thus, when comparing between groups or conditions, brain uptake or V_T should be corrected for differences in free fraction (not the fraction bound to proteins), as low absolute changes in free fraction can produce large proportional changes. For example, a change of bound fraction from 99.9 to 99.8 %, which could be caused by competitive binding by a drug, would correspond to a change of free fraction from 0.1 to 0.2 %, or a 100 % increase; such a phenomenon may have been the cause of about 17 % increased brain uptake of one radioligand when a coadministered drug caused about 10 % increased free fraction (Yasuno et al. 2008). Finally, it is generally assumed that metabolites more polar than the parent tracer are unable to cross the BBB. However, ligands for cannabinoid receptors have a higher lipophilicity than more typical PET tracers, and their metabolites, though relatively more polar, may retain a lipophilicity sufficient to cross the BBB. Thus, additional consideration should be made to the radiometabolite profile of cannabinoid PET tracers to avoid confounding results from pharmacokinetic modeling.

What does the data from CB_1 receptor radioligand studies imply physiologically? It is generally assumed that differences or changes to receptor binding are due to changes of receptor density; however, outcome measurements using PET alone cannot distinguish receptor density from receptor binding affinity; indeed, until recently few examples of decreased binding affinity had been reported (Itoh et al. 2009). Changes observed in studies using these radioligands are likely to demonstrate changes in receptor density, whether due to direct downregulation or by indirect downregulation due to increased endocannabinoid tone (Romero et al. 1995; Sim-Selley and Martin 2002). It is also assumed that the only receptors binding radioligand are membrane surface bound, which is particularly important for CB_1 receptors as a significant proportion of receptors may be internalized (e.g., 85 % in hippocampus) (Coutts et al. 2001). As GPCRs, cannabinoid receptors are found in both a protein-coupled or high-affinity and agonist-preferring state and an uncoupled or low-affinity inverse agonist-preferring state. As demonstrated by *in vitro* studies (Rinaldi-Carmona et al. 1996), high-affinity inverse agonists bind to all available receptors, and thus, it is assumed that at tracer doses inverse agonist

radioligand binding represents the entire population of available receptors. Regional changes relative to global distribution volume or brain uptake likely reflect local variations in CB₁ receptor availability or density, as tracer uptake is unlikely affected by regional flow effects. However, when relative values of brain uptake are taken alone, it could mask the absolute effect of receptor availability; e.g., does a local increase of tracer uptake in brain with globally decreased uptake represent a true, and potentially abnormal, increase in receptor availability, or does it represent a local sparing or preservation of receptor expression with global reductions? Such relative changes may be open to wider interpretation when presented without more absolute measurements, as can be obtained with V_T . Nevertheless, relative changes can be sensitive measures and may provide additional insight into regional alterations of CB₁ receptor availability or expression (Van Laere et al. 2002).

11.3.3.2 [¹¹C]OMAR

Following the successful results in rodents and baboons, [¹¹C]OMAR was tested in humans. Given the relatively fast kinetics of [¹¹C]OMAR, measurements of brain uptake can be quantified as V_T using two-tissue compartment modeling and is the preferred analytical method. Interestingly, human V_T was about 20 % of that in rhesus monkey, which may have been due to low estimations of brain entry (human K_1 parameter was approximately 25 % of that in monkey) (Normandin et al. 2010a). However, other studies have shown human CB₁ receptor density to be a similar fraction compared to nonhuman primate. An initial modeling study in baboons tested if the simpler reference tissue model could be used for [¹¹C]OMAR data analysis (Horti et al. 2006). When pons was used as a reference tissue, the resulting values of BP fluctuated by 10–20 %, further suggesting that it leads to low precision and is an unstable method to use for quantifying CB₁ receptors. An alternative candidate for use as a reference tissue, white matter, did not appear to reach equilibrium in the course of the scan and indeed had a small increase of radioactivity over the course of 90 min, eliminating it as a choice for analytic method.

Test-retest analysis of distribution volume in healthy human subjects demonstrated [¹¹C]OMAR has reasonably good precision (~3 % within-subject variability). Analysis of potential modeling errors suggested that measurement error in the input function is the likely source for variability in V_T . Both peak brain uptake and fraction of parent tracer in plasma were found to be higher in men than women. V_T was significantly higher in women than men, presumably due to the faster plasma clearance in women than in men (Normandin et al. 2010b). Full results on kinetic modeling and intersubject variability with [¹¹C]OMAR in human have been presented, but are yet to be published.

In healthy males, [¹¹C]OMAR demonstrated an age-related decline trending in nearly all regions and attaining statistical significance in the region with highest V_T (globus pallidus) (Wong et al. 2010a). [¹¹C]OMAR has also been used to measure CB₁ receptor occupancy by a novel antagonist (see Sect. 11.3.2.1) (Wong et al. 2010b).

Compared to healthy controls, patients with schizophrenia trended toward higher measurements of V_T (also see Sect. 11.3.2.1). There was no significant difference in

V_T between healthy controls and schizophrenia patients, with the exception of that in pons (Wong et al. 2010a); however, this finding was apparently not corrected for multiple comparisons. Patients in the study were on either olanzapine or risperidone monotherapy, and antipsychotics have been shown to have a mixed effect on CB_1 receptor binding or availability; in subgroup analysis, no difference was found between patients on the two medications. It was not reported if [^{11}C]OMAR was measured or corrected for free fraction in either healthy control or patient groups. Within the schizophrenia patient group, there was no association of V_T with Brief Psychotic Rating Score (BPRS); however, when scores were taken as ratio of positive over negative symptoms, there was a positive correlation with V_T in several areas of neocortex (Wong et al. 2008).

In alcohol-dependent patients, V_T of [^{11}C]OMAR was higher than that of healthy controls when measured 4 weeks after abstinence. Compared to healthy controls ($n=8$), alcohol-dependent patients ($n=8$) had approximately 20 % higher V_T in brain regions chosen a priori for their involvement in alcohol dependence. Analysis of other brain regions did not demonstrate any significant between-group differences. These findings were neither affected by age, body mass index (BMI), or use of tobacco nor did they correlate with any clinical measures (Neumeister et al. 2012).

The biodistribution and radiation dosimetry estimates for [^{11}C]OMAR have not yet been reported.

11.3.3.3 [^{18}F]MK-9470

[^{18}F]MK-9470 demonstrates many favorable properties for characterizing CB_1 receptors with in vivo imaging including good brain uptake and low nonspecific uptake. However, its slow pharmacokinetics has proven to be a challenge for modeling accepted outcome measures such as distribution volume. In both monkeys and humans, radioactivity increased in brain up to about 120 min after bolus injection with [^{18}F]MK-9470, and concentrations of radioactivity did not appear to decline, even though concentrations of the radioligand in arterial plasma decreased throughout the length of the scan (Burns et al. 2007). For these reasons, brain studies using [^{18}F]MK-9470 were analyzed using a pharmacokinetic method designed for irreversible PET radioligands (Koeppel et al. 1999) which simply uses the area under the curve (AUC) of radioactivity in brain after a period when measurements have stabilized (e.g., 120–180 min after injection), termed fractional uptake ratio (FUR). However, when challenged with another CB_1 inverse agonist, the radioactivity quickly washed out of brain, indicating that [^{18}F]MK-9470 undergoes reversible binding at the CB_1 receptor, which runs counter to the rationale of using an irreversible model.

Indeed, when scanning is continued for 12 h, a slow washout of the radioligand can be detected, and sufficient data is then available for 2-tissue compartment modeling (Sanabria-Bohorquez et al. 2010). However, even with this additional data, only macroparameters from modeling could be distinguished, and the individual parameter that is proportional to receptor density (k_3) could not be identified in any individual brain region. Using 2-tissue compartment modeling, the test-retest

variability of V_T was 10–30 %, indicating that it had poor precision. After making the assumption that dissociation from the receptor (k_4) is constant throughout the brain in vivo, multiple serial correlations were made linking V_T to irreversible measurements and to FUR . It was further assumed that in cases when plasma measurements are not statistically different, brain uptake measured as SUV or modified SUV ($mSUV$) is a sufficient outcome measurement, as they would correlate with FUR and be interpreted as CB_1 receptor availability. These models do not fully account for the full clearance of radioligand (i.e., AUC extrapolated to infinity) and therefore do not correct the amount of radioligand in brain to that in plasma, and, as previously discussed, dissociation from receptors is not always constant in vivo. Thus, while their precision can be assessed by test-retest studies, their accuracy remains uncertain, particularly in conditions where metabolic processes or changes in receptor density may affect radioligand concentration in plasma or the local dissociation rate. Nevertheless, using this analytical method, the authors found [^{18}F]MK-9470 had good precision (retest variability <7 % within 24 h) and intersubject variability (16–35 %) (Addy et al. 2008; Burns et al. 2007).

Preclinical studies using [^{18}F]MK-9470 in rodents have provided additional information on the radioligand's characterization and have hinted at potential clinical investigations. In rat brain, over half of radioactivity after injection of [^{18}F]MK-9470 is specific for CB_1 receptors, and approximately 10–30 % of radioactivity was attributed to metabolites that enter brain. Serial arterial blood sampling permitted kinetic modeling of both [^{18}F]MK-9470 and radioactive metabolites in brain and demonstrated that radiometabolites cause an overestimation of V_T . Measurements of V_T were better approximated after 10 h of scanning, which was independent of radiometabolites. Although it was concluded that compartmental modeling and measurements of V_T are superior to those of brain uptake alone, simplified measurements using SUV or $mSUV$ correlated with V_T and may be preferred over the onerous arterial sampling and extensive scan time required to measure V_T (Casteels et al. 2012). In male rats, [^{18}F]MK-9470 uptake was found to increase with age when comparing adolescent and adult rats, although this study was limited by its lack of kinetic modeling. Nevertheless, main effect was replicated with [3H]CP-55,940 (a CB_1 , CB_2 high-affinity agonist) in vitro binding, though with one quarter the magnitude (Verdurand et al. 2011). In a study examining the impact of nicotine on receptor binding, 2 weeks of nicotine exposure did not produce significant change in [^{18}F]MK-9470 uptake in rat brain (Gerard et al. 2010). Additional rodent studies demonstrated that anesthetics affected brain uptake of [^{18}F]MK-9470 and suggest an indirect action of $GABA_A$ receptors on CB_1 receptor binding (Casteels et al. 2010c). Following 2 weeks of treatment with antiepileptic agents, valproic acid produced a significant increase in [^{18}F]MK-9470 uptake while levetiracetam did not (Goffin et al. 2008). These results from rodents were not corrected for plasma concentrations of parent radioligand across conditions (i.e., drug treatments) which might be expected to change with altered hepatic metabolism and potentially confound independent measurements of brain uptake. Rodent models of Parkinson's disease using 6-hydroxydopamine showed decreased [^{18}F]MK-9470 uptake in bilateral striatum and contralateral cerebellum relative to the lesioned side. Additional

correlations were observed with an inverse relationship of tyrosine hydroxylase-containing neurons (i.e., dopaminergic neurons) to [^{18}F]MK-9470 uptake in ipsilateral cerebellum and a positive relationship of [^{18}F]MK-9470 uptake and contralateral limb impairment (i.e., disease severity) (Casteels et al. 2010d).

Gender-dependent increases of [^{18}F]MK-9470 uptake with age were measured in women but not in men, particularly in the basal ganglia and hippocampus (Van Laere et al. 2008b). These results were obtained with and without partial-volume correction of the brain images with presumably no loss of effect; partial-volume effects have been minimal and likely insignificant for other studies using [^{18}F]MK-9470. Metabolism of the radioligand was not dependent on age, although there were measured differences in metabolism between sexes. Similarly, sex-dependent differences were measured for the slow parameter of arterial input function (i.e., elimination phase of clearance). However, when applied to pharmacokinetic modeling, no significant difference was measured in arterial plasma input function using a three-parameter bi-exponential model. Larger intersubject variability (COV 15–20 %) and region-dependent differences (up to 230 %) were found than in the smaller sample size of the initial human study (Burns et al. 2007).

In part to assess this large variation within groups, additional information was obtained from subjects to find correlations between receptor availability and temperament traits, as have been shown for other receptor systems (Farde et al. 1997). Novelty-seeking traits were found to be inversely correlated to [^{18}F]MK-9470 uptake throughout the brain, with the strongest correlation in the left amygdala (Van Laere et al. 2009). The trait subtypes of extravagance and disorderliness maintained significance even after strict limitations, while trait subtypes of exploratory excitability and impulsiveness and trait types harm avoidance, reward dependence, and persistence failed to attain significant correlations with CB_1 receptor availability. As novelty-seeking traits are associated with thrill seeking, addiction behavior (including overeating and substance dependence), and impulsive aggression (Hiroi and Agatsuma 2005), their association with CB_1 receptor imaging, and particular location in the amygdala, is intriguing.

Given the high concentration of CB_1 receptors in the basal ganglia, neuropsychiatric and movement disorders known to affect those regions present themselves as potentially sensitive and particularly interesting targets for CB_1 receptor PET imaging. In two such neuropathological states, [^{18}F]MK-9470 has demonstrated changes in brain uptake. In Huntington's disease, [^{18}F]MK-9470 uptake was decreased in all areas of brain except white matter compared to healthy controls (Fig. 11.12) (Van Laere et al. 2010). Intriguingly, this was also observed in early symptomatic patients, even in areas with minimal volume loss. Decreased uptake was presumably due to reduced CB_1 receptor availability, as huntingtin is known to interfere with protein and receptor expression. Therefore, CB_1 PET imaging may be a useful tool to assess early symptomatic, and potentially presymptomatic, Huntington's disease onset. Similar reductions in [^{18}F]MK-9470 brain uptake were observed in a rat genetic model of Huntington's disease when compared to wild-type littermates (Casteels et al. 2011); however, this was observed in a regionally selective fashion limited to the basal ganglia, rather than the global reduction

described above for humans. A rat model using unilateral quinolinic acid lesion demonstrated a disproportionately modest decrease of [^{18}F]MK-9470 uptake compared to the severity of the lesion and an increase in contralateral basal ganglia and cerebellum, the latter of which corresponded to improved functional outcome (Casteels et al. 2010a).

In Parkinson's disease [^{18}F]MK-9470 uptake was altered in a region-specific pattern (Van Laere et al. 2012). In ventral midbrain (site of the substantia nigra), tracer uptake was decreased for early and late stages of Parkinson's disease patients compared to healthy controls, likely representing reduced CB_1 receptor expression in the pars reticulata, irrespective of disease progression, rather than simply a marker of neuronal loss. Whereas in putamen, prefrontal cortex, midcingulate, anterior insula, and hippocampus (regions correlating to dopaminergic projections), tracer uptake was increased relative to total brain uptake in comparison to healthy controls. Regionally increased CB_1 receptor availability could be explained by compensatory processes of reducing glutamatergic drive in the absence of normally inhibitory dopamine (in striatum) on glutamatergic neurons and disinhibition of dopaminergic neurons in the ventral tegmental area via a feedback mechanism from mesocortical and mesolimbic regions. Comparison of Parkinson's disease patients with or without levodopa-induced dyskinesias did not reveal any differences in [^{18}F]MK-9470 uptake, as was also shown in healthy rats receiving L-DOPA or bromocriptine (Casteels et al. 2010b).

Anorexia nervosa patients demonstrated globally increased [^{18}F]MK-9470 uptake in brain compared to healthy controls (Gerard et al. 2011). The amount of uptake was also significantly more than bulimia nervosa patients, though bulimia nervosa patients were not statistically different from controls. Uptake was relatively increased in insula for anorexia (right side) and bulimia (left side) patients and in areas of frontotemporal cortex in anorexia patients. In addition, scores rating drive for thinness in anorexia patients correlated with [^{18}F]MK-9470 uptake in one subregion. Increased uptake was interpreted as increased CB_1 receptor availability and therefore hypoactive endocannabinoid transmission. Similar results were found in rat models for anorexia, as released in two abstracts (Gerard et al. 2007, 2009).

An examination of patients with mesial temporal lobe epilepsy due to hippocampal sclerosis provided an *in vivo* perspective on the role of CB_1 receptors in a locally hyperexcitable and excitotoxic environment. Compared to healthy controls, [^{18}F]MK-9470 uptake was increased in the ipsilateral temporal lobe, and decreased in ipsilateral and, to a lesser extent, contralateral insula relative to the affected lobe (Goffin et al. 2011). Insufficient data is available to distinguish whether these changes are acute or chronic; however, there were significant correlations to relative uptake in the seizure focus: a positive correlation with number of seizures in the month prior to scanning and a negative correlation to the number of days since the last seizure before scanning.

In women with episodic migraine, [^{18}F]MK-9470 uptake was globally increased by about 16 %, with focal increases found in anterior cingulate, mesial temporal, prefrontal, and superior frontal cortices (Van der Schueren et al. 2011). No significant clinical correlations could be made between CB_1 receptor availability and

migraine characteristics (e.g., with or without aura, age of onset, migraine frequency).

In humans, [^{18}F]MK-9470 has shown to be useful in estimating receptor occupancy of other inverse agonists (Addy et al. 2008; Burns et al. 2007). Clinical trials of taranabant for weight loss showed that 10–40 % receptor occupancy was sufficient to produce significant amounts of weight loss in a dose-dependent fashion, which is in agreement with estimates from preclinical rodent studies.

Whole-body imaging studies using [^{18}F]MK-9470 demonstrated the radiation burden to be acceptable for completion of multiple brain studies per year ($22.8 \pm 4.3 \mu\text{Sv}/\text{MBq}$) and similar to that of other commonly used PET tracers (Van Laere et al. 2008c). Brain uptake of the radioligand was about 3.2–4.9 % of the total dose, and receptor occupancy was estimated to be well below 1 %. [^{18}F]MK-9470 undergoes predominantly hepatobiliary excretion, with significant radiation burden to the gallbladder which was the radiation dose-limiting organ. Although measured radioactivity in the periphery likely originates from a mixture of parent compound and its metabolites, an appreciable amount of radioactivity was measured in liver, small intestine, and red bone marrow, sites known to have CB_1 receptors.

11.3.3.4 [^{11}C]MePPEP and [^{18}F]FMPEP- d_2

Preclinical studies in rodents further defined the *in vivo* characteristics of [^{11}C]MePPEP (Terry et al. 2008). According to data from both genetic and pharmacologic rodent models, [^{11}C]MePPEP is not a substrate for P-gp and has high specificity for the CB_1 receptor if methods are used to correct for concentration of radioligand in plasma. Approximately two-thirds of radioactivity after injection of [^{11}C]MePPEP is specific for CB_1 receptors in mouse and rat brain, and serial arterial blood sampling permitted kinetic modeling of [^{11}C]MePPEP and measurements of CB_1 receptors as distribution volume within 70 min of scan time. A constant percentage (13 %) of the radioactivity present in rat brain was in the form of metabolites, which may cause a stable, overestimated value of distribution volume. High doses of CB_1 receptor agonists, including endocannabinoids and high-affinity synthetic cannabinoids, were unable to cause any displacement or blockade of [^{11}C]MePPEP binding in brain; these findings were independently confirmed by *ex vivo* experiments using mass spectrometry. Despite the much higher affinity of MePPEP over lower affinity agonists (e.g., endocannabinoids) for CB_1 receptors, the severalfold higher concentration of agonists would be expected to compete and potentially displace or block the tracer dose of radioligand. The inability of [^{11}C]MePPEP to be displaced by agonist *in vivo* suggests a large receptor reserve; that is, a small percentage of CB_1 receptors are in the high affinity, agonist preferring, state *in vivo*, as was previously shown *in vitro* (Gifford et al. 1999).

Initial scans in human brain using [^{11}C]MePPEP demonstrated that radioactivity concentrated in areas with high CB_1 receptor density and decreased slowly over the 150 min study (Terry et al. 2009). Despite the relatively low test-retest variability (8 %) and low intersubject variability (16 %) of brain uptake, when combined with concentrations of parent radioligand in arterial plasma to calculate V_T , the intersubject variability was much higher (>50 %). Assuming that the slow washout of [^{11}C]

MePPEP from brain limited a sufficient amount of pharmacokinetic data from being collected, an increased scan time of 210 min demonstrated that measurements of distribution volume were affected not by the washout rate of [^{11}C]MePPEP, but rather by the low concentration of [^{11}C]MePPEP in plasma and the radioactive half-life of ^{11}C ($t_{1/2}=20.4$ min). Thus, the relatively poor precision of the plasma measurements contributed to the higher within- and between-subject variabilities of V_T compared to those of brain uptake. Nevertheless, measurements of V_T were highly stable over time, and consistent values were observed 60 min after injection. The intraclass correlation coefficient (ICC) of V_T (i.e., the sensitivity of distinguishing variability between subjects from within subjects) was considered good to excellent (0.87) and better than that of brain uptake measured alone (0.77). Taken together, the stable measures of V_T , the high ICC of V_T , and the theoretically superior outcome measure of V_T compared to brain uptake suggest that V_T remains the more accurate index of CB_1 receptor density, in spite of the poor precision of plasma measurements. In simulations where CB_1 receptor density was varied, V_T was much more sensitive than brain uptake alone in measuring increases, but not sensitive for decreases, of receptor density, and therefore might be expected to require fewer sample points (i.e., study subjects) to detect significant differences between groups.

In an effort to develop a radioligand with improved measurements of radioactivity for an extended time, fluorinated analogs of [^{11}C]MePPEP were developed and tested in monkeys, yielding [^{18}F]FMPEP- d_2 as suitable for human studies (Terry et al. 2010b). Other fluorinated radioligands tested had either less specific binding or showed higher amounts of radioactivity bound to bone, presumably due to free [^{18}F]fluoride which was formed as a metabolite from the parent radioligand. Indeed, deuterium substitution on the fluoromethoxy radiolabel to inhibit defluorination resulted in about 1/3 less radioactivity uptake in bone than was observed after injection of the native hydrogen version. In test-retest studies similar to those done for [^{11}C]MePPEP, [^{18}F]FMPEP- d_2 yielded similar between-subject variability for brain uptake; however, [^{18}F]FMPEP- d_2 demonstrated a much better test-retest variability of plasma measurements (16 % vs. 58 % for [^{11}C]MePPEP). This increased precision of plasma measurements led to a much reduced intersubject variability of V_T (26 %) and, in conjunction with an extremely good ICC (0.89), suggests an improved accuracy of V_T . When changes of receptor density were simulated, V_T was shown to be more sensitive for detecting both increases and decreases of receptor density. The test-retest studies of both [^{11}C]MePPEP and [^{18}F]FMPEP- d_2 were conducted with at least 2 weeks intervals, strengthening the robustness of the radioligands' precision. In conclusion, using [^{18}F]FMPEP- d_2 to measure CB_1 receptor density as V_T was determined to be more precise, accurate, and sensitive than [^{11}C]MePPEP or using brain uptake alone as outcome measurement.

Two significant limitations of [^{18}F]FMPEP- d_2 were identified in early human studies. First, values of V_T increased after 120 min. While the exact cause was not identified, such a trend is consistent with an accumulation of radioactive metabolites in brain. Simulations demonstrated that radioactivity originating from neighboring bone would account for <2 % of the total amount. Fortunately, V_T was measured with consistent and stable values from 60 to 120 min after injection, and

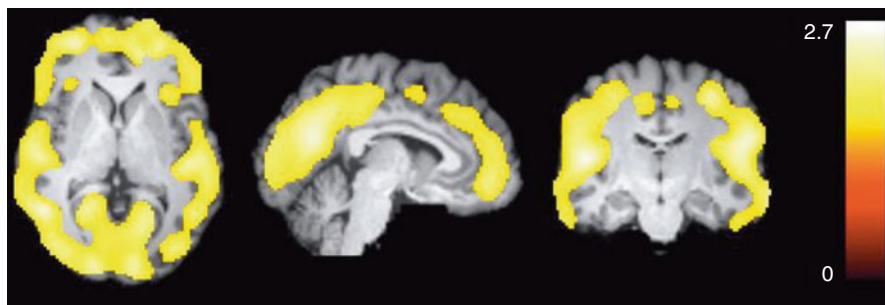


Fig. 11.13 Statistical parametric mapping (SPM) analysis of PET images with [^{18}F]FMPEP- d_2 shows lower V_T in chronic daily cannabis smokers ($n=30$) than in control subjects ($n=28$) at baseline as a large single cluster that includes only cortical regions. This cluster comprised of 67,513 voxels, had a maximum t value of 2.8 at $[-34, -78, 16]$, and had a cluster-level corrected p value of 0.043. Color bar represents t value in each voxel within the significant cluster (Reprinted from Hirvonen et al. (2012) with permission of Nature Publishing Group)

therefore limiting scan duration to 120 min should avoid confounding changes to the accuracy of V_T . Second, the plasma free fraction of both [^{11}C]MePPEP and [^{18}F]FMPEP- d_2 in humans is very low (approximately 0.05 and 0.63 %, respectively). The test-retest variability of plasma free fraction is excellent; however, the intersubject variability was quite large. This is likely due in part to the nature of such low values, since small differences would be disproportionately large in percentage. Since correction of V_T with free fraction (which would be a more correct quantitation of radioligand binding in brain) added too much noise to the final outcome measurements, it was excluded from the calculation of V_T . Thus, it is recommended that potential changes of free fraction be accounted for in future studies, particularly those with pharmacological challenges, as a proportionately large amount of radioligand could be displaced from plasma proteins and made available to enter brain.

[^{18}F]FMPEP- d_2 has been used to demonstrate a reversible downregulation of CB_1 receptors in chronic cannabis smokers (Hirvonen et al. 2010, 2012). Compared to healthy controls, V_T of [^{18}F]FMPEP- d_2 in chronic daily cannabis smokers was ~20 % lower in all regions of neocortex, but not subcortex, including basal ganglia (Fig. 11.13). Years of smoking correlated negatively with V_T (i.e., more years of smoking correlated with smaller V_T), as V_T of [^{18}F]FMPEP- d_2 was independent of age in healthy males. As there was no significant difference between groups for V_T in cerebellum, this tissue was used as a reference tissue for additional analysis; it should be noted that this was performed only after the lack of difference for V_T was established between groups using the standard method correcting for radioligand in plasma and may not be directly applicable to other between-group analyses. Following approximately 1 month of cannabis abstinence, V_T increased in all affected regions except hippocampus, demonstrating that the downregulation of CB_1 receptors was reversible. In addition, V_T correlated negatively with BMI; therefore, BMI was used as an adjustment variable in all findings. BMI or cannabis use did not correlate with free fraction of the radioligand, a potential confounding

variable of the study. Neither the initial V_T nor the amount of recovery of V_T after 4 weeks abstinence correlated with age of first use, amount of current daily use, or any clinical rating scales measuring withdrawal or craving. Tobacco smoking did not affect the results when included as a confounding variable in cannabis abusers; although not assessed in healthy controls, this suggests that nicotine does not affect CB_1 receptor binding or availability. Interestingly, three control subjects of Indian descent had significantly lower V_T , but there was no difference for subjects of African or European descent, compared to the rest of the control group.

In alcohol-dependent patients, [^{18}F]FMPEP- d_2 demonstrated reduced CB_1 receptor binding that did not recover after 2–4 weeks of abstinence. Compared to healthy controls ($n=19$), alcohol-dependent patients ($n=18$) had approximately 20–30 % lower V_T adjusted for BMI across all brain regions. Years of alcohol use correlated negatively with V_T , which was not confounded by age. Differences between controls and alcohol-dependent patients could not be accounted for by clinical rating scales for alcohol use or withdrawal, or by tobacco use, and remained significant after partial-volume correction. Repeat scans 2–4 weeks after abstinence did not result in any significant change in V_T . In both groups, those individuals carrying the *rs2023239 C* allele of *CNR1* had higher V_T (31 % higher in patients, 19 % in controls), although no statistical differences were detected between carriers and noncarriers based on demographic or clinical variables (Hirvonen et al. 2013). Whole-body imaging studies using [^{11}C]MePPEP and [^{18}F]FMPEP- d_2 demonstrated the radiation burden to be acceptable for both radioligands ($4.6 \pm 0.3 \mu Sv/MBq$ and $19.7 \pm 2.1 \mu Sv/MBq$, respectively) for completion of multiple brain studies per year (Terry et al. 2010a). Brain uptake of both radioligands was about 7–8 % of the total dose, and receptor occupancy is estimated to be well below 1 % (0.3 % for [^{11}C]MePPEP and 0.06 % for [^{18}F]FMPEP- d_2). Both radioligands undergo hepatobiliary excretion, [^{11}C]MePPEP exclusively, while [^{18}F]FMPEP- d_2 undergoes also some urinary excretion. Similar to [^{18}F]MK-9470, and as first reported for [^{11}C]OMAR, an appreciable amount of radioactivity was measured in red bone marrow. To determine if radioactivity was concentrated in bone tissue rather than bone marrow, additional analysis showed the pattern of accumulation in bone was consistent with areas rich in bone marrow, such as vertebrae, pelvis, and ribs. A comparison of bones rich in marrow to those devoid of marrow demonstrated that radioactivity was not largely due to accumulation in bone. In addition, studies using monkeys demonstrated that about 20 % of the radioactivity in bone marrow was due to specific binding to CB_1 receptors.

11.3.3.5 Considerations and Conclusions on the Use of Current CB_1 Receptor PET Radioligands

The development and evaluation of CB_1 receptor PET radioligands has presented both insight into CB_1 receptor pathophysiology and challenges to PET radiochemistry and pharmacokinetic modeling. For instance, CB_1 receptor density decreases after direct agonist stimulation (as cannabis abusers had lower V_T compared to controls) and in states regarded to have increased endocannabinoid tone (e.g., Huntington's disease), which was not due to direct competition with exogenous or

endogenous cannabinoids. Also, changes observed in CB₁ receptor density or availability were often region dependent, and in one case, a region-specific lesion resulted in contralateral changes (Casteels et al. 2010d); while unilateral lesions or comparisons across hemispheres are commonly performed for other tracers, findings from these CB₁ receptor imaging studies suggest that this may not always be an appropriate method. In terms of radiochemistry, the primary breakthrough in CB₁ receptor imaging was the development of ligands with lower lipophilicity and higher binding affinity. However, high lipophilicity continues to present challenges (see Sect. 11.3.3.1), and high binding affinity and slow clearance of the radioligands have presented new ones. The results from [¹¹C]OMAR and [¹¹C]MePPEP exemplify the need for accurate plasma measurements when determining V_T and that peak uptake alone is not an appropriate outcome measure when comparisons are made between subjects. Although not tested directly, distribution volume of [¹⁸F]FMPEP- d_2 obtained from controls and cannabis abusers, and of [¹¹C]OMAR and [¹⁸F]FMPEP- d_2 in alcohol-dependent subjects, was not significantly different in tobacco smokers compared to nonsmokers, which is consistent with rodent data obtained using [¹⁸F]MK-9470 after nicotine administration. Whether this holds as a non-confounding variable in larger studies remains to be shown. Finally, an inverse discrepancy has been reported for CB₁ receptor imaging in alcohol-dependent patients, in that [¹¹C]OMAR demonstrated a 20 % increase of V_T , while [¹⁸F]FMPEP- d_2 demonstrated a 20–30 % decrease. Whether this difference is due to study design or methods is unclear, and therefore, additional investigation is warranted.

The three radioligands presented above have their particular pros and cons (Table 11.4). [¹¹C]OMAR, with its relatively fast kinetics and C-11 radiolabel, has the advantage that subjects could quickly complete multiple PET studies in 1 day, and receptor density could be quantified by V_T . Its faster kinetics are attributed in part by its more modest binding affinity, which in turn likely contributes to less brain uptake and lower measures of V_T . [¹¹C]OMAR binding was shown to decrease with age, and thus, age should be analyzed as a clinical variable. [¹⁸F]MK-9470 has been studied extensively in healthy controls and in patients with several neuropsychiatric disorders, providing a wealth of data and observations. Its simplified outcome measure does not require arterial blood sampling, greatly easing subject burden and data analysis. However, this comes at the expense of potentially less accurate measurements, as differences in metabolism and excretion are not accounted for in the final outcome measurement. These initial studies also uncovered several clinical variables that should be accounted for when analyzing [¹⁸F]MK-9470 data, including age, sex, and weight. [¹⁸F]FMPEP- d_2 has high brain uptake which can be quantified by distribution volume and therefore is more likely to detect small changes in CB₁ receptor availability and more accurately measure an index of receptor density. It is available in C-11 form ([¹¹C]MePPEP) in addition to F-18 form, should same-day repeat studies be preferred, and studies with either radioligand can be completed with about 120 min of scanning. Longer scan times with [¹⁸F]FMPEP- d_2 may be vulnerable to radioactivity accumulation in the brain, possibly due to radioactive metabolites. Analysis of [¹⁸F]FMPEP- d_2 should account

Table 11.4 In vivo properties of CB₁ receptor radioligands in humans

Radioligand	[¹¹ C]OMAR	[¹⁸ F]MK-9470	[¹⁸ F]FMPEP- <i>d</i> ₂
Peak brain uptake (SUV)	~2	1.2	~4
Retest variability	–	~7 %	16 %
Intersubject variability	–	16 %	14 %
<i>V</i> _T (mL/cm ³)	~1.5	~22	~23
Retest variability	~3 %	10–30 %	14 %
Intersubject variability	–	(35 % with FUR)	26 %
Effective dose (μSv/MBq)	–	22.8	19.7
References	Normandin et al. (2010b), Wong et al. (2010a)	Addy et al. (2008), Burns et al. (2007), Van Laere et al. (2008b, c)	Terry et al. (2010a, b)

for BMI as a clinical variable. Due to their lipophilicity, the free fraction of all radioligands should be measured when comparing group differences or studying the effect of drugs. To date, partial-volume correction has not affected data for any of the radioligands.

Several uncertainties remain when interpreting data from CB₁ receptor imaging studies. It has been assumed that changes in [¹⁸F]MK-9470 uptake or [¹¹C]OMAR and [¹⁸F]FMPEP-*d*₂ *V*_T likely represent changes in receptor availability. However, it is unknown whether changes in uptake or *V*_T are due to altered receptor density, internalization, and/or changes in receptor trafficking (Cou tts et al. 2001) or changes in receptor binding affinity, as these cannot be distinguished with PET (Martin et al. 2004). Additionally, whether genetic polymorphisms of *CNR1* affect receptor density, binding affinity of the radioligands, or both remains to be assessed (Hutchison et al. 2008; Zhang et al. 2004). Finally, the results presented here were all obtained either in a single study or within a relatively short time span. Therefore, little information is available regarding longitudinal changes of CB₁ receptor expression over time, and the results may either suggest a causal relationship or merely significant correlations.

11.3.4 Current and Future Clinical Application in CB₁ Receptor Imaging

Given the multiple physiological and pathological roles of CB₁ receptors (see Sect. 11.1.4) and the long awaited arrival of specific radioligands to quantify them, there is much excitement and potential for their use. Neurological diseases, neurotransmitter imbalances, substance dependence, eating disorders, schizophrenia, and personality traits have been examined, whereas studies involving mood or anxiety disorders, dementia, stroke, neuroinflammation, or non-CNS diseases have yet to be reported using these radioligands. Several of the studies reviewed here have

generated data that is either contrary to some previous *in vitro* or *in vivo* studies or trended toward but did not achieve significance (Wong et al. 2010a); these may be worth repeating with either larger samples or an alternative radioligand. It also remains to be seen how the results from these studies can be generalized; for instance, would the results in cannabis smokers be seen with other substance-dependent subjects? Would the results reported for Huntington's or Parkinson's disease also be seen in asymptomatic patients with the same disease?

Slow pharmacokinetics have proved to be particularly troublesome for the CB₁ receptor radioligands ([¹¹C]MePPEP, [¹⁸F]MK-9470, and [¹⁸F]FMPEP-*d*₂) reviewed here and have impeded their accuracy and ease of use. [¹¹C]OMAR, a radioligand with improved properties, such as lower lipophilicity, modest binding affinity, and more rapid excretion, is helpful in avoiding long scans and poorly identified outcome measures. [¹¹C]SD5024 is another promising radioligand that may have faster pharmacokinetics, has been evaluated in monkey, and may be suitable for human use (Donohue et al. 2006). The development of additional radioligands with improved properties would be of value. To improve the measurements of parent ligand in plasma, alternative approaches with higher sensitivity could be used. Assays or spectroscopic methods with high accuracy for detecting very low concentrations of drug in plasma should be considered.

As demonstrated by [¹¹C]MePPEP, this class of radioligand is not displaced *in vivo* by endogenous or synthetic agonists. Therefore, these PET tracers can only be used for measuring changes or differences in receptor density or for measuring receptor occupancy by inverse agonists. They cannot be used for measuring receptor occupancy by agonists, and estimates of endocannabinoid tone are only assessed indirectly. Therefore, an agonist radioligand that demonstrates preference for the high-affinity state, and is therefore more susceptible to competition by endogenous agonists, would be of great value. For example, a radioligand for high-affinity dopamine D₂ receptors, [¹¹C]MNPA, is displaced nearly twice as much by dopamine than an antagonist, such as [¹¹C]raclopride (Seneca et al. 2006). Given that only a small proportion of receptors may be in the high-affinity state, the distribution and normal physiology of CB₁ receptors may appear quite different when an agonist radioligand is used for *in vivo* PET. Therefore, development of an agonist radiotracer may provide tremendous insight into the endocannabinoid system.

If an agonist radiotracer for the CB₁ receptor were developed, several experiments probing the endocannabinoid system could be conceived. First, increasing endocannabinoid concentrations by inhibiting their degradation or reuptake (via FAAH, MAG lipase, or other proteins) would provide better understanding of this dynamic and possibly regionally selective process. Second, studies involving stimulation or inhibition of the release of primary neurotransmitters could be performed to assess the relative response of endocannabinoids to neuromodulation of GABA, glutamate, and dopamine. Third, a radioligand sensitive to dynamic changes in endocannabinoid concentration would allow for *in vivo* studies with behavioral components, such as acute stress response (Gorzalka et al. 2008).

Development of an agonist radiotracer is likely to be difficult, primarily due to their high lipophilicity. Very few CB₁ agonists have the moderate lipophilicity

required for a PET tracer; a notable exception is the aminoalkylindole class of agonists, typified by WIN-55,212-2. In addition, most existing agonists do not have high selectivity for the CB₁ receptor. Indeed, one of the first attempts to develop a radioligand to image CB₁ receptors was [¹⁸F]Δ⁸-THC, which exhibited a prohibitively high lipophilicity and has nearly equal affinity for CB₁ and CB₂ receptors. Given the relatively low expression of CB₂ compared to CB₁ receptors and the availability of selective antagonists, it is unknown if high selectivity would be an absolute requirement for an agonist radioligand. Finally, the development of an agonist radioligand may face the complexities posed by partial agonism and functional selectivity, which may present the CB₁ receptor with altered binding conformations and possibly differing binding affinities for agonists depending on intracellular coupling of the receptor (Georgieva et al. 2008).

Lastly, there are many potential non-CNS applications for CB₁ receptor imaging, including liver fibrosis, metabolic diseases such as diabetes, and cancer. At present, insufficient data is available to determine if the existing CB₁ receptor radioligands would be optimal for use in imaging of diseases outside the CNS, and, if so, what the optimal method of analysis would be (radioactivity concentration vs. distribution volume). More research concerning the appropriate use of these tracers for imaging CB₁ receptors outside the brain needs to be performed.

11.4 Imaging of CB₂

The CB₂ receptor is expressed primarily by the immune system (Galiegue et al. 1995; Munro et al. 1993; Schatz et al. 1997), but recently it has been found in intact CNS tissue in tiny concentrations (Ashton et al. 2006; Gong et al. 2006; Van Sickle et al. 2005). Importantly, CB₂ receptors are highly expressed in disorders that are associated with inflammation including cancer, pain, osteoporosis, and liver diseases (see for review (Ashton 2007; Pertwee 2009; Pisanti and Bifulco 2009)). The entire functional role of CB₂ receptor expression in the inflammatory processes has yet to be clarified, though its upregulation makes CB₂ a unique biomarker of microglial/macrophage cell-specific activity in these neuroinflammatory processes.

Recent studies have demonstrated high expression of CB₂ receptors in CNS microglia in patients with various neuroinflammatory disorders (Benito et al. 2008). Postmortem tissue studies from patients with AD demonstrate dramatically increased expression of CB₂ receptors in areas of beta-amyloid (Aβ) plaque deposition (Benito et al. 2003). CB₂ receptor expression increases in striatal microglia of transgenic mouse models of Huntington's disease and patients with HD (Palazuelos et al. 2009). Better understanding of the immune-modifying role and principal mechanisms of CB₂ receptor agonists in the human CNS could facilitate the development of disease-modifying treatments and preventive agents, as proposed for AD (Tolon et al. 2009). Induced expression of CB₂ receptors in neuroinflammatory disease is also observed in tissue samples from human and animal models of HIV-induced encephalitis and multiple sclerosis (Benito et al. 2005) (see for review (Tolon et al. 2009)). Traumatic brain injury (TBI) leads to the release of

pro-inflammatory cytokines in the brain, which then cause neuronal cell death and secondary damage. Simultaneously, there is “on-demand” synthesis of cannabinoid receptors including CB₂, which in turn inhibit inflammatory responses (Shohami et al. 2011; Stella 2010).

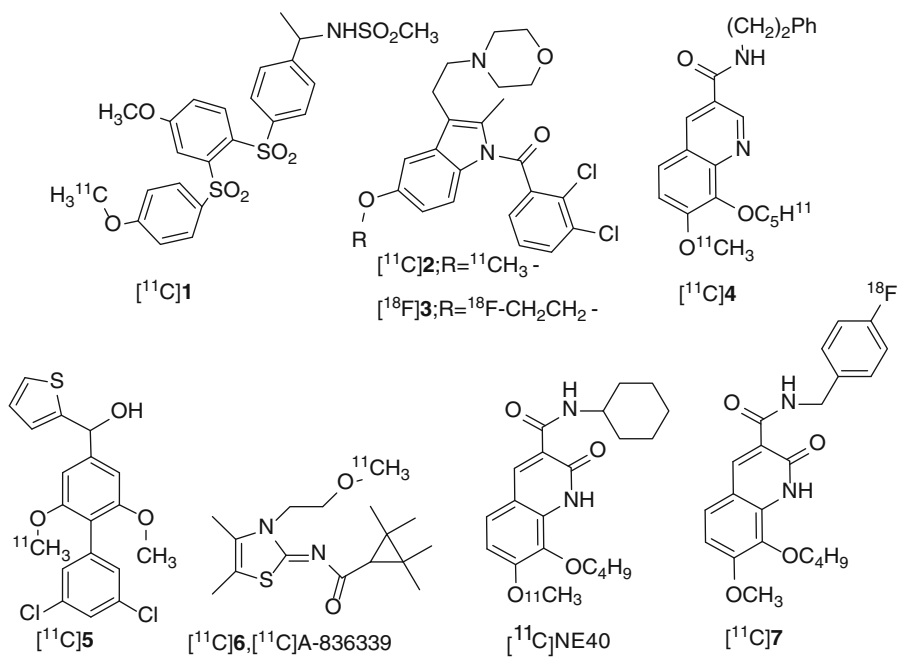
There are also unique therapeutic implications afforded by a better understanding of the endocannabinoid system and supported by recent studies of CB₂-specific agonists (Ehrhart et al. 2005; Tolon et al. 2009). Recent studies demonstrated that brain CB₂ receptors modulate cocaine’s rewarding and locomotor-stimulating effects (Xi et al. 2011). CB₂ is involved in some of the effects mediated by alcohol (Ishiguro et al. 2007) in rodent brains and expression of CB₂ in microglia increases in response to MDMA (“ecstasy”) treatment (Torres et al. 2010).

In summary, the CB₂ receptor that is nearly absent in the normal brain and highly expressed in activated microglia in neuroinflammation is an attractive target for PET imaging of a large variety of disorders that are associated with neuroinflammation. Although substantial progress has been made in the development of radioligands to image CB₁ with PET, the absence of suitable PET radioligands has hampered the noninvasive imaging of CB₂. Several CB₂ radioligands have recently been synthesized and evaluated in animals as potential PET radioligands (Evens et al. 2008, 2009a; Fujinaga et al. 2010; Gao et al. 2010).

11.4.1 Development of CB₂ Radioligands

CB₂ PET imaging and radioligand development are still in its early stage, but several research groups around the world are working in this direction; initial radioligand development has recently been described in an excellent review (Evens and Bormans 2010). Pioneer work of researchers from Canada and France revealed first selective CB₂ agonists (Gallant et al. 1996) and inverse agonists (Rinaldi-Carmona et al. 1998) with nanomolar affinity. In the last few years, a large number of selective high-affinity CB₂ ligands have been developed, and they were a basis for the recent development of CB₂ PET radioligands. The most representative CB₂ PET radioligands and their properties are shown in Tables 11.5 and 11.6. Table 11.5 lists physical-chemical properties that are linked to their imaging properties (Table 11.6).

The group from KU Leuven reported that [¹¹C]1 had high CB₂ binding affinity (Evens et al. 2008), but it exhibited low brain uptake (Tables 11.5 and 11.6). This is in accord with the high PSA value and high molecular weight (MW=540) of this radioligand that are above the conventional limits for passive BBB transport. However, brain uptake increased following the administration of cyclosporine A, which inhibits several BBB efflux transporters including P-gp, indicating that the radioligand is an efflux transporter substrate. No further studies on [¹¹C]1 have been published. Researchers from the same group presented radioligands based on the compound GW405833, [¹¹C]2 and [¹⁸F]3, which have more moderate CB₂ binding affinities (Table 11.5) (Evens et al. 2011). Both [¹¹C]2 and [¹⁸F]3 showed good BBB permeability (Table 11.6), in agreement with their molecular properties. Unfortunately, [¹⁸F]3 had much slower washout of radioactivity from mouse brain

Table 11.5 Physical-chemical properties of the recently developed CB₂ radioligands

Structure	M.W.	$clogD_{7.4}^a$	PSA	Experimental CB ₂ K _i , nM (CB ₂ /CB ₁ selectivity)	References
[¹¹ C]1	540	2.8	158	0.4 (2,263)	Evens et al. (2008)
[¹¹ C]2	447	4.5 2.5 ^b	44	35 (171)	Baekelandt et al. (2010), Evens et al. (2007), Evens and Bormans (2010)
[¹⁸ F]3	356	4.7 2.8 ^b	44	27 (370)	Evens and Bormans (2010), Evens et al. (2011)
[¹¹ C]4	393	3.6	60	6.9 (28)	Gao et al. (2010)
[¹¹ C]5	395	4.6	39	0.3 (3,333)	Fujinaga et al. (2010)
[¹¹ C]6	310	3.37 ± 0.08 ^b	42	0.7 (450)	Yao et al. (2009), Horti et al. (2010)
[¹¹ C]NE40	372	3.9 ± 0.01 ^b	77	9.6 (>100)	Evens et al. (2009a)
[¹⁸ F]7	398	4.4 ^b	77	3.4	Turkman et al. (2012)

^aLipophilicity $\log D_{7.4}$ and PSA values were calculated with ACD/Structure Designer Suite (Toronto, Canada)

^bExperimental data

than [¹¹C]2, which was due to a large fraction of radiometabolites in brain (50 % at 30 min after injection), limiting its further development.

The same group (Evens et al. 2009b; Vandeputte et al. 2011) took advantage of the low expression of CB₂ receptors in normal brain by using the CB₂/[¹¹C]2 reporter gene/reporter probe combination as a possible way to follow suitably transfected

Table 11.6 Imaging properties of the recently developed PET CB₂ radioligands

Radioligand	Spleen uptake, %ID/g	Brain uptake, %ID/g	Brain BP (animal model)	Reference
[¹¹ C]1	–	Low	–	Evens et al. (2008)
[¹¹ C]2	1 (2 min), 1 (1 h)	1.4 (2 min), 0.1(1 h)	>1 ^a	Evens and Bormans (2010)
[¹¹ C]3	0.9 (2 min), 0.7 (1 h)	1.7 (1 h)	–	Evens and Bormans (2010)
[¹¹ C]4	–	–	–	Gao et al. (2010)
[¹¹ C]5	n/a	1.9 (1 min), 0.7 (1 h)	–	Fujinaga et al. (2010)
[¹¹ C]6	1.3 (1 h) – control 0.6 (1 h) – CB ₂ block Control/block = 2.2	0.4 (1 h)	1.4 ^b , 2.5 ^c	Horti et al. (2010)
[¹¹ C]NE40	Control/block = 1.9	0.8 (2 min) 0.1 (60 min)	~3 ^a	Evens et al. (2012)
[¹⁸ F]7	Insignificant	–	~1 ^d	Turkman et al. (2012)

^aRat model of CB₂ overexpression

^bMouse model of Alzheimer's disease

^cLPS mouse model of neuroinflammation

^dU87/CB₂-expressing tumor in mice

cells. [¹¹C]2 is capable of selective CB₂ imaging in rats with an induced overexpression of the CB₂ receptor, but due to their relatively low binding affinity, both [¹¹C]2 and [¹⁸F]3 are unlikely candidates for imaging in neuroinflammatory disorders. Also, [¹¹C]2 exhibited low washout and high nonspecific binding in healthy monkey brain (Vandeputte et al. 2011).

A research group from Indiana synthesized a CB₂ ligand [¹¹C]4 (Gao et al. 2010) with moderate CB₂ binding affinity and low CB₂/CB₁ selectivity (Table 11.5). No animal studies have been published.

The Chiba University PET center presented a series of triaryl CB₂ radioligands (Fujinaga et al. 2010). One of these compounds [¹¹C]5 exhibited high binding affinity (Table 11.5). In a mouse study, [¹¹C]5 manifested good BBB penetration, but its slow brain washout suggests substantial nonspecific binding, which can be explained by the high lipophilicity of this radioligand (Tables 11.5 and 11.6).

The JHU group has recently synthesized [¹¹C]A836339 ([¹¹C]6) (Horti et al. 2010), a selective CB₂ agonist with high binding affinity, moderate lipophilicity, and an adequate PSA value for CNS activity (Table 11.5). In healthy control CD1 mice, [¹¹C]6 shows specific binding (Horti et al. 2010) (50 %, Table 11.6) in the spleen, an organ with high CB₂ receptor density. In control mice [¹¹C]6 exhibited good BBB permeability and little specific in vivo binding in the mouse brain, which is in agreement with low expression of CB₂ receptors in the intact brain (Munro et al. 1993; Schatz et al. 1997). The specific cerebral binding of [¹¹C]6 was studied in two animal models of neuroinflammation, a lipopolysaccharide (LPS)-induced mouse model (Qin et al. 2007) and a transgenic amyloid mouse model of AD (APP^{swE}/PS1dE9 mice). The dissection study (baseline and blockade (Horti et al. 2010))

showed that [^{11}C]6 exhibits high specific binding to CB_2 receptors (78–84 %) in LPS-treated mice. These results were also confirmed in a small animal PET/[^{11}C]6 study with control and LPS-treated mice (standardized uptake value (SUV)=0.7 and 2.3, respectively). The cerebral specific binding of [^{11}C]6 in the LPS-treated mice is in accordance with a previously found upregulation of CB_2 in this neuroinflammation model (Mukhopadhyay et al. 2006). The very high total cerebral uptake of [^{11}C]6 in LPS-treated mice may be associated in part with dysfunction of the BBB (Sumi et al. 2010). Brain distribution of [^{11}C]6 in the AD mouse model demonstrated that [^{11}C]6 displays significant specific CB_2 binding (29–33 %) in various brain regions, which is consistent with the distribution of the $\text{A}\beta$ plaques in this mouse model of AD. Previous *in vitro* studies showed that CB_2 receptors are abundantly and selectively expressed in microglia in human brain tissue from patients with AD, whereas the expression of the CB_1 subtype remains unchanged (Benito et al. 2003). These results suggest the potential of the CB_2 radioligand [^{11}C]6 for PET imaging of neuroinflammation in neurodegenerative disorders.

The latest compound of the KU Leuven group [^{11}C]NE40 (Evens et al. 2009a) displays favorable molecular properties for BBB transport, but its binding affinity is moderate (Table 11.5). [^{11}C]NE40 was successfully evaluated in a substantial number of preclinical safety studies (Evens et al. 2012). [^{11}C]NE40 showed specific CB_2 receptor binding in the spleen and blood of normal rats and high initial brain uptake in rhesus monkeys. In a rat model with local h- CB_2 receptor overexpression, [^{11}C]NE40 demonstrated specific and reversible binding to h- CB_2 receptors. [^{11}C]NE40 is the first CB_2 receptor PET radioligand that was selected for human PET studies. In healthy human brain, [^{11}C]NE40 exhibited rapid uptake and washout (Ahmad et al. 2011), but PET studies with [^{11}C]NE40 in disease have not yet been reported.

A group from MD Anderson Cancer Center has published a series of 2-oxoquinoline derivatives (Turkman et al. 2011) and reported one as a candidate for PET studies (Turkman et al. 2012). Designed to be a more metabolically stable fluorine-18 compound, [^{18}F]7 (Log P 4.4) had poor uptake in spleen, and only about 50 % specific binding on CB_2 receptor-positive tumor cells transfected into mouse. Both the preclinical applications and the clinical potential of this compound are limited by its poor solubility.

11.4.2 CB_2 Imaging Studies

Apart from initial demonstration of *in vivo* potential and proof of target, few CB_2 imaging studies have been reported. In animals, [^{11}C]6 has been shown to have sufficient brain uptake and receptor binding in models of substantial receptor expression; however, the preliminary findings were less favorable in rodent models of Alzheimer's-related neuroinflammation (Horti et al. 2010).

In animal studies [^{11}C]NE40 was shown to have rapid brain uptake and washout and relatively rapid plasma metabolism; however, at 10 min after injection, approximately 10 % of radioactivity in brain was due to radiometabolites (Horti et al. 2010). [^{11}C]NE40 has been used to demonstrate a PET reporter gene system in rats using

an adeno-associated viral vector, a potentially useful application in gene or stem cell therapy (Vandeputte et al. 2011).

The only PET radioligand for CB₂ receptors reported in human use is [¹¹C]NE40 (Ahmad et al. 2011). Although the full results have yet to be published, preliminary findings report rapid uptake and washout from brain, primarily hepatobiliary excretion, and an effective dose of 4.4 μSv/MBq in three healthy males. In addition to intestine, liver, and lungs, radioactivity was observed in lymph nodes and spleen, suggestive of CB₂ receptor localization. Results from humans with (neuro)inflammatory disorders, such as Huntington's disease, are pending.

To date, no pharmacokinetic modeling from *in vivo* imaging of CB₂ receptors has been reported; however, several predictions can be made based on preliminary studies and previous experience with CB₁ receptor imaging. Although CB₂ receptors are found at much lower density in brain than CB₁ receptors, image analysis and pharmacokinetic modeling of CB₂ receptor radioligands may have some potential sources of error. First, similar to CB₁ receptor ligands, CB₂ receptor radioligands are higher in lipophilicity than more commonly used PET tracers, and similar complications as described for CB₁ receptor radioligands should be anticipated. Second, many systemic or local inflammatory conditions can cause disruption of the BBB, causing brain uptake of the radioligand to be affected by flow in addition to specific binding. Third, given the low density of CB₂ receptors normally found in brain, simpler methods for quantifying receptor density might be employed (e.g., reference tissue modeling). However, such methods should be validated using compartmental modeling with plasma measurements prior to routine use of alternative methods, with particular attention to states of systemic inflammation, as increased expression of CB₂ receptors may not be a region-specific phenomenon. Fourth, specific binding may occur to circulating leukocytes in addition to nonspecific binding to plasma proteins, potentially complicating measurements of plasma free fraction. As an additional consequence, competition studies with cannabinoid ligands (agonists or inverse agonists) might be expected to have a more significant effect on plasma free fraction due to preferential displacement of radioligand from specific binding sites. Finally, it is unknown if the expression of CB₂ receptors during neuroinflammation or pathological conditions is consistently correlated to any clinical measures, making efforts toward quantitation both a challenge and an exciting prospect.

11.4.3 Potential Clinical Application of CB₂ Imaging

The paucity of reported results for CB₂ receptor imaging with PET is striking, as is its potential as a clinical biomarker. As reviewed in Sects. 11.1.2 and 11.1.4, multiple inflammatory conditions could be probed by a reliable CB₂ receptor radioligand. Multiple sclerosis, ALS, Huntington's disease, and Alzheimer's disease have already been discussed as neuroinflammatory conditions associated with CB₂ receptor upregulation. In particular, *in vivo* and dynamic monitoring of MS in response to treatment with cannabinoid agonists or other investigatory drugs may be of

particular interest. Vasculitis and cerebritis are often difficult to diagnose, in part due to their frequently normal appearance on conventional imaging, and can be difficult to treat. Thus, CB₂ receptor imaging could potentially provide assistance in both diagnosis and therapy monitoring. Certain types of cancer have demonstrated CB₂ receptor expression, and *in vivo* imaging could assist in identifying tumor type and grade prior to surgery and identify tumors susceptible to treatment with cannabinoids to induce apoptosis. Peripherally, CB₂ receptor imaging may assist in deepening an understanding of inflammation in atherosclerotic (Mach and Steffens 2008) and cardiovascular diseases (Patel et al. 2010). As described by Vandeputte et al. (2011), *in vivo* imaging of CB₂ receptors with a reporter gene/reporter probe system provides an excellent opportunity to monitor gene therapy with PET and may have other potential applications. Finally, inflammatory states have been associated with mood disorders, such as seen in patients treated with PEGylated interferon, and a genetic polymorphism of the CB₂ receptor has been associated with bipolar disorder (Minocci et al. 2011). Whether CB₂ receptors are a suitable *in vivo* biomarker for mood disorders remains unknown.

11.5 Imaging of FAAH

FAAH is an enzyme that is responsible for the breakdown of AEA. FAAH is found in the periphery and the CNS (Egertova et al. 1998; Thomas et al. 1997). FAAH inhibitors are considered to be an important therapeutic target (Otrubova et al. 2011). At this time, there are a relatively small number of publications on the PET imaging of FAAH. It should be noted that the FAAH inhibitory potency of unlabeled compounds that was used to predict specific binding of the corresponding radiotracers does not directly correlate with specific binding of these radiotracers. The lack of binding affinity data for the most promising FAAH inhibitors is an obstacle for development of FAAH radioligands for PET. Nevertheless, the latest studies revealed radioligands for imaging FAAH with adequate properties for PET quantification (Li et al. 2011; Wilson et al. 2011a).

Initial attempts of a group from Belgium to develop PET- and SPECT-labeled FAAH inhibitors have dealt with aryl analogs of AEA (Wyffels et al. 2009, 2010). Compounds [¹²³I]**8** and [¹²³I]**9** (Fig. 11.14) exhibited rapid deiodination in mice and were abandoned (Wyffels et al. 2009). Compounds [¹¹C]**10** and [¹¹C]**11** displayed moderate inhibitory potency of AEA metabolism (pIC₅₀=5.64 and 5.56, respectively) and demonstrated some brain uptake in mice (Wyffels et al. 2009), but no further *in vivo* evaluation has been presented. The latest FAAH PET tracer [¹¹C]**12**, a radiolabeled analog of URB597 (Fig. 11.15) from the same Belgian group, inhibited the hydrolysis of AEA with an IC₅₀ value of 436 nM and manifested good initial brain uptake, but no specific binding was observed in mouse biodistribution studies (Wyffels et al. 2010). It was concluded that this negative result is due to insufficient affinity of [¹¹C]**12**.

Researchers from Toronto have reported a series of ¹¹C-radiolabeled analogs of URB597 with low nanomolar inhibitory potency values (Wilson et al. 2011a, b).

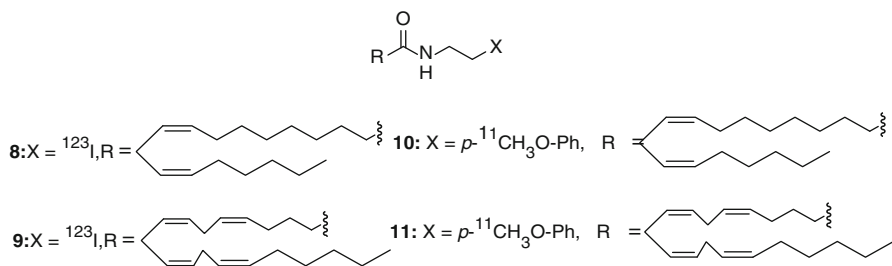


Fig. 11.14 Radiolabeled analogs of AEA for PET and SPECT imaging of FAAH

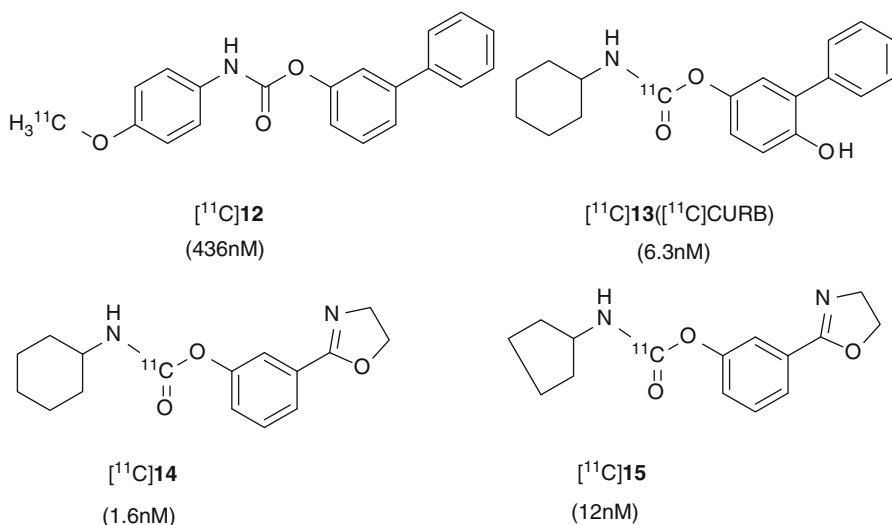


Fig. 11.15 Radiolabeled analogs of URB597

[^{11}C]CURB (Fig. 11.15) showed high brain uptake in rats (SUV of 1.6–2.4 at 5 min) with no washout, which is characteristic of irreversible binding. Regional distribution of radioactivity was found to be high in the cortex, intermediate in cerebellum, and low in the hypothalamus, which corresponds to the known distribution of FAAH in the rat brain (Egertova et al. 1998; Thomas et al. 1997). Pretreatment with the FAAH inhibitor URB597 reduced binding in all brain regions by 70–80%. The authors of the paper concluded that [^{11}C]CURB represents a highly promising radiotracer for imaging FAAH using PET (Wilson et al. 2011b) and started first human PET studies. The latest FAAH compounds reported by the same group ([^{11}C]14 and [^{11}C]15) also demonstrated irreversible high specific uptake in the rat brain (Wilson et al. 2011a), and they should be of interest for further PET imaging studies.

A group from Pfizer has released a series of publications on a novel FAAH inhibitor (Ahn et al. 2011; Johnson et al. 2010) and its closely related radiotracer, [^{18}F]PF-9811

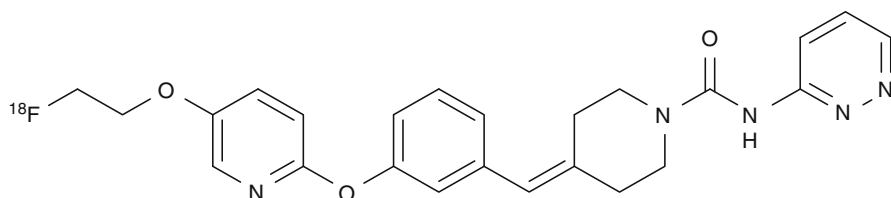
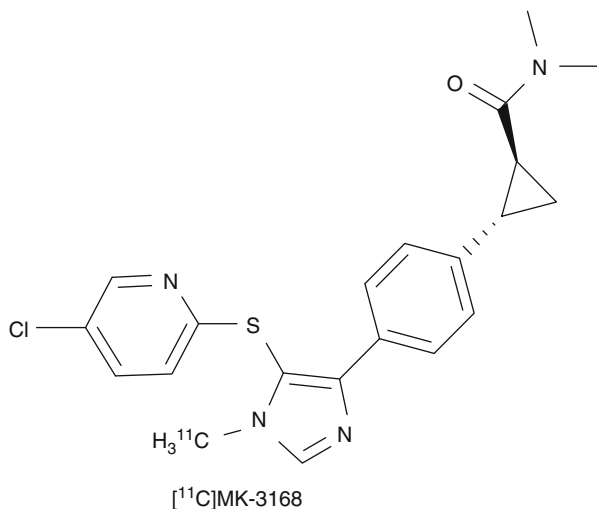


Fig. 11.16 [^{18}F]PF-9811, a novel PET radioligand for imaging FAAH

Fig. 11.17 [^{11}C]MK-3168,
first FAAH PET tracer for
imaging in human subjects



(Fig. 11.16). Using a three-step one-pot reaction sequence, [^{18}F]PF-9811 can be attained in high yield (~11 %). Using an activity-based protein profiling probe for FAAH, [^{18}F]PF-9811 achieved an IC_{50} =16 nM (compared to IC_{50} =3.2 nM for PF-04457845). Following injection of [^{18}F]PF-9811, distribution of radioactivity was as previously described for FAAH and [^{11}C]CURB in rat brain. Both *in vitro* and *in vivo* measurements of [^{18}F]PF-9811 were reduced after pretreatment with PF-04457845 in rats, with ~40 % reduction of SUV as measured by PET after 90 min (Skaddan et al. 2012).

Recently, the Merck PET group has presented data on [^{11}C]MK-3168 (Fig. 11.17), a radiolabeled inhibitor of FAAH (Li et al. 2011). The K_D value (0.8 nM human cortex) of the radiotracer was determined by an inhibition binding assay. Autoradiographic studies in rhesus monkey and human brain slices showed highest binding in striatum, frontal cortex, and hippocampus. PET studies in rhesus monkeys confirmed this uptake pattern, and the expected regional distribution of [^{11}C]MK-3168 was consistent with the *in vitro* autoradiography results. Preadministration of FAAH inhibitors provided evidence that *in vivo* binding of [^{11}C]MK-3168 is mediated by FAAH. Initial human PET/[^{11}C]MK-3168 studies demonstrated high brain uptake (peak SUV ~3–3.5), good test-retest variability, and acceptable radiation burden for PET studies.

11.6 Future

The complexity of the ECS and its seemingly unending connectivity to organ and biochemical systems affords it a vast potential for future development and investigations for in vivo imaging. With regard to radioligand development, targets such as GPR55 (the putative CB₃ receptor), MAG lipase, and the putative endocannabinoid transporter are all unexplored and would add to our knowledge of endocannabinoid physiology. The high density of CB₁ receptors in brain, which has proved a challenge, masks the true physiology of the receptor system; a series of radioligands that can distinguish their associated second messenger systems would provide additional information on the pathophysiology that has already been probed. Non-cannabinoid targets involved in the ECS, such as TRPV1, are likewise unexplored targets for radioligand development.

Conclusion

Herein we have described the utility of ECS imaging with PET, its historical development, the current understanding and experience with it, and its potential applications and developments in the future. Akin to its description as a nonclassical neurotransmitter system, it has pushed the boundaries of classical PET radioligand and pharmacokinetic techniques. Given the established roles of the ECS in physiological function, it is not surprising that direct in vivo imaging has provided a window into basic workings of the normal brain and a wide variety of neuropsychiatric diseases. It is therefore expected to continue yielding additional new insights for those, as well as for inflammatory, immunological, and non-CNS diseases.

Progress in the medicinal chemistry of cannabinoid drugs stimulated discovery of radiotracers for imaging the ECS. Most PET imaging studies on the ECS have been done with CB₁ receptor radioligands. There are at least three radiolabeled CB₁ receptor inverse agonists ([¹¹C]OMAR, [¹⁸F]MK-9470, and [¹⁸F]FMPEP-*d*₂) that are suitable for PET imaging in human subjects. All three radioligands are not free of drawbacks and better compounds are under development. Combination of excellent specific signal, high brain uptake, appropriate brain kinetics, absence of active radiometabolites, and radiochemical availability are a must for a successful radioligand for PET imaging in humans, but this is a tough nut to crack. Also, a useful radiolabeled CB₁ receptor agonist for PET imaging in humans remains to be discovered.

Several research groups are actively working on the development of CB₂ PET radioligands as potential probes for imaging inflammation in various disorders. Very low expression of CB₂ in the intact CNS dictates a necessity for a CB₂ PET radioligand with very high binding affinity. So far only one radioligand, [¹¹C]NE40, has been studied and reported in humans, but its binding affinity is rather moderate. To our knowledge, no PET imaging of CB₂ receptors in human disease has been published. The major obstacle in the development of CB₁ and CB₂ radioligands is a very high lipophilicity of compounds with sufficiently high binding affinities.

Discovery of FAAH PET radioligands is under way, and first human imaging studies have been recently reported. If the clinical potential of targeting FAAH remains hopeful, additional therapeutic compounds are likely to be discovered, and improved radioligands are likely to follow. As the depths of the ECS continue to be sounded, the drive for novel radioligands remains an exciting pursuit.

Acknowledgments The authors would like to thank Drs. Robert F. Dannals and Richard L. Wahl (Johns Hopkins University) for useful comments and continuous support and Mrs. Julia Buchanan (Johns Hopkins University) for editorial assistance.

The work on this chapter was supported in part by the NIH grant MH079017 (AGH) and the Division of Nuclear Medicine, Johns Hopkins School of Medicine.

Dr. Terry is supported by UCLA and the Resnick Neuropsychiatric Hospital.

References

- Addy C, Wright H, Van Laere K et al (2008) The acyclic CB1R inverse agonist taranabant mediates weight loss by increasing energy expenditure and decreasing caloric intake. *Cell Metab* 7:68–78
- Ahmad R, Evens N, Koole M et al (2011) Whole-body biodistribution and radiation dosimetry of the human cannabinoid type-2 receptor ligand [¹¹C]-NE40 in healthy subjects. *J Nucl Med* 52(Suppl 1):1470
- Ahn K, Smith SE, Liimatta MB et al (2011) Mechanistic and pharmacological characterization of PF-04457845: a highly potent and selective fatty acid amide hydrolase inhibitor that reduces inflammatory and noninflammatory pain. *J Pharmacol Exp Ther* 338:114–124
- Ambudkar SV, Kimchi-Sarfaty C, Sauna ZE et al (2003) P-glycoprotein: from genomics to mechanism. *Oncogene* 22:7468–7485
- Anand P, Whiteside G, Fowler CJ et al (2009) Targeting CB2 receptors and the endocannabinoid system for the treatment of pain. *Brain Res Rev* 60:255–266
- Ashton JC (2007) Cannabinoids for the treatment of inflammation. *Curr Opin Investig Drugs* 8:373–384
- Ashton JC, Friberg D, Darlington CL et al (2006) Expression of the cannabinoid CB2 receptor in the rat cerebellum: an immunohistochemical study. *Neurosci Lett* 396:113–116
- Ashton JC, Rahman RM, Nair SM et al (2007) Cerebral hypoxia-ischemia and middle cerebral artery occlusion induce expression of the cannabinoid CB2 receptor in the brain. *Neurosci Lett* 412:114–117
- Bacci A, Huguenard JR, Prince DA (2004) Long-lasting self-inhibition of neocortical interneurons mediated by endocannabinoids. *Nature* 431:312–316
- Baekelandt V, Bormans G, Debyser Z et al (2010) Reporter gene constructs and radioligand probes for PET, Patent application, WO 2010105315 A3
- Benito C, Nunez E, Tolon RM et al (2003) Cannabinoid CB2 receptors and fatty acid amide hydrolase are selectively overexpressed in neuritic plaque-associated glia in Alzheimer's disease brains. *J Neurosci* 23:11136–11141
- Benito C, Kim WK, Chavarria I et al (2005) A glial endogenous cannabinoid system is upregulated in the brains of macaques with simian immunodeficiency virus-induced encephalitis. *J Neurosci* 25:2530–2536
- Benito C, Romero JP, Tolon RM et al (2007) Cannabinoid CB1 and CB2 receptors and fatty acid amide hydrolase are specific markers of plaque cell subtypes in human multiple sclerosis. *J Neurosci* 27:2396–2402
- Benito C, Tolon RM, Pazos MR et al (2008) Cannabinoid CB2 receptors in human brain inflammation. *Br J Pharmacol* 153:277–285

- Benzinou M, Chevre JC, Ward KJ et al (2008) Endocannabinoid receptor 1 gene variations increase risk for obesity and modulate body mass index in European populations. *Hum Mol Genet* 17:1916–1921
- Berding G, Muller-Vahl K, Schneider U et al (2004) [123I]AM281 single-photon emission computed tomography imaging of central cannabinoid CB1 receptors before and after Delta9-tetrahydrocannabinol therapy and whole-body scanning for assessment of radiation dose in tourette patients. *Biol Psychiatry* 55:904–915
- Berding G, Schneider U, Gielow P et al (2006) Feasibility of central cannabinoid CB1 receptor imaging with [124I]AM281 PET demonstrated in a schizophrenic patient. *Psychiatry Res* 147:249–256
- Bertolini A, Ferrari A, Ottani A et al (2006) Paracetamol: new vistas of an old drug. *CNS Drug Rev* 12:250–275
- Bifulco M, Laezza C, Malfitano AM (2007) From anecdotal evidence of cannabinoids in multiple sclerosis to emerging new therapeutical approaches. *Mult Scler* 13:133–134
- Blazquez C, Chiarlone A, Sagredo O et al (2011) Loss of striatal type 1 cannabinoid receptors is a key pathogenic factor in Huntington's disease. *Brain* 134:119–136
- Bonhomme-Faivre L, Benyamina A, Reynaud M et al (2008) Disposition of Delta(9) tetrahydrocannabinol in CF1 mice deficient in mdr1a P-glycoprotein. *Addict Biol* 13(3–4):295–300
- Booth M (2005) Cannabis: a history. Picador, A Thomas Dunne Book, St. Martin's Press, New York
- Booz GW (2011) Cannabidiol as an emergent therapeutic strategy for lessening the impact of inflammation on oxidative stress. *Free Radic Biol Med* 51:1054–1061
- Burns HD, Van Laere K, Sanabria-Bohorquez S et al (2007) [18F]MK-9470, a positron emission tomography (PET) tracer for in vivo human PET brain imaging of the cannabinoid-1 receptor. *Proc Natl Acad Sci U S A* 104:9800–9805
- Cabral GA, Marciano-Cabral F (2005) Cannabinoid receptors in microglia of the central nervous system: immune functional relevance. *J Leukoc Biol* 78:1192–1197
- Cahill K, Ussher MH (2007) Cannabinoid type 1 receptor antagonists for smoking cessation. *Cochrane Database Syst Rev* (3):CD005353
- Caille S, Alvarez-Jaimes L, Polis I et al (2007) Specific alterations of extracellular endocannabinoid levels in the nucleus accumbens by ethanol, heroin, and cocaine self-administration. *J Neurosci* 27:3695–3702
- Calatozzolo C, Salmaggi A, Pollo B et al (2007) Expression of cannabinoid receptors and neurotrophins in human gliomas. *Neurol Sci* 28:304–310
- Carroll CB, Bain PG, Teare L et al (2004) Cannabis for dyskinesia in Parkinson disease: a randomized double-blind crossover study. *Neurology* 63:1245–1250
- Casanova ML, Blazquez C, Martinez-Palacio J et al (2003) Inhibition of skin tumor growth and angiogenesis in vivo by activation of cannabinoid receptors. *J Clin Invest* 111:43–50
- Caspi A, Moffitt TE, Cannon M et al (2005) Moderation of the effect of adolescent-onset cannabis use on adult psychosis by a functional polymorphism in the catechol-O-methyltransferase gene: longitudinal evidence of a gene X environment interaction. *Biol Psychiatry* 57:1117–1127
- Casteels C, Martinez E, Bormans G et al (2010a) Type 1 cannabinoid receptor mapping with [18F]MK-9470 PET in the rat brain after quinolinic acid lesion: a comparison to dopamine receptors and glucose metabolism. *Eur J Nucl Med Mol Imaging* 37:2354–2363
- Casteels C, Vanbilloen B, Vercammen D et al (2010b) Influence of chronic bromocriptine and levodopa administration on cerebral type 1 cannabinoid receptor binding. *Synapse* 64:617–623
- Casteels C, Bormans G, Van Laere K (2010c) The effect of anaesthesia on [(18)F]MK-9470 binding to the type 1 cannabinoid receptor in the rat brain. *Eur J Nucl Med Mol Imaging* 37:1164–1173
- Casteels C, Lauwers E, Baitar A et al (2010d) In vivo type 1 cannabinoid receptor mapping in the 6-hydroxydopamine lesion rat model of Parkinson's disease. *Brain Res* 1316:153–162
- Casteels C, Vandeputte C, Rangarajan JR et al (2011) Metabolic and type 1 cannabinoid receptor imaging of a transgenic rat model in the early phase of Huntington disease. *Exp Neurol* 229:440–449

- Casteels C, Koole M, Celen S et al (2012) Preclinical evaluation and quantification of [(18)F]MK-9470 as a radioligand for PET imaging of the type 1 cannabinoid receptor in rat brain. *Eur J Nucl Med Mol Imaging* 39:1467–1477
- Cencioni MT, Chiurchiu V, Catanzaro G et al (2010) Anandamide suppresses proliferation and cytokine release from primary human T-lymphocytes mainly via CB2 receptors. *PLoS One* 5:e8688
- Charalambous A, Marciniak G, Shiue CY et al (1991) PET studies in the primate brain and biodistribution in mice using (–)-5'-18F-delta 8-THC. *Pharmacol Biochem Behav* 40:503–507
- Chen K, Ratzliff A, Hilgenberg L et al (2003) Long-term plasticity of endocannabinoid signaling induced by developmental febrile seizures. *Neuron* 39:599–611
- Chhatwal JP, Davis M, Maguschak KA et al (2005) Enhancing cannabinoid neurotransmission augments the extinction of conditioned fear. *Neuropsychopharmacology* 30:516–524
- Cluny NL, Vemuri VK, Chambers AP et al (2010) A novel peripherally restricted cannabinoid receptor antagonist, AM6545, reduces food intake and body weight, but does not cause malaise, in rodents. *Br J Pharmacol* 161:629–642
- Compton DR, Rice KC, De Costa BR et al (1993) Cannabinoid structure-activity relationships: correlation of receptor binding and in vivo activities. *J Pharmacol Exp Ther* 265:218–226
- Compton WM, Thomas YF, Conway KP et al (2005) Developments in the epidemiology of drug use and drug use disorders. *Am J Psychiatry* 162:1494–1502
- Cooper SJ (2004) Endocannabinoids and food consumption: comparisons with benzodiazepine and opioid palatability-dependent appetite. *Eur J Pharmacol* 500:37–49
- Copeland J, Swift W (2009) Cannabis use disorder: epidemiology and management. *Int Rev Psychiatry* 21:96–103
- Corchero J, Manzanares J, Fuentes JA (2004) Cannabinoid/opioid crosstalk in the central nervous system. *Crit Rev Neurobiol* 16:159–172
- Cota D, Marsicano G, Lutz B et al (2003) Endogenous cannabinoid system as a modulator of food intake. *Int J Obes Relat Metab Disord* 27:289–301
- Cota D, Steiner MA, Marsicano G et al (2007) Requirement of cannabinoid receptor type 1 for the basal modulation of hypothalamic-pituitary-adrenal axis function. *Endocrinology* 148:1574–1581
- Coutts AA, Anavi-Goffer S, Ross RA et al (2001) Agonist-induced internalization and trafficking of cannabinoid CB1 receptors in hippocampal neurons. *J Neurosci* 21:2425–2433
- Croxford JL (2003) Therapeutic potential of cannabinoids in CNS disease. *CNS Drugs* 17:179–202
- Cupini LM, Bari M, Battista N et al (2006) Biochemical changes in endocannabinoid system are expressed in platelets of female but not male migraineurs. *Cephalalgia* 26:277–281
- Curtis A, Mitchell I, Patel S et al (2009) A pilot study using nabilone for symptomatic treatment in Huntington's disease. *Mov Disord* 24:2254–2259
- Dean B, Sundram S, Bradbury R et al (2001) Studies on [3H]CP-55940 binding in the human central nervous system: regional specific changes in density of cannabinoid-1 receptors associated with schizophrenia and cannabis use. *Neuroscience* 103:9–15
- Degenhardt L, Hall W, Lynskey M (2003) Exploring the association between cannabis use and depression. *Addiction* 98:1493–1504
- Degroot A, Nomikos GG (2007) In vivo neurochemical effects induced by changes in endocannabinoid neurotransmission. *Curr Opin Pharmacol* 7:62–68
- Deng H, Gifford AN, Zvonok AM et al (2005) Potent cannabinergic indole analogues as radioiodinatable brain imaging agents for the CB1 cannabinoid receptor. *J Med Chem* 48:6386–6392
- Deshpande LS, Blair RE, Ziobro JM et al (2007) Endocannabinoids block status epilepticus in cultured hippocampal neurons. *Eur J Pharmacol* 558:52–59
- Despres JP, Ross R, Boka G et al (2009) Effect of rimonabant on the high-triglyceride/ low-HDL-cholesterol dyslipidemia, intraabdominal adiposity, and liver fat: the ADAGIO-Lipids trial. *Arterioscler Thromb Vasc Biol* 29:416–423
- Devane WA, Dysarz FA 3rd, Johnson MR et al (1988) Determination and characterization of a cannabinoid receptor in rat brain. *Mol Pharmacol* 34:605–613

- Di Marzo V, De Petrocellis L (2010) Endocannabinoids as regulators of transient receptor potential (TRP) channels: a further opportunity to develop new endocannabinoid-based therapeutic drugs. *Curr Med Chem* 17:1430–1449
- Di Marzo V, Hill MP, Bisogno T et al (2000) Enhanced levels of endogenous cannabinoids in the globus pallidus are associated with a reduction in movement in an animal model of Parkinson's disease. *FASEB J* 14:1432–1438
- Di Marzo V, Goparaju SK, Wang L et al (2001) Leptin-regulated endocannabinoids are involved in maintaining food intake. *Nature* 410:822–825
- Di Marzo V, Bifulco M, De Petrocellis L (2004) The endocannabinoid system and its therapeutic exploitation. *Nat Rev Drug Discov* 3:771–784
- Di Marzo V, Piscitelli F, Mechoulam R (2011) Cannabinoids and endocannabinoids in metabolic disorders with focus on diabetes. *Handb Exp Pharmacol* 203:75–104
- Dinh TP, Carpenter D, Leslie FM et al (2002) Brain monoglyceride lipase participating in endocannabinoid inactivation. *Proc Natl Acad Sci U S A* 99:10819–10824
- Donohue S, Halldin C, Finnema S et al (2006) Synthesis and in vivo evaluation of a new PET radioligand for imaging the cannabinoid type-1 (CB1) receptors. *Neuroimage* 31:T50
- Donohue S, Halldin C, Schou M et al (2008a) Radiolabeling of a high potency cannabinoid subtype-1 receptor ligand, N-(4-fluoro-benzyl)-4-(3-(piperidin-1-yl)-indole-1-sulfonyl)benzamide (PipISB), with carbon-11 or fluorine-18. *J Label Compd Radiopharm* 51:146–152
- Donohue SR, Krushinski JH, Pike VW et al (2008b) Synthesis, ex vivo evaluation, and radiolabeling of potent 1,5-diphenylpyrrolidin-2-one cannabinoid subtype-1 receptor ligands as candidates for in vivo imaging. *J Med Chem* 51:5833–5842
- Donohue SR, Pike VW, Finnema SJ et al (2008c) Discovery and labeling of high-affinity 3,4-diarylpyrazolines as candidate radioligands for in vivo imaging of cannabinoid subtype-1 (CB1) receptors. *J Med Chem* 51:5608–5616
- Drysdale AJ, Platt B (2003) Cannabinoids: mechanisms and therapeutic applications in the CNS. *Curr Med Chem* 10:2719–2732
- Eckelman WC, Reba RC, Gibson RE (1979) Receptor-binding radiotracers: a class of potential radiopharmaceuticals. *J Nucl Med* 20:350–357
- Economidou D, Mattioli L, Cifani C et al (2006) Effect of the cannabinoid CB(1) receptor antagonist SR-141716A on ethanol self-administration and ethanol-seeking behaviour in rats. *Psychopharmacology (Berl)* 183:394–403
- Egertova M, Giang DK, Cravatt BF et al (1998) A new perspective on cannabinoid signalling: complementary localization of fatty acid amide hydrolase and the CB1 receptor in rat brain. *Proc Biol Sci* 265:2081–2085
- Eggan SM, Hashimoto T, Lewis DA (2008) Reduced cortical cannabinoid 1 receptor messenger RNA and protein expression in schizophrenia. *Arch Gen Psychiatry* 65:772–784
- Ehrhart J, Obregon D, Mori T et al (2005) Stimulation of cannabinoid receptor 2 (CB2) suppresses microglial activation. *J Neuroinflammation* 2:29
- Ellert-Miklaszewska A, Grajkowska W, Gabrusiewicz K et al (2007) Distinctive pattern of cannabinoid receptor type II (CB2) expression in adult and pediatric brain tumors. *Brain Res* 1137:161–169
- Elphick MR, Egertova M (2005) The phylogenetic distribution and evolutionary origins of endocannabinoid signalling. *Handb Exp Pharmacol* 168:283–297
- Ertl P (2008) Polar surface area. In: Mannhold R (ed) *Molecular drug properties. Measurements and predictions*. Wiley-VCH Verlag GmbH & Co, Weinheim, pp 111–126
- Eubanks LM, Rogers CJ, Beuscher AE 4th et al (2006) A molecular link between the active component of marijuana and Alzheimer's disease pathology. *Mol Pharm* 3:773–777
- Evens N, Bormans GM (2010) Non-invasive imaging of the type 2 cannabinoid receptor, focus on positron emission tomography. *Curr Top Med Chem* 10:1527–1543
- Evens N, Bosier B, Van Laere K et al (2007) Synthesis and evaluation of (2,3-dichloro-phenyl)-[5-[11C]methoxy-2-methyl-3-(2-morpholin-4-yl-ethyl)-indol-1-yl]-methanone as a PET radioligand with affinity for the CB2 receptor. *J Nucl Med* 48:133P
- Evens N, Bosier B, Lavey BJ et al (2008) Labelling and biological evaluation of [(11C)methoxy-Sch225336: a radioligand for the cannabinoid-type 2 receptor. *Nucl Med Biol* 35:793–800

- Evens N, Muccioli GG, Houbrechts N et al (2009a) Synthesis and biological evaluation of carbon-11- and fluorine-18-labeled 2-oxoquinoline derivatives for type 2 cannabinoid receptor positron emission tomography imaging. *Nucl Med Biol* 36:455–465
- Evens N, Vandeputte C, Toelen J et al (2009b) Validation of PET radioligands for visualisation of the type 2 cannabinoid receptor in a rat model with local cerebral CB2R overexpression. In: 2009 annual congress of the European Association of Nuclear Medicine. *Eur J Nucl Med Mol Imaging* (Barcelona, Spain) 36:OP337
- Evens N, Vandeputte C, Muccioli GG et al (2011) Synthesis, in vitro and in vivo evaluation of fluorine-18 labelled FE-GW405833 as a PET tracer for type 2 cannabinoid receptor imaging. *Bioorg Med Chem* 19:4499–4505
- Evens N, Vandeputte C, Coolen C et al (2012) Preclinical evaluation of [(11C)N]NE40, a type 2 cannabinoid receptor PET tracer. *Nucl Med Biol* 39:389–399
- Fan H, Ravert HT, Holt D et al (2006) Synthesis of 1-(2,4-dichlorophenyl)-4-cyano-5-(4-[11C]methoxyphenyl)-N-(piperidin-1-yl)-1H-pyrazole-3-carboxamide ([11C]JHU75528) and 1-(2-bromophenyl)-4-cyano-5-(4-[11C]methoxyphenyl)-N-(piperidin-1-yl)-1H-pyrazole-3-carboxamide ([11C]JHU75575) as potential radioligands for PET imaging of cerebral cannabinoid receptor. *J Label Compd Radiopharm* 49:1021–1036
- Fan H, Kotsikorou E, Hoffman AF et al (2009) Analogs of JHU75528, a PET ligand for imaging of cerebral cannabinoid receptors (CB1): development of ligands with optimized lipophilicity and binding affinity. *Eur J Med Chem* 44:593–608
- Farde L, Gustavsson JP, Jonsson E (1997) D2 dopamine receptors and personality traits. *Nature* 385:590
- Farkas S, Nagy K, Palkovits M et al (2012) [(1)(2)I]SD-7015 reveals fine modalities of CB cannabinoid receptor density in the prefrontal cortex during progression of Alzheimer's disease. *Neurochem Int* 60:286–291
- Felder CC, Dickason-Chesterfield AK, Moore SA (2006) Cannabinoids biology: the search for new therapeutic targets. *Mol Interv* 6:149–161
- Fernandez-Espejo E, Viveros MP, Nunez L et al (2009) Role of cannabis and endocannabinoids in the genesis of schizophrenia. *Psychopharmacology* (Berl) 206:531–549
- Fernandez-Ruiz J, Romero J, Velasco G et al (2007) Cannabinoid CB(2) receptor: a new target for controlling neural cell survival? *Trends Pharmacol Sci* 28:39–45
- Finnema SJ, Donohue SR, Zoghbi SS et al (2009) Evaluation of [11C]PipISB and [18F]PipISB in monkey as candidate radioligands for imaging brain cannabinoid type-1 receptors in vivo. *Synapse* 63:22–30
- Fowler CJ (2012) Anandamide uptake explained? *Trends Pharmacol Sci* 33:181–185
- Fox SH, Henry B, Hill M et al (2002) Stimulation of cannabinoid receptors reduces levodopa-induced dyskinesia in the MPTP-lesioned nonhuman primate model of Parkinson's disease. *Mov Disord* 17:1180–1187
- Frost JJ, Wagner HN Jr (1984) Kinetics of binding to opiate receptors in vivo predicted from in vitro parameters. *Brain Res* 305:1–11
- Fujinaga M, Kumata K, Yanamoto K et al (2010) Radiosynthesis of novel carbon-11-labeled triaryl ligands for cannabinoid-type 2 receptor. *Bioorg Med Chem Lett* 20:1565–1568
- Galiegue S, Mary S, Marchand J et al (1995) Expression of central and peripheral cannabinoid receptors in human immune tissues and leukocyte subpopulations. *Eur J Biochem* 232:54–61
- Gallant M, Dufresne C, Gareau Y et al (1996) New class of potent ligands for the human peripheral cannabinoid receptor. *J Med Chem* 6:2263–2268
- Gao M, Wang M, Miller KD et al (2010) Synthesis and in vitro biological evaluation of carbon-11-labeled quinoline derivatives as new candidate PET radioligands for cannabinoid CB2 receptor imaging. *Bioorg Med Chem* 18:2099–2106
- Gaoni Y, Mechoulam R (1964) Isolation, structure, and partial synthesis of an active constituent of hashish. *J Am Chem Soc* 86:1646–1647
- Gatley SJ, Gifford AN, Volkow ND et al (1996) 123I-labeled AM251: a radioiodinated ligand which binds in vivo to mouse brain cannabinoid CB1 receptors. *Eur J Pharmacol* 307:331–338

- Gatley SJ, Lan R, Volkow ND et al (1998) Imaging the brain marijuana receptor: development of a radioligand that binds to cannabinoid CB1 receptors in vivo. *J Neurochem* 70:417–423
- Gatley SJ, Gifford AN, Ding Y-S et al (2004) Development of PET and SPECT radioligands for cannabinoid receptors. In: Makriyannis A, Biegel D (eds) *Drug discovery strategies and methods*. Marcel Dekker, Inc., New York, pp 129–146
- George DT, Herion DW, Jones CL et al (2010) Rimonabant (SR141716) has no effect on alcohol self-administration or endocrine measures in nontreatment-seeking heavy alcohol drinkers. *Psychopharmacology (Berl)* 208:37–44
- Georgieva T, Devanathan S, Stropova D et al (2008) Unique agonist-bound cannabinoid CB1 receptor conformations indicate agonist specificity in signaling. *Eur J Pharmacol* 581:19–29
- Gerard N, Casteels C, Van Kuyck K et al (2007) In vivo overexpression of cerebral cannabinoid-type 1 receptors in a rodent model for anorexia nervosa: a microPET study. *J Nucl Med* 48(Suppl 2):8P
- Gerard N, Pottel L, Nuttin B et al (2009) Increased brain type 1 cannabinoid receptor availability in a rodent model for anorexia nervosa. *J Nucl Med* 50(Suppl 2):1204
- Gerard N, Ceccarini J, Bormans G et al (2010) Influence of chronic nicotine administration on cerebral type 1 cannabinoid receptor binding: an in vivo micro-PET study in the rat using [¹⁸F]MK-9470. *J Mol Neurosci* 42:162–167
- Gerard N, Pieters G, Goffin K et al (2011) Brain type 1 cannabinoid receptor availability in patients with anorexia and bulimia nervosa. *Biol Psychiatry* 70:777–784
- Gifford AN, Tang Y, Gatley SJ et al (1997) Effect of the cannabinoid receptor SPECT agent, AM 281, on hippocampal acetylcholine release from rat brain slices. *Neurosci Lett* 238:84–86
- Gifford AN, Bruneus M, Gatley SJ et al (1999) Large receptor reserve for cannabinoid actions in the central nervous system. *J Pharmacol Exp Ther* 288:478–483
- Giuffrida A, Parsons LH, Kerr TM et al (1999) Dopamine activation of endogenous cannabinoid signaling in dorsal striatum. *Nat Neurosci* 2:358–363
- Glass M, Dragunow M, Faull RL (1997) Cannabinoid receptors in the human brain: a detailed anatomical and quantitative autoradiographic study in the fetal, neonatal and adult human brain. *Neuroscience* 77:299–318
- Glass M, Dragunow M, Faull RL (2000) The pattern of neurodegeneration in Huntington's disease: a comparative study of cannabinoid, dopamine, adenosine and GABA(A) receptor alterations in the human basal ganglia in Huntington's disease. *Neuroscience* 97:505–519
- Glass M, van Dellen A, Blakemore C et al (2004) Delayed onset of Huntington's disease in mice in an enriched environment correlates with delayed loss of cannabinoid CB1 receptors. *Neuroscience* 123:207–212
- Gobbi G, Bambico FR, Mangieri R et al (2005) Antidepressant-like activity and modulation of brain monoaminergic transmission by blockade of anandamide hydrolysis. *Proc Natl Acad Sci U S A* 102:18620–18625
- Goffin K, Bormans G, Casteels C et al (2008) An in vivo [(18)F]MK-9470 microPET study of type 1 cannabinoid receptor binding in Wistar rats after chronic administration of valproate and levetiracetam. *Neuropharmacology* 54(7):1103–1106
- Goffin K, Van Paesschen W, Van Laere K (2011) In vivo activation of endocannabinoid system in temporal lobe epilepsy with hippocampal sclerosis. *Brain* 134:1033–1040
- Gong JP, Onaivi ES, Ishiguro H et al (2006) Cannabinoid CB2 receptors: immunohistochemical localization in rat brain. *Brain Res* 1071:10–23
- Gonzalez S, Valenti M, de Miguel R et al (2004) Changes in endocannabinoid contents in reward-related brain regions of alcohol-exposed rats, and their possible relevance to alcohol relapse. *Br J Pharmacol* 143:455–464
- Gozalka BB, Hill MN, Hillard CJ (2008) Regulation of endocannabinoid signaling by stress: implications for stress-related affective disorders. *Neurosci Biobehav Rev* 32:1152–1160
- Guindon J, De Lean A, Beaulieu P (2006) Local interactions between anandamide, an endocannabinoid, and ibuprofen, a nonsteroidal anti-inflammatory drug, in acute and inflammatory pain. *Pain* 121:85–93
- Hamill TG, Lin LS, Haggmann W et al (2009) PET imaging studies in rhesus monkey with the cannabinoid-1 (CB1) receptor ligand [(11)C]CB-119. *Mol Imaging Biol* 11(4):246–252

- Heimann AS, Gomes I, Dale CS et al (2007) Hemopressin is an inverse agonist of CB1 cannabinoid receptors. *Proc Natl Acad Sci U S A* 104:20588–20593
- Herance R, Rojas S, Abad S et al (2011) Positron emission tomographic imaging of the cannabinoid type 1 receptor system with [(11)C]OMAR ([[(11)C]JHU75528): improvements in image quantification using wild-type and knockout mice. *Mol Imaging* 10:481–487
- Herkenham M, Lynn AB, Little MD et al (1990) Cannabinoid receptor localization in brain. *Proc Natl Acad Sci U S A* 87:1932–1936
- Herkenham M, Lynn AB, Johnson MR et al (1991) Characterization and localization of cannabinoid receptors in rat brain: a quantitative in vitro autoradiographic study. *J Neurosci* 11:563–583
- Herrera B, Carracedo A, Diez-Zaera M et al (2005) p38 MAPK is involved in CB2 receptor-induced apoptosis of human leukaemia cells. *FEBS Lett* 579:5084–5088
- Hertzog DL (2004) Recent advances in the cannabinoids. *Expert Opin Ther Pat* 14:1435–1452
- Hill MN, McEwen BS (2009) Endocannabinoids: the silent partner of glucocorticoids in the synapse. *Proc Natl Acad Sci U S A* 106:4579–4580
- Hillard CJ, Weinlander KM, Stuhr KL (2011) Contributions of endocannabinoid signaling to psychiatric disorders in humans: genetic and biochemical evidence. *Neuroscience* 204:207–229
- Hiroi N, Agatsuma S (2005) Genetic susceptibility to substance dependence. *Mol Psychiatry* 10:336–344
- Hirvonen J, Terry GE, Halldin C et al (2010) Approaches to quantify radioligands that wash out slowly from target organs. *Eur J Nucl Med Mol Imaging* 37:917–919
- Hirvonen J, Goodwin RS, Li CT et al (2012) Reversible and regionally selective downregulation of brain cannabinoid CB(1) receptors in chronic daily cannabis smokers. *Mol Psychiatry* 17:642–649
- Hirvonen J, Zanotti-Fregonara P, Umhau JC et al (2013) Reduced cannabinoid CB(1) receptor binding in alcohol dependence measured with positron emission tomography. *Mol Psychiatry* 18:916–921
- Ho BC, Wassink TH, Ziebell S et al (2011) Cannabinoid receptor 1 gene polymorphisms and marijuana misuse interactions on white matter and cognitive deficits in schizophrenia. *Schizophr Res* 128:66–75
- Hogestatt ED, Jonsson BA, Ermund A et al (2005) Conversion of acetaminophen to the bioactive N-acylphenolamine AM404 via fatty acid amide hydrolase-dependent arachidonic acid conjugation in the nervous system. *J Biol Chem* 280:31405–31412
- Hohmann AG, Suplita RL 2nd (2006) Endocannabinoid mechanisms of pain modulation. *AAPS J* 8:E693–E708
- Horti AG, Van Laere K (2008) Development of radioligands for in vivo imaging of type 1 cannabinoid receptors (CB1) in human brain. *Curr Pharm Des* 14:3363–3383
- Horti AG, Fan H, Kuwabara H et al (2006) 11C-JHU75528: a radiotracer for PET imaging of CB1 cannabinoid receptors. *J Nucl Med* 47:1689–1696
- Horti AG, Gao Y, Ravert HT et al (2010) Synthesis and biodistribution of [11C]A-836339, a new potential radioligand for PET imaging of cannabinoid type 2 receptors (CB2). *Bioorg Med Chem* 18:5202–5207
- Howlett AC (1995) Pharmacology of cannabinoid receptors. *Annu Rev Pharmacol Toxicol* 35:607–634
- Howlett AC (2002) The cannabinoid receptors. *Prostaglandins Other Lipid Mediat* 68–69:619–631
- Howlett AC, Barth F, Bonner TI et al (2002) International Union of Pharmacology. XXVII. Classification of cannabinoid receptors. *Pharmacol Rev* 54:161–202
- Hsieh GC, Pai M, Chandran P et al (2011) Central and peripheral sites of action for CB receptor mediated analgesic activity in chronic inflammatory and neuropathic pain models in rats. *Br J Pharmacol* 162:428–440
- Huestis MA, Gorelick DA, Heishman SJ et al (2001) Blockade of effects of smoked marijuana by the CB1-selective cannabinoid receptor antagonist SR141716. *Arch Gen Psychiatry* 58:322–328

- Huffman JW, Zengin G, Wu MJ et al (2005) Structure-activity relationships for 1-alkyl-3-(1-naphthoyl) indoles at the cannabinoid CB(1) and CB(2) receptors: steric and electronic effects of naphthoyl substituents. New highly selective CB(2) receptor agonists. *Bioorg Med Chem* 13:89–112
- Hungund BL, Basavarajappa BS (2004) Role of endocannabinoids and cannabinoid CB1 receptors in alcohol-related behaviors. *Ann N Y Acad Sci* 1025:515–527
- Hutchison KE, Haughey H, Niculescu M et al (2008) The incentive salience of alcohol: translating the effects of genetic variant in CNR1. *Arch Gen Psychiatry* 65:841–850
- Innis RB, Cunningham VJ, Delforge J et al (2007) Consensus nomenclature for in vivo imaging of reversibly binding radioligands. *J Cereb Blood Flow Metab* 27:1533–1539
- Ishiguro H, Iwasaki S, Teasenfiz L et al (2007) Involvement of cannabinoid CB2 receptor in alcohol preference in mice and alcoholism in humans. *Pharmacogenomics J* 7:380–385
- Iskedjian M, Bereza B, Gordon A et al (2007) Meta-analysis of cannabis based treatments for neuropathic and multiple sclerosis-related pain. *Curr Med Res Opin* 23:17–24
- Itoh T, Abe K, Zoghbi SS et al (2009) PET measurement of the in vivo affinity of 11C-(R)-rolipram and the density of its target, phosphodiesterase-4, in the brains of conscious and anesthetized rats. *J Nucl Med* 50:749–756
- Iversen L (2003) Cannabis and the brain. *Brain* 126:1252–1270
- Jbilo O, Ravinet-Trillou C, Arnone M et al (2005) The CB1 receptor antagonist rimonabant reverses the diet-induced obesity phenotype through the regulation of lipolysis and energy balance. *FASEB J* 19:1567–1569
- Jin KL, Mao XO, Goldsmith PC et al (2000) CB1 cannabinoid receptor induction in experimental stroke. *Ann Neurol* 48:257–261
- Johnson DS, Stiff C, Lazerwith SE et al (2010) Discovery of PF-04457845: A Highly Potent, Orally Bioavailable, and Selective Urea FAAH Inhibitor. *ACS Med Chem Lett* 2:91–96
- Kaczocha M, Glaser ST, Deutsch DG (2009) Identification of intracellular carriers for the endocannabinoid anandamide. *Proc Natl Acad Sci U S A* 106:6375–6380
- Katoch-Rouse R, Chefer SI, Pavlova OA et al (2002) Development of C-11-NIDA-41020, a potential radiotracer for studying cerebral cannabinoid receptors (CB1) by PET. In: IX symposium on the Medical Applications of Cyclotrons, Turku
- Katoch-Rouse R, Pavlova OA, Caulder T et al (2003) Synthesis, structure-activity relationship, and evaluation of SR141716 analogues: development of central cannabinoid receptor ligands with lower lipophilicity. *J Med Chem* 46:642–645
- Kelly DL, Gorelick DA, Conley RR et al (2011) Effects of the cannabinoid-1 receptor antagonist rimonabant on psychiatric symptoms in overweight people with schizophrenia: a randomized, double-blind, pilot study. *J Clin Psychopharmacol* 31:86–91
- Kim K, Moore DH, Makriyannis A et al (2006) AM1241, a cannabinoid CB(2) receptor selective compound, delays disease progression in a mouse model of amyotrophic lateral sclerosis. *Eur J Pharmacol* 542(1–3):100–105
- Klein TW (2005) Cannabinoid-based drugs as anti-inflammatory therapeutics. *Nat Rev Immunol* 5:400–411
- Koeppel RA, Frey KA, Snyder SE et al (1999) Kinetic modeling of N-[11C]methylpiperidin-4-yl propionate: alternatives for analysis of an irreversible positron emission tomography trace for measurement of acetylcholinesterase activity in human brain. *J Cereb Blood Flow Metab* 19:1150–1163
- Kogan NM, Mechoulam R (2007) Cannabinoids in health and disease. *Dialogues Clin Neurosci* 9:413–430
- Kozak KR, Crews BC, Morrow JD et al (2002) Metabolism of the endocannabinoids, 2-arachidonylglycerol and anandamide, into prostaglandin, thromboxane, and prostacyclin glycerol esters and ethanolamides. *J Biol Chem* 277:44877–44885
- Kubinyi H (1995) The quantitative analysis of structure-activity relationships. In: Wolff ME (ed) *Burger's medicinal chemistry and drug discovery*. Wiley, New York, pp 497–571
- La Rana G, Russo R, Campolongo P et al (2006) Modulation of neuropathic and inflammatory pain by the endocannabinoid transport inhibitor AM404 [N-(4-hydroxyphenyl)-eicosa-5,8,11,14-tetraenamide]. *J Pharmacol Exp Ther* 317:1365–1371

- Lan R, Gatley SJ, Makriyannis A (1996) Preparation of iodine-123 labeled AM251: a potential SPECT radioligand for the brain cannabinoid CB1 receptor. *J Label Compd Radiopharm* 38:875–881
- Lan R, Liu Q, Fan P et al (1999) Structure-activity relationships of pyrazole derivatives as cannabinoid receptor antagonists. *J Med Chem* 42:769–776
- Laruelle M, Abi-Dargham A, al-Tikriti MS et al (1994) SPECT quantification of [¹²³I]iomazenil binding to benzodiazepine receptors in nonhuman primates: II. Equilibrium analysis of constant infusion experiments and correlation with in vitro parameters. *J Cereb Blood Flow Metab* 14:453–465
- Lastres-Becker I, Cebeira M, de Ceballos ML et al (2001) Increased cannabinoid CB1 receptor binding and activation of GTP-binding proteins in the basal ganglia of patients with Parkinson's syndrome and of MPTP-treated marmosets. *Eur J Neurosci* 14:1827–1832
- Lastres-Becker I, De Miguel R, Fernandez-Ruiz JJ (2003) The endocannabinoid system and Huntington's disease. *Curr Drug Targets CNS Neurol Disord* 2:335–347
- Laviolette SR, Grace AA (2006) The roles of cannabinoid and dopamine receptor systems in neural emotional learning circuits: implications for schizophrenia and addiction. *Cell Mol Life Sci* 63:1597–1613
- Le Foll B, Goldberg SR (2005) Cannabinoid CB1 receptor antagonists as promising new medications for drug dependence. *J Pharmacol Exp Ther* 312:875–883
- Le Foll B, Gorelick DA, Goldberg SR (2009) The future of endocannabinoid-oriented clinical research after CB1 antagonists. *Psychopharmacology (Berl)* 205:171–174
- Lee HK, Choi EB, Pak CS (2009) The current status and future perspectives of studies of cannabinoid receptor 1 antagonists as anti-obesity agents. *Curr Top Med Chem* 9:482–503
- Leroy S, Griffon N, Bourdel MC et al (2001) Schizophrenia and the cannabinoid receptor type 1 (CB1): association study using a single-base polymorphism in coding exon 1. *Am J Med Genet* 105:749–752
- Levenes C, Daniel H, Soubrie P et al (1998) Cannabinoids decrease excitatory synaptic transmission and impair long-term depression in rat cerebellar Purkinje cells. *J Physiol* 510(Pt 3):867–879
- Li Z, Gifford A, Liu Q et al (2005) Candidate PET radioligands for cannabinoid CB1 receptors: [18F]AM5144 and related pyrazole compounds. *Nucl Med Biol* 32:361–366
- Li W, Sanabria-Bohorquez S, Joshi A et al (2011) The discovery and characterization of [11C] MK-3168, a novel PET tracer for imaging fatty acid amide hydrolase (FAAH). *J Label Compd Radiopharm* 54(Suppl 1):S38
- Lin LS, Lanza TJ Jr, Jewell JP et al (2006) Discovery of N-[(1S,2S)-3-(4-Chlorophenyl)-2-(3-cyanophenyl)-1-methylpropyl]-2-methyl-2- {[5-(trifluoromethyl)pyridin-2-yl]oxy}propanamide (MK-0364), a novel, acyclic cannabinoid-1 receptor inverse agonist for the treatment of obesity. *J Med Chem* 49:7584–7587
- Lin LS, Ha S, Ball RG et al (2008) Conformational analysis and receptor docking of N-[(1S,2S)-3-(4-chlorophenyl)-2-(3-cyanophenyl)-1-methylpropyl]-2-methyl-2- {[5-(trifluoromethyl)pyridin-2-yl]oxy}propanamide (taranabant, MK-0364), a novel, acyclic cannabinoid-1 receptor inverse agonist. *J Med Chem* 51:2108–2114
- Liow JS, Lu S, McCarron JA et al (2007) Effect of a P-glycoprotein inhibitor, Cyclosporin A, on the disposition in rodent brain and blood of the 5-HT1A receptor radioligand, [11C](R)(-)-RWAY. *Synapse* 61:96–105
- Lynn AB, Herkenham M (1994) Localization of cannabinoid receptors and nonsaturable high-density cannabinoid binding sites in peripheral tissues of the rat: implications for receptor-mediated immune modulation by cannabinoids. *J Pharmacol Exp Ther* 268:1612–1623
- Mach F, Steffens S (2008) The role of the endocannabinoid system in atherosclerosis. *J Neuroendocrinol* 20(Suppl 1):53–57
- Makriyannis A, Deng H (2007) Cannabimimetic indole derivatives. Patent US 7,241,799
- Malone DT, Hill MN, Rubino T (2010) Adolescent cannabis use and psychosis: epidemiology and neurodevelopmental models. *Br J Pharmacol* 160:511–522

- Maresz K, Carrier EJ, Ponomarev ED et al (2005) Modulation of the cannabinoid CB2 receptor in microglial cells in response to inflammatory stimuli. *J Neurochem* 95:437–445
- Maresz K, Pryce G, Ponomarev ED et al (2007) Direct suppression of CNS autoimmune inflammation via the cannabinoid receptor CB1 on neurons and CB2 on autoreactive T cells. *Nat Med* 13:492–497
- Marsicano G, Goodenough S, Monory K et al (2003) CB1 cannabinoid receptors and on-demand defense against excitotoxicity. *Science* 302:84–88
- Martin BR, Sim-Selley LJ, Selley DE (2004) Signaling pathways involved in the development of cannabinoid tolerance. *Trends Pharmacol Sci* 25:325–330
- Martin-Santos R, Fagundo AB, Crippa JA et al (2010) Neuroimaging in cannabis use: a systematic review of the literature. *Psychol Med* 40:383–398
- Massa F, Storr M, Lutz B (2005) The endocannabinoid system in the physiology and pathophysiology of the gastrointestinal tract. *J Mol Med* 83:944–954
- Mathews WB, Ravert HT, Musachio JL et al (1999) Synthesis of [18 F] SR144385: a selective radioligand for positron emission tomographic studies of brain cannabinoid receptors. *J Labelled Compounds Radiopharm* 42:589–596
- Mathews WB, Scheffel U, Finley P et al (2000) Biodistribution of [18F] SR144385 and [18F] SR147963: selective radioligands for positron emission tomographic studies of brain cannabinoid receptors. *Nucl Med Biol* 27:757–762
- Mathews WB, Scheffel U, Rauseo PA et al (2002) Carbon-11 labeled radioligands for imaging brain cannabinoid receptors. *Nucl Med Biol* 29:671–677
- Matsuda LA, Lolait SJ, Brownstein MJ et al (1990) Structure of a cannabinoid receptor and functional expression of the cloned cDNA. *Nature* 346:561–564
- Minocci D, Masei J, Martino A et al (2011) Genetic association between bipolar disorder and 524A>C (Leu133Ile) polymorphism of CNR2 gene, encoding for CB2 cannabinoid receptor. *J Affect Disord* 134:427–430
- Monteleone P, Bifulco M, Di Filippo C et al (2009) Association of CNR1 and FAAH endocannabinoid gene polymorphisms with anorexia nervosa and bulimia nervosa: evidence for synergistic effects. *Genes Brain Behav* 8:728–732
- Moranta D, Esteban S, Garcia-Sevilla JA (2006) Ethanol desensitizes cannabinoid CB(1) receptors modulating monoamine synthesis in the rat brain in vivo. *Neurosci Lett* 392:58–61
- Moreira FA, Wotjak CT (2010) Cannabinoids and anxiety. *Curr Top Behav Neurosci* 2:429–450
- Moreira FA, Kaiser N, Monory K et al (2008) Reduced anxiety-like behaviour induced by genetic and pharmacological inhibition of the endocannabinoid-degrading enzyme fatty acid amide hydrolase (FAAH) is mediated by CB1 receptors. *Neuropharmacology* 54:141–150
- Morton GJ, Cummings DE, Baskin DG et al (2006) Central nervous system control of food intake and body weight. *Nature* 443:289–295
- Mukhopadhyay S, Das S, Williams EA et al (2006) Lipopolysaccharide and cyclic AMP regulation of CB(2) cannabinoid receptor levels in rat brain and mouse RAW 264.7 macrophages. *J Neuroimmunol* 181:82–92
- Munro S, Thomas KL, Abu-Shaar M (1993) Molecular characterization of a peripheral receptor for cannabinoids. *Nature* 365:61–65
- Murray RM, Morrison PD, Henquet C et al (2007) Cannabis, the mind and society: the hash realities. *Nat Rev Neurosci* 8:885–895
- Neumeister A, Normandin MD, Murrrough JW et al (2012) Positron emission tomography shows elevated cannabinoid CB (1) receptor binding in men with alcohol dependence. *Alcohol Clin Exp Res* 36:2104–2109
- Newell KA, Deng C, Huang XF (2006) Increased cannabinoid receptor density in the posterior cingulate cortex in schizophrenia. *Exp Brain Res* 172:556–560
- Nissen SE, Nicholls SJ, Wolski K et al (2008) Effect of rimonabant on progression of atherosclerosis in patients with abdominal obesity and coronary artery disease: the STRADIVARIUS randomized controlled trial. *JAMA* 299:1547–1560
- Nogueiras R, Veyrat-Durebex C, Suchanek PM et al (2008) Peripheral, but not central, CB1 antagonism provides food intake-independent metabolic benefits in diet-induced obese rats. *Diabetes* 57:2977–2991

- Nojiri Y, Ishiwata K, Qinggeletu et al (2008) Radiosynthesis and biodistribution in mice of a ¹⁸F-labeled analog of O-1302 for use in cerebral CB1 cannabinoid receptor imaging. *Biol Pharm Bull* 31:1274–1278
- Normandin MD, Weinzimmer DP, Ropchan J et al (2010a) Kinetic modeling of CB1 PET tracer [¹¹C]OMAR in rhesus monkeys and humans. *J Nucl Med* 51(Suppl 2):216
- Normandin MD, Zheng M-Q, Ropchan J et al (2010b) Test-retest reproducibility and gender differences in binding of CB1 PET tracer [¹¹C]OMAR in humans. *J Nucl Med* 51(Suppl 2):51
- Nowak KL, Vinod KY, Hungund BL (2006) Pharmacological manipulation of cb1 receptor function alters development of tolerance to alcohol. *Alcohol Alcohol* 41:24–32
- Oesch S, Walter D, Wachtel M et al (2009) Cannabinoid receptor 1 is a potential drug target for treatment of translocation-positive rhabdomyosarcoma. *Mol Cancer Ther* 8:1838–1845
- Onaivi ES, Ishiguro H, Gong JP et al (2006) Discovery of the presence and functional expression of cannabinoid CB2 receptors in brain. *Ann N Y Acad Sci* 1074:514–536
- Orgado JM, Fernandez-Ruiz J, Romero J (2009) The endocannabinoid system in neuropathological states. *Int Rev Psychiatry* 21:172–180
- Otrubova K, Ezzili C, Boger DL (2011) The discovery and development of inhibitors of fatty acid amide hydrolase (FAAH). *Bioorg Med Chem Lett* 21:4674–4685
- Pacher P, Batkai S, Kunos G (2006) The endocannabinoid system as an emerging target of pharmacotherapy. *Pharmacol Rev* 58:389–462
- Palazuelos J, Davoust N, Julien B et al (2008) The CB(2) cannabinoid receptor controls myeloid progenitor trafficking: involvement in the pathogenesis of an animal model of multiple sclerosis. *J Biol Chem* 283:13320–13329
- Palazuelos J, Aguado T, Pazos MR et al (2009) Microglial CB2 cannabinoid receptors are neuroprotective in Huntington's disease excitotoxicity. *Brain* 132:3152–3164
- Paldy E, Bereczki E, Santha M et al (2008) CB(2) cannabinoid receptor antagonist SR144528 decreases mu-opioid receptor expression and activation in mouse brainstem: role of CB(2) receptor in pain. *Neurochem Int* 53:309–316
- Papadopoulos V, Baraldi M, Guilarte TR et al (2006) Translocator protein (18kDa): new nomenclature for the peripheral-type benzodiazepine receptor based on its structure and molecular function. *Trends Pharmacol Sci* 27:402–409
- Paradisi A, Oddi S, Maccarrone M (2006) The endocannabinoid system in ageing: a new target for drug development. *Curr Drug Targets* 7:1539–1552
- Parmentier-Batteur S, Jin K, Mao XO et al (2002) Increased severity of stroke in CB1 cannabinoid receptor knock-out mice. *J Neurosci* 22:9771–9775
- Patel KD, Davison JS, Pittman QJ et al (2010) Cannabinoid CB(2) receptors in health and disease. *Curr Med Chem* 17:1393–1410
- Pertwee RG (1999) Pharmacology of cannabinoid receptor ligands. *Curr Med Chem* 6:635–664
- Pertwee RG (2009) Emerging strategies for exploiting cannabinoid receptor agonists as medicines. *Br J Pharmacol* 156:397–411
- Pertwee RG, Howlett AC, Abood ME et al (2010) International Union of Basic and Clinical Pharmacology. LXXIX. Cannabinoid receptors and their ligands: beyond CB and CB. *Pharmacol Rev* 62:588–631
- Pike VW (2009) PET radiotracers: crossing the blood-brain barrier and surviving metabolism. *Trends Pharmacol Sci* 30:431–440
- Piomelli D (2003) The molecular logic of endocannabinoid signalling. *Nat Rev Neurosci* 4:873–884
- Piomelli D, Tarzia G, Duranti A et al (2006) Pharmacological profile of the selective FAAH inhibitor KDS-4103 (URB597). *CNS Drug Rev* 12:21–38
- Pisanti S, Bifulco M (2009) Endocannabinoid system modulation in cancer biology and therapy. *Pharmacol Res* 60:107–116
- Pi-Sunyer FX, Aronne LJ, Heshmati HM et al (2006) Effect of rimonabant, a cannabinoid-1 receptor blocker, on weight and cardiometabolic risk factors in overweight or obese patients: RIO-North America: a randomized controlled trial. *JAMA* 295:761–775
- Pryce G, Baker D (2007) Control of spasticity in a multiple sclerosis model is mediated by CB1, not CB2, cannabinoid receptors. *Br J Pharmacol* 150:519–525

- Qamri Z, Preet A, Nasser MW et al (2009) Synthetic cannabinoid receptor agonists inhibit tumor growth and metastasis of breast cancer. *Mol Cancer Ther* 8:3117–3129
- Qin L, Wu X, Block ML et al (2007) Systemic LPS causes chronic neuroinflammation and progressive neurodegeneration. *Glia* 55:453–462
- Ramirez BG, Blazquez C, Gomez del Pulgar T et al (2005) Prevention of Alzheimer's disease pathology by cannabinoids: neuroprotection mediated by blockade of microglial activation. *J Neurosci* 25:1904–1913
- Riedel G, Davies SN (2005) Cannabinoid function in learning, memory and plasticity. *Handb Exp Pharmacol* 168:445–477
- Rinaldi-Carmona M, Barth F, Heaulme M et al (1994) SR141716A, a potent and selective antagonist of the brain cannabinoid receptor. *FEBS Lett* 350:240–244
- Rinaldi-Carmona M, Pialot F, Congy C et al (1996) Characterization and distribution of binding sites for [3H]-SR 141716A, a selective brain (CB1) cannabinoid receptor antagonist, in rodent brain. *Life Sci* 58:1239–1247
- Rinaldi-Carmona M, Barth F, Millan J et al (1998) SR 144528, the first potent and selective antagonist of the CB2 cannabinoid receptor. *J Pharmacol Exp Ther* 284:644–650
- Rodriguez de Fonseca F, Cebeira M, Ramos JA et al (1994) Cannabinoid receptors in rat brain areas: sexual differences, fluctuations during estrous cycle and changes after gonadectomy and sex steroid replacement. *Life Sci* 54:159–170
- Rog DJ, Nurmikko TJ, Friede T et al (2005) Randomized, controlled trial of cannabis-based medicine in central pain in multiple sclerosis. *Neurology* 65:812–819
- Romero J, Garcia L, Fernandez-Ruiz JJ et al (1995) Changes in rat brain cannabinoid binding sites after acute or chronic exposure to their endogenous agonist, anandamide, or to delta 9-tetrahydrocannabinol. *Pharmacol Biochem Behav* 51:731–737
- Rosenstock J, Hollander P, Chevalier S et al (2008) SERENADE: the study evaluating rimonabant efficacy in drug-naïve diabetic patients: effects of monotherapy with rimonabant, the first selective CB1 receptor antagonist, on glycemic control, body weight, and lipid profile in drug-naïve type 2 diabetes. *Diabetes Care* 31(11):2169–2176
- Rossi S, Bernardi G, Centonze D (2010) The endocannabinoid system in the inflammatory and neurodegenerative processes of multiple sclerosis and of amyotrophic lateral sclerosis. *Exp Neurol* 224:92–102
- Sagredo O, Gonzalez S, Aroyo I et al (2009) Cannabinoid CB2 receptor agonists protect the striatum against malonate toxicity: relevance for Huntington's disease. *Glia* 57:1154–1167
- Sanabria-Bohorquez SM, Hamill TG, Goffin K et al (2010) Kinetic analysis of the cannabinoid-1 receptor PET tracer [(18)F]MK-9470 in human brain. *Eur J Nucl Med Mol Imaging* 37:920–933
- Sapp E, Kegel KB, Aronin N et al (2001) Early and progressive accumulation of reactive microglia in the Huntington disease brain. *J Neuropathol Exp Neurol* 60:161–172
- Sarne Y, Mechoulam R (2005) Cannabinoids: between neuroprotection and neurotoxicity. *Curr Drug Targets CNS Neurol Disord* 4:677–684
- Schatz AR, Lee M, Condie RB et al (1997) Cannabinoid receptors CB1 and CB2: a characterization of expression and adenylate cyclase modulation within the immune system. *Toxicol Appl Pharmacol* 142:278–287
- Schlicker E, Kathmann M (2001) Modulation of transmitter release via presynaptic cannabinoid receptors. *Trends Pharmacol Sci* 22:565–572
- Secher A, Husum H, Holst B et al (2010) Risperidone treatment increases CB1 receptor binding in rat brain. *Neuroendocrinology* 91:155–168
- Segovia G, Mora F, Crossman AR et al (2003) Effects of CB1 cannabinoid receptor modulating compounds on the hyperkinesia induced by high-dose levodopa in the reserpine-treated rat model of Parkinson's disease. *Mov Disord* 18:138–149
- Seneca N, Finnema SJ, Farde L et al (2006) Effect of amphetamine on dopamine D2 receptor binding in nonhuman primate brain: a comparison of the agonist radioligand [11C]MNPDA and antagonist [11C]raclopride. *Synapse* 59:260–269

- Sevcik J, Masek K (2000) Potential role of cannabinoids in Parkinson's disease. *Drugs Aging* 16:391–395
- Shoemaker JL, Ruckle MB, Mayeux PR et al (2005) Agonist-directed trafficking of response by endocannabinoids acting at CB2 receptors. *J Pharmacol Exp Ther* 315:828–838
- Shoemaker JL, Seely KA, Reed RL et al (2007) The CB2 cannabinoid agonist AM-1241 prolongs survival in a transgenic mouse model of amyotrophic lateral sclerosis when initiated at symptom onset. *J Neurochem* 101:87–98
- Shohami E, Cohen-Yeshurun A, Magid L et al (2011) Endocannabinoids and traumatic brain injury. *Br J Pharmacol* 163:1402–1410
- Siegfried Z, Kanyas K, Latzer Y et al (2004) Association study of cannabinoid receptor gene (CNR1) alleles and anorexia nervosa: differences between restricting and binge/purging subtypes. *Am J Med Genet B Neuropsychiatr Genet* 125B:126–130
- Sieradzian KA, Fox SH, Hill M et al (2001) Cannabinoids reduce levodopa-induced dyskinesia in Parkinson's disease: a pilot study. *Neurology* 57:2108–2111
- Sim-Selley LJ, Martin BR (2002) Effect of chronic administration of R-(+)-[2,3-Dihydro-5-methyl-3-[(morpholinyl)methyl]pyrrolo[1,2,3-de]-1,4-benzoxazinyl]-1-naphthalenyl)methanone mesylate (WIN55,212-2) or delta(9)-tetrahydrocannabinol on cannabinoid receptor adaptation in mice. *J Pharmacol Exp Ther* 303:36–44
- Sipe JC, Chiang K, Gerber AL et al (2002) A missense mutation in human fatty acid amide hydrolase associated with problem drug use. *Proc Natl Acad Sci U S A* 99:8394–8399
- Sipe JC, Waalen J, Gerber A et al (2005) Overweight and obesity associated with a missense polymorphism in fatty acid amide hydrolase (FAAH). *Int J Obes Relat Metab Disord* 29(7):755–759
- Skaddan MB, Zhang L, Johnson DS et al (2012) The synthesis and in vivo evaluation of [(18)F]PF-9811: a novel PET ligand for imaging brain fatty acid amide hydrolase (FAAH). *Nucl Med Biol* 39(7):1058–1067
- Smith RA, Fathi Z (2005) Recent advances in the research and development of CB(1) antagonists. *IDrugs* 8:53–66
- Soyka M, Koller G, Schmidt P et al (2008) Cannabinoid receptor 1 blocker rimonabant (SR 141716) for treatment of alcohol dependence: results from a placebo-controlled, double-blind trial. *J Clin Psychopharmacol* 28:317–324
- Steffens S, Veillard NR, Arnaud C et al (2005) Low dose oral cannabinoid therapy reduces progression of atherosclerosis in mice. *Nature* 434:782–786
- Stella N (2010) Cannabinoid and cannabinoid-like receptors in microglia, astrocytes, and astrocytomas. *Glia* 58:1017–1030
- Sumi N, Nishioku T, Takata F et al (2010) Lipopolysaccharide-activated microglia induce dysfunction of the blood-brain barrier in rat microvascular endothelial cells co-cultured with microglia. *Cell Mol Neurobiol* 30:247–253
- Suter TM, Chesterfield AK, Bao C et al (2010) Pharmacological characterization of the cannabinoid CB receptor PET ligand ortholog, [(3)H]MePPEP. *Eur J Pharmacol* 649:44–50
- Tamagnan G, Lu XJ, Gao Y et al (1999) Potential SPECT radioligand for cannabinoid receptor. *J Label Compd Radiopharm* 43:S191–S193
- Teixeira-Clerc F, Julien B, Grenard P et al (2008) [The endocannabinoid system as a novel target for the treatment of liver fibrosis]. *Pathol Biol (Paris)* 56:36–38
- Terry G (2009) In vivo imaging of the cannabinoid CB1 receptor using positron emission tomography. The Department of Clinical Neuroscience, Karolinska Institutet, Stockholm
- Terry G, Liow JS, Chernet E et al (2008) Positron emission tomography imaging using an inverse agonist radioligand to assess cannabinoid CB1 receptors in rodents. *Neuroimage* 41:690–698
- Terry GE, Liow JS, Zoghbi SS et al (2009) Quantitation of cannabinoid CB1 receptors in healthy human brain using positron emission tomography and an inverse agonist radioligand. *Neuroimage* 48:362–370
- Terry GE, Hirvonen J, Liow JS et al (2010a) Biodistribution and dosimetry in humans of two inverse agonists to image cannabinoid CB1 receptors using positron emission tomography. *Eur J Nucl Med Mol Imaging* 37:1499–1506

- Terry GE, Hirvonen J, Liow JS et al (2010b) Imaging and quantitation of cannabinoid CB1 receptors in human and monkey brains using (18)F-labeled inverse agonist radioligands. *J Nucl Med* 51:112–120
- Thomas EA, Cravatt BF, Danielson PE et al (1997) Fatty acid amide hydrolase, the degradative enzyme for anandamide and oleamide, has selective distribution in neurons within the rat central nervous system. *J Neurosci Res* 50:1047–1052
- Thors L, Burston JJ, Alter BJ et al (2010) Biochanin A, a naturally occurring inhibitor of fatty acid amide hydrolase. *Br J Pharmacol* 160:549–560
- Timpone JG, Wright DJ, Li N et al (1997) The safety and pharmacokinetics of single-agent and combination therapy with megestrol acetate and dronabinol for the treatment of HIV wasting syndrome. The DATRI 004 Study Group. Division of AIDS Treatment Research Initiative. *AIDS Res Hum Retroviruses* 13:305–315
- Tolon RM, Nunez E, Pazos MR et al (2009) The activation of cannabinoid CB2 receptors stimulates in situ and in vitro beta-amyloid removal by human macrophages. *Brain Res* 1283:148–154
- Torres E, Gutierrez-Lopez MD, Borcel E et al (2010) Evidence that MDMA ('ecstasy') increases cannabinoid CB2 receptor expression in microglial cells: role in the neuroinflammatory response in rat brain. *J Neurochem* 113:67–78
- Turkman N, Shavrin A, Ivanov RA et al (2011) Fluorinated cannabinoid CB2 receptor ligands: Synthesis and in vitro binding characteristics of 2-oxoquinoline derivatives. *Bioorg Med Chem* 19:5698–5707
- Turkman N, Shavrin A, Paolillo V et al (2012) Synthesis and preliminary evaluation of [(18)F]-labeled 2-oxoquinoline derivatives for PET imaging of cannabinoid CB(2) receptor. *Nucl Med Biol* 39:593–600
- Ujike H, Morita Y (2004) New perspectives in the studies on endocannabinoid and cannabis: cannabinoid receptors and schizophrenia. *J Pharmacol Sci* 96:376–381
- Ujike H, Takaki M, Nakata K et al (2002) CNR1, central cannabinoid receptor gene, associated with susceptibility to hebephrenic schizophrenia. *Mol Psychiatry* 7:515–518
- Van der Schueren BJ, Van Laere K, Gerard N et al (2011) Interictal type 1 cannabinoid receptor binding is increased in female migraine patients. *Headache* 52:433–440
- van der Stelt M, Di Marzo V (2003) The endocannabinoid system in the basal ganglia and in the mesolimbic reward system: implications for neurological and psychiatric disorders. *Eur J Pharmacol* 480:133–150
- Van Gaal LF, Rissanen AM, Scheen AJ et al (2005) Effects of the cannabinoid-1 receptor blocker rimonabant on weight reduction and cardiovascular risk factors in overweight patients: 1-year experience from the RIO-Europe study. *Lancet* 365:1389–1397
- Van Laere K (2007) In vivo imaging of the endocannabinoid system: a novel window to a central modulatory mechanism in humans. *Eur J Nucl Med Mol Imaging* 34:1719–1726
- Van Laere KJ, Versijpt J, Koole M et al (2002) Experimental performance assessment of SPM for SPECT neuroactivation studies using a subresolution sandwich phantom design. *Neuroimage* 16:200–216
- Van Laere K, Casteels C, Lunskens S et al (2008a) In vivo PET brain imaging of the type 1 cannabinoid receptor in early and advanced Parkinson's disease. In: Annual meeting of European Association of Nuclear Medicine, Munich
- Van Laere K, Goffin K, Casteels C et al (2008b) Gender-dependent increases with healthy aging of the human cerebral cannabinoid-type 1 receptor binding using [(18)F]MK-9470 PET. *Neuroimage* 39:1533–1541
- Van Laere K, Koole M, Sanabria Bohorquez SM et al (2008c) Whole-body biodistribution and radiation dosimetry of the human cannabinoid type-1 receptor ligand 18F-MK-9470 in healthy subjects. *J Nucl Med* 49:439–445
- Van Laere K, Goffin K, Bormans G et al (2009) Relationship of type 1 cannabinoid receptor availability in the human brain to novelty-seeking temperament. *Arch Gen Psychiatry* 66:196–204
- Van Laere K, Casteels C, Dhollander I et al (2010) Widespread decrease of type 1 cannabinoid receptor availability in Huntington disease in vivo. *J Nucl Med* 51:1413–1417

- Van Laere K, Casteels C, Lunskens S et al (2012) Regional changes in type 1 cannabinoid receptor availability in Parkinson's disease in vivo. *Neurobiol Aging* 33:620, e621–e628
- Van Sickle MD, Duncan M, Kingsley PJ et al (2005) Identification and functional characterization of brainstem cannabinoid CB2 receptors. *Science* 310:329–332
- Vandeputte C, Evens N, Toelen J et al (2011) A PET brain reporter gene system based on type 2 cannabinoid receptors. *J Nucl Med* 52:1102–1109
- Varga EV, Georgieva T, Tumati S et al (2008) Functional selectivity in cannabinoid signaling. *Curr Mol Pharmacol* 1:273–284
- Verdurand M, Nguyen V, Stark D et al (2011) Comparison of cannabinoid CB(1) receptor binding in adolescent and adult rats: a positron emission tomography study using [18 F]MK-9470. *Int J Mol Imaging* 2011:548123
- Vickers SP, Kennett GA (2005) Cannabinoids and the regulation of ingestive behaviour. *Curr Drug Targets* 6:215–223
- Villares J (2007) Chronic use of marijuana decreases cannabinoid receptor binding and mRNA expression in the human brain. *Neuroscience* 145:323–334
- Vinod KY, Hungund BL (2006a) Role of the endocannabinoid system in depression and suicide. *Trends Pharmacol Sci* 27:539–545
- Vinod KY, Hungund BL (2006b) Cannabinoid-1 receptor: a novel target for the treatment of neuropsychiatric disorders. *Expert Opin Ther Targets* 10:203–210
- Waleh NS, Cravatt BF, Apte-Deshpande A et al (2002) Transcriptional regulation of the mouse fatty acid amide hydrolase gene. *Gene* 291:203–210
- Wallace MJ, Martin BR, DeLorenzo RJ (2002) Evidence for a physiological role of endocannabinoids in the modulation of seizure threshold and severity. *Eur J Pharmacol* 452:295–301
- Wallace MJ, Blair RE, Falenski KW et al (2003) The endogenous cannabinoid system regulates seizure frequency and duration in a model of temporal lobe epilepsy. *J Pharmacol Exp Ther* 307:129–137
- Wasmuth HE, Trautwein C (2007) CB1 cannabinoid receptor antagonism: a new strategy for the treatment of liver fibrosis. *Hepatology* 45:543–544
- Wei BQ, Mikkelsen TS, McKinney MK et al (2006) A second fatty acid amide hydrolase with variable distribution among placental mammals. *J Biol Chem* 281:36569–36578
- Willis PG, Katoch-Rouse R, Horti AG (2003) Regioselective F-18 radiolabeling of AM694, a CB1 cannabinoid receptor ligand. *J Labelled Compounds Radiopharm* 46:799
- Willis PG, Pavlova OA, Chefer SI et al (2005) Synthesis and structure-activity relationship of a novel series of aminoalkylindoles with potential for imaging the neuronal cannabinoid receptor by positron emission tomography. *J Med Chem* 48:5813–5822
- Wilson RI, Nicoll RA (2002) Endocannabinoid signaling in the brain. *Science* 296:678–682
- Wilson A, Garcia A, Parkes J et al (2011a) 3-oxazolinyphenyl N-alkylcarbamates as promising radiotracers for imaging fatty acid amide hydrolase (FAAH). *J Label Compd Radiopharm* 54(Suppl 1):S-37
- Wilson AA, Garcia A, Parkes J et al (2011b) [11 C]CURB: evaluation of a novel radiotracer for imaging fatty acid amide hydrolase by positron emission tomography. *Nucl Med Biol* 38:247–253
- Wong DF, Kuwabara H, Horti AG et al (2008) Imaging of human cannabinoid CB1 receptors with [11 C]OMAR. *J Nucl Med* 49(Suppl 1):131P
- Wong DF, Kuwabara H, Horti AG et al (2010a) Quantification of cerebral cannabinoid receptors subtype 1 (CB1) in healthy subjects and schizophrenia by the novel PET radioligand [11 C]OMAR. *Neuroimage* 52:1505–1513
- Wong DF, Kuwabara H, Hussain B et al (2010b) Evaluation of occupancy of cannabinoid CB1 receptors by a novel antagonist drug with [11 C]OMAR and PET. *Neuroimage* 52:S64
- Wyffels L, Muccioli GG, De Bruyne S et al (2009) Synthesis, in vitro and in vivo evaluation, and radiolabeling of aryl anandamide analogues as candidate radioligands for in vivo imaging of fatty acid amide hydrolase in the brain. *J Med Chem* 52:4613–4622

- Wyffels L, Muccioli GG, Kapanda CN et al (2010) PET imaging of fatty acid amide hydrolase in the brain: synthesis and biological evaluation of an ^{11}C -labelled URB597 analogue. *Nucl Med Biol* 37:665–675
- Xi ZX, Peng XQ, Li X et al (2011) Brain cannabinoid CB receptors modulate cocaine's actions in mice. *Nat Neurosci* 14:1160–1166
- Yao BB, Hsieh G, Daza AV et al (2009) Characterization of a cannabinoid CB2 receptor-selective agonist, A-836339 [2,2,3,3-tetramethyl-cyclopropanecarboxylic acid [3-(2-methoxy-ethyl)-4,5-dimethyl-3H-thiazol-(2Z)-ylidene]-amide], using in vitro pharmacological assays, in vivo pain models, and pharmacological magnetic resonance imaging. *J Pharmacol Exp Ther* 328:141–151
- Yasuno F, Brown AK, Zoghbi SS et al (2008) The PET radioligand [^{11}C]MePPEP binds reversibly and with high specific signal to cannabinoid CB1 receptors in nonhuman primate brain. *Neuropsychopharmacology* 33:259–269
- Yiangou Y, Facer P, Durrenberger P et al (2006) COX-2, CB2 and P2X7-immunoreactivities are increased in activated microglial cells/macrophages of multiple sclerosis and amyotrophic lateral sclerosis spinal cord. *BMC Neurol* 6:12
- Zavitsanou K, Garrick T, Huang XF (2004) Selective antagonist [^3H]SR141716A binding to cannabinoid CB1 receptors is increased in the anterior cingulate cortex in schizophrenia. *Prog Neuropsychopharmacol Biol Psychiatry* 28:355–360
- Zhang PW, Ishiguro H, Ohtsuki T et al (2004) Human cannabinoid receptor 1: 5' exons, candidate regulatory regions, polymorphisms, haplotypes and association with polysubstance abuse. *Mol Psychiatry* 9:916–931
- Zheng D, Bode AM, Zhao Q et al (2008) The cannabinoid receptors are required for ultraviolet-induced inflammation and skin cancer development. *Cancer Res* 68:3992–3998

Imaging Type 1 Glycine Transporters in the CNS Using Positron Emission Tomography

12

Jan Passchier, Roger N. Gunn, and Aren van Waarde

Contents

12.1	Introduction	321
12.2	Potential Utility of PET Imaging	322
12.3	Characteristics Required of a PET Probe for GlyT1	323
12.4	GlyT1 Tracer Development.....	324
12.4.1	[¹¹ C]ALX5407.....	324
12.4.2	[¹¹ C]GSK931145	324
12.4.3	[¹⁸ F]MK-6577.....	326
12.4.4	[¹¹ C]Ro5013853	326
12.4.5	[¹¹ C]- <i>N</i> -Methyl-SSR504734	327
12.4.6	[¹¹ C]-labelled CHIBA and SA Compounds	327
	Conclusions.....	328
	References.....	328

12.1 Introduction

Glycine is an inhibitory neurotransmitter acting through postsynaptic glycine receptors in caudal CNS regions and a positive modulator of glutamatergic neurotransmission as it is an essential co-agonist with D-serine at *N*-methyl-D-aspartate receptors (NMDAR). Extracellular concentrations of glycine are regulated by the glycine

J. Passchier (✉) • R.N. Gunn
Imanova Limited, Burlington Danes Building,
Imperial College London, Hammersmith Hospital,
Du Cane Road, London W12 0NN, UK
e-mail: jan.passchier@imanova.co.uk

A. van Waarde
Department of Nuclear Medicine and Molecular Imaging,
University Medical Center Groningen, University of Groningen,
Hanzeplein 1, Groningen 9713GZ, The Netherlands

transporters (GlyT1 and GlyT2) which are members of the Na⁺/Cl⁻-dependent transporter family and mediate the uptake of glycine from the extracellular space into the cytosol (Betz et al. 2006; Eulenburg et al. 2005).

Whereas GlyT1 is widely distributed throughout the CNS, GlyT2 has a much more limited distribution and is present mainly on nerve terminals of inhibitory glycinergic neurones. GlyT1 is likely to regulate glycine levels at both strychnine-insensitive NMDAR glycine sites and strychnine-sensitive inhibitory glycine receptors, whilst the main role of GlyT2 may be to replenish intracellular glycine stores in glycinergic nerve terminals (Gomez et al. 2003; Rousseau et al. 2008).

GlyT1 inhibition is currently under investigation for a number of pathological indications, notably schizophrenia where NMDAR hypofunction is believed to play an important role (Buchanan et al. 2007; Javitt 2002, 2006, 2008; Javitt et al. 2005; Lane et al. 2005; Lindsley et al. 2006). This is exemplified by the fact that very similar symptoms to those displayed by schizophrenia patients (e.g. enhanced motor activity, cognitive deficits and increased stereotyped behaviour) can be induced by NMDAR inhibitors such as phencyclidine (PCP). These symptoms can be reversed by the inhibition of GlyT1 as this leads to increased levels of glycine in the synapse and therefore improved NMDAR neurotransmission. Numerous efforts are being made to develop suitable drug candidates for GlyT1 inhibition and many have recently entered early phase clinical trials in man (Eulenburg et al. 2005; Betz et al. 2006; Javitt 2006). Examples of compounds developed for inhibition of the type 1 glycine transporter can be found in Harsing et al. (2006) and published international patent applications (Coulton et al. 2003; Bradley et al. 2006; Alberati et al. 2012, 2013).

12.2 Potential Utility of PET Imaging

Noninvasive nuclear imaging techniques can be used to obtain basic and diagnostic information about the physiology and biochemistry of living subjects – experimental animals, patients and healthy volunteers. These techniques rely on the use of imaging instruments that can detect radiation emitted from radiotracers administered to the subjects. Acquired information can be reconstructed to provide planar and tomographic images which reveal the distribution and/or concentration of the radiotracer as a function of time. Positron emission tomography (PET) offers the highest spatial and temporal resolution of all nuclear medicine imaging modalities and has the added advantage that it allows absolute quantification of tracer concentrations in the mammalian body. The technique involves the use of radiotracers, labelled with positron-emitting radionuclides, that are designed to have *in vivo* properties which permit measurement of parameters regarding the physiology or biochemistry of living tissue (see Chap. 2 of this book volume).

The availability of a PET imaging probe for GlyT1 has the promise to increase the understanding of the pathophysiology of diseases such as schizophrenia and aid in the drug development process at this target. Evaluation of brain penetration and

dose-occupancy relationships of candidate GlyT1 inhibitors will provide valuable information on which doses to select for early phase 2 proof of concept studies in patient populations. This is all the more pertinent for GlyT1 as there is an apparent narrow window for transporter occupancy with regard to beneficial effect on cognition in schizophrenia (Hashimoto 2010).

12.3 Characteristics Required of a PET Probe for GlyT1

Application of GlyT1 imaging in disease understanding is likely to focus, e.g. on baseline transporter availability in patients versus controls and/or differences in transporter efficiency following pharmacological perturbations. For this, the specific binding outcome measure for the PET ligand would need to have low coefficient of variation ($\%COV < \sim 10\%$) to enable the detection of small transporter availability differences across populations involving realistic n numbers. For application in drug development, where the aim is to understand the ability of novel drug candidates to interact with the target, the requirement on $\%COV$ can be relaxed. For this application, PET ligands still benefit from low $\%COV$ so as to allow for studies with small numbers of subjects, but ligands with $\%COV$ between 10 and 20% are acceptable. Indeed, ligands with poorer $\%COV$ (20–30%) can often still be used for occupancy studies, but the use of such tracers will lead to increased confidence intervals for the estimation of EC_{50} and a resulting need for larger scan numbers. If ligands become available in the first category which also meet the other requirements such as specificity of the signal and lack of brain penetrant metabolites, there is little or no need for continued radiopharmaceutical development, whereas such efforts are desirable when this is not the case.

Straightforward occupancy studies can be performed using either carbon-11- or fluorine-18-labelled PET ligands whereas more complicated study designs are best done with carbon-11 since the short half-life of this radionuclide allows scanning of the same volunteer or patient more than once a day (see Christian et al. 2004; Abanades et al. 2011; Gunn et al. 2011a, b). Carbon-11 is also preferred in cases where radiation dose constraints are severe. In radiochemistry, there is a trend towards accelerating development of fluorine-18-labelled radiopharmaceuticals. The rationale for this is often that carbon-11 does not lend itself to distribution and therefore cannot be used by groups who do not have the capability to produce their own tracers. There is clear value to this approach; however, prior to global use, much time and effort should be invested in verifying the validity of simplified analysis approaches that do not require a metabolite-corrected arterial input function – otherwise tracer application will be limited to a few high-end R&D centres that have the capability to perform full quantitative analysis.

Although no regional values for B_{max} have been reported for GlyT1 in the CNS, mRNA distribution, immunocytochemistry and immunohistochemistry experiments and autoradiography work using [3H]NFPS, [3H]-(*R*)-NPTS and [^{35}S]ACPPB indicate widespread localization of the transporter with highest densities in the spinal cord, cerebellum and midbrain and more moderate densities in cortical areas

(Zafra et al. 1995; Jursky and Nelson 1996; Lowe et al. 2003; Mallorga et al. 2003; Cubelos et al. 2005; Zeng et al. 2008). As a result, no proper reference region (brain area lacking GlyT1) is likely to be available, potentially complicating widespread utility of PET probes beyond dedicated and specialised research institutions, given the inherent need for determination of a metabolite-corrected arterial input function for each scan.

12.4 GlyT1 Tracer Development

Over the past 3 years, a number of PET probes have been developed and used for delineation of GlyT1 transporters in the mammalian brain. Structures and associated information for tracers that have been applied in humans or nonhuman primates are presented in Table 12.1.

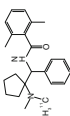
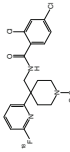
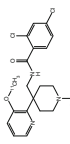
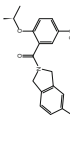
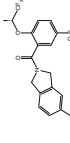
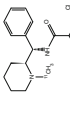
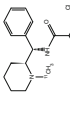
12.4.1 [¹¹C]ALX5407

The first GlyT1 inhibitor to be labelled with a PET isotope was [¹¹C]ALX5407 (Ravert et al. 2001), but no information on in vitro or in vivo evaluation has been provided subsequently, suggesting that this tracer was not successful as a PET ligand.

12.4.2 [¹¹C]GSK931145

In 2008, the imaging group at GSK reported the evaluation of three candidate PET ligands, [¹¹C]GSK931145, [¹¹C]GSK565710 and [¹¹C]GSK991022, in porcine CNS at the Society of Nuclear Medicine Annual Meeting in New Orleans (Passchier et al. 2008). Full data and additional results were published in 2010 (Passchier et al. 2010) and confirmed that out of the three labelled compounds, [¹¹C]GSK931145 showed promise as a potential PET ligand. Regional estimates of the total volume of distribution reflected the known rank order of GlyT1 distribution for [¹¹C]GSK931145 (brainstem > cortex) and were reduced to a homogeneous level following pre-administration of 0.5 mg/kg GSK565710. Calculation of binding potential (BP_{ND}), under the assumption of full block with 0.5 mg/kg GSK565710, indicated a $BP_{ND} \sim 2$ in the brainstem. Subsequent studies in nonhuman primates and human subjects confirmed suitable dosimetry for multiple scans in human subjects with a mean effective dose in humans of 4.02 μ Sv/MBq (male phantom) and 4.95 μ Sv/MBq (female phantom). Little or no urinary excretion was observed and the limiting organ was the liver with radiation absorbed dose estimates of 9.89 μ Gy/MBq and 13.05 μ Gy/MBq for male and female phantoms, respectively (Bullich et al. 2011). Further studies in healthy volunteers demonstrated the lack of a reference region devoid of specific binding. Test-retest variability of regional total volume of distribution (V_T) was poor (>30 %), and overall signal to noise was much reduced in man

Table 12.1 Structures and physicochemical properties for reported PET ligands

Tracer		[¹¹ C]GSK931145	[¹⁸ F]MK-6577	[¹¹ C]CMPyPB	[¹¹ C]RO501852	[¹¹ C]RO5013853	[¹¹ C]- <i>N</i> -Methyl_SSR504734 ([¹¹ C]GSK565710)
Structure							
MW	350.51	487.09	499.11	443.19	497.16	410.87	
Log <i>D</i> (pH7.4)	2.5	2.9	3.2	2.2	2.3	2.97	
p <i>K</i> ₅₀ (GlyT1)	8.4	8.7 (human)	8.4 (human)	NR	NR	8.3	
p <i>K</i> ₅₀ (GlyT2)	<4.6	<5	NR	NR	NR	5.4	
Affinity GlyT1	p <i>K</i> _i = 8.97 (rat cortex)	p <i>K</i> _i = 8.94 (human)	NR	<i>K</i> _D = 3.9 (rat); <i>K</i> _D = 3.7 (human)	<i>K</i> _D = 2 (rat); <i>K</i> _D = 1.7 (human)	p <i>K</i> _i = 9.09 (rat)	
<i>f</i> _p (%)	0.8 (human)	NR	NR	NR	NR	NR	
Primate	Yes	Yes	Yes	Yes	Yes	Yes	
Human	Yes	Yes	No	No	Yes	No	
%COV(<i>V</i> _T)	29–38 % (human)	–	–	–	1.2 % (human)	–	

NR not reported

compared to pig and primate. More detailed analysis pointed towards differences in plasma protein binding as the leading cause for the observed species differences. Although [^{11}C]GSK931145 does not appear suitable to investigate population differences (unless they are large), it can be used to determine occupancy and derive an EC_{50} value using a pseudo reference region approach (Gunn et al. 2011a), as demonstrated for the GlyT1 drug candidate GSK1018921.

12.4.3 [^{18}F]MK-6577

Hamill et al. (2011) reported the preclinical evaluation of [^{18}F]MK-6577 and [^{11}C]CMPyPB in rhesus monkey as potential PET ligands for delineation of GlyT1 in the CNS. Both tracers showed good brain uptake with a distribution that was in agreement with reported rank order of GlyT1 and with results obtained with [^{11}C]GSK931145 in primate brain. Although initial results looked promising, no further work was reported for [^{11}C]CMPyPB. Selectivity of MK-6577 for GlyT1 over GlyT2 was established by measuring inhibition of [^{14}C]glycine uptake in HEK cells expressing human GlyT2. A similar experiment was performed to determine selectivity for GlyT1 over the taurine transporter TauT in JAR cells. In addition, no off-target activities were observed when MK-6577 was screened against >100 known cerebral receptors, ion channels and enzymes. Blocking studies with (S)-CPyPBE resulted in rapid washout of [^{18}F]MK-6577 from all brain regions with near homogeneous tracer uptake throughout the brain. As observed for [^{11}C]GSK931145, reduction was seen for all brain regions. A subsequent chase study using (S)-CPyPBE demonstrated reversibility of [^{18}F]MK-6577 binding. Further papers have focused on quantification of GlyT1 availability using a model-based input function (Sanabria-Bohórquez et al. 2012), comparison of [^{18}F]MK6577 and [^{11}C]GSK931145 scan results in baboons (Zheng et al. 2013) and the use of [^{18}F]MK-6577 to estimate glycine transporter occupancy of drug candidates (Eddins et al. 2013), but to date no human data has been reported.

12.4.4 [^{11}C]Ro5013853

The radiosynthesis of another PET probe for GlyT1, [^{11}C]Ro5013853, was also reported in 2011 (Pinard et al. 2011). Recently, Borroni et al. (2013) and Wong et al. (2013) reported the preclinical and clinical characterization of this radiopharmaceutical as a novel PET tracer for GlyT1. Wong et al. (2012) and Borroni et al. (2013) also evaluated [^{11}C]Ro5013852, but although this compound did show a distribution in agreement with the previous PET ligands, [^{11}C]Ro5013853 displayed slightly higher brain uptake and a higher specific signal as determined using the occipital cortex as reference region. Thus, [^{11}C]Ro5013853 was selected for further studies.

The reported intra-subject variability (%COV) for V_T in baboon was good across brain regions, ranging from 18 % for pons to 10 % for cerebellum, thalamus and cortex. The characterization study in humans demonstrated that similar to [^{11}C]

GSK931145, regional brain V_T for [^{11}C]RO5013853 was substantially reduced in man compared to baboon. The BP_{ND} estimates in cerebellum, pons and thalamus were comparable to those obtained for [^{11}C]GSK931145; however, [^{11}C]RO5013853 test-retest variability was superior and can be smaller than 10 % (Wong et al. 2013). Although the authors claim that both [^{11}C]RO5013852 and [^{11}C]RO5013853 are selective for GlyT1 in a screen of more than 80 receptors, ion channels and enzymes widely distributed in the brain, no information of selectivity for GlyT1 over the anticipated closest pharmacology, GlyT2 was provided.

[^{11}C]RO5013853 was successfully applied to measuring the GlyT1 occupancy as a result of oral dosing of bitopertin in baboon and subsequently in man (Martin-Facklam et al. 2013).

12.4.5 [^{11}C]-*N*-Methyl-SSR504734

Most recently, Fuchigami et al. (2012) reported results in primate CNS for [^{11}C]-*N*-Methyl-SSR504734. This tracer was previously reported by Passchier et al. (2010) as [^{11}C]GSK565710 and evaluated in porcine brain where it was found to be inferior to [^{11}C]GSK931145. In cynomolgus monkey, the authors found [^{11}C]-*N*-Methyl-SSR504734 to be a promising potential GlyT1 PET ligand. Baseline V_T for the two monkeys followed the known rank order for GlyT1 distribution: thalamus > pons > cerebellum = putamen > cortical regions > white matter. Volumes of distribution for monkey 1 were ~2-fold higher than observed for monkey 2. Specific binding was characterised through pretreatment with SSR504734, leading to a reduction in V_T compared to baseline and an apparent occupancy of 45 and 74 % for doses of 1.5 and 4.5 mg/kg, respectively. Interestingly, thalamus seemed to behave differently from other regions which the authors propose may be due to a different non-displaceable component or a different GlyT1 occupancy. Further work using structurally different blocking agents will be required to confirm this finding. The authors plan to investigate the behaviour of this potential PET ligand in human volunteers.

12.4.6 [^{11}C]-labelled CHIBA and SA Compounds

Several structurally related non-sarcosine-based GlyT1 inhibitors have been labelled with ^{11}C and evaluated for GlyT1 imaging (Toyohara et al. 2011; Zhang et al. 2012). Although one of these compounds (^3H]CHIBA-3007) showed favourable pre-screening results, using in vitro autoradiography and binding assays in rat brain homogenates (Zhang et al. 2011), a subsequent in vivo study in mice indicated that [^{11}C]CHIBA-3007 and two of its analogs ([^{11}C]CHIBA-3009, [^{11}C]CHIBA-3011) are rapidly metabolised and demonstrate either low brain uptake or high nonspecific binding in vivo (Zhang et al. 2012). The low brain uptake of [^{11}C]CHIBA-3009 and [^{11}C]CHIBA-3011 was shown to be due to the fact that these compounds are substrates for the efflux transporter P-glycoprotein. Thus, these three CHIBA

compounds are not suitable for in vivo imaging of cerebral GlyT1 (Zhang et al. 2012). Three other structurally related [^{11}C]-labelled inhibitors (called [^{11}C]SA1, [^{11}C]SA2 and [^{11}C]SA3) have also been tested, [^{11}C]SA1 differing from [^{11}C]CHIBA-3007 only in the absence of a nitrogen atom in an aromatic ring. Of the latter three compounds, only [^{11}C]SA1 showed specific in vivo binding to GlyT1 in the mouse brain. [^{11}C]SA1 was therefore used for PET scans in conscious monkeys. The regional brain uptake of this compound corresponded closely to the known GlyT1 distribution in nonhuman primates. However, brain uptake was low with a high degree of variability and the authors suggest that further optimisation of the [^{11}C]SA1 structure would be required to achieve in vivo selective GlyT1 imaging (Toyohara et al. 2011).

Conclusions

1. Type 1 glycine transporters in the human brain remain an attractive and relevant target for PET imaging. Schizophrenia is a severe mental disorder with a significant impact on life expectancy and a relatively high incidence (0.03–0.07 % of global population). Partial inhibition of GlyT1 activity is proposed to improve cognitive impairment in schizophrenics.
2. In order to accurately understand the clinical relationship between the dose of a GlyT1 inhibitor and its effectiveness in cognitive models, an appropriate radioligand for use in PET or SPECT studies has to be available. There is thus an ongoing need for access to imaging tools which can be used in drug development and research focused on greater understanding of mechanisms underlying human disease.
3. Out of many currently reported radiopharmaceuticals for GlyT1, [^{11}C]Ro5013853 appears to be the best suitable for determination of transporter occupancy by nonradioactive drugs.
4. Data from a range of tracers indicate that GlyT1 is expressed throughout the brain with no available reference region, resulting in high tracer binding in cerebellum, pons, thalamus and white matter of the frontal cortex, with lower tracer binding in putamen, caudate and cortical grey matter.
5. Many tracer candidates have not yet been fully characterised. For [^{18}F]MK6577, [^{11}C]-N-methyl-SSR5-4734 and [^{11}C]SA1, human data are missing. The specificity of [^{11}C]Ro5013853 for GlyT1 vs GlyT2 has not yet been examined. Further radiopharmaceutical development is necessary to improve on the existing choice.

References

- Abanades S, van der Aart J, Barletta JA et al (2011) Prediction of repeat-dose occupancy from single-dose data: characterization of the relationship between plasma pharmacokinetics and brain target occupancy. *J Cereb Blood Flow Metab* 31:944–952
- Alberati D, Borroni EM, Hartung T et al (2012) Radiolabelled inhibitors of the glycine 1 transporter. US Patent 8,153,679 B2

- Alberati D, Borroni EM, Hartung T et al (2013) Radiolabelled inhibitors of the glycine 1 transporter. European Patent 2,342,197 B1
- Betz H, Gomeza J, Armsen W et al (2006) Glycine transporters: essential regulators of synaptic transmission. *Biochem Soc Trans* 34:55–58
- Borroni E, Zhou Y, Ostrowizki S et al (2013) Pre-clinical characterization of [¹¹C]Ro5013853 as a novel radiotracer for imaging of the glycine transporter type 1 by positron emission tomography. *Neuroimage* 75:291–300
- Bradley DM, Branch CL, Chan WN et al (2006) Glycine transport inhibitors, International Patent Application WO 2006 067423
- Buchanan RW, Javitt DC, Marder SR et al (2007) The cognitive and negative symptoms in schizophrenia trial (CONSIST): the efficacy of glutamatergic agents for negative symptoms and cognitive impairments. *Am J Psychiatry* 164:1593–1602
- Bullich S, Slifstein M, Passchier J et al (2011) Biodistribution and radiation dosimetry of the glycine transporter-1 ligand ¹¹C-GSK931145 determined from primate and human whole-body PET. *Mol Imaging Biol* 13:776–784
- Christian BT, Narayanan T, Shi B et al (2004) Measuring the in vivo binding parameters of [¹⁸F] fallypride in monkeys using a PET multiple-injection protocol. *J Cereb Blood Flow Metab* 24:309–322
- Coulton S, Hadley MS, Herdon HJ et al (2003) Glyt1 transporter inhibitors and uses thereof in treatment of neurological and neuropsychiatric disorders. International Patent Application WO 2003 055478
- Cubelos B, Giménez C, Zatra F (2005) Localization of the GLYT1 glycine transporter at glutamatergic synapses in the rat brain. *Cereb Cortex* 15:448–459
- Eddins D, Hamill TG, Puri V et al (2013) The relationship between glycine transporter 1 occupancy and the effects of the glycine transporter 1 inhibitor RG1678 or ORG25935 on object retrieval performance in scopolamine impaired rhesus monkey. *Psychopharmacology* DOI: 10.1007/s00213-013-3260-0
- Eulenburg V, Armsen W, Betz H et al (2005) Glycine transporters: essential regulators of neurotransmission. *Trends Biochem Sci* 30:325–333
- Fuchigami T, Takano A, Gulyás B et al (2012) Synthesis and evaluation of [¹¹C]N-methyl-SSR504734 as a PET radioligand for glycine transporter 1. *EJNMMI Res* 2:37
- Gomez J, Ohno K, Betz H (2003) Glycine transporter isoforms in the mammalian central nervous system: structures, functions and therapeutic promises. *Curr Opin Drug Discov Devel* 6:675–682
- Gunn RN, Murthy V, Catafau AM et al (2011a) Translational characterization of [¹¹C]GSK931145, a PET ligand for the glycine transporter type 1. *Synapse* 65:1319–1332
- Gunn RN, Qi G, Salinas CA et al (2011b) Advances in biomathematical modeling for PET neuro-receptor imaging. *Drug Discov Today Technol* 8:e45–e51
- Hamill TG, Eng W, Jennings A et al (2011) The synthesis and preclinical evaluation in rhesus monkey of [¹⁸F]MK-6577 and [¹¹C]CMPyPB glycine transporter 1 positron emission tomography radiotracers. *Synapse* 65:261–270
- Harsing LG, Juranyi Z, Gacsalyi I et al (2006) Glycine transporter type-1 and its inhibitors. *Curr Med Chem* 13:1017–1044
- Hashimoto K (2010) Glycine transport inhibitors for the treatment of schizophrenia. *Open Med Chem J* 4:10–19
- Javitt DC (2002) Glycine modulators in schizophrenia. *Curr Opin Investig Drugs* 3:1067–1072
- Javitt DC (2006) Is the glycine site half saturated or half unsaturated? Effects of glutamatergic drugs in schizophrenia patients. *Curr Opin Psychiatry* 19:151–157
- Javitt DC (2008) Glycine transport inhibitors and the treatment of schizophrenia. *Biol Psychiatry* 63:6–8
- Javitt DC, Hashim A, Sershen H (2005) Modulation of striatal dopamine release by glycine transport inhibitors. *Neuropsychopharmacology* 30:649–658
- Jursky F, Nelson N (1996) Developmental expression of the glycine transporters GLYT1 and GLYT2 in mouse brain. *J Neurochem* 67:336–344

- Lane HY, Chang YC, Liu YC et al (2005) Sarcosine or D-serine add-on treatment for acute exacerbation of schizophrenia: a randomized, double-blind, placebo-controlled study. *Arch Gen Psychiatry* 62:1196–1204
- Lindsley CW, Shipe WD, Wolkenberg SE et al (2006) Progress towards validating the NMDA receptor hypofunction hypothesis of schizophrenia. *Curr Top Med Chem* 6:771–785
- Lowe JA, Drozda SE, Fisher K et al (2003) [³H]-(R)-NPTS, a radioligand for the type 1 glycine transporter. *Bioorg Med Chem Lett* 13:1291–1292
- Mallorga PJ, Williams JB, Jacobson M et al (2003) Pharmacology and expression analysis of glycine transporter GlyT1 with [³H]-(N-[3-(4'-fluorophenyl)-3-(4'-phenylphenoxy)propyl] sarcosine. *Neuropharmacology* 45:585–593
- Martin-Facklam M, Pizzagalli F, Zhou Y et al (2013) Glycine transporter type 1 occupancy by bitopertin: a positron emission tomography study in healthy volunteers. *Neuropsychopharmacology* 38:504–512
- Passchier J, Murthy V, Catafau A et al (2008) Development and evaluation of [¹¹C]GSK931145, a new PET ligand for imaging type 1 glycine transporters (GlyT1) in the living human brain. *J Nucl Med* 49(Suppl 1):129P
- Passchier J, Gentile G, Porter R et al (2010) Identification and evaluation of [¹¹C]GSK931145 as a novel ligand for imaging the type 1 glycine transporter with positron emission tomography. *Synapse* 64:542–549
- Pinard E, Burner S, Cueni P et al (2011) Radiosynthesis of [¹¹C]Ro501383, a novel PET tracer for the glycine transporter type 1 (GlyT1). *J Label Comp Radiopharm* 54:702–707
- Ravert HT, Mathews WB, Klitenick MA et al (2001) Radiosynthesis of a ligand for studying the glycine transporter: [¹¹C]ALX-5407. *J Label Comp Radiopharm* 44:241–246
- Rousseau F, Aubrey KR, Supplisson S (2008) The glycine transporter GlyT2 controls the dynamics of synaptic vesicle refilling in inhibitory spinal cord neurons. *J Neurosci* 28:9755–9768
- Sanabria-Bohórquez SM, Joshi AD, Holahan M et al (2012) Quantification of the glycine transporter 1 in rhesus monkey brain using [¹⁸F]MK-6577 and a model-based input function. *Neuroimage* 59:2589–2599
- Toyohara J, Ishiwata K, Sakata M et al (2011) In vivo evaluation of carbon-11-labelled non-sarcosine-based glycine transporter 1 inhibitors in mice and conscious monkeys. *Nucl Med Biol* 38:517–527
- Wong DF, Borroni E, Ostrowitzki S et al (2012) Imaging biomarkers for the glycine transporter type 1. *J Nucl Med* 53(Suppl 1):199
- Wong DF, Ostrowitzki S, Zhou Y et al (2013) Characterization of [¹¹C]Ro5013853, a novel PET tracer for the glycine transporter type 1 (GlyT1) in humans. *Neuroimage* 75:282–290
- Zafra F, Gomeza J, Olivares L et al (1995) Regional distribution and developmental variation of the glycine transporters GLYT1 and GLYT2 in the rat CNS. *Eur J Neurosci* 7:1342–1352
- Zeng Z, O'Brien JA, Lemaire W et al (2008) A novel radioligand for glycine transporters: Characterization and use in autoradiographic and in vivo brain occupancy studies. *Nucl Med Biol* 35:315–325
- Zhang JC, Wu J, Toyohara J et al (2011) Characterization of [³H]CHIBA-3007 binding to glycine transporter 1 in the rat brain. *PLoS One* 6:e21322
- Zhang JC, Toyohara J, Wu J et al (2012) In vivo evaluation of three [¹¹C]labeled radioligands for glycine transporter 1 in the mouse brain. *Clin Psychopharmacol Neurosci* 10:34–43
- Zheng MQ, Holden D, Hamill T et al (2013) Comparative study of two glycine transporter 1 radiotracers, [¹¹C]GSK931145 and [¹⁸F]MK6577, in baboons. *J Nucl Med* 54(Suppl 2):414

Uta Funke, Danielle J. Vugts, Bieneke Janssen,
Arnold Spaans, Perry S. Kruijer, Adriaan A. Lammertsma,
Lars R. Perk, and Albert D. Windhorst

Contents

13.1	Introduction	332
13.2	Imaging of Histamine Receptors in CNS Using Non-histaminergic Radiopharmaceuticals	334
13.3	Imaging of the Histamine H ₁ Receptor	338
13.4	Imaging of the Histamine H ₂ Receptor	352
13.5	Imaging of the Histamine H ₃ Receptor	353
13.6	Imaging of the Histamine H ₄ Receptor	364
13.7	Summary and Conclusion	364
	References	365

Abstract

The histaminergic system contains four subtypes of G-protein-coupled receptors: H₁R, H₂R, H₃R and H₄R. In the central nervous system, they mediate the action of histamine in pituitary hormone secretion, wakefulness, motor and

U. Funke (✉)

Research and Development, BV Cyclotron VU, Amsterdam, The Netherlands

Department of Radiology and Nuclear Medicine, VU University Medical Center,
Amsterdam, The Netherlands

e-mail: u.funke@cyclotron.nl

D.J. Vugts • B. Janssen • A.A. Lammertsma

Department of Radiology and Nuclear Medicine, VU University Medical Center,
Amsterdam, The Netherlands

A. Spaans • P.S. Kruijer • L.R. Perk

Research and Development, BV Cyclotron VU, Amsterdam, The Netherlands

A.D. Windhorst

Department of Radiology and Nuclear Medicine, VU University Medical Center,
Amsterdam, The Netherlands

cognitive functions as well as in itch and nociception. Alterations in the cerebral histaminergic neurotransmission are associated with numerous neurological diseases, e.g. sleep/wake and eating disorders, epilepsy, neuropathic pain, neurodegeneration and neuroinflammation. Therefore, histamine receptors are a target of high interest, not only for therapy, but also for imaging and quantification using PET and SPECT. In addition to indirect flow and metabolism studies, this chapter provides a review of results of preclinical and clinical investigations with subtype-selective tracers.

13.1 Introduction

The endogenous short-acting biogenic amine histamine (2-(1*H*-imidazol-4-yl)ethanamine (Barger and Dale 1910; Windaus and Vogt 1907)) plays a key role in various physiological processes. In peripheral tissues, it acts as a mediator in immune reactions (Jutel et al. 2005; Thurmond 2010), smooth muscle contraction (Izzo et al. 1998; Karaki et al. 1997; Schoeffter and Godfraind 1989), gastric secretion (Barocelli and Ballabeni 2003; Sandvik et al. 1997) and sensation of itch as well as pain (Baraniuk 2012; Schmelz 2010; Shim and Oh 2008). In addition, histamine is a neurotransmitter (Haas et al. 2008; Nuutinen and Panula 2010) and a regulator of cell proliferation and differentiation (Molina-Hernández et al. 2012) in the central nervous system (CNS). This function is exerted by binding to the four known histamine receptor subtypes, H₁R, H₂R, H₃R and H₄R (Bongers et al. 2010; Hill et al. 1997; Parsons and Ganellin 2006), all belonging to the superfamily of G-protein-coupled receptors (GPCR).

Cerebral H₁R was shown to be functionally expressed with high levels in neocortex, claustrum, thalamus, hypothalamus and limbic system and lower levels in striatum and thalamus of both non-human primate and human brain (Kanba and Richelson 1984; Martinez-Mir et al. 1990). Alterations in H₁R-mediated neurotransmission result in disturbances of the circadian rhythm (Nowak 1994), feeding behaviour and energy metabolism (Deng et al. 2010; Masaki and Yoshimatsu 2006, 2010; Mercer et al. 1994; Morimoto et al. 2001; Sakata et al. 1997), wakefulness (Barbier and Bradbury 2007; Thakkar 2011) and cognitive functions (Alvarez 2009; Van Ruitenbeek et al. 2010). Finally, H₁R is involved in neuroinflammatory processes such as multiple sclerosis (Jadidi-Niaragh and Mirshafiey 2010; Passani and Ballerini 2012; Saligrama et al. 2012) and cerebral ischemia (Hu and Chen 2012).

Often found in co-expression with H₁R, H₂R was detected in guinea pig (Vizuete et al. 1997) and human brain (Martinez-Mir et al. 1990; Traiffort et al. 1992) with high levels in the basal ganglia, parietal and occipital cortex and limbic system, and in somewhat lower densities in thalamus, cerebellum and claustrum. It also mediates the action of histamine in brain ischemia (Adachi 2005; Hu and Chen 2012), multiple sclerosis (Jadidi-Niaragh and Mirshafiey 2010; Passani and Ballerini 2012; Saligrama et al. 2012) and cognition (Alvarez 2009). Based on pharmacological studies, both dysfunctional H₁R and H₂R have been suggested to play a role in

psychoses such as seen in schizophrenia, but none of the H₁ and H₂ receptor gene polymorphisms investigated showed an association with this disease (Arrang 2007; Haas et al. 2008; Ito 2004; Ito et al. 2000).

The H₃R was shown to be localized in various regions of the rodent brain, such as cerebral cortex, striatum, amygdala, hypothalamus, substantia nigra, nucleus accumbens and olfactory tubercle (Bonaventure et al. 2007; Chazot et al. 2001; Lovenberg et al. 1999). In contrast to postsynaptic H₁R and H₂R, the H₃R acts as pre- and postsynaptic heteroreceptor, and regulates the release of histamine and other neurotransmitters such as dopamine, acetylcholine, noradrenalin and serotonin (Leurs and Timmerman 1998). Therefore, its dysfunction is involved in numerous pathological conditions of the CNS (Esbenshade et al. 2006, 2008; Gemkow et al. 2009; Yu et al. 2010), such as Alzheimer's disease, attention-deficit hyperactivity disorder (Vohora and Bhowmik 2012), schizophrenia (Arrang 2007; Ito 2009), epilepsy, eating disorders (Deng et al. 2010; Masaki and Yoshimatsu 2010; Passani et al. 2011), insomnia and narcolepsy (Barbier and Bradbury 2007; Lin et al. 2011; Thakkar 2011). Like other histamine receptor subtypes, H₃R plays a role in neuronal injury and inflammation (Hu and Chen 2012; Jadidi-Niaragh and Mirshafiey 2010; Passani and Ballerini 2012; Saligrama et al. 2012).

The latter has been demonstrated also for the youngest member of the histamine receptor family, the H₄R (Passani and Ballerini 2012; del Rio et al. 2012). This role in neuroinflammation is confirmed by abundant H₄R expression on microglia (Ferreira et al. 2012), the resident macrophages of the brain and spinal cord (Kettenmann et al. 2011; Mrak and Griffin 2005). In addition, H₄R is involved in itch and nociception (Dunford et al. 2007; Hsieh et al. 2010; Yu et al. 2010). Neuronal expression of H₄R has been shown in cerebral cortex, cerebellum, hippocampus, thalamus and caudate putamen of the mouse and insular cortex of the human brain (Connelly et al. 2009).

The various neurological and neuropsychiatric disorders caused by affected histaminergic neurotransmission (Haas et al. 2008; Nuutinen and Panula 2010; Repka-Ramirez 2003) have stimulated great interest in histamine receptors not as target for therapy alone (Bongers et al. 2010; Passani and Blandina 2011; Tiligada et al. 2011). Histamine receptors have also been considered for *in vivo* imaging and quantification by positron emission tomography (PET) and single-photon emission computed tomography (SPECT). However, several former reviews including (Crouzel 1990; Duncan 1999; Nikolaus et al. 2009; Smith and Jakobsen 2009; Tashiro et al. 2008b) or focusing on histaminergic imaging (van der Goot and Timmerman 2000; Watanabe and Yanai 2001; Yanai et al. 2011b; Yanai and Tashiro 2007) were limited mainly to imaging H₁R. The purpose of this chapter is to provide an overview of previous and recent achievements in PET and SPECT imaging of all known histamine receptor subtypes.

As the chapter summarizes more than two decades of imaging research, nomenclature varies between publications. Within the context of the present review, where necessary, nomenclature was modified to comply with a recent consensus document (Innis et al. 2007).

13.2 Imaging of Histamine Receptors in CNS Using Non-histaminergic Radiopharmaceuticals

Various anti-allergy drugs act via H_1R inhibition and can cause undesirable CNS effects such as sleepiness and changed psychomotor speed (McDonald et al. 2008; Tannenbaum et al. 2012; Yanai et al. 2012). Amongst other PET studies (see Sect. 13.3), sedative effects of antihistamines have been investigated by measuring regional cerebral blood flow (rCBF) using [^{15}O]water. In particular, effects of the first-generation H_1R antagonist *d*-chlorpheniramine on task-related changes in rCBF were examined (Mochizuki et al. 2002; Okamura et al. 2000; Tashiro et al. 2008c).

In visual discrimination tasks in healthy human volunteers, administration of *d*-chlorpheniramine resulted in significantly increased reaction time and deteriorated accuracy, which was positively correlated with increased rCBF in right frontal cortex and decreased rCBF in temporal and frontal gyrus regions (Okamura et al. 2000). Performance of spatial discrimination induced significantly increased rCBF in right cingulate cortex and decreased rCBF in right parietal cortex (Fig. 13.1). The related fixation task showed a significant increase in rCBF in caudate nuclei and the temporal poles in the *d*-chlorpheniramine-treated subjects (Fig. 13.2), together with a decrease in right dorsolateral prefrontal cortex and the frontal eye field (Mochizuki et al. 2002). These high contrast [^{15}O]H $_2$ O perfusion patterns are thought to be a result of compensatory effects. Elevated activity in corresponding brain regions indicates increased efforts to perform a task and maintain motor control. It represents the counteraction to the sedative condition (Okamura et al. 2000) and deteriorated dexterity (Mochizuki et al. 2002) caused by H_1R inhibition.

These results have been confirmed by rCBF measurements during simulated car driving tests (Tashiro et al. 2008c). After application of *d*-chlorpheniramine, “driving” caused decreased change in perfusion (Δ rCBF, active driving vs. resting) in temporal, parietal and occipital cortices as well as cerebellum, compared to placebo-treated subjects, and enhanced activity in orbitofrontal cortex and cerebellar vermis (Fig. 13.3). The latter, signalling an attempt to optimize motor output based on visual inputs, again is considered as an indication of compensation of the disturbed visuospatial cognition and visuomotor coordination in the cortical areas. Altogether these findings overlap with results of specific H_1R binding and occupancy studies following administration of antihistamines (Sect. 13.3).

Furthermore, [^{18}F]FDG PET has been used to investigate the involvement of histaminergic signalling in energy regulation and metabolism (Wang et al. 2010). Wild-type (WT), H_1R ($H_1R^{-/-}$) and H_2R knockout mice ($H_2R^{-/-}$) were fed normal (NcD) as well as high-cholesterol (HcD) diets. Quantification by PET and after organ dissection revealed that only in the brains of NcD- and HcD-fed $H_1R^{-/-}$ mice [^{18}F]FDG uptake levels increased significantly (for HcD-fed mice see Fig. 13.4). This was accompanied and is assumed to be caused by increased leptin and glucose transporter type 4 expression in this knockout type and points to regulation of glucose allocation by the interaction of leptin and histaminergic neurons. $H_2R^{-/-}$ mice showed only a significant increase of [^{18}F]FDG uptake in skeletal muscle tissue.

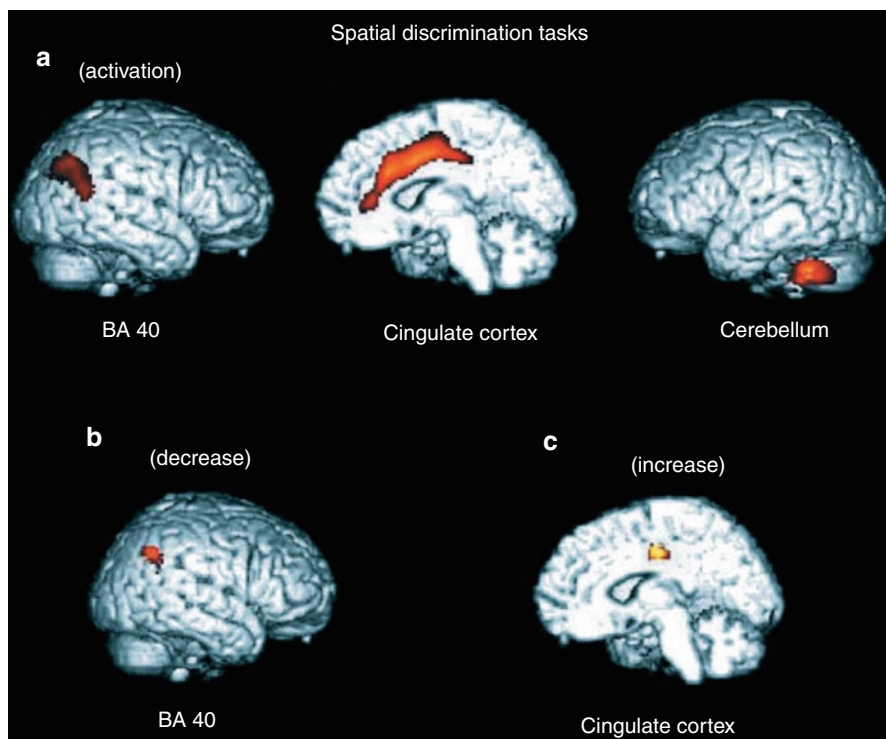


Fig. 13.1 Regions of significantly changed rCBF during spatial discrimination tasks in (a) a placebo group compared with results from a fixation task and (b, c) a *d*-chlorpheniramine-treated group compared with a placebo group. Brodmann's area (BA): supramarginal gyrus (BA40). Reprinted by permission of John Wiley & Sons Ltd from Mochizuki et al. 2002, Plate 1

Unfortunately, results for biodistribution of [^{18}F]FDG in HcD-fed normal mice, determined *ex vivo*, are not reported in this study. However, together with the development of an obese and visceral adipose phenotype with hyperleptinemia in $\text{H}_1\text{R}^{-/-}$, and according to the known neurobiological functions of histamine (Masaki and Yoshimatsu 2006, 2010), the results of Wang et al. (2010) emphasize a regulatory role of H_1R in feeding rhythms and energy metabolism.

Histamine H_3 and H_4 receptors are via their $\text{G}\alpha_{i/o}$ proteins negatively coupled to adenylate cyclase (AC) (Bongers et al. 2010) and play a part in the regulation of cyclic adenosine monophosphate (cAMP). This intracellular acting second-messenger molecule in turn is hydrolysed and so deactivated by phosphodiesterases (PDEs). Apart from studying effects of other neuroligands, Lourenco et al. followed this pathway in rats treated with the $\text{H}_3\text{R}/\text{H}_4\text{R}$ antagonist/inverse agonist thioperamide by measuring the biodistribution of (*R*)-[^{11}C]rolipram, a selective PDE4 inhibitor. Predosing with thioperamide (≥ 10 mg/kg) significantly increased specific radioligand binding in the brain in a dose-dependent manner (Lourenco et al. 2006).

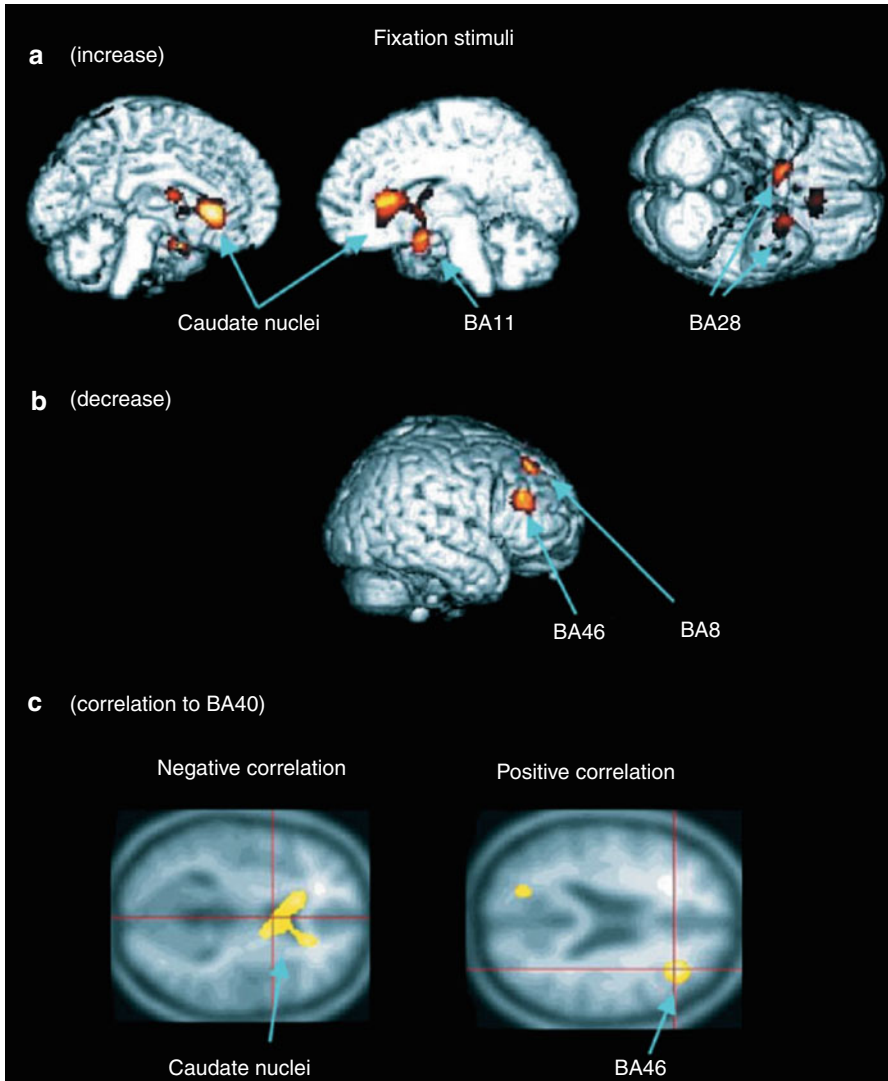


Fig. 13.2 Regions of significantly changed rCBF during fixation tests in a *d*-chlorpheniramine-treated group compared with a placebo group. (a) Increased rCBF in caudate nuclei, orbitofrontal cortex and temporal poles, and (b) decreased rCBF in prefrontal and dorsolateral prefrontal cortex. (c) Negative (*left*) and positive (*right*) correlation of caudate nuclei and dorsolateral prefrontal cortex to the activities of parietal cortex, respectively. Brodmann's areas (BA): frontal eye fields (BA8), orbitofrontal cortex (BA11), ventral entorhinal cortex (BA28), supramarginal gyrus (BA40), dorsolateral prefrontal cortex (BA46). Reprinted by permission of John Wiley & Sons Ltd from Mochizuki et al. 2002, Plate 2

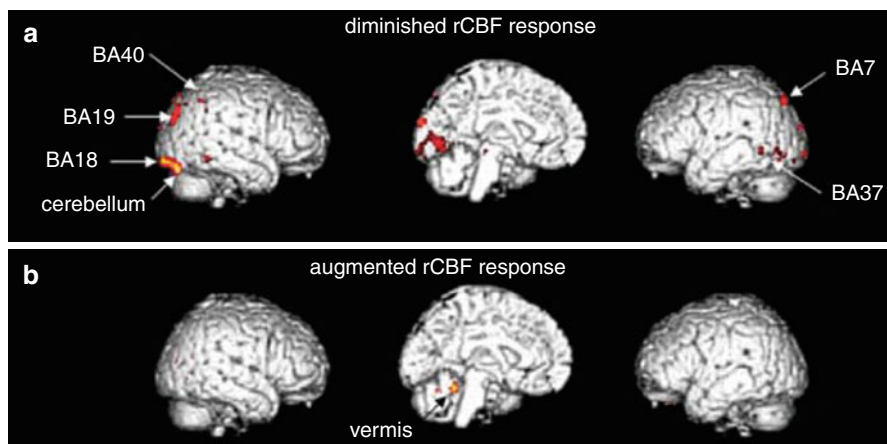


Fig. 13.3 Brain regions with altered rCBF responses ((a) diminished and (b) increased) in simulated car driving tests following *d*-chlorpheniramine treatment, superimposed onto standard MRI-rendered images. Brodmann's areas (BA): somatosensory association cortex (BA7), secondary (BA18) and associative visual cortex (BA19), fusiform (BA37) and supramarginal gyrus (BA40). Reprinted by permission of John Wiley & Sons Ltd from Tashiro et al. 2008c, Figure 4

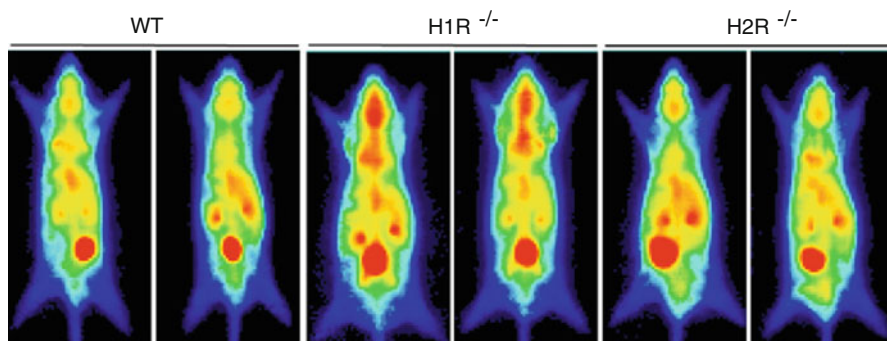


Fig. 13.4 Representative planar PET images, showing increased [¹⁸F]FDG uptake in H₁R^{-/-} mice brain after high-cholesterol feeding. Reprinted by permission of Elsevier Ltd from Wang et al. 2010, Figure 3

The authors explained this result by the H₃R antagonistic and histamine synthesis stimulating action of thioperamide (Gomez-Ramirez et al. 2002). However, inhibition of the presynaptic autoreceptor H₃R would increase histamine levels (Knigge et al. 1998; Leurs et al. 2005), thus increasing postsynaptic histamine receptor activity and decreasing cAMP concentrations. This, in turn, would cause diminished PDE4 expression and radioligand binding. It seems more likely that the increased (*R*)-[¹¹C] rolipram binding was due to the later discovered high affinity and antagonistic/inverse

agonistic action of thioperamide to the postsynaptic H₄R (Lim et al. 2005; Schnell et al. 2011). Inhibition of H₄R would cause an elevation of cAMP (Leurs et al. 2009; Thurmond et al. 2008) and thus PDE4 activity.

In summary, the few indirect imaging studies mentioned indicate the necessity for further studies of histamine receptors. This is needed to determine the role and relevance of histaminergic neurotransmission in normal physiological processes as well as in pathological conditions.

13.3 Imaging of the Histamine H₁ Receptor

Already at the end of the 1980s, two carbon-11-labelled ligands for imaging H₁R *in vivo* were reported: the pyridinyl-diamine [¹¹C]pyrilamine, also known as [¹¹C]mepyramine (Fig. 13.5), and the dibenzooxepinyl-amine [¹¹C]doxepin. Their nonradioactive analogues showed affinity for dog H₁R with inhibition constants (K_i) of ~11.7 and 2.8 nM, respectively (Yanai et al. 1990a). For human H₁R equilibrium dissociation constants (K_d) of 3.3 nM for pyrilamine and 0.17 nM for doxepin were determined (Cusack et al. 1994).

Both radioligands can be prepared by *N*-[¹¹C]methylation of the corresponding desmethyl-precursors. Depending on the approach, in about 20 min, nor-pyrilamine was converted with [¹¹C]methyl iodide to [¹¹C]pyrilamine in a decay-corrected radiochemical yield (RCY) of up to 34 %, a radiochemical purity (RCP) >99 % and a specific activity of up to 93 GBq/μmol (Dannals et al. 1989; Iwata et al. 1991; Yanai et al. 1988). Radiosynthesis of [¹¹C]doxepin has been accomplished by substitution of nor-doxepin with [¹¹C]methyl iodide (Cai et al. 2012; Dannals et al. 1989; Iwata et al. 1992; Ravert et al. 1992) as well as [¹¹C]methyl triflate. Nowadays, within about 40 min, automated preparation procedures approach RCYs of ~47 %, an RCP >97.5 % and a specific activity of ~45 GBq/μmol starting from [¹¹C]CH₃I (Cai et al. 2012). Starting from [¹¹C]CH₃OTf, an RCY >40 %, an RCP >99 % and a specific activity of around 100 GBq/μmol can be obtained within the same time (Ishiwata et al. 2004; Iwata et al. 2002; Mochizuki et al. 2004a; Yoshizawa et al. 2009).

In biodistribution studies [¹¹C]pyrilamine showed a brain uptake in mouse of ~5 % injected dose per gram of tissue (%ID/g) at 5 min p.i. but also fast clearance to ≤0.5 % at 60 min p.i. (Yanai et al. 1989). At 30 min p.i. the highest regional uptake was observed in hypothalamus, hippocampus, cortex and striatum with a ratio to cerebellum of 2, 1.8, 1.5 and 1.3, respectively (Yanai et al. 1988, 1989). [¹¹C]pyrilamine binding was specific, as demonstrated by [³H]pyrilamine saturation experiments. Further, [¹¹C]pyrilamine accumulation was blocked significantly by co-administration of the H₁R antagonist triprolidine (Yanai et al. 1988). Unfortunately, the latter was illustrated only by a reduced hypothalamus to cerebellum ratio from 1.4 to 1.2 at 15 min after application of the radioligand, and the dose of the inhibitor was not specified.

A decade later the first metabolism studies were undertaken, determining arterial plasma free and protein-bound fractions, parent compound and radiolabelled

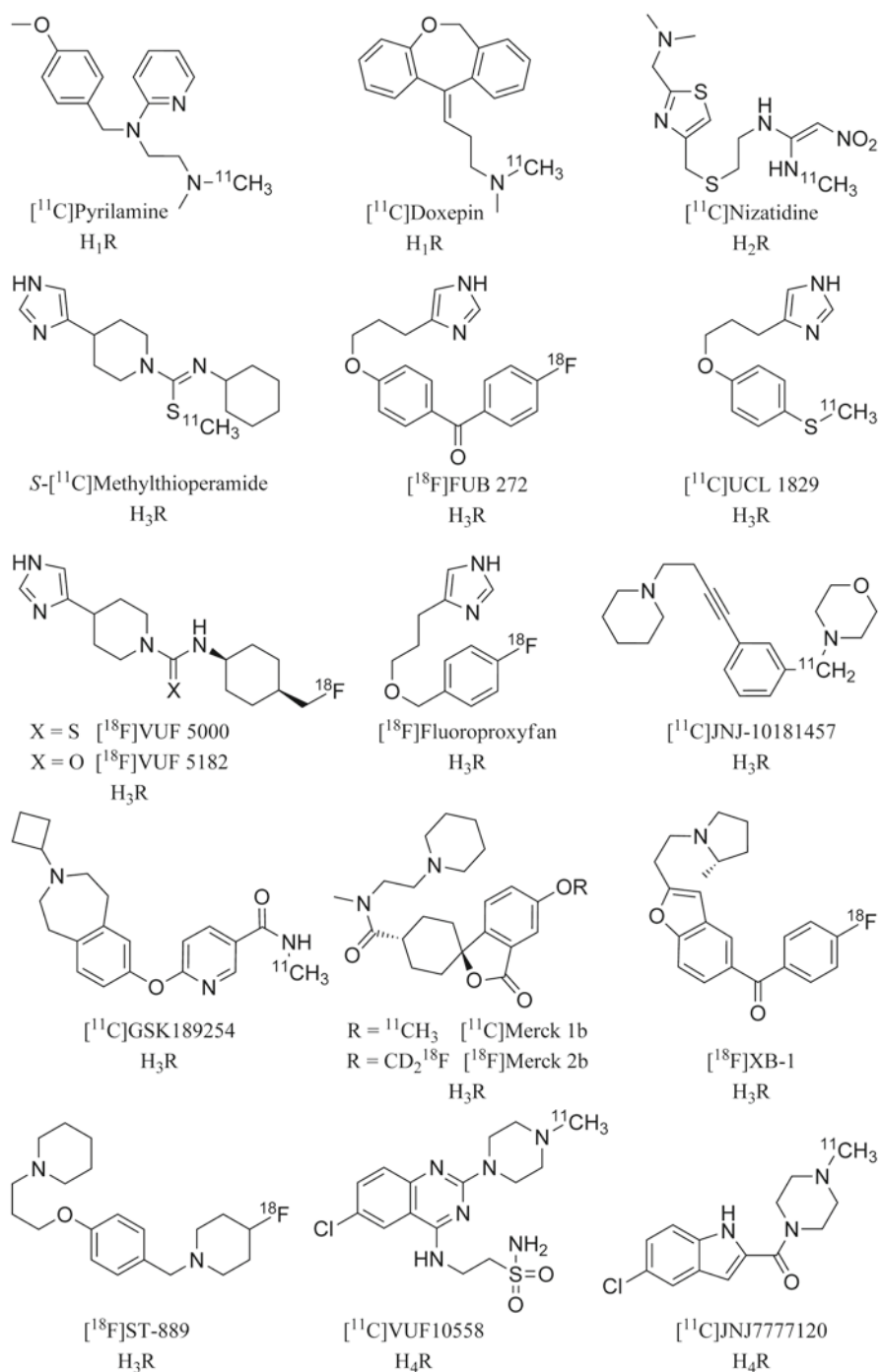


Fig. 13.5 Histamine receptor subtype-specific PET ligands

metabolite fractions for both [^{11}C]pyrilamine and [^{11}C]doxepin (Ishiwata et al. 1996). In healthy volunteers [^{11}C]pyrilamine showed low plasma protein binding. Correlating with that, rapid metabolism was observed, with only ~34 % of total plasma radioactivity corresponding with unchanged radiotracer at 15 min p.i. [^{11}C]Doxepin remained more stable with ~78 % of parent compound at 15 min p.i., whereof ~74 % were bound to plasma proteins. The latter seems to protect the radioligand from degradation, and the constant ratio of ~0.35 of unbound to bound plasma [^{11}C]doxepin appears to provide sufficient bioavailability for radioligand uptake and imaging of H_1R in the brain. In epileptic patients, medicated with anti-convulsants, the same free fraction in plasma was observed, but with only ~67 % of parent radioligand at 15 min p.i., suggesting an increase in [^{11}C]doxepin degradation (Ishiwata et al. 1996). This is supposed to be caused by elevated levels of hepatic microsomal metabolizing enzymes, such as cytochrome P450 (Anderson 2004; Spina and de Leon 2007), an issue that needs to be taken into account when scanning patients, especially if they are on medication.

Further it was investigated whether [^{11}C]pyrilamine metabolism had any effect on PET measurements in the brain (Kim et al. 1999). The amount of radiometabolites entering in human brain was inferred from rat brain homogenate analyses after [^{11}C]pyrilamine as well as radiometabolite administration. Injection of rat plasma containing 70–100 % metabolized [^{11}C]pyrilamine in rats revealed an initial brain uptake of <0.3 %ID/g for the radiometabolites at 5 min p.i. Extrapolating from that and human plasma metabolite analyses, only 1.8 % of the total radioactivity would correspond to radiometabolites in human brain at the time point of [^{11}C]pyrilamine peak uptake, even after an administration of 100 % metabolized radiotracer. Therefore no impact on PET imaging results was expected.

First visualization of H_1R by PET was performed in beagle dog brain using both [^{11}C]pyrilamine and [^{11}C]doxepin (Fig. 13.6) (Yanai et al. 1990a). Both radioligands showed suitable uptake (≥ 2 %ID/100 mL at 15 min p.i.). Successful blockade as well as displacement was observed after administration of 1 mg/kg triprolidine. The regional distribution of radiotracer uptake corresponded with the known expression of H_1R in various brain structures, being highest in cerebral cortex and olfactory bulb, and lowest in cerebellum. Of the two ligands, [^{11}C]doxepin showed the best imaging characteristics, as the images were higher in contrast (Fig. 13.6b), and the distribution remained constant during the scan.

Nevertheless, [^{11}C]pyrilamine was applied in various PET investigations of baboons and healthy human brain (Villemagne et al. 1991; Yanai et al. 1991). In baboon (Fig. 13.7), ~7 %ID/L peak uptake of [^{11}C]pyrilamine occurred at 20 min p.i. and decreased to ~6 %ID/L at 70 min p.i. in frontal cortex. This uptake was reduced by 33 % after pre-administration of 1 mg/kg of the antihistamine diphenhydramine and by 40 % after both 1 mg/kg and 5 mg/kg co-injected pyrilamine (Villemagne et al. 1991), suggesting that already 1 mg/kg of pyrilamine saturated the specific binding of the ligand (Quach et al. 1980; Yanai et al. 1988). In contrast to earlier studies, in baboon high [^{11}C]pyrilamine uptake was also observed in cerebellum with ~7.5 %ID/L at 20 min p.i. and ~6 %ID/L at 70 min p.i. Displacement with diphenhydramine and pyrilamine reduced this cerebellar uptake by 23 and 30 %, respectively.

Fig. 13.6 Transaxial PET images of dog brain, showing the distribution of (a) [^{11}C]pyrilamine and (b) [^{11}C]doxepin at 40–45 min p.i. Reprinted by permission of Elsevier Ltd from Yanai et al. 1990a, Figure 1

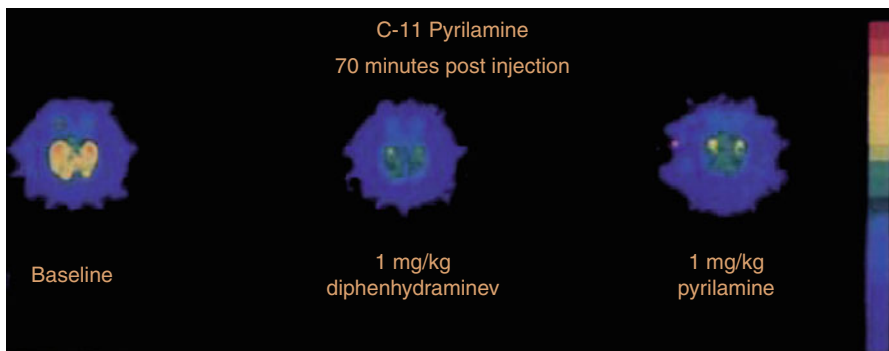
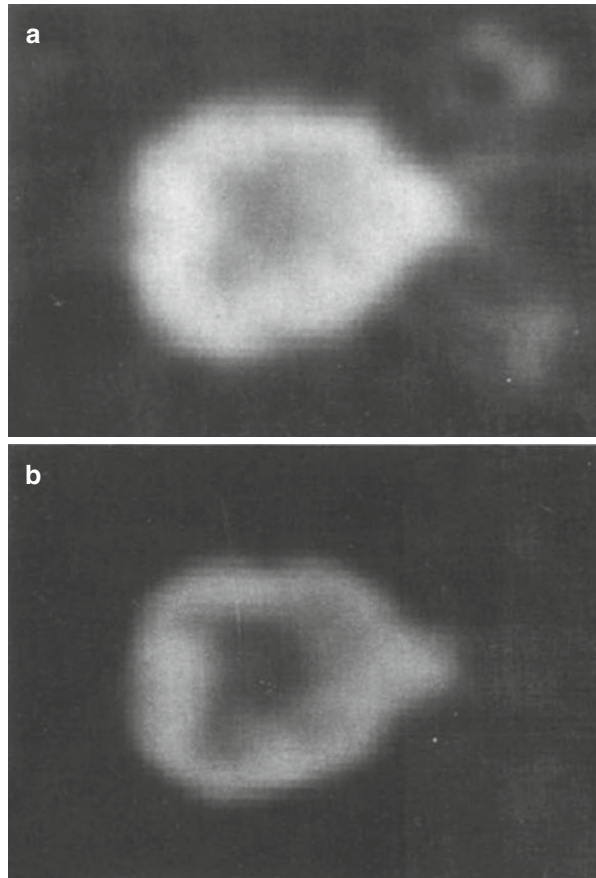


Fig. 13.7 Transaxial PET images from the lower hemisphere of baboon brains about 70 min p.i., demonstrating [^{11}C]pyrilamine distribution without (*left*) and after inhibition by pretreatment with 1 mg/kg diphenhydramine (*middle*) and co-injection of 1 mg/kg pyrilamine (*right*). Reprinted by permission of SNMMI from Villemagne et al. 1991, Figure 2

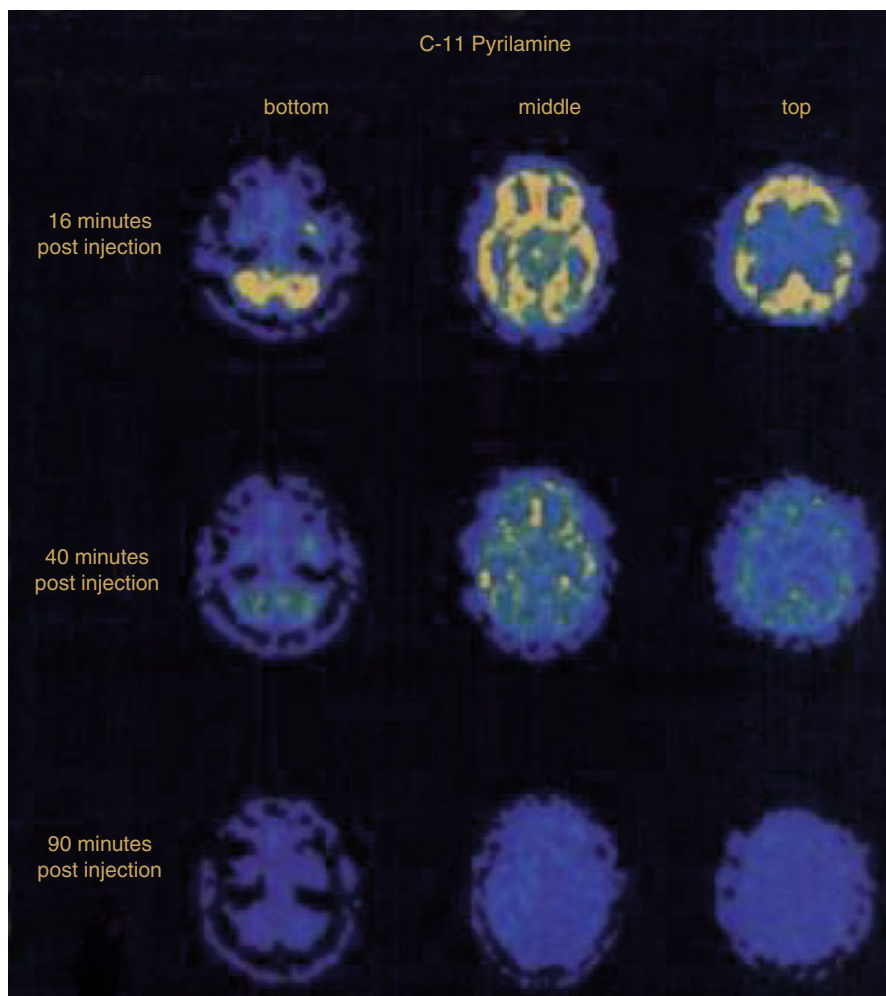


Fig. 13.8 Transversal PET images from a [^{11}C]pyrilamine study in healthy human brain at 16 min (*top*), 40 min (*middle*) and 90 min (*bottom*) p.i. of the radioligand, the latter including the administration of 0.7 mg/kg diphenhydramine at 45 min p.i. Reprinted by permission of SNMMI from Villemagne et al. 1991, Figure 5

In human brain (Fig. 13.8), peak uptake of [^{11}C]pyrilamine occurred somewhat earlier with around 3 %ID/L at 10–15 min p.i. in frontal cortex and cerebellum, and with a more rapid dissociation than in baboon. The displacement with 0.7 mg/kg of diphenhydramine (administered at 45 min p.i.) caused a slightly increased clearance of the radioligand, most notably in frontal cortex (around 1.5 %ID/L at 70 min p.i.) but also in cerebellum.

More conclusive results were obtained in a study in healthy male volunteers (Yanai et al. 1992b). [^{11}C]pyrilamine peak uptake at ~15 min p.i. was highest in

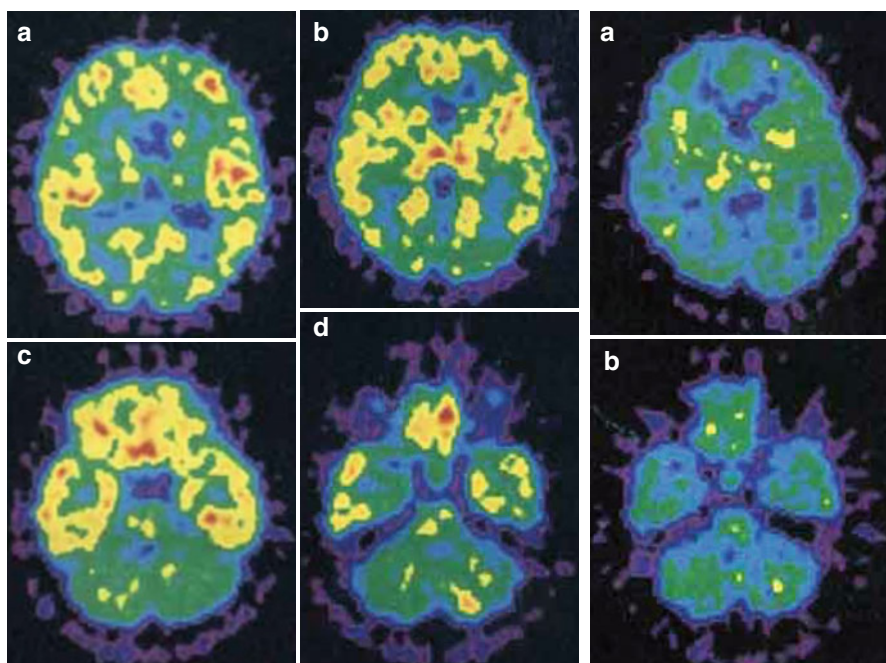


Fig. 13.9 Mapping of H_1R in a healthy human using $[^{11}C]$ pyrilamine. *Left*: transaxial PET images at 30–60 min p.i., with high radioactivity in temporal and frontal cortex, hippocampus and thalamus; localized above the orbitomeatal (*OM*) line at about 55 (a), 48 (b), 18 (c) and 11 (d) mm. *Right*: coronal PET images after administration of *d*-chlorpheniramine at 30–60 min p.i. with marginal reduction of activity in thalamus, striatum and cerebellum; localized above the *OM* line at about 48 (a) and 11 (b) mm. Reprinted by permission of John Wiley & Sons Ltd from Yanai et al. 1992b, Figure 1 and 2

thalamus and frontal as well as temporal cortex (Fig. 13.9, left) with ~ 8 and ~ 7 %ID/L, respectively, and lowest in striatum and cerebellum, both with ~ 6 %ID/L. Preadministered antihistamine *d*-chlorpheniramine (5 mg i.v.) induced increased initial uptake but also radioligand washout in cortices and thalamus (Fig. 13.9, right), which was only significant for the cortical regions (e.g. ~ 5.5 reduced to 4 %ID/L at 45 min p.i.). Investigated in parallel, $[^3H]$ pyrilamine binding on autopsy material revealed highest specific binding in cortex and highest nonspecific binding in thalamus (Yanai et al. 1992a, b).

Metabolite analysis showed strong metabolic degradation of $[^{11}C]$ pyrilamine in arterial plasma up to ~ 90 % at 30 min p.i. (Yanai et al. 1992b). However, based on the low content of $[^3H]$ pyrilamine metabolites in guinea pig brain (~ 8 % of total radioactivity at 60 min p.i.) (Yanai et al. 1990b), it was concluded that radiolabelled metabolites had no effects on $[^{11}C]$ pyrilamine binding results in human brain. Nevertheless, species differences should be taken in account, which were especially apparent in cerebellum. In guinea pig the highest radioligand uptake occurred in the cerebellar region, which was inhibited significantly by the antihistamine triprolidine (Yanai et al. 1990b). In humans, radioligand uptake in cerebellum was lower than in

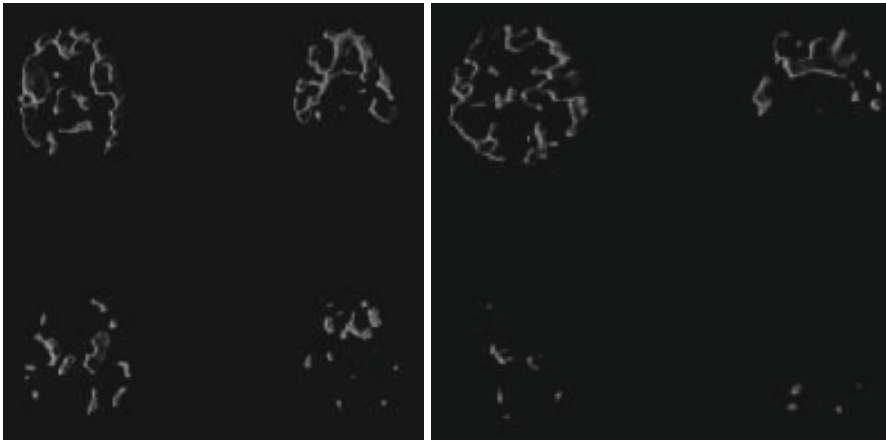


Fig. 13.10 Transaxial PET images obtained at 30–60 min after [^{11}C]pyrilamine (*left*) and 45–90 min after [^{11}C]doxepin injection (*right*) in young (25 and 20 years) and aged (69 and 80 years) subjects. The two images of each volunteer are localized at about 48 and 18 mm above the OM line. Reprinted by permission of Wolters Kluwer Health from Yanai et al. 1992a, Figure 1

other brain regions, and inhibition by *d*-chlorpheniramine was negligible (Yanai et al. 1992b), suggesting higher metabolic degradation of the radioligand or less H_1R expression and specific binding. The latter was in accordance with the lowest specific binding of [^3H]pyrilamine in the cerebellar fractions of human, dog and rat brain homogenates, respectively (Chang et al. 1979; Yanai et al. 1990a, 1992a, b).

The specific binding of [^{11}C]pyrilamine in the cortical regions appeared to be age dependent (Yanai et al. 1992b) and was examined more closely in a separate PET study of age-correlated H_1R binding in normal healthy volunteers (Fig. 13.10) (Yanai et al. 1992a). A decrease of [^{11}C]pyrilamine as well as [^{11}C]doxepin binding in frontal, parietal and temporal cortices about 13 % per decade was shown, implying a loss of H_1R density. This went along with age-dependent, significantly increased levels of histamine metabolites in human cerebrospinal fluid (Prell et al. 1988, 1991), indicating increased histaminergic activity. However, in postmortem human brain investigated, [^3H]pyrilamine affinity showed no significant differences depending on lifetime (Yanai et al. 1992a). This discrepancy was reasoned by possible tissue autolysis of the postmortem materials and a changed microenvironment of the receptors *in vitro*. The [^{11}C]pyrilamine PET study, however, offered the possibility to investigate H_1R density and activity in an intact physiological system.

To evaluate the kinetics of [^{11}C]pyrilamine in the human brain, factor analysis and compartmental modelling were used both under baseline conditions and after H_1R blockade (Szabo et al. 1993). Factor analysis conformed that data could be described by two tissue compartments, although the specific signal was small compared to the non-specific signal, as demonstrated by the blocking studies. In addition, metabolism of [^{11}C]pyrilamine was fast. Already at 20 min p.i., radioactivity in plasma was primarily due to radiolabelled metabolites. Only factor analysis was

able to detect a significant, although small, change between baseline and blocking conditions.

Moreover, data from this study were inserted into an artificial, self-organizing neural network (Resch and Szabo 1994). Within pixel time series, this network was then able to identify and separate receptor-rich from receptor-poor brain regions. It was therefore supposed to be a helpful tool in comparative analysis of multiple datasets, but there are no further applications of this network in the analysis of histaminergic PET imaging reported yet.

Although some specific signal was shown, [^{11}C]pyrilamine appeared to be less suitable for in vivo use than [^{11}C]doxepin. [^{11}C]Pyrilamine was included in only one more recent study, in which brain uptake of eight radioligands in mice was assessed after P-glycoprotein (P-gp) modulation (Ishiwata et al. 2007). Pretreatment with the immunosuppressant and P-gp modulator cyclosporine A (Linnet and Ejsing 2008; Saeki et al. 1993) (50 mg/kg i.v., 30 min prior to [^{11}C]pyrilamine) led to a significant increase in peak uptake in the brain (2.71–4.61 %ID/g at 15 min p.i.), but also in a decrease in brain-to-blood ratio (7.07–3.21 at 15 min p.i.). As an increase of both factors was defined as indication for P-gp modulation, the authors did not conclude [^{11}C]pyrilamine as to be modulated by P-gp (Ishiwata et al. 2007).

Incidentally, a comparative study demonstrated that imaging characteristics of [^{11}C]doxepin were superior over those of [^{11}C]pyrilamine, also in human (Yanai et al. 1992c). In five healthy subjects, both radioligands showed similar uptake patterns (Fig. 13.11, 1 and 2) in distinguished brain regions (cortices, hippocampus, thalamus), but differed in time-activity profiles and contrast. The highest uptake was observed within 45–90 min p.i. for [^{11}C]doxepin with 7.6 %ID/L and within 30–60 min p.i. for [^{11}C]pyrilamine with 4.7 %ID/L at 57.5 min p.i. in frontal cortex. This can be explained by the somewhat higher affinity for human H_1R ($K_i=1.9$ nM) and the better bioavailability of [^{11}C]doxepin (in plasma 60.4 % parent compound, 0.44 %ID/L, 60 min p.i.), as compared with [^{11}C]pyrilamine ($K_i=5.4$ nM; 9.5 % parent compound, 1.3 %ID/L). Nevertheless, also for [^{11}C]doxepin high non-specific binding was shown given the lack of blocking with *d*-chlorpheniramine in cerebellum (cf. Fig. 13.11, block 1 and 3).

Using several mammalian species, the correspondence between animal and human H_1R binding results was investigated (Ishiwata et al. 2004). Uptake expressed as %ID/g, standardized uptake value (SUV) and volume of distribution (V_T) under baseline and blocking conditions (230–3500 nmol/kg, *d*-chlorpheniramine i.v.) were determined in biodistribution (mouse, rat, guinea pig) and PET imaging (rabbit, monkey) experiments and compared with (reanalysed) data from previous studies in human (Yanai et al. 1992c). The fraction of total brain uptake representing H_1R specific binding of [^{11}C]doxepin was 10 % in mouse, 20 % in rat and rabbit, and 30 % in monkey compared with 36 % in human. This specific signal was absent in guinea pig. Besides the low specific binding, time-activity curves in mouse brain showed the highest divergence from the other species with a remarkably faster peak uptake than in human (15 vs. 60 min). As expected, both distribution and kinetics of [^{11}C]doxepin were most similar between monkey and human. The highest uptake

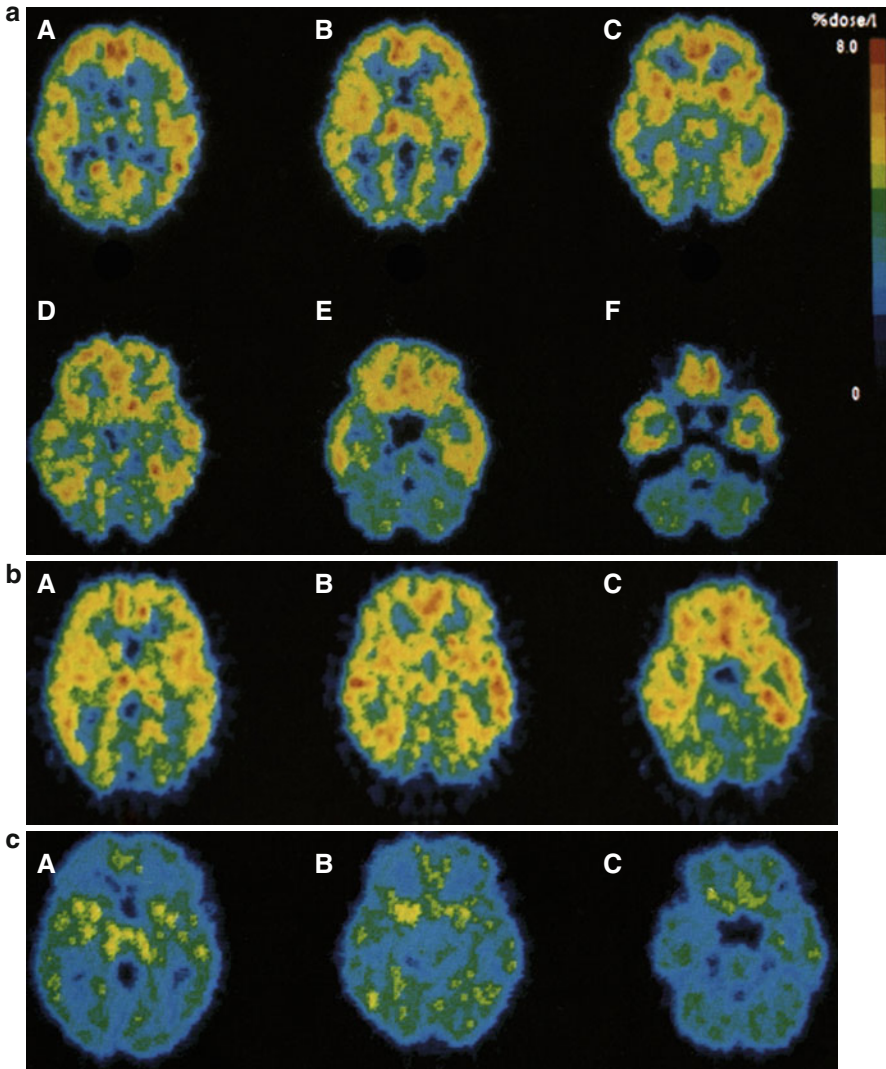


Fig. 13.11 (a) A–F Average transaxial [^{11}C]doxepin images (three healthy volunteers, 45–90 min p.i.). (b) A–C Average transaxial [^{11}C]pyrilamine images (three healthy volunteers, 30–60 min p.i.). (c) A–C Average transaxial [^{11}C]doxepin images after pretreatment with 5 mg *d*-chlorpheniramine i.v. (two healthy volunteers, 45–90 min p.i.). Reprinted by permission of Elsevier Ltd from Yanai et al. 1992c, Figure 1, 2, and 3

was observed in cortical regions, with a frontal cortex V_T of 49 in monkey and 37 in human. In the same brain region, also highest specific binding was detected, shown by reduced V_T values of 33 and ~26, respectively. Furthermore, there was a match in regions with the highest non-specific binding between both species with the lowest [^{11}C]doxepin inhibition in thalamus and cerebellum.

In a comprehensive study, V_T s of [^{11}C]doxepin uptake were determined for 13 brain regions in 12 healthy volunteers (Dogan et al. 2001a), confirming highest H_1R expression in anterior cingulate cortex ($V_T \sim 34.6$) and lowest in cerebellum ($V_T \sim 20.5$). Hence, it was concluded that cerebellum was a suitable reference region for calculating binding potentials.

In another study, the optimal compartmental model for analysing [^{11}C]doxepin kinetics was determined (Mochizuki et al. 2004a). PET scans of healthy volunteers were analysed using both two- and single-tissue compartment models. The latter model provided more stable outcome measures in both receptor-rich (cingulate cortex, tissue mass related $V_T = 37$ mL/g) and receptor-poor (cerebellum, tissue mass related $V_T = 26$ mL/g) brain regions. In addition, a single-tissue compartment model would be compatible with the rapid equilibration between bound and unbound compartment.

Acquiring an arterial plasma input function is cumbersome as it requires measurement of radiolabelled metabolites at several time points. In addition, it is inconvenient for the patient, as arterial sampling is an invasive procedure. In the first instance, a simplified PET protocol was developed, reducing blood collection to a single sample around 10 min after injection of the radioligand (Mochizuki et al. 2004b). Further, in this study [^{11}C]doxepin uptake in plasma input function normalized static PET images showed best correlation with V_T values within 70–90 min p.i. Therefore, PET scan time could be minimized to this timeframe. Next, implementation of Logan graphical analysis (Logan et al. 1996) with cerebellum as reference tissue enabled quantification of [^{11}C]doxepin binding in human brain without arterial blood sampling (Suzuki et al. 2005). Nevertheless, the high level of non-specific binding made it difficult to quantify [^{11}C]doxepin binding in regions with lower H_1R expression (Mochizuki et al. 2004a; Yanai et al. 1992c), and pathological conditions with changes in rCBF and BBB function could make it impossible to use a reference tissue model for [^{11}C]doxepin PET data analysis (Mochizuki et al. 2004b).

First investigations of H_1R expression and function under pathological conditions were performed in patients with Alzheimer's disease (AD), and results were compared with those in young and elderly healthy subjects (Higuchi et al. 2000). In general, analysis using a two-tissue compartment model revealed a diminished binding potential (BP_{ND}) of [^{11}C]doxepin in elderly healthy subjects and AD patients over young volunteers. Significantly, the BP_{ND} of frontal cortex decreased from young ($BP_{ND} \sim 0.4$) and old ($BP_{ND} \sim 0.2$) to mild ($BP_{ND} \sim 0.1$) and advanced AD ($BP_{ND} \sim 0.05$), whilst changes in BP_{ND} of thalamus and striatum showed no significance. Results were similar to those obtained by Logan graphical analysis (Logan et al. 1990) and agreed with values of rCBF ratios, estimated over cerebellum in the same study. rCBF ratios in frontal cortex were significantly diminished in old and AD versus young volunteers (Fig. 13.12), however, to a lower rate than the changes in BP_{ND} s. Further, no changes in rCBF ratios were observed in striatum and thalamus, suggesting that changes in [^{11}C]doxepin binding are mainly based on altered H_1R levels. Altogether this study confirmed not only previous reports of decreased H_1R activity in aged brain (Higuchi et al. 1998; Yanai et al. 1992a, b) but also relevant loss of H_1R expression and/or histaminergic neurons in AD. Therefore, next to PET imaging of acetylcholinesterase and amyloid load, it was actually proposed to

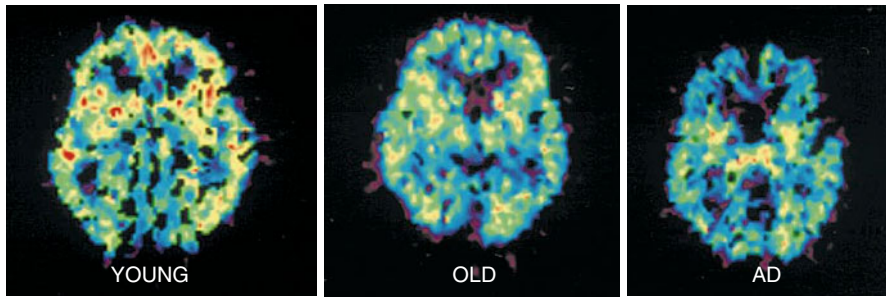


Fig. 13.12 Parametric images of BP_{ND} of [^{11}C]doxepin in young (22 years), old (64 years) and AD (early state with 66 years) subjects, generated using Logan graphical analysis. Reprinted by permission of Elsevier Ltd from Higuchi et al. 2000, Figure 2

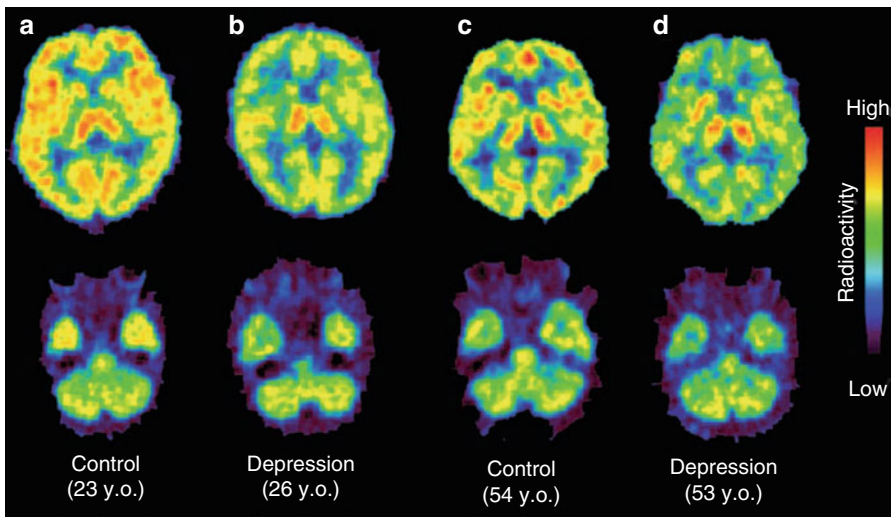


Fig. 13.13 Individual PET images at the thalamic and cerebellar level at 45–90 min after injection of [^{11}C]doxepin in a young healthy (a), a young depressed (b) and a middle-aged healthy (c) as well as a depressed (d) volunteer. Reprinted by permission of John Wiley & Sons Ltd from Kano et al. 2004, Figure 1

include H_1R expression in the procedures for diagnosing AD (Okamura and Yanai 2009; Yanai et al. 2007).

In male patients with major depressive disorder and of varying age (Fig. 13.13), BP_{ND} values of [^{11}C]doxepin significantly decreased in cortical frontal ($BP_{ND} \sim 0.15$) and anterior cingulate ($BP_{ND} \sim 0.25$) areas compared with the same regions in healthy subjects (BP_{ND} around 0.2 and 0.35, respectively) (Kano et al. 2004). In these brain regions, BP values also showed a significant negative correlation with individually rated values on a scale for the severity of depression symptoms (Zung 1965). The latter also included phenomena such as disturbances in sleep behaviour

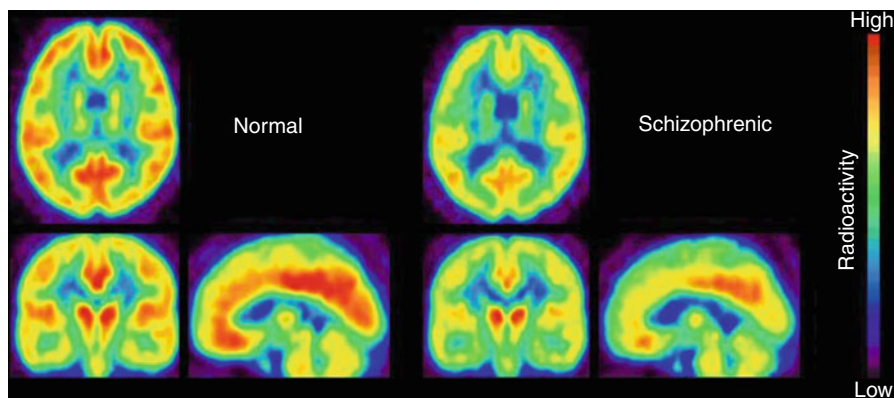


Fig. 13.14 Average transaxial, coronal and sagittal PET images of [^{11}C]doxepin uptake in brains of schizophrenic patients and healthy control subjects, 45–90 min p.i. Reprinted by permission of Elsevier Ltd from Iwabuchi et al. 2005, Figure 1

and attention, attributed to H_1R dysfunction, as mentioned above (see Sect. 13.1), and associated with frontal and anterior cortical brain regions. Although not completely clarifying the underlying pathology (stress-related increase of histamine release or region-specific reduction of H_1R expression), this study confirmed an involvement of altered histaminergic neurotransmission in depression.

In particular frontal cortical areas showed diminished H_1R activity in schizophrenia (Iwabuchi et al. 2003, 2005). In young schizophrenic adults, BP_{ND} of [^{11}C]doxepin was significantly reduced from ~ 0.2 (controls) to ~ 0.1 in prefrontal cortex and from ~ 0.3 (controls) to ~ 0.15 in the cingulate region (Fig. 13.14). This was in accordance with reduced H_1R density in frontal brain areas of schizophrenic patients, determined postmortem. In contrast to the findings in depression (see above), [^{11}C]doxepin images in schizophrenic patients did not correlate with a symptom scale, but the causative pathophysiology could be deduced. In the cerebrospinal fluid of schizophrenic patients, significantly increased levels of N-methylhistamine were found (Prell et al. 1995), whereas an H_1R promoter gene variant appeared without significance (Mancama et al. 2002). Therefore, the downregulated H_1R expression, demonstrated by reduced [^{11}C]doxepin binding in the schizophrenic brain, was supposed to be a response to increased presynaptic histamine release (Iwabuchi et al. 2005).

Significantly higher [^{11}C]doxepin binding was observed in the left lentiform nucleus ($\text{BP}_{\text{ND}} \sim 0.35$) and right amygdala ($\text{BP}_{\text{ND}} \sim 4$) of young female anorexia nervosa (AN) patients (Fig. 13.15), compared with female ($\text{BP}_{\text{ND}} \sim 0.25$ and 0.2 , respectively) as well as male ($\text{BP}_{\text{ND}} \sim 0.25$ and 0.05 , respectively) healthy volunteers (Yoshizawa et al. 2009). Even though there was no compliance with body mass indexes or length of disease, BP_{ND} of [^{11}C]doxepin in thalamus and left amygdala showed a significant negative correlation with results of an eating behaviour inquiring self-report (Garner et al. 1982; Garner and Garfinkel 1979). Despite the strong association of H_1R activity and nutrition, it remained unclear in this study whether AN is a cause or effect of alterations in histaminergic neurotransmission. Histamine

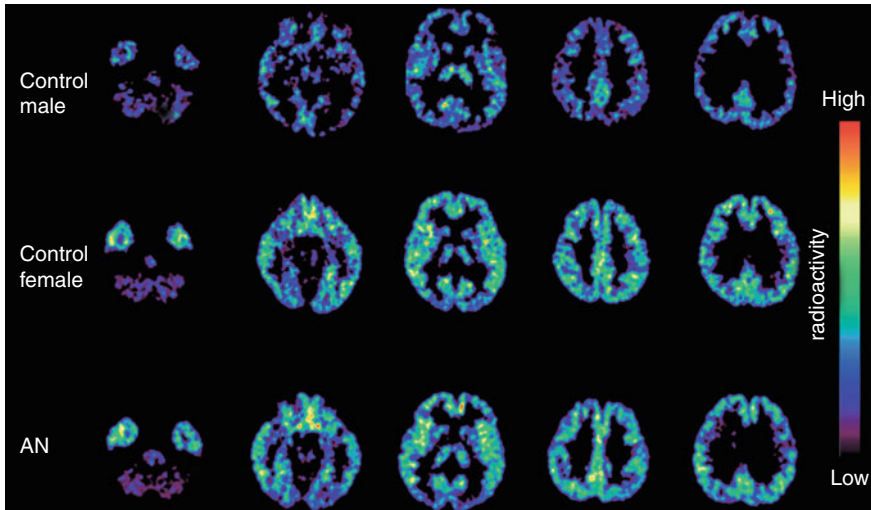


Fig. 13.15 Transaxial PET images of the [^{11}C]doxepin distribution in the brain of control subjects and anorexia nervosa (AN) patients. Reprinted by permission of Elsevier Ltd from Yoshizawa et al. 2009, Figure 1

levels were shown to be significantly increased in, for instance, food-deprived activity stress in rats (Endou et al. 2001), which means forced physical activity under limited food access, and led to a slow, but also significant decrease in H_1R expression. On the other hand, inhibition of histamine metabolism significantly decreased food intake, and a low-protein diet led to upregulated H_1R levels in rats (Mercer et al. 1996). Later results of increased [^{18}F]FDG uptake in H_1R gene knockout mice (Wang et al. 2010), however, revealed a causative role of decreased H_1R expression in the development of obesity (see Sect. 13.1) and would support the concept that AN can result from increased H_1R density.

This study also revealed significant gender differences in H_1R expression (Fig. 13.15) in accordance with results of other [^{11}C]doxepin PET studies in humans (Kato et al. 2009; Yanai et al. 2011a). Analysis of data from healthy female volunteers resulted in BP_{ND} values of ~ 0.4 in cortical regions, 0.2 in amygdala and 0.2 in hippocampus, in comparison with ~ 0.3 , 0.1 and 0.1, respectively, in healthy men (Yoshizawa et al. 2009). These differences coincided with significantly higher levels of histamine metabolites in female cerebrospinal fluid (Prell et al. 1991) and emphasized that a higher incidence of eating disorders in women compared with men (Pawluck and Gorey 1998; Smink et al. 2012) is not exclusively the result of social and psychological factors.

Moreover, attempts to assess the role of H_1R in attentive waking and circadian rhythm were performed using [^{11}C]doxepin PET (Shibuya et al. 2012). Healthy male volunteers showed slightly decreased BP_{ND} values in the morning than in the afternoon (e.g. $BP_{ND} \sim 0.55$ and ~ 0.45 , respectively, in anterior cingulate gyrus). During calculation tasks, BP_{ND} decreased as well, e.g. from ~ 0.6 (resting state)

to ~0.55 (attentive state), in posterior cingulate gyrus. However, this reduction in [¹¹C]doxepin binding was not observed in all cortical brain regions investigated. Consequently, involvement of H₁R activity in alertness and cognition could not be established. This lack of involvement also follows from the delayed response of H₁R to stress-related histamine release, pointing to the more rapidly downregulated H₃R (Endou et al. 2001) as a better target for imaging altered histaminergic neurotransmission (see section 5). Nevertheless, the results demonstrated the good reproducibility of [¹¹C]doxepin PET studies.

The majority of [¹¹C]doxepin investigations, however, were performed to examine potential cognitive side effects of antihistamines, such as affected attention and psychomotor skills (Van Ruitenbeek et al. 2010; Theunissen et al. 2006). As a parameter, receptor occupancy (RO) (Gillman et al. 2009) in human brain following administration of antihistamines was determined. Several antihistamines were evaluated, also taking in account effects of dose and long-term administration (Buczyłko 2009; Dogan et al. 2001b; Tagawa et al. 2001; Tashiro et al. 2006; Yanai et al. 1995a, b, 2008, 2011a). Combination of these studies with investigations of sleepiness and cognitive performance (Kubo et al. 2011; Okamura et al. 2000; Senda et al. 2009; Tashiro et al. 2002a, b, 2004, 2008a, 2009; Yanai et al. 1999; Zhang et al. 2010) and comparison with other effects of antihistamines, such as rCBF (Mochizuki et al. 2002; Okamura et al. 2000; Tashiro et al. 2008c) (see Sect. 13.1), provided the means to correlate RO with neurological effects and/or subjective perception. To give an example, oral administration of the first-generation antihistamine diphenhydramine (30 mg, 120–180 min prior to [¹¹C]doxepin) caused significant subjective sleepiness compared with the second-generation antihistamine bepotastine (10 mg) or placebo (lactobacteria preparation, 6 mg) in healthy humans (Tashiro et al. 2008a; Yanai et al. 2011b). At the same time, cortical H₁R RO (BP_{ND} in Fig. 13.16) was significantly lower for bepotastine (14.7 %) than for diphenhydramine (56.4 %). These values also correlated significantly with drug plasma concentrations, 71.0 and 16.3 ng/mL at 120 min after administration, demonstrating low blood–brain barrier (BBB) permeability for bepotastine and high brain uptake of diphenhydramine, respectively (Tashiro et al. 2008a).

In general, PET results were in line with those reflecting individual perception (Izumi et al. 2008b), although the relationship between RO by an antihistamine and a sedative effect was not significant in all cases (Izumi et al. 2008b; Senda et al. 2009; Tashiro et al. 2002a, 2004, 2009; Yanai et al. 1999; Zhang et al. 2010). One possible explanation could be individual differences in subjective notion (Tashiro et al. 2009; Yanai et al. 1999). In addition, a dependency on type of disease, treated with an antihistamine, was discovered (Izumi et al. 2008a), and several studies also reported mild stimulating effects on attention and task performance by some H₁R antagonists (Theunissen et al. 2006). It should also be noted that PET measurements of RO cannot discriminate between occupancy by parent compounds and that by pharmacologically active metabolites (Gillman et al. 2009).

Nonetheless, based on the results of these comprehensive PET studies, a classification of antihistamines in sedative (RO of H₁R >50 %, high BBB permeability), less sedative (RO of 20–50 %, BBB permeability moderate) and non-sedative (RO <20 %, low BBB permeable) was proposed (Yanai et al. 2011b). Despite the

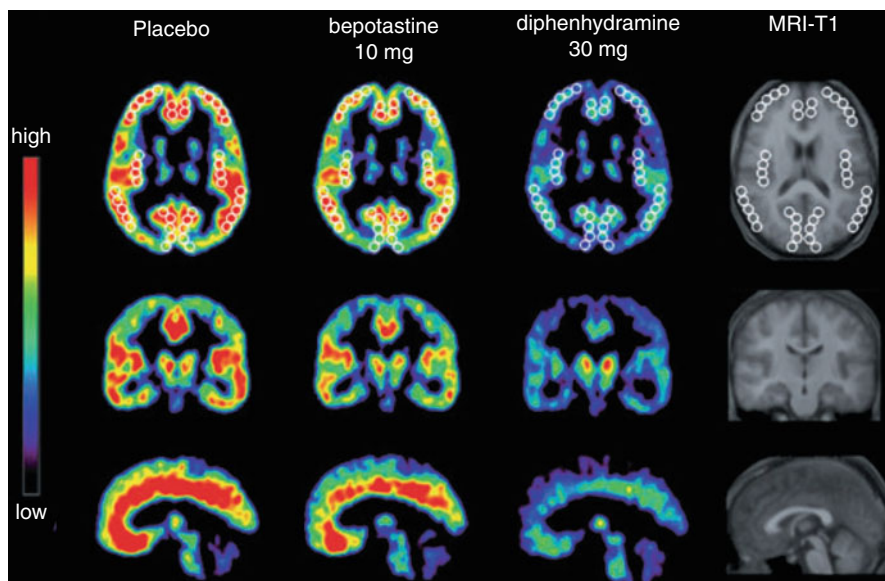


Fig. 13.16 Transaxial (*top*), coronal (*middle*) and sagittal (*bottom*) images of mean BP_{NDs} of [^{11}C]doxepin in the human brain of healthy male subjects ($n=8$), about 160 min after oral administrations of placebo or an antihistamine. *White circles* in the transaxial images indicate ROIs, used for quantitative analysis in the corresponding study. Reprinted by permission of John Wiley & Sons Ltd from Tashiro et al. 2008a, Figure 2

existence of several caveats, antihistamine evaluation based on quantification of H_1R occupancy supports the idea that PET can play an important role in drug development and safety evaluation of new pharmaceuticals (Wong and Pomper 2003).

13.4 Imaging of the Histamine H_2 Receptor

Via its $G\alpha_s$ protein, H_2R stimulates adenylyl cyclase to cAMP production and hence activation of cationic channels, such as I_h , I_{AHP} and $Kv3.2$. It is involved in the accommodation (or adjustment) of neural action potentials and cell proliferation, for example in brain development (Molina-Hernández et al. 2012). Despite its proven excitatory and proliferative function, over the years H_2R has turned out to be a challenge for brain mapping. H_2R is widely distributed across all brain regions, often co-expressed with H_1R (Martinez-Mir et al. 1990). This conflicts with the prevalently deficient subtype selectivity of H_2R targeting ligands (Bongers et al. 2010; Hill et al. 1997). In addition, most H_2R ligands are polar compounds and as such exhibit limited BBB permeability, and radiolabelling of the compounds of interest is cumbersome (Crouzel 1990; Hill et al. 1997).

Nevertheless, one carbon-11-labelled ligand has been synthesized and evaluated *in vivo* in mice (Yanai et al. 1994). The H_2R antagonist [^{11}C]nizatidine (Fig. 13.5) was synthesized via conversion of its *N*-desmethyl-precursor with [^{11}C]CH₃I.

Unfortunately, this radioligand did not show sufficient uptake in the brain. Instead, it was proposed to use it for imaging H₂R in peripheral tissues, but no reports are available yet.

In the periphery H₂R is supposed to be involved in smooth muscle relaxation, such as in cardiovascular, airway and gastric systems, and in gastric acid secretion (Hill et al. 1997; Parsons and Ganellin 2006). Nevertheless, only one attempt to image peripheral H₂R has been reported using indirect SPECT imaging with [^{99m}Tc] pertechnetate and an [¹¹¹In]indium-diethylenetriaminepentaacetic acid-containing liquid meal to investigate effects of the H₂R antagonist ranitidine on gastric motor function (Madsen and Graff 2008). In healthy male volunteers, injection of a 50 mg bolus of ranitidine caused neither a change of gastric volume nor gastric emptying before, during and after administration of the meal. This result is comparable with clinical studies of dyspepsia treatment, where H₂R antagonism not necessarily had a significant effect over treatment with placebo (Bytzer 2002). It demonstrates the difficulty in correlating a specific physiological function with a single receptor, in this case H₂R.

13.5 Imaging of the Histamine H₃ Receptor

In the past two decades, numerous compounds have been developed for targeting H₃R (Leurs et al. 2005; Stark et al. 2004; Tiligada et al. 2011). Amongst them, the imidazole-based H₃R antagonist thioperamide binds to human H₃R with a K_i of 7.14 nM (Esbenshade et al. 2003) and a pK_i of 7.3 (Lim et al. 2005), and is considered to be the classical H₃R antagonist. Its carbimidothioate analogue *S*-[¹¹C]methylthioperamide (Fig. 13.5) was the first H₃R targeting PET ligand to be synthesized and evaluated in mice (Yanai et al. 1994). This radioligand was prepared by *S*-[¹¹C]methylation using an automated synthesis method (Iwata et al. 1992). With low uptake in mouse brain, however, *S*-[¹¹C]methylthioperamide was shown to be inappropriate for cerebral imaging in vivo.

Deriving from potent lead compounds, various tritiated and radioiodinated compounds have been developed for pharmacological H₃R studies. Nevertheless, developing PET tracers with sufficient brain penetration and specific binding remained difficult for many years (Windhorst et al. 1998). Several miscellaneous radioligands have been evaluated as unsuitable for brain PET, such as the imidazolylbenzophenone [¹⁸F]FUB 272 (Fig. 13.5), the first reported fluorine-18-labelled H₃R ligand (Ponchant et al. 1997). Radiosynthesis was based on nucleophilic aromatic substitution (S_NAr) of the corresponding nitro precursor, yielding 65 % of [¹⁸F]FUB 272 with a specific activity of 70.3 GBq/μmol. In rat brain, uptake of [¹⁸F]FUB 272 appeared very low, i.e. ≤0.7 %ID/g, with a homogeneous distribution. Uptake in cerebellum indicated nonspecific binding or presence of radiolabelled metabolites in the brain. Comparable results were obtained for the carbon-11-labelled methylthio-phenoxy analogue [¹¹C]UCL 1829 (Ponchant et al. 1997). Synthesized via *S*-[¹¹C]methylation using [¹¹C]CH₃I, this radioligand could be produced with a specific activity of 35 GBq/μmol. Also in this case, however, biodistribution experiments in rats resulted in low and homogenous brain uptake.

Analogues of *S*-[¹¹C]methylthioperamide, such as fluorine-18-labelled thioperamide derivatives, were developed and investigated *in vivo*. [¹⁸F]VUF 5000 and [¹⁸F]VUF 5182 (Fig. 13.5) were synthesized in multistep radiosyntheses, starting from *cis*-4-[¹⁸F]fluoromethylcyclohexylamine as radiolabelled synthon (Windhorst et al. 1999a, c). In a total synthesis time of 3.5–4 h, these radioligands were obtained in RCYs of 23 and 12 %, respectively, and with RCPs >99 %. Specific activity for [¹⁸F]VUF 5000 was determined with >95 GBq/μmol (Windhorst et al. 1999c). A K_i value of 2.3 nM for the inhibition of rat H₃R and high selectivity of VUF 5000 over various other targets, a $\log D_{7,2}$ of 1.88, and fast blood clearance of [¹⁸F]VUF 5000 in rats pointed to good imaging properties (Windhorst et al. 1999a). Nevertheless, both radioligands showed very low uptake in rat brain of ~0.01 %ID/g at 30 min p.i.

With [¹⁸F]fluoroproxyfan (Fig. 13.5) another imidazole-based PET ligand was investigated. In a multistep radiosynthesis, starting with radiofluorination of benzaldehyde and a synthesis time of less than 100 min, this radioligand was prepared in an RCY of ~10 %, a specific activity ≥ 150 GBq/μmol and an RCP >99 % (Funaki et al. 2007; Iwata et al. 2000). After *i.v.* injection in rats, [¹⁸F]fluoroproxyfan distributed heterogeneously in rat brain. The highest uptake was observed in hypothalamus (ratio to cerebellum of 1.9 at 60 min p.i.). In blocking studies, radioligand binding decreased with an increasing dose of nonradioactive compound, resulting in a reduced hypothalamus to cerebellum ratio from 1.6 to 1.0 at 30 min p.i. after pre-administration of 0.5 mg/kg fluoroproxyfan p.i. However, cortex to cerebellum ratios did not change (Funaki et al. 2007). As 94 % of the brain activity at 30 min p.i. was represented by parent compound, interaction of [¹⁸F]fluoroproxyfan with binding sites unrelated to H₃R was indicated. This was in accordance with the results of a SPECT study using structurally related [¹²³I]iodoproxyfan (Windhorst et al. 1999b), where binding was not inhibited by pretreatment with [*R*]- α -methylhistamine (see below).

Non-imidazole-based H₃R antagonists turned to be more promising clinical candidate pharmaceuticals (Leurs et al. 2005; Zhang et al. 2005), as in general they possess higher target selectivity and less drug-drug interactions. The benzylmorpholine [¹¹C]JNJ-10181457 (Fig. 13.5) was the first reported non-imidazole-based radioligand (Airaksinen et al. 2006). Its nonradioactive analogue was identified as a highly potent ($K_i=0.8$ nM, human) and selective (Apodaca et al. 2003) H₃R antagonist, and the moderate lipophilicity ($\log D_{7,4}=1.54$) indicated sufficient uptake via the BBB. The multistep radiosynthesis of [¹¹C]JNJ-10181457 was carried out in a one-pot procedure, starting with [¹¹C]carboxylation of an *in situ* generated phenyllithium precursor and providing radioligand in 67 min with an RCY of ≥ 20 %, an RCP >99 % and a specific activity ≥ 30 GBq/μmol (Airaksinen et al. 2006). This radioligand showed sufficient accumulation in rat brain with up to 1.7 %ID/g in cerebral cortex and 1.4 %ID/g in hippocampus, whilst the lowest uptake was observed in cerebellum with 0.8 %ID/g at 30 min p.i. Unfortunately, uptake could not be significantly inhibited, neither by pre-administration of nonradioactive compound nor by the H₃R antagonist JNJ-5207852 (10 mg/kg *i.p.*). With around 13 %ID/g in the cerebral cortex at 30 min p.i., uptake of [¹¹C]JNJ-10181457 was remarkably high in H₃R gene knockout mice. These results, on the one hand, pointed

to a high level of non-specific binding. On the other hand, they correlate well with results of investigations of H₃R involvement in neuroinflammatory diseases, where H₃R and H₃H₄R gene knockout mice demonstrated increased BBB permeability (Saligrama et al. 2012; Teuscher et al. 2007).

As the only radioligand succeeding in H₃R imaging in humans, most progress has been made with the benzoazepane [¹¹C]GSK189254 (Fig. 13.5). The H₃R antagonist GSK189254 showed high affinity for human H₃R with a pK_i of 9.59 and a >10,000-fold selectivity over other histamine receptor subtypes (Medhurst et al. 2007). Synthesis of the radiotracer was achieved by [¹¹C]methylation of the corresponding desmethyl-amide. Starting from [¹¹C]CH₃I, [¹¹C]GSK189254 could be produced with an RCY of up to 80 % (Plisson et al. 2009), an RCP >99 %, a specific activity of 50–500 GBq/μmol (Jucaite et al. 2013; Plisson et al. 2006, 2009) and up to 20 % uncorrected RCY in a total synthesis time of 27 min (Ashworth et al. 2010). A second approach by means of [¹¹C]CH₃OTf resulted in a maximum RCY of 60 % (based on [¹¹C]CO₂) and a specific activity of up to 740 GBq/μmol at EOB in a total synthesis time of 40 min (Wang et al. 2012). Good BBB permeability of [¹¹C]GSK189254, indicated by a log*D*_{7.4} of 1.74 (Plisson et al. 2009) and log*P* of 2.24 (Wang et al. 2012), led to high brain uptake in first PET experiments in porcine (Fig. 13.17). With 9.0 %ID/L at 20 min p.i. (Plisson et al. 2009), the radiotracer showed the highest accumulation in known H₃R-rich regions such as striatum and cortices (Fig. 13.17b). Resulting ratios of striatum and frontal cortex over cerebellum were 4.7 and 2.9 at 85 min p.i., respectively (Plisson et al. 2006).

Investigation of metabolism in plasma samples showed degradation of [¹¹C]GSK189254 up to 58 % at 30 min p.i. Radiolabelled metabolites, however, did not affect imaging results in pig brain, as radioligand binding was inhibited in a dose-dependent manner by both co-administration of the H₃R inverse agonist/antagonist ciproxifan (Fig. 13.17c–f) and of GSK189254 (0.08–50 μg/kg). The latter experiment enabled in vivo determination of [¹¹C]GSK189254 affinity for pig H₃R with a K_d of 0.1 nM. H₃R expression levels were determined with B_{max} values of 2.65 in striatum and 2.05 nM in cortex (Plisson et al. 2009). The resulting bound-to-free radioligand ratio of B_{max}/K_d ≥ 10 pointed to high suitability for determining H₃R alterations using [¹¹C]GSK189254 (Eckelman 1998).

High metabolic stability was observed in humans with ~86 % of parent radioligand present at 75 min p.i. (Ashworth et al. 2010). [¹¹C]GSK189254 rapidly entered the brain and distributed heterogeneously (Fig. 13.18, top). The highest uptake was measured in caudate with a total V_T of around 95, which was displaced with 50 μg of non-labelled GSK189254 p.o. (Fig. 13.18, middle; 4 h prior to radioligand) to a V_T ~22. Cerebellar uptake, however, with a V_T ~22, was diminished less conspicuous to a V_T of ~11. The resulting lack of a reference region to determine RO values could be overcome by application of the Lassen plot (Cunningham et al. 2010; Lassen et al. 1995; Lassen 1992).

[¹¹C]GSK189254 showed minor washout in regional time-activity curves and a significantly diminished partition between tissue and plasma in the second scans of test-retest studies (e.g. in putamen from V_T of 120–68, Δt 2 h). Therefore, an alternative reversible two-tissue compartment model was applied, taking account of

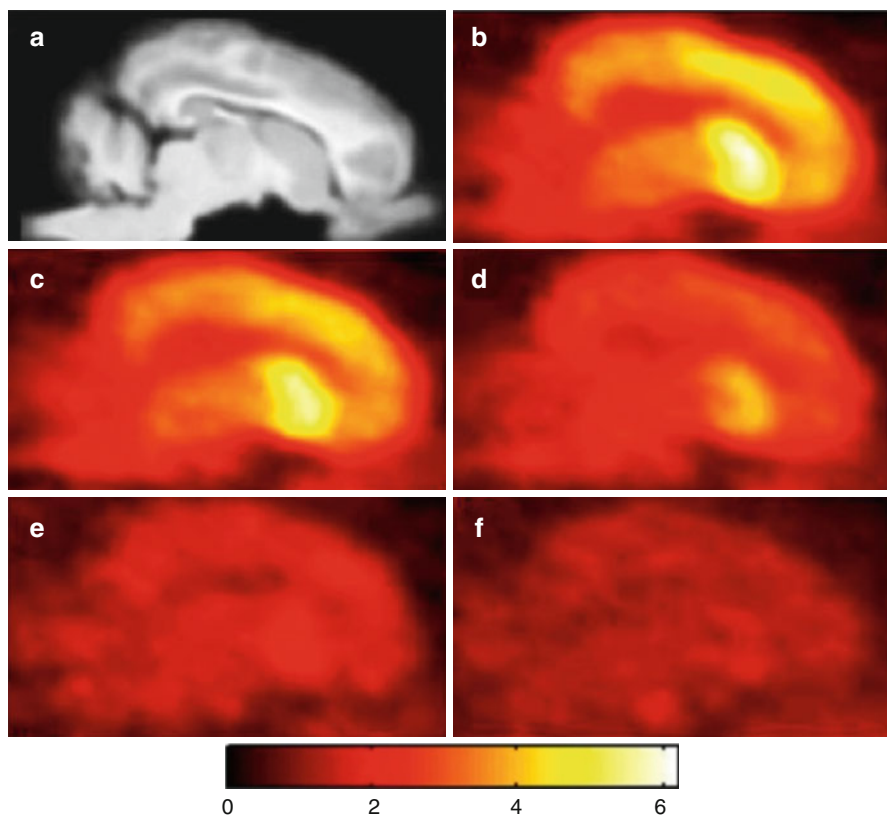


Fig. 13.17 Summed (0–90 min p.i.) sagittal porcine brain images after administration of $[^{11}\text{C}]\text{GSK189254}$. (a) Aligned MR image. (b) Baseline PET scan. (c) + 0.006 mg/kg ciproxifan. (d) + 0.06 mg/kg ciproxifan. (e) + 0.6 mg/kg ciproxifan. (f) + 2.0 mg/kg ciproxifan. Reprinted by permission of SNMMI from Plisson et al. 2009, Figure 3

GSK189254 carryover from the first to the second scan (Ashworth et al. 2010; Slifstein 2010). In the same study, an affinity (K_d) for human H_3R of 0.01 nM and a B_{max} in putamen of 3.8 nM were determined. Subsequently, it was demonstrated that the injected dose of $[^{11}\text{C}]\text{GSK189254}$ led to an estimated H_3R occupancy of >5 %, which exceeds tracer conditions. Hence, $[^{11}\text{C}]\text{GSK189254}$ PET studies require high specific activity in order to limit the administered dose of GSK189254 to 0.003 $\mu\text{g}/\text{mg}$. Alternatively, studies should take into account mass dose effects when analysing data (Ashworth et al. 2010), especially for the determination of RO by other H_3R targeting compounds.

This was considered in a $[^{11}\text{C}]\text{GSK189254}$ PET study of RO by an H_3R antagonist in baboon (Logan et al. 2012). Radioligand accumulation was corrected for radiometabolite fractions and tracer mass, and RO was determined using the Lassen plot. Uptake was highest in striatum with a V_T of around 130 (Fig. 13.19, left). The diazepam JNJ-39220675, inhibiting H_3R with a K_i of 1.4 nM (Letavic et al. 2010), blocked around 90 % of $[^{11}\text{C}]\text{GSK189254}$ binding after intravenous and oral

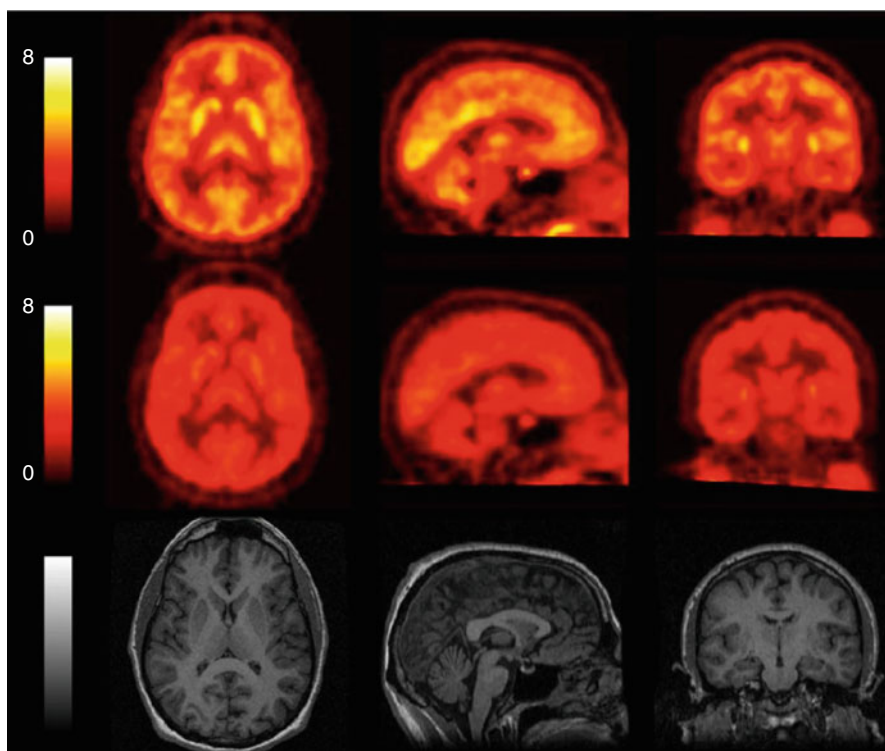


Fig. 13.18 [¹¹C]GSK189254 uptake in a healthy human subject. Mean SUV images (0–90 min) before (*top*) and 4 h after (*middle*) a 50 µg oral dose of GSK189254 are shown together with structural MR images of the same subject (*bottom*). Reprinted by permission of SNMMI from Ashworth et al. 2010, Figure 1

administration of 1 mg/kg (Fig. 13.19, right). Together with results of preclinical studies, showing reduced alcohol preference in abusive rats (Galici et al. 2011), good BBB permeability and stable H₃R blockade by JNJ-39220675 justify further preclinical studies in the treatment of alcoholism (Logan et al. 2012).

In a recently published [¹¹C]GSK189254 PET study in humans, the highly selective H₃R antagonist AZD5213 (undisclosed structure and pharmacological data) was investigated with respect to a dose-dependent effect on circadian rhythm (Jucaite et al. 2013). Taking into account the semi-reversible binding characteristics, means slow dissociation of [¹¹C]GSK189254 (Ashworth et al. 2010), examinations were extended to 120 min. The arterial input function was corrected for dispersion and radiolabelled metabolites. In baseline scans, the highest radioactivity was observed in thalamus. Although known as highly H₃R expressing regions and showing high radioligand accumulation (Fig. 13.20), caudate and putamen were excluded from quantitative analyses, as they did not reach equilibrium.

After administration of single oral doses of 0.05–30 mg of AZD5213, [¹¹C]GSK189254 measurements were undertaken at 2–4 or 24–26 h p.o. and H₃R

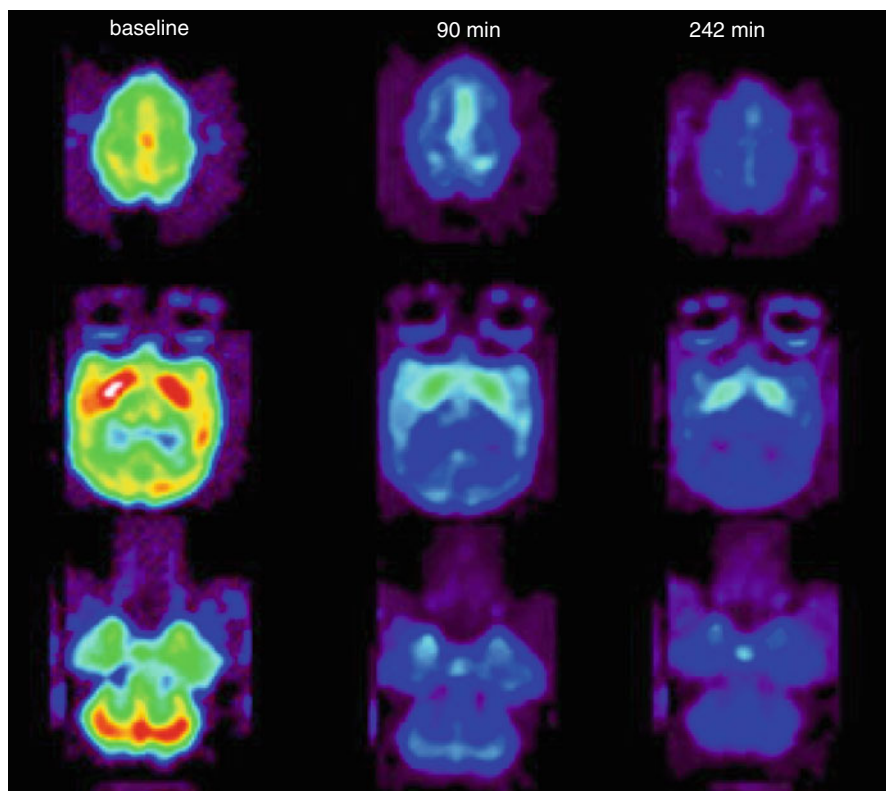


Fig. 13.19 Transaxial [^{11}C]GSK189254 PET images showing the effect of oral administration of JNJ 39220675 (1 mg/kg) in baboon brain at the level of the striatum. Reprinted by permission of Springer Science + Business Media from Logan et al. 2012, Figure 5

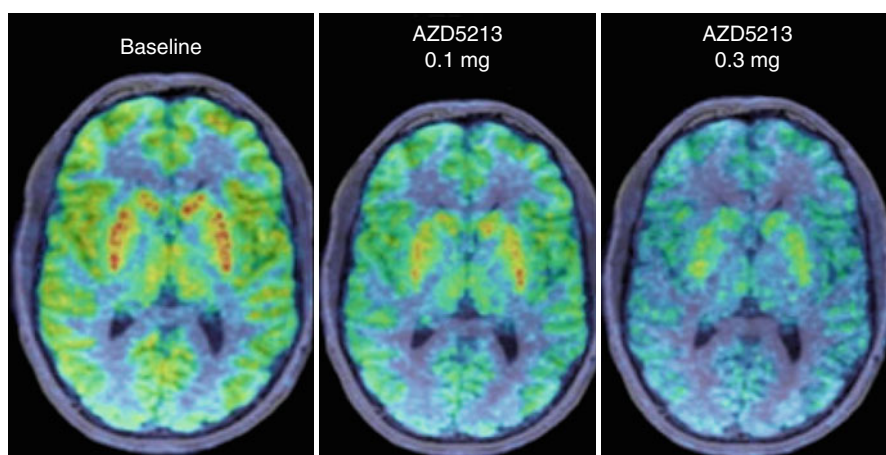


Fig. 13.20 Three summed [^{11}C]GSK189254 PET images (0–120 min p.i.) in one subject, superimposed on corresponding MR images, showing binding to H_3R at baseline and 2–4 h after administration of 0.1 and 0.3 mg AZD5213. Reprinted by permission of Cambridge University Press from Jucaite et al. 2012, Figure 2

ROs estimated by Lassen plot (Lassen et al. 1995; Lassen 1992). The highest RO of about 90 % was observed at 2–4 h with 1–30 mg of AZD5213 and the lowest RO of 16 % at 24–26 h in one subject with 2 mg of AZD5213. For the latter dose, results are debatable, as in the group with 2 mg dosage ROs ranged from 16 to 56 % at 24–26 h p.o. Additionally, the values cross ROs of ~55 % with 0.05 mg and ~40 % with 0.1 mg of AZD5213 at 2–4 h p.o. However, plotting them against each other, H₃R ROs were shown to coincide with the corresponding plasma concentrations of the drug. Further, model-based time courses of ROs in all subjects after receiving a single oral dose of 1–2 mg of AZD5213 showed comparatively high daytime followed by low nighttime RO. Therewith, still maintaining its daytime efficacy, the influence of AZD5213 on the circadian rhythm and the risk of sleep disruption is expected to be low (Jucaite et al. 2013).

Taking together, these studies demonstrated clinical applicability of [¹¹C]GSK189254 PET and showed the feasibility to include measurement of H₃R occupancy in the pharmacological characterization of new H₃R antagonistic drug candidates.

Another approach for PET radioligands has been H₃R inverse agonists based on spiro-isobenzofuranones. Two derivatives were found to be highly potent inhibitors: a 5-methoxy (IC₅₀ of 0.54 nM) (Jitsuoka et al. 2008) and a 5-fluoromethoxy (IC₅₀ of 0.90 nM) (Hamill et al. 2009) derivative. Based on these compounds, a 5-[¹¹C]methoxy and a 5-[¹⁸F]fluorodideuteromethoxy derivative have been synthesized and evaluated in rhesus monkey (Bao et al. 2012), depicted as [¹¹C]Merck 1b and [¹⁸F]Merck 2b, respectively (Fig. 13.5). By alkylation of the corresponding phenolic precursor with [¹¹C]methyl iodide, [¹¹C]Merck 1b was obtained in a non-decay-corrected RCY of up to 37 % with an RCP of more than 98 % and a specific activity of around 150 GBq/μmol. [¹⁸F]Merck 2b was synthesized starting from the same precursor by substitution with [¹⁸F]fluoromethyl bromide-d₂, resulting in ~4 % non-decay-corrected RCY, an RCP >98 % and a specific activity of around 85 GBq/μmol (Hamill et al. 2009).

According to the log*D*_{7,4} of 2.2 for [¹¹C]Merck 1b and 2.1 for [¹⁸F]Merck 2b, combined with their low P-glycoprotein affinity as shown by in vitro transcellular transport ratios of 2.3 and 1.9, both radioligands entered the rhesus monkey brain sufficiently for [¹¹C]Merck 1b (see Fig. 13.21a). The highest uptake was observed in striatum and frontal cortex, which was accompanied by a notably slow washout. Standardized uptake values (SUV) for [¹¹C]Merck 1b occurred somewhat higher, peaking at 30 min with an SUV of ~2.3 in striatal regions, compared to an SUV ~1.2 for [¹⁸F]Merck 2b. The caudate/cerebellum ratio was ~2 for [¹¹C]Merck 1b and ~1.8 for [¹⁸F]Merck 2b at 70 min p.i. Blocking studies with a quinazolinone-based H₃R inverse antagonist (Nagase et al. 2008) caused efficient inhibition for [¹¹C]Merck 1b (see Fig. 13.21b). In caudate, blocked to unblocked uptake ratios of ~5:1 for [¹¹C]Merck 1b and ~4:1 for [¹⁸F]Merck 2b at 70 min p.i. demonstrated low levels of non-specific binding for both radioligands. Furthermore, in the [¹¹C]Merck 1b blockade experiments, the required plasma concentration for the H₃R-inhibiting quinazolinone to achieve 50 % RO was determined to be ~17 nM. Therefore, it was decided that both radioligands investigated could be useful tools for both imaging H₃R and determining potencies of various H₃R inverse antagonists in the brain in vivo.

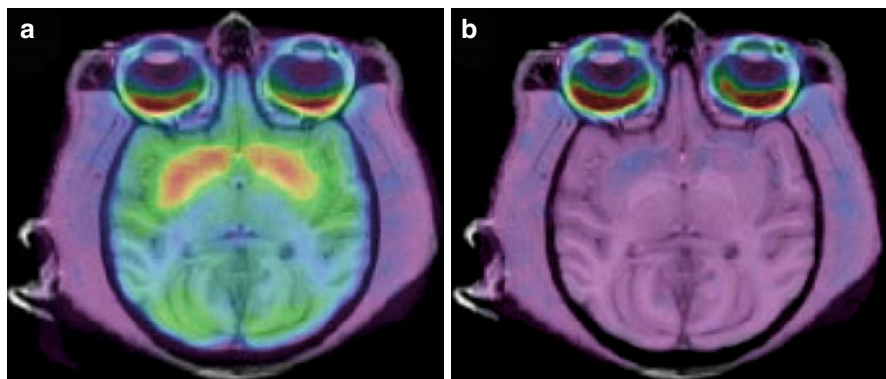


Fig. 13.21 Transaxial, fused MRI/PET images of a rhesus monkey brain after i.v. administration of [^{11}C]Merck 1b. (a) Baseline and (b) blockade with an H_3R inverse antagonist (bolus i.v. 1 h prior to the radioligand, 0.33 mg/kg, 0.16 mg/kg/h). Reprinted by permission of John Wiley & Sons Ltd and Merck Sharp & Dohme Corp. from Hamill et al. 2009, Figure 6

Metabolic degradation in vivo was investigated only for [^{11}C]Merck 1b, showing $\sim 35\%$ parent compound in plasma at 60 min p.i. The role of metabolism of [^{18}F]Merck 2b, however, could be of interest, as for fluoromethylated derivatives increased metabolism has been determined in vitro, thereby potentially reducing radioligand uptake in the brain (Hamill et al. 2009). In addition, lacking a suitable reference region with, e.g. an SUV ~ 0.9 , in cerebellum at 30 min p.i. for [^{11}C]Merck 2b diminished to ~ 0.5 by pretreatment with another H_3R inverse agonist, the Lassen plot (Cunningham et al. 2010) could be useful for data analysis.

A structurally related development was achieved with radiofluorinated 2-aminoethylbenzofuran [^{18}F]XB-1 (Fig. 13.5). The underlying antagonist/inverse agonist was shown to bind to human H_3R with a pK_i of 9.57 (Coward et al. 2005) and a K_i of 1.9 nM (Bao et al. 2012), and to possess a >100 -fold lower affinity for other histamine receptor subtypes as well as various other receptors and transporters. Its radiosynthesis proceeded by [^{18}F]fluoride substitution of the corresponding nitro precursor in a total synthesis time of about 110 min, resulting in an RCY of around 9%, a specific activity of ~ 49 GBq/ μmol and an RCP $>99\%$ (Bao et al. 2012; Xiaofeng et al. 2011). As expected from a $\log D_{7.4}$ of 2.95, [^{18}F]XB-1 showed fast uptake in mice brain (Bao et al. 2012) with a peak SUV of 3.36 at about 6.5 min p.i., which slowly declined to an SUV ~ 2.3 at 90 min p.i. Pretreatment with 1.0 mg/kg i.v. of XB-1 or the nitro-precursor (K_i to human H_3R of 0.4 nM), 30 min prior to [^{18}F]XB-1 injection, increased initial uptake to an SUV >4 at 3.5 min p.i. and caused reduction to an SUV <1.2 at 90 min p.i. The level of non-specific binding of about 50% derived from this study was confirmed by blocking studies with ciproxifan (2.0 mg/kg i.v., 30 min prior PET scan), which diminished [^{18}F]XB-1 levels to an SUV of ~ 1.09 at 90 min p.i. Pretreatment with ciproxifan also caused a decrease in peak uptake in mouse brain to an SUV of ~ 1.98 at 4.5 min p.i., demonstrating the H_3R specific binding of [^{18}F]XB-1.

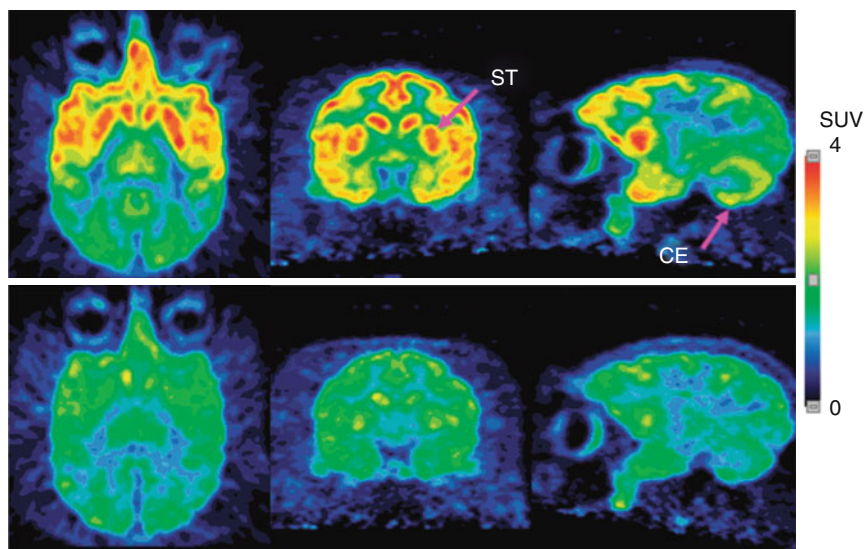


Fig. 13.22 PET images of rhesus monkey brain at the level of the striatum from 0 to 180 min after intravenous injection of [^{18}F]XB-1. *Top*: baseline scan, *bottom*: after treatment with XB-1 (1.0 mg/kg, i.v.). Reprinted by permission of ACS from Bao et al. 2012, Figure 3

Therefore, the radioligand was further evaluated in rhesus monkey (Fig. 13.22) and showed moderately high brain accumulation. Peak uptake was highest in striatum with an SUV of 4.45 at 27.5 min and lowest in cerebellum with an SUV of 2.76 at 31 min. Analysis using a two-tissue compartment model with metabolite-corrected input function in 2 subjects revealed the highest V_T of 64.1 in frontal cortex and the lowest of 28.5 in cerebellum. In striatum and cerebellum, V_T values decreased by 26 % after pretreatment with 2.0 mg/kg i.v. ciproxifan, 30 min prior to [^{18}F]XB-1, and in other brain regions such as frontal cortex by ~33 %. This low inhibition was ascribed to the ~50-fold lower affinity of ciproxifan for human H_3R ($K_i=63$ nM) and a possible underdose. Despite the promising properties of [^{18}F]XB-1, such as sufficient brain uptake and no radiodefluorination in vivo, the lowest blockade of radioligand uptake in the highly H_3R expressing striatum remains unexplained. Further evaluation of this radioligand in displacement studies is recommended.

To date, the most recently published radioligand development for histaminergic PET imaging in the brain is the 4- ^{18}F fluor-piperidine [^{18}F]ST-889 (Fig. 13.5) (Selivanova et al. 2012). This H_3R antagonist possesses high affinity for human H_3R with a K_i of 0.094 nM (Isensee et al. 2009). Via direct radiofluorination of the corresponding mesyl precursor, the radioligand could be obtained in a total synthesis time of around 100 min, RCYs of up to 20 %, an RCP >99 % and with a specific activity ≥ 65 GBq/ μmol (Selivanova et al. 2012). A relatively low lipophilicity with a $\log D_{7.4}$ of ~0.35 and a low passive permeation with a low permeability coefficient (P_{app}) of 1.6 from apical to basal ($P_{\text{app}A \rightarrow B}$) implied low uptake of [^{18}F]ST-889 via

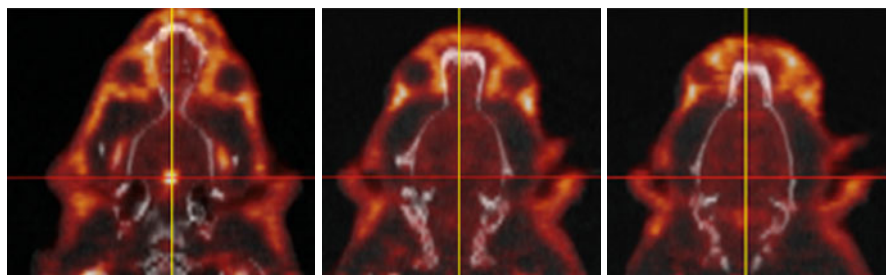


Fig. 13.23 Representative horizontal PET/CT images of rat cranium after i.v. administration of [^{18}F]ST-889, obtained by reconstructing data from 0 to 60 min p.i. (averaged). Yellow colouring in the PET images indicates highest radioactivity concentration. Reprinted by permission of Elsevier Ltd from Selivanova et al. 2012, Figure 6

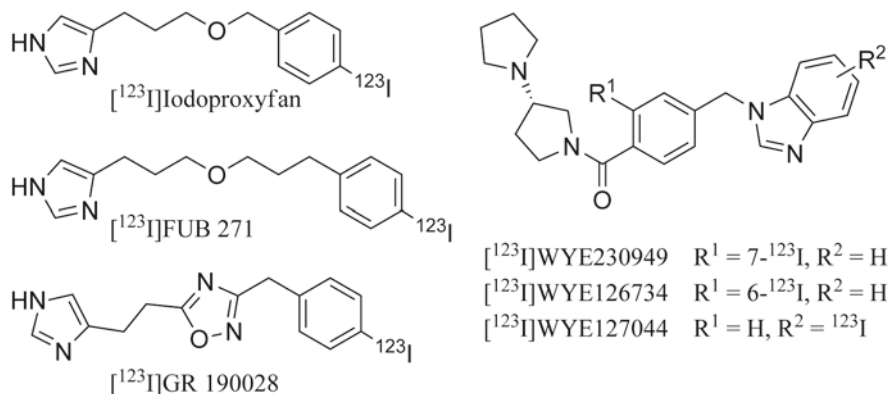


Fig. 13.24 H_3R -specific SPECT ligands

the BBB. But as the radioligand was also shown to be no substrate for P-glycoprotein with a $P_{\text{app}}A \rightarrow B/P_{\text{app}}B \rightarrow A$ ratio of 0.8, no efflux from the brain was expected.

However, PET imaging in rats demonstrated only a negligible level of cortical uptake of [^{18}F]ST-889, accompanied by a remarkably high and persistent glandular accumulation and no significant washout (Fig. 13.23). This was not caused by uptake and binding of radiometabolites, as [^{18}F]ST-889 was shown to be stable in vivo over 30 min. Co-administered H_3R antagonists ST-900 (1 mg/kg i.v.) and ciproxifan (2 mg/kg i.v.) did not inhibit radioligand binding, but rather increased its uptake in some brain regions, indicating that this radioligand is inappropriate for imaging H_3R in the brain.

In contrast to the other histamine receptor subtypes, for imaging H_3R also iodine-123-labelled SPECT ligands have been developed. The first SPECT ligands investigated in vivo were based on imidazole-containing structures: [^{123}I]iodoproxyfan, [^{123}I]FUB 271 and [^{123}I]GR 190028 (Fig. 13.24, left). These very potent and selective antagonists and partial agonists exhibited high affinities at rodent H_3R with pK_i values of 9.0, 8.1 and 8.2, respectively (Clitherow et al. 1996; Stark et al. 1996).

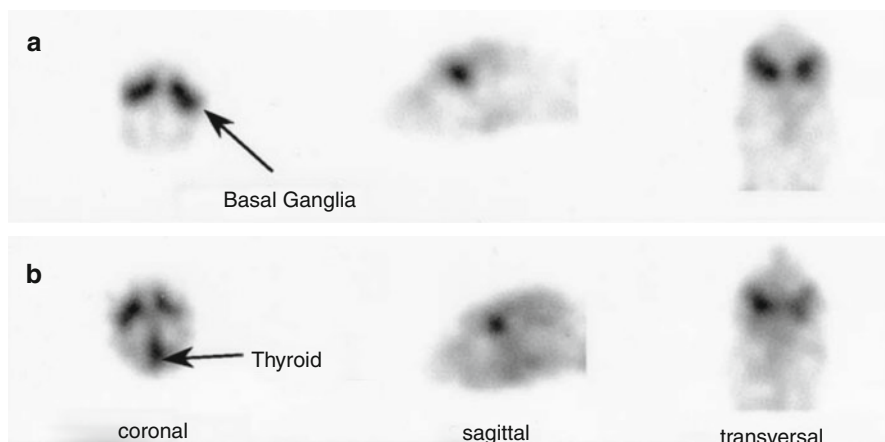


Fig. 13.25 Reconstructed SPECT images of the cerebral distribution of [^{123}I]iodoproxyfan in the rabbit at 10 min p.i.; coronal, sagittal and transversal slices (*left to right*). (a) Without pretreatment. (b) Pretreatment with 15 mg/kg of [R]- α -methylhistamine, 60 min before radioligand application. Thyroid uptake indicates presence of [^{123}I]I $_2$ as metabolite of the baseline scan, which was performed 2 days before the blockade experiment. Reprinted by permission of Elsevier Ltd from Windhorst et al. 1999b, Figure 5

Radiolabelling occurred via isotopic exchange on the corresponding nonradioactive analogues with RCYs of 93, 87 and 46 % and specific activities of >4.4, 5.2 and 1.5 GBq/ μmol , respectively (Windhorst et al. 1999b). The lipophilicity of these radioligands ($\log D_{7.2}$ values of 2.02, 2.37 and 3.12, respectively) suggested sufficient BBB permeability.

Nevertheless, injected in rat i.v., only [^{123}I]iodoproxyfan showed sufficient brain uptake, e.g. with a %ID/g ratio of striatum/cerebellum of 1.86 at 30 min p.i. A subsequent pilot SPECT study in rabbit revealed high uptake of the compound in the basal ganglia (Fig. 13.25a). Unfortunately, pretreatment with i.v. injected 15 mg/kg of [R]- α -methylhistamine (Fig. 13.25b) did not block this uptake and suggested off-target binding. This was confirmed by the inability to block uptake in rats with 25 mg/kg of [R]- α -methylhistamine or thioperamide, injected i.p. 60 min before [^{123}I]iodoproxyfan and resulting, e.g. in striatal uptake of ~ 0.7 %ID/g vs. ~ 0.7 or 0.9 %ID/g, respectively. In the end none of the three radioligands investigated proved to be suitable for in vivo imaging of H $_3$ R in the brain.

More recently the radiosynthesis of three further potential SPECT ligands has been reported. The benzimidazole-based [^{123}I]WYE230949, [^{123}I]WYE126734 and [^{123}I]WYE127044 (Fig. 13.24, right) were radiolabelled via [^{123}I]iododestannylation of the corresponding precursors in incorporation yields >70 % and RCPs of around 80 % (Champion et al. 2011). Detailed results of an evaluation of these radioligands in vivo have not been published yet. However, low brain uptake (0.11 %ID/g) of the iodine-125-labelled analogue [^{125}I]WYE230949 (Lewis et al. 2010) is not a promising feature for neuronal SPECT imaging.

13.6 Imaging of the Histamine H₄ Receptor

The H₄R is the most recently identified histamine receptor subtype (Nijmeijer et al. 2012). Its high clinical potential has encouraged the development of a growing number of high-affinity H₄R compounds (Kiss and Keserű 2012; Marson 2011; Nijmeijer et al. 2012; Smits et al. 2009). These antagonists and agonists provide various leads for radiotracer development, both for carbon-11 and fluorine-18, but less so for iodine-123-labelled compounds. However, at present it is not known whether they are able to cross the BBB, as they were developed for treatment of H₄R effects in the periphery.

To date, two ¹¹C-labelled radioligands were developed and investigated *in vivo* for imaging of H₄R using PET. These ligands are based on the highly potent and H₄R-selective compounds VUF10558 (Smits et al. 2010) ($pK_i=8.35$, human) and JNJ7777120 (Jablonski et al. 2003) ($pK_i=8.4$, human). Both radioligands (Fig. 13.5) were synthesized by *N*-¹¹C-methylation of the piperazinyli moiety, resulting in RCYs of 40 %, RCPs >99 % and specific activities of 20–40 GBq/μmol (Leurs et al. 2008). Whilst [¹¹C]VUF10558 showed no uptake in the brain, [¹¹C]JNJ7777120 did pass the BBB, and further PET studies using this radioligand are warranted.

13.7 Summary and Conclusion

During the century since the discovery and of exploring histamine and its receptors, histaminergic neurotransmission has always been of high interest for therapeutic and diagnostic approaches. In view of their involvement in numerous (patho)physiological processes, it was logical that histamine receptors would also become targets for functional and molecular imaging studies of the brain.

Whilst development of histamine receptor subtype-specific SPECT ligands has been limited to a few H₃R targeting compounds, neuronal PET imaging has been widely used in preclinical and clinical investigations of the histaminergic system. Apart from the quantification of histamine receptor binding, cerebral blood flow ([¹⁵O]H₂O) and metabolism ([¹⁸F]FDG) were measured to investigate functional effects of histamine-regulated neurophysiological processes. Although limited in number, imaging results correlated well with underlying physiological processes, and the resulting information could be useful in interpreting studies with histamine receptor subtype-specific radiotracers.

The latter started with the development of H₁R-specific ligands more than two decades ago. Radiosyntheses and in-depth *in vivo* investigations of two carbon-11-labelled H₁R ligands have been reported, showing unfavourable properties such as high non-specific binding. Nevertheless, PET imaging of H₁R in the human brain has been established successfully using the tricyclic oxepin [¹¹C]doxepin. Apart from determining the role of H₁R in neurological and neuropsychiatric disorders, this radiotracer has also been used to study and assess side effects of new pharmaceuticals. In particular, antihistamines have been evaluated, quantifying H₁R occupancy in the human brain. This can be seen as a typical example of the added value of quantitative molecular imaging in drug development.

So far, the H₂R could not be visualized using PET, neither in CNS nor in peripheral tissues. The only reported H₂R-selective ligand [¹¹C]nizatidine only showed minor accumulation in mouse brain. In contrast, there are numerous reports on the development of radioligands for H₃R. From these investigations some useful compounds emerged, such as ¹¹C- and ¹⁸F-labelled (iso)benzofuran(ones). They showed different amounts of non-specific binding but also apparent H₃R-specific accumulation in the brain of rhesus monkeys. Further studies are planned to verify the suitability of these ligands for clinical studies. Besides that, using the benzoazepane [¹¹C]GSK189254, H₃R could already be quantified in human brain under normal as well as treatment conditions. Therewith the first PET tracer could be provided for extensive investigation of the H₃R in clinical research and drug development.

Reports of PET studies targeting the most recently discovered histamine receptor, H₄R, are still very limited. One carbon-11-labelled compound, the indolylopi-piperazine [¹¹C]JNJ7777120, is currently under investigation *in vivo*. Fortunately, a growing number of high-affinity H₄R compounds provide further leads for potential radioligands. Together with the increased clinical interest in the role of H₄R in the brain, this should encourage development of novel H₄R-selective PET and SPECT tracers.

In summary, histamine receptor subtype-specific imaging by PET is useful for elucidating biochemical and physiological sources of CNS diseases and for determining effects of drugs on neurological functions. Further investigations are expected to provide more insights in the complexity and large number of neurological processes in which histamine receptors are involved.

Acknowledgements The compilation of this literature review was supported by funding from the European Union's Seventh Framework Programme (FP7/2007-2013) under grant agreement n° HEALTH-F2-2011-278850 (INMiND).

References

- Adachi N (2005) Cerebral ischemia and brain histamine. *Brain Res Rev* 50:275–286. doi:[10.1016/j.brainresrev.2005.08.002](https://doi.org/10.1016/j.brainresrev.2005.08.002)
- Airaksinen AJ, Jablonowski JA, van der Mey M et al (2006) Radiosynthesis and biodistribution of a histamine H₃ receptor antagonist 4-[3-(4-piperidin-1-yl-but-1-ynyl)-[¹¹C]benzyl]-morpholine: evaluation of a potential PET ligand. *Nucl Med Biol* 33:801–810. doi:[10.1016/j.nucmedbio.2006.05.008](https://doi.org/10.1016/j.nucmedbio.2006.05.008)
- Alvarez EO (2009) The role of histamine on cognition. *Behav Brain Res* 199:183–189. doi:[10.1016/j.bbr.2008.12.010](https://doi.org/10.1016/j.bbr.2008.12.010)
- Anderson GD (2004) Pharmacogenetics and enzyme induction/inhibition properties of antiepileptic drugs. *Neurology* 63:S3–S8. doi:[10.1212/WNL.63.10_suppl_4.S3](https://doi.org/10.1212/WNL.63.10_suppl_4.S3)
- Apodaca R, Xiao W, Jablonoski JA (2003) Phenylalkynes. WO Patent WO/2003/050099
- Arrang J-M (2007) Histamine and schizophrenia. *Int Rev Neurobiol* 78:247–287. doi:[10.1016/S0074-7742\(06\)78009-6](https://doi.org/10.1016/S0074-7742(06)78009-6)
- Ashworth S, Rabiner EA, Gunn RN et al (2010) Evaluation of ¹¹C-GSK189254 as a novel radioligand for the H₃ receptor in humans using PET. *J Nucl Med* 51:1021–1029. doi:[10.2967/jnumed.109.071753](https://doi.org/10.2967/jnumed.109.071753)

- Bao X, Lu S, Liow J-S et al (2012) Radiosynthesis and evaluation of an ^{18}F -labeled positron emission tomography (PET) radioligand for brain histamine subtype-3 receptors based on a non-imidazole 2-aminoethylbenzofuran chemotype. *J Med Chem* 55:2406–2415. doi:[10.1021/jm201690h](https://doi.org/10.1021/jm201690h)
- Baraniuk JN (2012) Rise of the sensors: nociception and pruritus. *Curr Allergy Asthma Rep* 12:104–114. doi:[10.1007/s11882-012-0245-8](https://doi.org/10.1007/s11882-012-0245-8)
- Barbier AJ, Bradbury MJ (2007) Histaminergic control of sleep-wake cycles: recent therapeutic advances for sleep and wake disorders. *CNS Neurol Disord Drug Targets* 6:31–43. doi:<http://dx.doi.org/10.2174/187152707779940790>
- Barger G, Dale HH (1910) CCLXV.-4- β -Aminoethylglyoxaline (β -Iminazolyethylamine) and the other active principles of Ergot. *J Chem Soc Trans* 97:2592–2595. doi:[10.1039/CT9109702592](https://doi.org/10.1039/CT9109702592)
- Barocelli E, Ballabeni V (2003) Histamine in the control of gastric acid secretion: a topic review. *Pharmacol Res* 47:299–304. doi:[http://dx.doi.org/10.1016/S1043-6618\(03\)00009-4](http://dx.doi.org/10.1016/S1043-6618(03)00009-4)
- Bonaventure P, Letavic M, Dugovic C et al (2007) Histamine H_3 receptor antagonists: from target identification to drug leads. *Biochem Pharmacol* 73:1084–1096. doi:[10.1016/j.bcp.2006.10.031](https://doi.org/10.1016/j.bcp.2006.10.031)
- Bongers G, de Esch I, Leurs R (2010) Molecular pharmacology of the four histamine receptors. *Adv Exp Med Biol* 709:11–19. doi:[10.1007/978-1-4419-8056-4_2](https://doi.org/10.1007/978-1-4419-8056-4_2)
- Buczylko K (2009) Application of antihistamines in ear, nose and throat disorders. *Post Dermatol Alergol XXVI*:382–384
- Bytzer P (2002) H_2 receptor antagonists and prokinetics in dyspepsia: a critical review. *Gut* 50:iv58–iv62. doi:[10.1136/gut.50.suppl_4.iv58](https://doi.org/10.1136/gut.50.suppl_4.iv58)
- Cai H, Mangner TJ, Muzik O et al (2012) Fully automated production of ^{11}C -doxepin for PET imaging histamine H_1 receptor. *Mol Imaging Biol* 14:546–552. doi:[10.1007/s11307-011-0535-x](https://doi.org/10.1007/s11307-011-0535-x)
- Champion S, Gross J, Robichaud AJ, Pimlott S (2011) Radiosynthesis of ^{123}I -labelled benzimidazoles as novel single-photon emission computed tomography tracers for the histamine H_3 receptor. *J Label Compd Radiopharm* 54:674–677. doi:[10.1002/jlcr.1899](https://doi.org/10.1002/jlcr.1899)
- Chang RS, Tran VT, Snyder SH (1979) Heterogeneity of histamine H_1 -receptors: species variations in [^3H]mepyramine binding of brain membranes. *J Neurochem* 32:1653–1663. doi:[10.1111/j.1471-4159.1979.tb02276.x](https://doi.org/10.1111/j.1471-4159.1979.tb02276.x)
- Chazot PL, Hann V, Wilson C et al (2001) Immunological identification of the mammalian H_3 histamine receptor in the mouse brain. *Neuroreport* 12:259–262. doi:<http://ovidsp.tx.ovid.com/sp-3.7.1b/ovidweb.cgi?&S=FPMC/FPOCNDDDLFPCNCPKFBALBNNCBAA00&Abstract=S.sh.18%7c1%7c1>
- Clitherow JW, Beswick P, Irving WJ et al (1996) Novel 1, 2, 4-oxadiazoles as potent and selective histamine H_3 receptor antagonists. *Bioorg Med Chem Lett* 6:833–838. doi:[10.1016/0960-894X\(96\)00122-9](https://doi.org/10.1016/0960-894X(96)00122-9)
- Connelly WM, Shenton FC, Lethbridge N et al (2009) The histamine H_4 receptor is functionally expressed on neurons in the mammalian CNS. *Br J Pharmacol* 157:55–63. doi:[10.1111/j.1476-5381.2009.00227.x](https://doi.org/10.1111/j.1476-5381.2009.00227.x)
- Cowart M, Faghhi R, Curtis MP et al (2005) 4-(2-[2-(2(R)-methylpyrrolidin-1-yl)ethyl]benzofuran-5-yl)benzotrile and related 2-aminoethylbenzofuran H_3 receptor antagonists potently enhance cognition and attention. *J Med Chem* 48:38–55. doi:[10.1021/jm040118g](https://doi.org/10.1021/jm040118g)
- Crouzel C (1990) Positron emitter labeling of ligands for receptor studies. *Acta Radiol Suppl* 374:43–46
- Cunningham VJ, Rabiner EA, Slifstein M et al (2010) Measuring drug occupancy in the absence of a reference region: the Lassen plot re-visited. *J Cereb Blood Flow Metab* 30:46–50. doi:[10.1038/jcbfm.2009.190](https://doi.org/10.1038/jcbfm.2009.190)
- Cusack B, Nelson A, Richelson E (1994) Binding of antidepressants to human brain receptors: focus on newer generation compounds. *Psychopharmacology (Berl)* 114:559–565. doi:[10.1007/BF02244985](https://doi.org/10.1007/BF02244985)
- Dannals RF, Yanai K, Wilson AA et al (1989) Synthesis of radiotracers for studying histamine-1 receptors: carbon-11 labeled doxepin and pyrilamine. *J Label Compd Radiopharm* 26:213–214. doi:[10.1002/jlcr.2580260196](https://doi.org/10.1002/jlcr.2580260196)

- Del Rio R, Noubade R, Saligrama N et al (2012) Histamine H₄ receptor optimizes T regulatory cell frequency and facilitates anti-inflammatory responses within the central nervous system. *J Immunol* 188:541–547. doi:[10.4049/jimmunol.1101498](https://doi.org/10.4049/jimmunol.1101498)
- Deng C, Weston-Green K, Huang X-F (2010) The role of histaminergic H₁ and H₃ receptors in food intake: a mechanism for atypical antipsychotic-induced weight gain? *Prog Neuropsychopharmacol Biol Psychiatry* 34:1–4. doi:[10.1016/j.pnpbp.2009.11.009](https://doi.org/10.1016/j.pnpbp.2009.11.009)
- Dogan AS, Catafau AM, Zhou Y et al (2001a) In vivo histamine H-1 receptor mapping in normal human brain using ¹¹C-doxepin PET. *Eur J Nucl Med Mol Imaging* 28:973. doi:[10.1007/BF02832651](https://doi.org/10.1007/BF02832651)
- Dogan AS, Catafau AM, Zhou Y et al (2001b) In vivo cerebral histamine receptor occupancy of three antihistamine drugs: A ¹¹C-doxepin PET study. *Eur J Nucl Med Mol Imaging* 28:974. doi:[10.1007/BF02832651](https://doi.org/10.1007/BF02832651)
- Duncan JS (1999) Positron emission tomography receptor studies in epilepsy. *Rev Neurol* 155:482–488. doi:[RNE-07-1999-155-6-7-0000-0000-101019-ART58](https://doi.org/10.1016/j.neuro.1999.155.6.7-0000-0000-101019-ART58)
- Dunford PJ, Williams KN, Desai PJ et al (2007) Histamine H₄ receptor antagonists are superior to traditional antihistamines in the attenuation of experimental pruritus. *J Allergy Clin Immunol* 119:176–183. doi:[10.1016/j.jaci.2006.08.034](https://doi.org/10.1016/j.jaci.2006.08.034)
- Eckelman WC (1998) Sensitivity of new radiopharmaceuticals. *Nucl Med Biol* 25:169–173
- Endou M, Yanai K, Sakurai E et al (2001) Food-deprived activity stress decreased the activity of the histaminergic neuron system in rats. *Brain Res* 891:32–41. doi:[http://dx.doi.org/10.1016/S0006-8993\(00\)03226-1](http://dx.doi.org/10.1016/S0006-8993(00)03226-1)
- Esbenshade TA, Krueger KM, Miller TR et al (2003) Two novel and selective nonimidazole histamine H₃ receptor antagonists A-304121 and A-317920: I. In vitro pharmacological effects. *J Pharmacol Exp Ther* 305:887–896. doi:[10.1124/jpet.102.047183](https://doi.org/10.1124/jpet.102.047183)
- Esbenshade TA, Fox GB, Cowart MD (2006) Histamine H₃ receptor antagonists: preclinical promise for treating obesity and cognitive disorders. *Mol Interv* 6:77–88. doi:[10.1124/mi.6.2.5](https://doi.org/10.1124/mi.6.2.5)
- Esbenshade TA, Browman KE, Bitner RS et al (2008) The histamine H₃ receptor: an attractive target for the treatment of cognitive disorders. *Br J Pharmacol* 154:1166–1181. doi:[10.1038/bjp.2008.147](https://doi.org/10.1038/bjp.2008.147)
- Ferreira R, Santos T, Gonçalves J et al (2012) Histamine modulates microglia function. *J Neuroinflammation* 9:90. doi:[10.1186/1742-2094-9-90](https://doi.org/10.1186/1742-2094-9-90)
- Funaki Y, Sato K, Kato M et al (2007) Evaluation of the binding characteristics of [¹⁸F]fluoroproxyfan in the rat brain for in vivo visualization of histamine H₃ receptor. *Nucl Med Biol* 34:981–987. doi:[10.1016/j.nucmedbio.2007.07.012](https://doi.org/10.1016/j.nucmedbio.2007.07.012)
- Galici R, Rezvani AH, Aluisio L et al (2011) JNJ-39220675, a novel selective histamine H₃ receptor antagonist, reduces the abuse-related effects of alcohol in rats. *Psychopharmacology (Berl)* 214:829–841. doi:[10.1007/s00213-010-2092-4](https://doi.org/10.1007/s00213-010-2092-4)
- Garner DM, Garfinkel PE (1979) The eating attitudes test: an index of the symptoms of anorexia nervosa. *Psychol Med* 9:273–279. doi:[10.1017/S0033291700030762](https://doi.org/10.1017/S0033291700030762)
- Garner DM, Olmsted MP, Bohr Y, Garfinkel PE (1982) The eating attitudes test: psychometric features and clinical correlates. *Psychol Med* 12:871–878. doi:[10.1017/S0033291700049163](https://doi.org/10.1017/S0033291700049163)
- Gemkow MJ, Davenport AJ, Harich S et al (2009) The histamine H₃ receptor as a therapeutic drug target for CNS disorders. *Drug Discov Today* 14:509–515. doi:[10.1016/j.drudis.2009.02.011](https://doi.org/10.1016/j.drudis.2009.02.011)
- Gillman S, Gillard M, Strolin Benedetti M (2009) The concept of receptor occupancy to predict clinical efficacy: a comparison of second generation H₁ antihistamines. *Allergy Asthma Proc* 30:366–376. doi:[10.2500/aap.2009.30.3226](https://doi.org/10.2500/aap.2009.30.3226)
- Gomez-Ramirez J, Ortiz J, Blanco I (2002) Presynaptic H₃ autoreceptors modulate histamine synthesis through cAMP pathway. *Mol Pharmacol* 61:239–245. doi:[10.1124/mol.61.1.239](https://doi.org/10.1124/mol.61.1.239)
- Haas HL, Sergeeva OA, Selbach O (2008) Histamine in the nervous system. *Physiol Rev* 88:1183–1241. doi:[10.1152/physrev.00043.2007](https://doi.org/10.1152/physrev.00043.2007)
- Hamill TG, Sato N, Jitsuoka M et al (2009) Inverse agonist histamine H₃ receptor PET tracers labelled with carbon-11 or fluorine-18. *Synapse* 63:1122–1132. doi:[10.1002/syn.20689](https://doi.org/10.1002/syn.20689)
- Higuchi M, Itoh M, Yanai K et al (1998) Chapter 31 – Brain mapping of the effects of aging on histamine H₁ receptors in humans: a PET study with [¹¹C] doxepin. In: Carson RE, Daube-

- Witherspoon ME, Herscovitch P (eds) Quantitative functional brain imaging with positron emission tomography. Academic, San Diego, pp 207–214
- Higuchi M, Yanai K, Okamura N et al (2000) Histamine H₁ receptors in patients with Alzheimer's disease assessed by positron emission tomography. *Neuroscience* 99:721–729. doi:[10.1016/S0306-4522\(00\)00230-X](https://doi.org/10.1016/S0306-4522(00)00230-X)
- Hill SJ, Ganellin CR, Timmerman H et al (1997) International Union of Pharmacology. XIII. Classification of histamine receptors. *Pharmacol Rev* 49:253–278
- Hsieh GC, Chandran P, Salyers AK et al (2010) H₄ receptor antagonism exhibits anti-nociceptive effects in inflammatory and neuropathic pain models in rats. *Pharmacol Biochem Behav* 95:41–50. doi:[10.1016/j.pbb.2009.12.004](https://doi.org/10.1016/j.pbb.2009.12.004)
- Hu W-W, Chen Z (2012) Role of histamine and its receptors in cerebral ischemia. *ACS Chem Neurosci* 3:238–247. doi:[10.1021/cn200126p](https://doi.org/10.1021/cn200126p)
- Innis RB, Cunningham VJ, Delforge J et al (2007) Consensus nomenclature for in vivo imaging of reversibly binding radioligands. *J Cereb Blood Flow Metab* 27:1533–1539. doi:[10.1038/sj.jcbfm.9600493](https://doi.org/10.1038/sj.jcbfm.9600493)
- Isensee K, Amon M, Garlapati A et al (2009) Fluorinated non-imidazole histamine H₃ receptor antagonists. *Bioorg Med Chem Lett* 19:2172–2175. doi:[10.1016/j.bmcl.2009.02.110](https://doi.org/10.1016/j.bmcl.2009.02.110)
- Ishiwata K, Yanai K, Iwata R et al (1996) Analysis of plasma metabolites during human PET studies with three receptor ligands, [¹¹C]YM-09151-2, [¹¹C]doxepin and [¹¹C]pyrilamine. *Tohoku J Exp Med* 178:129–136. doi:[10.1620/tjem.178.129](https://doi.org/10.1620/tjem.178.129)
- Ishiwata K, Kawamura K, Wang W-F et al (2004) Evaluation of in vivo selective binding of [¹¹C]doxepin to histamine H₁ receptors in five animal species. *Nucl Med Biol* 31:493–502. doi:[10.1016/j.nucmedbio.2003.11.005](https://doi.org/10.1016/j.nucmedbio.2003.11.005)
- Ishiwata K, Kawamura K, Yanai K, Hendrikse NH (2007) In vivo evaluation of P-glycoprotein modulation of 8 PET radioligands used clinically. *J Nucl Med* 48:81–87
- Ito C (2004) The role of the central histaminergic system on schizophrenia. *Drug News Perspect* 17:383–387
- Ito C (2009) Histamine H₃-receptor inverse agonists as novel antipsychotics. *Cent Nerv Syst Agents Med Chem* 9:132–136
- Ito C, Morisset S, Krebs MO et al (2000) Histamine H₂ receptor gene variants: lack of association with schizophrenia. *Mol Psychiatry* 5:159–164. doi:[10.1038/sj.mp.4000664](https://doi.org/10.1038/sj.mp.4000664)
- Iwabuchi K, Ito C, Kubota Y et al (2003) Neuroimaging of histamine H₁-receptor in the schizophrenic human brain by positron emission tomography. *Int Clin Psychopharmacol* 18:180. doi:[10.1097/00004850-200305000-00016](https://doi.org/10.1097/00004850-200305000-00016)
- Iwabuchi K, Ito C, Tashiro M et al (2005) Histamine H₁ receptors in schizophrenic patients measured by positron emission tomography. *Eur Neuropsychopharmacol* 15:185–191. doi:[10.1016/j.euroneuro.2004.10.001](https://doi.org/10.1016/j.euroneuro.2004.10.001)
- Iwata R, Hatano K, Yanai K et al (1991) A semi-automated synthesis system for routine preparation of [¹¹C]YM-09151-2 and [¹¹C]pyrilamine from [¹¹C]methyl iodide. *Int J Radiat Appl Instrum Part A* 42:202–205. doi:[10.1016/0883-2889\(91\)90075-C](https://doi.org/10.1016/0883-2889(91)90075-C)
- Iwata R, Pascali C, Yuasa M et al (1992) On-line [¹¹C]methylation using [¹¹C]methyl iodide for the automated preparation of ¹¹C-radiopharmaceuticals. *Int J Radiat Appl Instrum Part A* 43:1083–1088. doi:[10.1016/0883-2889\(92\)90048-J](https://doi.org/10.1016/0883-2889(92)90048-J)
- Iwata R, Horváth G, Pascali C et al (2000) Synthesis of 3-[1H-imidazol-4-yl]propyl 4-[18F]fluorobenzyl ether ([¹⁸F]fluoroproxyfan): a potential radioligand for imaging histamine H₃ receptors. *J Label Compd Radiopharm* 43:873–882. doi:[10.1002/1099-1344\(200008\)43:9<873::AID-JLCR371>3.0.CO;2-A](https://doi.org/10.1002/1099-1344(200008)43:9<873::AID-JLCR371>3.0.CO;2-A)
- Iwata R, Pascali C, Bogani A et al (2002) A combined loop-SPE method for the automated preparation of [¹¹C]doxepin. *J Label Compd Radiopharm* 45:271–280. doi:[10.1002/jlcr.557](https://doi.org/10.1002/jlcr.557)
- Izumi N, Mizuguchi H, Umehara H et al (2008a) Analysis of disease-dependent sedative profiles of H(1)-antihistamines by large-scale surveillance using the visual analog scale. *Methods Find Exp Clin Pharmacol* 30:225–230
- Izumi N, Mizuguchi H, Umehara H et al (2008b) Evaluation of efficacy and sedative profiles of H(1) antihistamines by large-scale surveillance using the visual analogue scale (VAS). *Allergol Int* 57:257–263. doi:[10.2332/allergolint.O-07-525](https://doi.org/10.2332/allergolint.O-07-525)

- Izzo AA, Costa M, Mascolo N, Capasso F (1998) The role of histamine H₁, H₂ and H₃ receptors on enteric ascending synaptic transmission in the guinea pig ileum. *J Pharmacol Exp Ther* 287:952–957
- Jablonowski JA, Grice CA, Chai W et al (2003) The first potent and selective non-imidazole human histamine H₄ receptor antagonists. *J Med Chem* 46:3957–3960. doi:[10.1021/jm0341047](https://doi.org/10.1021/jm0341047)
- Jadidi-Niaragh F, Mirshafiey A (2010) Histamine and histamine receptors in pathogenesis and treatment of multiple sclerosis. *Neuropharmacology* 59:180–189. doi:[10.1016/j.neuropharm.2010.05.005](https://doi.org/10.1016/j.neuropharm.2010.05.005)
- Jitsuoka M, Tsukahara D, Ito S et al (2008) Synthesis and evaluation of a spiro-isobenzofuranone class of histamine H₃ receptor inverse agonists. *Bioorg Med Chem Lett* 18:5101–5106. doi:[10.1016/j.bmcl.2008.07.125](https://doi.org/10.1016/j.bmcl.2008.07.125)
- Jucaite A, Takano A, Boström E et al (2013) AZD5213: a novel histamine H₃ receptor antagonist permitting high daytime and low nocturnal H₃ receptor occupancy, a PET study in human subjects. *Int J Neuropsychopharmacol* 6:1231–1239. doi:[10.1017/S1461145712001411](https://doi.org/10.1017/S1461145712001411)
- Jutel M, Blaser K, Akdis CA (2005) Histamine in allergic inflammation and immune modulation. *Int Arch Allergy Immunol* 137:82–92. doi:[10.1159/000085108](https://doi.org/10.1159/000085108)
- Kanba S, Richelson E (1984) Histamine H₁ receptors in human brain labelled with [³H]doxepin. *Brain Res* 304:1–7. doi:[10.1016/0006-8993\(84\)90856-4](https://doi.org/10.1016/0006-8993(84)90856-4)
- Kano M, Fukudo S, Tashiro A et al (2004) Decreased histamine H₁ receptor binding in the brain of depressed patients. *Eur J Neurosci* 20:803–810. doi:[10.1111/j.1460-9568.2004.03540.x](https://doi.org/10.1111/j.1460-9568.2004.03540.x)
- Karaki H, Ozaki H, Hori M et al (1997) Calcium movements, distribution, and functions in smooth muscle. *Pharmacol Rev* 49:157–230
- Kato M, Tashiro M, Yoshizawa M et al (2009) Gender difference in histamine H₁ receptors in the human brain: a human PET study. *J Pharmacol Sci* 109:281P
- Kettenmann H, Hanisch U-K, Noda M, Verkhratsky A (2011) Physiology of microglia. *Physiol Rev* 91:461–553. doi:[10.1152/physrev.00011.2010](https://doi.org/10.1152/physrev.00011.2010)
- Kim SE, Szabo Z, Seki C et al (1999) Effect of tracer metabolism on PET measurement of [¹¹C]pyrilamine binding to histamine H₁ receptors. *Ann Nucl Med* 13:101–107. doi:[10.1007/BF03164885](https://doi.org/10.1007/BF03164885)
- Kiss R, Keserű GM (2012) Histamine H₄ receptor ligands and their potential therapeutic applications: an update. *Expert Opin Ther Pat* 22:205–221. doi:[10.1517/13543776.2012.665447](https://doi.org/10.1517/13543776.2012.665447)
- Knigge U, Kjaer A, Jørgensen H, Warberg J (1998) H₃ receptor modulation of neuroendocrine responses to histamine and stress. In: Leurs R, Timmerman H (eds) *The histamine H₃ receptor A target for new drugs*. Elsevier, Amsterdam/New York, pp 41–58. doi:[10.1016/S0165-7208\(98\)80024-X](https://doi.org/10.1016/S0165-7208(98)80024-X)
- Kubo N, Senda M, Ohsumi Y et al (2011) Brain histamine H₁ receptor occupancy of loratadine measured by positron emission topography: comparison of H₁ receptor occupancy and proportional impairment ratio. *Hum Psychopharmacol* 26:133–139. doi:[10.1002/hup.1184](https://doi.org/10.1002/hup.1184)
- Lassen NA (1992) Neuroreceptor quantitation in vivo by the steady-state principle using constant infusion or bolus injection of radioactive tracers. *J Cereb Blood Flow Metab* 12:709–716. doi:[10.1038/jcbfm.1992.101](https://doi.org/10.1038/jcbfm.1992.101)
- Lassen NA, Bartenstein PA, Lammertsma AA et al (1995) Benzodiazepine receptor quantification in vivo in humans using [¹¹C]flumazenil and PET: application of the steady-state principle. *J Cereb Blood Flow Metab* 15:152–165. doi:[10.1038/jcbfm.1995.17](https://doi.org/10.1038/jcbfm.1995.17)
- Letavic MA, Aluisio L, Atack JR et al (2010) Pre-clinical characterization of aryloxyppyridine amides as histamine H₃ receptor antagonists: identification of candidates for clinical development. *Bioorg Med Chem Lett* 20:4210–4214. doi:[10.1016/j.bmcl.2010.05.041](https://doi.org/10.1016/j.bmcl.2010.05.041)
- Leurs R, Timmerman H (1998) *The histamine H₃ receptor – a target for new drugs*, vol 30, 1st edn. Elsevier, Amsterdam/New York, pp 1–291
- Leurs R, Bakker RA, Timmerman H, de Esch IJP (2005) The histamine H₃ receptor: from gene cloning to H₃ receptor drugs. *Nat Rev Drug Discov* 4:107–120. doi:[10.1038/nrd1631](https://doi.org/10.1038/nrd1631)
- Leurs R, Smits R, Mooijer M et al (2008) Synthesis and in-vivo evaluation of human histamine H₄ receptor modulators [¹¹C]JNJ777120 and [¹¹C]VUF10558 for monitoring inflammatory processes using PET. EHRs XXXVIIth annual meeting, Stockholm, P26:87

- Leurs R, Chazot PL, Shenton FC et al (2009) Molecular and biochemical pharmacology of the histamine H₄ receptor. *Br J Pharmacol* 157:14–23. doi:[10.1111/j.1476-5381.2009.00250.x](https://doi.org/10.1111/j.1476-5381.2009.00250.x)
- Lewis DY, Champion S, Dewar D et al (2010) Characterisation of novel histamine H₃ receptor tracers for SPECT. *Mol Imaging Biol* 12(S1):S122. doi:[10.1007/s11307-009-0251-y](https://doi.org/10.1007/s11307-009-0251-y)
- Lim HD, van Rijn RM, Ling P et al (2005) Evaluation of histamine H₁-, H₂-, and H₃-receptor ligands at the human histamine H₄ receptor: identification of 4-methylhistamine as the first potent and selective H₄ receptor agonist. *J Pharmacol Exp Ther* 314:1310–1321. doi:[10.1124/jpet.105.087965](https://doi.org/10.1124/jpet.105.087965)
- Lin J-S, Sergeeva OA, Haas HL (2011) Histamine H₃ receptors and sleep-wake regulation. *J Pharmacol Exp Ther* 336:17–23. doi:[10.1124/jpet.110.170134](https://doi.org/10.1124/jpet.110.170134)
- Linnert K, Ejsing TB (2008) A review on the impact of P-glycoprotein on the penetration of drugs into the brain. Focus on psychotropic drugs. *Eur Neuropsychopharmacol* 18:157–169. doi:[10.1016/j.euroneuro.2007.06.003](https://doi.org/10.1016/j.euroneuro.2007.06.003)
- Logan J, Fowler JS, Volkow ND et al (1990) Graphical analysis of reversible radioligand binding from time-activity measurements applied to [N-11C-methyl]-(-)-cocaine PET studies in human subjects. *J Cereb Blood Flow Metab* 10:740–747. doi:[10.1038/jcbfm.1990.127](https://doi.org/10.1038/jcbfm.1990.127)
- Logan J, Fowler JS, Volkow ND et al (1996) Distribution volume ratios without blood sampling from graphical analysis of PET data. *J Cereb Blood Flow Metab* 16:834–840. doi:[10.1097/00004647-199609000-00008](https://doi.org/10.1097/00004647-199609000-00008)
- Logan J, Carruthers NI, Letavic MA et al (2012) Blockade of the brain histamine H₃ receptor by JNJ-39220675: preclinical PET studies with [¹¹C]GSK189254 in anesthetized baboon. *Psychopharmacology (Berl)* 223:447–455. doi:[10.1007/s00213-012-2733-x](https://doi.org/10.1007/s00213-012-2733-x)
- Lourenco CM, Kenk M, Beanlands RS, DaSilva JN (2006) Increasing synaptic noradrenaline, serotonin and histamine enhances in vivo binding of phosphodiesterase-4 inhibitor (R)-[11C] rolipram in rat brain, lung and heart. *Life Sci* 79:356–364. doi:[10.1016/j.lfs.2006.01.010](https://doi.org/10.1016/j.lfs.2006.01.010)
- Lovenberg TW, Roland BL, Wilson SJ et al (1999) Cloning and functional expression of the human histamine H₃ receptor. *Mol Pharmacol* 55:1101–1107
- Madsen JL, Graff J (2008) Effects of the H₂-receptor antagonist ranitidine on gastric motor function after a liquid meal in healthy humans. *Scand J Clin Lab Invest* 68:681–684. doi:[10.1080/00365510802047685](https://doi.org/10.1080/00365510802047685)
- Mancama D, Arranz MJ, Munro J et al (2002) Investigation of promoter variants of the histamine 1 and 2 receptors in schizophrenia and clozapine response. *Neurosci Lett* 333:207–211. doi:[http://dx.doi.org/10.1016/S0304-3940\(02\)00178-7](http://dx.doi.org/10.1016/S0304-3940(02)00178-7)
- Marson CM (2011) Targeting the histamine H₄ receptor. *Chem Rev* 111:7121–7156. doi:[10.1021/cr900166w](https://doi.org/10.1021/cr900166w)
- Martinez-Mir MI, Pollard H, Moreau J et al (1990) Three histamine receptors (H₁, H₂ and H₃) visualized in the brain of human and non-human primates. *Brain Res* 526:322–327. doi:[http://dx.doi.org/10.1016/0006-8993\(90\)91240-H](http://dx.doi.org/10.1016/0006-8993(90)91240-H)
- Masaki T, Yoshimatsu H (2006) The hypothalamic H₁ receptor: a novel therapeutic target for disrupting diurnal feeding rhythm and obesity. *Trends Pharmacol Sci* 27:279–284. doi:[10.1016/j.tips.2006.03.008](https://doi.org/10.1016/j.tips.2006.03.008)
- Masaki T, Yoshimatsu H (2010) Neuronal histamine and its receptors: implication of the pharmacological treatment of obesity. *Curr Med Chem* 17:4587–4592. doi:<http://dx.doi.org/10.2174/092986710794182944>
- McDonald K, Trick L, Boyle J (2008) Sedation and antihistamines: an update. Review of inter-drug differences using proportional impairment ratios. *Hum Psychopharmacol* 23:555–570. doi:[10.1002/hup.962](https://doi.org/10.1002/hup.962)
- Medhurst AD, Atkins AR, Beresford IJ et al (2007) GSK189254, a novel H₃ receptor antagonist that binds to histamine H₃ receptors in Alzheimer's disease brain and improves cognitive performance in preclinical models. *J Pharmacol Exp Ther* 321:1032–1045. doi:[10.1124/jpet.107.120311](https://doi.org/10.1124/jpet.107.120311)
- Mercer LP, Kelley DS, Humphries LL, Dunn JD (1994) Manipulation of central nervous system histamine or histaminergic receptors (H₁) affects food intake in rats. *J Nutr* 124:1029–1036
- Mercer LP, Kelley DS, Haq A, Humphries LL (1996) Dietary induced anorexia: a review of involvement of the histaminergic system. *J Am Coll Nutr* 15:223–230

- Mochizuki H, Tashiro M, Tagawa M et al (2002) The effects of a sedative antihistamine, *d*-chlorpheniramine, on visuomotor spatial discrimination and regional brain activity as measured by positron emission tomography (PET). *Hum Psychopharmacol* 17:413–418. doi:[10.1002/hup.430](https://doi.org/10.1002/hup.430)
- Mochizuki H, Kimura Y, Ishii K et al (2004a) Quantitative measurement of histamine H₁ receptors in human brains by PET and [¹¹C]doxepin. *Nucl Med Biol* 31:165–171. doi:[10.1016/j.nucmedbio.2003.08.010](https://doi.org/10.1016/j.nucmedbio.2003.08.010)
- Mochizuki H, Kimura Y, Ishii K et al (2004b) Simplified PET measurement for evaluating histamine H₁ receptors in human brains using [¹¹C]doxepin. *Nucl Med Biol* 31:1005–1011. doi:[10.1016/j.nucmedbio.2004.06.009](https://doi.org/10.1016/j.nucmedbio.2004.06.009)
- Molina-Hernández A, Díaz NF, Arias-Montaño J-A (2012) Histamine in brain development. *J Neurochem* 122:872–882. doi:[10.1111/j.1471-4159.2012.07863.x](https://doi.org/10.1111/j.1471-4159.2012.07863.x)
- Morimoto T, Yamamoto Y, Yamatodani A (2001) Brain histamine and feeding behavior. *Behav Brain Res* 124:145–150. doi:[10.1016/S0166-4328\(01\)00225-X](https://doi.org/10.1016/S0166-4328(01)00225-X)
- Mrak RE, Griffin WST (2005) Glia and their cytokines in progression of neurodegeneration. *Neurobiol Aging* 26:349–354. doi:[10.1016/j.neurobiolaging.2004.05.010](https://doi.org/10.1016/j.neurobiolaging.2004.05.010)
- Nagase T, Mizutani T, Ishikawa S et al (2008) Synthesis, structure-activity relationships, and biological profiles of a quinazolinone class of histamine H₃ receptor inverse agonists. *J Med Chem* 51:4780–4789. doi:[10.1021/jm8003834](https://doi.org/10.1021/jm8003834)
- Nijmeijer S, de Graaf C, Leurs R, Vischer HF (2012) Molecular pharmacology of histamine H₄ receptors. *Front Biosci* 17:2089–2106. doi:[10.2741/4039](https://doi.org/10.2741/4039)
- Nikolaus S, Antke C, Müller H-W (2009) In vivo imaging of synaptic function in the central nervous system: II. Mental and affective disorders. *Behav Brain Res* 204:32–66. doi:[10.1016/j.bbr.2009.06.009](https://doi.org/10.1016/j.bbr.2009.06.009)
- Nowak JZ (1994) Histamine in the central nervous system: its role in circadian rhythmicity. *Acta Neurobiol Exp* 54(Suppl):65–82
- Nuutinen S, Panula P (2010) Histamine in neurotransmission and brain diseases. In: Thurmond RL (ed) *Histamine in inflammation*. Springer, New York, pp 95–107. doi:[10.1007/978-1-4419-8056-4_10](https://doi.org/10.1007/978-1-4419-8056-4_10)
- Okamura N, Yanai K (2009) Molecular PET imaging of acetylcholine esterase, histamine H₁ receptor and amyloid deposits in Alzheimer disease. In: Lim CT, Goh JCH, Magjarevic R (eds) *13th international conference on biomedical engineering*. Springer, Berlin/Heidelberg, pp 2181–2183
- Okamura N, Yanai K, Higuchi M et al (2000) Functional neuroimaging of cognition impaired by a classical antihistamine, *d*-chlorpheniramine. *Br J Pharmacol* 129:115–123. doi:[10.1038/sj.bjp.0702994](https://doi.org/10.1038/sj.bjp.0702994)
- Parsons ME, Ganellin CR (2006) Histamine and its receptors. *Br J Pharmacol* 147:S127–S135. doi:[10.1038/sj.bjp.0706440](https://doi.org/10.1038/sj.bjp.0706440)
- Passani MB, Ballerini C (2012) Histamine and neuroinflammation: insights from murine experimental autoimmune encephalomyelitis. *Front Syst Neurosci* 6:32. doi:[10.3389/fnsys.2012.00032](https://doi.org/10.3389/fnsys.2012.00032)
- Passani MB, Blandina P (2011) Histamine receptors in the CNS as targets for therapeutic intervention. *Trends Pharmacol Sci* 32:242–249. doi:[10.1016/j.tips.2011.01.003](https://doi.org/10.1016/j.tips.2011.01.003)
- Passani MB, Blandina P, Torrealba F (2011) The histamine H₃ receptor and eating behavior. *J Pharmacol Exp Ther* 336:24–29. doi:[10.1124/jpet.110.171306](https://doi.org/10.1124/jpet.110.171306)
- Pawluck DE, Gorey KM (1998) Secular trends in the incidence of anorexia nervosa: integrative review of population-based studies. *Int J Eat Disord* 23:347–352. doi:[10.1002/\(SICI\)1098-108X\(199805\)23:4<347::AID-EAT1>3.0.CO;2-I](https://doi.org/10.1002/(SICI)1098-108X(199805)23:4<347::AID-EAT1>3.0.CO;2-I)
- Plisson C, Bender D, Ashworth S et al (2006) PET imaging of the CNS histamine H₃ receptor using [¹¹C]GSK189254A. *Neuroimage* 31:T47. doi:[10.1016/j.neuroimage.2006.04.038](https://doi.org/10.1016/j.neuroimage.2006.04.038)
- Plisson C, Gunn RN, Cunningham VJ et al (2009) [¹¹C]-GSK189254: a selective radioligand for in vivo central nervous system imaging of histamine H₃ receptors by PET. *J Nucl Med* 50:2064–2072. doi:[10.2967/jnumed.109.062919](https://doi.org/10.2967/jnumed.109.062919)
- Ponchant M, Demphel S, Fuseau C et al (1997) Radiosynthesis and biodistribution of two potential antagonists of cerebral histamine H₃ receptors for PET studies: [¹⁸F]FUB 272 and [¹¹C]UCL 1829. *J Label Compd Radiopharm* 40:605–607. doi:[10.1002/jlcr.2580400901](https://doi.org/10.1002/jlcr.2580400901)

- Prell GD, Khandelwal JK, Burns RS et al (1988) Elevated levels of histamine metabolites in cerebrospinal fluid of aging, healthy humans. *Compr Gerontol A* 2:114–119
- Prell GD, Khandelwal JK, Burns RS et al (1991) Influence of age and gender on the levels of histamine metabolites and pros-methylimidazoleacetic acid in human cerebrospinal fluid. *Arch Gerontol Geriatr* 12:1–12. doi:[10.1016/0167-4943\(91\)90002-8](https://doi.org/10.1016/0167-4943(91)90002-8)
- Prell GD, Green JP, Kaufmann CA et al (1995) Histamine metabolites in cerebrospinal fluid of patients with chronic schizophrenia: their relationships to levels of other aminergic transmitters and ratings of symptoms. *Schizophr Res* 14:93–104. doi:[http://dx.doi.org/10.1016/0920-9964\(95\)00090-9](http://dx.doi.org/10.1016/0920-9964(95)00090-9)
- Quach TT, Duchemin AM, Rose C, Schwartz JC (1980) Labeling of histamine H₁-receptors in the brain of the living mouse. *Neurosci Lett* 17:49–54. doi:[10.1016/0304-3940\(80\)90060-9](https://doi.org/10.1016/0304-3940(80)90060-9)
- Ravert HT, Dannals RF, Wilson AA, Wagner HN (1992) (N-[¹¹C]-Methyl)doxepin: Synthesis of a radiotracer for studying the histamine H-1 receptor. *J Label Compd Radiopharm* 31:403–407. doi:[10.1002/jlcr.2580310510](https://doi.org/10.1002/jlcr.2580310510)
- Repka-Ramirez MS (2003) New concepts of histamine receptors and actions. *Curr Allergy Asthma Rep* 3:227–231. doi:[10.1007/s11882-003-0044-3](https://doi.org/10.1007/s11882-003-0044-3)
- Resch CL, Szabo Z (1994) Analysis of dynamic positron emission tomography images using a neural network. *J Hopkins APL Tech Dig* 15:265–268
- Saeki T, Ueda K, Tanigawara Y et al (1993) Human P-glycoprotein transports cyclosporin A and FK506. *J Biol Chem* 268:6077–6080
- Sakata T, Yoshimatsu H, Kurokawa M (1997) Hypothalamic neuronal histamine: implications of its homeostatic control of energy metabolism. *Nutrition* 13:403–411. doi:[10.1016/S0899-9007\(97\)91277-6](https://doi.org/10.1016/S0899-9007(97)91277-6)
- Saligrama N, Noubade R, Case LK et al (2012) Combinatorial roles for histamine H₁-H₂ and H₃-H₄ receptors in autoimmune inflammatory disease of the central nervous system. *Eur J Immunol* 42:1536–1546. doi:[10.1002/eji.201141859](https://doi.org/10.1002/eji.201141859)
- Sandvik AK, Brenna E, Waldum HL (1997) Review article: the pharmacological inhibition of gastric acid secretion–tolerance and rebound. *Aliment Pharmacol Ther* 11:1013–1018. doi:[10.1046/j.1365-2036.1997.00257.x](https://doi.org/10.1046/j.1365-2036.1997.00257.x)
- Schmelz M (2010) Itch and pain. *Neurosci Biobehav Rev* 34:171–176. doi:[10.1016/j.neubiorev.2008.12.004](https://doi.org/10.1016/j.neubiorev.2008.12.004)
- Schoeffter P, Godfraind T (1989) Histamine receptors in the smooth muscle of human internal mammary artery and saphenous vein. *Pharmacol Toxicol* 64:64–71. doi:[10.1111/j.1600-0773.1989.tb00603.x](https://doi.org/10.1111/j.1600-0773.1989.tb00603.x)
- Schnell D, Brunskole I, Ladova K et al (2011) Expression and functional properties of canine, rat, and murine histamine H₄ receptors in Sf9 insect cells. *Naunyn Schmiedebergs Arch Pharmacol* 383:457–470. doi:[10.1007/s00210-011-0612-3](https://doi.org/10.1007/s00210-011-0612-3)
- Selivanova SV, Honer M, Combe F et al (2012) Radiofluorinated histamine H₃ receptor antagonist as a potential probe for in vivo PET imaging: Radiosynthesis and pharmacological evaluation. *Bioorg Med Chem* 20:2889–2896. doi:[10.1016/j.bmc.2012.03.024](https://doi.org/10.1016/j.bmc.2012.03.024)
- Senda M, Kubo N, Adachi K et al (2009) Cerebral histamine H₁ receptor binding potential measured with PET under a test dose of olopatadine, an antihistamine, is reduced after repeated administration of olopatadine. *J Nucl Med* 50:887–892. doi:[10.2967/jnumed.108.058537](https://doi.org/10.2967/jnumed.108.058537)
- Shibuya K, Funaki Y, Hiraoka K et al (2012) [¹¹C]Doxepin binding to histamine H₁ receptors in living human brain: reproducibility during attentive waking and circadian rhythm. *Front Syst Neurosci* 6:1–7. doi:[10.3389/fnsys.2012.00045](https://doi.org/10.3389/fnsys.2012.00045)
- Shim W-S, Oh U (2008) Histamine-induced itch and its relationship with pain. *Mol Pain* 4:29. doi:[10.1186/1744-8069-4-29](https://doi.org/10.1186/1744-8069-4-29)
- Slifstein M (2010) When reversible ligands do not reverse, and other modelers' dilemmas. *J Nucl Med* 51:1005–1008. doi:[10.2967/jnumed.109.073445](https://doi.org/10.2967/jnumed.109.073445)
- Smink FRE, van Hoeken D, Hoek HW (2012) Epidemiology of eating disorders: incidence, prevalence and mortality rates. *Curr Psychiatry Rep* 14:406–414. doi:[10.1007/s11920-012-0282-y](https://doi.org/10.1007/s11920-012-0282-y)
- Smith DF, Jakobsen S (2009) Molecular tools for assessing human depression by positron emission tomography. *Eur Neuropsychopharmacol* 19:611–628. doi:[10.1016/j.euroneuro.2009.04.005](https://doi.org/10.1016/j.euroneuro.2009.04.005)
- Smits RA, Leurs R, de Esch IJP (2009) Major advances in the development of histamine H₄ receptor ligands. *Drug Discov Today* 14:745–753. doi:[10.1016/j.drudis.2009.05.007](https://doi.org/10.1016/j.drudis.2009.05.007)

- Smits RA, Adami M, Istyastono EP et al (2010) Synthesis and QSAR of quinazoline sulfonamides as highly potent human histamine H₄ receptor inverse agonists. *J Med Chem* 53:2390–2400. doi:[10.1021/jm901379s](https://doi.org/10.1021/jm901379s)
- Spina E, de Leon J (2007) Metabolic drug interactions with newer antipsychotics: a comparative review. *Basic Clin Pharmacol Toxicol* 100:4–22. doi:[10.1111/j.1742-7843.2007.00017.x](https://doi.org/10.1111/j.1742-7843.2007.00017.x)
- Stark H, Purand K, Hüls A et al (1996) [¹²⁵I]iodoproxyfan and related compounds: a reversible radioligand and novel classes of antagonists with high affinity and selectivity for the histamine H₃ receptor. *J Med Chem* 39:1220–1226. doi:[10.1021/jm9504767](https://doi.org/10.1021/jm9504767)
- Stark H, Kathmann M, Schlicker E et al (2004) Medicinal chemical and pharmacological aspects of imidazole-containing histamine H₃ receptor antagonists. *Mini Rev Med Chem* 4: 965–977
- Suzuki A, Tashiro M, Kimura Y et al (2005) Use of reference tissue models for quantification of histamine H₁ receptors in human brain by using positron emission tomography and [¹¹C]doxepin. *Ann Nucl Med* 19:425–433. doi:[10.1007/BF02985569](https://doi.org/10.1007/BF02985569)
- Szabo Z, Ravert HT, Gözükarı I et al (1993) Noncompartmental and compartmental modeling of the kinetics of carbon-11 labeled pyrilamine in the human brain. *Synapse* 15:263–275. doi:[10.1002/syn.890150403](https://doi.org/10.1002/syn.890150403)
- Tagawa M, Kano M, Okamura N et al (2001) Neuroimaging of histamine H₁-receptor occupancy in human brain by positron emission tomography (PET): a comparative study of ebastine, a second-generation antihistamine, and (+)-chlorpheniramine, a classical antihistamine. *Br J Clin Pharmacol* 52:501–509. doi:[10.1046/j.1365-2125.2001.01471.x](https://doi.org/10.1046/j.1365-2125.2001.01471.x)
- Tannenbaum C, Paquette A, Hilmer S et al (2012) A systematic review of amnesic and non-amnesic mild cognitive impairment induced by anticholinergic, antihistamine, GABAergic and opioid drugs. *Drugs Aging* 29:639–658. doi:[10.2165/11633250-000000000-00000](https://doi.org/10.2165/11633250-000000000-00000)
- Tashiro M, Mochizuki H, Iwabuchi K et al (2002a) Roles of histamine in regulation of arousal and cognition: functional neuroimaging of histamine H₁ receptors in human brain. *Life Sci* 72:409–414. doi:[10.1016/S0024-3205\(02\)02276-2](https://doi.org/10.1016/S0024-3205(02)02276-2)
- Tashiro M, Sakurada Y, Mochizuki H et al (2002b) Study on CNS side effects of fexofenadine and cetirizine: measurement of histamine H₁ receptor occupancy using positron emission tomography. *J Clin Pharmacol* 42:1071
- Tashiro M, Sakurada Y, Iwabuchi K et al (2004) Central effects of fexofenadine and cetirizine: measurement of psychomotor performance, subjective sleepiness, and brain histamine H₁-receptor occupancy using ¹¹C-doxepin positron emission tomography. *J Clin Pharmacol* 44:890–900. doi:[10.1177/0091270004267590](https://doi.org/10.1177/0091270004267590)
- Tashiro M, Mochizuki H, Sakurada Y et al (2006) Brain histamine H receptor occupancy of orally administered antihistamines measured by positron emission tomography with ¹¹C-doxepin in a placebo-controlled crossover study design in healthy subjects: a comparison of olopatadine and ketotifen. *Br J Clin Pharmacol* 61:16–26. doi:[10.1111/j.1365-2125.2005.02514.x](https://doi.org/10.1111/j.1365-2125.2005.02514.x)
- Tashiro M, Duan X, Kato M et al (2008a) Brain histamine H₁ receptor occupancy of orally administered antihistamines, bepotastine and diphenhydramine, measured by PET with ¹¹C-doxepin. *Br J Clin Pharmacol* 65:811–821. doi:[10.1111/j.1365-2125.2008.03143.x](https://doi.org/10.1111/j.1365-2125.2008.03143.x)
- Tashiro M, Fukuda H, Itoh M et al (2008b) Molecular imaging at Tohoku University: from cancer to neuroreceptors. *Curr Med Imaging Rev* 4:8–13. doi:[10.2174/157340508783502796](https://doi.org/10.2174/157340508783502796)
- Tashiro M, Sakurada Y, Mochizuki H et al (2008c) Effects of a sedative antihistamine, D-chlorpheniramine, on regional cerebral perfusion and performance during simulated car driving. *Hum Psychopharmacol* 23:139–150. doi:[10.1002/hup.909](https://doi.org/10.1002/hup.909)
- Tashiro M, Kato M, Miyake M et al (2009) Dose dependency of brain histamine H(1) receptor occupancy following oral administration of cetirizine hydrochloride measured using PET with [¹¹C]doxepin. *Hum Psychopharmacol* 24:540–548. doi:[10.1002/hup.1051](https://doi.org/10.1002/hup.1051)
- Teuscher C, Subramanian M, Noubade R et al (2007) Central histamine H₃ receptor signaling negatively regulates susceptibility to autoimmune inflammatory disease of the CNS. *Proc Natl Acad Sci U S A* 104:10146–10151. doi:[10.1073/pnas.0702291104](https://doi.org/10.1073/pnas.0702291104)
- Thakkar MM (2011) Histamine in the regulation of wakefulness. *Sleep Med Rev* 15:65–74. doi:[10.1016/j.smr.2010.06.004](https://doi.org/10.1016/j.smr.2010.06.004)

- Theunissen EL, Vermeeren A, Vuurman EFPM, Ramaekers JG (2006) Stimulating effects of H₁-antagonists. *Curr Pharm Des* 12:2501–2509
- Thurmond RL (2010) Histamine in inflammation, 1st edn. Springer, New York. doi:[10.1007/978-1-4419-8056-4](https://doi.org/10.1007/978-1-4419-8056-4)
- Thurmond RL, Gelfand EW, Dunford PJ (2008) The role of histamine H₁ and H₄ receptors in allergic inflammation: the search for new antihistamines. *Nat Rev Drug Discov* 7:41–53. doi:[10.1038/nrd2465](https://doi.org/10.1038/nrd2465)
- Tiligada E, Kyriakidis K, Chazot PL, Passani MB (2011) Histamine pharmacology and new CNS drug targets. *CNS Neurosci Ther* 17:620–628. doi:[10.1111/j.1755-5949.2010.00212.x](https://doi.org/10.1111/j.1755-5949.2010.00212.x)
- Traiffort E, Pollard H, Moreau J et al (1992) Pharmacological characterization and autoradiographic localization of histamine H₂ receptors in human brain identified with [¹²⁵I]iodoaminopotentidine. *J Neurochem* 59:290–299. doi:[10.1111/j.1471-4159.1992.tb08903.x](https://doi.org/10.1111/j.1471-4159.1992.tb08903.x)
- Van der Goot H, Timmerman H (2000) Selective ligands as tools to study histamine receptors. *Eur J Med Chem* 35:5–20. doi:[10.1016/S0223-5234\(00\)00101-X](https://doi.org/10.1016/S0223-5234(00)00101-X)
- Van Ruitenbeek P, Vermeeren A, Riedel WJ (2010) Cognitive domains affected by histamine H(1)-antagonism in humans: a literature review. *Brain Res Rev* 64:263–282. doi:[10.1016/j.brainresrev.2010.04.008](https://doi.org/10.1016/j.brainresrev.2010.04.008)
- Villemagne VL, Dannals RF, Sánchez-Roa PM et al (1991) Imaging histamine H₁ receptors in the living human brain with carbon-11-pyramine. *J Nucl Med* 32:308–311
- Vizuete ML, Traiffort E, Bouthenet ML et al (1997) Detailed mapping of the histamine H₂ receptor and its gene transcripts in guinea-pig brain. *Neuroscience* 80:321–343. doi:[http://dx.doi.org/10.1016/S0306-4522\(97\)00010-9](http://dx.doi.org/10.1016/S0306-4522(97)00010-9)
- Vohora D, Bhowmik M (2012) Histamine H₃ receptor antagonists/inverse agonists on cognitive and motor processes: relevance to Alzheimer's disease, ADHD, schizophrenia, and drug abuse. *Front Syst Neurosci* 6:1–10. doi:[10.3389/fnsys.2012.00072](https://doi.org/10.3389/fnsys.2012.00072)
- Wang K-Y, Tanimoto A, Yamada S et al (2010) Histamine regulation in glucose and lipid metabolism via histamine receptors: model for nonalcoholic steatohepatitis in mice. *Am J Pathol* 177:713–723. doi:[10.2353/ajpath.2010.091198](https://doi.org/10.2353/ajpath.2010.091198)
- Wang M, Gao M, Steele BL et al (2012) A new facile synthetic route to [¹¹C]GSK189254, a selective PET radioligand for imaging of CNS histamine H(3) receptor. *Bioorg Med Chem Lett* 22:4713–4718. doi:[10.1016/j.bmcl.2012.05.076](https://doi.org/10.1016/j.bmcl.2012.05.076)
- Watanabe T, Yanai K (2001) Studies on functional roles of the histaminergic neuron system by using pharmacological agents, knockout mice and positron emission tomography. *Tohoku J Exp Med* 195:197–217. doi:[10.1620/tjem.195.197](https://doi.org/10.1620/tjem.195.197)
- Windaus A, Vogt W (1907) Synthese des Imidazolyl-Äthylamins. *Ber d Chem Gesell* 40:3691–3695. doi:[10.1002/cber.190704003164](https://doi.org/10.1002/cber.190704003164)
- Windhorst AD, Leurs R, Menge WMPB et al (1998) Synthesis of radioligands for the histamine H₃ receptor. In: Leurs R, Timmerman H (eds) *The histamine H₃ receptor A target for new drugs*. Elsevier, Amsterdam/New York, p 159–174. doi:[10.1016/S0165-7208\(98\)80029-9](https://doi.org/10.1016/S0165-7208(98)80029-9)
- Windhorst AD, Timmerman H, Klok RP et al (1999a) Evaluation of [¹⁸F]VUF 5000 as a potential PET ligand for brain imaging of the histamine H₃ receptor. *Bioorg Med Chem* 7:1761–1767. doi:[10.1016/S0968-0896\(99\)00108-X](https://doi.org/10.1016/S0968-0896(99)00108-X)
- Windhorst AD, Timmerman H, Klok RP et al (1999b) Radiosynthesis and biodistribution of ¹²³I-labeled antagonists of the histamine H₃ receptor as potential SPECT ligands. *Nucl Med Biol* 26:651–659. doi:[10.1016/S0969-8051\(99\)00014-1](https://doi.org/10.1016/S0969-8051(99)00014-1)
- Windhorst AD, Timmerman H, Menge WMPB et al (1999c) Synthesis, in vitro pharmacology and radiosynthesis of N-(cis-4-fluoromethylcyclohexyl)-4-(1(H)-imidazol-4-yl)piperidine-11-thiocarbamide (VUF 5000), a potential PET ligand for the histamine H₃ receptor. *J Label Compd Radiopharm* 42:293–307. doi:[10.1002/\(SICI\)1099-1344\(199903\)42:3<293::AID-JLCR191>3.0.CO;2-B](https://doi.org/10.1002/(SICI)1099-1344(199903)42:3<293::AID-JLCR191>3.0.CO;2-B)
- Wong DF, Pomper MG (2003) Predicting the success of a radiopharmaceutical for in vivo imaging of central nervous system neuroreceptor systems. *Mol Imaging Biol* 5:350–362. doi:[10.1016/j.mibio.2003.09.011](https://doi.org/10.1016/j.mibio.2003.09.011)
- Xiaofeng B, Shuiyu L, Liow J-S et al (2011) Radiolabeling and evaluation of [F-18]XB-1 in monkey as a prospective histamine subtype 3 receptor PET radioligand. *J Label Compd Radiopharm* 54:S83. doi:[10.1002/jlcr.1925](https://doi.org/10.1002/jlcr.1925)

- Yanai K, Tashiro M (2007) The physiological and pathophysiological roles of neuronal histamine: an insight from human positron emission tomography studies. *Pharmacol Ther* 113:1–15. doi:[10.1016/j.pharmthera.2006.06.008](https://doi.org/10.1016/j.pharmthera.2006.06.008)
- Yanai K, Dannals RF, Wilson AA et al (1988) (N-methyl-[11C])pyrilamine, a radiotracer for histamine H₁ receptors: radiochemical synthesis and biodistribution study in mice. *Int J Radiat Appl Instrum Part B* 15:605–610. doi:[10.1016/0883-2897\(88\)90050-5](https://doi.org/10.1016/0883-2897(88)90050-5)
- Yanai K, Dannals RF, Wilson AA et al (1989) Biodistribution and radiation absorbed dose of (N-methyl[11C])pyrilamine: a histamine H₁ receptor radiotracer. *Int J Radiat Appl Instrum Part B* 16:361–363. doi:[10.1016/0883-2897\(89\)90100-1](https://doi.org/10.1016/0883-2897(89)90100-1)
- Yanai K, Watanabe T, Hatazawa J et al (1990a) Visualization of histamine H₁ receptors in dog brain by positron emission tomography. *Neurosci Lett* 118:41–44. doi:[10.1016/0304-3940\(90\)90244-4](https://doi.org/10.1016/0304-3940(90)90244-4)
- Yanai K, Yagi N, Watanabe T et al (1990b) Specific binding of [³H]pyrilamine to histamine H₁ receptors in guinea pig brain in vivo: determination of binding parameters by a kinetic four-compartment model. *J Neurochem* 55:409–420. doi:[10.1111/j.1471-4159.1990.tb04152.x](https://doi.org/10.1111/j.1471-4159.1990.tb04152.x)
- Yanai K, Watanabe T, Itoh M et al (1991) Labeling of histamine H₁-receptors in vivo: a compartment model analysis and positron emission tomographic imaging. *Agents Actions Suppl* 33:381–386
- Yanai K, Watanabe T, Meguro K et al (1992a) Age-dependent decrease in histamine H₁ receptor in human brains revealed by PET. *Neuroreport* 3:433–436. doi:[10.1097/00001756-199205000-00014](https://doi.org/10.1097/00001756-199205000-00014)
- Yanai K, Watanabe T, Yokoyama H et al (1992b) Mapping of histamine H₁ receptors in the human brain using [11C]pyrilamine and positron emission tomography. *J Neurochem* 59:128–136. doi:[10.1111/j.1471-4159.1992.tb08883.x](https://doi.org/10.1111/j.1471-4159.1992.tb08883.x)
- Yanai K, Watanabe T, Yokoyama H et al (1992c) Histamine H₁ receptors in human brain visualized in vivo by [¹¹C]doxepin and positron emission tomography. *Neurosci Lett* 137:145–148. doi:[10.1016/0304-3940\(92\)90390-S](https://doi.org/10.1016/0304-3940(92)90390-S)
- Yanai K, Ryu JH, Watanabe T et al (1994) Labelling of histamine H₁, H₂, and H₃ receptor antagonists with carbon-11 using on-line methylation system: potential radiopharmaceuticals for PET studies. *J Label Compd Radiopharm* 35:520. doi:[10.1002/jlcr.2580350107](https://doi.org/10.1002/jlcr.2580350107)
- Yanai K, Ryu JH, Watanabe T et al (1995a) Positron emission tomographic study of central histamine H₁-receptor occupancy in human subjects treated with epinastine, a second-generation antihistamine. *Methods Find Exp Clin Pharmacol* 17:64–69
- Yanai K, Ryu JH, Watanabe T et al (1995b) Histamine H₁ receptor occupancy in human brains after single oral doses of histamine H₁ antagonists measured by positron emission tomography. *Br J Pharmacol* 116:1649–1655
- Yanai K, Okamura N, Tagawa M et al (1999) New findings in pharmacological effects induced by antihistamines: from PET studies to knock-out mice. *Clin Exp Allergy* 29:29–36. doi:[10.1046/j.1365-2222.1999.00008.x-i1](https://doi.org/10.1046/j.1365-2222.1999.00008.x-i1)
- Yanai K, Okamura N, Kudo Y et al (2007) Molecular pet imaging of acetylcholine esterase, histamine H₁ receptor and amyloid deposits in Alzheimer disease. *J Neurochem* 102:92. doi:[10.1111/j.0022-3042.2007.04727.x](https://doi.org/10.1111/j.0022-3042.2007.04727.x)
- Yanai K, Zhang D, Manabu T, Shibuya K (2008) Evaluation of residual sedative effect of antihistamines by measuring central histamine H₁ receptor occupancy using ¹¹C-doxepin -PET. *Acta Derm Venereol* 89:707. doi:[10.2340/00015555-0751](https://doi.org/10.2340/00015555-0751)
- Yanai K, Nakamura T, Tashiro M, Watanabe T (2011a) Imaging histamine H₁ receptors using PET and [11C]doxepin: further progress. *Inflamm Res* 60:S347. doi:[10.1007/s00011-011-0371-0](https://doi.org/10.1007/s00011-011-0371-0)
- Yanai K, Zhang D, Tashiro M et al (2011b) Positron emission tomography evaluation of sedative properties of antihistamines. *Expert Opin Drug Saf* 10:613–622. doi:[10.1517/14740338.2011.562889](https://doi.org/10.1517/14740338.2011.562889)
- Yanai K, Rogala B, Chugh K et al (2012) Safety considerations in the management of allergic diseases: focus on antihistamines. *Curr Med Res Opin* 28:623–642. doi:[10.1185/03007995.2012.672405](https://doi.org/10.1185/03007995.2012.672405)
- Yoshizawa M, Tashiro M, Fukudo S et al (2009) Increased brain histamine H₁ receptor binding in patients with anorexia nervosa. *Biol Psychiatry* 65:329–335. doi:[10.1016/j.biopsych.2008.08.012](https://doi.org/10.1016/j.biopsych.2008.08.012)
- Yu F, Bonaventure P, Thurmond RL (2010) The future antihistamines: histamine H(3) and H(4) receptor ligands. *Adv Exp Med Biol* 709:125–140. doi:[10.1007/978-1-4419-8056-4_12](https://doi.org/10.1007/978-1-4419-8056-4_12)

- Zhang M, Ballard ME, Pan L et al (2005) Lack of cataleptogenic potentiation with non-imidazole H₃ receptor antagonists reveals potential drug-drug interactions between imidazole-based H₃ receptor antagonists and antipsychotic drugs. *Brain Res* 1045:142–149. doi:[10.1016/j.brainres.2005.03.018](https://doi.org/10.1016/j.brainres.2005.03.018)
- Zhang D, Tashiro M, Shibuya K et al (2010) Next-day residual sedative effect after nighttime administration of an over-the-counter antihistamine sleep aid, diphenhydramine, measured by positron emission tomography. *J Clin Psychopharmacol* 30:694–701. doi:[10.1097/JCP.0b013e3181fa8526](https://doi.org/10.1097/JCP.0b013e3181fa8526)
- Zung WW (1965) A self-rating depression scale. *Arch Gen Psychiatry* 12:63–70

Mohammed A. Khayum, Janine Doorduyn, Andor W.J.M. Glaudemans, Rudi A.J.O. Dierckx, and Erik F.J. de Vries

Contents

14.1	Introduction	379
14.2	Steroid Hormones in Brain Disorders	380
14.2.1	Estrogens	380
14.2.2	Progestins	381
14.2.3	Androgens	382
14.2.4	Corticosteroids	383
14.3	Steroid Hormone Receptors in Brain Disorders.....	384
14.4	Imaging of Steroid Hormone Receptors	386
14.4.1	Radiopharmaceuticals for Estrogen Receptor Imaging	387
14.4.2	Radiopharmaceuticals for Progesterone Receptor Imaging.....	390
14.4.3	Radiopharmaceuticals for Androgen Receptor Imaging.....	392
14.4.4	Radiopharmaceuticals for Corticoid Receptor Imaging.....	394
14.5	Imaging of Steroid Hormone Receptors in the Brain.....	397
14.6	Conclusion and Perspectives	399
	References	400

Abstract

Steroid hormones like estrogens, progestins, androgens, and corticosteroids are involved in normal brain function. They are able to exert both neuroprotective and neurotrophic effects. In addition, steroid hormones play a crucial role in

M.A. Khayum • J. Doorduyn • Andor W.J.M. Glaudemans • E.F.J. de Vries (✉)
Department of Nuclear Medicine and Molecular Imaging, University Medical Center
Groningen, University of Groningen, Hanzeplein 1, Groningen 9713 GZ, The Netherlands
e-mail: e.f.j.de.vries@umcg.nl

R.A.J.O. Dierckx
Department of Nuclear Medicine and Molecular Imaging, University Medical Center
Groningen, University of Groningen, Hanzeplein 1, Groningen 9713 GZ, The Netherlands

Department of Nuclear Medicine, University Hospital Gent, University of Gent,
De Pintelaan 185, 9000 Gent, Belgium

mood disorders by interacting with different neurotransmitter systems in the brain. Steroid hormones produce their physiological effects by binding to their corresponding hormone receptors. To better understand the role of steroid hormones, knowledge of the expression of steroid hormone receptors in the brain may provide important insights. In animal experiments, it is possible to perform invasive measurement of steroid hormone receptors both in healthy and in pathological conditions, but noninvasive measurement of steroid receptors in the brain is required in humans. PET and SPECT are techniques that may allow noninvasive measurements of the expression of steroid hormone receptors. This chapter addresses the role of steroid hormone receptors in both physiological and pathological conditions and provides an overview of the current status of PET and SPECT imaging methods for steroid hormone receptors.

Abbreviations

(Z)-[¹²³ I]MIVE	(20Z)-11beta-methoxy-17alpha-[¹²³ I]iodovinylestradiol
[¹²³ I]IES	16alpha-[¹²³ I]iodo-17beta-estradiol
[¹²³ I]IVMMNT	17alpha-[¹²³ I] iodovinyl-18-methyl-11-methylene-19-nortestosterone
[¹²³ I]TAM	[¹²³ I]iodotamoxifen
[¹²⁵ I]IVNT	(20Z)-17alpha-[¹²⁵ I]iodovinyl-19-nortestosterone
[¹²⁵ I]MIE	16alpha-[¹²⁵ I]iodo-11beta-methoxy-17beta-estradiol
[¹⁸ F]betaFMOX	17alpha-ethynyl-11beta-methoxy-estradiol
[¹⁸ F]FDHT	16beta-[¹⁸ F]fluorodihydrotestosterone
[¹⁸ F]FENP	21-[¹⁸ F]fluoro-16alpha-ethyl-19-norprogesterone
[¹⁸ F]FES	16alpha-[¹⁸ F]fluoro-17beta-estradiol
[¹⁸ F]FFNP	21-[¹⁸ F]fluoro-16alpha,17alpha-[(R)-(1'alpha-furylmethylidene)dioxy]-19-norpregn-4-ene-3,20-dione
[¹⁸ F]FMDHT	7alpha-[¹⁸ F]fluoro-17-methyl-5-dihydrotestosterone
[¹⁸ F]FMNP	21-[¹⁸ F]fluoro-16alpha-methyl-19-norprogesterone
[¹⁸ F]FPTP	4-[¹⁸ F]fluoropropyl-tanaproget
[¹⁸ F]FTX	[¹⁸ F]Fluoromethyl- <i>N,N</i> -dimethyltamoxifen
16alpha-[¹⁸ F]FMNT	16alpha-[¹⁸ F]fluoro-7alpha-methyl-19-nortestosterone
16beta-[¹⁸ F]FMNT	16beta-[¹⁸ F]fluoro-7alpha-methyl-19-nortestosterone
16beta-[¹⁸ F]FT	16beta-[¹⁸ F]fluorotestosterone
20-[¹⁸ F]Fmib	20-[¹⁸ F]fluoromibolone
4F-M[¹⁸ F]FES	11beta-methoxy-4,16alpha-[¹⁸ F]difluoroestradiol
7alpha-[¹²⁵ I]IDHT	7alpha-[¹²⁵ I]iodo-5alpha-dihydrotestosterone
8beta-[¹⁸ F]FEE	8beta-(2-[¹⁸ F]fluoroethyl)estradiol
AR	Androgen receptors
CNS	Central nervous system
DES	Diethylstilbestrol
ER	Estrogen receptors
GR	Glucocorticoid receptors

HPA axis	Hypothalamic-pituitary-adrenal axis
MR	Mineralocorticoid receptors
PR	Progesterone receptors
SHBG	Sex hormone-binding protein
SHR	Steroid hormone receptors

14.1 Introduction

Hormones are messenger molecules that are produced and secreted by endocrine glands in the body. Hormones travel through the blood stream to those parts of the body where they induce their specific cellular responses. Hormones are generally classified into two classes: steroidal and nonsteroidal hormones. Structurally all steroid hormones consist of a steroidal scaffold, which is composed of three six-membered rings and one five-membered ring; nonsteroidal hormones lack this steroid scaffold. Examples of steroid hormones are estrogens, progesterones, androgens, and corticosteroids. Steroid hormones are responsible for biological responses in a wide range of endocrine processes, including sexual differentiation, reproductive physiology, glucose metabolism, and maintenance of salt and water balance. Examples of nonsteroidal hormones are insulin, glucagon, thyroid-stimulating hormone, follicular-stimulating hormone, catecholamines, and eicosanoids.

The brain is an important target organ for circulating steroid hormones that are secreted from peripheral organs, such as adrenal cortex, testes, and ovaries. Steroid hormones are highly lipophilic and therefore can easily pass through the blood-brain barrier by passive diffusion. However, the brain itself is now known to synthesize steroid hormones *de novo* from cholesterol (Fig. 14.1). After surgical removal of peripheral organs that produce steroid hormones (e.g., castration, like orchiectomy or ovariectomy), constant levels of these neurosteroids are maintained in the brain (Corpéchet et al. 1983; Robel and Baulieu 1985). The most important neuroactive steroids include not only neurosteroids produced by the brain like pregnenolone, dehydroepiandrosterone, and 3 α -hydroxy-5 α -pregnane-20-one but also classical steroid hormones, such as 17 β -estradiol, testosterone, and progesterone. Neurosteroids produce their effects by autocrine or endocrine pathways (Baulieu 1998). Steroid hormones produced in the CNS are allosteric modulators of different neurotransmitter receptors. The major functions of neuroactive steroids have been reviewed by Rupprecht (2003).

In the central nervous system (CNS), neuroactive steroids/neurosteroids play a crucial role in neuronal development and plasticity. Neuroactive steroids can act as allosteric modulators of ligand-gated ion channels (GABA_A), NMDA, and sigma receptors. Because of these interactions, neuroactive steroids have been implicated to have sleep-inducing, anticonvulsant, anesthetic, nootropic, and antipsychotic properties (Rupprecht 2003). They are also associated with processes like learning, memory, emotion, behavior, synaptic transmission, and neuroprotection (Giatti et al. 2012). Because of these neuroprotective properties, steroid hormones may

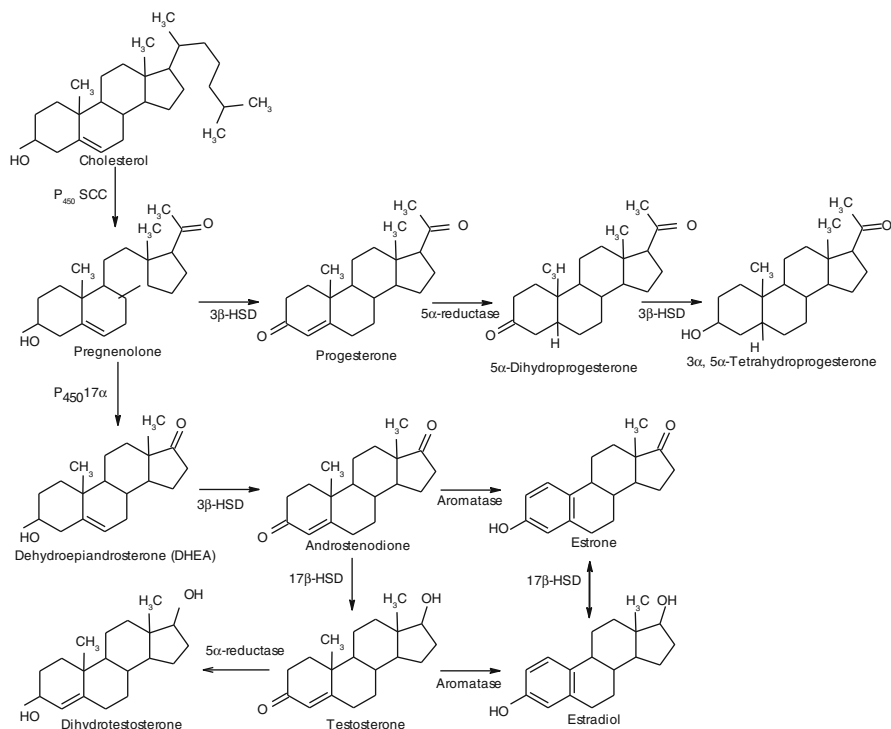


Fig. 14.1 Neurosteroidogenesis: Steroidogenesis follows a sequential, highly compartmentalized reaction, with the translocation of cholesterol from cytoplasm to mitochondria in the cells of CNS, which is mediated by steroidogenic acute regulatory protein (StAR) and an 18 kDa translocator protein (TSPO). In the mitochondria, P450 side-chain cleavage (P450SCC) cleaves the side chain from cholesterol, resulting in the formation of pregnenolone. Pregnenolone is subsequently converted to progesterone and dehydroepiandrosterone in endoplasmic reticulum. The lipophilic nature of these compounds allows them to diffuse from one cell to another. Progesterone and dehydroepiandrosterone are further metabolized to form other neuroactive metabolites like testosterone, estrone, and estradiol

have a beneficial effect in neurodegenerative diseases, including Alzheimer's disease, multiple sclerosis, Parkinson's disease, and Huntington's disease. However, steroid hormones are also implicated in psychiatric disorders, due to their role in cognition and behavior.

14.2 Steroid Hormones in Brain Disorders

14.2.1 Estrogens

Women have a higher prevalence of reduced cognitive function, depression, panic disorder, generalized anxiety disorder, social phobia, eating disorders, and some

personality traits than men (Holsen et al. 2011). This difference in prevalence between sexes suggests that female sex steroid hormones may be involved in these conditions. This hypothesis is supported by the observation that several mental changes occur during the transition of women from pre- to postmenopause. These changes include reduced sexual drive, premenstrual and perimenopausal dysphoria induced by oral contraceptives or hormone replacement therapy (Eriksson et al. 2002; Rubinow and Schmidt 2006; Steiner et al. 2003). These symptoms are associated with altered levels of circulating estrogens. At menopause, levels of circulating estrogens are strongly reduced. This reduction in estrogen levels is associated with social and psychological changes in women, like anxiety, irritability, stress, memory loss, lack of concentration, and loss of libido. Eventually, this may culminate into depression (Bryant et al. 2012). The effects of estrogen changes are likely the result of an altered interaction of estrogens with other neurotransmitters like acetylcholine, dopamine, noradrenaline, and serotonin (McEwen 2001). Moreover, prolonged deficiency of estrogens increases the risk to develop dementia (Sherman et al. 2005) and Alzheimer's disease (Pike et al. 2009).

As a consequence, maintenance of steady levels of estrogens seems essential for normal physiological and mental status. In fact, estrogen replacement therapy was found to improve learning, memory, and cognition in postmenopausal women (Sherwin 1997) and to prevent depression both in peri- and postmenopausal women (Grigoriadis and Kennedy 2002). Furthermore, estrogen replacement therapy was also found to have a protective effect against neurodegenerative disorders. This protective effect was ascribed to the anti-inflammatory activity of estrogens (Resnick and Henderson 2002; Vegeto et al. 2008; Yaffe et al. 1998). Neurosteroids produced by activated microglia are able to shift a pro-inflammatory immune response into an anti-inflammatory phenotype (Giatti et al. 2012). The shift between pro- and anti-inflammatory effects of estrogens seems to be dependent upon both the expression level and the extent of stimulation of estrogen receptors (ER) in the CNS. It is also evident from recent literature that the anti-inflammatory effects are associated with suppression of ER-mediated pro-inflammatory cytokine and chemokine production (Benedusi et al. 2012; Brown et al. 2010).

14.2.2 Progestins

Progestins have been demonstrated to play an important role in neuroprotection as observed in experimental models and clinical trials in patients with stroke and traumatic brain injury (Stein 2011a, b). Progestins can easily pass through the blood-brain barrier and exert their neuroprotective effects inside the brain. A few studies were performed to assess the role of PR in experimental animal models of stroke and traumatic brain injury. Liu et al. found that ischemia to the brain for 6 h resulted in a rapid increase in the progesterone and 5 α -dihydroprogesterone levels both in wild-type and PR knockout mice, suggesting a possible role of progestins in the salvage of neurons at risk (Liu et al. 2012). Changes in steroid hormone levels affected the expression of membrane PR, specifically PR alpha, in rats

and mice. Upon treatment with estradiol or progesterone, significant expression of PR alpha was observed in neurons of olfactory bulb, striatum, cortex, thalamus, hypothalamus, septum, hippocampus, and cerebellum, but not on oligodendrocytes or astrocytes. Traumatic brain injury induced the expression of PR alpha not only on neurons but also on oligodendrocytes, astrocytes, and reactive microglia, suggesting a role of progestins and PR in inflammation in the injured brain (Meffre et al. 2013).

The neuroprotective mechanisms and anti-inflammatory effects of progestins have been reviewed by several authors (Giatti et al. 2012; Luoma et al. 2012; De Nicola et al. 2009; Sayeed and Stein 2009; Singh and Su 2012; Stein et al. 2008). Progestins may prevent brain damage by controlling edema formation (vasogenic or cytogenic) via modulation of the expression of the aquaporin-4 water transporter, moderating Ca^{2+} flux caused by excitotoxicity, and reconstitution of the blood-brain barrier. Progestins also have antioxidant properties that can prevent cellular insults by oxidative stress induced by free radical formation. Progestins can inhibit the activation of microglia, which prevents NO and TNF-alpha production and the release of other inflammatory cytokines, such as IL-1 beta, TNF-alpha, and IL-6, complement factor C3 and C5, and macrophage-inducing factor-1. In addition, progestins have anti-apoptotic properties. Besides the aforementioned roles in neuroprotection, progestins also play a role in neuronal remodelling by upregulating several neurotrophic factors, such as brain-derived neurotrophic factor (BDNF), Na/K ATPase, microtubule-associated protein 2 (MAP-2), choline acetyltransferase (ChAT), and glial-derived neurotrophic factor (GDNF).

To investigate progestin as neuroprotectant in patients, a clinical trial (phase IIa) was conducted in 100 male and female patients with blunt head trauma with moderate-to-severe damage. Treatment with progesterone showed significant reduction in mortality compared to vehicle group (Wright et al. 2007). Two large-scale studies on progesterone treatment are now in process. A phase III clinical trial investigates the effects in moderate-to-severe traumatic brain injury in 1,200 patients. Another phase III trial studies the effect on brain injury in pediatric patients (Stein 2011b). Administration of progestins in combination with estrogens was found to be an effective treatment for postmenopausal symptoms. The combination of progestins and estrogens showed efficacy in the treatment of multiple sclerosis in both animal models and in patients. The beneficial effect was mediated by modulation of peripheral and brain-intrinsic immune responses and regulation of local growth factor supply, oligodendrocytes, and astrocytes (Kipp et al. 2012).

14.2.3 Androgens

The most common central effect of androgens is the induction of aggression. Excessive levels of testosterone are known to induce aggression in both sexes. Exposure to high testosterone levels at young age is associated with a reduction in

feminine characteristics in women. Moreover, testosterone is converted to estradiol in the CNS, which plays a pivotal role in the feedback regulation in the hypothalamus. The hypothalamus plays a positive role in hormone release by endocrine system through the pituitary. In analogy to menopause in women, aging men may experience andropause (hypogonadism), which is a condition characterized by very low circulating androgen concentrations. This reduction in androgen levels may be accompanied by decreased cell survival in the hippocampus (Spritzer and Galea 2007) and a decrease in cognitive functions and increased risk to develop depression and Alzheimer's disease (Irie et al. 2006; Seidman 2007). Testosterone treatment was found to reduce many mood- and cognition-related symptoms in hypogonadal men (Zitzmann 2006) and to enhance hippocampal neurogenesis through increased cell survival in rodents (Spritzer and Galea 2007). Androgen treatment combined with estrogens in postmenopausal women provides more improvement in psychologic and sexual symptoms than does estrogen alone (Sarrel 1999).

14.2.4 Corticosteroids

Corticosteroids, such as glucocorticoids and mineralocorticoids, are produced by the adrenal glands, liver, and during pregnancy by placenta and maternal glands. In stressful conditions, the glucocorticoid, cortisol, is rapidly synthesized and secreted in response to adrenocorticotrophic hormone released from the pituitary and corticotrophin-releasing hormone secreted by the hypothalamus. Cortisol stimulates the production of energy-rich compounds such as glucose, free fatty acids, and amino acids. The mineralocorticoid aldosterone is produced in response to angiotensin II and promotes sodium reabsorption and fluid retention. Besides their role in glucose and mineral metabolism, corticosteroids are also implicated in the regulation of sleep, ingestive behavior, behavioral adaptation, learning, and memory. In addition, corticosteroid receptors play a significant role in brain damage, aging (De Kloet et al. 1986), mood, mental performance, and the pathogenesis of neuropsychiatric disorders, such as depression and Alzheimer's disease (McEwen and Sapolsky 1995; Sapolsky 2004). Both cortisol and aldosterone release are controlled by the hypothalamic-pituitary-adrenal (HPA) axis. The HPA axis is a neuroendocrine system that has complex interactions with brain serotonergic, noradrenergic, and dopaminergic systems. An important role of the HPA axis is the regulation of the body's response to stress. Overactivity of the HPA axis or enlargement of the pituitary or adrenal gland causes an increase in cortisol levels, which in turn leads to hypercortisolemia. The overactivity of the HPA axis in stressful conditions may lead to dysregulation of the serotonergic system and is one of the most important predictors of suicide attempts in depressed patients (Pompili et al. 2010). Depression, on the other hand, is one of the major causes of hypercortisolemia, characterized by increased cortisol levels. Hypercortisolemia may lead to neurotoxicity and reduced neurogenesis in the hippocampus in depressed patients (Sapolsky 1996).

14.3 Steroid Hormone Receptors in Brain Disorders

Steroid hormones exert their biological effects through specific steroid hormone receptors (SHR) that are expressed by the target cells. To date, two estrogen receptor subtypes (ER alpha and ER beta) with several isoforms (Koike et al. 1987; Kuiper et al. 1996; Ma 2000; Menuet et al. 2002), two progesterone receptors (PR) subtypes (PR_A and PR_B) with several splice variants (Brinton et al. 2008; Misrahi et al. 1987), and two types of androgen receptor (AR) subtypes have been identified (AR_A and AR_B) (Chang et al. 1988; Wilson and McPhaul 1994). The corticosteroid receptors may be divided into two classes: mineralocorticoid receptors (MR) (Arriza et al. 1987) and glucocorticoid receptors (GR) (Hollenberg et al. 1985). All SHR share similar functional domains but differ in the length of the amino acid chain (Fig. 14.2).

In steroid-responsive cells, SHR are mainly present in the cytoplasm and the nucleus, although SHR are also found on the cell membrane (Jensen et al. 1968; Walsh et al. 1990). When SHR are activated by the corresponding steroid hormone, they dimerize and move into the nucleus of the cell, where they bind to hormone-responsive element in the promoter region of specific target genes. SHR may act as transcriptional activators or transcriptional repressors, resulting in the induction or suppression of the expression of hormone-responsive genes. These responsive genes may evoke a wide variety of physiological responses. Some rapid actions of estrogens and progestins are directly mediated by cell surface receptors in a non-genomic manner (Fig. 14.3). Although the involvement of steroid hormones in various brain disorders has been demonstrated, the mechanisms with which they exert their effects are still largely unknown.

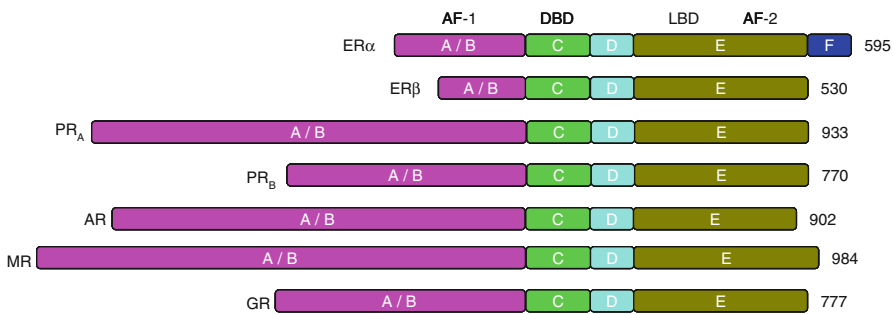


Fig. 14.2 Functional domains of steroid hormone receptors (SHR). All the SHRs consists of common structural domains, in particular an N-terminal transcription activation-1 domain (A/B), which regulates the ligand-independent transcription; a DNA binding domain (C) which recognizes and binds with the steroid hormone response elements on DNA; a flexible hinge domain (D) which carries information for the posttranscriptional modification; and a multifunctional ligand binding domain (E) which recognizes and binds the ligand and acts as a ligand-dependent transcription activation function. Numbers represent the number of amino acids in each receptor. ER alpha contains an extra region (F). ER estrogen receptor, PR progesterone receptor, AR androgen receptor, MR mineralocorticoid receptor, GR glucocorticoid receptor, AF activation function, DBD DNA-binding domain, LBD ligand binding domain

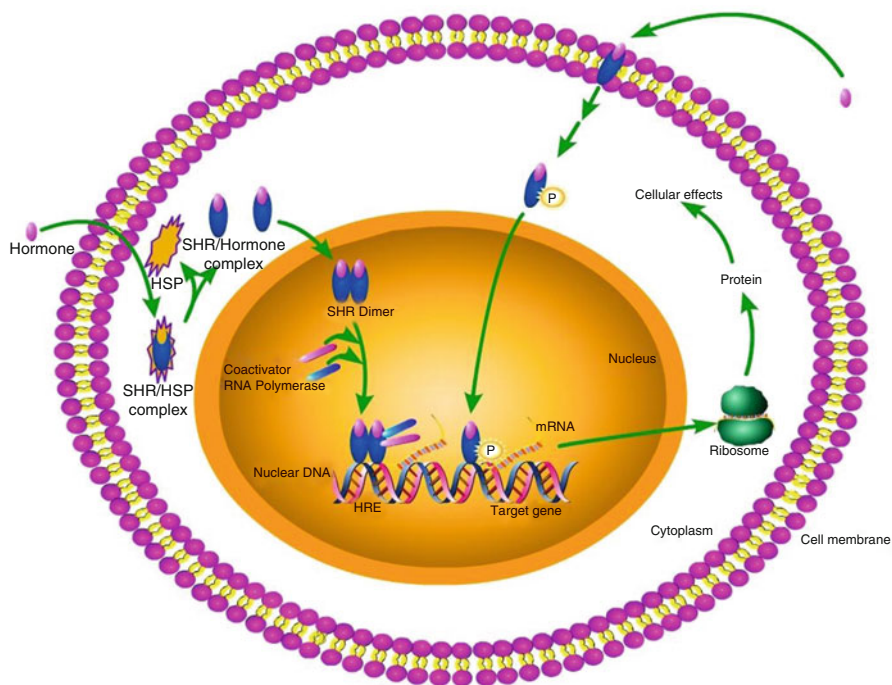


Fig. 14.3 Mode of action of steroid hormone receptors. All the steroid hormone receptors mediate their action by a common genomic pathway. In the cytoplasm, they exist as complexes with heat shock proteins in an inactive form. When a steroid hormone binds, the receptor complex releases the heat shock proteins and becomes activated. The activated receptor forms a homodimer or heterodimer, which subsequently enters into the nucleus. The dimer binds to the specific hormone response element in DNA and initiates or inhibits the process of gene transcription

Western blotting and immunohistochemical studies in experimental animals and postmortem human brains have shown that receptors for different steroid hormones are expressed in different regions of the brain. ER, PR, and AR are expressed in those brain areas that are associated with emotion, cognition, and behavior, such as the hypothalamus, amygdala, cerebral cortex, hippocampus, and brainstem. This expression pattern is in agreement with the association of sex hormones with psychiatric disorders. The neuroprotective effects of estrogens are mainly due to ER alpha-mediated signaling (Ooishi et al. 2012), whereas the effect on mood and cognitive functions in depression and schizophrenia is mainly mediated by ER beta (Foster 2012). A study on patients with depression or schizophrenia, who committed suicide, showed downregulation of ER beta expression in the limbic system (Ostlund et al. 2003). To our knowledge, no data exist on altered expression of PR and AR in the human brain in mood and behavioral disorders.

Not only SHR expression, but also polymorphisms in the SHR genes were found to be implicated in psychiatric diseases. SHR polymorphisms have been associated with an increased risk for schizophrenia, depression, anxiety traits, and cognitive

impairment. Association of polymorphisms in estrogen and androgen receptors associated with psychiatric disorders has been reviewed recently by Westbert and Eriksson (2008).

Corticosteroids affect behavioral changes by engaging with either MR or GR. MR are mainly expressed in the limbic system, hypothalamus, and circumventricular organs and to lesser extent in other parts of the brain. The expression of GR, on the other hand, is mainly observed in the subfields of the cerebral cortex, olfactory cortex, hippocampus, amygdala, dorsal thalamus, hypothalamus, cerebellar cortex, trapezoid body, locus coeruleus, and dorsal raphe nucleus in rats (Morimoto et al. 1996). Both the corticosteroid receptors are co-expressed in the hippocampus, amygdala, inferior frontal gyrus, cingulate gyrus, and nucleus accumbens in human brain, whereas predominantly MR were found in the hippocampus (Klok et al. 2011). A reduction in both MR and GR expression and an increase in corticosteroid levels were observed in the brains of patients with bipolar disorder or schizophrenia who committed suicide and in subjects exposed to stressful conditions (Xing et al. 2004). Furthermore, decreased MR expression in the hippocampus of suicide victims was observed in another study (López et al. 1998). Decreased MR expression was also demonstrated in depressed subjects after treatment with the MR antagonist, spironolactone. Spironolactone treatment led to an increase in cortisol levels in both controls and depressed patients. However, in depressed patients, cortisol levels were significantly higher than in controls (Young et al. 2003).

Increased production of the cortisol also causes desensitization of the GR, resulting in a downregulation of these receptors. Downregulation of GR in turn leads to an increase in the levels of cortisol (Hansen-Grant et al. 1998). Prolonged stress has been reported to downregulate the expression of GR in the prefrontal cortex in rats (Chiba et al. 2012). Likewise, stress leads to a reduction in the GR mRNA in the basolateral/lateral nuclei in patients with schizophrenia or bipolar disorder (Perlman et al. 2004, 2007).

14.4 Imaging of Steroid Hormone Receptors

Hitherto, almost all information about the role of SHR in healthy and diseased brain is obtained from experimental animals and postmortem human studies, because brain biopsy in patients is generally not feasible or highly undesirable. To better understand the role of steroid hormones in neurodegenerative and psychiatric diseases, it is therefore of invaluable importance to have a noninvasive tool to measure the expression of SHR in the brain. PET and SPECT are noninvasive nuclear imaging techniques that allow measurement of receptor expression and receptor occupancy in the living brain. Until now, several PET and SPECT tracers have been developed to image the SHR. Most of these radiopharmaceuticals, however, were developed for applications in oncology, in particular for imaging of receptor expression and occupancy in steroid hormone-sensitive tumors like breast and prostate cancer (Hospers et al. 2008; De Vries et al. 2007). So far, only a few studies on imaging of SHR in the brain have been reported. However, it is expected that most

radiopharmaceuticals that have been developed for tumor imaging may also be applied in brain imaging. Although many tracers have been described for each SHR, most of these tracers did not provide satisfactory results and consequently did not enter clinical studies. In the following paragraphs, we will not provide a complete overview of all tracers for SHR that have been reported, but only discuss the most promising candidate tracers for PET and SPECT imaging of SHR in the brain.

14.4.1 Radiopharmaceuticals for Estrogen Receptor Imaging

ER is the most widely studied SHR. Although literature exists on Western blotting and in situ hybridization studies to determine the expression of the ER in the rodent brain, hardly any data exists on ER expression in the human brain. For this purpose, imaging methods to measure ER expression could certainly be of added value. Several tracers have been developed for PET and SPECT imaging of ER, in particular for imaging breast cancer.

14.4.1.1 PET

16Alpha-[¹⁸F]fluoro-17beta-estradiol ([¹⁸F]FES) was introduced for imaging of ER in the 1980 and is now used in both clinical trials and in patient care for diagnosis and monitoring of anticancer treatment efficacy in ER-positive breast cancer. In rats and mice, highest [¹⁸F]FES uptake was observed in tissues with high ER expression, such as the uterus and ovaries (Aliaga et al. 2004; Kiesewetter et al. 1984; Sasaki et al. 2000; Seimbille et al. 2002; Yoo et al. 2005). [¹⁸F]FES uptake in ER-rich organs could be blocked with unlabeled estradiol in a dose-dependent manner, indicating that the tracer uptake is ER-mediated (Katzenellenbogen et al. 1993). A recent study demonstrated that treatment with fulvestrant, an irreversible ER antagonist, also reduced the uptake of [¹⁸F]FES in ER-positive breast tumors in mice (Fowler et al. 2012). PET imaging studies in rodents showed a good correlation of [¹⁸F]FES tumor uptake with ER density, as determined in vitro (Aliaga et al. 2004). In breast cancer patients, [¹⁸F]FES PET has been applied successfully to determine the ER status of tumor lesions. ER expression was clearly visualized in primary breast tumors and in metastases. The accumulation of [¹⁸F]FES in these tumors correlated well with ER density, as determined by immunohistochemistry (Dehdashti et al. 1995; Mintun et al. 1988). The radiation burden associated with [¹⁸F]FES PET is within the normal range of other clinical nuclear medicine procedures: a typical dose of 200 MBq (6 mCi) causes a radiation burden to the patient of 4.4 mSv (Mankoff et al. 2001; Mortimer et al. 1996; Peterson et al. 2008). [¹⁸F]FES preferentially binds to the alpha subtype of the ER, as its affinity is 6.3-fold higher for ER alpha than for ER beta (Yoo et al. 2005). ER alpha is overexpressed in many breast tumors, where it is associated with tumor growth and development. The ER beta isoform was found to be co-expressed with ER alpha in breast tumors (Dotzlaw et al. 1997; Järvinen et al. 2000), but the function of ER beta in breast cancer is not well understood yet. The discovery of ER beta in breast cancer initiated the search for ER beta-selective PET tracers. Several attempts have been made to develop ER

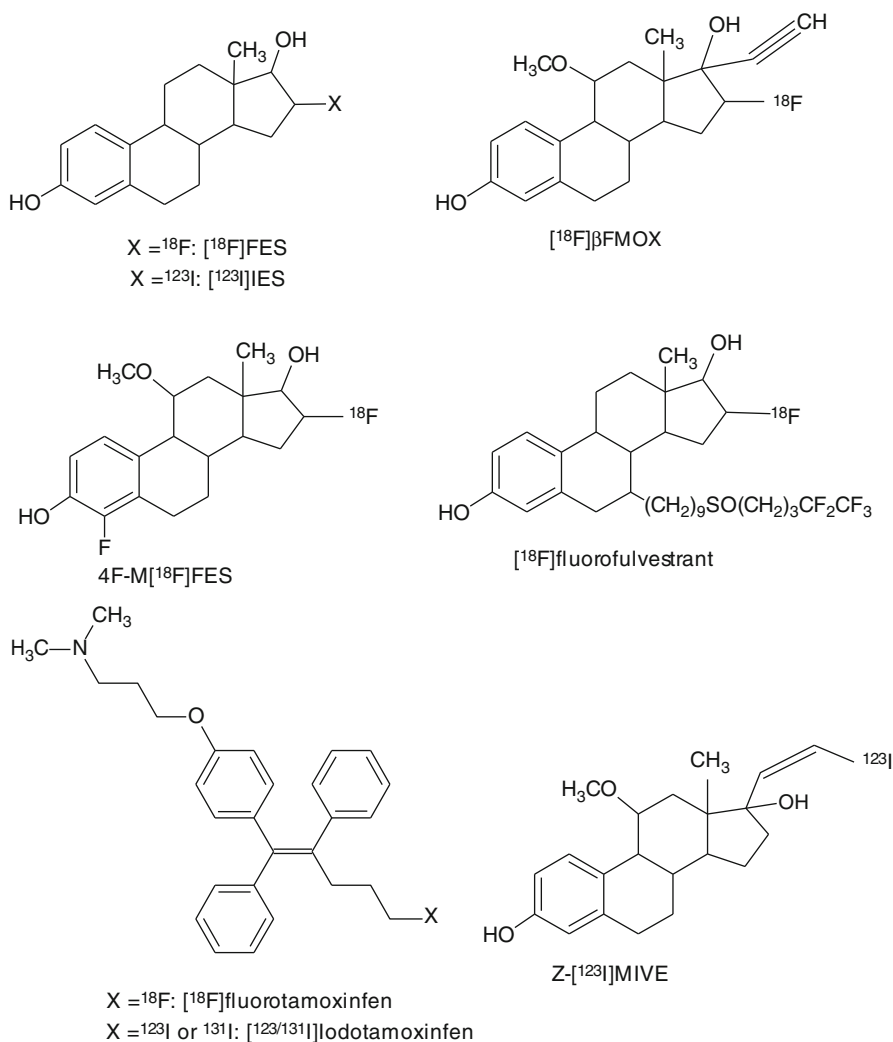


Fig. 14.4 Chemical structures of tracers that have been evaluated for PET or SPECT imaging of estrogen receptors

beta-selective tracers. Recently, 8beta-(2-[^{18}F]fluoroethyl)estradiol (8beta-[^{18}F]FEE), a derivative of the potent ER beta-selective steroid 8beta-vinylestradiol, was evaluated as a selective PET tracer for ER beta. In addition, the nonsteroidal ER beta ligand ERB-041 was labeled with ^{76}Br , yielding [^{76}Br]BrERB-041 as a potential ER beta-selective PET tracer. Although both 8beta-[^{18}F]FEE and [^{76}Br]BrERB-041 showed high binding affinities in a radiometric assay, ex vivo biodistribution studies in rats and mice could not demonstrate ER beta-mediated uptake (Lee et al. 2012). So far, no suitable PET tracer of imaging of ER beta is available.

Besides [^{18}F]FES, several radiolabeled estradiol derivatives and ER-targeting anticancer drugs have been evaluated as candidate PET tracers for imaging ER density and occupancy (Fig. 14.4). The potent estrogen 17 α -ethynyl-11 β -methoxy-estradiol ([^{18}F]betaFMOX) showed promising results in rodents with a fourfold higher uptake in immature rat uterus than [^{18}F]FES. [^{18}F]betaFMOX was considered to be a highly sensitive tracer for imaging of the ER, as [^{18}F]betaFMOX also exhibited specific binding in organs with low ER density, such as the kidney, muscle, and thymus (VanBrocklin et al. 1993a, b). Despite the promising results in rodents, [^{18}F]betaFMOX PET studies failed to detect ER-positive lesions in human breast cancer patients. This lack of sensitivity in humans may be due to the fast metabolism of the tracer, because it exhibited low binding to sex hormone-binding protein (SHBG), which protects steroids from metabolic degradation (Jonson et al. 1999). Other ethynyl analogues of FES also showed better target-to-background ratios but were also associated with faster degradation *in vivo*, because of low SHBG binding (VanBrocklin et al. 1992).

In order to increase the binding affinity and *in vivo* stability of the tracer, several analogues of [^{18}F]FES were developed. One of these candidates, 11 β -methoxy-4,16 α -[^{18}F]difluoroestradiol (4F-M[^{18}F]FES), showed high uptake and high target-to-background ratios in ER-rich organs like the uterus (VanBrocklin et al. 1994). 4F-M[^{18}F]FES has a low affinity towards the SHBG, but studies in humans showed a significant, potentially ER-mediated uterus uptake in both pre- and postmenopausal women (Beauregard et al. 2009). However, no other human studies with 4F-M[^{18}F]FES have been published since.

In addition to estradiol derivatives, radiolabeled derivatives of anticancer drugs, such as tamoxifen and fulvestrant, were evaluated for imaging of ER. Tamoxifen is a partial agonist of the ER and used as a drug in the treatment of ER-positive breast cancer. ^{18}F -labeled tamoxifen, [^{18}F]fluoromethyl-*N,N*-dimethyltamoxifen ([^{18}F]FTX), exhibited specific uptake in the uterus and mammary tumors, which could be blocked with an excess of estradiol (Yang et al. 1994). In a clinical study in 10 ER-positive breast cancer patients, [^{18}F]FTX uptake appeared to correlate with tamoxifen treatment outcome (Inoue et al. 1996). So far, no additional studies have been performed to prove the clinical utility of [^{18}F]FTX. Labeling of fulvestrant, a full antagonist of the ER, with ^{18}F reduced its binding affinity. Consequently, ^{18}F -labeled fulvestrant is not suitable for PET imaging of ER (Seimille et al. 2004).

14.4.1.2 SPECT

In addition to PET tracers, some SPECT tracers were developed for imaging of ER (Fig. 14.4). Amongst the promising SPECT tracers for ER was 16 α -[^{125}I]iodo-11 β -methoxy-17 β -estradiol ([^{125}I]MIE) (Zielinski et al. 1986). In rodents, [^{125}I]MIE was found to accumulate in ER-rich areas, such as the uterus. [^{125}I]MIE showed higher uterus-to-blood ratios than 16 α -[^{125}I]iodoestradiol. 16 α -[^{123}I]iodo-17 β -estradiol ([^{123}I]IES) and (20 Z)-11 β -methoxy-17 α -[^{123}I]iodovinylestradiol (*Z*-[^{123}I]MIVE) have not only been applied in animals but also in clinical studies. [^{123}I]IES showed ER-mediated uptake in the rabbit reproductive system and in ER-positive tumors in breast cancer patients, but no specificity or

sensitivity data were reported (Kenady et al. 1993; Pavlik et al. 1990; Scheidhauer et al. 1991; Schober et al. 1990). Both stereoisomers of [^{123}I]MIVE were evaluated for ER imaging. (Z)-[^{123}I]MIVE showed highest ER-mediated specific uptake in rodents and in clinical studies in breast cancer patients. The tracer uptake could be blocked by saturation of the ER with tamoxifen (Bennink et al. 2001, 2004; Rijks et al. 1997a, b). Although both [^{123}I]IES and (Z)-[^{123}I]MIVE showed ER-mediated specific uptake, these tracers also displayed fast metabolism and low SHBG binding (Nachar et al. 1999; Rijks et al. 1998b). For both tracers, no further studies are available to support their utility for brain imaging.

Attempts have been made to generate a SPECT tracer for ER by labeling derivatives of the anticancer drug tamoxifen. In rodents, the uptake of [^{123}I]iodotamoxifen ([^{123}I]TAM) was found to be high in ER-rich organs. In clinical studies, [^{123}I]TAM showed ER-specific uptake in breast tumors (Hanson and Seitz 1982; Van de Wiele et al. 2001). Recently tamoxifen was also labeled with ^{131}I ([^{131}I]TAM). Biodistribution studies in rodents proved that the uptake of this tracer was ER-mediated in the uterus and breast tissue (Muftuler et al. 2008). No further studies on iodine-labeled tamoxifen have been published lately.

Estradiol and anticancer drug derivatives have also been labeled with $^{99\text{m}}\text{Tc}$. A few of them have even been successfully evaluated in rodents (Arterburn et al. 2003; Nayak et al. 2008; Ramesh et al. 2006; Takahashi et al. 2007a, b; Yurt et al. 2009; Zhu et al. 2010). However, the usefulness of these tracers for brain imaging would be questionable, because of the high hydrophilicity of the $^{99\text{m}}\text{Tc}$ conjugates, which likely precludes efficient brain penetration.

Consequently, at this moment [^{18}F]FES remains the only validated tracer for molecular imaging of ER expression that is currently used in clinical studies. Even though its characteristics are not ideal, [^{18}F]FES still is an adequate tracer for PET imaging of ER in humans (Van Kruchten et al. 2012). Efforts to develop better alternatives for [^{18}F]FES are still made but yielded disappointing results so far.

14.4.2 Radiopharmaceuticals for Progesterone Receptor Imaging

14.4.2.1 PET

A few substrates of PR have been labeled with ^{18}F , ^{76}Br , ^{123}I , and ^{125}I for imaging of PR with PET and SPECT (Fig. 14.5). The ^{18}F -labeled candidate PET tracers for PR include 21-[^{18}F]fluoro-16 α -ethyl-19-norprogesterone ([^{18}F]FENP) (Dehdashti et al. 1991; Jonson and Welch 1998; Pomper et al. 1988; Verhagen et al. 1991a), 21-[^{18}F]fluoro-16 α -methyl-19-norprogesterone ([^{18}F]FMNP) (Verhagen et al. 1991b), and 21-[^{18}F]fluoro-16 α ,7 α -[(R)-(1' α -furylethylidene)dioxy]-19-norpregn-4-ene-3,20-dione (Buckman et al. 1995). [^{18}F]FMNP exhibited PR-mediated uptake in the uterus and tumors in rats (Verhagen et al. 1991b), but no further studies in humans were reported. [^{18}F]FENP showed highly selective PR-mediated uptake in the uterus of estrogen-primed rats (Pomper et al. 1988) and in PR-positive carcinoma in mice (Verhagen et al. 1991a). In eight breast cancer patients, however, [^{18}F]FENP could only detect 50 % of PR-positive lesions, and

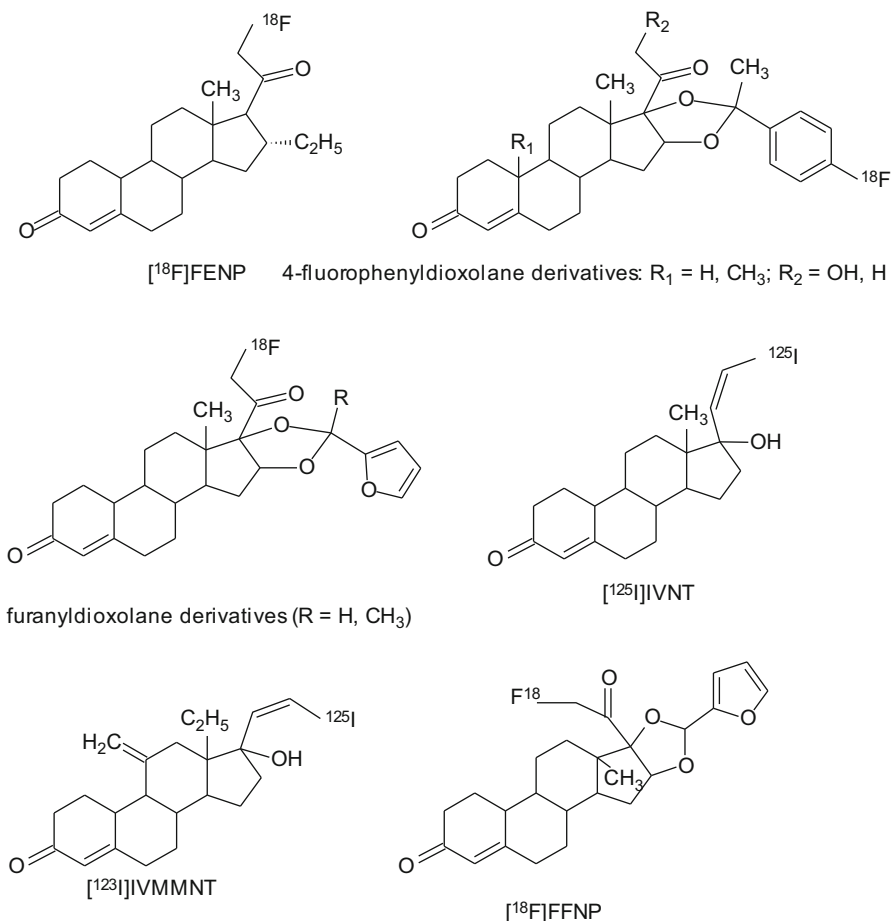


Fig. 14.5 Chemical structures of tracers that have been evaluated for PET or SPECT imaging of progesterone receptors

tracer uptake did not correlate with PR expression (Dehdashti et al. 1991). The major reason for failure of [¹⁸F]FENP in clinical studies was its extensive metabolism in humans (Verhagen et al. 1994). To overcome this problem, several ketals of 16 α ,17 α -dihydroxyprogesterone were labeled with positron-emitting isotopes (Buckman et al. 1995; Vijaykumar et al. 2002; Zhou et al. 2006). One of these ketals is 21-¹⁸F-fluoro-16 α ,17 α -[(R)-(1'- α -furylmethylidene)dioxy]-19-norpregn-4-ene-3,20-dione ([¹⁸F]FFNP). In a study performed in mice with mammary tumors, treatment with estradiol, letrozole, or fulvestrant showed treatment-induced changes in the uptake of [¹⁸F]FFNP, suggesting that early evaluation of response to the anticancer treatment could be feasible (Fowler et al. 2012). Recently, a study in breast cancer patients showed that [¹⁸F]FFNP PET is a safe, noninvasive method to evaluate the tumor's PR status in vivo (Dehdashti et al.

2012). Brain uptake of [^{18}F]FFNP seems to be acceptable, but further studies are needed to prove its suitability for brain imaging.

Another series of candidate PET tracers for PR imaging were the derivatives of the nonsteroidal PR agonist tanaproget. Several derivatives of tanaproget were evaluated (Zhou et al. 2010), and 4-[^{18}F]fluoropropyl-tanaproget ([^{18}F]FPTP) demonstrated highest uptake in the target tissues like uterus and ovaries. The biodistribution pattern of [^{18}F]FPTP in rats was comparable with other PR tracers, such as FENP and FFNP (Lee et al. 2010).

14.4.2.2 SPECT

A few iodinated tracers for PR imaging have been developed, but none of these candidate tracers showed promising results. (20Z)-17alpha-[^{125}I]iodovinyl-19-nortestosterone ([^{125}I]IVNT) had interesting binding properties but lacked selectivity in vivo (Ali et al. 1994). Later, both isomers of 17alpha-iodovinyl-18-methyl-11-methylene-19-nortestosterone ([^{123}I]IVMMNT) were investigated in rats and rabbits. (Z)-[^{123}I]IVMMNT displayed highest in vivo binding in target organs, such as in uterus and ovaries. The uptake of (Z)-[^{123}I]IVMMNT was found to be PR-mediated (Rijks et al. 1998a). So far, no human data exist to prove the feasibility of PR imaging with these tracers.

At the moment, [^{18}F]FFNP seems to be the most promising candidate tracer for imaging PR, but more studies are required to validate the utility of this tracer in humans.

14.4.3 Radiopharmaceuticals for Androgen Receptor Imaging

14.4.3.1 PET

The existing PET tracers for imaging AR expression are depicted in Fig. 14.6. 20-[^{18}F]fluoromibolone (20-[^{18}F]Fmib) was the first radiolabeled PET tracer for AR that showed promising uptake in the prostate of diethylstilbestrol (DES)-primed rats (Liu et al. 1991). Several other fluorinated compounds have been developed, and some of them showed promising results, such as 16beta-[^{18}F]fluorodihydrotestosterone ([^{18}F]FDHT), 16beta-[^{18}F]fluorotestosterone (16beta-[^{18}F]FT), 16beta-[^{18}F]fluoro-7alpha-methyl-19-nortestosterone (16beta-[^{18}F]FMNT), 16alpha-[^{18}F]fluoro-7alpha-methyl-19-nortestosterone (16alpha-[^{18}F]FMNT), and 20-[^{18}F]fluorometribolone (20-[^{18}F]R1881) (Liu et al. 1992). Most of these tracers showed quick clearance from the body and rapid metabolism. Best results in baboons and rats were obtained for [^{18}F]FDHT. Uptake of [^{18}F]FDHT in the prostate was specific and AR-mediated. Metabolism of [^{18}F]FDHT was slower than metabolism of the other candidate tracers (Bonasera et al. 1996; Choe et al. 1995). [^{18}F]FDHT was able to detect AR-positive tumor lesions in prostate cancer patients, and tracer uptake was proven to be AR-mediated in humans as well (Dehdashti et al. 2005; Larson et al. 2004). Another interesting candidate PET tracer is 7alpha-[^{18}F]fluoro-17-methyl-5-dihydrotestosterone ([^{18}F]FMDHT), although the first results reported for this tracer were not very promising. The uptake of [^{18}F]FMDHT in the prostate

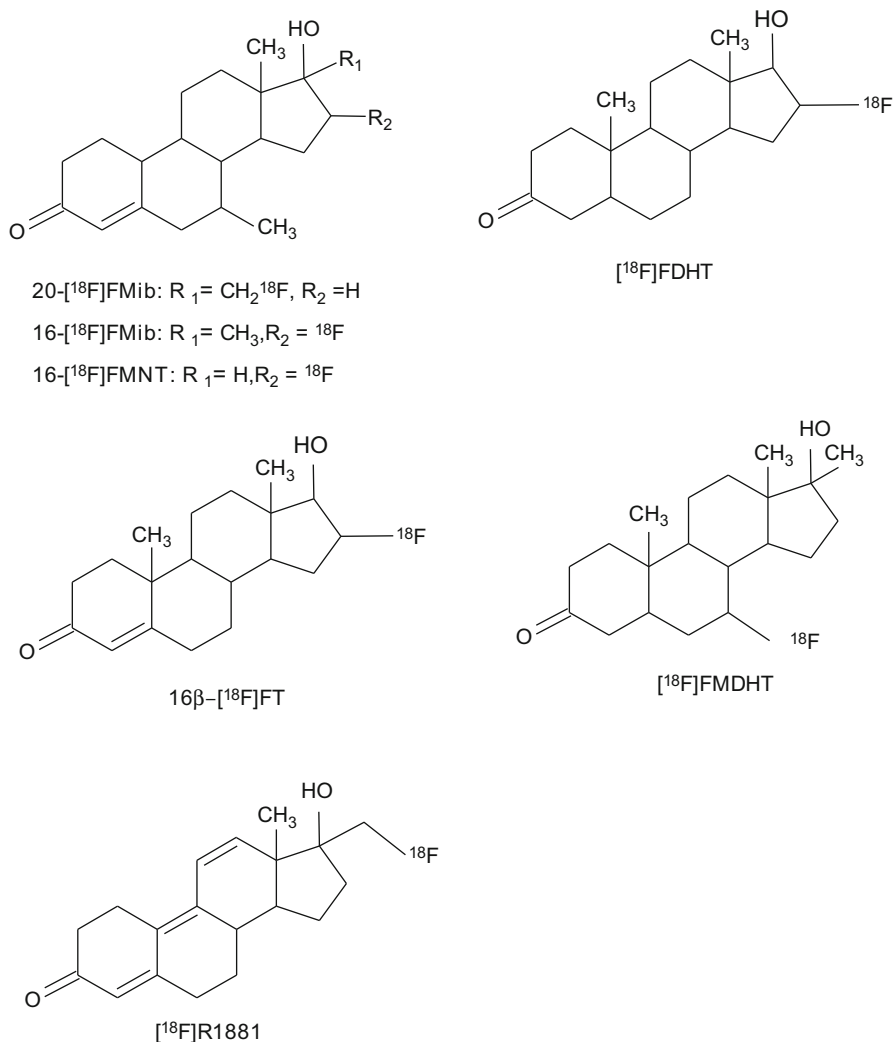


Fig. 14.6 Chemical structures of tracers that have been evaluated for PET or SPECT imaging of androgen receptors

was low; results were not reproducible and not comparable with other labeled steroids like $[^{18}\text{F}]\text{FDHT}$. In these first experiments, $[^{18}\text{F}]\text{FMDHT}$ was investigated in rats treated with DES to suppress endogenous testosterone production (Garg et al. 2001). The same authors reevaluated the suitability of $[^{18}\text{F}]\text{FMDHT}$ for AR imaging in chemically castrated rats. In this animal model, uptake in the prostate was proven to be AR-mediated. Prostate uptake was comparable to other ^{18}F -labeled steroids and twofold higher than $[^{18}\text{F}]\text{FMDHT}$ uptake in DES-treated rats (Garg et al. 2008).

Currently, [^{18}F]FDHT is the only PET tracer that has proceeded into the clinical evaluation phase (Beattie et al. 2010; Dehdashti et al. 2005; Larson et al. 2004; Zanzonico et al. 2004). The radiation burden associated with [^{18}F]FDHT PET is within the normal range of other clinical nuclear medicine procedures: 0.018 mSv/MBq; for the maximum administered dose of 331 MBq, the total radiation burden is 6.0 mSv. The major drawback of [^{18}F]FDHT is its rapid metabolism. This led to the investigation of nonsteroidal derivatives with better in vivo stability, like propanamide derivatives a selective androgen receptor modulator (SARM) with ^{11}C (Gao et al. 2011).

Some nonsteroidal antagonists of AR have been radiolabeled, such as a ^{11}C -labeled diethylamine flutamide derivative (Jacobson et al. 2006), a ^{18}F -labeled hydroxyflutamide derivative (Jacobson et al. 2005), 3- ^{76}Br]bromohydroxyflutamide (Parent et al. 2006), [^{18}F]bicalutamide, 4- ^{76}Br]bromobicalutamide, and ^{76}Br]bromo-thiobicalutamide (Parent et al. 2007). However, none of these compounds showed promising results that warranted further evaluation.

14.4.3.2 SPECT

The radioiodinated steroid 2alpha- ^{125}I]dihydrotestosterone was the first SPECT tracer showing high uptake in AR-rich organs like the prostate, epididymis, and testis in rats. Pretreatment with dihydrotestosterone reduced the uptake in these organs, suggesting that tracer uptake is specific and AR-mediated (Tarle et al. 1981). 7alpha- ^{125}I]iodo-5alpha-dihydrotestosterone (7alpha- ^{125}I]IDHT) is another analogue of testosterone that was labeled with ^{125}I . 7alpha- ^{125}I]IDHT showed AR-mediated uptake in the prostate of rats. In vitro autoradiography of 7alpha- ^{125}I]IDHT produced excellent autoradiograms with low nonspecific binding in the prostate of rats (Labaree et al. 1997), but no further studies were published to demonstrate the use of this tracer in vivo.

Some steroid and flutamide derivatives have been labeled with $^{99\text{m}}\text{Tc}$ and tested as SPECT tracers for AR. However, in vivo evaluation in rats did not show any AR-mediated specific binding for any of these compounds (Dallagi et al. 2010; Dhyani et al. 2011).

So far, [^{18}F]FDHT is the only AR tracer that has proceeded into the clinical evaluation phase. Clinical studies confirmed that this tracer is suitable for AR imaging in cancer patients. However, it still remains to be evaluated whether [^{18}F]FDHT PET is also able to monitor AR expression in the human brain. Preclinical data of [^{18}F]FMDHT suggest that it might have favorable characteristics for AR imaging as well, but further evaluation is still required to establish the merit of this tracer.

14.4.4 Radiopharmaceuticals for Corticoid Receptor Imaging

14.4.4.1 Radiopharmaceuticals for Glucocorticoid Receptor Imaging

So far, only a few GR ligands have been synthesized and evaluated for the potential use as imaging tracer (Fig. 14.7). Most of these candidate tracers showed disappointing results in rodents and baboons. The first labeled compound that was introduced as ligand for the imaging of GR was 21- ^{18}F]fluoroprednisone. 21- ^{18}F]

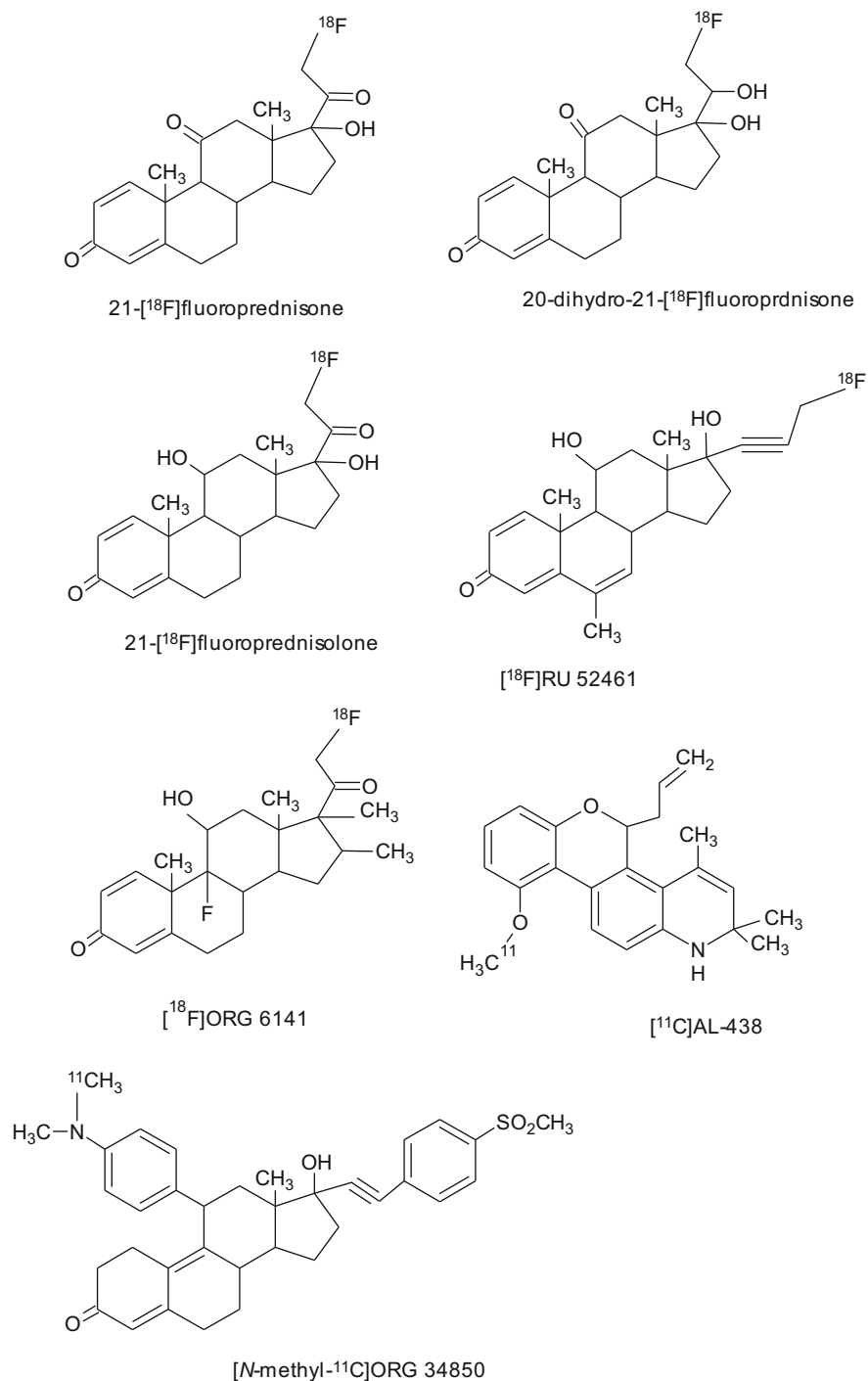


Fig. 14.7 Chemical structures of tracers that have been evaluated for PET or SPECT imaging of glucocorticoid receptors

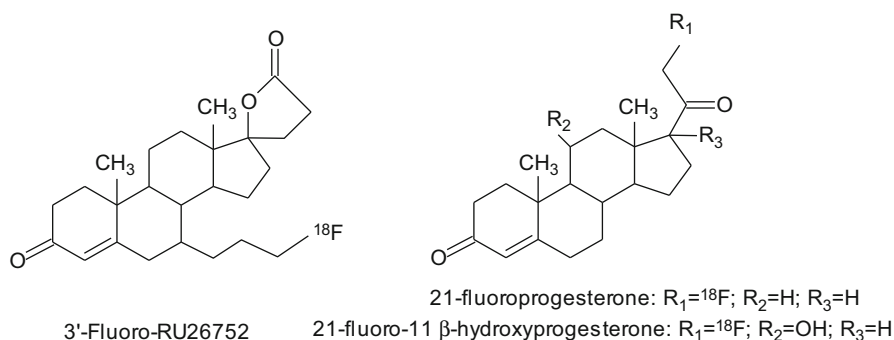


Fig. 14.8 Chemical structures of tracers that have been evaluated for PET imaging of mineralocorticoid receptors

floroprednisone was rapidly metabolized, leading to low uptake in rat brain (Feliu and Rottenberg 1987).

The biodistribution of [^{18}F]RU 52461, an analogue of the selective GR agonist RU28362, showed high GR-mediated uptake in the adrenals and pituitary in rats. PET imaging studies in baboons, however, showed low uptake of [^{18}F]RU 52461 in the brain (Dasilva et al. 1992). In another study in rats, [^{18}F]RU 52461 uptake in the hippocampus could only be partially blocked with an excess of the unlabeled ligand, whereas complete blocking of tracer uptake in peripheral organs was observed (Pomper et al. 1992).

The potent GR ligand [^{18}F]ORG 6141 was evaluated in adrenalectomized and sham-operated rats. Ex vivo biodistribution 3 h postinjection revealed higher uptake of tracer in the hippocampus and brain stem of adrenalectomized animals as compared to sham-operated controls. However, GR-mediated specific retention of activity in these brain areas could not be demonstrated (Visser et al. 1995).

Wuest et al. synthesized a series of novel 4-fluorophenylpyrazolo steroids and tested their binding affinities to GR. Some of these compounds showed binding affinities up to 56 % relative to dexamethasone (100 %) (Wüst et al. 2003). One of these compounds, 2'-(4-fluorophenyl)-21- ^{18}F -20-oxo-11 β ,17 α -dihydroxy-pregn-4-eno[3,2-c]pyrazole, was evaluated in rats using autoradiography and small animal PET imaging. Brain uptake of this tracer was found to be constant between 5 and 60 min after tracer injection. However, brain uptake was not specifically GR-mediated (Wüst et al. 2005), but only due to nonspecific binding.

The high-affinity GR antagonist Org 34850 was labeled with ^{11}C . [N-methyl- ^{11}C]Org 34850 was found to rapidly metabolize in rats. Ex vivo biodistribution and small animal PET studies demonstrated that [N-methyl- ^{11}C]Org 34850 was not able to penetrate the blood-brain barrier (Wuest et al. 2009).

The nonsteroidal selective GR modulator AL-438 was labeled with ^{11}C . The biodistribution of [^{11}C]AL-438 showed high uptake in the pituitary and the brain, but treatment with a high dose of the GR antagonist corticosterone did not result in any blocking of tracer uptake, suggesting that the uptake was not GR-mediated (Wuest et al. 2007).

Thus, none of the aforementioned studies were successful, and consequently suitable tracers for imaging GR expression are currently not available.

14.4.4.2 Radiopharmaceuticals for Mineralocorticoid Receptor Imaging

There is only one report that describes a series of MR-specific compounds that have been labeled with fluorine-18 for PET imaging. These compounds include 21-[¹⁸F] fluoroprogestosterone, 21-[¹⁸F]fluoro-11beta-hydroxyprogesterone, and 3'-fluoro-RU 26752 (Fig. 14.8). Unfortunately, none of these compounds displayed the characteristics that are required for PET imaging of MR (Pomper et al. 1992).

14.5 Imaging of Steroid Hormone Receptors in the Brain

Despite several tracers for imaging of SHR have now been applied in humans, hardly any studies on imaging of these receptors in the brain have been published. So far, only tracers for ER have been successfully used in rodents for imaging SHR in the brain. 16alpha-[¹²⁵I]iodoestradiol and [¹²⁵I]MIE₂ have only been used in autoradiography studies, whereas [¹⁸F]FES has also been used for ex vivo biodistribution and PET imaging of the rat brain.

An ex vivo brain autoradiography study in prepubertal Sprague Dawley rats injected with 16alpha-[¹²⁵I]iodoestradiol showed high concentrations of activity at the marginal zone of the mid-region anterior lobe of the pituitary at 1 h post tracer injection, whereas the intermediate lobe and most cells in the anterior lobe showed only a weak signal. Also the dorsocaudal paraventricular nucleus and the medial amygdaloid region showed only a weak signal, whereas a high signal was observed in preoptic neurons. Long-term exposure of the photographic plate allowed topographical recognition of tracer binding to cells in medial amygdala, mediodorsal and cortical nuclei, and the piriform cortex. However, 16alpha-[¹²⁵I]iodoestradiol uptake in the brain was not significantly blocked by an excess of unlabeled estradiol, which was ascribed to deiodination of the tracer, leading to nonspecific binding of ¹²⁵I within the myelin sheaths (Stumpf et al. 1987).

11beta-methoxy-16alpha-[¹²⁵I]iodoestradiol ([¹²⁵I]MIE₂) has been evaluated in binding and displacement studies in rat, rabbit, and human brain slices. [¹²⁵I]MIE₂ showed specific binding to the ER with no cross-reactivity with the other SHR. Moreover, a dose-dependent uptake of [¹²⁵I]MIE₂ in pituitary and brain cell nuclei was observed after in vivo administration in 25-day-old female rats (Brown et al. 1989). In another study, ER expression during the brain development was studied with [¹²⁵I]MIE₂ in mice of both sexes. This study demonstrated the presence of ER-positive cells in the early postnatal cortex and showed a profound change in the topography and number of ER-positive cells during development (Shughrue et al. 1990). Recently, the effect of long-term treatment (21–60 days) with estradiol and tamoxifen on ER occupancy in the brain was evaluated by ex vivo autoradiography with [¹²⁵I]MIE₂. The distribution of [¹²⁵I]MIE₂ uptake was in agreement with the expected ER distribution in the ovariectomized rats: highest uptake in the preoptic

and hypothalamic nuclei, followed by the amygdala, hippocampus, midbrain, and frontal cortex. In the tamoxifen-treated rats, a reduction in [125 I]MIE₂ binding was mainly seen in ER alpha-dominated regions like the cortical amygdala, central gray, and anterior paraventricular thalamus. A moderate inhibition of tracer uptake was found in the regions where both ER subtypes are expressed, like the ventrolateral-ventromedial hypothalamus, medial preoptic area, medial amygdala, and arcuate nucleus. After estradiol treatment, [125 I]MIE₂ showed a low and homogenous uptake in the brain, with an overall reduction in ER binding of 87 % as compared to untreated controls (Pareto et al. 2004).

Fluoroestradiol ([18 F]FES) is the only PET tracer that has been used to assess ER expression in rat brain. In a very detailed study, the suitability of [18 F]FES for in vivo quantification of ER was performed by both equilibrium and dynamic kinetic analysis (Moresco et al. 1995). The uptake of [18 F]FES was mainly seen in ER-rich regions in the brain, such as in the pituitary and hypothalamus. Maximum uptake was observed between 25 and 30 min postinjection reaching a pseudoequilibrium at 30 min. Blocking with increasing doses of unlabeled estradiol reduced the accumulation in the pituitary and hypothalamus in a dose-dependent manner, whereas no effect was observed in the hippocampus, cortex, and striatum. The specific binding of [18 F]FES was calculated by equilibrium analysis considering the striatum as a reference tissue where the expression of the ER was expected to be very low. The equilibrium analysis showed saturable binding in the pituitary and hypothalamus with highest binding potential (B_{\max}/K_d) in the pituitary (16.11) and hypothalamus (1.97). The B_{\max} and the K_d were found to be much higher in pituitary (124.01 ± 12.36 pmol/g and 7.70 ± 1.07) than in hypothalamus (11.85 ± 0.16 pmol/g and 6.01 ± 0.41). The in vivo quantification of ER gave similar results in the pituitary and hypothalamus when either equilibrium or graphical analysis was used (Moresco et al. 1995). In another study, the effect of long-term treatment of estradiol and tamoxifen on ER occupancy in rat brain was studied by ex vivo autoradiography with [18 F]FES. Although this study showed marked reduction in the uptake of [18 F]FES in ER-rich areas, such as the hypothalamus, preoptic area, amygdala, and frontal cortex in the treatment groups, no differences in cerebellar uptake was observed (Pareto et al. 2004).

All the aforementioned studies were performed by ex vivo measurement of tracer uptake, without the use of in vivo imaging. We recently studied the feasibility of [18 F]FES to monitor ER in the rat brain by small animal PET. The brain time-activity curves of [18 F]FES showed a quick peak uptake immediately after intravenous tracer injection, which was followed by a washout leading to a state of pseudoequilibrium after 25 min. Highest uptake was seen in the pituitary gland, followed by the hypothalamus. All other areas of the brain showed low uptake. Blocking of the receptor with an excess of estradiol resulted in a statistically significant reduction in tracer uptake only in the pituitary gland (90 %, $p < 0.001$) and hypothalamus (70 %, $p < 0.001$). A statistically significant higher volume of distribution and binding potential was found in the pituitary, when compared to other brain regions. [18 F]FES uptake was not significantly affected by differences in plasma estrogen levels.

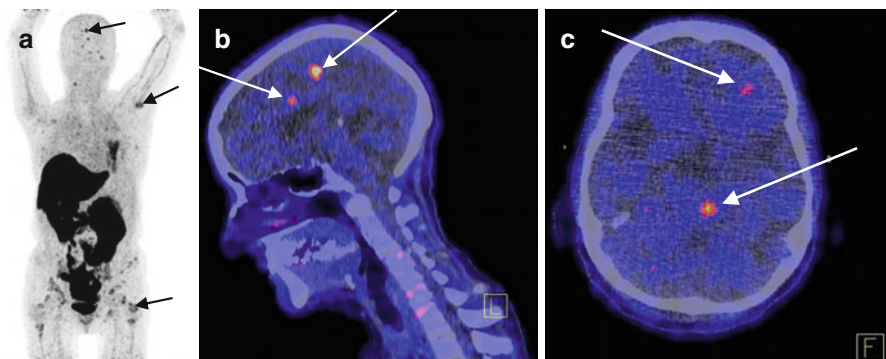


Fig. 14.9 [^{18}F]FES PET image of a patient with metastasized breast cancer. (a) Maximum intensity projection (MIP) coronal [^{18}F]FES PET image, showing the physiological uptake in the liver and normal excretion by the gallbladder and bile ducts into the intestines and some excretion via kidneys and urinary bladder. Multiple bone, lymph node, and cerebral metastases (arrows), (b) fused FES PET and CT sagittal slice showing two cerebral metastases (arrows), and (c) fused FES PET and CT transversal slice showing two cerebral metastases (arrows)

So far, [^{18}F]FES is the only tracer that was tested for *in vivo* visualization of ER in the brain of rats. [^{18}F]FES showed promising results, as it displayed highest uptake in the regions of the brain with high expression of ER. In an ongoing study in breast cancer patients at University Medical Center Groningen, it was found that [^{18}F]FES can be used to visualize the brain metastases (Fig. 14.9). But further research is necessary to validate this tracer for ER imaging in human brain. Moreover, the availability of a new ER beta-selective tracer would be highly desirable, since the different isoforms of ER have different expression patterns and different functions in neuroprotection, mood, and memory (Foster 2012; Ooishi et al. 2012).

[^{18}F]FPTP is the only tracer that could visualize PR both in humans and in experimental animals so far, but further evaluation of the tracer for brain imaging is required. More recently, [^{18}F]FFNP PET was found to be a safe, noninvasive method to evaluate tumor PR *in vivo* in patients with breast cancer. This tracer may also be of interest for brain research. [^{18}F]FDHT is the only tracer that has successfully been applied for AR imaging in humans but still needs to be validated for its use in brain imaging. Unfortunately, no selective tracers for the different isoforms of the PR and AR are available yet. No suitable tracers for GR and MR imaging are available yet either.

14.6 Conclusion and Perspectives

Despite a growing insight into several functions of SHR, many questions still remain unanswered. PET and SPECT imaging are attractive tools to investigate SHR function in the brain in living subjects. Several PET and SPECT tracers have been

already evaluated for detection of SHR in various applications in oncology, and few of them have already entered into the clinical settings. It is evident that SHR are not only associated with cancers, but they are also associated with neurological and psychiatric disorders, such as depression and neurodegenerative disorders. Research on brain SHR is still a largely unexplored area, in which these PET and SPECT tracers may be valuable tools. Tracers that are already used for diagnosis and monitoring of therapy response in hormone-sensitive cancers may probably easily be validated for applications in neurological and psychiatric disorders as well. So far, [^{18}F]FES, [^{18}F]FFNP, and [^{18}F]FDHT have been used successfully in cancer patients for imaging of ER, PR, and AR, respectively. These compounds are now available as potential tracers for imaging of SHR in the human brain. In addition, new tracers for SHR are still under development.

Development of tracers for corticoid receptors has long been attempted, but these efforts did not produce any promising results yet. When tracers for corticoid receptors finally become available, however, they will be valuable assets for research in stress, mood, and neuropsychiatric disorders that are known to be associated with overactivity of the HPA axis.

Aging and the lifestyle-associated stress are known to change SHR expression. Imaging of SHR in the brain could be a valuable tool to study the disease mechanisms associated with the age and stress-related changes in expressional levels of SHR, which can ultimately culminate into neurological and psychiatric disorders. Understanding the disease mechanism could provide a rationale for treatment regimens based on hormone replacement or the use of selective SHR modulators. PET and SPECT imaging of SHR could also be helpful in drug discovery for individual SHR-associated disorders. Based on the occupancy studies of a new drug, PET and SPECT may provide information about the amount of drug that binds to the target and about the residence time of the drug in the brain. Such information about a new drug is highly valuable for decision making in drug development and optimizing the dose and route of administration. Another benefit of PET and SPECT imaging could be patient stratification based on the receptor status of a patient before inclusion in a clinical trial. Thus, studies can be performed in a more homogenous population, which reduces variability and may reduce the costs of drug development.

In the future, PET and SPECT imaging of SHR will not only be helpful in the diagnosis of neurological and psychiatric disorders associated with altered SHR expression, but could also be instrumental in providing a better understanding of disease mechanisms and the development of new intervention strategies.

References

- Ali H, Rousseau AJ, Van Lier JE (1994) Synthesis of (17 alpha,20E/Z)iodovinyl testosterone and 19-nortestosterone derivatives as potential radioligands for androgen and progesterone receptors. *J Steroid Biochem Mol Biol* 49:15–29
- Aliaga A, Rousseau JA, Ouellette R et al (2004) Breast cancer models to study the expression of estrogen receptors with small animal PET imaging. *Nucl Med Biol* 31:761–770. doi:[10.1016/j.nucmedbio.2004.02.011](https://doi.org/10.1016/j.nucmedbio.2004.02.011)

- Arriza JL, Weinberger C, Cerelli G et al (1987) Cloning of human mineralocorticoid receptor complementary DNA: structural and functional kinship with the glucocorticoid receptor. *Science* 237:268–275
- Arterburn JB, Corona C, Rao KV et al (2003) Synthesis of 17- α -substituted estradiol-pyridin-2-yl hydrazine conjugates as effective ligands for labeling with Alberto's complex fac-[Re(OH)₂3(CO)₃]⁺ in water. *J Org Chem* 68:7063–7070. doi:10.1021/jo034780g
- Baulieu EE (1998) Neurosteroids: a novel function of the brain. *Psychoneuroendocrinology* 23:963–987
- Beattie BJ, Smith-Jones PM, Jhanwar YS et al (2010) Pharmacokinetic assessment of the uptake of 16 β -18F-fluoro-5 α -dihydrotestosterone (FDHT) in prostate tumors as measured by PET. *J Nucl Med* 51:183–192. doi:10.2967/jnumed.109.066159
- Beauregard J-M, Croteau E, Ahmed N et al (2009) Assessment of human biodistribution and dosimetry of 4-fluoro-11 β -methoxy-16 α -18F-fluoroestradiol using serial whole-body PET/CT. *J Nucl Med* 50:100–107. doi:10.2967/jnumed.108.057000
- Benedusi V, Meda C, Della Torre S et al (2012) A lack of ovarian function increases neuroinflammation in aged mice. *Endocrinology* 153:2777–2788. doi:10.1210/en.2011-1925
- Bennink RJ, Rijks LJ, Van Tienhoven G et al (2001) Estrogen receptor status in primary breast cancer: iodine 123-labeled cis-11 β -methoxy-17 α -iodovinyl estradiol scintigraphy. *Radiology* 220:774–779
- Bennink RJ, Van Tienhoven G, Rijks LJ et al (2004) In vivo prediction of response to antiestrogen treatment in estrogen receptor-positive breast cancer. *J Nucl Med* 45:1–7
- Bonaser TA, O'Neil JP, Xu M et al (1996) Preclinical evaluation of fluorine-18-labeled androgen receptor ligands in baboons. *J Nucl Med* 37:1009–1015
- Brinton RD, Thompson RF, Foy MR et al (2008) Progesterone receptors: form and function in brain. *Front Neuroendocrinol* 29:313–339. doi:10.1016/j.yfrne.2008.02.001
- Brown TJ, MacLusky NJ, Toran-Allerand CD et al (1989) Characterization of 11 β -methoxy-16 α -[125I]iodoestradiol binding: neuronal localization of estrogen-binding sites in the developing rat brain. *Endocrinology* 124:2074–2088
- Brown CM, Mulcahey TA, Filipek NC, Wise PM (2010) Production of proinflammatory cytokines and chemokines during neuroinflammation: novel roles for estrogen receptors α and β . *Endocrinology* 151:4916–4925. doi:10.1210/en.2010-0371
- Bryant C, Judd FK, Hickey M (2012) Anxiety during the menopausal transition: a systematic review. *J Affect Disord* 139:141–148. doi:10.1016/j.jad.2011.06.055
- Buckman BO, Bonaser TA, Kirschbaum KS et al (1995) Fluorine-18-labeled progestin 16 α , 17 α -dioxolanes: development of high-affinity ligands for the progesterone receptor with high in vivo target site selectivity. *J Med Chem* 38:328–337
- Chang CS, Kokontis J, Liao ST (1988) Molecular cloning of human and rat complementary DNA encoding androgen receptors. *Science* 240:324–326
- Chiba S, Numakawa T, Ninomiya M et al (2012) Chronic restraint stress causes anxiety- and depression-like behaviors, downregulates glucocorticoid receptor expression, and attenuates glutamate release induced by brain-derived neurotrophic factor in the prefrontal cortex. *Prog Neuropsychopharmacol Biol Psychiatry* 39:112–119. doi:10.1016/j.pnpbp.2012.05.018
- Choe YS, Lidström PJ, Chi DY et al (1995) Synthesis of 11 β -[18F]fluoro-5 α -dihydrotestosterone and 11 β -[18F]fluoro-19-nor-5 α -dihydrotestosterone: preparation via halofluorination-reduction, receptor binding, and tissue distribution. *J Med Chem* 38:816–825
- Corpéchet C, Synguelakis M, Talha S et al (1983) Pregnenolone and its sulfate ester in the rat brain. *Brain Res* 270:119–125
- Dallagi T, Top S, Masi S et al (2010) Synthesis and biodistribution of [99mTc]-N-[4-nitro-3-trifluoromethyl-phenyl] cyclopentadienyltricarbonyltechnetium carboxamide, a nonsteroidal antiandrogen flutamide derivative. *Metallomics* 2:289–293. doi:10.1039/b925224j
- Dasilva JN, Crouzel C, Stulzaft O et al (1992) Synthesis, tissue distribution in rats and PET studies in baboon brain of no-carrier-added [18F]RU 52461: in vivo evaluation as a brain glucocorticoid receptor radioligand. *Int J Rad Appl Instrum B* 19:167–173

- De Kloet ER, Reul JM, De Ronde FS et al (1986) Function and plasticity of brain corticosteroid receptor systems: action of neuropeptides. *J Steroid Biochem* 25:723–731
- De Nicola AF, Labombarda F, Deniselle MCG et al (2009) Progesterone neuroprotection in traumatic CNS injury and motoneuron degeneration. *Front Neuroendocrinol* 30:173–187. doi:[10.1016/j.yfrne.2009.03.001](https://doi.org/10.1016/j.yfrne.2009.03.001)
- De Vries EFJ, Rots MG, Hoppers GAP (2007) Nuclear imaging of hormonal receptor status in breast cancer: a tool for guiding endocrine treatment and drug development. *Curr Cancer Drug Targets* 7:510–519
- Dehdashti F, McGuire AH, Van Brocklin HF et al (1991) Assessment of 21-[18F]fluoro-16 alpha-ethyl-19-norprogesterone as a positron-emitting radiopharmaceutical for the detection of progesterin receptors in human breast carcinomas. *J Nucl Med* 32:1532–1537
- Dehdashti F, Mortimer JE, Siegel BA et al (1995) Positron tomographic assessment of estrogen receptors in breast cancer: comparison with FDG-PET and in vitro receptor assays. *J Nucl Med* 36:1766–1774
- Dehdashti F, Picus J, Michalski JM et al (2005) Positron tomographic assessment of androgen receptors in prostatic carcinoma. *Eur J Nucl Med Mol Imaging* 32:344–350. doi:[10.1007/s00259-005-1764-5](https://doi.org/10.1007/s00259-005-1764-5)
- Dehdashti F, Laforest R, Gao F et al (2012) Assessment of progesterone receptors in breast carcinoma by PET with 21-18F-fluoro-16 α ,17 α -[(R)-(1'- α -furylmethylidene)dioxy]-19-norpregn-4-ene-3,20-dione. *J Nucl Med* 53:363–370. doi:[10.2967/jnumed.111.098319](https://doi.org/10.2967/jnumed.111.098319)
- Dhyani MV, Satpati D, Korde A, Banerjee S (2011) Synthesis and preliminary bioevaluation of 99mTc(CO)₃-17 α -triazolylandrost-4-ene-3-one derivative prepared via click chemistry route. *Cancer Biother Radiopharm* 26:539–545. doi:[10.1089/cbr.2011.0966](https://doi.org/10.1089/cbr.2011.0966)
- Dotzlaw H, Leygue E, Watson PH, Murphy LC (1997) Expression of estrogen receptor-beta in human breast tumors. *J Clin Endocrinol Metab* 82:2371–2374
- Eriksson E, Andersch B, Ho HP et al (2002) Diagnosis and treatment of premenstrual dysphoria. *J Clin Psychiatry* 63(Suppl 7):16–23
- Feliu AL, Rottenberg DA (1987) Synthesis and evaluation of fluorine-18 21-fluoroprednisone as a potential ligand for neuro-PET studies. *J Nucl Med* 28:998–1005
- Foster TC (2012) Role of estrogen receptor alpha and beta expression and signaling on cognitive function during aging. *Hippocampus* 22:656–669. doi:[10.1002/hipo.20935](https://doi.org/10.1002/hipo.20935)
- Fowler AM, Chan SR, Sharp TL et al (2012) Small-animal PET of steroid hormone receptors predicts tumor response to endocrine therapy using a preclinical model of breast cancer. *J Nucl Med* 53:1119–1126. doi:[10.2967/jnumed.112.103465](https://doi.org/10.2967/jnumed.112.103465)
- Gao M, Wang M, Miller KD, Zheng Q-H (2011) Facile radiosynthesis of new carbon-11-labeled propanamide derivatives as selective androgen receptor modulator (SARM) radioligands for prostate cancer imaging. *Steroids* 76:1505–1512. doi:[10.1016/j.steroids.2011.08.005](https://doi.org/10.1016/j.steroids.2011.08.005)
- Garg PK, Labaree DC, Hoyte RM, Hochberg RB (2001) [7 α -18F]fluoro-17 α -methyl-5 α -dihydrotestosterone: a ligand for androgen receptor-mediated imaging of prostate cancer. *Nucl Med Biol* 28:85–90
- Garg S, Doke A, Black KW, Garg PK (2008) In vivo biodistribution of an androgen receptor avid PET imaging agent 7- α -fluoro-17 α -methyl-5- α -dihydrotestosterone ([18F] FMDHT) in rats pretreated with cetorelix, a GnRH antagonist. *Eur J Nucl Med Mol Imaging* 35:379–385. doi:[10.1007/s00259-007-0610-3](https://doi.org/10.1007/s00259-007-0610-3)
- Giatti S, Boraso M, Melcangi RC, Viviani B (2012) Neuroactive steroids, their metabolites, and neuroinflammation. *J Mol Endocrinol* 49:R125–R134. doi:[10.1530/JME-12-0127](https://doi.org/10.1530/JME-12-0127)
- Grigoriadis S, Kennedy SH (2002) Role of estrogen in the treatment of depression. *Am J Ther* 9:503–509
- Hansen-Grant S, Pariante C, Kalin N, Miller A (1998) Neuroendocrine and immune system pathology in psychiatric disease. In: Schatzberg A, Nemeroff C (eds) *Textbook of psychopharmacology*, 2nd edn. American Psychiatric Press, Washington, DC, pp 171–194
- Hanson RN, Seitz DE (1982) Tissue distribution of the radiolabeled antiestrogen [125I]iodotamoxifen. *Int J Nucl Med Biol* 9:105–107
- Hollenberg SM, Weinberger C, Ong ES et al (1985) Primary structure and expression of a functional human glucocorticoid receptor cDNA. *Nature* 318:635–641

- Holsen LM, Spaeth SB, Lee J-H et al (2011) Stress response circuitry hypoactivation related to hormonal dysfunction in women with major depression. *J Affect Disord* 131:379–387. doi:[10.1016/j.jad.2010.11.024](https://doi.org/10.1016/j.jad.2010.11.024)
- Hospers GAP, Helmond FA, De Vries EGE et al (2008) PET imaging of steroid receptor expression in breast and prostate cancer. *Curr Pharm Des* 14:3020–3032
- Inoue T, Kim EE, Wallace S et al (1996) Positron emission tomography using [¹⁸F]fluorotamoxifen to evaluate therapeutic responses in patients with breast cancer: preliminary study. *Cancer Biother Radiopharm* 11:235–245
- Irie F, Strozyk D, Peila R et al (2006) Brain lesions on MRI and endogenous sex hormones in elderly men. *Neurobiol Aging* 27:1137–1144. doi:[10.1016/j.neurobiolaging.2005.05.015](https://doi.org/10.1016/j.neurobiolaging.2005.05.015)
- Jacobson O, Bechor Y, Icar A et al (2005) Prostate cancer PET bioprobes: synthesis of [¹⁸F]-radiolabeled hydroxyflutamide derivatives. *Bioorg Med Chem* 13:6195–6205. doi:[10.1016/j.bmc.2005.06.033](https://doi.org/10.1016/j.bmc.2005.06.033)
- Jacobson O, Laky D, Carlson KE et al (2006) Chiral dimethylamine flutamide derivatives—modeling, synthesis, androgen receptor affinities and carbon-11 labeling. *Nucl Med Biol* 33:695–704. doi:[10.1016/j.nucmedbio.2006.05.010](https://doi.org/10.1016/j.nucmedbio.2006.05.010)
- Järvinen TA, Peltö-Huikko M, Holli K, Isola J (2000) Estrogen receptor beta is coexpressed with ERalpha and PR and associated with nodal status, grade, and proliferation rate in breast cancer. *Am J Pathol* 156:29–35
- Jensen EV, Suzuki T, Kawashima T et al (1968) A two-step mechanism for the interaction of estradiol with rat uterus. *Proc Natl Acad Sci U S A* 59:632–638
- Jonson SD, Welch MJ (1998) PET imaging of breast cancer with fluorine-18 radiolabeled estrogens and progestins. *Q J Nucl Med* 42:8–17
- Jonson SD, Bonasera TA, Dehdashti F et al (1999) Comparative breast tumor imaging and comparative in vitro metabolism of 16alpha-[¹⁸F]fluoroestradiol-17beta and 16beta-[¹⁸F]fluoromoxestrol in isolated hepatocytes. *Nucl Med Biol* 26:123–130
- Katzenellenbogen JA, Mathias CJ, VanBrocklin HF et al (1993) Titration of the in vivo uptake of 16 alpha-[¹⁸F]fluoroestradiol by target tissues in the rat: competition by tamoxifen, and implications for quantitating estrogen receptors in vivo and the use of animal models in receptor-binding radiopharmaceutical development. *Nucl Med Biol* 20:735–745
- Kenady DE, Pavlik EJ, Nelson K et al (1993) Images of estrogen-receptor-positive breast tumors produced by estradiol labeled with iodine I 123 at 16 alpha. *Arch Surg* 128:1373–1381
- Kiesewetter DO, Kilbourn MR, Landvatter SW et al (1984) Preparation of four fluorine-18-labeled estrogens and their selective uptakes in target tissues of immature rats. *J Nucl Med* 25:1212–1221
- Kipp M, Amor S, Krauth R, Beyer C (2012) Multiple sclerosis: neuroprotective alliance of estrogen-progesterone and gender. *Front Neuroendocrinol* 33:1–16. doi:[10.1016/j.yfme.2012.01.001](https://doi.org/10.1016/j.yfme.2012.01.001)
- Klok MD, Alt SR, Irurzun Lafitte AJM et al (2011) Decreased expression of mineralocorticoid receptor mRNA and its splice variants in postmortem brain regions of patients with major depressive disorder. *J Psychiatr Res* 45:871–878. doi:[10.1016/j.jpsychires.2010.12.002](https://doi.org/10.1016/j.jpsychires.2010.12.002)
- Koike S, Sakai M, Muramatsu M (1987) Molecular cloning and characterization of rat estrogen receptor cDNA. *Nucleic Acids Res* 15:2499–2513
- Kuiper GG, Enmark E, Peltö-Huikko M et al (1996) Cloning of a novel receptor expressed in rat prostate and ovary. *Proc Natl Acad Sci U S A* 93:5925–5930
- Labaree DC, Brown TJ, Hoyte RM, Hochberg RB (1997) 7 alpha-iodine-125-iodo-5 alpha-dihydrotestosterone: a radiolabeled ligand for the androgen receptor. *J Nucl Med* 38:402–409
- Larson SM, Morris M, Gunther I et al (2004) Tumor localization of 16beta-18F-fluoro-5alpha-dihydrotestosterone versus 18F-FDG in patients with progressive, metastatic prostate cancer. *J Nucl Med* 45:366–373
- Lee JH, Zhou H, Dence CS et al (2010) Development of [¹⁸F]-fluorine-substituted Tanaproget as a progesterone receptor imaging agent for positron emission tomography. *Bioconjug Chem* 21:1096–1104. doi:[10.1021/bc1001054](https://doi.org/10.1021/bc1001054)
- Lee JH, Peters O, Lehmann L et al (2012) Synthesis and biological evaluation of two agents for imaging estrogen receptor β by positron emission tomography: challenges in PET imaging of a low abundance target. *Nucl Med Biol* 39:1105–1116. doi:[10.1016/j.nucmedbio.2012.05.011](https://doi.org/10.1016/j.nucmedbio.2012.05.011)

- Liu AJ, Katzenellenbogen JA, VanBrocklin HF et al (1991) 20-[18F]fluoromibolerone, a positron-emitting radiotracer for androgen receptors: synthesis and tissue distribution studies. *J Nucl Med* 32:81–88
- Liu A, Dence CS, Welch MJ, Katzenellenbogen JA (1992) Fluorine-18-labeled androgens: radiochemical synthesis and tissue distribution studies on six fluorine-substituted androgens, potential imaging agents for prostatic cancer. *J Nucl Med* 33:724–734
- Liu A, Margail I, Zhang S et al (2012) Progesterone receptors: a key for neuroprotection in experimental stroke. *Endocrinology* 153:3747–3757. doi:[10.1210/en.2012-1138](https://doi.org/10.1210/en.2012-1138)
- López JF, Chalmers DT, Little KY, Watson SJ (1998) A.E. Bennett Research Award. Regulation of serotonin1A, glucocorticoid, and mineralocorticoid receptor in rat and human hippocampus: implications for the neurobiology of depression. *Biol Psychiatry* 43:547–573
- Luoma JI, Stern CM, Mermelstein PG (2012) Progesterone inhibition of neuronal calcium signaling underlies aspects of progesterone-mediated neuroprotection. *J Steroid Biochem Mol Biol* 131:30–36. doi:[10.1016/j.jsmb.2011.11.002](https://doi.org/10.1016/j.jsmb.2011.11.002)
- Ma C (2000) CDNA cloning and expression of a novel estrogen receptor β -subtype in goldfish (*Carassius auratus*). *Biochim Biophys Acta* 1490:145–152. doi:[10.1016/S0167-4781\(99\)00235-3](https://doi.org/10.1016/S0167-4781(99)00235-3)
- Mankoff DA, Peterson LM, Tewson TJ et al (2001) [18F]fluoroestradiol radiation dosimetry in human PET studies. *J Nucl Med* 42:679–684
- McEwen BS (2001) Invited review: estrogens effects on the brain: multiple sites and molecular mechanisms. *J Appl Physiol* (1985) 91:2785–2801
- McEwen BS, Sapolsky RM (1995) Stress and cognitive function. *Curr Opin Neurobiol* 5:205–216
- Meffre D, Labombarda F, Delespierre B et al (2013) Distribution of membrane progesterone receptor alpha in the male mouse and rat brain and its regulation after traumatic brain injury. *Neuroscience* 231:111–124. doi:[10.1016/j.neuroscience.2012.11.039](https://doi.org/10.1016/j.neuroscience.2012.11.039)
- Menuet A, Pellegrini E, Anglade I et al (2002) Molecular characterization of three estrogen receptor forms in zebrafish: binding characteristics, transactivation properties, and tissue distributions. *Biol Reprod* 66:1881–1892
- Mintun MA, Welch MJ, Siegel BA et al (1988) Breast cancer: PET imaging of estrogen receptors. *Radiology* 169:45–48
- Misrahi M, Atger M, D' Aurio L et al (1987) Complete amino acid sequence of the human progesterone receptor deduced from cloned cDNA. *Biochem Biophys Res Commun* 143:740–748
- Moresco RM, Casati R, Lucignani G et al (1995) Systemic and cerebral kinetics of 16 alpha [18F] fluoro-17 beta-estradiol: a ligand for the in vivo assessment of estrogen receptor binding parameters. *J Cereb Blood Flow Metab* 15:301–311. doi:[10.1038/jcbfm.1995.35](https://doi.org/10.1038/jcbfm.1995.35)
- Morimoto M, Morita N, Ozawa H et al (1996) Distribution of glucocorticoid receptor immunoreactivity and mRNA in the rat brain: an immunohistochemical and in situ hybridization study. *Neurosci Res* 26:235–269
- Mortimer JE, Dehdashti F, Siegel BA et al (1996) Positron emission tomography with 2-[18F] fluoro-2-deoxy-D-glucose and 16alpha-[18F]fluoro-17beta-estradiol in breast cancer: correlation with estrogen receptor status and response to systemic therapy. *Clin Cancer Res* 2:933–939
- Muftuler FZB, Unak P, Teksoz S et al (2008) 131I labeling of tamoxifen and biodistribution studies in rats. *Appl Radiat Isot* 66:178–187. doi:[10.1016/j.apradiso.2007.08.005](https://doi.org/10.1016/j.apradiso.2007.08.005)
- Nachar O, Rousseau JA, Lefebvre B et al (1999) Biodistribution, dosimetry and metabolism of 11beta-methoxy-(17alpha,20E/Z)-[123I]iodovinylestradiol in healthy women and breast cancer patients. *J Nucl Med* 40:1728–1736
- Nayak TK, Hathaway HJ, Ramesh C et al (2008) Preclinical development of a neutral, estrogen receptor-targeted, tridentate 99mTc(I)-estradiol-pyridin-2-yl hydrazine derivative for imaging of breast and endometrial cancers. *J Nucl Med* 49:978–986. doi:[10.2967/jnumed.107.048546](https://doi.org/10.2967/jnumed.107.048546)
- Ooishi Y, Kawato S, Hojo Y et al (2012) Modulation of synaptic plasticity in the hippocampus by hippocampus-derived estrogen and androgen. *J Steroid Biochem Mol Biol* 131:37–51. doi:[10.1016/j.jsmb.2011.10.004](https://doi.org/10.1016/j.jsmb.2011.10.004)

- Ostlund H, Keller E, Hurd YL (2003) Estrogen receptor gene expression in relation to neuropsychiatric disorders. *Ann N Y Acad Sci* 1007:54–63
- Parent EE, Jenks C, Sharp T et al (2006) Synthesis and biological evaluation of a nonsteroidal bromine-76-labeled androgen receptor ligand 3-[76Br]bromo-hydroxyflutamide. *Nucl Med Biol* 33:705–713. doi:[10.1016/j.nucmedbio.2006.05.009](https://doi.org/10.1016/j.nucmedbio.2006.05.009)
- Parent EE, Dence CS, Jenks C et al (2007) Synthesis and biological evaluation of [18F]bicalutamide, 4-[76Br]bromobicalutamide, and 4-[76Br]bromo-thiobicalutamide as non-steroidal androgens for prostate cancer imaging. *J Med Chem* 50:1028–1040. doi:[10.1021/jm060847r](https://doi.org/10.1021/jm060847r)
- Pareto D, Alvarado M, Hanrahan SM, Biegion A (2004) In vivo occupancy of female rat brain estrogen receptors by 17beta-estradiol and tamoxifen. *Neuroimage* 23:1161–1167. doi:[10.1016/j.neuroimage.2004.07.036](https://doi.org/10.1016/j.neuroimage.2004.07.036)
- Pavlik EJ, Nelson K, Gallion HH et al (1990) Characterization of high specific activity [16 alpha-123I]iodo-17 beta-estradiol as an estrogen receptor-specific radioligand capable of imaging estrogen receptor-positive tumors. *Cancer Res* 50:7799–7805
- Perlman WR, Webster MJ, Kleinman JE, Weickert CS (2004) Reduced glucocorticoid and estrogen receptor alpha messenger ribonucleic acid levels in the amygdala of patients with major mental illness. *Biol Psychiatry* 56:844–852. doi:[10.1016/j.biopsych.2004.09.006](https://doi.org/10.1016/j.biopsych.2004.09.006)
- Perlman WR, Webster MJ, Herman MM et al (2007) Age-related differences in glucocorticoid receptor mRNA levels in the human brain. *Neurobiol Aging* 28:447–458. doi:[10.1016/j.neurobiolaging.2006.01.010](https://doi.org/10.1016/j.neurobiolaging.2006.01.010)
- Peterson LM, Mankoff DA, Lawton T et al (2008) Quantitative imaging of estrogen receptor expression in breast cancer with PET and 18F-fluoroestradiol. *J Nucl Med* 49:367–374. doi:[10.2967/jnumed.107.047506](https://doi.org/10.2967/jnumed.107.047506)
- Pike CJ, Carroll JC, Rosario ER, Barron AM (2009) Protective actions of sex steroid hormones in Alzheimer's disease. *Front Neuroendocrinol* 30:239–258. doi:[10.1016/j.yfrne.2009.04.015](https://doi.org/10.1016/j.yfrne.2009.04.015)
- Pomper MG, Katzenellenbogen JA, Welch MJ et al (1988) 21-[18F]fluoro-16 alpha-ethyl-19-norprogesterone: synthesis and target tissue selective uptake of a progestin receptor based radiotracer for positron emission tomography. *J Med Chem* 31:1360–1363
- Pomper MG, Kochanny MJ, Thieme AM et al (1992) Fluorine-substituted corticosteroids: synthesis and evaluation as potential receptor-based imaging agents for positron emission tomography of the brain. *Int J Rad Appl Instrum B* 19:461–480
- Pompili M, Serafini G, Innamorati M et al (2010) The hypothalamic-pituitary-adrenal axis and serotonin abnormalities: a selective overview for the implications of suicide prevention. *Eur Arch Psychiatry Clin Neurosci* 260:583–600. doi:[10.1007/s00406-010-0108-z](https://doi.org/10.1007/s00406-010-0108-z)
- Ramesh C, Bryant B, Nayak T et al (2006) Linkage effects on binding affinity and activation of GPR30 and estrogen receptors ERalpha/beta with tridentate pyridin-2-yl hydrazine tricarbonyl-Re/(99m)Tc(I) chelates. *J Am Chem Soc* 128:14476–14477. doi:[10.1021/ja066360p](https://doi.org/10.1021/ja066360p)
- Resnick SM, Henderson VW (2002) Hormone therapy and risk of Alzheimer disease: a critical time. *JAMA* 288:2170–2172
- Rijks LJ, Bakker PJ, Van Tienhoven G et al (1997a) Imaging of estrogen receptors in primary and metastatic breast cancer patients with iodine-123-labeled Z-MIVE. *J Clin Oncol* 15:2536–2545
- Rijks LJ, Boer GJ, Endert E et al (1997b) The Z-isomer of 11 beta-methoxy-17 alpha-[123I]iodovinylestradiol is a promising radioligand for estrogen receptor imaging in human breast cancer. *Nucl Med Biol* 24:65–75
- Rijks LJ, Van den Bos JC, Van Doremalen PA et al (1998a) New iodinated progestins as potential ligands for progesterone receptor imaging in breast cancer. Part 2: in vivo pharmacological characterization. *Nucl Med Biol* 25:791–798
- Rijks LJ, Busemann Sokole E, Stabin MG et al (1998b) Biodistribution and dosimetry of iodine-123-labelled Z-MIVE: an oestrogen receptor radioligand for breast cancer imaging. *Eur J Nucl Med* 25:40–47
- Robel P, Baulieu EE (1985) Neuro-steroids: 3?-hydroxy-?(5)-derivatives in the rodent brain. *Neurochem Int* 7:953–958
- Rubinow DR, Schmidt PJ (2006) Gonadal steroid regulation of mood: the lessons of premenstrual syndrome. *Front Neuroendocrinol* 27:210–216. doi:[10.1016/j.yfrne.2006.02.003](https://doi.org/10.1016/j.yfrne.2006.02.003)

- Rupprecht R (2003) Neuroactive steroids: mechanisms of action and neuropsychopharmacological properties. *Psychoneuroendocrinology* 28:139–168
- Sapolsky R (1996) Stress, glucocorticoids, and damage to the nervous system: the current state of confusion. *Stress* 1:1–19. doi:[10.3109/10253899609001092](https://doi.org/10.3109/10253899609001092)
- Sapolsky RM (2004) Is impaired neurogenesis relevant to the affective symptoms of depression? *Biol Psychiatry* 56:137–139. doi:[10.1016/j.biopsych.2004.04.012](https://doi.org/10.1016/j.biopsych.2004.04.012)
- Sarrel PM (1999) Psychosexual effects of menopause: role of androgens. *Am J Obstet Gynecol* 180:S319–S324
- Sasaki M, Fukumura T, Kuwabara Y et al (2000) Biodistribution and breast tumor uptake of 16alpha-[18F]-fluoro-17beta-estradiol in rat. *Ann Nucl Med* 14:127–130
- Sayed I, Stein DG (2009) Progesterone as a neuroprotective factor in traumatic and ischemic brain injury. *Prog Brain Res* 175:219–237. doi:[10.1016/S0079-6123\(09\)17515-5](https://doi.org/10.1016/S0079-6123(09)17515-5)
- Scheidhauer K, Müller S, Smolarz K et al (1991) Tumor scintigraphy using 123I-labeled estradiol in breast cancer—receptor scintigraphy. *Nuklearmedizin* 30:84–99
- Schober O, Scheidhauer K, Jankisch C et al (1990) Breast cancer imaging with radioiodinated oestradiol. *Lancet* 335:1522
- Seidman SN (2007) Androgens and the aging male. *Psychopharmacol Bull* 40:205–218
- Seimille Y, Rousseau J, Bénard F et al (2002) 18F-labeled difluoroestradiols: preparation and pre-clinical evaluation as estrogen receptor-binding radiopharmaceuticals. *Steroids* 67:765–775
- Seimille Y, Bénard F, Rousseau J et al (2004) Impact on estrogen receptor binding and target tissue uptake of [18F]fluorine substitution at the 16alpha-position of fulvestrant (faslodex; ICI 182,780). *Nucl Med Biol* 31:691–698. doi:[10.1016/j.nucmedbio.2004.02.010](https://doi.org/10.1016/j.nucmedbio.2004.02.010)
- Sherman S, Miller H, Nerurkar L, Schiff I (2005) Research opportunities for reducing the burden of menopause-related symptoms. *Am J Med* 118 Suppl:166–171. doi:[10.1016/j.amjmed.2005.12.004](https://doi.org/10.1016/j.amjmed.2005.12.004)
- Sherwin BB (1997) Estrogen effects on cognition in menopausal women. *Neurology* 48:S21–S26
- Shughrue PJ, Stumpf WE, MacLusky NJ et al (1990) Developmental changes in estrogen receptors in mouse cerebral cortex between birth and postweaning: studied by autoradiography with 11 beta-methoxy-16 alpha-[125I]iodoestradiol. *Endocrinology* 126:1112–1124
- Singh M, Su C (2012) Progesterone, brain-derived neurotrophic factor and neuroprotection. *Neuroscience*. doi:[10.1016/j.neuroscience.2012.09.056](https://doi.org/10.1016/j.neuroscience.2012.09.056)
- Spritzer MD, Galea LAM (2007) Testosterone and dihydrotestosterone, but not estradiol, enhance survival of new hippocampal neurons in adult male rats. *Dev Neurobiol* 67:1321–1333. doi:[10.1002/dneu.20457](https://doi.org/10.1002/dneu.20457)
- Stein DG (2011a) Progesterone in the treatment of acute traumatic brain injury: a clinical perspective and update. *Neuroscience* 191:101–106. doi:[10.1016/j.neuroscience.2011.04.013](https://doi.org/10.1016/j.neuroscience.2011.04.013)
- Stein DG (2011b) Is progesterone a worthy candidate as a novel therapy for traumatic brain injury? *Dialogues Clin Neurosci* 13:352–359
- Stein DG, Wright DW, Kellermann AL (2008) Does progesterone have neuroprotective properties? *Ann Emerg Med* 51:164–172. doi:[10.1016/j.annemergmed.2007.05.001](https://doi.org/10.1016/j.annemergmed.2007.05.001)
- Steiner M, Dunn E, Born L (2003) Hormones and mood: from menarche to menopause and beyond. *J Affect Disord* 74:67–83
- Stumpf WE, Morin JK, Ennis BW et al (1987) Utility of [16 alpha-125I] iodoestradiol for autoradiography for the study of cellular and regional distribution of receptors. *J Histochem Cytochem* 35:87–92
- Takahashi N, Yang DJ, Kohanim S et al (2007a) Targeted functional imaging of estrogen receptors with 99mTc-GAP-EDL. *Eur J Nucl Med Mol Imaging* 34:354–362. doi:[10.1007/s00259-006-0191-6](https://doi.org/10.1007/s00259-006-0191-6)
- Takahashi N, Yang DJ, Kurihara H et al (2007b) Functional imaging of estrogen receptors with radiolabeled-GAP-EDL in rabbit endometriosis model. *Acad Radiol* 14:1050–1057. doi:[10.1016/j.acra.2007.05.020](https://doi.org/10.1016/j.acra.2007.05.020)
- Tarle M, Padovan R, Spaventi S (1981) The uptake of radioiodinated 5 alpha-dihydrotestosterone by the prostate of intact and castrated rats. *Eur J Nucl Med* 6:79–83
- Van de Wiele C, Cocquyt V, VandenBroecke R et al (2001) Iodine-labeled tamoxifen uptake in primary human breast carcinoma. *J Nucl Med* 42:1818–1820

- Van Kruchten M, Glaudemans AWJM, De Vries EFJ et al (2012) PET imaging of estrogen receptors as a diagnostic tool for breast cancer patients presenting with a clinical dilemma. *J Nucl Med* 53:182–190. doi:[10.2967/jnumed.111.092734](https://doi.org/10.2967/jnumed.111.092734)
- VanBrocklin HF, Pomper MG, Carlson KE et al (1992) Preparation and evaluation of 17-ethynyl-substituted 16 alpha-[18F]fluoroestradiols: selective receptor-based PET imaging agents. *Int J Rad Appl Instrum B* 19:363–374
- VanBrocklin HF, Carlson KE, Katzenellenbogen JA, Welch MJ (1993a) 16 beta-([18F]fluoro) estrogens: systematic investigation of a new series of fluorine-18-labeled estrogens as potential imaging agents for estrogen-receptor-positive breast tumors. *J Med Chem* 36:1619–1629
- VanBrocklin HF, Rocque PA, Lee HV et al (1993b) 16 beta-[18F]fluoromoxestrol: a potent, metabolically stable positron emission tomography imaging agent for estrogen receptor positive human breast tumors. *Life Sci* 53:811–819
- VanBrocklin HF, Liu A, Welch MJ et al (1994) The synthesis of 7 alpha-methyl-substituted estrogens labeled with fluorine-18: potential breast tumor imaging agents. *Steroids* 59:34–45
- Vegeto E, Benedusi V, Maggi A (2008) Estrogen anti-inflammatory activity in brain: a therapeutic opportunity for menopause and neurodegenerative diseases. *Front Neuroendocrinol* 29:507–519. doi:[10.1016/j.yfrne.2008.04.001](https://doi.org/10.1016/j.yfrne.2008.04.001)
- Verhagen A, Elsinga PH, De Groot TJ et al (1991a) A fluorine-18 labeled progestin as an imaging agent for progesterin receptor positive tumors with positron emission tomography. *Cancer Res* 51:1930–1933
- Verhagen A, Luurtsema G, Pesser JW et al (1991b) Preclinical evaluation of a positron emitting progestin ([18F]fluoro-16 alpha-methyl-19-norprogesterone) for imaging progesterone receptor positive tumours with positron emission tomography. *Cancer Lett* 59:125–132
- Verhagen A, Studeny M, Luurtsema G et al (1994) Metabolism of a [18F]fluorine labeled progestin (21-[18F]fluoro-16 alpha-ethyl-19-norprogesterone) in humans: a clue for future investigations. *Nucl Med Biol* 21:941–952
- Vijaykumar D, Mao W, Kirschbaum KS, Katzenellenbogen JA (2002) An efficient route for the preparation of a 21-fluoro progestin-16 alpha,17 alpha-dioxolane, a high-affinity ligand for PET imaging of the progesterone receptor. *J Org Chem* 67:4904–4910
- Visser GM, Krugers HJ, Luurtsema G et al (1995) Synthesis and organ distribution of [18F]fluoro-*Org* 6141 in the rat: a potential glucocorticoid receptor ligand for positron emission tomography. *Nucl Med Biol* 22:915–920
- Walsh PJ, Teasdale J, Cowen PN (1990) Ultrastructural localisation of oestrogen receptor in breast cancer cell nuclei. *Histochemistry* 95:205–207
- Westberg L, Eriksson E (2008) Sex steroid-related candidate genes in psychiatric disorders. *J Psychiatry Neurosci* 33:319–330
- Wilson CM, McPhaul MJ (1994) A and B forms of the androgen receptor are present in human genital skin fibroblasts. *Proc Natl Acad Sci U S A* 91:1234–1238
- Wright DW, Kellermann AL, Hertzberg VS et al (2007) ProTECT: a randomized clinical trial of progesterone for acute traumatic brain injury. *Ann Emerg Med* 49:391–402, 402.e1–2. doi:[10.1016/j.annemergmed.2006.07.932](https://doi.org/10.1016/j.annemergmed.2006.07.932)
- Wuest F, Kniess T, Bergmann R et al (2007) Synthesis and radiopharmacological characterization of [11C]JAL-438 as a nonsteroidal ligand for imaging brain glucocorticoid receptors. *Bioorg Med Chem Lett* 17:4035–4039. doi:[10.1016/j.bmcl.2007.04.094](https://doi.org/10.1016/j.bmcl.2007.04.094)
- Wuest F, Kniess T, Henry B et al (2009) Radiosynthesis and radiopharmacological evaluation of [N-methyl-11C]Org 34850 as a glucocorticoid receptor (GR)-binding radiotracer. *Appl Radiat Isot* 67:308–312. doi:[10.1016/j.apradiso.2008.10.014](https://doi.org/10.1016/j.apradiso.2008.10.014)
- Wüst F, Carlson KE, Katzenellenbogen JA (2003) Synthesis of novel arylpyrazolo corticosteroids as potential ligands for imaging brain glucocorticoid receptors. *Steroids* 68:177–191
- Wüst F, Kniess T, Kretschmar M, Bergmann R (2005) Synthesis and radiopharmacological evaluation of 2'-(4-fluorophenyl)-21-[18F]fluoro-20-oxo-11beta,17alpha-dihydroxy-pregn-4-eno[3,2-c]pyrazole as potential glucocorticoid receptor ligand for positron emission tomography (PET). *Bioorg Med Chem Lett* 15:1303–1306. doi:[10.1016/j.bmcl.2005.01.033](https://doi.org/10.1016/j.bmcl.2005.01.033)

- Xing G-Q, Russell S, Webster MJ, Post RM (2004) Decreased expression of mineralocorticoid receptor mRNA in the prefrontal cortex in schizophrenia and bipolar disorder. *Int J Neuropsychopharmacol* 7:143–153. doi:[10.1017/S1461145703004000](https://doi.org/10.1017/S1461145703004000)
- Yaffe K, Sawaya G, Lieberburg I, Grady D (1998) Estrogen therapy in postmenopausal women: effects on cognitive function and dementia. *JAMA* 279:688–695
- Yang DJ, Li C, Kuang LR et al (1994) Imaging, biodistribution and therapy potential of halogenated tamoxifen analogues. *Life Sci* 55:53–67
- Yoo J, Dence CS, Sharp TL et al (2005) Synthesis of an estrogen receptor beta-selective radioligand: 5-[18F]fluoro-(2R,3S)-2,3-bis(4-hydroxyphenyl)pentanenitrile and comparison of in vivo distribution with 16alpha-[18F]fluoro-17beta-estradiol. *J Med Chem* 48:6366–6378. doi:[10.1021/jm050121f](https://doi.org/10.1021/jm050121f)
- Young EA, Lopez JF, Murphy-Weinberg V et al (2003) Mineralocorticoid receptor function in major depression. *Arch Gen Psychiatry* 60:24–28
- Yurt A, Muftuler FZB, Unak P et al (2009) Synthesis of a novel antiestrogen radioligand (99mTc-TOR-DTPA). *Cancer Biother Radiopharm* 24:707–716. doi:[10.1089/cbr.2009.0656](https://doi.org/10.1089/cbr.2009.0656)
- Zanzonico PB, Finn R, Pentlow KS et al (2004) PET-based radiation dosimetry in man of 18F-fluorodihydrotestosterone, a new radiotracer for imaging prostate cancer. *J Nucl Med* 45:1966–1971
- Zhou D, Carlson KE, Katzenellenbogen JA, Welch MJ (2006) Bromine- and iodine-substituted 16alpha,17alpha-dioxolane progestins for breast tumor imaging and radiotherapy: synthesis and receptor binding affinity. *J Med Chem* 49:4737–4744. doi:[10.1021/jm060348q](https://doi.org/10.1021/jm060348q)
- Zhou H-B, Lee JH, Mayne CG et al (2010) Imaging progesterone receptor in breast tumors: synthesis and receptor binding affinity of fluoroalkyl-substituted analogues of tanaproget. *J Med Chem* 53:3349–3360. doi:[10.1021/jm100052k](https://doi.org/10.1021/jm100052k)
- Zhu H, Huang L, Zhang Y et al (2010) Design, synthesis, and evaluation of cyclofenil derivatives for potential SPECT imaging agents. *J Biol Inorg Chem* 15:591–599. doi:[10.1007/s00775-010-0627-0](https://doi.org/10.1007/s00775-010-0627-0)
- Zielinski JE, Yabuki H, Pahuja SL et al (1986) 16 Alpha-[125I]iodo-11 beta-methoxy-17 beta-estradiol: a radiochemical probe for estrogen-sensitive tissues. *Endocrinology* 119:130–139
- Zitzmann M (2006) Testosterone and the brain. *Aging Male* 9:195–199. doi:[10.1080/13685530601040679](https://doi.org/10.1080/13685530601040679)

Current Radioligands for the PET Imaging of Metabotropic Glutamate Receptors

15

Linjing Mu and Simon M. Ametamey

Contents

15.1	Introduction	411
15.1.1	Glutamate Receptors	411
15.1.2	PET	412
15.1.3	General Requirements for CNS Radiotracers	413
15.2	mGluR1 PET Tracers.....	415
15.2.1	¹¹ C-Labeled mGluR1 Tracers.....	416
15.2.2	¹⁸ F-Labeled mGluR1 Tracers	419
15.3	mGluR5 PET Tracers.....	422
15.3.1	MPEP-Derived mGluR5 Tracers	423
15.3.2	MTEP-Derived mGluR5 Tracers	427
15.3.3	ABP688-Related mGluR5 Tracers.....	430
15.4	Other mGluR PET Tracers	434
15.5	Application of mGluRs Tracers	435
	References.....	436

Abstract

Glutamate receptors are divided into two main groups: ionotropic glutamate receptors (iGluRs) and metabotropic glutamate receptors (mGluRs). Modulation of iGluRs and mGluRs has potential for the treatment of psychiatric and neurological diseases such as depression, anxiety, schizophrenia, and Parkinson's disease. Positron emission tomography (PET) might offer the possibility to visualize

L. Mu

Department of Nuclear Medicine, Center for Radiopharmaceutical Sciences of ETH, PSI and USZ, University Hospital Zürich, CH-8091 Zürich, Switzerland
e-mail: linjing.mu@usz.ch

S.M. Ametamey (✉)

Department of Chemistry and Applied Biosciences, Center for Radiopharmaceutical Sciences of ETH, PSI and USZ, ETH Zurich, CH-8093 Zurich, Switzerland
e-mail: simon.ametamey@pharma.ethz.ch

glutamate receptors and presents an interesting tool for studying these receptors under physiologic and pathologic conditions. mGluR PET radioligands reported till April 2012 are outlined alongside their in vitro/in vivo properties and clinical applications. Emphasis is given to mGluR1 and mGluR5, two receptor subtypes for which most advances in radioligand development have been accomplished.

Abbreviations

ABP688	3-(6-methyl-pyridin-2-ylethynyl)-cyclohex-2-enonemethyl-oxime
AMPA	2-amino-3-(3-hydroxy-5-methyl-isoxazol-4-yl)-propionic acid
BBB	Blood-brain barrier
B_{\max}	Maximal binding capacity
BP_{ND}	Binding potential relative to the no displaceable compartment
Bq	Becquerel
BSA	Bovine serum albumin
CAMP	Cyclic adenosine monophosphate
CNS	Central nervous system
DMF	Dimethylformamide
DMSO	Dimethyl sulfoxide
EOB	End of bombardment
EOS	End of synthesis
Et_3N	Triethylamine
GPCR	G-protein-coupled receptor
HBD	Hydrogen bond donors
HPLC	High-pressure liquid chromatography
i.v	Intravenous
IC_{50}	Inhibition constant required for displacement of 50 % of radioligand binding
ID	Injected dose
IDnorm./g	Injected dose normalized to body weight per tissue weight
iGluR	Ionotropic glutamate receptor
K_d	Dissociation constant
K_i	Inhibition constant
ko	Knockout
LTP	Long-term potentiation
MeI	Methyl iodide
M-FPEP	2-methyl-6-(3-fluoro-phenylethynyl)-pyridine
mGluR	Metabotropic glutamate receptor
mGluR5	Metabotropic glutamate receptor subtype 5
min	Minute(s)
M-MPEP	2-methyl-6-((methoxyphenyl)ethynyl)-pyridine
MPEP	6-methyl-2-(phenylethynyl)-pyridine
MW	Microwave
NAC	<i>N</i> -acetylcysteine

NMDA	<i>N</i> -methyl-D-aspartate
NMDAR	<i>N</i> -methyl-D-aspartate receptor
p.i.	Postinjection
PBS	Phosphate buffered saline
PET	Positron emission tomography
P-gp	P-glycoprotein
PI	Phosphoinositol
PLC	Phospholipase C
ROI	Region of interest
RT	Room temperature
SAR	Structure–activity relationship
SUV	Standard uptake value
TAC	Time activity curve
TEMPO	2,2,6,6-tetramethylpiperidine-1-oxyl
THF	Tetrahydrofuran
TM	Transmembrane domain
TPSA	Topological polar surface area
wt	Wild-type

15.1 Introduction

15.1.1 Glutamate Receptors

Glutamate (L-glutamic acid) serves as the neurotransmitter at the majority of excitatory synapses in the mammalian central nervous system (CNS). Glutamate receptors are divided into two main groups, namely, ionotropic glutamate receptors (iGluRs) and metabotropic glutamate receptors (mGluRs) (Fig. 15.1).

The iGluRs are the principal mediators of excitatory neurotransmission. These are ligand-gated cationic-selective channels which are permeable to Na⁺, K⁺, and Ca²⁺ ions. They are subdivided into three major classes based on structural similarities and named according to the type of synthetic agonist that activates them. These three selective agonists are: NMDA (*N*-methyl-D-aspartate), AMPA (α -amino-3-hydroxy-5-methyl-isoxazole-4-propionate), and kainate (Bettler and Mülle 1995; Mori and Mishina 1995). Native receptors of all of these families are likely heteromeric assemblies comprising more than one type of subunit. *N*-methyl-D-aspartate (NMDA) tetrameric receptors consist of subunits NR1 and NR2. There are four NR2 subunit types, NR2A, B, C, and D. AMPA receptors are composed of a four-subunit family (GluR1–4) with members that are products of separate genes and are believed to assemble as functional tetramers. Kainate receptors are composed of two related subunit families, GluR5–7 and KA-1 and 2.

Metabotropic glutamate receptors (mGluRs) are G-protein-coupled receptors (GPCR), which activate intracellular secondary messenger systems when bound by the physiological ligand glutamate. From a structural viewpoint, mGluRs belong to the seven-transmembrane protein family and have been classified into three

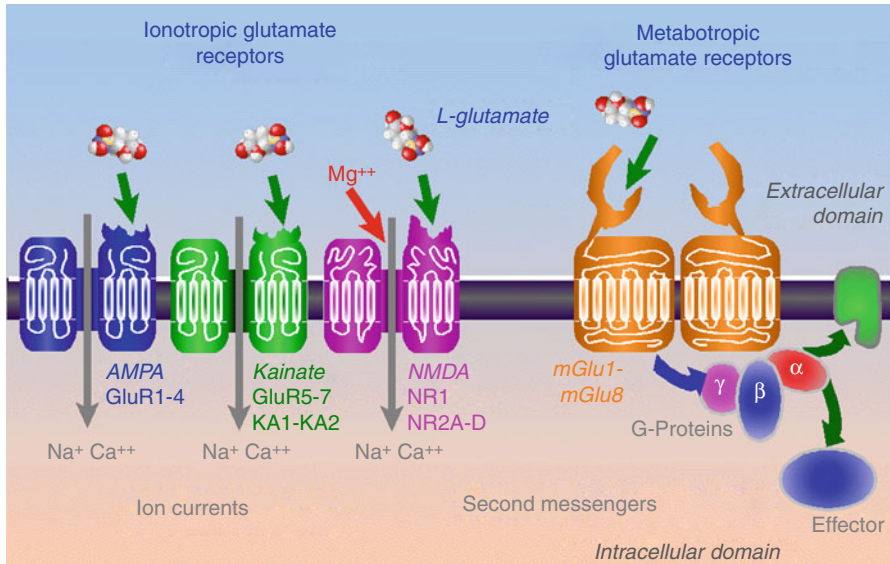


Fig. 15.1 Ionotropic and metabotropic glutamate receptors (Source: <http://www.ucl.ac.uk/iao/research/salt/glutam.htm> (Prof. Tom Salt))

subgroups. Group I mGluRs (mGluR1 and mGluR5) are coupled to phospholipase C and upregulate or downregulate neuronal excitability (Gereau and Conn 1995). Group II (mGluR2 and mGluR3) and group III (mGluR4 and mGluR6–8) inhibit adenylate cyclase and hence reduce synaptic transmission (Bradley et al. 2000; Ritzen et al. 2005). The mGluRs are expressed on neuronal and glial cells, with each receptor subtype exhibiting distinct spatial and temporal expression profiles in the brain (Shigemoto et al. 1997; Thomas et al. 2001), with the exception of mGluR6 existing in the retina. In neurons, group I mGluRs are mainly localized in somato-dendritic domains and postsynaptically regulate neuronal excitability and synaptic transmission via several intracellular second messenger systems, whereas group II and III mGluRs are predominantly localized in axonal domains and axon terminals to presynaptically regulate neurotransmitter release (Cartmell and Schoepp 2000). mGluRs function as dimers, with two glutamate molecules being required for full receptor activation (Tsuchiya et al. 2002; Shin et al. 2008; Ono et al. 2012).

15.1.2 PET

Positron emission tomography (PET) is a noninvasive imaging technology, allowing for the quantitative imaging of physiologic and pathophysiologic processes in vivo (Talbot and Laruelle 2002; Schubiger et al. 2007; Ametamey et al. 2008). High resolution of about 1–2 mm can be achieved with small animal imaging systems and 4–6 mm for clinical PET scanners. The visualization of biological targets and systems is of

special interest in this research field. Specific PET tracers for labeling such targets are potential future diagnostics of various diseases and provide elegant tools for drug development (Fowler et al. 1999), especially for the development of drugs with less side effects. Besides oncologic and cardiac applications, there is a growing demand for specific and selective radiopharmaceuticals in the field of neuroscience. PET can be used to image receptor distribution, concentration, and functions in normal and pathological states and has proven to be a powerful technique in neurological research (Passchier et al. 2002). Due to the convenient half-lives of carbon-11 and fluorine-18 and their chemical properties, most effort has been put into the development of tracers labeled with one of these isotopes. In general, carbon-11 and fluorine-18 are produced by nuclear reactions which require the bombardment of convenient stable isotopes with high energetic protons provided by a cyclotron. Carbon-11 can easily be introduced into biologically interesting compounds without changing their biochemical and pharmacological properties. The relatively short physical half-life of ^{11}C (20 min) allows for multiple imaging studies in a short period of time, which makes it advantageous for sequential investigations with short time intervals in the same individual (animal or human), thereby allowing the subject to serve as its own control. Therefore ^{11}C -labeled compounds can be used for instance in a receptor occupancy paradigm or in cognitive intervention studies where several PET investigations are usually needed within a few hours apart from each other. The short half-life of ^{11}C , however, is disadvantageous for commercial production. Fluorine-18 has long physical half-life of 110 min allowing more complex synthesis, extended in vivo investigation, and, most importantly, satellite distribution of the radiotracer to clinical PET centers that do not have radiochemistry facilities. In addition, it shows better imaging characteristics than carbon-11 due to its lower positron energy (0.64 MeV vs. 0.96 MeV for ^{11}C). The larger the positron energy, the larger the average distance the positron travels before annihilating and as such more loss in spatial resolution will be expected. Thus, efforts have been put into developing ^{18}F -labeled radiotracers. Radiolabeling methods with either carbon-11 or fluorine-18 will not be discussed in this chapter. Several review papers on this topic can be found in the literature (Ametamey et al. 2008; Cai et al. 2008; Miller et al. 2008; Li and Conti 2010).

15.1.3 General Requirements for CNS Radiotracers

The general requirements for successful PET radiotracers for the imaging of specific brain targets such as transporters, receptors, and enzymes also hold true for glutamate receptors. Several excellent review papers have been published on this topic (Waterhouse 2003; Eckelman et al. 2006; Eckelman and Mathis 2006b; Patel and Gibson 2008; Tavares et al. 2012). A summary of some of the most major points is provided below.

15.1.3.1 High Affinity and Selectivity

The affinity of the radiotracer relative to the concentration of binding site present in the target tissue is an important characteristic of site-specific radiotracers

(Eckelman et al. 2006). The ability to image a receptor is determined by delivery, by retention at the specific binding site, and by washout of nonspecifically associated radiotracer. Two terms are related to the affinity of a ligand towards its target, and depending on how the value is obtained, the K_d (equilibrium dissociation constant) and the K_i (inhibition constant) express the affinity of a ligand to the target. Usually, binding affinities should be in the low nanomolar to subnanomolar range. With regard to selectivity, the radioligand in question should have the highest affinity for the actual target and only low affinity for any other binding site.

15.1.3.2 Concentration of Target Sites (B_{\max})

A high ratio of binding site concentration towards radiotracer concentration is a requirement for a valid response to changes in binding site concentration caused by diseases or drug occupancy during a PET experiment. Therefore, it is important that the B_{\max} value exceeds the affinity (K_d) of the radioligand, and this positively affects the target-to-nontarget ratio and the imaging quality. It is considered that PET tracers with an in vitro B_{\max}/K_d ratio (also called binding potential) of at least ten have a high chance of providing a specific signal in vivo. A high level of nondisplaceable binding in vivo may require an in vitro B_{\max}/K_d much greater than ten to provide a useful specific signal in vivo (Eckelman and Mathis 2006b).

15.1.3.3 BBB Permeability

Lipophilicity is a measure of how much of a compound partitions into a lipid environment compared to an aqueous environment. CNS compounds have to pass the blood-brain barrier (BBB) and ideally should therefore have $\log P$ values well above 1 to allow free diffusion across the BBB. Nonspecific binding is known to be higher with increasing lipophilicity, and high nonspecific binding in target tissues reduces the signal-to-noise ratio, and thus, the ability to detect the specific signal (Pike 2009). It has been recommended that the $\log P$ values of potential CNS compounds should be between 1 and 3.5 (Clark 2003; Waterhouse 2003). It should also be pointed out that lipophilicity values (normally $\log P$ or $\log D$) are highly variable, depending on the methodology used for their determination. Values obtained using the traditional “shake-flask” method tends to be lower than those obtained by the HPLC, C18, and calculation methods. $\log P$ values determined using *in silico* methodology are also highly variable, depending on the algorithm used. Therefore, it has been suggested that $\log P$ should not be relied upon as a sole predictor of BBB penetration during brain radiotracer discovery. HPLC measurement of permeability, percentage of plasma protein binding, and membrane interactions may be potentially useful in predicting a radioligand’s in vivo performance (Tavares et al. 2012). Additionally, the BBB possesses efflux pumps which can prevent compounds from effectively accumulating in the brain, of which P-glycoprotein (P-gp) is a key efflux pump (Ohe et al. 2003). Therefore, a PET tracer should not be a substrate for P-gp. There are in vitro assays to determine whether a compound is a P-gp substrate or not (Horio et al. 1989; Braun et al. 2000; Wanger-Baumann et al. 2011).

15.1.3.4 In Vivo Stability

The formation of radioactive metabolites which might enter into the brain and confound the brain signals is undesired. Unfavorable is also the metabolic elimination of the radioactive nuclide from the radiotracer. Thus, the radioligand should be resistant to unfavorable metabolism for the acquisition time, and radioactive metabolites should not be taken up in the target area.

15.1.3.5 Efficient Radiosynthesis

Due to the short half-lives of common PET nuclides, a rapid and efficient radiolabeling process is crucial. The best radiosynthetic scheme should incorporate the radionuclide at the last synthetic step and occur on a time scale similar to the half-life of the radioisotope. Typically, the reaction time for synthetic schemes with multiple steps should be accomplished within two half-lives of the radioisotope. The establishment of a one-step radiosynthesis is desired for obtaining high radiochemical yields with high specific activities. The ratio between labeled and unlabeled tracer is defined by the specific activity. Low specific activities result in low-quality PET images especially for saturable systems such as enzymes, transporter proteins, and receptors. For receptors with low binding sites (low B_{\max}), very high specific activity is required in order to exclude substantial occupation of target sites by unlabeled ligand and the saturation of the biological system of interest.

It should be stressed that these criteria do not necessarily guarantee a successful glutamate radiotracer. They are merely guidelines to assist in the selection of potentially useful CNS imaging ligands. Recently, multiparameter optimization methods have been used to assess ligands which have central nervous drug-like properties. The parameters are (1) lipophilicity, calculated distribution coefficient ($ClogP$); (2) calculated distribution coefficient at pH=7.4 ($ClogD$); (3) molecular weight (MW); (4) topological polar surface area (TPSA); (5) number of hydrogen bond donors (HBD); and (6) pK_a (Wager et al. 2010, 2011). It is obvious that this multiparameter optimization might also find utility for developing successful CNS PET tracers.

When a potential radiotracer has been selected and a radiolabeling method has been developed, some preclinical evaluations and acute toxicity studies have to be performed prior to PET studies in humans. The characterization of a new radioligand includes autoradiography, biodistribution, and metabolite studies as well as pretreatment and displacement studies, using *in vitro*, *in vivo*, and *ex vivo* techniques. With the increasing ability to carry out PET studies in rodents, using dedicated small animal PET cameras, the evaluation of PET tracers is simplified and serves as an important bridge between laboratory and clinical science (Myers 2001; Lancelot and Zimmer 2010; Xi et al. 2011).

15.2 MGLuR1 PET Tracers

MGLuR1 has been implicated in neuroprotection, chronic and neuropathic pain, multiple sclerosis, motor dysfunction, epilepsy, cerebral ischemia, and cerebellar long-term depression (Neugebauer 2002; Swanson et al. 2005; Schkeryantz et al.

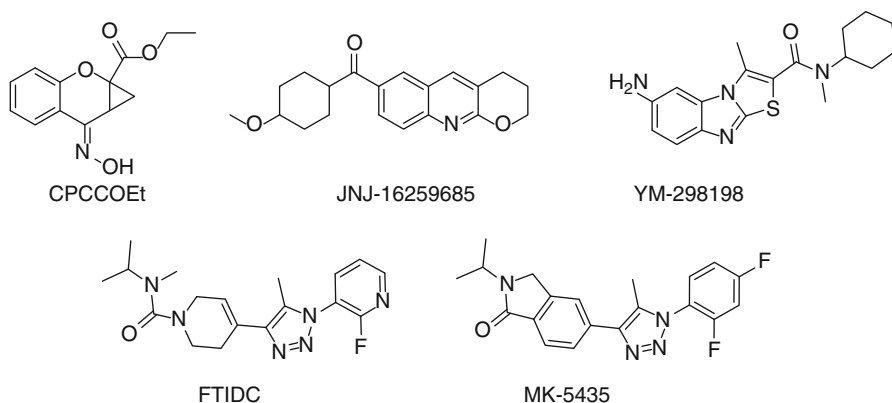


Fig. 15.2 Structures of some mGluR1 allosteric antagonists

2007; Wu et al. 2007; Kohara et al. 2008; Ito et al. 2009). Hence, monitoring mGluR1 *in vivo* and noninvasively would lead to a better understanding of the role of this receptor in the pathophysiology of biological processes mediated through glutamatergic pathways. It has been reported that the highest expression of mGluR1 in rat brain is in the cerebellum; moderate or low level in the thalamus, striatum, hippocampus, and cerebral cortex; and very low level in the brain stem (Fotuhi et al. 1993; Lavreysen et al. 2004a). Since noncompetitive ligands do not bind to the evolutionarily conserved glutamate binding site, they offer the potential for improved selectivity for mGluR subtypes (Parmentier et al. 2000). Therefore, potent and selective allosteric mGluR1 antagonists such as CPCCOEt (Annoura et al. 1996), JNJ-16259685 (Lavreysen et al. 2004b), YM-298198 (Kohara et al. 2005), FTIDC (Suzuki et al. 2007), and MK-5435 (Ito et al. 2009) have been developed (Fig. 15.2). Subsequently, several radiolabeled ligands for PET studies were synthesized and evaluated for their utility as potential imaging agents for the mGluR1 (Fig. 15.3).

15.2.1 ^{11}C -Labeled mGluR1 Tracers

The most important carbon-11 radioligands for mGluR1 are described below.

(3-ethyl-2- ^{11}C -methyl-6-quinolinyl)(cis-4-methoxycyclohexyl)-methanone, also denoted as ^{11}C JNJ-16567083, was the first reported allosteric antagonist PET tracer for imaging mGluR1 in the rodent brain (Huang et al. 2005). High binding affinity of JNJ-16567083 towards rat mGluR1 receptor was discovered with a K_i value of 0.87 nM. ^{11}C JNJ-16567083 was synthesized via palladium-mediated Stille coupling of the trialkyltin precursor with ^{11}C methyl iodide (Scheme 15.1). Biodistribution studies in rats under baseline and blockade conditions showed that ^{11}C JNJ-16567083 is selective and binds specifically to the mGluR1. Among the brain regions examined, the cerebellum, a region with the highest expression of the

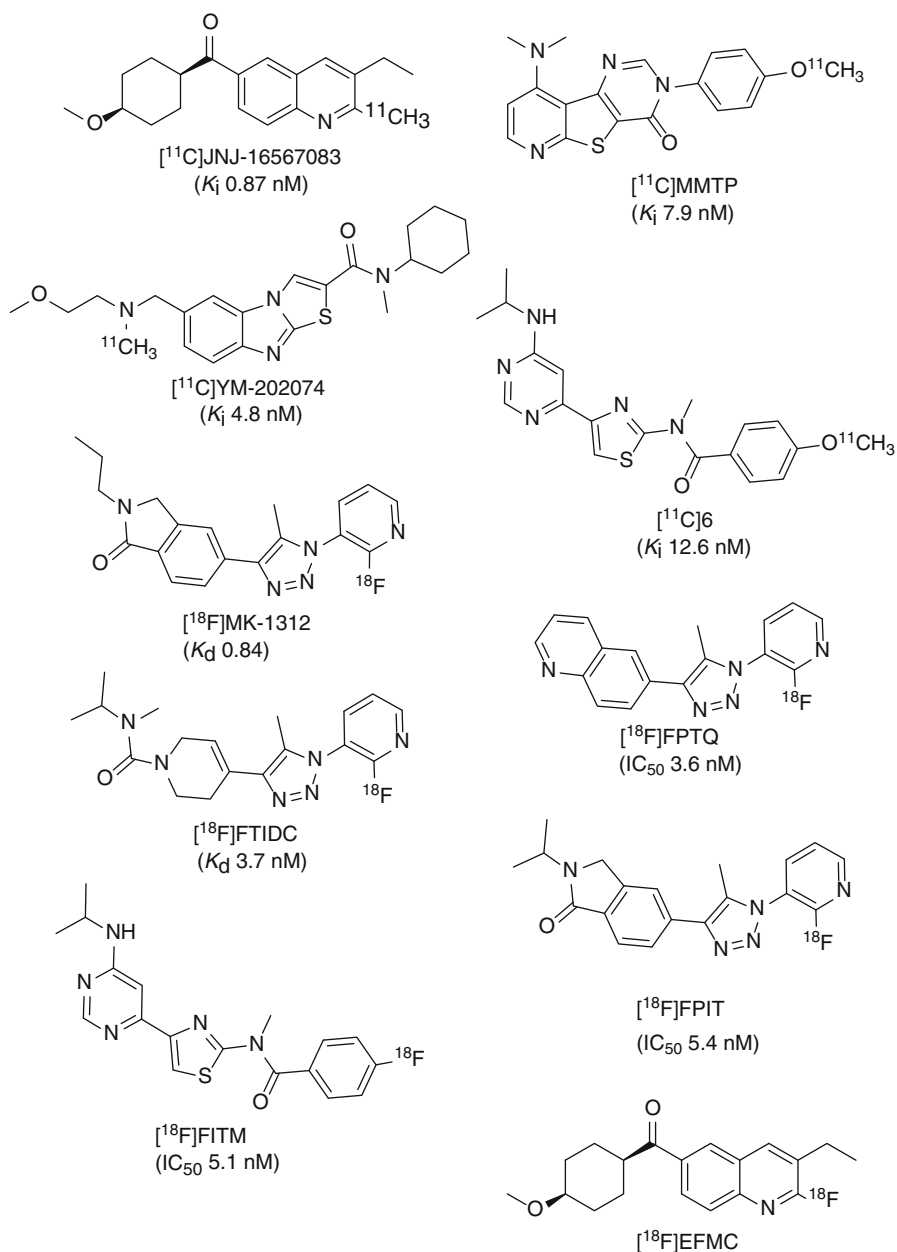
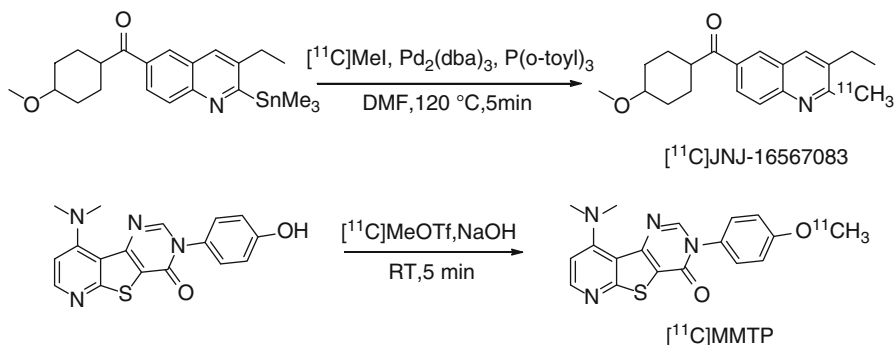


Fig. 15.3 Structures of some important mGluR1 PET tracers

mGluR1, exhibited the highest uptake of radioactivity and highest specific binding of 81 %. Since the publication of Huang et al., no further evaluation of this radioligand in higher species has been reported.



Scheme 15.1 Radiosyntheses of [¹¹C]JNJ-16567083 and [¹¹C]MMTP

[¹¹C]MMTP, [*O*-methyl-¹¹C]dimethylamino-3(4-methoxyphenyl)-3H-pyrido[3',2':4,5]thieno[3,2-d]pyrimidin-4-one, is another promising carbon-11-labeled mGluR1 PET radioligand, which was synthesized by methylation of the corresponding desmethyl precursor using [¹¹C]MeOTf in the presence of NaOH at room temperature (Scheme 15.1) (Prabhakaran et al. 2010). [¹¹C]MMTP selectively labeled mGluR1 binding sites in postmortem human brain slices containing the cerebellum, hippocampus, frontal cortex, and striatum using phosphor imaging autoradiography. The densities of binding sites (B_{\max}) for the various brain regions estimated from these autoradiography studies were 140, 110, 85, and 20 fmol/cm² for cerebellum, hippocampus, frontal cortex, and striatum, respectively. The authors performed PET studies in a baboon and showed that [¹¹C]MMTP penetrates the BBB and accumulated in mGluR1-rich regions. The highest uptake was observed in the cerebellum, a region known to have the highest level of mGluR1 expression.

N-cyclohexyl-6- $\{[N-(2\text{-methoxyethyl})-N\text{-methylamino}]methyl-N\text{-methylthiazolo}[3,2-a]benzimidazole-2\text{-carboxamide}$ (YM-202074) is a derivative of YM-298198 (Fig. 15.2) and exhibits an inhibition constant (K_i) of 4.8 nM towards mGluR1 and no inhibition up to 1 μ M for mGluR5 (Kohara et al. 2008). [¹¹C]YM-202074 was synthesized by *N*-[¹¹C] methylation of its desmethyl precursor with [¹¹C] methyl iodide in DMF at 90 °C for 3 min. [¹¹C]YM-202074 exhibited optimal lipophilicity with a log D value of 2.7. High specific binding of [¹¹C]YM-202074 for mGluR1 in rat brain was confirmed by in vitro autoradiography under blockade conditions with nonradioactive mGluR1 antagonists YM-202074, JNJ-16259685, and CPCCOEt. However, ex vivo autoradiography and PET study showed that the in vivo radioactivity distribution of [¹¹C]YM-202074 in rat brain region did not reflect the distribution pattern expected from the in vitro autoradiographic results. It was suggested that the discrepancy between in vitro and in vivo distributions might be caused by radiometabolite(s) of [¹¹C]YM-202074 in the brain, and less than 10 % intact compound was found in mouse plasma at 30 min p.i. Therefore, it was concluded that [¹¹C]YM-202074 may not be a useful PET ligand for the in vivo imaging of mGluR1 (Yanamoto et al. 2010).

N-(4-(6-(isopropylamino)pyrimidin-4-yl)-1,3-(thiazol-2-yl)-4- $^{[11]C}$ methoxy-*N*-methylbenzamide ($^{[11]C}$ 6, Fig. 15.3) was prepared by reacting the corresponding phenolic precursor with $^{[11]C}$ MeI (Fujinaga et al. 2012b). A K_i value of 12.6 nM was determined towards mGluR1 using rat brain homogenates in competition binding experiments. The $\log D$ value of $^{[11]C}$ 6 was 2.57 using shake-flask method in octanol/phosphate buffer at pH 7.4. In vitro autoradiography on sagittal section of rat brain slices showed heterogeneous distribution of $^{[11]C}$ 6, with highest uptake in the cerebellum, moderate radioactivity in the thalamus, and low in the striatum. The lowest radioactivity was detected in the brain stem. The in vivo PET results confirmed the expected distribution pattern of $^{[11]C}$ 6 in rat brain with highest uptake in the cerebellum, followed by thalamus and striatum. Pretreatment with unlabeled 6 (1 mg/kg) significantly reduced the uptake compared to the control group, and the distribution of radioactivity became fairly uniform throughout the brain. The maximum reduction of radioactivity uptake exceeded 85 % in the thalamus and striatum, demonstrating that $^{[11]C}$ 6 binds specifically to mGluR1 in the rat brain. The specificity of binding of $^{[11]C}$ 6 was also confirmed in mGluR1-knockout mouse brain. Although rapid metabolism was observed in the plasma, > 80 % total radioactivity in the rat brain homogenate was intact $^{[11]C}$ 6 (Fujinaga et al. 2012b). Further (pre) clinical evaluation of this promising radioligand is warranted.

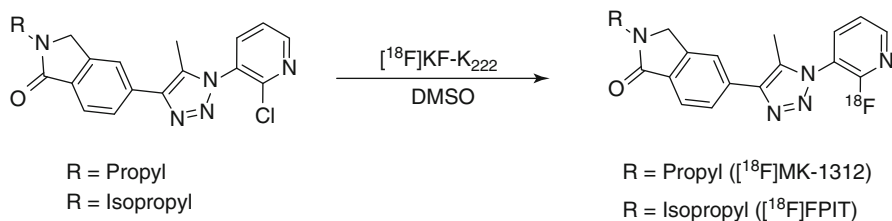
15.2.2 ^{18}F -Labeled mGluR1 Tracers

A number of fluorine-18-labeled compounds have been evaluated as potential PET ligands for imaging mGluR1. Some of the most important ^{18}F -labeled mGluR1 radioligands reported so far are described below.

15.2.2.1 ^{18}F -Labeled Triazole Analogues

Based on the structure of MK-5435, a potent and selective mGluR1 allosteric antagonist (Ito et al. 2009), several pyridyl triazole derivatives have been developed for imaging mGluR1. Depicted in Fig. 15.3 are the structures of four triazole analogues $^{[18]F}$ MK-1312, $^{[18]F}$ FPTQ, $^{[18]F}$ FTIDC, and $^{[18]F}$ FPIT.

$^{[18]F}$ MK-1312 was synthesized via reaction of $^{[18]F}$ KF with the corresponding chloropyridine in DMSO with microwave heating (Scheme 15.2) (Hostetler et al.

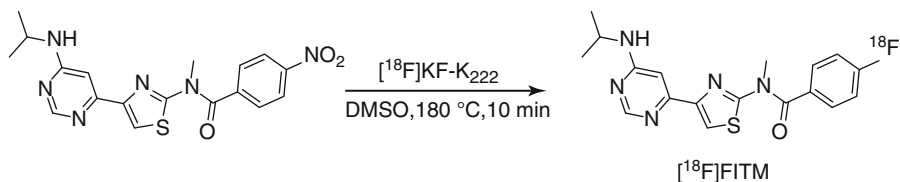


Scheme 15.2 Radiosynthetic scheme for $^{[18]F}$ MK-1312 and $^{[18]F}$ FPIT

2011). Saturation binding studies in cerebellum homogenates with [^{18}F]MK-1312 revealed a K_d value of 0.40 and 0.84 nM for rhesus monkey and human cerebellum, respectively. Autoradiography was performed with both human and monkey brain slices. The cerebellum exhibited the highest accumulation of activity for both species. Baseline PET studies in a monkey showed that this radiotracer rapidly penetrates the BBB, which is in line with its optimal lipophilicity value of 2.3. The distribution of [^{18}F]MK-1312 was heterogeneous, with highest uptake observed in the cerebellum and moderate uptake in the thalamus and striatum. Displacement studies with an mGluR1 allosteric antagonist, MK-5435, indicated specific binding of [^{18}F]MK-1312 to mGluR1 in the cerebellum of rhesus monkey, and blockade was concentration dependent (Hostetler et al. 2011). Measurement of in vivo tracer metabolism in plasma revealed that 17 % of plasma radioactivity was due to [^{18}F]MK-1312 at the end of a 90-min baseline PET scan. [^{18}F]MK-1312 possesses the desired characteristics for a potential mGluR1 PET tracer with respect to its lipophilicity, affinity, and specificity towards mGluR1.

[^{18}F]FPTQ, 6-[1-(2-[^{18}F]fluoro-3-pyridyl)-5-methyl-1H-1,2,3-triazol-4-yl]quinolone, was synthesized by heating the bromo precursor with [^{18}F]KF in anhydrous DMSO at 150 °C for 10 min. High binding affinities (IC_{50} values) of FPTQ towards mouse and human mGluR1 of 1.4 and 3.6 nM, respectively, have been reported (Suzuki et al. 2009). In vitro autoradiographic results showed that the distribution pattern of [^{18}F]FPTQ in the brain of rats was consistent with the distribution of mGluR1 reported previously (Lavreysen et al. 2004a). The specific binding of [^{18}F]FPTQ accounted for higher than 97 % of total binding, as determined by incubating with unlabeled FPTQ or mGluR1-selective JNJ-16259685 in rat brain slices. PET imaging showed that the distribution and uptake of [^{18}F]FPTQ in the rat brain was consistent with the results obtained by dissection as well as by in vitro autoradiography. The maximum standard uptake values (SUV) were 2.3 in the cerebellum, 2.1 in the thalamus, and ranged from 1.1 to 1.5 in the hippocampus, striatum, cerebral cortex, and medulla. However, the presence of a radiolabeled metabolite in the brain may confound the specific binding of this radioligand in vivo. Thus, [^{18}F]FPTQ may be of limited utility for the in vivo investigation of mGluR1 (Fujinaga et al. 2011).

[^{18}F]FTIDC, [4-[1-(2-[^{18}F]fluoropyridine-3-yl)-5-methyl-1H-1,2,3-triazol-4-yl]-*N*-isopropyl-*N*-methyl-3,6-dihydropyridine-1(2H)-carboxamide], was labeled with [^{18}F]fluoride by a halogen exchange reaction with the corresponding bromine derivative. Compound FTIDC was identified as a potent and selective mGluR1 allosteric antagonist (Suzuki et al. 2007). It showed high selectivity and equal inhibitory activity towards recombinant human, rat, and mouse mGluR1. The tritiated mGluR1-selective allosteric antagonist, [^3H]FTIDC, was identified as a radioligand having high affinity for mGluR1-expressing CHO cells ($K_d=2.1$ nM) and mouse cerebellum ($K_d=3.7$ nM) (Suzuki et al. 2009). Brain uptake of [^{18}F]FTIDC in mice was high. The highest accumulation was in the mGluR1-rich cerebellum at 10 min postinjection and was about two to three times higher than any other brain regions (Ohgami et al. 2009). Although the preliminary studies were promising, no further results have been reported.



Scheme 15.3 Radiosynthetic scheme for $[^{18}\text{F}]\text{FITM}$

$[^{18}\text{F}]\text{FPIT}$, 1-(2- $[^{18}\text{F}]\text{fluoro}$ -3-pyridyl)-4-(2-isopropyl-1-oxoisindolin-5-yl)-5-methyl-1H-1,2,3-triazole, an analogue of $[^{18}\text{F}]\text{MK-1312}$, was synthesized by reacting the bromo precursor with $[^{18}\text{F}]\text{KF}$ in anhydrous DMSO at 150 °C for 10 min (Scheme 15.2). FPIT was shown to have an IC_{50} value of 5.4 nM for mGluR1 and 2,500 nM for mGluR5 (Hostetler et al. 2011). The experimentally determined $\log D$ value of $[^{18}\text{F}]\text{FPIT}$ was 2.53, suggesting good BBB penetration. Autoradiography showed that the binding of $[^{18}\text{F}]\text{FPIT}$ is consistent with the reported distribution of mGluR1 with high specific binding in the cerebellum and thalamus of rat and monkey brains. $[^{18}\text{F}]\text{FPIT}$ displayed a similar distribution of radioactivity in both monkey and rat brains. The sequence of radioactivity level in the brain regions was cerebellum >thalamus >hippocampus >cerebral cortex >striatum >pons-medulla. Pretreatment with FPIT or JNJ-16259865 showed substantial inhibition of $[^{18}\text{F}]\text{FPIT}$ binding in these brain regions to a level close to or lower than that in the pons-medulla and almost diminished the difference in radioactivity among all brain regions. As indicated by the authors, a disadvantage of $[^{18}\text{F}]\text{FPIT}$ is its slow kinetics in the monkey brain and also the generation of a radiolabeled metabolite in the brain that could hamper accurate modeling and quantification with PET (Fujinaga et al. 2012a).

15.2.2.2 $[^{18}\text{F}]\text{FITM}$

$[^{18}\text{F}]\text{FITM}$ (4- $[^{18}\text{F}]\text{fluoro}$ -*N*-[4-[6-(isopropylamino)pyrimidin-4-yl]-1,3-thiazol-2-yl]-*N*-methylbenzamide) has a novel chemical structure that does not contain a triazole ring. Moreover, instead of the 2- $[^{18}\text{F}]\text{fluoropyridine}$ ring, $[^{18}\text{F}]\text{FITM}$ contains a $[^{18}\text{F}]\text{fluorobenzene}$ ring, which is expected to be stable against defluorination. $[^{18}\text{F}]\text{FITM}$ was synthesized by $[^{18}\text{F}]\text{fluorination}$ of its corresponding nitro precursor with $[^{18}\text{F}]\text{KF}$ in the presence of Kryptofix 222 (Scheme 15.3). FITM was shown to have potent antagonistic activity against human mGluR1 with an IC_{50} value of 5.1 nM. Excellent selectivity over other subtypes has been reported whereby the IC_{50} values were 7,000 nM for human mGluR5, >10,000 nM for mGluR2, and >10,000 nM for mGluR8 (Satoh et al. 2009). The distribution coefficient ($\log D$) of $[^{18}\text{F}]\text{FITM}$ was 1.46 using the shake-flask method at pH 7.4. Strong signals of radioactivity were found in known mGluR1-rich regions such as the cerebellum and thalamus in *in vitro* autoradiographic studies using rat brain sections. By co-incubation with the nonradioactive reference FITM or mGluR1 antagonist JNJ-16259685, radioactivity throughout the brain section decreased significantly compared with those in the control section. Upon co-incubation with MPEP, an antagonist for mGluR5, no change in radioactivity accumulation was observed. The signals of radioactivity in *ex vivo* autoradiography in

the brain sections of rat co-injected with JNJ-16259685 decreased by 86–91 % in mGluR1-rich regions compared with those of the control, indicating the tracer was specifically bound to mGluR1 (Yamasaki et al. 2011). Very recently, the same research group reported on the further evaluation of [^{18}F]FITM in a monkey brain. High in vivo stability was also observed. The uptake of [^{18}F]FITM in the monkey brain was not only high in mGluR1-rich cerebellum but also in brain regions such as the thalamus and hippocampus which have moderate expression levels of mGluR1. Specific binding of [^{18}F]FITM could be demonstrated in all the aforementioned brain regions by pretreatment with JNJ-16259685 (Yamasaki et al. 2012).

15.2.2.3 [^{18}F]EFMC

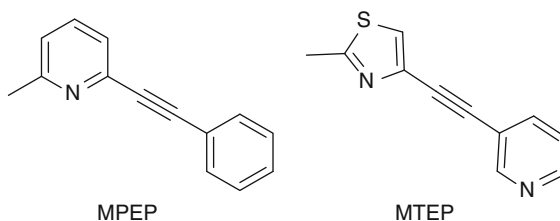
(3-Ethyl-2-[^{18}F]fluoroquinolin-6-yl) cis-(4-methoxycyclohexyl)methanone ([^{18}F]EFMC), the ^{18}F -labeled analogue of JNJ-16567083, was prepared by Br- ^{18}F exchange in DMSO in the presence of Kryptofix 222 at 100 °C for 5 min, followed by semi-HPLC purification (Lee et al. 2012). The radiochemical yield of [^{18}F]EFMC was 29 %. No degradation of [^{18}F]EFMC was found in MeCN/H $_2$ O (1:1) after 4 h at room temperature, and 90 % intact compound was present in human serum after 2 h of incubation at 37 °C. In biodistribution studies, the brain uptake of [^{18}F]EFMC was found to be 4.35 ± 0.32 % ID/g at 10 min after injection. Highest uptake of [^{18}F]EFMC was observed in the cerebellum in a PET study. Pretreatment with unlabeled EFMC led to a remarkable decrease of cerebellum uptake indicating specific binding towards mGluR1 in mice brain.

So far, mGluR1 PET ligands such as [^{18}F]FTIDC, [^{18}F]MK-1312, [^{18}F]FPIT, and [^{18}F]FPQT containing a triazole and a 2-[^{18}F]fluoropyridine ring have shown high specific binding to mGluR1-rich regions in rodent and primate brains in vitro and in vivo. For example, [^{18}F]FPIT had about fivefold higher SUV value than [^{11}C]YM-202074 (Yanamoto et al. 2010) and 0.5-fold lower uptake (SUV) than [^{11}C]JNJ-16567083 (Huang et al. 2005) in the rat cerebellum. However, to the best of our knowledge, none of these radioligands has progressed into a clinical setting. Based on the currently available results, it is suggested that radioligands containing a triazole and 2-[^{18}F]fluoropyridine ring are metabolized through similar in vivo elimination systems, and therefore ligands of this structural type may not be suitable for in vivo quantitative analysis of mGluR1. Among all the mGluR1 ligands evaluated so far, [^{18}F]FITM, a pyrimidine analogue, appears to show the most promising in vivo characteristics due to its higher metabolic stability and in vivo specificity. Thus, the expectations are that [^{18}F]FITM will soon find application in the clinic as a useful PET ligand for determining the distribution of mGluR1 expression in humans and also to ascertain the density of mGluR1 in pathological states in which mGluR1 is implicated.

15.3 MGLU5 PET Tracers

MGLU5 is an important target for PET imaging with potential for applications in drug development, diagnosis, and therapy monitoring. Metabotropic glutamate subtype 5 receptor (mGluR5) was cloned in 1992 and exists as a covalently bound

Fig. 15.4 Chemical structures of MPEP and MTEP



homodimer in heterologous expression system as well as in native tissue (Abe et al. 1992; Romano et al. 1996). It is expressed in brain regions such as the hippocampus, basal ganglia (striatum and nucleus accumbens), amygdala, and cortex (Romano et al. 1995; Gupta et al. 2005). mGluR5 has been implicated in a number of central nervous system disorders including depression, anxiety, addiction, schizophrenia, Parkinson's disease, and fragile X syndrome (Ohnuma et al. 1998; Rouse et al. 2000; Spooren et al. 2000, 2003; Tatarczynska et al. 2001; Spooren and Gasparini 2004; Bear 2005; Palucha et al. 2005; Tsai et al. 2005; Pietraszek et al. 2007; Carroll 2008). As such, this receptor provides a novel target for the development of therapeutic drugs for the aforementioned neurological disorders. A number of noncompetitive mGluR5 ligands have been developed during the past years, and their potential as therapeutic drugs for some of the abovementioned CNS disorders has been investigated (Varney et al. 2002; Augelli-Szafran and Schwarz 2003; Chua et al. 2005; Porter et al. 2005; Szydłowska et al. 2007; Carroll 2008; Chen and Conn 2008; Gasparini et al. 2008; Jaeschke et al. 2008; Kulkarni et al. 2009; Lindsley and Emmitte 2009; Ritzen et al. 2009; Emmitte 2011; Lindemann et al. 2011). In addition to CNS disorders, mGluR5 was found to be upregulated in CNS tumors and some non-CNS tumors (Brocke et al. 2010; Choi et al. 2011), participating in tumor growth and aggression.

The first potent and selective noncompetitive mGluR5 antagonists reported were the diaryl alkynes, 2-methyl-6-(phenylethynyl)pyridine (MPEP) (Gasparini et al. 1999; Lea and Faden 2006), and 3-[(2-methyl-1,3-thiazol-4-yl)ethynyl]pyridine (MTEP) (Fig. 15.4) (Cosford et al. 2002, 2003a, b). Since their publication, MPEP and MTEP have been used as templates for the design of noncompetitive mGluR5 antagonists. Also a series of PET radioligands based on their core structures have been labeled with either carbon-11 or fluorine-18 and evaluated in in vitro and in vivo studies. Two reviews providing an overview on available mGluR5 PET ligands have recently been published (Yu 2007; Mu et al. 2010).

15.3.1 MPEP-Derived mGluR5 Tracers

MPEP and its methyl analogue M-MPEP have been identified as potent, highly selective, noncompetitive antagonists for mGluR5. Derivatives of MPEP that have been labeled with either carbon-11 or fluorine-18 are depicted in Fig. 15.5.

The high binding affinity of MPEP (IC_{50} 20 nM) (Gasparini et al. 1999, 2002) to the heptahelical domain mGluR5 initiated the first radiolabeling of this compound

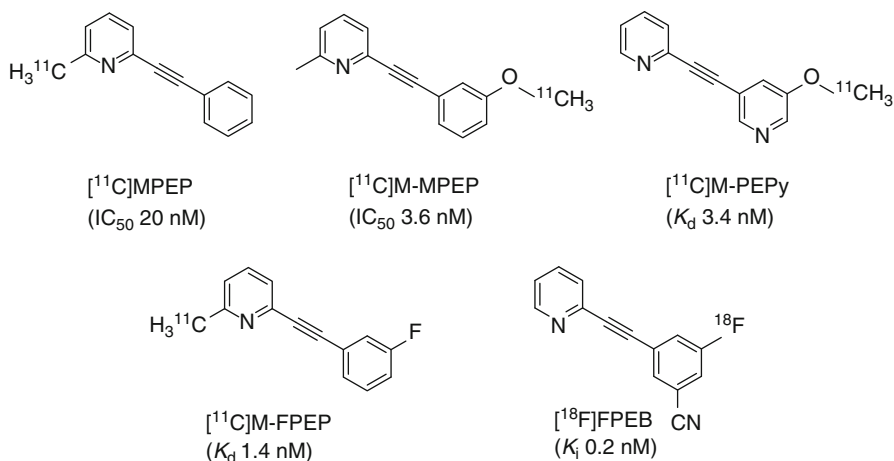
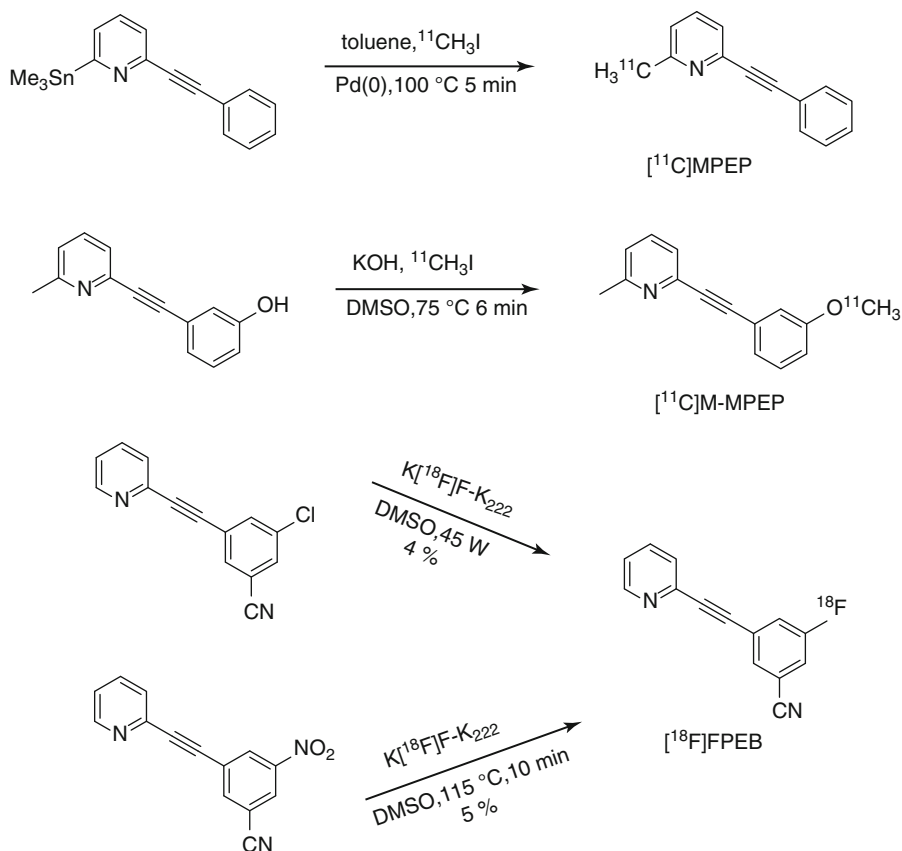


Fig. 15.5 Chemical structures of ^{11}C - and ^{18}F -labeled MPEP derivatives

with tritium. The identification of high-affinity analogues of M-MPEP (2-(2-(3-methoxyphenyl)ethynyl)pyridine, IC_{50} 3.6 nM) (Gasparini et al. 2002) and M-PEPy (3-methoxy-5-pyridin-2ylethynyl)pyridine, K_d 3.4 nM) (Anderson et al. 2003; Cosford et al. 2003a; Patel et al. 2003) prompted the radiolabeling of these derivatives with carbon-11 for evaluation as potential candidates for imaging mGluR5.

$[\text{C}^{11}]\text{MPEP}$ was prepared via Stille coupling reaction of 2-(phenylethynyl)-6-(trimethylstannyl)pyridine with $[\text{C}^{11}]\text{MeI}$ (Scheme 15.4) in high radiochemical purity and good specific radioactivity (33–44 GBq/ μmol) (Yu et al. 2005). In vivo PET imaging studies of $[\text{C}^{11}]\text{MPEP}$ in Sprague–Dawley rats showed high accumulation of $[\text{C}^{11}]\text{MPEP}$ in brain areas such as the olfactory bulb, striatum, hippocampus, frontal cortex, and cerebellum. Pre-administration of unlabeled MPEP (10 mg/kg) 5 min prior to administration of $[\text{C}^{11}]\text{MPEP}$ led to a decreased $[\text{C}^{11}]\text{MPEP}$ binding in the olfactory bulb. In contrast, an increased uptake was noted for the hippocampus and striatum suggesting that $[\text{C}^{11}]\text{MPEP}$ binds nonspecifically to these brain regions. No reasons have been provided by the authors to explain this phenomenon. For the olfactory bulb, the extent of specific binding was 45 and 61 % at 5 and 40 min postinjection, respectively.

The radiosynthesis of $[\text{C}^{11}]\text{M-MPEP}$ was accomplished by reacting $[\text{C}^{11}]\text{MeI}$ with phenolic precursor in the presence of solid KOH powder in 85 % radiochemical yield and 98 % radiochemical purity (Scheme 15.4) (Yu et al. 2005). Moderate uptake was observed after tail vein injection of $[\text{C}^{11}]\text{M-MPEP}$ into rats. Pre-administration of MPEP (10 mg/kg) induced a 60 % decrease in $[\text{C}^{11}]\text{M-MPEP}$ binding in the olfactory bulb 5 min postinjection. In other brain regions, the mGluR5 antagonist, MPEP, decreased $[\text{C}^{11}]\text{M-MPEP}$ binding only during the early time points: 45 % in the cortex, 14 % in the hippocampus, and 29 % in the striatum at 5 min postinjection. At 40 min postinjection, a binding ratio of olfactory bulb to



Scheme 15.4 Radiosyntheses of [^{11}C]MPEP, [^{11}C]M-MPEP, and [^{18}F]FPEB

cerebellum was 4.2. Kocic et al. also reported on the radiosynthesis and the *in vivo* evaluation of [^{11}C]M-MPEP albeit in an abstract (Kocic et al. 2001). In their study, Kocic and colleagues found an increased uptake of [^{11}C]M-MPEP radioactivity 30 min postinjection in the rat brain after co-injection with unlabeled M-MPEP (1 mg/kg). However, no information was provided on radioactivity uptake in the olfactory bulb.

[^{11}C]M-PEPy was obtained by reacting the desmethyl precursor with either [^{11}C]MeI (Yu et al. 2005) or [^{11}C]CH₃OTf (Severance et al. 2006) in the presence of KOH or NaOH in moderate radiochemical yield. *In vitro* phosphor imaging with [^{11}C]M-PEPy using human and rat brain tissues demonstrated high specific binding in the hippocampus, striatum, and cortex with minimal specific binding in the cerebellum. The hippocampus-to-cerebellum ratio found in this study was 37 in rats and 8 in humans. However, further *in vivo* micro-PET studies in rats using urethane anesthesia, PET studies in baboons using isoflurane anesthesia, and *ex vivo* studies in rats showed little specific binding in the brain and very fast tracer washout

Table 15.1 Lipophilicity, in vitro binding affinity, and specificity of ^{11}C -labeled MPEP derivatives

Compd	CLog P^a	IC $_{50}$	Specificity (brain)
[^{11}C]MPEP	3.6	20 nM	No
[^{11}C]M-MPEP	3.7	3.6 nM	Low
[^{11}C]M-PEPy	1.5	3.4 nM (K_d) ^b	Middle
[^{11}C]M-FPEP	2.5	1.4 nM (K_d) ^b	No

^aCLog P values were calculated based on ChemBioDraw software

^bObtained from saturation assays using [^3H]M-FPEP or [^{11}C]M-FPEP

(Severance et al. 2006). One possible explanation is that [^{11}C]M-PEPy is actively extruded from the brain by P-gp or some other multidrug-resistant like transport protein in the blood-brain barrier. Despite the promising in vitro results, the low signal-to-noise ratio found in vivo did not justify the use of [^{11}C]M-PEPy as a PET radiotracer in humans (Severance et al. 2006).

Kessler labeled 2-methyl-6-(3-fluoro-phenylethynyl)-pyridine (M-FPEP), another analogue of MPEP, with ^{11}C (Kessler 2004). [^{11}C]M-FPEP was prepared in good radiochemical yields and high specific radioactivity starting from its bromopyridine precursor. Saturation assays of [^{11}C]M-FPEP binding resulted in a single high-affinity binding site with a K_d of 1.4 ± 0.1 nM and a B_{max} value of 563 ± 190 fmol/mg protein. Dynamic PET studies in a rat indicated rapid uptake of [^{11}C]M-FPEP in rat brain, followed by a fast clearance. Classical biodistribution studies in rats showed a homogeneous distribution of [^{11}C]M-FPEP in all brain regions examined, suggesting nonspecific uptake in the brain, which was also confirmed in blocking studies.

Based on the data summarized in Table 15.1, although moderate to high binding affinities towards mGluR5 for all the ^{11}C -labeled MPEP derivatives have been observed, their utility as mGluR5 imaging agents has been limited due to their unfavorable in vivo properties. The radiosynthesis of [^{18}F]FPEB ([^{18}F]3-fluoro-5-[(pyridin-3-yl)ethynyl] benzonitrile), a structural analogue of M-FPEP, was accomplished via a nucleophilic aromatic substitution reaction using either nitro or Cl^- as a leaving group under conventional or microwave heating conditions (Hamill et al. 2005; Patel et al. 2007; Wang et al. 2007; Belanger et al. 2008). Low radiochemical yields were obtained under both conditions (Scheme 15.4). The low radiochemical yields may be due to the position of the leaving group which is not activated enough for aromatic nucleophilic substitution. High binding affinities of [^{18}F]FPEB towards mGluR5 in rat, rhesus, and human brain sections have been reported ($K_d = 0.1\text{--}0.15$ nM, $n \geq 3$) (Patel et al. 2007). [^{18}F]FPEB showed an approximately 70 % specific signal in the cortex and caudate-putamen of rat, rhesus, and human brain (Patel et al. 2007). Small animal PET imaging studies using Sprague-Dawley rats demonstrated that [^{18}F]FPEB accumulated in mGluR5-rich regions of the brain such as striatum and hippocampus with 77 % specific binding after 20 min postinjection (Patel et al. 2005). In blocking studies of [^{18}F]FPEB, pretreatment with 3 mg/kg, MTEP did not result in identical residual uptake in all regions. When [^{18}F]FPEB was blocked with 10 mg/kg MTEP, nearly homogeneous uptake of tracer

in all regions was observed, indicating full blockade had been achieved. It was also found that blocking mGluR5 is more efficient with MTEP than MPEP under the same conditions (Wang et al. 2007). PET imaging studies in a monkey also showed that [^{18}F]FPEB readily enters the brain and provides mGluR5-specific signal in all gray matter regions, including the cerebellum (Hamill et al. 2005). Initial human studies have been reported by Tamagnan et al. (2009). Dynamic PET images of six human subjects examined so far revealed excellent penetration of [^{18}F]FPEB into human brain with initial visualization of anterior cingulate, thalamus, caudate, and midbrain, while cerebellum showed low uptake.

15.3.2 MTEP-Derived mGluR5 Tracers

Structural modification of MTEP (Fig. 15.4) led to M-MTEP (4-(5-methoxypyridin-3-yl)ethynyl-2-methyl-4,5-dihydrothiazole, K_i 2.0 nM) (Cosford et al. 2003a; Patel et al. 2005) and M-MTEB (3-methyl-5-[(2-methyl-1,3-thiazol-4-yl)ethynyl]benzonitrile, K_i 0.23 nM) with improved binding affinity to mGluR5. The corresponding carbon-11- and fluorine-18-labeled PET radioligands derived from MTEP are shown in Fig. 15.6.

[^{11}C]M-MTEP was synthesized by reacting the cesium salt of 5-((2-methyl-4,5-dihydrothiazol-4-yl)ethynyl)pyridin-3-ol with [^{11}C]MeI in 39 % radiochemical yield (Patel et al. 2005). The [^{11}C]methyl group in [^{11}C]M-MTEB can be introduced by using either Stille (Suzuki et al. 1997) or Suzuki (Hostetler and Burns 2003) coupling reaction with [^{11}C]MeI as shown in Scheme 15.5. However, due to the ease of precursor synthesis and radiolabeling, the Suzuki route (Scheme 15.5, pathway

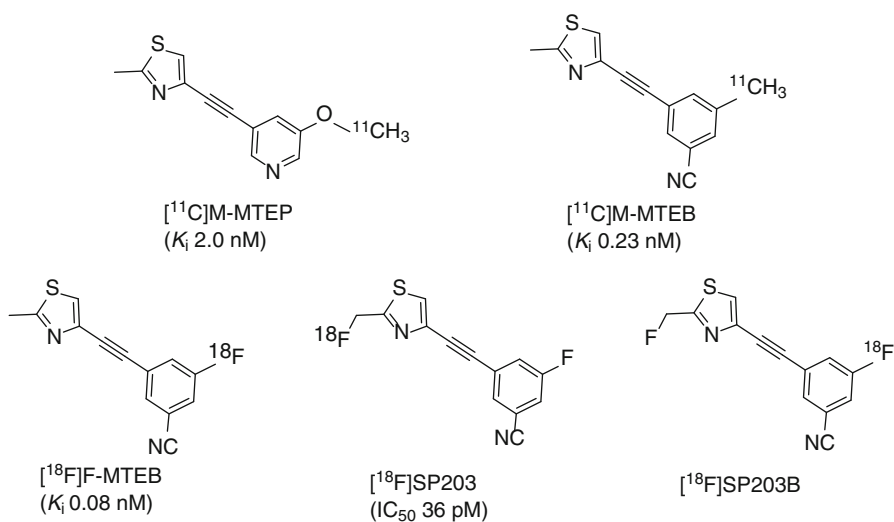
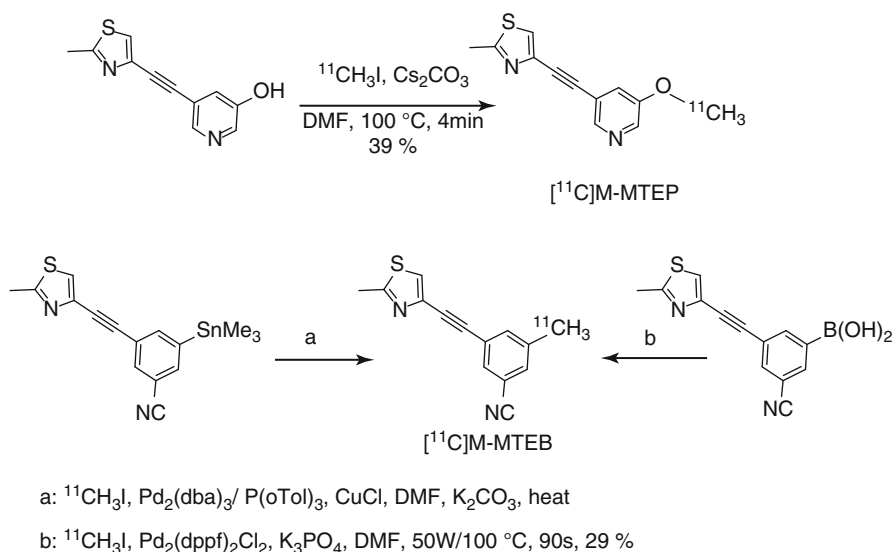


Fig. 15.6 Chemical structures of ^{11}C - and ^{18}F -labeled MTEP derivatives

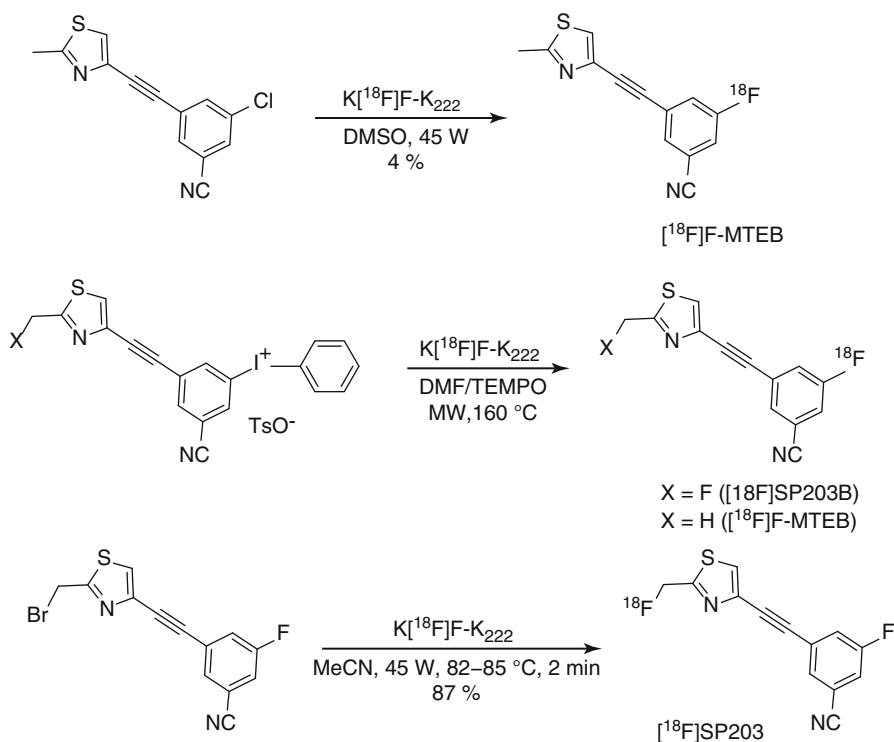


Scheme 15.5 Radiosynthetic routes to $[\text{1}^{11}\text{C}]\text{M-MTEP}$ and $[\text{1}^{11}\text{C}]\text{M-MTEB}$

b) with aryl boronic acid as the precursor was chosen (Hamill et al. 2005). A radiochemical yield of 29 % was obtained for $[\text{1}^{11}\text{C}]\text{M-MTEB}$ using DMF as solvent. The total synthesis time was ~20–23 min, and the specific radioactivity achieved was 70 GBq/ μmol .

PET imaging studies with $[\text{1}^{11}\text{C}]\text{M-MTEP}$ in a rat and a rhesus monkey showed a uniform distribution across most cerebral regions, and its clearance from the brain was also rapid, suggesting little retention by mGluR5 (Hamill et al. 2003; Krause et al. 2003). More promising results were obtained with $[\text{1}^{11}\text{C}]\text{M-MTEB}$. $[\text{1}^{11}\text{C}]\text{M-MTEB}$ showed rapid uptake into the brain of rhesus monkey and provided large, long-lasting specific signals in mGluR5-rich regions such as the striatum, lower uptake in the frontal cortex, but surprisingly also specific uptake in the cerebellum, a region known to contain low densities of mGluR5. Species differences in the distribution of mGluR5 may account for this uptake in the cerebellum (Hamill et al. 2005).

$[\text{1}^{18}\text{F}]\text{F-MTEB}$ ($[\text{1}^{18}\text{F}]\text{3-Fluoro-5-[(2-methyl-1,3-thiazol-4-yl)ethynyl]benzotrile}$) was synthesized (Scheme 15.6) by the same synthetic route as shown for $[\text{1}^{18}\text{F}]\text{FPEB}$ (Scheme 15.4) in low radiochemical yields (Hamill et al. 2005; Patel et al. 2005). The binding affinity (K_i) of F-MTEB towards mGluR5 was in the subnanomolar range (80 pM). High-quality mGluR5-specific images in rat and rhesus monkey PET studies were obtained with $[\text{1}^{18}\text{F}]\text{F-MTEB}$. The low radiochemical yield of 4 % would limit its application in human subjects; however, the recently reported high yielding method that uses iodonium salt as a precursor in the presence of TEMPO could increase the RCY of $[\text{1}^{18}\text{F}]\text{F-MTEB}$ threefold to 20 % (Telu et al. 2011). This is a step forward which would make possible the application of $[\text{1}^{18}\text{F}]\text{F-MTEB}$ in humans (Telu et al. 2011).



Scheme 15.6 Radiosynthetic routes to $[^{18}F]$ F-MTEB, $[^{18}F]$ SP203, and $[^{18}F]$ SP203B

3-Fluoro-5-(2-(2-(fluoromethyl)thiazol-4-yl)ethynyl) benzonitrile (designated SP203) an analogue of F-MTEB was found to have unusually high affinity ($IC_{50}=36$ pM) and potency in a phosphoinositol hydrolysis assay ($IC_{50}=0.71$ pM) for mGluR5 (Simeon et al. 2007). SP203 was labeled with fluorine-18 by treatment of its bromomethyl analogue with $[^{18}F]$ -fluoride in high radiochemical yield (87 %, Scheme 15.6).

The PET evaluation of $[^{18}F]$ SP203 in a monkey demonstrated that a high proportion of radioactivity in brain was bound to mGluR5. However, radioactivity also accumulated in the bone, suggesting *in vivo* defluorination (Simeon et al. 2007). *Ex vivo* analysis of metabolites in rat brain extracts indicated that defluorination of $[^{18}F]$ SP203 occurs by glutathionylation at the 2-fluoromethyl group in $[^{18}F]$ SP203 (Shetty et al. 2008). $[^{18}F]$ SP203 was further evaluated in human subjects by the same group (Brown et al. 2008; Kimura et al. 2010). The results showed that defluorination of $[^{18}F]$ SP203 was relatively small and that brain uptake could be robustly quantified. A recent study in nine healthy subjects using a bolus plus constant infusion protocol (equilibrium method) showed that this method is a viable alternative method and is slightly more precise than the standard bolus injection and kinetic modeling method (Kimura et al. 2012). To circumvent the problem of *in vivo*

radiodefluorination, the aryl fluorine part of SP203 was recently labeled with ^{18}F at the meta-position on the aromatic ring (Telu et al. 2011). Because this position is not activated enough towards aromatic nucleophilic substitution, iodonium salt was used as a precursor. A radiochemical yield of 33 % was obtained (Scheme 15.6). Compared to ^{18}F SP203, it is expected that ^{18}F SP203B will show a higher in vivo stability with respect to in vivo ^{18}F -defluorination.

15.3.3 ABP688-Related mGluR5 Tracers

Chemical modification of the original MPEP series allowed the identification of ABP688, a derivative in which the aromatic ring of the MPEP series is replaced by a functionalized cyclohexanone moiety (Fig. 15.7).

^{11}C ABP688 (3-(6-methyl-pyridin-2-ylethynyl)-cyclohex-2-enone- O - ^{11}C -methyl-oxime) was described in 2006 by Ametamey et al. (2006). The radiosynthesis of ABP688 was accomplished by reacting desmethyl-ABP688 in anhydrous DMF with ^{11}C MeI at 90 °C for 5 min using sodium hydride as a base (Scheme 15.7). ^{11}C ABP688 showed an optimal $\log D$ value of 2.4 and high binding affinity to mGluR5 (K_d 1.7 nM in rat) with a B_{\max} value of 231 ± 18 pmol/mg protein. Ex vivo autoradiography in wild-type mice and rats showed that the brain uptake of ^{11}C ABP688 was highly selective and specific, with high heterogeneous accumulation in known mGluR5-rich regions such as the hippocampus, caudate putamen, and cortex. The specificity of ^{11}C ABP688 binding was confirmed by blockade studies with M-MPEP (1 mg/kg), an antagonist for mGluR5. Up to 80 % reduction in radioactivity uptake in mGluR5-rich regions (hippocampus, striatum) was observed; however, no blocking effect was observed in the cerebellum. The observed heterogeneity of tracer uptake is consistent with the known distribution of mGluR5 in the brain. The specificity of binding of ^{11}C ABP688 was also confirmed in

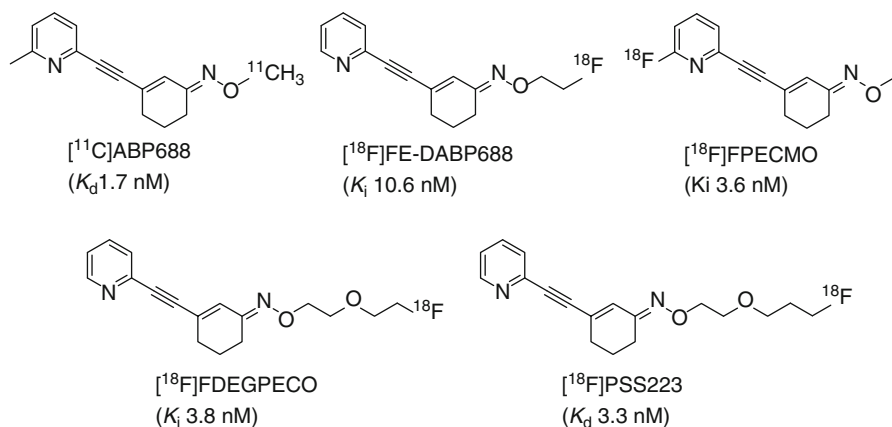
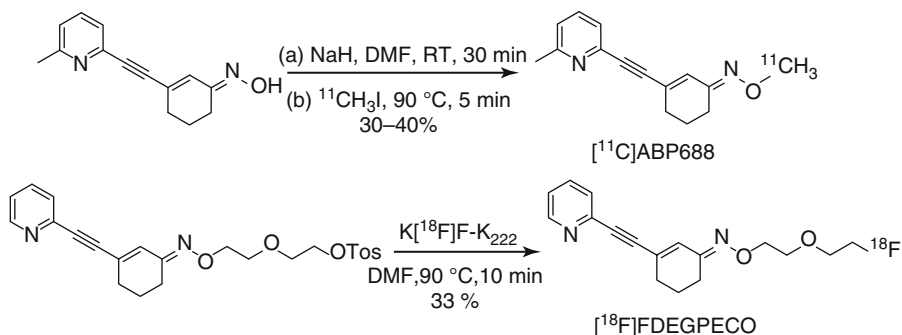


Fig. 15.7 Chemical structures of ^{11}C - and ^{18}F -labeled ABP derivatives



Scheme 15.7 Radiosyntheses of $[^{11}\text{C}]$ ABP688 and $[^{18}\text{F}]$ FDEGPECO

mGluR5-knockout mouse brain. Using the cerebellum as a reference region, radioactivity uptake ratios of 6.6 ± 0.1 , 5.4 ± 0.1 , and 4.6 ± 0.1 were obtained for the striatum, hippocampus, and cortex, respectively.

PET studies in rats and mice using a small animal PET scanner also demonstrated receptor-specific uptake in the brain regions known to be rich in mGluR5.

The first human PET studies on six healthy male volunteers using $[^{11}\text{C}]$ ABP688 as the PET tracer were reported by the same group (Ametamey et al. 2007; Treyer et al. 2008). Relatively high radioactivity concentrations were observed in mGluR5-rich brain regions such as the anterior cingulate, medial temporal lobe, amygdala, caudate, and putamen, whereas radioactivity uptake in the cerebellum and white matter, regions known to contain low densities of mGluR5, was low (Fig. 15.8). Specific distribution volume as an outcome measure of mGluR5 density in the various brain regions ranged from 5.45 ± 1.47 (anterior cingulate) to 1.91 ± 0.32 (cerebellum), and the rank order of the corresponding specific distribution volumes of $[^{11}\text{C}]$ ABP688 in cortical regions was temporal >frontal >occipital >parietal. The rank order of specific distribution volume obtained was in accordance with the reported distribution pattern of mGluR5 in rodents and humans. These results indicated that $[^{11}\text{C}]$ ABP688 has suitable characteristics in humans and is a promising PET ligand for imaging mGluR5 distribution in humans.

Encouraged by the animal and human PET imaging results of $[^{11}\text{C}]$ ABP688, several novel ^{18}F -labeled ABP688 derivatives have been evaluated as potential mGluR5 imaging agents by the group that first reported on $[^{11}\text{C}]$ ABP688 (Honer et al. 2007; Lucatelli et al. 2009; Baumann et al. 2010; Wanger-Baumann et al. 2011; Sephton Milicevic et al. 2012).

$[^{18}\text{F}]$ FE-DABP688 was produced by reacting 2- $[^{18}\text{F}]$ -fluoroethyl tosylate with the sodium salt of 3-(pyridin-2-ylethynyl)-cyclohex-2-enone-oxime in dry DMF. The isolated radiochemical yield was $25 \pm 8\%$ (Honer et al. 2007). Saturation assays of $[^{18}\text{F}]$ FE-DABP688 revealed a single high-affinity binding site with a K_d of 1.6 nM and a B_{max} value of 119 ± 24 fmol/mg protein. Biodistribution and PET studies of $[^{18}\text{F}]$ FE-DABP688 in rats indicated radioactivity uptake in mGluR5-rich regions such as the hippocampus, striatum, and cortex, while radioactivity

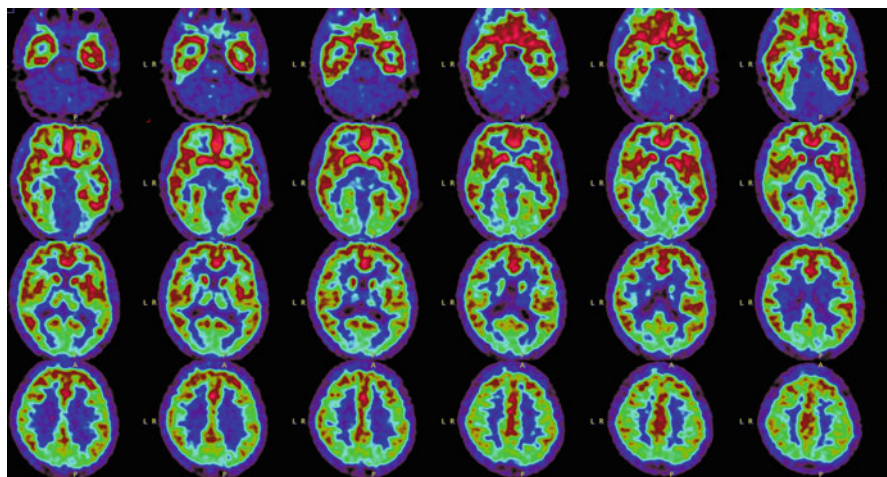


Fig. 15.8 Uptake of [^{11}C]ABP688 in a healthy volunteer

accumulation in the cerebellum was significantly low. Although the obtained PET image quality of [^{18}F]FE-DABP688 was comparable to that of [^{11}C]ABP688, [^{18}F]FE-DABP688 displayed unfavorable pharmacokinetics in the anesthetized rat with a fast washout from the forebrain resulting in a relatively short-lived signal. Consequently, [^{18}F]FE-DABP688 was abandoned and was not further exploited in primates.

^{18}F -(*E*)-3-((6-Fluoropyridin-2-yl)ethynyl)cyclohex-2-enone *O*-methyl oxime ([^{18}F]FPECMO) is another derivative of [^{11}C]ABP688 (Lucatelli et al. 2009). It was synthesized in a one-step reaction sequence by reacting $\text{K}[^{18}\text{F}]\text{F}-\text{K}_{222}$ complex with (*E*)-3-((6-bromopyridin-2-yl)ethynyl)cyclohex-2-enone *O*-methyl oxime in dry DMSO. The radiochemical yield after semi-preparative HPLC was 35 %, and specific activity was greater than 240 GBq/ μmol . [^{18}F]FPECMO exhibited optimal lipophilicity ($\log D = 2.1$) and high metabolic stability in vitro. Displacement studies revealed a K_i value of 3.6 nM for FPECMO. Biodistribution studies and ex vivo autoradiographies confirmed this specificity revealing highest radioactivity accumulation in mGluR5-rich brain regions. Despite high metabolic stability in various in vitro test systems, a rapid defluorination of the radiolabeled substance was observed in rats in vivo.

[^{18}F]FDEGPECO (*E*)-3-(pyridin-2-ylethynyl)cyclohex-2-enone *O*-2-(2-fluoroethoxy)ethyl oxime is one of the most recently developed ABP688 derivatives (Baumann et al. 2010; Wanger-Baumann et al. 2011). A K_i value of 3.8 ± 0.4 ($n=3$) nM was obtained for FDEGPECO, and the radioligand was synthesized in one-step reaction sequence by reacting $\text{K}[^{18}\text{F}]\text{F}-\text{K}_{222}$ complex with the corresponding tosyl precursor in anhydrous DMF (Scheme 15.7) in good radiochemical yield and high specific radioactivity. Scatchard plot analysis indicated two affinity binding sites with dissociation constants of 0.6 ± 0.2 nM and 13.7 ± 4.7 nM ($n=3$) and $B_{\text{max}1}$ and $B_{\text{max}2}$ values ranging from 470 to 1,870 fmol/mg and from 4.0 to 15.6 pmol/

mg protein, respectively. The in vitro autoradiography on rat brain slices showed a heterogeneous uptake consistent with the distribution of mGluR5 in the rat brain. PET imaging on rats revealed specific uptake of radioactivity in the mGluR5-rich brain regions. Postmortem biodistribution studies in rats that received intravenous injections of 8–16 MBq [^{18}F]FDEGPECO at 15 min p.i. confirmed the distribution pattern observed in PET. The highest radioactivity concentrations were observed in mGluR5-rich brain regions. The hippocampus/cerebellum and striatum/cerebellum ratios were 2.8 and 3.3, respectively. [^{18}F]FDEGPECO is one of the most promising fluorine-18-labeled ABP688 analogues so far although its background activity is relatively high and the radioactivity ratios when compared to [^{11}C]ABP688 (Ametamey et al. 2006) are lower.

[^{18}F]PSS223 ((E)-3-(pyridin-2-ylethynyl)cyclohex-2-enone *O*-(2-(3- ^{18}F -fluoropropoxy)ethyl) oxime), an [^{18}F]FDEGPECO analogue, was designed with the aim to increase the lipophilicity of the ligand, in which the side chain was extended by one methylene group (Sephton Milicevic et al. 2012). [^{18}F]PSS223 was obtained in 20 % decay-corrected radiochemical yield. Experimentally determined $\log D$ value of [^{18}F]PSS223 was 1.89, which is 0.2 log units higher than that of [^{18}F]FDEGPECO (Baumann et al. 2010) as expected. The in vitro binding affinity of [^{18}F]PSS223 was measured directly in a Scatchard assay to give a K_d value of 3.34 ± 2.05 nM. In vitro autoradiography on horizontal rat brain slices showed heterogeneous distribution of [^{18}F]PSS223 with the highest accumulation in brain regions where mGluR5 is highly expressed (hippocampus, striatum, and cortex). Autoradiography in vitro under blockade conditions with ABP688 also confirmed the high specificity of [^{18}F]PSS223 for mGluR5. Under the same blocking conditions but using the mGluR1 antagonist, JNJ-16259685, no blockade was observed demonstrating the selectivity of [^{18}F]PSS223 for mGluR5 over mGluR1. [^{18}F]PSS223 was stable in PBS and rat plasma but was significantly metabolized by rat liver microsomal enzymes and to a lesser extent by human liver microsomes. Within 60 min, 90 and 20 % of [^{18}F]PSS223 were metabolized by rat and human microsome enzymes, respectively. PET studies showed that [^{18}F]PSS223 has a fast clearance and only a weak accumulation in mGluR5-rich brain regions. A significant accumulation of radioactivity in the skull and jaws was also observed suggesting in vivo defluorination of [^{18}F]PSS223. Consequently a clear-cut visualization of mGluR5-rich brain regions in vivo in rats was not possible.

The difference in the in vivo behavior of [^{18}F]PSS223 and [^{18}F]FDEGPECO could be attributed to the β -heteroatom effect (French et al. 1993), by which primary aliphatic ^{18}F -atoms in a β -position to heteroatom (e.g., [^{18}F]FCH₂CH₂OR) are found to be metabolized at a slower rate. This is in line with the absence of defluorination of [^{18}F]FDEGPECO in vivo.

Among all the abovementioned mGluR5 PET ligands, [^{11}C]ABP688 is the most successful and widely used PET tracer for imaging mGluR5 in humans. Two potential ^{18}F -labeled mGluR5 tracers [^{18}F]FPEB and [^{18}F]SP203 are currently being validated in ongoing clinical trials, and the results of these clinical studies are eagerly awaited.

15.4 Other mGluR PET Tracers

The widely diverse and heterogeneous distribution of mGluR subtypes provides an opportunity for selectively targeting individual mGluR subtypes involved in CNS functions for the development of novel treatment strategies for psychiatric and neurological disorders. Many PET radioligands have been developed for group I subtypes (mGluR1 and mostly mGluR5), very few PET tracers for imaging group II mGluRs (mGluR2 and mGluR3). [^{11}C]CMGDE (Fig. 15.9) (*S,S,S*)-2-(2-carboxycyclopropyl)-2-(3- [^{11}C]methoxyphenethyl) glycine dimethyl ester, a pro-drug with affinity for both mGluR2 and mGluR3, was radiosynthesized in two steps with a radiochemical purity of more than 96 % (Wang et al. 2012). Small animal PET imaging studies demonstrated that [^{11}C]CMGDE readily penetrated into the brain and the radiotracer generated from [^{11}C]CMGDE, i.e., [^{11}C]CMG, had fast reversible binding to mGluR2- and mGluR3-rich regions including the striatum, hippocampus, and different cortical areas. Blocking studies with LY341495 showed only 20–30 % decrease in the binding of the radiotracer generated from [^{11}C]CMGDE in all brain areas with the highest decrease in the striatum 31.5 ± 3.2 %. As expected, PET imaging studies with [^{11}C]CMG showed no brain penetration in the male Sprague–Dawley rats. [^{11}C]CMGDE is the first PET tracer in this class that is brain penetrating; however, its specificity is not high enough to permit the in vivo imaging of mGluR2/3. At the recent SNM 2012 meeting in Miami, [^{11}C]JNJ-42491293 (structure not disclosed in the abstracts) was presented as a novel PET tracer for imaging mGluR2 (Celen et al. 2012; Van Laere et al. 2012). JNJ-42491293 was selected based on its affinity and selectivity towards mGluR2 and its favorable physicochemical properties. [^{11}C]JNJ-42491293 was obtained by alkylation of the phenolic precursor with [^{11}C]MeI followed by semi-HPLC purification. Preliminary biological evaluation of [^{11}C]JNJ-42491293 in rat brain demonstrated specific and reversible binding to mGluR2 allosteric site in the brain. The further evaluation of [^{11}C]JNJ-42491293 in 20 healthy male subjects showed that this new ligand readily enters the brain. High radioactivity uptake was observed in the striatum and cerebellum, consistent with the reported distribution pattern of mGluR2 in the human brain. These results strongly suggest that [^{11}C]JNJ-42491293 is a highly promising PET tracer for measuring mGluR2 availability in humans and may be suitable for assessing occupancy of drug candidates targeting this receptor.

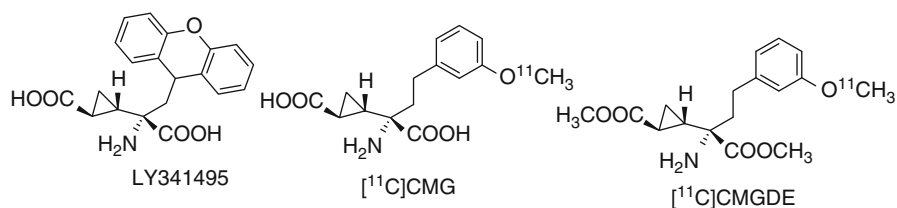


Fig. 15.9 Structures of GluR2/3 ligands

15.5 Application of mGluRs Tracers

With the availability of suitable mGluR5 radioligands, the utility of mGluR5 PET radioligands for drug development and the study of psychiatric and neurological diseases have recently been demonstrated. It was demonstrated that mGluR5 is upregulated in the striatum of parkinsonian primates using [^{11}C]M-PEPy. This supports interest in therapeutic exploration of mGluR5 antagonists in Parkinson's disease (Sanchez-Pernaute et al. 2008). [^{11}C]ABP688, a highly selective allosteric antagonist of mGluR5, was also used to study the level of mGluR5 expression in depressive patients. In this study, it was shown that mGluR5 is downregulated in the hippocampus of patients with depression (Deschwandten et al. 2011). This finding suggests that neurotransmission at mGluR5 is reduced in depression, possibly as a result of basal or compensatory changes in glutamate system activity. Implications of these findings are that mGluR5 receptor expression might be well suited for use as a biomarker for depression and as a target for novel antidepressant medications. A pilot study performed in baboons showed that extrasynaptic glutamate release by *N*-acetylcysteine (NAC) administration resulted in a decrease of [^{11}C]ABP688 uptake (Miyake et al. 2011). Thus [^{11}C]ABP688 PET imaging with a pharmacological, challenge might be a potential tool for detecting changes in glutamate levels in vivo. Furthermore, [^{11}C]ABP688 was used to determine the reproducibility of mGluR5 quantification in rats (Elmenhorst et al. 2012), and the results show that quantification of mGluR5 with [^{11}C]ABP688 is reliable and reproducible. Intraindividual variability of mGluR5 expression and specificity of [^{11}C]ABP688 uptake in baboons have also been reported (DeLorenzo et al. 2011b). The results in baboons indicated that the specificity of [^{11}C]ABP688 is high and that ligand binding can be effectively blocked by the highly specific mGluR5 antagonist, MTEP. With regard to reproducibility, an absolute variability of 11.5 % was reported for the two baboons investigated. Occupancy studies of mGluR5 using [^{11}C]ABP688 appear to be feasible in baboons (DeLorenzo et al. 2011b). However, in the test–retest studies in humans, high within-subject variability was observed (DeLorenzo et al. 2011a). As this type of high variation was not observed in [^{11}C]ABP688 baboon test–retest studies, the authors speculated it may be because of glutamate level variation in response to the stress of the PET scans. If PET imaging with [^{11}C]ABP688 could detect such differences, as preliminary evidence suggests, it could be used to help uncover the role of glutamate in the pathophysiology of brain disorders (DeLorenzo et al. 2011a).

In summary, a number of group I mGluRs ligands have been successfully used to label mGluR1 and mGluR5 in vitro. The development of these ligands into useful PET tracers in vivo, however, in most cases failed due to high nonspecific binding, unfavorable brain uptake kinetics, and/or limited metabolic stability. So far, three mGluR5 PET radioligands have been applied for clinical studies. [^{18}F]FITM, the most promising mGluR1 PET tracer, might be tested soon in a clinical setting. [^{11}C]JNJ-42491293, the first mGluR2 PET ligand used in humans, might also find clinical utility. Currently, radioligands for group III subtypes are lacking. Different mGluR subtype PET radioligands would have high utility in the drug development

programs by supporting the selection of appropriate doses of clinically relevant drugs and the determination of receptor occupancy of drugs, guiding proof of concept studies, and characterizing various disease states related to the type of receptor involved. Furthermore, they will have great implications for the identification of potential molecular therapeutic targets, in the development of new treatment strategies, and in helping to understand psychiatric and neurological diseases.

References

- Abe T, Sugihara H, Nawa H, Shigemoto R, Mizuno N, Nakanishi S (1992) Molecular characterization of a novel metabotropic glutamate receptor mGluR5 coupled to inositol phosphate/Ca²⁺ signal transduction. *J Biol Chem* 267:13361–13368
- Ametamey SM, Kessler LJ, Honer M, Wyss MT, Buck A, Hintermann S, Auberson YP, Gasparini F, Schubiger PA (2006) Radiosynthesis and preclinical evaluation of C-11-ABP688 as a probe for imaging the metabotropic glutamate receptor subtype 5. *J Nucl Med* 47:698–705
- Ametamey SM, Treyer V, Streffer J, Wyss MT, Schmidt M, Blagojev M, Hintermann S, Auberson Y, Gasparini F, Fischer UC, Buck A (2007) Human PET studies of metabotropic glutamate receptor subtype 5 with C-11-ABP688. *J Nucl Med* 48:247–252
- Ametamey SM, Honer M, Schubiger PA (2008) Molecular imaging with PET. *Chem Rev* 108:1501–1516
- Anderson JJ, Bradbury MJ, Giracello DR, Chapman DF, Holtz G, Roppe J, King C, Cosford NDP, Varney MA (2003) In vivo receptor occupancy of mGlu5 receptor antagonists using the novel radioligand [H-3]3-methoxy-5-(pyridin-2-ylethynyl)pyridine. *Eur J Pharmacol* 473:35–40
- Annoura H, Fukunaga A, Uesugi M, Tatsuoka T, Horikawa Y (1996) A novel class of antagonists for metabotropic glutamate receptors, 7-(hydroxyimino)cyclopropa[b]chromen-1a-carboxylates. *Bioorg Med Chem Lett* 6:763–766
- Augelli-Szafran CE, Schwarz RD (2003) Metabotropic glutamate receptors: agonists, antagonists and allosteric modulators. *Ann Rep Med Chem* 38:21–30
- Baumann CA, Mu L, Johannsen S, Honer M, Schubiger PA, Ametamey SM (2010) Structure-activity relationships of fluorinated (E)-3-((6-methylpyridin-2-yl)ethynyl)cyclohex-2-enone-O-methylxime (ABP688) derivatives and the discovery of a high affinity analogue as a potential candidate for imaging metabotropic glutamate receptors subtype 5 (mGluR5) with positron emission tomography (PET). *J Med Chem* 53:4009–4017
- Bear MF (2005) Therapeutic implications of the mGluR theory of fragile X mental retardation. *Genes Brain Behav* 4:393–398
- Belanger MJ, Krause SM, Ryan C, Sanabria-Bohorquez S, Li WP, Hamill TG, Burns HD (2008) Biodistribution and radiation dosimetry of [F-18]F-PEB in nonhuman primates. *Nucl Med Commun* 29:915–919
- Bettler B, Mülle C (1995) Review: neurotransmitter receptors. II. AMPA and kainate receptors. *Neuropharmacology* 34:123–139
- Bradley SR, Marino MJ, Wittmann M, Rouse ST, Awad H, Levey AI, Conn PJ (2000) Activation of group II metabotropic glutamate receptors inhibits synaptic excitation of the substantia nigra pars reticulata. *J Neurosci* 20:3085–3094
- Braun A, Hammerle S, Suda K, Rothen-Rutishauser B, Gunther M, Kramer SD, Wunderli-Allenspach H (2000) Cell cultures as tools in biopharmacy. *Eur J Pharmaceut Sci* 11(Suppl 2):S51–S60
- Brocke KS, Stauffer C, Luksch H, Geiger KD, Stepulak A, Marzahn J, Schackert G, Temme A, Ikonomidou C (2010) Glutamate receptors in pediatric tumors of the central nervous system. *Cancer Biol Ther* 9:455–468
- Brown AK, Kimura Y, Zoghbi SS, Simeon FG, Liow J-S, Kreisl WC, Tau A, Fujita M, Pike VW, Innis RB (2008) Metabotropic glutamate subtype 5 receptors are quantified in the human brain with a novel radioligand for PET. *J Nucl Med* 49:2042–2048

- Cai LS, Lu SY, Pike VW (2008) Chemistry with [F-18]fluoride ion. *Eur J Org Chem* 17:2853–2873
- Carroll FI (2008) Antagonists at metabotropic glutamate receptor subtype 5 structure activity relationships and therapeutic potential for addiction. *Addiction Reviews* 1141:221–232
- Cartmell J, Schoepp DD (2000) Regulation of neurotransmitter release by metabotropic glutamate receptors. *J Neurochem* 75:889–907
- Celen S, Koole M, Alcazar J, De Angelis M, Schmidt M, Van Laere K, Verbruggen A, Langlois X, Andres JI, Bormans G (2012) Preliminary biological evaluation of [¹¹C]JNJ42491293 as a radioligand for PET imaging of mGluR2 in brain. *J Nucl Med* 53(Suppl 1):286
- Chen YL, Conn PJ (2008) mGluR(5) positive allosteric modulators. *Drug Future* 33:355–360
- Choi KY, Chang K, Pickel JM, Badger JD 2nd, Roche KW (2011) Expression of the metabotropic glutamate receptor 5 (mGluR5) induces melanoma in transgenic mice. *Proc Natl Acad Sci U S A* 108:15219–15224
- Chua PC, Nagasawa JY, Bleicher LS, Munoz B, Schweiger EJ, Tehrani L, Anderson JJ, Cramer M, Chung J, Green MD, King CD, Reyes-Manalo G, Cosford NDP (2005) Cyclohexenyl- and dehydropiperidinyl-alkynyl pyridines as potent metabotropic glutamate subtype 5 (mGlu5) receptor antagonists. *Bioorg Med Chem Lett* 15:4589–4593
- Clark DE (2003) In silico prediction of blood-brain barrier permeation. *Drug Discov Today* 8:927–933
- Cosford NDP, Tehrani L, Arruda J, King C, McDonald IA, Munoz B, Roppe J, Anderson E, Bristow L, Brodtkin J, Rao S, Siegel R, Tattersall D, Washburn M, Prasit P, Varney M (2002) 3-[(2-methyl-1,3-thiazol-4-yl)ethynyl]pyridine (MTEP): design and synthesis of a potent and highly selective metabotropic glutamate subtype 5 (mGlu5) receptor antagonist with anxiolytic activity. *Neuropharmacology* 43:282–283
- Cosford NDP, Roppe J, Tehrani L, Schweiger EJ, Seiders TJ, Chaudary A, Rao S, Varney MA (2003a) [H-3]-methoxymethyl-MTEP and [H-3]-methoxy-PEPy: potent and selective radioligands for the metabotropic glutamate subtype 5 (mGlu5) receptor. *Bioorg Med Chem Lett* 13:351–354
- Cosford NDP, Tehrani L, Roppe J, Schweiger E, Smith ND, Anderson J, Bristow L, Brodtkin J, Jiang XH, McDonald I, Rao S, Washburn M, Varney MA (2003b) 3-[(2-Methyl-1,3-thiazol-4-yl)ethynyl]-pyridine: a potent and highly selective metabotropic glutamate subtype 5 receptor antagonist with anxiolytic activity. *J Med Chem* 46:204–206
- DeLorenzo C, Kumar JSD, Mann JJ, Parsey RV (2011a) In vivo variation in metabotropic glutamate receptor subtype 5 binding using positron emission tomography and [(11)C]ABP688. *J Cereb Blood Flow Metab* 31:2169–2180
- DeLorenzo C, Milak MS, Brennan KG, Kumar JSD, Mann JJ, Parsey RV (2011b) In vivo positron emission tomography imaging with [(11)C]ABP688: binding variability and specificity for the metabotropic glutamate receptor subtype 5 in baboons. *Eur J Nucl Med Mol Imaging* 38:1083–1094
- Deschwanden A, Karolewicz B, Feyissa AM, Treyer V, Ametamey SM, Johayem A, Burger C, Auberson YP, Sovago J, Stockmeier CA, Buck A, Hasler G (2011) Reduced metabotropic glutamate receptor 5 density in major depression determined by [(11)C]ABP688 PET and post-mortem study. *Am J Psychiatry* 168:727–734
- Eckelman WC, Mathis CA (2006b) Targeting proteins in vivo: in vitro guidelines. *Nucl Med Biol* 33:161–164
- Eckelman WC, Kilbourn MR, Mathis CA (2006) Discussion of targeting proteins in vivo: in vitro guidelines. *Nucl Med Biol* 33:449–451
- Elmenhorst D, Aliaga A, Bauer A, Rosa-Neto P (2012) Test-retest stability of cerebral mGluR(5) quantification using [(11)C]ABP688 and positron emission tomography in rats. *Synapse* 66:552–560
- Emmitte KA (2011) Recent advances in the design and development of novel negative allosteric modulators of mGlu(5). *ACS Chem Neurosci* 2:411–432
- Fotuhi M, Sharp AH, Glatt CE, Hwang PM, von Krosigk M, Snyder SH, Dawson TM (1993) Differential localization of phosphoinositide-linked metabotropic glutamate receptor (mGluR1) and the inositol 1,4,5-trisphosphate receptor in rat brain. *J Neurosci* 13:2001–2012

- Fowler JS, Volkow ND, Wang GJ, Ding YS, Dewey SL (1999) PET and drug research and development. *J Nucl Med* 40:1154–1163
- French AN, Napolitano E, VanBrocklin HF, Hanson RN, Welch MJ, Katzenellenbogen JA (1993) Synthesis, radiolabeling and tissue distribution of 11 beta-fluoroalkyl- and 11 beta-fluoroalkoxy-substituted estrogens: target tissue uptake selectivity and defluorination of a homologous series of fluorine-18-labeled estrogens. *Nucl Med Biol* 20:31–47
- Fujinaga M, Yamasaki T, Kawamura K, Kumata K, Hatori A, Yui J, Yanamoto K, Yoshida Y, Ogawa M, Nengaki N, Maeda J, Fukumura T, Zhang MR (2011) Synthesis and evaluation of 6-[1-(2-[(18)F]fluoro-3-pyridyl)-5-methyl-1H-1,2,3-triazol-4-yl]quinoline for positron emission tomography imaging of the metabotropic glutamate receptor type 1 in brain. *Bioorg Med Chem* 19:102–110
- Fujinaga M, Maeda J, Yui J, Hatori A, Yamasaki T, Kawamura K, Kumata K, Yoshida Y, Nagai Y, Higuchi M, Suhara T, Fukumura T, Zhang MR (2012a) Characterization of 1-(2-[(18)F]fluoro-3-pyridyl)-4-(2-isopropyl-1-oxo-isoindoline-5-yl)-5-methyl-1H-1,2,3-triazole, a PET ligand for imaging the metabotropic glutamate receptor type 1 in rat and monkey brains. *J Neurochem* 121:115–124
- Fujinaga M, Yamasaki T, Yui J, Hatori A, Xie L, Kawamura K, Asagawa C, Kumata K, Yoshida Y, Ogawa M, Nengaki N, Fukumura T, Zhang MR (2012b) Synthesis and evaluation of novel radioligands for positron emission tomography imaging of metabotropic glutamate receptor subtype 1 (mGluR1) in rodent brain. *J Med Chem* 55:2342–2352
- Gasparini F, Lingenhoehl K, Flor PJ, Stoehr N, Stierlin C, Heinrich M, Vranesic I, Allgeier H, Biollaz M, Heckendorn R, Urwyler S, Schmutz M, Spooren W, Varney MA, Johnson EC, Hess SD, Sakaan A, Santori E, Velicelebi G, Kuhn R (1999) Discovery of 2-methyl-6-(phenylethynyl)-pyridine (MPEP): a highly potent and selective mGluR5 antagonist. *Neuropharmacology* 38:52
- Gasparini F, Andres H, Flor PJ, Heinrich M, Inderbitzin W, Lingenhohl K, Muller H, Munk VC, Omilusik K, Stierlin C, Stoehr N, Vranesic I, Kuhn R (2002) [H-3]-M-MPEP, a potent, subtype-selective radioligand for the metabotropic glutamate receptor subtype 5. *Bioorg Med Chem Lett* 12:407–409
- Gasparini F, Bilbe G, Gomez-Mancilla B, Spooren W (2008) mGluR5 antagonists: discovery, characterization and drug development. *Curr Opin Drug Discov Devel* 11:655–665
- Gereau RW, Conn PJ (1995) Roles of specific metabotropic glutamate-receptor subtypes in regulation of hippocampal Ca1 pyramidal cell excitability. *J Neurophysiol* 74:122–129
- Gupta DS, McCullumsmith GE, Beneyto M, Haroutunian V, Davis KL, Meador-Woodruff JH (2005) Metabotropic glutamate receptor protein expression in the prefrontal cortex and striatum in schizophrenia. *Synapse* 57:123–131
- Hamill TG, Seiders TJ, Krause S, Ryan C, Sanabria S, Gibson RE, Patel S, Cosford NDP, Roppe J, Yang J, King C, Hargreaves RJ, Burns HD (2003) The synthesis and characterization of mGluR5 receptor PET ligands. *J Labelled Compd Rad* 46:S184
- Hamill TG, Krause S, Ryan C, Bonnefous C, Govek S, Seiders TJ, Cosford NDP, Roppe J, Kamenecka T, Patel S, Gibson RE, Sanabria S, Riffel K, Eng WS, King C, Yang XQ, Green MD, O'Malley SS, Hargreaves R, Burns HD (2005) Synthesis, characterization, and first successful monkey imaging studies of metabotropic glutamate receptor subtype 5 (mGluR5) PET radiotracers. *Synapse* 56:205–216
- Honer M, Stoffel A, Kessler LJ, Schubiger PA, Ametamey SM (2007) Radiolabeling and in vitro and in vivo evaluation of [F-18]-FE-DABP688 as a PET radioligand for the metabotropic glutamate receptor subtype 5. *Nucl Med Biol* 34:973–980
- Horio M, Chin KV, Currier SJ, Goldenberg S, Williams C, Pastan I, Gottesman MM, Handler J (1989) Trans-epithelial transport of drugs by the multidrug transporter in cultured Madin-Darby canine kidney-cell epithelia. *J Biol Chem* 264:14880–14884
- Hostetler ED, Burns HD (2003) An improved synthesis of substituted [C-11]toluenes via Suzuki coupling with [C-11]methyl iodide. *J Labelled Compd Rad* 46:S75
- Hostetler ED, Eng W, Joshi AD, Sanabria-Bohorquez S, Kawamoto H, Ito S, O'Malley S, Krause S, Ryan C, Patel S, Williams M, Riffel K, Suzuki G, Ozaki S, Ohta H, Cook J, Burns HD,

- Hargreaves R (2011) Synthesis, characterization, and monkey PET studies of [(18)F]MK-1312, a PET tracer for quantification of mGluR1 receptor occupancy by MK-5435. *Synapse* 65:125–135
- Huang YY, Narendran R, Bischoff F, Guo NN, Zhu ZH, Bae SA, Lesage AS, Laruelle M (2005) A positron emission tomography radioligand for the in vivo labeling of metabotropic glutamate 1 receptor: (3-ethyl-2-[C-11]methyl-6-quinoliny) (cis-4-methoxycyclohexyl)methanone. *J Med Chem* 48:5096–5099
- Ito S, Hirata Y, Nagatomi Y, Satoh A, Suzuki G, Kimura T, Satow A, Maehara S, Hikichi H, Hata M, Ohta H, Kawamoto H (2009) Discovery and biological profile of isoindolinone derivatives as novel metabotropic glutamate receptor 1 antagonists: a potential treatment for psychotic disorders. *Bioorg Med Chem Lett* 19:5310–5313
- Jaeschke G, Wettstein JG, Nordquist RE, Spooen W (2008) mGlu5 receptor antagonists and their therapeutic potential. *Expert Opin Ther Pat* 18:123–142
- Kessler LJ (2004) Development of novel ligands for PET imaging of metabotropic glutamate receptor subtype 5 (mGluR5). Dissertation No 15633, ETH-Zürich
- Kimura Y, Simeon FG, Hatazawa J, Mozley PD, Pike VW, Innis RB, Fujita M (2010) Biodistribution and radiation dosimetry of a positron emission tomographic ligand, (18)F-SP203, to image metabotropic glutamate subtype 5 receptors in humans. *Eur J Nucl Med Mol Imaging* 37:1943–1949
- Kimura Y, Simeon FG, Zoghbi SS, Zhang Y, Hatazawa J, Pike VW, Innis RB, Fujita M (2012) Quantification of metabotropic glutamate subtype 5 receptors in the brain by an equilibrium method using ¹⁸F-SP203. *Neuroimage* 59:2124–2130
- Kohara A, Toya T, Tamura S, Watabiki T, Nagakura Y, Shitaka Y, Hayashibe S, Kawabata S, Okada M (2005) Radioligand binding properties and pharmacological characterization of 6-amino-N-cyclohexyl-N,3-dimethylthiazolo[3,2-a] benzimidazole-2-carboxamide (YM-298198), a high-affinity, selective, and noncompetitive antagonist of metabotropic glutamate receptor type 1. *J Pharmacol Exp Ther* 315:163–169
- Kohara A, Takahashi M, Yatsugi S, Tamura S, Shitaka Y, Hayashibe S, Kawabata S, Okada M (2008) Neuroprotective effects of the selective type 1 metabotropic glutamate receptor antagonist YM-202074 in rat stroke models. *Brain Res* 1191:168–179
- Kocic M, Honer M, Ametamey SM, Gasparini F, Andres H, Bischoff F, Flor PJ, Heinrich M, Vranesic I, Spooen W, Kuhn R, Schubiger PA (2001) Radiolabeling and in vivo evaluation of ¹¹C-M-MPEP as a PET radioligand for the imaging of the metabotropic glutamate receptor 5 (mGluR5). *J Labelled Compd Rad* 44:S231–S232
- Krause SM, Hamill TG, Seiders TJ, Ryan C, Sanabria S, Gibson RE, Patel S, Cosford NDP, Roppe JR, Hargreaves RJ, Burns HD (2003) In vivo characterization of PET ligands for the mGluR5 receptor in rhesus monkey. *Mol Imaging Biol* 5:166
- Kulkarni SS, Zou MF, Cao JJ, Deschamps JR, Rodriguez AL, Conn PJ, Newman AH (2009) Structure-activity relationships comparing N-(6-methylpyridin-yl)-substituted aryl amides to 2-methyl-6-(substituted-arylethynyl)pyridines or 2-methyl-4-(substituted-arylethynyl)thiazoles as novel metabotropic glutamate receptor subtype 5 antagonists. *J Med Chem* 52:3563–3575
- Lancelot S, Zimmer L (2010) Small-animal positron emission tomography as a tool for neuropharmacology. *Trends Pharmacol Sci* 31:411–417
- Lavreysen H, Pereira SN, Leysen JE, Langlois X, Lesage AS (2004a) Metabotropic glutamate 1 receptor distribution and occupancy in the rat brain: a quantitative autoradiographic study using [³H]R214127. *Neuropharmacology* 46:609–619
- Lavreysen H, Wouters R, Bischoff F, Nobrega Pereira S, Langlois X, Blokland S, Somers M, Dillen L, Lesage AS (2004b) JNJ16259685, a highly potent, selective and systemically active mGlu1 receptor antagonist. *Neuropharmacology* 47:961–972
- Lea PM, Faden AI (2006) Metabotropic glutamate receptor subtype 5 antagonists MPEP and MTEP. *CNS Drug Rev* 12:149–166
- Lee B, Kim YK, Jeong J, Lee YS, Lee JY, Lee JS, Lee DS, Chung JK, Lee M (2012) Study of a novel PET tracer for type 1 metabotropic glutamate receptor (mGluR1) imaging in brain. *J Nucl Med* 53(Suppl 1):400

- Li Z, Conti PS (2010) Radiopharmaceutical chemistry for positron emission tomography. *Adv Drug Deliv Rev* 62:1031–1051
- Lindemann L, Jaeschke G, Michalon A, Vieira E, Honer M, Spooren W, Porter R, Hartung T, Kolczewski S, Buttelmann B, Flament C, Diener C, Fischer C, Gatti S, Prinssen EP, Parrott N, Hoffmann G, Wettstein JG (2011) CTEP: a novel, potent, long-acting, and orally bioavailable metabotropic glutamate receptor 5 inhibitor. *J Pharmacol Exp Ther* 339:474–486
- Lindsley CW, Emmitte KA (2009) Recent progress in the discovery and development of negative allosteric modulators of mGluR5. *Curr Opin Drug Discov Dev* 12:446–457
- Lucatelli C, Honer M, Salazar JF, Ross TL, Schubiger PA, Ametamey SM (2009) Synthesis, radiolabeling, in vitro and in vivo evaluation of [F-18]-FPECMO as a positron emission tomography radioligand for imaging the metabotropic glutamate receptor subtype 5. *Nucl Med Biol* 36:613–622
- Miller PW, Long NJ, Vilar R, Gee AD (2008) Synthesis of ^{11}C , ^{18}F , ^{15}O , and ^{13}N radiolabels for positron emission tomography. *Angew Chem* 47:8998–9033
- Miyake N, Skinbjerg M, Easwaramoorthy B, Kumar D, Girgis RR, Xu XY, Slifstein M, Abi-Dargham A (2011) Imaging changes in glutamate transmission in vivo with the metabotropic glutamate receptor 5 tracer [(11)C] ABP688 and N-acetylcysteine challenge. *Biol Psychiatry* 69:822–824
- Mori H, Mishina M (1995) Structure and function of the NMDA receptor channel. *Neuropharmacology* 34:1219–1237
- Mu L, Schubiger PA, Ametamey SM (2010) Radioligands for the PET imaging of metabotropic glutamate receptor subtype 5 (mGluR5). *Curr Top Med Chem* 10:1558–1568
- Myers R (2001) The biological application of small animal PET imaging. *Nucl Med Biol* 28:585–593
- Neugebauer V (2002) Metabotropic glutamate receptors—important modulators of nociception and pain behavior. *Pain* 98:1–8
- Ohe T, Sato M, Tanaka S, Fujino N, Hata M, Shibata Y, Kanatani A, Fukami T, Yamazaki M, Chiba M, Ishii Y (2003) Effect of P-glycoprotein-mediated efflux on cerebrospinal fluid/plasma concentration ratio. *Drug Metab Dispos* 31:1251–1254
- Ohgami M, Haradahira T, Takai N, Zhang M, Kawamura K, Yamasaki T, Yanagimoto K (2009) [^{18}F]FTIDC: a new PET radioligand for metabotropic glutamate receptor 1. *Eur J Nucl Med Mol Imaging* 36:S310
- Ohnuma T, Augood SJ, Arai H, McKenna PJ, Emson PC (1998) Expression of the human excitatory amino acid transporter 2 and metabotropic glutamate receptors 3 and 5 in the prefrontal cortex from normal individuals and patients with schizophrenia. *Mol Brain Res* 56:207–217
- Ono M, Ohgami M, Haratake M, Saji H, Nakayama M (2012) A novel bifunctional chelating agent based on bis(hydroxamamide) for $^{99\text{m}}\text{Tc}$ labeling of polypeptides. *J Labelled Comp Rad* 55:71–79
- Palucha A, Branski P, Szewczyk B, Wieronska JM, Klak K, Pilc A (2005) Potential antidepressant-like effect of MTEP, a potent and highly selective mGluR5 antagonist. *Pharmacol Biochem Behav* 81:901–906
- Parmentier ML, Galvez T, Acher F, Peyre B, Pellicciari R, Grau Y, Bockaert J, Pin JP (2000) Conservation of the ligand recognition site of metabotropic glutamate receptors during evolution. *Neuropharmacology* 39:1119–1131
- Passchier J, Gee A, Willemsen A, Vaalburg W, van Waarde A (2002) Measuring drug-related receptor occupancy with positron emission tomography. *Methods* 27:278–286
- Patel S, Gibson R (2008) In vivo site-directed radiotracers: a mini-review. *Nucl Med Biol* 35:805–815
- Patel S, Krause SM, Hamill T, Chaudhary A, Burns DH, Gibson RA (2003) In vitro characterization of [H-3]MethoxyPyEP, an mGluR5 selective radioligand. *Life Sci* 73:371–379
- Patel S, Ndbuzio O, Hamill T, Chaudhary A, Burns HD, Hargreaves R, Gibson RE (2005) Screening cascade and development of potential positron emission tomography radiotracers for mGluR5: in vitro and in vivo characterization. *Mol Imaging Biol* 7:314–323
- Patel S, Hamill TG, Connolly B, Jagoda E, Li W, Gibson RE (2007) Species differences in mGluR5 binding sites in mammalian central nervous system determined using in vitro binding with [F-18]F-PEB. *Nucl Med Biol* 34:1009–1017

- Pietraszek M, Nagel J, Gravius A, Schafer D, Danysz W (2007) The role of group I metabotropic glutamate receptors in schizophrenia. *Amino Acids* 32:173–178
- Pike VW (2009) PET radiotracers: crossing the blood-brain barrier and surviving metabolism. *Trends Pharmacol Sci* 30:431–440
- Porter RHP, Jaeschke G, Spooren W, Ballard TM, Buttelmann B, Kolczewski S, Peters JU, Prinssen E, Wichmann J, Vieira E, Muhlemann A, Gatti S, Mutel V, Malherbe P (2005) Fenobam: a clinically validated nonbenzodiazepine anxiolytic is a potent, selective, and non-competitive mGlu5 receptor antagonist with inverse agonist activity. *J Pharmacol Exp Ther* 315:711–721
- Prabhakaran J, Majo VJ, Milak MS, Kassir SA, Palner M, Savenkova L, Mali P, Arango V, Mann JJ, Parsey RV, Kumar JSD (2010) Synthesis, in vitro and in vivo evaluation of [(11)C]MMTP: a potential PET ligand for mGluR1 receptors. *Bioorg Med Chem Lett* 20:3499–3501
- Ritzen A, Mathiesen JM, Thomsen C (2005) Molecular pharmacology and therapeutic prospects of metabotropic glutamate receptor allosteric modulators. *Basic Clin Pharmacol Toxicol* 97:202–213
- Ritzen A, Sindet R, Hentzer M, Svendsen N, Brodbeck RM, Bundgaard C (2009) Discovery of a potent and brain penetrant mGluR5 positive allosteric modulator. *Bioorg Med Chem Lett* 19:3275–3278
- Romano C, Sesma MA, McDonald CT, Omalley K, Vandenpol AN, Olney JW (1995) Distribution of Metabotropic Glutamate-Receptor Mglur5 Immunoreactivity in Rat-Brain. *J Comp Neurol* 355:455–469
- Romano C, Yang WL, O Malle KL (1996) Metabotropic glutamate receptor 5 is a disulfide-linked dimer. *J Biol Chem* 271:28612–28616
- Rouse ST, Marino MJ, Bradley SR, Awad H, Wittmann M, Conn PJ (2000) Distribution and roles of metabotropic glutamate receptors in the basal ganglia motor circuit: implications for treatment of Parkinson's disease and related disorders. *Pharmacol Ther* 88:427–435
- Sanchez-Pernaute R, Wang JQ, Kuruppu D, Cao L, Tueckmantel W, Kozikowski A, Isacson O, Brownell AL (2008) Enhanced binding of metabotropic glutamate receptor type 5 (mGluR5) PET tracers in the brain of Parkinsonian primates. *Neuroimage* 42:248–251
- Satoh A, Nagatomi Y, Hirata Y, Ito S, Suzuki G, Kimura T, Maehara S, Hikichi H, Satow A, Hata M, Ohta H, Kawamoto H (2009) Discovery and in vitro and in vivo profiles of 4-fluoro-N-[4-[6-(isopropylamino)pyrimidin-4-yl]-1,3-thiazol-2-yl]-N-methylbenzamide as novel class of an orally active metabotropic glutamate receptor 1 (mGluR1) antagonist. *Bioorg Med Chem Lett* 19:5464–5468
- Schkeryantz JM, Kingston AE, Johnson MP (2007) Prospects for metabotropic glutamate 1 receptor antagonists in the treatment of neuropathic pain. *J Med Chem* 50:2563–2568
- Schubiger PA, Lehmann L, Friebe M (2007) PET chemistry: the driving force in molecular imaging. Springer, Berlin/New York
- Sephton Milicevic S, Denmler P, Leutwiler DS, Mu L, Wanger-Baumann CA, Schibli R, Krämer SD, Ametamey SM (2012) Synthesis, radiolabelling and in vitro and in vivo evaluation of a novel fluorinated ABP688 derivative for the PET imaging of metabotropic glutamate receptor subtype 5. *Am J Nucl Med Mol Imaging* 2:14–28
- Severance AJ, Parsey RV, Kumar JSD, Underwood MD, Arango V, Majo VJ, Prabhakaran J, Simpson NR, Van Heertum RL, Mann JJ (2006) In vitro and in vivo evaluation of [C-11] MPEPy as a potential PET ligand for mGlu(5) receptors. *Nucl Med Biol* 33:1021–1027
- Shetty HU, Zoghbi SS, Simeon FG, Liow JS, Brown AK, Kannan P, Innis RB, Pike VW (2008) Radiodefluorination of 3-fluoro-5-(2-(2-[F-18](fluoromethyl)-thiazol-4-yl) ethynyl)benzotrile ([F-18]SP203), a radioligand for imaging brain metabotropic glutamate subtype-5 receptors with positron emission tomography, occurs by glutathionylation in rat brain. *J Pharmacol Exp Ther* 327:727–735
- Shigemoto R, Kinoshita A, Wada E, Nomura S, Ohishi H, Takada M, Flor PJ, Neki A, Abe T, Nakanishi S, Mizuno N (1997) Differential presynaptic localization of metabotropic glutamate receptor subtypes in the rat hippocampus. *J Neurosci* 17:7503–7522
- Shin SS, Martino JJ, Chen S (2008) Metabotropic glutamate receptors (mGlu) and cellular transformation. *Neuropharmacology* 55:396–402

- Simeon FG, Brown AK, Zoghbi SS, Patterson VM, Innis RB, Pike VW (2007) Synthesis and simple F-18-labeling of 3-fluoro-5-(2-(2-(fluoromethyl)thiazol-4-yl)ethynyl)benzotrile as a high affinity radioligand for imaging monkey brain metabotropic glutamate subtype-5 receptors with positron emission tomography. *J Med Chem* 50:3256–3266
- Spooren W, Gasparini F (2004) mGluS receptor antagonists: a novel class of anxiolytics? *Drug News Perspect* 17:251–257
- Spooren WPJM, Vassout A, Neijt HC, Kuhn R, Gasparini F, Roux S, Porsolt RD, Gentsch C (2000) Anxiolytic-like effects of the prototypical metabotropic glutamate receptor 5 antagonist 2-methyl-6-(phenylethynyl)pyridine in rodents. *J Pharmacol Exp Ther* 295:1267–1275
- Spooren W, Ballard T, Gasparini F, Amalric M, Mutel V, Schreiber R (2003) Insight into the function of group I and group II metabotropic glutamate (mGlu) receptors: behavioural characterization and implications for the treatment of CNS disorders. *Behav Pharmacol* 14:257–277
- Suzuki M, Doi H, Bjorkman M, Andersson Y, Langstrom B, Watanabe Y, Noyori R (1997) Rapid coupling of methyl iodide with aryltributylstannanes mediated by palladium(0) complexes: a general protocol for the synthesis of (CH₃)-C-11-labeled PET tracers. *Chem-Eur J* 3:2039–2042
- Suzuki G, Kimura T, Satow A, Kaneko N, Fukuda J, Hikichi H, Sakai N, Maehara S, Kawagoe-Takaki H, Hata M, Azuma T, Ito S, Kawamoto H, Ohta H (2007) Pharmacological characterization of a new, orally active and potent allosteric metabotropic glutamate receptor 1 antagonist, 4-[1-(2-fluoropyridin-3-yl)-5-methyl-1H-1,2,3-triazol-4-yl]-N-isopropyl-N-methyl-3,6-dihydropyridine-1(2H)-carboxamide (FTIDC). *J Pharmacol Exp Ther* 321:1144–1153
- Suzuki G, Kawagoe-Takaki H, Inoue T, Kimura T, Hikichi H, Murai T, Satow A, Hata M, Maehara S, Ito S, Kawamoto H, Ozaki S, Ohta H (2009) Correlation of receptor occupancy of metabotropic glutamate receptor subtype 1 (mGluR1) in mouse brain with in vivo activity of allosteric mGluR1 antagonists. *J Pharmacol Sci* 110:315–325
- Swanson CJ, Bures M, Johnson MP, Linden AM, Monn JA, Schoepp DD (2005) Metabotropic glutamate receptors as novel targets for anxiety and stress disorders. *Nat Rev Drug Discov* 4:131–144
- Szydłowska K, Kaminska B, Baude A, Parsons CG, Danysz W (2007) Neuroprotective activity of selective mGlu1 and mGlu5 antagonists in vitro and in vivo. *Eur J Pharmacol* 554:18–29
- Talbot PS, Laruelle M (2002) The role of in vivo molecular imaging with PET and SPECT in the elucidation of psychiatric drug action and new drug development. *Eur Neuropsychopharmacol* 12:503–511
- Tamagnan GD, Batis J, Koren AO, Lee H, Alagille D, Jennings D, Russell D, Carson R, Marek K, Seibyl JP (2009) Initial human studies of [18]-FPEB, a selective metabotropic glutamate receptor 5. *Eur J Nucl Med Mol Imaging* 36(Suppl 2):S223
- Tatarczynska E, Klodzinska A, Chojnacka-Wojcik E, Palucha A, Gasparini F, Kuhn R, Pilc A (2001) Potential anxiolytic- and antidepressant-like effects of MPEP, a potent, selective and systemically active mGlu5 receptor antagonist. *Br J Pharmacol* 132:1423–1430
- Tavares AA, Lewsey J, Dewar D, Pimlott SL (2012) Radiotracer properties determined by high performance liquid chromatography: a potential tool for brain radiotracer discovery. *Nucl Med Biol* 39:127–135
- Telu S, Chun J, Simeon FG, Lu S, Pike VW (2011) Syntheses of an mGluR5 PET radioligands through the radiofluorination of a diaryliodonium tosylates. *Org Biomol Chem* 9:6629–6638
- Thomas NK, Wright RA, Howson PA, Kingston AE, Schoepp DD, Jane DE (2001) (S)-3,4-DCPG, a potent and selective mGlu8a receptor agonist, activates metabotropic glutamate receptors on primary afferent terminals in the neonatal rat spinal cord. *Neuropharmacology* 40:311–318
- Treyer V, Streffer J, Ametamey SM, Bettio A, Blauenstein P, Schmidt M, Gasparini F, Fischer U, Hock C, Buck A (2008) Radiation dosimetry and biodistribution of ¹¹C-ABP688 measured in healthy volunteers. *Eur J Nucl Med Mol Imaging* 35:766–770
- Tsai VWW, Scott HL, Lewis RJ, Dodd PR (2005) The role of group I metabotropic glutamate receptor's in neuronal excitotoxicity in Alzheimer's disease. *Neurotox Res* 7:125–141
- Tsuchiya D, Kunishima N, Kamiya N, Jingami H, Morikawa K (2002) Structural views of the ligand-binding cores of a metabotropic glutamate receptor complexed with an antagonist and both glutamate and Gd³⁺. *Proc Natl Acad Sci U S A* 99:2660–2665

- Van Laere K, Koole M, de Hoon J, Van Hecken A, Langlois X, Andres JJ, Bormans G, Schmidt M (2012) Biodistribution, dosimetry and kinetic modeling of [¹¹C]JNJ-42491293, a PET tracer for the mGluR2 receptor in the human brain. *J Nucl Med* 53(Suppl 1):355
- Varney M, Anderson J, Bradbury M, Bristow L, Brodtkin J, Giracello D, Jachec C, Holtz G, Prasit P, Rao S, Chapman D, Cosford NDP (2002) 3-[(2-Methyl-1,3-thiazol-4-yl)ethynyl]pyridine (MTEP): a potent and highly selective metabotropic glutamate subtype 5 (mGlu5) receptor antagonist with anxiolytic activity. *Neuropharmacology* 43:311–311
- Wager TT, Hou XJ, Verhoest PR, Villalobos A (2010) Moving beyond rules: the development of a central nervous system multi-parameter optimization (CNS MPO) approach to enable alignment of drug-like properties. *ACS Chem Neurosci* 1(6):435–449
- Wager TT, Villalobos A, Verhoest PR, Hou X, Shaffer CL (2011) Strategies to optimize the brain availability of central nervous system drug candidates. *Exp Opin Drug Discov* 6:371–381
- Wang JQ, Tueckmantel W, Zhu AJ, Pellegrino D, Brownell AL (2007) Synthesis and preliminary biological evaluation of 3-[F-18]fluoro-5-(2-pyridinylethynyl)benzotrile as a PET radiotracer for imaging metabotropic glutamate receptor subtype 5. *Synapse* 61:951–961
- Wang JQ, Zhang Z, Kuruppu D, Brownell AL (2012) Radiosynthesis of PET radiotracer as a pro-drug for imaging group II metabotropic glutamate receptors in vivo. *Bioorg Med Chem Lett* 22:1958–1962
- Wanger-Baumann CA, Mu L, Honer M, Belli S, Alf MF, Schubiger PA, Kramer SD, Ametamey SM (2011) In vitro and in vivo evaluation of [F-18]-FDEGPECO as a PET tracer for imaging the metabotropic glutamate receptor subtype 5 (mGluR5). *Neuroimage* 56:984–991
- Waterhouse RN (2003) Determination of lipophilicity and its use as a predictor of blood-brain barrier penetration of molecular imaging agents. *Mol Imaging Biol* 5:376–389
- Wu WL, Burnett DA, Domalski M, Greenlee WJ, Li C, Bertorelli R, Fredduzzi S, Lozza G, Veltri A, Reggiani A (2007) Discovery of orally efficacious tetracyclic metabotropic glutamate receptor 1 (mGluR1) antagonists for the treatment of chronic pain. *J Med Chem* 50:5550–5553
- Xi W, Tian M, Zhang H (2011) Molecular imaging in neuroscience research with small-animal PET in rodents. *Neurosci Res* 70:133–143
- Yamasaki T, Fujinaga M, Yoshida Y, Kumata K, Yui JJ, Kawamura K, Hatori A, Fukumura T, Zhang MR (2011) Radiosynthesis and preliminary evaluation of 4-[(¹⁸F)fluoro-N-[4-[6-(isopropylamino)pyrimidin-4-yl]-1,3-thiazol-2-yl]-N-methylbenzamide as a new positron emission tomography ligand for metabotropic glutamate receptor subtype 1. *Bioorg Med Chem Lett* 21:2998–3001
- Yamasaki T, Fujinaga M, Maeda J, Kawamura K, Yui J, Hatori A, Yoshida Y, Nagai Y, Tokunaga M, Higuchi M, Suhara T, Fukumura T, Zhang MR (2012) Imaging for metabotropic glutamate receptor subtype 1 in rat and monkey brains using PET with [(¹⁸F)FITM]. *Eur J Nucl Med Mol Imaging* 39:632–641
- Yanamoto K, Konno F, Odawara C, Yamasaki T, Kawamura K, Hatori A, Yui J, Wakizaka H, Nengaki N, Takei M, Zhang MR (2010) Radiosynthesis and evaluation of [(¹¹C)YM-202074 as a PET ligand for imaging the metabotropic glutamate receptor type 1. *Nucl Med Biol* 37:615–624
- Yu M (2007) Recent developments of the PET imaging agents for metabotropic glutamate receptor subtype 5. *Curr Top Med Chem* 7:1800–1805
- Yu MX, Tueckmantel W, Wang XK, Zhu AJ, Kozikowski AP, Brownell AL (2005) Methoxyphenylethynyl, methoxypyridylethynyl and phenylethynyl derivatives of pyridine: synthesis, radiolabeling and evaluation of new PET ligands for metabotropic glutamate subtype 5 receptors. *Nucl Med Biol* 32:631–640

Hideo Tsukada

Contents

16.1	Introduction	446
16.2	Development of [¹¹ C](+)-3-MPB and Its Analogues.....	448
16.2.1	Assessment of [¹¹ C](+)-3-MPB in Comparison with [¹¹ C]4-MPB.....	448
16.2.2	<i>N</i> -Substitution Analogues of [¹¹ C](+)-3-MPB with Longer Alkyl Chain Length.....	450
16.3	Detection of Aging Effects on mAChR with [¹¹ C](+)-3-MPB	452
16.4	Cognitive Function and mAChR	456
16.5	A Clinical Application of [¹¹ C](+)-3-MPB in Chronic Fatigue Syndrome	459
	Conclusion	461
	References.....	461

Abstract

We have successfully developed a novel PET ligand for muscarinic acetylcholine receptors (mAChR), (+)-*N*-[¹¹C]methyl-3-piperidyl benzilate ([¹¹C](+)-3-MPB), and evaluated this in the brain of conscious monkeys using high-resolution positron emission tomography (PET). (+)-3-MPB had relatively low selectivity to the subtype of mAChR, showing K_i values of 1.3, 1.1, 2.8, 1.7, and 5.9 nM for M1, M2, M3, M4, and M5, respectively, of the human receptors. The regional cortical distribution of [¹¹C](+)-3-MPB was found to be consistent with mAChR density in the monkey brain as reported *in vitro*. Time-activity curves of [¹¹C](+)-3-MPB peaked in all brain regions, suggesting that this PET probe bound reversibly to the mAChR. Administration of scopolamine, a mAChR antagonist, reduced the radioactivity of [¹¹C](+)-3-MPB in all regions except the cerebellum, and the reduction of [¹¹C](+)-3-MPB uptake was well correlated with the degree of

H. Tsukada
 Central Research Laboratory, Hamamatsu Photonics K.K.,
 5000 Hirakuchi, Hamakita, Hamamatsu, Shizuoka 434-8601, Japan
 e-mail: tsukada0412@nifty.com

impairment of working memory performance ($R^2=0.55$ and 0.84 in hippocampus and brainstem, respectively) assessed in conscious monkeys. Based on these preclinical studies, we recently demonstrated in clinical study that chronic fatigue syndrome (CFS) patients with positive serum autoantibody against mAChR showed significantly lower [^{11}C](+)-3-MPB binding than negative patients and normal controls. These results demonstrated that PET imaging with [^{11}C](+)-3-MPB could be useful for diagnosis of neurological diseases associated with impaired mAChR function and cognitive function.

16.1 Introduction

Neurodegenerative diseases are characterized by selective loss of neuronal populations in the central nervous system (CNS). The central muscarinic acetylcholine (mAChR) receptor system plays an important role in memory and cognitive functions. Alzheimer-type dementia has been neuropathologically characterized by the presence of neurofibrillary tangles and senile plaques (Katzman 1986; Selkoe 1990). Moreover, there is a loss of cholinergic neurons in the forebrain, reduced cholinergic activity in the hippocampus, and a cortical loss of choline acetyltransferase, and the severity of these cholinergic abnormalities is closely correlated with the degree of dementia (Perry 1986; Höhmann et al. 1998). Among several cholinergic neuronal systems, reduced central mAChR has been reported in Alzheimer-type dementia (Rinne et al. 1985; Reinikainen et al. 1987; Terry and Buccafusco 2003).

Positron emission tomography (PET) has been widely applied for investigation of the cerebral distribution of positron emitter-labeled neurotransmitter-specific receptor probes. Several antagonist-based [^{11}C]-labeled probes for imaging mAChR in the CNS have been developed and evaluated, including [^{11}C]scopolamine (Vora et al. 1983; Mulholland et al. 1988b; Frey et al. 1992), [^{11}C]dextimide (Dannals et al. 1988), [^{11}C]quinuclidinyl benzilate (QNB) (Prenant et al. 1989), [^{11}C]benztropine (Dewey et al. 1990a), and [^{11}C]tropanyl benzilate (TRB) (Mulholland et al. 1992; Koeppe et al. 1994). These labeled ligands for muscarinic receptors, however, show poor selectivity for mAChR subtypes, relatively low uptake to the brain, and also slow dissociation rates from receptor binding sites, which may limit estimation of the density of mAChR in vivo (Koeppe et al. 1994). Slow dissociation rate from mAChR makes analysis difficult, because true equilibrium cannot be obtained within PET scanning time with short half-lives of positron emitters. A radiolabeled mAChR probe, *N*-[^{11}C]methyl-4-piperidyl benzilate ([^{11}C]4-MPB) (Fig. 16.1), was proposed (Mulholland et al. 1988a), showing more favorable kinetic properties than previously labeled compounds for mAChR in humans (Zubieta et al. 1998).

Thereafter, Takahashi et al. proposed another novel mAChR probe, *N*-[^{11}C]methyl-3-piperidyl benzilate ([^{11}C]3-MPB) (Takahashi et al. 1997) (Fig. 16.1). Since its chemical structure contained a chiral carbon, it provided two stereoisomers, the active form as [^{11}C](+)-3-MPB and inactive one as [^{11}C](−)-3-MPB, and even active [^{11}C](+)-3-MPB revealed relatively low affinity to mAChR as determined

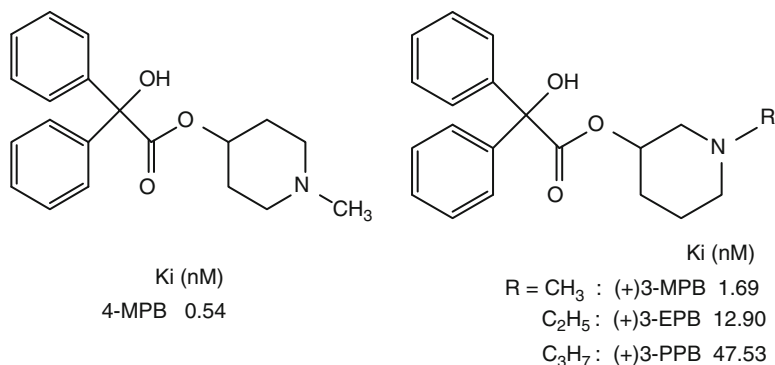


Fig. 16.1 Chemical structures of 4-MPB (*left*), (+)3-MPB and its *N*-alkyl substitution analogues, (+)3-EPB and (+)3-PPB (*right*). Affinity (K_i) values of each compound were determined by *in vitro* assay with [³H]QNB

by *in vitro* binding assay (Takahashi et al. 1997). To extend prior work in the rat brain, [¹¹C](+)3-MPB was evaluated for quantification of cerebral mAChR binding in the monkey brain (Tsukada et al. 2001c). With [¹¹C](+)3-MPB and its analogues (Nishiyama et al. 2001), we determined the aging effects on mAChR binding in the monkey brain (Tsukada et al. 2001a, 2004). In addition, the temporal relationship between the occupancy level of central mAChR by scopolamine and anticholinergic drugs for overactive bladder (OAB) treatment, as measured by [¹¹C](+)3-MPB, and cognitive impairment, as assessed by a delayed matching to sample task, was determined in conscious monkeys (Yamamoto et al. 2011a, b). These monkey PET imaging studies were conducted with a high-resolution animal PET scanner which allowed us to image the brain under conscious conditions.

The PET studies reported in this chapter have been conducted with monkeys in conscious condition. Anesthetics have been used in nonhuman primate PET studies, because it is necessary to fix animal during PET scanning. However, anesthetics affect several neuronal functions, resulting in an alteration of neuronal activities in the central nervous system. Thus, the indices of brain function as well as the pharmacological actions as measured by PET should be affected by the anesthetics. In order to avoid these anesthetic effects, we developed a sophisticated total PET system (Hamamatsu SHR-7700, Watanabe et al. 1997) to conduct an “activation study” with conscious behaving monkeys (Onoe et al. 2001; Yokoyama et al. 2005; Nishimura et al. 2007). Its gantry including optical detectors can tilt up to 90° at any angle, and brain images of monkey sitting on a monkey chair can be measured even in the conscious condition. This PET system enabled us to conduct PET imaging of mAChR with [¹¹C](+)3-MPB without any effects of anesthetics, making it easier to conduct the translational research of [¹¹C](+)3-MPB from animals to humans.

Based on the conscious monkey PET studies, we have just started translational studies with [¹¹C](+)3-MPB from preclinical level with experimental animals to clinical levels with humans. We checked the safety issue of [¹¹C](+)3-MPB

based on the microdose concept and recently reported that chronic fatigue syndrome (CFS) patients with positive serum autoantibody against mAChR showed significantly lower [^{11}C](+)-3-MPB binding than negative patients and normal controls.

16.2 Development of [^{11}C](+)-3-MPB and Its Analogues

16.2.1 Assessment of [^{11}C](+)-3-MPB in Comparison with [^{11}C]4-MPB

[^{11}C](+)-3-MPB and its stereoisomer [^{11}C](−)-3-MPB were evaluated and compared with the conventional muscarinic receptor ligand [^{11}C]4-MPB for quantification of cerebral muscarinic receptors in the monkey brain. To minimize the effects of anesthetics on receptor binding, conscious monkeys were utilized in the present study (Tsukada et al. 2000a, 2001b; Ohba et al. 2009).

Positron emitting carbon-11 (^{11}C) was produced by $^{14}\text{N}(\text{p},\alpha)^{11}\text{C}$ nuclear reaction using a cyclotron and chemical converted to [^{11}C]methyl iodide. [^{11}C](+)-3-MPB and its stereoisomer [^{11}C](−)-3-MPB were labeled by *N*-methylation of their respective nor-compounds, (+)-3-PB and (−)-3-PB, with [^{11}C]methyl iodide (Takahashi et al. 1997; Tsukada et al. 2001c). As a reference, [^{11}C]4-MPB (Mulholland et al. 1988a; Zubieta et al. 1998) was also labeled by *N*-methylation of 4-PB.

PET imaging data were collected on a high-resolution PET scanner (HAMAMATSU SHR-7700) with transaxial resolution of 2.6 mm full width at half maximum (FWHM) and a center-to-center distance of 3.6 mm (Watanabe et al. 1997).

Monkeys (*Macaca mulatta*) were trained to sit on a chair with head motion restriction using a specially designed head holder twice a week for more than 3 months (Onoe et al. 1994). After an overnight fast, a monkey was seated on the monkey chair under conscious condition and fixed with stereotactic coordinates aligned parallel to the orbitomeatal (OM) line. Each labeled compound (100–120 MBq/kg body weight) was injected through the venous cannula. The radioactive purity of each labeled compound used in this study was greater than 99 % and the specific radioactivity ranged from 61.7 to 92.4 for [^{11}C](+)-3-MPB, from 60.0 to 79.5 for [^{11}C](−)-3-MPB, and from 34.4 to 75.9 GBq/ μmol for [^{11}C]4-MPB. Each labeled compound was injected through the venous cannula, and a PET scan was made for 91 min. Regions of interest (ROI) were identified according to MR images of each monkey brain, and time-activity curves for these ROIs were calculated. To measure the input function of each labeled compound into the brain, arterial blood samples were obtained, the ratio of radioactivity in the unmetabolized fraction to that in total plasma was determined with a thin layer chromatography (TLC) plate. Logan (Logan et al. 1990) and Patlak's (Patlak et al. 1983) graphical analyses were applied to measure the net accumulation of tracer in the reversible and irreversible compartment, respectively.

In Fig. 16.2, typical PET images of [^{11}C](+)-3-MPB (A), [^{11}C](−)-3-MPB (B), and [^{11}C]4-MPB (C) are shown obtained in the same monkey under conscious condition. The regional uptake pattern of [^{11}C](+)-3-MPB was high in the striatum; intermediate in the occipital, temporal, and frontal cortices and hippocampus and thalamus;

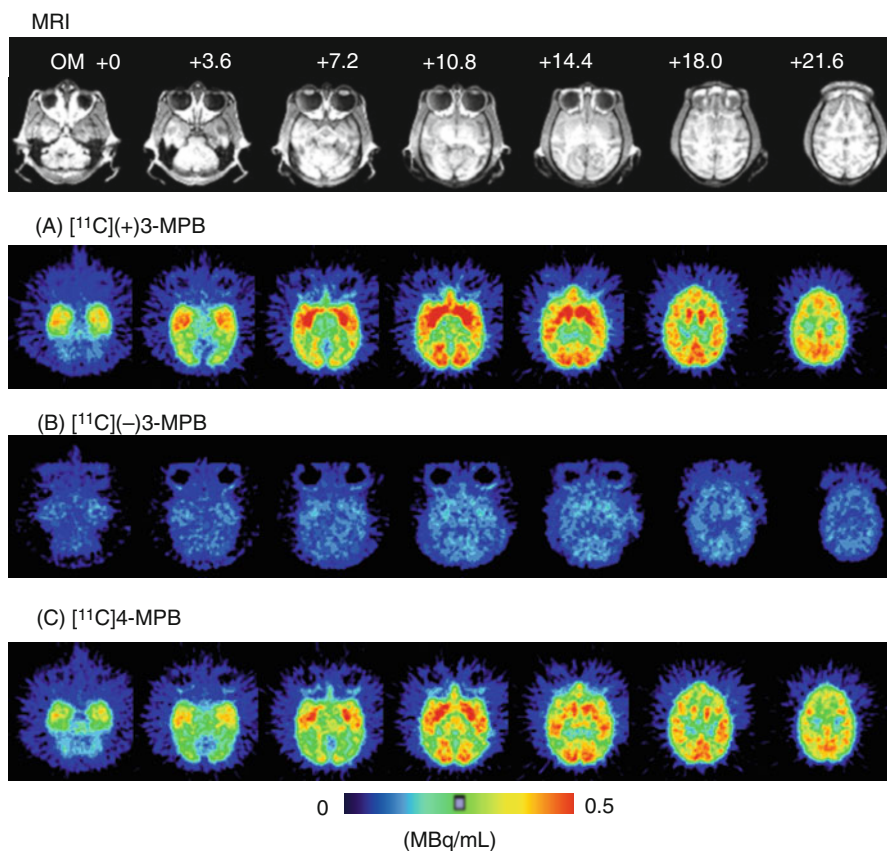


Fig. 16.2 MRI and PET images of [^{11}C](+)3-MPB (A), [^{11}C](-)3-MPB (B), and [^{11}C]4-MPB (C) in the monkey brain. MR images of monkeys were obtained with a Toshiba MRT-50A/II (0.5 T). PET data were collected in the conscious state with a high-resolution PET scanner (HAMAMATSU SHR-7700) with a transaxial resolution of 2.6 mm (FWHM). Each labeled compound (100–120 MBq/kg body weight) was injected through the venous cannula. PET scans were performed for 91 min, and each PET image was generated by summation of image data from 60 to 94 min postinjection

and low in the cerebellum (Fig. 16.2A). In contrast, the level of [^{11}C](-)3-MPB was much lower than those of [^{11}C](+)3-MPB in all regions of the brain (Fig. 16.2B). The patterns of distribution of [^{11}C]4-MPB (Fig. 16.2C) were almost identical to that of [^{11}C](+)3-MPB.

The time-activity curves of [^{11}C](+)3-MPB in the frontal, temporal, and occipital cortices reached their peaks 40 min after injection, whereas the striatal and hippocampal regions reached peak values 60 min after injection (Fig. 16.3a). In contrast, the time-activity curves of [^{11}C](-)3-MPB showed similar patterns in all regions of the brain (Fig. 16.3b). Uptake of [^{11}C]4-MPB in all regions except the thalamus and cerebellum gradually increased with time during the scan until 91 min after injection (Fig. 16.3c).

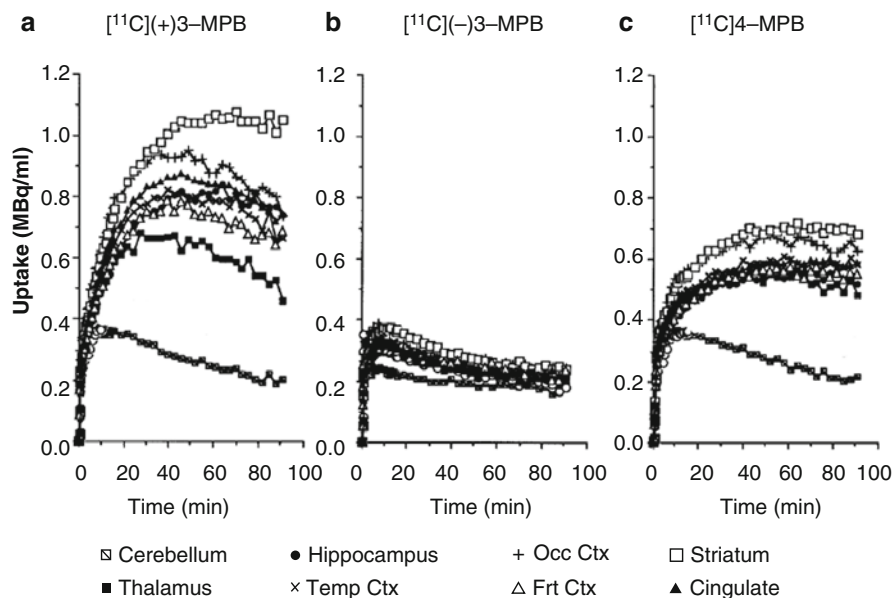


Fig. 16.3 Time-activity curves (TAC) of [^{11}C](+)-3-MPB (a), [^{11}C](−)-3-MPB (b), and [^{11}C]4-MPB (c) in the conscious monkey brain. PET scans were performed as shown in the legend of Fig. 16.2. Regions of interest (ROIs) were identified according to a MRI scan of the each animal

Patlak's plot analysis demonstrated that [^{11}C]4-MPB provided linear regression curves in all regions evaluated, while [^{11}C](+)-3-MPB provided nonlinear curves showing slope=0 in late phase, suggesting that the dissociation rate constant (k_d) from muscarinic cholinergic receptors was not negligible for [^{11}C](+)-3-MPB. Therefore, Logan plot analysis was applied to investigate the *in vivo* binding of [^{11}C](+)-3-MPB. The ratio of Logan slopes of [^{11}C](+)-3-MPB in each region against the cerebellum as reference region, and Patlak's slope of [^{11}C]4-MPB were correlated with the data of muscarinic cholinergic receptor density (B_{max}) as measured by the *in vitro* assay (Snyder et al. 1975). These results demonstration that [^{11}C](+)-3-MPB was a more suitable [^{11}C]labeled ligand for the quantification of muscarinic cholinergic receptors in the brain with PET than conventional [^{11}C]labeled ligands such as [^{11}C]4-MPB and [^{11}C]scopolamine.

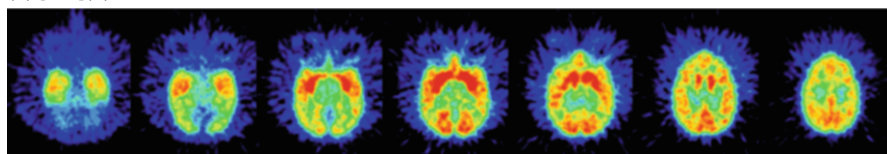
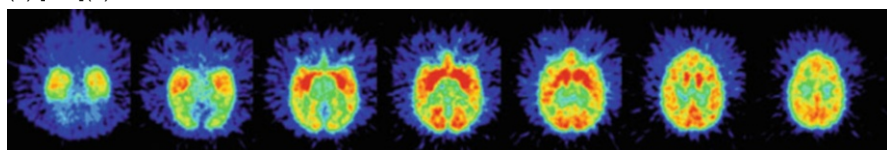
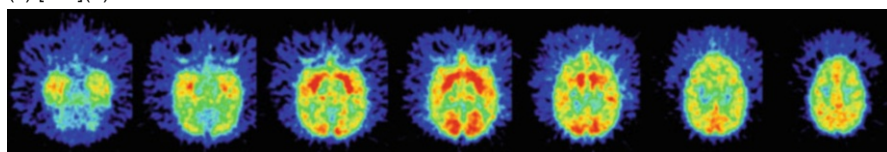
16.2.2 N-Substitution Analogues of [^{11}C](+)-3-MPB with Longer Alkyl Chain Length

The assessment of neurotransmitter release in the living brain should be very important from the neuroscientific and pharmacological points of view. Microdialysis method is the classical method to evaluate neurotransmitter release; however, since insertion of the needle-shaped dialysis probe into the brain is quite invasive, human

studies would be difficult to justify. In the last decade, interactions between endogenous neurotransmitters released into the synaptic cleft and the binding of labeled compounds have been examined by neuroimaging with PET/SPECT, especially in the dopaminergic system (for review, see Laruelle 2000; Tsukada et al. 2000a, b). Thus, the changes in synaptic neurotransmitters could be measured noninvasively by PET using labeled compounds, which have moderate affinity for their specific receptors. In order to develop a PET probe to assess acetylcholine release into the synaptic cleft, we developed two *N*-substitution analogues of [¹¹C](+)-3-MPB, (+)-*N*-[¹¹C]ethyl-3-piperidyl benzilate ([¹¹C](+)-3-EPB) and (+)-*N*-[¹¹C]propyl-3-piperidyl benzilate ([¹¹C](+)-3-PPB), and evaluated their specificity, affinity, and kinetics in comparison with original [¹¹C](+)-3-MPB in the conscious monkeys (Nishiyama et al. 2001) (Fig. 16.1). Since previous studies have suggested that *N*-substitution of 4-PB with longer alkyl chain length affected their affinities in vitro and anticholinergic potencies in vivo (Tejani-Butt et al. 1990), the affinities of (+)-3-MPB, (+)-3-EPB, and (+)-3-PPB for mAChR were assessed with in vitro competition binding assay of [³H]quinuclidinyl benzilate (QNB) using rat brain coronal slices before PET study, resulting in K_i values of 1.7, 12.9, and 47.5 nM, respectively.

Carbon-11 (¹¹C) was produced by ¹⁴N(p,α)¹¹C nuclear reaction using a cyclotron and chemically converted into [¹¹C]ethyl or [¹¹C]propyl iodide by reaction with the appropriate Grignard reagent (Långström et al. 1986). [¹¹C](+)-3-EPB or [¹¹C](−)-3-EPB was synthesized by *N*-ethylation or *N*-propylation of (+)-3-PB with [¹¹C]ethyl iodide or [¹¹C]propyl iodide using an automated synthesizer developed in our laboratory (Nishiyama et al. 2001). PET data acquisition, cortical TAC, and plasma metabolic analyses were conducted as described in Sect. 16.2.1. TACs for metabolite-corrected arterial plasma (input function) and for each ROI were fitted to a three-compartment model with a least-square fitting method to estimate the kinetic parameters, and the values of binding potential ($BP = k_3/k_4$) for mAChR in each region were calculated.

Figure 16.4 shows typical PET images of [¹¹C](+)-3-MPB (a), [¹¹C](+)-3-EPB (b), and [¹¹C](+)-3-PPB (c) in the conscious monkey brain. The regional distribution patterns of these three labeled compounds were well correlated with data on mAChR density as measured by in vitro assay (Snyder et al. 1975). The time-activity curves demonstrated that the peak times shifted earlier implying a faster clearance rate after injection of ligands with longer [¹¹C]alkyl chain lengths (Fig. 16.5). Kinetic analysis revealed that labeling with longer [¹¹C]alkyl chain length induced lower binding potential ($BP = k_3/k_4$ in Frontal cortex; 2.4, 2.0, and 1.4 for [¹¹C](+)-3-MPB, [¹¹C](+)-3-EPB, and [¹¹C](+)-3-PPB, respectively), consistent with the rank order of affinity of these ligands determined by an in vitro assay. The administration of Aricept, a cholinesterase inhibitor, increased acetylcholine level in extracellular fluid of the frontal cortex (ca. 150 and 175 % of baseline at 50 and 150 μg/kg, respectively) as measured by microdialysis in the conscious condition (Nishiyama et al. 2001) according to the method previously reported (Tsukada et al. 2000c). The binding of [¹¹C](+)-3-PPB with the lowest affinity to the receptors was displaced by the endogenous acetylcholine induced by cholinesterase inhibition, while [¹¹C](+)-3-MPB with the highest affinity was not significantly affected (Fig. 16.6). These

(a) [^{11}C](+)-MPB(b) [^{11}C](+)-3-EPB(c) [^{11}C](+)-3-PPB


0  0.5
(MBq/mL)

Fig. 16.4 MRI and PET images of [^{11}C](+)-3-MPB (a), [^{11}C](+)-3-EPB (b), and [^{11}C](+)-3-PPB (c). MR images of monkeys were obtained with a Toshiba MRT-50A/II (0.5 T). PET data were collected in the conscious state with a high-resolution PET scanner (HAMAMATSU SHR-7700). Each labeled compound (100–120 MBq/kg body weight) was injected through the venous cannula. PET scans were performed for 91 min, and each PET image was generated by summation of image data from 60 to 94 min postinjection (Tsukada et al. 2001b)

results suggested that increasing [^{11}C]alkyl chain length did alter the kinetic properties of PET probes by reducing the affinity to mAChR, which might make it possible to assess the interaction between the endogenous neurotransmitter acetylcholine and ligand-receptor binding in vivo as measured by PET.

16.3 Detection of Aging Effects on mAChR with [^{11}C](+)-3-MPB

Clinical PET studies with [^{11}C]benztropine, [^{11}C]4-MPB, and [^{11}C]tropanyl benzilate quantitatively detected the neurological alterations of mAChR in aging (Dewey et al. 1990b; Suhara et al. 1993; Lee et al. 1996; Yoshida et al. 1998). The PET probes for mAChR listed above, however, showed relatively low uptake to the brain and also slow dissociation rates from receptor binding sites, which may limit estimation of the density of binding sites in vivo (Koeppel et al. 1994). So, we tried to assess the age-related changes in mAChR with [^{11}C](+)-3-MPB in the living brains of young (ca. 6 years old) and aged (ca. 20 years old) monkeys in the

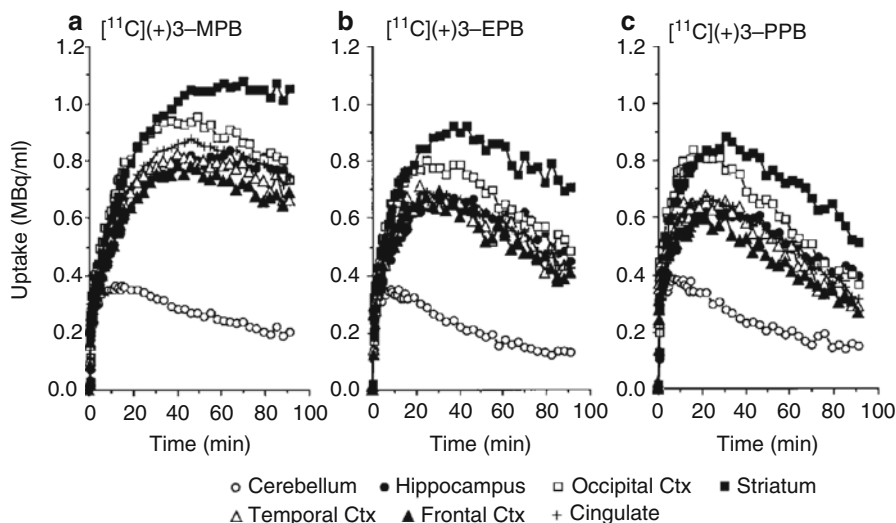


Fig. 16.5 Time-activity curves of $[^{11}\text{C}](+)\text{-3-MPB}$ (a), $[^{11}\text{C}](+)\text{-3-EPB}$ (b), and $[^{11}\text{C}](+)\text{-3-PPB}$ (c) in the conscious monkey brain. PET scans were performed as described in the legend of Fig. 16.4. Regions of interest (ROIs) were identified according to a MRI scan of each animal

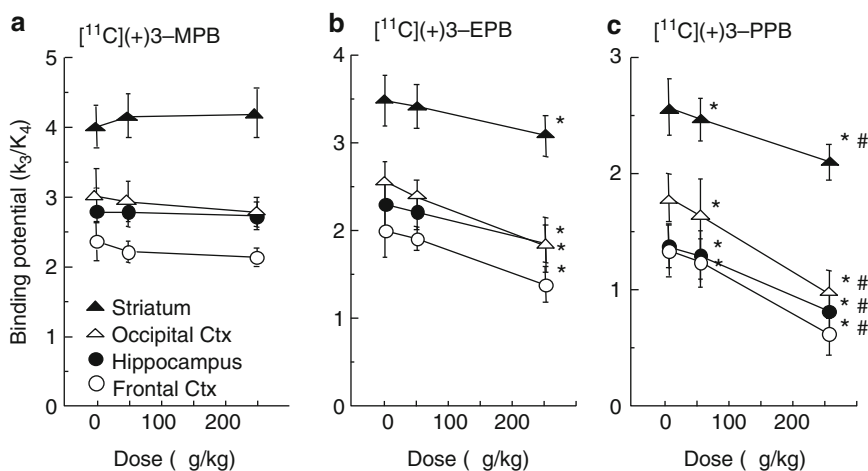


Fig. 16.6 Dose-dependent effects of Aricept on the binding potential ($\text{BP} = k_3/k_4$) of $[^{11}\text{C}](+)\text{-3-MPB}$ (a), $[^{11}\text{C}](+)\text{-3-EPB}$ (b), and $[^{11}\text{C}](+)\text{-3-PPB}$ (c) in the cortical regions of the conscious monkey brain. PET scans were performed as shown in the legend of Fig. 16.4. Receptor binding of each labeled compound was analyzed based on a three-compartment model with metabolite-corrected plasma time-activity curve. Data are expressed as means \pm SD for five animals per treatment condition. * $P < 0.01$ vs. Saline. # $P < 0.01$ vs. 50 $\mu\text{g}/\text{kg}$ Aricept

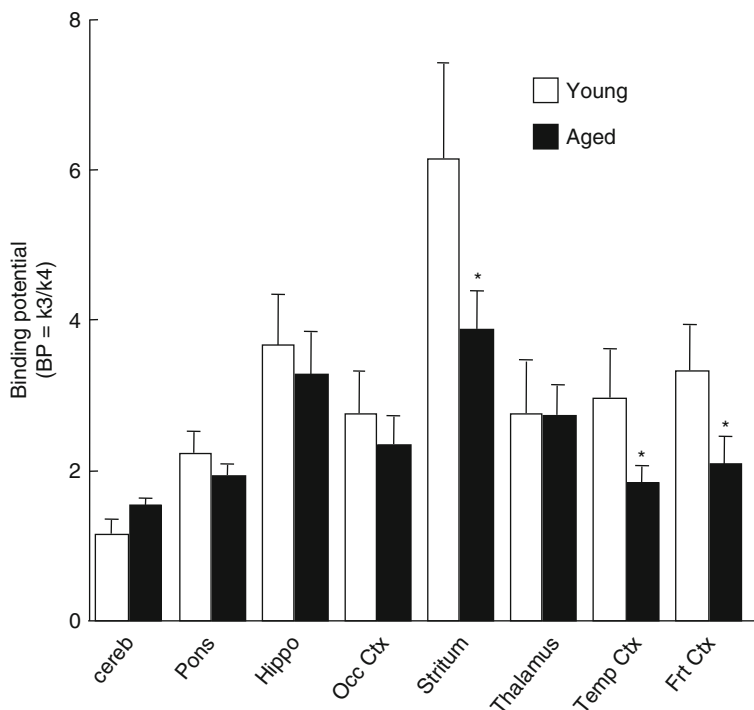


Fig. 16.7 Age-related changes in cerebral muscarinic cholinergic receptor binding in vivo. PET scans were performed as shown in the legend of Fig. 16.4. Receptor binding of each labeled compound was analyzed based on a three-compartment model with metabolite-corrected plasma time-activity curve. Data represent means \pm SD for seven animals per group. * $P < 0.05$ vs. young animals

conscious state (Tsukada et al. 2001a). In addition, the effects of Aricept, a cognitive enhancer, on mAChR binding as well as cholinesterase inhibitor activity were evaluated with [^{11}C](+)-3-PPB and *N*-[^{11}C]methyl-4-piperidyl acetate ([^{11}C]MP4A) (Tsukada et al. 2004).

[^{11}C]MP4A was labeled by *N*-methylation of its nor-compound with [^{11}C]methyl iodide (Irie et al. 1996). The synthesis of [^{11}C](+)-3-MPB, PET data acquisition, cortical TAC, and plasma metabolic analyses were conducted as described in Sect. 16.2.1, and the synthesis of [^{11}C](+)-3-PPB and data analysis were done as shown in Sect. 16.2.2.

In aged monkeys, the time-activity curves of [^{11}C](+)-3-MPB in regions rich in muscarinic receptors peaked at earlier time points and showed faster elimination rates than those in young monkeys, while curves in the cerebellum showed no significant difference between young and aged animals. When analyzed using the three-compartment model with arterial input function, significant age-related alterations of the in vivo binding of [^{11}C](+)-3-MPB were observed in the temporal and frontal cortices and the striatum (Fig. 16.7, $P < 0.05$ vs. young animals in each region). In contrast, the previous studies demonstrated when expressed relative to

the cerebellum as assumed nonspecific and free tracer reference region, age-related reduction of mAChR was observed in almost all cerebral regions in humans as measured by [^{11}C]benztropine (Dewey et al. 1990b) and [^{11}C]4-MPB (Suhara et al. 1993; Yoshida et al. 1998). It should be noted that there were trends toward reduced cerebral mAChR binding and toward elevated cerebellar binding with aging in humans as measured by a kinetic analysis method using [^{11}C]tropanyl benzilate in conjunction with arterial blood sampling (Lee et al. 1996). Although we cannot exclude species differences (monkeys vs. humans) and of differences in labeled compounds used for analysis, the combination of opposing cortical and cerebellar changes of receptor binding with aging may have led to the previous conclusion that the loss of mAChR was more substantial than that reported here.

Furthermore, we evaluated the effects of Aricept, a cognitive enhancer with AChE inhibition, on the central cholinergic neuronal system in aged monkeys. The degree of AChE inhibition by Aricept was assayed by [^{11}C]MP4A as well as a microdialysis method. The effect of increased acetylcholine on mAChR binding was demonstrated by [^{11}C](+)-3-PPB, which was sensitive to synaptic acetylcholine levels (Nishiyama et al. 2001). In aged monkeys, when Aricept was administered at the doses of 50 and 250 $\mu\text{g}/\text{kg}$, the k_3 value of [^{11}C]MP4A in the neocortical regions decreased in a dose-dependent manner, suggesting the suppression of AChE activity. The suppression of AChE activity by Aricept in the cortex was also confirmed by microdialysis analysis. The mAChR binding evaluated with [^{11}C](+)-3-PPB showed age-dependent reduction in all regions as shown with [^{11}C](+)-3-MPB previously, and Aricept at a dose of 250 $\mu\text{g}/\text{kg}$ resulted in a significant reduction in BP of [^{11}C](+)-3-PPB in all regions assayed. Aged monkeys showed impaired working memory performance compared to young monkeys, and the impaired performance was partly improved by the administration of Aricept, due to the facilitation of the cholinergic neuronal system by AChE inhibition (Data not shown). These results demonstrated that the PET imaging technique with specific labeled compounds in combination with microdialysis and a behavioral cognition task could be a useful method to clarify the mechanism of drugs in the living brains of experimental animals.

Because of poor selectivity of [^{11}C](+)-3-MPB for mAChR subtypes, it was unclear which subtype was exclusively affected by aging. To compensate the poor selectivity, a selective PET probe for M2 receptor, 3-(3-(3-[^{18}F]fluoropropylthio)-1,2,5-thiadiazol-4-yl)-1,2,5,6-tetrahydro-1-methylpyridine ([^{18}F]FP-TZTP), was proposed as a probe with an *in vitro* affinity (K_i) of 2.2 and 7.4 nM for M2 and M1, respectively (Kiesewetter et al. 1995). The advantage of F-18-labeled compounds is that they do not always require an in-house cyclotron. The cortical binding of [^{18}F]FP-TZTP was decreased by physostigmine, a cholinesterase inhibitor, consistent with increased endogenous ACh competition (Carson et al. 1998). Of interest, an age-related increase binding of [^{18}F]FP-TZTP was determined (Podruchny et al. 2003), which was completely opposite results obtained with agonist-based [^{11}C]benztropine (Dewey et al. 1990b), [^{11}C]4-MPB (Suhara et al. 1993; Yoshida et al. 1998), and [^{11}C](+)-3-MPB (Tsukada et al. 2001a). The authors speculated that a lower concentration of ACh in the synapse was one possible explanation for the age-related increase in [^{18}F]FP-TZTP binding (Podruchny et al. 2003). It is of interest that the opposite

effects of aging on mAChR binding were demonstrated between agonist-based and antagonist-based PET probes. We recently have also reported the opposite effects of stress on dopamine D₂ receptor binding between agonist-based and antagonist-based PET probes, [¹¹C]MNPA and [¹¹C]raclopride (Tsukada et al. 2011). These results suggest that when we attempt to develop novel PET probes, we should take into account the chemical property of agonist or antagonist.

16.4 Cognitive Function and mAChR

Neurotransmission through mAChR in the brain has been recognized to be involved in human cognitive function including attention and working memory (Collerton 1986). Abnormalities of the central mAChR system in Alzheimer disease are well correlated with the degree of dementia (Perry 1986; Höhmann et al. 1998), and several mAChR agonists were reported to improve cognitive function in Alzheimer-type dementia (Bodick et al. 1997) and schizophrenia (Raedler et al. 2003). Pharmacological manipulation has been a useful strategy for demonstrating the importance of the role of central mAChR in learning and memory functions in humans (Collerton 1986). Although it had been well known that blockade of the mAChR with scopolamine, a specific mAChR antagonist, resulted in transient cognitive impairment, there were no study revealing the relationship between the occupancy level of central mAChRs and the degree of cognitive impairment induced by scopolamine in primates. We recently reported the time-dependent effects of scopolamine on the occupancy level of central mAChR and cognitive impairment in conscious monkeys (Yamamoto et al. 2011b).

The synthesis of [¹¹C](+)-3-MPB, PET data acquisition, and cortical TAC analysis were conducted as described in Sect. 16.2.1. Quantitative analysis of [¹¹C](+)-3-MPB binding to mAChR in the brain was carried out with the Logan reference tissue method, which had already been validated in our previous study (Yamamoto et al. 2010), and the occupancy of mAChR in the brain was calculated. The cognitive impairment was determined by a titration version of delayed matching to sample (T-DMS) task (Hudzik and Wenger 1993).

DMS task is one method for evaluating potential drug effects on cognitive functions. Typically, a sample visual stimulus is presented to the animal for a short time. Following a delay interval, the sample and another test stimulus are presented simultaneously. The subject is required to choose the sample visual stimulus to be rewarded. One limitation of conventional DMS task is that the maximal delay interval is fixed for all subjects, although cognitive abilities differ among them. With T-DMS task test, at the control condition, the monkeys' correct response levels will depend on each animal's working memory capacity as determined by the maximal delay interval. The memory assessment was serially conducted 2, 6, 24, and 48 h after administration of scopolamine at the dose of 0.01 and 0.03 mg/kg, respectively. Scopolamine decreased the memory performance in a dose-dependent manner 2 h after administration, followed by a gradual recovery at 24 h and later after scopolamine administration as shown in Fig. 16.8. In addition to T-DMS task test,

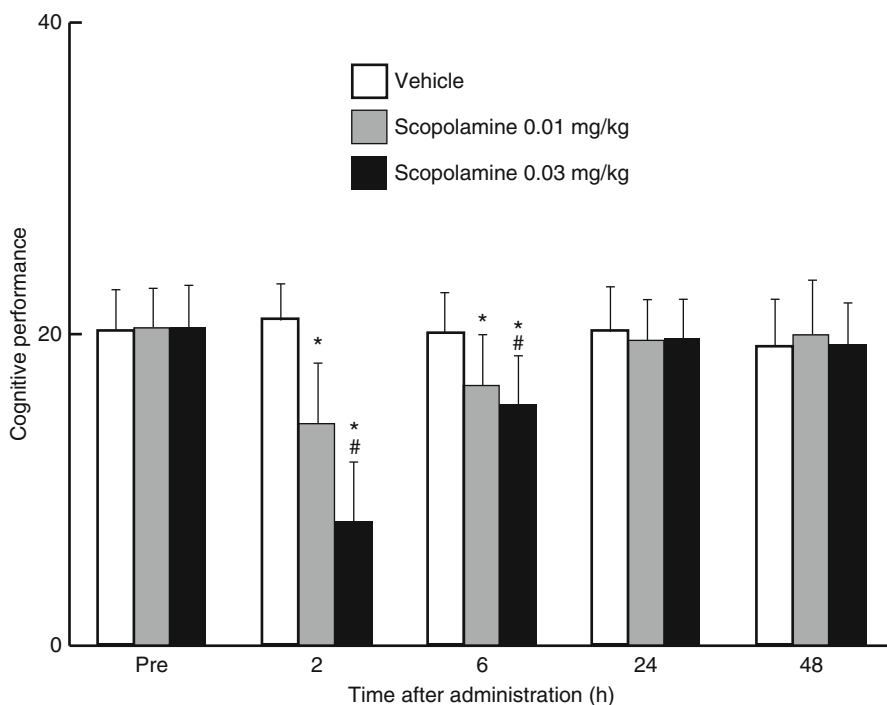


Fig. 16.8 Effects of scopolamine on titration-delayed match to sample (T-DMS) task. Time course of the cognitive index was serially monitored 2, 6, 24, and 48 h following administration of vehicle or scopolamine at the doses of 0.01 and 0.03 mg/kg. * $P < 0.01$ vs. Saline. # $P < 0.01$ vs. 0.01 mg/kg Scopolamine

the time-dependent changes in occupancy of mAChR by scopolamine were simultaneously observed with serial PET measurements with [^{11}C](+)-3-MPB. Occupancy levels of mAChR were maximal 2 h after scopolamine administration in the cortical regions innervated primarily by the basal forebrain, thalamus, and brainstem (Fig. 16.9). As shown in Fig. 16.10, mAChR occupancy and the degree of cognitive impairment were significantly and positively correlated in all brain regions. It should be noted that the highest significant correlation was observed in the brainstem. Although memory research has generally focused on the basal forebrain cholinergic systems (Collerton 1986; Everitt and Robbins 1997), a significant role of the brainstem cholinergic system in attention, learning, and memory has been reported (Inglis et al. 2001; Kozak et al. 2005). The present study demonstrated that the muscarinic cholinergic system in the brainstem was clearly involved with maintenance of an alert cognitive state in primates. Cognitive impairment induced by scopolamine persisted for 6 h and was followed by complete recovery to normal levels 24 h later. However, it was very interesting that some mAChR occupancy was still observed in most brain areas except the brainstem 24 h after scopolamine administration, suggesting the existence of a threshold (ca. 25 %) of mAChR

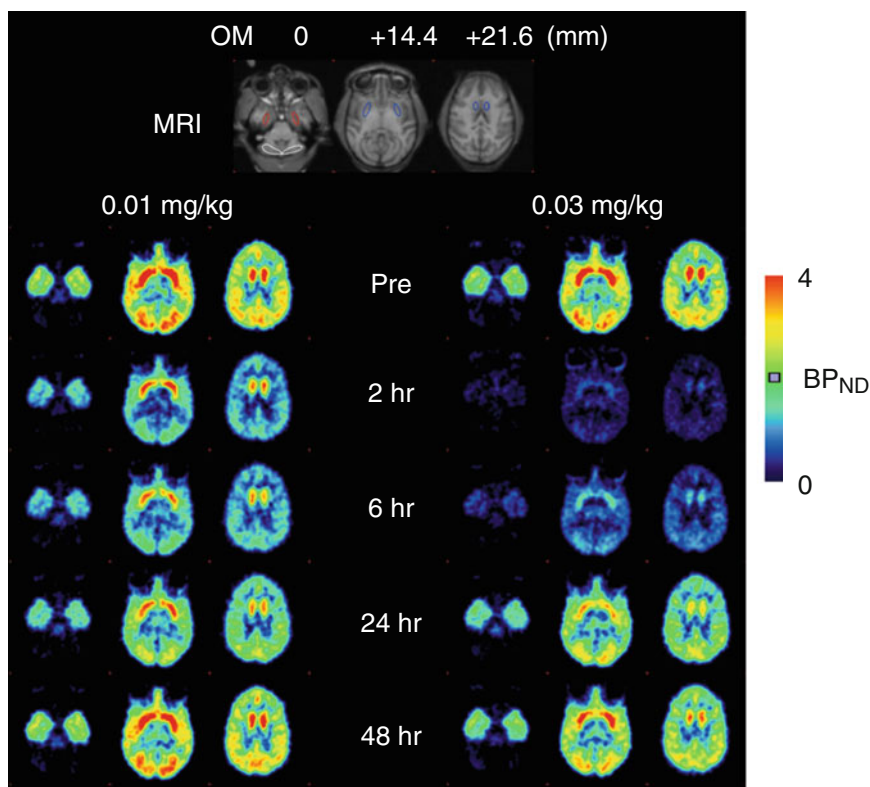


Fig. 16.9 Typical MRI and parametric PET images of [^{11}C](+)-3-MPB binding in monkey brain. PET data were collected in the conscious state with a high-resolution PET scanner (HAMAMATSU SHR-7700). Each labeled compound (100–120 MBq/kg body weight) was injected through the venous cannula. PET scans were performed for 91 min. Parametric maps (BP_{ND} of [^{11}C](+)-3-MPB) were calculated by the Logan plot reference tissue method with the cerebellum as the reference region. ROIs determined on the individual MRI image were superimposed on the parametric PET images to obtain BP_{ND} values

occupancy to induce cognitive impairment. This interpretation was consistent with our previous PET study with [^{11}C](+)-3-MPB which demonstrated 30–40 % reduction of mAChR in aged monkeys (ca. 20 years old) compared to young-adult monkeys (ca. 6 years old) (Tsukada et al. 2001a), associated with an impaired working memory performance (Tsukada et al. 2004).

The first study combining PET ([^{11}C](+)-3-MPB) and a behavioral test (T-DMS task) demonstrated that some degree of mAChR occupancy is needed to induce cognitive impairment, and a major involvement of brainstem mAChR occupancy in working memory. Based on this knowledge, we proposed important insights regarding the side effects of anticholinergic drugs for treatment of overactive bladder (Yamamoto et al. 2011a). Thus, we propose that the thresholds of mAChR occupancy to produce cognitive impairment by antimuscarinic agents are ca. 30–40 % in

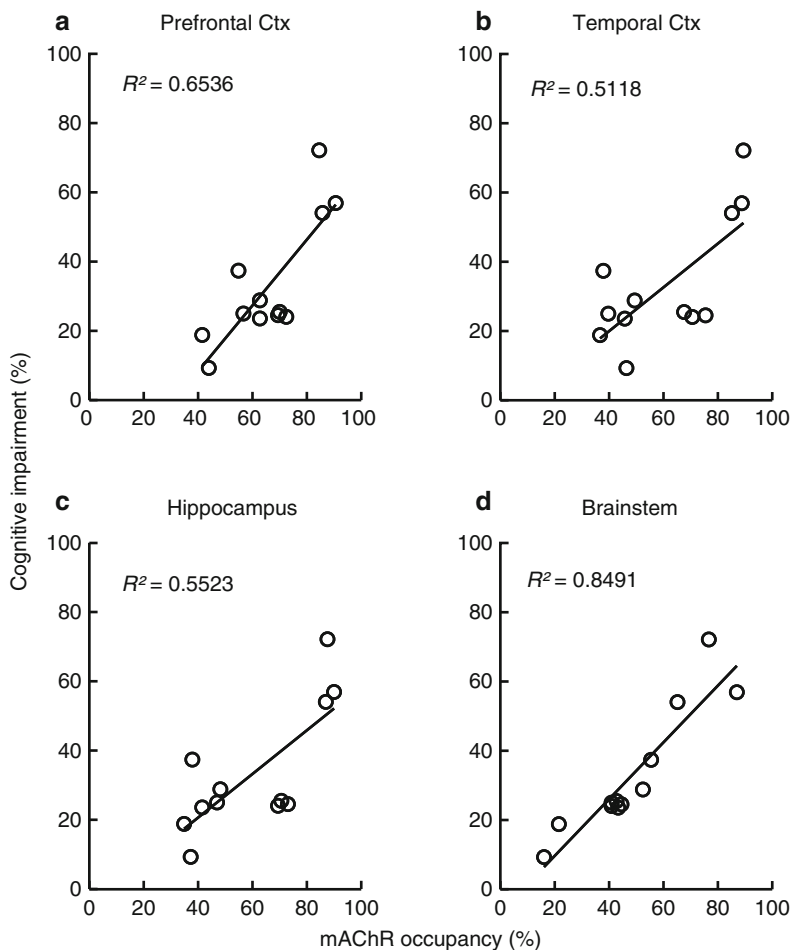


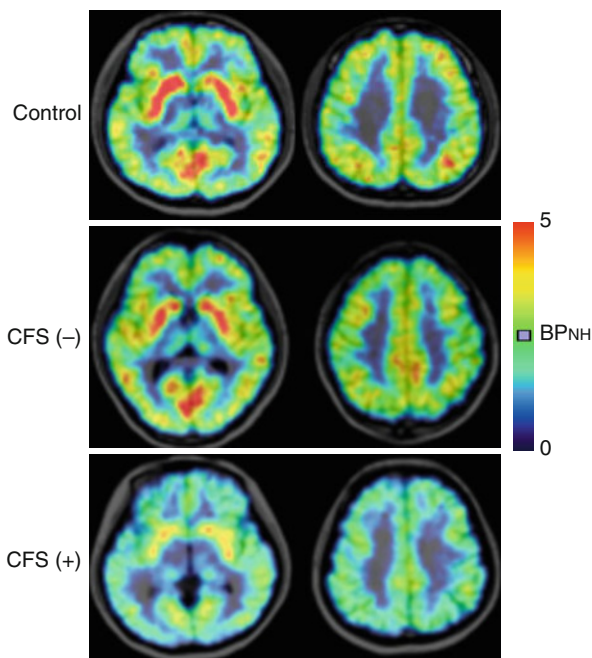
Fig. 16.10 Relationship between mAChR occupancy and cognitive impairment. Occupancy levels for prefrontal cortex (a), temporal cortex (b), hippocampus (c), and brainstem (d) were assessed 2 and 6 h after scopolamine administration at the doses of 0.01 and 0.03 mg/kg

cortices and ca. 20–30 % in brainstem, and a desirable drug for OAB treatment should not occupy central mAChR above these thresholds.

16.5 A Clinical Application of [^{11}C](+)-3-MPB in Chronic Fatigue Syndrome

Chronic fatigue syndrome (CFS) is a heterogeneous disorder characterized by persistent fatigue accompanied by rheumatologic, cognitive, and infectious-appearing symptoms. Associations between brain-reactive antibodies and neurological or

Fig. 16.11 PET images with [^{11}C](+)-3-MPB among normal control (NC) and CFS(-) and CFS(+) patients. Representative parametric PET images of each group were superimposed on the individual MRI. MR images were obtained with a 3.0-T scanner (HITACHI MRP7000AD). PET data were collected with a high-resolution PET scanner (HAMAMATSU SHR-12000) with a transaxial resolution of 2.9 mm (FWHM). After a bolus injection of [^{11}C](+)-3-MPB (ca. 350 MBq), PET scans were performed for 92 min, and the distribution volume ratio (DVR) images were calculated by Logan reference tissue method



psychiatric symptoms have been proposed. CFS researchers have showed abnormal cytokine levels including tumor necrosis factor, interleukin-1, interleukin-6, and increased markers of inflammation (Raison et al. 2009). Serum autoantibody against mAChR was increased in some CFS patients or psychiatric disease. We assessed the effects of serum autoantibody against mAChR on the central mAChR binding using PET and [^{11}C](+)-3-MPB in CFS patients with positive [CFS(+)] and negative [CFS(-)] autoantibodies (Yamamoto et al. 2012).

Five CFS(+) and six CFS(-) patients as well as 11 normal control subjects underwent a series of PET measurements with [^{11}C](+)-3-MPB for the mAChR binding and [^{11}C]MP4A for acetylcholinesterase (AChE) activity. The syntheses of [^{11}C](+)-3-MPB and [^{11}C]MP4A, PET data acquisitions, and cortical TAC analyses were conducted as described in Sects. 16.2.1 and 16.3. The radioligand assay of autoantibody to mAChR was conducted according to methods described in the previously published study (Tanaka et al. 2003). Cognitive function and fatigue scores of all subjects were assessed by neuropsychological tests (National Adult Reading Test, Wisconsin Card Sorting Test, etc.) and Advanced Trail-Making Test, respectively.

Radioligand assay in serum samples collected on the PET experiment demonstrated that 5 CFS(+) patients whose serum autoantibody was higher than the cutoff value shown as a dashed line, and 6 CFS(-) patients. In normal controls, there were no subjects with positive autoantibody against the mAChR. Fatigue scores were similar between CFS(+) and CFS(-) patients. There were no significant differences among the three groups in all the neuropsychological assessments. The binding of [^{11}C](+)-3-MPB in each brain of CFS(+) patients were significantly lower than those

in CFS(−) patients and control subjects (Fig. 16.11). Compared with controls, a 10–25 % reduction of binding to mAChR was observed in CFS(+) patients. In contrast, AChE activity did not differ among the three groups, suggesting the specific effects of autoantibody to mAChR, not to general cholinergic neuronal system.

Because the mAChR has a significant role in cognitive function, we predicted cognitive impairment in CFS(+) patients. However, there were no regions in which the binding of [¹¹C](+)-3-MPB significantly correlated with any neuropsychological indices even in CFS(+) patients. One plausible explanation is that reduction in the level of [¹¹C](+)-3-MPB binding occurs within a range of preserved cognitive function. Indeed, as described in Sect. 16.4, we reported the relationship between binding of [¹¹C](+)-3-MPB and cognitive function in conscious monkeys, showing that there were thresholds (ca. 30–40 % in cortex and ca. 20–30 % in brainstem) of activity of the brain mAChR to induce cognitive impairment (Yamamoto et al. 2011a, b).

Conclusion

We developed [¹¹C](+)-3-MPB with suitable kinetic properties for quantitative imaging of mAChR with PET in the living brains of rodents and nonhuman primates. The results of our studies described above strongly suggested the usefulness of this probe for pathophysiological and neurological assessments of neurological/mental disorders. We have checked the safety issue of this probe based on the microdose concept and started several clinical investigations of neurological/mental diseases not only Alzheimer-type dementia but also chronic fatigue syndrome (CFS).

References

- Bodick NC, Offen WW, Levey AI et al (1997) Effects of xanomeline, a selective muscarinic receptor agonist, on cognitive function and behavioral symptoms in Alzheimer disease. *Arch Neurol* 54:465–473
- Carson RE, Kiesewetter DO, Jagoda E et al (1998) Muscarinic cholinergic receptor measurements with [¹⁸F]FP-TZTP: control and competition studies. *J Cereb Blood Flow Metab* 18:1130–1142
- Collerton D (1986) Cholinergic function and intellectual decline in Alzheimer's disease [Review]. *Neuroscience* 19:1–28
- Dannals RF, Långström B, Ravert HT et al (1988) Synthesis of radiotracers for studying muscarinic cholinergic receptors in the living human brain using positron emission tomography: [¹¹C]dextetimide and [¹¹C]levetimidate. *Appl Radiat Isot* 39:291–295
- Dewey SL, MacGregor RR, Brondie JD et al (1990a) Mapping muscarinic receptors in human and baboon brain using [*N*-¹¹C-methyl]benztropine. *Synapse* 5:213–223
- Dewey SL, Volkow ND, Logan J et al (1990b) Age-related decrease in muscarinic cholinergic receptor binding in the human brain measured with positron emission tomography (PET). *J Neurosci Res* 27:569–575
- Everitt BJ, Robbins TW (1997) Central cholinergic systems and cognition. *Annu Rev Psychol* 48:649–684
- Frey KA, Koeppe RA, Mulholland GK et al (1992) In vivo muscarinic cholinergic receptor imaging in human brain with [¹¹C]scopolamine and positron emission tomography. *J Cereb Blood Flow Metab* 12:147–1541

- Höhhmann C, Antuono P, Coyle JT (1998) Basal forebrain cholinergic neurons and Alzheimer's disease. In: Iversen LL, Iversen SD, Snyder SD (eds) *Psychopharmacology of the aging nervous system*. Plenum, New York
- Hudzik TJ, Wenger GR (1993) Effects of drugs of abuse and cholinergic agents on delayed matching-to-sample responding in the squirrel monkey. *J Pharmacol Exp Ther* 265:120–127
- Inglis WL, Olmstead MC, Robbins TW (2001) Selective deficits in attentional performance on the 5-choice serial reaction time task following pedunclopontine tegmental nucleus lesions. *Behav Brain Res* 123:117–131
- Irie T, Fukushi K, Namba H et al (1996) Brain acetylcholinesterase activity: validation of a PET tracer in a rat model of Alzheimer's disease. *J Nucl Med* 37:649–655
- Katzman R (1986) Alzheimer's disease. *N Engl J Med* 314:964–973
- Kieseewetter DO, Lee J, Lang L et al (1995) Preparation of ^{18}F -labeled muscarinic agonist with M2 selectivity. *J Med Chem* 38:5–8
- Koeppel RA, Frey KA, Mulholland GK et al (1994) [^{11}C]Tropanyl benzilate binding to muscarinic cholinergic receptors: methodology and kinetic modeling alterations. *J Cereb Blood Flow Metab* 14:85–99
- Kozak R, Bowman EM, Latimer MP (2005) Excitotoxic lesions of the pedunclopontine tegmental nucleus in rats impair performance on a test of sustained attention. *Exp Brain Res* 162:257–264
- Långström B, Antoni G, Gullberg P et al (1986) The synthesis of ^{11}C -labeled ethyl, propyl, butyl and isobutyl iodides and examples of alkylation reactions. *Appl Radiat Isot* 37:1141–1145
- Laruelle M (2000) Imaging synaptic neurotransmission with in vivo binding competition techniques: a critical review. *J Cereb Blood Flow Metab* 20:423–451
- Lee KS, Frey KA, Koeppel RA et al (1996) In vivo quantification of cerebral muscarinic receptors in normal human aging using positron emission tomography and [^{11}C]tropanyl benzilate. *J Cereb Blood Flow Metab* 16:303–310
- Logan J, Fowler J, Volkow N et al (1990) Graphical analysis of reversible radioligand binding from time-activity measurements applied to N - ^{11}C -methyl(-)-cocaine PET studies in human subjects. *J Neurochem* 10:740–747
- Mulholland GK, Jewett DW, Otto CA et al (1988a) Synthesis and regional brain distribution of [^{11}C]N-methyl-4-piperidyl benzilate ([^{11}C]NMPB) in the rat. *J Nucl Med* 29:768
- Mulholland GK, Jewett DW, Toorongian SA (1988b) Routine synthesis of N -[^{11}C -methyl]scopolamine by phosphate mediated reductive methylation with [^{11}C]formaldehyde. *Appl Radiat Isot* 39:373–379
- Mulholland GK, Otto CA, Jewett DW et al (1992) Synthesis, rodent biodistribution, dosimetry, metabolism and monkey images of carbon-11-labeled (+)- 2α -tropanyl benzilate: a central muscarinic receptor imaging agent. *J Nucl Med* 33:423–430
- Nishimura Y, Onoe H, Morichika Y et al (2007) Time-dependent central compensatory mechanism of finger dexterity after spinal-cord injury. *Science* 318:1150–1155
- Nishiyama S, Tsukada H, Sato K et al (2001) Evaluation of PET ligands (+)N-[^{11}C]ethyl-3-piperidyl benzilate and (+)N-[^{11}C]propyl-3-piperidyl benzilate for muscarinic cholinergic receptors: a PET study with microdialysis in comparison with (+)N-[^{11}C]methyl-3-piperidyl benzilate in the conscious monkey brain. *Synapse* 40:159–169
- Ohba H, Harada N, Nishiyama S et al (2009) Ketamine/xylozine anesthesia alters [^{11}C]MNPA binding to dopamine D_2 receptors and response to methamphetamine challenge in monkey brain. *Synapse* 63:534–537
- Onoe H, Inoue O, Suzuki K et al (1994) Ketamine increases the striatal N - ^{11}C -methylspiperone binding in vivo: positron emission tomography study using conscious rhesus monkey. *Brain Res* 663:191–198
- Onoe H, Komori M, Onoe K et al (2001) Cortical networks recruited for time perception: a monkey positron emission tomography (PET) study. *Neuroimage* 13:37–45
- Patlak C, Blasberg RG, Fenstermacher JD (1983) Graphical evaluation of blood-to-brain transfer constants from multiple-time uptake data. *J Cereb Blood Flow Metab* 3:1–7
- Perry EK (1986) The cholinergic hypothesis – ten years on [Review]. *Br Med Bull* 42:63–69

- Podruchny TA, Connolly C, Bokde A et al (2003) In vivo muscarinic 2 receptor imaging in cognitively normal young and older volunteers. *Synapse* 48:39–44
- Prenant C, Barre L, Crouzel C (1989) Synthesis of n.c.a. [¹¹C]QNB. *J Labelled Compd Radiopharm* 26:199–201
- Raedler TJ, Knable MB, Jones DW et al (2003) In vivo determination of muscarinic acetylcholine receptor availability in schizophrenia. *Am J Psychiatry* 160:118–127
- Raison CL, Lin JM, Reeves WC et al (2009) Association of peripheral inflammatory markers with chronic fatigue in a population-based sample. *Brain Behav Immun* 23:327–337
- Reinikainen KJ, Riekkinen PJ, Halonen T, Laakso M (1987) Decreased muscarinic receptor binding in cerebral cortex and hippocampus in Alzheimer's disease. *Life Sci* 41:453–461
- Rinne JO, Laakso K, Lönnberg P et al (1985) Brain muscarinic receptors in senile dementia. *Brain Res* 336:19–25
- Selkoe DJ (1990) Deciphering Alzheimer's disease: the amyloid precursor protein yields new clues. *Science* 248:1058–1060
- Snyder SH, Chang KJ, Kuhar MJ et al (1975) Biochemical identification of the mammalian muscarinic cholinergic receptor. *Feder Proc* 34:1915–1921
- Suhara T, Inoue O, Kobayashi K et al (1993) Age-related changes in human muscarinic acetylcholine receptors measured by positron emission tomography. *Neurosci Lett* 149:225–228
- Takahashi K, Murakami M, Miura S et al (1997) Radiosynthesis and biodistribution of [¹¹C]3NMPB enantiomers in rats for studying muscarinic cholinergic receptors using PET. *J Labelled Compd Radiopharm* 40:613–615
- Tanaka S, Kuratsune H, Hidaka Y et al (2003) Autoantibodies against muscarinic cholinergic receptor in chronic fatigue syndrome. *Int J Mol Med* 12:225–230
- Tejani-Butt SM, Luthin GR, Wolfe BB et al (1990) *N*-substituted derivatives of 4-piperidinyll benzilate: affinities for brain muscarinic acetylcholine receptors. *Life Sci* 47:841–848
- Terry AV Jr, Buccafusco JJ (2003) The cholinergic hypothesis of age and Alzheimer's disease-related cognitive deficits: recent challenges and their implications for novel drug development. *J Pharmacol Exp Ther* 306:821–827
- Tsukada H, Harada N, Nishiyama S et al (2000a) Ketamine decreased striatal [¹¹C]raclopride binding with no alteration in static dopamine concentrations in the striatal extracellular fluid in the monkey brain: multi-parametric PET studies combined with microdialysis analysis. *Synapse* 37:95–103
- Tsukada H, Harada N, Nishiyama S et al (2000b) Cholinergic neuronal modulation alters dopamine D₂ receptor availability in vivo by regulating receptor affinity induced by facilitated synaptic dopamine turnover: PET studies with microdialysis in the conscious monkey brain. *J Neurosci* 20:7067–7073
- Tsukada H, Sato K, Kakiuchi T et al (2000c) Age-related impairment of coupling mechanism between neuronal activation and functional cerebral blood flow response was restored by cholinesterase inhibition: PET study with microdialysis in the awake monkey brain. *Brain Res* 857:158–164
- Tsukada H, Kakiuchi T, Nishiyama S et al (2001a) Age differences in muscarinic cholinergic receptors assayed with (+)*N*-[¹¹C]methyl-3-piperidyl benzilate in the brains of conscious monkeys. *Synapse* 41:248–257
- Tsukada H, Nishiyama S, Kakiuchi T et al (2001b) Ketamine alters the availability of striatal dopamine transporter as measured by [¹¹C]β-CFT and [¹¹C]β-CIT-FE in the monkey brain. *Synapse* 42:273–280
- Tsukada H, Takahashi K, Miura S et al (2001c) Evaluation of novel PET ligands (+)*N*-[¹¹C]methyl-3-piperidyl benzilate ([¹¹C](+)-3-MPB) and its stereoisomer [¹¹C](–)-3-MPB for muscarinic cholinergic receptors in the conscious monkey brain: a PET study in comparison with [¹¹C]4-MPB. *Synapse* 39:182–192
- Tsukada H, Nishiyama S, Fukumoto D et al (2004) Effects of acute acetylcholinesterase inhibition on the cerebral cholinergic neuronal system and cognitive function: functional imaging of the conscious monkey brain using animal PET in combination with microdialysis. *Synapse* 52:1–10

- Tsukada H, Ohba H, Nishiyama S, Kakiuchi T (2011) Differential effects of stress on [¹¹C]raclopride and [¹¹C]MNPA binding to striatal D₂/D₃ dopamine receptors: a PET study in conscious monkeys. *Synapse* 64:84–89
- Vora MM, Finn RD, Boothe TE (1983) [*N*-methyl-¹¹C]scopolamine: synthesis and distribution in rat brain. *J Labelled Compd Radiopharm* 20:1229–1234
- Watanabe M, Okada H, Shimizu K et al (1997) A high resolution animal PET scanner using compact PS-PMT detectors. *IEEE Trans Nucl Sci* 44:1277–1282
- Yamamoto S, Ohba H, Nishiyama S et al (2010) Validation of reference tissue model of PET ligand [¹¹C](+)-3-MPB for the muscarinic cholinergic receptor in the living brain of conscious monkey. *Synapse* 65:548–551
- Yamamoto S, Maruyama S, Ito Y et al (2011a) Effect of oxybutynin and imidafenacin on central muscarinic receptor occupancy and cognitive function: a monkey PET study with [¹¹C](+)-3-MPB. *Neuroimage* 58:1–9
- Yamamoto S, Nishiyama S, Kawamata M et al (2011b) Muscarinic receptor occupancy and cognitive impairment: a PET study with [¹¹C](+)-3-MPB and scopolamine in conscious monkeys. *Neuropsychopharmacology* 36:1455–1465
- Yamamoto S, Ouchi Y, Nakatsuka D et al (2012) Reduction of [¹¹C](+)-3-MPB binding in brain of chronic fatigue syndrome with serum autoantibody against muscarinic cholinergic receptor. *PLoS ONE* 7:e51515
- Yokoyama C, Tsukada H, Watanabe Y, Onoe H (2005) A dynamic shift of neural network activity before and after learning-set formation. *Cereb Cortex* 15:796–801
- Yoshida T, Kuwabara Y, Ichiya Y et al (1998) Cerebral muscarinic acetylcholinergic receptor measurement in Alzheimer's disease patient on ¹¹C-methyl-4-piperidyl benzilate – comparison with cerebral blood flow and cerebral glucose metabolism. *Ann Nucl Med* 12:35–42
- Zubieta JK, Koeppe RA, Mulholland GK et al (1998) Quantification of muscarinic cholinergic receptors with [¹¹C]NMPB and positron emission tomography: method development and differentiation of tracer delivery from receptor binding. *J Cereb Blood Flow Metab* 18:619–631

Peter Brust, Winnie Deuther-Conrad, Cornelius K. Donat,
Henryk Barthel, Patrick Riss, Louise Paterson,
Alexander Höpping, Osama Sabri, and Paul Cumming

Contents

17.1	Introduction	466
17.2	Advances in Animal PET and SPECT Technology	470
17.3	PET and SPECT Radioligands Targeting nAChR.....	472
17.3.1	Radioligands for $\alpha 4\beta 2$ nAChRs	472
17.3.2	Imaging of Heteromeric $\beta 4$ -Containing nAChR Subtype.....	484
17.3.3	Radioligands for $\alpha 7$ nAChRs	484
17.4	Imaging of Neurodegenerative Diseases	488
17.4.1	Alzheimer's Disease.....	488
17.4.2	Parkinson's Disease and Further Neurodegenerative Diseases.....	489
17.5	Imaging of Stroke and Neuroinflammation.....	491
17.6	Imaging of Traumatic Brain Injury	492
17.7	Imaging of Addiction and Psychiatric Disorders.....	493
17.7.1	Physiological Effects of Nicotine in the Context of Addiction.....	493
17.7.2	Schizophrenia and Depression.....	495
17.8	Potential Role of Nicotinic Receptor Studies for Measurement of Endogenous Acetylcholine	496
	Conclusion	497
	References.....	498

P. Brust, PhD (✉) • W. Deuther-Conrad • C.K. Donat
Department of Neuroradiopharmaceuticals, Institute of Radiopharmaceutical
Cancer Research, Helmholtz-Zentrum Dresden – Rossendorf, Research Site Leipzig,
Permoserstraße 15, 04318 Leipzig, Germany
e-mail: p.brust@hzdr.de

H. Barthel • O. Sabri
Department of Nuclear Medicine, University Hospital Leipzig, University of Leipzig,
Liebigstrasse 18, 04103 Leipzig, Germany

P. Riss
Department of Clinical Neurosciences, Wolfson Brain Imaging Centre,
Cambridge University, Manchester, UK

L. Paterson
Division of Experimental Medicine, Imperial College London, London, UK

A. Höpping • P. Cumming
ABX Pharmaceuticals, Radeberg, Germany

Abstract

Recent developments in radiochemistry have opened new vistas for investigations of nicotinic acetylcholine receptors (nAChRs) in living brain by positron emission tomography (PET) and by single photon emission computed tomography (SPECT). In parallel, dedicated instrumentation for molecular imaging in small animals has facilitated preclinical investigations in a number of models in which perturbations in nAChR signalling are implicated, notably Alzheimer's disease and other neurodegenerative conditions, schizophrenia and other neuropsychiatric disorders, substance abuse and traumatic brain injury. The nAChRs are members of a family of ligand-gated ion channels composed of five subunits, most commonly occurring in the central nervous system as heteropentamers designated $\alpha 4\beta 2$, with lesser amounts of the $\alpha 7$ homopentamer. We present a systematic review of preclinical findings with the diverse nAChR ligands which have been investigated to date. Molecular imaging of the $\alpha 4\beta 2$ nAChR subtype by PET has been successfully achieved by 2-[^{18}F]fluoro-A-85380. Newer agents such as (-)-[^{18}F]flubatine permit quantitation of $\alpha 4\beta 2$ receptors with PET recordings not exceeding 90 min, without the toxicity characteristic of earlier epibatidine derivatives. Imaging studies of $\alpha 7$ nAChRs have been hampered by inadequate pharmacological specificity of available ligands and by the low natural abundance of this receptor subtype in the brain. However, a continued search for optimal ligands is justified by the particular association of $\alpha 7$ nAChRs with aspects of cognitive function. We note that no molecular imaging ligands have been developed for $\alpha 6$ -containing nAChRs, despite their importance for the psychopharmacology of nicotine actions in the basal ganglia. Finally, we review the competitive binding model, in which the availability of $\alpha 4\beta 2$ binding sites is altered by competition from endogenous acetylcholine, noting that this approach has yet to be applied for monitoring acetylcholine release in disease models.

17.1 Introduction

Nicotine is an addictive drug named after the French diplomat Jean Nicot, who introduced cultivation of the tobacco plant (*Nicotiana tabacum*) in Europe. As early as 1828, nicotine was characterised as the major pharmacologically active substance of this solanaceous herb (Posselt and Reimann 1828); elucidation of its chemical structure followed 60 years later (Pinner and Wolffenstein 1891; Pinner 1893), and soon thereafter the first successful synthesis was obtained by Amé Pictet (1903). The stimulation of sympathetic ganglia by nicotine, first observed by John Newport Langley in Cambridge (Langley 1901), led to the concept of receptors that mediate drug actions (Langley 1905; Bennett 2000) and ultimately to the modern concept of molecular neurotransmission.

Nicotine and related alkaloids are present in other solanaceae such as tomato, potato, peppers and eggplant and also in tea leaves (Schep et al. 2009), such that the mean daily dietary nicotine intake is about 1.4 $\mu\text{g}/\text{day}$ (Siegmund et al. 1999); nicotine absorption in the gut is rapid, and its extraction at the blood–brain barrier is

extensive (Oldendorf et al. 1979; Allen and Lockman 2003). Indeed, inhaled nicotine reaches the brain within seconds (Rose et al. 2010), which may account for the perniciousness of smoking as a vehicle for nicotine self-administration. Within the brain, nicotine binds with high affinity to heteromeric (mainly the $\alpha 4\beta 2$ subtype) and homomeric (mainly the $\alpha 7$ subtype) nicotinic acetylcholine receptors (nAChRs) (Changeux 2010), which are the focus of this chapter. Signalling by the endogenous agonist acetylcholine via cerebral nAChRs mediates aspects of attention and cognition, locomotion, vigilance control and reward mechanisms (Changeux 2010; Graef et al. 2011). Modulation by nAChRs of dopamine release in the basal ganglia (Pradhan et al. 2002; Cumming et al. 2003) may contribute to the addictive potential of nicotine and tobacco smoking (Hogg et al. 2003). Furthermore there is evidence that nAChRs play a major role in brain development (Hruska et al. 2009; Ross et al. 2010). Nicotinic receptors, in particular the $\alpha 7$ subtype, are expressed by many classes of neurons and indeed by virtually all cell types of the brain, including astrocytes (Sharma and Vijayaraghavan 2001), microglia (De Simone et al. 2005; Suzuki et al. 2006), oligodendrocyte precursor cells (Sharma and Vijayaraghavan 2002) and endothelial cells (Hawkins et al. 2005). Perhaps consistent with this protean cellular distribution, dysfunction of nAChRs has been implicated in diverse human diseases such as schizophrenia, attention-deficit hyperactivity disorder, depression, anxiety disorders and degenerative conditions such as Huntington's disease, Alzheimer's disease, Parkinson's disease and traumatic brain injury, all of which motivates the present search for optimal molecular imaging agents.

The nAChRs belong to the Cys-loop super family of pentameric ligand-gated ion channels, which also includes the serotonin 5-HT₃, γ -aminobutyric acid (GABA_A and GABA_C) and glycine receptors, as has been reviewed in detail (Paterson and Nordberg 2000; Taly et al. 2009). Functional nAChRs are formed as pentamers of homologous or heterologous subunits forming a central cation channel permeable for Na⁺, K⁺ and Ca²⁺ ions. There are at least 17 genes encoding the following subunits: $\alpha 1$ –10, $\beta 1$ –4, δ , ϵ and γ (Karlin 2002), all of which occur in mammals except for the avian $\alpha 8$ subunit. Each monomer possesses an extracellular N-terminal domain, four transmembrane helices and a small cytoplasmic region (Karlin 2002). Recently, the 1.76 Å-resolution X-ray structure of a nAChR homologue, the prokaryotic acetylcholine binding protein (AChBP), has been reported (Brejc et al. 2001; Bourne et al. 2005; Hibbs et al. 2009), and a refined model of the membrane-associated nAChR from *Torpedo electric organ* based on 4 Å-resolution electron microscopy data has been presented (Unwin 2005).

The consensus nomenclature for nAChRs is based on the predominant subunit composition of the receptor. Although most functional receptors are heteromers, the $\alpha 7$ –10 subunits form functional homomers *in vivo*. Most neuronal nAChRs contain α - and β -subunits only (δ , ϵ and γ are expressed in peripheral tissues). Of the various possible $\alpha\beta$ permutations, nAChRs with six of the α -subunits (2–7) and three of the β -subunits (2–4) have been identified in mammalian brain, with heteromeric $\alpha 4\beta 2$ nAChRs predominating (Gotti et al. 2006). The next most abundant cerebral nAChR is the homomeric $\alpha 7$ subtype, which is functionally distinct from the heteromeric nAChRs due to its lower affinity for the agonists acetylcholine and

nicotine and higher affinity for α -bungarotoxin, an antagonist derived from snake venom. Indeed, radiolabelled α -bungarotoxin serves admirably for selective $\alpha 7$ autoradiography in vitro (Clarke et al. 1984). The $\alpha 7$ nAChR shows relatively fast activation and has the highest permeability to Ca^{2+} of all nAChR subtypes, whereas the $\alpha 4\beta 2$ hetero-oligomer is characterised by a high affinity for ACh and slow desensitisation (Changeux 2010). In general, activation of nAChRs requires cooperativity between subunits, with the agonist binding sites being located at subunit interfaces (Taylor et al. 1994). Activation of AChR heteromers requires binding of two ACh molecules at orthosteric binding sites, which are formed within the hydrophilic extracellular domain from three peptide domains on the α -subunit and three domains on the adjacent subunits (β or other) (Kalamida et al. 2007). Homomers have five acetylcholine binding sites, one between each α - α subunit interface (Millar and Harkness 2008).

As noted above, the nAChRs can shift between functionally distinct conformational states, four of which have been identified: resting (R), activated (A) with rapid opening within 1 ms and low affinity (μM to mM) for agonists and two desensitised, closed channel states which are refractory to opening for intervals lasting ms (I, insensitive) or minutes (D, desensitised), although still possessing high affinity (pM to nM) for receptor agonists (Decker et al. 2000). Thus, binding of ligands either at the orthosteric site or any of several allosteric sites alters the functional state of nAChRs, by favouring particular conformational states, consequently modifying the equilibrium between the four states of the receptor (Taly et al. 2009). Activation of nAChRs increases Ca^{2+} influx, which induces a spectrum of consequences, including (1) immediate effects, such as neurotransmitter release; (2) short-term effects, such as receptor desensitisation and recovery; and (3) long-lasting adaptive effects, such as neuroprotection or brain plasticity via altered gene expression (Radcliffe and Dani 1998; Leonard 2003; Shen and Yakel 2009). The particular pathways of intracellular signalling evoked by activation of nAChRs are complex and cell specific (Frazier et al. 1998; Schilström et al. 2000; Berg and Conroy 2002).

Neuronal nAChRs in the brain have been localised at post-, pre-, peri- and extra-synaptic sites of cholinergic or other neurones, affording multiple ways in which to modulate brain function. Regulation of the expression of these receptors is unusual in that prolonged exposure to agonists (e.g. nicotine) results in upregulation of functional receptors (i.e. an increase in the number of [^3H]nicotine binding sites) rather than downregulation as often seen with G-protein-coupled receptors. This upregulation is thought to occur by virtue of altered nAChR turnover, i.e. an increase in the number of receptors inserted in the cell membrane or a decrease in the removal of receptors from the cell membrane via altered endocytotic trafficking or degradation rates (Peng et al. 1994; Darsow et al. 2005). The predominant nAChRs in the brain, $\alpha 4\beta 2$ and $\alpha 7$, seem particularly sensitive to this form of post-translational regulation.

The total abundance of nAChRs in membrane homogenates from rodent brain is between 8 and 15 pmol/g tissue (Wang et al. 2011) and in human brain up to 10 pmol/g tissue (Shimohama et al. 1985; Marutle et al. 1998), calculated assuming

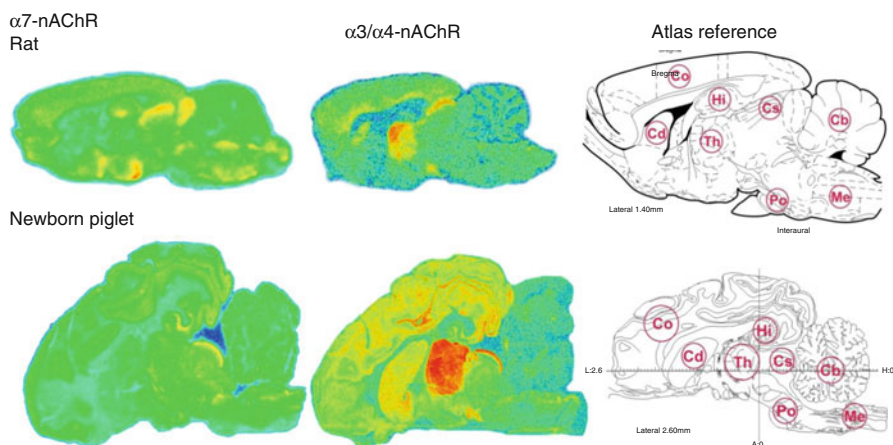


Fig. 17.1 Representative autoradiograms of rat (*upper row*) and neonate pig brains (*lower row*) obtained with an $\alpha 7$ nAChR ligand ($[^{125}\text{I}]\alpha$ -bungarotoxin) and the semi-selective $\alpha 3\beta 2$ ligand $[^3\text{H}]$ epibatidine. For anatomic reference, the right-hand side of the figure shows comparable sagittal planes modified from the rat brain atlas (Paxinos and Watson 1998) and the pig brain atlas (Felix et al. 1999). Structures marked in the reference atlases are Co cerebral cortex, Cd caudate nucleus, Cs superior colliculus, Cb cerebellum, Hi hippocampus, Th thalamus, Po pons, Me medulla oblongata

that protein constitutes 10 % of brain weight. The predominant heteromeric $\alpha 3\beta 2$ nAChR receptors account for some 80 % of the total abundance of brain nAChRs (Wang et al. 2011). For the less abundant $\alpha 7$ nAChRs, a B_{max} of 5 pmol/g tissue has been described in mice (Whiteaker et al. 1999), while levels of $[^{125}\text{I}]\alpha$ -bungarotoxin binding in the temporal cortex were only 1 pmol/g tissue for human and monkey (Gotti et al. 2006). Notably, these studies are based on tissue homogenates. However, a recent study has shown that the native environment of nAChRs is important for accurate quantitation of nAChRs in the brain (Wang et al. 2011); a very similar phenomenon has been described for dopamine receptors (Cumming 2011) suggesting that many receptors may be lost during the preparation of membranes or that not all receptors are externalised in the plasma membrane. Therefore, to predict the potential of nAChR radioligands for molecular imaging, binding to nAChRs should in general be tested by autoradiographic analysis of sections from frozen, intact brain.

The relatively few quantitative autoradiographic studies consistently report higher nAChR densities than homogenate-based studies. Autoradiographic studies with ligands for heteromeric $\alpha 3\beta 2$ nAChRs characteristically reveal particularly intense binding in the thalamus (Fig. 17.1). Using $[^{18}\text{F}]$ FNEP, the B_{max} for heteromeric nAChRs in human thalamus autoradiograms was 20 pmol/g tissue (Gatley et al. 1998), which is comparable to the density of binding sites of 2- $[^{18}\text{F}]$ F-A-85380 in porcine thalamus, 46 pmol/g tissue (Deuther-Conrad et al. 2006). In quantitative receptor autoradiographic studies with the $\alpha 7$ -selective ligands $[^3\text{H}]$ MLA and $[^{125}\text{I}]\alpha$ -bungarotoxin, densities were as high as 40 pmol/g tissue in mouse brain

(Whiteaker et al. 1999), whereas other studies with [125 I] α -bungarotoxin have indicated densities of 4–20 pmol/g tissue in rat and 2–10 pmol/g tissue in neonate pig (Hoffmeister et al. 2011). Across species, autoradiographic studies have revealed a characteristic distribution pattern for α 7 nAChRs (Fig. 17.1), which is rather diffuse, but with focally high density in hippocampus, the colliculi and the hypothalamus (except in newborn piglet), with moderate radiotracer binding in thalamus, and low expression in cerebellum (Breese et al. 1997; Whiteaker et al. 1999; Hoffmeister et al. 2011). The regional distribution of [3 H]AZ11637326, a novel α 7 nAChR radiotracer, determined in rat brain by autoradiography *ex vivo*, defined here as administration of the radioligand prior to euthanasia, was consistent with autoradiography findings *in vitro* (Maier et al. 2011).

The aspects of receptor imaging *in vivo* as discussed in this review relate exclusively to the use of radiolabelled receptor ligands, although we note that optical imaging has been used to investigate the cholinergic system (Prakash and Frostig 2005). Furthermore, clinical imaging of α 4 β 2 nAChR in human brain is reviewed elsewhere in this volume (see Sabri et al. in: PET and SPECT in Neurology). Therefore, the current review is focussed primarily on preclinical aspects including parts on instrumentation and radiotracer development.

17.2 Advances in Animal PET and SPECT Technology

The abundance of nAChRs can be measured *in vitro* and *ex vivo* using selective radioligands in conjunction with quantitative autoradiography. However, molecular imaging with positron emission tomography (PET) or single photon emission computed tomography (SPECT) makes possible the detection of neuroreceptors in the living brain. Contrary to autoradiography *in vitro*, *in vivo* imaging procedures allow for longitudinal studies in individual animals, thereby minimising issues arising from intersubject variability and allowing intervention or challenge studies. Until recently, animal PET studies were carried out using clinical scanners, most of which having a spatial resolution of approximately 5 mm; this is hardly adequate for resolution of structures within rodent brain. Only in the past 10 years have dedicated small-animal PET scanners become widely available. The best current instruments can attain a spatial resolution of little more than 1 mm full width at half maximum (FWHM) in the centre of the field of view, which is adequate to resolve structures as small as the mouse striatum.

PET technology is based upon coincident detection of two gamma photons (511 keV) arising from positron-electron annihilation subsequent to positron emission by decay of a neutron-deficient radionuclide incorporated in the tracer molecule. As such, the positron range prior to annihilation ultimately limits the spatial resolution of small-animal PET. The positron range is somewhat greater for positrons arising from the decay of carbon-11 than for the less energetic positrons emitted by fluorine-18. Iterative image reconstruction algorithms can approach a final resolution for 18 F sources of little more than 0.7 mm FWHM (Reader 2008).

Some of the dedicated small-animal scanners such as the Focus 120 (Siemens) are designed to be readily movable between research units (Tai et al. 2001). Other

systems, e.g. the microPET P4, Focus 220 (Siemens) and ClearPET (Raytest), can accommodate rodents and small non-human primates, whereas the larger Hamamatsu SHR-7700 instrument is designed specifically for non-human primate studies. The aperture and field of view of PET imaging systems designed for animal studies allow simultaneous recordings from up to eight mice (Rominger et al. 2010a), which should present a considerable economy in the experimental design of studies with transgenic animals. The most recent generation of preclinical PET scanners, such as the Inveon® PET-CT (Siemens), affords a considerable advantage in terms of anatomic information provided by the CT modality, but at the expense of lesser mobility for the hybrid scanners.

Small-animal PET and SPECT images are frequently characterised by a lack of anatomic information. In order to interpret the emission images, it has generally been necessary to employ some manual procedure for registration of the emission images to digitised brain atlases, based on histology or magnetic resonance imaging (MRI) atlases for rodent brain (Jupp et al. 2007; Rominger et al. 2010b). Contemporary multimodal imaging systems combine small-animal PET with SPECT, X-ray computed tomography (CT) and/or MRI. As noted above, PET-CT presents a great advantage for brain studies in that a high-resolution structural brain image in perfect registration with the PET image is obtained for each individual animal, rather than resorting to some standard atlas. In addition, the CT scan can be used to correct the PET images for attenuation by tissue, thus providing absolute quantitation of radioactivity concentrations in the brain without requiring an additional time-consuming transmission scan. MRI offers better tissue contrast than CT, but the combining of PET and MRI instrumentation has presented a greater technical challenge, due to incompatibility of traditional electronic components with a strong magnetic field. Nonetheless, a number of prototype PET/MRI scanners have been constructed, including the split magnet design in an animal microPET^(R)MR system at the University of Cambridge (Lucas et al. 2007). A commercial PET/MRI system for rats and mice was developed by Mediso; its 1 T permanent magnet limits MRI applications but offers great flexibility for animal PET studies.

At the cutting edge of small-animal imaging is the head-mounted PET detector developed at Brookhaven (“ratCAP”), which is compatible with imaging in awake, behaving rats (Schulz et al. 2011). This technology promises to revolutionise preclinical molecular brain imaging, by avoiding the well-known pharmacological confounds presented by anaesthesia. The ratCAP has recently been tested within the bore of a very high-field microMRI scanner, with minimal loss of sensitivity arising from the requirement for gating of the PET acquisition (Maramraju et al. 2011). Likewise, a SPECT camera which can be placed within an MRI magnet has recently been developed for small-animal studies (Meier et al. 2011). Whereas attenuation correction is usually obtained by CT scanning, MR-based attenuation correction has been demonstrated for PET and SPECT imaging using clinical scanners (Marshall et al. 2011) but has yet to be developed for small-animal studies. Although this technology remains at an early stage of development, hybrid PET-SPECT should eventually be permissive to multiple tracer studies with simultaneous acquisitions.

17.3 PET and SPECT Radioligands Targeting nAChR

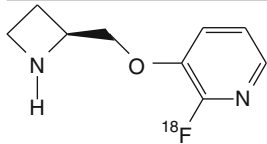
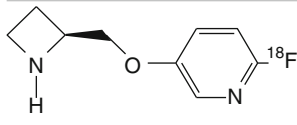
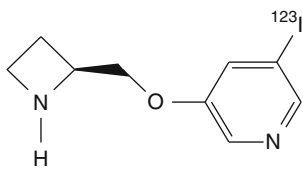
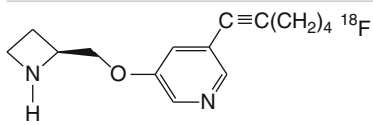
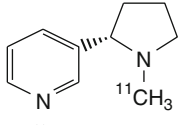
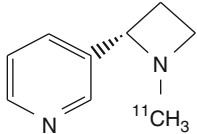
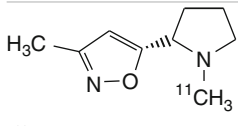
Many autoradiographic studies of nAChRs particularly in human brain have focussed on comparing the agonist-sensitive sites using rather non-selective ligands such as [³H]acetylcholine, [³H]nicotine, [³H/¹²⁵I]epibatidine or [³H]cytisine with those of the α 7-selective antagonist [³H/¹²⁵I] α -bungarotoxin (Paterson and Nordberg 2000). This approach suggested the existence of at least three native receptor subtypes with multiple affinity states, such that the α -bungarotoxin-sensitive receptors predominantly represent homomeric α 7 nAChRs, whereas the acetylcholine/nicotine binding sites represent mainly heteromeric α 4 β 2 nAChRs and a small population of heteromeric receptors containing the α 3 subunit. Given the predominance α 4 β 2 and the α 7 subtypes in the brain as documented above, they have presented the main targets for molecular imaging of nAChRs. The available information on the distribution, density and functional role of other subtypes in the brain is relatively sparse (Gotti et al. 2006; Sharma and Vijayaraghavan 2008). Furthermore, the current emphasis on α 4 β 2 and the α 7 subtypes as targets for pharmaceutical development may account for the paucity of selective high-affinity drugs for the other subtypes (Gündisch and Eibl 2011).

17.3.1 Radioligands for α 4 β 2 nAChRs

Reviews summarising the history of ligand development for the nAChRs (Sihver et al. 2000a, b; Ding and Fowler 2005; Horti and Villemagne 2006; Horti et al. 2010) have helped galvanise research groups to generate new lead compounds for molecular imaging and therapeutics. Radiolabelled imaging agents successfully applicable for the quantitative visualisation of neuronal nicotinic receptors in living systems have to fulfil a multitude of criteria: (1) high target affinity in the subnanomolar range and specificity towards nontarget nAChR subtypes, (2) low non-specific binding and absence of confounding metabolism generating brain permeant radiometabolites, (3) rapid clearance from non-specific areas and plasma to reduce background in the target tissue and (4) high membrane permeability as well as (5) high permeability and low efflux at the blood–brain barrier.

The vast majority of novel tracers for α 4 β 2 nAChRs have been derived from three compounds: nicotine, epibatidine and 3-piridyl ether. Four of these compounds have so far been used successfully to image α 4 β 2 receptors in human brain (Sihver et al. 2000b): nicotine (Nordberg 1993); the two halogen-substituted derivatives of A-85380, namely, 2-fluoro-A-85380 (Kimes et al. 2003) and 6-fluoro-A-85380 (Horti et al. 2000); and the epibatidine derivative flubatine (Sabri et al. 2011). Receptor-ligand interactions frequently entail stereoselective features (Smith and Jakobsen 2007), as has been formally demonstrated for the case of nAChRs in human PET studies with the two stereoisomers of [¹¹C]nicotine (Nordberg et al. 1991; Nordberg et al. 1992) and also several of the radioligands discussed below. A summary of the compounds that have been investigated for imaging of α 4 β 2 nAChRs is given in Table 17.1.

Table 17.1 Results of biodistribution *ex vivo* and PET imaging studies *in vivo* of the cerebral binding of $\alpha 4\beta 2$ nAChR-selective radioligands

	Main findings
 2- ¹⁸ F]fluoro-A-85380	Thalamic uptake of radioactivity in rat and baboon peaked at 60 min. In humans, cerebral uptake pattern consistent with the known distribution of $\alpha 4\beta 2$ nAChRs in human brain. Total distribution volume significantly higher in smokers than in non-smokers, except the thalamus. Radioactivity in the brain reached steady state by 6 h (Dollé et al. 1999; Kimes et al. 2003, 2008; Mukhin et al. 2008)
 6- ¹⁸ F]fluoro-A-85380	In baboon dynamic PET, faster peak uptake and clearance as well as higher thalamus-to-cerebellum ratios than that obtained for 2- ¹⁸ F]fluoro-A-85380 (Ding et al. 2000b)
 5- ¹²³ I]iodo-A-85380	In rhesus dynamic PET, regional distribution in the brain consistent with the known nAChR distribution pattern. Relatively slow kinetics, with maximal binding ratios at more than 4 h. In baboon, significant displacement of radioactivity from cerebellum by cytosine, indicating this region inappropriate as reference region (Chefer et al. 1998; Fujita et al. 2000)
 [¹⁸ F]-ZW-104	In baboon dynamic PET, rather slow kinetics in thalamus. High affinity towards multiple $\beta 2$ -containing nAChR subtypes (Valette et al. 2009)
 S- ¹¹ C]nicotine	In human and rhesus dynamic PET, binding was less selective for nAChR subtypes than was [¹¹ C]MPA (Sihver et al. 1999b)
 [¹¹ C]MPA	Specific binding in rhesus monkey proven by nicotine displacement in dynamic PET, but specific binding rather low (Sihver et al. 1999b)
 [¹¹ C]ABT418	In rhesus dynamic PET, low uptake and rapid washout, with no evidence for displacement by unlabelled ABT-418. Increased uptake following S(-)-nicotine pretreatment (Valette et al. 1997; Sihver et al. 1999b)

(continued)

Table 17.1 (continued)

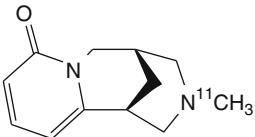
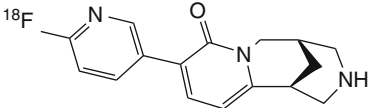
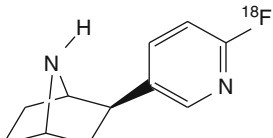
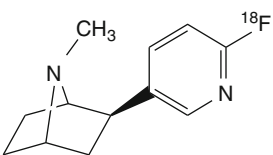
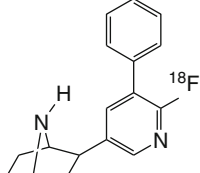
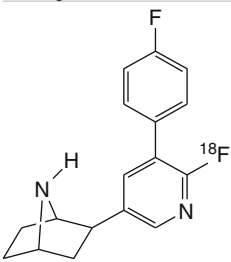
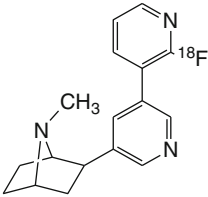
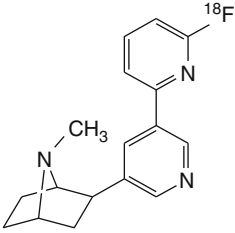
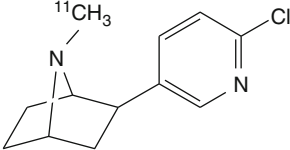
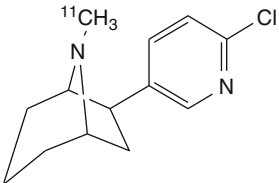
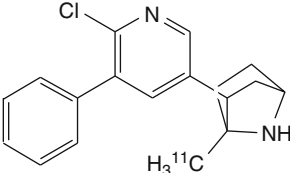
	Main findings
 <p><i>N</i>-[¹¹C]methylcytisine</p>	No evidence of specific binding in rhesus monkey brain by dynamic PET (Valette et al. 1997)
 <p>[¹⁸F]FPyCYT</p>	In rat biodistribution study, low (0.3 % ID/g) and uniform brain uptake, with little evidence of specific binding (Roger et al. 2003)
 <p>[¹⁸F]NFEP</p>	High brain uptake by mouse biodistribution and baboon PET studies and clear indication of specific binding. Applications in humans limited by high toxicity (Ding et al. 1996, 1999; Villemagne et al. 1997; Dolci et al. 1999)
 <p>[¹⁸F]<i>N</i>-methyl-NFEP</p>	In baboon dynamic PET, higher peak uptake in all brain regions than for [¹⁸ F]NFEP. Despite milder toxicity than [¹⁸ F]NFEP, evidence against safe use in humans (Ding et al. 1999)
 <p>[¹⁸F]FphEP</p>	In baboon dynamic PET, more favourable kinetics than 2-[¹⁸ F]fluoro-A-85380. Peak uptake at 20 min, but no evidence for displacement by nicotine challenge (Roger et al. 2006; Valette et al. 2007)
 <p>[¹⁸F]F₂PhEP</p>	Dynamic PET in baboon did not indicate reduction in brain distribution volume following pretreatment with nicotine (Valette et al. 2007)

Table 17.1 (continued)

	Main findings
 <p>¹⁸F]XTRA</p>	Dynamic PET showed peak activity in baboon thalamus at 75 min after bolus, requiring several hours for steady-state measurement (Horti and Wong 2009)
 <p>¹⁸F]AZAN</p>	Baboon dynamic PET showed rapid brain kinetics, favourable metabolic profile and high BP _{ND} , reliably measured with 90 min scans. However, part of in vivo binding could be related to other nAChRs with β-subunits (Gao et al. 2008b; Kuwabara et al. 2012)
 <p>N-[¹¹C]methylepipibatidine</p>	Different kinetics of brain uptake and washout seen for the stereoisomers in rats and mice. Dynamic PET showed high enrichment of radioactivity in the thalamus of the pig, but steady state not attained during 60 min scans. Applications in humans limited by high toxicity (Patt et al. 1999; Spang et al. 2000)
 <p>N-[¹¹C]methylhomoepipibatidine</p>	In pig dynamic PET, the (–)-enantiomer showed a regional distribution and high accumulation in the thalamus consistent with representative for the α4β2 nAChR, which could be displaced by cytosine. Distribution of the (+)-enantiomer, non-specific. Applications in humans limited by high toxicity (Patt et al. 2001)
 <p>[¹¹C]2-(6-chloro-5-phenylpyridin-3-yl)-methyl-7-azabicyclo[2.2.1]heptane</p>	Rat biodistribution study showed high displaceable binding. Dynamic baboon PET showed rapid peak in thalamus, but increasing ratio relative to cerebellum over at least 2 h (Huang et al. 2004)

(continued)

Table 17.1 (continued)

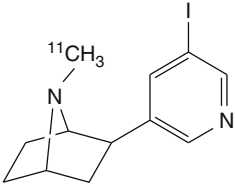
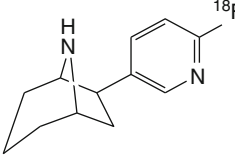
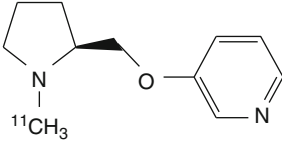
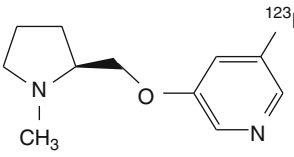
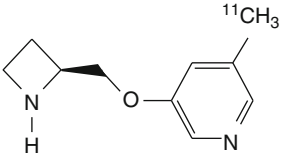
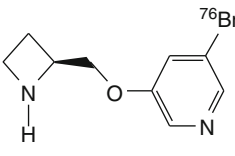
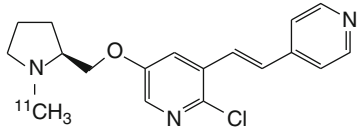
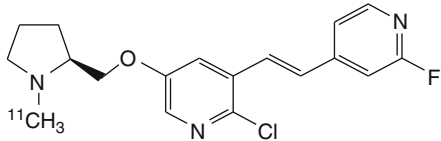
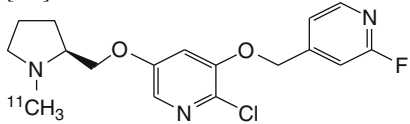
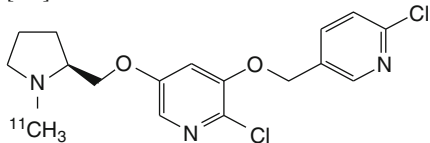
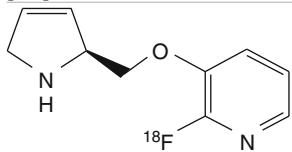
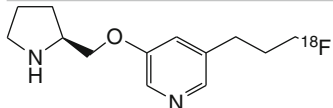
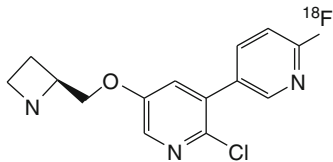
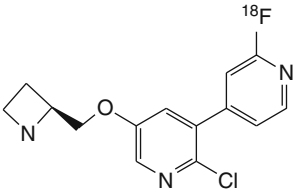
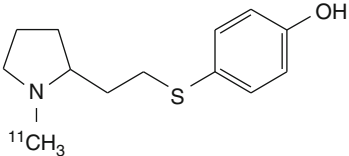
	Main findings
 <p>¹¹CH₃</p> <p>[¹¹C]NMI-EPB</p>	Baboon dynamic PET showed high uptake and displaceable thalamic binding. Higher uptake and faster kinetics than 2-[¹⁸ F]fluoro-A-85380; however, (–)-enantiomer did not reach steady state within 90 min post-injection (Ding et al. 2006; Gao et al. 2008a)
 <p>¹⁸F</p> <p>[¹⁸F]flubatine</p>	Higher uptake of radioactivity in mouse than for 2-[¹⁸ F]fluoro-A-85380. Binding equilibrium of the (–)-enantiomer was reached significantly earlier (~60 min p.i.) than that of the (+)-enantiomer (Brust et al. 2008; Deuther-Conrad et al. 2008)
 <p>¹¹CH₃</p> <p>[¹¹C]-A-84543</p>	Mouse biodistribution showed high brain uptake and a distribution consistent with the density of α4β2 nAChRs (Kassiou et al. 1998)
 <p>¹²³I</p> <p>5-[¹²³I]iodo-A-84543</p>	Nearly homogeneous distribution in mouse brain, likewise seen in baboon dynamic PET (Fan et al. 2001; Henderson et al. 2004)
 <p>¹¹CH₃</p> <p>5-[¹¹C]methyl-A-85380</p>	Mouse biodistribution consistent with α4β2 nAChRs. Rhesus monkey dynamic PET showed high non-specific binding (Iida et al. 2004)
 <p>⁷⁶Br</p> <p>[⁷⁶Br]BAP</p>	In comparison to rat biodistribution, baboon dynamic PET showed higher non-specific binding with nicotine of cystine displacement (Sihver et al. 1999a)
 <p>⁷⁶Br</p> <p>[⁷⁶Br]BrPH</p>	Rat biodistribution and baboon dynamic PET showed binding to nAChRs, but without subtype selectivity (Kassiou et al. 2002)

Table 17.1 (continued)

	Main findings
 <p>¹¹C]Me-<i>p</i>-PVC</p>	Rapid accumulation in mice <i>ex vivo</i> , and rhesus PET studies, thus quantifiable with 2-h recordings, but BP _{ND} slightly lower than for 2-[¹⁸ F]fluoro-A-85380 (Brown et al. 2004)
 <p>¹¹C]JHU85270</p>	In baboon dynamic PET, thalamic BP _{ND} lower than that of 2-[¹⁸ F]fluoro-A-85380 (Gao et al. 2009)
 <p>¹¹C]JHU85208</p>	
 <p>¹¹C]JHU85157</p>	
 <p>¹⁸F]nifene</p>	In rhesus dynamic PET, fast kinetics with peak thalamic binding at less than 10 min, thalamus-to-cerebellum ratio of ~2 (Pichika et al. 2006)
 <p>¹⁸F]nifrolidine</p>	In rhesus dynamic PET good labelling of thalamus, with slightly faster kinetics than for 2-[¹⁸ F]fluoro-A-85380, with maximal binding at 70 min and with plateau thalamus-to-cerebellum ratio of 1.7 at 2 h (Chattopadhyay et al. 2005)
 <p>¹⁸F]NIDA52189</p>	In rhesus dynamic PET, distribution consistent with $\alpha 4\beta 2$ nAChRs, but BP _{ND} 2.5 times higher than for 2-[¹⁸ F]fluoro-A-85380 (Zhang et al. 2004)

(continued)

Table 17.1 (continued)

	Main findings
 <p>¹⁸F NIDA522131</p>	In rhesus dynamic PET BP _{ND} in thalamus, 3–4-fold greater than with 2-[¹⁸ F] fluoro-A-85380, but at least 8-h recordings required for stable estimation (Chefer et al. 2008)
 <p>¹¹CH₃ [¹¹C]-SIB-1553A</p>	In rat biodistribution study, 0.5 %ID/g at 10 min and 0.25 %ID/g at 30 min, but no evidence of specific binding discernible against high background (Sobrio et al. 2008)

17.3.1.1 Nicotine Derivatives

The tracer *S*-[¹¹C]nicotine, one of the very first positron-emitting receptor ligands (Maziere et al. 1976), was initially developed to investigate the *in vivo* distribution of nicotine in the context of tobacco addiction, for investigation of diabetes insipidus and for insecticide research (Soloway 1976; Gündisch 2000). With the advent of PET, *S*-[¹¹C]nicotine was tested for imaging nAChRs in human brain (Nordberg 1993). However, co-administration of unlabelled nicotine failed to displace much of the radioligand, indicating that the PET signal did not sensitively reveal specific binding to $\alpha 4\beta 2$ nAChRs (Nybäck et al. 1994); cerebral *S*-[¹¹C]nicotine uptake proved mainly to be determined by blood flow, rather than local abundance of nAChRs *in vivo* (Gündisch 2000).

17.3.1.2 Cytisine Derivatives

The nAChR agonist [³H]cytisine is a useful radioligand for characterisation of $\alpha 4\beta 2$ nAChRs *in vitro*. However, the cytisine derivatives [¹¹C]ABT-418 and *N*-[¹¹C]methylcytisine (Valette et al. 1997) failed *in vivo* due to low cerebral uptake and rapid washout. Another derivative, [¹¹C]MPA, showed high-affinity binding (~10–100-fold higher than [¹¹C]ABT-418 and *S*-[¹¹C]nicotine) in membranes from rat forebrain (Sihver et al. 1998). Furthermore [¹¹C]MPA showed rapid uptake into monkey brain, to a similar extent as that of [¹¹C]ABT-418 and *S*-[¹¹C]nicotine. Pre-administration of unlabelled *S*-nicotine (0.02 mg/kg) decreased the peak uptake of [¹¹C]MPA in monkey brain by about 20 %, indicating the presence of some specific binding to nAChRs (Sihver et al. 1999b), but no further studies have been published with this ligand. [¹⁸F]fluoropyridinylcytisine was developed as another candidate radioligand for $\alpha 4\beta 2$ nAChR imaging. However, its *in vivo* distribution in rats did not resemble the regional distribution of nAChRs, and blocking studies with nicotine failed to demonstrate specific binding of this tracer (Roger et al. 2003).

17.3.1.3 Epibatidine Derivatives

Epibatidine has long been known for its high affinity to heteromeric nAChRs (Daly 1998). However it has a rather high toxicity arising from its potency and capacity to activate many different neuronal nAChR subtypes (Avalos et al. 2002). Pharmacological effects of epibatidine related in part to its affinity to the $\alpha 3\beta 4$ nAChR (Tomizawa et al. 2001; Avalos et al. 2002) have limited the application of radiolabelled epibatidine derivatives in human PET studies (Bohnen and Frey 2007). In theory, subtype-specific analogues of epibatidine could present favourable tracer properties with lesser toxicity (Avalos et al. 2002). Although [^{18}F]NFEP ([^{18}F]FPH, norchlorofluoroepibatidine) and [^{18}F]N-Me-NFEP showed good brain uptake and signal-to-background ratios in mouse and baboon brain (Ding et al. 1996; Dolci et al. 1999), their toxicity was considered to be too high for use in man (Horti et al. 1997; Molina et al. 1997; Villemagne et al. 1997; Ding et al. 1999). However, Horti and co-workers successfully synthesised epibatidine derivatives with lesser toxicity, thereby supporting the view that epibatidine could serve as a chemical lead for developing nAChR ligands applicable in PET (Horti et al. 1998a).

Fluorine-18-labelled FPhEP (Roger et al. 2006), a functional antagonist with much reduced toxicity, had faster brain kinetics in baboon than did 2-[^{18}F]fluoro-A-85380 (discussed below), whereas its fluorophenyl analogue [^{18}F]F₂PhEP possessed a higher specific binding (Valette et al. 2007), which was quantified as *binding potential*, which is designated BP_{ND} , and is proportional to the ratio $B_{\text{max}}/K_{\text{d}}$. However, neither radioligand was adequately displaced by nicotine, which indicated poor specific binding. Patt and co-workers developed [^{11}C]N-methylepibatidine and N-[^{11}C]methylhomoepibatidine (Patt et al. 1999, 2001). The enantiomers of [^{11}C]N-methylepibatidine were compared in vivo in mouse, rat and pig brain. Whereas the (–)-enantiomer showed slower uptake and gradual accumulation in the brain, the (+)-enantiomer showed very rapid uptake and washout. A different mechanism of binding of the enantiomers to nAChRs was proposed as a possible explanation for this difference (Patt et al. 1999). Because of its better kinetics and higher selectivity, [^{11}C]N-methyl(–)epibatidine was investigated in pigs by PET, which showed high brain uptake. However, steady-state binding in thalamus, the region with the highest binding, was not attained within the investigation time (1 h), which may present a significant disadvantage for carbon-11-labelled tracers, due to the 20 min physical half-life. Furthermore high toxicity was observed, precluding its use in humans (Patt et al. 1999). The analogue N-[^{11}C]methylhomoepibatidine had an improved toxicity profile; as was the case with [^{11}C]N-methylepibatidine, the (–)-enantiomer of N-[^{11}C]methylhomoepibatidine showed high uptake in pig brain, while the (+)-enantiomer was rapidly washed out. Although the binding characteristics of N-[^{11}C]methyl(–)-homoepibatidine in porcine brain suggested suitability for PET imaging studies, its toxicity in mice and rats was comparable to that of N-methylepibatidine, again precluding its use in humans (Patt et al. 2001).

Further development of epibatidine derivatives have focussed on maintaining or improving kinetic profiles while reducing toxicity. One such compound, [^{11}C]2-(6-chloro-5-phenylpyridin-3-yl)-7-methyl-7-azabicyclo[2.2.1]-heptane, showed a thalamus-to-cerebellum ratio of 4.2 at 90 min after injection, indicating high

specific binding in rat brain, which was displaceable by pretreatment with nicotine (1 mg/kg). A preliminary PET study of this tracer in a baboon revealed fast brain uptake and a distribution pattern consistent with $\alpha 4\beta 2$ nAChR binding. However binding equilibrium was not reached within 2 h, which is the limit for PET recordings with ^{11}C -labelled radioligands (Huang et al. 2004).

Mu et al. synthesised another series of epibatidine and homoepibatidine analogues (Mu et al. 2006). Of these, the 8- ^{11}C methyl-8-azabicyclo[3.2.1]octane derivative with a double bond conjugated with the pyridine nucleus, thus restricting free rotation of the pyridine ring, showed high affinity (2 nM) in vitro and at least 100-fold selectivity for $\alpha 4\beta 4$ over $\alpha 7$ nAChRs. Furthermore, it had 50-fold lesser toxicity than epibatidine. Although this radioligand promises to be useful for PET studies, no further experimental data on its evaluation in vivo are available. The antagonistic epibatidine derivative (\pm)- ^{11}C NMI-EPB (Ding et al. 2006) had 2.5-fold higher uptake in the baboon brain than did the 3-pyridil ether 2- ^{18}F fluoro-A-85380, discussed below (Ding et al. 2006). Surprisingly, separation of the (\pm)- ^{11}C NMI-EPB enantiomers did not reveal one to be a superior radiotracer: (+)- ^{11}C NMI-EPB had fast kinetics and low affinity, whereas (-)- ^{11}C NMI-EPB had slow kinetics (Gao et al. 2007a).

More recently, two further sets of epibatidine analogues (Gao et al. 2007a, b) were developed by the group from Johns Hopkins University, including (-)- ^{18}F JHU87522 (more recently termed ^{18}F AZAN) (Gao et al. 2008b; Horti et al. 2010), which displayed promising properties with respect to brain uptake, kinetics, metabolic stability and toxicity. Toxicology and radiation dosimetry experiments in human PET have been reported (Horti et al. 2010). PET studies in baboons confirmed that ^{18}F AZAN rapidly entered the brain and reached a steady state within 90 min after injection (Kuwabara et al. 2012). Furthermore, blocking experiments with cytisine demonstrated that ^{18}F AZAN binds specifically with $\beta 2$ -containing (predominantly $\alpha 4\beta 2$) nAChRs, supporting its suitability for nicotinic drug evaluation. Another epibatidine analogue, (-)- ^{18}F JHU86428 (^{18}F XTRA), was proposed, based on its exceptionally high affinity in vitro, as a potential tracer for the less abundant extrathalamic $\alpha 4\beta 2$ nAChRs (Gao et al. 2008b; Horti et al. 2010). An improved radiosynthesis methodology has been reported (Gao et al. 2010), but no further information is available about the ligand's binding properties in vivo.

Given that toxicity of epibatidine analogues may be related to high affinity for $\alpha 3\beta 4$ receptors, ligands with a higher selectivity ratio of $\alpha 4\beta 2$ relative to $\alpha 3\beta 4$ are needed. To this end, ^{18}F -labelled stereoisomers of the chloro-fluoro-substituted homoepibatidine analogue, flubatine (previously called NCFHEB), have been synthesised. The two enantiomers of flubatine bind with subnanomolar affinities to membranes from rat thalamus or HEK293 cells expressing the human $\alpha 4\beta 2$ nAChR (Deuther-Conrad et al. 2004). The (+)-enantiomer had twofold higher affinity than did the other stereoisomer. Previous studies have shown that fluoro and norchloro analogues of epibatidine have selectivity for $\beta 2$ -containing receptors (Avalos et al. 2002). Indeed, both enantiomers of flubatine had affinities to $\alpha 4\beta 2$ nAChRs comparable to that of epibatidine, but had 20–60-fold lower affinities to ganglionic $\alpha 3\beta 4$

nAChRs (Deuther-Conrad et al. 2004). The increase in subtype selectivity of flubatine seemingly results in decreased pharmacological side effects compared to epibatidine; injection of 25 µg/kg (+)-flubatine or (-)-flubatine to awake mice was without important pharmacological effects (Deuther-Conrad et al. 2008). The doses expected in a human PET study with [¹⁸F]flubatine are more than three orders of magnitude lower (Vaupel et al. 2005), which entails a considerable margin of safety. In addition to its selectivity for $\alpha 4\beta 2$ over $\alpha 3\beta 4$, (-)-flubatine and (+)-flubatine also had considerably better selectivity of $\alpha 4\beta 2$ over $\alpha 7$ receptors than did (-)-epibatidine (Deuther-Conrad et al. 2004).

N-methyl- and *N*-ethyl-derivatives of flubatine have been synthesised, but displayed lower target affinities and were consequently not considered for radiolabelling (Deuther-Conrad et al. 2004). Similar distribution patterns for (+)-[¹⁸F]flubatine and (-)-[¹⁸F]flubatine were observed in mice, rat and porcine brain (Brust et al. 2008; Deuther-Conrad et al. 2008; Sabri et al. 2008). Allen et al. provided evidence that nicotine analogues are transported into the brain via the blood–brain barrier (BBB) choline transporter (Allen et al. 2003); this mechanism may also be involved in the brain uptake of epibatidine and homoepibatidine derivatives (Deuther-Conrad et al. 2008). Indeed, addition of flubatine to the incubation medium inhibited the uptake of [³H]choline in immortalised rat brain endothelial cells, which are known to express the blood–brain barrier (BBB) choline transporter (Friedrich et al. 2001), with an IC_{50} of 370 ± 90 µM (Deuther-Conrad et al. 2008). This result is comparable to the K_i of 65 µM obtained for hemicholinium-3 in the same experimental system (Friedrich et al. 2001). Furthermore, *in vivo* experiments in rats have confirmed the postulated interaction of flubatine with the BBB choline transporter; 50 µM flubatine reduced the transport rate of [³H]choline by 21 %, whereas equimolar epibatidine resulted in a ~40 % reduction (Deuther-Conrad et al. 2008). The stronger interaction of epibatidine is consistent with its higher uptake in mouse brain (London et al. 1995) compared to (+)-[¹⁸F]flubatine or (-)-[¹⁸F]flubatine.

PET studies in young pigs were performed to compare the brain uptake and kinetics of (+)-[¹⁸F]flubatine and (-)-[¹⁸F]flubatine with that of 2-[¹⁸F]fluoro-A-85380, a 3-pyridyl ether discussed in detail below. The brain uptake of both enantiomers proved to be two- to threefold higher than that of 2-[¹⁸F]fluoro-A-85380. The binding equilibrium of (-)-[¹⁸F]flubatine was reached significantly earlier (~60 min *p.i.*) than that of the (+)-enantiomer (Brust et al. 2008), consistent with its lesser affinity *in vitro*. The specific binding of (-)-[¹⁸F]flubatine in porcine brain was comparable to that of 2-[¹⁸F]fluoro-A-85380, but (+)-[¹⁸F]flubatine displayed about twofold higher specific binding. Thus, both [¹⁸F]flubatine enantiomers may present advantages over 2-[¹⁸F]fluoro-A-85380 for application in human PET studies, especially as pertains to the time to equilibrium binding.

17.3.1.4 3-Pyridyl Ethers

First developed for treatment of Alzheimer's disease, the 3-pyridyl ethers have long been regarded as promising radioligands for imaging of nAChRs *in vivo* (Gündisch 2000; Horti and Villemagne 2006; Horti et al. 2010). The 3-pyridyl ethers are equipotent to epibatidine at [³H]cytisine binding sites in the brain, which mainly bind

$\alpha 4\beta 2$ nAChRs, but are 100-fold less potent than epibatidine as agonists at $\alpha 3\beta 4$ nAChR receptors (Abreo et al. 1996). This property predicts larger dose margins and minimal cardiovascular or other toxic side effects. The prototype compound A-85380 has similar binding affinities at recombinant $\alpha 2\beta 2$, $\alpha 3\beta 2$ and $\alpha 4\beta 2$ nAChRs in vitro (Xiao and Kellar 2004). In addition, the iodinated derivative 5-[^{125}I] iodo-A-85380 binds with high affinity to $\alpha 6\beta 2\beta 3$ nAChRs in monkey and rat striatum (Kulak et al. 2002). Therefore, 3-pyridyl ethers are properly regarded as $\beta 2$ -selective compounds (Jensen et al. 2005; Lai et al. 2005), furthermore possessing little affinity or efficacy at the $\alpha 7$ nAChR (Sullivan et al. 1996).

As noted above, 2-[^{18}F]fluoro-A-85380 and 6-[^{18}F]fluoro-A-85380 (Horti et al. 1998b, 2000) showed early promise for PET imaging, with a better toxicity profile than epibatidine analogues. Of the two, 6-[^{18}F]fluoro-A-85380 (Scheffel et al. 2000) had superior kinetics, characterised by earlier peak and faster clearance from the brain (Ding et al. 2004), and better target-to-background ratios than were obtained with 2-[^{18}F]fluoro-A-85380 in a comparative study in baboon (Ding et al. 2000a). Although 6-[^{18}F]fluoro-A-85380 has nonetheless not yet found wide use, both derivatives proved successful in human brain imaging (see Sabri et al. in: PET and SPECT in Neurology). The SPECT analogue 5-[^{123}I]iodo-85380 was tested in rhesus monkey (Chefer et al. 1998) and baboon (Fujita et al. 2000). Although hindered by slow kinetics, the radioligand seemed sensitive to changes in the endogenous acetylcholine level (Fujita et al. 2003), a property which will be discussed in some detail below. The methyl-substituted derivative 5-[^{123}I]iodo-A-84543 (Henderson et al. 2004) displayed faster kinetics, but homogenous uptake of radioactivity in baboon brain, in contrast to the spatially heterogeneous pattern of specific binding for the analogue [^{11}C]-A-84543 seen in mouse brain (Kassiou et al. 1998). PET studies in pigs with [^{11}C]-A-186253, a structurally similar tracer, revealed little displacement by cytosine in the thalamus and cortex, indicating excessive non-specific binding (Itier et al. 2004).

The comparably low brain uptake of 2-[^{18}F]fluoro-A-85380 was similar to that previously found with 5-[^{11}C]methyl-A-85380 (2.2 % ID/g brain tissue at 30 min p.i. (Iida et al. 2004)). This may be related to the rather high polarity of these compounds (Zhang et al. 2004), which is regarded as a critical parameter for brain radiotracer uptake (Waterhouse 2003). Nevertheless 2-[^{18}F]fluoro-A-85380 has been successfully used to image nAChRs in non-human primates (Chefer et al. 1999, 2003; Valette et al. 1999; Le Foll et al. 2007) and in rat microPET studies (Vaupel et al. 2007). An optimised radiosynthesis of 2-[^{18}F]fluoro-A-85380 and improved analytical techniques (Mitkovski et al. 2005; Schmaljohann et al. 2005; Kimes et al. 2008) have facilitated its use in human imaging studies (Ellis et al. 2009) (Lotfipour et al. 2012). Despite slow binding kinetics requiring interrupted or continuous PET recordings lasting at least 6 h (Gallezot et al. 2005; Horti and Villemagne 2006), 2-[^{18}F]fluoro-A-85380 remains the most utilised nAChR ligand in human PET studies (see Sabri et al. in: PET and SPECT in Neurology); despite its limitations, it is to some extent the standard against which other PET ligands have been compared.

A series of 5-substituted-6-halogeno derivatives of A-85380 with potentially improved lipophilicity and affinity has been generated (Zhang et al. 2004). PET

studies in rhesus monkey with two [^{18}F]-labelled derivatives revealed that their lipophilicity exceeding that of the rather hydrophilic 2- ^{18}F fluoro-A-85380, resulting in enhanced target-to-background ratios. Imaging studies with another 5-substituted A-85380 derivative, [^{11}C]5-MA (Iida et al. 2004), demonstrated lower total brain uptake and target-to-background ratios than that seen with 2- or 6- ^{18}F fluoro-A-85380. A further analogue, [^{18}F]ZW-104, is still under investigation (Kozikowski et al. 2005; Valette et al. 2009; Saba et al. 2010). In baboon PET studies, this tracer showed regional radioactivity distribution similar to that of 2- ^{18}F fluoro-A-85380 and some superior properties, including higher accumulation in the brain, earlier peak uptake in the thalamus and faster washout kinetics. However, it also displayed considerable affinity for $\alpha 3\beta 2$ and $\alpha 2\beta 2$ receptors in vitro (Valette et al. 2009) and rather high non-displaceable (by nicotine) uptake in the striatum, a region with comparably low density of nAChRs.

Many further derivatives were tested in rodent and non-human primate PET studies: [^{76}Br]BAP (Sihver et al. 1999a); [^{76}Br]BrPH (Kassiou et al. 2002); [^{11}C] Me-*p*-PVC (Brown et al. 2004) and its analogues [^{11}C]JHU85208, [^{11}C] JHU85157 and [^{11}C]JHU85270 (Gao et al. 2007b, 2009); [^{18}F]nifene (Pichika et al. 2006; Easwaramoorthy et al. 2007); and two carbon-11- and fluorine-18-labelled isotopomers of one pyridine-derived ligand. While some of these ligands displayed improved kinetics relative to 2- ^{18}F fluoro-A-85380, insufficient binding potential or high levels of non-specific binding prevented their further development for human imaging (Easwaramoorthy et al. 2007). Interestingly, specific binding of [^{18}F]nifene could be attributed entirely to $\alpha 4\beta 2$ nAChRs based on studies in $\beta 2$ -knockout mice (Bieszczad et al. 2012). PET imaging of $\alpha 4\beta 2$ nAChRs using the pyridyl ether analogue [^{18}F]nifrolidine has been initiated in rhesus monkey (Chattopadhyay et al. 2005). Although having favourable kinetics, the thalamus-to-cerebellum ratio was lower than that of other $\alpha 4\beta 2$ -targeting pyridyl ether analogues (Chattopadhyay et al. 2005), and no further investigations have yet been reported with this compound. Similarly, there have been no follow-up reports on the nifrolidine homologue [^{18}F]nifzetidine (Mukherjee et al. 2004).

The series of pyridyl ether-based compounds [^{18}F]NIDA52189, [^{18}F]NIDA522131 and [^{18}F]NIDA52289 have been synthesised and evaluated by PET in rhesus monkeys (Horti and Villemagne 2006) for imaging of extrathalamic $\alpha 4\beta 2$ nAChRs. Among these, [^{18}F]NIDA52189 (Zhang et al. 2004) and [^{18}F]NIDA522131 (Chefer et al. 2008) were deemed superior to 2- ^{18}F -FA with respect to extrathalamic binding, but suffered from slow kinetics in vivo.

17.3.1.5 Non-epibatidine- and Non-A-85380-Related Compounds

Carbon-11-labelled Me-*p*-PVC (Brown et al. 2002) and *p*-PVP-MEMA, which were selected from the class of (4-pyridinyl)vinylpyridines developed by Abbott Laboratories, possessed picomolar affinity towards $\alpha 4\beta 2$ receptors. Nevertheless, [^{11}C]Me-*p*-PVC had low binding potential in rhesus monkey thalamus (Brown et al. 2004), and a low target-to-background ratio was obtained in baboon brain for [^{11}C]p-PVP-MEMA in a preliminary PET study (Dollé et al. 2008).

17.3.2 Imaging of Heteromeric $\beta 4$ -Containing nAChR Subtype

The putative $\beta 4$ -selective agonist [^{11}C]-SIB-1553A was assessed by biodistribution and ex vivo brain autoradiography in rats (Sobrio et al. 2008). Its low specific binding suggested a limited potential for further development, although no attempt was made to separate and individually investigate the enantiomers of this racemic radioligand.

17.3.3 Radioligands for $\alpha 7$ nAChRs

Efforts to develop a radiopharmaceutical for PET imaging of $\alpha 7$ nAChR have met with only partial success. The steric and electronic requirements of this site are met by structurally diverse classes of compounds, as reviewed recently (Toyohara et al. 2010b). As noted above, the cerebral expression of $\alpha 7$ nAChR is comparatively low, constituting perhaps one quarter of the density for $\alpha 4\beta 2$ receptors (Spurden et al. 1997; Whiteaker et al. 1999; Hellström-Lindhahl and Court 2000). Because of this low natural abundance of $\alpha 7$ sites, high affinity is particularly important for an effective PET tracer. Binding properties of various $\alpha 7$ tracers tested to date are summarised in Table 17.2.

17.3.3.1 Quinuclidine-Based Ligands

The lead compound of a series of azabicyclic carbamate $\alpha 7$ receptor agonists developed by Astra Laboratories has been labelled with carbon-11 and evaluated in rats (Dollé et al. 2001a). Despite having relatively good brain uptake, no regionally selective or specific binding could be seen. Another series of potential $\alpha 7$ -selective imaging agents based on the quinuclidine moiety has been labelled with carbon-11 and iodine-125 (Pomper et al. 2005). Target selectivities of these compounds were modest, and the most affine compounds had significant binding to the 5-HT₃ receptor, a structural homologue of $\alpha 7$ nAChR (Zwart et al. 2004).

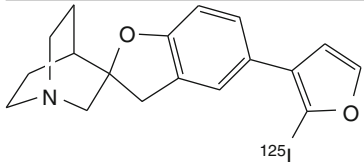
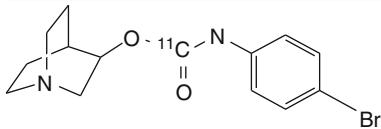
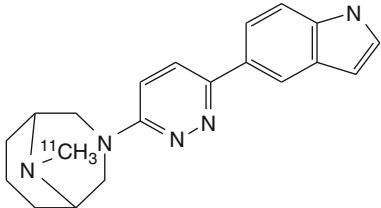
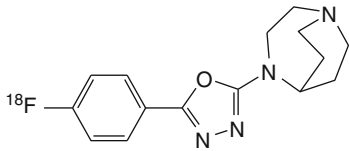
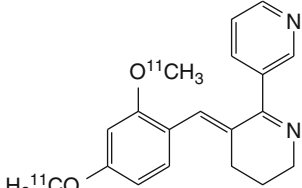
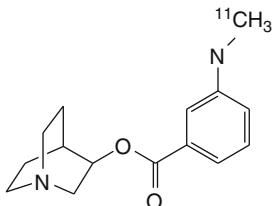
17.3.3.2 GTS-21

Other potential ligands originate from, for example, benzylidene anabaseine compounds such as GTS-21 (de Fiebre et al. 1995; Meyer et al. 1998). GTS-21 (3-(2,4-dimethoxybenzylidene)-anabaseine) is one of the most promising $\alpha 7$ nAChR agonist drugs currently being evaluated clinically for improving cognition in patients with schizophrenia (Freedman et al. 2008; Tregellas et al. 2011). It has been labelled with iodine-123 (Zhang et al. 2001) and carbon-11 (Kim et al. 2007b). Consistent with the relatively low affinity and specificity of GTS-21 for $\alpha 7$ nAChR, the distribution and kinetics of [^{123}I]GTS-21 and [^{11}C]GTS-21 in vivo in both baboon and mice were dominated by non-specific binding (Kim et al. 2007a).

17.3.3.3 Diazabicyclononane Derivatives

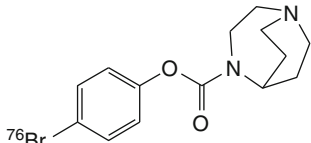
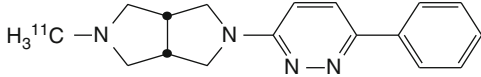
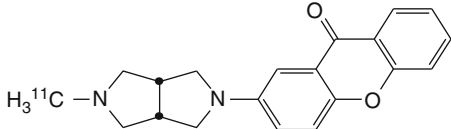
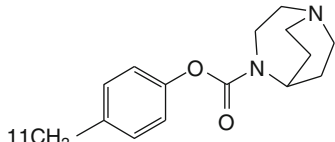
Recently, the 1,4-diazabicyclo-[3.2.2]nonane skeleton (Bunnelle et al. 2004) has been identified as new structure to improve the $\alpha 7$ receptor-ligand interaction, and

Table 17.2 Results of biodistribution ex vivo and PET imaging studies in vivo of the cerebral binding of $\alpha 7$ nAChR-selective radioligands

	Main findings
 <p>^{125}I4</p>	Biodistribution in CD1 mice showed very limited uptake in the brain and no evidence of displaceable binding (Pomper et al. 2005)
 <p>^{11}C1</p>	Biodistribution study in rats showed no regionally selective or specific binding (Dollé et al. 2001b)
 <p>^{11}CNS12857</p>	High uptake in pig brain by dynamic PET, but lack of displacement in vivo (Lehel et al. 2009)
 <p>^{18}FNS10743</p>	High uptake in the pig brain by dynamic PET, with clear evidence of displaceable binding in regions of relatively high tracer accumulation (Deuther-Conrad et al. 2011)
 <p>2/4-methoxy-^{11}CGTS21</p>	In baboon dynamic PET, very high initial uptake followed by rapid clearance; relatively little evidence for specific $\alpha 7$ nAChR binding. Brain-penetrating radiometabolites detected in plasma (Kim et al. 2007b)
 <p>^{11}CMeQAA</p>	In rhesus monkey dynamic PET, the <i>R</i> -enantiomer had high cerebral uptake and distribution consistent with $\alpha 7$ nAChRs (Ogawa et al. 2010)

(continued)

Table 17.2 (continued)

	Main findings
 $[^{76}\text{Br}]\text{SSR180711}$	In rhesus monkey dynamic PET, substantial and heterogeneous brain accumulation. Binding globally reduced to level seen in cerebellum by pretreatment with the $\alpha 7$ nAChR agonist SSR180711 (Hashimoto et al. 2008)
 $[^{11}\text{C}]\text{A-582941}$	In rhesus monkey dynamic PET studies, evidence for regional distribution consistent with $\alpha 7$ nAChR expression (Toyohara et al. 2010a)
 $[^{11}\text{C}]\text{A-844606}$	
 $[^{11}\text{C}]\text{CHIBA-1001}$	In a PET study of one healthy human, evidence for preferential in the hippocampus, cortex and basal ganglia, with slow washout, and least binding in cerebellum (Toyohara et al. 2009)

the two novel diazabicyclononane-derived PET ligands $[^{76}\text{Br}]\text{SSR180711}$ and $[^{11}\text{C}]\text{CHIBA-1001}$ were evaluated by PET in conscious non-human primates, with testing in a model of schizophrenia (Hashimoto et al. 2008). Of the two tracers, $[^{11}\text{C}]\text{CHIBA-1001}$ demonstrated superior accumulation in the brain, revealing a heterogeneous regional distribution consistent with the localisation of $\alpha 7$ in monkey brain; specific binding was blocked by selective $\alpha 7$ but not $\alpha 4\beta 2$ agonists. Furthermore, it was suggested that this radioligand could be used for measuring occupancy by pharmaceuticals at $\alpha 7$ nAChRs. A first clinical PET study confirmed the suitability of $[^{11}\text{C}]\text{CHIBA-1001}$, although the regional binding differences were small in the human brain and $\alpha 7$ -specific binding could not be demonstrated (Toyohara et al. 2009). There was no displacement of 30 nM $[^3\text{H}]\text{-CHIBA}$ binding from rat brain membranes by 1 μM α -bungarotoxin in vitro (Tanibuchi et al. 2010). Furthermore, differences in the regional distribution of the binding sites of CHIBA-1001 relative to $[^{125}\text{I}]\alpha$ -bungarotoxin were evident in monkey and human brain samples (Tanibuchi et al. 2010). Another rodent study reported low in vitro binding affinity of $[^3\text{H}]\text{-CHIBA}$ and poor in vivo selectivity to $\alpha 7$ nAChRs in rodent brain (Ding et al. 2012).

Among the most promising PET ligands for imaging of cerebral $\alpha 7$ nAChR are the 1,4-diazabicyclo[3.2.2]nonane derivatives developed by NeuroSearch (Peters et al. 2007). Two carbon-11 radioligands were developed, $[^{11}\text{C}]\text{NS12857}$ (Lehel

et al. 2009) and [^{11}C]NS14492 (Ettrup et al. 2011), along with the fluorine-18 compound [^{18}F]NS10743 (Deuther-Conrad et al. 2009). Evaluation of the latter tracer in mice showed it to permeate readily into brain, obtaining a heterogeneous pattern matching the $\alpha 7$ distribution; this binding was blocked by pre-administration of a selective $\alpha 7$ agonist. The brain uptake of these three 1,4-diazabicyclo[3.2.2]nonane derivatives is generally higher than that of [^{11}C]CHIBA-1001. Although the uptake of [^{11}C]NS12857 was not blocked by pretreatment with $\alpha 7$ nAChR-selective compounds, specific binding was clearly evident for [^{11}C]NS14492 and [^{18}F]NS10743, the two ligands with higher target affinity (Brust et al. 2012).

The general suitability of these derivatives for PET imaging of $\alpha 7$ nAChR was shown by preclinical PET studies in pigs (Lehel et al. 2009; Deuther-Conrad et al. 2011; Ettrup et al. 2011), although the magnitude of BP_{ND} , about 0.5, is the absolute minimum for a useful PET tracer. However, in view of the low expression density of $\alpha 7$ nAChR in the brain, a substantial increase in $\alpha 7$ affinity of PET radiotracers may be required for sensitive quantitation (Brust et al. 2012); target affinities of [^{11}C]CHIBA-1001 ($K_i \sim 35$ nM) (Hashimoto et al. 2008; Toyohara et al. 2009) and [^{18}F]NS10743 ($K_i \sim 10$ nM) (Deuther-Conrad et al. 2009) do not predict adequate specific signal in vivo, given the low B_{max} (Koeppel 2001). NS14490, a novel diazabicyclononane derivative, with a K_i of 3 nM may be more promising in this regard (Brust and Deuther-Conrad 2012). The distribution of [^{18}F]NS14490 binding in mouse brain autoradiograms correlated with the known pattern of $\alpha 7$ nAChR expression and was displaced with the $\alpha 7$ nAChR ligand methyllycaconitine (Brust and Deuther-Conrad 2012). Very recently, a new highly affine radioligand ($K_i = 0.3$ nM), [^{18}F]DBT10, has been studied in pigs and showed BP values in brain between 2 and 5 (Teodoro et al. 2014, unpublished).

17.3.3.4 [^{11}C]A-582941 and [^{11}C]A-844606

Recently, a new series of octahydropyrrolo[3,4-c]pyrrole derivatives was described by Abbott Laboratories, two of which were selected for labelling with carbon-11 (Toyohara et al. 2010a). Whereas no regional heterogeneity or displaceable binding was evident in mouse brain ex vivo, pretreatment with an $\alpha 7$ -specific agonist decreased the total distribution volumes of both tracers in conscious monkey PET studies, indicative of a BP_{ND} close to 0.5, as with the NeuroSearch compounds cited above.

17.3.3.5 [^{125}I]I-TSA

A diazabicyclooctane-derived PET ligand with high affinity and selectivity has been radiolabelled and evaluated in mice (Ogawa et al. 2006). Despite a subnanomolar affinity, the high non-specific binding made [^{125}I]I-TSA inadequate for imaging of brain $\alpha 7$ receptors.

17.3.3.6 R-[^{11}C]MeQAA

The two enantiomers of [^{11}C]MeQAA, an azabicyclooctylester-derived compound, were evaluated in mice and conscious monkey PET studies (Ogawa et al. 2009). Although R-[^{11}C]MeQAA showed target-specific accumulation, the in vivo selectivity was insufficient due to binding to the serotonin 5HT $_3$ -R.

17.4 Imaging of Neurodegenerative Diseases

Reductions in cortical nAChR binding have been found in patients with diverse forms of dementia, including Alzheimer's disease, Parkinson's disease, Lewy body disease, progressive supranuclear palsy and Down's syndrome (Perry et al. 1986; Picciotto and Zoli 2002). However, there have been few preclinical PET and SPECT studies of nAChRs in animal models of neurodegenerative disease. This is attributable to two considerations: First, models in transgenic mice have only recently become available for some of these diseases while remaining lacking for others, and second, the spatial resolution of small-animal PET and SPECT instruments has until recently been inadequate for regional analysis of neuroreceptors in rodent brain, such that the majority of such investigations have been conducted using autoradiography *in vitro*. Furthermore, interpretation of preclinical imaging studies are hindered by the occurrence of species differences (Pauly et al. 1989; Quik et al. 2000; Han et al. 2003). Despite these limitations, molecular imaging is emerging as a powerful tool for investigating pathophysiological changes in animal models of neurodegenerative diseases, especially when conducted in conjunction with techniques such as *in vivo* microdialysis, electrophysiology and histopathology (Higuchi et al. 2012).

17.4.1 Alzheimer's Disease

A link between cognitive performance and $\alpha 4\beta 2$ nAChR expression in forebrain of healthy rats has been demonstrated in a PET study using the ligand [^{18}F]nifene (Bieszczad et al. 2012), as confirmed by autoradiography *ex vivo* and *in vitro*. The three imaging methods showed the same rank order of specific binding by brain region. We anticipate that [^{18}F]nifene PET should allow tracking of dynamic changes in nAChRs during learning acquisition and memory consolidation, in rodents and also in large-brained animals. In contrast to the case for humans (Zanardi et al. 2002), normal aging does not seem to reduce nAChR density in rat brain (Picciotto and Zoli 2002; Schliebs and Arendt 2011).

The hallmark histopathological features of Alzheimer's disease are extraneuronal amyloid plaques composed of aggregated β -amyloid peptides ($\text{A}\beta$), and intraneuronal neurofibrillary tangles, which are composed largely of hyperphosphorylated forms of tau, a microtubule-associated protein (Thal and Braak 2005). Molecular imaging studies in animal models have primarily targeted fibrillar protein assemblies such as β -amyloid and tau depositions, neuroinflammatory processes and cerebral glucose metabolism (Higuchi et al. 2012). However, these features are closely related to cholinergic hypofunction found in Alzheimer's disease and relevant animal models (Schliebs and Arendt 2011). Cognitive impairment in Alzheimer's disease is at least partially associated with loss of cortical nAChRs, which may arise due to toxicity of soluble β -amyloid (Zanardi et al. 2002; Schliebs 2005; Schliebs and Arendt 2011). Nicotine treatment in a transgenic mouse model (3xTg-AD) can mediate increased tau phosphorylation and decreased β -amyloid load (Rubio et al. 2006).

Impaired cholinergic neurotransmission has been described in the brain of Tg2576 mice, which express the Swedish mutation of human β -amyloid precursor protein (Apelt et al. 2002). Enzyme activities for acetylcholine synthesis (choline acetyltransferase) and degradation (acetylcholine esterase, AChE) did not differ between transgenic mice and non-transgenic littermates. However, a reduction of high-affinity choline uptake and M_1 -muscarinic receptor density was observed. Autoradiography with [3 H]cytisine revealed a significant 20 % loss of $\alpha 4$ -containing nAChRs in cingulate and parietal cortices of these animals at an age of 17 months. However, there was no change in the number of basal forebrain cholinergic neurons in the transgenic mice, compared to age-matched wild-type animals.

Evidence for an involvement of $\alpha 7$ nAChR in Alzheimer's disease was first presented three decades ago (Davies and Feisullin 1981). More recently, a very high-affinity binding of (soluble) β -amyloid to $\alpha 7$ nAChRs has been described in vitro (Wang et al. 2000), supporting the hypothesis that β -amyloid at very low concentrations may initiate neuronal degeneration via an $\alpha 7$ nAChR-mediated inflammatory process (Bencherif and Lippiello 2010). A 20 % reduction in $\alpha 7$ nAChRs labelled with [125 I] α -bungarotoxin was evident in the hippocampus, retrosplenial and parietal cortices and thalamus of 3xTg-AD mice at 6 months of age. There was a significant correlation between intraneuronal β -amyloid and reduced $\alpha 7$ nAChR binding in the same mouse model (Oddo et al. 2005). Whereas chronic nicotine administration did not alter $\alpha 7$ nAChR in these mice, there was an increase in $\alpha 4\beta 2$ nAChRs labelled with [125 I]epibatidine (Oddo et al. 2005). In contrast to the earlier report, no alteration in $\alpha 7$ nAChR binding was noted in a subsequent study of the triple transgenic 3xTg-AD mice, which closely emulate several features of natural Alzheimer's disease (Hedberg et al. 2010); this unexpected negative finding was attributed to unknown environmental and/or genetic factors.

The abundance of $\alpha 7$ nAChRs was determined using nanogold-conjugated α -bungarotoxin in the APP_(SWE) mouse model of Alzheimer's disease (Jones et al. 2004). Interestingly, the $\alpha 7$ nAChR binding increased in the transgenic animals until 9 months of age, but had declined at 12 months, most notably in areas of gliosis associated with β -amyloid plaques (Jones et al. 2006). Also [125 I] α -bungarotoxin binding decreased in APP_(SWE) mice between 9 months of age and 16 months (Hellström-Lindahl et al. 2004).

17.4.2 Parkinson's Disease and Further Neurodegenerative Diseases

Parkinson's disease is, after Alzheimer's disease, the second most common neurodegenerative disorder. The hallmark neuropathology of Parkinson's disease is selective degeneration of midbrain dopaminergic neurons of the substantia nigra pars compacta (SNpc) and the presence of intra-cytoplasmic inclusions (Lewy bodies) consisting of aggregated α -synuclein (Spillantini et al. 1997) in surviving dopamine neurons. In a 2-[18 F]fluoro-A-85380 PET study, the density of $\alpha 4\beta 2$ nAChRs was slightly reduced in the basal ganglia of non-smoking Parkinson's disease patients

(Kas et al. 2009). Another 2-^[18F]fluoro-A-85380 PET study of Parkinson's disease patients reported a widespread reduction of $\alpha 4\beta 2$ nAChR availability in cortical and subcortical regions, which correlated with the severity of mild cognitive or depressive symptoms (Meyer et al. 2009).

Neurotoxins such as MPTP and 6-hydroxydopamine have been used in animal models emulating the nigrostriatal degeneration of Parkinson's disease (Quik 2004). Lesions of the nigrostriatal pathway in rats reveal a population of [³H]nicotine binding sites on dopamine terminals (Clarke and Pert 1985). More recently, the stimulation of striatal dopamine release by nicotine has been linked specifically to $\alpha 6\beta 2\beta 3$ and $\alpha 6\alpha 4\beta 2\beta 3$ nAChRs, which predominate in the basal ganglia (Quik et al. 2011). Quantitative analysis with the $\alpha 6\beta 2$ nAChR subtype ligand [¹²⁵I] α -conotoxin MII in conjunction with dopamine transport measurements in MPTP-lesioned mice shows an association with presynaptic nigrostriatal terminals (Quik et al. 2003). In that study, much smaller reductions in the binding of [¹²⁵I]epibatidine (multiple sites) and 5-^[125I]iodo-A-85380 ($\beta 2$ -sites) were noted after lesioning, while no change was detected in $\alpha 7$ nAChRs measured with [¹²⁵I] α -bungarotoxin binding after nigrostriatal lesions. Displacement of [¹²⁵I]- α -conotoxin MII binding with the analogue E11A was biphasic, allowing resolution of the $\alpha 6\beta 2\beta 3$ and $\alpha 6\alpha 4\beta 2\beta 3$ components (Bordia et al. 2007); autoradiographic studies in MPTP-treated mouse and non-human primates, as well as in material from idiopathic Parkinson's disease patients, revealed the $\alpha 6\alpha 4\beta 2\beta 3$ nAChR subtype population to be selectively vulnerable to nigrostriatal damage. Chronic oral nicotine administration was able to protect nicotinic receptors and also dopaminergic markers in MPTP-treated monkeys (Bordia et al. 2006; Quik et al. 2006). There is a current lack of agents for molecular imaging of the particular $\alpha 6$ -containing nAChRs subtypes of greatest relevance to Parkinson's disease.

Huntington's disease is an autosomal dominant hereditary disorder proceeding to severe cognitive impairment and motor symptoms, notably hyperkinetic involuntary movements (chorea) (Roos 2010). A transgenic rat model of HD, which carries a truncated huntingtin cDNA fragment with 51 CAG repeats under control of the native rat huntingtin promoter, has been developed (von Horsten et al. 2003). Early investigations of nicotinic receptors in post-mortem brain from Huntington's disease patients did not reveal any significant changes (Perry et al. 1987; Whitehouse and Kellar 1987). However, autoradiographic assessment of 2-year-old transgenic rats revealed significant increase of nAChR in various regions in heterozygous but not homozygous animals (Bauer et al. 2005).

Some forms of epilepsy have recently been associated with alterations of $\alpha 4$ nAChR subtype expression (Raggenbass and Bertrand 2002), and there is experimental evidence that the $\alpha 7$ nAChR may play a role in epileptogenesis (Dobelis et al. 2003). The autosomal dominant nocturnal frontal lobe epilepsy (ADNFLE) can be caused by mutations in the neuronal nicotinic acetylcholine receptor (nAChR) subunit genes CHRNA4 and CHRNB2 (Steinlein et al. 1995; Phillips et al. 2001). Relative to age-matched non-smoking subjects, there was a 10–20 % increase in the binding of 2-^[18F]fluoro-A-85380 to $\alpha 4\beta 2$ receptors in the brain of patients with autosomal dominant nocturnal frontal lobe epilepsy (Picard et al. 2006); knock-in

mice bearing a culprit mutant $\alpha 4$ gene have been prepared (Lipovsek et al. 2008), but have not been investigated by receptor autoradiography or PET.

17.5 Imaging of Stroke and Neuroinflammation

Stroke is the leading cause of adult disability in the United States and Europe and the second leading cause of death worldwide. Stroke is characterised by a loss of brain functions due to rapid disturbances in cerebral blood supply, either as reduced blood flow by thrombosis or embolism (ischemic stroke) or blood leakage (haemorrhagic stroke). Hyperacute mechanisms of stroke-related brain tissue damage, such as excitotoxicity, can be discriminated from delayed factors such as inflammation and apoptosis. Cellular components of the so-called neurovascular unit, which includes neurons, astrocytes and endothelial cells, all express nAChRs (Paulson et al. 2010). Insofar as long-term tobacco smoking is a risk factor for ischemic stroke (Hawkins et al. 2002), it may be relevant that nAChRs were altered in a post-mortem study of smokers; $\alpha 4$ expression was increased in neurons and dendritic processes and $\alpha 7$ expression was decreased in hippocampal neurons and astrocytes (Teakong et al. 2004). In hypertensive stroke-prone rats, cortical $\alpha 7$ nAChRs are reduced, without concomitant changes in the $\alpha 4\beta 2$ nAChRs (Ferrari et al. 1999). Activation of nAChRs by nicotine promotes endothelial cell proliferation (Villablanca 1998) and leucocyte migration (Yong et al. 1997), which together may increase thrombotic risk. However, nAChR agonism was neuroprotective against excitotoxicity in vitro, an effect which was mediated by growth factors (Belluardo et al. 1998) and also by inactivation of the toxins (O'Neill et al. 2002). These effects were blocked by the $\alpha 7$ nAChR antagonist α -bungarotoxin (Donnelly-Roberts et al. 1996). Interestingly, nicotine increased oedema/infarct size in a rodent stroke model (Paulson et al. 2010). A particular contribution of $\alpha 7$ nAChRs to stroke-related excitotoxicity might reflect their high Ca^{2+} permeability, especially under depolarising conditions. Treatment with the acetylcholinesterase inhibitor methanesulfonyl fluoride attenuated stroke-induced learning and memory deficits in rats (Borlongan et al. 2005).

These rather discordant findings of effects of nAChR agonism in stroke models may reflect the different contributions of excitotoxicity and also neuroinflammatory processes. The $\alpha 7$ nAChRs expressed on microglia (Shytle et al. 2004) seem particularly posed to mediate inflammatory responses. Nicotinic agonism at these sites suppressed inflammation by decreasing TNF- α production, while nicotine antagonists had the opposite effect (Shytle et al. 2004). In addition to central mechanisms, cholinergic signalling in the “cholinergic anti-inflammatory pathway” involving the vagus nerve may suppress the release of pro-inflammatory cytokines and influence migration T cells from the periphery to brain areas affected by stroke or multiple sclerosis (Borovikova et al. 2000) by a mechanism sensitive to α -bungarotoxin (Pavlov et al. 2003).

Despite this extensive background, there have been very few molecular imaging studies of nAChRs in relevant neuroinflammatory models. We have undertaken PET

studies to assess $\alpha 7$ nAChR alterations in the sheep stroke model (Boltze et al. 2008). Recently, we measured [^{18}F]NS10743 binding at 6 months after permanent medial cerebral artery occlusion (pMCAO) by dynamic PET imaging using a clinical tomograph (unpublished data). We found reduced tracer uptake in cortex ipsilateral to the lesion, but increased uptake in the brainstem. The declining $\alpha 7$ nAChR availability doubtless indicates degeneration of neurons in the infarct area, but the distal increases are of uncertain significance. Ongoing studies aim to establish better the time course and histological correlates of the $\alpha 7$ nAChR changes in our stroke model.

17.6 Imaging of Traumatic Brain Injury

Traumatic brain injury is a permanent or temporary impairment of brain functions with an associated diminished or altered state of consciousness caused by external mechanical force. In the western world, it is the most important cause of death in young adults (Olesen and Leonardi 2003). In a human post-mortem study, performed after traumatic brain injury, reduced choline acetyl transferase activity and synaptophysin immunoreactivity in cerebral cortex were found, indicating damage of the cholinergic innervation, but nAChR binding determined by either [^3H]nicotine or α -[^{125}I]bungarotoxin was unchanged (Murdoch et al. 1998), suggesting mainly presynaptic mechanisms.

Among various animal models which have been developed to experimentally investigate traumatic brain injury, the fluid-percussion (FPI), weight drop and controlled cortical impact (CCI) models are the most common. The FPI model, which entails transduction of mechanical force to the brain via a fluidic wave (Thompson et al. 2005), causes injuries resembling those observed in the clinic. The CCI model, which was first developed in small animals (Lighthall 1988) and later used in pigs (Duhaime et al. 2000; Alessandri et al. 2003; Manley et al. 2006), entails a piston strike, which results in more focal brain injury than is afforded by the FPI model.

Early evidence of the involvement of the cholinergic system in traumatic brain injury was obtained in dogs and cats, in which increased acetylcholine concentration was noted in cerebrospinal fluid up to 48 h post-injury (Bornstein 1946). In a more recent autoradiographic study of rats with traumatic brain injury, there were widespread and substantial bilateral reductions in cortical and hippocampal $\alpha 7$ nAChRs labelled with α -[^{125}I]bungarotoxin, in contrast to lesser, more focal and ipsilateral effects on heteromeric nAChRs labelled with [^3H]epibatidine (Verbois et al. 2000); we have seen a similar decline in $\alpha 7$ binding in the brain of rats and neonate piglets following FP injuries (Donat et al. 2008, 2010a, b; Hoffmeister et al. 2011). In a saturation binding study, the reductions were linked to declines in B_{max} , rather than affinity changes (Verbois et al. 2002), an issue that must always be considered in autoradiographic or PET studies performed with a single ligand concentration. Peak effects occurred at 2 days post-injury, but persisted for as long as 2 weeks.

Cognitive impairment was demonstrated in the rat FP model (Scheff et al. 1997), suggesting that the $\alpha 7$ nAChR reductions may contribute to these cognitive deficits caused by brain trauma. Also in the FP paradigm, prolonged treatment with nicotine

partially attenuated the cognitive deficits seen in the Morris Water Maze performance and reduced the magnitude and spatial extent of the $\alpha 7$ changes (Verbois et al. 2003a, b). Indeed, nicotine has been effective in a number of other brain lesion models (Visanji et al. 2006; Huang et al. 2009; Zafonte et al. 2009; Quik et al. 2010). However, investigations in $\alpha 7$ knockout mice failed to show much effect of $\alpha 7$ receptor expression on lesion volume or microglia activation (Kelso et al. 2006). Nonetheless, dietary choline supplements partially rescued the spatial memory deficits and $\alpha 7$ receptor deficits after CCI (Guseva et al. 2008).

17.7 Imaging of Addiction and Psychiatric Disorders

17.7.1 Physiological Effects of Nicotine in the Context of Addiction

Whereas acetylcholine is rapidly inactivated by AChE, nicotine exerts prolonged agonism due to its metabolic stability. This property accounts for the well-known phenomenon of desensitisation of nicotinic receptors by nicotine (Govind et al. 2012), in which inactivated receptors concentrate in the plasma membrane due first to agonist-evoked conformational changes, which is followed by decreased degradation of subunits (Govind et al. 2012). In the case of $\alpha 4\beta 2$ nAChRs, upregulation is mediated by activation of protein kinase C, which results in phosphorylation of the $\alpha 4$ subunit (Wecker et al. 2010). This mechanism is supported by studies in rats and 3xT_d-AD mice showing upregulation of $\alpha 4\beta 2$ nAChR after chronic nicotine administration (Flores et al. 1992; Oddo et al. 2005). Chronic nicotine treatment persistently increased the binding of the $\alpha 4\beta 2$ ligand 5-[¹²³I]iodo-A-85380 by approximately 50 % in the brain of baboons (Kassiou et al. 2001). Similarly, a 2-[¹⁸F]fluoro-A-85380 PET study in chronic smokers abstinent for at least 24 h revealed upregulation of $\alpha 4\beta 2$ nAChR throughout the brain (Mukhin et al. 2008); these findings stress the requirement for strict control of exposure to nicotine in the design of clinical and preclinical imaging studies of nAChRs. Thus, exposure of rats to tobacco smoke not only induced nicotine dependence but also increased the $\alpha 7$ nAChR density in the CA2/3 area (+25 %) and the stratum oriens (+18 %) of the hippocampus (Small et al. 2010).

Since the nAChRs are ligand-gated cation channels, their activation facilitates depolarisation and enhances the release of dopamine and other neurotransmitters. Consistent with the increased energy demands associated with depolarisation, acute challenge with nicotine increases the cerebral metabolic rate for glucose (CMR_{glc}) as measured by [¹⁴C]-deoxyglucose autoradiography; these effects are most notable in the thalamus and other rat brain regions in which nicotinic receptors are most abundant (London et al. 1988; Marengo et al. 2000). Despite the phenomenon of upregulation/desensitisation of nAChRs, stimulation of CMR_{glc} in rat brain was still evident after reinstatement of nicotine following a period of withdrawal (Schröck and Kuschinsky 1991). Effects of nicotine on CMR_{glc} are poorly documented in human brain, but one PET study showed that nicotine-evoked stimulation

of [^{18}F]fluorodeoxyglucose uptake in non-smokers was dependent on the hostility trait, as was also seen in smoking subjects treated with a higher dose of nicotine (Fallon et al. 2004). The latter finding seems consistent with desensitisation of the cerebrometabolic response to nicotine challenge in the smoking group.

Baseline levels of 2- ^{18}F fluoro-A-85380 binding in the brainstem of healthy squirrel monkeys predicted their motivation to subsequently self-administer nicotine, as indicated by the number of bar presses (Le Foll et al. 2009), suggesting that nAChRs mediate a trait vulnerability specifically for nicotine abuse. It is unclear whether this association with nicotine addiction generalises to other addictive drugs. However, activation of nAChRs on dopamine neurons and terminals is central to the reinforcing and addictive properties of nicotine. Stimulation of striatal dopamine release by nicotine has recently been linked to $\alpha 6\beta 2\beta 3$ and $\alpha 6\alpha 4\beta 2\beta 3$ nAChRs, which predominate in the basal ganglia (Quik et al. 2011). Activation of these receptors increases the firing rate and augments phasic bursting of midbrain dopamine neurons (De Biasi and Dani 2011). It has been suggested that $\alpha 7$ nAChRs in the ventral tegmental area mediate nicotine's stimulatory effect on mesolimbocortical dopaminergic function and consequently its reinforcing and dependence-producing properties (Nomikos et al. 2000).

Altered dopamine release can be detected in PET studies with [^{11}C]raclopride and other benzamide antagonists of $D_{2/3}$ receptors, wherein ligand binding is reduced by competition from endogenous dopamine (Laruelle 2000; Cumming et al. 2003). Whereas powerful psychostimulants such as amphetamine can evoke 30 % decreases in striatal [^{11}C]raclopride binding, challenge with nicotine reduced this binding by only 5–10 % in striatum of anaesthetised pigs, most notably in the ventral striatum (Cumming et al. 2003); effects of similar magnitude are noted in the brain of non-human primates (Marengo et al. 2004), although others were unable to see this effect in PET scans of awake monkeys (Tsukada et al. 2002), suggesting a confounding pharmacological effect of general anaesthesia. Similarly, intranasal administration of nicotine was without robust effect on [^{11}C]raclopride binding in healthy habitual smokers, although baseline binding correlated with scores of nicotine dependence, and there was a positive relationship between binding changes and individual reports of pleasant subjective experience (Montgomery et al. 2007), as likewise seen in an independent [^{11}C]raclopride PET study of smokers (Barrett et al. 2004). In general, motivational aspects of nicotine may be imperfectly emulated in preclinical studies with noncontingent pharmacological challenge.

Dopamine synthesis capacity in living striatum can be measured by PET studies with DOPA decarboxylase substrates such as [^{11}C]DOPA or [^{18}F]fluoro-DOPA (FDOPA). Whereas acute nicotine treatment had no effect on [^{11}C]DOPA utilisation in striatum of awake monkeys, this utilisation was reduced by one third after overnight abstinence in monkey habituated to nicotine and normalised rapidly following reinstatement of nicotine treatment (Domino et al. 2009). On the other hand, in an isolated clinical PET finding, FDOPA utilisation was 20–30 % increased in striatum of human smokers (Salokangas et al. 2000); this difference might reflect the chronic nature of smoking in humans or alternately the complex psychopharmacology of tobacco smoke as compared to nicotine injections, as in the monkey study.

17.7.2 Schizophrenia and Depression

Nicotine addiction is notoriously prevalent among patients with schizophrenia (Lohr and Flynn 1992), a chronic psychiatric disease characterised by behavioural changes, which are difficult to model in experimental animals. The DSM-IV criteria for schizophrenia consist of a complex of positive symptoms (such as agitation, paranoia and hallucinations), negative symptoms (including emotional blunting, avolition and social withdrawal) and specific cognitive and psychomotor deficits (Goldman-Rakic and Selemon 1997). A greater appreciation in recent years of the importance of cognitive changes has led to search for interventions ameliorating cognitive deficits such as processing speed, attention/vigilance and working memory (Nuechterlein et al. 2004; Heinrichs 2005), in the context of a hypothesis implicating gene-mediated dysfunction of $\alpha 7$ nAChRs (Freedman et al. 1997; Stephens et al. 2009; Dome et al. 2010) in the underlying impairments seen in schizophrenia (Nomikos et al. 2000). Indeed, in one post-mortem study, the hippocampal α -[125 I]bungarotoxin binding was decreased in a schizophrenic patient population containing a single non-smoker (Freedman et al. 1995). Furthermore significant differences in $\alpha 7$ neuronal nicotinic receptor gene (*CHRNA7*) expression at both mRNA and protein level between schizophrenic smokers and schizophrenic non-smokers were found (Mexal et al. 2010).

Nicotinic receptors and treatments have been investigated in a number of murine models emulating aspects of schizophrenia. An auditory gating defect in dilute brown non-agouti (DBA/2) mice is rectified by treatment with an $\alpha 4\beta 2$ agonist (Wildeboer and Stevens 2008), but other nAChR subtypes such as $\alpha 7$ may also mediate sensory gating in these mice (Radek et al. 2006). Mice lacking the dopamine transporter show hyperactivity and cognitive deficits and are hypersensitive to the locomotor stimulant effect of nicotine, which is taken to model schizophrenia. Treatment of these mice with nicotine improved their performance in tasks of spatial and cued learning (Weiss et al. 2007a), whereas autoradiographic studies showed a small decline in the $\beta 2$ subunit, a large decrease in $\beta 6$ and a substantial increase in $\alpha 7$ receptors in these mice (Weiss et al. 2007b). Deficiency of the microtubule-stabilising protein STOP results in impaired hippocampal plasticity and behavioural hypersensitivity to psychostimulants, likewise associated with a decrease in $\beta 6$, and a substantial increase in $\alpha 7$ receptors (Bouvrais-Veret et al. 2007), suggesting a common nicotinic pathway in these two models of schizophrenia.

Availability of $\alpha 4\beta 2$ nAChR binding sites was globally reduced in a 5-[123 I]iodo-A-85380 SPECT study of patients with major depression (Saricicek et al. 2012). Changes in behaviour and in endocrine, immune and neurotransmitter systems modelling symptoms of patients with major depression have been described in rats following bilateral olfactory bulbectomy (Song and Leonard 2005). Such rats present characteristic alterations in cholinergic function (Hozumi et al. 2003). Although degeneration of cholinergic neurons has suggested to be the cause of the observed impairment of learning and memory-related behaviour in the olfactory bulbectomy rats, densities of nAChRs have not yet been investigated in this model.

17.8 Potential Role of Nicotinic Receptor Studies for Measurement of Endogenous Acetylcholine

The competition model for measuring dopamine release by molecular imaging has enabled substantial insights into the role of dopamine in the pathophysiology of schizophrenia and nicotine addiction. However, attempts to generalise the dopamine competition model to other neurotransmitter systems have met with mixed success (Paterson et al. 2010). A molecular imaging assay for fluctuations in extracellular acetylcholine would be a useful tool for evaluating new pharmacological treatments for Alzheimer's disease and other diseases. Besides approaches to measure those changes in the level of endogenous acetylcholine by radioligands, targeting muscarinic acetylcholine receptors (Dewey et al. 1993; Suhara et al. 1994; Ma et al. 2004; Eckelman 2006) for sensitivity to endogenous acetylcholine is an important validation for any new nAChR ligands.

In analogy to the case for dopamine receptors (Cumming 2011), the occurrence of multiple affinity states of nAChRs differentially sensitive to agonist and antagonist ligands is a factor in the competition model. Exposure to acetylcholine and other agonists can alter the affinity states of the nAChR receptor and influence receptor translocation (Darsow et al. 2005; Kumari et al. 2008; Govind et al. 2009; Lester et al. 2009). In consideration of these issues, all of the nAChR ligands tested so far in a competition paradigm have been agonists. Treatment with AChE inhibitors, an important class of compounds used for alleviation of Alzheimer's disease symptoms, affords a convenient way of enhancing acetylcholine levels in living brain in tests of the competition model.

In the first such study, the uptake of 2-[¹⁸F]fluoro-A-85380 in rat thalamus measured *ex vivo* was 45 % reduced by pretreatment with the AChE inhibitor physostigmine (Dollé et al. 1999); decreases of similar magnitude were seen in animals treated with typical $\alpha 4\beta 2$ ligands (fluoro-A-85380, nicotine, epibatidine and cytisine) but not by $\alpha 7$ - or 5-HT₃-specific antagonists. Previous microdialysis studies had confirmed that the same dose of physostigmine (300 $\mu\text{g}/\text{kg}$) caused large increases in interstitial acetylcholine (Cuadra et al. 1994), thus substantiating the competition model.

In a PET study, Ding et al. investigated whether modulation of acetylcholine levels could modulate [¹⁸F]NFEP binding in the baboon (Ding et al. 2000b). As predicted, a reduction in binding was observed following physostigmine administration. Relative to baseline, the treatment reduced the [¹⁸F]NFEP distribution volume by 25 % in thalamus and striatum, the regions in which the effect was greatest. Furthermore the dopamine D_{2/3} antagonist raclopride reduced the striatal binding of [¹⁸F]NFEP by 22 %, whereas the agonist quinpirole increased striatal binding by 26 %. Selective dopamine D₁ drugs had no such effects. These findings were consistent with results of cerebral microdialysis studies showing that dopamine D_{2/3} receptors tonically inhibit acetylcholine release in striatum (Damsma et al. 1991; DeBoer et al. 1996).

In a 5-[¹²³I]iodo-A-85380 SPECT study in baboon, a bolus plus constant infusion paradigm was intended to obtain an equilibrium before bolus injection of

physostigmine (Fujita et al. 2003). Due to unstable plasma levels of 5-[¹²³I] iodo-A-85380 following physostigmine administration, the BP_{ND} was not calculated, but a 14–17 % decrease in thalamic tracer uptake was observed, independent of the physostigmine dose administered, suggesting a ceiling effect in the competition. In a subsequent 2-[¹⁸F]fluoro-A-85380 study, a more prolonged infusion of physostigmine was employed so as to minimise the hemodynamic changes partially confounding the earlier study (Valette et al. 2005). Here, the treatment evoked a 40 % reduction in 2-[¹⁸F]fluoro-A-85380 distribution volume in putamen and more modest reduction in cerebral cortex. The effect was not dose dependent, and infusion of galantamine, a weaker AChE inhibitor, did not alter 2-[¹⁸F]fluoro-A-85380 binding, which again suggests a fairly narrow relationship between interstitial acetylcholine concentration and increased competition.

Competitive acetylcholine binding at nAChRs from rat brain has been tested *in vitro* with [¹⁸F]nifene and [³H]cytosine (Easwaramoorthy et al. 2007). Addition of acetylcholine to the incubation medium displaced both binding ligands when in the additional presence of an AChE inhibitor such as physostigmine or galantamine. These findings highlight the rapid hydrolysis of endogenous acetylcholine in the presence of native AChE and raised the consideration that inactivation/upregulation of nAChRs may arise from “supernormal” activation during AChE inhibition or during exposure to nicotine or other long-lived agonists. Released acetylcholine is normally cleared on a time scale of seconds (Bruno et al. 2006). As such, the PET observations described above cannot unambiguously be ascribed to the competition model; some of the decreases in receptor binding after treatment with AChE inhibitors might be attributable to transition of the receptors to a low affinity state. This is especially a consideration in studies with ligands with slow kinetics, such as in the above reports.

The competition model is scantily documented in human studies. Despite this limitation presented by low specific signal, the group of Nordberg recently published a S-[¹¹C]nicotine study of the effect of the AChE inhibitor rivastigmine on the availability of brain nAChRs in patients with mild Alzheimer’s disease. They reported a general increase in radioligand retention in cerebral cortex, which persisted after long-term rivastigmine treatment and correlated positively with scores in a test of attention (Kadir et al. 2007). It has been suggested that [¹¹C]CHIBA-1001 binding to $\alpha 7$ nAChRs may be sensitive to competition from acetylcholine (Hashimoto et al. 2008), but this was not investigated in detail. As of yet, the fitness of $\alpha 7$ nAChR ligand for detecting changes in acetylcholine release is poorly documented. This merits further investigation, although the low receptor abundance in the brain and the relatively low affinity of acetylcholine for this receptor may predict for low sensitivity.

Conclusion

The development of selective ligands for nAChRs has been challenging due to the diversity of subtypes existing in the brain and due to the unfavourable kinetics and toxicity profiles of some lead compounds. Promising novel tracers targeting $\alpha 4\beta 2$ receptors include [¹⁸F]AZAN and both the (–) and (+) enantiomers of

[¹⁸F]flubatine (previously called NCFHEB). For the $\alpha 7$ receptor, [¹¹C]NS14492, [¹⁸F]NS10743, and [¹⁸F]DBT10 are promising candidates, but it remains to be seen whether these will prove successful for human receptor imaging. Despite the importance of $\alpha 6$ nAChRs in the action of nicotine on dopamine release, selective tracers for this target remain elusive.

References

- Abreo MA, Lin NH, Garvey DS et al (1996) Novel 3-pyridyl ethers with subnanomolar affinity for central neuronal nicotinic acetylcholine receptors. *J Med Chem* 39:817–825
- Alessandri B, Heimann A, Filippi R et al (2003) Moderate controlled cortical contusion in pigs: effects on multi-parametric neuromonitoring and clinical relevance. *J Neurotrauma* 20:1293–1305
- Allen DD, Lockman PR (2003) The blood–brain barrier choline transporter as a brain drug delivery vector. *Life Sci* 73:1609–1615
- Allen DD, Lockman PR, Roder KE et al (2003) Active transport of high-affinity choline and nicotine analogs into the central nervous system by the blood–brain barrier choline transporter. *J Pharmacol Exp Ther* 304:1268–1274
- Apelt J, Kumar A, Schliebs R (2002) Impairment of cholinergic neurotransmission in adult and aged transgenic Tg2576 mouse brain expressing the Swedish mutation of human beta-amyloid precursor protein. *Brain Res* 953:17–30
- Avalos M, Parker MJ, Maddox FN et al (2002) Effects of pyridine ring substitutions on affinity, efficacy, and subtype selectivity of neuronal nicotinic receptor agonist epibatidine. *J Pharmacol Exp Ther* 302:1246–1252
- Barrett SP, Boileau I, Okker J et al (2004) The hedonic response to cigarette smoking is proportional to dopamine release in the human striatum as measured by positron emission tomography and [¹¹C]raclopride. *Synapse* 54:65–71
- Bauer A, Zilles K, Matusch A et al (2005) Regional and subtype selective changes of neurotransmitter receptor density in a rat transgenic for the Huntington's disease mutation. *J Neurochem* 94:639–650
- Belluardo N, Blum M, Mudo G et al (1998) Acute intermittent nicotine treatment produces regional increases of basic fibroblast growth factor messenger RNA and protein in the tel- and diencephalon of the rat. *Neuroscience* 83:723–740
- Bencherif M, Lippello PM (2010) Alpha7 neuronal nicotinic receptors: the missing link to understanding Alzheimer's etiopathology? *Med Hypotheses* 74:281–285
- Bennett MR (2000) The concept of transmitter receptors: 100 years on. *Neuropharmacology* 39:523–546
- Berg DK, Conroy WG (2002) Nicotinic $\alpha 7$ receptors: synaptic options and downstream signaling in neurons. *J Neurobiol* 53:512–523
- Bieszczad KM, Kant R, Constantinescu CC et al (2012) Nicotinic acetylcholine receptors in rat forebrain that bind ¹⁸F-nifene: relating PET imaging, autoradiography, and behavior. *Synapse* 66:418–434
- Bohnen NI, Frey KA (2007) Imaging of cholinergic and monoaminergic neurochemical changes in neurodegenerative disorders. *Mol Imaging Biol* 9:243–257
- Boltze J, Forschler A, Nitzsche B et al (2008) Permanent middle cerebral artery occlusion in sheep: a novel large animal model of focal cerebral ischemia. *J Cereb Blood Flow Metab* 28:1951–1964
- Bordia T, Parameswaran N, Fan H et al (2006) Partial recovery of striatal nicotinic receptors in 1-methyl-4-phenyl-1,2,3,6-tetrahydropyridine (MPTP)-lesioned monkeys with chronic oral nicotine. *J Pharmacol Exp Ther* 319:285–292
- Bordia T, Grady SR, McIntosh JM et al (2007) Nigrostriatal damage preferentially decreases a subpopulation of alpha6beta2* nAChRs in mouse, monkey, and Parkinson's disease striatum. *Mol Pharmacol* 72:52–61

- Borlongan CV, Sumaya IC, Moss DE (2005) Methanesulfonyl fluoride, an acetylcholinesterase inhibitor, attenuates simple learning and memory deficits in ischemic rats. *Brain Res* 1038:50–58
- Bornstein MB (1946) Presence and action of acetylcholine in experimental brain trauma. *J Neurophysiol* 9:349–366
- Borovikova LV, Ivanova S, Zhang M et al (2000) Vagus nerve stimulation attenuates the systemic inflammatory response to endotoxin. *Nature* 405:458–462
- Bourne Y, Talley TT, Hansen SB et al (2005) Crystal structure of a Cbtx-AChBP complex reveals essential interactions between snake α -neurotoxins and nicotinic receptors. *EMBO J* 24:1512–1522
- Bouvrais-Veret C, Weiss S, Andrieux A et al (2007) Sustained increase of $\alpha 7$ nicotinic receptors and choline-induced improvement of learning deficit in STOP knock-out mice. *Neuropharmacology* 52:1691–1700
- Breese CR, Adams C, Logel J et al (1997) Comparison of the regional expression of nicotinic acetylcholine receptor $\alpha 7$ mRNA and [125I]- α -bungarotoxin binding in human postmortem brain. *J Comp Neurol* 387:385–398
- Brejci K, van Dijk WJ, Klaassen RV et al (2001) Crystal structure of an ACh-binding protein reveals the ligand-binding domain of nicotinic receptors. *Nature* 411:269–276
- Brown LL, Kulkarni S, Pavlova OA et al (2002) Synthesis and evaluation of a novel series of 2-chloro-5-((1-methyl-2-(S)-pyrrolidinyl)methoxy)-3-(2-(4-pyridinyl)vinyl) pyridine analogues as potential positron emission tomography imaging agents for nicotinic acetylcholine receptors. *J Med Chem* 45:2841–2849
- Brown L, Chefer S, Pavlova O et al (2004) Evaluation of 5-(2-(4-pyridinyl)vinyl)-6-chloro-3-(1-methyl-2-(S)-pyrrolidinylmethoxy)pyridine and its analogues as PET radioligands for imaging nicotinic acetylcholine receptors. *J Neurochem* 91:600–612
- Bruno JP, Gash C, Martin B et al (2006) Second-by-second measurement of acetylcholine release in prefrontal cortex. *Eur J Neurosci* 24:2749–2757
- Brust P, Deuther-Conrad W (2012) Molecular imaging of $\alpha 7$ nicotinic acetylcholine receptors in vivo: current status and perspectives. In: Bright P (ed) *Neuroimaging – clinical applications*. In Tech, Rijeka
- Brust P, Patt JT, Deuther-Conrad W et al (2008) In vivo measurement of nicotinic acetylcholine receptors with [¹⁸F]norchloro-fluoro-homoepibatidine. *Synapse* 62:205–218
- Brust P, Peters D, Deuther-Conrad W (2012) Development of radioligands for the imaging of $\alpha 7$ nicotinic acetylcholine receptors with positron emission tomography. *Curr Drug Targets* 13:594–601
- Bunnelle WH, Dart MJ, Schrimpf MR (2004) Design of ligands for the nicotinic acetylcholine receptors: the quest for selectivity. *Curr Top Med Chem* 4:299–334
- Changeux JP (2010) Nicotine addiction and nicotinic receptors: lessons from genetically modified mice. *Nat Rev Neurosci* 11:389–401
- Chattopadhyay S, Xue B, Collins D et al (2005) Synthesis and evaluation of nicotine $\alpha 4\beta 2$ receptor radioligand, 5-(3'-¹⁸F-fluoropropyl)-3-(2-(S)-pyrrolidinylmethoxy)pyridine, in rodents and PET in nonhuman primate. *J Nucl Med* 46:130–140
- Chefer SI, Horti AG, Lee KS et al (1998) In vivo imaging of brain nicotinic acetylcholine receptors with 5-[¹²³I]iodo-A-85380 using single photon emission computed tomography. *Life Sci* 63:PL355–PL360
- Chefer SI, Horti AG, Koren AO et al (1999) 2-[¹⁸F]F-A-85380: a PET radioligand for $\alpha 4\beta 2$ nicotinic acetylcholine receptors. *Neuroreport* 10:2715–2721
- Chefer SI, London ED, Koren AO et al (2003) Graphical analysis of 2-[¹⁸F]FA binding to nicotinic acetylcholine receptors in rhesus monkey brain. *Synapse* 48:25–34
- Chefer SI, Pavlova OA, Zhang Y et al (2008) NIDA522131, a new radioligand for imaging extrathalamic nicotinic acetylcholine receptors: in vitro and in vivo evaluation. *J Neurochem* 104:306–315
- Clarke PB, Pert A (1985) Autoradiographic evidence for nicotine receptors on nigrostriatal and mesolimbic dopaminergic neurons. *Brain Res* 348:355–358
- Clarke PB, Pert CB, Pert A (1984) Autoradiographic distribution of nicotine receptors in rat brain. *Brain Res* 323:390–395

- Cuadra G, Summers K, Giacobini E (1994) Cholinesterase inhibitor effects on neurotransmitters in rat cortex in vivo. *J Pharmacol Exp Ther* 270:277–284
- Cumming P (2011) Absolute abundances and affinity states of dopamine receptors in mammalian brain: a review. *Synapse* 65:892–909
- Cumming P, Rosa-Neto P, Watanabe H et al (2003) Effects of acute nicotine on hemodynamics and binding of [¹¹C]raclopride to dopamine D_{2,3} receptors in pig brain. *Neuroimage* 19:1127–1136
- Daly JW (1998) Thirty years of discovering arthropod alkaloids in amphibian skin. *J Nat Prod* 61:162–172
- Damsma G, Robertson GS, Tham CS et al (1991) Dopaminergic regulation of striatal acetylcholine release: importance of D1 and N-methyl-D-aspartate receptors. *J Pharmacol Exp Ther* 259:1064–1072
- Darsow T, Booker TK, Pina-Crespo JC et al (2005) Exocytic trafficking is required for nicotine-induced up-regulation of $\alpha 4\beta 2$ nicotinic acetylcholine receptors. *J Biol Chem* 280:18311–18320
- Davies P, Feisullin S (1981) Postmortem stability of α -bungarotoxin binding sites in mouse and human brain. *Brain Res* 216:449–454
- De Biasi M, Dani JA (2011) Reward, addiction, withdrawal to nicotine. *Annu Rev Neurosci* 34:105–130
- de Fiebre CM, Meyer EM, Henry JC et al (1995) Characterization of a series of anabaseine-derived compounds reveals that the 3-(4)-dimethylaminocinnamylidene derivative is a selective agonist at neuronal nicotinic $\alpha 7/^{125}\text{I}$ - α -bungarotoxin receptor subtypes. *Mol Pharmacol* 47:164–171
- De Simone R, Ajmone-Cat MA, Carnevale D et al (2005) Activation of $\alpha 7$ nicotinic acetylcholine receptor by nicotine selectively up-regulates cyclooxygenase-2 and prostaglandin E2 in rat microglial cultures. *J Neuroinflammation* 2:1–10
- DeBoer P, Heeringa MJ, Abercrombie ED (1996) Spontaneous release of acetylcholine in striatum is preferentially regulated by inhibitory dopamine D2 receptors. *Eur J Pharmacol* 317:257–262
- Decker MW, Sullivan JP, Americ SP et al (2000) Neuronal nicotinic acetylcholine receptors: novel targets for CNS therapeutics. In: Bloom FE, Kupfer DJ (eds) *Psychopharmacology: fourth generation of progress*. Raven Press, New York. <http://www.acnp.org/publications/psychogen4generation.aspx>
- Deuther-Conrad W, Patt JT, Feuerbach D et al (2004) Norchloro-fluoro-homoepibatidine: specificity to neuronal nicotinic acetylcholine receptor subtypes in vitro. *Farmacology* 59:785–792
- Deuther-Conrad W, Wevers A, Becker G et al (2006) Autoradiography of 2-[¹⁸F]F-A-85380 on nicotinic acetylcholine receptors in the porcine brain in vitro. *Synapse* 59:201–210
- Deuther-Conrad W, Patt JT, Lockman PR et al (2008) Norchloro-fluoro-homoepibatidine (NCFHEB) – a promising radioligand for neuroimaging nicotinic acetylcholine receptors with PET. *Eur Neuropsychopharmacol* 18:222–229
- Deuther-Conrad W, Fischer S, Hiller A et al (2009) Molecular imaging of $\alpha 7$ nicotinic acetylcholine receptors: design and evaluation of the potent radioligand [¹⁸F]NS10743. *Eur J Nucl Med Mol Imaging* 36:791–800
- Deuther-Conrad W, Fischer S, Hiller A et al (2011) Assessment of $\alpha 7$ nicotinic acetylcholine receptor availability in porcine brain with [¹⁸F]NS10743. *Eur J Nucl Med Mol Imaging* 38:1541–1549
- Dewey SL, Smith GS, Logan J et al (1993) Modulation of central cholinergic activity by GABA and serotonin: PET studies with 11C-benzotrope in primates. *Neuropsychopharmacology* 8:371–376
- Ding YS, Fowler J (2005) New-generation radiotracers for nAChR and NET. *Nucl Med Biol* 32:707–718
- Ding YS, Gatley SJ, Fowler JS et al (1996) Mapping nicotinic acetylcholine receptors with PET. *Synapse* 24:403–407
- Ding YS, Molina PE, Fowler JS et al (1999) Comparative studies of epibatidine derivatives [¹⁸F]NFEP and [¹⁸F]N-methyl-NFEP: kinetics, nicotine effect, and toxicity. *Nucl Med Biol* 26:139–148

- Ding Y, Liu N, Wang T et al (2000a) Synthesis and evaluation of 6-[¹⁸F]fluoro-3-[2(S)-azetidylmethoxy]pyridine as a PET tracer for nicotinic acetylcholine receptors. *Nucl Med Biol* 27:381–389
- Ding YS, Logan J, Bermel R et al (2000b) Dopamine receptor-mediated regulation of striatal cholinergic activity: positron emission tomography studies with norchloro[¹⁸F]fluoroepibatidine. *J Neurochem* 74:1514–1521
- Ding YS, Fowler JS, Logan J et al (2004) 6-[¹⁸F]Fluoro-A-85380, a new PET tracer for the nicotinic acetylcholine receptor: studies in the human brain and in vivo demonstration of specific binding in white matter. *Synapse* 53:184–189
- Ding YS, Kil KE, Lin KS et al (2006) A novel nicotinic acetylcholine receptor antagonist radioligand for PET studies. *Bioorg Med Chem Lett* 16:1049–1053
- Ding M, Ghanekar S, Elmore CS et al (2012) [³H]Chiba-1001(methyl-SSR180711) has low in vitro binding affinity and poor in vivo selectivity to nicotinic alpha-7 receptor in rodent brain. *Synapse* 66:315–322
- Dobelis P, Hutton S, Lu Y et al (2003) GABAergic systems modulate nicotinic receptor-mediated seizures in mice. *J Pharmacol Exp Ther* 306:1159–1166
- Dolci L, Dolle F, Valette H et al (1999) Synthesis of a fluorine-18 labeled derivative of epibatidine for in vivo nicotinic acetylcholine receptor PET imaging. *Bioorg Med Chem* 7:467–479
- Dollé F, Dolci L, Valette H et al (1999) Synthesis and nicotinic acetylcholine receptor in vivo binding properties of 2-fluoro-3-[2(S)-2-azetidylmethoxy]pyridine: a new positron emission tomography ligand for nicotinic receptors. *J Med Chem* 42:2251–2259
- Dollé F, Valette H, Hinnen F et al (2001) Synthesis and preliminary evaluation of a carbon-11-labelled agonist of the $\alpha 7$ nicotinic acetylcholine receptor. *J Label Compd Radiopharm* 44:785–795
- Dollé F, Langle S, Roger G et al (2008) Synthesis and in-vivo evaluation of [(11C)p-PVP-MEMA as a PET radioligand for imaging nicotinic receptors. *Aust J Chem* 61:438–445
- Dome P, Lazary J, Kalapos MP et al (2010) Smoking, nicotine and neuropsychiatric disorders. *Neurosci Biobehav Rev* 34:295–342
- Domino EF, Tsukada H, Harada N (2009) Positron emission tomographic measure of brain dopamine dependence to nicotine as a model of drugs of abuse. *Psychopharmacology (Berl)* 204:149–153
- Donat CK, Schuhmann MU, Voigt C et al (2008) Time-dependent alterations of cholinergic markers after experimental traumatic brain injury. *Brain Res* 1246:167–177
- Donat CK, Walter B, Deuther-Conrad W et al (2010a) Alterations of cholinergic receptors and the vesicular acetylcholine transporter after lateral fluid percussion injury in newborn piglets. *Neuropathol Appl Neurobiol* 36:225–236
- Donat CK, Walter B, Kayser T et al (2010b) Effects of lateral fluid percussion injury on cholinergic markers in the newborn piglet brain. *Int J Dev Neurosci* 28:31–38
- Donnelly-Roberts DL, Xue IC, Arneric SP et al (1996) In vitro neuroprotective properties of the novel cholinergic channel activator (ChCA), ABT-418. *Brain Res* 719:36–44
- Duhaime AC, Margulies SS, Durham SR et al (2000) Maturation-dependent response of the piglet brain to scaled cortical impact. *J Neurosurg* 93:455–462
- Easwaramoorthy B, Pichika R, Collins D et al (2007) Effect of acetylcholinesterase inhibitors on the binding of nicotinic $\alpha_4\beta_2$ receptor PET radiotracer, ¹⁸F-nifene: a measure of acetylcholine competition. *Synapse* 61:29–36
- Eckelman WC (2006) Imaging of muscarinic receptors in the central nervous system. *Curr Pharm Des* 12:3901–3913
- Ellis JR, Nathan PJ, Villemagne VL et al (2009) Galantamine-induced improvements in cognitive function are not related to alterations in $\alpha 4\beta 2$ nicotinic receptors in early Alzheimer's disease as measured in vivo by 2-[¹⁸F]Fluoro-A-85380 PET. *Psychopharmacology (Berl)* 202:79–91
- Ettrup A, Mikkelsen JD, Lehel S et al (2011) [¹¹C]NS14492 as a novel PET ligand for imaging cerebral $\alpha 7$ nicotinic receptors: in vivo evaluation and drug occupancy measurements. *J Nucl Med* 52:1449–1456

- Fallon JH, Keator DB, Mbogori J et al (2004) Hostility differentiates the brain metabolic effects of nicotine. *Brain Res Cogn Brain Res* 18:142–148
- Fan H, Scheffel UA, Rauseo P et al (2001) [¹²⁵I/²³I] 5-Iodo-3-pyridyl ethers. Syntheses and binding to neuronal nicotinic acetylcholine receptors. *Nucl Med Biol* 28:911–921
- Felix B, Leger ME, Albe-Fessard D et al (1999) Stereotaxic atlas of the pig brain. *Brain Res Bull* 49:1–137
- Ferrari R, Frasoldati A, Leo G et al (1999) Changes in nicotinic acetylcholine receptor subunit mRNAs and nicotinic binding in spontaneously hypertensive stroke prone rats. *Neurosci Lett* 277:169–172
- Flores CM, Rogers SW, Pabreza LA et al (1992) A subtype of nicotinic cholinergic receptor in rat brain is composed of $\alpha 4$ and $\beta 2$ subunits and is up-regulated by chronic nicotine treatment. *Mol Pharmacol* 41:31–37
- Frazier CJ, Rollins YD, Breese CR et al (1998) Acetylcholine activates an α -bungarotoxin-sensitive nicotinic current in rat hippocampal interneurons, but not pyramidal cells. *J Neurosci* 18:1187–1195
- Freedman R, Hall M, Adler LE et al (1995) Evidence in postmortem brain tissue for decreased numbers of hippocampal nicotinic receptors in schizophrenia. *Biol Psychiatry* 38:22–33
- Freedman R, Coon H, Myles-Worsley M et al (1997) Linkage of a neurophysiological deficit in schizophrenia to a chromosome 15 locus. *Proc Natl Acad Sci U S A* 94:587–592
- Freedman R, Olincy A, Buchanan RW et al (2008) Initial phase 2 trial of a nicotinic agonist in schizophrenia. *Am J Psychiatry* 165:1040–1047
- Friedrich A, George RL, Bridges CC et al (2001) Transport of choline and its relationship to the expression of the organic cation transporters in a rat brain microvessel endothelial cell line (RBE4). *Biochim Biophys Acta* 1512:299–307
- Fujita M, Tamagnan G, Zoghbi SS et al (2000) Measurement of $\alpha 4\beta 2$ nicotinic acetylcholine receptors with [¹²³I]5-I-A-85380 SPECT. *J Nucl Med* 41:1552–1560
- Fujita M, Al-Tikriti MS, Tamagnan G et al (2003) Influence of acetylcholine levels on the binding of a SPECT nicotinic acetylcholine receptor ligand [¹²³I]5-I-A-85380. *Synapse* 48:116–122
- Gallezot JD, Bottlaender M, Gregoire MC et al (2005) In vivo imaging of human cerebral nicotinic acetylcholine receptors with 2-[¹⁸F]-fluoro-A-85380 and PET. *J Nucl Med* 46:240–247
- Gao Y, Horti AG, Kuwabara H et al (2007a) Derivatives of (–)-7-methyl-2-(5-(pyridinyl)pyridin-3-yl)-7-azabicyclo[2.2.1]heptane are potential ligands for positron emission tomography imaging of extrathalamic nicotinic acetylcholine receptors. *J Med Chem* 50:3814–3824
- Gao Y, Ravert HT, Holt D et al (2007b) 6-Chloro-3-(((1-[¹¹C]methyl)-2-(S)-pyrrolidinyl)methoxy)-5-(2-fluoropyridin-4-yl)pyridine ([¹¹C]JHU85270), a potent ligand for nicotinic acetylcholine receptor imaging by positron emission tomography. *Appl Radiat Isot* 65:947–951
- Gao Y, Horti AG, Kuwabara H et al (2008a) New synthesis and evaluation of enantiomers of 7-methyl-2-exo-(3'-iodo-5'-pyridinyl)-7-azabicyclo[2.2.1]heptane as stereoselective ligands for PET imaging of nicotinic acetylcholine receptors. *Bioorg Med Chem Lett* 18:6168–6170
- Gao Y, Kuwabara H, Spivak CE et al (2008b) Discovery of (–)-7-methyl-2-exo-[3'-(6-[¹⁸F]fluoropyridin-2-yl)-5'-pyridinyl]-7-azabicyclo[2.2.1]heptane, a radiolabeled antagonist for cerebral nicotinic acetylcholine receptor ($\alpha 4\beta 2$ -nAChR) with optimal positron emission tomography imaging properties. *J Med Chem* 51:4751–4764
- Gao Y, Ravert HT, Kuwabara H et al (2009) Synthesis and biological evaluation of novel carbon-11 labeled pyridyl ethers: candidate ligands for in vivo imaging of $\alpha 4\beta 2$ nicotinic acetylcholine receptors ($\alpha 4\beta 2$ -nAChRs) in the brain with positron emission tomography. *Bioorg Med Chem* 17:4367–4377
- Gao Y, Wang H, Mease RC et al (2010) Improved syntheses of precursors for PET radioligands [¹⁸F]XTRA and [¹⁸F]AZAN. *Tetrahedron Lett* 51:5333–5335
- Gatley SJ, Ding YS, Brady D et al (1998) In vitro and ex vivo autoradiographic studies of nicotinic acetylcholine receptors using ¹⁸F fluoronochloroepibatidine in rodent and human brain. *Nucl Med Biol* 25:449–454
- Goldman-Rakic PS, Selemon LD (1997) Functional and anatomical aspects of prefrontal pathology in schizophrenia. *Schizophr Bull* 23:437–458

- Gotti C, Zoli M, Clementi F (2006) Brain nicotinic acetylcholine receptors: native subtypes and their relevance. *Trends Pharmacol Sci* 27:482–491
- Govind AP, Vezina P, Green WN (2009) Nicotine-induced upregulation of nicotinic receptors: underlying mechanisms and relevance to nicotine addiction. *Biochem Pharmacol* 78:756–765
- Govind AP, Walsh H, Green WN (2012) Nicotine-induced upregulation of native neuronal nicotinic receptors is caused by multiple mechanisms. *J Neurosci* 32:2227–2238
- Graef S, Schönknecht P, Sabri O et al (2011) Cholinergic receptor subtypes and their role in cognition, emotion, and vigilance control: an overview of preclinical and clinical findings. *Psychopharmacology (Berl)* 215:205–229
- Gündisch D (2000) Nicotinic acetylcholine receptors and imaging. *Curr Pharm Des* 6:1143–1157
- Gündisch D, Eibl C (2011) Nicotinic acetylcholine receptor ligands, a patent review (2006–2011). *Expert Opin Ther Pat* 21:1867–1896
- Guseva MV, Hopkins DM, Scheff SW et al (2008) Dietary choline supplementation improves behavioral, histological, and neurochemical outcomes in a rat model of traumatic brain injury. *J Neurotrauma* 25:975–983
- Han ZY, Zoli M, Cardona A et al (2003) Localization of [³H]nicotine, [³H]cytisine, [³H]jepibatidine, and [¹²⁵I]alpha-bungarotoxin binding sites in the brain of *Macaca mulatta*. *J Comp Neurol* 461:49–60
- Hashimoto K, Nishiyama S, Ohba H et al (2008) [¹¹C]CHIBA-1001 as a novel PET ligand for $\alpha 7$ nicotinic receptors in the brain: a PET study in conscious monkeys. *PLoS One* 3:e3231
- Hawkins BT, Brown RC, Davis TP (2002) Smoking and ischemic stroke: a role for nicotine? *Trends Pharmacol Sci* 23:78–82
- Hawkins BT, Egleton RD, Davis TP (2005) Modulation of cerebral microvascular permeability by endothelial nicotinic acetylcholine receptors. *Am J Physiol Heart Circ Physiol* 289:H212–H219
- Hedberg MM, Clos MV, Ratia M et al (2010) Effect of huprine X on β -amyloid, synaptophysin and $\alpha 7$ neuronal nicotinic acetylcholine receptors in the brain of 3xTg-AD and APPsw transgenic mice. *Neurodegener Dis* 7:379–388
- Heinrichs RW (2005) The primacy of cognition in schizophrenia. *Am Psychol* 60:229–242
- Hellström-Lindahl E, Court JA (2000) Nicotinic acetylcholine receptors during prenatal development and brain pathology in human aging. *Behav Brain Res* 113:159–168
- Hellström-Lindahl E, Court J, Keverne J et al (2004) Nicotine reduces A beta in the brain and cerebral vessels of APPsw mice. *Eur J Neurosci* 19:2703–2710
- Henderson DJ, Eberl S, Thomson S et al (2004) 3-Pyridyl ethers as SPECT radioligands for imaging nicotinic acetylcholine receptors. *Appl Radiat Isot* 60:669–676
- Hibbs RE, Sulzenbacher G, Shi J et al (2009) Structural determinants for interaction of partial agonists with acetylcholine binding protein and neuronal $\alpha 7$ nicotinic acetylcholine receptor. *EMBO J* 28:3040–3051
- Higuchi M, Maeda J, Ji B et al (2012) PET applications in animal models of neurodegenerative and neuroinflammatory disorders. *Curr Top Behav Neurosci* 11:45–64
- Hoffmeister PG, Donat CK, Schuhmann MU et al (2011) Traumatic brain injury elicits similar alterations in $\alpha 7$ nicotinic receptor density in two different experimental models. *Neuromolecular Med* 13:44–53
- Hogg RC, Ragenbass M, Bertrand D (2003) Nicotinic acetylcholine receptors: from structure to brain function. *Rev Physiol Biochem Pharmacol* 147:1–46
- Horti AG, Villemagne VL (2006) The quest for Eldorado: development of radioligands for in vivo imaging of nicotinic acetylcholine receptors in human brain. *Curr Pharm Des* 12:3877–3900
- Horti AG, Wong DF (2009) Clinical perspective and recent development of PET radioligands for imaging cerebral nicotinic acetylcholine receptors. *PET Clin*. 4:89–100
- Horti A, Scheffel U, Stathis M et al (1997) Fluorine-18-FPH for PET imaging of nicotinic acetylcholine receptors. *J Nucl Med* 38:1260–1265
- Horti AG, Scheffel U, Kimes AS et al (1998a) Synthesis and evaluation of N-[¹¹C]methylated analogues of epibatidine as tracers for positron emission tomographic studies of nicotinic acetylcholine receptors. *J Med Chem* 41:4199–4206
- Horti AG, Scheffel U, Koren AO et al (1998b) 2-[¹⁸F]Fluoro-A-85380, an in vivo tracer for the nicotinic acetylcholine receptors. *Nucl Med Biol* 25:599–603

- Horti AG, Chefer SI, Mukhin AG et al (2000) 6-[¹⁸F]Fluoro-A-85380, a novel radioligand for in vivo imaging of central nicotinic acetylcholine receptors. *Life Sci* 67:463–469
- Horti AG, Gao Y, Kuwabara H et al (2010) Development of radioligands with optimized imaging properties for quantification of nicotinic acetylcholine receptors by positron emission tomography. *Life Sci* 86:575–584
- Hozumi S, Nakagawasai O, Tan-No K et al (2003) Characteristics of changes in cholinergic function and impairment of learning and memory-related behavior induced by olfactory bulbectomy. *Behav Brain Res* 138:9–15
- Hruska M, Keefe J, Wert D et al (2009) Prostate stem cell antigen is an endogenous lynx1-like prototoxin that antagonizes $\alpha 7$ -containing nicotinic receptors and prevents programmed cell death of parasympathetic neurons. *J Neurosci* 29:14847–14854
- Huang Y, Zhu Z, Narendran R et al (2004) Pharmacological evaluation of [C-11]2-[3-(6-chloro-5-phenyl)pyridinyl]-7-methyl-7-aza-bicyclo[2.2.1]heptane, a new PET radioligand for the nicotinic acetylcholine receptors. *Neuroimage* 22(S2):T113
- Huang LZ, Parameswaran N, Bordia T et al (2009) Nicotin is neuroprotective when administered before but not after nigrostriatal damage in rats and monkeys. *J Neurochem* 109:826–837
- Iida Y, Ogawa M, Ueda M et al (2004) Evaluation of 5-¹¹C-methyl-A-85380 as an imaging agent for PET investigations of brain nicotinic acetylcholine receptors. *J Nucl Med* 45:878–884
- Itier V, Schonbachler R, Tribollet E et al (2004) A-186253, a specific antagonist of the $\alpha 4\beta 2$ nAChRs: its properties and potential to study brain nicotinic acetylcholine receptors. *Neuropharmacology* 47:538–557
- Jensen AA, Frolund B, Liljefors T et al (2005) Neuronal nicotinic acetylcholine receptors: structural revelations, target identifications, and therapeutic inspirations. *J Med Chem* 48:4705–4745
- Jones IW, Barik J, O'Neill MJ et al (2004) Alpha bungarotoxin-1.4 nm gold: a novel conjugate for visualising the precise subcellular distribution of $\alpha 7^*$ nicotinic acetylcholine receptors. *J Neurosci Methods* 134:65–74
- Jones IW, Westmacott A, Chan E et al (2006) $\alpha 7$ nicotinic acetylcholine receptor expression in Alzheimer's disease: receptor densities in brain regions of the APP(SWE) mouse model and in human peripheral blood lymphocytes. *J Mol Neurosci* 30:83–84
- Jupp B, Williams J, Binns D et al (2007) Imaging small animal models of epileptogenesis. *Neurosci Asia* 12(Suppl 1):51–54
- Kadir A, Darreh-Shori T, Almkvist O et al (2007) Changes in brain ¹¹C-nicotinic binding sites in patients with mild Alzheimer's disease following rivastigmine treatment as assessed by PET. *Psychopharmacology (Berl)* 191:1005–1014
- Kalamida D, Poulas K, Avramopoulou V et al (2007) Muscle and neuronal nicotinic acetylcholine receptors. Structure, function and pathogenicity. *FEBS J* 274:3799–3845
- Karlin A (2002) Emerging structure of the nicotinic acetylcholine receptors. *Nat Rev Neurosci* 3:102–114
- Kas A, Bottlaender M, Gallezot JD et al (2009) Decrease of nicotinic receptors in the nigrostriatal system in Parkinson's disease. *J Cereb Blood Flow Metab* 29:1601–1608
- Kassiou M, Scheffel UA, Ravert HT et al (1998) Pharmacological evaluation of [¹¹C]A-84543: an enantioselective ligand for in vivo studies of neuronal nicotinic acetylcholine receptors. *Life Sci* 63:PL13–PL18
- Kassiou M, Eberl S, Meikle SR et al (2001) In vivo imaging of nicotinic receptor upregulation following chronic (–)-nicotine treatment in baboon using SPECT. *Nucl Med Biol* 28:165–175
- Kassiou M, Bottlaender M, Loc'h C et al (2002) Pharmacological evaluation of a Br-76 analog of epibatidine: a potent ligand for studying brain nicotinic acetylcholine receptors. *Synapse* 45:95–104
- Kelso ML, Wehner JM, Collins AC et al (2006) The pathophysiology of traumatic brain injury in $\alpha 7$ nicotinic cholinergic receptor knockout mice. *Brain Res* 1083:204–210
- Kim SW, Ding YS, Alexoff D et al (2007) Synthesis and positron emission tomography studies of C-11-labeled isotopomers and metabolites of GTS-21, a partial $\alpha 7$ nicotinic cholinergic agonist drug. *Nucl Med Biol* 34:541–551

- Kimes AS, Horti AG, London ED et al (2003) 2-[¹⁸F]F-A-85380: PET imaging of brain nicotinic acetylcholine receptors and whole body distribution in humans. *FASEB J* 17:1331–1333
- Kimes AS, Chefer SI, Matochik JA et al (2008) Quantification of nicotinic acetylcholine receptors in the human brain with PET: bolus plus infusion administration of 2-[¹⁸F]F-A85380. *Neuroimage* 39:717–727
- Koeppel RA (2001) A panel discussion on the future of pharmacology and experimental tomography. In: Gjedde A, Hansen SB, Knudsen GM, Paulson OB (eds) *Physiological imaging of the brain with PET*. Academic, New York
- Kozikowski A, Musachio J, Kellar K et al (2005) Inventors; Georgetown University, assignee. Ligands for nicotinic acetylcholine receptors, and methods of making and using them. WO 2005/000806
- Kulak JM, Sum J, Musachio JL et al (2002) 5-Iodo-A-85380 binds to α -conotoxin MII-sensitive nicotinic acetylcholine receptors (nAChRs) as well as $\alpha 4\beta 2$ subtypes. *J Neurochem* 81:403–406
- Kumari S, Borroni V, Chaudhry A et al (2008) Nicotinic acetylcholine receptor is internalized via a Rac-dependent, dynamin-independent endocytic pathway. *J Cell Biol* 181:1179–1193
- Kuwabara H, Wong DF, Gao Y et al (2012) PET Imaging of nicotinic acetylcholine receptors in baboons with 18F-AZAN, a radioligand with improved brain kinetics. *J Nucl Med* 53:121–129
- Lai A, Parameswaran N, Khwaja M et al (2005) Long-term nicotine treatment decreases striatal $\alpha 6^*$ nicotinic acetylcholine receptor sites and function in mice. *Mol Pharmacol* 67:1639–1647
- Langley JN (1901) On the stimulation and paralysis of nerve-cells and of nerve-endings: part I. *J Physiol* 27:224–236
- Langley JN (1905) On the reaction of cells and of nerve-endings to certain poisons, chiefly as regards the reaction of striated muscle to nicotine and to curari. *J Physiol* 33:374–413
- Laruelle M (2000) Imaging synaptic neurotransmission with in vivo binding competition techniques: a critical review. *J Cereb Blood Flow Metab* 20:423–451
- Le Foll B, Chefer SI, Kimes AS et al (2007) Validation of an extracerebral reference region approach for the quantification of brain nicotinic acetylcholine receptors in squirrel monkeys with PET and 2-18F-fluoro-A-85380. *J Nucl Med* 48:1492–1500
- Le Foll B, Chefer SI, Kimes AS et al (2009) Baseline expression of $\alpha 4\beta 2^*$ nicotinic acetylcholine receptors predicts motivation to self-administer nicotine. *Biol Psychiatry* 65:714–716
- Lehel S, Madsen J, Etrup A et al (2009) [¹¹C]NS-12857: a novel PET ligand for $\alpha 7$ -nicotinic receptors. *J Label Compd Radiopharm* 52:S379
- Leonard S (2003) Consequences of low levels of nicotinic acetylcholine receptors in schizophrenia for drug development. *Drug Dev Res* 60:127–136
- Lester HA, Xiao C, Srinivasan R et al (2009) Nicotine is a selective pharmacological chaperone of acetylcholine receptor number and stoichiometry. Implications for drug discovery. *AAPS J* 11:167–177
- Lighthall JW (1988) Controlled cortical impact: a new experimental brain injury model. *J Neurotrauma* 5:1–15
- Lipovsek M, Plazas P, Savino J et al (2008) Properties of mutated murine $\alpha 4\beta 2$ nicotinic receptors linked to partial epilepsy. *Neurosci Lett* 434:165–169
- Lohr JB, Flynn K (1992) Smoking and schizophrenia. *Schizophr Res* 8:93–102
- London ED, Connolly RJ, Szikszay M et al (1988) Effects of nicotine on local cerebral glucose utilization in the rat. *J Neurosci* 8:3920–3928
- London ED, Scheffel U, Kimes AS et al (1995) In vivo labeling of nicotinic acetylcholine receptors in brain with [³H]epibatidine. *Eur J Pharmacol* 278:R1–R2
- Lotfipour S, Mandelkern M, Alvarez-Estrada M et al (2012) A single administration of low-dose varenicline saturates $\alpha 4\beta 2^*$ nicotinic acetylcholine receptors in the human brain. *Neuropsychopharmacology* 37:1738–1748
- Lucas A, Hawkes R, Ansorge R et al (2007) Development of a combined microPET^(R)MR system. Workshop on Medical Instrumentation Signal and Imaging, Aveiro Portugal, 11–12 Apr 2007, p 827

- Ma B, Sherman PS, Moskwa JE et al (2004) Sensitivity of [¹¹C]N-methylpyrrolidinyl benzilate ([¹¹C]NMPYB) to endogenous acetylcholine: PET imaging vs tissue sampling methods. *Nucl Med Biol* 31:393–397
- Maier DL, Hill G, Ding M et al (2011) Pre-clinical validation of a novel alpha-7 nicotinic receptor radiotracer, [³H]AZ11637326: target localization, biodistribution and ligand occupancy in the rat brain. *Neuropharmacology* 61:161–171
- Manley GT, Rosenthal G, Lam M et al (2006) Controlled cortical impact in swine: pathophysiology and biomechanics. *J Neurotrauma* 23:128–139
- Maramraju SH, Smith SD, Junnarkar SS et al (2011) Small animal simultaneous PET/MRI: initial experiences in a 9.4 T microMRI. *Phys Med Biol* 56:2459–2480
- Marengo T, Bernstein S, Cumming P et al (2000) Effects of nicotine and chlorisondamine on cerebral glucose utilization in immobilized and freely-moving rats. *Br J Pharmacol* 129:147–155
- Marengo S, Carson RE, Berman KF et al (2004) Nicotine-induced dopamine release in primates measured with [¹¹C]raclopride PET. *Neuropsychopharmacology* 29:259–268
- Marshall HR, Stodilka RZ, Theberge J et al (2011) A comparison of MR-based attenuation correction in PET versus SPECT. *Phys Med Biol* 56:4613–4629
- Marutle A, Warpman U, Bogdanovic N et al (1998) Regional distribution of subtypes of nicotinic receptors in human brain and effect of aging studied by (+/-) ³H epibatidine. *Brain Res* 801:143–149
- Maziere M, Comar D, Marazano C et al (1976) Nicotine-11C: synthesis and distribution kinetics in animals. *Eur J Nucl Med* 1:255–258
- Meier D, Wagenaar DJ, Chen S et al (2011) A SPECT camera for combined MRI and SPECT for small animals. *Nucl Instrum Methods Phys Res A* 652:731–734
- Mexal S, Berger R, Logel J et al (2010) Differential regulation of α7 nicotinic receptor gene (*CHRNA7*) expression in schizophrenic smokers. *J Mol Neurosci* 40:185–195
- Meyer EM, Kuryatov A, Gerzanich V et al (1998) Analysis of 3-(4-hydroxy, 2-methoxybenzylidene) anabaseine selectivity and activity at human and rat α7 nicotinic receptors. *J Pharmacol Exp Ther* 287:918–925
- Meyer PM, Strecker K, Kendziorra K et al (2009) Reduced α4β2*-nicotinic acetylcholine receptor binding and its relationship to mild cognitive and depressive symptoms in Parkinson disease. *Arch Gen Psychiatry* 66:866–877
- Millar NS, Harkness PC (2008) Assembly and trafficking of nicotinic acetylcholine receptors (review). *Mol Membr Biol* 25:279–292
- Mitkovski S, Villemagne VL, Novakovic KE et al (2005) Simplified quantification of nicotinic receptors with 2[¹⁸F]F-A-85380 PET. *Nucl Med Biol* 32:585–591
- Molina PE, Ding YS, Carroll FI et al (1997) Fluoro-norchloroepibatidine: preclinical assessment of acute toxicity. *Nucl Med Biol* 24:743–747
- Montgomery AJ, Lingford-Hughes AR, Egerton A et al (2007) The effect of nicotine on striatal dopamine release in man: a [¹¹C]raclopride PET study. *Synapse* 61:637–645
- Mu L, Drandarov K, Bisson WH et al (2006) Synthesis and binding studies of epibatidine analogues as ligands for the nicotinic acetylcholine receptors. *Eur J Med Chem* 41:640–650
- Mukherjee J, Pichika R, Leslie FM et al (2004) Design and development of novel new PET imaging agents for α4β2 nicotinic receptors: 18F-nifrolidine and 18F-nifzetidine. *NeuroImage* 22 S2:T124–T125
- Mukhin AG, Kimes AS, Chefer SI et al (2008) Greater nicotinic acetylcholine receptor density in smokers than in nonsmokers: a PET study with 2-18F-FA-85380. *J Nucl Med* 49:1628–1635
- Murdoch I, Perry EK, Court JA et al (1998) Cortical cholinergic dysfunction after human head injury. *J Neurotrauma* 15:295–305
- Nomikos GG, Schilström B, Hildebrand BE et al (2000) Role of α7 nicotinic receptors in nicotine dependence and implications for psychiatric illness. *Behav Brain Res* 113:97–103
- Nordberg A (1993) Clinical studies in Alzheimer patients with positron emission tomography. *Behav Brain Res* 57:215–224
- Nordberg A, Hartvig P, Lilja A et al (1991) Nicotine receptors in the brain of patients with Alzheimer's disease. Studies with ¹¹C-nicotine and positron emission tomography. *Acta Radiol Suppl* 376:165–166

- Nordberg A, Lilja A, Lundqvist H et al (1992) Tacrine restores cholinergic nicotinic receptors and glucose metabolism in Alzheimer patients as visualized by positron emission tomography. *Neurobiol Aging* 13:747–758
- Nuechterlein KH, Barch DM, Gold JM et al (2004) Identification of separable cognitive factors in schizophrenia. *Schizophr Res* 72:29–39
- Nyback H, Halldin C, Ahlin A et al (1994) PET studies of the uptake of (S)- and (R)-[¹¹C]nicotine in the human brain: difficulties in visualizing specific receptor binding in vivo. *Psychopharmacology (Berl)* 115:31–36
- O'Neill MJ, Murray TK, Lakics V et al (2002) The role of neuronal nicotinic acetylcholine receptors in acute and chronic neurodegeneration. *Curr Drug Targets CNS Neurol Disord* 1:399–411
- Oddo S, Caccamo A, Green KN et al (2005) Chronic nicotine administration exacerbates tau pathology in a transgenic model of Alzheimer's disease. *Proc Natl Acad Sci U S A* 102:3046–3051
- Ogawa M, Tatsumi R, Fujio M et al (2006) Synthesis and evaluation of [¹²⁵I]-TSA as a brain nicotinic acetylcholine receptor $\alpha 7$ subtype imaging agent. *Nucl Med Biol* 33:311–316
- Ogawa M, Tsukada H, Hatano K et al (2009) Central in vivo nicotinic acetylcholine receptor imaging agents for positron emission tomography (PET) and single photon emission computed tomography (SPECT). *Biol Pharm Bull* 32:337–340
- Ogawa M, Nishiyama S, Tsukada H et al (2010) Synthesis and evaluation of new imaging agent for central nicotinic acetylcholine receptor $\alpha 7$ subtype. *Nucl Med Biol* 37:347–355
- Oldendorf W, Braun L, Cornford E (1979) pH dependence of blood–brain barrier permeability to lactate and nicotine. *Stroke* 10:577–581
- Olesen J, Leonardi M (2003) The burden of brain diseases in Europe. *Eur J Neurol* 10:471–477
- Paterson D, Nordberg A (2000) Neuronal nicotinic receptors in the human brain. *Prog Neurobiol* 61:75–111
- Paterson LM, Tyacke RJ, Nutt DJ et al (2010) Measuring endogenous 5-HT release by emission tomography: promises and pitfalls. *J Cereb Blood Flow Metab* 30:1682–1706
- Patt JT, Spang JE, Westera G et al (1999) Synthesis and in vivo studies of [¹¹C]-N-methylepipibatidine: comparison of the stereoisomers. *Nucl Med Biol* 26:165–173
- Patt JT, Spang JE, Buck A et al (2001) Synthesis and in vivo studies of the stereoisomers of N-[¹¹C]methyl-homoepibatidine. *Nucl Med Biol* 28:645–655
- Paulson JR, Yang T, Selvaraj PK et al (2010) Nicotine exacerbates brain edema during in vitro and in vivo focal ischemic conditions. *J Pharmacol Exp Ther* 332:371–379
- Pauly JR, Stitzel JA, Marks MJ et al (1989) An autoradiographic analysis of cholinergic receptors in mouse brain. *Brain Res Bull* 22:453–459
- Pavlov VA, Wang H, Czura CJ et al (2003) The cholinergic anti-inflammatory pathway: a missing link in neuroimmunomodulation. *Mol Med* 9:125–134
- Paxinos G, Watson C (1998) The rat brain in stereotaxic coordinates. Academic, New York
- Peng X, Gerzanich V, Anand R et al (1994) Nicotine-induced increase in neuronal nicotinic receptors results from a decrease in the rate of receptor turnover. *Mol Pharmacol* 46:523–530
- Perry EK, Perry RH, Smith CJ et al (1986) Cholinergic receptors in cognitive disorders. *Can J Neurol Sci* 13:521–527
- Perry EK, Perry RH, Smith CJ et al (1987) Nicotinic receptor abnormalities in Alzheimer's and Parkinson's diseases. *J Neurol Neurosurg Psychiatry* 50:806–809
- Peters D, Olsen GM, Nielsen EO et al (2007) Inventors; NeuroSearch A/S, assignee. Novel 1,4-diaza-bicyclo[3.2.2]nonyl oxadiazolyl derivatives and their medical use, WO/2007/138037
- Phillips HA, Favre I, Kirkpatrick M et al (2001) CHRN2 is the second acetylcholine receptor subunit associated with autosomal dominant nocturnal frontal lobe epilepsy. *Am J Hum Genet* 68:225–231
- Picard F, Bruel D, Servent D et al (2006) Alteration of the in vivo nicotinic receptor density in ADNFLE patients: a PET study. *Brain* 129:2047–2060
- Picciotto MR, Zoli M (2002) Nicotinic receptors in aging and dementia. *J Neurobiol* 53:641–655

- Pichika R, Easwaramoorthy B, Collins D et al (2006) Nicotinic $\alpha 4\beta 2$ receptor imaging agents part II. Synthesis and biological evaluation of 2-[^{18}F]fluoro-3-[2-((S)-3-pyrrolinyl)methoxy]pyridine (^{18}F -nifene) in rodents and imaging by PET in nonhuman primate. *Nucl Med Biol* 33:295–304
- Pictet A (1903) Synthese de la nicotine. *Comptes Rendus de l'Academie des Sciences* 137:860–862
- Pinner A (1893) Ueber Nicotin. Die Constitution des Alkaloids. V. Mittheilung. *Berichte der deutschen chemischen Gesellschaft* 26:292–305
- Pinner A, Wolfenstein R (1891) Ueber Nicotin. *Berichte der deutschen chemischen Gesellschaft* 24:61–67
- Pomper MG, Phillips E, Fan H et al (2005) Synthesis and biodistribution of radiolabeled $\alpha 7$ nicotinic acetylcholine receptor ligands. *J Nucl Med* 46:326–334
- Posselt W, Reimann L (1828) Chemische Untersuchungen des Tabaks und Darstellung des eigenthümlichen wirksamen Principis dieser Pflanze. *Geiger's Magazin für Pharmacie und die dahin einschlagenden Wissenschaften* 24:138–161
- Pradhan AA, Cumming P, Clarke PB (2002) [^{125}I]Epibatidine-labelled nicotinic receptors in the extended striatum and cerebral cortex: lack of association with serotonergic afferents. *Brain Res* 954:227–236
- Prakash N, Frostig RD (2005) What has intrinsic signal optical imaging taught us about NGF-induced rapid plasticity in adult cortex and its relationship to the cholinergic system? *Mol Imaging Biol* 7:14–21
- Quik M (2004) Smoking, nicotine and Parkinson's disease. *Trends Neurosci* 27:561–568
- Quik M, Polonskaya Y, Gillespie A et al (2000) Localization of nicotinic receptor subunit mRNAs in monkey brain by in situ hybridization. *J Comp Neurol* 425:58–69
- Quik M, Sum JD, Whiteaker P et al (2003) Differential declines in striatal nicotinic receptor subtype function after nigrostriatal damage in mice. *Mol Pharmacol* 63:1169–1179
- Quik M, Parameswaran N, McCallum SE et al (2006) Chronic oral nicotine treatment protects against striatal degeneration in MPTP-treated primates. *J Neurochem* 98:1866–1875
- Quik M, Campos C, Parameswaran N et al (2010) Chronic nicotine treatment increases nAChRs and microglial expression in monkey substantia nigra after nigrostriatal damage. *J Mol Neurosci* 40:105–113
- Quik M, Perez XA, Grady SR (2011) Role of $\alpha 6$ nicotinic receptors in CNS dopaminergic function: relevance to addiction and neurological disorders. *Biochem Pharmacol* 82:873–882
- Radcliffe KA, Dani JA (1998) Nicotinic stimulation produces multiple forms of increased glutamatergic synaptic transmission. *J Neurosci* 18:7075–7083
- Radek RJ, Miner HM, Bratcher NA et al (2006) $\alpha 4\beta 2$ nicotinic receptor stimulation contributes to the effects of nicotine in the DBA/2 mouse model of sensory gating. *Psychopharmacology (Berl)* 187:47–55
- Raggenbass M, Bertrand D (2002) Nicotinic receptors in circuit excitability and epilepsy. *J Neurobiol* 53:580–589
- Reader AJ (2008) The promise of new PET image reconstruction. *Phys Med* 24:49–56
- Roger G, Lagnel B, Rouden J et al (2003) Synthesis of a [2-pyridinyl- ^{18}F]-labelled fluoro derivative of (–)-cytisine as a candidate radioligand for brain nicotinic $\alpha 4\beta 2$ receptor imaging with PET. *Bioorg Med Chem* 11:5333–5343
- Roger G, Saba W, Valette H et al (2006) Synthesis and radiosynthesis of [^{18}F]FPhEP, a novel $\alpha 4\beta 2$ -selective, epibatidine-based antagonist for PET imaging of nicotinic acetylcholine receptors. *Bioorg Med Chem* 14:3848–3858
- Rominger A, Mille E, Zhang S et al (2010a) Validation of the octamouse for simultaneous ^{18}F -fallypride small-animal PET recordings from 8 mice. *J Nucl Med* 51:1576–1583
- Rominger A, Wagner E, Mille E et al (2010b) Endogenous competition against binding of [^{18}F]DMFP and [^{18}F]fallypride to dopamine $D_{2/3}$ receptors in brain of living mouse. *Synapse* 64:313–322
- Roos RA (2010) Huntington's disease: a clinical review. *Orphanet J Rare Dis* 5:40

- Rose JE, Mukhin AG, Lokitz SJ et al (2010) Kinetics of brain nicotine accumulation in dependent and nondependent smokers assessed with PET and cigarettes containing ^{11}C -nicotine. *Proc Natl Acad Sci U S A* 107:5190–5195
- Ross RG, Stevens KE, Proctor WR et al (2010) Research review: cholinergic mechanisms, early brain development, and risk for schizophrenia. *J Child Psychol Psychiatry* 51:535–549
- Rubio A, Perez M, Avila J (2006) Acetylcholine receptors and tau phosphorylation. *Curr Mol Med* 6:423–428
- Saba W, Valette H, Granon S et al (2010) [^{18}F]ZW-104, a new radioligand for imaging $\alpha 2$ - $\alpha 3$ - $\alpha 4$ / $\beta 2$ central nicotinic acetylcholine receptors: Evaluation in mutant mice. *Synapse* 64:570–572
- Sabri O, Kendziorra K, Wolf H et al (2008) Acetylcholine receptors in dementia and mild cognitive impairment. *Eur J Nucl Med Mol Imaging* 35(Suppl 1):S30–S45
- Sabri O, Wilke S, Gräf S et al (2011) Cerebral alpha4beta2 nicotinic acetylcholine receptors (nAChRs) in early Alzheimer disease (AD) assessed with the new PET tracer (-)-[^{18}F]-norchlorofluoro-homoepibatidine (NCFHEB). *J Nucl Med* 52(Suppl 1):1267
- Salokangas RK, Vilkmann H, Ilonen T et al (2000) High levels of dopamine activity in the basal ganglia of cigarette smokers. *Am J Psychiatry* 157:632–634
- Saricicek A, Esterlis I, Maloney KH et al (2012) Persistent beta2*-nicotinic acetylcholinergic receptor dysfunction in major depressive disorder. *Am J Psychiatry* 169:851–859
- Scheff SW, Baldwin SA, Brown RW et al (1997) Morris water maze deficits in rats following traumatic brain injury: lateral controlled cortical impact. *J Neurotrauma* 14:615–627
- Scheffel U, Horti AG, Koren AO et al (2000) 6-[^{18}F]Fluoro-A-85380: an in vivo tracer for the nicotinic acetylcholine receptor. *Nucl Med Biol* 27:51–56
- Schep LJ, Slaughter RJ, Beasley DM (2009) Nicotinic plant poisoning. *Clin Toxicol (Philadelphia)* 47:771–781
- Schilström B, Fagerquist MV, Zhang X et al (2000) Putative role of presynaptic $\alpha 7^*$ nicotinic receptors in nicotine stimulated increases of extracellular levels of glutamate and aspartate in the ventral tegmental area. *Synapse* 38:375–383
- Schliebs R (2005) Basal forebrain cholinergic dysfunction in Alzheimer's disease – interrelationship with beta-amyloid, inflammation and neurotrophin signaling. *Neurochem Res* 30:895–908
- Schliebs R, Arendt T (2011) The cholinergic system in aging and neuronal degeneration. *Behav Brain Res* 221:555–563
- Schmaljohann J, Gundisch D, Minnerop M et al (2005) A simple and fast method for the preparation of n.c.a. 2-[^{18}F]F-A85380 for human use. *Appl Radiat Isot* 63:433–435
- Schröck H, Kuschinsky W (1991) Effects of nicotine withdrawal on the local cerebral glucose utilization in conscious rats. *Brain Res* 545:234–238
- Schulz D, Southekal S, Junnarkar SS et al (2011) Simultaneous assessment of rodent behavior and neurochemistry using a miniature positron emission tomograph. *Nat Methods* 8:347–352
- Sharma G, Vijayaraghavan S (2001) Nicotinic cholinergic signaling in hippocampal astrocytes involves calcium-induced calcium release from intracellular stores. *Proc Natl Acad Sci U S A* 98:4148–4153
- Sharma G, Vijayaraghavan S (2002) Nicotinic receptor signaling in nonexcitable cells. *J Neurobiol* 53:524–534
- Sharma G, Vijayaraghavan S (2008) Nicotinic receptors: role in addiction and other disorders of the brain. *Subst Abus* 2008:81
- Shen JX, Yakel JL (2009) Nicotinic acetylcholine receptor-mediated calcium signaling in the nervous system. *Acta Pharmacol Sin* 30:673–680
- Shimohama S, Taniguchi T, Fujiwara M et al (1985) Biochemical characterization of the nicotinic cholinergic receptors in human brain: binding of (-)-[^3H]nicotine. *J Neurochem* 45:604–610
- Shytle RD, Mori T, Townsend K et al (2004) Cholinergic modulation of microglial activation by $\alpha 7$ nicotinic receptors. *J Neurochem* 89:337–343
- Siegmund B, Leitner E, Pfannhauser W (1999) Determination of the nicotine content of various edible nightshades (Solanaceae) and their products and estimation of the associated dietary nicotine intake. *J Agric Food Chem* 47:3113–3120

- Silver W, Fasth KJ, Ögren M et al (1998) In vitro evaluation of ¹¹C-labeled (S)-nicotine, (S)-3-methyl-5-(1-methyl-2-pyrrolidinyl)isoxazole, and (R, S)-1-methyl-2-(3-pyridyl)azetidone as nicotinic receptor ligands for positron emission tomography studies. *J Neurochem* 71:1750–1760
- Silver W, Fasth KJ, Horti AG et al (1999a) Synthesis and characterization of binding of 5-[⁷⁶Br] bromo-3-[[2(S)-azetidynyl]methoxy]pyridine, a novel nicotinic acetylcholine receptor ligand, in rat brain. *J Neurochem* 73:1264–1272
- Silver W, Fasth KJ, Ögren M et al (1999b) In vivo positron emission tomography studies on the novel nicotinic receptor agonist [¹¹C]MPA compared with [¹¹C]ABT-418 and (S)(–) [¹¹C]nicotine in rhesus monkeys. *Nucl Med Biol* 26:633–640
- Silver W, Langström B, Nordberg A (2000a) Ligands for in vivo imaging of nicotinic receptor subtypes in Alzheimer brain. *Acta Neurol Scand Suppl* 176:27–33
- Silver W, Nordberg A, Langström B et al (2000b) Development of ligands for in vivo imaging of cerebral nicotinic receptors. *Behav Brain Res* 113:143–157
- Small E, Shah HP, Davenport JJ et al (2010) Tobacco smoke exposure induces nicotine dependence in rats. *Psychopharmacology (Berl)* 208:143–158
- Smith DF, Jakobsen S (2007) Stereoselective neuroimaging in vivo. *Eur Neuropsychopharmacol* 17:507–522
- Sobrio F, Quentin T, Dhilly M et al (2008) Radiosynthesis and ex vivo evaluation of [¹¹C]-SIB-1553A as a PET radiotracer for $\beta 4$ selective subtype nicotinic acetylcholine receptor. *Nucl Med Biol* 35:377–385
- Soloway SB (1976) Naturally occurring insecticides. *Environ Health Perspect* 14:109–117
- Song C, Leonard BE (2005) The olfactory bulbectomized rat as a model of depression. *Neurosci Biobehav Rev* 29:627–647
- Spang JE, Patt JT, Westera G et al (2000) Comparison of N-[¹¹C]methyl-norchloroepibatidine and N-[¹¹C]methyl-2-(2-pyridyl)-7-azabicyclo[2.2.1]heptane with N-[¹¹C]methyl-epibatidine in small animal PET studies. *Nucl Med Biol* 27:239–247
- Spillantini MG, Schmidt ML, Lee VM et al (1997) α -Synuclein in Lewy bodies. *Nature* 388:839–840
- Spurden DP, Court JA, Lloyd S et al (1997) Nicotinic receptor distribution in the human thalamus: autoradiographical localization of [³H]nicotine and [¹²⁵I] alpha-bungarotoxin binding. *J Chem Neuroanat* 13:105–113
- Steinlein OK, Mulley JC, Propping P et al (1995) A missense mutation in the neuronal nicotinic acetylcholine receptor alpha 4 subunit is associated with autosomal dominant nocturnal frontal lobe epilepsy. *Nat Genet* 11:201–203
- Stephens SH, Logel J, Barton A et al (2009) Association of the 5'-upstream regulatory region of the $\alpha 7$ nicotinic acetylcholine receptor subunit gene (CHRNA7) with schizophrenia. *Schizophr Res* 109:102–112
- Suhara T, Inoue O, Kobayashi K et al (1994) An acute effect of triazolam on muscarinic cholinergic receptor binding in the human brain measured by positron emission tomography. *Psychopharmacology (Berl)* 113:311–317
- Sullivan JP, Donnelly-Roberts D, Briggs CA et al (1996) A-85380 [3-(2(S)-azetidynylmethoxy)pyridine]: in vitro pharmacological properties of a novel, high affinity $\alpha 4\beta 2$ nicotinic acetylcholine receptor ligand. *Neuropharmacology* 35:725–734
- Suzuki T, Hide I, Matsubara A et al (2006) Microglial $\alpha 7$ nicotinic acetylcholine receptors drive a phospholipase C/IP3 pathway and modulate the cell activation toward a neuroprotective role. *J Neurosci Res* 83:1461–1470
- Tai YC, Chatziioannou A, Siegel S et al (2001) Performance evaluation of the microPET P4: a PET system dedicated to animal imaging. *Phys Med Biol* 46:1845–1862
- Taly A, Corringier PJ, Guedin D et al (2009) Nicotinic receptors: allosteric transitions and therapeutic targets in the nervous system. *Nat Rev Drug Discov* 8:733–750
- Tanibuchi Y, Wu J, Toyohara J et al (2010) Characterization of [³H]CHIBA-1001 binding to $\alpha 7$ nicotinic acetylcholine receptors in the brain from rat, monkey, and human. *Brain Res* 1348:200–208

- Taylor P, Radic Z, Kreienkamp HJ et al (1994) Expression and ligand specificity of acetylcholinesterase and the nicotinic receptor: a tale of two cholinergic sites. *Biochem Soc Trans* 22:740–745
- Teaktong T, Graham AJ, Johnson M et al (2004) Selective changes in nicotinic acetylcholine receptor subtypes related to tobacco smoking: an immunohistochemical study. *Neuropathol Appl Neurobiol* 30:243–254
- Thal DR, Braak H (2005) Post-mortem diagnosis of Alzheimer's disease (in German). *Pathologie* 26:201–213
- Thompson HJ, Lifshitz J, Marklund N et al (2005) Lateral fluid percussion brain injury: a 15-year review and evaluation. *J Neurotrauma* 22:42–75
- Tomizawa M, Cowan A, Casida JE (2001) Analgesic and toxic effects of neonicotinoid insecticides in mice. *Toxicol Appl Pharmacol* 177:77–83
- Toyohara J, Sakata M, Wu J et al (2009) Preclinical and the first clinical studies on [¹¹C]CHIBA-1001 for mapping $\alpha 7$ nicotinic receptors by positron emission tomography. *Ann Nucl Med* 23:301–309
- Toyohara J, Ishiwata K, Sakata M et al (2010a) In vivo evaluation of $\alpha 7$ nicotinic acetylcholine receptor agonists [¹¹C]A-582941 and [¹¹C]A-844606 in mice and conscious monkeys. *PLoS One* 5:e8961
- Toyohara J, Wu J, Hashimoto K (2010b) Recent development of radioligands for imaging $\alpha 7$ nicotinic acetylcholine receptors in the brain. *Curr Top Med Chem* 10:1544–1557
- Tregellas JR, Tanabe J, Rojas DC et al (2011) Effects of an alpha 7-nicotinic agonist on default network activity in schizophrenia. *Biol Psychiatry* 69:7–11
- Tsukada H, Miyasato K, Kakiuchi T et al (2002) Comparative effects of methamphetamine and nicotine on the striatal [¹¹C]raclopride binding in unanesthetized monkeys. *Synapse* 45:207–212
- Unwin N (2005) Refined structure of the nicotinic acetylcholine receptor at 4 Å resolution. *J Mol Biol* 346:967–989
- Valette H, Bottlaender M, Dollé F et al (1997) An attempt to visualize baboon brain nicotinic receptors with N-[¹¹C]ABT-418 and N-[¹¹C]methyl-cytisine. *Nucl Med Commun* 18:164–168
- Valette H, Bottlaender M, Dollé F et al (1999) Imaging central nicotinic acetylcholine receptors in baboons with [¹⁸F]fluoro-A-85380. *J Nucl Med* 40:1374–1380
- Valette H, Bottlaender M, Dollé F et al (2005) Acute effects of physostigmine and galantamine on the binding of [¹⁸F]fluoro-A-85380: a PET study in monkeys. *Synapse* 56:217–221
- Valette H, Dollé F, Saba W et al (2007) [¹⁸F]FPhEP and [¹⁸F]F2PhEP, two new epibatidine-based radioligands: evaluation for imaging nicotinic acetylcholine receptors in baboon brain. *Synapse* 61:764–770
- Valette H, Xiao Y, Peyronneau MA et al (2009) 18F-ZW-104: a new radioligand for imaging neuronal nicotinic acetylcholine receptors—in vitro binding properties and PET studies in baboons. *J Nucl Med* 50:1349–1355
- Vaupel DB, Tella SR, Huso DL et al (2005) Pharmacological and toxicological evaluation of 2-fluoro-3-(2(S)-azetidylmethoxy)pyridine (2-F-A-85380), a ligand for imaging cerebral nicotinic acetylcholine receptors with positron emission tomography. *J Pharmacol Exp Ther* 312:355–365
- Vaupel DB, Stein EA, Mukhin AG (2007) Quantification of $\alpha 4\beta 2^*$ nicotinic receptors in the rat brain with microPET(R) and 2-[¹⁸F]F-A-85380. *Neuroimage* 34:1352–1362
- Verbois SL, Sullivan PG, Scheff SW et al (2000) Traumatic brain injury reduces hippocampal alpha7 nicotinic cholinergic receptor binding. *J Neurotrauma* 17:1001–1011
- Verbois SL, Scheff SW, Pauly JR (2002) Time-dependent changes in rat brain cholinergic receptor expression after experimental brain injury. *J Neurotrauma* 19:1569–1585
- Verbois SL, Hopkins DM, Scheff SW et al (2003a) Chronic intermittent nicotine administration attenuates traumatic brain injury-induced cognitive dysfunction. *Neuroscience* 119:1199–1208
- Verbois SL, Scheff SW, Pauly JR (2003b) Chronic nicotine treatment attenuates alpha 7 nicotinic receptor deficits following traumatic brain injury. *Neuropharmacology* 44:224–233

- Villablanca AC (1998) Nicotine stimulates DNA synthesis and proliferation in vascular endothelial cells in vitro. *J Appl Physiol* 84:2089–2098
- Villemagne VL, Horti A, Scheffel U et al (1997) Imaging nicotinic acetylcholine receptors with fluorine-18-FPH, an epibatidine analog. *J Nucl Med* 38:1737–1741
- Visanji NP, O'Neill MJ, Duty S (2006) Nicotine, but neither the alpha4beta2 ligand RJR2403 nor an alpha7 nAChR subtype selective agonist, protects against a partial 6-hydroxydopamine lesion of the rat median forebrain bundle. *Neuropharmacology* 51:506–516
- von Horsten S, Schmitt I, Nguyen HP et al (2003) Transgenic rat model of Huntington's disease. *Hum Mol Genet* 12:617–624
- Wang HY, Lee DH, D'Andrea MR et al (2000) β -Amyloid(1–42) binds to $\alpha 7$ nicotinic acetylcholine receptor with high affinity. Implications for Alzheimer's disease pathology. *J Biol Chem* 275:5626–5632
- Wang MH, Yoshiki H, Anisuzzaman AS et al (2011) Re-evaluation of nicotinic acetylcholine receptors in rat brain by a tissue-segment binding assay. *Front Pharmacol* 2:65
- Waterhouse RN (2003) Determination of lipophilicity and its use as a predictor of blood–brain barrier penetration of molecular imaging agents. *Mol Imaging Biol* 5:376–389
- Wecker L, Pollock VV, Pacheco MA et al (2010) Nicotine-induced up regulation of alpha4beta2 neuronal nicotinic receptors is mediated by the protein kinase C-dependent phosphorylation of alpha4 subunits. *Neuroscience* 171:12–22
- Weiss S, Nosten-Bertrand M, McIntosh JM et al (2007a) Nicotine improves cognitive deficits of dopamine transporter knockout mice without long-term tolerance. *Neuropsychopharmacology* 32:2465–2478
- Weiss S, Tzavara ET, Davis RJ et al (2007b) Functional alterations of nicotinic neurotransmission in dopamine transporter knock-out mice. *Neuropharmacology* 52:1496–1508
- Whiteaker P, Davies AR, Marks MJ et al (1999) An autoradiographic study of the distribution of binding sites for the novel $\alpha 7$ -selective nicotinic radioligand [3 H]-methyllycaconitine in the mouse brain. *Eur J Neurosci* 11:2689–2696
- Whitehouse PJ, Kellar KJ (1987) Nicotinic and muscarinic cholinergic receptors in Alzheimer's disease and related disorders. *J Neural Transm Suppl* 24:175–182
- Wildeboer KM, Stevens KE (2008) Stimulation of the alpha4beta2 nicotinic receptor by 5-I A-85380 improves auditory gating in DBA/2 mice. *Brain Res* 1224:29–36
- Xiao Y, Kellar KJ (2004) The comparative pharmacology and up-regulation of rat neuronal nicotinic receptor subtype binding sites stably expressed in transfected mammalian cells. *J Pharmacol Exp Ther* 310:98–107
- Yong T, Zheng MQ, Linthicum DS (1997) Nicotine induces leukocyte rolling and adhesion in the cerebral microcirculation of the mouse. *J Neuroimmunol* 80:158–164
- Zafonte R, Friedewald WT, Lee SM et al (2009) The citicoline brain injury treatment (COBRIT) trial: design and methods. *J Neurotrauma* 26:2207–2216
- Zanardi A, Leo G, Biagini G et al (2002) Nicotine and neurodegeneration in ageing. *Toxicol Lett* 127:207–215
- Zhang JH, Akula MR, Kabalka GW (2001) 3-((2,4-dimethyl-5-[125 I]iodo)benzylidene)-anabaseine: a potent SPECT agent for imaging lung cancer. *J Label Compd Radiopharm* 44:S359–S361
- Zhang Y, Pavlova OA, Chefer SI et al (2004) 5-substituted derivatives of 6-halogeno-3-((2-(S)-azetidyl)methoxy)pyridine and 6-halogeno-3-((2-(S)-pyrrolidinyl)methoxy)pyridine with low picomolar affinity for $\alpha 4\beta 2$ nicotinic acetylcholine receptor and wide range of lipophilicity: potential probes for imaging with positron emission tomography. *J Med Chem* 47:2453–2465
- Zwart R, Bodkin M, Broad LM et al (2004) Common structural and pharmacological properties of 5-HT₃ receptors and $\alpha 7$ nicotinic acetylcholine receptors. In: Silman I, Soreq H, Anglister L, Michaelson D, Fisher A (eds) *Cholinergic mechanisms: function and dysfunction*. Taylor & Francis, London

Development of Radioligands for In Vivo Imaging of NMDA Receptors

18

Takeshi Fuchigami, Morio Nakayama,
and Yasuhiro Magata

Contents

18.1	Introduction	515
18.2	Radioligands for PCP-Binding Site	518
18.2.1	Dissociative Anesthetic Derivatives	518
18.2.2	Diarylguanidine Derivatives	525
18.2.3	Other Open Channel Blocker Derivatives	529
18.3	Radioligands for Glycine Site	531
18.3.1	Radioligands Based on Cyclic Amino Acids	531
18.3.2	5-Aminomethylquinoxaline-2,3-Dione Derivative	534
18.3.3	4-Hydroxyquinolone Derivatives	534
18.4	Development of Radioligands for Ifenprodil-Binding Site	539
18.4.1	Ifenprodil Derivatives	540
18.4.2	Non-ifenprodil-Related NR2B Antagonist Derivatives	545
18.5	Conclusion and Perspectives	548
	References	551

Abstract

N-methyl-D-aspartate receptors (NMDARs) play an important role in the neuro-transmission of the central nervous system (CNS). On the other hand, aberrant functioning of the NMDARs has been implicated in various CNS disorders. Positron emission tomography (PET) and single photon emission computed tomography (SPECT) imaging of NMDARs may provide novel insights on CNS functions and various CNS disorders that could lead to the discovery of potential drug therapies. Despite numerous efforts to develop a number of radioligands for

T. Fuchigami • M. Nakayama
Pharmaceutical Sciences, Graduate School of Biomedical Sciences,
Nagasaki University, Nagasaki 852-8521, Japan
e-mail: t-fuchi@nagasaki-u.ac.jp; morio@nagasaki-u.ac.jp

Y. Magata (✉)
Medical Photonics Research Center, Hamamatsu University School of Medicine,
Hamamatsu 431-3192, Japan
e-mail: magata@hama-med.ac.jp

NMDARs since the late 1980s, none have been deemed satisfactory as in vivo imaging probes. In this chapter, we summarize the progress in the development of PET and SPECT imaging agents for NMDARs and discuss the prospects in this field.

Abbreviations

% ID/g	Percent injected dose per gram of tissue
% ID/mL	Percent injected dose per milliliter of tissue
3MPICA	3-[2-[(3-methoxyphenylamino)carbonyl]ethenyl]-4,6-dichloroindole-2-carboxylic acid
AD	Alzheimer's disease
BBB	Blood-brain barrier
BP	Binding potential
CBZ	Benzyloxycarbonyl
<i>cis</i> -HPTC	<i>cis</i> -2-hydroxymethyl- <i>r</i> -1-(<i>N</i> -piperidyl)-1-(2-thienyl)cyclohexane
CNS	Central nervous system
CNS 1261	<i>N</i> -(1-naphthyl)- <i>N'</i> -(3-iodophenyl)- <i>N'</i> -methylguanidine
CNS 5161	<i>N</i> -(2-chloro-5-(methylmercapto)phenyl)- <i>N'</i> -methylguanidine monohydrochloride
CP-101,606	(<i>1S,2S</i>)-1-(4-hydroxyphenyl)-2-(4-hydroxy-4-phenylpiperidino)-1-propanol
DAO	D-amino acid oxidase
DCKA	5,7-dichlorokynurenic acid
DTG	1,3-di- <i>o</i> -tolylguanidine
EMD-95885	6-3-4-(4-fluorobenzyl)piperidinopropionyl-3H-benzoxazol-2-one
GMOM	<i>N</i> -(2-chloro-5-thiomethylphenyl)- <i>N'</i> -(3-methoxy-phenyl)- <i>N'</i> -methylguanidine
GV150526A	3-(2-((phenylamino)carbonyl)ethenyl)-4,6-dichloroindol-2-carboxylic acid
HON0001	7-hydroxy-6-methoxy-2-methyl-1-(2-(4-(trifluoromethyl)phenyl)ethyl)-1,2,3,4-tetrahydroisoquinoline hydrochloride
HPLC	High-performance liquid chromatography
Ifenprodil	4-[2-(4-benzylpiperidin-1-yl)-1-hydroxypropyl]phenol
Ketamine	(<i>R,S</i>)-2-(2-chlorophenyl)-2-(methylamino)cyclohexanone
Kryptofix 2.2.2	4,7,13,16,21,24-hexaoxa-1,10-diazabicyclo[8.8.8]-hexacosane
L-689,560	<i>trans</i> -2-carboxy-5,7-dichloro-4-phenylaminocarbonylamino-1,2,3,4-tetrahydroquinoline
L-703,717	3-[3-(4-methoxybenzyl)phenyl]-4-hydroxy-7-chloroquinolin-2(1H)-one
MDL-104,653	3-phenyl-4-hydroxy-7-chloro-quinolin-2(1H)-one
MDL-105519	(<i>Z</i>)-2-carboxy-4,6-dichloroindole-3-(2'-phenyl-2'-carboxy)-ene
MEM	1-amino-3-fluoromethyl-5-methyl-adamantane
Memantine	3,5-dimethyladamantan-1-amine

MK-0657	(3 <i>S</i> ,4 <i>R</i>)-4-methylbenzyl methyl piperidine-1-carboxylate	3-fluoro-4-((pyrimidin-2-ylamino) methyl) piperidine-1-carboxylate
MK-801	dizocilpine maleate	{(+)-10,11-dihydro-5-methyl-5 <i>H</i> -dibenzo[<i>a,d</i>] cyclohepten-5,10-diyl]diammonium maleate}
NCAM	<i>N</i> -[2-(<i>N</i> -(2-mercaptoethyl)) amino ethyl]- <i>N</i> -(2-mercaptoethyl)-3,5-dimethyl acetamide	amantadine
NHAM	1-[<i>N</i> -[<i>N</i> -(2-mercaptoethyl)]- <i>N</i> -[2-(2-mercaptoethyl)amino] amino ethyl] amino-3,5-dimethyladamantane	
NMDAR	<i>N</i> -methyl- <i>D</i> -aspartate receptors	
NPS 1506	[3-fluoro- γ -(3-fluorophenyl)- <i>N</i> -methylbenzenepropamine]	
PAMQX	(<i>D</i>)-7-iodo- <i>N</i> -(1-phosphonoethyl)-5-aminomethylquinoxaline-2,3-dione	
PCP	Phencyclidine {1-(1-phenylcyclohexyl) piperidine}	
PD	Parkinson's disease	
PET	Positron emission tomography	
rCBF	Regional cerebral blood flow	
RGH-896	2-[4-[(4-fluorophenyl)methyl]piperidin-1-yl]-2-oxo- <i>N</i> -(2-oxo- <i>N</i> -3 <i>H</i> -1,3-benzoxazol-6-yl)acetamide	
Ro 25-6981	[(\pm)-(α R, β S)]- α -(4-Hydroxyphenyl)- β -methyl-4-(phenylmethyl)-1-piperidine propanol	
Ro-647312	[2-(3,4-dihydro-1 <i>H</i> -isoquinolin-2-yl)-pyridin-4-yl]-dimethylamine	
SAR	Structure activity relationship	
SPECT	Single photon emission computed tomography	
TCP	<i>N</i> -[1-(2-Thienyl)cyclohexyl]-3,4-piperidine	
TLC	Thin-layer chromatography	
VT	Total volume of distribution	

18.1 Introduction

N-methyl-*D*-aspartate receptors (NMDARs) are glutamate gated ion channels that play a central role in excitatory neurotransmission and are known to be involved in learning, memory, and synaptic plasticity (Riedel et al. 2003; Lau and Zukin 2007; Traynelis et al. 2010). On the other hand, excessive glutamate causes overactivation of NMDARs, which results in an increase of intracellular calcium. Subsequent downstream events, including activation of nitric oxide synthase, calcium-sensitive proteases, and mitochondrial damage, can induce neuronal death. This glutamate excitotoxicity is thought to be implicated in the pathophysiology of various neurological diseases, including epilepsy, ischemia, stroke, and neurodegenerative disorders, such as Parkinson's disease (PD), Alzheimer's disease (AD), and Huntington's disease. Hypofunction of NMDARs has been suggested to be related to the pathology of schizophrenia. Therefore, NMDARs have been considered to be attractive therapeutic targets for these diseases (Kemp and McKernan 2002; Kalia et al. 2008; Lau and Tymianski 2010).

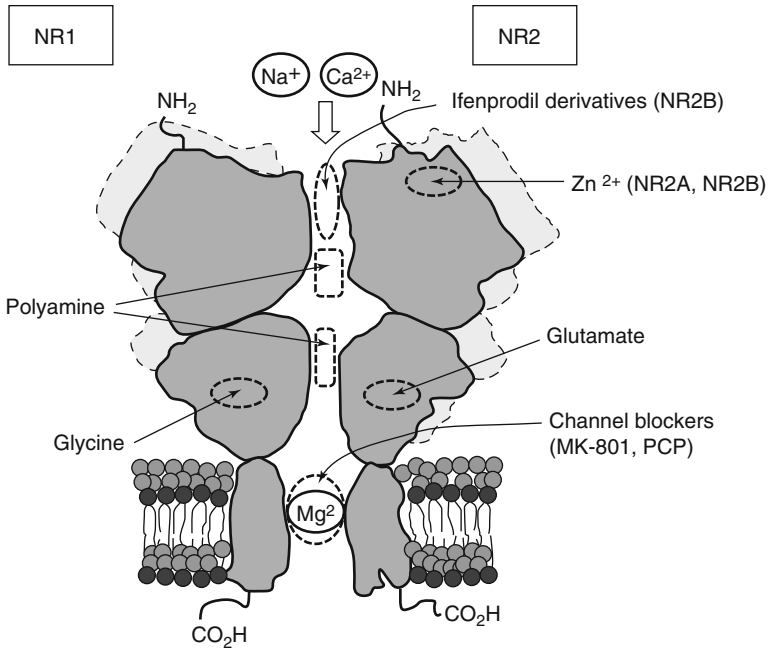


Fig. 18.1 Structure of NMDARs and location of ligand-binding site

NMDARs are unique ligand-gated ion channels. Activation of the receptors not only requires simultaneous binding of two amino acids, glycine and glutamate, but also removal of magnesium (Mg^{2+}) blockade by membrane depolarization. These events lead to the opening of the receptor pore, followed by calcium influx into cells. Consequently, Ca^{2+} -dependent signal transduction cascades trigger the modulation of many aspects of neuronal function (Dingledine et al. 1999, Traynelis et al. 2010). Functional NMDARs require assembly of two NR1 subunits (also named GluN1) together with either two NR2 subunits (GluN2) or a combination of NR2 subunits and NR3 subunits (GluN3) (Laube et al. 1998; Furukawa et al. 2005; Ulbrich and Isacoff 2008). NR1 subunits have only one gene (eight splice variants) with ubiquitous distribution in the brain. NR2 subunits are divided into four types (NR2A, NR2B, NR2C, NR2D). These subunits show distinct anatomical distribution in the brain which determines the biophysical and pharmacological properties of the NMDARs (Köhr 2006; Paoletti and Neyton 2007). NR3 subunits have glycine-binding sites, and glycine alone is sufficient to activate NR1/NR3 receptors. However, the function of NR3-containing NMDARs remains to be fully elucidated (Low and Wee 2010).

The NMDAR's architecture has been reported to be clamshell-like with several binding sites for endogenous and exogenous ligands as shown in Fig. 18.1. While the glutamate-binding site is exhibited on the NR2 subunit, the glycine-binding site is located on the NR1 or NR3 subunit (Furukawa and Gouaux 2003; Furukawa

et al. 2005; Yao et al. 2008). Zinc (Zn^{2+}) has been reported to bind to NR2A or NR2B subunit and inhibits the ion-channel activity in a noncompetitive manner (Rachline et al. 2005; Karakas et al. 2009). Polyamines are allosteric potentiators of NR2B subunit-containing NMDARs, presumably through recognition of the dimer interface of NR1 and NR2B subunits (Mony et al. 2009). A number of exogenous ligands for the several binding sites of NMDARs have been developed as neuroprotective agents. Numerous small compounds have been identified to exhibit binding on the glutamate-binding sites or glycine-binding sites in a competitive manner (Danysz and Parsons 1998; Dingledine et al. 1999). Aliphatic cyclic amines, such as dizocilpine maleate (MK-801) and phencyclidine (PCP), have been reported to inhibit NMDARs strongly in a noncompetitive and voltage-dependent manner (Anis et al. 1983; Foster and Wong 1987). These compounds are called open channel blockers because the blocking effect on NMDARs is caused by binding to the channel pore region near the Mg^{2+} -binding site (Kashiwagi et al. 1997). Recently, ifenprodil and related compounds, which are NR2B selective antagonists, have been identified to bind at the interface between NR1 and NR2B subunits (Karakas et al. 2011).

Positron emission tomography (PET) and single photon emission computed tomography (SPECT) imaging for NMDARs could be powerful tools for obtaining information about the functional mechanism of the NMDA ion channel in the living brain, the pathophysiology of related neurological disorders, and in vivo occupancy of agonists or antagonists of NMDARs. Although a conclusive relationship between NMDAR expression and neurodegenerative disease has yet be elucidated, several reports suggested that NMDAR expression is deregulated in neurological patients. It is reported that mRNA and protein levels of NMDAR NR2A and NR2B subunits were decreased in AD patients (Hynd et al. 2004; Jacob et al. 2007). In addition, [3H]Ro 25-6981 (NR2B selective ligand as described below) binding was increased in the putamen of PD patients experiencing motor complications (Calon et al. 2003), and protein levels of the NR1 subunit were decreased in the postmortem left hippocampus in schizophrenic patients (Vrajová et al. 2010). Therefore, nuclear medicine imaging of NMDARs could lead to characterization of disease progression and early diagnosis of such diseases.

Development of imaging agents for NMDARs has been extensively reviewed previously (Waterhouse 2003a; Sobrio et al. 2010). General strategies for the development of radioligands for NMDARs have been based on the structural modification of NMDAR antagonists for application in PET or SPECT imaging. Thus, the target sites for the radioligands could be divided into three classes as follows: (1) PCP-binding site (channel blocker-binding site), (2) glycine-binding site, and (3) ifenprodil-binding site (NR2B negative modulator binding site). Because most competitive antagonists for the glutamate-binding site have an acid moiety that may cause low brain uptake, no radioligands for this site have been published in the literature. Despite enormous efforts, there are still no satisfactory radioligands for the visualization of NMDARs in the living brain. In this chapter, we summarize the history and present status of radioligands for these three sites.

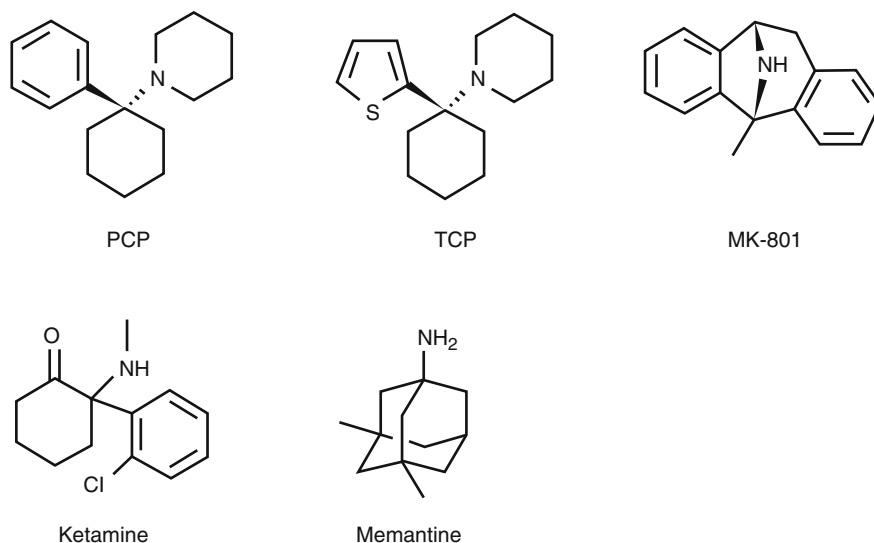


Fig. 18.2 Chemical structure of open channel blockers of NMDARs

18.2 Radioligands for PCP-Binding Site

Open channel blockers of NMDARs, such as MK-801 and PCP derivatives (Fig. 18.2), have been reported to bind to NMDARs in a receptor activation-dependent manner (Loo et al. 1986; Foster and Wong 1987; Wong et al. 1988). Thus, *in vivo* imaging of the PCP-binding site of NMDARs would provide not only quantification of NMDAR density in the living brain but also allow receptor activation under normal and pathophysiological conditions to be monitored. In recent decades, a number of reports have emerged regarding the development of radioligands based on dissociative anesthetics (PCP, MK-801, ketamine, memantine derivatives, diarylguanidines) as shown in Fig. 18.2.

18.2.1 Dissociative Anesthetic Derivatives

18.2.1.1 PCP and TCP Derivatives

PCP, one of the dissociative anesthetics, has been found to inhibit the actions of NMDARs by blocking the ion channel (Anis et al. 1983). On the other hand, TCP ([2-thienyl]-cyclohexyl-PCP), one of the PCP derivatives, has been reported to show severalfold higher affinity than PCP itself toward the PCP-binding site (Vincent et al. 1979; Tsukiyama et al. 1991).

In structure-activity relationship (SAR) studies of PCP derivatives, the binding affinity of the compounds was expressed as $K_{0.5}$, which means the half maximal (50 %) inhibitory concentration of [^3H]PCP binding. Methoxy analogs **1** and **2** (Fig. 18.3) showed a higher binding affinity (**1**; $K_{0.5}$ =90 nM, **2**; $K_{0.5}$ =58 nM) than

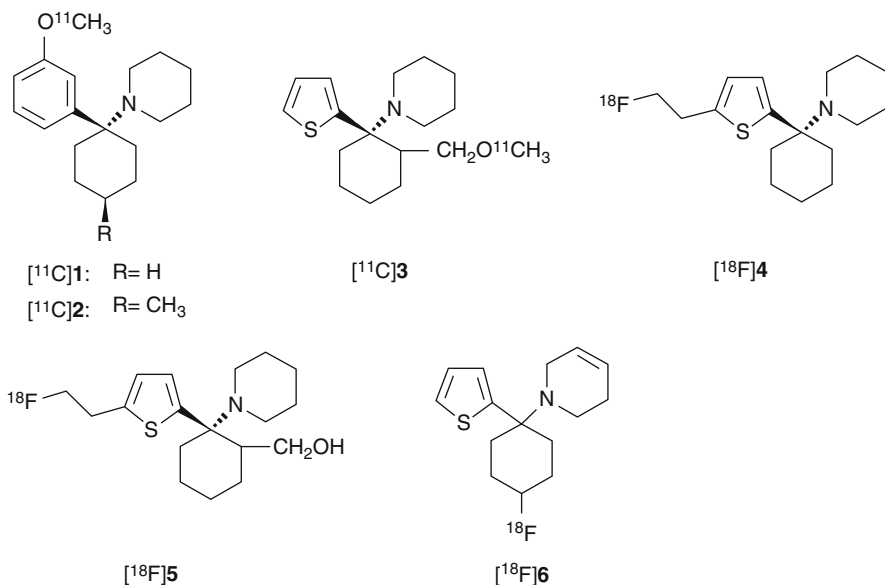


Fig. 18.3 Chemical structure of radiolabeled PCP and TCP derivatives

PCP itself (PCP; $K_{0.5}=250$ nM) (Chaudieu et al. 1989). The IC_{50} value of methoxy-methyl analog of TCP (**3**, Fig. 18.3) for the [³H]TCP-binding site was 16 nM, which was slightly weaker than TCP ($IC_{50}=7.9$ nM) but stronger than PCP ($IC_{50}=52$ nM) (Tsukiyama et al. 1991). These compounds were labeled with C-11 and then evaluated as PET radioligands for the PCP-binding site of NMDARs (Haradahira et al. 1998). The [¹¹C]-radiotracers were prepared from hydroxyl precursors reacting with [¹¹C]CH₃I to reach a specific activity of more than 41 GBq/μmol. In the biodistribution studies in mice, initial uptake of the TCP analog [¹¹C]**3** was twofold higher (2.6–2.9 % ID/g at 1 min) than the PCP analogs [¹¹C]**1** (1.4–1.6 % ID/g at 1 min) and [¹¹C]**2** (1.1–1.5 % ID/g at 1 min). On the other hand, [¹¹C]**3** showed faster clearance in the brain than [¹¹C]**1** and [¹¹C]**2**. However, there was no significant difference in the accumulated radioactivity level between the NMDAR-rich regions and NMDAR-poor regions. These results indicated that the radioligands had no small binding interaction with brain components other than PCP-binding site. Since no blocking studies using the PCP-binding site antagonists were performed, it is unclear whether these radioligands bound specifically in certain brain regions (Haradahira et al. 1998).

Orita et al. developed [¹⁸F]fluoroethyl analog of TCP ([¹⁸F]**4**, Fig. 18.3) with IC_{50} values of 61 nM for the PCP-binding site of NMDARs. The [¹⁸F]**4** showed heterogeneous in vivo distribution that was similar to NMDAR expression. In addition, co-injection of high-affinity ion-channel blocker *cis*-HPTC (1.7 μmol/kg) yielded reduction of regional cerebral distribution of [¹⁸F]**4** (Fig. 18.4). However, this tracer may be an unsuitable PET radioligand for NMDARs because of the high nonspecific binding in brain tissues (Orita et al. 1993).

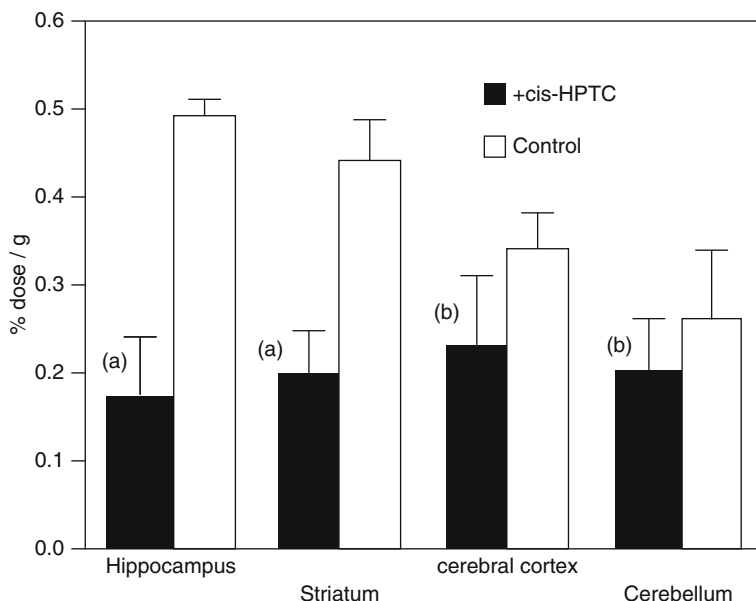


Fig. 18.4 Regional brain distribution of radioactivity in rats at 15 min after injection of [^{18}F]**4**. In the blocking study, *cis*-HPTC (1.7 mmol/kg) was pre-injected 5 min before administration of [^{18}F]**4**. Student's *t*-test with respect to the control, (a) $P < 0.01$, (b) not significant (Orita et al. 1993)

Another [^{18}F]fluoroethyl analog of TCP ([^{18}F]**5**, Fig. 18.3) has been synthesized by nucleophilic substitution of mesylate precursor with $^{18}\text{F}^-$ at a specific activity of >31 GBq/ μmol . Biodistribution analysis in rats revealed that [^{18}F]**5** exhibited peak uptake (0.25 % ID/g) in the brain at 10 min. However, no regional difference was observed in the brain tissues, and the blocking effect of *cis*-HPTC (1.7 $\mu\text{mol}/\text{kg}$) was not observed for all the tissues investigated. Nonspecific brain distribution of [^{18}F]**5** could be attributed to the hydrophobic property and low affinity for NMDARs ($\text{IC}_{50} = 1.5$ μM vs [^3H]TCP) of these ligands (Shibayama et al. 1996).

Ouyang et al. has reported a fluorocyclohexyl analog of TCP ([^{18}F]**6**, Fig. 18.3) with IC_{50} value of 97 nM for the PCP-binding site (vs [^3H]MK-801). The [^{18}F]**6** was prepared by nucleophilic substitution of corresponding tosylate precursor with a specific activity of 19–37 GBq/ μmol . In PET studies in the rhesus monkey, [^{18}F]**6** showed up to 0.08 %ID/mL of brain uptake, but the radioactivity was cleared rapidly from all regions of the brain indicative of little or no retention of the radiotracer in the receptor-rich regions (Fig. 18.5) (Ouyang et al. 1996). Because [^{18}F]**6** has only moderate affinity and the specificity for NMDARs has not been confirmed, new radioligands with significant improvement of binding affinity and target specificity have to be developed.

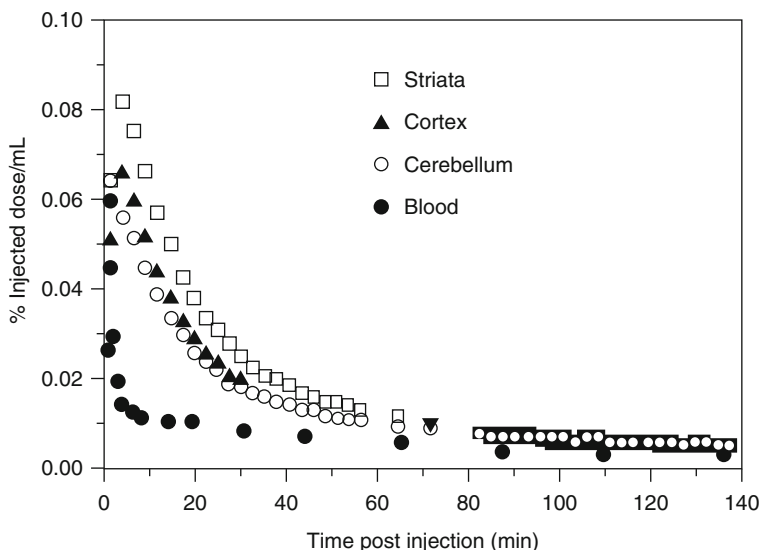


Fig. 18.5 PET data on the binding of [^{18}F]6 in a rhesus monkey brain (Ouyang et al. 1996)

18.2.1.2 MK-801 Derivatives

The anticonvulsant MK-801 (Fig. 18.2) has been identified as a potent and selective noncompetitive NMDAR antagonist (Wong et al. 1986). Because MK-801 has high binding affinity for the PCP-binding site of NMDARs (Wong et al. 1988) and easy penetrability into the brain (Clineschmidt et al. 1982), MK-801 analogs were expected to be suitable as in vivo imaging probes for NMDARs. Several MK-801 derivatives labeled with ^{11}C , ^{18}F , or ^{123}I have been synthesized and evaluated as PET or SPECT radioligands for NMDARs.

Blin et al. reported the preparation of [^{18}F]fluoromethyl analog of MK-801 ([^{18}F]FMM, Fig. 18.6) and PET studies on baboons (Blin et al. 1991). In the baseline PET studies, initial accumulation into the brain of [^{18}F]FMM was marked with peak uptake values as high as 0.03 %ID/mL. However, the ratios of [^{18}F]FMM in the cerebral cortex and striatum (NMDAR-rich regions) to the cerebellum (NMDAR-poor regions) were only minimal (maximal ratios ranging from 1.1 to 1.6 during the first 20–40 min). In addition, there was no clear reduction in the brain uptake and target-to-nontarget ratios by pretreatment of the open channel blockers (PCP or MK-801). Because binding of [^3H]MK-801 to the PCP-binding site has been enhanced severalfold in the presence of high amount of glutamate (Wong et al. 1988), the authors investigated further using PET studies of [^{18}F]FMM on ischemic baboons with excessive glutamate activation. However, the brain kinetics of [^{18}F]FMM was not significantly different between the ischemic and control groups. It can be concluded that [^{18}F]FMM is an unsuitable radioligand for the PCP-binding site of NMDARs (Blin et al. 1991). Ransom et al. developed the 3- ^{123}I iodo analog of MK-801 ([^{123}I]3-iodo-MK-801, Fig. 18.6) as a SPECT imaging agent. Over 95 % of [^{123}I]3-iodo-MK-801 binding was specific in rat brain homogenates. MK-801

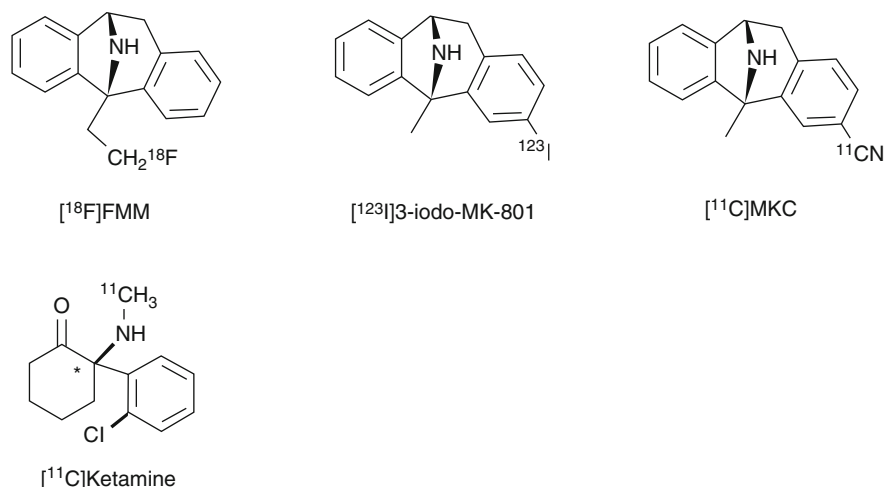


Fig. 18.6 Chemical structure of radiolabeled MK-801 derivatives and $[^{11}\text{C}]\text{ketamine}$

derivatives were shown to bind with high affinity for the $[^{123}\text{I}]\text{3-iodo-MK-801}$ -binding site {3-iodo-MK-801: $\text{IC}_{50} = 3.4 \text{ nM}$, (+)-MK-801: $\text{IC}_{50} = 5.6 \text{ nM}$ } indicating excellent binding affinity of this tracer for the PCP-binding site (Ransom et al. 1990). These positive *in vitro* results prompted further *in vivo* imaging studies. Owens et al. reported the clinical SPECT investigation of $[^{123}\text{I}]\text{3-iodo-MK-801}$. In normal subjects, $[^{123}\text{I}]\text{3-iodo-MK-801}$ showed rapid uptake into the brain, but the tracer has a high nonspecific retention in the brain tissues probably due to its high lipophilicity (Owens et al. 1997). Brown et al. reported the clinical SPECT studies of $[^{123}\text{I}]\text{3-iodo-MK-801}$ in Alzheimer's diseases (AD) and healthy subjects. There were slight difference in the brain uptake/rCBF (regional cerebral blood flow) ratio and wash out of $[^{123}\text{I}]\text{3-iodo-MK-801}$ between the AD patients and control groups, which suggested that the binding of this tracer in the brain was increased in AD patients. However, the authors concluded that $[^{123}\text{I}]\text{3-iodo-MK-801}$ did not provide accurate measurement of NMDARs since the alteration was not significant, and the brain distribution of this tracer was homogenous in both AD and control groups (Brown et al. 1997).

Andersson et al. successfully synthesized 3- $[^{11}\text{C}]\text{cyano}$ analog of MK-801 ($[^{11}\text{C}]\text{MKC}$, Fig. 18.6) with high specific activity (220–600 GBq/ μmol) from 3-iodo precursor using palladium(0)-promoted $[^{11}\text{C}]\text{-cyanation}$ (Andersson et al. 1998). Saturation assay in rat cortical membranes revealed that $[^{11}\text{C}]\text{MKC}$ had a single high-affinity binding site with a K_d of 8.2 nM and a B_{max} of 1.6 pmol/mg protein (Sihver et al. 1998). *In vitro* autoradiography demonstrated that the highest specific binding in rat slices of $[^{11}\text{C}]\text{MKC}$ was observed in the hippocampus and frontal cortex. Moderate binding was found in the caudate putamen and thalamus. Low-density binding sites were observed in the cerebellum, pons, midbrain, and brainstem (Fig. 18.7). This correlated with the distribution of $[^3\text{H}]\text{MK-801}$ (Bowery et al.

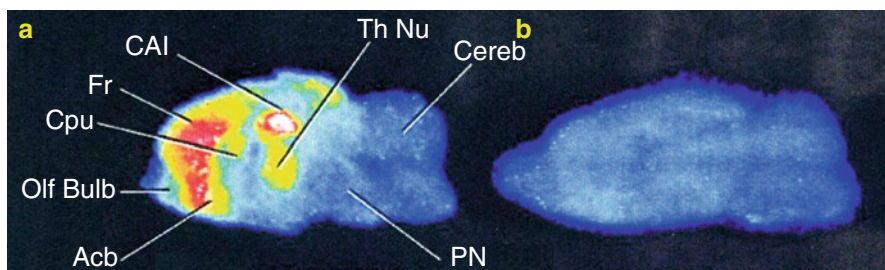


Fig. 18.7 In vitro autoradiography of [^{11}C]MKC in the rat brain slices. Total binding (a) and non-specific binding (b) are shown in sagittal planes. Nonspecific binding was measured in the presence of MK-801 (1 mM). Abbreviations: *Acb* accumbens nucleus, *CAI* CA1 of hippocampus, *Cereb* cerebellum, *Cpu* caudate putamen, *Fr* frontal cortex, *Olf bulb* olfactory bulb, *PN* pontine nuclei, *Th Nu* thalamic nuclei (Sihver et al. 1998)

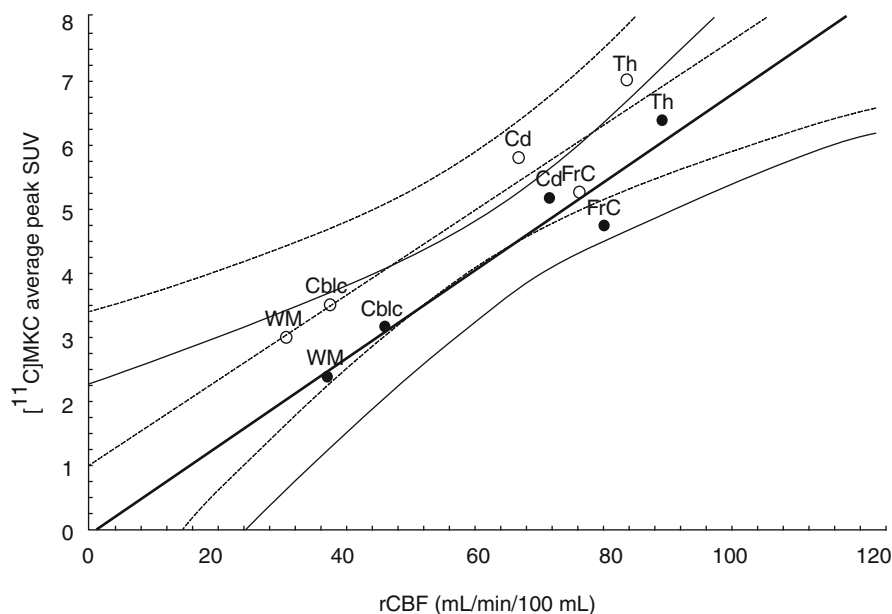


Fig. 18.8 Typical graph presenting the relation between peak [^{11}C]MKC uptake and rCBF in the same regions in the baseline measurement (*open circles and dotted lines*) and ketamine-pretreatment measurement (*closed circles and continuous lines*). Curved lines indicate 95 % confidence. Abbreviations: *FrC* frontal cortex, *Cd* right caudate nucleus, *Th* thalamic nuclei, *Cblc* cerebellar cortex, *WM* white matter (Sihver et al. 1998)

1988). The in vivo PET studies demonstrated that [^{11}C]MKC showed a rapid and high uptake in the brain tissues. In addition, the radioactivity level was higher in the frontal cortex than cerebellar cortex, but the brain distribution pattern was well correlated with the rCBF (Fig. 18.8). Neither MK801 (0.1 mg/kg) nor ketamine (2.5 mg/kg) as pretreatment dose caused a significant change in regional brain

kinetics. These results could be caused by the very low-specific binding fraction of [^{11}C]MKC under in vivo conditions (Sihver et al. 1998). Development of new radioligands with lower lipophilicity and higher NMDAR selectivity should be tried to reduce nonspecific binding.

18.2.1.3 [^{11}C]Ketamine

Ketamine (Fig. 18.2) is known as a PCP-like anesthetic drug which has a weak binding affinity for the PCP-binding site of NMDARs (Lodge and Johnson 1990). In the displacement assay using pig brain homogenates, the K_i values of (*S*)-ketamine and (*R*)-ketamine for [^3H]MK-801-binding site of NMDARs were 1.2 and 5.0 μM , respectively (Oye et al. 1992). [^{11}C]-labeled (*R,S*)-ketamine ([^{11}C]ketamine, Fig. 18.6) and its enantiomers were synthesized, then in vivo evaluation was performed (Hartvig et al. 1994; Shiue et al. 1997). Although [^{11}C]ketamine showed high blood–brain barrier (BBB) permeability (2.80 % ID/g at 5 min after injection) in mice brain, unchanged [^{11}C]ketamine was only 50 % at 5 min. PET studies in a baboon demonstrated that the influx of [^{11}C]ketamine and its enantiomers into the brain was high for the first few minutes, but radioactivity then declined rapidly and a similar uptake in the striatum and cerebellum was observed. In addition, these three tracers were also metabolized rapidly in the baboon plasma. Because [^{11}C]ketamine and its enantiomers were revealed to be metabolically unstable and had inconsistent binding with NMDAR expression, these tracers failed to act as useful radioligands for in vivo imaging of NMDARs (Shiue et al. 1997).

18.2.1.4 Memantine Derivatives

Memantine (Fig. 18.2) is a drug used in the treatment of various neurological and psychiatric disorders, including Parkinson's disease and Alzheimer's disease. Memantine has been identified as a noncompetitive open channel blocker of NMDARs with good BBB permeability (Parsons et al. 1993; Lipton 2004). Therefore, several radiolabeled memantine derivatives have been developed as imaging agents for NMDARs.

Synthesis of 3-[^{18}F]fluoromethyl analog of memantine ([^{18}F]MEM, Fig. 18.9) was achieved from *N*-Boc-protected tosylate precursor by nucleophilic radiofluorination in two steps. The MEM showed a slightly weaker inhibitory activity to the current response to NMDARs ($\text{IC}_{50}=6.0 \mu\text{M}$) than memantine ($\text{IC}_{50}=2.9 \mu\text{M}$) and PCP ($\text{IC}_{50}=1.0 \mu\text{M}$). In the biodistribution studies in mice, [^{18}F]MEM showed an excellent brain uptake (3.6 % ID/g at 60 min) and the accumulation in the frontal cortex and hippocampus was higher than in the cerebellum. In addition, co-injection of MK-801 (0.10 mg/kg) led to 25–36 % reduction of radioactivity in NMDAR-rich regions. PET studies in a rhesus monkey revealed that [^{18}F]MEM displayed high brain uptake and low clearance of the radiotracer from the brain tissues. Pretreatment with memantine (0.50 and 1 mg/kg) yielded a reduction of uptake of up to 32 % from 60 min in the examined brain regions. However, the highest uptake was observed in the cerebellum, which is an NMDAR-poor region. In addition, pretreatment with haloperidol, which is a ligand with high affinity for dopamine D2 and sigma receptors, also caused similar reduction of radioactivity in the brain (Samnick

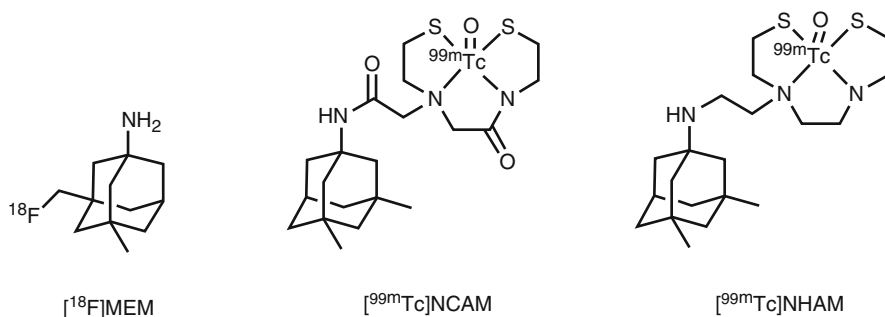


Fig. 18.9 Chemical structure of radiolabeled memantine derivatives

et al. 1998). In clinical PET studies, $[^{18}\text{F}]\text{MEM}$ showed perfusion-dependent uptake in the brain rather than NMDAR expression (Ametamey et al. 2002). Because of inconsistent binding with NMDAR expression and low specificity for NMDARs, it would appear that $[^{18}\text{F}]\text{MEM}$ is an unsuitable radioligand (Samnick et al. 1998; Ametamey et al. 2002). However, the different brain distribution pattern of $[^{18}\text{F}]\text{MEM}$ observed among species was noteworthy. New technetium-labeled memantine derivatives such as $[^{99\text{m}}\text{Tc}]\text{NCAM}$ and $[^{99\text{m}}\text{Tc}]\text{NHAM}$ have recently been reported as novel SPECT imaging probes (Fig. 18.9). The $[^{99\text{m}}\text{Tc}]\text{NCAM}$ had a single binding site with a K_d of 701 nM. Furthermore, the in vitro binding of $[^{99\text{m}}\text{Tc}]\text{NCAM}$ was blocked by ketamine and MK-801 in a competitive manner. In the bio-distribution studies in mice, $[^{99\text{m}}\text{Tc}]\text{NCAM}$ showed 1.2 % ID/g brain uptake at 5 min and the target (frontal cortex, hippocampus) to nontarget (cerebellum) ratio of radioactivity reached 2.5–3.0 at 60 min. The in vivo blocking studies were not so far reported in the literature (Zhou et al. 2012).

18.2.2 Diarylguanidine Derivatives

Initially reported imaging probes, such as PCP and MK-801 analogs, suffered from high nonspecific in vivo accumulation, which was probably due to the high lipophilicity and lack of selectivity for NMDARs. Diarylguanidine derivatives were discovered as NMDAR open channel blockers with high potency and selectivity. These compounds showed therapeutic effect in various brain disease model animals (Reddy et al. 1994; Hu et al. 1997). Because most diarylguanidines are more hydrophilic than PCP and MK-801, several radiolabeled diarylguanidine analogs were developed for PET or SPECT imaging of NMDARs. In the first study, $[^{125}\text{I}]\text{CNS 1261}$ (Fig. 18.10) was developed as a high-affinity imaging agent for NMDARs with a K_i value of 4.2 nM for the $[^3\text{H}]\text{MK-801}$ -binding site with moderate lipophilicity ($\log D=2.19$). Binding assays to other neurotransmitter receptors demonstrated that CNS 1261 had a weaker binding affinity for the other 41 neurotransmitter receptors. Ex vivo autoradiography studies with normal rats showed that the $[^{125}\text{I}]\text{CNS 1261}$ uptake in the hippocampus was 2.4–2.9-fold higher than that in the

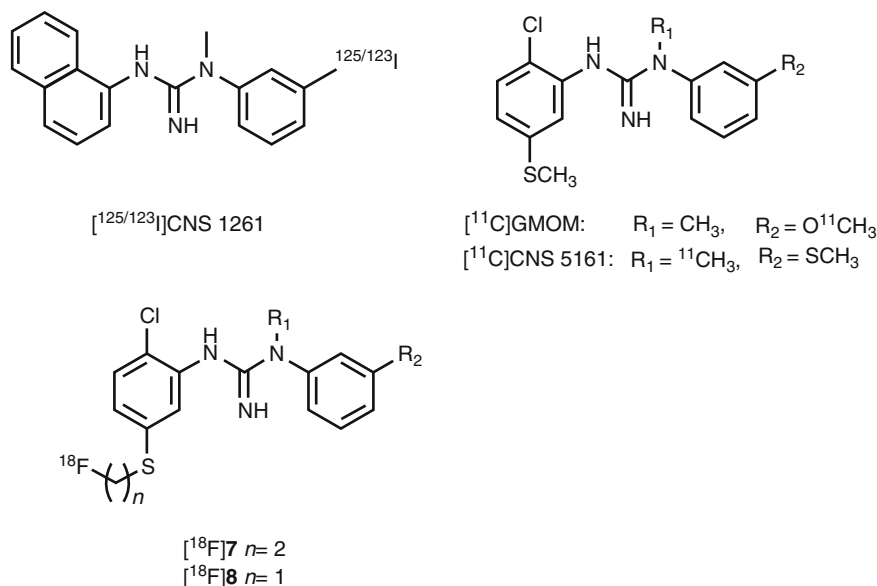


Fig. 18.10 Chemical structure of radiolabeled diarylguanidine derivatives

cerebellum, in which the accumulation matched the distribution of NMDARs. In the ischemic rat brain, $[^{125}\text{I}]\text{CNS } 1261$ uptake was considerably increased in the neocortex and striatum, with a twofold higher uptake in the ischemic hemisphere of the caudate nucleus uptake than the same regions on the contralateral nonischemic hemisphere (Fig. 18.11). This suggested that $[^{125}\text{I}]\text{CNS } 1261$ could recognize the areas of NMDAR activation (Owens et al. 2000). Based on these results, several clinical SPECT studies of $[^{123}\text{I}]\text{CNS } 1261$ were conducted. SPECT imaging of $[^{123}\text{I}]\text{CNS } 1261$ in healthy volunteers were conducted by using both bolus and bolus plus constant infusion paradigms. Total volume of distribution (V_T) values was approximately the same in the NMDAR-rich regions (striatum, hippocampus, frontal cortex) and NMDAR-poor region (cerebellum). The V_T value in the thalamus, which is a region with considerably high expression of NMDARs, was slightly higher than in other regions (Fig. 18.12) (Erlandsson et al. 2003; Bressan et al. 2004). Bolus plus infusion of ketamine in healthy volunteers caused a global reduction in V_T of $[^{123}\text{I}]\text{CNS } 1261$ compared with placebo in most brain regions, including the putamen, temporal, and pericallosal regions (Stone et al. 2006). Subsequent work by the same group demonstrated that the degree of reduction in the V_T values of $[^{123}\text{I}]\text{CNS } 1261$ correlated with the negative symptoms of schizophrenia in all brain regions examined (Stone et al. 2008). In addition, they reported that drug-free patients with schizophrenia had reduced binding of $[^{123}\text{I}]\text{CNS } 1261$ in the left hippocampus relative to the whole cortex compared with healthy controls (Pilowsky et al. 2006). In contrast, the same group found that the V_T values of $[^{123}\text{I}]\text{CNS } 1261$ did not differ between healthy normal volunteers and drug-free or typical antipsychotic-treated

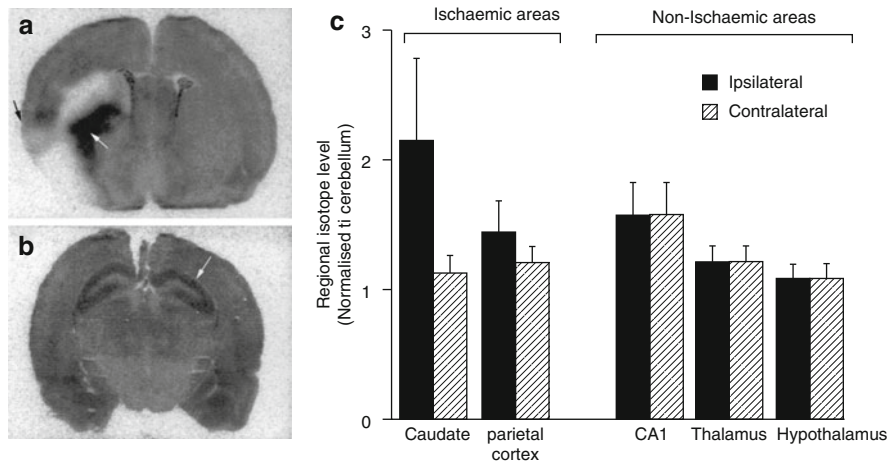


Fig. 18.11 Ex vivo autoradiography of [¹²⁵I]CNS 1261 in coronal sections of rat brain at the level of (a) caudate nucleus (*white arrow*) and circumscribed zones of cerebral cortex (*black arrow*) (b) CA1 region of hippocampus (*white arrow*). The animals were injected with [¹²⁵I]CNS 1261 15 min after permanent occlusion of the middle cerebral artery (left hemisphere) and sacrificed 120 min after tracer injection. (c) Accumulated radioactivity levels in ROIs to cerebellum (Owens et al. 2000)

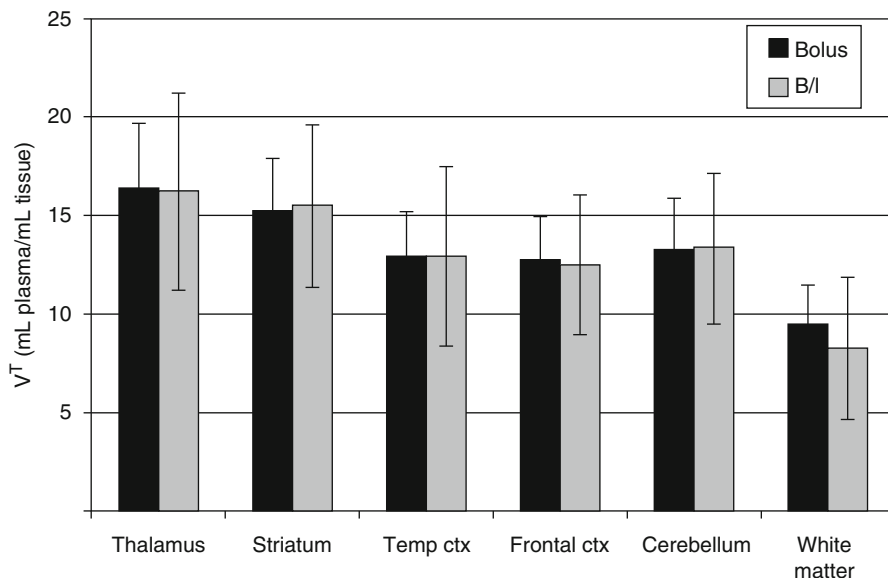


Fig. 18.12 The mean V_T values (\pm SD) of [¹²⁵I]CNS 1261 for ROIs from healthy volunteers scanned with the bolus protocol ($n=7$) (*dark bars*) and with the bolus/infusion protocol ($n=6$) (*light bars*) (Bressan et al. 2004)

schizophrenia patients. On the other hand, clozapine-treated patients showed a significant reduction of V_T in all brain regions examined, which indicated a decrease of NMDAR activation in this group. However, the regional brain distribution of [123 I] CNS 1261 was almost homogenous in all groups (Bressan et al. 2005). Although there was no conclusive evidence that [123 I]CNS 1261 could recognize NMDAR activation, these reports suggested that protein expression levels of NMDARs could be reduced in the brain of schizophrenia patients. Numerous reports indicated the involvement of NMDAR hypofunction in the pathophysiology of positive and negative symptoms of schizophrenia (Kantrowitz and Javitt 2010; Lin et al. 2012). Recently, Knol et al. reported further in vivo studies of [123 I]CNS 1261 using rats. The [123 I]CNS 1261 showed higher accumulation in the NMDAR-rich regions such as hippocampus and frontal cortex than that of NMDAR-poor cerebellum, in which the ratio was maximum (about 1.4) at 2 h postinjection. Pretreatment with the NMDAR co-agonist, D-serine, (10 mg/kg) led to no significant change in the hippocampus/cerebellar ratio. On the other hand, treatment with D-serine and MK-801 resulted in a significantly lower hippocampus/cerebellar ratio, which indicated the existence of specific trapping of a certain amount [123 I]CNS 1261 in the NMDAR-rich regions. However, the authors concluded that the use of [123 I]CNS 1261 would be limited in terms of quantification and detection of small changes in receptor availability because of a considerable amount of nonspecific binding of this tracer (Knol et al. 2009).

To provide potential PET radioligands for the PCP-binding site, [11 C]-labeled diarylguanidine derivatives have been synthesized and evaluated. [11 C]GMOM (Fig. 18.10) with a high affinity for NMDARs ($K_i=5.2$ nM) was prepared from the corresponding hydroxyl precursor with a specific activity of 46 GBq/ μ mol. In rats, brain uptake of [11 C]GMOM was high and peaked during the early part of the study. Regional brain distribution at 10 min was 1.23, 0.93, and 0.74 % ID/g for the frontal cortex, hippocampus, and cerebellum, respectively, as regards the appearance of contrast in the NMDAR-rich and NMDAR-poor regions. Pretreatment with open channel blockers GMOM or MK-801 (1 mg/kg) or the NB2B-selective NMDAR modulator Ro 25-6981 led to a moderate and uniform decrease of [11 C]GMOM uptake in brain regions. On the other hand, NMDAR co-agonist D-serine increased [11 C]GMOM binding in all regions. PET imaging in baboons revealed that [11 C]GMOM exhibited high BBB penetration. However, the brain distribution of [11 C]GMOM was almost homogenous and pre-administration of MK801 did not reduce regional V_T 's or regional V_T ratios. The authors hypothesized that these inconsistent results could be caused by the blocking effect of anesthesia (ketamine and isoflurane) to NMDAR activity (Waterhouse et al. 2004). Further PET investigations of [11 C]GMOM in other conditions, such as in a conscious state, have not been reported so far.

Another diarylguanidine derivative, CNS 5161 (Fig. 18.10), has been shown to exhibit high affinity for the PCP-binding site ($K_i=1.9$ nM) (Hu et al. 1997; Dumont et al. 2002). Clinical trials using CNS 5161 have been evaluated in the treatment of neuropathic pain (Walters et al. 2002; Forst et al. 2007). The [3 H]CNS 5161 showed a heterogeneous in vivo brain distribution in rats and a cortex/cerebellum ratio of

1.4. Pretreatment of NMDA increased the ratio in the hippocampus/cerebellum to 1.6–1.9, while MK801 diminished this increase that resulted in ratios close to 1. [^3H]CNS 5161 appeared to be unstable in arterial blood, as 65 % of the parent compound was metabolized to several more hydrophilic compounds even 20 min after tracer injection (Biegon et al. 2007). The [^{11}C]CNS 5161 was synthesized by [^{11}C] methylation of the desmethyl guanidine precursor with low specific activity (41GBq/mmol) (Zhao et al. 2006). In human PET studies, [^{11}C]CNS 5161 exhibited the largest uptake in the putamen and thalamus and the lowest uptake in the cerebellum, but relatively lower radioactivity was observed in the hippocampus compared with other gray matter regions. Similar to rats, the metabolism of [^{11}C]CNS 5161 was rapid in human plasma. No blocking studies were reported in the literature (Asselin et al. 2004). Recently, clinical PET studies of [^{11}C]CNS 5161 were carried out to assess the effect of levodopa on striatal and cortical NMDAR activity in patients with Parkinson's disease with and without dyskinesias (Ahmed et al. 2011). The levodopa-treated dyskinetic patients had higher [^{11}C]CNS 5161 uptake in the caudate, putamen, and precentral gyrus compared with patients without dyskinesias. These results are consistent with reports that upregulation of NMDARs has been associated with the development of levodopa-induced dyskinesias in animal models of Parkinsonism (Oh et al. 1998). However, no significant increase in [^{11}C]CNS 5161 uptake was observed in patients with Parkinson's disease when compared with control subjects. In addition, relatively high uptake of [^{11}C]CNS 5161 in the cerebellum was observed, which was inconsistent with the brain distribution of [^{11}C]CNS 5161 in a previous clinical PET study reported by Asselin et al. (2004). Further investigations are necessary in order to prove the usefulness of these diarylguanidines as radioligands for measuring NMDAR function by PET or SPECT.

Recently, ^{18}F -labeled S-fluoroalkyl diarylguanidines were synthesized and used for in vitro evaluation. Among them, [^{18}F]7 and [^{18}F]8 showed high affinity for the PCP-binding site ($K_d=2.4$ nM for [^{18}F]7 and $K_d=1.4$ nM for [^{18}F]8). Further studies could not be performed on [^{18}F]8 owing to low stability of this ligand. A broad receptor-binding assay for 60 receptors demonstrated that [^{18}F]7 had high selectivity for the PCP-binding site of NMDARs (Robins et al. 2010). No in vivo studies of [^{18}F]7 have been reported so far.

18.2.3 Other Open Channel Blocker Derivatives

The 6,11-ethanobenzo[b]quinolizinium derivatives are highly hydrophilic compounds reported to exhibit high affinity and specificity to the PCP-binding site of the NMDARs (Mallamo et al. 1994). Based on the SAR studies, new fluorine-18 radioligands ([^{18}F]9 and [^{18}F]10) and a carbon-11 ligand ([^{11}C]11) have been developed as novel PET radioligands for the PCP-binding site of NMDARs as shown in Fig. 18.13 (Sasaki et al. 1998; Ishibashi et al. 2000). These compounds showed moderate binding affinity for the PCP-binding site (9: $\text{IC}_{50}=47$ nM, 10: $\text{IC}_{50}=89$ nM, 11: $\text{IC}_{50}=19$ nM vs [^3H]TCP) (Sasaki et al. 1998). In the preliminary radiosynthesis of [^{18}F]9 and [^{18}F]10, nucleophilic radiofluorination of mesylate was unsuccessful

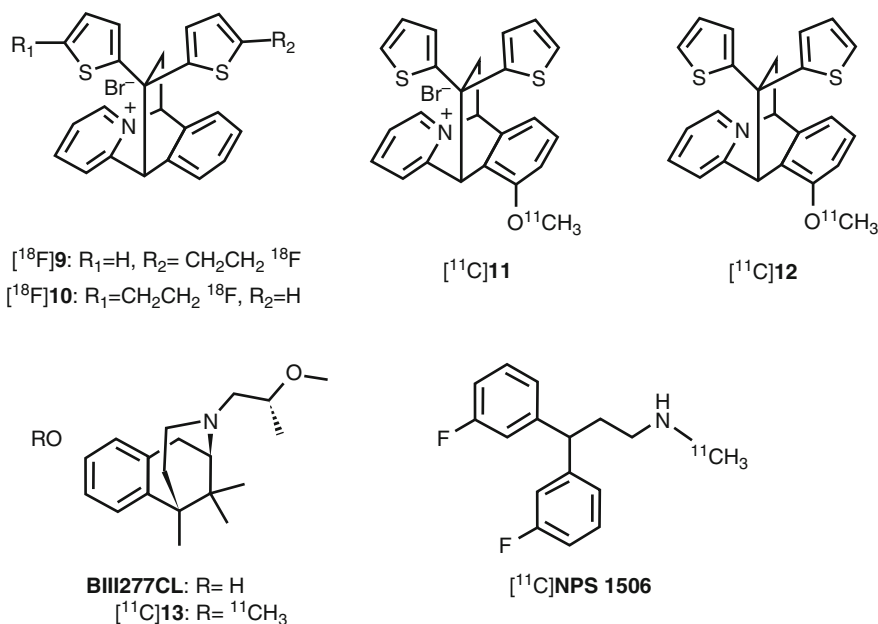


Fig. 18.13 Chemical structure of other radiolabeled open channel blocker derivatives

probably due to trapping of $^{18}\text{F}^-$ anion by the ammonium cation. An alternative synthetic route, including early fluorination of dienophile prior to the Diels-Alder reaction permitted successful radiosynthesis of $[^{18}\text{F}]\mathbf{9}$ and $[^{18}\text{F}]\mathbf{10}$ (Sasaki et al. 1998; Ishibashi et al. 2000). However, the specific activity of $[^{18}\text{F}]\mathbf{9}$ and $[^{18}\text{F}]\mathbf{10}$ was relatively low (>263 MBq/ μmol). The $[^{11}\text{C}]\mathbf{11}$ was prepared by *O*-methylation of the hydroxyl precursor. The specific activity of $[^{11}\text{C}]\mathbf{11}$ was about 63 GBq/mmol. Values were approximately a 1,000-fold lower than the theoretical specific activity of C-11 ligands starting from $[^{11}\text{C}]\text{CO}_2$. In vivo biodistribution studies demonstrated that these three radioligands showed a quite low BBB permeability (0.02–0.05 % ID/g at 15 min) presumably because of their cationic property and extremely low lipophilicity (Ishibashi et al. 2000). To improve brain uptake and receptor specificity, the reduced derivative $[^{11}\text{C}]\mathbf{12}$ was developed as a prodrug for $[^{11}\text{C}]\mathbf{11}$. In the preliminary in vivo studies, cationic $[^{14}\text{C}]\mathbf{12}$ was easily metabolized to neutral $[^{14}\text{C}]\mathbf{11}$ at 15 min after injection. However, most of $[^{14}\text{C}]\mathbf{11}$ was cleared from the brain at 45 min. Although $[^{11}\text{C}]\mathbf{12}$ showed a higher BBB penetration (0.7–0.8 % ID/g at 15 min) than that of $[^{14}\text{C}]\mathbf{11}$, no regional difference was observed between the forebrain regions and cerebellum (Sasaki et al. 2001). Although $[^{11}\text{C}]\mathbf{12}$ was not confirmed to be a useful PET ligand for NMDARs, this prodrug strategy can be applied to the development of in vivo imaging agents.

BIII277CL (Fig. 18.13), a potent anticonvulsant and neuroprotective agent, has been reported to have high affinity ($K_i=4.5$ nM vs $[^3\text{H}]\text{MK-801}$) at the PCP-binding site of NMDARs (Grauert et al. 1997, 1998). Kocic et al. have developed a methyl

analog of BIII277CL (**13**, Fig. 18.13) with substantial affinity for the PCP-binding site ($K_i=49$ nM vs [^3H]TCP) as a candidate imaging agent for NMDARs. [^{11}C]**13** was prepared by *O*-[^{11}C] methylation of BIII277CL with a specific activity of 30–60 GBq/ μmol . PET studies of [^{11}C]**13** in pigs revealed homogenous localization in the cortex and cerebellum. The kinetic analysis using one-tissue compartment model revealed that V_T of [^{11}C]**13** was approximately 1 in both the cortex and cerebellum. These results indicated a lack of specific binding of [^{11}C]**13** for NMDARs (Kokic et al. 2002).

NPS 1506 (Fig. 18.13) has been reported noncompetitive NMDAR antagonist with moderate affinity ($\text{IC}_{50}=664$ nM vs [^3H]MK-801). The NPS 1506 is neuroprotective in a variety of animal models of stroke and head injury with no PCP-like psychotomimetic effects at doses between 1 and 5 mg/kg i.p. in rats (Mueller et al. 1999). Considering such a pharmacological profile, which is different from the previous NMDAR antagonists, NPS 1506 was labeled with carbon-11 and evaluated as a novel PET tracer for the PCP-binding site of NMDARs. The [^{11}C]NPS 1506 was prepared by *N*-[^{11}C] methylation of primary amine precursor with a specific activity of around 50 GBq/ μmol . Biodistribution of [^{11}C]NPS 1506 in mice and rat demonstrated that uptake into the brain was rapid and occurred at high levels. However, the regional brain distribution was fairly uniform and did not clearly reflect the known localization of NMDARs in the rodent brain. In addition, treatment with unlabeled NPS 1506 did not cause any change in uptake in the mouse brain compared with the control group. An activator of NMDARs, 3-nitropropionic acid (20 mg/kg), did not produce any change in the regional uptake in the hippocampus nor the striatum. Therefore, [^{11}C]NPS 1506 may be an unsuitable in vivo tracer for NMDARs because of its large nonspecific binding fraction and low in vitro binding affinity for NMDARs (Fuchigami et al. 2003).

18.3 Radioligands for Glycine Site

Because glycine and/or D-serine are essential co-agonists for NMDA ion-channel activation, various classes of glycine-binding site antagonists (Fig. 18.14) have been reported as anticonvulsant and neuroprotective agents (Danysz and Parsons 1998). Hypofunction of NMDARs is considered to be associated with the pathophysiology of schizophrenia. Indeed, it was reported that the enhancement of NMDAR activity via glycine site was efficacious in the treatment of schizophrenia (Millan 2005). Imaging of the glycine site of NMDARs was considered useful for obtaining information about the functional mechanism of the glycine site in the living brain and in the diagnosis of various neurological disorders.

18.3.1 Radioligands Based on Cyclic Amino Acids

7-Chloro-5-iodokynurenic acid (**14**, Fig. 18.15) has been identified as a potent (IC_{50} vs [^3H]glycine binding, 32 nM) and selective antagonist for the glycine site of NMDARs (Leeson et al. 1991). The [^{123}I]**14** was successfully synthesized by

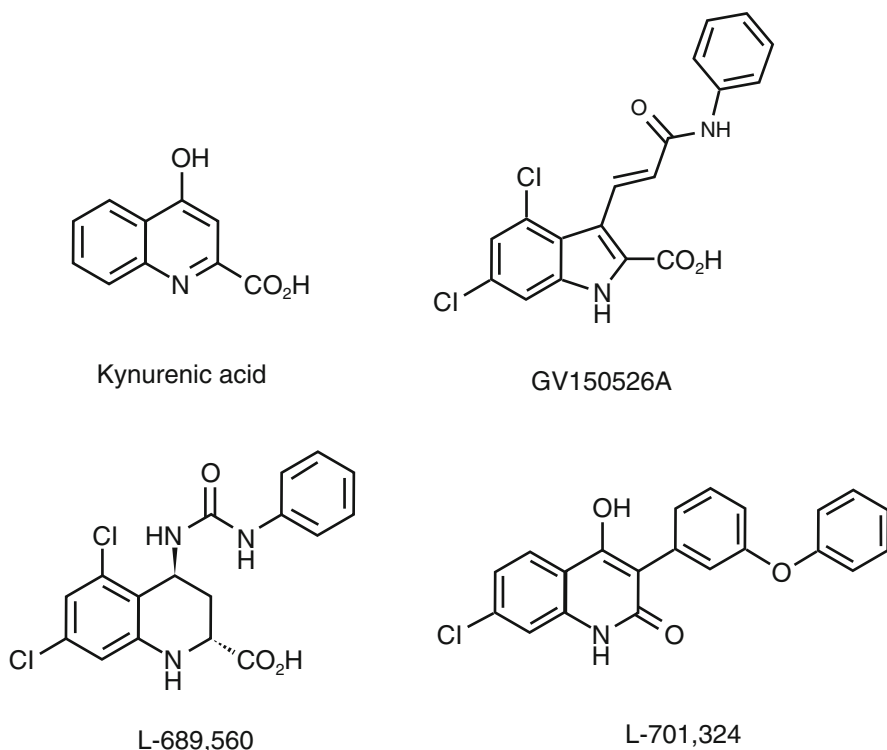


Fig. 18.14 Chemical structure of glycine-binding site antagonists

halogen exchange reaction of a mixture of 5-bromo-7-chloro- and 7-bromo-5-chlorokynurenic acid at a specific activity of 37 GBq/ μmol . In the biodistribution studies in mice, [^{123}I]**14** showed fast deiodination (85 % of parent compound was changed to $^{123}\text{I}^-$) and low brain uptake (0.61 % ID/g at 5 min). The [^{123}I]**14** had been demonstrated to be an unsuitable *in vivo* tracer (Dumont and Slegers 1997).

GV150526A (Fig. 18.14) is one of the most potent glycine site antagonists ($K_i=3.2$ nM vs [^3H]glycine) with reasonable lipophilicity ($\log P=2.24$) (Di Fabio et al. 1997). Based on the report, Waterhouse et al. developed a *meta*-methoxy derivative [^{11}C]3MPICA (Fig. 18.15) with high affinity for the glycine site ($K_i=4.8$ nM vs [^3H]MDL 105,519). The [^{11}C]3MPICA was prepared by *O*-[^{11}C] methylation of the corresponding desmethyl derivative with a specific activity of 44 GBq/ μmol (Waterhouse et al. 2002a). In the biodistribution studies in rats, regional uptake of [^{11}C]3MPICA at 2 min ranged from 0.11 to 0.18 % ID/g. The radioactivity cleared rapidly from all brain regions examined. Blocking studies using unlabeled compound (1 mg/kg) did not cause a marked reduction in the ratio of the brain tissues/blood. Treatment with warfarin (100 mg/kg) led to reduction in blood radioactivity concentrations while brain uptake was not changed significantly,

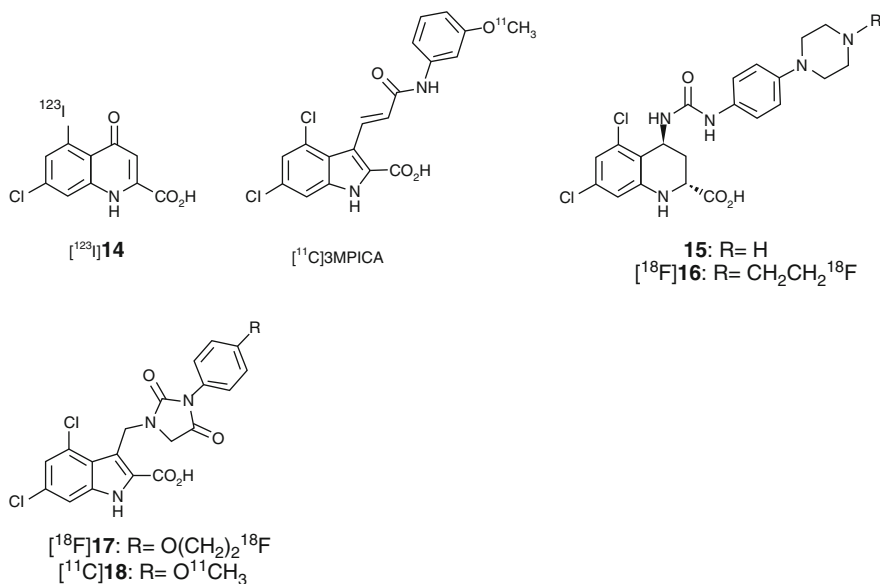
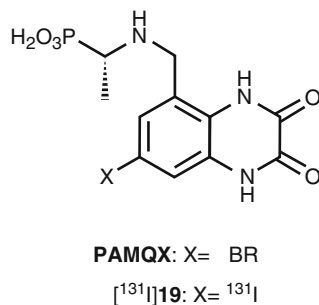


Fig. 18.15 Chemical structure of radiolabeled cyclic amino acid derivatives

which indicated that factors other than binding to serum albumin could prevent BBB penetration of $[^{11}\text{C}]$ 3MPICA (Waterhouse et al. 2002b).

Trans-5,7-dichloro-4-substituted-2-carboxytetrahydroquinolines such as **15** (Fig. 18.15) showed high affinities ($K_i=6.0$ nM vs $[^3\text{H}]$ 5,7-dichlorokynurenic acid) for the glycine site of NMDARs (Leeson et al. 1992). Based on the SAR studies, fluoroethyl derivative $[^{18}\text{F}]$ **16** (Fig. 18.15) was designed, synthesized, and evaluated as a PET radioligand for glycine site. The **16** had a relatively low lipophilicity ($\log D=1.3$) and high affinity ($K_i=12$ nM vs $[^3\text{H}]$ MDL 105,519) for the glycine-binding site. The radiosynthesis of $[^{18}\text{F}]$ **16** was achieved by *N*- $[^{18}\text{F}]$ fluoroethylation of a piperidine precursor with 2- $[^{18}\text{F}]$ fluoroethyltosylate followed by hydrolysis of methyl ester. Biodistribution studies revealed that $[^{18}\text{F}]$ **16** showed homogenous low levels of accumulation in all considered brain regions. Because the difference in regional brain distribution of $[^{18}\text{F}]$ **16** could not be detected, no blocking experiments were performed (Piel et al. 2003). Recently, hydantoin-substituted indole carboxylic acids were developed as novel PET ligands for the glycine-binding site with a higher lipophilicity than **16**. Compound **17** and **18** showed moderate affinity for the glycine site ($K_i=53$ nM for **17** and $K_i=31$ for **18** in $[^3\text{H}]$ MDL 105,519 binding assay). The $\log D$ values of **17** and **18** were 2.07 and 2.26, respectively. $[^{18}\text{F}]$ **17** and $[^{11}\text{C}]$ **18** were successfully synthesized with overall decay-corrected radiochemical yields of 5–7 and 6–9 % and specific activities of 24–67 GBq/ μmol and 8–26 GBq/ μmol , respectively (Bauman et al. 2011). No further in vivo evaluations of these radioligands have been reported so far.

Fig. 18.16 Chemical structure of PAMQX and radioiodinated PAMQX derivative



18.3.2 5-Aminomethylquinoxaline-2,3-Dione Derivative

(*S*)-7-Bromo-*N*-(1-phosphonoethyl)-5-aminomethylquinoxaline-2,3-dione (PAMQX, Fig. 18.16) has been discovered as a selective and high-affinity glycine site antagonist with an IC_{50} value of 6 nM against [^3H]MDL-105519 binding (Auberson et al. 1999). The 7-iodo derivative of PAMQX (**19**, Fig. 18.16) exhibited comparable affinity (IC_{50} =8 nM vs [^3H]MDL-105,519) for the glycine site with PAMQX (Ametamey et al. 2000). Radiosynthesis of [^{131}I]**19** was achieved by iododestannylation of *N*-CBZ-protected tributylstannyl precursor followed by deprotection of CBZ group. Biodistribution studies of [^{123}I]**19** in mice revealed an extremely low BBB permeability of [^{123}I]**19** (0.03 % ID/g at 30 min) probably due to its high polarity and low $\log D_{7,4}$ value ($\log D_{7,4} = -2.5$) (Ametamey et al. 2000).

18.3.3 4-Hydroxyquinolone Derivatives

The radioligands consisting of carboxylic acids showed poor brain penetration due to the highly polar nature of the charged carboxylate. The 4-hydroxyquinolones (4-HQs)-devised carboxylic bioisostere had been developed as one of the most potent antagonists for the glycine-binding site of NMDARs. As expected, this series showed *in vivo* anticonvulsant activity, which suggested an ability to penetrate the BBB (Kulagowski et al. 1994; Rowley et al. 1997). In line with this, Morris et al. synthesized [^{11}C]L-703,717 (Fig. 18.17), one of the most potent glycine site antagonists (IC_{50} =4.5 nM vs [^3H]L-689,560), by *O*-[^{11}C] methylation of phenol precursor using [^{11}C]CH $_3$ I containing K $_2$ CO $_3$ /Kryptofix 2.2.2 as a base, but the radiochemical yield was very low (7 %) (Morris et al. 1997). The labeling precursor has three possible sites (amide, enol, and phenol) which could be reacted with [^{11}C]CH $_3$ I. Therefore, regioselective methylation at the phenol position was required to prepare [^{11}C]L-703,717 for high yield and purity. Haradahira et al. succeeded in the synthesis of [^{11}C]L-703,717 by using 5 eq of NaH as a base in high yields (87 %) with a specific activity of 47–53 GBq/ μmol . The excess amount of NaH can give the triply deprotonated species, then the most accessible terminal phenol can be preferentially methylated (Haradahira et al. 1999). In the biodistribution study in mice, [^{11}C]

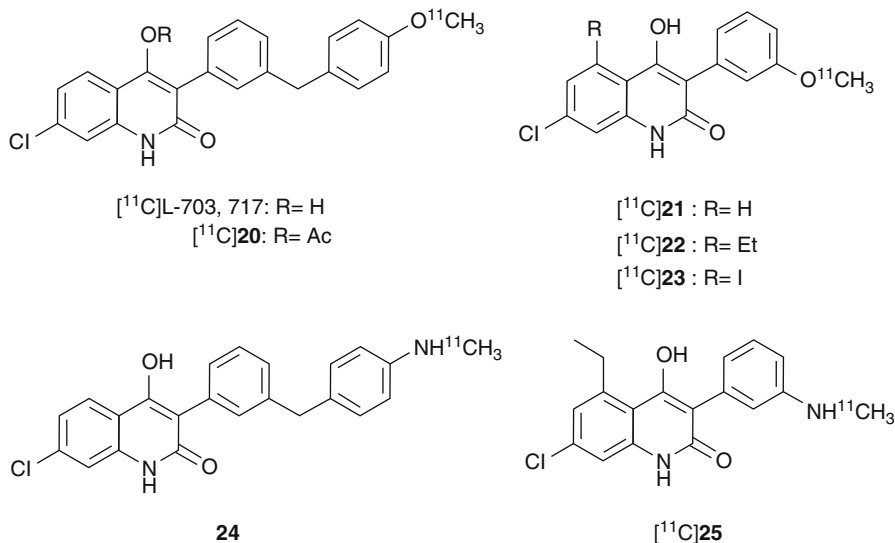


Fig. 18.17 Chemical structure of radiolabeled 4-hydroxyquinolone derivatives

L-703,717 showed low BBB permeability (0.32–0.36 % ID/g at 1 min) and extremely high blood concentration presumably due to high affinity for the warfarin-binding site of plasma protein. Indeed, warfarin led to a dose-dependent enhancement of the initial brain uptake of $[^{11}\text{C}]\text{L-703,717}$ that resulted in a fivefold increase in the brain radioactivity at the dose of 200 mg of warfarin. However, the radioactivity in the cerebrum was rapidly decreased (0.2 % ID/g) with some retention observed in the cerebellum (0.65 % ID/g) at 30 min after injection. This suggested inconsistent binding with known distribution of NMDARs. In addition, a significant blocking effect by nonradioactive L-703,717 (2 mg/kg) was observed only in the cerebellum (Haradahira et al. 2000). To improve brain penetration of $[^{11}\text{C}]\text{L-703,717}$, acetyl derivative of L-703,717 ($[^{11}\text{C}]\text{20}$, Fig. 18.17) was prepared and evaluated as prodrug of $[^{11}\text{C}]\text{L-703,717}$. Initial brain uptake of $[^{11}\text{C}]\text{20}$ (0.71 % ID/g) was twofold higher than that of $[^{11}\text{C}]\text{L-703,717}$ (0.36 % ID/g). Metabolism experiments of $[^{11}\text{C}]\text{20}$ in rat brain homogenates confirmed that about 80 % of $[^{11}\text{C}]\text{20}$ was converted to $[^{11}\text{C}]\text{L-703,717}$ at 20 min after injection. Ex vivo autoradiography demonstrated that $[^{11}\text{C}]\text{20}$ exhibited similar cerebellar localization of radioactivity to $[^{11}\text{C}]\text{20}$ (Haradahira et al. 2001). Further in vivo evaluation revealed that the specific cerebellar binding of $[^{11}\text{C}]\text{L-703,717}$ was abolished in the NR2C-deficient mice as shown in Fig. 18.18a–c. This result suggested that the in vivo cerebellar localization of $[^{11}\text{C}]\text{L-703,717}$ could be caused by preferential binding to the NR2C subunit-containing NMDARs predominantly expressed in the cerebellum. However, $[^{11}\text{C}]\text{L-703,717}$ exhibited high specific localization in the hippocampus and cerebral cortex under in vitro condition as shown in Fig. 18.18d–f, indicative of the absence of intrinsic selectivity for the NR2C subunit-containing NMDARs in the cerebellum (Haradahira et al. 2002b). Thus, the authors next hypothesized that

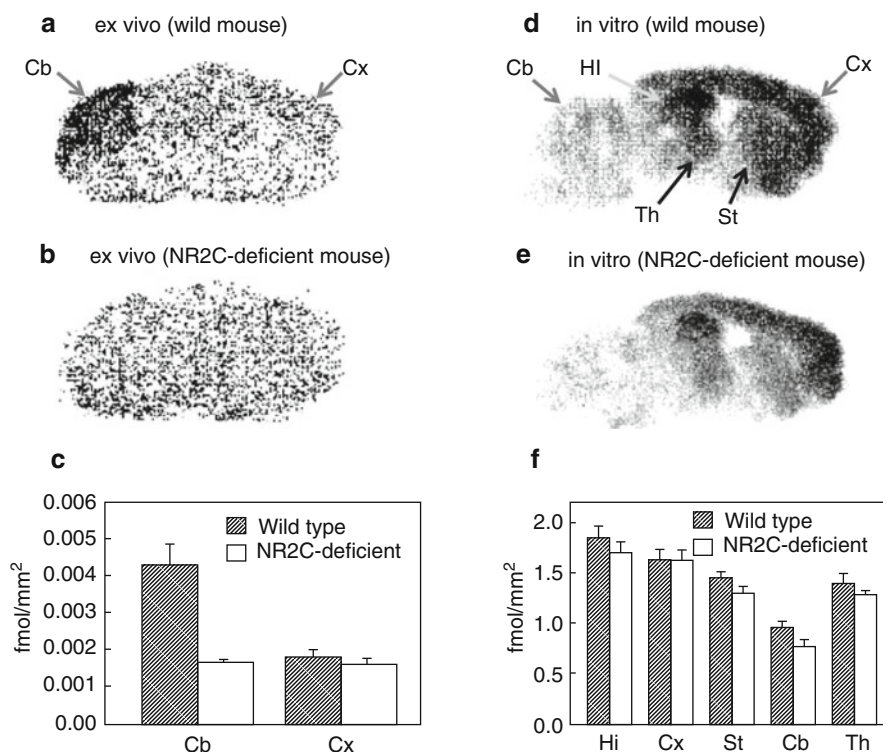
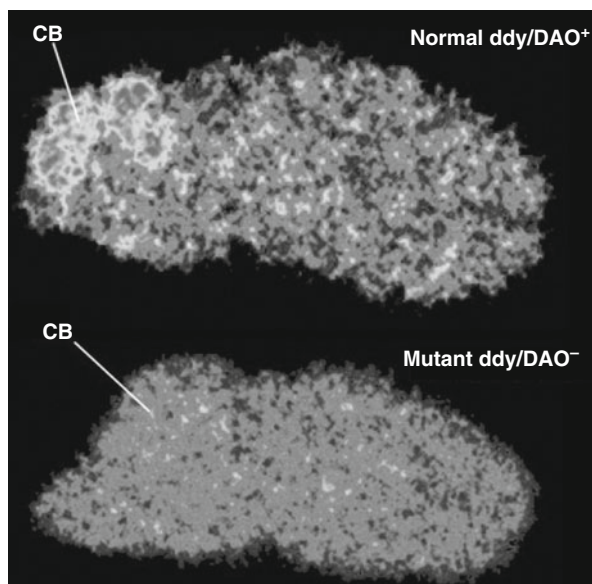


Fig. 18.18 Ex vivo and in vitro autoradiograms of [¹¹C]L-703,717 in sagittal sections of wild-type and NR2C-deficient mice brain. (a, b) Ex vivo images obtained at 20 min after injection of [¹¹C]L-703,717 and warfarin (60 mg/kg). (c) Quantified values of the ex vivo binding in cerebral cortex (Cx) and cerebellum (Cb). (d, e) In vitro images of [¹¹C]L-703,717. (f) Quantified values of the in vitro bindings in hippocampus (Hi), cerebral cortex (Cx), striatum (St), cerebellum (Cb), and thalamus (Th) (Haradahira et al. 2002b)

endogenous NMDAR co-agonists might play a key role in the unusual localization in the cerebellum of [¹¹C]L-703,717. Both glycine and D-serine are known as co-agonists of NMDARs and exist in micromolar level. Glycine is distributed throughout the brain, while D-serine is localized only in the forebrain regions (Hashimoto et al. 1993; Schell et al. 1997). D-serine is reported to be nearly undetectable in cerebellum due to the highest level of D-amino acid oxidase (DAO) activity (Schell et al. 1995). Haradahira et al. demonstrated that the cerebellar localization of [¹¹C]L-703,717 was abolished in mutant ddY/DAO^{-/-} mice, in which the D-serine level in cerebellum was markedly increased (Fig. 18.19). Hence, the authors proposed that the low level of [¹¹C]L-703,717 binding in forebrain regions could be explained by the strong inhibition of high amount of endogenous D-serine; whereas, specific localization in the cerebellum might be due to the lack of D-serine (Haradahira et al. 2003). Considering that [¹¹C]L-703,717 has been demonstrated to recognize cerebellar NMDARs to some extent, clinical PET studies of [¹¹C]20 (a prodrug of [¹¹C]

Fig. 18.19 Ex vivo autoradiogram of [^{11}C] L-703,717 in the brain of normal ddY/DAO $^{+}$ and mutant ddY/DAO $^{-}$ mice. The brain slices (50 μm) were obtained at 30 min after injection of [^{11}C]L-703,717 and warfarin (60 mg/kg) (Haradahira et al. 2003)



L-703,717) were performed for the visualization of NMDARs in the cerebellum (Matsumoto et al. 2007). Binding potential (BP) calculated from white matter as a reference region in the cerebellar cortex was twofold higher than in the cerebral cortices (cerebellar cortex; BP=2.2, cerebral cortices; BP= 1.1). Regional brain distributions were consistent with previous reports of rodents (Haradahira et al. 2001). However, the brain uptake of [^{11}C]20 was too low for the visualization of the cerebellar NMDAs by PET (Matsumoto et al. 2007).

The 3-methoxy-MDL-104,653 (21, Fig. 18.17) has been reported as a weak antagonist (IC_{50} =204 nM vs [^3H]L-689,560) for the glycine site of NMDARs (Rowley et al. 1997). PET studies on monkeys demonstrated that [^{11}C]21 exhibited higher localization in the cortex regions than in the cerebellum, in which binding was not blocked by glycine site agonists (Haradahira et al. 2002c). It is reported that glycine site agonists and antagonists bind to overlapping but different sites on the NMDARs (Kuryatov et al. 1994; Wafford et al. 1995). Previous studies on [^{11}C] L-703,717 suggested that most radioligands for the glycine site were susceptible to inhibition by endogenous agonists (agonist-sensitive) and resulted in strong inhibition of in vivo binding by agonists (Haradahira et al. 2002b, 2003). On the other hand, [^{11}C]20 might be an atypical glycine site antagonist, in which the binding site overlaps with the glycine antagonist-binding site, but not with the agonist-binding site, namely, agonist-insensitive ligand. Although insufficient BBB permeability and high nonspecific binding limited further investigations of [^{11}C]21, structural optimization of [^{11}C]21 in order to increase BBB permeability, as well as improve in vivo specificity, would produce a useful agonist-insensitive radioligand for the glycine site of NMDARs, especially in the forebrain regions which play crucial roles in various brain functions. On the basis of SAR studies, we developed 5-ethyl

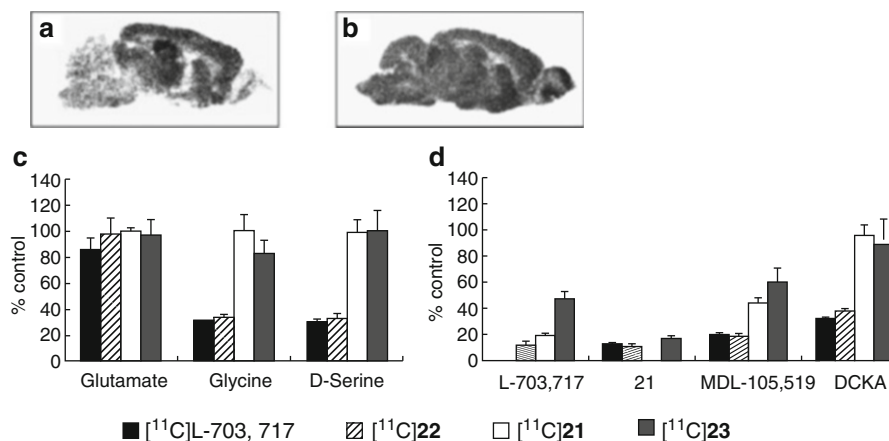


Fig. 18.20 Typical autoradiogram of in vitro binding of $[^{11}\text{C}]\mathbf{22}$ (a) and $[^{11}\text{C}]\mathbf{23}$ (b). Effect of NMDAR agonists (c) and antagonists (d) on in vitro-specific $[^{11}\text{C}]$ 4-hydroxyquinolones binding to hippocampus. Abbreviations: *DCKA* 5,7-dichlorokynurenic acid (Fuchigami et al. 2008)

(**22**) and 5-iodine (**23**) derivative of $[^{11}\text{C}]\mathbf{21}$ (Fig. 18.17) with high affinity for the glycine site ($K_i=7.2$ and 10.3 nM vs $[^3\text{H}]\text{MDL-105,519}$, respectively). In vitro autoradiography demonstrated that $[^{11}\text{C}]\mathbf{22}$ and $[^{11}\text{C}]\mathbf{23}$ displayed quite different binding properties. The $[^{11}\text{C}]\mathbf{22}$ showed high accumulation in the forebrain regions but lowest in the cerebellum. The binding was inhibited both by glycine site antagonists and agonists as shown in Fig. 18.20a, c and d which suggested that $[^{11}\text{C}]\mathbf{22}$ is an agonist-sensitive ligand. On the other hand, $[^{11}\text{C}]\mathbf{23}$ exhibited homogeneous accumulation throughout the brain and the binding was inhibited by glycine site antagonists but not by agonists as shown in Fig. 18.20b–d which suggested that $[^{11}\text{C}]\mathbf{23}$ is an agonist-insensitive ligand (Fuchigami et al. 2008). These results indicated that 4-HQs could be divided into two groups “agonist-sensitive ligands ($[^{11}\text{C}]\text{L-703,717}$ and $[^{11}\text{C}]\mathbf{22}$)” and “agonist-insensitive ligands ($[^{11}\text{C}]\mathbf{21}$ and $[^{11}\text{C}]\mathbf{23}$).” It is possible that the agonist-insensitive ligands can bind the glycine antagonist-preferring site, such as homomeric NR1 or inactivated NR1/NR2 site, of the NMDARs. On the other hand, the agonist-sensitive ligand can preferentially bind to the functional and heteromeric NMDARs, which is localized in the forebrain regions rather than in the cerebellum and therefore is sensitive to agonist binding. Unfortunately, $[^{11}\text{C}]\mathbf{22}$ and $[^{11}\text{C}]\mathbf{23}$ did not exhibit a significant increase in brain uptake compared with $[^{11}\text{C}]\text{L-703,717}$ and $[^{11}\text{C}]\mathbf{21}$, although $[^{11}\text{C}]\mathbf{22}$ and $[^{11}\text{C}]\mathbf{23}$ had moderate lipophilicity ($\log P=2.25$ for **22** and 1.81 for **23**). Consistent with previous reports (Haradahira et al. 2002c), agonist-sensitive $[^{11}\text{C}]\mathbf{22}$ showed higher localization in the cerebellum; whereas, agonist-insensitive $[^{11}\text{C}]\mathbf{23}$ showed homogeneous brain uptake. However, poor brain uptake and high nonspecific binding of $[^{11}\text{C}]\mathbf{22}$ and $[^{11}\text{C}]\mathbf{23}$ limited further detailed in vivo investigations. Because warfarin increased brain uptake of $[^{11}\text{C}]\mathbf{22}$ and $[^{11}\text{C}]\mathbf{23}$, the binding of these tracers for serum albumin should have considerable effect on in vivo brain uptake (Fuchigami et al.

2008). The 4-HQs are all acidic with pK_a values of around 5 or below (Rowley et al. 1997) and more amenable to binding with plasma proteins than nonacidic compounds, which result in poor BBB permeability. Introduction of the basic amino group into 4-HQs was expected to increase the pK_a value and reduce unsuitable protein binding, which could increase brain uptake. We synthesized and evaluated several amino 4-HQ derivatives as new PET radioligand candidates for the glycine site. Among these ligands, methylamino derivatives of 4-HQs (**24** and **25**, Fig. 18.17) have been identified as high-affinity glycine site ligands (K_d values; 11.7 nM for **24** and 11.8 nM for **25**). In vitro autoradiography experiments demonstrated that both of [^{11}C]**24** and [^{11}C]**25** showed higher accumulation in the forebrain regions than cerebellum, which was consistent with known NMDAR distribution. Furthermore, the in vitro binding of [^{11}C]**24** and [^{11}C]**25** was strongly inhibited by both glycine agonists and antagonists, which suggests that these tracers are agonist-sensitive glycine site ligands. Although no agonist-insensitive ligands for glycine site were obtained, further in vivo characterization of [^{11}C]**24** and [^{11}C]**25** were performed. In the biodistribution studies in mice, cerebellum-to-blood ratio of both [^{11}C]**24** and [^{11}C]**25** at 30 min was about 0.06 at 30 min after injection, which indicated poor BBB penetration of these radioligands. Although the plasma protein-binding ratio of [^{11}C]**25** was much lower than that of methoxy analogs (71 % vs 94–98 %, respectively), [^{11}C]**25** still bound with plasma protein strongly (Fuchigami et al. 2009). Further SAR studies are required for developing favorable PET ligands for the glycine site of NMDARs with improved BBB permeability.

18.4 Development of Radioligands for Ifenprodil-Binding Site

In the adult brain, NR2B expression has been reported to be restricted to the forebrain areas, including the cortex, hippocampus, striatum, thalamus, and olfactory bulb (Monyer et al. 1994; Akazawa et al. 1994). Since NR2B subunit has been suggested to play a key role in various diseases such as ischemic stroke, Parkinson's disease, Alzheimer's disease, and neuropathic pain, a number of organic compounds that target the NR2B subunit have been developed for the treatment of such diseases (Gogas 2006; Mony et al. 2009). Ifenprodil was initially discovered as an NR2B-selective negative modulator of NMDARs ($K_d=34$ nM for NR1a/NR2B receptors); however, it showed poor selectivity for NMDARs over other receptors such as α 1-adrenergic and σ receptors (Williams 1993; Karbon et al. 1990; Contreras et al. 1990; Hashimoto and London 1995; Grimwood et al. 2000). Accordingly, several series of NR2B antagonists with improved selectivity and affinity for NR2B-containing NMDARs have been developed (Chazot 2004; Gogas 2006; Mony et al. 2009). These compounds are divided into two classes, the "ifenprodil derivatives" and the "non-ifenprodil-related compounds" as shown in Fig. 18.21. Ifenprodil derivatives are likely to share the same site with ifenprodil on the interlobe cleft of the NR2B subunit (Malherbe et al. 2003). However, whether non-ifenprodil-related NR2B-selective antagonists have a similar binding mode to ifenprodil is unclear.

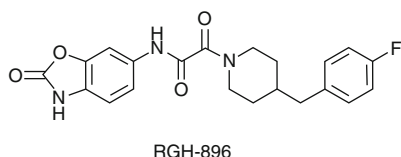
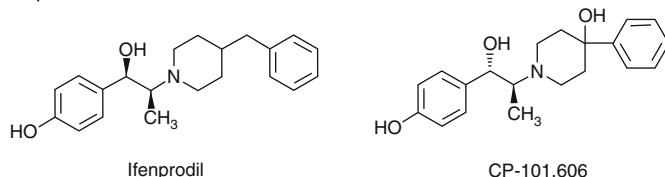
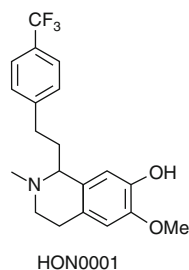
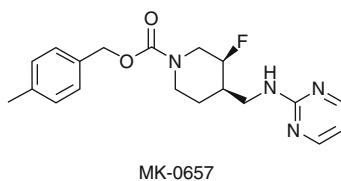
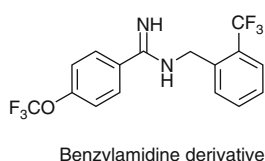
Ifenprodil derivativesNon ifenprodil-related compounds

Fig. 18.21 Chemical structure of NR2B selective NMDAR antagonists

In vivo imaging of NR2B-containing NMDARs is considered useful for obtaining information about various psychiatric diseases and facilitating drug development, as well as in vivo occupancy. Development of PET or SPECT imaging probes for NR2B subunit has been conducted based on these NR2B selective antagonists as described below.

18.4.1 Ifenprodil Derivatives

It has been shown that CP-101,606 is a potent NMDAR antagonist highly selective for NR2B subunit-containing receptors with K_d values of 10 nM (Menniti et al. 1997). A carbon-11 labeled methoxyl analog of CP-101,606 ($[^{11}\text{C}]\mathbf{26}$, Fig. 18.22) was developed for PET imaging of the NR2B subunit-containing NMDARs (Haradahira et al. 2002a). The $[^{11}\text{C}]\mathbf{26}$ was prepared by *O*- $[^{11}\text{C}]$ methylation of a phenol precursor with $[^{11}\text{C}]\text{CH}_3\text{I}$ and subsequent deprotection of phenolic TIPS ether. The specific radioactivity of $[^{11}\text{C}]\mathbf{26}$ ranged from 55 to 85 GBq/ μmol . In vitro autoradiography in rat brain slices revealed an extremely high localization of $[^{11}\text{C}]\mathbf{26}$ in the forebrain regions and very low in the cerebellum as shown in Fig. 18.23a. The in vitro distribution pattern of $[^{11}\text{C}]\mathbf{26}$ matched previously reported $[^3\text{H}]\text{CP-101,606}$

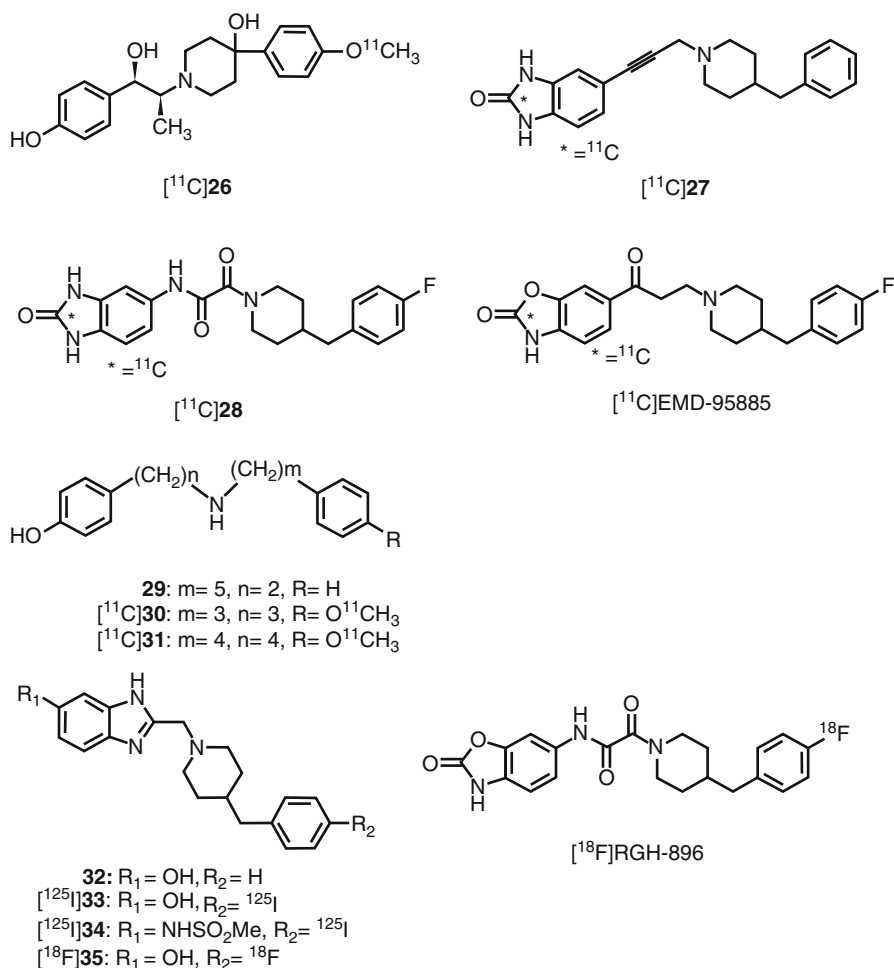


Fig. 18.22 Chemical structure of radiolabeled ifenprodil derivatives and bis(phenylalkyl)-amines

binding (Menniti et al. 1997) and NR2B subunit expression (Mori and Mishina 1995). Nonspecific binding of $[^{11}\text{C}]26$ was found to be less than 5 % as shown in Fig. 18.23b. The binding of $[^{11}\text{C}]26$ was displaced by CP-101,606 and ifenprodil in a competitive manner. Treatment of spermine and Zn^{2+} (1 mM) markedly decreased in vitro binding of $[^{11}\text{C}]26$ (74–82 %). It is suggested that ifenprodil and Zn^{2+} share the binding site on the interlobe cleft of NR2B subunit (Rachline et al. 2005). These results indicated that this tracer recognizes the ifenprodil-binding site on the NR2B subunit under in vitro condition. In contrast, in vivo biodistribution studies on mice and PET studies on monkeys demonstrated that this tracer exhibited a moderate brain uptake, but no apparent specific localization of the radioactivity was observed in any of the brain regions as shown in Fig. 18.23c (Haradahira et al. 2002a).

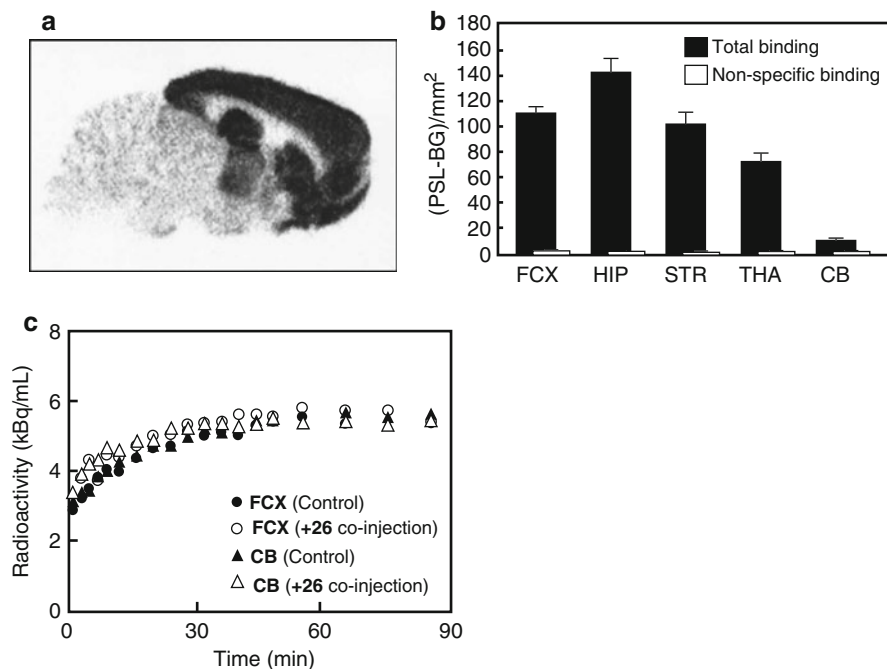


Fig. 18.23 (a) In vitro autoradiogram of [¹¹C]26 in sagittal sections of rat brain. (b) Quantified values of the autoradiogram in frontal cortex (FCX), hippocampus (HIP), striatum (STR), thalamus (THA), and cerebellum (CB). Nonspecific binding was determined in the presence of (+) CP-101,606 (10 μM). (PSL-BG)/mm² means photostimulated-luminescence (PSL) values per mm². Background PSL values (BG) were subtracted from the total PSL values on ROIs. (c) Time radioactivity curves in frontal cortex (FCX) and cerebellum (CB) after i.v. injection of [¹¹C]26 into monkey. Nonradioactive 26 (2 mg/kg) was injected simultaneously with [¹¹C]26 into the same monkey (Haradahira et al. 2002c)

The 1-(aryllalkynyl)-4-benzylpiperidine derivative **27** (Fig. 18.22) has been discovered as highly potent (IC₅₀ = 5.3 nM) NR2B subunit selective NMDAR antagonist (Wright et al. 2000). The [¹¹C]27 was successfully synthesized by cyclization reaction of benzene-1,2-diamine precursor with [¹¹C]COCl₂ with radiochemical yields of 3.5–7.0%. The specific activity of [¹¹C]27 was 37–74 GBq/μmol. The in vivo brain uptake of [¹¹C]27 in rats was fairly low (0.07% ID/g at 30 min) and localization was inconsistent with known NR2B expression with highest uptake in the cerebellum and lowest in the striata. Pretreatment with ifenprodil (20 mg/kg, ip) did not cause a prominent change in brain tissues/plasma ratio of radioactivity, which suggested a high nonspecific binding of [¹¹C]27 (Roger et al. 2003). Barta-Szalai et al. developed oxamides derived from indole-2-carboxamides as potent NR2B selective NMDA receptor antagonists. Among them, Compound **28** showed the best affinity in this series with an IC₅₀ of 5 nM in the [³H]Ro-25,6981 binding assay (Barta-Szalai et al. 2004). Recently, [¹¹C]28 was synthesized by the same method for [¹¹C]27 using [¹¹C]phosgene. [¹¹C]28 was obtained with a radiochemical

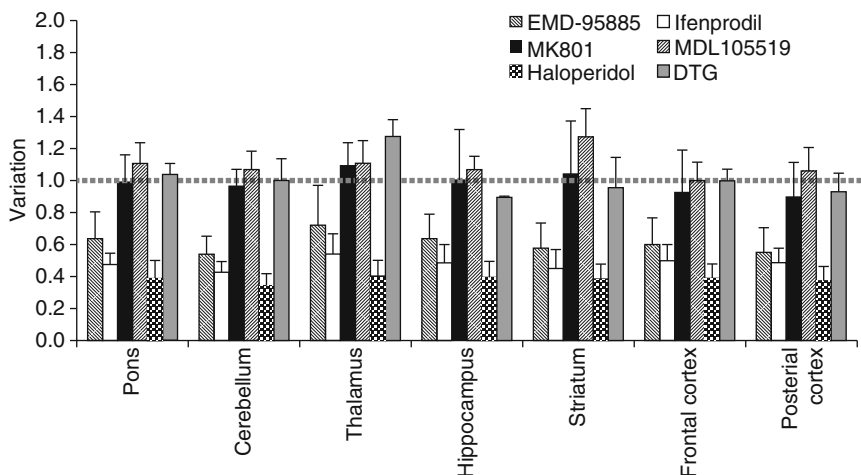


Fig. 18.24 Effect of various drugs on in vivo localization of [^{11}C]EMD-95885 in rat brain. The y-axis labeled as “Variation” means ratio of the binding in the presence of blocker to the binding in the absence of blocker in each brain region (Roger et al. 2004)

yield of 30–40 % with high specific radioactivity (72–127 GBq/ μmol) (Labas et al. 2010). Further in vitro and in vivo studies of [^{11}C]28 have not yet been published. Another 4-benzylpiperidine derivative, EMD-95885 (Fig. 18.22), has been reported to exhibit high affinity ($\text{IC}_{50} = 3.9 \text{ nM}$) and is a selective NR2B antagonist (Leibrock et al. 1997). The [^{11}C] EMD-95885 was prepared by a similar method used for [^{11}C]27 using [^{11}C]COCl $_2$ with a specific activity of 37–74 GBq/ μmol . Radiosensitive β -microprobe acquisition and biodistribution studies in rats revealed that [^{11}C] EMD-95885 displayed five to ninefold higher BBB penetration than [^{11}C]27. However, the distribution was almost homogeneous in all brain structures studied. Pretreatment with nonradioactive 27 or ifenprodil led to a considerable reduction in brain uptake of [^{11}C]EMD-95885; whereas, other site ligands such as MK-801, MDL-105,519, and DTG (1,3-di-*o*-tolylguanidine) had no blocking effect (Fig. 18.24), suggesting some specific binding in the brain tissues (Roger et al. 2004). It should be taken into consideration that the blocking effects of [^{11}C]EMD-95885 binding were observed not only in NR2B-rich regions, such as the hippocampus and frontal cortex, but also in NR2B-poor region, such as cerebellum. Although treatment with ifenprodil-like compounds resulted in a decrease of in vivo [^{11}C] EMD-95885 binding, this tracer was not a promising PET radioligand for the NR2B subunit.

The bis(phenylalkyl)amines were reported to be selective antagonists of NR1A/2B receptors. The most potent of this series, compound 29 (Fig. 18.22), has an IC_{50} value of 8 nM and >1,000-fold selectivity for NR1A/2B receptors over other subunit-containing receptors (Tamiz et al. 1998). Thus, two ^{11}C -labeled analogs of bis(phenylalkyl)amine, bis(phenylpropyl)amine ([^{11}C]30) and bis(phenylbutyl)amine ([^{11}C]31), were synthesized and evaluated by Sasaki et al.

These [^{11}C]-ligands were prepared by *O*-methylation on the corresponding diphenol precursors with [^{11}C]CH $_3$ I with a specific activity of around 75 GBq/ μmol . In the in vitro autoradiography studies, both [^{11}C]**30** and [^{11}C]**31** displayed almost homogeneous distribution throughout the brain. Treatment with nonradioactive **30** and **31** led to only 50 and 40 % reduction in the in vitro binding of [^{11}C]**30** and [^{11}C]**31**, respectively. Both spermine and ifenprodil caused 30–40 % reduction of these tracers, which indicated that these bis(phenylalkyl)amines shared the binding site with ifenprodil. Further in vivo studies in rodents demonstrated that [^{11}C]**30** exhibited homogenous accumulation and non-labeled **30** increased the brain uptake. Because of the high nonspecific binding both in vitro and in vivo, [^{11}C]**30** and [^{11}C]**31** are unsuitable radiotracers for NR1A/2B receptors (Sasaki et al. 2004). A new series of benzimidazole derivatives such as compound **32** [K_i = 1.5 nM vs [^3H]{(*E*)-*N* 1 -(2-methoxybenzyl) cinnamidine (compound **36** as described below)}] was developed as highly potent NR2B antagonists (McCauley et al. 2004). Based on the article, we developed 4'-radioiodinated benzimidazoles as SPECT imaging agents for the NR2B subunit. The compounds **33** and **34** showed high affinity for NR2B subunit with K_i values of 7.3 nM and 5.8 nM, respectively (vs [^3H]ifenprodil). In vitro autoradiography revealed that both [^{125}I]**33** and [^{125}I]**34** exhibited high accumulation in the forebrain regions but low in the cerebellum as shown in Fig. 18.25a. These regional distributions of the radioligands were consistent with the expression of the NR2B subunit. The in vitro binding of these tracers was blocked by NR2B antagonist but not by other site ligands, which suggested the high selectivity of [^{125}I]**33** and [^{125}I]**34** for the NR2B subunit. However, the specific binding of these [^{125}I]benzimidazoles were lower than CP-101,606 analog [^{11}C]**26** as shown in Fig. 18.25b probably due to high lipophilicity of these [^{125}I]ligands. In mice, [^{125}I]**33** and [^{125}I]**34** showed moderate brain uptake at 5–180 min after administration (0.42–0.56 % and 0.44–0.67 % ID/g, respectively). The brain-to-blood ratio of [^{125}I]**33** led to 34 % reduction in the presence of nonradioactive **33** and 59 % reduction in the presence of the NR2B ligand Ro 25–6981 as shown in Fig. 18.25c. Although these radioligands showed poor BBB permeability and inconsistent distribution with NR2B subunit, [^{125}I]**33** may be partially bound to the NR2B subunit under in vivo conditions. Compound **33** may be a potential scaffold for further structural modification in order to develop potential imaging probes for the NR2B subunit-containing NMDARs (Fuchigami et al. 2010). More recently, high-affinity NR2B antagonists benzimidazole derivative (**35**, Fig. 18.22) and RGH-896 (Fig. 18.22) were successfully labeled with ^{18}F by an aromatic nucleophilic radiofluorination followed by a reduction of the para-position carbonyl function (Labas et al. 2011). Despite modification of synthetic conditions, both [^{18}F]**35** and [^{18}F]RGH-896 were obtained with poor specific activities of 1.7 and 1.2 GBq/ μmol , respectively. In vivo brain uptakes of [^{18}F]**35** or [^{18}F]RGH-896 in rats were quite low at 120 min after injection of radiotracers (0.035 and 0.054 % ID/g, respectively). High accumulation of radioactivity in the bone and further metabolic analysis of [^{18}F]fluorobenzyl piperidine fragment implicated that [^{18}F]**35** and [^{18}F]RGH-896 seemed to be rapidly defluorinated by hydroxylation in the benzyl ring followed by glucuronidation (Labas et al. 2011).

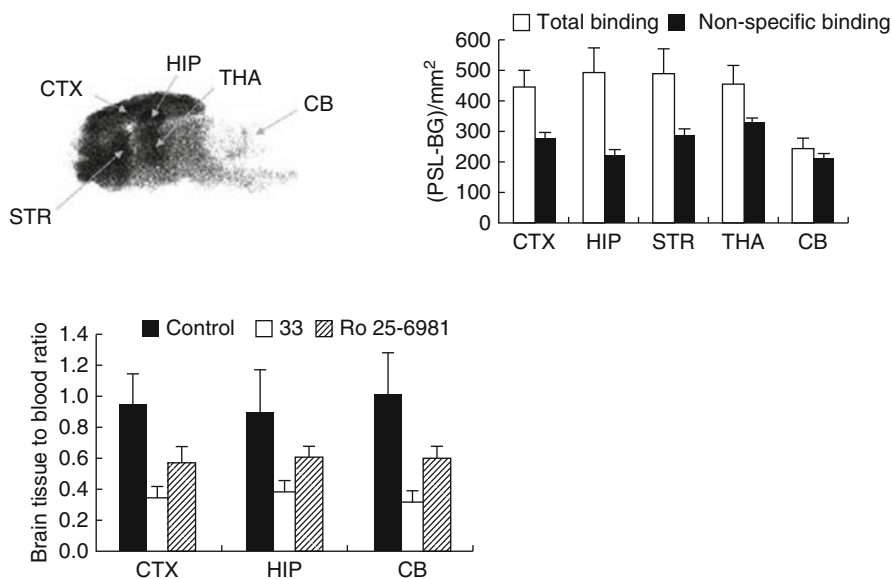


Fig. 18.25 (a) In vitro autoradiogram of [¹²⁵I]**33** in sagittal sections of rat brain. (b) Quantified values of the autoradiogram in cerebral cortex (CTX), hippocampus (HIP), striatum (STR), thalamus (THA), and cerebellum (CB). Nonspecific binding was determined in the presence of nonradioactive **33** (10 μM). (c) Effect of nonradioactive **33** and Ro 25–6981 (NR2B antagonist) on the brain tissue to blood ratio in mice at 180 min after intravenous injection of [¹²⁵I]**33**. Drugs were pretreated 30 min before the tracer injection. * $P < 0.01$ in comparison to the control group (Fuchigami et al. 2010)

18.4.2 Non-ifenprodil-Related NR2B Antagonist Derivatives

A series of 2-(3,4-dihydro-1H-isoquinolin-2-yl)-pyridines have been identified as a new class of selective NR1/2B NMDAR antagonists. Among them, Ro-647312 (Fig. 18.26) displayed high affinity and selectivity for NR2B-containing NMDARs ($K_i = 8$ nM vs [³H]Ro 25–6981) (Büttelmann et al. 2003). The [¹¹C]Ro-647312 was synthesized using [¹¹C]methyl triflate from the nor-methyl compound with a specific activity of 37–129 GBq/μmol. Biodistribution studies of [¹¹C]Ro-647312 in rats demonstrated that the distribution of radioactivity was homogeneous in all brain structures, which correlated poorly with known distribution of NR2B subunits (Dollé et al. 2004). Benzylamidines were discovered as novel series of highly potent NR2B-selective NMDAR antagonists. From this series, (*E*)-styrene derivative (**36**, Fig. 18.26) and 2-naphthyl derivative (**37**, Fig. 18.26) displayed excellent high affinity for NR2B subunit with K_i value of 0.7 and 1.3 nM (vs [³H]ifenprodil), respectively (Curtis et al. 2003; Claiborne et al. 2003). The 4-trifluoromethoxyphenyl derivative (**38**, Fig. 18.26) was identified as a highly potent NR2B antagonist with K_i value of 5.7 nM as determined by patch-clamp experiments of NR1a/NR2B

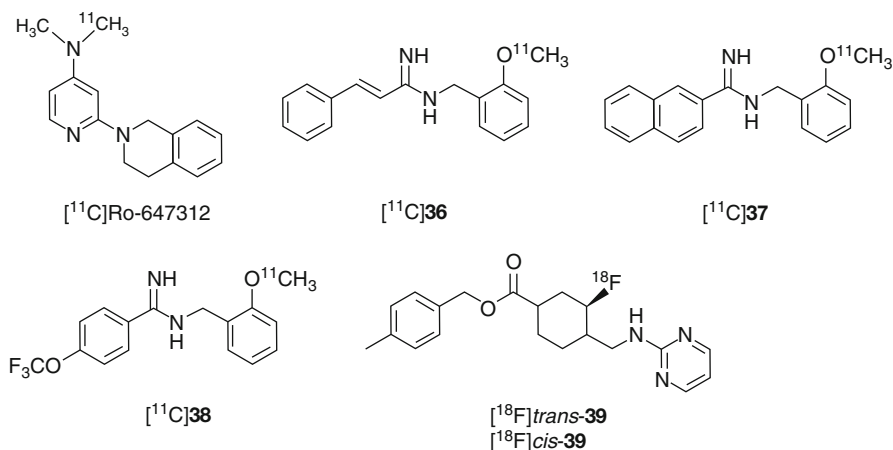


Fig. 18.26 Chemical structure of radiolabeled non-ifenprodil-related derivatives

receptors (Claiborne et al. 2003). The [¹¹C]-ligands were prepared from hydroxyl precursors with [¹¹C]CH₃I, which led to the specific activity of more than 74 GBq/μmol. In vitro autoradiography studies showed consistent brain localization of [¹¹C]38 with distribution of NR2B subunit. In addition, the in vitro binding of [¹¹C]38 was strongly inhibited (over 75 %) by nonradioactive 38 and ifenprodil (100 μM) (Fig. 18.27), which suggested the high specific binding toward NR2B subunit-containing NMDARs. The [¹¹C]36 and [¹¹C]37 showed moderate initial brain uptake (about 1.0 % ID/g at 5 min), while [¹¹C]38 exhibited higher brain uptake with 1.8 % ID/g. Metabolite analysis demonstrated that only 31 and 37 % of intact [¹¹C]36 and [¹¹C]37, respectively, were detected in the brain; whereas, 49 % of authentic [¹¹C]38 remained in the brain at 40 min. Because of metabolic instability, it can be stated that these radiotracers are unsuitable imaging agents for the NR2B subunit (Arstad et al. 2006). Our independent studies of [¹¹C]36 and [¹¹C]37 agreed with the study by Arstad et al. The percentage of unchanged radioligands was very low not only in the blood but also in the brain. These data implicated that the metabolite of the radiotracers could enter the brain tissue. Indeed, radio TLC analysis of [¹¹C]37 in the whole brain demonstrated that the metabolite deemed as the amide derivative of [¹¹C]37, which could pass easily through BBB, was detected (Haradahira et al. 2005). MK-0657 (Fig. 18.26) was reported as a highly potent NR2B antagonist (IC₅₀=3.6 nM). Clinical trial of MK-0657 has begun for the treatment of neuropathic pain, Parkinson's disease and major depression (Mony et al. 2009; Addy et al. 2009). Most recently, two radiofluorinated diastereoisomers of MK-0657 ([¹⁸F]trans-39 and [¹⁸F]cis-39) have been developed as PET radioligands for NR2B subunit. Radiofluorination of these tracers were achieved by a one-step nucleophilic substitution reaction of the mesylate precursor with specific radioactivities of 236 and 170 GBq/μmol for [¹⁸F]trans-50 and [¹⁸F]cis-39, respectively. Both ligands displayed high affinity for NR2B subunit

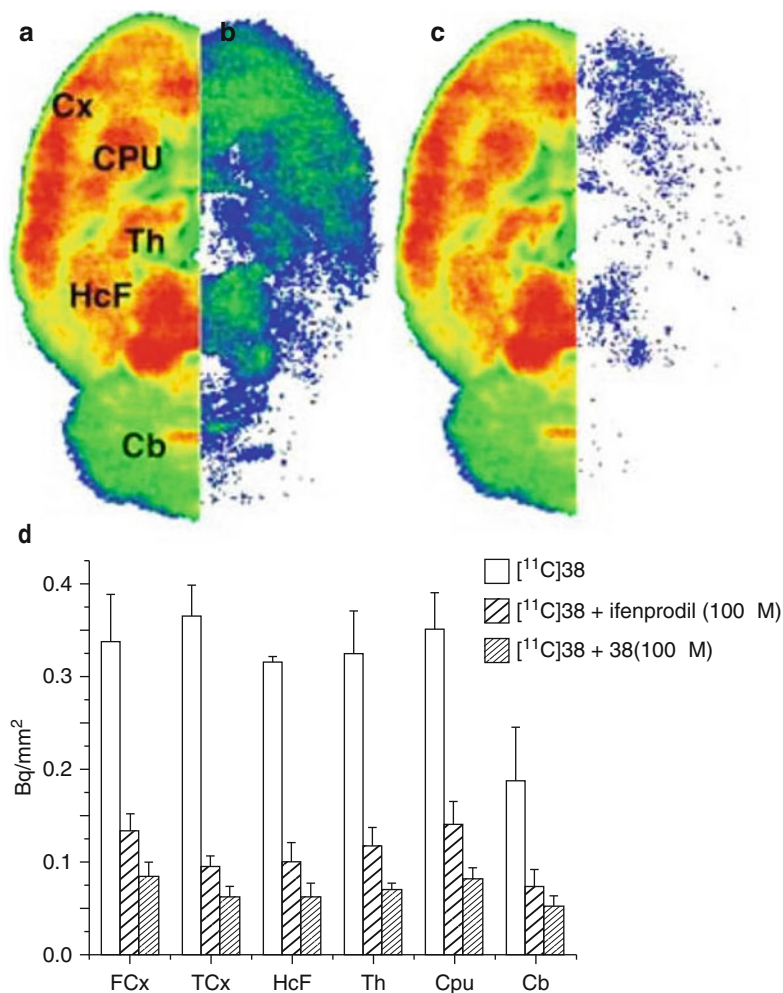


Fig. 18.27 In vitro autoradiogram of [¹¹C]38 in sagittal sections of rat brain, under control conditions (a), in the presence of 100 μM ifenprodil (b) or nonradioactive 49 (c), and quantified values of the autoradiogram under the above three conditions (d). Abbreviations. Cx cortex, FCx frontal cortex, TCx temporal cortex, Cpu caudate putamen, Th thalamus, HcF hippocampal formation, Cb cerebellum (Arstad et al. 2006)

with K_d values ranging from 1.9 to 7.1 nM for [¹⁸F]trans-39 and 5.9–15.2 nM for [¹⁸F]cis-39, respectively. In vitro autoradiography experiments on rat brain slices showed similar localization of [¹⁸F]trans-39 and [¹⁸F]cis-39 to the known distribution pattern of NR2B subunit as shown in Fig. 18.28a, b. The in vitro binding of these ligands was strongly inhibited by Ro 25–6981 (10 μM), which led to low nonspecific binding in all brain regions as shown in Fig. 18.28c (Koudih et al. 2012). These promising in vitro results could lead to further in vivo evaluation of [¹⁸F]trans-39 and [¹⁸F]cis-39 in the future.

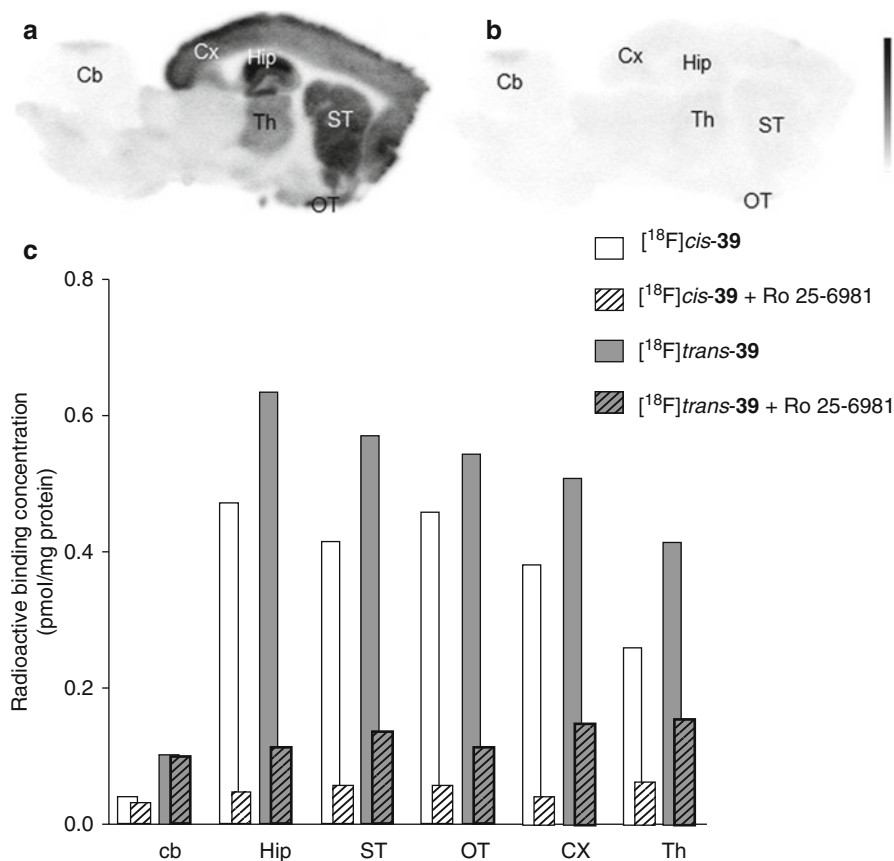


Fig. 18.28 In vitro autoradiogram of [¹⁸F]cis-39 in sagittal sections of rat brain, under control conditions (a), in the presence of 10 μM Ro 25-6981 (b). Radioligands concentration in brain structure after in vitro binding of [¹⁸F]cis-39 or [¹⁸F]trans-39 alone or co-incubation with Ro 25-6981 (10 μM) on rat brain sections (c). Abbreviations: Cb cerebellum, Cx cortex, Hip hippocampus, ST striatum, OT olfactory tubercle, Th thalamus (Koudih et al. 2012)

18.5 Conclusion and Perspectives

Despite considerable efforts, no radioligands have been confirmed as potential in vivo imaging agents for NMDARs by PET or SPECT imaging. Because NMDARs form complex systems with ligand-gated ion channels including two agonist-binding sites, a transmembrane ion permeation pore, and various allosteric modulators binding sites, it could be difficult to apply the strategy of developing radioligands for other neurotransmitter receptors that can be successfully visualized by PET or SPECT imaging.

Initially developed radiolabeled dissociative anesthetic derivatives, which are noncompetitive NMDAR open channel blockers, were shown to exhibit high

nonspecific in vivo accumulation probably due to high lipophilicity and/or lack of selectivity for NMDARs. Among these dissociative anesthetics, only MK-801 has been confirmed as a NMDAR-specific ligand (Wong et al. 1986). Although several radiolabeled MK-801 derivatives showed consistent in vitro brain localization with NMDAR expression, these ligands exhibited high nonspecific binding under in vivo conditions. It should be noted that [^3H]MK-801 exhibited high specific binding (78 %) in vivo if the brain tissue was homogenized, filtered, and washed. In addition, the specific binding was abolished by omission of the washing procedures (Price et al. 1988). These results indicated that although [^3H]MK-801 has a certain in vivo-specific binding component to NMDARs, the high adsorption property of this ligand on brain tissue may hamper in vivo imaging of NMDARs, probably owing to high lipophilicity of [^3H]MK-801. Radiolabeled MK-801 derivatives with optimized lipophilicity and binding affinity for the PCP-binding site may be potential imaging agents for NMDARs. Radiolabeled diarylguanidine derivatives were developed as more hydrophilic imaging agents for the PCP-binding site of NMDARs. In vivo studies of ischemic rats demonstrated that pathological activation of NMDARs led to an increase in [^{125}I]CNS 1261 binding (Owens et al. 2000). However, the possibility that this change was caused by change in cerebral blood flow and/or input function of these tracers could not be excluded. In vivo displacement effect of open channel blockers for [$^{123/125}\text{I}$]CNS 1261 binding in the brain tissues has not yet been confirmed. In addition, rapid in vivo metabolism of [^{125}I]CNS 1261 (half-life: 2.2 min in rat plasma) should be taken into consideration (Owens et al. 2000). Nevertheless, altered in vivo pharmacokinetics of [^{123}I]CNS 1261 in patients with schizophrenia compared with healthy controls was noteworthy (Pilowsky et al. 2006). Radiolabeled diarylguanidine derivatives with high metabolic stability could be attractive imaging agent candidates for the PCP-binding site of NMDARs. Because it is suggested that only 30 % NMDARs are under open states (Jahr 1992), imaging PCP-binding site by such activity dependent-binding radioligands would be difficult. Nonetheless, further studies on the development of new imaging probes for the PCP-binding site should be undertaken. Radioligands for this site could detect activated NMDARs in the living brain including various brain disorders.

Another possibility is that the poor in vivo results of radioligands for the PCP-binding site could be caused by their restricted in vivo access to the inside of the ion channel. Compared with the PCP-binding site, glycine- and ifenprodil-binding sites were reported to be located outside of the receptor. Accordingly, these two sites have been considered as attractive targets for visualization of NMDARs by PET or SPECT imaging.

Several radioligands for the glycine-binding site showed promising in vitro results. In contrast, in vivo results revealed quite low brain uptake and unusual cerebellar localization of these tracers. The difference between in vitro and in vivo studies could be explained by the influence by endogenous glycine site agonists. The in vivo binding of [^{11}C]L-703,717 was strongly affected by endogenous D-SERINE concentration (Haradahira et al. 2003). On the other hand, in most of the in vitro experiments, brain slices or homogenates were well washed, which resulted

in the removal of endogenous glycine and D-serine. Considering these results, we hypothesized that the agonist-insensitive radioligands with high affinity for glycine site radioligands could be useful for in vivo imaging of NMDARs. Fuchigami and Magata et al. developed high-affinity “agonist-insensitive” glycine site ligand [^{11}C]23, but BBB passage was too low to obtain reliable in vivo results (Fuchigami et al. 2008). Further investigations should be carried out for the development of new imaging probes with high BBB penetration to allow for the binding mechanism of glycine antagonists to be identified.

Radioligands for the ifenprodil-binding site showed consistent localization with the expression of NR2B subunit and high specificity to NR2B-rich region only under in vitro condition but not in vivo. It is suggested that ifenprodil could exhibit higher affinity for the agonist-bound activated or desensitized state of NMDARs relative to the agonist-unbound state (Kew et al. 1996). It is demonstrated that neuroprotective effects of NR2B antagonists were much more potent at pH=6.5 than at pH=7.5 (Mott et al. 1998). In the ischemic tissue with NMDAR-activated state, pH value was reported to be around 6.5 (Silver and Erecińska 1992). Therefore, it is possible that the radioligands for the ifenprodil-binding site could recognize only agonist-bound and/or activated NMDAR-like PCP-binding site ligands. Nonetheless, new radioligands with optimized lipophilicity, metabolic stability, and binding affinity could show different pharmacokinetics from reported radioligands. Continuous efforts should be undertaken in order to develop promising in vivo imaging agents for the ifenprodil-binding site. Although benzimidazole derivative [^{125}I]33 showed inconsistent in vivo localization with NR2B subunit expression, this tracer could exhibit partial specific binding for NR2B subunit (Fuchigami et al. 2010). Further SAR studies of benzimidazoles could provide promising radioligands for the ifenprodil-binding site of NMDARs. Radiolabeled benzylamidines showed excellent high specific binding for the NR2B subunit under in vitro conditions (Arstad et al. 2006). Optimized benzylamine derivatives with high metabolic stability and moderate lipophilicity could be attractive imaging probe candidates for ifenprodil-binding site of NMDARs. Recently, new series of antagonists for the ifenprodil-binding site, such as MK-0657 and HON0001, were reported (Suetake-Koga et al. 2006; Addy et al. 2009). Indeed, [^{18}F] labeled MK-0657 derivatives showed promising in vitro results (Koudih et al. 2012). New generation radioligands could be potential in vivo imaging agents for NR2B subunit-containing NMDARs.

In general, higher B_{\max}/K_d of radioligands could give higher target-to-nontarget (T/N) binding ratios. Eckelman et al. suggested that PET tracers should have B_{\max}/K_d ratio greater than 10 to provide a useful specific in vivo signal (Eckelman et al. 1979, 2006). B_{\max} values of the PCP-binding site in the dentate gyrus of the rat brain and CA1 stratum radiatum of the human brain using [^3H]MK-801 were demonstrated to be 173 and 141 fmol/mg protein, respectively (Bowery et al. 1988). Accordingly, K_d values below 1.73 and 1.41 nM may be required for PCP-binding site ligands in the rat and human brain, respectively, to obtain a B_{\max}/K_d ratio over 10. The B_{\max} value of the glycine-binding site in rat brain membranes using [^3H] MDL 105,519 was calculated to be 12.1 pmol/mg protein (Baron et al. 1996).

Therefore, a K_d below 121 nM may be required for glycine-binding site ligands in the rat brain to obtain a B_{\max}/K_d ratio over 10. The B_{\max} value of the ifenprodil-binding site in rat brain membranes using [^3H]Ro 25-6981 was estimated to be 1.6 pmol/mg protein (Mutel et al. 1998). Thus, a K_d below 16 nM may be required for glycine-binding site ligands in the rat brain to obtain a B_{\max}/K_d ratio over 10. Although several radioligands for NMDARs met the above conditions, numerous factors decrease the reliability of in vivo images such as the low plasma-free fraction of radioligands and Pgp efflux. It has been suggested that radiotracers with low molecular weight (<500 Da) and moderate lipophilicity (log $D_{7.4}$ values; 2.0–3.5) could have optimal BBB permeability (Waterhouse 2003b; Pike 2009). Therefore, newly developed radioligands should be at least within the above range. Furthermore, exhaustive binding assays of these ligands for various receptors and transporters expressed in the brain should be carried out to screen NMDAR-specific radioligands.

Another interpretation is that the discrepancy between the in vitro and in vivo brain localization of radioligands for NMDARs could be caused by dynamic plasticity of NMDARs. It has been suggested that considerable structural change of NMDARs occurs following binding of both endogenous agonists and exogenous ligands (Traynelis et al. 2010). It is reported that the number of NMDARs on the cell surface frequently changed by tyrosine phosphorylation and/or cysteine palmitoylation of C-terminus of NMDARs with an alteration in subunit composition (Vallano et al. 1996; Roche et al. 2001; Hayashi et al. 2009). Further investigations, such as in vivo imaging studies of genetically modified or drug-treated animals with various conditions of NMDARs would be needed to clarify the discrepancy between the in vitro and in vivo experiments. In addition, novel screening systems other than traditional in vitro assays should be used. Using living brain slices as a screening method (Matsumura et al. 1995) may lead to the development of promising radioligands for NMDARs.

References

- Addy C, Assaid C, Hreniuk D et al (2009) Single-dose administration of MK-0657, an NR2B-selective NMDA antagonist, does not result in clinically meaningful improvement in motor function in patients with moderate Parkinson's disease. *J Clin Pharmacol* 49:856–864
- Ahmed I, Bose SK, Pavese N et al (2011) Glutamate NMDA receptor dysregulation in Parkinson's disease with dyskinesias. *Brain* 134:979–986
- Akazawa C, Shigemoto R, Bessho Y et al (1994) Differential expression of five N-methyl-D-aspartate receptor subunit mRNAs in the cerebellum of developing and adult rats. *J Comp Neurol* 347:150–160
- Ametamey SM, Kocic M, Carrey-Rémy N et al (2000) Synthesis, radiolabelling and biological characterization of (D)-7-iodo- N-(1-phosphonoethyl)-5- aminomethylquinoxaline-2,3-dione, a glycine-binding site antagonist of NMDA receptors. *Bioorg Med Chem Lett* 10:75–78
- Ametamey SM, Bruehlmeier M, Kneifel S et al (2002) PET studies of ^{18}F -memantine in healthy volunteers. *Nucl Med Biol* 29:227–231
- Andersson Y, Tyrefors N, Sihver S et al (1998) Synthesis of a ^{11}C -labelled derivative of the N-Methyl-D-Aspartate receptor antagonist MK-801. *J Label Compd Radiopharm* 41:567–576

- Anis NA, Berry SC, Burton NR et al (1983) The dissociative anaesthetics, ketamine and phencyclidine, selectively reduce excitation of central mammalian neurones by N-methyl-aspartate. *Br J Pharmacol* 79:565–575
- Arstad E, Platzer S, Berthele A et al (2006) Towards NR2B receptor selective imaging agents for PET-synthesis and evaluation of N-[¹¹C]-(2-methoxy)benzyl (E)-styrene-, 2-naphthyl- and 4-trifluoromethoxyphenylamidine. *Bioorg Med Chem* 14:6307–6313
- Asselin MC, Hammer A, Turton D et al (2004) Initial kinetic analysis of the in vivo binding of the putative NMDA receptor ligand [¹¹C]CNS 5161 in humans. *Neuroimage* 22:T137
- Auberson YP, Acklin P, Bischoff S et al (1999) N-phosphonoalkyl-5-aminomethylquinoline-2,3-diones: in vivo active AMPA and NMDA(glycine) antagonists. *Bioorg Med Chem Lett* 9:249–254
- Baron BM, Siegel BW, Harrison BL et al (1996) [³H]MDL 105,519, a high-affinity radioligand for the N-methyl-D-aspartate receptor-associated glycine recognition site. *J Pharmacol Exp Ther* 279:62–68
- Barta-Szalai G, Borza I, Bozó E et al (2004) Oxamides as novel NR2B selective NMDA receptor antagonists. *Bioorg Med Chem Lett* 14:3953–3956
- Bauman A, Piel, M, Höhnemann S et al (2011) Synthesis, labelling and evaluation of hydantoin-substituted indole carboxylic acids as potential ligands for positron emission tomography imaging of the glycine binding site of the N-methyl-d-aspartate receptor. *J Label Compd Radiopharm* 54:645–656
- Biegon A, Gibbs A, Alvarado M et al (2007) In vitro and in vivo characterization of [³H]CNS-5161-a use-dependent ligand for the N-methyl-D-aspartate receptor in rat brain. *Synapse* 61:577–586
- Blin J, Denis A, Yamaguchi T et al (1991) PET studies of [¹⁸F]methyl-MK-801, a potential NMDA receptor complex radioligand. *Neurosci Lett* 121:183–186
- Bowery NG, Wong EH, Hudson AL (1988) Quantitative autoradiography of [³H]-MK-801 binding sites in mammalian brain. *Br J Pharmacol* 93:944–954
- Bressan RA, Erlandsson K, Mulligan RS et al (2004) A bolus/infusion paradigm for the novel NMDA receptor SPET tracer [¹²³I]CNS 1261. *Nucl Med Biol* 31:155–164
- Bressan RA, Erlandsson K, Stone JM et al (2005) Impact of schizophrenia and chronic antipsychotic treatment on [¹²³I]CNS-1261 binding to N-methyl-D-aspartate receptors in vivo. *Biol Psychiatry* 58:41–46
- Brown DR, Wyper DJ, Owens J et al (1997) ¹²³Iodo-MK-801: a SPECT agent for imaging the pattern and extent of glutamate (NMDA) receptor activation in Alzheimer's disease. *J Psychiatr Res* 31:605–619
- Büttelmann B, Alanine A, Bourson A et al (2003) 2-(3,4-Dihydro-1H-isoquinolin-2yl)-pyridines as a novel class of NR1/2B subtype selective NMDA receptor antagonists. *Bioorg Med Chem Lett* 13:829–832
- Calon F, Rajput AH, Hornykiewicz O et al (2003) Levodopa-induced motor complications are associated with alterations of glutamate receptors in Parkinson's disease. *Neurobiol Dis* 14:404–416
- Chaudieu I, Vignon J, Chicheportiche M et al (1989) Role of the aromatic group in the inhibition of phencyclidine binding and dopamine uptake by PCP analogs. *Pharmacol Biochem Behav* 32:699–705
- Chazot PL (2004) The NMDA receptor NR2B subunit: a valid therapeutic target for multiple CNS pathologies. *Curr Med Chem* 11:389–396
- Claiborne CF, McCauley JA, Libby BE et al (2003) Orally efficacious NR2B-selective NMDA receptor antagonists. *Bioorg Med Chem Lett* 13:697–700
- Clineschmidt BV, Martin GE, Bunting PR (1982) Anticonvulsant activity of (+)-5-methyl-10,11-dihydro-5H-dibenzof[a, d]cyclohepten-5, 10-imine (MK-801), a substance with potent anticonvulsant, central sympathomimetic, and apparent anxiolytic properties. *Drug Dev Res* 2:123–134
- Contreras PC, Bremer ME, Gray NM (1990) Ifenprodil and SL 82.0715 potently inhibit binding of [³H](+)-3-PPP to sigma binding sites in rat brain. *Neurosci Lett* 116:190–193

- Curtis NR, Diggle HJ, Kulagowski JJ et al (2003) Novel N¹-(benzyl)cinnamamide derived NR2B subtype-selective NMDA receptor antagonists. *Bioorg Med Chem Lett* 13:693–696
- Danysz W, Parsons CG (1998) Glycine and N-methyl-D-aspartate receptors: physiological significance and possible therapeutic applications. *Pharmacol Rev* 50:597–664
- Di Fabio R, Capelli AM, Conti N et al (1997) Substituted indole-2-carboxylates as in vivo potent antagonists acting as the strychnine-insensitive glycine binding site. *J Med Chem* 40:841–850
- Dingledine R, Borges K, Bowie D et al (1999) The glutamate receptor ion channels. *Pharmacol Rev* 51:7–61
- Dollé F, Valette H, Demphel S et al (2004) Radiosynthesis and in vivo evaluation of [¹¹C] Ro-647312: a novel NR1/2B subtype selective NMDA receptor radioligand. *J Label Compd Radiopharm* 47:911–920
- Dumont F, Slegers G (1997) Synthesis and in vivo evaluation of 7-chloro-5-[¹²³I]iodo-4-oxo-1,4-dihydroquinoline-2-carboxylic acid. *Appl Radiat Isot* 48:1173–1177
- Dumont F, Sultana A, Waterhouse RN (2002) Synthesis and in vitro evaluation of N,N'-diphenyl and N-naphthyl-N'-phenylguanidines as N-methyl-D-aspartate receptor ion-channel ligands. *Bioorg Med Chem Lett* 12:1583–1586
- Eckelman WC, Gibson RE, Rzeszotarski WJ et al (1979) The design of receptor binding radiotracers. In: *Principles of radiopharmacology*. CRC Press, New York, pp 251–274
- Eckelman WC, Kilbourn MR, Mathis CA (2006) Discussion of targeting proteins in vivo: in vitro guidelines. *Nucl Med Biol* 33:449–451
- Erlandsson K, Bressanb RA, Mulligana RS et al (2003) Kinetic modelling of [¹²³I]CNS 1261—a potential SPET tracer for the NMDA receptor. *Nucl Med Biol* 30:441–454
- Forst T, Smith T, Schütte K et al (2007) CNS 5161 Study Group. Dose escalating safety study of CNS 5161 HCl, a new neuronal glutamate receptor antagonist (NMDA) for the treatment of neuropathic pain. *Br J Clin Pharmacol* 64:75–82
- Foster AC, Wong EH (1987) The novel anticonvulsant MK-801 binds to the activated state of the N-methyl-D-aspartate receptor in rat brain. *Br J Pharmacol* 91:403–409
- Fuchigami T, Haradahira T, Arai T et al (2003) Synthesis and brain regional distribution of [¹¹C] NPS 1506 in mice and rat: an N-methyl-D-aspartate (NMDA) receptor antagonist. *Biol Pharm Bull* 26:1570–1573
- Fuchigami T, Haradahira T, Fujimoto N et al (2008) Difference in brain distributions of carbon 11-labeled 4-hydroxy-2(1H)-quinolones as PET radioligands for the glycine-binding site of the NMDA ion channel. *Nucl Med Biol* 35:203–212
- Fuchigami T, Haradahira T, Fujimoto N et al (2009) Development of N-[¹¹C] methylamino 4-hydroxy-2(1H)-quinolone derivatives as PET radioligands for the glycine-binding site of NMDA receptors. *Bioorg Med Chem* 17:5665–5675
- Fuchigami T, Yamaguchi H, Ogawa M et al (2010) Synthesis and biological evaluation of radioiodinated benzimidazoles as SPECT imaging agents for NR2B subtype of NMDA receptor. *Bioorg Med Chem* 18:7497–7506
- Furukawa H, Gouaux E (2003) Mechanisms of activation, inhibition and specificity: crystal structures of the NMDA receptor NR1 ligand-binding core. *EMBO J* 22:2873–2885
- Furukawa H, Singh SK, Mancusso R et al (2005) Subunit arrangement and function in NMDA receptors. *Nature* 438:185–192
- Gogas KR (2006) Glutamate-based therapeutic approaches: NR2B receptor antagonists. *Curr Opin Pharmacol* 6:68–74
- Grauert M, Bechtel WD, Ensinger HA et al (1997) Synthesis and structure-activity relationships of 6,7-benzomorphan derivatives as antagonists of the NMDA receptor-channel complex. *J Med Chem* 40:2922–2930
- Grauert M, Rho JM, Subramaniam S et al (1998) N-methyl-D-aspartate receptor channel block by the enantiomeric 6,7-benzomorphans BIII 277 CL and BIII 281 CL. *J Pharmacol Exp Ther* 285:767–776
- Grimwood S, Richards P, Murray F et al (2000) Characterisation of N-methyl-D-aspartate receptor-specific [³H]ifenprodil binding to recombinant human NR1a/NR2B receptors compared with native receptors in rodent brain membranes. *J Neurochem* 75:2455–2463

- Haradahira T, Sasaki S, Maeda M et al (1998) Synthesis and brain distribution of carbon-11 labeled analogs of antagonists for the NMDA receptor coupled PCP-binding site. *J Label Compd Radiopharm* 41:843–858
- Haradahira T, Suzuki K et al (1999) An improved synthesis of [¹¹C]L-703,717 as a radioligand for the glycine site of the NMDA receptor. *Nucl Med Biol* 26:245–247
- Haradahira T, Zhang M, Maeda J et al (2000) A strategy for increasing the brain uptake of a radioligand in animals: use of a drug that inhibits plasma protein binding. 27:357–360
- Haradahira T, Zhang MR, Maeda J et al (2001) A prodrug of NMDA/glycine site antagonist, L-703,717, with improved BBB permeability: 4-acetoxy derivative and its positron-emitter labeled analog. *Chem Pharm Bull (Tokyo)* 49:147–150
- Haradahira T, Maeda J, Okauchi T et al (2002a) Synthesis, in vitro and in vivo pharmacology of a C-11 labeled analog of CP-101,606, (+/-)threo-1-(4-hydroxyphenyl)-2-[4-hydroxy-4-(p-[¹¹C] methoxyphenyl)piperidino]-1-propanol, as a PET tracer for NR2B subunit-containing NMDA receptors. *Nucl Med Biol* 29:517–525
- Haradahira T, Okauchi T, Maeda J et al (2002b) A positron-emitter labeled glycine(B) site antagonist, [¹¹C]L-703,717, preferentially binds to a cerebellar NMDA receptor subtype consisting of GluR epsilon3 subunit in vivo, but not in vitro. *Synapse* 43:131–133
- Haradahira T, Sahara S, Okauchi T et al (2002c) Developments of PET radioligands for NMDA receptors. *World J Nucl Med* 1:S183–S184
- Haradahira T, Okauchi T, Maeda J et al (2003) Effects of endogenous agonists, glycine and D-serine, on in vivo specific binding of [¹¹C]L-703,717, a PET radioligand for the glycine-binding site of NMDA receptors. *Synapse* 50:130–136
- Haradahira T, Fuchigami T, Fujimoto N et al (2005) In vitro and in vivo binding characteristics of C-11 labeled antagonists for NR2B subunit of NMDA receptors. *J Label Compd Radiopharm* 48(suppl. 1):S92
- Hartvig P, Valtysson J, Antoni G et al (1994) Brain kinetics of (R)- and (S)-[N-methyl-¹¹C]ketamine in the rhesus monkey studied by positron emission tomography (PET). *Nucl Med Biol* 21:927–934
- Hashimoto K, London ED (1995) Interactions of erythro-ifenprodil, threo-ifenprodil, erythro-iodifenprodil, and eliprodil with subtypes of sigma receptors. *Eur J Pharmacol* 273:307–310
- Hashimoto A, Nishikawa T, Oka T et al (1993) Endogenous D-serine in rat brain: N-methyl-D-aspartate receptor-related distribution and aging. *J Neurochem* 60:783–786
- Hayashi T, Thomas GM, Haganir RL (2009) Dual palmitoylation of NR2 subunits regulates NMDA receptor trafficking. *Neuron* 64:213–226
- Hu LY, Guo J, Magar SS et al (1997) Synthesis and pharmacological evaluation of N-(2,5-disubstituted phenyl)-N'-(3-substituted phenyl)-N'-methylguanidines as N-methyl-D-aspartate receptor ion-channel blockers. *J Med Chem* 40:4281–4289
- Hynd MR, Scott HL, Dodd PR (2004) Differential expression of N-methyl-D-aspartate receptor NR2 isoforms in Alzheimer's disease. *J Neurochem* 90:913–919
- Ishibashi N, Kuwamura T, Sano H et al (2000) Synthesis and evaluation of ¹⁸F- and ¹¹C-labelled 9,10-ethanobenzo[b]quinolizinium derivatives for imaging of the NMDA receptor at the TCP-binding site. *J Label Compd Radiopharm* 43:375–383
- Jacob CP, Koutsilieri E, Bartl J (2007) Alterations in expression of glutamatergic transporters and receptors in sporadic Alzheimer's disease. *J Alzheimers Dis* 11:97–116
- Jahr CE (1992) High probability opening of NMDA receptor channels by L-glutamate. *Science* 255:470–472
- Kalia LV, Kalia SK, Salter MW (2008) NMDA receptors in clinical neurology: excitatory times ahead. *Lancet Neurol* 7:742–755
- Kantrowitz JT, Javitt DC (2010) N-methyl-D-aspartate (NMDA) receptor dysfunction or dysregulation: the final common pathway on the road to schizophrenia? *Brain Res Bull* 83(3–4):108–121
- Karakas E, Simorowski N, Furukawa H (2009) Structure of the zinc-bound amino-terminal domain of the NMDA receptor NR2B subunit. *EMBO J* 28:3910–3920
- Karakas E, Simorowski N, Furukawa H (2011) Subunit arrangement and phenylethanolamine binding in GluN1/GluN2B NMDA receptors. *Nature* 475:249–253

- Karbon EW, Patch RJ, Pontecorvo MJ et al (1990) Ifenprodil potently interacts with [^3H](+)-3-PPP-labeled sigma binding sites in guinea pig brain membranes. *Eur J Pharmacol* 176:247–248
- Kashiwagi K, Pahk AJ, Masuko T et al (1997) Block and modulation of N-methyl-D-aspartate receptors by polyamines and protons: role of amino acid residues in the transmembrane and pore-forming regions of NR1 and NR2 subunits. *Mol Pharmacol* 52:701–713
- Kemp JA, McKernan RM (2002) NMDA receptor pathways as drug targets. *Nat Neurosci* 5(Suppl):1039–1042
- Kew JN, Trube G, Kemp JA (1996) A novel mechanism of activity-dependent NMDA receptor antagonism describes the effect of ifenprodil in rat cultured cortical neurones. *J Physiol* 497:761–772
- Knol RJ, de Bruin K, van Eck-Smit BL (2009) In vivo [^{123}I]CNS-1261 binding to D-serine-activated and MK801-blocked NMDA receptors: a storage phosphor imaging study in rats. *Synapse* 63:557–564
- Köhr G (2006) NMDA receptor function: subunit composition versus spatial distribution. *Cell Tissue Res* 326:439–446
- Kokic M, Honer M, Kessler LJ et al (2002) Synthesis and in vitro and in vivo evaluation of [^{11}C]methyl-BIII277CL for imaging the PCP-binding site of the NMDA receptor by PET. *J Recept Signal Transduct Res* 22:123–139
- Koudih R, Gilbert G, Dhilly M et al (2012) Synthesis and in vitro characterization of trans- and cis-[^{18}F]-4-methylbenzyl 4-[(pyrimidin-2-ylamino)methyl]-3-fluoropiperidine-1-carboxylates as new potential PET radiotracer candidates for the NR2B subtype N-methyl-D-aspartate receptor. *Eur J Med Chem* 53C:408–415
- Kulagowski JJ, Baker R, Curtis NR et al (1994) 3'-(Arylmethyl)- and 3'-(aryloxy)-3-phenyl-4-hydroxyquinolin-2(1H)-ones: orally active antagonists of the glycine site on the NMDA receptor. *J Med Chem* 37:1402–1405
- Kuryatov A, Laube B, Betz H et al (1994) Mutational analysis of the glycine-binding site of the NMDA receptor: structural similarity with bacterial amino acid-binding proteins. *Neuron* 12:1291–1300
- Labas R, Sobrio F, Bramoullé Y et al (2010) Radiosynthesis of N-[4-(4-fluorobenzyl) piperidin-1-yl]-N'-(2-[^{11}C]oxo-1,3-dihydrobenzimidazol-5-yl)oxamide, a NR2B-selective NMDA receptor antagonist. *J Label Compd Radiopharm* 53:63–67
- Labas R, Gilbert G, Nicole O et al (2011) Synthesis, evaluation and metabolic studies of radiotracers containing a 4-(4-[^{18}F]-fluorobenzyl)piperidin-1-yl moiety for the PET imaging of NR2B NMDA receptors. *Eur J Med Chem* 46:2295–2309
- Lau A, Tymianski M (2010) Glutamate receptors, neurotoxicity and neurodegeneration. *Pflugers Arch* 460:525–542
- Lau CG, Zukin RS (2007) NMDA receptor trafficking in synaptic plasticity and neuropsychiatric disorders. *Nat Rev Neurosci* 8:413–426
- Laube B, Kuhse J, Betz H (1998) Evidence for a tetrameric structure of recombinant NMDA receptors. *J Neurosci* 18:2954–2961
- Leeson PD, Baker R, Carling RW et al (1991) Kynurenic acid derivatives. Structure-activity relationships for excitatory amino acid antagonism and identification of potent and selective antagonists at the glycine site on the N-methyl-D-aspartate receptor. *J Med Chem* 34:1243–1252
- Leeson PD, Carling RW, Moore KW et al (1992) 4-Amido-2-carboxytetrahydroquinolines. Structure-activity relationships for antagonism at the glycine site of the NMDA receptor. *J Med Chem* 35:1954–1968
- Leibrock J, Prücher H, Rautenberg W et al (1997) EMD 95885, a new eliprodil analogue with higher affinity for the N-methyl-D-aspartate (NMDA) receptor. *Pharmazie* 52:479–480
- Lin CH, Lane HY, Tsai GE (2012) Glutamate signaling in the pathophysiology and therapy of schizophrenia. *Pharmacol Biochem Behav* 100:665–677
- Lipton SA (2004) Paradigm shift in NMDA receptor antagonist drug development: molecular mechanism of uncompetitive inhibition by memantine in the treatment of Alzheimer's disease and other neurologic disorders. *J Alzheimers Dis* 6(6 Suppl):S61–S74
- Lodge D, Johnson KM (1990) Noncompetitive excitatory amino acid receptor antagonists. *Trends Pharmacol Sci* 11:81–86

- Loo P, Braunwalder A, Lehmann J et al (1986) Radioligand binding to central phencyclidine recognition sites is dependent on excitatory amino acid receptor agonists. *Eur J Pharmacol* 123:467–468
- Low CM, Wee KS (2010) New insights into the not-so-new NR3 subunits of N-methyl-D-aspartate receptor: localization, structure, and function. *Mol Pharmacol* 78:1–11
- Malherbe P, Mutel V, Broger C et al (2003) Identification of critical residues in the amino terminal domain of the human NR2B subunit involved in the RO 25–6981 binding pocket. *J Pharmacol Exp Ther* 307:897–905
- Mallamo JP, Earley WG, Kumar V et al (1994) Identification, synthesis, and characterization of a unique class of N-methyl-D-aspartate antagonists. The 6,11-ethanobenzo[b]quinolizinium cation. *J Med Chem* 37:4438–4448
- Matsumoto R, Haradahira T, Ito H et al (2007) Measurement of glycine binding site of N-methyl-D-aspartate receptors in living human brain using 4-acetoxy derivative of L-703,717, 4-acetoxy-7-chloro-3-[3-(4-[¹¹C] methoxybenzyl) phenyl]-2(1H)-quinolone (AcL703) with positron emission tomography. *Synapse* 61:795–800
- Matsumura K, Bergström M, Onoe H et al (1995) In vitro positron emission tomography (PET): use of positron emission tracers in functional imaging in living brain slices. *Neurosci Res* 22:219–229
- McCauley JA, Theberge CR, Romano JJ et al (2004) NR2B-selective N-methyl-D-aspartate antagonists: synthesis and evaluation of 5-substituted benzimidazoles. *J Med Chem* 47:2089–2096
- Menniti F, Chenard B, Collins M et al (1997) CP-101,606, a potent neuroprotectant selective for forebrain neurons. *Eur J Pharmacol* 331:117–126
- Millan MJ (2005) N-Methyl-D-aspartate receptors as a target for improved antipsychotic agents: novel insights and clinical perspectives. *Psychopharmacology (Berl)* 179:30–53
- Mony L, Kew JN, Gunthorpe MJ et al (2009) Allosteric modulators of NR2B-containing NMDA receptors: molecular mechanisms and therapeutic potential. *Br J Pharmacol* 157:1301–1317
- Monyer H, Burnashev N, Laurie DJ et al (1994) Developmental and regional expression in the rat brain and functional properties of four NMDA receptors. *Neuron* 12:529–540
- Mori H, Mishina M (1995) Structure and function of the NMDA receptor channel. *Neuropharmacology* 34:1219–1237
- Morris HJ, Luthra SK, Brown DJ et al (1997) Synthesis of [¹¹C]L-703,717, a potential ligand for PET studies of the glycine site of the NMDA receptor. *J Label Compd Radiopharm* 40:640–641
- Mott DD, Doherty JJ, Zhang S et al (1998) Phenylethanolamines inhibit NMDA receptors by enhancing proton inhibition. *Nat Neurosci* 1:659–667
- Mueller AL, Artman LD, Balandrin MF et al (1999) NPS 1506, a novel NMDA receptor antagonist and neuroprotectant. Review of preclinical and clinical studies. *Ann N Y Acad Sci* 890:450–457
- Mutel V, Buchy D, Klingelschmidt A et al (1998) In vitro binding properties in rat brain of [³H]RO 25–6981, a potent and selective antagonist of NMDA receptors containing NR2B subunits. *J Neurochem* 70:2147–2155
- Oh JD, Russell DS, Vaughan CL et al (1998) Enhanced tyrosine phosphorylation of striatal NMDA receptor subunits: effect of dopaminergic denervation and L-DOPA administration. *Brain Res* 813:150–159
- Orita K, Sasaki S, Maeda M et al (1993) Synthesis and evaluation of 1-(1-[5-(2'-[¹⁸F]fluoroethyl)-2-thienyl]-cyclohexyl)piperidine as a potential in vivo radioligand for the NMDA receptor-channel complex. *Nucl Med Biol* 20:865–873
- Ouyang X, Mukherjee J, Yang ZY (1996) Synthesis, radiosynthesis, and biological evaluation of fluorinated thienylcyclohexyl piperidine derivatives as potential radiotracers for the NMDA receptor-linked calcium ionophore. *Nucl Med Biol* 23:315–324
- Owens J, Wyper DJ, Patterson J et al (1997) First SPET images of glutamate (NMDA) receptor activation in vivo in cerebral ischaemia. *Nucl Med Commun* 18:149–158
- Owens J, Tebbutt AA, McGregor AL et al (2000) Synthesis and binding characteristics of N-(1-naphthyl)-N'-(3-[¹²⁵I]-iodophenyl)-N'-methylguanidine ([¹²⁵I]-CNS 1261): a potential SPECT agent for imaging NMDA receptor activation. *Nucl Med Biol* 27:557–564

- Oye I, Paulsen O, Maurset A (1992) Effects of ketamine on sensory perception: evidence for a role of N-methyl-D-aspartate receptors. *J Pharmacol Exp Ther* 260:1209–1213
- Paoletti P, Neyton J (2007) NMDA receptor subunits: function and pharmacology. *Curr Opin Pharmacol* 7:39–47
- Parsons CG, Gruner R, Rozental J et al (1993) Patch clamp studies on the kinetics and selectivity of N-methyl-D-aspartate receptor antagonism by memantine (1-amino-3,5-dimethyladamantane). *Neuropharmacology* 32:1337–1350
- Piel M, Schirmacher R, Höhnemann S et al (2003) Synthesis and evaluation of 5,7-dichloro-4-(3-{4-[4-(2-[¹⁸F]fluoroethyl)-piperazin-1-yl]-phenyl}-ureido)-1,2,3,4-tetrahydroquinoline-2-carboxylic acid as a potential NMDA ligand to study glutamatergic neurotransmission in vivo. *J Label Compd Radiopharm* 46:645–659
- Pike VW (2009) PET radiotracers: crossing the blood–brain barrier and surviving metabolism. *Trends Pharmacol Sci* 30:431–440
- Pilowsky LS, Bressan RA, Stone JM et al (2006) First in vivo evidence of an NMDA receptor deficit in medication-free schizophrenic patients. *Mol Psychiatry* 11:118–119
- Price GW, Ahier RG, Middlemiss DN et al (1988) *In vivo* labelling of the NMDA receptor channel complex by [³H]MK-801. *Eur J Pharmacol* 158:279–282
- Rachline J, Le Perin-Dureau F, Goff A et al (2005) The micromolar zinc-binding domain on the NMDA receptor subunit NR2B. *J Neurosci* 25:308–317
- Ransom RW, Eng WS, Burns HD et al (1990) (+)-3-[¹²³I]Iodo-MK-801: synthesis and characterization of binding to the N-methyl-D-aspartate receptor complex. *Life Sci* 46:1103–1110
- Reddy NL, Hu LY, Cotter RE et al (1994) Synthesis and structure-activity studies of N, N'-diarylguanidine derivatives N-(1-naphthyl)-N'-(3-ethylphenyl)-N'-methylguanidine: a new, selective noncompetitive NMDA receptor antagonist. *J Med Chem* 37:260–267
- Riedel G, Platt B et al (2003) Glutamate receptor function in learning and memory. *Behav Brain Res* 140:1–47
- Robins EG, Zhao Y, Khan I et al (2010) Synthesis and in vitro evaluation of ¹⁸F-labelled S-fluoroalkyl diarylguanidines: novel high-affinity NMDA receptor antagonists for imaging with PET. *Bioorg Med Chem Lett* 20:1749–1751
- Roche KW, Standley S, McCallum J et al (2001) Molecular determinants of NMDA receptor internalization. *Nat Neurosci* 4:794–802
- Roger G, Lagnel B, Besret L et al (2003) Synthesis, radiosynthesis and in vivo evaluation of 5-[3-(4-benzylpiperidin-1-yl)prop-1-ynyl]-1,3-dihydrobenzimidazol-2-[¹¹C] one, as a potent NR_{1A}/2B subtype selective NMDA PET radiotracer. *Bioorg Med Chem* 11:5401–5408
- Roger G, Dollé F, De Bruin B et al (2004) Radiosynthesis and pharmacological evaluation of [¹¹C] EMD-95885: a high affinity ligand for NR2B-containing NMDA receptors. *Bioorg Med Chem* 12:3229–3237
- Rowley M, Kulagowski JJ, Watt AP et al (1997) Effect of plasma protein binding on in vivo activity and brain penetration of glycine/NMDA receptor antagonists. *J Med Chem* 40:4053–4068
- Samnick S, Ametamey S, Leenders KL et al (1998) Electrophysiological study, biodistribution in mice, and preliminary PET evaluation in a rhesus monkey of 1-amino-3-[¹⁸F]fluoromethyl-5-methyl-adamantane (¹⁸F-MEM): a potential radioligand for mapping the NMDA-receptor complex. *Nucl Med Biol* 25:323–330
- Sasaki S, Ishibashi N, Kuwamura T et al (1998) Excellent acceleration of the Diels-Alder reaction by microwave irradiation for the synthesis of new fluorine-substituted ligands of NMDA receptor. *Bioorg Med Chem Lett* 8:2983–2986
- Sasaki S, Kanda T, Ishibashi N et al (2001) 4,5,9,10-Tetrahydro-1,4-ethanobenz[b]quinolizine as a prodrug for its quinolizinium cation as a ligand to the open state of the TCP-binding site of NMDA receptors. *Bioorg Med Chem Lett* 11:519–521
- Sasaki S, Kurosaki F, Haradahira T et al (2004) Synthesis of ¹¹C-labelled bis(phenylalkyl)amines and their in vitro and in vivo binding properties in rodent and monkey brains. *Biol Pharm Bull* 27:531–537
- Schell MJ, Molliver ME, Snyder SH (1995) D-serine, an endogenous synaptic modulator: localization to astrocytes and glutamate-stimulated release. *Proc Natl Acad Sci U S A* 92:3948–3952

- Schell MJ, Brady RO Jr, Molliver ME et al (1997) D-serine as a neuromodulator: regional and developmental localizations in rat brain glia resemble NMDA receptors. *J Neurosci* 17:1604–1615
- Shibayama Y, Sasaki S, Tomita U et al (1996) Synthesis and evaluation of new ^{18}F -labelled thienylcyclohexylpiperidine (TCP) analogues as radioligands for the NMDA receptor-channel complex. *J Label Compd Radiopharm* 38:77–86
- Shiue CY, Vallabhahosula S, Wolf AP et al (1997) Carbon-11 labelled ketaminesynthesis, distribution in mice and PET studies in baboons. *Nucl Med Biol* 24:145–150
- Sihver S, Sihver W, Andersson Y et al (1998) In vitro and in vivo characterization of (+)-3-[^{11}C]cyano-dizocilpine. *J Neural Transm* 105:117–131
- Silver IA, Erecińska M (1992) Ion homeostasis in rat brain in vivo: intra- and extracellular [Ca^{2+}] and [H^{+}] in the hippocampus during recovery from short-term, transient ischemia. *J Cereb Blood Flow Metab* 12:759–772
- Sobrio F, Gilbert G, Perrio C et al (2010) PET and SPECT imaging of the NMDA receptor system: an overview of radiotracer development. *Mini Rev Med Chem* 10:870–886
- Stone JM, Erlandsson K, Arstad E et al (2006) Ketamine displaces the novel NMDA receptor SPET probe [^{123}I]CNS-1261 in humans in vivo. *Nucl Med Biol* 33:239–243
- Stone JM, Erlandsson K, Arstad E et al (2008) Relationship between ketamine-induced psychotic symptoms and NMDA receptor occupancy: a [^{123}I]CNS-1261 SPET study. *Psychopharmacology (Berl)* 197:401–408
- Suetake-Koga S, Shimazaki T, Takamori K et al (2006) In vitro and antinociceptive profile of HON0001, an orally active NMDA receptor NR2B subunit antagonist. *Pharmacol Biochem Behav* 84:134–141
- Tamiz AP, Whittemore ER, Zhou ZL et al (1998) Structure-activity relationships for a series of bis(phenylalkyl)amines: potent subtype-selective inhibitors of N-methyl-D-aspartate receptors. *J Med Chem* 41:3499–3506
- Traynelis SF, Wollmuth LP et al (2010) Glutamate receptor ion channels: structure, regulation, and function. *Pharmacol Rev* 62:405–496
- Tsukiyama S, Hashimoto A, Katayama S et al (1991) Fluoromethylated and hydroxymethylated derivatives of N-methyl-D-aspartate receptor antagonist 1-[1-(2-thienyl)cyclohexyl]piperidine. *Chem Pharm Bull (Tokyo)* 39:1581–1584
- Ulbrich MH, Isacoff EY (2008) Rules of engagement for NMDA receptor subunits. *Proc Natl Acad Sci U S A* 105:14163–14168
- Vallano ML, Lambolez B, Audinat E et al (1996) Neuronal activity differentially regulates NMDA receptor subunit expression in cerebellar granule cells. *J Neurosci* 16:631–639
- Vincent JP, Kartalovski B, Geneste P et al (1979) Interaction of phencyclidine (“angel dust”) with a specific receptor in rat brain membranes. *Proc Natl Acad Sci U S A* 76:4678–4682
- Vrajová M, Stastný F, Horáček J et al (2010) Expression of the hippocampal NMDA receptor GluN1 subunit and its splicing isoforms in schizophrenia: postmortem study. *Neurochem Res* 35:994–1002
- Wafford KA, Kathoria M, Bain CJ et al (1995) Identification of amino acids in the N-methyl-D-aspartate receptor NR1 subunit that contribute to the glycine-binding site. *Mol Pharmacol* 47:374–380
- Walters MR, Bradford APJ, Fischer J et al (2002) Early clinical experience with the novel NMDA receptor antagonist CNS 5161. *Br J Clin Pharmacol* 53:305–311
- Waterhouse RN (2003a) Imaging the PCP site of the NMDA ion channel. *Nucl Med Biol* 30:869–878
- Waterhouse RN (2003b) Determination of lipophilicity and its use as a predictor of blood–brain barrier penetration of molecular imaging agents. *Mol Imaging Biol* 5:376–389
- Waterhouse RN, Sultana A, Guo N et al (2002a) Synthesis and characterization of 4,6-dichloroindole-based radioligands for imaging the glycine site of the NMDA ion channel. *J Label Compd Radiopharm* 45:91–102
- Waterhouse RN, Sultana A, Laruelle M et al (2002b) In vivo evaluation of [^{11}C]-3-[2-[(3-methoxyphenylamino)carbonyl]ethenyl]-4,6-dichloroindole-2-carboxylic acid ([^{11}C]3MPICA)

- as a PET radiotracer for the glycine site of the NMDA ion channel. *Nucl Med Biol* 29:791–794
- Waterhouse RN, Slifstein M, Dumont F et al (2004) In vivo evaluation of [¹¹C]N-(2-chloro-5-thiomethylphenyl)-N'-(3-methoxy-phenyl)-N'-methylguanidine ([¹¹C] GMOM) as a potential PET radiotracer for the PCP/NMDA receptor. *Nucl Med Biol* 31:939–948
- Williams K (1993) Ifenprodil discriminates subtypes of the N-methyl-D-aspartate receptor: selectivity and mechanisms at recombinant heteromeric receptors. *Mol Pharmacol* 44:851–859
- Wong EH, Kemp JA, Priestley T et al (1986) The anticonvulsant MK-801 is a potent N-methyl-D-aspartate antagonist. *Proc Natl Acad Sci U S A* 83:7104–7108
- Wong EH, Knight AR, Woodruff GN (1988) [³H]MK-801 labels a site on the N-methyl-D-aspartate receptor channel complex in rat brain membranes. *J Neurochem* 50:274–281
- Wright JL, Gregory TF, Kesten SR et al (2000) Subtype-selective N-methyl-D-aspartate receptor antagonists: synthesis and biological evaluation of 1-(heteroarylalkynyl)-4-benzylpiperidines. *J Med Chem* 43:3408–3419
- Yao Y, Harrison CB, Freddolino PL et al (2008) Molecular mechanism of ligand recognition by NR3 subtype glutamate receptors. *EMBO J* 27:2158–2170
- Zhao Y, Robins E, Turton D et al (2006) Synthesis and characterization of N-(2-chloro-5-methylthiophenyl)-N'-(3-methylthiophenyl)-N'-[¹¹C]methylguanidine [¹¹C]CNS 5161, a candidate PET tracer for functional imaging of NMDA receptors. *J Label Compd Radiopharm* 49:163–170
- Zhou X, Zhang J, Yan C et al (2012) Preliminary studies of ^{99m}Tc-memantine derivatives for NMDA receptor imaging. *Nucl Med Biol* 39:1034–1041

Progress in PET Imaging of the Norepinephrine Transporter System

19

Yu-Shin Ding

Contents

19.1	Introduction	562
19.2	Challenges in NET Imaging of the Brain.....	562
19.2.1	NET Has a Relatively Lower Density in the Brain.....	562
19.2.2	NET Has a Widespread Distribution in the Brain.....	562
19.2.3	NET Has a Lower Contrast Between NET-Poor and NET-Rich Regions.....	563
19.2.4	The Locus Coeruleus (LC), the Highest NET Density Region, Has a Small Structure that Makes It Difficult to be Delineated and Quantitated.....	563
19.3	Translational PET Imaging Studies of NET	563
19.3.1	NET in Substance Abuse	564
19.3.2	NET in ADHD	566
19.3.3	NET in PTSD	573
19.3.4	NET in Alcohol Dependence	573
19.3.5	NET in Obesity and Brown Adipose tissue (Brown Fat).....	574
19.3.6	NET in Aging.....	575
19.3.7	Kinetic Modeling for NET Imaging Studies in Brain.....	576
19.4	Summary and Outlook	577
	References.....	579

Abstract

The norepinephrine transporter (NET) has long been recognized to play a role in various neurological and psychiatric disorders, e.g., ADHD, substance abuse, depression, alcoholism, obesity, addiction, Alzheimer's, and Parkinson's diseases. However, many of the important findings resulted from studies in vitro using postmortem tissues have never been verified via in vivo methods due to the lack of suitable radioligands, preventing the brain imaging of NET in living

Y.-S. Ding, PhD
Departments of Radiology, Psychiatry, and Chemistry,
New York University School of Medicine, New York, NY 10016, USA
e-mail: yushin.ding@nyumc.org

systems. We have identified the superiority of (*S,S*)-[¹¹C]MRB and the suitability of the MRB analogs as potential NET ligands for PET translational studies from preclinical investigation in animals to clinical research in humans. In this review article, progress in these translational research studies will be discussed, including the role of NET in ADHD, substance abuse, depression, posttraumatic stress disorder (PTSD), alcohol dependence, obesity, and aging.

19.1 Introduction

In a previous review article (Ding et al. 2006), we provided background and clinical relevance of the norepinephrine transporter (NET) to support the need to develop novel radiotracers to study the brain NET system in order to better understand its role in brain function and diseases. We also discussed the design and biological evaluation of several radioligands for imaging the brain NET system with PET. Based on these characterization studies (Ding et al. 2003, 2005; Lin et al. 2005), including C-11 labeled desipramine (DMI), 2-hydroxy-desipramine (HDMI), talopram, talsupram, nioxetine (Nis), oxaprotiline (Oxap), lortalamine (Lort), and C-11 and F-18 derivatives of reboxetine (RB), methylreboxetine (MRB), and their individual (*R,R*) and (*S,S*) enantiomers, in conjunction with studies using radiolabeled 4-iodo-tomoxetine and 2-iodo-nioxetine, we have identified the superiority of (*S,S*)-[¹¹C]MRB and the suitability of the MRB analogs as potential NET ligands for PET translational studies from preclinical investigation in animals to clinical research in humans. In this review article, progress in this translational research will be discussed.

19.2 Challenges in NET Imaging of the Brain

NET possesses several intrinsic disadvantages as a molecular imaging target as compared to the other monoamine transporters (dopamine transporter (DAT) and serotonin transporter (SERT)). These disadvantages have presented drawbacks, described below, and hindered for decades progress in ligand development and imaging of NET in the living human brain.

19.2.1 NET Has a Relatively Lower Density in the Brain

B_{max} for NET is ~5–150 fmol/mg tissue (Smith et al. 2006; Tejani-Butt 1992); however, DAT has more than 50-fold higher density, and SERT is over five to ten-fold higher (Kaufman et al. 1991; Zeng et al. 2006).

19.2.2 NET Has a Widespread Distribution in the Brain

Studies in rodents, cats, nonhuman primates, and humans have indicated that noradrenergic terminals in the central nervous system (CNS) are widespread. Highest

levels occur in the locus coeruleus complex (LC) and raphe nuclei, moderate levels in the hypothalamus, midline thalamic nuclei, bed nucleus of the stria terminalis, central nucleus of the amygdala and brainstem nuclei, and low levels in the basolateral amygdala and cortical and striatal regions (Tejani-Butt 1992; Charnay et al. 1995; Ding et al. 2003, 2010; Ding and Fowler 2005; Gallezot et al. 2007, 2008, 2010; Hannestad et al. 2010).

19.2.3 NET Has a Lower Contrast Between NET-Poor and NET-Rich Regions

Two detrimental effects on NET imaging as the result of the widespread distribution of NET in the brain are (1) lower contrast and (2) lack of an obvious reference region. In contrast, a significant difference in the density between the transporter-rich and transporter-poor regions for both DAT and SERT systems offers much better contrast for PET imaging of DAT/SERT and simplifies data analysis methods by using a reference region approach.

19.2.4 The Locus Coeruleus (LC), the Highest NET Density Region, Has a Small Structure that Makes It Difficult to be Delineated and Quantitated

We and other research groups have been making progress towards ligand development for PET imaging of NET. After over two decades of effort, (*S,S*)-[¹¹C]MRB and its analogs are considered by far the most promising NET ligands for PET imaging (Ding et al. 2006 and references within). In several early publications, including the very first reports about this novel radioligand, (*S,S*)-[¹¹C]MRB was called (*S,S*)-[¹¹C]MeNER (Wilson et al. 2003; Schou et al. 2003; Ghose et al. 2005). This ligand has been used to study the role of NET in humans. How best to carry out these translational research studies and how best to normalize data from the NET-PET studies to obtain a measure related to NET availability have been the subjects of our recent work. Specific examples of tracer applications in the neurosciences (mainly in brain) are given in the following sections.

19.3 Translational PET Imaging Studies of NET

The NET has been suggested to play a role in numerous disorders such as substance abuse and withdrawal, ADHD, depression, schizophrenia, Alzheimer's disease, Parkinson's disease, as well as aging; however, in vivo brain imaging studies of NET have not been possible due to the lack of suitable radioligands (Ding et al. 2006 and references within). We have evaluated the suitability of (*S,S*)-[¹¹C]MRB in preclinical models and further evaluated it in humans. The results show that (*S,S*)-[¹¹C]MRB possesses properties that are highly favorable for the imaging of brain NET as a PET tracer, including (a) a regional distribution consistent with the known

distribution of NET in the brain; (b) high test/retest reproducibility in nonhuman primates and humans; (c) excellent specificity and selectivity for NET over other monoamine transporters, namely, DAT and SERT; and (d) the short half-life of its ^{11}C label ($t_{1/2} = 20$ min), enabling multiple assessments (e.g., baseline and drug intervention) in the same subject on the same day. So far, we have carried out over 300 scans using (*S,S*)- ^{11}C]MRB, including preclinical and clinical studies, to investigate cocaine abuse, alcoholism, depression, posttraumatic stress disorder (PTSD), obesity, brown adipose tissue (brown fat), and diabetes-related studies (studies related to drug occupancy of several novel pharmaceuticals targeting the NET system during their phase I clinical trials are not included). These studies have facilitated our better understanding of the role of NET in brain function and diseases. Furthermore, the use of PET with a suitable NET ligand to study drug occupancy and drug mechanisms will assist in the development of the next generation of effective drugs for the treatment of various NET-related disorders. Here we present a few examples to illustrate the progress in PET imaging of the NET system using (*S,S*)- ^{11}C]MRB (abbreviated henceforth as ^{11}C]MRB).

19.3.1 NET in Substance Abuse

Cocaine inhibits neurotransmitter uptake of human monoamine transporters, including NET, DAT, and SERT, with comparable potency. Alterations in NET concentration in the CNS following cocaine exposure have been identified in rats, nonhuman primate models, and postmortem human studies in cocaine users (Beveridge et al. 2005; Macey et al. 2003; Mash et al. 2005). Although these observations point to potentially important dysregulations in NET and NET-mediated neuroenergetics in response to chronic cocaine use (Weinshenker and Schroeder 2007), *in vivo* studies of NET regulation in clinical populations have yet to be explored. Thus, our aim was to use ^{11}C]MRB to determine the alterations in brain NET concentration in chronic cocaine users (Ding et al. 2010).

19.3.1.1 NET Abnormalities in Cocaine Dependence

In this pilot study, 12 healthy control subjects (HC) (6 M and 6 F; range 25–54) and 10 cocaine-dependent individuals (COC) (7M, 3F; range 39–49) were recruited (Ding et al. 2010). COC subjects were studied either as inpatients or outpatients, with cocaine abstinence at the time of PET scanning established by 24-h inpatient supervision and/or negative urine toxicology testing, respectively. All subjects participated in magnetic resonance imaging (structural MRI, 3 T) and PET scanning (high-resolution research tomograph (HRRT), 207 slices, resolution ~ 2.5 mm FWHM in 3D acquisition mode) on two different days. Binding potential (BP_{ND}) parametric images were computed using the simplified reference tissue model (SRTM2) with the occipital cortex as reference region. BP_{ND} values were compared between the two groups.

High-resolution imaging of brain NET using ^{11}C]MRB and HRRT clearly delineated the fine-scale regional distribution of ^{11}C]MRB in small brain regions known

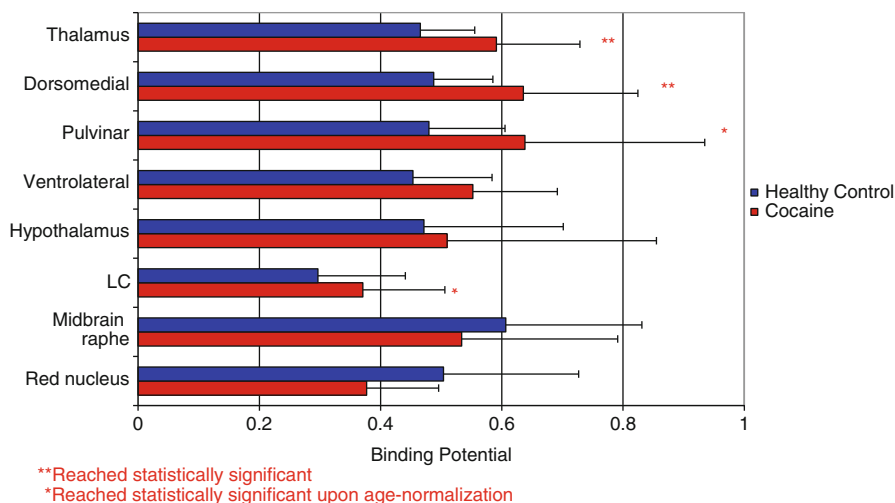


Fig. 19.1 Effect of cocaine dependence on [¹¹C]MRB binding in humans. BP_{ND} (binding potential) values were compared between healthy control and cocaine-dependent individuals

to have high NET concentrations, including the hypothalamus, red nucleus, midbrain raphe, pontine raphe, thalamus and its subnuclei (dorsomedial thalamic nucleus, ventrolateral thalamic nucleus, pulvinar), and the area of locus coeruleus (LC). The BP_{ND} was significantly increased in thalamus (27 %; $P < 0.02$) and dorsomedial thalamic nuclei (30 %; $P < 0.03$) in COC as compared to HC. We also found that there was an age effect on NET concentrations in HC. Thus, group comparison in a covariance analysis to account for the differences in age between groups was also performed. Upon age normalization, the upregulation of NET in COC also reached significance in LC (63 %, $P < 0.01$) and pulvinar (55 %, $P < 0.02$) regions (Fig. 19.1).

19.3.1.2 Duration of Abstinence Effect on NET Binding

In a subsequent study, we looked into the duration of the effect of abstinence on NET binding. Regional brain NET binding potential (BP_{ND} , MRTM2) was measured with [¹¹C]-MRB PET scanning in healthy controls ($n = 12$, 38 ± 11 years) and patients with chronic cocaine dependence (total $n = 15$, 43 ± 6 years, with 22 ± 7 years of cocaine use) after 1 week ($n = 4$), 2 weeks ($n = 6$), and 3–5 weeks ($n = 5$) of abstinence.

Our results served to reproduce our previous finding that NET is upregulated in chronic cocaine users after recent abstinence, as compared with controls. In addition, we found that subjects with cocaine dependence had higher NET BP_{ND} values after 1 week of abstinence in the ventral lateral thalamus (70 %; $P < 0.05$); and that remained elevated (85 %; $P < 0.01$) during the second week of abstinence. By the third week, NET levels slowly declined (11 %; $P = 0.60$) (Lee et al. 2012). Similar significant patterns were observed in the measurement of the whole thalamus and the midbrain raphe nuclei.

The observations of an increased binding of [^{11}C]MRB in our in vivo PET imaging studies of chronic COC subjects is consistent with previously published in vitro data in rodents, rhesus monkeys, and postmortem human brains (Beveridge et al. 2005; Macey et al. 2003; Mash et al. 2005). Our results are also in agreement with an in vitro study in which an upregulation of NET mRNA in the LC was observed in rats following chronic binge administration of cocaine (Burchett and Bannon 1997). Interestingly, in this rat study an alteration was observed in an opposite direction for the other two monoamine transporters, i.e., a decrease in SERT mRNA (in raphe) and DAT mRNA (in midbrain) following a binge regimen of chronic COC.

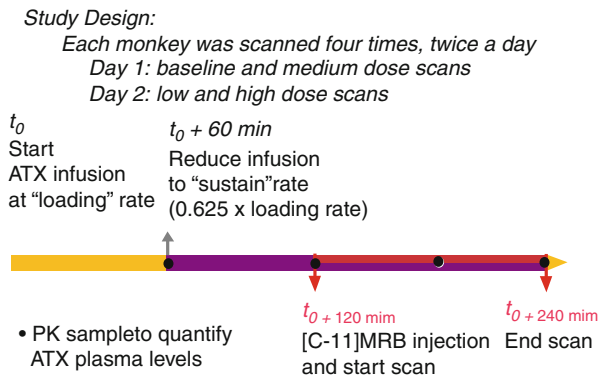
19.3.2 NET in ADHD

Attention-deficit hyperactivity disorder (ADHD), a complex developmental behavioral and cognitive disorder that affects approximately 3–7 % of school-age boys and 2–4 % of adults, is associated with impaired academic and occupational achievements, problem behaviors, increased risk for accidents, and substance abuse (American Psychiatric Press 1994; Barkley 1997; Dopheide and Pliszka 2009). The core features of ADHD – inattention, hyperactivity, and impulsivity – can be attributed to dysfunction in neural systems that regulate attention, executive function, motor control, and reward (Makris et al. 2009; Bush 2010); however, effective treatments remain elusive and the neurochemical mechanisms of this disorder are poorly understood (Bush 2010). The three therapeutic classes of pharmacologic treatments for ADHD – (a) psychostimulants (e.g., methylphenidate hydrochloride, MPH), (b) non-stimulant catecholamine reuptake inhibitors (e.g., atomoxetine, ATX), and (c) $\alpha 2$ adrenergic receptor agonists (e.g., guanfacine) – all modulate DA and NE neurotransmission (Makris et al. 2009; Bush 2010; Biederman et al. 2008; Dickstein et al. 2006; Madras et al. 2005). Small changes in extracellular NE or DA concentration affect networks of pyramidal cells in the prefrontal cortex (PFC) which regulates and sustains attention. The beneficial effects of DA occur at D1 receptors, while those of NE are believed to occur at $\alpha 2$ receptors (Arnsten 2009). Here we present several of our translational research studies of drug occupancy designed directly towards developing a better understanding of the mechanisms that contribute to the therapeutic effects of pharmacologic treatments for ADHD.

19.3.2.1 ATX Occupancy Study on NET in Humans and Nonhuman Primates

Atomoxetine (ATX, Strattera), a potent NET reuptake inhibitor ($K_i \sim 5$ nM), is the first non-stimulant drug that was approved for the treatment of ADHD (Bymaster et al. 2002; Michelson et al. 2001; Swanson and Volkow 2009; Chamberlain et al. 2007a; Volkow et al. 2001; Del Campo et al. 2011; Arnsten 2006; Spencer et al. 2002). When [^{11}C]MRB was initially tested in a drug occupancy study in humans using atomoxetine (ATX), a reduction in [^{11}C]MRB binding was observed, but there was no obvious dose-dependent effect (Logan et al. 2007). One hypothesis was that

Fig. 19.2 Study design for the 2-day, four-dose studies to measure ATX occupancy of NET in nonhuman primates using [^{11}C]MRB



the doses of ATX examined in the human PET study (oral, 25, 50 or 100 mg), though clinically relevant, were too high. That is, the three tested doses all reached saturation, the plateau portion of the corresponding dose-occupancy curve, and as a result there was no obvious dose-dependent effect. Another occupancy study of ATX using [^{18}F]FMENR-D2 in rhesus monkeys showed a reasonable dose-dependent occupancy, though only in one of the two monkeys studied and the IC_{50} (or ED_{50}) was not determined (Seneca et al. 2006).

Thus, the suitability of [^{11}C]MRB for occupancy studies was further evaluated by carrying out investigations in a nonhuman primate model (rhesus macaque) using lower doses of ATX than those used in the previous PET study with [^{11}C]MRB (Logan et al. 2007) and with a continuous ATX infusion paradigm to maintain a constant concentration of ATX in the plasma during the PET acquisition time (120 min). Ten PET studies were performed in three anesthetized rhesus monkeys following an infusion of ATX or placebo.

For each PET study, two infusion rates were used as follows: ATX infusion at a "loading" rate was first given for 1 h starting at 2 h before the injection of [^{11}C]MRB; then ATX was given at a "maintenance" rate (37.5 % lower than the "loading" rate) at 1 h before the injection of [^{11}C]MRB. This infusion rate was maintained until the end of the 2-h PET scan (i.e., 3 h at "maintenance" rate) (Fig. 19.2). Three doses of "maintenance" rate were used: 0.01 mg/kg/h (low dose), 0.03 mg/kg/h (medium dose), and 0.09 mg/kg/h (high dose) (i.e., each monkey had four PET scans, including the baseline scan with placebo). The design was to have each monkey have four PET scans on two study days. These two study days were scheduled at least 3 weeks apart to allow recovery from the effect of the anesthesia and blood drawing. On each study day, two PET scans were acquired, beginning 4 h apart. The first study day consisted of the baseline and medium-dose scans, the second study day consisted of the low- and high-dose scans.

A dose-dependent reduction of [^{11}C]MRB volume of distribution was observed after correction for [^{11}C]MRB plasma free fraction. Although the slow clearance of [^{11}C]MRB in NET-rich regions such as the thalamus posed a concern for kinetic modeling, the combination of the suitably designed infusion study paradigm,

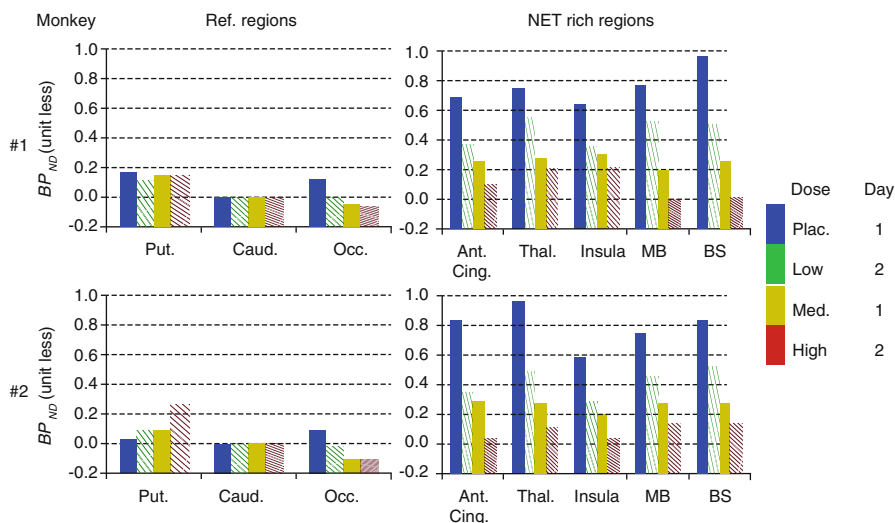


Fig. 19.3 Dose-dependent occupancy of ATX in NET-rich regions in two monkeys using [^{11}C]MRB after the placebo (*Plac.*), low, medium, and high ATX doses. BP_{ND} (binding potential) values were measured for NET-poor regions (putamen (*put.*) and occipital cortex (*Occ.*)) and NET-rich regions (anterior cingulate (*Ant. Cing.*), thalamus (*Thal.*), insular, midbrain (*MB*), and brain stem (*BS*)), using caudate as a reference region

and refined kinetic modeling methods, an unequivocal dose-dependent occupancy of atomoxetine was obtained (Fig. 19.3) clearly demonstrating the suitability of [^{11}C]MRB for drug occupancy studies of the NET (Gallezot et al. 2010).

Based on this study, ATX IC_{50} was estimated to be 32 ± 13 ng/mL plasma, corresponding to an effective dose (ED_{50}) of 0.13 mg/kg, which is much lower than the therapeutic dose of ATX in ADHD (1.0–1.5 mg/kg). In the previous ATX occupancy study in humans, three clinically relevant doses were used (oral, 25, 50, or 100 mg), the blood levels of ATX (in ng/mL plasma) averaged over subjects were 116 (25 mg ATX), 206 (50 mg ATX), and 421 (100 mg ATX), which were significantly higher than the estimated IC_{50} for ATX in plasma (~ 30 ng/mL). This suggests that the lack of an obvious dose-dependent effect in the previous study was indeed because the three clinically relevant doses all reached saturation with over 78–93 % occupancy, i.e., the plateau portion of the corresponding dose-occupancy curve (Logan et al. 2007). Taken together, our results clearly indicate the importance of dose selection for PET occupancy studies, especially when observation of dose-dependency of the study drug is one of the goals for the outcome measurement.

19.3.2.2 ATX Occupancy Study on SERT, Implication on Treatment of Depression and ADHD

The development of ATX and its approval for the treatment of ADHD by the Food and Drug Administration (Faraone et al. 2005) was based on the rationale that it selectively blocks the NET (Barton 2005) and increases the availability of

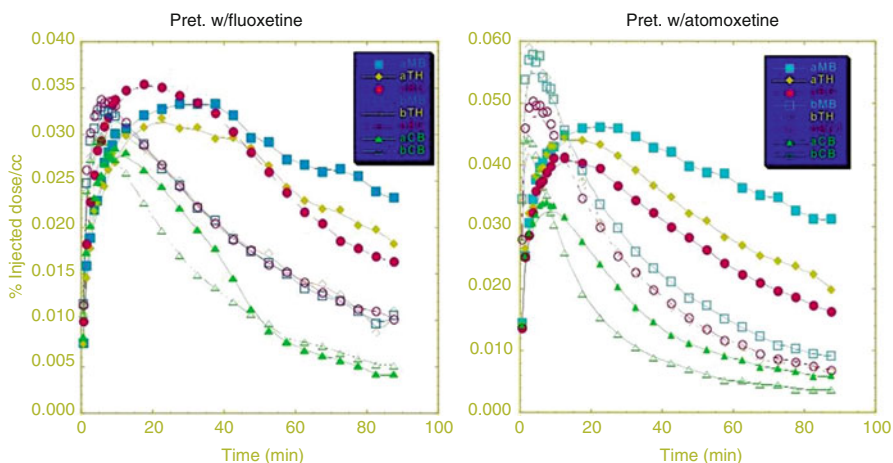


Fig. 19.4 ATX displayed a blocking effect similar to fluoxetine (a selective SERT inhibitor) on binding of [^{11}C]DASB (a selective SERT ligand), questioning the in vivo selectivity of ATX

intrasympathetic NE, resulting in the improvement of high-level cognitive functions that are often impaired in ADHD, such as working memory and inhibitory response control (Robbins and Arnsten 2009). In principle, ATX may offer clinical advantages by virtue of its limited effects on subcortical dopamine, which is thought to be responsible for the abuse potential of psychostimulant treatment (Volkow 2006). Furthermore, this single NE pathway of drug mechanism may facilitate further drug research and development.

The noradrenergic action also exerts an important clinical effect in different antidepressant classes such as desipramine and nortriptyline (tricyclics with prevalent noradrenergic effect). Thus, ATX has also been used to improve responses to treatment of depression (Dell'Osso et al. 2010; O'Sullivan et al. 2009).

Serendipitously, we discovered that ATX displayed a blocking effect similar to fluoxetine (a selective SERT inhibitor) on binding of [^{11}C]DASB (Ding and Fowler 2005), a selective SERT ligand (Houle et al. 2000) (Fig. 19.4). These results suggested that ATX not only binds to NET but also binds to SERT with high affinity. To date, whether the therapeutic effects of ATX in the treatment of either ADHD or depression are due to inhibitory effects on one (NET) or two transporters (NET and SERT) is not known. Therefore, we took on this investigation by carrying out comparative occupancy studies with [^{11}C]MRB (a NET ligand, as described above) (Gallezot et al. 2008, 2010) and [^{11}C]AFM (a SERT ligand) (Huang et al. 2002) to evaluate the in vivo IC_{50} of ATX for both NET and SERT in nonhuman primates using PET.

The continuous infusion protocol with [^{11}C]AFM was similar to our previous study with [^{11}C]MRB (see above) (Gallezot et al. 2008, 2010). Two monkeys were scanned with maintenance rates: 0.045 mg/kg/h (low dose), 0.135 mg/kg/h (medium dose), and 0.405 mg/kg/h (high dose). One monkey was scanned with the higher

maintenance rates: 0.135 mg/kg/h (medium dose), 0.405 mg/kg/h (high dose), and 1.054 mg/kg/h (very-high dose) (details of this study will be published elsewhere).

19.3.2.3 Summary of the Comparative Occupancy Studies of ATX for NET (Using [^{11}C]MRB) and SERT (Using [^{11}C]AFM)

ATX displayed dose-dependent occupancy of both NET and SERT, with a higher occupancy of NET: IC_{50} of 31 ± 10 and 99 ± 21 ng/mL plasma for NET and SERT, respectively. At a clinically relevant dose (1.8 mg/kg, ~ 600 ng/mL plasma), ATX would occupy $>95\%$ of NET and occupy $>85\%$ of SERT. It is worth noting that this value of 3.2 for the selectivity ratio of ATX towards NET vs. SERT measured via in vivo PET imaging in nonhuman primates (NHP) is similar to a value of 4.5 for the selectivity ratio derived from the previously reported in vitro K_d values using human NET and SERT tissue homogenates (8.9 and 2 nM for SERT and NET, respectively) (Tatsumi et al. 1997). Based on these data, we propose that ATX at clinically relevant doses occupies high proportions of both NET and SERT. Thus, the interpretation of the therapeutic mode of action of ATX for treatment of depression and ADHD may be more complex than selective blockade of the NET.

19.3.2.4 The Mechanisms of Action of ATX in ADHD and Depression

It has been shown that response inhibition (the ability to exert high-level inhibitory control over motor responses so as to suppress unwanted actions) is impaired in subjects with ADHD and is one of the most robust cognitive findings in ADHD research (Lijffijt et al. 2005). Response inhibition (aka impulsivity) can be measured by the stop-signal task (SST), and quantified by the stop-signal reaction time (SSRT), an estimate of the time taken to inhibit the prepotent motor response (Aron et al. 2003a). The research group at Cambridge, UK, found that single doses of atomoxetine (60 mg) were able to improve response inhibition in humans and in rats (Chamberlain et al. 2006, 2007a; Eagle et al. 2008; Bari et al. 2009). By contrast, serotonin manipulations with citalopram, a SERT blocker (Chamberlain et al. 2006; Del Campo et al. 2011), or with buspirone, a serotonin 5-HT_{1A} receptor agonist (Chamberlain et al. 2006, 2007b), appear to have no behavioral effects on the SSRT. These results suggest that atomoxetine enhances stopping selectively via actions on NE uptake and that NET drugs may be more suited to ameliorating impaired response inhibition as an ADHD therapeutic target.

Taken together, the inhibitory effect of ATX on NET plays a crucial role on its therapeutic effect on ADHD, while the inhibitory effect of ATX on SERT may play a more important role on its therapeutic effect on depression. Further studies to elucidate the actual relationship between the drug mechanisms and drug therapeutic effects are needed.

19.3.2.5 MPH Occupancy Study on NET in Humans

The effects of MPH on the DA system have been studied extensively. Our previous PET studies have demonstrated that MPH's pharmacological effects reside in *d-threo*-MPH, the active enantiomer (Ding et al. 1997), and that at clinical doses MPH significantly occupies DAT in vivo in humans (Swanson and Volkow 2009;

Volkow et al. 1998), suggesting that DA reuptake inhibition may be an important therapeutic mechanism in ADHD. However, MPH has shown higher in vitro affinity for NET than DAT ($K_i=38$ nM vs. 193 nM) (Eshleman et al. 1999). The potential role of NE in ADHD was supported by animal and human data (Biederman et al. 2008). Low doses of MPH increase levels of NE in the PFC in animals (Berridge et al. 2006), and low doses of MPH improve performance of PFC tasks in subjects with ADHD (Aron et al. 2003b). The absence of a suitable NET tracer has delayed similar in vivo PET studies of NET until now.

We used [^{11}C]MRB to determine the effective dose 50 (ED_{50}) of MPH for NET (Hannestad et al. 2010). We first conducted a preliminary duration study to determine how much time it takes from oral MPH administration to maximum occupancy of brain NET. As peak displacement of [^{11}C]MRB by MPH (oral, 40 mg, i.e., 0.35–0.55 mg/kg, the average clinical maintenance dose of MPH) was achieved in 75 min, we chose 75 min as the time between oral MPH dosing and [^{11}C]MRB injection for the subsequent occupancy study. Based on our previous experience with ATX occupancy studies in humans, dose selection is critical if dose-dependent occupancy is one of the goals to be achieved. Thus, in this within-subject design study, healthy subjects ($n=11$) received oral, single-blind placebo and 2.5, 10, and 40 mg of MPH 75 min prior to [^{11}C]MRB injection. Dynamic PET imaging was performed for 2 h with HRRT. Three regions with known lowest density of NET (occipital cortex, caudate, and putamen) were investigated (Logan et al. 2005) further as reference regions by comparing the distribution volume (V_T) in these three regions between the placebo and 40 mg MPH conditions (Hannestad et al. 2010). We found no significant change of V_T (or V_T/f_p) (f_p : plasma free fraction) in these three regions between the placebo and 40 mg MPH conditions, and the putamen and occipital had similar V_T values. Thus, the multilinear reference tissue model with occipital cortex as the reference region was used to estimate binding potential (BP_{ND}) in the thalamus and other NET-rich regions.

We found that BP_{ND} was reduced by MPH in a dose-dependent manner in the thalamus and other NET-rich regions (Fig. 19.5). The global ED_{50} was estimated to be 0.14 mg/kg; therefore the average clinical maintenance dose of MPH (0.35–0.55 mg/kg) produces 70–80 % occupancy of NET. This is the first in vivo study in humans showing that clinically relevant doses of MPH occupy significant levels of NET, despite the fact that MPH has been used for the treatment of ADHD for decades. The ED_{50} is lower than that for DAT (0.25 mg/kg), suggesting the potential relevance of NET inhibition in the therapeutic effects of MPH in ADHD.

Previous studies also suggested that effects on delayed responding and working memory are mediated by noradrenergic afferents from LC (the highest NET density region) to PFC (Biederman et al. 2008; Solanto 1998). However, limited studies were able to link brain process with attention and ADHD. It has also been shown that the temporal, parietal, and prefrontal (PFC) association cortices mediate different aspects of attention and that treatments for ADHD enhance catecholamine actions in PFC and improve PFC functions (Arnsten 2009). Although the density of NET in PFC is very low, we were able to detect dose-dependent displacement of [^{11}C]MRB by MPH in two cortical regions in which NET densities were high enough: paracentral lobule and

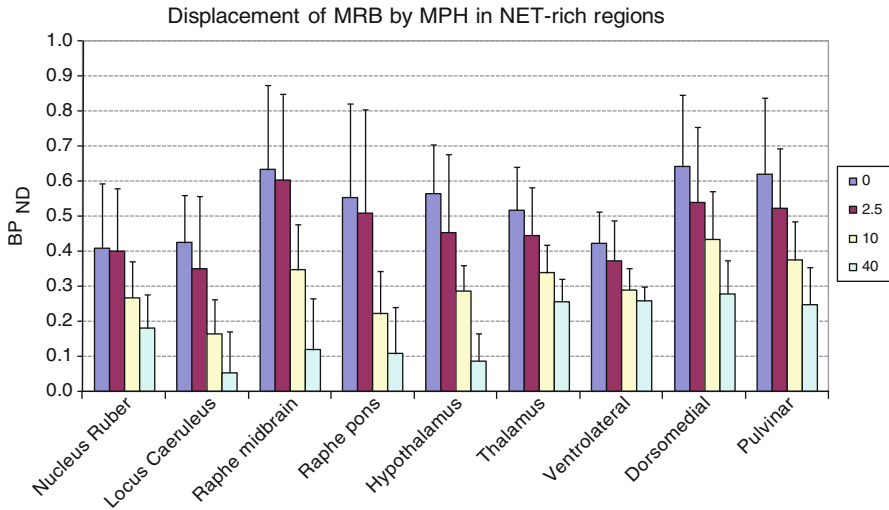


Fig. 19.5 BP_{ND} values were reduced by methylphenidate in a dose-dependent manner in NET-rich regions after four doses of oral methylphenidate (0, 2.5, 10, 40 mg)

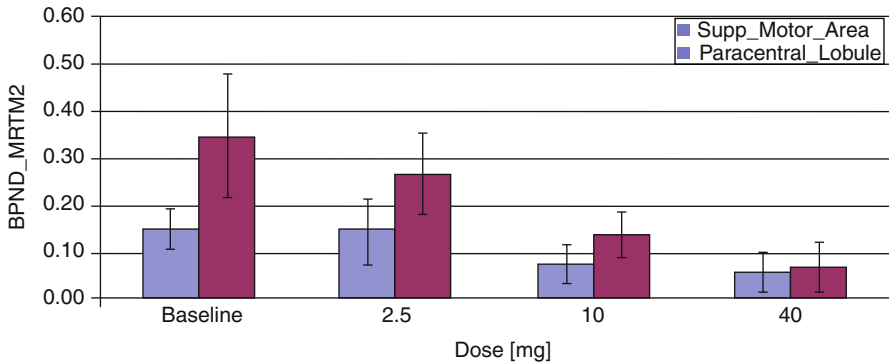


Fig. 19.6 Dose-dependent displacement of $[^{11}C]$ MRB by methylphenidate in two cortical regions (paracentral lobule and the supplementary motor area (SMA)) was also detected after four doses of oral methylphenidate (0, 2.5, 10, 40 mg). *MTRM2* multilinear reference tissue model with two parameters (Ichise et al. 2003)

the supplementary motor area (SMA) (Fig. 19.6), which are areas involved in the response to MPH and inhibition control during cognitive tasks, respectively (Hannestad et al. 2010; Volkow et al. 2008; Li et al. 2006). Although we cannot assess the effect of MPH in the PFC directly, our assumption is that the global ED_{50} calculated using NET-rich regions, including the neocortical paracentral lobule, is similar to the ED_{50} in regions with lower NET density, such as the PFC. It is also important to fill the gap by combining PET (offers specificity) and other modality such as fMRI (offers spatial and temporal resolution) to explore the underlying molecular processes.

19.3.3 NET in PTSD

Termination of the action of NE on adrenergic receptors is accomplished primarily by NE reuptake into the presynaptic terminal via the NE transporters (NET). Animal studies and postmortem studies in humans have implicated reductions in NET expression in depression, which is often comorbid with PTSD. While acute stress does not alter NET density, there is evidence from rodent studies that repeated stress decreases NET density in the locus coeruleus (LC) and limbic brain regions (Zafar et al. 1997). These important findings, however, have not yet been confirmed in humans using in vivo methods because brain imaging of NET in living humans has been hampered for over 20 years by the lack of suitable radioligands. Given that the NET is a suitable target for antidepressants and the established role of noradrenergic mechanisms in PTSD, additional research on the distribution and function of NET in the brain of patients with PTSD is important to better understand the hypothesized dysregulations in NE function in PTSD. Thus, the hypothesis that lower NET density may be related to the development of mood and anxiety disorders (Moron et al. 2002; Liprando et al. 2004; Miner et al. 2006; Arnsten and Li 2005) was investigated using the most promising NET ligand, [^{11}C]MRB. In order to evaluate whether trauma exposure and PTSD would be associated with lower NET density in the locus coeruleus (LC), we conducted PET studies using [^{11}C]MRB in three groups of individuals: 18 healthy adults (healthy controls: HC), 16 adults exposed to trauma who did not develop PTSD (trauma control: TC), and 22 adults exposed to trauma who developed PTSD. As a secondary aim, we evaluated the relation between NET availability in LC and a contemporary phenotypic model of PTSD symptomatology, namely, a five factor model comprised of reexperiencing, avoidance, numbing, dysphoric arousal, and anxious arousal (Pietrzak et al. 2012; Armour et al. 2012; Elhai et al. 2011). Our study results revealed that both the PTSD group and the TC group had significantly lower NET density than the HC group (41 % lower with Cohen's $d=1.04$ for the PTSD group and 31 % lower with Cohen's $d=0.77$ for the TC group, respectively), while NET density was not significantly different between the TC and PTSD groups (15 % lower in PTSD versus TC group, Cohen's $d=0.27$). In the PTSD group, NET density in the LC was independently positively associated with the severity of anxious arousal (i.e., hypervigilance symptoms, $r=0.52$), but not with any of the other symptom clusters. Results of this study suggest that TC and PTSD are associated with significant reductions in NET availability in LC and that NET density in this brain region is associated with increased severity of anxious arousal symptoms among individuals with PTSD (Pietrzak et al. 2013).

19.3.4 NET in Alcohol Dependence

We investigated the role of NET in alcohol dependence in human subjects, in vivo, using [^{11}C]MRB and PET. Unmedicated, recently abstinent (4–6 weeks abstinence to compensate for acute alcohol withdrawal effects) non-obese men and women meeting DSM-IV (First et al. 1996) criteria for current alcohol dependence ($n=15$)

and age- and sex-matched healthy control subjects ($n=15$) were studied and compared. Our hypothesis was that in areas of highest NET density, we would detect lower ligand binding commensurate with NET downregulation due to chronic alcohol exposure. We identified two brain regions in alcoholics, the thalamus and locus coeruleus, which exhibited reduced NET binding potential (BP_{ND}). We have postulated that these regions are involved in alcohol craving, acquisition, and ingestion and that they may serve as biomarkers of altered NET expression in alcohol dependence disorders and as potential therapeutic targets for drug development (unpublished results; details of this study will be published elsewhere).

19.3.5 NET in Obesity and Brown Adipose tissue (Brown Fat)

We have conducted studies in humans to investigate the role of NET in obesity. The preliminary data suggest that there is lower NET binding in the thalamus (including pulvinar) in obese subjects (body mass index (BMI) of 34.7 ± 2.6) as compared to matched lean subjects (BMI of 23.1 ± 1.4) (unpublished results, details of this study will be published elsewhere).

Obesity is characterized by impaired energy expenditure associated with adaptive thermogenesis (Camastra et al. 1999; Golay et al. 1986; Yeckel et al. 2009, Jequier and Schutz 1985). Brown adipose tissue (BAT, brown fat), one of the primary tissues responsible for adaptive non-shivering thermogenesis in mammals (Wijers et al. 2009), was previously thought to disappear in humans as part of development into adulthood. The recent confirmation that BAT still exists in adult humans provides a renewed interest in this tissue; however, the relative importance of BAT activity to adult human whole-body energy expenditure is still unknown. Lessons learned from steps taken to reduce undesirable FDG-labeling during many false-positive clinical scans (Nedergaard et al. 2007; Hany et al. 2002; Christensen et al. 2006) demonstrate that repeat scans after beta-adrenergic blockade eliminate the interfering BAT signal (Agrawal et al. 2009). These data suggest the presence of strong sympathetic nervous system (SNS) activation of BAT in humans and the potential involvement of the noradrenergic system in the regulation of BAT activity. Thus, in addition to a NET obesity study in brain, we also carried out a pilot study to look into the NET involvement in both central and peripheral SNS function and to determine whether BAT can be visualized with NET-PET imaging and whether NET binding in BAT can be quantified under both basal and activated conditions in humans.

Based on [^{18}F]FDG-PET imaging data, [^{18}F]FDG-imaging requires subjects under cold stimulation during the PET imaging, and BAT does not appear to be visualized with [^{18}F]FDG-PET at room temperature (Saito et al. 2009; van Marken Lichtenbelt et al. 2009). The BAT metabolic activity is related to age, gender, BMI, cold exposure and medications (Cypess et al. 2009). Thus, the [^{18}F]FDG-PET approach may not be suitable for imaging BAT at the basal state, i.e., room temperature. Since BAT activation appears to be dynamic, expressing large variability due to thermal sensitivity, individual differences in BAT activation due to variations in thermal response are likely to make comparisons between obese and normal-weight

subjects difficult. Moreover, [^{18}F]FDG is not specific to BAT nor is glucose the primary substrate for BAT heat production. The [^{18}F]FDG-PET strategy will not address regulatory mechanisms that are related to the specific SNS modulation features of BAT, which are likely to be key features to understanding potential dysfunction. Therefore, it is important to develop new and more specific methods to address both the plasticity of BAT activation and the basal characteristics that do not require stimulation or that could alternatively be used in combination with strategies that highlight BAT stimulated activity.

We first conducted both ex vivo and in vivo evaluation in rats using [^{11}C]MRB to determine BAT imaging in the basal state of BAT (at room temperature, r.t.), which is not achievable with [^{18}F]FDG (Lin et al. 2012). In the ex vivo study, awake male Sprague-Dawley rats were administered intravenous [^{18}F]FDG or [^{11}C]MRB after exposing to cold (4 °C for 4 h, $n=9$) or remaining at r.t. ($n=9$) and were sacrificed at 20, 40, and 60 min postinjection. The results demonstrate that the uptake of [^{11}C]MRB in BAT was three times higher than [^{18}F]FDG at r.t. ($P=0.0088$) and the cold exposure increased [^{18}F]FDG uptake in BAT tenfold compared to the r.t. control (1.6 ± 0.3 vs. 0.2 ± 0.05 %ID/g, $P=0.0009$) while no significant thermal effect was observed with [^{11}C]MRB BAT uptake (0.87 ± 0.18 vs. 0.63 ± 0.09 %ID/g, $P=0.082$). In addition to the brain and heart, BAT exhibited specific [^{11}C]MRB uptake that was significantly reduced to near baseline levels ($P=0.0013$) by pretreatment with unlabeled MRB or nisoxetine. These results were concordant with the in vivo PET imaging of anesthetized rats, which clearly demonstrated intense [^{11}C]MRB uptake in the interscapular BAT of both r.t. and cold-exposed rats; in contrast, [^{18}F]FDG in BAT was only detected in rats treated with cold (Fig. 19.7). HPLC analysis revealed that 94–99 % of total radioactivity in BAT represented unchanged [^{11}C]MRB, which further supports the NET-PET strategy for imaging BAT in humans at basal conditions. This NET-PET imaging strategy for BAT will help to provide insight into whether BAT is a pivotal target tissue for therapeutic interventions designed to reduce human obesity and will also help to elucidate mechanisms related to its function/dysfunction. Our choice of the [^{11}C]MRB ligand also has other specific advantages. Studies have shown that disruption of NET function directly impacts both autonomic function and mental health (Esler et al. 1991; Ganguly et al. 1986; Haenisch et al. 2009; Hahn et al. 2003, 2005, 2008, 2009) and that NET function is regulated both centrally and peripherally by insulin (Robertson et al. 2010). Unlike many other NET ligands, [^{11}C]MRB is able to cross the blood-brain barrier, allowing for simultaneous central and peripheral imaging. Thus, using [^{11}C]MRB may help to further elucidate mechanisms of BAT action and the role of NET in energy balance of obesity and insulin resistance by simultaneously correlating the CNS and peripheral SNS functions. Imaging BAT in humans is currently under investigation.

19.3.6 NET in Aging

It may be worth mentioning that there appears to be a significant age effect on NET concentrations in healthy control subjects (HC). A pilot study with a small sample

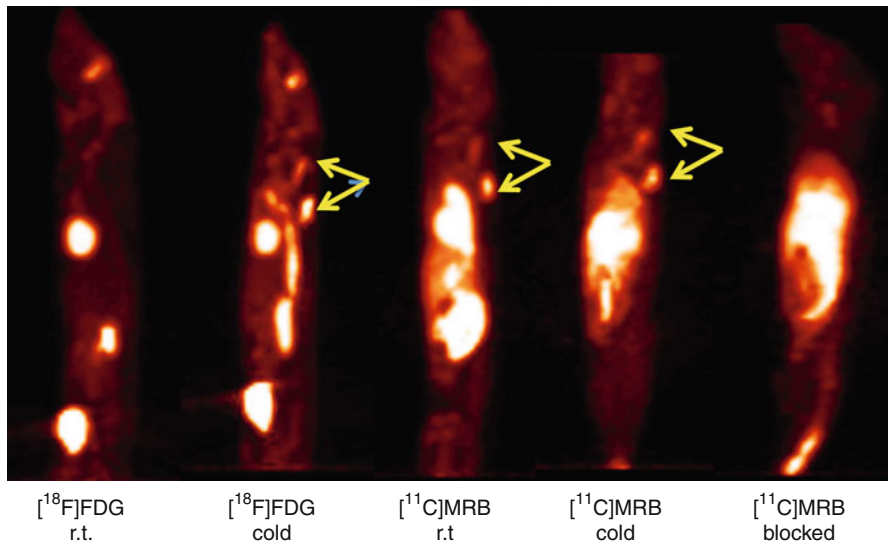


Fig. 19.7 PET images (50–70 min postinjection) on isoflurane-anesthetized rats from left to right: $[^{18}\text{F}]\text{FDG}$ room temperature control, $[^{18}\text{F}]\text{FDG}$ cold-exposed rat, $[^{11}\text{C}]\text{MRB}$ room temperature control, $[^{11}\text{C}]\text{MRB}$ cold-exposed rat, and $[^{11}\text{C}]\text{MRB}$ following blockade by unlabeled MRB. Brown adipose tissue (BAT) is denoted by *arrows*. The amounts of injected activity from left to right were 10.7, 10.9, 29.2, 31.5, and 40.9 MBq

size ($n=12$, age range 25–54) showed that LC, hypothalamus, and pulvinar displayed a significant inverse correlation with age among HC ($P=0.04$, 0.009, 0.03, respectively). According to our previous study, the % BP_{ND} change for DAT was approx. 0.7 % per year (Volkow et al. 1996); however, the % BP_{ND} change per year for NET was about threefold higher based on our pilot study (Ding et al. 2010). These intriguing results warrant further investigation with a larger sample size.

19.3.7 Kinetic Modeling for NET Imaging Studies in Brain

It is important to point out that arterial input function measurement was conducted for almost all of our PET-NET brain imaging studies using $[^{11}\text{C}]\text{MRB}$ (Logan et al. 2005; Ding et al. 2010; Gallezot et al. 2010; Hannestad et al. 2010). This made it possible to quantify the volume of distribution (V_T) of $[^{11}\text{C}]\text{MRB}$ using multilinear analysis MA1 (Ichise et al. 2002) and a direct comparison of the quantification of $[^{11}\text{C}]\text{MRB}$ binding potential (BP_{ND}) without arterial blood sampling using either MRTM2 (Ichise et al. 2003) or SRTM2. With these validation techniques (Gallezot et al. 2010; Hannestad et al. 2010), we evaluated several candidate reference regions so that placement of arterial lines may not be needed for future NET imaging studies using $[^{11}\text{C}]\text{MRB}$.

As described above, one of the intrinsic challenges for imaging NET is its wide distribution throughout the brain, with relatively low contrast between

transporter-poor and transporter-rich regions. It has been shown that the lowest NET densities measured by autoradiography in rhesus monkeys were in putamen and caudate (Smith et al. 2006); while the lowest concentration of NET in humans was found in the occipital cortex, based on one in vitro autoradiography study in humans using [^{18}F]F-MeNER-D2 (Schou et al. 2005). Thus, evaluation of caudate, putamen, and occipital cortex as potential reference regions was conducted in both rhesus monkeys and humans.

Based on our [^{11}C]MRB studies in nonhuman primates (NHP), we found that the use of caudate as the reference region in NHP leads to the least bias. This bias is not significant as compared to the “gold standard” IC_{50} estimate obtained using only V_T or V_T/f_P values (Gallezot et al. 2010). Moreover, similar results were obtained while using the binding potentials BP_F and BP_{ND} (Innis et al. 2007). The latter could be estimated without arterial blood sampling by using MRTM2 and provided results equivalent to those obtained with the arterial data, i.e., without introducing further bias. Based on our [^{11}C]MRB studies in both NHP and humans, it seems that the fraction of displaceable binding in the occipital cortex for [^{11}C]MRB is higher in rhesus monkeys than in humans.

Interestingly, the issue of selecting a reference region seems to be less troublesome in humans since all three NET-poor regions (caudate, putamen, and occipital) were considered as reasonable reference regions based on the results of our occupancy study of methylphenidate in humans (Hannestad et al. 2010), and see above discussion. The occipital cortex has lower levels of NET than the striatum (Schou et al. 2005) and is a relatively bigger region with a simpler shape than the caudate and putamen, making it more suitable as the reference region for human studies, especially when ROIs are delineated with an automated template. Thus, using MRTM2 with a reference region to quantify [^{11}C]MRB binding without arterial sampling for occupancy studies is feasible in nonhuman primates and adequate in humans.

19.4 Summary and Outlook

The main purpose of this review article is to outline the progress that has been made on PET imaging of the NET system during the past decade, starting from ligand development, ligand characterization, toxicology evaluation, ligand validation, and approval for human studies (Ding et al. 2006), leading to the translational research in humans. A few specific applications using [^{11}C]MRB in the scope of evaluation of disease abnormality, determination of drug occupancy, understanding biological processes, and interpretation of drug mechanisms have been explored. Our pilot investigations clearly indicated how little we know about the role of NET in various CNS disorders. As previously mentioned, many of the important findings resulted from studies in vitro using postmortem tissues and have suggested the implication of NET in various neurological and psychiatric disorders, but they have never been verified via in vivo methods due to the lack of suitable radioligands.

We have just begun to learn the role of NET in the pathophysiology and the treatment of several disorders, including cocaine abuse, ADHD, depression, PTSD,

alcohol dependence, obesity, and also in normal aging. For example, cocaine is the most abused drug with highest reinforcing ability. Its effect on the dopamine system has been well characterized; however, its effect on NET in humans has never been investigated. Our studies on cocaine abusers and the effect of duration of abstinence on NET binding provide the first evidence of NET abnormalities in cocaine dependence.

Our occupancy studies of MPH demonstrate that clinically relevant doses block 70–80 % of NET, whereas only 60–70 % of DAT is blocked at similar doses. Despite of the fact that MPH has been the most prescribed drug for the treatment of ADHD over the last 50 years, our study provides the first evidence questioning the traditional thinking that the therapeutic effect of MPH is mainly due to its inhibition of DAT.

Our PET imaging studies on ATX unveiled its high *in vivo* affinity towards both NET and SERT, questioning the traditional thinking that ATX is a selective NET inhibitor. These results suggest a cautious interpretation of the therapeutic mode of action of ATX for the treatment of depression and ADHD, as the therapeutic effect of ATX may be more complex than selective blockade of the NET.

It is important to point out that most of our investigations to evaluate disease abnormality are pilot studies with relatively small sample sizes. Further studies employing larger samples are needed to confirm the results. Furthermore, other important aspects (e.g., gender) that have been linked to various disorders may be revealed.

Though the major focus of this chapter was on our translational research using [^{11}C]MRB, its F-18 analogs, such as [^{18}F]fluoromethyl ((*S,S*)-[F]FMeNER) (Schou et al. 2004; Takano et al. 2009) and [^{18}F]fluoroethyl analogs, ((*S,S*)-[^{18}F]FRB) (Ding et al. 2005, 2006; Lin et al. 2005) also showed promising results. Unfortunately, their relatively lower binding affinity and defluorination problems precluded their further translational research in humans (Ding et al. 2005, 2006; Lin et al. 2005; Takano et al. 2008). NET ligand development work is ongoing. Future studies using PET ligands with greater affinity and specificity towards NET may help to further examine the role of noradrenergic function in various CNS disorders and facilitate our understanding of the role of NET in living humans, without having to rely solely on the results from postmortem studies.

New strategies are being developed for synergistic PET/MR imaging using simultaneous data acquisition capabilities of a combined PET/MR scanner (e.g., Siemens mMR) in order to take advantage of the spatial resolution of MRI with the biochemical and functional information from PET. This state-of-the-art PET/MR combined modality would facilitate co-registration, for example, the locus coeruleus (LC), which plays an important role in various CNS disorders and is the region of highest NET density, is a very small structure that poses a challenge to NET imaging due to difficulties encountered during PET and MRI co-registration when separate PET and MRI scans are collected – a problem that can be addressed by simultaneous MR and PET data acquisition. Furthermore, it would permit simultaneous imaging of physiologic and pathophysiologic processes and avoid the potential confounding effects of day-to-day and status variations. It would also provide an

unprecedented opportunity to correlate PET measures with MR-detected patterns of neural synchrony in both cortical and subcortical regions, facilitating the search process for optimal biomarkers for various CNS disorders. For example, we have demonstrated the dose-dependent occupancy of MPH in LC, subcortical, and cortical regions by using NET-PET imaging (see above Sect. 19.3.2.5). The use of PET/MR with simultaneous acquisition after the treatment with MPH may facilitate our understanding of the functional connectivity among the brain regions by linking the effect of MPH from LC to its projection into cortical regions, including PFC.

Acknowledgements This research was supported by the National Institutes of Health (National Institute for Biomedical Imaging and Bioengineering RO1 EB002630-29 (Ding); National Institute on Drug Abuse, DA-06278, 9 R01 DA019062-31, 5R56DA019062-33 (Ding); NIH/NCRR U54 (IRC) Interdisciplinary Research Consortium on Stress Self-Control and Addiction (Sinha/Neumeister); 1RL 1AA 017540-01 (Neumeister); VA Merit Award (Neumeister); and National Institute of Diabetes and Digestive and Kidney Diseases (1R21DK090764-01A1, Ding)), GlaxoSmithKline, and Pfizer. The author is grateful to the PET group at Brookhaven National Laboratory and the PET Center team at Yale University School of Medicine for their assistance.

References

- Agrawal A, Nair N, Baghel NS (2009) A novel approach for reduction of brown fat uptake on FDG PET. *Br J Radiol* 82:626–631
- American Psychiatric Press (1994 and 2000) Diagnostic and statistical manual of mental disorders, 4th edn. American Psychiatric Association, Washington, DC
- Armour C, Elhai JD, Richardson D et al (2012) Assessing a five factor model of PTSD: is dysphoric arousal a unique PTSD construct showing differential relationships with anxiety and depression? *J Anxiety Disord* 26:368–376
- Arnsten AF (2006) Fundamentals of attention-deficit/hyperactivity disorder: circuits and pathways. *J Clin Psychiatry* 67(Suppl 8):7–12
- Arnsten AF (2009) Toward a new understanding of attention-deficit hyperactivity disorder pathophysiology: an important role for prefrontal cortex dysfunction. *CNS Drugs* 23(Suppl 1):33–41
- Arnsten AF, Li BM (2005) Neurobiology of executive functions: catecholamine influences on prefrontal cortical functions. *Biol Psychiatry* 57:1377–1384
- Aron AR, Dowson JH, Sahakian BJ et al (2003a) Methylphenidate improves response inhibition in adults with attention-deficit/hyperactivity disorder. *Biol Psychiatry* 54:1465–1468
- Aron AR, Fletcher PC, Bullmore ET et al (2003b) Stop-signal inhibition disrupted by damage to right inferior frontal gyrus in humans. *Nat Neurosci* 6:115–116
- Bari A, Eagle DM, Mar AC et al (2009) Dissociable effects of noradrenaline, dopamine, and serotonin uptake blockade on stop task performance in rats. *Psychopharmacology (Berl)* 205:273–283
- Barkley RA (1997) Attention deficit hyperactivity disorder: a handbook for diagnosis and treatment. The Guilford Press, New York
- Barton J (2005) Atomoxetine: a new pharmacotherapeutic approach in the management of attention deficit/hyperactivity disorder. *Arch Dis Child* 90(Suppl 1):i26–i29
- Berridge CW, Devilbiss DM, Andrzejewski ME et al (2006) Methylphenidate preferentially increases catecholamine neurotransmission within the prefrontal cortex at low doses that enhance cognitive function. *Biol Psychiatry* 60:1111–1120
- Beveridge TJ, Smith HR, Nader MA et al (2005) Effects of chronic cocaine self-administration on norepinephrine transporters in the nonhuman primate brain. *Psychopharmacology (Berl)* 180:781–788

- Biederman J, Melmed RD, Patel A et al (2008) A randomized, double-blind, placebo-controlled study of guanfacine extended release in children and adolescents with attention-deficit/hyperactivity disorder. *Pediatrics* 121:e73–e84
- Burchett SA, Bannon MJ (1997) Serotonin, dopamine and norepinephrine transporter mRNAs: heterogeneity of distribution and response to “binge” cocaine administration. *Brain Res Mol Brain Res* 49:95–102
- Bush G (2010) Attention-deficit/hyperactivity disorder and attention networks. *Neuropsychopharmacology* 35:278–300
- Bymaster FP, Katner JS, Nelson DL et al (2002) Atomoxetine increases extracellular levels of norepinephrine and dopamine in prefrontal cortex of rat: a potential mechanism for efficacy in attention deficit/hyperactivity disorder. *Neuropsychopharmacology* 27:699–711
- Camasta S, Bonora E, Del Prato S et al (1999) Effect of obesity and insulin resistance on resting and glucose-induced thermogenesis in man. EGIR (European Group for the Study of Insulin Resistance). *Int J Obes Relat Metab Disord* 23:1307–1313
- Chamberlain SR, Müller U, Blackwell AD et al (2006) Neurochemical modulation of response inhibition and probabilistic learning in humans. *Science* 311:861–863
- Chamberlain SR, Del Campo N, Dowson J et al (2007a) Atomoxetine improved response inhibition in adults with attention deficit/hyperactivity disorder. *Biol Psychiatry* 62:977–984
- Chamberlain SR, Müller U, Deakin JB et al (2007b) Lack of deleterious effects of buspirone on cognition in healthy male volunteers. *J Psychopharmacol* 21:210–215
- Charnay Y, Leger L, Vallet PG et al (1995) [³H]Nisoxetine binding sites in the cat brain: an autoradiographic study. *Neuroscience* 69:259–270
- Christensen CR, Clark PB, Morton KA (2006) Reversal of hypermetabolic brown adipose tissue in F-18 FDG PET imaging. *Clin Nucl Med* 31:193–196
- Cypess AM, Lehman S, Williams G et al (2009) Identification and importance of brown adipose tissue in adult humans. *N Engl J Med* 360:1509–1517
- Del Campo N, Chamberlain SR, Sahakian BJ et al (2011) The roles of dopamine and noradrenaline in the pathophysiology and treatment of attention-deficit/hyperactivity disorder. *Biol Psychiatry* 69:e145–e157
- Dell’Osso B, Palazzo MC, Oldani L et al (2010) The noradrenergic action in antidepressant treatments: pharmacological and clinical aspects. *CNS Neurosci Ther* 17:723–732
- Dickstein SG, Bannon K, Castellanos FX et al (2006) The neural correlates of attention deficit hyperactivity disorder: an ALE meta-analysis. *J Child Psychol Psychiatry* 47:1051–1062
- Ding YS, Fowler JS (2005) New generation radiotracers for nAChR and NET. In: proceedings of the third La Jolla conference “the magic bullet a century later”. *Nucl Med Biol* 32:707–718
- Ding YS, Fowler JS, Volkow ND et al (1997) Chiral drugs: comparison of the pharmacokinetics of [¹⁴C]d-threo and L-threo-methylphenidate in the human and baboon brain. *Psychopharmacology (Berl)* 131:71–78
- Ding YS, Lin KS, Garza V et al (2003) Evaluation of a new norepinephrine transporter PET ligand in baboons, both in brain and peripheral organs. *Synapse* 50:345–352
- Ding YS, Lin KS, Logan J et al (2005) Comparative evaluation of positron emission tomography radiotracers for imaging the norepinephrine transporter: (S, S) and (R, R) enantiomers of reboxetine analogs ([¹¹C]methylreboxetine, 3-Cl-[¹¹C]methylreboxetine and [18F]fluororeboxetine), (R)-[¹¹C]nisoxetine, [¹¹C]oxaprotiline and [¹¹C]lortalamine. *J Neurochem* 94:337–351
- Ding YS, Lin KS, Logan J (2006) PET imaging of norepinephrine transporters. *Curr Pharm Des* 12:3831–3845
- Ding YS, Singhal T, Planeta-Wilson B et al (2010) PET imaging of the effects of age and cocaine on the norepinephrine transporter in the human brain using (S, S)-[(¹¹C)O-methylreboxetine and HRRT. *Synapse* 64:30–38
- Dopheide JA, Pliszka SR (2009) Attention-deficit-hyperactivity disorder: an update. *Pharmacotherapy* 29:656–679
- Eagle DM, Bari A, Robbins TW (2008) The neuropsychopharmacology of action inhibition: cross-species translation of the stop-signal and go/no-go tasks. *Psychopharmacology (Berl)* 199:439–456

- Elhai JD, Biehn TL, Armour C et al (2011) Evidence for a unique PTSD construct represented by PTSD's D1-D3 symptoms. *J Anxiety Disord* 25:340–345
- Eshleman AJ, Carmolli M, Cumbay M et al (1999) Characteristics of drug interactions with recombinant biogenic amine transporters expressed in the same cell type. *J Pharmacol Exp Ther* 289:877–885
- Esler MD, Wallin G, Dorward PK et al (1991) Effects of desipramine on sympathetic nerve firing and norepinephrine spillover to plasma in humans. *Am J Physiol* 260:R817–R823
- Faraone SV, Biederman J, Spencer T et al (2005) Efficacy of atomoxetine in adult attention-deficit/hyperactivity disorder: a drug-placebo response curve analysis. *Behav Brain Funct* 1:16
- First M, Gibbon M, Spitzer R et al (1996) Structured clinical interview for DSM-IV axis I disorders: non-patient edition (SCID-I/NP). Biometrics Department, New York State Psychiatric Institute, New York
- Gallezot JD, Planeta-Wilson B, Wang GK et al (2007) Parametric imaging of the NET radioligand [C-11]MRB in humans: a test-retest study. *J Nucl Med* 48:159P
- Gallezot JD, Weinzimmer D, Nabulsi N et al (2008) Evaluation of [C-11]MRB for receptor occupancy studies of norepinephrine transporters. *Neuroimaging* 41:T49
- Gallezot JD, Weinzimmer D, Nabulsi N et al (2010) Evaluation of [¹¹C]MRB for assessment of occupancy of norepinephrine transporters: studies with atomoxetine in non-human primates. *Neuroimage* 56:268–279
- Ganguly PK, Dhalla KS, Innes IR et al (1986) Altered norepinephrine turnover and metabolism in diabetic cardiomyopathy. *Circ Res* 59:684–693
- Ghose S, Fujita M, Morrison P et al (2005) Specific in vitro binding of (S, S)-[3H]MeNER to norepinephrine transporters. *Synapse* 56:100–104
- Golay A, Schutz Y, Felber JP et al (1986) Lack of thermogenic response to glucose/insulin infusion in diabetic obese subjects. *Int J Obes* 10:107–116
- Haenisch B, Linsel K, Bruss M et al (2009) Association of major depression with rare functional variants in norepinephrine transporter and serotonin1A receptor genes. *Am J Med Genet B Neuropsychiatr Genet* 150B:1013–1016
- Hahn MK, Robertson D, Blakely RD (2003) A mutation in the human norepinephrine transporter gene (SLC6A2) associated with orthostatic intolerance disrupts surface expression of mutant and wild-type transporters. *J Neurosci* 23:4470–4478
- Hahn MK, Mazei-Robison MS, Blakely RD (2005) Single nucleotide polymorphisms in the human norepinephrine transporter gene affect expression, trafficking, antidepressant interaction, and protein kinase C regulation. *Mol Pharmacol* 68:457–466
- Hahn MK, Blackford JU, Haman K et al (2008) Multivariate permutation analysis associates multiple polymorphisms with subphenotypes of major depression. *Genes Brain Behav* 7:487–495
- Hahn MK, Steele A, Couch RS et al (2009) Novel and functional norepinephrine transporter protein variants identified in attention deficit hyperactivity disorder. *Neuropharmacology* 57:694–701
- Hannestad J, Gallezot JD, Planeta-Wilson B et al (2010) Clinically relevant doses of methylphenidate significantly occupy the norepinephrine transporter in humans in vivo. *Biol Psychiatry* 6:854–860
- Hany TF, Gharehpapagh E, Kamel EM et al (2002) Brown adipose tissue: a factor to consider in symmetrical tracer uptake in the neck and upper chest region. *Eur J Nucl Med Mol Imaging* 29:1393–1398
- Houle S, Ginovart N, Hussey D et al (2000) Imaging the serotonin transporter with positron emission tomography: initial human studies with [¹¹C]DAPP and [¹¹C]DASB. *Eur J Nucl Med* 27:1719–1722
- Huang Y, Hwang DR, Narendran R et al (2002) Comparative evaluation in nonhuman primates of five PET radiotracers for imaging the serotonin transporters: [¹¹C]McN 5652, [¹¹C]ADAM, [¹¹C]DASB, [¹¹C]DAPA, and [¹¹C]AFM. *J Cereb Blood Flow Metab* 22:1377–1398
- Ichise M, Toyama H, Innis RB et al (2002) Strategies to improve neuroreceptor parameter estimation by linear regression analysis. *J Cereb Blood Flow Metab* 22:1271–1281
- Ichise M, Liow JS, Lu JQ et al (2003) Linearized reference tissue parametric imaging methods: application to [¹¹C]DASB positron emission tomography studies of the serotonin transporter in human brain. *J Cereb Blood Flow Metab* 23:1096–1112

- Innis RB, Cunningham VJ, Delforge J et al (2007) Consensus nomenclature for in vivo imaging of reversibly binding radioligands. *J Cereb Blood Flow Metab* 27:1533–1539
- Jequier E, Schutz Y (1985) New evidence for a thermogenic defect in human obesity. *Int J Obes* 9(Suppl 2):1–7
- Kaufman MJ, Speelman RD, Madras BK (1991) Distribution of cocaine recognition sites in monkey brain: I. In vitro autoradiography with [³H]CFT. *Synapse* 9:177–187
- Lee DE, Planeta-Wilson B, Gallezot JD et al (2012) Imaging norepinephrine transporter (NET) in abstinent cocaine users using (S, S)-[¹¹C]O-methylreboxetine. *J Nucl Med* 53(Suppl 1):474P
- Li CSR, Huang C, Constable RT et al (2006) Imaging response inhibition in a stop signal task – neural correlates independent of signal monitoring and post-response processing. *J Neurosci* 26:186–192
- Lijffijt M, Kenemans JL, Verbaten MN et al (2005) A metaanalytic review of stopping performance in attention-deficit/hyperactivity disorder: deficient inhibitory motor control? *J Abnorm Psychol* 114:216–222
- Lin KS, Ding YS, Kim SW et al (2005) Synthesis, enantiomeric resolution, F-18 labeling and biodistribution of reboxetine analogs: promising radioligands for imaging the norepinephrine transporter with positron emission tomography. *Nucl Med Biol* 32:415–422
- Lin S-F, Fan X, Yeckel CW et al (2012) Ex vivo and in vivo evaluation of the norepinephrine transporter ligand [¹¹C]MRB for brown adipose tissue imaging. *Nucl Med Biol* 39:1081–1086
- Liprando LA, Miner LH, Blakely RD et al (2004) Ultrastructural interactions between terminals expressing the norepinephrine transporter and dopamine neurons in the rat and monkey ventral tegmental area. *Synapse* 54:233–244
- Logan J, Ding YS, Lin KS et al (2005) Modeling and analysis of PET studies with norepinephrine transporter ligands: the search for a reference region. *Nucl Med Biol* 32:531–542
- Logan J, Wang GJ, Telang F et al (2007) Imaging the norepinephrine transporter in humans with (S, S)-[¹¹C]O-methyl reboxetine and PET: problems and progress. *Nucl Med Biol* 34:667–679
- Macey DJ, Smith HR, Nader MA et al (2003) Chronic cocaine self-administration upregulates the norepinephrine transporter and alters functional activity in the bed nucleus of the stria terminalis of the rhesus monkey. *J Neurosci* 23:12–16
- Madras BK, Miller GM, Fischman AJ (2005) The dopamine transporter and attention-deficit/hyperactivity disorder. *Biol Psychiatry* 57:1397–1409
- Makris N, Biederman J, Monuteaux MC et al (2009) Towards conceptualizing a neural systems-based anatomy of attention-deficit/hyperactivity disorder. *Dev Neurosci* 31:36–49
- Mash DC, Ouyang Q, Qin Y et al (2005) Norepinephrine transporter immunoblotting and radioligand binding in cocaine abusers. *J Neurosci Methods* 143:79–85
- Michelson D, Faries D, Wernicke J et al, Atomoxetine ADHD Study Group (2001) Atomoxetine in the treatment of children and adolescents with attention-deficit/hyperactivity disorder: a randomized, placebo-controlled, dose-response study. *Pediatrics* 108:E83
- Miner LH, Jedema HP, Moore FW et al (2006) Chronic stress increases the plasmalemmal distribution of the norepinephrine transporter and the coexpression of tyrosine hydroxylase in norepinephrine axons in the prefrontal cortex. *J Neurosci* 26:1571–1578
- Moron JA, Brockington A, Wise RA (2002) Dopamine uptake through the norepinephrine transporter in brain regions with low levels of the dopamine transporter: evidence from knock-out mouse lines. *J Neurosci* 22:389–395
- Nedergaard J, Bengtsson T, Cannon B (2007) Unexpected evidence for active brown adipose tissue in adult humans. *Am J Physiol Endocrinol Metab* 293:E444–E452
- O'Sullivan JB, Ryan KM, Curtin NM et al (2009) Noradrenaline reuptake inhibitors limit neuroinflammation in rat cortex following a systemic inflammatory challenge: implications for depression and neurodegeneration. *Int J Neuropsychopharmacol* 12:687–699
- Pietrzak RH, Tsai J, Harpaz-Rotem I et al (2012) Support for a novel five-factor model of post-traumatic stress symptoms in three independent samples of Iraq/Afghanistan veterans: a confirmatory factor analytic study. *J Psychiatr Res* 46:317–322
- Pietrzak RH, Gallezot JD, Ding YS et al (2013) Association of posttraumatic stress disorder with reduced in vivo norepinephrine transporter availability in the locus coeruleus. *JAMA Psychiatry* 70:1199–1205

- Robbins TW, Arnsten AF (2009) The neuropsychopharmacology of fronto-executive function: monoaminergic modulation. *Annu Rev Neurosci* 32:267–287
- Robertson SD, Matthies HJG, Owens WA et al (2010) Insulin reveals Akt signaling as a novel regulator of norepinephrine transporter trafficking and norepinephrine homeostasis. *J Neurosci* 30:11305–11316
- Saito M, Okamatsu-Ogura Y, Matsushita M et al (2009) High incidence of metabolically active brown adipose tissue in healthy adult humans: effects of cold exposure and adiposity. *Diabetes* 58:1526–1531
- Schou M, Halldin C, Sovago J et al (2003) Specific in vivo binding to the norepinephrine transporter demonstrated with the PET radioligand, (S, S)-[11C]MeNER. *Nucl Med Biol* 30:707–714
- Schou M, Halldin C, Sovago J et al (2004) PET evaluation of novel radiofluorinated reboxetine analogs as norepinephrine transporter probes in the monkey brain. *Synapse* 53:57–67
- Schou M, Halldin C, Pike VW et al (2005) Post-mortem human brain autoradiography of the norepinephrine transporter using (S, S)-[18F]FMeNER-D2. *Eur Neuropsychopharmacol* 15:517–520
- Seneca N, Gulyás B, Varrone A et al (2006) Atomoxetine occupies the norepinephrine transporter in a dose-dependent fashion: a PET study in nonhuman primate brain using (S, S)-[18F]FMeNER-D2. *Psychopharmacology (Berl)* 188:119–127
- Smith HR, Beveridge TJ, Porrino LJ (2006) Distribution of norepinephrine transporters in the non-human primate brain. *Neuroscience* 138:703–714
- Solanto MV (1998) Neuropsychopharmacological mechanisms of stimulant drug action in attention-deficit hyperactivity disorder: a review and integration. *Behav Brain Res* 94:127–152
- Spencer TJ, Biederman J, Wilens TE et al (2002) Novel treatments for attentiondeficit/hyperactivity disorder in children. *J Clin Psychiatry* 63(Suppl 12):16–22
- Swanson JM, Volkow ND (2009) Psychopharmacology: concepts and opinions about the use of stimulant medications. *J Child Psychol Psychiatry* 50:180–193
- Takano A, Gulyás B, Varrone A et al (2008) Imaging the norepinephrine transporter with positron emission tomography: initial human studies with (S, S)-[18F]FMeNER-D2. *Eur J Nucl Med Mol Imaging* 35:153–157
- Takano A, Gulyás B, Varrone A et al (2009) Comparative evaluations of norepinephrine transporter radioligands with reference tissue models in rhesus monkeys: (S, S)-[18F]FMeNER-D2 and (S, S)-[11C]MeNER. *Eur J Nucl Med Mol Imaging* 36:1885–1891
- Tatsumi M, Groshan K, Blakely RD et al (1997) Pharmacological profile of antidepressants and related compounds at human monoamine transporters. *Eur J Pharmacol* 340:249–258
- Tejani-Butt SM (1992) [3H]nisoxetine: a radioligand for quantitation of norepinephrine uptake sites by autoradiography or by homogenate binding. *J Pharmacol Exp Ther* 260:427–436
- van Marken Lichtenbelt WD, Vanhommerig JW et al (2009) Cold-activated brown adipose tissue in healthy men. *N Engl J Med* 360:1500–1508
- Volkow ND (2006) Stimulant medications: how to minimize their reinforcing effects? *Am J Psychiatry* 163:359–361
- Volkow ND, Ding Y-S, Fowler JS et al (1996) Dopamine transporters decrease with age. *J Nucl Med* 37:554–559
- Volkow ND, Wang GJ, Fowler JS et al (1998) Dopamine transporter occupancies in the human brain induced by therapeutic doses of oral methylphenidate. *Am J Psychiatry* 155:1325–1331
- Volkow ND, Wang GW, Fowler JS et al (2001) Therapeutic doses of oral methylphenidate significantly increase extracellular dopamine in the human brain. *J Neurosci* 21:RC121
- Volkow ND, Fowler JS, Wang GJ et al (2008) Methylphenidate decreased the amount of glucose needed by the brain to perform a cognitive task. *PLoS One* 3:e2017
- Weinshenker D, Schroeder JP (2007) There and back again: a tale of norepinephrine and drug addiction. *Neuropsychopharmacology* 32:1433–1451
- Wijers SL, Saris WH, van Marken Lichtenbelt WD (2009) Recent advances in adaptive thermogenesis: potential implications for the treatment of obesity. *Obes Rev* 10:218–226

- Wilson AA, Johnson DP, Mozley D et al (2003) Synthesis and in vivo evaluation of novel radiotracers for the in vivo imaging of the norepinephrine transporter. *Nucl Med Biol* 30:85–92
- Yeckel CW, Gulanski B, Zgorski ML et al (2009) Simple exercise recovery index for sympathetic overactivity is linked to insulin resistance. *Med Sci Sports Exerc* 41:505–515
- Zafar HM, Pare WP, Tejani-Butt SM (1997) Effect of acute or repeated stress on behavior and brain norepinephrine system in Wistar-Kyoto (WKY) rats. *Brain Res Bull* 44:289–295
- Zeng Z, Chen TB, Miller PJ et al (2006) The serotonin transporter in rhesus monkey brain: comparison of DASB and Citalopram binding sites. *Nucl Med Biol* 33:555–563

Positron Emission Tomography (PET) Imaging of Opioid Receptors

20

Aren van Waarde, Anthony R. Absalom,
Anniek K.D. Visser, and Rudi A.J.O. Dierckx

Contents

20.1	Introduction	586
20.2	Opioid Receptor Ligands for PET: A Historical Overview	587
20.3	Characteristics of Widely Used Radioligands.....	591
20.3.1	Cyclofoxy.....	591
20.3.2	CFN.....	593
20.3.3	DPN.....	594
20.3.4	MeNTI.....	595
20.3.5	GR103545	595
20.4	PET Studies in Healthy Volunteers	596
20.4.1	Influence of Gender, Hormonal Status, and Age	596
20.4.2	Personality Traits	597
20.4.3	Affective Responses.....	597
20.4.4	Pain.....	598
20.4.5	Vestibular Processing	600
20.4.6	Myocardial Opioid Receptors	600
20.4.7	Occupancy Studies.....	600

A. van Waarde (✉) • A.K.D. Visser
Department of Nuclear Medicine and Molecular Imaging, University Medical Center
Groningen, University of Groningen, Hanzeplein 1, 9713GZ Groningen, The Netherlands
e-mail: a.van.waarde@umcg.nl

A.R. Absalom
Department of Anaesthesiology, University Medical Center Groningen,
University of Groningen, Hanzeplein 1, 9713GZ Groningen, The Netherlands

R.A.J.O. Dierckx
Department of Nuclear Medicine and Molecular Imaging, University Medical Center
Groningen, University of Groningen, Hanzeplein 1, 9713GZ Groningen, The Netherlands

Department of Nuclear Medicine, University Hospital Gent, University of Gent,
De Pintelaan 185, 9000, Ghent, Belgium
e-mail: r.a.dierckx@umcg.nl

20.5	PET Studies in Patients and Drug Addicts.....	602
20.5.1	Major Depressive, Borderline Personality, and Posttraumatic Stress Disorder	602
20.5.2	Pain.....	603
20.5.3	Pain Treatment	605
20.5.4	Substance Abuse	606
20.5.5	Eating Disorders.....	609
20.5.6	Epilepsy.....	609
20.5.7	Neurodegenerative Diseases	611
20.5.8	Opioid Receptor Expression in Lung Tumors	612
	Conclusion	612
	References.....	612

Abstract

The opioid system consists of opioid receptors (which mediate the actions of opium), their endogenous ligands (the enkephalins, endorphins, endomorphins, dynorphin, and nociceptin), and the proteins involved in opioid production, transport, and degradation. PET tracers for the various opioid receptor subtypes are available, and changes in regional opioidergic activity have been assessed during both sensory and affective processing in healthy individuals and in various disease conditions such as chronic pain, neurodegeneration, epilepsy, eating disorders, and substance abuse. It is not always clear whether observed changes of tracer binding reflect altered release of endogenous opioids or altered opioid receptor expression. Some radioligands for opioid receptors have suboptimal kinetics (i.e., slow dissociation from their target protein) or can induce undesired side effects even at low administered doses (sedation, respiratory arrest). There remains a need for PET tracers with improved properties, which can selectively visualize changes of the apparent density of a single opioid receptor subtype. Yet, PET offers the unique opportunity of quantifying opioid receptor-mediated signaling in the human central nervous system *in vivo*.

20.1 Introduction

The term “opioid” is derived from opium: dried latex from the opium poppy (*Papaver somniferum*) which has been used since ancient times as an analgesic and recreational drug (Kalant 1997). An opioid is either a synthetic narcotic that has similar activities as opium or a naturally occurring peptide that has such activities. Several classes of endogenous opioids have been discovered, viz., the enkephalins (Hughes et al. 1975), endorphins (Cox et al. 1976; Simantov and Snyder 1976), endomorphins (Zadina et al. 1997), dynorphins (Goldstein et al. 1979), and nociceptin (Meunier et al. 1995; Reinscheid et al. 1995). These messenger substances bind to G-protein-coupled opioid receptors in the brain, the spinal cord, and the digestive tract. Agonist binding to opioid receptors results in a decrease of the activity of adenylyl cyclase (Snyder and Pasternak 2003; Trescot et al. 2008; Waldhoer et al. 2004).

At least four broad subclasses of opioid receptors have been identified by the use of selective ligands (Dhawan et al. 1996). Assessment of antagonist potencies against the actions of various opioid agonists in different tissue preparations resulted in the identification of the mu, delta, and kappa subclasses (Lord et al. 1977; Martin et al. 1976). Later, mRNAs for these three subtypes were cloned and characterized (Chen et al. 1993; Evans et al. 1992; Kieffer et al. 1992; Yasuda et al. 1993). Mu opioid receptors (μ OR) are named after morphine, the alkaloid which is the active compound in opium (Martin et al. 1976). Kappa opioid receptors (κ OR) derive their name from the drug ketocyclazocine (Martin et al. 1976). Delta opioid receptors (δ OR) were initially characterized in the murine vas deferens (Lord et al. 1977). μ OR are β -endorphin preferring, κ OR dynorphin preferring, and δ OR enkephalin preferring (Minami and Satoh 1995). Nonclassical, nociceptin- or opiate-like receptors 1 (ORL1) bind nociceptin (Meunier et al. 1995; Reinscheid et al. 1995).

β -Endorphin binds with nM affinity to μ OR and δ OR (K_i about 1 nM) but with low affinity to κ OR ($K_i=52$ nM) (Raynor et al. 1994). In contrast, dynorphin A has sub-nM affinity to κ OR ($K_i=0.5$ nM), low affinity to μ OR ($K_i=32$ nM), and negligible affinity to δ OR ($K_i>1$ μ M) (Raynor et al. 1994). Enkephalins have sub-nM or nM affinity to δ OR and μ OR (K_i values 0.6–4 nM) but negligible affinity to κ OR ($K_i>1$ μ M) (Raynor et al. 1994). Endomorphins are very potent and selective μ OR agonists ($K_i=0.3$ – 0.7 nM) (Hackler et al. 1997). Stimulation of μ OR or δ OR generally results in analgesia and reward, whereas κ OR stimulation may have negative consequences, such as dysphoria and hallucinations.

Opioids and their receptors play important roles in a large spectrum of physiological processes, including learning and memory, reward, mood, appetite, circadian rhythms, sexual activity, pregnancy, locomotion, cardiovascular, gastrointestinal, renal and hepatic function, respiration, regulation of body temperature, and immunological response (Vaccharino and Kastin 2001). Well known is their involvement in regulating the sensation of pain; opiates are clinically employed to produce analgesia.

20.2 Opioid Receptor Ligands for PET: A Historical Overview

Several radioligands for PET imaging of opioid receptors have been prepared. These include subtype-selective and non-subtype-selective agonists and antagonists (see Table 20.1). Several comprehensive reviews on opioid receptor imaging were published between 2000 and 2008 (Frost 2001; Hammers and Lingford-Hughes 2006; Henriksen and Willoch 2008; Koeppe and Duncan 2000; Lever 2007; Ravert et al. 2004; Sprenger et al. 2005).

The first attempt at *in vivo* labeling of opioid receptors was made in 1975. Investigators at Johns Hopkins University administered a labeled opioid receptor antagonist, [3 H]naloxone, to living rats. In the excised brain tissue of these animals, they observed a regional distribution of radioactivity which corresponded to the known distribution of opioid receptors in the rodent brain (striatum>hindbrain>cerebellum).

Table 20.1 PET probes for the opioid system

Name	Action	Abbreviation	Initial publication
[¹⁸ F]Cyclofoxy	Antagonist, μ OR, and κ OR	–	Pert et al. (1984)
[¹¹ C]Diprenorphine	Antagonist, non-subtype selective	DPN	Luthra et al. (1985)
[¹⁸ F]Diprenorphine	Antagonist, non-subtype selective	FDPN	Wester et al. (2000)
[¹¹ C]Buprenorphine	Mixed agonist/antagonist, non-subtype selective	BPN	Luthra et al. (1987)
[¹⁸ F]-FE-PEO	Full agonist, non-subtype selective	–	Riss et al. (2013)
[¹¹ C]Carfentanil	Agonist, μ OR	CFN	Dannals et al. (1985)
[¹¹ C]Methylnaltrindole	Antagonist, δ OR	MeNTI	Lever et al. (1992)
[¹¹ C]GR103545	Agonist, κ OR	–	Talbot et al. (2005)
[¹¹ C]MeJDTic	Antagonist, κ OR	–	Poisnel et al. (2008)
[¹¹ C]LY2795050	Antagonist, κ OR	–	Zheng et al. (2013)
[¹¹ C]NOP-1A	Antagonist, ORL1	–	Pike et al. (2011)
[¹⁸ F]MK-0911	Antagonist, ORL1	–	Hostetler et al. (2013)

Because of strong nonspecific binding of [³H]naloxone, acceptable target-to-nontarget ratios of radioactivity could only be reached after *ex vivo* washing of brain slices to remove nonspecifically bound tracer. Yet, this seminal study paved the way for all later imaging of neuroreceptors in the living brain (Pert and Snyder 1975).

The first successful PET probe for opioid receptors was prepared in 1984 (Channing et al. 1985; Pert et al. 1984). After intravenous administration of [¹⁸F]3-acetylcyclofoxy (3-acetyl-6-deoxy-6- β -[¹⁸F]-fluoronaltraxone), a regional distribution of radioactivity was observed which corresponded to the regional distribution of opioid receptors in the rat and baboon brain. Bound tracer in the baboon brain was completely displaced by the active (–)enantiomer of naloxone, whereas an identical dose of the inactive (+)enantiomer (0.13 mg/kg) had no effect (Pert et al. 1984).

Since [³H]naloxone showed a low ratio of specific-to-nonspecific binding, an antagonist with a higher affinity ([³H]diprenorphine, [³H]DPN) was prepared and successfully applied in autoradiography (review in Frost (2001)). However, labeling DPN with ¹¹C proved difficult. Because of these difficulties, radiochemists focused their attention on other opioid ligands, and a method was developed to label carfentanil (CFN) with ¹¹C, using a carboxylic acid analog of carfentanil as a precursor (Dannals et al. 1985). The resulting tracer, [¹¹C]CFN, was used to acquire the very first images of opioid receptors in the human brain (Frost et al. 1985). At baseline, a regional distribution of radioactivity was observed which corresponded to the known regional densities of μ OR. After treatment of the volunteer with naloxone (1 mg/kg), cerebral uptake of the tracer was strongly suppressed, indicating that [¹¹C]CFN binds to μ OR in the living brain *in vivo* (Frost et al. 1985). A regional distribution of radioactivity consistent with μ OR binding and blockade of tracer uptake by naloxone were also observed in the mouse brain. Thus, [¹¹C]CFN is suitable for studies of μ OR in rodents (Saji et al. 1992).

In the same year that the first images of opioid receptors in the human brain were acquired, radiochemists developed a method for preparation of [^{11}C]DPN. The compound was labeled at the N-carbon atom of its cyclopropylmethyl group (Luthra et al. 1985). A study with [^{11}C]DPN in four healthy volunteers indicated that the tracer is rapidly washed out from brain regions with a low density of opioid receptors, whereas activity is retained in receptor-rich target areas. Eighty to ninety percent of tracer binding in target regions is naloxone reversible, suggesting that [^{11}C]DPN is suitable for studies of opioid receptors in man (Jones et al. 1988).

A different method to prepare ^{11}C -DPN was later published. That method involves [^{11}C]-*O*-methylation of 3-*O*-*t*-butyldimethylsilyl-(6-*O*-desmethyl) diprenorphine with [^{11}C]methyl iodide, followed by acidic deprotection of the reaction product (Lever et al. 1987). The advantage of this approach compared to the previously published method is its greater radiochemical yield.

The non-subtype-selective opioid ligand buprenorphine (BPN) has also been labeled with ^{11}C . The first published method involved the reaction of an *N*-(decyclopropylmethyl) precursor of buprenorphine with [^{11}C]cyclopropanecarbonyl chloride followed by reduction with lithium aluminum hydride (Luthra et al. 1987). Later, a more facile synthesis of [^{11}C]BPN was reported, in which the drug was labeled with ^{11}C at the 6-methoxy position, using a methylation reaction with [^{11}C]iodomethane (Lever et al. 1990). In a preclinical study in a baboon, the cerebral kinetics of [^{11}C]BPN and [^{11}C]DPN were directly compared. (–)Naloxone-sensitive binding of both ligands was observed in the striatum but not in the cerebellum. Uptake values and time courses in the target region were similar. The investigators concluded that [^{11}C]DPN shows better kinetics than [^{11}C]BPN since [^{11}C]DPN is cleared more rapidly from brain areas devoid of opioid receptors (Shiue et al. 1991). [^{11}C]BPN shows a regional distribution in the baboon brain consistent with regional opioid receptor density, whereas bound radioactivity in target areas can be displaced by naloxone. Moreover, [^{11}C]BPN binding in the striatum shows a good (~10 %) short-term test-retest variability (Galyunker et al. 1996).

A non-subtype-selective agonist radioligand for opioid receptor imaging has recently become available. This compound, called ^{18}F -FE-PEO, binds with K_i values of 0.4–1.6 nM to all opioid receptor subtypes. The distribution of radioactivity in the rat brain corresponds to regional opioid receptor levels, but nonspecific binding is rather high (≥ 33 % even in target areas). ^{18}F -FE-PEO is relatively slowly metabolized (60 % parent in rat plasma after 3 h), and radioactive metabolites do not enter the brain (Riss et al. 2013).

The first successful radioligand for δOR was the antagonist $\text{N}1'-(^{11}\text{C})\text{methyl}$ naltrindole ($[^{11}\text{C}]\text{MeNTI}$). [^{11}C]MeNTI was synthesized by alkylation of 3-*O*-benzylnaltrindole with [^{11}C]methyl iodide followed by removal of the protecting benzyl moiety. [^{11}C]MeNTI binding in the brain of living mice was blocked (up to 75 %) by naltrindole (δOR antagonist), but not by cyprodine (μOR antagonist) nor by U50,488 (κOR agonist). Regional tracer uptake showed a linear, close correlation to δOR densities known from autoradiography. These data indicated that [^{11}C]MeNTI binds selectively to δOR in the mouse brain in vivo (Lever et al. 1992).

An attempt to label the delta-1 subtype of δ OR in the mouse brain with the selective ligand [3 H]benzylidenenaltrexone (BNTX) was only partially successful. Although some specific binding of the compound was observed in vivo and tracer uptake could be blocked with the appropriate compounds, ratios of specific-to-nonspecific binding were very poor (Lever et al. 1996). Fluorinated analogs of naltrindole (N1'-fluoroethyl-naltrindole or BU97001 and N1'-fluoroethyl-(14-formylamino)-naltrindole or BU97018) have been proposed for PET imaging. BU97001 has been tritiated and used successfully for autoradiography of the rat brain; it shows sub-nM affinity to δ OR (K_d 0.42 nM) (Tyacke et al. 2002). However, PET data for [18 F]BU97001 have not yet been reported.

A 11 C-labeled N-substituted quinolinimide derivative with much higher subtype selectivity than [11 C]MeNTI has been tested as a potential ligand for in vivo imaging of δ OR. The compound was rapidly degraded in both plasma and brain tissue after intravenous injection in rats, and specific binding could not be detected in vivo (Bourdier et al. 2007). A radiofluorinated δ OR antagonist based on the Dmt-Tic pharmacophore has also been prepared. Although the compound showed significant binding to δ OR in brain slices, it failed to cross the blood-brain barrier in living rats (Ryu et al. 2008). Three benzamide δ OR agonists have been labeled with 11 C and subjected to preclinical testing. All compounds showed a very low brain uptake and no regional specific binding in mice. One of the compounds, called [11 C]SNC80, was also tested in a monkey. Results in this primate were similar to those seen previously in mice, i.e., low blood-brain barrier permeability and a uniform distribution of radioactivity throughout the brain, indicating nonspecific binding (Pichika et al. 2010).

Initial attempts at developing subtype-selective radioligands for κ OR were not successful. 18 F-labeled analogs of U-50488 were prepared by fluoroalkyl substitution, but the labeling procedure resulted in a very strong (≥ 100 -fold) loss of affinity with reference to the parent compound (Chesis et al. 1990b). A successful agonist radioligand for κ OR, [11 C]GR89696, was finally prepared in 1999 (Ravert et al. 1999). The R enantiomer, later called [11 C]GR103545, shows an excellent hypothalamus/cerebellum ratio of 11.4 in the mouse brain at 90 min after injection, in contrast to the S enantiomer which is inactive (target/nontarget ratio=1) (Ravert et al. 2002). Using subtype-selective opioid receptor ligands in blocking studies, the binding of [11 C]GR103545 was shown to be κ OR selective and saturable. Preclinical evaluation in baboons also indicated that [11 C]GR103545 is a promising tracer for imaging of κ OR. A regional distribution of radioactivity is observed that is consistent with the regional density of κ OR. Naloxone pretreatment reduces tracer uptake in all brain regions to the level observed in the cerebellum. In vivo binding of the tracer is stereoselective, and significant washout occurs within the time frame of a PET scan (Talbot et al. 2005). A one-pot radiosynthesis for preparation of [11 C]GR103545 with high specific radioactivity has recently been described (Nabulsi et al. 2011).

Antagonist radioligands for κ OR have also been proposed. [11 C]MeJDTic was prepared by methylation of the precursor JDTic with [11 C]methyl triflate. In a pre-clinical study in mice, high uptake of the tracer was noted in target organs (lung,

hypothalamus). Blocking and displacement studies with nonradioactive kappa, mu, and delta ligands suggested that [^{11}C]MeJDTic binds specifically to κOR in the brain of living mice *in vivo* (Poinsel et al. 2008). Yet, no follow-up studies with [^{11}C]MeJDTic have been reported. Another antagonist, [^{11}C]LY2795050, was evaluated in Sprague–Dawley rats, wild-type and κOR knockout mice, and rhesus monkeys. Specific binding of the probe to cerebral κOR was observed; this binding was completely blocked by pretreatment of monkeys with naloxone (1 mg/kg) and dose-dependently inhibited by the selective κOR antagonist LY2456302. Tracer metabolism in primates is moderate (40 % parent remaining in monkey plasma at 30 min), and tracer pharmacokinetics appears favorable; thus, [^{11}C]LY2795050 is the first successful antagonist radioligand for κOR (Zheng et al. 2013).

The last subclass of the opioid system for which imaging probes have been developed is the nociceptin/orphanin or opiate-like receptor (ORL1). [^{11}C]Methyl-Ro64-6198 failed as a radioligand for this subtype since its *in vivo* binding in the mouse brain was largely nonspecific (Ogawa et al. 2001). A second probe, [^{11}C]CPEB, showed some saturable *in vivo* binding but lack of specificity to ORL1 (Ogawa et al. 2003).

The first successful ORL1 ligand was [^{11}C]NOP-1A, a specific antagonist with sub-nM affinity (0.15 nM). This compound was selected from a library of ORL1 antagonists developed by Eli Lilly & Co. (Pedregal et al. 2012). After intravenous administration of [^{11}C]NOP-1A to rhesus monkeys, a regional cerebral distribution of radioactivity is observed consistent with binding of the probe to its target. Brain uptake is reduced by 50–70 % after pretreatment of animals with the ORL1 antagonist SB-612111 (Kimura et al. 2011; Pike et al. 2011). The regional distribution of [^{11}C]NOP-1A in the human brain resembles that in the monkey brain. Regional distribution volume of the tracer can be reliably estimated using a 2-tissue compartment model with arterial sampling or Ichise's noncompartmental bilinear analysis (Lohith et al. 2012).

Another ORL1 antagonist for PET imaging has recently been developed by Merck. Their compound [^{18}F]MK-0911 shows a regional distribution in the monkey and human brain consistent with the regional expression of ORL1. Binding in the monkey brain is inhibited after pretreatment of animals with several structurally diverse ORL1 antagonists (MK-0584, MK-0337, MK-5757). Dose-dependent occupancy of ORL1 in the human brain by nonradioactive MK-5757 could be assessed with [^{18}F]MK-0911 and PET (Hostetler et al. 2013).

20.3 Characteristics of Widely Used Radioligands

20.3.1 Cyclofoxy

[^3H]Cyclofoxy, the parent compound of [^{18}F]cyclofoxy, labels both μOR and κOR in the autoradiography of the rat and guinea pig brain (McLean et al. 1987; Rothman and McLean 1988). The regional pattern of radioactivity in the rat brain after *in vivo* injection of [^3H]cyclofoxy corresponds to the regional distribution of these opioid

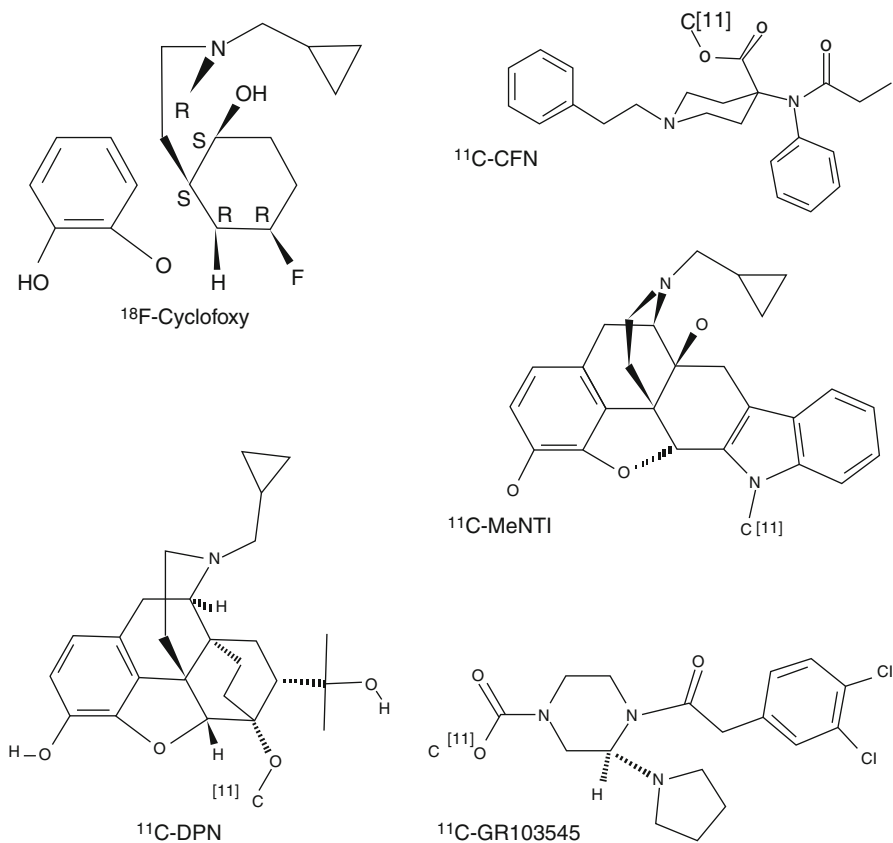


Fig. 20.1 Chemical structures of widely used opioid radioligands

receptor subtypes (Ostrowski et al. 1987; Rothman and McLean 1988), and brain radioactivity is reduced to background levels after pretreatment of animals with unlabeled naloxone (Ostrowski et al. 1987). K_i values of (–)cyclofoxy for μ OR, κ OR, and δ OR in rat brain membranes are 2.6, 9.3, and 89 nM, respectively, whereas the (+)enantiomer is essentially inactive (K_i values > 10 μ M) (Rothman et al. 1988). Consistent with these in vitro data, uptake of the radiofluorinated (–)enantiomer in the rat brain shows striking regional differences consistent with tracer binding to opioid receptors, whereas the tritiated (+)enantiomer is rather homogeneously distributed and shows low brain uptake. Pretreatment of animals with unlabeled (–)cyclofoxy reduces the uptake of [¹⁸F](–)cyclofoxy in all regions to the level of the tritiated (+) enantiomer (Kawai et al. 1990). Thus, [¹⁸F]cyclofoxy visualizes μ OR and κ OR in the living brain (Fig. 20.1).

Kinetic analysis of [³H]cyclofoxy uptake in the rat brain suggested an in vivo K_d of 2.1–5.2 nM in different brain areas and a B_{max} ranging from 1 pmol/g in the cerebellum to 78 pmol/g in the thalamus. Binding was reversible on a PET time scale

(Sawada et al. 1991). In a follow-up study, a combination of bolus injection and constant infusion of [^{18}F]cyclofoxy was applied to estimate the receptor-ligand parameters in a condition of “true” tissue-blood equilibrium, which was reached after 60 min. K_d values of 1.4–2.9 nM were measured and B_{max} in target areas ranged from 15 to 74 pmol/g tissue. Rodent cerebellum could not be used as a reference region since the level of nonspecific binding in the cerebellum was different from that in other parts of the brain (Kawai et al. 1991). Bolus plus continuous infusion of [^{18}F]cyclofoxy was also advantageous in baboons, as it resulted in shorter scan times, a simplified protocol for blood sampling, and more accurate receptor measurements (Carson et al. 1993).

20.3.2 CFN

In vitro binding assays in human thalamic membranes indicated a K_d of 0.08 nM for ^3H -CFN (Titeler et al. 1989). In the rat brain, K_i values of 0.051, 4.7, and 13 nM were measured at μOR , δOR , and κOR , respectively (Frost et al. 1985). For the guinea pig brain, the corresponding values were 0.024, 3.28, and 43.1 nM (Cometta-Morini et al. 1992). In vitro competition studies using opioid ligands with a wide range of subtype selectivities confirmed that [^3H]CFN selectively labels μOR , in both the rat and human brain (Titeler et al. 1989). Thus, CFN is a potent and selective μOR agonist.

A study which applied compartment modeling for the analysis of ^{11}C -CFN binding in the human brain showed that the occipital cortex can be considered as a region with low or negligible receptor density. Target region-to-occipital cortex ratios of radioactivity at late time points can be used instead of ratios of k_3/k_4 when tracer kinetic modeling is not feasible, e.g., in clinical research protocols (Frost et al. 1989). However, Logan graphical analysis or a simplified reference tissue model approach can provide more accurate estimates of ^{11}C -CFN binding to μOR in the human brain than the ratio method (Endres et al. 2003). A test-retest study which assessed ^{11}C -CFN binding in the brain of healthy volunteers twice, on a single day, indicated that both the regional two-tissue compartment model distribution volume (V_T) of the tracer and binding potential (BP_{ND}) are reproducible (variability <6 and $<10\%$, respectively) (Hirvonen et al. 2009).

Administration of ^{11}C -CFN can induce somnolence and sedation and, at higher dose, respiratory arrest. These pharmacological effects are related to the fact that CFN is an opioid agonist. The upper limit for the administered mass of CFN is about 0.1 $\mu\text{g}/\text{kg}$ (Frost 2001). [^{11}C]CFN binding in the human brain is affected by polymorphisms of the μOR gene. Carriers of the G allele (Asn40Asp variant, which may contribute to the development of alcohol dependence) have lower global binding potential than subjects homozygous for the A allele (Weerts et al. 2013).

Radiofluorinated analogs of carfentanil with subnanomolar affinities to μOR have been prepared (Henriksen et al. 2005b). *N*-[4-(methoxymethyl)-1-[2-(2-thienyl)ethyl]-4-piperidinyl]-*N*-phenyl-2-(\pm)-[^{18}F]fluoropropanamide ([^{18}F]sufentanil) showed a high brain uptake in living mice and a distribution of radioactivity

corresponding to regional μ OR expression. The compound was rapidly metabolized in plasma (only 21 % parent remaining at 40 min), but the metabolites appeared to not enter the brain in significant amounts (Henriksen et al. 2005a).

20.3.3 DPN

Another widely applied radioligand for opioid receptor mapping is [^{11}C]DPN. [^3H]DPN binds with subnanomolar (K_d 0.22–0.23 nM) affinity to opioid receptors in the rat brain (Chang et al. 1981) and in the human frontal cortex (Pfeiffer et al. 1982). K_i values of DPN for μ OR, δ OR, and κ OR in the rat brain are 0.20, 0.18, and 0.47 nM, respectively (Chang et al. 1981). Thus DPN is a non-subtype-selective opioid antagonist.

Using RB101, an inhibitor of enkephalin-degrading enzymes, the *in vivo* binding of [^3H]DPN to opioid receptors in the mouse brain was shown to be sensitive to competition by endogenous enkephalins. Although RB101 is devoid of affinity to opioid receptors, the compound dose-dependently inhibits [^3H]DPN binding in the unstressed mouse brain up to a maximum of 30 %. When mice were stressed by a warm-swim test, a greater inhibition of [^3H]DPN binding by RB101 was observed (maximally 45 %). These effects of RB101 are probably related to increased levels of endogenous enkephalins (Ruiz-Gayo et al. 1992).

A validation study using [^3H]DPN in rats showed that compartment modeling of PET data with the cerebellum as reference region can provide accurate measurements of regional opioid receptor B_{\max} and K_d , although K_d values estimated *in vivo* are an order of magnitude higher than those determined *in vitro*, probably due to diffusion gradients in tissue or protein binding of the radioligand (Cunningham et al. 1991). However, the cerebellum cannot be considered as a region devoid of opioid receptors in human studies since μ OR and κ OR are expressed at low levels in this area of the human brain (Schadrack et al. 1999).

The kinetics of [^{11}C]DPN and [^{11}C]CFN in the brain of human volunteers have been directly compared (Frost et al. 1990; Villemagne et al. 1994). Binding of both ligands in the thalamus (an area containing mainly μ OR) was not significantly different, but [^{11}C]DPN showed significantly greater binding than [^{11}C]CFN in the striatum, cingulate, and frontal cortex. Dissociation of [^{11}C]CFN from its binding sites was observed, but dissociation of [^{11}C]DPN was hardly noticeable. [^{11}C]CFN binding reached a plateau, whereas [^{11}C]DPN uptake showed a steady increase (Frost et al. 1990). Total radioactivity in the human brain (SUV) and the ratio of total/nonspecific binding were twice as great after administration of [^{11}C]DPN than [^{11}C]CFN. The dose of naloxone required to fully block [^{11}C]DPN binding was ten times greater than that required for [^{11}C]CFN (Villemagne et al. 1994). Thus, [^{11}C]DPN appeared to label δ OR and KOR in addition to the μ OR which are selectively labeled by [^{11}C]CFN.

Both the regional density (B_{\max}) and radioligand affinity (K_d) of opioid receptors can be assessed by applying a two-injection protocol, in which [^{11}C]DPN is administered at high (20–160 TBq/mmol) and low (1–3 TBq/mmol) specific

radioactivities (Sadzot et al. 1991) or by a pulse-chase protocol (Jones et al. 1994b). Parametric images of [^{11}C]DPN binding can be prepared, using both conventional spectral analysis and rank shaping (Hammers et al. 2007b).

Radiofluorinated analogs of DPN have been prepared. *N*-(3-[^{18}F]Fluoropropyl)-*N*-nordiprenorphine (FPND) showed rather limited brain uptake (Bai et al. 1990) but a striatum/cerebellum ratio of 3.3 ± 0.7 at 30 min postinjection which was reduced to unity after pretreatment of animals with naloxone (1 mg/kg). The tracer was extensively metabolized (<25 % parent remaining in blood at 30 min), but not significantly defluorinated (Chesis et al. 1990a). 6-*O*-(3-[^{18}F]Fluoroethyl)-6-*O*-desmethyldiprenorphine ([^{18}F]DPN) showed a regional binding pattern in the human brain similar to that of [^{11}C]DPN (Wester et al. 2000). FDPN binds to μOR , δOR , and κOR in rat brain slices like the parent tracer, DPN (Wester et al. 2000). A scan duration of at least 90 min is required for reliable estimates of tracer distribution volume (Boecker et al. 2005). If metabolite-corrected plasma data are used as input function, individualized metabolite correction should be performed since women metabolize FDPN significantly faster than men (Henriksen et al. 2006).

20.3.4 MeNTI

K_i values of MeNTI at δOR , μOR , and κOR in guinea pig brain membranes are 0.02, 14, and 65 nM, respectively (Portoghesi et al. 1990). Thus, MeNTI is a very potent and subtype-selective δOR antagonist.

In the human brain, [^{11}C]MeNTI shows regional kinetics concordant with selective binding of the tracer to δOR . Prolonged retention of radioactivity is observed in receptor-rich areas, whereas the ligand is rapidly washed out from nontarget areas of the brain. The regional distribution of radioactivity is closely correlated with local δOR densities but not with regional densities of μ or κ binding sites. Tracer uptake is blocked after pretreatment of volunteers with naltrexone (up to 73 %) (Madar et al. 1996).

[^{11}C]MeNTI shows irreversible binding characteristics in the human brain during a 90-min scanning period. A constrained three-compartment kinetic model is superior to other data-analytical techniques for quantification of the in vivo binding of the tracer to δOR (Smith et al. 1999).

20.3.5 GR103545

The subtype selectivity of [^{11}C]GR103545 has been determined in HEK-239 cells expressing human κOR , CHO-K1 cells expressing human μOR , and CHO cells expressing human δOR . K_i values at the three OR subtypes were 0.02, 16.2, and 536 nM, respectively (Schoultz et al. 2010). Thus, [^{11}C]GR103545 is an extremely potent and subtype-selective κOR agonist.

In a preclinical study in awake rhesus macaques, [^{11}C]GR103545 showed a regional volume of distribution in the brain which corresponded to regional κOR

densities (Schoultz et al. 2010). In a more recent study, the use of a bolus-plus-continuous-infusion protocol was shown to permit estimation of both B_{\max} and K_d of κ OR in the monkey brain in vivo (Tomasi et al. 2013). The cerebellum was used as the reference region in kinetic analysis.

A low injected mass of [^{11}C]GR103545 is essential since this κ OR agonist can induce respiratory depression, reductions of heart rate, and sedation even at very low administered doses of 0.3 $\mu\text{g}/\text{kg}$. Based on the K_d value estimated for the radioligand in nonhuman primates, a dose of 1.4 μg (3.38 nmol) was estimated as an acceptable dose limit in human studies for subjects with a body mass of 70 kg (Tomasi et al. 2013).

20.4 PET Studies in Healthy Volunteers

20.4.1 Influence of Gender, Hormonal Status, and Age

^{11}C -CFN-PET has been applied for the study of changes of opioid receptor binding in the brain of women during the menstrual cycle. No significant differences in tracer binding were noted between the follicular and luteal phases of the cycle, but follicular levels of estradiol in the circulation were negatively correlated with ^{11}C -CFN binding potential in the amygdala and hypothalamus. These results, combined with measurements of luteinizing hormone pulse, suggested that μ OR in the amygdala modulate gonadal steroid hormone pulsatility, whereas circulating estradiol regulates μ OR function in the brain (Smith et al. 1998). Neuroimaging has shown that black cohosh, a herbal extract used to treat menopausal symptoms, affects the endogenous opioid receptor system. Significant increases in ^{11}C -CFN binding potential (10–61 %) were noted in the cortical areas, thalamus, and nucleus accumbens of the brain of postmenopausal women (Reame et al. 2008). In the thalamus and nucleus accumbens, similar effects were observed after estrogen replacement therapy (Smith et al. 2006).

A PET study with ^{11}C -CFN, involving 50 subjects, indicated that the cerebral binding of ^{11}C -CFN is affected both by gender and by age. Binding potential of the radioligand increased with age in the neocortex and putamen. Women showed higher ^{11}C -CFN binding than men of the same age in several cortical and subcortical areas; however, in postmenopausal women μ OR binding in the thalamus and amygdala declined to levels lower than in age-matched men (Zubieta et al. 1999). A PET study with [^{18}F]cyclofoxy confirmed that opioid receptor binding in the thalamus of females is lower than in males, both in healthy aged subjects and in patients with Alzheimer disease (Cohen et al. 2000). MRI-based partial volume correction is required for the accurate assessment of receptor densities in small structures of the human brain. Applying such correction to ^{11}C -CFN data for the left temporal cortex, binding of the radioligand appeared to increase with age (0.9 % per year), consistent with B_{\max} values from postmortem autoradiography. Without partial volume correction, the effect of aging could not be observed (Bencherif et al. 2004a).

20.4.2 Personality Traits

Several PET studies have explored relationships between opioid receptor availability in the human brain and personality traits. Using the tracer [^{18}F]DPN, German investigators scanned 23 healthy male volunteers under resting conditions. Subsequently, the subjects were psychologically tested for novelty seeking, harm avoidance, reward dependence, and persistence. A significant correlation was detected between the score for reward dependence (a personality trait predisposing for addictive behavior) and tracer binding potential in the bilateral ventral striatum with nucleus accumbens (Schreckenberger et al. 2008). A later study from the USA involved scanning of 19 young healthy male volunteers with the μOR ligand [^{11}C]CFN and PET. Subjects were scanned both at baseline and during receipt of a painful stress challenge (infusion of hypertonic saline solution in the left masseter muscle). High scores for impulsiveness and low deliberation scores were associated with significantly higher baseline μOR availability and greater stress-induced endogenous opioid system activation, measured as a reduction of [^{11}C]CFN binding potential. These differences were noted in several brain areas (prefrontal and orbitofrontal cortices, anterior cingulate, thalamus, nucleus accumbens, and basolateral amygdala). Thus, μOR binding potential appears to predict an individual's vulnerability to risky behaviors, such as the development of substance abuse (Love et al. 2009). An interesting study from Finland measured brain μOR availability with [^{11}C]CFN under resting conditions in 22 healthy volunteers: 10 individuals scoring in the upper and 12 individuals scoring in the lowest quartile for harm avoidance. A high score for harm avoidance (particularly in the subscales shyness with strangers, fatigability, and asthenia) was associated with high μOR availability (or low endogenous μ -opioid drive) in the anterior cingulate cortex, ventromedial and dorsolateral prefrontal cortices, and anterior insular cortex. Thus, high μOR availability may be related to vulnerability for affective disorders (Tuominen et al. 2012).

20.4.3 Affective Responses

The opioid system appears to play an important role in the regulation of affective responses. An initial PET study examined [^{11}C]CFN binding and blood flow (uptake of ^{15}O -water) in the brain of 12 healthy male volunteers, which viewed either aversive images (facial mutilation, wounds, dead bodies) or neutral images (common objects, benign scenes, normal faces). Higher baseline μOR binding potential in the left temporal pole of the subjects was associated with lower blood flow in this region during presentation of the aversive emotional stimuli. This finding was interpreted as evidence for an inhibitory or anxiolytic role of the opioid system in limbic regions of the brain (Liberzon et al. 2002).

A second study examined healthy female volunteers, using ^{11}C -CFN and PET. Sustained neutral and sadness states were elicited by the recall of an autobiographical event associated with these emotions. Sustained sadness caused an increase of μOR availability in the rostral anterior cingulate, ventral pallidum, amygdala, and

inferior temporal cortex which was interpreted as reflecting a reduction of the release of endogenous opioids due to deactivation of opioid neurotransmission (Zubieta et al. 2003).

Long-distance runners have often reported to enter a state of euphoria while running, commonly referred to as “runner’s high.” In order to examine possible mechanisms underlying this phenomenon, ten athletes were scanned with [^{18}F]DPN and PET, both at rest and after 2 h of endurance running (in random order). By SPM2 analysis, reductions of tracer binding were noted in several brain areas after exercise. Reported levels of euphoria were inversely correlated with [^{18}F]DPN binding in the prefrontal/orbitofrontal cortices, anterior cingulate cortex, bilateral insula, parainsular cortex, and temporoparietal regions. These findings support the idea that running is associated with increased release of endorphins, resulting in positive mood changes (Boecker et al. 2008).

Whereas sustained sadness in healthy volunteers is associated with a reduction in the release of endogenous opioids, positive emotion appears to be associated with an increase of that release. An interesting study from London scanned 25 healthy male volunteers with [^{11}C]DPN and PET, both during positive mood induction (sexually oriented video clip, listening to favorite music, reading positive statements, unexpected gift of 30 GBP) and during neutral mood (nature movie, listening to unknown classical music, reading neutral statements, no gift). Significant reductions of [^{11}C]DPN binding were noted in the hippocampus during positive mood induction, and the magnitude of positive mood change was negatively correlated with DPN binding in the amygdala (Koepp et al. 2009).

20.4.4 Pain

Opioid receptor expression ([^{11}C]DPN or [^{18}F]DPN binding) is high in projections of the medial and part of the lateral pain system of the human brain (Baumgartner et al. 2006; Jones et al. 1991). The lateral network is believed to be associated with the sensory aspects and the medial network with the affective aspects of pain perception. Reductions in receptor availability have been observed in healthy volunteers suffering pain. These data can be interpreted as decreases of regional receptor availability because of release of endogenous opioids, although internalization or downregulation of opioid receptors can also occur. Released opioids may mediate antinociception.

Sustained masseter muscle pain in 20 healthy volunteers was associated with significant declines of the binding of [^{11}C]CFN in several cortical and subcortical brain regions (Zubieta et al. 2001). When capsaicin was applied to the dorsal side of the left hand of eight healthy volunteers, a pain-related decrease in [^{11}C]CFN binding was measured in the contralateral thalamus (Bencherif et al. 2002). In eight healthy volunteers who received painful heat stimulation through the right forearm, a significant reduction of [^{18}F]DPN binding was noted in the limbic and paralimbic areas of the brain, including the rostral anterior cingulate cortex and the insula (Sprenger et al. 2006a).

The duration of pain-induced changes in μ OR binding potential has been examined in a PET study with [^{11}C]CFN. Three subsequent 90-min scans were made in 14 healthy male volunteers; the first scan consisted of two 45-min baseline intervals, the second scan involved a 45-min period of sustained muscle pain followed by a 45-min baseline interval, and the third scan consisted again of two 45-min baseline intervals. Robust decreases of [^{11}C]CFN binding were noted in several cortical and subcortical regions during the pain challenge. However, these changes did not persist in a subsequent scan. Pain-induced alterations of opioid release and/or μ OR internalization are therefore short lasting (Scott et al. 2007b).

In a study involving 14 male and 14 female healthy individuals subjected to sustained masseter muscle pain (infusion of hypertonic saline), men demonstrated larger declines of [^{11}C]CFN binding in the anterior thalamus, ventral basal ganglia, and amygdala. Conversely, women showed greater declines of the PET signal in the nucleus accumbens. Thus, opioid receptor-mediated antinociceptive responses show gender differences (Zubieta et al. 2002).

Opioid release is also involved in placebo analgesia. In a PET study with [^{11}C]CFN, healthy subjects were scanned under four different conditions: painful skin heat with placebo cream, painful skin heat under control conditions, nonpainful warmth with placebo cream, and nonpainful warmth under control conditions. In all cases, the volunteers were told that the placebo cream was a powerful analgesic. Placebo treatment resulted in significant decreases of [^{11}C]CFN binding in several brain regions known to be involved in pain and affect; thus, endogenous opioid release appears to be part of the mechanism by which expectancies regulate the perception of pain (Wager et al. 2007). A later study from the same group examined placebo and nocebo effects, i.e., the subjects expected the placebo cream to either ameliorate or exacerbate their pain. Placebo and nocebo effects were found to be associated with opposite opioid and dopaminergic responses. A placebo-activated opioid neurotransmission in the anterior cingulate, orbitofrontal and insular cortices, nucleus accumbens, amygdala, and periaqueductal gray, whereas dopaminergic neurotransmission was activated in the ventral basal ganglia including the nucleus accumbens. Nocebo responses consisted of a deactivation of opioid and dopamine release. The magnitude of opioid and dopamine activation was correlated with the anticipated and subjectively perceived placebo effect (Scott et al. 2008).

When heat pain was combined with either acupuncture or placebo needle stimulation in healthy volunteers, acupuncture was shown to result in altered binding of [^{11}C]DPN (mainly decreases) in the orbitofrontal cortex, medial prefrontal cortex, insula, thalamus, and anterior cingulate cortex (Dougherty et al. 2008).

Opioid receptor availability at baseline conditions appears to be a predictor of human sensitivity to both painful (cold pressor test) and mechanical stimuli (touch, vibration). Greater sensitivity was associated with a lower BP of [^{18}F]DPN in various cortical areas (Mueller et al. 2010). In a later study on 12 healthy male volunteers, a significant correlation was observed between baseline binding potential of [^{11}C]CFN (μ OR binding) in the striatum and the cold pressor pain threshold (Hagelberg et al. 2012).

20.4.5 Vestibular Processing

An interesting study examined involvement of the opioid system in vestibular neurotransmission in humans. Ten right-handed healthy volunteers were scanned with the ligand [^{18}F]DPN, both under baseline conditions and during caloric stimulation of the right ear. Each 90-min scan session consisted of three subsequent phases: a prestimulation period (30 min), a stimulation or sham period (30 min), and a follow-up period (30 min). During the stimulation period, warm (44 °C) and cold (30 °C) air were alternated at 5-min intervals in order to avoid habituation; during the sham period the tubing was fixed to the subjects head in such a way that the air flow passed beside the ear. A decrease in tracer binding was noted in the right posterior insular cortex and the postcentral region during stimulation, indicating release of endogenous opioids and involvement of the opioid system in vestibular processing (Baier et al. 2010).

20.4.6 Myocardial Opioid Receptors

Both ^{11}C -*N*-methyl-naltrindole (^{11}C -MeNTI) and ^{11}C -CFN show specific binding in the human heart. However, the reduction of myocardial distribution volume and binding potential of these opioid ligands after pretreatment of volunteers with naloxone is only minor (14–21 and 19–25 %, respectively), suggesting low levels of δOR and μOR expression and poor signal-to-noise ratios in PET (Villemagne et al. 2002).

20.4.7 Occupancy Studies

PET offers the unique opportunity of measuring the fraction of receptor populations occupied by nonradioactive drugs in the living brain and relating measured levels of occupancy to the magnitude of the therapeutic effect or to unwanted side effects. Receptor occupancy is estimated by assessing competition of a nonradioactive drug with the radioligand for the same binding sites. The basic idea was already published in 1980 (Homey et al. 1980).

Using the radioligand [^{11}C]CFN, a half-life of μOR blockade of 72–108 h was measured in the brain of healthy volunteers after a single oral dosing of naltrexone, corresponding to the duration of pharmacological effects when the drug is used for treatment of heroin dependence (Lee et al. 1988).

A later study with ^{11}C -CFN compared the duration of occupancy of μOR in the human brain by the antagonists nalmefene and naloxone. Clearance half-lives were 28.7 h after administration of 1 mg of nalmefene and 2.0 h for 2 mg of naloxone. The longer blockade by nalmefene could represent an advantage in the clinical use of this compound for reversal of opioid anesthesia or for treatment of drug addicts after an opioid overdose (Kim et al. 1997). Nalmefene has also been proposed for treatment of alcoholism. The decline of μOR occupancy in the human brain after

single or repeated nalmefene dosing was found to be slower than the decline in plasma concentration of the drug or its metabolites, indicating slow dissociation of receptor-bound nalmefene *in vivo* (Ingman et al. 2005).

Buprenorphine is used for the treatment of heroin dependence. Buprenorphine occupancy of μ OR in the human brain has been examined, using ^{11}C -CFN and PET. Four hours after administration of 2 mg buprenorphine, receptor occupancy ranged from 36 to 50 %. When the buprenorphine dose was raised to 16 mg, levels of occupancy increased to 79–95 %. Placebo-treated heroin abusers had greater μ OR binding potential in the inferofrontal and anterior cingulate cortex compared to matched healthy controls (Zubieta et al. 2000). Increasing doses of buprenorphine were associated both with decreased μ OR availability and with decreased withdrawal symptoms. The highest dose of buprenorphine (32 mg) caused virtually complete μ OR occupancy (Greenwald et al. 2003). The duration of action of buprenorphine was examined in ten heroin-dependent subjects after termination of a 16-mg/day dose of the drug. Relative to a control group of heroin-dependent subjects maintained on placebo, μ OR occupancy was 70, 46, 33, and 18 % at 4, 28, 52, and 76 h after last use of the drug. Receptor occupancy was correlated with withdrawal symptoms; an occupancy of 50–60 % appeared necessary for adequate symptom suppression (Greenwald et al. 2007).

Although the dose- and time-dependent opioid receptor occupancy by antagonists and partial agonists can be assessed with PET, measurements of receptor occupancy by full agonists may be problematic. No difference in [^{11}C]DPN binding was found in the brain of opioid-dependent subjects stable on methadone (18–90 mg daily, PET scan performed at peak plasma levels of the agonist) as compared to healthy controls. In rats receiving increased doses of methadone, no dose-dependent reduction of the cerebral binding of [^{11}C]DPN was observed. These negative findings were explained by assuming that methadone is already efficacious at very low levels of receptor occupancy (<10 %, i.e., below the detection limit of PET) (Melichar et al. 2005). In a subsequent preclinical study, rats were pretreated with antinociceptive doses of oxycodone (μ OR and κ OR agonist), morphine (μ OR agonist), and buprenorphine (δ OR and κ OR antagonist, μ OR partial agonist). Full agonists did not reduce the brain uptake of [^{11}C]DPN at all, whereas buprenorphine administration resulted in a strong reduction (up to 90 %) of tracer binding (Hume et al. 2007). Opioid receptor occupancy by the antagonist naloxone could also be measured with [^{11}C]DPN and PET, a drug dose of 13 $\mu\text{g}/\text{kg}$ resulting in 50 % occupancy (Melichar et al. 2003). The reason for the negative findings with exogenous full agonists is not clear, since endogenous enkephalins have been shown to compete with [^{11}C]DPN for OR binding in the human brain (Ruiz-Gayo et al. 1992). Moreover, an early PET study reported 19–32 % lower binding of [^{18}F]cyclofoxy in various brain regions of long-term methadone-treated former heroin addicts as compared to controls (22 h after the last dose), and the reduction of tracer binding in caudate and putamen correlated with levels of methadone in plasma (Kling et al. 2000). Since the observed competition is both tracer and agonist dependent, these PET data may indicate the presence of multiple, different agonist binding sites on opioid receptor proteins or upregulation of subclasses of opioid receptors in heroin-dependent subjects.

Opioid receptor (particularly μ OR) agonists increase and antagonists decrease feeding and other rewarding behaviors in animal models. A [11 C]CFN-PET study examined cerebral μ OR occupancy in 26 healthy male volunteers after single oral doses of either GSK1521498 (μ OR inverse agonist, candidate drug for the treatment of overeating) or naltrexone (μ OR and κ OR antagonist). Activation of the amygdala by a palatable food stimulus (fruit drink) was examined in the same volunteers, using fMRI. Although a dose-dependent occupancy of μ OR was observed for both compounds, GSK1521498 significantly attenuated activation of the amygdala by the food stimulus, in contrast to naltrexone. This difference may be related to the fact that μ OR and κ OR signaling have different effects on feeding behavior and reward processing (Rabiner et al. 2011).

Naloxone administration triggers activity of the hypothalamic-pituitary-adrenal (HPA) axis by blocking opioid inhibitory tone at corticotropin-releasing factor (CRF) neurons in the paraventricular nucleus of the hypothalamus. These neurons regulate the secretion of adrenocorticotropic hormone (ACTH) and cortisol. An interesting study measured μ OR binding potential in the brain of 18 healthy subjects using [11 C]CFN and PET. The following day, ACTH and cortisol responses to an incremental naloxone challenge were tested in the same subject group. Cortisol responses to naloxone were negatively correlated to [11 C]CFN binding potential in several brain areas (ventral striatum, putamen, caudate, hypothalamus). Apparently, subjects with higher binding potential have lower endogenous occupancy of μ OR by β -endorphin and thus place less inhibitory tone on the HPA axis; therefore these subjects show a smaller cortisol response to naloxone (Wand et al. 2011).

20.5 PET Studies in Patients and Drug Addicts

20.5.1 Major Depressive, Borderline Personality, and Posttraumatic Stress Disorder

Using the sustained neutral and sadness state paradigm, μ OR availability in the brain of healthy female volunteers and patients with major depressive disorder (MDD) has been compared. Healthy controls showed an increase of μ OR availability in the anterior cingulate during the sustained sadness condition indicating deactivation of μ OR-mediated neurotransmission, but in patients who did not respond to antidepressant treatment after PET imaging, sustained sadness was associated with a *decreased* binding of 11 C-CFN in this region, i.e., activation of the opioid system. Patients with MDD showed significantly lower μ OR binding potential in the posterior thalamus than healthy controls during the neutral state. These PET data indicated that endogenous opioid neurotransmission is altered in MDD (Kennedy et al. 2006). A later study from the same group showed that in MDD patients but not in healthy subjects, plasma levels of the inflammatory cytokine IL-18 are positively correlated with baseline μ OR binding potential and with activation of μ OR-mediated neurotransmission during a sadness challenge (Prossin et al. 2011). Thus, there may be a link between peripheral stress-activated

proinflammatory mechanisms and central stress-activated neurotransmitter systems, such as the opioid system.

A later study from the same group examined responses of the μ OR system to sustained sadness in patients with borderline personality disorder. During the baseline (neutral) state, patients showed greater [^{11}C]CFN binding than healthy controls in the bilateral orbitofrontal cortex, caudate, and nucleus accumbens besides the left amygdala, but lower binding in the posterior thalamus. Induction of sadness caused greater declines of [^{11}C]CFN binding potential in the pregenual anterior cingulate, left orbitofrontal cortex, left ventricular pallidum, left amygdala, and left inferior prefrontal cortex of the patients than of healthy controls and greater increases of binding potential in the left nucleus accumbens, the hypothalamus, and the right hippocampus/parahippocampus. Apparently, the opioid system of patients with borderline personality disorder differs from healthy, age- and sex-matched control subjects both at baseline and in its response to a negative emotional challenge (Prossin et al. 2010).

An interesting study compared μ OR binding in the brain of 14 healthy male volunteers, 15 males with combat exposure but without posttraumatic stress disorder (PTSD), and 16 male patients with PTSD, using [^{11}C]CFN and PET. The two groups which had been exposed to war trauma showed lower μ OR binding in the amygdala, nucleus accumbens, dorsal frontal cortex, and insular cortex than healthy volunteers but higher μ OR binding in the orbitofrontal cortex. PTSD patients showed a significant reduction of μ OR binding in the anterior cingulate cortex compared with both other groups. Combat-exposed subjects without PTSD had lower μ OR binding in the amygdala but higher binding in the orbitofrontal cortex than either PTSD patients or healthy controls. Thus, the opioid system of the brain shows specific changes both after trauma and in PTSD (Liberzon et al. 2007).

20.5.2 Pain

In a group of four patients with rheumatoid arthritis, regional cerebral opioid receptor binding of [^{11}C]DPN was quantified both during a period of pain and during a period when the subjects were out of pain. Significant decreases of [^{11}C]DPN binding were seen in many brain areas when subjects suffered pain (particularly straight gyrus and frontal, cingulate, and temporal cortex) (Jones et al. 1994a). In a patient with central poststroke pain which developed after a small pontine hemorrhagic infarction, a reduction of the binding of [^{11}C]DPN was also noted, and this reduction was more striking than the hypometabolism of [^{18}F]FDG on the lateral cortical surface contralateral to the symptoms (Willoch et al. 1999).

Changes of [^{11}C]DPN binding in the brain of six patients after surgical relief of trigeminal neuralgia pain were examined in a later study. The volume of distribution of the tracer in several cortical areas (prefrontal, insular, perigenual, midcingulate, inferior parietal), basal ganglia, and the thalamus was found to be significantly increased after surgery (Jones et al. 1999). These data and the findings in the previous studies were interpreted as evidence for the release of opioid peptides during

various forms of pain resulting in a reduction of the fraction of receptors available for ligand binding. However, changes of opioid receptor numbers (upregulation after surgery or after the disappearance of pain) could not be ruled out.

In a later study involving four patients with central neuropathic pain (mainly poststroke) and age-matched controls, patients were found to have significantly less [^{11}C]DPN binding in the dorsolateral, anterior cingulate, and insula cortices, the thalamus, and the inferior parietal cortex. These reductions were not a direct consequence of their cerebral lesions, since these were located in other brain areas. The authors interpreted the PET data as evidence for reduced damping of nociceptor activity in the patients and as a possible explanation for the fact that high doses of opiates are frequently required to achieve optimal analgesia in subjects with central neuropathic pain (Jones et al. 2004). Essentially similar findings were reported in a study from another institution, using the same tracer and involving five patients with central poststroke pain and 12 healthy volunteers (Willoch et al. 2004).

An interesting study compared changes of [^{11}C]DPN binding in the brain of patients with peripheral neuropathic pain and central poststroke pain. Peripheral neuropathic pain patients showed bilateral and symmetric decreases of [^{11}C]DPN binding, in contrast to central poststroke pain patients where an asymmetric decrease was noted, which was most prominent in the contralateral hemisphere. The symmetric and bilateral decline in the former patient group may reflect endogenous opioid release, whereas the lateralized decrease in the latter group suggests a loss of opioid receptors (Maarrawi et al. 2007a). Thus, central and peripheral forms of neuropathic pain may have different effects on the opioid system of the brain.

In a group of ten patients with restless legs syndrome (RLS), significant negative correlations were observed between [^{11}C]DPN binding in areas serving the medial pain system and RLS severity or pain scores. These findings suggested release of endogenous opioids within the medial pain system related to the severity of the syndrome (von Spiczak et al. 2005).

Changes of the opioid system in patients with cluster headache were also examined, using the tracer [^{11}C]DPN and PET. When patients as a group were compared with healthy volunteers, a striking (>50 %) decrease of tracer binding was noted in the pineal gland but not in any other brain area. Within the patient group, opioid receptor availability in the ipsilateral hypothalamus and anterior cingulate cortex was negatively correlated to the duration of the headache disorder. The patients did not experience acute pain during or immediately before the study; thus, the observed alterations of [^{11}C]DPN binding appear not to represent an effect of acute pain processing but rather alterations in the opioid system related to the development of the disease. Opioidergic dysfunction in circuitries generating the biologic clock may be a mechanism underlying cluster headache (Sprenger et al. 2006b).

In patients with complex regional pain syndrome (CRPS), a chronic pain condition which can develop after limb trauma, binding of the non-subtype-selective OR ligand [^{18}F]DPN was found to be reduced in the contralateral amygdala and parahippocampal gyri but increased in the contralateral prefrontal cortical areas. Ligand binding in the ipsilateral temporal cortex and midcingulate cortex was negatively correlated with pain scores, but ligand binding in the contralateral temporal cortex

was positively correlated with anxiety and depression scales (Klega et al. 2010). These findings suggest that the endogenous opioid system is implied in both chronic pain and its psychiatric comorbidity.

A recent study with the tracer [^{11}C]CFN compared μOR binding in the brain of four patients with trigeminal neuropathic pain and eight gender- and age-matched healthy controls. Patients showed reduced tracer binding in the left nucleus accumbens, and binding potential in this area was negatively correlated with their pain ratings. This finding was interpreted as evidence for downregulation of μOR after persistent activation of opioid neurotransmission in chronic pain (DosSantos et al. 2012b).

20.5.3 Pain Treatment

Monitoring the relationship between opioid receptor occupancy and pain relief could be useful in the development of improved techniques for the treatment of pain (Sadzot et al. 1990; Sadzot and Frost 1990). This study paradigm has been employed in several recent reports.

An initial study examined the contribution of the endogenous opioid system to pain relief induced by motor cortex stimulation (MCS). Eight patients with refractory neuropathic pain were scanned three times with [^{11}C]DPN and PET: twice preoperatively with a 2-week interval and once after 7 months of chronic MCS. The preoperative test-retest scans did not show any significant differences, but comparison of the last scan with the two preoperative scans revealed significant decreases of tracer binding in the anterior middle cingulate cortex, periaqueductal gray, prefrontal cortex, and cerebellum. The magnitude of the changes in the first two brain areas was significantly correlated with pain relief. These findings were interpreted as evidence for the release of endogenous opioids in brain structures involved in pain processing after MCS (Maarrawi et al. 2007b).

The effects of traditional Chinese acupuncture and placebo needle stimulation have been compared in chronic pain patients diagnosed with fibromyalgia. [^{11}C]CFN-PET scans were made at both the beginning and the end of the 4-week treatment period. Acupuncture was shown to result in both short- and long-term increases in [^{11}C]CFN binding potential in multiple pain and sensory processing regions. In the sham group, small reductions of [^{11}C]CFN binding were observed, consistent with previously reported placebo effects. The long-term increases after acupuncture were correlated with reductions in clinical pain. Thus, acupuncture and sham acupuncture may have different effects on cerebral μOR binding and alterations of μOR binding potential may be involved in the analgesic effect of acupuncture (Harris et al. 2009).

A recent case study reported that transcranial direct current stimulation (tDCS) of the motor cortex in a trigeminal neuropathic pain patient considerably decreased the binding potential of [^{11}C]CFN in several brain areas compared to sham tDCS. The effect was particularly striking in the posterior thalamus. tDCS increased the threshold for experimental cold pain in the patient but did not improve her clinical

pain. The authors suggested that the release of endogenous opioids is immediately increased by tDCS, but repetitive tDCS sessions are required to revert neuroplastic changes related to the neuropathic pain (DosSantos et al. 2012a).

20.5.4 Substance Abuse

20.5.4.1 Cocaine Dependence

The endogenous opioid system appears to play a role in the reinforcing actions of non-opioid drugs. American investigators examined μ OR binding in the brain of cocaine addicts, 1–4 days after their last use of cocaine, using ^{11}C -CFN and PET. An increase of tracer binding was observed, particularly in the frontal cortex and caudate nucleus, and this increase persisted even after 4 weeks of drug abstinence. The magnitude of ^{11}C -CFN uptake was positively correlated with the severity of cocaine craving experienced by the subjects. These findings confirmed the involvement of the opioid system in cocaine dependence (Zubieta et al. 1996).

Increases of μ OR binding potential in the anterior cingulate and anterior frontal cortex of cocaine users during abstinence are not only positively correlated with the intensity of cocaine craving, but the elevation of ^{11}C -CFN binding in these areas is also correlated with the percentage of days with cocaine use and the amount of cocaine used per day before the study period (Gorelick et al. 2005).

Regional increases of μ OR binding appear to be related not only to the intensity of cocaine craving but also to the time interval before relapse to cocaine use after discharge from a closed research ward. In an interesting study, 15 cocaine-dependent subjects were housed in this ward for 12 weeks of monitored abstinence. During this period, regional brain μ OR binding was measured at 1 and 12 weeks, using ^{11}C -CFN and PET. A shorter time interval before relapse was associated with increased μ OR binding in the frontal and temporal cortex in both PET scans and with a lesser decrease in binding between 1 and 12 weeks. The significance of this correlation persisted even after accounting for clinical variables. Thus, increased μ OR binding in the frontal and temporal cortex is a predictor of time to relapse to cocaine use (Gorelick et al. 2008).

A recent PET study examined regional μ OR ($[^{11}\text{C}]\text{CFN}$) binding in the brain of treatment-seeking cocaine users before the onset of treatment and correlated this parameter with subsequent treatment outcome. Elevated μ OR binding in brain regions associated with reward sensitivity correlated with greater cocaine use during treatment and shorter duration of cocaine abstinence. Thus, μ OR binding in these brain areas was a significant independent predictor of treatment outcome (Ghitza et al. 2010).

The mechanism of action of psychostimulant drugs in the mammalian brain appears to involve the release of endogenous opioids (endorphins) in the reward system. Two recent PET studies have attempted to obtain experimental proof for this mechanism by administering d-amphetamine to healthy volunteers (i.v.) and examining the impact of this challenge on $[^{11}\text{C}]\text{CFN}$ binding in the brain. A Swedish study in which ten subjects were scanned under three conditions (baseline, placebo, amphetamine 0.3 mg/kg) could not detect any significant differences in the binding

potential of [^{11}C]CFN after the amphetamine challenge (Guterstam et al. 2013). However, another study in which 12 subjects were scanned before and 3 h after an amphetamine challenge (either a high dose, 0.5 mg/kg, or an ultralow dose 0.017 mg/kg) reported that [^{11}C]CFN binding was reduced after the high but not the ultralow dose in the frontal cortex, putamen, caudate, thalamus, anterior cingulate cortex, and insula (Colasanti et al. 2012).

20.5.4.2 Opioid Dependence

Similar changes of opioid receptor binding as were reported for cocaine addicts have also been observed in early abstinence from opioid (heroin) dependence. Compared with 20 healthy controls, ten subjects with opioid dependence who had completed inpatient detoxification showed increased [^{11}C]DPN binding in the whole brain and in 15 out of 21 studied brain areas (Williams et al. 2007).

20.5.4.3 Alcohol Dependence

Whereas studies in cocaine and heroin addicts suggest increases of opioid receptor binding during abstinence, studies in alcohol dependence have produced conflicting results. In an early PET study with [^{11}C]CFN, μOR binding potential was measured in eight male alcohol-dependent subjects during alcohol withdrawal and eight matched healthy controls. Contrary to the findings in cocaine abusers, alcoholics showed *reductions* of μOR binding potential in the right dorsal lateral prefrontal cortex, right anterior frontal cortex, and right parietal cortex. Lower μOR binding potential was associated with higher craving and with depressive symptoms in the subjects (Bencherif et al. 2004b). Based on the findings in subsequent studies, one could speculate that alcohol abstinence and depression have different effects on μOR binding (an increase and a decrease, respectively), the latter effect predominating in this early investigation.

Opposite results were reported in a German study. The authors examined [^{11}C]CFN binding in the brain of alcoholics after 1–3 weeks of abstinence. Significantly *higher* binding was observed in the ventral striatum of the patients compared with healthy controls. This increase persisted up to 5 weeks, and its magnitude was significantly correlated with the intensity of alcohol craving. Elevated availability of μOR in the striatum was considered as a neuronal correlate of alcohol urge since the ventral striatum is known to be an important part of the reward system in the human brain (Heinz et al. 2005). Similar results were reported in a large study involving 25 alcohol-dependent subjects who were scanned on day 5 of abstinence and 30 healthy controls. Alcohol-dependent subjects had a significantly higher binding potential of [^{11}C]CFN in many brain regions. There was a significant inverse relationship between [^{11}C]CFN binding in several brain regions and the intensity of craving in the alcohol-dependent group. No significant group differences in binding of the δOR ligand [^{11}C]MeNTI were observed, but the binding potential of this ligand in the caudate nucleus was positively correlated with recent drinking in alcohol-dependent subjects (Weerts et al. 2011).

In alcohol-dependent subjects completing a 19-day inpatient protocol (alcohol abstinence followed by naltrexone treatment, 50 mg daily, on days 15–19),

a virtually complete (95 %) occupancy of μ OR by naltrexone was observed, using [^{11}C]CFN and PET. However, a much lower and highly variable (0–50 %) occupancy of δ OR was detected in [^{11}C]MeNTI scans. The relationship between δ OR occupancy and treatment outcome could be explored in future studies (Weerts et al. 2008).

A British study with the non-subtype-selective opioid ligand [^{11}C]DPN reported a trend towards increased tracer binding in 11 alcohol-dependent subjects during early abstinence, compared to healthy controls, although this trend did not reach statistical significance. A significant correlation between alcohol craving and the global and regional distribution volume of [^{11}C]DPN was noted in the alcohol-dependent subjects (Williams et al. 2009).

A recent study examined [^{11}C]CFN binding in the human brain before and immediately after alcohol consumption in 13 heavy drinkers and an age-matched control group of 12 healthy subjects. Drinking alcohol reduced tracer binding in the nucleus accumbens and orbitofrontal cortex, indicating release of endogenous opioids in brain areas involved in the valuation of reward. The magnitude of change in the orbitofrontal cortex was significantly correlated with problem alcohol use and with subjective high in the drinker group. Thus, the release of endogenous opioids by ethanol promotes further alcohol consumption, and altered function of the opioid system appears to contribute to alcohol abuse (Mitchell et al. 2012).

20.5.4.4 Nicotine Dependence

Several PET studies have examined the relationship between opioid neurotransmission and smoking. In an initial, groundbreaking publication, six healthy male smokers and six age- and sex-matched nonsmokers were scanned with both [^{11}C]CFN and the dopamine receptor ligand [^{11}C]raclopride. Smokers abstained from smoking for 12 h prior to the study. They first smoked a denicotinized cigarette, 2 and 12 min after scan onset, followed by a normal cigarette after 40 and 50 min. Total scan duration was 90 min. Thus, each scan period consisted of an initial, denicotinized phase and a later, average nicotine phase. Nonsmokers were subjected to the same scanning protocol but were only scanned at baseline (i.e., they did not smoke anything). In the smoker group, significant declines of [^{11}C]CFN binding in the right anterior cingulate cortex were noted during transition from the first to the second phase of the scan, indicating activation of opioid neurotransmission by nicotine. A simultaneous decline of [^{11}C]raclopride binding was noted in the ventral basal ganglia, and the magnitude of this decline correlated with nicotine dependence score. Increases of the release of endogenous opioids and dopamine are probably involved in the rewarding effect of nicotine. Smokers had lower μ OR binding potential in the cingulate cortex, thalamus, ventral basal ganglia, and amygdala compared to nonsmokers during the first phase of the scan; these reductions were reversed in the thalamus, ventral basal ganglia, and amygdala after nicotine smoking (Scott et al. 2007a).

A later study with [^{11}C]CFN examined the relationship between smoking and the relief of negative affect. Twenty-two smokers were scanned after overnight abstinence, once after smoking a denicotinized cigarette and at another scanning day after smoking a normal cigarette. Higher μ OR availability in the amygdala was

correlated with greater motivation to smoke in order to relieve negative affect, but not with changes in affect after smoking (Falcone et al. 2012).

Polymorphisms of the μ OR gene affect both the levels of μ OR expression in the human brain and smoking behavior. Smokers homozygous for the wild-type *OPRM1* A allele show significantly higher [^{11}C]CFN binding in the bilateral amygdala, left thalamus, and left anterior cingulate cortex than smokers carrying the *OPRM1* A118G allele. In bearers of the G polymorphism, the extent of reward difference between smoking a normal and a denicotinized cigarette was significantly associated with the change of [^{11}C]CFN binding potential in the right amygdala, caudate, anterior cingulate cortex, and thalamus, but in smokers homozygous for the wild-type gene, this association could not be observed (Ray et al. 2011).

A recent PET study examined whether individual differences in μ OR availability in alcohol-dependent subjects are associated with tobacco use, nicotine dependence, and level of nicotine craving. Subjects had withdrawn from alcohol use under medical supervision. They were not allowed to smoke but received transdermal nicotine maintenance (21 mg/day). Higher scores in a nicotine dependence test were found to be associated with a lower binding potential of [^{11}C]CFN in the amygdala, cingulate, globus pallidus, thalamus, and insula. The number of cigarettes which subjects had used per day prior to the study was also negatively correlated with [^{11}C]CFN binding potential in these areas. Thus, smoking intensity and severity of nicotine dependence appear to be related to reduced μ OR binding potential in several brain regions of alcohol-dependent subjects (Weerts et al. 2012).

20.5.5 Eating Disorders

Bulimia nervosa, a disorder characterized by cycles of food restriction, binge eating, and vomiting, shares certain phenomena with addiction and substance abuse. Compared with controls, bulimic individuals show significantly decreased μ OR binding in the left insular cortex, a brain area involved in taste discrimination and eating reward. This finding may reflect either downregulation of μ OR in the bulimic state as a consequence of chronically increased release of opioid peptides or a personality trait that increases the reward value of dieting (Bencherif et al. 2005).

20.5.6 Epilepsy

Opioid receptors and endogenous opioid peptides are known to play a role in the mechanisms underlying seizures. Many PET studies with opioid receptor ligands have been performed in patients with epilepsy. The first of these involved ^{11}C -CFN and subjects with complex partial seizures due to unilateral temporal seizure foci. ^{11}C -CFN binding in the temporal neocortex was greater on the side of the focus than on the contralateral side. This increase was interpreted as evidence for involvement of μ OR in a tonic anticonvulsant system that limits the spread of electrical activity (Frost et al. 1988). In contrast to ^{11}C -CFN binding, ^{11}C -DPN uptake (Mayberg et al.

1991) and [^{18}F]cyclofoxy (Theodore et al. 1992) uptake in the ipsilateral and contralateral lobes were not significantly different, suggesting that opioid receptor subtypes are differentially regulated in temporal lobe epilepsy. Evidence for differential regulation was obtained in a later study in which subjects with temporal lobe epilepsy were scanned both with the δOR ligand ^{11}C -methylnaltrindole (^{11}C -MeNTI) and with the μOR ligand ^{11}C -CFN. Binding of both ligands was increased in the ipsilateral temporal cortex, but the regional pattern of the changes was different (more extended for ^{11}C -MeNTI than for ^{11}C -CFN). Upregulation of δOR may indicate an anticonvulsant action for this receptor subtype (Madar et al. 1997). A more recent study examined [^{11}C]DPN binding in the brain of patients with temporal lobe epilepsy both shortly (within a few hours) after spontaneous epileptic seizures and interictally. In 14 healthy controls, no changes of [^{11}C]DPN binding were observed as a function of time, but in the patients, an increase of tracer binding was noted in the ipsilateral temporal pole and fusiform gyrus, shortly after seizures. The magnitude of this increase was inversely correlated to the interval that had elapsed since the last seizure, suggesting an increase of receptor binding during seizures followed by a gradual return to baseline (Hammers et al. 2007a). Thus, results from PET studies with three different ligands ([^{11}C]CFN, [^{11}C]MeNTI, and [^{11}C]DPN) support the idea that the opioid system is involved in seizure control.

The interictal distribution volume of [^{11}C]DPN in the cortex and thalamus of eight patients with childhood and juvenile absence epilepsy was found to be not significantly different from values in healthy age-matched controls; thus, there appeared to be no overall abnormality of opioid receptors in this patient group (Prettet et al. 1994). To examine whether absence seizures are associated with release of endogenous opioids, investigators scanned eight patients with primary generalized epilepsy and eight control subjects with ^{11}C -DPN and PET. Serial absences were precipitated in the patients by hyperventilation for 10 min, starting 30–40 min after injection of the tracer. Increased washout of DPN was observed in the association cortex but not in other brain areas during seizures, as compared with control subjects and patients scanned without provocation of absences. Pharmacokinetic modeling suggested that absence seizures resulted in a significant, 15–41 % decrease in the rate constant of association (k_3) of the tracer. These data were interpreted as evidence for the release of endogenous opioids in the association cortex at the time of absences, leading to increased opioid receptor occupancy (Bartenstein et al. 1993).

A later study involved five patients with reading epilepsy who were scanned both at baseline (reading a string of symbols) and during seizure activation (reading a scientific paper). The latter condition was associated with significantly lower binding of ^{11}C -DPN in the left parietotemporal-occipital cortex of the patients as compared with six healthy controls, suggesting release of endogenous opioids as part of a mechanism to terminate reading-induced seizures (Koepp et al. 1998).

Two patients with mesobasal temporal lobe epilepsy have been scanned with ^{11}C -DPN, before and after selective amygdalohippocampectomy. After removal of the epileptic focus, ^{11}C -DPN binding in the ipsilateral frontal cortex was found to be reduced, suggesting either downregulation of opioid receptors in the absence of seizures or postoperative neuronal dysfunction (Bartenstein et al. 1994).

20.5.7 Neurodegenerative Diseases

Losses of opioid receptors with different regional patterns have been observed in several neurodegenerative diseases.

20.5.7.1 Huntington's Disease

Significant decreases of [^{11}C]DPN binding (24–40 %) were noted in the caudate and putamen of Huntington's disease (HD) patients using striatum-to-occipital cortex uptake ratios, spectral analysis, voxelwise parametric analysis, and statistical parametric mapping (SPM) for quantification (Weeks et al. 1997).

20.5.7.2 Alzheimer Disease

Decreases of opioid receptor binding (up to 40 %) have been detected in the brain of Alzheimer disease (AD) patients using the tracer [^{18}F]cyclofoxy, and these changes were not correlated with decreases in regional cerebral blood flow (Cohen et al. 1997).

20.5.7.3 Parkinson Disease and Related Disorders

An initial study on eight clinically defined Parkinson disease (PD) patients, seven subjects with the striatonigral degeneration type of multiple system atrophy and six subjects with Steele-Richardson-Olszewski (SRO) syndrome examined opioid receptor binding in the human striatum with the tracer [^{11}C]DPN and PET. In the PD patient group, tracer binding was not significantly altered compared to healthy controls. Striatonigral degeneration was associated with reduced binding of [^{11}C]DPN in the putamen, but not in the caudate. In the SRO syndrome group, both caudate and putamen opioid receptor binding were significantly reduced. The binding pattern of [^{11}C]DPN may thus help to differentiate between various akinetic-rigid syndromes (Burn et al. 1995). In ten patients with the olivopontocerebellar variant of multiple system atrophy, a significant 12 % reduction of the caudate-occipital ratio and a 15 % reduction of the putamen-occipital uptake ratio of [^{11}C]DPN were noted. The latter decline was correlated to loss of [^{18}F]DOPA uptake in the putamen (average reduction 29 %) (Rinne et al. 1995).

Using [^{11}C]DPN-PET and either a region-of-interest (ROI) or an SPM approach, a significantly reduced opioid receptor binding was later noted in the striatum and thalamus of PD patients with levodopa-induced dyskinesias but not in non-dyskinetic subjects (Piccini et al. 1997). No difference in striatal dopamine D_1 or D_2 receptor binding was found between the two subgroups, and measurements with PET and [^{15}O]water showed that rCBF after oral administration of levodopa was increased during dyskinesias in lentiform nuclei and motor, premotor, and dorsal prefrontal cortex. Thus, dyskinesias appear to arise not from a disturbance of dopamine receptor availability but rather from overactivity of opioid transmission, particularly the basal ganglia-frontal projections (Brooks et al. 2000).

In bilaterally 1-methyl-4-phenyl-1,2,3,6-tetrahydropyridine (MPTP)-lesioned monkeys which had clinically recovered from the acute motor effects of dopaminergic neuron lesioning, a 65 % decrease in the accumulation of [^{18}F]DOPA was noted

in the basal ganglia. This decrease was associated with a 30–35 % decline of [^{18}F]cyclofoxy binding in the caudate, anterior putamen, thalamus, and amygdala. The authors concluded that altered opioid receptor signaling (probably increased levels of Met-enkephalin) had contributed to the behavioral changes which were observed in the animals, i.e., the masking of their motor symptoms (Cohen et al. 1998). A later study from the same group showed that in unilaterally MPTP-lesioned monkeys with parkinsonian symptoms, opioid receptor availability is reduced by 30–35 % on both the lesioned and the non-lesioned sides of the brain (Cohen et al. 1999).

In contrast to the decreases of opioid receptor binding which were observed in akinetic-rigid syndromes and PD patients with dyskinesias, no abnormalities of [^{11}C]DPN binding were noted in patients with primary torsion dystonia (carriers of the DYT1 gene), and no correlation between the severity of dystonia and opioid binding could be detected (Whone et al. 2004).

20.5.8 Opioid Receptor Expression in Lung Tumors

A pilot PET study involving seven patients with lung carcinomas examined the feasibility of tumor imaging with the radioligands [^{11}C]MeNTI and [^{11}C]CFN. Four of these patients were also scanned with [^{18}F]FDG for clinical indications. All tumors showed an accumulation of opioid receptor ligands above background. The tumor-to-nontumor binding ratio of the δ OR ligand [^{11}C]MeNTI (4.3 ± 1.3) was greater than that of the μ OR ligand [^{11}C]CFN (2.4 ± 1.2) but lower than that of [^{18}F]FDG (7.7 ± 0.5). About 50 % of [^{11}C]MeNTI uptake and 44 % of [^{11}C]CFN uptake in the tumors could be blocked by naloxone. Particularly [^{11}C]MeNTI appears suitable for investigation of lung carcinoma biology, since δ OR may be involved in tumor invasion and metastasis (Madar et al. 2007).

Conclusion

PET imaging has provided insight in the involvement of opioid system in affective and sensory processing. Changes of opioid receptor expression related to increasing age and altered hormonal status have also been reported. Moreover, OR imaging has been successfully applied in the study of the pharmacokinetics and pharmacodynamics of novel and existing drugs.

Regional changes of OR availability have been observed in psychiatric and neurodegenerative disorders, epilepsy, pain, bulimia nervosa, and substance abuse. PET imaging may contribute to the development of improved techniques for the treatment of pain (and addiction) by monitoring the relationship between OR occupancy and symptom relief.

References

- Bai LQ, Teng RR, Shiue CY, Wolf AP, Dewey SL, Holland MJ, Simon EJ (1990) No-carrier-added (NCA) N-(3-[^{18}F]fluoropropyl)-N-norbuprenorphine and N-(3-[^{18}F]fluoropropyl)-N-nordiprenorphine – synthesis, anatomical distribution in mice and rats, and tomographic studies in a baboon. *Int J Rad Appl Instrum B* 17:217–227

- Baier B, Bense S, Birklein F, Buchholz HG, Mischke A, Schreckenberger M, Dieterich M (2010) Evidence for modulation of opioidergic activity in central vestibular processing: a [(18)F] diprenorphine PET study. *Hum Brain Mapp* 31:550–555
- Bartenstein PA, Duncan JS, Preveit MC, Cunningham VJ, Fish DR, Jones AK, Luthra SK, Sawle GV, Brooks DJ (1993) Investigation of the opioid system in absence seizures with positron emission tomography. *J Neurol Neurosurg Psychiatry* 56:1295–1302
- Bartenstein PA, Preveit MC, Duncan JS, Hajek M, Wieser HG (1994) Quantification of opiate receptors in two patients with mesiobasal temporal lobe epilepsy, before and after selective amygdalohippocampectomy, using positron emission tomography. *Epilepsy Res* 18:119–125
- Baumgartner U, Buchholz HG, Bellosevich A, Magerl W, Siessmeier T, Rolke R, Hohmann S, Piel M, Rosch F, Wester HJ, Henriksen G, Stoeter P, Bartenstein P, Treede RD, Schreckenberger M (2006) High opiate receptor binding potential in the human lateral pain system. *Neuroimage* 30:692–699
- Bencherif B, Fuchs PN, Sheth R, Dannals RF, Campbell JN, Frost JJ (2002) Pain activation of human supraspinal opioid pathways as demonstrated by [11C]-carfentanil and positron emission tomography (PET). *Pain* 99:589–598
- Bencherif B, Stumpf MJ, Links JM, Frost JJ (2004a) Application of MRI-based partial-volume correction to the analysis of PET images of mu-opioid receptors using statistical parametric mapping. *J Nucl Med* 45:402–408
- Bencherif B, Wand GS, McCaul ME, Kim YK, Ilgin N, Dannals RF, Frost JJ (2004b) Mu-opioid receptor binding measured by [11C]carfentanil positron emission tomography is related to craving and mood in alcohol dependence. *Biol Psychiatry* 55:255–262
- Bencherif B, Guarda AS, Colantuoni C, Ravert HT, Dannals RF, Frost JJ (2005) Regional mu-opioid receptor binding in insular cortex is decreased in bulimia nervosa and correlates inversely with fasting behavior. *J Nucl Med* 46:1349–1351
- Boecker H, Sprenger T, Henriksen G, Toelle TR, Spilker ME (2005) Optimal duration of PET studies with 18F-fluoroethyl-diprenorphine. *J Nucl Med* 46:2092–2096
- Boecker H, Sprenger T, Spilker ME, Henriksen G, Koppenhoefer M, Wagner KJ, Valet M, Berthele A, Tolle TR (2008) The runner's high: opioidergic mechanisms in the human brain. *Cereb Cortex* 18:2523–2531
- Bourdier T, Poisnel G, Dhilly M, Delamare J, Henry J, Debruyne D, Barre L (2007) Synthesis and biological evaluation of N-substituted quinolinimides, as potential ligands for in vivo imaging studies of delta-opioid receptors. *Bioconj Chem* 18:538–548
- Brooks DJ, Piccini P, Turjanski N, Samuel M (2000) Neuroimaging of dyskinesias. *Ann Neurol* 47:S154–S158
- Burn DJ, Rinne JO, Quinn NP, Lees AJ, Marsden CD, Brooks DJ (1995) Striatal opioid receptor binding in Parkinson's disease, striatonigral degeneration and Steele-Richardson-Olszewski syndrome, A [11C]diprenorphine PET study. *Brain* 118(Pt 4):951–958
- Carson RE, Channing MA, Blasberg RG, Dunn BB, Cohen RM, Rice KC, Herscovitch P (1993) Comparison of bolus and infusion methods for receptor quantitation: application to [18F] cyclofoxy and positron emission tomography. *J Cereb Blood Flow Metab* 13:24–42
- Chang KJ, Hazum E, Cuatrecasas P (1981) Novel opiate binding sites selective for benzomorphan drugs. *Proc Natl Acad Sci U S A* 78:4141–4145
- Channing MA, Eckelman WC, Bennett JM, Burke TR Jr, Rice KC (1985) Radiosynthesis of [18F]3-acetylcyclofoxy: a high affinity opiate antagonist. *Int J Appl Radiat Isot* 36:429–433
- Chen Y, Mestek A, Liu J, Hurley JA, Yu L (1993) Molecular cloning and functional expression of a mu-opioid receptor from rat brain. *Mol Pharmacol* 44:8–12
- Chesis PL, Welch MJ (1990) Synthesis and in vitro characterization of fluorinated U-50488 analogs for PET studies of kappa opioid receptors. *Int J Rad Appl Instrum A* 41:267–273
- Chesis PL, Hwang DR, Welch MJ (1990) N-(3-[18F]fluoropropyl)-N-nordiprenorphine: synthesis and characterization of a new agent for imaging opioid receptors with positron emission tomography. *J Med Chem* 33:1482–1490
- Cohen RM, Andreason PJ, Doudet DJ, Carson RE, Sunderland T (1997) Opiate receptor avidity and cerebral blood flow in Alzheimer's disease. *J Neurol Sci* 148:171–180
- Cohen RM, Carson RE, Aigner TG, Doudet DJ (1998) Opiate receptor avidity is reduced in non-motor impaired MPTP-lesioned rhesus monkeys. *Brain Res* 806:292–296

- Cohen RM, Carson RE, Wyatt RJ, Doudet DJ (1999) Opiate receptor avidity is reduced bilaterally in rhesus monkeys unilaterally lesioned with MPTP. *Synapse* 33:282–288
- Cohen RM, Carson RE, Sunderland T (2000) Opiate receptor avidity in the thalamus is sexually dimorphic in the elderly. *Synapse* 38:226–229
- Colasanti A, Searle GE, Long CJ, Hill SP, Reiley RR, Quelch D, Erritzoe D, Tziortzi AC, Reed LJ, Lingford-Hughes AR, Waldman AD, Schruers KR, Matthews PM, Gunn RN, Nutt DJ, Rabiner EA (2012) Endogenous opioid release in the human brain reward system induced by acute amphetamine administration. *Biol Psychiatry* 72:371–377
- Cometta-Morini C, Maguire PA, Loew GH (1992) Molecular determinants of mu receptor recognition for the fentanyl class of compounds. *Mol Pharmacol* 41:185–196
- Cox BM, Goldstein A, Hi CH (1976) Opioid activity of a peptide, beta-lipotropin-(61–91), derived from beta-lipotropin. *Proc Natl Acad Sci U S A* 73:1821–1823
- Cunningham VJ, Hume SP, Price GR, Ahier RG, Cremer JE, Jones AK (1991) Compartmental analysis of diprenorphine binding to opiate receptors in the rat in vivo and its comparison with equilibrium data in vitro. *J Cereb Blood Flow Metab* 11:1–9
- Dannals RF, Ravert HT, Frost JJ, Wilson AA, Burns HD, Wagner HN Jr (1985) Radiosynthesis of an opiate receptor binding radiotracer: [11C]carfentanil. *Int J Appl Radiat Isot* 36:303–306
- Dhawan BN, Cesselin F, Raghbir R, Reisine T, Bradley PB, Portoghese PS, Hamon M (1996) International union of pharmacology. XII. Classification of opioid receptors. *Pharmacol Rev* 48:567–592
- DosSantos MF, Love TM, Martikainen IK, Nascimento TD, Fregni F, Cumiford C, Deboer MD, Zubieta JK, Dasilva AF (2012a) Immediate effects of tDCS on the mu-opioid system of a chronic pain patient. *Front Psychiatry* 3:93
- DosSantos MF, Martikainen IK, Nascimento TD, Love TM, Deboer MD, Maslowski EC, Monteiro AA, Vincent MB, Zubieta JK, Dasilva AF (2012b) Reduced basal ganglia mu-opioid receptor availability in trigeminal neuropathic pain: a pilot study. *Mol Pain* 8:74
- Dougherty DD, Kong J, Webb J, Webb M, Bonab AA, Fischman AJ, Gollub RL (2008) A combined [11C] diprenorphine PET study and fMRI study of acupuncture analgesia. *Behav Brain Res* 193:63–68
- Endres CJ, Bencherif B, Hilton J, Madar I, Frost JJ (2003) Quantification of brain mu-opioid receptors with [11C]carfentanil: reference-tissue methods. *Nucl Med Biol* 30:177–186
- Evans CJ, Keith DE Jr, Morrison H, Magendzo K, Edwards RH (1992) Cloning of a delta opioid receptor by functional expression. *Science* 258:1952–1955
- Falcone M, Gold AB, Wileyto EP, Ray R, Ruparel K, Newberg A, Dubroff J, Logan J, Zubieta JK, Blendy JA, Lerman C (2012) mu-Opioid receptor availability in the amygdala is associated with smoking for negative affect relief. *Psychopharmacology (Berl)* 222:701–708
- Frost JJ (2001) PET imaging of the opioid receptor: the early years. *Nucl Med Biol* 28:509–513
- Frost JJ, Wagner HN Jr, Dannals RF, Ravert HT, Links JM, Wilson AA, Burns HD, Wong DF, McPherson RW, Rosenbaum AE et al (1985) Imaging opiate receptors in the human brain by positron tomography. *J Comput Assist Tomogr* 9:231–236
- Frost JJ, Mayberg HS, Fisher RS, Douglass KH, Dannals RF, Links JM, Wilson AA, Ravert HT, Rosenbaum AE, Snyder SH et al (1988) Mu-opiate receptors measured by positron emission tomography are increased in temporal lobe epilepsy. *Ann Neurol* 23:231–237
- Frost JJ, Douglass KH, Mayberg HS, Dannals RF, Links JM, Wilson AA, Ravert HT, Crozier WC, Wagner HN Jr (1989) Multicompartmental analysis of [11C]-carfentanil binding to opiate receptors in humans measured by positron emission tomography. *J Cereb Blood Flow Metab* 9:398–409
- Frost JJ, Mayberg HS, Sadzot B, Dannals RF, Lever JR, Ravert HT, Wilson AA, Wagner HN Jr, Links JM (1990) Comparison of [11C]diprenorphine and [11C]carfentanil binding to opiate receptors in humans by positron emission tomography. *J Cereb Blood Flow Metab* 10:484–492
- Galynker I, Schlyer DJ, Dewey SL, Fowler JS, Logan J, Gatley SJ, MacGregor RR, Ferrieri RA, Holland MJ, Brodie J, Simon E, Wolf AP (1996) Opioid receptor imaging and displacement studies with [6-O-[11C] methyl]buprenorphine in baboon brain. *Nucl Med Biol* 23:325–331

- Ghitza UE, Preston KL, Epstein DH, Kuwabara H, Endres CJ, Bencherif B, Boyd SJ, Copersino ML, Frost JJ, Gorelick DA (2010) Brain mu-opioid receptor binding predicts treatment outcome in cocaine-abusing outpatients. *Biol Psychiatry* 68:697–703
- Goldstein A, Tachibana S, Lowney LI, Hunkapiller M, Hood L (1979) Dynorphin-(1–13), an extraordinarily potent opioid peptide. *Proc Natl Acad Sci U S A* 76:6666–6670
- Gorelick DA, Kim YK, Bencherif B, Boyd SJ, Nelson R, Copersino M, Endres CJ, Dannals RF, Frost JJ (2005) Imaging brain mu-opioid receptors in abstinent cocaine users: time course and relation to cocaine craving. *Biol Psychiatry* 57:1573–1582
- Gorelick DA, Kim YK, Bencherif B, Boyd SJ, Nelson R, Copersino ML, Dannals RF, Frost JJ (2008) Brain mu-opioid receptor binding: relationship to relapse to cocaine use after monitored abstinence. *Psychopharmacology (Berl)* 200:475–486
- Greenwald MK, Johanson CE, Moody DE, Woods JH, Kilbourn MR, Koeppe RA, Schuster CR, Zubieta JK (2003) Effects of buprenorphine maintenance dose on mu-opioid receptor availability, plasma concentrations, and antagonist blockade in heroin-dependent volunteers. *Neuropsychopharmacology* 28:2000–2009
- Greenwald M, Johanson CE, Bueller J, Chang Y, Moody DE, Kilbourn M, Koeppe R, Zubieta JK (2007) Buprenorphine duration of action: mu-opioid receptor availability and pharmacokinetic and behavioral indices. *Biol Psychiatry* 61:101–110
- Guterstam J, Jayaram-Lindstrom N, Cervenka S, Frost JJ, Farde L, Halldin C, Franck J (2013) Effects of amphetamine on the human brain opioid system – a positron emission tomography study. *Int J Neuropsychopharmacol* 16:763–769
- Hackler L, Zadina JE, Ge LJ, Kastin AJ (1997) Isolation of relatively large amounts of endomorphin-1 and endomorphin-2 from human brain cortex. *Peptides* 18:1635–1639
- Hagelberg N, Aalto S, Tuominen L, Pesonen U, Nagren K, Hietala J, Scheinin H, Pertovaara A, Martikainen IK (2012) Striatal mu-opioid receptor availability predicts cold pressor pain threshold in healthy human subjects. *Neurosci Lett* 521:11–14
- Hammers A, Lingford-Hughes A (2006) Opioid imaging. *Neuroimaging Clin N Am* 16:529–552, vii
- Hammers A, Asselin MC, Hinz R, Kitchen I, Brooks DJ, Duncan JS, Koeppe MJ (2007a) Upregulation of opioid receptor binding following spontaneous epileptic seizures. *Brain* 130:1009–1016
- Hammers A, Asselin MC, Turkheimer FE, Hinz R, Osman S, Hotton G, Brooks DJ, Duncan JS, Koeppe MJ (2007b) Balancing bias, reliability, noise properties and the need for parametric maps in quantitative ligand PET: [(11)C]diprenorphine test-retest data. *Neuroimage* 38:82–94
- Harris RE, Zubieta JK, Scott DJ, Napadow V, Gracely RH, Clauw DJ (2009) Traditional Chinese acupuncture and placebo (sham) acupuncture are differentiated by their effects on mu-opioid receptors (MORs). *Neuroimage* 47:1077–1085
- Heinz A, Reimold M, Wrase J, Hermann D, Croissant B, Mundle G, Dohmen BM, Braus DF, Schumann G, Machulla HJ, Bares R, Mann K (2005) Correlation of stable elevations in striatal mu-opioid receptor availability in detoxified alcoholic patients with alcohol craving: a positron emission tomography study using carbon 11-labeled carfentanil. *Arch Gen Psychiatry* 62:57–64
- Henriksen G, Willoch F (2008) Imaging of opioid receptors in the central nervous system. *Brain* 131:1171–1196
- Henriksen G, Platzer S, Hauser A, Willoch F, Berthele A, Schwaiger M, Wester HJ (2005a) 18F-labeled sufentanil for PET-imaging of mu-opioid receptors. *Bioorg Med Chem Lett* 15:1773–1777
- Henriksen G, Platzer S, Marton J, Hauser A, Berthele A, Schwaiger M, Marinelli L, Lavecchia A, Novellino E, Wester HJ (2005b) Syntheses, biological evaluation, and molecular modeling of 18F-labeled 4-anilidopiperidines as mu-opioid receptor imaging agents. *J Med Chem* 48:7720–7732
- Henriksen G, Spilker ME, Sprenger T, Hauser AI, Platzer S, Boecker H, Toelle TR, Schwaiger M, Wester HJ (2006) Gender dependent rate of metabolism of the opioid receptor-PET ligand [18F]fluoroethylidiprenorphine. *Nuklearmedizin* 45:197–200

- Hirvonen J, Aalto S, Hagelberg N, Maksimow A, Ingman K, Oikonen V, Virkkala J, Nagren K, Scheinin H (2009) Measurement of central mu-opioid receptor binding in vivo with PET and [¹¹C]carfentanil: a test-retest study in healthy subjects. *Eur J Nucl Med Mol Imaging* 36:275–286
- Homcy CJ, Strauss HW, Kopiwoda S (1980) Beta receptor occupancy. Assessment in the intact animal. *J Clin Invest* 65:1111–1118
- Hostetler ED, Sanabria-Bohorquez S, Eng W, Joshi AD, Patel S, Gibson RE, O'Malley S, Krause SM, Ryan C, Riffel K, Bi S, Okamoto O, Kawamoto H, Ozaki S, Ohta H, de Groot T, Bormans G, Depre M, de Hoon J, De Lepeleire I, Reynders T, Cook JJ, Burns HD, Egan M, Cho W, van Laere K, Hargreaves RJ (2013) Evaluation of [(18)F]MK-0911, a positron emission tomography (PET) tracer for opioid receptor-like 1 (ORL1), in rhesus monkey and human. *Neuroimage* 68:1–10
- Hughes J, Smith TW, Kosterlitz HW, Fothergill LA, Morgan BA, Morris HR (1975) Identification of two related pentapeptides from the brain with potent opiate agonist activity. *Nature* 258:577–580
- Hume SP, Lingford-Hughes AR, Nataf V, Hirani E, Ahmad R, Davies AN, Nutt DJ (2007) Low sensitivity of the positron emission tomography ligand [¹¹C]diprenorphine to agonist opiates. *J Pharmacol Exp Ther* 322:661–667
- Ingman K, Hagelberg N, Aalto S, Nagren K, Juhakoski A, Karhuvaara S, Kallio A, Oikonen V, Hietala J, Scheinin H (2005) Prolonged central mu-opioid receptor occupancy after single and repeated nalmefene dosing. *Neuropsychopharmacology* 30:2245–2253
- Jones AK, Luthra SK, Maziere B, Pike VW, Loc'h C, Cruzel C, Syrota A, Jones T (1988) Regional cerebral opioid receptor studies with [¹¹C]diprenorphine in normal volunteers. *J Neurosci Methods* 23:121–129
- Jones AK, Qi LY, Fujirawa T, Luthra SK, Ashburner J, Bloomfield P, Cunningham VJ, Itoh M, Fukuda H, Jones T (1991) In vivo distribution of opioid receptors in man in relation to the cortical projections of the medial and lateral pain systems measured with positron emission tomography. *Neurosci Lett* 126:25–28
- Jones AK, Cunningham VJ, Ha-Kawa S, Fujiwara T, Luthra SK, Silva S, Derbyshire S, Jones T (1994a) Changes in central opioid receptor binding in relation to inflammation and pain in patients with rheumatoid arthritis. *Br J Rheumatol* 33:909–916
- Jones AK, Cunningham VJ, Ha-Kawa SK, Fujiwara T, Liyui Q, Luthra SK, Ashburner J, Osman S, Jones T (1994b) Quantitation of [¹¹C]diprenorphine cerebral kinetics in man acquired by PET using presaturation, pulse-chase and tracer-only protocols. *J Neurosci Methods* 51:123–134
- Jones AK, Kitchen ND, Watabe H, Cunningham VJ, Jones T, Luthra SK, Thomas DG (1999) Measurement of changes in opioid receptor binding in vivo during trigeminal neuralgic pain using [¹¹C] diprenorphine and positron emission tomography. *J Cereb Blood Flow Metab* 19:803–808
- Jones AK, Watabe H, Cunningham VJ, Jones T (2004) Cerebral decreases in opioid receptor binding in patients with central neuropathic pain measured by [¹¹C]diprenorphine binding and PET. *Eur J Pain* 8:479–485
- Kalant H (1997) Opium revisited: a brief review of its nature, composition, non-medical use and relative risks. *Addiction* 92:267–277
- Kawai R, Sawada Y, Channing M, Dunn B, Newman AH, Rice KC, Blasberg RG (1990) Kinetic analysis of the opiate antagonist cyclofoxy in rat brain: simultaneous infusion of active and inactive enantiomers. *J Pharmacol Exp Ther* 255:826–835
- Kawai R, Carson RE, Dunn B, Newman AH, Rice KC, Blasberg RG (1991) Regional brain measurement of Bmax and KD with the opiate antagonist cyclofoxy: equilibrium studies in the conscious rat. *Blood Flow Metab* 11:529–544
- Kennedy SE, Koeppe RA, Young EA, Zubieta JK (2006) Dysregulation of endogenous opioid emotion regulation circuitry in major depression in women. *Arch Gen Psychiatry* 63:1199–1208
- Kieffer BL, Befort K, Gaveriaux-Ruff C, Hirth CG (1992) The delta-opioid receptor: isolation of a cDNA by expression cloning and pharmacological characterization. *Proc Natl Acad Sci U S A* 89:12048–12052

- Kim S, Wagner HN Jr, Villemagne VL, Kao PF, Dannals RF, Ravert HT, Joh T, Dixon RB, Civelek AC (1997) Longer occupancy of opioid receptors by nalmefene compared to naloxone as measured in vivo by a dual-detector system. *J Nucl Med* 38:1726–1731
- Kimura Y, Fujita M, Hong J, Lohith TG, Gladding RL, Zoghbi SS, Tauscher JA, Goebel N, Rash KS, Chen Z, Pedregal C, Barth VN, Pike VW, Innis RB (2011) Brain and whole-body imaging in rhesus monkeys of ¹¹C-NOP-1A, a promising PET radioligand for nociceptin/orphanin FQ peptide receptors. *J Nucl Med* 52:1638–1645
- Klega A, Eberle T, Buchholz HG, Maus S, Maihofner C, Schreckenberger M, Birklein F (2010) Central opioidergic neurotransmission in complex regional pain syndrome. *Neurology* 75:129–136
- Kling MA, Carson RE, Borg L, Zametkin A, Matochik JA, Schluger J, Herscovitch P, Rice KC, Ho A, Eckelman WC, Kreek MJ (2000) Opioid receptor imaging with positron emission tomography and [¹⁸F]cyclofexy in long-term, methadone-treated former heroin addicts. *J Pharmacol Exp Ther* 295:1070–1076
- Koepp MJ, Duncan JS (2000) PET: opiate neuroreceptor mapping. *Adv Neurol* 83:145–156
- Koepp MJ, Richardson MP, Brooks DJ, Duncan JS (1998) Focal cortical release of endogenous opioids during reading-induced seizures. *Lancet* 352:952–955
- Koepp MJ, Hammers A, Lawrence AD, Asselin MC, Grasby PM, Bench CJ (2009) Evidence for endogenous opioid release in the amygdala during positive emotion. *Neuroimage* 44:252–256
- Lee MC, Wagner HN Jr, Tanada S, Frost JJ, Bice AN, Dannals RF (1988) Duration of occupancy of opiate receptors by naltrexone. *J Nucl Med* 29:1207–1211
- Lever JR (2007) PET and SPECT imaging of the opioid system: receptors, radioligands and avenues for drug discovery and development. *Curr Pharm Des* 13:33–49
- Lever JR, Dannals RF, Wilson AA, Ravert HT, Wagner HN Jr (1987) Synthesis of carbon-11 labeled diprenorphine: a radioligand for positron emission tomographic studies of opiate receptors. *Tetrahedron Lett* 28:4015–4018
- Lever JR, Mazza SM, Dannals RF, Ravert HT, Wilson AA, Wagner HN Jr (1990) Facile synthesis of [¹¹C]buprenorphine for positron emission tomographic studies of opioid receptors. *Int J Rad Appl Instrum A* 41:745–752
- Lever JR, Scheffel U, Kinter CM, Ravert HT, Dannals RF, Wagner HN Jr, Frost JJ (1992) In vivo binding of N¹'-([¹¹C]methyl)naltrexone to delta-opioid receptors in mouse brain. *Eur J Pharmacol* 216:459–460
- Lever JR, Stathis M, Kinter CM, Scheffel U (1996) In vivo labeling of delta opioid receptors in mouse brain by [³H]benzylidenenaltrexone, a ligand selective for the delta 1 subtype. *Life Sci* 58:L331–L336
- Liberzon I, Zubieta JK, Fig LM, Phan KL, Koeppe RA, Taylor SF (2002) mu-opioid receptors and limbic responses to aversive emotional stimuli. *Proc Natl Acad Sci U S A* 99:7084–7089
- Liberzon I, Taylor SF, Phan KL, Britton JC, Fig LM, Bueller JA, Koeppe RA, Zubieta JK (2007) Altered central micro-opioid receptor binding after psychological trauma. *Biol Psychiatry* 61:1030–1038
- Lohith TG, Zoghbi SS, Morse CL, Araneta MF, Barth VN, Goebel NA, Tauscher JT, Pike VW, Innis RB, Fujita M (2012) Brain and whole-body imaging of nociceptin/orphanin FQ peptide receptor in humans using the PET ligand ¹¹C-NOP-1A. *J Nucl Med* 53:385–392
- Lord JA, Waterfield AA, Hughes J, Kosterlitz HW (1977) Endogenous opioid peptides: multiple agonists and receptors. *Nature* 267:495–499
- Love TM, Stohler CS, Zubieta JK (2009) Positron emission tomography measures of endogenous opioid neurotransmission and impulsiveness traits in humans. *Arch Gen Psychiatry* 66:1124–1134
- Luthra SK, Pike VW, Brady F (1985) The preparation of carbon-11 labeled diprenorphine: a new radioligand for the study of the opiate receptor system in vivo. *J Chem Soc Chem Commun* 1423–1425
- Luthra SK, Pike VW, Brady F, Horlock PL, Prenant C, Crouzel C (1987) Preparation of [¹¹C]buprenorphine – a potential radioligand for the study of the opiate receptor system in vivo. *Int J Rad Appl Instrum A* 38:65–66

- Maarrawi J, Peyron R, Mertens P, Costes N, Magnin M, Sindou M, Laurent B, Garcia-Larrea L (2007a) Differential brain opioid receptor availability in central and peripheral neuropathic pain. *Pain* 127:183–194
- Maarrawi J, Peyron R, Mertens P, Costes N, Magnin M, Sindou M, Laurent B, Garcia-Larrea L (2007b) Motor cortex stimulation for pain control induces changes in the endogenous opioid system. *Neurology* 69:827–834
- Madar I, Lever JR, Kinter CM, Scheffel U, Ravert HT, Musachio JL, Mathews WB, Dannals RF, Frost JJ (1996) Imaging of delta opioid receptors in human brain by N1'-([11C]methyl)naltrindole and PET. *Synapse* 24:19–28
- Madar I, Lesser RP, Krauss G, Zubieta JK, Lever JR, Kinter CM, Ravert HT, Musachio JL, Mathews WB, Dannals RF, Frost JJ (1997) Imaging of delta- and mu-opioid receptors in temporal lobe epilepsy by positron emission tomography. *Ann Neurol* 41:358–367
- Madar I, Bencherif B, Lever J, Heitmiller RF, Yang SC, Brock M, Brahmmer J, Ravert H, Dannals R, Frost JJ (2007) Imaging delta- and mu-opioid receptors by PET in lung carcinoma patients. *J Nucl Med* 48:207–213
- Martin WR, Eades CG, Thompson JA, Huppler RE, Gilbert PE (1976) The effects of morphine- and nalorphine-like drugs in the nondependent and morphine-dependent chronic spinal dog. *J Pharmacol Exp Ther* 197:517–532
- Mayberg HS, Sadzot B, Meltzer CC, Fisher RS, Lesser RP, Dannals RF, Lever JR, Wilson AA, Ravert HT, Wagner HN Jr et al (1991) Quantification of mu and non-mu opiate receptors in temporal lobe epilepsy using positron emission tomography. *Ann Neurol* 30:3–11
- McLean S, Rice KC, Lessor R, Rothman RB (1987) [3H]cyclofoxy, a ligand suitable for positron emission tomography, labels mu and kappa opioid receptors. *Neuropeptides* 10:235–239
- Melichar JK, Nutt DJ, Malizia AL (2003) Naloxone displacement at opioid receptor sites measured in vivo in the human brain. *Eur J Pharmacol* 459:217–219
- Melichar JK, Hume SP, Williams TM, Daglish MR, Taylor LG, Ahmad R, Malizia AL, Brooks DJ, Myles JS, Lingford-Hughes A, Nutt DJ (2005) Using [11C]diprenorphine to image opioid receptor occupancy by methadone in opioid addiction: clinical and preclinical studies. *J Pharmacol Exp Ther* 312:309–315
- Meunier JC, Mollereau C, Toll L, Suaudeau C, Moisand C, Alvinerie P, Butour JL, Guillemot JC, Ferrara P, Monsarrat B et al (1995) Isolation and structure of the endogenous agonist of opioid receptor-like ORL1 receptor. *Nature* 377:532–535
- Minami M, Satoh M (1995) Molecular biology of the opioid receptors: structures, functions and distributions. *Neurosci Res* 23:121–145
- Mitchell JM, O'Neil JP, Janabi M, Marks SM, Jagust WJ, Fields HL (2012) Alcohol consumption induces endogenous opioid release in the human orbitofrontal cortex and nucleus accumbens. *Sci Transl Med* 4:116ra6
- Mueller C, Klega A, Buchholz HG, Rolke R, Magerl W, Schirrmacher R, Schirrmacher E, Birckle F, Treede RD, Schreckenberger M (2010) Basal opioid receptor binding is associated with differences in sensory perception in healthy human subjects: a [18F]diprenorphine PET study. *Neuroimage* 49:731–737
- Nabulsi NB, Zheng MQ, Ropchan J, Labaree D, Ding YS, Blumberg L, Huang Y (2011) [11C] GR103545: novel one-pot radiosynthesis with high specific activity. *Nucl Med Biol* 38:215–221
- Ogawa M, Hatano K, Kawasumi Y, Wichmann J, Ito K (2001) Synthesis and in vivo evaluation of [11C]methyl-Ro 64–6198 as an ORL1 receptor imaging agent. *Nucl Med Biol* 28:941–947
- Ogawa M, Hatano K, Kawasumi Y, Ishiwata K, Kawamura K, Ozaki S, Ito K (2003) Synthesis and evaluation of 1-[(3R,4R)-1-cyclooctylmethyl-3-hydroxymethyl-4-piperidyl]-3-[11C]ethyl-1,3-dihydro-2H-benzimidazol-2-one as a brain ORL1 receptor imaging agent for positron emission tomography. *Nucl Med Biol* 30:51–59
- Ostrowski NL, Burke TR Jr, Rice KC, Pert A, Pert CB (1987) The pattern of [3H]cyclofoxy retention in rat brain after in vivo injection corresponds to the in vitro opiate receptor distribution. *Brain Res* 402:275–286
- Pedregal C, Joshi EM, Toledo MA, Lafuente C, Diaz N, Martinez-Grau MA, Jimenez A, Benito A, Navarro A, Chen Z, Mudra DR, Kahl SD, Rash KS, Statnick MA, Barth VN (2012)

- Development of LC-MS/MS-based receptor occupancy tracers and positron emission tomography radioligands for the nociceptin/orphanin FQ (NOP) receptor. *J Med Chem* 55:4955–4967
- Pert CB, Snyder SH (1975) Identification of opiate receptor binding in intact animals. *Life Sci* 16:1623–1634
- Pert CB, Danks JA, Channing MA, Eckelman WC, Larson SM, Bennett JM, Burke TR Jr, Rice KC (1984) 3-[18F]Acetylcyclofoxy: a useful probe for the visualization of opiate receptors in living animals. *FEBS Lett* 177:281–286
- Pfeiffer A, Pasi A, Mehraein P, Herz A (1982) Opiate receptor binding sites in human brain. *Brain Res* 248:87–96
- Piccini P, Weeks RA, Brooks DJ (1997) Alterations in opioid receptor binding in Parkinson's disease patients with levodopa-induced dyskinesias. *Ann Neurol* 42:720–726
- Pichika R, Jewett DM, Sherman PS, Traynor JR, Husbands SM, Woods JH, Kilbourn MR (2010) Synthesis and in vivo brain distribution of carbon-11-labeled delta-opioid receptor agonists. *Nucl Med Biol* 37:989–996
- Pike VW, Rash KS, Chen Z, Pedregal C, Statnick MA, Kimura Y, Hong J, Zoghbi SS, Fujita M, Toledo MA, Diaz N, Gackenhaimer SL, Tauscher JT, Barth VN, Innis RB (2011) Synthesis and evaluation of radioligands for imaging brain nociceptin/orphanin FQ peptide (NOP) receptors with positron emission tomography. *J Med Chem* 54:2687–2700
- Poisnel G, Oueslati F, Dhilly M, Delamare J, Perrio C, Debruyne D, Barre L (2008) [11C]-MeJDTic: a novel radioligand for kappa-opioid receptor positron emission tomography imaging. *Nucl Med Biol* 35:561–569
- Portoghese PS, Sultana M, Takemori AE (1990) Design of peptidomimetic delta opioid receptor antagonists using the message-address concept. *J Med Chem* 33:1714–1720
- Prevett MC, Cunningham VJ, Brooks DJ, Fish DR, Duncan JS (1994) Opiate receptors in idiopathic generalised epilepsy measured with [11C]diprenorphine and positron emission tomography. *Epilepsy Res* 19:71–77
- Prossin AR, Love TM, Koeppe RA, Zubieta JK, Silk KR (2010) Dysregulation of regional endogenous opioid function in borderline personality disorder. *Am J Psychiatry* 167:925–933
- Prossin AR, Koch AE, Campbell PL, McInnis MG, Zalcmann SS, Zubieta JK (2011) Association of plasma interleukin-18 levels with emotion regulation and mu-opioid neurotransmitter function in major depression and healthy volunteers. *Biol Psychiatry* 69:808–812
- Rabiner EA, Beaver J, Makwana A, Searle G, Long C, Nathan PJ, Newbould RD, Howard J, Miller SR, Bush MA, Hill S, Reiley R, Passchier J, Gunn RN, Matthews PM, Bullmore ET (2011) Pharmacological differentiation of opioid receptor antagonists by molecular and functional imaging of target occupancy and food reward-related brain activation in humans. *Mol Psychiatry* 16:826–835, 785
- Ravert HT, Mathews WB, Musachio JL, Scheffel U, Finley P, Dannals RF (1999) [11C]-methyl 4-[(3,4-dichlorophenyl)acetyl]-3-[(1-pyrrolidinyl)-methyl]-1-piperazinecarboxylate ([11C] GR89696): synthesis and in vivo binding to kappa opiate receptors. *Nucl Med Biol* 26:737–741
- Ravert HT, Scheffel U, Mathews WB, Musachio JL, Dannals RF (2002) [(11)C]-GR89696, a potent kappa opiate receptor radioligand; in vivo binding of the R and S enantiomers. *Nucl Med Biol* 29:47–53
- Ravert HT, Bencherif B, Madar I, Frost JJ (2004) PET imaging of opioid receptors in pain: progress and new directions. *Curr Pharm Des* 10:759–768
- Ray R, Ruparel K, Newberg A, Wileyto EP, Loughhead JW, Divgi C, Blendy JA, Logan J, Zubieta JK, Lerman C (2011) Human Mu Opioid Receptor (OPRM1 A118G) polymorphism is associated with brain mu-opioid receptor binding potential in smokers. *Proc Natl Acad Sci U S A* 108:9268–9273
- Raynor K, Kong H, Chen Y, Yasuda K, Yu L, Bell GI, Reisine T (1994) Pharmacological characterization of the cloned kappa-, delta-, and mu-opioid receptors. *Mol Pharmacol* 45:330–334
- Reame NE, Lukacs JL, Padmanabhan V, Eyvazzadeh AD, Smith YR, Zubieta JK (2008) Black cohosh has central opioid activity in postmenopausal women: evidence from naloxone blockade and positron emission tomography neuroimaging. *Menopause* 15:832–840

- Reinscheid RK, Nothacker HP, Bourson A, Ardati A, Henningsen RA, Bunzow JR, Grandy DK, Langen H, Monsma FJ Jr, Civelli O (1995) Orphanin FQ: a neuropeptide that activates an opioidlike G protein-coupled receptor. *Science* 270:792–794
- Rinne JO, Burn DJ, Mathias CJ, Quinn NP, Marsden CD, Brooks DJ (1995) Positron emission tomography studies on the dopaminergic system and striatal opioid binding in the olivopontocerebellar atrophy variant of multiple system atrophy. *Ann Neurol* 37:568–573
- Riss PJ, Hong YT, Marton J, Caprioli D, Williamson DJ, Ferrari V, Saigal N, Roth BL, Henriksen G, Fryer TD, Dalley JW, Aigbirhio FI (2013) Synthesis and evaluation of 18F-FE-PEO in rodents: an 18F-labeled full agonist for opioid receptor imaging. *J Nucl Med* 54:299–305
- Rothman RB, McLean S (1988) An examination of the opiate receptor subtypes labeled by [³H] cycloFOXY: an opiate antagonist suitable for positron emission tomography. *Biol Psychiatry* 23:435–458
- Rothman RB, Bykov V, Reid A, De Costa BR, Newman AH, Jacobson AE, Rice KC (1988) A brief study of the selectivity of norbinaltorphimine, (–)-cyclofoxy, and (+)-cyclofoxy among opioid receptor subtypes in vitro. *Neuropeptides* 12:181–187
- Ruiz-Gayo M, Baamonde A, Turcaud S, Fournie-Zaluski MC, Roques BP (1992) In vivo occupation of mouse brain opioid receptors by endogenous enkephalins: blockade of enkephalin degrading enzymes by RB 101 inhibits [³H]diprenorphine binding. *Brain Res* 571:306–312
- Ryu EK, Wu Z, Chen K, Lazarus LH, Marczak ED, Sasaki Y, Ambo A, Salvadori S, Ren C, Zhao H, Balboni G, Chen X (2008) Synthesis of a potent and selective (18F)-labeled delta-opioid receptor antagonist derived from the Dmt-Tic pharmacophore for positron emission tomography imaging. *J Med Chem* 51:1817–1823
- Sadzot B, Frost JJ (1990) Pain and opiate receptors: considerations for the design of positron emission tomography studies. *Anesth Prog* 37:113–120
- Sadzot B, Mayberg HS, Frost JJ (1990) Detection and quantification of opiate receptors in man by positron emission tomography. Potential applications to the study of pain. *Neurophysiol Clin* 20:323–334
- Sadzot B, Price JC, Mayberg HS, Douglass KH, Dannals RF, Lever JR, Ravert HT, Wilson AA, Wagner HN Jr, Feldman MA et al (1991) Quantification of human opiate receptor concentration and affinity using high and low specific activity [¹¹C]diprenorphine and positron emission tomography. *J Cereb Blood Flow Metab* 11:204–219
- Saji H, Tsutsumi D, Magata Y, Iida Y, Konishi J, Yokoyama A (1992) Preparation and biodistribution in mice of [¹¹C]carfentanil: a radiopharmaceutical for studying brain mu-opioid receptors by positron emission tomography. *Ann Nucl Med* 6:63–67
- Sawada Y, Kawai R, McManaway M, Otsuki H, Rice KC, Patlak CS, Blasberg RG (1991) Kinetic analysis of transport and opioid receptor binding of [³H](–)-cyclofoxy in rat brain in vivo: implications for human studies. *J Cereb Blood Flow Metab* 11:183–203
- Schadrack J, Willoch F, Platzer S, Bartenstein P, Mahal B, Dworzak D, Wester HJ, Zieglgansberger W, Tolle TR (1999) Opioid receptors in the human cerebellum: evidence from [¹¹C]diprenorphine PET, mRNA expression and autoradiography. *Neuroreport* 10:619–624
- Schultz BW, Hjernevik T, Willoch F, Marton J, Noda A, Murakami Y, Miyoshi S, Nishimura S, Arstad E, Drzezga A, Matsunari I, Henriksen G (2010) Evaluation of the kappa-opioid receptor-selective tracer [(11C)GR103545 in awake rhesus macaques. *Eur J Nucl Med Mol Imaging* 37:1174–1180
- Schreckenberger M, Klega A, Grunder G, Buchholz HG, Scheurich A, Schirmacher R, Schirmacher E, Muller C, Henriksen G, Bartenstein P (2008) Opioid receptor PET reveals the psychobiologic correlates of reward processing. *J Nucl Med* 49:1257–1261
- Scott DJ, Domino EF, Heitzeg MM, Koeppe RA, Ni L, Guthrie S, Zubieta JK (2007a) Smoking modulation of mu-opioid and dopamine D2 receptor-mediated neurotransmission in humans. *Neuropsychopharmacology* 32:450–457
- Scott DJ, Stohler CS, Koeppe RA, Zubieta JK (2007b) Time-course of change in [¹¹C]carfentanil and [¹¹C]raclopride binding potential after a nonpharmacological challenge. *Synapse* 61:707–714
- Scott DJ, Stohler CS, Egnatuk CM, Wang H, Koeppe RA, Zubieta JK (2008) Placebo and nocebo effects are defined by opposite opioid and dopaminergic responses. *Arch Gen Psychiatry* 65:220–231

- Shiue CY, Bai LQ, Teng RR, Arnett CD, Dewey SL, Wolf AP, McPherson DW, Fowler JS, Logan J, Holland MJ et al (1991) A comparison of the brain uptake of N-(cyclopropyl[11C]methyl) norbuprenorphine ([11C]buprenorphine) and N-(cyclopropyl[11C]methyl)nordiprenorphine ([11C]diprenorphine) in baboon using PET. *Int J Rad Appl Instrum B* 18:281–288
- Simantov R, Snyder SH (1976) Morphine-like peptides in mammalian brain: isolation, structure elucidation, and interactions with the opiate receptor. *Proc Natl Acad Sci U S A* 73:2515–2519
- Smith YR, Zubieta JK, del Carmen MG, Dannals RF, Ravert HT, Zacur HA, Frost JJ (1998) Brain opioid receptor measurements by positron emission tomography in normal cycling women: relationship to luteinizing hormone pulsatility and gonadal steroid hormones. *J Clin Endocrinol Metab* 83:4498–4505
- Smith JS, Zubieta JK, Price JC, Flesher JE, Madar I, Lever JR, Kinter CM, Dannals RF, Frost JJ (1999) Quantification of delta-opioid receptors in human brain with N1'-(11C)methyl naltrindole and positron emission tomography. *J Cereb Blood Flow Metab* 19:956–966
- Smith YR, Stohler CS, Nichols TE, Bueller JA, Koeppe RA, Zubieta JK (2006) Pronociceptive and antinociceptive effects of estradiol through endogenous opioid neurotransmission in women. *J Neurosci* 26:5777–5785
- Snyder SH, Pasternak GW (2003) Historical review: opioid receptors. *Trends Pharmacol Sci* 24:198–205
- Sprenger T, Berthele A, Platzer S, Boecker H, Tolle TR (2005) What to learn from in vivo opioidergic brain imaging? *Eur J Pain* 9:117–121
- Sprenger T, Valet M, Boecker H, Henriksen G, Spilker ME, Willloch F, Wagner KJ, Wester HJ, Tolle TR (2006a) Opioidergic activation in the medial pain system after heat pain. *Pain* 122:63–67
- Sprenger T, Willloch F, Miederer M, Schindler F, Valet M, Berthele A, Spilker ME, Forderreuther S, Straube A, Stangier I, Wester HJ, Tolle TR (2006b) Opioidergic changes in the pineal gland and hypothalamus in cluster headache: a ligand PET study. *Neurology* 66:1108–1110
- Talbot PS, Narendran R, Butelman ER, Huang Y, Ngo K, Slifstein M, Martinez D, Laruelle M, Hwang DR (2005) 11C-GR103545, a radiotracer for imaging kappa-opioid receptors in vivo with PET: synthesis and evaluation in baboons. *J Nucl Med* 46:484–494
- Theodore WH, Carson RE, Andreasen P, Zametkin A, Blasberg R, Leiderman DB, Rice K, Newman A, Channing M, Dunn B et al (1992) PET imaging of opiate receptor binding in human epilepsy using [18F]cyclofoxy. *Epilepsy Res* 13:129–139
- Titeler M, Lyon RA, Kuhar MJ, Frost JF, Dannals RF, Leonhardt S, Bullock A, Rydelek LT, Price DL, Struble RG (1989) Mu opiate receptors are selectively labelled by [3H]carfentanil in human and rat brain. *Eur J Pharmacol* 167:221–228
- Tomasi G, Nabulsi N, Zheng MQ, Weinzimmer D, Ropchan J, Blumberg L, Brown-Proctor C, Ding YS, Carson RE, Huang Y (2013) Determination of in vivo Bmax and Kd for 11C-GR103545, an agonist PET tracer for kappa-opioid receptors: a study in nonhuman primates. *J Nucl Med* 54:1–9
- Trescot AM, Datta S, Lee M, Hansen H (2008) Opioid pharmacology. *Pain Physician* 11:S133–S153
- Tuominen L, Salo J, Hirvonen J, Nagren K, Laine P, Melartin T, Isometsa E, Viikari J, Raitakari O, Keltikangas-Jarvinen L, Hietala J (2012) Temperament trait Harm Avoidance associates with mu-opioid receptor availability in frontal cortex: a PET study using [(11)C]carfentanil. *Neuroimage* 61:670–676
- Tyacke RJ, Robinson ES, Schnabel R, Lewis JW, Husbands SM, Nutt DJ, Hudson AL (2002) N1'-fluoroethyl-naltrindole (BU97001) and N1'-fluoroethyl-(14-formylamino)-naltrindole (BU97018) potential delta-opioid receptor PET ligands. *Nucl Med Biol* 29:455–462
- Vaccarino AL, Kastin AJ (2001) Endogenous opiates: 2000. *Peptides* 22:2257–2328
- Villemagne VL, Frost JJ, Dannals RF, Lever JR, Tanada S, Natarajan TK, Wilson AA, Ravert HT, Wagner HN Jr (1994) Comparison of [11C]diprenorphine and [11C]carfentanil in vivo binding to opiate receptors in man using a dual detector system. *Eur J Pharmacol* 257:195–197
- Villemagne PS, Dannals RF, Ravert HT, Frost JJ (2002) PET imaging of human cardiac opioid receptors. *Eur J Nucl Med Mol Imaging* 29:1385–1388

- von Spiczak S, Whone AL, Hammers A, Asselin MC, Turkheimer F, Tings T, Happe S, Paulus W, Trenkwalder C, Brooks DJ (2005) The role of opioids in restless legs syndrome: an [¹¹C]diprenorphine PET study. *Brain* 128:906–917
- Wager TD, Scott DJ, Zubieta JK (2007) Placebo effects on human mu-opioid activity during pain. *Proc Natl Acad Sci U S A* 104:11056–11061
- Waldhoer M, Bartlett SE, Whistler JL (2004) Opioid receptors. *Annu Rev Biochem* 73:953–990
- Wand GS, Weerts EM, Kuwabara H, Frost JJ, Xu X, McCaul ME (2011) Naloxone-induced cortisol predicts mu opioid receptor binding potential in specific brain regions of healthy subjects. *Psychoneuroendocrinology* 36:1453–1459
- Weeks RA, Cunningham VJ, Piccini P, Waters S, Harding AE, Brooks DJ (1997) ¹¹C-diprenorphine binding in Huntington's disease: a comparison of region of interest analysis with statistical parametric mapping. *J Cereb Blood Flow Metab* 17:943–949
- Weerts EM, Kim YK, Wand GS, Dannals RF, Lee JS, Frost JJ, McCaul ME (2008) Differences in delta- and mu-opioid receptor blockade measured by positron emission tomography in naltrexone-treated recently abstinent alcohol-dependent subjects. *Neuropsychopharmacology* 33:653–665
- Weerts EM, Wand GS, Kuwabara H, Munro CA, Dannals RF, Hilton J, Frost JJ, McCaul ME (2011) Positron emission tomography imaging of mu- and delta-opioid receptor binding in alcohol-dependent and healthy control subjects. *Alcohol Clin Exp Res* 35:2162–2173
- Weerts EM, Wand GS, Kuwabara H, Xu X, Frost JJ, Wong DF, McCaul ME (2012) Association of smoking with mu-opioid receptor availability before and during naltrexone blockade in alcohol-dependent subjects. *Addict Biol*. doi:10.1111/adb.12022
- Weerts EM, McCaul ME, Kuwabara H, Yang X, Xu X, Dannals RF, Frost JJ, Wong DF, Wand GS (2013) Influence of OPRM1 Asn40Asp variant (A118G) on [¹¹C]carfentanil binding potential: preliminary findings in human subjects. *Int J Neuropsychopharmacol* 16:47–53
- Wester HJ, Willoch F, Tolle TR, Munz F, Herz M, Oye I, Schadrack J, Schwaiger M, Bartenstein P (2000) 6-O-(2-[¹⁸F]fluoroethyl)-6-O-desmethyldiprenorphine ([¹⁸F]DPN): synthesis, biologic evaluation, and comparison with [¹¹C]DPN in humans. *J Nucl Med* 41:1279–1286
- Whone AL, von Spiczak S, Edwards M, Valente EM, Hammers A, Bhatia KP, Brooks DJ (2004) Opioid binding in DYT1 primary torsion dystonia: an ¹¹C-diprenorphine PET study. *Mov Disord* 19:1498–1503
- Williams TM, Daglish MR, Lingford-Hughes A, Taylor LG, Hammers A, Brooks DJ, Grasby P, Myles JS, Nutt DJ (2007) Brain opioid receptor binding in early abstinence from opioid dependence: positron emission tomography study. *Br J Psychiatry* 191:63–69
- Williams TM, Davies SJ, Taylor LG, Daglish MR, Hammers A, Brooks DJ, Nutt DJ, Lingford-Hughes A (2009) Brain opioid receptor binding in early abstinence from alcohol dependence and relationship to craving: an [¹¹C]diprenorphine PET study. *Eur Neuropsychopharmacol* 19:740–748
- Willoch F, Tolle TR, Wester HJ, Munz F, Petzold A, Schwaiger M, Conrad B, Bartenstein P (1999) Central pain after pontine infarction is associated with changes in opioid receptor binding: a PET study with ¹¹C-diprenorphine. *AJNR Am J Neuroradiol* 20:686–690
- Willoch F, Schindler F, Wester HJ, Empl M, Straube A, Schwaiger M, Conrad B, Tolle TR (2004) Central poststroke pain and reduced opioid receptor binding within pain processing circuitries: a [¹¹C]diprenorphine PET study. *Pain* 108:213–220
- Yasuda K, Raynor K, Kong H, Breder CD, Takeda J, Reisine T, Bell GI (1993) Cloning and functional comparison of kappa and delta opioid receptors from mouse brain. *Proc Natl Acad Sci U S A* 90:6736–6740
- Zadina JE, Hackler L, Ge LJ, Kastin AJ (1997) A potent and selective endogenous agonist for the mu-opiate receptor. *Nature* 386:499–502
- Zheng MQ, Nabulsi N, Kim SJ, Tomasi G, Lin SF, Mitch C, Quimby S, Barth V, Rash K, Masters J, Navarro A, Seest E, Morris ED, Carson RE, Huang Y (2013) Synthesis and evaluation of ¹¹C-LY2795050 as a kappa-opioid receptor antagonist radiotracer for PET imaging. *J Nucl Med* 54:455–463

- Zubieta JK, Gorelick DA, Stauffer R, Ravert HT, Dannals RF, Frost JJ (1996) Increased mu opioid receptor binding detected by PET in cocaine-dependent men is associated with cocaine craving. *Nat Med* 2:1225–1229
- Zubieta JK, Dannals RF, Frost JJ (1999) Gender and age influences on human brain mu-opioid receptor binding measured by PET. *Am J Psychiatry* 156:842–848
- Zubieta J, Greenwald MK, Lombardi U, Woods JH, Kilbourn MR, Jewett DM, Koeppe RA, Schuster CR, Johanson CE (2000) Buprenorphine-induced changes in mu-opioid receptor availability in male heroin-dependent volunteers: a preliminary study. *Neuropsychopharmacology* 23:326–334
- Zubieta JK, Smith YR, Bueller JA, Xu Y, Kilbourn MR, Jewett DM, Meyer CR, Koeppe RA, Stohler CS (2001) Regional mu opioid receptor regulation of sensory and affective dimensions of pain. *Science* 293:311–315
- Zubieta JK, Smith YR, Bueller JA, Xu Y, Kilbourn MR, Jewett DM, Meyer CR, Koeppe RA, Stohler CS (2002) mu-opioid receptor-mediated antinociceptive responses differ in men and women. *J Neurosci* 22:5100–5107
- Zubieta JK, Ketter TA, Bueller JA, Xu Y, Kilbourn MR, Young EA, Koeppe RA (2003) Regulation of human affective responses by anterior cingulate and limbic mu-opioid neurotransmission. *Arch Gen Psychiatry* 60:1145–1153

PET Imaging of ABC Transporters in the BBB

21

Marcel Benadiba, Heli Savolainen, Nicola A. Colabufo,
Albert D. Windhorst, Aren van Waarde,
and Gert Luurtsema

Contents

21.1	ABC Transporter Expression at the Blood–Brain Barrier in Neurological Diseases ...	626
21.2	PET.....	629
21.3	P-gp Substrate, Inhibitor, and Modulator Terminology Overview.....	629
21.4	PET Tracers for Imaging of ABC Transporter Function and Expression in the BBB..	630
21.4.1	Background.....	630
21.4.2	Substrates as Tracers for Measuring P-gp Function	631
21.4.3	Inhibitors as Tracers for Measuring P-gp Expression.....	634
21.4.4	PET Studies with [¹¹ C]Verapamil in Neurological Diseases	636
21.4.5	Comparative Studies of [¹¹ C]Verapamil and Its Carbon-11-Labeled Metabolite D617 in BBB Using PET	637
21.4.6	Comparative Studies of [¹¹ C]Verapamil and [¹¹ C]dLop in BBB Using PET.....	638
21.4.7	¹⁸ F-Labeled Compounds to Assess P-gp Function and Expression	639
21.4.8	Use of P-gp Stimulator Compounds as a Strategy for Treatment of Neurodegenerative Diseases	639
21.5	Targeting ABC Transporter Regulation in the BBB: Considerations for Further Investigations with New Tracers and Treatment Outcomes.....	640
21.6	Mechanism of Action of ABC Transporter-Binding Substances.....	641
21.7	Discussion and Concluding Remarks.....	643
	References.....	644

M. Benadiba • H. Savolainen • A. van Waarde • G. Luurtsema (✉)
Department of Nuclear Medicine and Molecular Imaging, University Medical Center
Groningen, University of Groningen, Hanzeplein 1, Groningen 9713GZ, The Netherlands
e-mail: g.luurtsema@umcg.nl

N.A. Colabufo
Department of Pharmacochimistry, University of Bari, Bari, Italy

A.D. Windhorst
Nuclear Medicine and PET Research, Free University, Amsterdam, The Netherlands

Department of Radiology and Nuclear Medicine, VU University Medical Center,
Amsterdam, The Netherlands

Abstract

Neuroscience has never been so close to early diagnosis of complex neurological disorders like Alzheimer's and Parkinson's disease. As a consequence, new treatments can now be designed and pharmacotherapy be prescribed with better promise of a favorable clinical outcome, especially for resistant neurodegenerative diseases. Protein expression and function (particularly of membrane-bound receptors or enzymes) can be imaged and quantified in a noninvasive manner with positron emission tomography (PET). This technique can also be applied to the ABC transporter family of proteins, among which P-glycoprotein (P-gp) and breast cancer resistance protein (BCRP) have been major topics of study. [¹¹C] Verapamil, for example, is a widely used radiotracer to assess P-gp functionality in the blood–brain barrier (BBB) using PET. However, significant limitations of this tracer have led to the search for new radiopharmaceuticals for exploring BBB transporter function. This search aims to identify an optimal tracer to specifically assess P-gp function and expression at the BBB. Translating *in vitro* results to the *in vivo* situation may be difficult. Thus, studies in different animal species and strains are of great value. Transporter imaging may help clinicians with a more reliable early diagnosis of neurodegenerative syndromes such as Alzheimer's and Parkinson's disease with greater accuracy, preferably in a presymptomatic stage of the disease and before pharmacoresistance has developed.

21.1 ABC Transporter Expression at the Blood–Brain Barrier in Neurological Diseases

The ATP-binding cassette (ABC) transporters are a family of proteins implicated in the maintenance of the tissue homeostasis and are especially associated with blood–brain barrier (BBB) integrity. ABC proteins use energy from ATP hydrolysis to transport endogenous and exogenous compounds across cell membranes (Dean et al. 2001; Dean and Allikmets 2001; Thiebaut et al. 1987). To date, there are 49 ABC membrane proteins divided in seven subfamilies, and 44 of these are functionally characterized as membrane transporters for lipids, ions, peptides, or xenobiotics. In addition, there are 4 translation factors without transport activity, as they lack transmembrane domains (TD), and one pseudogene protein product (Barbet et al. 2012). Since ABC transporters are involved in the maintenance of cellular and tissue homeostasis, they strongly contribute to the development of the multidrug resistance (MDR) phenotype in neurological diseases (Agarwal et al. 2011; Bartels 2011; Löscher et al. 2011; Rosenhagen and Uhr 2011). In general terms, transporters at the BBB are essential for tissue detoxification and as a corollary of their biological function constitute a major barrier for pharmacotherapy for treatment of brain diseases.

Because of the MDR phenotype, ABC transporters are also known as multidrug resistance-associated proteins (MRP) or simply MDR/MRP transporters. ABCB1, also named MDR1 or P-glycoprotein (P-gp), was the first ABC transporter described and is found in both luminal and abluminal membranes of endothelial cells of the

Table 21.1 ABC transporters and brain disorders

CNS disease	ABC transporters examined in the context of this disease	References
Ischemic stroke	ABCB1, ABCC1	ElAli and Hermann (2010), Kilic et al. (2008), Spudich et al. (2006)
Epilepsy	ABCB1, various ABCCs, ABCG2	Kubota et al. (2006), Löscher and Potschka (2005), Seegers et al. (2002)
Brain cancer	ABCB1, ABCC1, ABCC4, ABCC5, ABCG2	Bronger et al. (2005), Porro et al. (2010)
Parkinson's disease, progressive supranuclear palsy, multiple system atrophy	ABCB1	Bartels et al. (2008b), Westerlund et al. (2008)
Alzheimer's disease	ABCA1, ABCA2, ABCB1, ABCC4, ABCG2	van Assema et al. (2012b), Cotte et al. (2009), Kuhnke et al. (2007), Lam et al. (2001), Macé et al. (2005), Riddell et al. (2007), Wijesuriya et al. (2010)
Adrenoleukodystrophy	ABCD1	Morita et al. (2011), Mosser et al. (1993)
Multiple sclerosis	ABCB1, ABCG2	Kooij et al. (2010), Xiong et al. (2009)
Brain metabolic disorders	ABCA1, ABCA2, ABCC8 (SUR1), ABCC9 (SUR2), ABCG1, ABCG4	Bojanic et al. (2010), Kaminski et al. (2006), Kim et al. (2008), Sakai et al. (2007)

Updated from ElAli and Hermann (2011)

human and rat brain vasculature (Bendayan et al. 2006) although it is also localized in the nuclear envelope of rat brain cells (Babakhanian et al. 2007). ABCC1, another important MRP, is present at the luminal side of human brain capillary endothelial cells (Gazzin et al. 2008; Nies et al. 2004). ABCC4 and ABCC5 are also expressed with high density at the luminal side of the BBB (Nies et al. 2004). Dauchy et al. demonstrated that ABCC1, ABCC4, ABCC5, ABCC6, ABCC11, and ABCC12 mRNAs are present in isolated brain microvessels, but their expression levels are lower than those of ABCB1 and ABCG2 (or BCRP1—breast cancer resistance protein) (Dauchy et al. 2008). In summary, ABCB1/MDR1 (P-gp), ABCC4/MRP4, ABCC5/MRP5, and ABCG2/BCRP1 appear to be the main ABC transporters expressed at the human BBB. The expression of these proteins can be altered depending on their microenvironmental conditions.

An overview of ABC transporters associated with brain disorders is given in Table 21.1. For example, in disorders such as epilepsy, the genes encoding ABCB1, ABCC2, and ABCC5 are all overexpressed in brain microvessels, in contrast to ABCC1 (Dombrowski et al. 2001). Another study comparing human nonmalignant brain tissue and human glioblastoma multiforme tumors showed that the expression levels of ABCG2 and ABCC1 were similar and higher than the expression of ABCB1 in the whole human brain (Zhang et al. 2003). In addition, these authors

demonstrated that ABCG2 is upregulated in brain tumor vessels and participates in directional drug efflux *in vitro*.

As polymorphisms of these genes are critical for prediction of neurological diseases, their pharmacogenetic data is also of great value. The ABCB1 gene contains more than 50 single nucleotide polymorphisms (SNP), some of them linked to changes in the expression and/or function of this ABC transporter (Sharom 2007). However, the difficulty in replicating results associating polymorphisms with the risk of developing diseases complicates this area of research. For example, many studies have investigated the relationship between ABCB1 polymorphisms and the risk of developing Parkinson's disease (PD), but to date only few studies have established such a direct association (Drożdżik et al. 2003; Lee et al. 2004; Westerlund et al. 2009). Therefore, ABCB1 variants are now thought to act rather indirectly as a susceptibility factor or modulator of the risk of PD in conjunction with the exposure to known risk factors such as pesticides (Brown et al. 2006). Noteworthy, three studies of genetic polymorphisms related to P-gp have underscored the increased risk of developing PD for carriers of variant C3435T or G2677[A,T] ABCB1 alleles who have also been exposed to pesticides (Drożdżik et al. 2003; Dutheil et al. 2010; Zschiedrich et al. 2009).

In relation to Alzheimer's disease (AD), ABCB1 and ABCG2 have recently been linked to the transport of A β peptides at the BBB. However, Vogelgesang et al. found no significant association between ABCB1 polymorphisms in humans and the risk of AD, but they demonstrated an inverse correlation between A β deposition rates and the cerebrovascular ABCB1 expression (Vogelgesang et al. 2002, 2004). Another recent study showed that besides the age-related decrease of P-gp expression, the A β 1-42 peptide itself is able to downregulate the expression of P-gp (Brenn et al. 2011). In contrast, the amount of ABCG2 in the brains of AD and CAA (cerebral amyloid angiopathy) patients was higher than in age-matched controls. Furthermore, the brains of Abcg2-null mice significantly accumulated more A β peptides compared to wild-type mice (Xiong et al. 2009), confirming that this transporter plays a protecting role against A β overload in the brain. In addition, the implication of both ABCB1 and ABCG2 in preventing A β from entering the brain was already confirmed by *in vitro* studies (Candela et al. 2010; Tai et al. 2009). This coordinated action between these two transporters is now the object of study of several research groups (Agarwal et al. 2011, 2012; Agarwal and Elmquist 2012; Kodaira et al. 2010), which certainly will provide a better understanding of their function at the BBB.

Since many *in vitro* results about ABC transporters may not be representative for the *in vivo* situation, functional imaging of these transporters at the BBB with an *in vivo* PET assay will increase our knowledge on the role of these proteins in physiological and pathophysiological conditions.

It has been established that considerable species differences exist concerning the expression of several ABC transporters in the BBB (Hermann and Bassetti 2007; Soontornmalai et al. 2006). A recent proteomic analysis conducted by Uchida and colleagues in both human and mouse brain microvessels lends support to this conclusion, and several examples illustrate this fact. Expression of BCRP protein was almost twice as high (1.85-fold) in humans as in mice. In contrast, MDR1 and

MRP4 protein expressions were smaller in humans than in mice, 2.33- and 8.15-fold, respectively (Uchida et al. 2011). Thus, imaging of ABC transporters and comparison of the data from different animal strains and from animal and human tissues will certainly expand our knowledge in this field. In addition, it will facilitate the translation of pharmacological findings from one animal strain to another, as well as from animals to humans.

21.2 PET

Positron emission tomography (PET) and single-photon emission computed tomography (SPECT) together with magnetic resonance imaging (MRI) and computed tomography (CT) are imaging techniques that allow noninvasive tracking of pathophysiological processes in various neuropsychiatric disorders. Molecular imaging has also been used in various aspects of drug development (Willmann et al. 2008). For an efficient visualization, characterization, and measurement of biological processes at the molecular, cellular, whole organ, or body level, specific imaging probes are needed. These probes are also known as tracers, due to the sub-pharmacological amounts administered. They provide an analytical signal which is detected by a particular method resulting in either a two- or three-dimensional image. PET is the most sensitive technique for in vivo imaging and quantification of biological and pathophysiological processes. However, the spatial resolution of PET is relatively low, and the additional use of CT or MRI imaging is required to provide high-resolution structural images that can be fused with the functional PET image. This will give both anatomical and functional information in a single scanning session.

The decay of these radionuclides occurs by the emission of a positively charged particle called positron. When emitted from the nucleus, the positron travels a very short distance (positron range, 3–5 mm) in the surrounding tissue before it annihilates by combining with an electron. Then, the mass of the positron and electron are converted to energy resulting in two 511 keV γ -rays which are emitted simultaneously at approximately 180° to each other. The pair of γ -rays is detected by rings of detectors in the PET scanner. The acquisition of a large number of coincident events provides data which can be reconstructed to an image with information on the spatial distribution of radioactivity as a function of time.

21.3 P-gp Substrate, Inhibitor, and Modulator Terminology Overview

In relation to P-gp binding (usually a reversible, noncovalent binding), a terminology overview is necessary. When a *substrate* (sometimes called a P-gp activator) binds to P-gp (in the substrate site of the P-gp molecule) or to another ABC transporter (depending on the molecular affinity), it is pumped out of the cell in an ATP-dependent manner. On the other hand, P-gp *inhibitors* bind to P-gp (or other ABC transporters, depending on the specificity of the molecule) and then block its

activity, preventing P-gp-mediated drug transport and allowing lipophilic molecules to get into the cells. A P-gp *modulator* also increases the tissue penetration of drugs transported by these proteins, but by a different mechanism of action. Modulators usually bind (noncovalently) to specific regulatory site(s) on the transporter molecule, thus causing a conformational alteration of the P-gp tertiary structure which is known as allosteric modulation (in this case a negative allosteric modulation of the transporter occurs). Modulators can bind to other regulatory site(s) of the P-gp structure as well and cause activation instead of inhibition by a process called positive allosteric modulation. It is important to consider that P-gp substrates such as verapamil and cyclosporine A can also bind to site(s) other than the substrate site, resulting in inhibition of P-gp activity (Maki and Dey 2006). For the more recent second- and third-generation inhibitors, the modes of action are yet to be determined. Based on experimental evidence, there is a growing consensus in favor of an allosteric mode of action for some of these compounds. Independent studies (Dey et al. 1997, 1998, 1999) suggested the existence of distinct modulator site(s) within the P-gp molecule that are linked to substrate site(s) either by negative or positive heterotropic cooperativity (heterotropic when the modulator is a molecule other than the substrate, otherwise it should be called homotropic cooperativity). Finally, it should be noted that conformational changes of the P-gp molecule can be induced by both ligand and ATP (Moaddel and Wainer 2007).

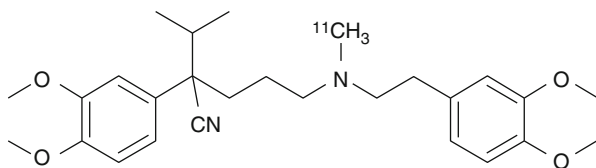
21.4 PET Tracers for Imaging of ABC Transporter Function and Expression in the BBB

21.4.1 Background

Positron emission tomography (PET) is a widely used technique that allows measurement of the expression or function of proteins involved in many neurological diseases including cancer. The most demanding challenge to date is to synthesize the best tracer for a trustworthy clinical diagnosis (Kannan et al. 2009). In relation to ABC transporters, and especially to P-gp, there are three criteria for the selection of the optimal tracer: high radiochemical purity, high selectivity for P-gp, and a large-magnitude signal (Kannan et al. 2009). Combinations of several radiolabeled and nonradioactive P-gp inhibitors are currently used in order to obtain a more specific imaging analysis, allowing the tracer to enter the brain tissue (see text below).

It is important to note that, beyond the scope of diagnosis, P-gp inhibitors have also been widely studied in order to improve treatment outcome in conditions of chemoresistance. Many clinical trials have attempted to overcome the MDR phenomenon by pharmacological inhibition of P-gp (McHugh et al. 2008; McHugh 2008). However, 30 years of such trials have yielded little or no success (Kannan et al. 2009), mainly because of a poor inhibitor selectivity. Other ABC transporters not involved in MDR are affected by the drug treatment which may lead to severe side effects, and the CYP3A4 enzyme that is responsible for metabolism of chemotherapeutic agents is inhibited (van Zuylen et al. 2000). Hence the search for more

Fig. 21.1 Structure of [^{11}C] verapamil



potent, efficacious, and selective P-gp inhibitors continues, for both diagnostic and treatment purposes.

In theory, P-gp inhibitors can be used to image P-gp expression, whereas P-gp substrates will image P-gp function (Dörner et al. 2011). However, in practice, these compounds do not show the same behavior *in vivo* and *in vitro*, which is a great challenge for neuroimaging studies. An important point to consider is membrane fluidity that is influenced by age and diet composition. In addition, sphingolipids can modulate membrane composition and properties through reciprocal interconversions and specific lipid–protein interactions (Posse de Chaves and Sipione 2010). This can alter the structure and spatial conformation of membrane proteins, conferring them distinct ligand-binding aspects.

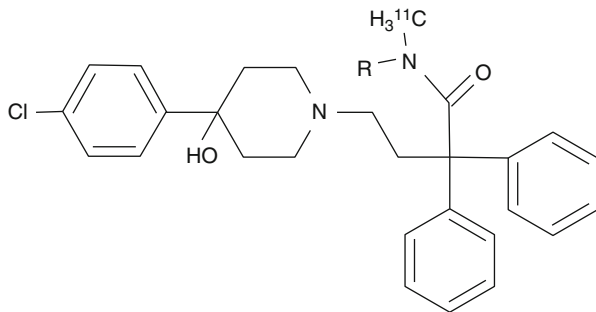
Several PET tracers have been synthesized for monitoring the function and expression of P-gp at the BBB. Some of them were initially described as P-gp substrates such as [^{11}C]verapamil (Luurtsema et al. 2003) and [^{11}C]N-desmethylloperamide (Lazarova et al. 2008). Others are P-gp inhibitors such as [^{11}C]laniquidar (Luurtsema et al. 2009), [^{11}C]elacridar (Dörner et al. 2009; Kawamura et al. 2011a), [^{11}C]tariquidar (Bauer et al. 2010; Kawamura et al. 2010), and [^{11}C]MC18 (van Waarde et al. 2009).

21.4.2 Substrates as Tracers for Measuring P-gp Function

21.4.2.1 [^{11}C]Verapamil

The L-type calcium channel blocker verapamil [2,8-bis(3,4-dimethoxyphenyl)-6-methyl-2-isopropyl-6-azaocitanitrile] is widely used in the treatment of hypertension (McTavish and Sorkin 1989), angina pectoris, and cardiac arrhythmias. Verapamil metabolizes preferentially to norverapamil via N-demethylation (Kroemer et al. 1993). After oral administration, the (*S*)-enantiomer of verapamil is metabolized more actively than (*R*)-verapamil in humans, resulting in a 2.5 times higher concentration of the (*R*)-enantiomer in plasma (Häussermann et al. 1991). (*R*)-verapamil has only 5–10% of the calcium channel blocking activity of the (*S*)-enantiomer. However, the (*R*)-enantiomer is equipotent to racemic verapamil and (*S*)-verapamil in its efficacy to inhibit MDR. Verapamil is metabolized by cytochrome P450 enzymes and some of the radioactive metabolites are themselves substrates and inhibitors of P-gp (Pauli-Magnus et al. 2000). In addition, polar radiolabeled metabolites are formed, which may result in a non-P-gp-mediated signal (Luurtsema et al. 2005). Quantification of racemic [^{11}C]verapamil (Fig. 21.1) is difficult because the enantiomers have different pharmacokinetic properties

Fig. 21.2 Structures of [^{11}C]loperamide and [^{11}C]dLop



R = Me, [^{11}C]Loperamide

R = H, [^{11}C]N-desmethyl-loperamide ([^{11}C]dLop)

(Laberge et al. 2001). Therefore PET studies need to be performed with an optically pure enantiomer. (*R*)- and (*S*)-[^{11}C]verapamil were prepared from (*R*)- and (*S*)-desmethylverapamil by methylation with no-carrier added [^{11}C]methyl iodide or [^{11}C]methyl triflate (Luurtsema et al. 2002). However, no difference in transport for P-gp between (*R*)- and (*S*)-verapamil was found (Luurtsema et al. 2003). (*R*)-[^{11}C]verapamil had a low brain uptake at baseline both in humans and other vertebrate species, but coadministration with inhibitor cyclosporin A (CsA) or tariquidar increased distribution volume (DV) and kinetic constant k_1 (Bankstahl et al. 2008b; Muzi et al. 2009). The increase in brain DV was approximately +300 % in rats and +24 ± 15 % in humans after administration of tariquidar (Kuntner et al. 2010; Wagner et al. 2009), which points to a pronounced species difference regarding the tariquidar effect. Three different PET tracers, including [^{11}C]verapamil, have been tested in five different mammals. The brain uptake of all radioligands was clearly higher in humans, monkeys, and minipigs than in rats or guinea pigs (Sylvänen et al. 2009).

21.4.2.2 [^{11}C]N-desmethyl-Loperamide

Loperamide is an antidiarrheal agent that acts through agonism of gut μ -opioid receptors (Awouters et al. 1993). This drug is normally without harmful central effects because P-gp expels it from the brain. [^{11}C]Loperamide is avidly metabolized to [*N*-methyl- ^{11}C]N-desmethyl-loperamide ([^{11}C]dLop) via demethylation (Fig. 21.2) (Zoghbi et al. 2008). This metabolite also behaves as a substrate for P-gp and it has been used as a PET tracer instead of [^{11}C]loperamide. Demethylation of [^{11}C]dLop may also occur, but it will lead only to single-carbon radiometabolites such as [^{11}C]methanol. These metabolites will be oxidized and ultimately expired as [^{11}C]carbon dioxide. They should not accumulate in brain tissue and will therefore not cause problems in biomathematical analysis of the acquired PET data. The uptake of [^{11}C]dLop-derived radioactivity at 30 min was about 3.5-fold higher in the forebrain of P-gp knockout mice compared to wild-type mice supporting the results from previous studies which indicate that [^{11}C]dLop is a substrate of P-gp (Lazarova

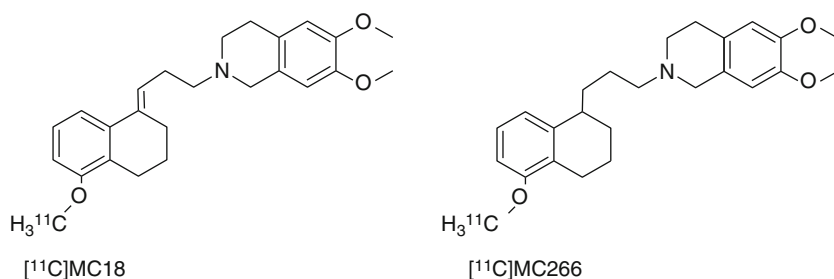


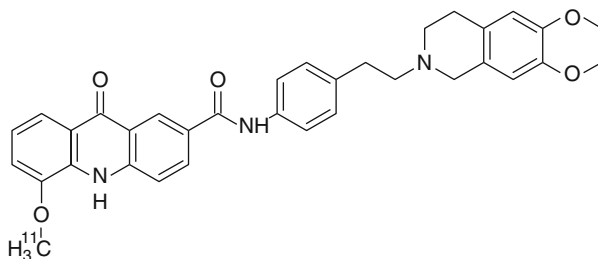
Fig. 21.3 Structures of $[^{11}\text{C}]\text{MC18}$ and $[^{11}\text{C}]\text{MC266}$

et al. 2008). Similar results were found in monkeys. $[^{11}\text{C}]\text{dLop}$ was found to be selective for P-gp when tested in human cell lines that overexpress P-gp, MRP1, or BCRP and also in P-gp knockout mice (Kannan et al. 2010). At low concentrations (≤ 1 nM) dLop acts only as a substrate, but at higher concentrations (≥ 20 μM) it acts as a competitive substrate (both a substrate and an inhibitor). Because low concentrations of radiotracer are used in PET imaging, $[^{11}\text{C}]\text{dLop}$ will act only as a selective substrate for P-gp at the BBB.

Pretreatment with the inhibitor tariquidar increases the brain uptake of $[^{11}\text{C}]\text{dLop}$ markedly in monkeys and humans (Kreisl et al. 2010). After entry of $[^{11}\text{C}]\text{dLop}$ into the brain, it is trapped and doesn't wash out. Although dLop is an opiate agonist, its trapping is not a result of high-affinity binding to the opiate receptor. Brain uptake of $[^{11}\text{C}]\text{dLop}$ cannot be displaced by receptor-saturating doses of an opiate agonist or antagonist (Lazarova et al. 2008). This irreversible trapping amplifies the PET signal so it is advantageous from an imaging perspective. dLop has a pK_a of 7.3 and may be trapped by passive diffusion into acidic organelles, mainly lysosomes, followed by protonation within the organelle (Kaufmann and Krise 2007; MacIntyre and Cutler 1988). To test this hypothesis the accumulation of $[^3\text{H}]\text{dLop}$ was measured in human cell lines and compared with the uptake of other weak bases (Kannan et al. 2011a). $[^{11}\text{C}]\text{dLop}$ was found to be ionically trapped in acidic lysosomes and tariquidar competed for lysosomal accumulation, both in vitro and in vivo. This interaction is problematic in peripheral organs but not in the brain. Thus $[^{11}\text{C}]\text{dLop}$ can still be used, either alone or in combination with tariquidar, to measure the function of P-gp at the BBB.

The low baseline uptake of radiolabeled substrates in the brain because of a very large capacity of pumping systems in the BBB is still an important issue, since it hampers the detection of subtle changes in function (particularly an upregulation of P-gp). Thus, novel PET ligands for P-gp with improved kinetics are still required. MC266 is a tracer of P-gp function with higher baseline uptake than $[^{11}\text{C}]\text{verapamil}$ (van Waarde et al. 2009). Thus, upregulation of P-gp function in response to treatment may be detectable using MC266 (Fig. 21.3) and PET. Another alternative is the P-gp inhibitor $[^{11}\text{C}]\text{MC18}$ (Fig. 21.3), a unique tracer of P-gp expression which shows specific binding in the brain and several peripheral target organs. However, a derivative with higher affinity for P-gp may be required for quantitative imaging (van Waarde et al. 2009).

Fig. 21.4 Structure of [^{11}C] elacridar



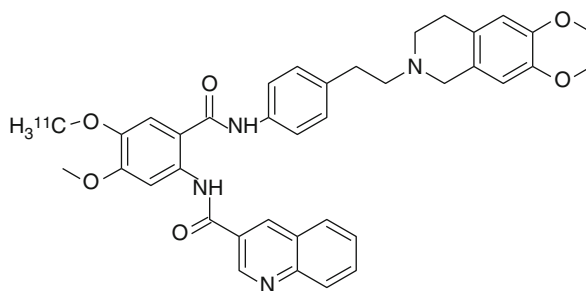
21.4.3 Inhibitors as Tracers for Measuring P-gp Expression

Because currently available PET tracers are high-affinity substrates for P-gp, they are efficiently kept out of the brain by P-gp-mediated transport and therefore show low brain uptake. Low brain uptake makes it difficult to use these probes for the mapping of regional differences in cerebral P-gp activity, which are expected to occur, for example, in medically refractory epilepsy. A promising complementary approach to the use of radiolabeled substrates for assessing P-gp *in vivo* would be the use of radiolabeled inhibitors, which bind with nanomolar affinity to the pump without being transported. Such tracers are expected to show a signal increase rather than a signal reduction in brain regions that overexpress P-gp.

21.4.3.1 [^{11}C]Elacridar

[^{11}C]Elacridar (Fig. 21.4) displayed high metabolic stability and displaceable binding to rat brain slices *in vitro* (Dörner et al. 2009). During subsequent *in vivo* studies, tracer concentration was about ten times higher in the brain of wild-type mice than in rat brain. This difference can most likely be explained by the severalfold higher blood activity levels in mice as compared to rats. [^{11}C]Elacridar is a nontransported inhibitor of P-gp but also inhibits breast cancer resistance protein (BCRP, ABCG2) at comparable concentrations as it inhibits P-gp. However, elacridar does not inhibit multidrug resistance-associated proteins (MRPs) such as MRP1. Experiments in wild-type and *mdr1a/b* knockout mice showed comparable blood activity levels of the PET tracer, but in knockout animals brain uptake of [^{11}C]elacridar was 2.5 times higher. Following administration of unlabeled elacridar, brain uptake of [^{11}C]elacridar in rats was increased by a factor of 5 and in wild-type mice by a factor of 2.5. Similar results were obtained in rats and mice, but the optimal blood concentration (EC90) of elacridar in guinea pigs was tenfold higher, suggesting the existence of species differences in rodents (Cutler et al. 2006). Elacridar, as well as tariquidar (see below), was able to increase [^{11}C]verapamil distribution in rat brain up to 11-fold over baseline at maximum effective doses and was about three times more potent than tariquidar (Kuntner et al. 2010), probably because of its dual action on both P-gp and BCRP. Further studies aimed at detecting P-gp and BCRP function were conducted by Dörner et al. who used 1-[^{18}F]fluoroelacridar (Dörner et al. 2011). In conclusion, [^{11}C]elacridar is not specific for P-gp and its signal magnitude is low.

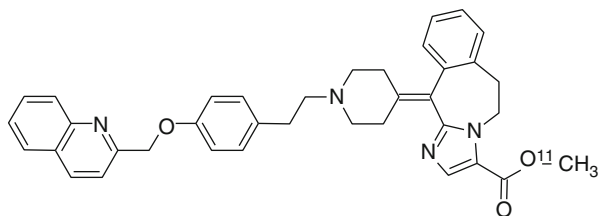
Fig. 21.5 Structure of [^{11}C] tariquidar



21.4.3.2 [^{11}C]Tariquidar

Tariquidar is at low concentrations a noncompetitive inhibitor of P-gp and a substrate for breast cancer resistance protein (BCRP, ABCG2). At higher concentrations (≥ 100 nM) tariquidar acts as an inhibitor of both P-gp and BCRP (Kannan et al. 2011b; Kühnle et al. 2009). For this reason [^{11}C]tariquidar is not a suitable PET tracer for mapping of cerebral BCRP expression (Mairinger et al. 2010). Tariquidar does not inhibit multidrug resistance-associated proteins (MRPs) such as MRP1 (Mistry et al. 2001). In the presence of unlabeled ligand, an increased influx of radioactivity into the brain has been observed (Bauer et al. 2010). Unlabeled tariquidar may have displaced labeled tariquidar from its binding site and may have resulted in passive diffusion of [^{11}C]tariquidar (Fig. 21.5) into the brain. Advantages of [^{11}C]tariquidar are the apparent lack of nonspecific binding to other membrane proteins and good metabolic stability. One hour after injection in rats, 96 % of plasma radioactivity represents unchanged parent compound (Bauer et al. 2010). Further experiments are needed to clarify if [^{11}C]tariquidar behaves as a transported or as a nontransported P-gp/BCRP inhibitor in vivo. A new tariquidar-like compound has been synthesized as a BCRP-selective inhibitor (see Mairinger et al. 2010 for molecular structure). Regional differences in tariquidar-induced modulation of [^{11}C]verapamil brain uptake indicate regional differences of P-gp function in rat brain (Kuntner et al. 2010). In addition, the use of 2 mg/kg body weight (BW) of tariquidar in rats demonstrated a P-gp inhibition comparable to that obtained in humans with 3 mg/kg (Kuntner et al. 2010). In contrast, other studies demonstrated that 6 mg/kg of tariquidar was the minimum dosage necessary to obtain a significant increase in the brain uptake of [^{11}C]dLop (Kreisl et al. 2010). Noteworthy, Kurnik et al., who did not use PET, failed to demonstrate a significant effect of the 2 mg/kg dose of tariquidar on central opioid effects of loperamide in humans because of the greater resistance of brain P-gp to inhibition as compared to T lymphocytes (Kurnik et al. 2008). Tariquidar-induced P-gp modulation at the human BBB appears to be transient (depending on the species, tracers, and tissue), and its magnitude is directly proportional to serum drug exposure. Thus, higher plasma concentrations of tariquidar could be safely obtained in the clinic in order to overcome drug resistance and to achieve higher levels of cerebral P-gp inhibition (Wagner et al. 2009).

Fig. 21.6 Structure of [^{11}C]laniquidar



21.4.3.3 [^{11}C]Laniquidar

Laniquidar is a noncompetitive inhibitor which has been used in Phase I and II clinical trials (van Zuylen et al. 2000; 2002) as well as in animal studies (Bardelmeijer et al. 2004). Laniquidar lacks interactions with cytochrome P450 isoenzymes which should result in low levels of labeled metabolites (Thomas and Coley 2003). Lipophilicity of laniquidar is rather high ($\log P = 6.89$) (Wang et al. 2003). A potential explanation of low cerebral uptake could be high binding to plasma proteins, resulting in a low free fraction of [^{11}C]laniquidar (Fig. 21.6) in plasma. When [^{11}C]laniquidar is injected in tracer amounts, it may act as a substrate rather than an inhibitor (Moerman et al. 2012). This is supported by pretreatment with cyclosporin A in rats which yielded in higher brain uptake of [^{11}C]laniquidar (Luurtsema et al. 2009). Studies in WT mice demonstrate statistically higher brain uptake of [^{11}C]laniquidar when administered with the cold compound as a carrier, representing a therapeutic dose of 60 mg/kg laniquidar (Moerman et al. 2012).

It is important to mention that besides species differences, there are also some important factors that can influence P-gp expression/activity which must be taken into account. For example, estrogens may induce increases of P-gp function (see below). Thus, PET data obtained from female animals must be interpreted with care. In addition, isoflurane can cause an increase in neuroreceptor ligand binding although its effect on P-gp is unknown (Elfving et al. 2003; Harada et al. 2004).

21.4.4 PET Studies with [^{11}C]Verapamil in Neurological Diseases

Kortekaas et al. showed that the intracerebral transfer of [^{11}C]verapamil was significantly increased in the midbrain of patients with Parkinson's disease (PD), when compared to healthy volunteers. Since verapamil is a P-gp substrate, this result supports a dysfunctional BBB as a correlated mechanism in this brain disease (Kortekaas et al. 2005). Bartels et al. found in ten advanced PD patients (5 ± 2 years runtime disease) treated with levodopa and dopaminergic agonists an increase of cerebral [^{11}C]verapamil distribution in white matter of the frontal cortex, in comparison with healthy controls (Bartels et al. 2008a). On the other hand, ten young de novo PD patients presented a decrease of cerebral [^{11}C]verapamil uptake in the brain stem, indicating a localized upregulation of P-gp at the onset of PD (Bartels et al. 2008a). So, the authors highlighted a delayed decrease of P-gp functionality, related with disease progression, and a similar change is observed even during normal aging.

A decrease in P-gp activity at the blood–brain barrier level and in peripheral mononuclear blood cells was found in elderly healthy volunteers, in comparison to young healthy subjects (Bartels et al. 2008b; Toornvliet et al. 2006). In addition, a recent study using [^{11}C]verapamil also found decreased P-gp function in patients with sporadic Alzheimer’s disease (van Assema et al. 2012b). However, this kind of studies should be interpreted with caution because of the possibility of drug substances, stress, and emotions affecting P-gp functionality. Using [^{11}C]verapamil to assess BBB P-gp function in rats, de Klerk et al. showed that the antidepressant venlafaxine increases P-gp function whereas chronic stress inhibits it (de Klerk et al. 2010a). An interesting study revealed that the clearance of [^{11}C]verapamil from the brain is significantly greater in younger monkeys than in adults. It was also shown that the brain penetration of [^{11}C]oseltamivir changed with development and was slightly higher in younger monkeys (Takashima et al. 2011). The authors pointed out that this change may be related to the observed difference in drug responses in the brains of children and human adults. Taken together, these results suggest that besides disease, other factors can affect P-gp status. P-gp is a vulnerable protein; toxic substances can change its activity or expression depending on how much exposure is encountered during life.

The contribution of P-gp to regional drug distribution in healthy human brains was assessed using PET (Muzi et al. 2009; Sasongko et al. 2005). Fairly uniform P-gp activity was observed in all brain regions that are protected by the BBB and negligible activity in the pituitary, which is situated outside the BBB (Eyal et al. 2010).

Patients with chronic schizophrenia treated with antipsychotic drugs show a significant decrease in [^{11}C]verapamil uptake in the temporal cortex, the basal ganglia, and the amygdala compared with healthy controls, and a trend towards a significant decrease is found throughout the brain. Such a decrease correlates with an increased activity of P-gp (de Klerk et al. 2010b), which may contribute to drug resistance in schizophrenia, induced by antipsychotics (Colabufo et al. 2010). So, because both pathology and medication can cause alterations in cell homeostasis and consequently in P-gp function and expression, drug-naïve patients should be examined besides medicated patients, although recruitment of such subjects is quite difficult.

21.4.5 Comparative Studies of [^{11}C]Verapamil and Its Carbon-11-Labeled Metabolite D617 in BBB Using PET

Cerebral kinetics of the recently synthesized compound [^{11}C]D617, a metabolite of [^{11}C]verapamil, has been studied before and after administration of tariquidar. This study used Sprague–Dawley and Wistar rats in order to assess possible differences in tariquidar-induced effects between these two strains. The results showed an approximately twofold increase in the cerebral volume of distribution (V_T) of [^{11}C]D617 after intravascular administration of tariquidar in both rat strains. Results also indicated that the lack of a tariquidar-induced effect in the ex vivo biodistribution study was due to the route of administration. Comparison with previously reported

[¹¹C]verapamil data showed that, at baseline, the kinetics of [¹¹C]D617 and (*R*)-[¹¹C]verapamil are similar (Verbeek et al. 2012). It is important to note that a tenfold increase of [¹¹C]verapamil uptake has been observed after treatment with the same dose of tariquidar, indicating that [¹¹C]verapamil is a better P-gp substrate than [¹¹C]D617. The similar kinetics of [¹¹C]D617 and [¹¹C]verapamil at baseline provides support for use of the kinetic model for analysis of [¹¹C]verapamil data (Lubberink et al. 2007). Nevertheless, the authors argued that the different kinetics of [¹¹C]D617 and [¹¹C]verapamil after P-gp inhibition indicates that assumption about kinetics should be made with care, and further simulation studies are needed to assess the impact of such differences under different conditions (Verbeek et al. 2012). It is important to mention that a recent study already measured the test–retest (TRT) variability of regional [¹¹C]verapamil uptake in addition to variability of total brain uptake (Lubberink et al. 2007). This work showed that reproducibility of [¹¹C]verapamil PET studies was best if V_T derived from single-tissue (global TRT 6 %) and constrained two-tissue (global TRT 9 %) compartment models was used as the outcome parameter. Thus, the two-tissue compartment model is the kinetic model of choice with the volume of distribution V_T as the preferred outcome measure (van Assema et al. 2012a).

21.4.6 Comparative Studies of [¹¹C]Verapamil and [¹¹C]dLop in BBB Using PET

[¹¹C]Verapamil generates more brain-penetrating radiometabolites than [¹¹C]dLop in rats. Approximately 30 % of brain radioactivity reflects radiometabolites (Luurtsema et al. 2005), compared to less than 10 % after administration of [¹¹C]dLop (Lazarova et al. 2008). In healthy human subjects, [¹¹C]verapamil has a fourfold higher brain uptake than [¹¹C]dLop (70 % vs. 15 % SUV – standardized uptake value, respectively), suggesting the generation of radiometabolites from [¹¹C]verapamil (Ikoma et al. 2006; Seneca et al. 2009). In addition, the K_1 of [¹¹C]verapamil (0.05 mLcm⁻³min⁻¹) is about fivefold greater than that of [¹¹C]dLop (0.009 mLcm⁻³min⁻¹) (Seneca et al. 2009). [¹¹C]dLop, as well as [¹¹C]loperamide, is an avid substrate for P-gp (Zoghbi et al. 2008). In monkeys, the brain uptake of [¹¹C]dLop is high (>40 %) when P-gp is inhibited and is dependent on regional blood flow (Liow et al. 2009). Such result was followed by the demonstration that P-gp function appears fairly uniformly distributed in the monkey brain (Liow et al. 2009). At baseline conditions, almost no [¹¹C]dLop enters the brain because of the high capacity of P-gp. Thus, the baseline uptake of [¹¹C]dLop is not sensitive to increases of P-gp function (Kannan et al. 2011a). However, it may be possible to use [¹¹C]dLop in combination with nonradioactive tariquidar to detect regional increases of P-gp function after partial inhibition of the efflux pump. Extensive research is ongoing to check if this approach is feasible in human subjects. The study of pathological conditions with increased P-gp function (e.g., drug-resistant epilepsy) will also benefit from this approach. However, for brain disorders in which P-gp function may be reduced, such as Alzheimer’s disease (Vogelgesang

et al. 2002, 2004), [^{11}C]dLop may be advantageous because it may enter the brain and may provide a strong signal, as it is irreversibly trapped in lysosomes (Kannan et al. 2011a).

21.4.7 ^{18}F -Labeled Compounds to Assess P-gp Function and Expression

Several studies with ^{18}F probes for P-gp have been reported. Such probes have a longer physical half-life in comparison to [^{11}C]labeled compounds (110 min vs. 20 min) and can be transported to other PET sites which lack GMP (good manufacturing practice)-compliant radiopharmaceutical production facilities. The synthesis and in vivo evaluation of [^{18}F]fluoroethyl elacridar and tariquidar as PET probes for assessing the function of drug efflux transporters P-gp and BCRP have been reported by Kawamura et al. Results of the two new ^{18}F -labeled compounds were compared to those of the two [^{11}C]labeled parent molecules that were tested in previous studies (Kawamura et al. 2010, 2011b). In addition, radioactivity levels in mice brain after injection of [^{18}F]elacridar and [^{18}F]tariquidar were increased when the function of drug efflux transporters was inhibited. The increase of the uptake of these two compounds was similar to that of their [^{11}C]labeled analogs. In metabolite analyses of mice brain and plasma, [^{18}F]tariquidar proved metabolically more stable than [^{18}F]elacridar. The authors concluded that [^{18}F]tariquidar may be more suitable than ^{18}F -elacridar to evaluate the in vivo function of drug efflux transporters (Kawamura et al. 2011a), but that probe concentration needs to be chosen carefully in order to assess both P-gp and BCRP function (Kannan et al. 2011b).

21.4.8 Use of P-gp Stimulator Compounds as a Strategy for Treatment of Neurodegenerative Diseases

Recently a benzopyrane derivative was synthesized which demonstrated a potent P-gp ligand activity with increased selectivity for P-gp over the MRP1 pump when compared to the lead compound MC18 (Contino et al. 2012). However, initial results indicated that 1,2,3,4-tetrahydro-2-((3,4-dihydro-6-methoxy-2H-chromen-3-yl)-methyl)-6,7-dimethoxyisoquinoline is a P-gp-inducing agent, whereas MC18 is a potent P-gp inhibitor (Contino et al. 2012). Because of these findings the authors pointed to the potential application of P-gp stimulators in treating Alzheimer's disease (AD) and Parkinson's disease (PD), as such compounds could stimulate the clearance of β -amyloid or α -synuclein, respectively, in AD and PD (Contino et al. 2012). A noteworthy previous study using widely known compounds including rifampicin, dexamethasone, caffeine, verapamil, hyperforin, β -estradiol, and pentylenetetrazole already demonstrated the ability of these substances to improve the efflux of β -amyloid, which may slow down the progression of neurodegenerative disease (Abuznait et al. 2011a). Furthermore, a galloyl benzamide molecule has been successfully used to design new potent galloyl-based selective P-gp and MRP1 modulators (Pellicani et al. 2012).

21.5 Targeting ABC Transporter Regulation in the BBB: Considerations for Further Investigations with New Tracers and Treatment Outcomes

The notion that ABC transporters can be regulated by endogenous as well as exogenous factors is already well established. For example, focusing on endothelin receptor-1 (ET-1) signaling through the endothelin receptor type B (ETB), nitric oxide synthase (NOS), and protein kinase C (PKC) rapidly decreases P-gp activity in isolated rat brain capillaries (Hartz et al. 2004). Another report showed that BBB P-gp expression is regulated by the inflammatory mediators LPS, tumor necrosis factor- α (TNF- α), and ET-1, which activated toll-like receptor 4 (TLR4), TNF receptor 1 (TNFR1), ETB receptor, NOS, and PKC, leading to reduced P-gp activity (Hartz et al. 2006). Moreover, glutamate, cyclooxygenase-2, and prostaglandin E2-EP1 receptor signaling were implicated in seizure-induced upregulation of P-gp (Bankstahl et al. 2008a; Pekcec et al. 2009; Zibell et al. 2009). Not only P-gp but also other ABC transporters can be regulated by inflammatory mediators. Recently, it was shown that HIV-1 envelope glycoprotein gp120 and TNF-alpha are able to upregulate MRP1 expression in cultured astrocytes, and both NF-kappaB and c-Jun N-terminal kinase (JNK) signaling were involved in this regulation (Ronaldson et al. 2010). In addition, further studies demonstrated that BCRP mRNA levels and activity are significantly reduced by interleukin-1 β (IL-1 β), interleukin-6 (IL-6), and TNF- α (Poller et al. 2010). In a follow-up study, Rigor et al. identified PKC beta(I) as the responsible PKC isoform for downregulation of P-gp activity (Rigor et al. 2010). Importantly, this study demonstrated that targeting PKC beta(I) increases brain uptake of the P-gp substrate verapamil. Hawkins et al. made a similar observation using injection of vascular endothelial growth factor (VEGF). It was shown that VEGF decreased P-gp activity in rat brain capillaries via activation of VEGF receptors flk-1 and Src, probably through Src-mediated phosphorylation of caveolin-1 (Hawkins et al. 2010a). More studies are needed to determine whether targeting these pathways will improve the delivery of tracers across the BBB and into the brain.

Recently, sexual hormones have been implicated in efflux transporter modulation, especially estrogens (Sui et al. 2011). It was already demonstrated that estrogens play a key role in BCRP regulation (Imai et al. 2002). Estrone and 17 β -estradiol reverse BCRP-mediated drug resistance, and the latter triggers posttranscriptional downregulation of BCRP in human breast cancer cell lines. Ee et al. identified an estrogen response element (ERE) in the BCRP promoter region and showed ERE activation by binding of the 17 β -estradiol/estrogen receptor- α complex, which upregulated BCRP mRNA expression (Ee et al. 2004). In addition, Hartz et al. found that 17 β -estradiol reduces BCRP transport activity in brain capillaries in a rapid way. Since this effect occurs within minutes and does not involve transcription, translation, or proteasomal degradation, a nongenomic mechanism is indicated (Hartz et al. 2010a). It is important to mention that P-gp activity is also upregulated by β -estradiol (Abuznait et al. 2011a, b). Thus, these results support the observation of gender-related differences in PET studies of P-gp function (van Assema et al. 2012c; Bebawy and Chetty 2009).

Importantly, a recent study in a mouse model of AD demonstrated that targeting intracellular signals that upregulate BBB P-gp caused an increase in A β clearance from the brain and reduce A β brain accumulation in early stages of the disease (Hartz et al. 2010b). Activation of the crucial P-gp regulator nuclear receptor pregnane X receptor (PXR) (Bauer et al. 2004) by pregnenolone-16 α -carbonitrile restored P-glycoprotein expression and transport activity in brain capillaries and significantly reduced brain A β levels compared with untreated control mice. Interestingly, both orphan nuclear receptors, human PXR (hPXR), and human constitutive androstane receptor (hCAR) are involved in the regulation of P-gp expression (Chan et al. 2011). In addition, Chan et al. demonstrated that the activity of hPXR and hCAR can be pharmacologically modified by selective inhibitors (i.e., A-792611 and meclizine) which suggests that P-gp induction can be prevented (Chan et al. 2011). Signals that increase and decrease P-gp expression are illustrated in Figs. 21.7 and 21.8, respectively. Taken together, these results showed the importance of knowing the mechanisms of ABC transporter regulation in order to improve imaging and also the design of new tracers as well as new drugs to treat neurological diseases. Better imaging of ABC transporters will also improve the monitoring of disease progression. Furthermore, multi-tracer PET studies aimed at other targets besides ABC transporters will increase knowledge in this field as well as improve diagnostic and treatment outcome.

21.6 Mechanism of Action of ABC Transporter-Binding Substances

It is important to be aware of the fact that some compounds do not only interact with their primary target molecules but also with organelles present in the cytoplasm. For example, a recent report showed that *N*-desmethyl-loperamide (dLop) is trapped in lysosomes which can result in accumulation of PET signal (Kannan et al. 2011a). Although the trapping property of a substrate radiotracer, such as [¹¹C]dLop, is beneficial for measuring P-gp function in the brain, the authors pointed out that trapping of an inhibitor radiotracer intended to measure P-gp density, such as [¹¹C] tariquidar, is not desirable because simultaneous binding to the transporter and trapping of the probe in lysosomes complicates interpretation of the PET signal of weak base inhibitors. The authors also warn against overestimation of P-gp density in the brain. Although [¹¹C]dLop fulfills the three prerequisites for an ideal radiolabeled substrate, the extremely low baseline uptake of [¹¹C]dLop limits its application to disorders where P-gp function is reduced (e.g., Alzheimer's or Parkinson's disease) (Kannan 2012).

It has become clear that elacridar and tariquidar are not P-gp specific, but at higher concentrations also inhibit BCRP (Maliapaard et al. 2001; Mistry et al. 2001; Robey et al. 2004). In addition, Kannan et al. showed that at low concentrations tariquidar acts selectively as an inhibitor of P-gp and a substrate of BCRP. At much higher concentrations (≥ 100 nM), tariquidar acts as an inhibitor of both P-gp and BCRP (Kannan et al. 2011b). Because of these results [¹¹C]tariquidar does not enter

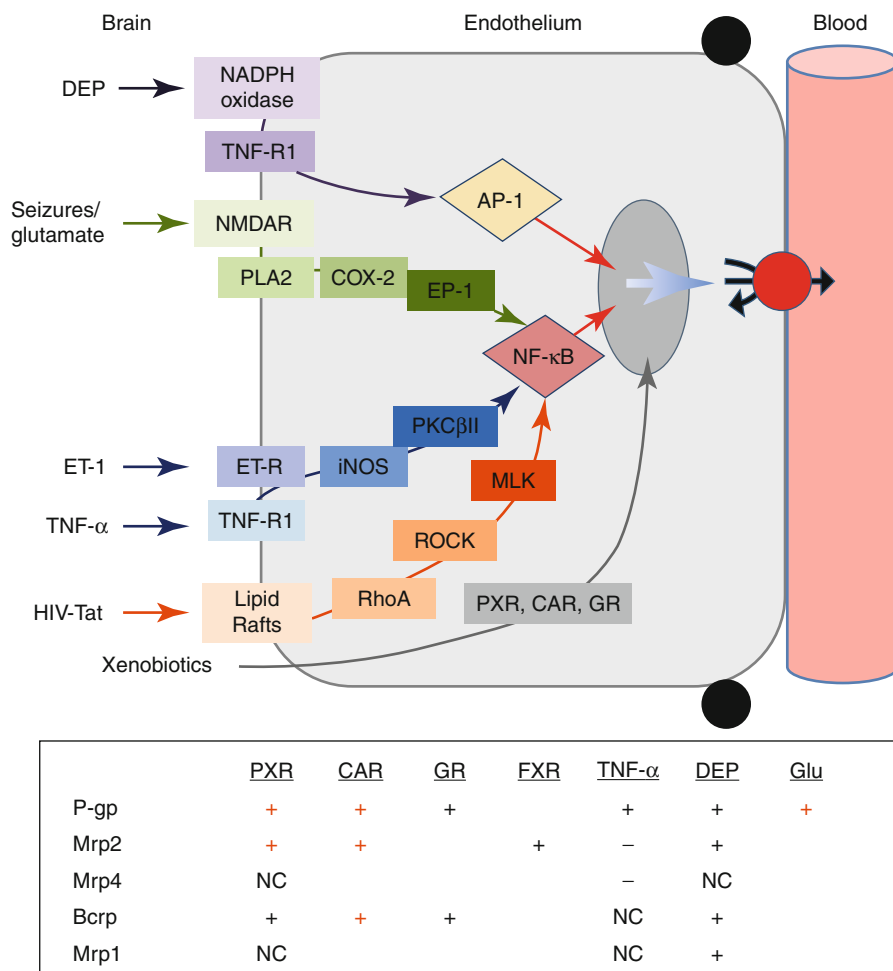


Fig. 21.7 Signaling pathways and key transcription factors that alter expression of P-glycoprotein and other ABC transporters at the BBB (Reprinted with permission)

the brain of WT mice. Its uptake is reported to be high only in triple P-gp and BCRP KO [*mdr1a(-/-)*, *mdr1b(-/-)*, *bcrp(-/-)*] mice (Bauer et al. 2010; Kawamura et al. 2010). Although [^{11}C]tariquidar is a P-gp inhibitor with one of the highest affinities available, its binding potential (product of receptor density and affinity) is low. Future inhibitors used to measure P-gp density may require a tenfold (for imaging in mice) or 50-fold (for imaging in humans) higher affinity than tariquidar (Kannan 2012). However, [^{11}C]tariquidar may be useful for other purposes. A recent study demonstrated that it was the best tracer for assessment of P-gp expression in murine breast cancer in small-animal PET in comparison with [^{11}C]elacridar and (*R*)-[^{11}C]verapamil (Wanek et al. 2012).

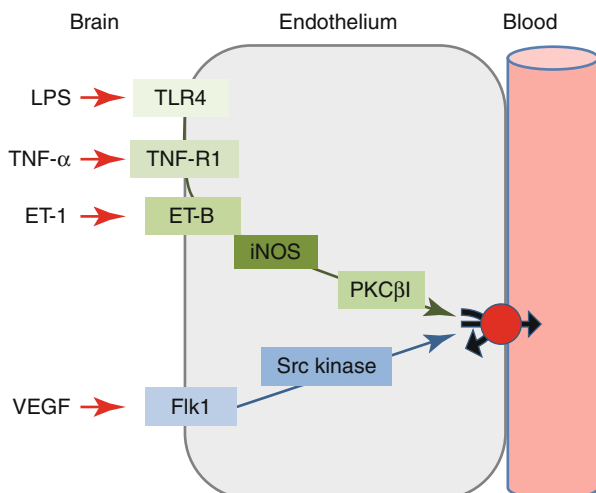


Fig. 21.8 Signals that rapidly decrease P-glycoprotein transport activity at the BBB. Two signaling pathways (proinflammatory and VEGF induced) were initially identified in rat brain capillaries using pharmacological tools. They have been validated *in vivo*, in that activating each of the pathways rapidly and substantially increases brain uptake of the P-glycoprotein substrates verapamil and morphine (Hartz et al. 2004, 2006; Hawkins et al. 2010b; Rigor et al. 2010). Because signaling through these pathways has the potential to rapidly and transiently reduce P-glycoprotein activity without altering P-gp expression, targeting of downstream steps provides a strategy for improving the brain delivery of drugs that are P-glycoprotein substrates (Reprinted with permission)

21.7 Discussion and Concluding Remarks

Early and progression-related events in neurodegenerative disease and other brain disorders are only partly known due to the complex cellular and molecular mechanisms underlying their pathogenesis. Impaired cellular homeostasis in the BBB caused by several factors such as hypoxia, inflammation, drugs, diet, stress, or disease may compromise the effective clearance of toxic substances from the brain by efflux transporters (Hawkins and Davis 2005). In addition, genetic or heredity-related alterations may impair the homeostasis-restoring mechanisms (Cascorbi and Haenisch 2010), hampering the removal of toxic compounds from the cells. Unfortunately, in a clinical setting the symptoms of the majority of neurological diseases became manifest only in a late phase of the disease, when homeostasis is already severely impaired, which negatively affects treatment outcomes. Thus, early diagnostic protocols are of paramount importance in order to start treatment prior to irreversible brain damage.

PET is a widely used diagnostic technique that may increase our knowledge regarding the function and expression of proteins involved in neurological diseases including efflux transporters. Recent advances have been made towards a better understanding of the function of these BBB proteins in neurological disorders.

These studies are aimed at an earlier detection of the disease in order to improve treatment outcome. In summary, the use of PET has provided important information about the function of BBB transporters, especially P-gp, in both physiological and pathological conditions. For example, [¹¹C]verapamil PET revealed important changes of P-gp functionality in aging healthy brains, lesioned brains, neuroinflammation, and neurodegenerative or neuropsychiatric diseases (depending on the progression of the disease) (van Assema et al. 2012b, c; Bartels et al. 2008b; Carvey et al. 2005; de Klerk et al. 2010a, b; Zibell et al. 2009). This knowledge would not exist without the use of imaging. Novel, more specific tracers will certainly expand this knowledge and further improve the diagnosis and treatment of patients suffering from neurological diseases.

References

- Abuznait AH, Cain C, Ingram D et al (2011a) Up-regulation of P-glycoprotein reduces intracellular accumulation of beta amyloid: investigation of P-glycoprotein as a novel therapeutic target for Alzheimer's disease. *J Pharm Pharmacol* 63:1111–1118. doi:[10.1111/j.2042-7158.2011.01309.x](https://doi.org/10.1111/j.2042-7158.2011.01309.x)
- Abuznait AH, Patrick SG, Kaddoumi A (2011b) Exposure of LS-180 cells to drugs of diverse physicochemical and therapeutic properties up-regulates P-glycoprotein expression and activity. *J Pharm Pharm Sci* 14:236–248
- Agarwal S, Elmquist WF (2012) Insight into the cooperation of P-glycoprotein (ABCB1) and breast cancer resistance protein (ABCG2) at the blood-brain barrier: a case study examining sorafenib efflux clearance. *Mol Pharm* 9:678–684. doi:[10.1021/mp200465c](https://doi.org/10.1021/mp200465c)
- Agarwal S, Hartz AMS, Elmquist WF, Bauer B (2011) Breast cancer resistance protein and P-glycoprotein in brain cancer: two gatekeepers team up. *Curr Pharm Des* 17:2793–2802
- Agarwal S, Uchida Y, Mittapalli RK et al (2012) Quantitative proteomics of transporter expression in brain capillary endothelial cells isolated from P-gp, BCRP, and P-gp/BCRP knockout mice. *Drug Metab Dispos* 40(6):1164–1169. doi:[10.1124/dmd.112.044719](https://doi.org/10.1124/dmd.112.044719)
- Awouters F, Megens A, Verlinden M et al (1993) Loperamide. Survey of studies on mechanism of its antidiarrheal activity. *Dig Dis Sci* 38:977–995
- Babakhanian K, Bendayan M, Bendayan R (2007) Localization of P-glycoprotein at the nuclear envelope of rat brain cells. *Biochem Biophys Res Commun* 361:301–306. doi:[10.1016/j.bbrc.2007.06.176](https://doi.org/10.1016/j.bbrc.2007.06.176)
- Bankstahl JP, Hoffmann K, Bethmann K, Löscher W (2008a) Glutamate is critically involved in seizure-induced overexpression of P-glycoprotein in the brain. *Neuropharmacology* 54:1006–1016. doi:[10.1016/j.neuropharm.2008.02.008](https://doi.org/10.1016/j.neuropharm.2008.02.008)
- Bankstahl JP, Kuntner C, Abraham A et al (2008b) Tariquidar-induced P-glycoprotein inhibition at the rat blood-brain barrier studied with (R)-¹¹C-verapamil and PET. *J Nucl Med* 49:1328–1335. doi:[10.2967/jnumed.108.051235](https://doi.org/10.2967/jnumed.108.051235)
- Barbet R, Peiffer I, Hutchins JRA et al (2012) Expression of the 49 human ATP binding cassette (ABC) genes in pluripotent embryonic stem cells and in early- and late-stage multipotent mesenchymal stem cells: possible role of ABC plasma membrane transporters in maintaining human stem cell pluripotency. *Cell cycle* 11:1–10
- Bardelmeijer HA, Ouwehand M, Beijnen JH et al (2004) Efficacy of novel P-glycoprotein inhibitors to increase the oral uptake of paclitaxel in mice. *Invest New Drugs* 22:219–229. doi:[10.1023/B:DRUG.0000026248.45084.21](https://doi.org/10.1023/B:DRUG.0000026248.45084.21)
- Bartels AL (2011) Blood-brain barrier P-glycoprotein function in neurodegenerative disease. *Curr Pharm Des* 17:2771–2777
- Bartels AL, van Berckel BNM, Lubberink M et al (2008a) Blood-brain barrier P-glycoprotein function is not impaired in early Parkinson's disease. *Parkinsonism Relat Disord* 14:505–508. doi:[10.1016/j.parkreldis.2007.11.007](https://doi.org/10.1016/j.parkreldis.2007.11.007)

- Bartels AL, Willemsen AT, Kortekaas R et al (2008b) Decreased blood-brain barrier P-glycoprotein function in the progression of Parkinson's disease, PSP and MSA. *J Neural Transm* 115:1001–1009. doi:[10.1007/s00702-008-0030-y](https://doi.org/10.1007/s00702-008-0030-y)
- Bauer B, Hartz AMS, Fricker G, Miller DS (2004) Pregnane X receptor up-regulation of P-glycoprotein expression and transport function at the blood-brain barrier. *Mol Pharmacol* 66:413–419. doi:[10.1124/mol.66.3](https://doi.org/10.1124/mol.66.3)
- Bauer F, Kuntner C, Bankstahl JP et al (2010) Synthesis and in vivo evaluation of [¹¹C]tariquidar, a positron emission tomography radiotracer based on a third-generation P-glycoprotein inhibitor. *Bioorg Med Chem* 18:5489–5497. doi:[10.1016/j.bmc.2010.06.057](https://doi.org/10.1016/j.bmc.2010.06.057)
- Bebawy M, Chetty M (2009) Gender differences in p-glycoprotein expression and function: effects on drug disposition and outcome. *Curr Drug Metab* 10:322–328
- Bendayan R, Ronaldson PT, Gingras D, Bendayan M (2006) In situ localization of P-glycoprotein (ABCB1) in human and rat brain. *J Histochem Cytochem* 54:1159–1167. doi:[10.1369/jhc.5A6870.2006](https://doi.org/10.1369/jhc.5A6870.2006)
- Bojancic DD, Tarr PT, Gale GD et al (2010) Differential expression and function of ABCG1 and ABCG4 during development and aging. *J Lipid Res* 51:169–181. doi:[10.1194/M900250-JLR200](https://doi.org/10.1194/M900250-JLR200)
- Brenn A, Grube M, Peters M et al (2011) Beta-amyloid downregulates MDR1-P-glycoprotein (Abcb1) expression at the blood-brain barrier in mice. *Int J Alzheimers Dis* 2011:690121. doi:[10.4061/2011/690121](https://doi.org/10.4061/2011/690121)
- Bronger H, König J, Kopplow K et al (2005) ABCC drug efflux pumps and organic anion uptake transporters in human gliomas and the blood-tumor barrier. *Cancer Res* 65:11419–11428. doi:[10.1158/0008-5472.CAN-05-1271](https://doi.org/10.1158/0008-5472.CAN-05-1271)
- Brown TP, Rumsby PC, Capleton AC et al (2006) Pesticides and Parkinson's disease—is there a link? *Environ Health Perspect* 114:156–164. doi:[10.1289/ehp.8095](https://doi.org/10.1289/ehp.8095)
- Candela P, Gosselet F, Saint-Pol J et al (2010) Apical-to-basolateral transport of amyloid- β peptides through blood-brain barrier cells is mediated by the receptor for advanced glycation end-products and is restricted by P-glycoprotein. *J Alzheimers Dis* 22:849–859. doi:[10.3233/JAD-2010-100462](https://doi.org/10.3233/JAD-2010-100462)
- Carvey PM, Zhao CH, Hendey B et al (2005) 6-Hydroxydopamine-induced alterations in blood-brain barrier permeability. *Eur J Neurosci* 22:1158–1168. doi:[10.1111/j.1460-9568.2005.04281.x](https://doi.org/10.1111/j.1460-9568.2005.04281.x)
- Cascorbi I, Haenisch S (2010) In: Zhou J (ed) *Pharmacogenetics of ATP-binding cassette transporters and clinical implications*. Humana Press, Clifton, *Methods Mol Biol*. Vol. 596, pp 95–121. doi:[10.1007/978-1-60761-416-6_6](https://doi.org/10.1007/978-1-60761-416-6_6)
- Chan GNY, Hoque MT, Cummins CL, Bendayan R (2011) Regulation of P-glycoprotein by orphan nuclear receptors in human brain microvessel endothelial cells. *J Neurochem* 118:163–175. doi:[10.1111/j.1471-4159.2011.07288.x](https://doi.org/10.1111/j.1471-4159.2011.07288.x)
- Colabufo NA, Berardi F, Cantore M et al (2010) Perspectives of P-glycoprotein modulating agents in oncology and neurodegenerative diseases: pharmaceutical, biological, and diagnostic potentials. *J Med Chem* 53:1883–1897. doi:[10.1021/jm900743c](https://doi.org/10.1021/jm900743c)
- Contino M, Cantore M, Capparelli E et al (2012) A benzopyrane derivative as a P-glycoprotein stimulator: a potential agent to decrease β -amyloid accumulation in Alzheimer's disease. *ChemMedChem* 7:391–395. doi:[10.1002/cmdc.201100469](https://doi.org/10.1002/cmdc.201100469)
- Cotte S, von Ahesen N, Kruse N et al (2009) ABC-transporter gene-polymorphisms are potential pharmacogenetic markers for mitoxantrone response in multiple sclerosis. *Brain* 132:2517–2530. doi:[10.1093/brain/awp164](https://doi.org/10.1093/brain/awp164)
- Cutler L, Howes C, Deeks NJ et al (2006) Development of a P-glycoprotein knockout model in rodents to define species differences in its functional effect at the blood-brain barrier. *J Pharm Sci* 95:1944–1953. doi:[10.1002/jps.20658](https://doi.org/10.1002/jps.20658)
- Dauchy S, Dutheil F, Weaver RJ et al (2008) ABC transporters, cytochromes P450 and their main transcription factors: expression at the human blood-brain barrier. *J Neurochem* 107:1518–1528. doi:[10.1111/j.1471-4159.2008.05720.x](https://doi.org/10.1111/j.1471-4159.2008.05720.x)
- de Klerk OL, Bosker FJ, Willemsen ATM et al (2010a) Chronic stress and antidepressant treatment have opposite effects on P-glycoprotein at the blood-brain barrier: an experimental PET study in rats. *J Psychopharmacol* 24:1237–1242. doi:[10.1177/0269881109349840](https://doi.org/10.1177/0269881109349840)

- de Klerk OL, Willemsen ATM, Bosker FJ et al (2010b) Regional increase in P-glycoprotein function in the blood-brain barrier of patients with chronic schizophrenia: a PET study with [(11)C] verapamil as a probe for P-glycoprotein function. *Psychiatry Res* 183:151–156. doi:[10.1016/j.psychres.2010.05.002](https://doi.org/10.1016/j.psychres.2010.05.002)
- Dean M, Allikmets R (2001) Complete characterization of the human ABC gene family. *J Bioenerg Biomembr* 33:475–479
- Dean M, Hamon Y, Chimini G (2001) The human ATP-binding cassette (ABC) transporter superfamily. *J Lipid Res* 42:1007–1017
- Dey S, Ramachandra M, Pastan I et al (1997) Evidence for two nonidentical drug-interaction sites in the human P-glycoprotein. *Proc Natl Acad Sci U S A* 94:10594–10599
- Dey S, Ramachandra M, Pastan I et al (1998) Photoaffinity labeling of human P-glycoprotein: effect of modulator interaction and ATP hydrolysis on substrate binding. *Methods Enzymol* 292:318–328
- Dey S, Hafkemeyer P, Pastan I, Gottesman MM (1999) A single amino acid residue contributes to distinct mechanisms of inhibition of the human multidrug transporter by stereoisomers of the dopamine receptor antagonist flupentixol. *Biochemistry* 38:6630–6639. doi:[10.1021/bi983038I](https://doi.org/10.1021/bi983038I)
- Dombrowski SM, Desai SY, Marroni M et al (2001) Overexpression of multiple drug resistance genes in endothelial cells from patients with refractory epilepsy. *Epilepsia* 42:1501–1506
- Dörner B, Kuntner C, Bankstahl JP et al (2009) Synthesis and small-animal positron emission tomography evaluation of [11C]-elacridar as a radiotracer to assess the distribution of P-glycoprotein at the blood-brain barrier. *J Med Chem* 52:6073–6082. doi:[10.1021/jm900940f](https://doi.org/10.1021/jm900940f)
- Dörner B, Kuntner C, Bankstahl JP et al (2011) Radiosynthesis and in vivo evaluation of 1-[18F] fluoroelacridar as a positron emission tomography tracer for P-glycoprotein and breast cancer resistance protein. *Bioorg Med Chem* 19:2190–2198. doi:[10.1016/j.bmc.2011.02.039](https://doi.org/10.1016/j.bmc.2011.02.039)
- Drożdżik M, Białocka M, Myśliwiec K et al (2003) Polymorphism in the P-glycoprotein drug transporter MDR1 gene: a possible link between environmental and genetic factors in Parkinson's disease. *Pharmacogenetics* 13:259–263. doi:[10.1097/01.fpc.0000054087.48725.d9](https://doi.org/10.1097/01.fpc.0000054087.48725.d9)
- Dutheil F, Jacob A, Dauchy S et al (2010) ABC transporters and cytochromes P450 in the human central nervous system: influence on brain pharmacokinetics and contribution to neurodegenerative disorders. *Expert Opin Drug Metab Toxicol* 6:1161–1174. doi:[10.1517/17425255.2010.510832](https://doi.org/10.1517/17425255.2010.510832)
- Ee PLR, Kamalakaran S, Tonetti D et al (2004) Identification of a novel estrogen response element in the breast cancer resistance protein (ABCG2) gene. *Cancer Res* 64:1247–1251. doi:[10.1158/0008-5472.CAN-03-3583](https://doi.org/10.1158/0008-5472.CAN-03-3583)
- EIAlì A, Hermann DM (2010) Apolipoprotein E controls ATP-binding cassette transporters in the ischemic brain. *Sci Signal* 3:ra72. doi:[10.1126/scisignal.2001213](https://doi.org/10.1126/scisignal.2001213)
- EIAlì A, Hermann DM (2011) ATP-binding cassette transporters and their roles in protecting the brain. *Neuroscientist* 17:423–436. doi:[10.1177/1073858410391270](https://doi.org/10.1177/1073858410391270)
- Elfving B, Bjørnholm B, Knudsen GM (2003) Interference of anaesthetics with radioligand binding in neuroreceptor studies. *Eur J Nucl Med Mol Imaging* 30:912–915. doi:[10.1007/s00259-003-1171-8](https://doi.org/10.1007/s00259-003-1171-8)
- Eyal S, Ke B, Muzi M et al (2010) Regional P-glycoprotein activity and inhibition at the human blood-brain barrier as imaged by positron emission tomography. *Clin Pharmacol Ther* 87:579–585. doi:[10.1038/clpt.2010.11](https://doi.org/10.1038/clpt.2010.11)
- Gazzin S, Strazielle N, Schmitt C et al (2008) Differential expression of the multidrug resistance-related proteins ABCB1 and ABCC1 between blood-brain interfaces. *J Comp Neurol* 510:497–507. doi:[10.1002/cne.21808](https://doi.org/10.1002/cne.21808)
- Gottesman MM, Fojo T, Bates SE (2002) Multidrug resistance in cancer: role of ATP-dependent transporters. *Nat Rev Cancer* 2:48–58. doi:[10.1038/nrc706](https://doi.org/10.1038/nrc706)
- Harada N, Ohba H, Fukumoto D et al (2004) Potential of [(18)F]beta-CFT-FE (2beta-carbomethoxy-3beta-(4-fluorophenyl)-8-(2-[(18)F]fluoroethyl)nortropane) as a dopamine transporter ligand: a PET study in the conscious monkey brain. *Synapse* 54:37–45. doi:[10.1002/syn.20059](https://doi.org/10.1002/syn.20059)
- Hartz AMS, Bauer B, Fricker G, Miller DS (2004) Rapid regulation of P-glycoprotein at the blood-brain barrier by endothelin-1. *Mol Pharmacol* 66:387–394. doi:[10.1124/mol.104.001503](https://doi.org/10.1124/mol.104.001503)

- Hartz AMS, Bauer B, Fricker G, Miller DS (2006) Rapid modulation of P-glycoprotein-mediated transport at the blood-brain barrier by tumor necrosis factor- α and lipopolysaccharide. *Mol Pharmacol* 69:462–470. doi:[10.1124/mol.105.017954](https://doi.org/10.1124/mol.105.017954)
- Hartz AMS, Mahringer A, Miller DS, Bauer B (2010a) 17- β -Estradiol: a powerful modulator of blood-brain barrier BCRP activity. *J Cereb Blood Flow Metab* 30:1742–1755. doi:[10.1038/jcbfm.2010.36](https://doi.org/10.1038/jcbfm.2010.36)
- Hartz AMS, Miller DS, Bauer B (2010b) Restoring blood-brain barrier P-glycoprotein reduces brain amyloid-beta in a mouse model of Alzheimer's disease. *Mol Pharmacol* 77:715–723. doi:[10.1124/mol.109.061754](https://doi.org/10.1124/mol.109.061754)
- Häussermann K, Benz B, Gekeler V et al (1991) Effects of verapamil enantiomers and major metabolites on the cytotoxicity of vincristine and daunomycin in human lymphoma cell lines. *Eur J Clin Pharmacol* 40:53–59
- Hawkins BT, Davis TP (2005) The blood-brain barrier/neurovascular unit in health and disease. *Pharmacol Rev* 57:173–185. doi:[10.1124/pr.57.2.4](https://doi.org/10.1124/pr.57.2.4)
- Hawkins BT, Rigor RR, Miller DS (2010a) Rapid loss of blood-brain barrier P-glycoprotein activity through transporter internalization demonstrated using a novel in situ proteolysis protection assay. *J Cereb Blood Flow Metab* 30:1593–1597. doi:[10.1038/jcbfm.2010.117](https://doi.org/10.1038/jcbfm.2010.117)
- Hawkins BT, Sykes DB, Miller DS (2010b) Rapid, reversible modulation of blood-brain barrier P-glycoprotein transport activity by vascular endothelial growth factor. *J Neurosci* 30:1417–1425. doi:[10.1523/JNEUROSCI.5103-09.2010](https://doi.org/10.1523/JNEUROSCI.5103-09.2010)
- Hermann DM, Bassetti CL (2007) Implications of ATP-binding cassette transporters for brain pharmacotherapies. *Trends Pharmacol Sci* 28:128–134. doi:[10.1016/j.tips.2007.01.007](https://doi.org/10.1016/j.tips.2007.01.007)
- Ikoma Y, Takano A, Ito H et al (2006) Quantitative analysis of ¹¹C-verapamil transfer at the human blood-brain barrier for evaluation of P-glycoprotein function. *J Nucl Med* 47:1531–1537
- Imai Y, Tsukahara S, Ishikawa E et al (2002) Estrone and 17 β -estradiol reverse breast cancer resistance protein-mediated multidrug resistance. *Jpn J Cancer Res* 93:231–235
- Kaminski WE, Piehler A, Wenzel JJ (2006) ABC A-subfamily transporters: structure, function and disease. *Biochim Biophys Acta* 1762:510–524. doi:[10.1016/j.bbadis.2006.01.011](https://doi.org/10.1016/j.bbadis.2006.01.011)
- Kannan P, Brimacombe KR et al (2010) N-desmethyl-Loperamide Is Selective for P-Glycoprotein among Three ATP-Binding Cassette Transporters at the Blood-Brain Barrier. *Drug Metab Dispos* 38:917–922. doi:[10.1124/dmd.109.031161](https://doi.org/10.1124/dmd.109.031161)
- Kannan P (2012) Pharmacological properties of radiotracers that measure p – glycoprotein function and density. Karolinska Institutet, Stockholm. p 41
- Kannan P, John C, Zoghbi SS et al (2009) Imaging the function of P-glycoprotein with radiotracers: pharmacokinetics and in vivo applications. *Clin Pharmacol Ther* 86:368–377. doi:[10.1038/clpt.2009.138](https://doi.org/10.1038/clpt.2009.138)
- Kannan P, Brimacombe KR, Kreisl WC et al (2011a) Lysosomal trapping of a radiolabeled substrate of P-glycoprotein as a mechanism for signal amplification in PET. *Proc Natl Acad Sci U S A* 108:2593–2598. doi:[10.1073/pnas.1014641108](https://doi.org/10.1073/pnas.1014641108)
- Kannan P, Telu S, Shukla S et al (2011b) The “specific” P-glycoprotein inhibitor tariquidar is also a substrate and an inhibitor for breast cancer resistance protein (BCRP/ABCG2). *ACS Chem Neurosci* 2:82–89. doi:[10.1021/cn100078a](https://doi.org/10.1021/cn100078a)
- Kaufmann AM, Krise JP (2007) Lysosomal sequestration of amine-containing drugs : analysis and therapeutic implications. *J Pharm Sci* 96:729–746. doi:[10.1002/jps](https://doi.org/10.1002/jps)
- Kawamura K, Konno F, Yui J et al (2010) Synthesis and evaluation of [¹¹C]XR9576 to assess the function of drug efflux transporters using PET. *Ann Nucl Med* 24:403–412. doi:[10.1007/s12149-010-0373-y](https://doi.org/10.1007/s12149-010-0373-y)
- Kawamura K, Yamasaki T, Konno F et al (2011a) Synthesis and in vivo evaluation of ¹⁸F-fluoroethyl GF120918 and XR9576 as positron emission tomography probes for assessing the function of drug efflux transporters. *Bioorg Med Chem* 19:861–870. doi:[10.1016/j.bmc.2010.12.004](https://doi.org/10.1016/j.bmc.2010.12.004)
- Kawamura K, Yamasaki T, Konno F et al (2011b) Evaluation of limiting brain penetration related to P-glycoprotein and breast cancer resistance protein using [(11)C]GF120918 by PET in mice. *Mol Imaging Biol* 13:152–160. doi:[10.1007/s11307-010-0313-1](https://doi.org/10.1007/s11307-010-0313-1)

- Kilic E, Spudich A, Kilic U et al (2008) ABCC1: a gateway for pharmacological compounds to the ischaemic brain. *Brain* 131:2679–2689. doi:[10.1093/brain/awn222](https://doi.org/10.1093/brain/awn222)
- Kim WS, Weickert CS, Garner B (2008) Role of ATP-binding cassette transporters in brain lipid transport and neurological disease. *J Neurochem* 104:1145–1166. doi:[10.1111/j.1471-4159.2007.05099.x](https://doi.org/10.1111/j.1471-4159.2007.05099.x)
- Kodaira H, Kusuhara H, Ushiki J et al (2010) Kinetic analysis of the cooperation of P-glycoprotein (P-gp/Abcb1) and breast cancer resistance protein (Bcrp/Abcg2) in limiting the brain and testis penetration of erlotinib, flavopiridol, and mitoxantrone. *J Pharmacol Exp Ther* 333:788–796. doi:[10.1124/jpet.109.162321](https://doi.org/10.1124/jpet.109.162321)
- Kooij G, van Horsen J, de Lange ECM et al (2010) T lymphocytes impair P-glycoprotein function during neuroinflammation. *J Autoimmun* 34:416–425. doi:[10.1016/j.jaut.2009.10.006](https://doi.org/10.1016/j.jaut.2009.10.006)
- Kortekaas R, Leenders KL, van Oostrom JCH et al (2005) Blood-brain barrier dysfunction in parkinsonian midbrain in vivo. *Ann Neurol* 57:176–179. doi:[10.1002/ana.20369](https://doi.org/10.1002/ana.20369)
- Kreisl WC, Liow J-S, Kimura N et al (2010) P-glycoprotein function at the blood-brain barrier in humans can be quantified with the substrate radiotracer 11C-N-desmethyl-loperamide. *J Nucl Med* 51:559–566. doi:[10.2967/jnumed.109.070151](https://doi.org/10.2967/jnumed.109.070151)
- Kroemer HK, Gautier JC, Beaune P et al (1993) Identification of P450 enzymes involved in metabolism of verapamil in humans. *Naunyn Schmiedeberg Arch Pharmacol* 348:332–337
- Kubota H, Ishihara H, Langmann T et al (2006) Distribution and functional activity of P-glycoprotein and multidrug resistance-associated proteins in human brain microvascular endothelial cells in hippocampal sclerosis. *Epilepsy Res* 68:213–228. doi:[10.1016/j.epilepsyres.2005.11.011](https://doi.org/10.1016/j.epilepsyres.2005.11.011)
- Kuhnke D, Jedlitschky G, Grube M et al (2007) MDR1-P-Glycoprotein (ABCB1) Mediates Transport of Alzheimer's amyloid-beta peptides—implications for the mechanisms of Abeta clearance at the blood-brain barrier. *Brain Pathol* 17:347–353. doi:[10.1111/j.1750-3639.2007.00075.x](https://doi.org/10.1111/j.1750-3639.2007.00075.x)
- Kühnle M, Egger M, Müller C et al (2009) Potent and selective inhibitors of breast cancer resistance protein (ABCG2) derived from the p-glycoprotein (ABCB1) modulator tariquidar. *J Med Chem* 52:1190–1197. doi:[10.1021/jm8013822](https://doi.org/10.1021/jm8013822)
- Kuntner C, Bankstahl JP, Bankstahl M et al (2010) Dose–response assessment of tariquidar and elacridar and regional quantification of P-glycoprotein inhibition at the rat blood-brain barrier using (R)-[(11)C]verapamil PET. *Eur J Nucl Med Mol Imaging* 37:942–953. doi:[10.1007/s00259-009-1332-5](https://doi.org/10.1007/s00259-009-1332-5)
- Kurnik D, Sofowora GG, Donahue JP et al (2008) Tariquidar, a selective P-glycoprotein inhibitor, does not potentiate loperamide's opioid brain effects in humans despite full inhibition of lymphocyte P-glycoprotein. *Anesthesiology* 109:1092–1099. doi:[10.1097/ALN.0b013e31818d8f28](https://doi.org/10.1097/ALN.0b013e31818d8f28)
- Laberge P, Martineau P, Sebahang H, Lalonde G (2001) Verapamil intoxication after substitution of immediate-release for extended-release verapamil. *Am J Health Syst Pharm* 58:402–405
- Lam FC, Liu R, Lu P et al (2001) beta-Amyloid efflux mediated by p-glycoprotein. *J Neurochem* 76:1121–1128
- Lazarova N, Zoghbi SS, Hong J et al (2008) Synthesis and evaluation of [N-methyl-11C] N-desmethyl-loperamide as a new and improved PET radiotracer for imaging P-gp function. *J Med Chem* 51:6034–6043. doi:[10.1021/jm800510m](https://doi.org/10.1021/jm800510m)
- Lee CGL, Tang K, Cheung YB et al (2004) MDR1, the blood-brain barrier transporter, is associated with Parkinson's disease in ethnic Chinese. *J Med Genet* 41:e60
- Liow J-S, Kreisl W, Zoghbi SS et al (2009) P-glycoprotein function at the blood-brain barrier imaged using 11C-N-desmethyl-loperamide in monkeys. *J Nucl Med* 50:108–115. doi:[10.2967/jnumed.108.056226](https://doi.org/10.2967/jnumed.108.056226)
- Löscher W, Potschka H (2005) Drug resistance in brain diseases and the role of drug efflux transporters. *Nat Rev Neurosci* 6:591–602. doi:[10.1038/nrn1728](https://doi.org/10.1038/nrn1728)
- Löscher W, Luna-Tortós C, Römermann K, Fedrowitz M (2011) Do ATP-binding cassette transporters cause pharmacoresistance in epilepsy? Problems and approaches in determining which antiepileptic drugs are affected. *Curr Pharm Des* 17:2808–2828

- Lubberink M, Luurtsema G, van Berckel BNM et al (2007) Evaluation of tracer kinetic models for quantification of P-glycoprotein function using (R)-[11C]verapamil and PET. *J Cereb Blood Flow Metab* 27:424–433. doi:[10.1038/sj.jcbfm.9600349](https://doi.org/10.1038/sj.jcbfm.9600349)
- Luurtsema G, Windhorst AD, Mooijer MPJ et al (2002) Fully automated high yield synthesis of (R)- and (S)-[11C]verapamil for measuring P-glycoprotein function with positron emission tomography. *J Labelled Comp Radiopharm* 45:1199–1207. doi:[10.1002/jlcr.632](https://doi.org/10.1002/jlcr.632)
- Luurtsema G, Molthoff CFM, Windhorst AD et al (2003) (R)- and (S)-[11C]verapamil as PET-tracers for measuring P-glycoprotein function: in vitro and in vivo evaluation. *Nucl Med Biol* 30:747–751. doi:[10.1016/S0969-8051\(03\)00078-7](https://doi.org/10.1016/S0969-8051(03)00078-7)
- Luurtsema G, Molthoff CFM, Schuit RC et al (2005) Evaluation of (R)-[11C]verapamil as PET tracer of P-glycoprotein function in the blood-brain barrier: kinetics and metabolism in the rat. *Nucl Med Biol* 32:87–93. doi:[10.1016/j.nucmedbio.2004.06.007](https://doi.org/10.1016/j.nucmedbio.2004.06.007)
- Luurtsema G, Schuit RC, Klok RP et al (2009) Evaluation of [11C]laniquidar as a tracer of P-glycoprotein: radiosynthesis and biodistribution in rats. *Nucl Med Biol* 36:643–649. doi:[10.1016/j.nucmedbio.2009.03.004](https://doi.org/10.1016/j.nucmedbio.2009.03.004)
- Macé S, Cousin E, Ricard S et al (2005) ABCA2 is a strong genetic risk factor for early-onset alzheimer's disease. *Neurobiol Dis* 18:119–125. doi:[10.1016/j.nbd.2004.09.011](https://doi.org/10.1016/j.nbd.2004.09.011)
- MacIntyre AC, Cutler DJ (1988) The potential role of lysosomes in tissue distribution of weak bases. *Biopharm Drug Dispos* 9:513–526
- Mairinger S, Langer O, Kuntner C et al (2010) Synthesis and in vivo evaluation of the putative breast cancer resistance protein inhibitor [11C]methyl 4-((4-(2-(6,7-dimethoxy-1,2,3,4-tetrahydroisoquinolin-2-yl)ethyl)phenyl)amino-carbonyl)-2-(quinoline-2-carbonylamino)benzoate. *Nucl Med Biol* 37:637–644. doi:[10.1016/j.nucmedbio.2010.02.008](https://doi.org/10.1016/j.nucmedbio.2010.02.008)
- Maki N, Dey S (2006) Biochemical and pharmacological properties of an allosteric modulator site of the human P-glycoprotein (ABCB1). *Biochem Pharmacol* 72:145–155. doi:[10.1016/j.bcp.2006.04.008](https://doi.org/10.1016/j.bcp.2006.04.008)
- Maliepaard M, Gastelen MAV, Tohgo A, Waardenburg RCAMV (2001) Circumvention of breast cancer resistance protein (BCRP) – mediated resistance to camptothecins in vitro using non-substrate drugs or the BCRP inhibitor GF120918. *Clin Cancer Res* 7:935–941
- McHugh K, Callaghan, R. (2008) 7 Clinical trials on MDR reversal agents. *Clin Trials J* 661(2): 1–33
- McHugh K, Callaghan R, Colabufo NA (2008) Clinical trials on MDR reversal agents. In multi-drug resistance: biological and pharmaceutical advances in antitumour treatment (ed. Colabufo, NA). Research Signpost, India, pp 321–354
- McTavish D, Sorkin EM (1989) Verapamil. An updated review of its pharmacodynamic and pharmacokinetic properties, and therapeutic use in hypertension. *Drugs* 38:19–76
- Mistry P, Stewart AJ, Dangerfield W et al (2001) In vitro and in vivo reversal of P-glycoprotein-mediated multidrug resistance by a novel potent modulator, XR9576. *Cancer* 61:749–758
- Moaddel R, Wainer IW (2007) Conformational mobility of immobilized proteins. *J Pharm Biomed Anal* 43:399–406. doi:[10.1016/j.jpba.2006.08.021](https://doi.org/10.1016/j.jpba.2006.08.021)
- Moerman L, Dumolyn C, Boon P, De Vos F (2012) The influence of mass of [11C]-laniquidar and [11C]-N-desmethyl-loperamide on P-glycoprotein blockage at the blood-brain barrier. *Nucl Med Biol* 39:121–125. doi:[10.1016/j.nucmedbio.2011.06.009](https://doi.org/10.1016/j.nucmedbio.2011.06.009)
- Morita M, Shimozawa N, Kashiwayama Y et al (2011) ABC subfamily D proteins and very long chain fatty acid metabolism as novel targets in adrenoleukodystrophy. *Curr Drug Targets* 12:694–706
- Mosser J, Douar AM, Sarde CO et al (1993) Putative X-linked adrenoleukodystrophy gene shares unexpected homology with ABC transporters. *Nature* 361:726–730. doi:[10.1038/361726a0](https://doi.org/10.1038/361726a0)
- Muzi M, Mankoff DA, Link JM et al (2009) Imaging of cyclosporine inhibition of P-glycoprotein activity using 11C-verapamil in the brain: studies of healthy humans. *J Nucl Med* 50:1267–1275. doi:[10.2967/jnumed.108.059162](https://doi.org/10.2967/jnumed.108.059162)
- Nies AT, Jedlitschky G, König J et al (2004) Expression and immunolocalization of the multidrug resistance proteins, MRP1-MRP6 (ABCC1-ABCC6), in human brain. *Neuroscience* 129:349–360. doi:[10.1016/j.neuroscience.2004.07.051](https://doi.org/10.1016/j.neuroscience.2004.07.051)

- Pauli-Magnus C, von Richter O, Burk O et al (2000) Characterization of the major metabolites of verapamil as substrates and inhibitors of P-glycoprotein. *J Pharmacol Exp Ther* 293:376–382
- Pekcec A, Unkru B, Schlichtiger J et al (2009) Targeting prostaglandin E 2 EP1 receptors prevents seizure-associated P-glycoprotein up-regulation. *Pharmacology* 330:939–947. doi:[10.1124/jpet.109.152520.2002](https://doi.org/10.1124/jpet.109.152520.2002)
- Pellicani RZ, Stefanachi A, Niso M et al (2012) Potent galloyl-based selective modulators targeting multidrug resistance associated protein 1 and P-glycoprotein. *J Med Chem* 55:424–436. doi:[10.1021/jm201305y](https://doi.org/10.1021/jm201305y)
- Poller B, Drewe J, Krähenbühl S et al (2010) Regulation of BCRP (ABCG2) and P-glycoprotein (ABCB1) by cytokines in a model of the human blood-brain barrier. *Cell Mol Neurobiol* 30:63–70. doi:[10.1007/s10571-009-9431-1](https://doi.org/10.1007/s10571-009-9431-1)
- Porro A, Haber M, Diolaiti D et al (2010) Direct and coordinate regulation of ATP-binding cassette transporter genes by Myc factors generates specific transcription signatures that significantly affect the chemoresistance phenotype of cancer cells. *J Biol Chem* 285:19532–19543. doi:[10.1074/jbc.M109.078584](https://doi.org/10.1074/jbc.M109.078584)
- Posse de Chaves E, Sipione S (2010) Sphingolipids and gangliosides of the nervous system in membrane function and dysfunction. *FEBS Lett* 584:1748–1759. doi:[10.1016/j.febslet.2009.12.010](https://doi.org/10.1016/j.febslet.2009.12.010)
- Riddell DR, Zhou H, Comery TA et al (2007) The LXR agonist TO901317 selectively lowers hippocampal Abeta42 and improves memory in the Tg2576 mouse model of Alzheimer's disease. *Mol Cell Neurosci* 34:621–628. doi:[10.1016/j.mcn.2007.01.011](https://doi.org/10.1016/j.mcn.2007.01.011)
- Rigor RR, Hawkins BT, Miller DS (2010) Activation of PKC isoform beta(I) at the blood-brain barrier rapidly decreases P-glycoprotein activity and enhances drug delivery to the brain. *J Cereb Blood Flow Metab* 30:1373–1383. doi:[10.1038/jcbfm.2010.21](https://doi.org/10.1038/jcbfm.2010.21)
- Robey RW, Steadman K, Polgar O et al (2004) Pheophorbide is a specific probe for ABCG2 function and inhibition. *Cancer Res* 64:1242–1246. doi:[10.1158/0008-5472.CAN-03-3298](https://doi.org/10.1158/0008-5472.CAN-03-3298)
- Ronaldson PT, Ashraf T, Bendayan R (2010) Regulation of multidrug resistance protein 1 by tumor necrosis factor alpha in cultured glial cells: involvement of nuclear factor-kappa B and c-Jun N-terminal kinase signaling pathways. *Mol Pharmacol* 77:644–659. doi:[10.1124/mol.109.059410.proteins](https://doi.org/10.1124/mol.109.059410.proteins)
- Rosenhagen MC, Uhr M (2011) The clinical impact of ABCB1 polymorphisms on the treatment of psychiatric diseases. *Curr Pharm Des* 17:2843–2851
- Sakai H, Tanaka Y, Tanaka M et al (2007) ABCA2 deficiency results in abnormal sphingolipid metabolism in mouse brain. *J Biol Chem* 282:19692–19699. doi:[10.1074/jbc.M611056200](https://doi.org/10.1074/jbc.M611056200)
- Sasongko L, Link JM, Muzi M et al (2005) Imaging P-glycoprotein transport activity at the human blood-brain barrier with positron emission tomography. *Clin Pharmacol Ther* 77:503–514. doi:[10.1016/j.cpt.2005.01.022](https://doi.org/10.1016/j.cpt.2005.01.022)
- Seegers U, Potschka H, Löscher W (2002) Transient increase of P-glycoprotein expression in endothelium and parenchyma of limbic brain regions in the kainate model of temporal lobe epilepsy. *Epilepsy Res* 51:257–268
- Seneca N, Zoghbi SS, Liow J-S et al (2009) Human brain imaging and radiation dosimetry of ¹¹C-N-desmethyl-loperamide, a PET radiotracer to measure the function of P-glycoprotein. *J Nucl Med* 50:807–813. doi:[10.2967/jnumed.108.058453](https://doi.org/10.2967/jnumed.108.058453)
- Sharom FJ (2007) ABC multidrug transporters: structure, function and role in chemoresistance. *Pharmacogenomics* 9:105–127. doi:[10.2217/14622416.9.1.105](https://doi.org/10.2217/14622416.9.1.105)
- Soontornmalai A, Vlaming MLH, Fritschy J-M (2006) Differential, strain-specific cellular and subcellular distribution of multidrug transporters in murine choroid plexus and blood-brain barrier. *Neuroscience* 138:159–169. doi:[10.1016/j.neuroscience.2005.11.011](https://doi.org/10.1016/j.neuroscience.2005.11.011)
- Spudich A, Kilic E, Xing H et al (2006) Inhibition of multidrug resistance transporter-1 facilitates neuroprotective therapies after focal cerebral ischemia. *Nat Neurosci* 9:487–488. doi:[10.1038/nn1676](https://doi.org/10.1038/nn1676)
- Sui M, Zhang H, Fan W (2011) The role of estrogen and estrogen receptors in chemoresistance. *Curr Med Chem* 18:4674–4683

- Syvänen S, Lindhe O, Palner M et al (2009) Species differences in blood-brain barrier transport of three positron emission tomography radioligands with emphasis on P-glycoprotein transport. *Drug Metab Dispos* 37:635–643. doi:[10.1124/dmd.108.024745](https://doi.org/10.1124/dmd.108.024745)
- Tai LM, Reddy PS, Lopez-Ramirez MA et al (2009) Polarized P-glycoprotein expression by the immortalised human brain endothelial cell line, hCMEC/D3, restricts apical-to-basolateral permeability to rhodamine 123. *Brain Res* 1292:14–24. doi:[10.1016/j.brainres.2009.07.039](https://doi.org/10.1016/j.brainres.2009.07.039)
- Takashima T, Yokoyama C, Mizuma H et al (2011) Developmental changes in P-glycoprotein function in the blood-brain barrier of nonhuman primates: PET study with R-11C-verapamil and 11C-oseltamivir. *J Nucl Med* 52:950–957. doi:[10.2967/jnumed.110.083949](https://doi.org/10.2967/jnumed.110.083949)
- Thiebaut F, Tsuroo T, Hamada H et al (1987) Cellular localization of the multidrug-resistance gene product P-glycoprotein in normal human tissues. *Proc Natl Acad Sci U S A* 84:7735–7738
- Thomas H, Coley HM (2003) Overcoming multidrug resistance in cancer: an update on the clinical strategy of inhibiting p-glycoprotein. *Cancer Control* 10:159–165. PubMed 12712010
- Toornvliet R, van Berckel BNM, Luurtsema G et al (2006) Effect of age on functional P-glycoprotein in the blood-brain barrier measured by use of (R)-[(11)C]verapamil and positron emission tomography. *Clin Pharmacol Ther* 79:540–548. doi:[10.1016/j.cpt.2006.02.004](https://doi.org/10.1016/j.cpt.2006.02.004)
- Uchida Y, Ohtsuki S, Katsukura Y et al (2011) Quantitative targeted absolute proteomics of human blood-brain barrier transporters and receptors. *J Neurochem* 117:333–345. doi:[10.1111/j.1471-4159.2011.07208.x](https://doi.org/10.1111/j.1471-4159.2011.07208.x)
- van Assema DM, Lubberink M, Boellaard R et al (2012a) Reproducibility of quantitative (R)-[(11)C]verapamil studies. *EJNMMI Res* 2:1. doi:[10.1186/2191-219X-2-1](https://doi.org/10.1186/2191-219X-2-1)
- van Assema DME, Lubberink M, Bauer M et al (2012b) Blood-brain barrier P-glycoprotein function in Alzheimer's disease. *Brain* 135:181–189. doi:[10.1093/brain/awr298](https://doi.org/10.1093/brain/awr298)
- van Assema DME, Lubberink M, Boellaard R et al (2012c) P-glycoprotein function at the blood-brain barrier: effects of age and gender. *Mol Imaging Biol*. doi:[10.1007/s11307-012-0556-0](https://doi.org/10.1007/s11307-012-0556-0)
- van Waarde A, Ramakrishnan NK, Rybczynska AA et al (2009) Synthesis and preclinical evaluation of novel PET probes for P-glycoprotein function and expression. *J Med Chem* 52:4524–4532. doi:[10.1021/jm900485a](https://doi.org/10.1021/jm900485a)
- van Zuylen L, Sparreboom A, van der Gaast A et al (2000) The orally administered P-glycoprotein inhibitor R101933 does not alter the plasma pharmacokinetics of docetaxel. *Clin Cancer Res* 6:1365–1371
- van Zuylen L, Sparreboom A, van der Gaast A et al (2002) Disposition of docetaxel in the presence of P-glycoprotein inhibition by intravenous administration of R101933. *Eur J Cancer* 38:1090–1099. doi:[10.1016/S0959-8049\(02\)00035-7](https://doi.org/10.1016/S0959-8049(02)00035-7)
- Verbeek J, Syvänen S, Schuit RC et al (2012) Synthesis and preclinical evaluation of [(11)C]D617, a metabolite of (R)-[(11)C]verapamil. *Nucl Med Biol*. doi:[10.1016/j.nucmedbio.2011.10.017](https://doi.org/10.1016/j.nucmedbio.2011.10.017)
- Vogelgesang S, Cascorbi I, Schroeder E et al (2002) Deposition of Alzheimer's beta-amyloid is inversely correlated with P-glycoprotein expression in the brains of elderly non-demented humans. *Pharmacogenetics* 12:535–541
- Vogelgesang S, Warzok RW, Cascorbi I et al (2004) The role of P-glycoprotein in cerebral amyloid angiopathy; implications for the early pathogenesis of Alzheimer's disease. *Curr Alzheimer Res* 1:121–125
- Wagner CC, Bauer M, Karch R et al (2009) A pilot study to assess the efficacy of tariquidar to inhibit P-glycoprotein at the human blood-brain barrier with (R)-11C-verapamil and PET. *J Nucl Med* 50:1954–1961. doi:[10.2967/jnumed.109.063289](https://doi.org/10.2967/jnumed.109.063289)
- Wanek T, Kuntner C, Bankstahl JP et al (2012) A comparative small-animal PET evaluation of [(11)C]tariquidar, [(11)C]elacridar and (R)-[(11)C]verapamil for detection of P-glycoprotein-expressing murine breast cancer. *Eur J Nucl Med Mol Imaging* 39:149–159. doi:[10.1007/s00259-011-1941-7](https://doi.org/10.1007/s00259-011-1941-7)
- Wang RB, Kuo CL, Lien LL, Lien EJ (2003) Structure-activity relationship: analyses of p-glycoprotein substrates and inhibitors. *J Clin Pharm Ther* 28:203–228
- Westerlund M, Belin AC, Olson L, Galter D (2008) Expression of multi-drug resistance 1 mRNA in human and rodent tissues: reduced levels in Parkinson patients. *Cell Tissue Res* 334:179–185. doi:[10.1007/s00441-008-0686-5](https://doi.org/10.1007/s00441-008-0686-5)

- Westerlund M, Belin AC, Anvret A et al (2009) Association of a polymorphism in the ABCB1 gene with Parkinson's disease. *Parkinsonism Relat Disord* 15:422–424. doi:[10.1016/j.parkreldis.2008.11.010](https://doi.org/10.1016/j.parkreldis.2008.11.010)
- Wijesuriya HC, Bullock JY, Faull RLM et al (2010) ABC efflux transporters in brain vasculature of Alzheimer's subjects. *Brain Res* 1358:228–238. doi:[10.1016/j.brainres.2010.08.034](https://doi.org/10.1016/j.brainres.2010.08.034)
- Willmann JK, van Bruggen N, Dinkelborg LM, Gambhir SS (2008) Molecular imaging in drug development. *Nat Rev Drug Discov* 7:591–607. doi:[10.1038/nrd2290](https://doi.org/10.1038/nrd2290)
- Xiong H, Callaghan D, Jones A et al (2009) ABCG2 is upregulated in Alzheimer's brain with cerebral amyloid angiopathy and may act as a gatekeeper at the blood-brain barrier for Abeta(1–40) peptides. *J Neurosci* 29:5463–5475. doi:[10.1523/JNEUROSCI.5103-08.2009](https://doi.org/10.1523/JNEUROSCI.5103-08.2009)
- Zhang W, Mojsilovic-Petrovic J, Andrade MF et al (2003) The expression and functional characterization of ABCG2 in brain endothelial cells and vessels. *FASEB J* 17:2085–2087. doi:[10.1096/fj.02-1131fje](https://doi.org/10.1096/fj.02-1131fje)
- Zibell G, Unkrüer B, Pekcec A et al (2009) Prevention of seizure-induced up-regulation of endothelial P-glycoprotein by COX-2 inhibition. *Neuropharmacology* 56:849–855. doi:[10.1016/j.neuropharm.2009.01.009](https://doi.org/10.1016/j.neuropharm.2009.01.009)
- Zoghbi SS, Liow J-S, Yasuno F et al (2008) 11C-loperamide and its N-desmethyl radiometabolite are avid substrates for brain permeability-glycoprotein efflux. *J Nucl Med* 49:649–656. doi:[10.2967/jnumed.107.047308](https://doi.org/10.2967/jnumed.107.047308)
- Zschiechrich K, König IR, Brüggemann N et al (2009) MDR1 variants and risk of Parkinson disease. Association with pesticide exposure? *J Neurol* 256:115–120. doi:[10.1007/s00415-009-0089-x](https://doi.org/10.1007/s00415-009-0089-x)

David J. Brooks

Contents

22.1	Introduction	654
22.2	Imaging TSPO with PET	655
22.3	TSPO Imaging in Alzheimer's Disease.....	656
22.4	Inflammation in Frontotemporal Dementia and Motor Neurone Disease.....	658
22.5	Parkinsonian Syndromes and TSPO Imaging	659
22.6	Huntington's Disease and Microglial Activation.....	660
22.7	Measuring Inflammation in Multiple Sclerosis.....	661
22.8	Traumatic Brain Injury.....	662
22.9	Stroke and Microglial Activation.....	662
22.10	Psychosis.....	663
	Conclusions.....	663
	References.....	664

Abstract

Microglia provide the intrinsic immune defence of the brain and are activated by any injurious process. As such they provide a nonspecific marker of disease activity. Their function can be both detrimental and beneficial as they release cytokines which can drive disease progression but also release restorative growth factors, can help clear cellular debris and abnormal protein aggregations and can remodel connections as an adaptive response to brain damage. Activated microglia express translocator protein (TSPO), and this allows them to be imaged in vivo with positron emission tomography (PET) radioligands which are substrates. In this chapter, the role of TSPO imaging with PET is discussed in neurodegenerative and inflammatory brain diseases and in focal brain injury due to trauma or stroke.

D.J. Brooks

Department of Medicine, Imperial College London, London, UK

Department of Nuclear Medicine, Aarhus University, Aarhus, Denmark

e-mail: davidjbrooks@sky.com

22.1 Introduction

The 18 kDa translocator protein (TSPO), previously known as the peripheral benzodiazepine receptor (PBR), is present in many peripheral organs including the liver, spleen, adrenals and myocardium (Banati 2002b). It is expressed only at low levels in the normal brain, but if microglial cells become activated, TSPO can be detected in their outer mitochondrial membrane. The TSPO serves a number of functions including transport of cholesterol, anions and porphyrin; maintenance of mitochondrial membrane potential; regulation of cell apoptosis and proliferation; and immunomodulation (Papadopoulos et al. 2006). The protein expresses a binding site for benzodiazepines and isoquinolines such as PK11195, and this has allowed detection of TSPO *in vivo* with ^{11}C -PK11195 PET. Newer PET biomarkers are now available to image TSPO expression which include phenoxyarylacetamides such as $^{11}\text{C}/^{18}\text{F}$ -DAA1106, ^{11}C -PBR28, ^{18}F -PBR06, ^{18}F -PBR111 and ^{18}F -FEPPA; pyrazolo[1,5-a]pyrimidines such as ^{11}C -DPA713 and ^{18}F -DPA714; the vinca alkaloid ^{11}C -vinpocetine; and the imidazo[1,2a]pyridines $^{11}\text{C}/^{18}\text{F}$ -CLINDE (Dolle et al. 2009; Doorduyn et al. 2008).

Microglia account for around 15 % of the cerebral white cell population and are normally in a resting state sending out long ramified processes which contact neighbouring neurones and astrocytes (Kreutzberg 1996; Ransohoff and Perry 2009). It is, therefore, likely that the function of resting microglia is to monitor changes in the local brain milieu – for an excellent review see Hanisch and Kettenmann (2007). Microglia are cells of monocyte lineage and are protected from antigens in the plasma by the blood-brain barrier. They form the natural immune defence of the brain and exposure to plasma proteins such as fibrinogen following blood-brain barrier disruption, or to intrinsic excitotoxic agents such as raised glutamate, nitric oxide or cytokines, causes them to become activated taking on amoeboid or rodlike morphology. When activated, the microglia express MHC class 1 and 2 antigens and release cytokines such as $\text{TNF}\alpha$, $\text{IL}1\beta$ and $\text{IL}6$ and growth factors such as $\text{TGF-}\beta 1$. They become phagocytic and can strip and remodel synapses. It is now considered that activated microglia may exist as two primary phenotypes: M1 which is associated with the release of cidal cytokines promoting cell damage and M2 which is associated with phagocytosis of dead tissue, synaptic remodelling and growth factor release promoting neurogenesis (Boche et al. 2012; Varnum and Ikezu 2012). These two phenotypes may well be interconvertible, have overlapping functions and predominate at different disease phases. After an acute stroke activated, microglia act locally to wall off, remove dead tissue and remodel connections, while in chronic neurodegenerative diseases they may release cytokines where disease is locally active but remodel distant connections in the brainstem and thalamus. The advent of TSPO PET agents has allowed us to image *in life* the distribution of activated microglia in the brain. Currently, TSPO ligands are unable to discriminate between M1 and M2 phenotypes, and so they provide a measure of total activated microglia load.

22.2 Imaging TSPO with PET

The ligand that has seen the greatest use for imaging TSPO in the brain is isoquinoline ^{11}C -PK11115. The rat unilateral facial nerve axonopathy model results in activated microglia in the ipsilateral facial nucleus. Autoradiography studies have shown that ^3H -PK11195 binds selectively to these activated microglia which are involved in remodelling connections to restore facial muscle function (Banati et al. 1997). A human equivalent of this rodent model is Bell's palsy where the facial nerve becomes unilaterally compressed due to local inflammation as it passes through the auditory canal. ^{11}C -PK11115 PET studies have demonstrated tracer uptake in the facial nerve nucleus ipsilateral to the paralysed facial muscles (Banati 2002b). Human subjects with acquired upper limb amputations develop phantom limb phenomena where the absent limb still feels to be present but may be telescoped into the stump. In these subjects one can detect thalamic inflammation contralateral to the missing limb with ^{11}C -PK11115 PET (Banati 2002a). These studies, therefore, reveal the microglial activation resulting from disconnection of brain nuclei due to peripheral injury, presumably playing an active role in the remodelling of connections. It remains to be determined whether these cells are expressing the M2 phenotype.

In the majority of brain disorders, ^{11}C -PK11115 PET reveals microglial activation due to both local disease activity and the effects of downstream disconnection. Additionally, as endothelial cells also express TSPO, tracer binding is seen in the lateral and sagittal venous sinuses, and this signal can spill over into adjacent brain tissue – particularly the cerebellum – due to the 5 mm spatial resolution of most commercial PET cameras. This can make quantitative modelling of ^{11}C -PK11115 PET problematic as there is no single brain region that can provide a tissue reference for nonspecific tracer uptake. The use of an arterial plasma input function with this tracer is also problematic as ^{11}C -PK11115 sticks to plastic tubing, and it can be difficult to obtain wash-in and washout blood time-activity curves allowing accurate measurement of peak height, delay and dispersion. For these reasons, a modelling approach has been developed that uses cluster analysis to define a collection of grey matter voxels in the subject's brain that have a time-activity curve (TAC) similar to that of normal grey matter TAC in a population of healthy controls (Anderson et al. 2007). This reference cluster can then be used to define nonspecific ^{11}C -PK11115 uptake in other clusters where retention is occurring. At the same time, signal due to vascular tracer binding, which shows the most rapid uptake, is separated from brain parenchymal signal. The ^{11}C -PK11115 binding potentials (BPs) are computed using a standard simplified reference tissue model (SRTM) with brain-specific and nonspecific compartments. ^{11}C -PK11195 binding increases in the normal thalamus and cortex with age, and so it is important to age match healthy controls to patients when assessing levels of inflammation in disease states (Cagnin et al. 2001).

Recently, new higher-affinity tracers have been developed with lower nonspecific signal in order to provide a more sensitive detection of microglial activation

and facilitate modelling approaches. However, with these new tracers has come the realisation that TSPO imaging is influenced by which polymorphisms of the TSPO gene are expressed by individuals (Owen et al. 2012). The most influential of these is the rs6971 polymorphism where a homozygous Ala147Thr substitution results in subjects becoming low-affinity binders of these novel TSPO ligands while heterozygotes are mixed-affinity binders. In Caucasian populations around 60 % of individuals are high, 10 % low and 30 % mixed-affinity binders for the newer TSPO ligands. ^{11}C -PK11115 affinity for TSPO, however, appears to be of little influenced by genotype. ^{11}C -PBR28 shows a 50-fold difference in affinity for TSPO between high (Kd 4nM)- and low (Kd 200nM)-affinity binders. The PET tracers ^{11}C -DAA1106, ^{11}C -DPA713 and ^{18}F -PBR111 show four to fivefold differences in affinity for TSPO between high and low binders. Mixed-affinity binders express high- and low-affinity TSPO binding sites in equal proportions. If one is to use these newer TSPO PET markers, then low- and mixed-affinity binders may need to be excluded or stratified in studies by prior genetic screening and findings compared with appropriate control populations with similar genotype.

22.3 TSPO Imaging in Alzheimer's Disease

Dementia affects 10 % of the over sixties, the prevalence rising to 30 % of the over eighties. It is characterised clinically by progressive impairment of memory, speech and perception along with personality change in the absence of altered conscious level. Sixty percent of dementia cases have Alzheimer pathology with fibrillar extracellular amyloid plaques and intraneuronal neurofibrillary tangles of hyperphosphorylated tau at postmortem. Activated microglia are seen surrounding the amyloid plaques which target the association cortex, cingulate and striatum (Braak and Braak 1997; Dickson 1997). They are also found in brain areas with denser tau pathology but fewer plaques such as the entorhinal cortex and hippocampus.

Raised levels of microglial activation can be detected in vivo in Alzheimer's disease (AD) patients with ^{11}C -PK11195 PET, binding potentials rising by up to 50 % in association cortex – see Fig. 22.1a (Cagnin et al. 2001; Schuitmaker et al. 2013). Uptake of the TSPO ligand ^{11}C -DAA1106 has also been reported to be elevated by up to 33 % in AD (Yasuno et al. 2008). The cortical distribution of raised ^{11}C -PK11195 uptake parallels that of the amyloid deposition detected with ^{11}C -PIB PET, a thioflavin marker of fibrillar amyloid load (Edison et al. 2007a). Interestingly, while levels of cortical ^{11}C -PK11195 uptake in AD have been reported to correlate with cognitive impairment rated with the mini-mental state examination (MMSE), there was no correlation between amyloid load and cognitive status (Edison et al. 2007b; Yokokura et al. 2011). This suggests that it may be the cortical microglial activation rather than amyloid plaques in AD that are detrimental to cognitive function, possibly due to cytokine release by these cells. Along with raised cortical ^{11}C -PK11195 signal, activated microglia can also be detected in the thalamus, cerebellum and brainstem of Alzheimer's patients. As these subcortical areas are not targeted by plaques, the ^{11}C -PK11195 signal there is likely to reflect microglial activation either

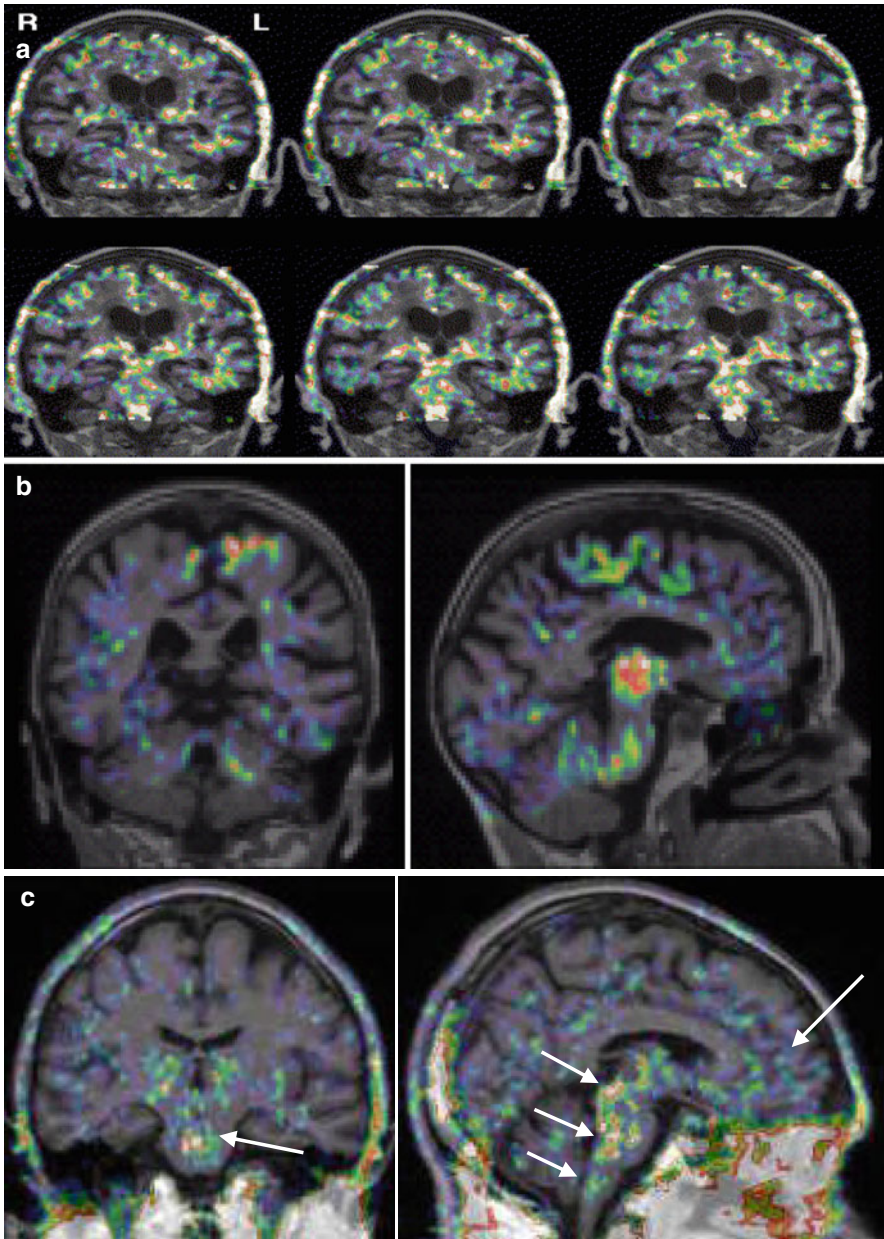


Fig. 22.1 ^{11}C -PK11195 PET images of microglial activation in patients with (a) Alzheimer's disease, (b) motor neurone disease, (c) Parkinson's disease, (d) multiple sclerosis

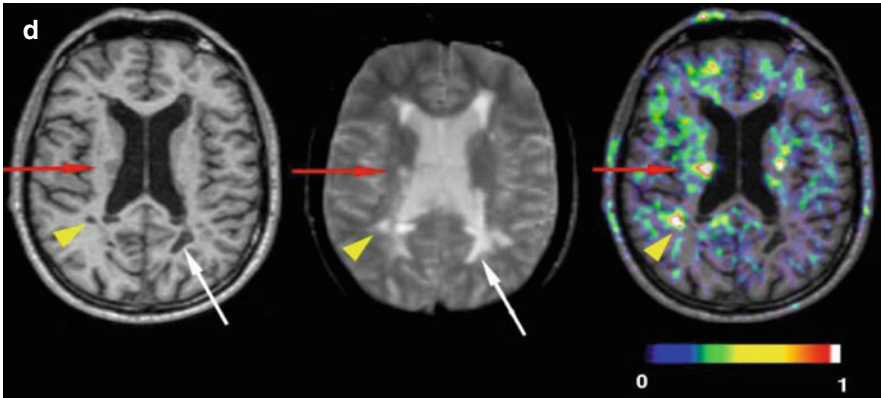


Fig.22.1 (continued)

due to local tangle disease or in response to cortical disconnection, the cells possibly acting to remodel connections.

^{11}C -PK11195 and ^{11}C -DAA1106 PET have also been reported to detect the presence of microglial activation in amnesic mild cognitive impairment (MCI). These subjects have isolated recall problems that are not severe enough to interfere with activities of daily living, but 60 % of these cases progress to develop Alzheimer's disease (Petersen et al. 2001). In one series it was reported that ^{11}C -PK11195 PET detected microglial activation in 40 % of amnesic MCI cases, while 60 % showed evidence of amyloid plaque deposition with ^{11}C -PIB PET (Okello et al. 2009). However, others have failed to detect microglial activation in amnesic MCI with ^{11}C -PK11195 PET (Schuitemaker et al. 2013). When a group of seven MCI cases were studied with ^{11}C -DAA1106 PET, there was a significant mean of 27 % increase in tracer uptake across brain regions, and two cases individually had microglial activation elevated more than 2 SD above the control mean (Yasuno et al. 2012). Five of the seven MCI subjects with ^{11}C -DAA1106 uptake raised more than 0.5 standard deviations above the normal mean progressed to frank dementia over a 2-year follow-up period.

22.4 Inflammation in Frontotemporal Dementia and Motor Neurone Disease

Dementia of the frontotemporal type affects around 10 % of dementia cases, and clinically it typically presents as personality change, praxis and language difficulties with memory becoming impaired later on. The pathology can involve Pick bodies containing three-repeat tau, TDP-43 protein inclusions or spongiform degeneration which targets the frontal and inferior temporal lobes. This dementia is not associated with amyloid plaque formation. A PET series has reported raised frontotemporal uptake of ^{11}C -PK11195 in five FTLD cases (Cagnin et al. 2004).

There is both a clinical and pathological overlap between frontotemporal dementia and motor neurone disease (amyotrophic lateral sclerosis). The neuropathology of

both can be associated with cortical TDP-43 inclusions and spongiform degeneration, and neuropsychological and imaging studies have indicated that dysfunction extends beyond the motor system in ALS. Ten probable or definite (El Escorial criteria) ALS patients and 14 healthy controls have been studied with ^{11}C -PK11195 PET (Turner et al. 2004). Significantly increased microglial activation was seen in the motor cortex, brainstem, thalamus, dorsolateral prefrontal cortex and occipital lobes of the ALS patients – see Fig. 22.1b. There was a significant correlation between ^{11}C -PK11195 uptake in the motor cortex and severity of upper motor neurone signs clinically.

22.5 Parkinsonian Syndromes and TSPO Imaging

Parkinson's disease (PD) is the second most common neurodegenerative disorder after dementia, affecting around 1 % of those over sixties. It manifests as asymmetrical limb bradykinesia, rigidity and tremor, and these symptoms are usually responsive to levodopa. The pathology is characterised by Lewy body inclusions in neurones which contain aggregated alpha-synuclein and neurofilaments.

While the dopamine neurones of the substantia nigra compacta are targeted by the Lewy body pathology, it is now thought that the pathology first affects the dorsal motor nucleus of the vagus in the medulla and then ascends through the brainstem to the cortex in stages (Braak et al. 2004). In stage 2 the locus coeruleus, pedunculopontine nucleus and median raphe in the pons become involved, while the dopamine neurones of the substantia nigra compacta in the midbrain only become targeted in stage 3 along with the cholinergic nucleus basalis. The limbic cortex and cingulate are involved by stage 4 and the association and primary neocortex in stages 5 and 6.

At postmortem microglial activation has been reported to accompany Lewy body pathology in both subcortical and cortical affected regions (Imamura et al. 2003; McGeer et al. 1993). It has been shown *in vitro* that aggregated alpha-synuclein fibrils can stimulate microglial activation, but the relationship between this inflammatory process and disease progression remains uncertain. In an initial PET study, it was reported that levels of increased midbrain ^{11}C -PK11195 uptake in PD correlated with reductions in putamen dopamine transporter (DAT) binding measured with ^{11}C -CFT PET (Ouchi et al. 2005). The authors suggested that this provided evidence for involvement of microglia in the loss of dopaminergic function that characterises PD. Later ^{11}C -PK11195 PET series, however, have failed to detect consistent microglial activation in the substantia nigra of PD cases or to replicate an association between midbrain ^{11}C -PK11195 signals and loss of dopaminergic function in PD. It is conceivable that the dopaminergic drugs used to treat PD may have an influence on the levels of microglial activation. Although none of these agents directly act to suppress microglial activation, it has been suggested that both dopamine agonists and monoamine oxidase B inhibitors have neuroprotective properties (Schapira and Olanow 2004). This claim is, however, controversial, and currently there is no hard evidence that therapy for PD influences levels of the inflammatory response.

Microglial activation is known to be widespread in PD, and raised ^{11}C -PK11195 uptake has been reported in the brainstem, basal ganglia and cortical regions of non-demented cases, regions which are all targeted by Lewy body pathology in later

disease stages – Fig. 22.1c (Gerhard et al. 2006a). We have recently found that levels of striatal ^{11}C -PK11195 uptake in PD correlated with disability rated with the Unified Parkinson's Disease Rating Scale (UPDRS), while impaired verbal fluency was associated with raised frontal and insular ^{11}C -PK11195 activity (Simpson et al. 2012). This suggests that microglial activation may well reflect disease activity and is in line with the dying back theory of PD pathology which suggests that nigrostriatal terminals may become dysfunctional ahead of nigral cell body loss.

The level of ^{11}C -PK11195 uptake appears to remain static over a 2-year follow-up period despite ongoing clinical deterioration and loss of putamen ^{18}F -dopa storage of PD cases (Gerhard et al. 2006a). It has been suggested that microglial activation is an early phenomenon in PD and may act to drive disease progression and superadded dementia that can follow although levels of inflammation remain fixed. In favour of this viewpoint, it was noted that PD cases with late dementia had similar cortical levels of microglial activation to similarly disabled non-demented cases.

Neurodegenerative disorders that are associated with atypical parkinsonian disorders include multiple system atrophy (MSA) and progressive supranuclear palsy (PSP). MSA is associated with asymmetric parkinsonism along with early autonomic dysfunction, postural instability and ataxia. The pathology is characterised by argyrophilic glial cytoplasmic inclusions (GCIs) that contain alpha-synuclein and target the substantia nigra, putamen, pontocerebellar connections and the lateral columns of the spinal cord. Microglial activation is known to be associated with MSA pathology, and ^{11}C -PK11195 PET has revealed raised binding in the putamen, pallidum, pons, substantia nigra and dorsolateral prefrontal cortex at higher levels than that associated with PD (Gerhard et al. 2003).

In a proteolipid protein-alpha-synuclein overexpression (PLP- α SYN) transgenic mouse model of MSA, a correlation between levels of nigral microglial activation and dopamine neurone loss has been reported (Stefanova et al. 2007). Minocycline administration was protective, both suppressing the inflammation and preserving dopamine neurones in the mouse. A human trial was subsequently performed to determine the neuroprotective efficacy of minocycline in MSA. The drug failed clinically to alter disease progression at clinically licensed doses; however, those MSA cases receiving active medication showed a 30 % reduction in brain ^{11}C -PK11195 uptake relative to placebo-treated cases (Dodel et al. 2010).

Three PSP patients have been studied with ^{11}C -PK11195 PET and reported to show significantly increased signal in their caudate nucleus, putamen, pallidum, midbrain, substantia nigra, frontal lobe and cerebellum (Gerhard et al. 2006b). One of these patients was rescanned after 10 months and their level of microglial activation had remained stable.

22.6 Huntington's Disease and Microglial Activation

Huntington's disease is an autosomal dominant inherited progressive neurodegenerative disorder associated with motor, cognitive and psychiatric symptoms. It is associated with an abnormal CAG triplet-repeat expansion of the huntingtin gene

on chromosome 4 which leads to an elongated polyglutamine chain at the terminus of the huntingtin protein. The effect of this is to cause intranuclear aggregations of huntingtin to form resulting in progressive loss of medium spiny striatal GABAergic neurones (Sapp et al. 1997). These neurones express either dopamine D1 or D2 receptors, and so striatal dysfunction can be detected prior to symptom onset as a loss of availability of these sites for ligand binding (Andrews et al. 1999).

The loss of striatal neurones in HD is associated with microglial activation (Sapp et al. 2001) which can potentially be detected with ^{11}C -PK11195 PET. Levels of striatal microglial activation correlate with loss of dopamine D2 receptors measured with ^{11}C -raclopride PET and also with locomotor disability rated with the Unified Huntington's Disease Rating Scale (UHDRS) (Pavese et al. 2006). This suggests that microglial activation may play a role in driving the disease process. In favour of this viewpoint, ^{11}C -PK11195 PET studies have reported raised microglial activation in a majority of asymptomatic adult HD gene carriers (Tai et al. 2007). Those carriers with active disease also showed reduced dopamine D2 binding with ^{11}C -raclopride PET. Cortical microglial activation can also be detected in pre-manifesting HD carriers confirming that this is not a purely basal ganglia disorder (Politis et al. 2011). Levels of striatal ^{11}C -PK11195 uptake have been shown to correlate with the predicted time of clinical disease onset (Politis et al. 2011; Tai et al. 2007).

22.7 Measuring Inflammation in Multiple Sclerosis

Multiple sclerosis (MS) is a disease characterised clinically by relapsing and remitting neurological episodes followed by a progressive phase of disability. Pathologically central inflammatory demyelination is seen as white matter plaques associated with axonal degeneration. MS targets young adults and is the most common cause of non-traumatic disability in the Western world (Compston and Coles 2008). Active plaques of demyelination contain blood-borne B and T lymphocytes and macrophages that have invaded the disrupted blood-brain barrier. However, there is also an intrinsic immune reaction to the disease process manifested as involvement of activated microglia (Benveniste 2007). Postmortem investigations have detected activated microglia not just in white matter plaques but also in the cortex and apparently normal-appearing brain areas (De Groot et al. 2001; Peterson et al. 2001). In progressive MS activated microglia are seen surrounding degenerating myelinated axons (Magliozzi et al. 2010).

^{11}C -PK11195 PET has been used to demonstrate the extent of microglial activation in MS patients – Fig. 22.1d (Banati et al. 2000; Debruyne et al. 2003). PET findings have been validated with ^3H -PK11195 autoradiographic studies on human brain slices which showed that this tracer binds to activated microglia rather than astrocytes or lymphocytes in plaques of demyelination (Banati et al. 2000). PET reveals that not only can raised ^{11}C -PK11195 uptake be seen in active plaques, where there is altered T2 signal and gadolinium enhancement on MRI, but also in normal-appearing white and grey matter (Banati et al. 2000; Debruyne et al. 2003;

Versijpt et al. 2005). This finding supports the hypothesis that in early MS microglial activation may initiate the inflammatory process prior to invasion of the damaged blood-brain barrier by lymphocytes. The activated microglial load at baseline may well be the critical factor when predicting outcome in MS patients (Confavreux et al. 2000). ^{11}C -PK11195 uptake has been reported to be higher in secondary progressive than relapsing-remitting MS. Additionally, a significant correlation was reported between levels of ^{11}C -PK11195 binding in cortical grey matter and locomotor disability in patients with secondary progressive MS (Politis et al. 2012).

TSPO expression in MS has also been examined with ^{11}C -PBR28 PET (Oh et al. 2010). Overall brain ^{11}C -PBR28 uptake was increased in the MS cohort. Focal increases in binding, corresponding to areas of active inflammation and blood-brain barrier breakdown on gadolinium contrast-enhanced magnetic resonance imaging (MRI), were also evident. Increases in ^{11}C -PBR28 binding preceded the appearance of contrast enhancement on magnetic resonance imaging in some lesions, suggesting that glial activation is an early phenomenon in MS lesion formation. Global levels of ^{11}C -PBR28 binding correlated with disease duration but not with locomotor disability.

22.8 Traumatic Brain Injury

Recovery from concussive traumatic brain injury (TBI) is highly variable. With ^{11}C -PK11195 PET it has been demonstrated that an inflammatory response is present in many of these cases years after their original injury. In a recent series ten patients had ^{11}C -PK11195 PET at least 11 months after moderate to severe TBI, and binding was calculated in and around the site of focal brain damage and in selected distant and subcortical brain regions (Ramlackhansingh et al. 2011). Microglial activation was significantly raised in the thalami, putamen, occipital cortices, and posterior limb of the internal capsules after TBI though there was no increase in binding at the original site of the focal brain injury. Levels of thalamic ^{11}C -PK11195 uptake were correlated with impairment on executive tasks but not with either the time since the injury or the amount of structural brain injury. The authors concluded that increased microglial activation can persist up to 17 years after TBI in distant brain areas from the original focal lesion, particularly in subcortical regions. They suggested that a chronic inflammatory response to TBI develops over time and that anti-microglial strategies may still be beneficial months to years after the original insult.

22.9 Stroke and Microglial Activation

Stroke is associated with microglial activation both around the infarct, which develops within hours of the event, but also later in disconnected brain regions including the thalamus and brainstem. In one series six patients were examined with ^{11}C -PK11195 PET between 3 and 150 days after their infarct, and increased microglial activation was present in all the patients examined (Gerhard et al. 2005). In the first 6 days following the stroke, the PET lesions were generally smaller and adjacent to the MRI lesion with little spatial overlap. The size of the local area of microglial

activation then increased over the next month overlapping with the MRI lesion as the blood-brain barrier became disrupted and invasion by macrophages binding ^{11}C -PK11195 alongside local microglial activation occurred. By 6 months after the initial stroke, local microglial activation was subsiding, whereas distant areas of ^{11}C -PK11195 uptake could be seen beyond the primary infarct site into connected areas of the same hemisphere, the thalamus and the brainstem. The cortical area with maximal ^{11}C -PK11195 binding became atrophic during that 6-month interval.

22.10 Psychosis

Both dementia and Parkinson's disease are associated with secondary psychosis related to cortical pathology and possibly the presence of cortical and limbic inflammation that can be detected in these disorders. Schizophrenia is a primary psychosis but has also been reported to be associated with low levels of brain inflammation at postmortem. In a recent series, seven schizophrenic patients in the recovery phase from a psychotic episode were studied with ^{11}C -PK11195 PET (Doorduyn et al. 2009). Conventional T1- and T2-weighted MRI had shown no significant abnormalities. PET revealed a 51 % increase in mean hippocampal and a 30 % increase in global cortical ^{11}C -PK11195 binding in the schizophrenic subjects compared with age-matched cortical controls. Three of the subjects individually showed significantly raised levels of cortical inflammation. Previously, low-level inflammation in the cortex of schizophrenic cases in remission has been reported (van Berckel et al. 2008). The present authors suggested that active episodes of psychosis may be related to an increase in background inflammatory activity.

Conclusions

Microglial activation is a nonspecific reaction to all forms of brain injury and can be detected with PET in inflammatory, vascular, traumatic, degenerative and psychotic brain disorders. The role of activated microglia after stroke and trauma appears to be primarily restorative, the cells adopting a phagocytic phenotype removing debris and remodelling connections. However, in chronic neurodegenerative diseases the role of activated microglia is less certain. Initially these cells could act to ingest misfolded proteins and release growth factors, but in later disease this action could fail and local release of cytokines predominates leading to neuronal death and disease progression. In downstream disconnected areas microglia could have a beneficial action leading to remodelling of connections as an adaptive response.

Currently PET imaging of activated microglia relies in the use of TSPO radioligands. While these provide a valuable *in vivo* tool for detecting disease activity and tracking the progression of neuroinflammation, binding of the newer ligands is influenced by TSPO polymorphisms expressed – 40 % of Caucasians are either non- or mixed-affinity binders. As a consequence, despite its higher nonspecific signal and rapid washout, ^{11}C -PK11195 PET still provides a pragmatic approach for measuring brain inflammation. TSPO imaging does not have diagnostic potential as raised microglial activation is not specific to any one neurological

disorder. However, the early detection of microglia with PET provides a potential biomarker for measuring both disease activity and the efficacy of neuroprotective strategies designed to suppress the inflammatory response to local injury or neurodegenerative processes. In the future hopefully there will be development of both TSPO tracers uninfluenced by the genotype along with other markers of microglial activation, such as cannabinoid CB2 expression, allowing us to improve our understanding of the role of activated microglia in CNS disease.

References

- Anderson AN, Pavese N, Edison P, Tai YF, Hammers A, Gerhard A, Brooks DJ, Turkheimer FE (2007) A systematic comparison of kinetic modelling methods generating parametric maps for [(11)C]-(R)-PK11195. *Neuroimage* 36:28–37
- Andrews TC, Weeks RA, Turjanski N, Gunn RN, Watkins LHA, Sahakian B, Hodges JR, Rosser AE, Wood NW, Brooks DJ (1999) Huntington's disease progression PET and clinical observations. *Brain* 122:2353–2363
- Banati RB (2002a) Brain plasticity and microglia: is transsynaptic glial activation in the thalamus after limb denervation linked to cortical plasticity and central sensitisation? *J Physiol Paris* 96:289–299
- Banati RB (2002b) Visualising microglial activation in vivo. *Glia* 40:206–217
- Banati RB, Myers R, Kreutzberg GW (1997) PK ('peripheral benzodiazepine')-binding sites in the CNS indicate early and discrete brain lesions: microautoradiographic detection of [3H] PK11195 binding to activated microglia. *J Neurocytol* 26:77–82
- Banati RB, Newcombe J, Gunn RN, Cagnin A, Turkheimer F, Heppner F, Price G, Wegner F, Giovannoni G, Miller DH, Perkin GD, Smith T, Hewson AK, Bydder G, Kreutzberg GW, Jones T, Cuzner ML, Myers R (2000) The peripheral benzodiazepine binding site in the brain in multiple sclerosis: quantitative in vivo imaging of microglia as a measure of disease activity. *Brain* 123(Pt 11):2321–2337
- Benveniste EN (2007) Role of macrophages/microglia in multiple sclerosis and experimental allergic encephalomyelitis. *J Molecular Medicine* 75:165–173
- Boche D, Perry VH, Nicoll JA (2013) Activation patterns of microglia and their identification in the human brain. *Neuropathol Appl Neurobiol* 39(1):3–18
- Braak H, Braak E (1997) Frequency of stages of Alzheimer-related lesions in different age categories. *Neurobiol Aging* 18:351–357
- Braak H, Ghebremedhin E, Rub U, Bratzke H, Del Tredici K (2004) Stages in the development of Parkinson's disease-related pathology. *Cell Tissue Res* 318:121–134
- Cagnin A, Brooks DJ, Kennedy AM, Gunn RN, Myers R, Turkheimer FE, Jones T, Banati RB (2001) In-vivo measurement of activated microglia in dementia. *Lancet* 358:461–467
- Cagnin A, Rossor M, Sampson EL, Mackinnon T, Banati RB (2004) In vivo detection of microglial activation in frontotemporal dementia. *Ann Neurol* 56:894–897
- Compston A, Coles A (2008) Multiple sclerosis. *Lancet* 372:1502–1517
- Confavreux C, Vukusic S, Moreau T, Adeleine P (2000) Relapses and progression of disability in multiple sclerosis. *N Engl J Med* 343:1430–1438
- De Groot CJ, Bergers E, Kamphorst W, Ravid R, Polman CH, Barkhof F, van der Valk P (2001) Post-mortem MRI-guided sampling of multiple sclerosis brain lesions: increased yield of active demyelinating and (p)reactive lesions. *Brain* 124:1635–1645
- Debruyne JC, Versijpt J, Van Laere KJ, De Vos F, Keppens J, Strijckmans K, Achten E, Slegers G, Dierckx RA, Korf J, De Reuck JL (2003) PET visualization of microglia in multiple sclerosis patients using [(11)C]PK11195. *Eur J Neurol* 10:257–264
- Dickson DW (1997) The pathogenesis of senile plaques. *J Neuropathol Exp Neurol* 56:321–339

- Dodel R, Spottke A, Gerhard A, Reuss A, Reinecker S, Schimke N, Trenkwalder C, Sixel-Doring F, Herting B, Kamm C, Gasser T, Sawires M, Geser F, Kollensperger M, Seppi K, Kloss M, Krause M, Daniels C, Deuschl G, Böttger S, Naumann M, Lipp A, Gruber D, Kupsch A, Du Y, Turkheimer F, Brooks DJ, Klockgether T, Poewe W, Wenning G, Schade-Brittinger C, Oertel WH, Eggert K (2010) Minocycline 1-year therapy in multiple-system-atrophy: effect on clinical symptoms and [(11)C] (R)-PK11195 PET (MEMSA-trial). *Mov Disord* 25:97–107
- Dolle F, Luus C, Reynolds A, Kassiou M (2009) Radiolabelled molecules for imaging the translocator protein (18 kDa) using positron emission tomography. *Curr Med Chem* 16:2899–2923
- Doorduyn J, de Vries EF, Dierckx RA, Klein HC (2008) PET imaging of the peripheral benzodiazepine receptor: monitoring disease progression and therapy response in neurodegenerative disorders. *Curr Pharm Des* 14:3297–3315
- Doorduyn J, de Vries EF, Willemsen AT, de Groot JC, Dierckx RA, Klein HC (2009) Neuroinflammation in schizophrenia-related psychosis: a PET study. *J Nucl Med* 50:1801–1807
- Edison P, Archer H, Hinz R, Fox N, Kennedy A, Rossor M, Brooks DJ (2007a) Relationship between the distribution of microglial activation and amyloid deposition in Alzheimer's disease: an 11C-PK11195 and 11C-PIB PET study. *J Neurol Neurosurg Psychiatry* 78:219–219
- Edison P, Archer HA, Hinz R, Hammers A, Pavese N, Tai YF, Hotton G, Cutler D, Fox N, Kennedy A, Rossor M, Brooks DJ (2007b) Amyloid, hypometabolism, and cognition in Alzheimer disease – an [11C]PIB and [18F]FDG PET study. *Neurology* 68:501–508
- Gerhard A, Banati RB, Goerres GB, Cagnin A, Myers R, Gunn RN, Turkheimer F, Good CD, Mathias CJ, Quinn N, Schwarz J, Brooks DJ (2003) [(11)C](R)-PK11195 PET imaging of microglial activation in multiple system atrophy. *Neurology* 61:686–689
- Gerhard A, Schwarz J, Myers R, Wise R, Banati RB (2005) Evolution of microglial activation in patients after ischemic stroke: a [(11)C](R)-PK11195 PET study. *Neuroimage* 24:591–595
- Gerhard A, Pavese N, Hotton G, Turkheimer F, Es M, Hammers A, Eggert K, Oertel W, Banati RB, Brooks DJ (2006a) In vivo imaging of microglial activation with [(11)C](R)-PK11195 PET in idiopathic Parkinson's disease. *Neurobiol Dis* 21:404–412
- Gerhard A, Trender-Gerhard I, Turkheimer F, Quinn NP, Bhatia KP, Brooks DJ (2006b) In vivo imaging of microglial activation with [(11)C](R)-PK11195 PET in progressive supranuclear palsy. *Mov Disord* 21:89–93
- Hanisch UK, Kettenmann H (2007) Microglia: active sensor and versatile effector cells in the normal and pathological brain. *Nat Neurosci* 10:1387–1394
- Imamura K, Hishikawa N, Sawada M, Nagatsu T, Yoshida M, Hashizume Y (2003) Distribution of major histocompatibility complex class II-positive microglia and cytokine profile of Parkinson's disease brains. *Acta Neuropathol* 106:518–526
- Kreutzberg GW (1996) Microglia: a sensor for pathological events in the CNS. *Trends Neurosci* 19:312–318
- Magliozzi R, Howell OW, Reeves C, Roncaroli F, Nicholas R, Serafini B, Aloisi F, Reynolds R (2010) A gradient of neuronal loss and meningeal inflammation in multiple sclerosis. *Ann Neurol* 68:477–493
- McGeer P, Kawamata T, Walker DG, Akiyama H, Tooyama I, McGeer EG (1993) Microglia in degenerative disease. *Glia* 7:84–92
- Oh U, Fujita M, Ikonomidou VN, Evangelou IE, Matsuura E, Harberts E, Ohayon J, Pike VW, Zhang Y, Zoghbi SS, Innis RB, Jacobson S (2011) Translocator protein PET imaging for glial activation in multiple sclerosis. *J Neuroimmune Pharmacol* 6(3):354–361
- Okello A, Edison P, Archer HA, Turkheimer FE, Kennedy J, Bullock R, Walker Z, Kennedy A, Fox N, Rossor M, Brooks DJ (2009) Microglial activation and amyloid deposition in mild cognitive impairment: a PET study. *Neurology* 72:56–62
- Ouchi Y, Yoshikawa E, Sekine Y, Futatsubashi M, Kanno T, Ogusu T, Torizuka T (2005) Microglial activation and dopamine terminal loss in early Parkinson's disease. *Ann Neurol* 57:168–175
- Owen DR, Yeo AJ, Gunn RN, Song K, Wadsworth G, Lewis A, Rhodes C, Pulford DJ, Bennacef I, Parker CA, StJean PL, Cardon LR, Mooser VE, Matthews PM, Rabiner EA, Rubio JP (2012) An 18-kDa translocator protein (TSPO) polymorphism explains differences in binding affinity of the PET radioligand PBR28. *J Cereb Blood Flow Metab* 32:1–5

- Papadopoulos V, Baraldi M, Guilarte TR, Knudsen TB, Lacapere JJ, Lindemann P, Norenberg MD, Nutt D, Weizman A, Zhang MR, Gavish M (2006) Translocator protein (18 kDa): new nomenclature for the peripheral-type benzodiazepine receptor based on its structure and molecular function. *Trends Pharmacol Sci* 27:402–409
- Pavese N, Gerhard A, Tai YF, Ho AK, Turkheimer F, Barker RA, Brooks DJ, Piccini P (2006) Microglial activation correlates with severity in Huntington disease: a clinical and PET study. *Neurology* 66:1638–1643
- Petersen RC, Doody R, Kurz A, Mohs RC, Morris JC, Rabins PV, Ritchie K, Rossor M, Thal L, Winblad B (2001) Current concepts in mild cognitive impairment. *Arch Neurol* 58:1985–1992
- Peterson JW, Bo L, Mork S, Chang A, Trapp BD (2001) Transected neurites, apoptotic neurons, and reduced inflammation in cortical multiple sclerosis lesions. *Ann Neurol* 50:389–400
- Politis M, Pavese N, Tai YF, Kiferle L, Mason SL, Brooks DJ, Tabrizi SJ, Barker RA, Piccini P (2011) Microglial activation in regions related to cognitive function predicts disease onset in Huntington's disease: a multimodal imaging study. *Hum Brain Mapp* 32:258–270
- Politis M, Giannetti P, Su P, Turkheimer F, Keihaninejad S, Wu K, Waldman A, Malik O, Matthews PM, Reynolds R, Nicholas R, Piccini P (2012) Increased PK11195 PET binding in the cortex of patients with MS correlates with disability. *Neurology* 79(6):523–530
- Ramlackhansingh AF, Brooks DJ, Greenwood RJ, Bose SK, Turkheimer FE, Kinnunen KM, Gentleman S, Heckemann RA, Gunanayagam K, Gelosa G, Sharp DJ (2011) Inflammation after trauma: microglial activation and traumatic brain injury. *Ann Neurol* 70(3):374–383
- Ransohoff RM, Perry VH (2009) Microglial physiology: unique stimuli, specialized responses. *Ann Rev Immunol* 27:119–145
- Sapp E, Schwarz C, Chase K, Bhide PG, Young AB, Penney J, Vonsattel JP, Aronin N, DiFiglia M (1997) Huntingtin localization in brains of normal and Huntington's disease patients. *Ann Neurol* 42:604–612
- Sapp E, Kegel KB, Aronin N, Hashikawa T, Uchiyama Y, Tohyama K, Bhide PG, Vonsattel JP, DiFiglia M (2001) Early and progressive accumulation of reactive microglia in the Huntington disease brain. *J Neuropathol Exp Neurol* 60:161–172
- Schapira AH, Olanow CW (2004) Neuroprotection in Parkinson disease: mysteries, myths, and misconceptions. *JAMA* 291:358–364
- Schuitemaker A, Kropholler MA, Boellaard R, van der Flier WM, Kloet RW, van der Doef TF, Knol DL, Windhorst AD, Luurtsema G, Barkhof F, Jonker C, Lammertsma AA, Scheltens P, van Berckel BN (2013) Microglial activation in Alzheimer's disease: an (R)-[(1)(1)C]PK11195 positron emission tomography study. *Neurobiol Aging* 34:128–136
- Simpson BS, Pavese N, Ramlackhansingh AF, Breen DP, Barker RA, Brooks DJ (2012) Clinical correlates of brain inflammation in Parkinson's disease: a PET study. *Mov Disord* 27:775
- Stefanova N, Reindl M, Neumann M, Kahle PJ, Poewe W, Wenning GK (2007) Microglial activation mediates neurodegeneration related to oligodendroglial alpha-synucleinopathy: implications for multiple system atrophy. *Mov Disord* 22:2196–2203
- Tai YF, Pavese N, Gerhard A, Tabrizi SJ, Barker RA, Brooks DJ, Piccini P (2007) Microglial activation in presymptomatic Huntington's disease gene carriers. *Brain* 130:1759–1766
- Turner MR, Cagnin A, Turkheimer FE, Miller CC, Shaw CE, Brooks DJ, Leigh PN, Banati RB (2004) Evidence of widespread cerebral microglial activation in amyotrophic lateral sclerosis: an [11C](R)-PK11195 positron emission tomography study. *Neurobiol Dis* 15:601–609
- van Berckel BN, Bossong MG, Boellaard R, Kloet R, Schuitemaker A, Caspers E, Luurtsema G, Windhorst AD, Cahn W, Lammertsma AA, Kahn RS (2008) Microglia activation in recent-onset schizophrenia: a quantitative (R)-[11C]PK11195 positron emission tomography study. *Biol Psychiatry* 64:820–822
- Varnum MM, Ikezu T (2012) The classification of microglial activation phenotypes on neurodegeneration and regeneration in Alzheimer's disease brain. *Arch Immunol Ther Exp (Warsz)* 60:251–266
- Versijpt J, Debruyne JC, Van Laere KJ, De Vos F, Keppens J, Strijckmans K, Achten E, Slegers G, Dierckx RA, Korf J, De Reuck JL (2005) Microglial imaging with positron emission

tomography and atrophy measurements with magnetic resonance imaging in multiple sclerosis: a correlative study. *Mult Scler* 11:127–134

Yasuno F, Ota M, Kosaka J, Ito H, Higuchi M, Doronbekov TK, Nozaki S, Fujimura Y, Koeda M, Asada T, Suhara T (2008) Increased binding of peripheral benzodiazepine receptor in Alzheimer's disease measured by positron emission tomography with [11C]DAA1106. *Biol Psychiatry* 64:835–841

Yasuno F, Kosaka J, Ota M, Higuchi M, Ito H, Fujimura Y, Nozaki S, Takahashi S, Mizukami K, Asada T, Suhara T (2012) Increased binding of peripheral benzodiazepine receptor in mild cognitive impairment-dementia converters measured by positron emission tomography with [(11)C]DAA1106. *Psychiatry Res* 203:67–74

Yokokura M, Mori N, Yagi S, Yoshikawa E, Kikuchi M, Yoshihara Y, Wakuda T, Sugihara G, Takebayashi K, Suda S, Iwata Y, Ueki T, Tsuchiya KJ, Suzuki K, Nakamura K, Ouchi Y (2011) In vivo changes in microglial activation and amyloid deposits in brain regions with hypometabolism in Alzheimer's disease. *Eur J Nucl Med Mol Imaging* 38:343–351

Imaging of the Serotonin System: Radiotracers and Applications in Memory Disorders

23

Gitte Moos Knudsen and Steen G. Hasselbalch

Contents

23.1	Introduction	670
23.1.1	5-HT Targets for PET and SPECT	670
23.2	Current Radioligands for In Vivo Brain Imaging of the 5-HT System	671
23.2.1	5-HT _{1A} Receptor	671
23.2.2	5-HT _{1B} Receptor	672
23.2.3	5-HT _{2A} Receptor	672
23.2.4	5-HT _{2B} and 5-HT _{2C} Receptors	673
23.2.5	5-HT ₃ Receptors	673
23.2.6	5-HT ₄ Receptors	673
23.2.7	5-HT ₅ Receptors	674
23.2.8	5-HT ₆ Receptors	674
23.2.9	5-HT ₇ Receptors	675
23.2.10	SERT	675
23.3	PET Imaging of the Serotonergic System in Alzheimer's Disease	676
23.3.1	5-HT _{1A} Receptor in AD	677
23.3.2	5-HT _{2A} Receptor Binding in AD	677
23.3.3	5-HT ₄ Receptor Binding in AD	678
23.3.4	5-HT ₆ Receptor Binding in AD	679
23.3.5	SERT Binding in AD	679
23.4	Can Serotonergic Dysfunction Explain AD Symptomatology?	680
	References	681

G.M. Knudsen (✉)

Neurobiology Research Unit, Center for Integrated Molecular Brain Imaging, Rigshospitalet, University of Copenhagen, Blegdamsvej 9, Copenhagen DK-2100, Denmark
e-mail: gmk@nru.dk

S.G. Hasselbalch

Neurobiology Research Unit, Center for Integrated Molecular Brain Imaging, Rigshospitalet, University of Copenhagen, Blegdamsvej 9, Copenhagen DK-2100, Denmark

Memory Disorders Research Group, Department of Neurology, Neuroscience Center, Danish Dementia Research Center, Copenhagen University Hospital, Rigshospitalet, University of Copenhagen, Copenhagen, Denmark

Abstract

The serotonergic system plays a key modulatory role in the brain and is the target for many drug treatments for brain disorders either through reuptake blockade or via interactions at the 14 subtypes of serotonin (5-HT) receptors. This chapter provides the current status of radioligands used for positron emission tomography (PET) and single-photon emission computerised tomography (SPECT) imaging of the human brain 5-HT receptors and the 5-HT transporter (SERT) with particular emphasis on the applications in Alzheimer's disease (AD).

Currently available radioligands for in vivo brain imaging of the 5-HT system in humans include radiolabelled compounds for the 5-HT_{1A}, 5-HT_{1B}, 5-HT_{2A}, 5-HT₄ and to some extent 5-HT₆ receptors, and for SERT. Imaging of serotonergic targets in humans has given invaluable insight into the normal brain function and into brain disorders where the serotonergic system is perturbed. One example of the latter is given here.

Imaging studies show that the 5-HT_{1A} receptor binding is increased and 5-HT_{2A} receptor binding is decreased in mild cognitive impairment (MCI). In early AD, 5-HT₄ receptor binding is increased, whereas in early and more advanced AD, SERT and the 5-HT_{1A} and 5-HT_{2A} receptor binding is reduced in a region-specific manner. Future studies should focus on the association between serotonergic dysfunction and symptomatology in order to increase our understanding of the neurobiological background for neuropsychiatric symptoms in neurodegenerative and neuropsychiatric disorders.

23.1 Introduction

The serotonergic (5-HT) system plays a key modulatory role in many brain functions. The serotonin transporter and 14 serotonergic receptor subtypes result in a complex pattern of modulatory control over various physiological, emotional and cognitive processes. These include, e.g. mood, sleep, diurnal rhythms, cognition, learning, memory and appetite. Serotonergic dysfunction has been implicated in the aetiology of many psychiatric and neurological disorders, e.g. affective disorders, anxiety, schizophrenia, Alzheimer's disease, migraine and epilepsy. The development of in vivo brain imaging techniques, such as positron emission tomography (PET) and single-photon emission computerised tomography (SPECT), increasingly allows the study of the serotonergic system in the human brain; for review, see Jones and Rabiner (2012) and Paterson et al. (2013).

This review covers the current status of which PET and SPECT radioligands are available for imaging serotonergic targets within the brain. Secondly, as an example of one of the applications of PET imaging, the current knowledge about disturbances of the serotonergic system in Alzheimer's disease is given.

23.1.1 5-HT Targets for PET and SPECT

The 5-HT receptors are amongst the most diverse group of neurotransmitter receptors in the human genome, and the 5-HT system is also one of the

phylogenetically oldest systems. Currently, 14 structurally and pharmacologically distinct mammalian 5-HT receptor subtypes have been described. Based on their structure, affinity for different ligands and second messenger pathway, they are assigned to one of seven families, 5-HT₁₋₇ (Hoyer et al. 2002). All 5-HT receptors, except the 5-HT₃ receptor, are G-protein-coupled seven transmembrane spanning receptors (GPCRs). The 5-HT₃ receptor is a ligand-gated sodium ion channel. In addition, the 5-HT transporters (SERTs) responsible for 5-HT reuptake and 5-HT synthetic enzymes, especially tryptophan hydroxylase, are also targets for tracer development. Significant discoveries of the 5-HT system in the human brain have been made following the development of selective PET and SPECT radioligands, some examples are given in a recent review (Jones and Rabiner 2012).

23.2 Current Radioligands for In Vivo Brain Imaging of the 5-HT System

A multitude of radioligands exist for in vitro studies of serotonergic targets, and over the last decade, we have seen an impressive increase in the number of useful PET and SPECT radioligands. Published PET and SPECT radioligands for imaging the serotonergic system have recently been extensively reviewed (Paterson et al. 2013), but here, we will only summarise some of the to date most utilised radiotracers.

23.2.1 5-HT_{1A} Receptor

The 5-HT_{1A} receptor is one of the best characterised receptors in the serotonergic family; its role as an inhibitory autoreceptor in the raphe nuclei and the possible implications of this role for the treatment of depression and anxiety with serotonin reuptake inhibitors are well known (King et al. 2008).

Many of the 5-HT_{1A} radioligands were based on WAY-100635 (*N*-[2-[4-(2-methoxyphenyl)piperazin-1-yl]ethyl]-*N*-pyridin-2-ylcyclohexanecarboxamide), which in its *carbonyl*-¹¹C-labelled form is widely used for 5-HT_{1A} receptor imaging. Currently, four radioligands are used for PET studies of the 5-HT_{1A} receptor in humans: [*carbonyl*-¹¹C]WAY-100635, [¹⁸F]MPPF, [¹⁸F]FCWAY and [¹¹C]CUMI-101. [*carbonyl*-¹¹C]WAY-100635 is so far the most widely used 5-HT_{1A} receptor radioligand. It has a high target to background ratio, but its fast systemic metabolism makes it difficult to quantify accurately. [¹⁸F]MPPF has the advantage of the longer lived ¹⁸F-label, and it also selectively labels the 5-HT_{1A} receptors with a low non-specific binding. Its major disadvantage is its low brain uptake. [¹⁸F]FCWAY is rarely used, probably because of issues with defluorination of the parent compound which leads to high bone uptake of radioactivity (Ryu et al. 2007). [¹¹C]CUMI-101 is a high-affinity 5-HT_{1A} (partial) agonist radioligand that displays high specific binding and seems suitable for imaging the high-affinity site within the human brain (Milak et al. 2008; Pinborg et al. 2012).

23.2.2 5-HT_{1B} Receptor

The 5-HT_{1B} receptor is of particular interest in relation to obesity (Halford et al. 2007) and migraine (Tfelt-Hansen 2012). No less than two PET radiotracers for imaging the 5-HT_{1B} receptor have recently been introduced for use in humans: [¹¹C]AZ10419369 and [¹¹C]P943. [¹¹C]AZ10419369 (5-methyl-8-(4-[¹¹C]methyl-piperazin-1-yl)-4-oxo-4*H*-chromene-2-carboxylic acid(4-morpholin-4-yl-phenyl)-amide) is a 5-HT_{1B} partial agonist used in humans (Varnas et al. 2011); it has a slow systemic metabolism. The high-affinity 5-HT_{1B} antagonist radioligand, [¹¹C]P943 (*R*-1-[4-(2-methoxyisopropyl)-phenyl]-3-[2-(4-methyl-piperazin-1-yl)benzyl]-pyrrolidin-2-one), also shows good properties for quantification in the human brain (Gallezot et al. 2010). For both radiotracers, it seems that cerebellum constitutes an acceptable reference region, and from studies in non-human primates, there is some evidence that the radiotracers are sensitive to displacement by endogenous 5-HT (Finnema et al. 2010; Ridler et al. 2011). The first normative healthy individual studies are now emerging (Savli et al. 2012), and an 8 % decline in 5-HT_{1B} receptor binding per decade, but no gender-related differences, has been reported (Matuskey et al. 2012).

23.2.3 5-HT_{2A} Receptor

5-HT_{2A} receptors are of interest for many reasons: they are a primary target of psychedelic compounds (Lee and Roth 2012), contribute to the efficacy of antipsychotic medications and are involved in the aetiology or treatment of various psychiatric disorders (Leysen 2004).

Several different radioligands for imaging the brain 5-HT_{2A} receptor have successfully been used in human PET studies, e.g. [¹⁸F]altanserin; [¹⁸F]setoperone; [¹¹C]NMSP; [¹¹C]MDL 100,907; and [¹¹C]Cimbi-36. In addition, the SPECT-tracer [¹²³I]-R91150 is used in imaging studies, but the radiotracer displays a lower signal-to-noise ratio compared to the available PET radioligands.

Despite its lipophilic radiometabolite, [¹⁸F]altanserin continues to be the most widely used PET radiotracer. One of the reasons for this is that ¹⁸F-labelling – because of the longer half-life – facilitates the application of a bolus/infusion paradigm that in turn enables subtraction of the lipophilic brain metabolite (Pinborg et al. 2003). Imaging data obtained from [¹⁸F]altanserin binding in the human brain are highly reproducible (Haugbol et al. 2007), and the large number of publications based on this radioligand provides a convenient reference for new findings.

[¹¹C]NMSP (*N*-methylspiperone, 8-[4-(4-fluorophenyl)-4-oxobutyl]-2-methyl-4-phenyl-2,4,8-triazaspiro[4.5]decan-1-one) is a dual D₂/5-HT₂ receptor ligand. As [¹⁸F]setoperone, NMSP has high affinity for both receptors, but since the density of D₂ receptors is low and that of 5-HT₂ receptors is high in the cortical brain regions, then the majority of specific binding in neocortex is due to 5-HT₂ receptor binding. For subcortical brain regions, the reverse is true (Lyon et al. 1986). [¹¹C]NMSP has been used primarily as an imaging tool to visualise D₂ receptor binding in the striatum but was also used in early PET studies to estimate changes in cortical 5-HT₂

receptor binding in, for example, aging (Wong et al. 1984). At that time, the more selective PET radioligand, [^{18}F]altanserin, had not yet been fully developed.

The radioligand [^{18}F]setoperone (6-[2-[4-(4-[^{18}F]fluorobenzoyl)piperidin-1-yl]ethyl]-7-methyl-2,3-dihydro-[1,3]thiazolo[3,2-a]pyrimidin-5-one) is less selective than [^{18}F]altanserin and is being used less and less, perhaps due to its lack of specificity for the 5-HT_{2A} receptors.

Following the positive validation studies, [^{18}F]altanserin was used to determine changes in 5-HT_{2A} receptor density in relation to aging (Erritzoe et al. 2009), and a database of 5-HT_{2A} receptor binding in healthy volunteers was published (Adams et al. 2004), and it has been reported that binding in healthy subjects correlates with the body mass index (Erritzoe et al. 2009) but does not vary with gender (Frokjaer et al. 2009). Furthermore, twin studies have shown that [^{18}F]altanserin binding is strongly genetically determined (Pinborg et al. 2008).

Based on *in vitro* data (Kristiansen et al. 2005), [^{11}C]MDL 100,907 is more selective for the 5-HT_{2A} receptor than [^{18}F]altanserin, but it is questionable if this has any practical implications because of the scarcity of 5-HT_{2B} and to some extent 5-HT_{2C} receptors, and in any instance, [^{11}C]MDL 100,907 is much less widely used as a 5-HT_{2A} receptor radioligand than [^{18}F]altanserin. The reason for this could be that arterial blood sampling is required for correct quantification of [^{11}C]MDL 100,907 (Talbot et al. 2012). Another promising radioligand is [^{11}C]Cimbi-36 (Ettrup et al. 2011) which is the first 5-HT_{2A} receptor agonist radioligand that has proven successful in humans (personal communication).

23.2.4 5-HT_{2B} and 5-HT_{2C} Receptors

To date, it is questionable if 5-HT_{2B} receptors are expressed in the brain in sufficient amounts to allow for imaging. This is not the case for 5-HT_{2C} receptors, but currently, all radiolabelled 5-HT_{2C} receptor ligands have shared pharmacology with other receptors. No radiotracers have been developed for SPECT or PET imaging of 5-HT_{2B} or 5-HT_{2C} receptors.

23.2.5 5-HT₃ Receptors

Despite a number of research centres undertaking a concerted effort to develop 5-HT₃-selective PET and SPECT tracers, it seems that the very discrete localisation and relatively low levels of 5-HT₃ receptors that are localised with highest densities in the brainstem (Parker et al. 1996) make it a very difficult target to image *in vivo*.

23.2.6 5-HT₄ Receptors

5-HT₄ receptors are involved in learning and memory and are potential targets for the treatment of Alzheimer's disease (for a review, see (Bockaert et al. 2004)). So

far, there is one PET ligand, [^{11}C]SB207145 (8-amino-7-chloro-(*N*-[^{11}C]methyl-4-piperidylmethyl)-1,4-benzodioxan-5-carboxylate), that has been successfully evaluated in humans.

The 5-HT₄ receptor antagonist SB207145 was initially radiolabelled with C-11 (Gee et al. 2008) and evaluated for its potential as a PET radioligand for 5-HT₄ imaging. [^{11}C]SB207145 was subsequently successfully quantified for use in human brain studies (Marner et al. 2009). In this study, a comprehensive quantification of the binding of [^{11}C]SB207145 to cerebral 5-HT₄ receptors in the human brain *in vivo* was further provided. Distribution volumes and binding potentials of [^{11}C]SB207145 showed good test–retest reproducibility and time stability. The blocking study with piboserod confirmed that the cerebellum is a suitable reference region devoid of specific binding and that reference tissue models apply. Subsequently, it was shown that [^{11}C]SB207145 is not to any significant degree displaceable by acutely increased levels of endogenous 5-HT (Marner et al. 2010), but cautions need to be taken to ensure that the injected mass of SB207145 does not exceed 4.5 μg (Madsen et al. 2011c). That is, [^{11}C]SB207145 can be used for quantitative PET measurements of 5-HT₄ receptors in the human brain, and normative data on age- and sex-related variations have been published (Madsen et al. 2011b).

23.2.7 5-HT₅ Receptors

The 5-HT₅ receptor has two subtypes, the 5-HT_{5A} and the 5-HT_{5B} receptors. The 5-HT_{5A} receptor has been identified in the human brain, but the 5-HT_{5B} receptor is not expressed in humans because the coding sequence is interrupted by stop codons (Nelson 2004). The 5-HT_{5A} receptor shows a particularly high presence in raphe and other brainstem and pons nuclei (Volk et al. 2010). There are no available radioligands for either of the 5-HT₅ receptors.

23.2.8 5-HT₆ Receptors

5-HT₆ receptors are found exclusively in the CNS and are predominantly expressed in the striatum, limbic system and cortex (Woolley et al. 2004). They are of particular interest because of their involvement in learning and memory (King et al. 2008). So far, only one non-selective radioligand for PET imaging of the 5-HT₆ receptor has made its way into humans, namely, [^{11}C]GSK215083 (3-[(3-fluorophenyl)sulfonyl]-8-(4-[^{11}C]methyl-1-piperazinyl)quinoline (Parker et al. 2012). GSK215083 has high affinity for 5-HT₆ (*in vitro* K_i , 0.16 nM) but also has high 5-HT_{2A} affinity (*in vitro* K_i , 0.79 nM). However, the differential localisation of 5-HT_{2A} and 5-HT₆ receptors (predominantly cortical and striatal, respectively) combined with the ~5-fold difference in affinity means that discrimination between these two receptor types can be done to some extent.

23.2.9 5-HT₇ Receptors

Several research centres are attempting to develop 5-HT₇-selective PET and SPECT tracers, but so far, these efforts have not resulted in a radiotracer that has been taken into humans.

23.2.10 SERT

SERT is the serotonin transporter and it receives considerable interests, not the least due to the success of its inhibitors in the treatment of depression and anxiety disorders. Several PET and SPECT ligands have been developed for this purpose and a detailed review of SERT imaging by PET and SPECT can be found in Huang et al. (2010).

Initially, images of SERT in the human brain came from the non-selective cocaine derivative SPECT ligand [¹²³I]β-CIT and later with the selective but kinetically irreversible PET ligand [¹¹C](+)McN5652. Today, the most successful line of SERT radioligands are those developed from diarylsulfides such as [¹²³I]ADAM, and especially [¹¹C]MADAM, and [¹¹C]DASB.

The currently most appropriate SPECT radioligand for SERT imaging is [¹²³I]ADAM (2-((2-((dimethylamino)methyl)phenyl)thio)-5-iodophenylamine), which is potent, selective and has a high target to background ratio in human studies (Newberg et al. 2004). Quantification of the SERT binding with [¹²³I]ADAM SPECT is most often done with a ratio method, based on data acquired from 200 to 240 min. This has, however, been shown to overestimate the specific binding by about 10 %. The most reliable outcome is based on a 0–120 min SPECT acquisition followed by Logan non-invasive modelling (Frokjaer et al. 2008).

The first selective PET radioligand for imaging SERT in the human brain was [¹¹C](+)McN5652 (*trans*-1,2,3,5,6,10-β-hexahydro-6-[4-(methylthio)phenyl]pyrrolo-[2,1-*a*]isoquinoline) (Szabo et al. 1995). Its use has been limited by a relatively low target to background ratio in vivo, as well as a slow brain uptake and irreversible kinetics that complicate quantification in high binding regions (Frankle et al. 2004). Despite this, [¹¹C](+)McN5652 PET has been used to investigate SERT binding in humans in more than 20 published studies (Pubmed November 2012).

[¹¹C]DASB (3-amino-4-(2-dimethylamino-methyl-phenylsulfanyl)-benzonitrile) is one of a series of ¹¹C-labelled arylthiobenzylamines developed by Wilson and Houle (1999). [¹¹C]DASB displays good selectivity and high affinity and is to date the most widely used radiotracer for in vivo imaging of SERT, with more than 150 hits on Pubmed. [¹¹C]DASB PET can be quantified with reference tissue models (Ginovart et al. 2001); this is the most frequently used way of quantifying [¹¹C]DASB. Furthermore, test–retest data showed high reproducibility and reliability (Kim et al. 2006). [¹¹C]DASB PET normative data are available (Erritzoe et al. 2009, 2010), and apart from a multitude of patient studies, it has also been used to measure SERT occupancy at clinical doses of selective reuptake inhibitors, e.g. citalopram and paroxetine (Meyer et al. 2004).

[¹¹C]MADAM (*N,N*-dimethyl-2-(2-amino-4-methylphenylthio)-benzylamine) is yet another PET radioligand that has made its way into humans (Lundberg et al. 2005). When done several weeks apart, test–retest reproducibility of [¹¹C]MADAM is excellent (Lundberg et al. 2006). As for [¹¹C]DASB, [¹¹C]MADAM has been used to estimate relative SERT occupancy of citalopram and escitalopram (Lundberg et al. 2007) and to investigate the relationship between 5-HT_{1A} and SERT binding in healthy young men and women (Henningsson et al. 2009; Jovanovic et al. 2008). [¹¹C]DASB and [¹¹C]MADAM thus seem comparable in terms of their pharmacological and kinetic profile.

The primary reason why new radioligands are still being developed is that the low density of SERT-binding sites in the neocortex is challenging for accurate measurement and it would also be valuable to have an ¹⁸F-labelled SERT radioligand.

23.3 PET Imaging of the Serotonergic System in Alzheimer's Disease

As an example of the application of PET imaging in neurology and psychiatry, studies of the serotonergic system in Alzheimer's disease (AD) will be reviewed in this section. With increasing incidence and prevalence worldwide, AD presents a unique challenge to researchers in order to provide better diagnostic tools, as well as a better understanding of the pathophysiology of the disease. Biomarkers such as medial temporal lobe atrophy on magnetic resonance imaging, glucose metabolism measured with PET or beta-amyloid and tau in cerebrospinal fluid become increasingly incorporated into the diagnostic process (Dubois et al. 2010). Therefore, the focus of neuroreceptor imaging with PET has changed in the direction of better understanding of the pathophysiology behind the symptomatology of AD (Xu et al. 2012). The ultimate goal of this research is better and more specific treatment options.

Postmortem and clinical studies have shown widespread dysfunction of the serotonergic transmitter system in AD. Thus, postmortem brain studies have consistently found significant loss of serotonin-producing neurons or reductions in the presynaptically located serotonin transporter (SERT) in the raphe nuclei (Aletrino et al. 1992; Halliday et al. 1992; Hendricksen et al. 2004; Tejani-Butt et al. 1995) and in serotonergic neuronal projections (Tejani-Butt et al. 1995; Thomas et al. 2006; Tsang et al. 2003). Also, in several postmortem studies, postsynaptic receptor subtypes have been found reduced: 5-HT_{1A} (Lai et al. 2003b), 5-HT_{1B} (Garcia-Alloza et al. 2004), 5-HT_{2A} (Bowen et al. 1989; Cheng et al. 1991; Lai et al. 2005; Lorke et al. 2006) and 5-HT₆ receptors (Lorke et al. 2006). Since serotonergic dysfunction and neuropsychiatric symptoms have been linked to mood disorders, disturbances in the serotonergic system could be related to the presence of neuropsychiatric symptoms in AD. This would be especially relevant for depressive symptoms, which are frequent in AD (Ballard et al. 1996; Lyketsos et al. 2002). Serotonin may, however, also play a role in normal cognitive functions (for review, see Schmitt and co-workers (Schmitt et al. 2006)). More recently, the involvement of

serotonin in cognition has further been substantiated by studies in healthy young subjects, showing an association between high SERT binding in fronto-striatal regions and better performance on tasks involving executive function and logical reasoning (Madsen et al. 2011a) and an inverse association between 5-HT₄ receptor binding in the hippocampus and memory performance (Haahr et al. 2013). Thus, serotonergic dysfunction could partly be responsible for not only neuropsychiatric symptomatology but also cognitive impairment in patients with AD.

23.3.1 5-HT_{1A} Receptor in AD

Using [¹⁸F]MPPF, Kepe and co-workers found significant reductions in 5-HT_{1A} receptor densities in both the hippocampus and raphe nuclei in patients with mild cognitive impairment (MCI) (24 %) and AD patients (49 %) (Kepe et al. 2006). They interpreted their findings as secondary to neocortical degeneration of synapses and neurons, because a positive association of 5-HT_{1A} receptor binding with glucose metabolism was found in the hippocampus. Further, 5-HT_{1A} receptor binding was negatively correlated with [¹⁸F]FDDNP, a marker of tau pathology (Kepe et al. 2006). Interestingly, using the same tracer, Truchot and co-workers found a biphasic change in 5-HT_{1A} receptor binding in the hippocampus, parahippocampus and inferior temporal cortex with upregulation in MCI and a marked reduction (approx. 50 %) in AD (Truchot et al. 2007) which may suggest a compensatory upregulation due to lower serotonin levels in the pre-dementia stage of AD. Following this upregulation, 5-HT_{1A} receptor binding may eventually decrease in early to moderate stages of AD due to neurodegeneration, as suggested by Kepe et al. (2006).

23.3.2 5-HT_{2A} Receptor Binding in AD

Several studies have found widespread reduction in 5-HT_{2A} receptor binding in mild to moderate AD. Using PET and [¹⁸F]setoperone in patients with AD, Blin and colleagues found a 35–69 % reduction in temporoparietal cortical 5-HT₂ receptor binding (Blin et al. 1993). In a similar patient group (mean MMSE 20), but using [¹⁸F]altanserin, Meltzer and colleagues found reductions of approximately 30 % in the anterior cingulate, prefrontal and sensorimotor cortices (Meltzer et al. 1999). In two consecutive [¹⁸F]altanserin studies in MCI and AD patients, these findings were corroborated by widespread neocortical reductions in receptor binding (MCI: 22–29 % and AD: 28–39 %) (Hasselbalch et al. 2008; Marner et al. 2011). Importantly, all three [¹⁸F]altanserin studies employed correction for partial volume error due to atrophy, and atrophy did not explain the findings.

In contrast to the 5-HT_{1A} receptor findings above, the reductions in 5-HT_{2A} receptor are widespread and occur early in the course of the disease (Hasselbalch et al. 2008), but the reason for this reduction is largely unexplained. It is unlikely that loss of serotonergic neurons projecting to neocortex has any major impact on the post-synaptic 5-HT_{2A} receptor reductions, since reductions in 5-HT_{2A} receptors are not

accompanied by similar reductions in presynaptic serotonin transporter binding (Marner et al. 2012). One plausible explanation for the diffused neocortical 5-HT_{2A} receptor reductions could be that local AD pathology, especially in the form of widespread beta-amyloid accumulation, is responsible for the reduction in 5-HT_{2A} receptors. Beta-amyloid accumulation has a spatial distribution similar to the reduction in 5-HT_{2A} receptor binding, whereas neurodegeneration in the form of tau accumulation follows a different pattern (Braak and Braak 1991). As an indirect support of the proposed beta-amyloid/5HT_{2A} receptor association, Marner and co-workers found a nonsignificant 5–10 % reduction in ¹⁸F-altanserin binding in neocortical regions in a 2-year follow-up study of 15 MCI patients (Marner et al. 2011). This reduction inversely mirrors the small increase in beta-amyloid accumulation found in early AD in most studies (Jack et al. 2010). Further, experimental studies have shown an association between increased beta-amyloid load and decreased 5-HT_{2A} receptor binding (Christensen et al. 2008; Holm et al. 2010). Thus, 5-HT_{2A} receptor may be especially sensitive to beta-amyloid pathology, but the nature of this interaction needs to be clarified in future studies.

23.3.3 5-HT₄ Receptor Binding in AD

The 5-HT₄ receptor is especially interesting in AD as it is both linked to memory function and beta-amyloid accumulation. There is ample evidence for pro-cognitive actions of agonists to the 5-HT₄ receptor. Thus, in animals, pre-task systemic injections of 5-HT₄ receptor agonists have shown to improve performance in a variety of memory tasks such as olfactory associative learning (Marchetti et al. 2000; Marchetti-Gauthier et al. 1997), place and object recognition (Lamirault and Simon 2001), the Morris water maze (Lelong et al. 2001), and matching-to-sample (Terry et al. 1998). In the only study in healthy humans, using [¹¹C]SB207145 and Rey's Auditory Verbal Learning Test in healthy young subjects, Haahr and co-workers found significant negative associations between the immediate and delayed recall scores and hippocampal 5-HT₄ receptor binding (Haahr et al. 2013). This paradoxical finding was explained by upregulation of 5-HT₄ receptor levels to partially compensate for lower hippocampal 5-HT levels in subjects with poorer memory function (Haahr et al. 2013). In early AD, Madsen and co-workers found some support for this hypothesis: In mild stage AD patients, beta-amyloid imaging with [¹¹C]PiB and 5-HT₄ receptor imaging using [¹¹C]SB207145 was performed in the same subjects (Madsen et al. 2011d). PiB-positive individuals had 13 % higher 5-HT₄ receptor binding compared to PiB-negative individuals. The 5-HT₄ receptor binding was positively correlated to beta-amyloid burden and negatively to the MMSE score (Mini-Mental State Examination - a measure of global cognitive function) of the AD patients. These findings suggest that cerebral 5-HT₄ receptor upregulation starts at a preclinical stage of AD and continues while dementia is still at a mild stage, which contrasts other receptor subtypes. As in the study of healthy subjects mentioned above, it was speculated that the upregulation was a compensatory effect of decreased levels of interstitial 5-HT in early AD (Madsen et al. 2011d). Further,

agonism of the 5-HT₄ receptor increases alpha-secretase activity and thus promotes non-amyloidogenic degradation of the amyloid precursor protein (APP) (Cachard-Chastel et al. 2007). Therefore, an upregulation of the 5-HT₄ receptor level in early AD may serve to counteract beta-amyloid accumulation, but further studies are needed to elucidate these rather speculative interactions.

23.3.4 5-HT₆ Receptor Binding in AD

The 5-HT₆ receptor has been implicated in memory functions, as 5-HT₆ antagonism can reverse scopolamine-induced episodic memory dysfunction (de Bruin et al. 2011), although the effect may be strongest for working memory and aversive learning (Da Silva Costa-Aze et al. 2012). The pro-cognitive effects of 5-HT₆ antagonism are currently investigated in clinical trials of mild-to-moderate AD (Maher-Edwards et al. 2010). In the postmortem AD brains, reductions in 5-HT₆ binding have been found in frontal as well as temporal cortical areas (Garcia-Alloza et al. 2004; Lorke et al. 2006). As described above, a PET tracer for the 5-HT₆ receptor is currently being evaluated (Parker et al. 2012), but so far, no human studies (in healthy subjects or in AD) have been published.

23.3.5 SERT Binding in AD

As described above, several studies in the postmortem AD brains have shown significant losses of serotonin-producing neurons or reductions in the presynaptically located SERT in the raphe nuclei and in serotonergic neuronal projections (Aletrino et al. 1992; Halliday et al. 1992; Hendricksen et al. 2004; Tejani-Butt et al. 1995; Thomas et al. 2006; Tsang et al. 2003). However, only two studies have investigated the SERT binding in AD in vivo by PET in AD. Ouchi and co-workers used [¹¹C]DASB in 15 mild to moderately demented AD patients, of whom seven also had depressive symptoms (Ouchi et al. 2009). They found that [¹¹C]DASB binding in the dense SERT regions (the midbrain, including the raphe nuclei, nucleus accumbens, putamen, and thalamus) of the depressed AD group was significantly lower than that in an age-matched control group SERT (Ouchi et al. 2009). In the midbrain, the reduction amounted to 33 %. In the nondepressed group, a significant SERT reduction was found only in the putamen. In contrast, in 12 mild-to-moderate AD patients, Marner and co-workers did not find reductions in [¹¹C]DASB binding in the raphe nuclei (Marner et al. 2012). In this study, SERT binding was reduced in mesial temporal lobe only, whereas 5-HT_{2A} receptor binding measured using ¹⁸F-altanserin was globally reduced by 28–39 % in the same subjects. The discrepancies between these two studies may arise from methodological differences and also from patient selection, where only four subjects in the study by Marner et al. (2012) had neuropsychiatric symptomatology (score >5 on the Neuropsychiatric Inventory). With no SERT reduction in the raphe nuclei, it is unlikely that a presynaptic serotonergic dysfunction, i.e. reduction in the number of serotonergic neurons

projecting to the neocortex, can explain the marked loss of 5-HT_{2A} receptor binding. Also, the combination of reduced [¹¹C]DASB binding in the mesial temporal lobes and seemingly preserved serotonergic cell bodies in the midbrain suggests a selective loss of projecting serotonergic axons in the mesial temporal lobe, perhaps due to retrograde neurodegeneration in that area. In conclusion, in end-stage AD, post-mortem studies clearly document degeneration of serotonergic neurons in the raphe and in serotonergic neuronal projections, but in early AD, it is still unclear to what extent the serotonergic neurons and projections are affected.

23.4 Can Serotonergic Dysfunction Explain AD Symptomatology?

As described above, dysfunction of the serotonergic transmitter system has been documented in AD. The important question is whether this dysfunction explains part of the symptomatology of the disorder. In postmortem studies of AD, low densities of neocortical SERT and 5-HT_{1A} receptors have been associated with depression and aggression, respectively (Chen et al. 1996; Lai et al. 2003a). Also, Garcia-Alloza et al. found associations between cognition and frontal cortex 5-HT_{1B} binding and between behavioural symptoms and temporal 5-HT₆ binding (Garcia-Alloza et al. 2004). Postmortem studies are associated with problems regarding time interval between symptom evaluation and receptor binding analyses, and also, they represent an end stage of the disease. But in vivo studies have so far not been able to give a clear answer to the question. Although Kepe et al. (2006) demonstrated a correlation between hippocampal 5-HT_{1A} receptor binding and MMSE, they interpreted this association as secondary to the well-known correlation between neurodegeneration and cognitive function. No correlation between MMSE score and 5-HT_{2A} receptor binding was found in two studies of MCI and AD patients (Hasselbalch et al. 2008; Meltzer et al. 1999). However, these studies included rather small sample sizes, and also, the limited range of cognitive dysfunction may have made it difficult to determine correlations between serotonergic and cognitive dysfunction. In a SPECT study of AD patients (Versijpt et al. 2003), a correlation between MMSE scores and 5-HT_{2A} receptor binding in the left orbitofrontal region was found, but the relevance of this finding is not clear. Patients with significant neuropsychiatric symptoms can be very difficult to include in PET studies, and generally, patients covering the spectrum from mild to severe neuropsychiatric symptoms are lacking in in vivo studies. Meltzer and co-workers found no difference in 5-HT_{2A} receptor binding in AD subjects with depression compared to AD subjects without depression. Further, in the depressed patients, there was no correlation between 5-HT_{2A} receptor binding and Hamilton Depression Scale score (Meltzer et al. 1999). Likewise, an inverse correlation between neuropsychiatric symptoms scored by Neuropsychiatric Inventory (NPI) and striatal 5-HT_{2A} receptor binding observed in MCI (Hasselbalch et al. 2008; Marner et al. 2011) could not be corroborated in with the same methodology in a sample of AD patients (Marner et al. 2012). Similarly, SERT findings have been controversial: In a postmortem study of depressive versus nondepressive AD patients,

Hendricksen et al. (2004) found no differences in raphe pathology. In contrast, Ouchi and co-workers found significant correlations between SERT high-binding regions (the midbrain, striatum and thalamus) and Geriatric Depressions scores when grouping depressed and nondepressed AD patients (Ouchi et al. 2009). However, Marner and co-workers did not find significant associations between measures of depression and SERT binding in AD patients, but in this study, patients had less cognitive and neuropsychiatric symptoms (Marner et al. 2012) as compared to Ouchi et al. (2009). Thus, postmortem and in vivo imaging data are only consistent when it comes to the association between reduced SERT expression in the midbrain and depressive symptoms in AD (Chen et al. 1996; Ouchi et al. 2009). No clear picture emerges from other in vivo studies, which may stem from several methodological problems, and future in vivo studies need to include larger samples of patients with a spectrum of cognitive and neuropsychiatric symptoms. Even when doing so, the complex neuropathology and the interaction between several affected transmitter systems may make the aim of establishing associations between serotonin receptor subtypes and symptomatology too simplistic. However, once the pathophysiology of AD symptoms is further elucidated, in vivo imaging studies may help us to determine available drug targets. Thus, the relatively well-preserved SERT and 5-HT₄ receptors in mild to moderate AD suggest these binding sites are potentially available for new treatment strategies.

Acknowledgements This work was supported by the Lundbeck Foundation center grant to Center for Integrated Molecular Brain Imaging (Cimbi).

References

- Adams KH, Pinborg LH, Svarer C, Hasselbalch SG, Holm S, Haugbol S, Madsen K, Frokjaer V, Martiny L, Paulson OB, Knudsen GM (2004) A database of [(18)F]-altanserin binding to 5-HT_{2A} receptors in normal volunteers: normative data and relationship to physiological and demographic variables. *Neuroimage* 21:1105–1113
- Aletrino MA, Vogels OJ, Van Domburg PH, Ten Donkelaar HJ (1992) Cell loss in the nucleus raphes dorsalis in Alzheimer's disease. *Neurobiol Aging* 13:461–468
- Ballard C, Bannister C, Solis M, Oyebode F, Wilcock G (1996) The prevalence, associations and symptoms of depression amongst dementia sufferers. *J Affect Disord* 36:135–144
- Blin J, Baron JC, Dubois B, Crouzel C, Fiorelli M, Ittar-Levy D, Pillon B, Fournier D, Vidailhet M, Agid Y (1993) Loss of brain 5-HT₂ receptors in Alzheimer's disease. In vivo assessment with positron emission tomography and [18F]setoperone. *Brain* 116(Pt 3):497–510
- Bockaert J, Claeysen S, Compan V, Dumuis A (2004) 5-HT₄ receptors. *Curr Drug Targets CNS Neurol Disord* 3:39–51
- Bowen DM, Najlerahim A, Procter AW, Francis PT, Murphy E (1989) Circumscribed changes of the cerebral cortex in neuropsychiatric disorders of later life. *Proc Natl Acad Sci U S A* 86:9504–9508
- Braak H, Braak E (1991) Neuropathological staging of Alzheimer-related changes. *Acta Neuropathol* 82:239–259
- Cachard-Chastel M, Lezoualc'h F, Dewachter I, Delomenie C, Croes S, Devijver H, Langlois M, Van LF, Sicsic S, Gardier AM (2007) 5-HT₄ receptor agonists increase sAPP α levels in the cortex and hippocampus of male C57BL/6j mice. *Br J Pharmacol* 150:883–892

- Chen CP, Alder JT, Bowen DM, Esiri MM, McDonald B, Hope T, Jobst KA, Francis PT (1996) Presynaptic serotonergic markers in community-acquired cases of Alzheimer's disease: correlations with depression and neuroleptic medication. *J Neurochem* 66:1592–1598
- Cheng AV, Ferrier IN, Morris CM, Jabeen S, Sahgal A, McKeith IG, Edwardson JA, Perry RH, Perry EK (1991) Cortical serotonin-5₂ receptor binding in Lewy body dementia, Alzheimer's and Parkinson's diseases. *J Neurol Sci* 106:50–55
- Christensen R, Marcussen AB, Wortwein G, Knudsen GM, Aznar S (2008) Abeta(1–42) injection causes memory impairment, lowered cortical and serum BDNF levels, and decreased hippocampal 5-HT(2A) levels. *Exp Neurol* 210:164–171
- Da Silva Costa-Aze V, Quideville A, Boulouard M, Dauphin F (2012) 5-HT₆ receptor blockade differentially affects scopolamine-induced deficits of working memory, recognition memory and aversive learning in mice. *Psychopharmacology (Berl)* 222:99–115
- de Bruin NM, Prickaerts J, van Loevezijn A, Venhorst J, de Groote L, Houba P, Reneerkens O, Akkerman S, Kruse CG (2011) Two novel 5-HT₆ receptor antagonists ameliorate scopolamine-induced memory deficits in the object recognition and object location tasks in Wistar rats. *Neurobiol Learn Mem* 96:392–402
- Dubois B, Feldman HH, Jacova C, Cummings JL, Dekosky ST, Barberger-Gateau P, Delacourte A, Frisoni G, Fox NC, Galasko D, Gauthier S, Hampel H, Jicha GA, Meguro K, O'Brien J, Pasquier F, Robert P, Rossor M, Salloway S, Sarazin M, de Souza LC, Stern Y, Visser PJ, Scheltens P (2010) Revising the definition of Alzheimer's disease: a new lexicon. *Lancet Neurol* 9:1118–1127
- Erritzoe D, Frokjaer VG, Haugbol S, Marnner L, Svarer C, Holst K, Baare WF, Rasmussen PM, Madsen J, Paulson OB, Knudsen GM (2009) Brain serotonin 2A receptor binding: relations to body mass index, tobacco and alcohol use. *Neuroimage* 46:23–30
- Erritzoe D, Holst K, Frokjaer VG, Licht CL, Kalbitzer J, Nielsen FA, Svarer C, Madsen J, Knudsen G (2010) A nonlinear relationship between cerebral serotonin transporter and 5-HT_{2A} receptor binding: an in vivo molecular imaging study in humans. *J Neurosci* 30:3391–3397
- Ettrup A, Hansen M, Santini MA, Paine J, Gillings N, Palner M, Lehel S, Herth MM, Madsen J, Kristensen J, Begtrup M, Knudsen GM (2011) Radiosynthesis and in vivo evaluation of a series of substituted 11C-phenethylamines as 5-HT (2A) agonist PET tracers. *Eur J Nucl Med Mol Imaging* 38:681–693
- Finnema SJ, Varrone A, Hwang TJ, Gulyas B, Pierson ME, Halldin C, Farde L (2010) Fenfluramine-induced serotonin release decreases [¹¹C]AZ10419369 binding to 5-HT_{1B}-receptors in the primate brain. *Synapse* 64:573–577
- Frankle WG, Huang Y, Hwang DR, Talbot PS, Slifstein M, Van HR, bi-Dargham A, Laruelle M (2004) Comparative evaluation of serotonin transporter radioligands 11C-DASB and 11C-McN 5652 in healthy humans. *J Nucl Med* 45:682–694
- Frokjaer VG, Pinborg LH, Madsen J, de Nijs R, Svarer C, Wagner A, Knudsen GM (2008) Evaluation of the serotonin transporter ligand 123I-ADAM for SPECT studies on humans. *J Nucl Med* 49:247–254
- Frokjaer VG, Erritzoe D, Madsen J, Paulson OB, Knudsen GM (2009) Gender and the use of hormonal contraception in women are not associated with cerebral cortical 5-HT 2A receptor binding. *Neuroscience* 163:640–645
- Gallezot JD, Nabulsi N, Neumeister A, Planeta-Wilson B, Williams WA, Singhal T, Kim S, Maguire RP, McCarthy T, Frost JJ, Huang Y, Ding YS, Carson RE (2010) Kinetic modeling of the serotonin 5-HT(1B) receptor radioligand [(11C)]P943 in humans. *J Cereb Blood Flow Metab* 30:196–210
- Garcia-Alloza M, Hirst WD, Chen CP, Lasheras B, Francis PT, Ramirez MJ (2004) Differential involvement of 5-HT(1B/1D) and 5-HT₆ receptors in cognitive and non-cognitive symptoms in Alzheimer's disease. *Neuropsychopharmacology* 29:410–416
- Gee AD, Martarello L, Passchier J, Wishart M, Parker C, Matthews J, Comley R, Hopper R, Gunn R (2008) Synthesis and evaluation of [¹¹C]SB207145 as the first in vivo serotonin 5-HT₄ receptor radioligand for PET imaging in man. *Curr Radiopharm* 1:110–114
- Ginovart N, Wilson AA, Meyer JH, Hussey D, Houle S (2001) Positron emission tomography quantification of [(11C)]-DASB binding to the human serotonin transporter: modeling strategies. *J Cereb Blood Flow Metab* 21:1342–1353

- Haahr ME, Fisher P, Holst K, Madsen K, Jensen CG, Mamer L, Lehel S, Baare W, Knudsen G, Hasselbalch S (2013) The 5-HT₄ receptor levels in hippocampus correlates inversely with memory test performance in humans. *Hum Brain Mapp* 34:3066–3074
- Halford JC, Harrold JA, Boyland EJ, Lawton CL, Blundell JE (2007) Serotonergic drugs: effects on appetite expression and use for the treatment of obesity. *Drugs* 67:27–55
- Halliday GM, McCann HL, Pamphlett R, Brooks WS, Creasey H, McCusker E, Cotton RG, Broe GA, Harper CG (1992) Brain stem serotonin-synthesizing neurons in Alzheimer's disease: a clinicopathological correlation. *Acta Neuropathol* 84:638–650
- Hasselbalch SG, Madsen K, Svarer C, Pinborg LH, Holm S, Paulson OB, Waldemar G, Knudsen GM (2008) Reduced 5-HT_{2A} receptor binding in patients with mild cognitive impairment. *Neurobiol Aging* 29:1830–1838
- Haugbol S, Pinborg LH, Arfan HM, Frokjaer VM, Madsen J, Dyrby TB, Svarer C, Knudsen GM (2007) Reproducibility of 5-HT_{2A} receptor measurements and sample size estimations with [¹⁸F]altanserin PET using a bolus/infusion approach. *Eur J Nucl Med Mol Imaging* 34:910–915
- Hendricksen M, Thomas AJ, Ferrier IN, Ince P, O'Brien JT (2004) Neuropathological study of the dorsal raphe nuclei in late-life depression and Alzheimer's disease with and without depression. *Am J Psychiatry* 161:1096–1102
- Henningsson S, Borg J, Lundberg J, Bah J, Lindstrom M, Ryding E, Jovanovic H, Saijo T, Inoue M, Rosen I, Traskman-Bendz L, Farde L, Eriksson E (2009) Genetic variation in brain-derived neurotrophic factor is associated with serotonin transporter but not serotonin-1A receptor availability in men. *Biol Psychiatry* 66:477–485
- Holm P, Ettrup A, Klein AB, Santini MA, El-Sayed M, Elvang AB, Stensbol TB, Mikkelsen JD, Knudsen GM, Aznar S (2010) Plaque deposition dependent decrease in 5-HT_{2A} serotonin receptor in AbetaPP^{swe}/PS1^{ΔE9} amyloid overexpressing mice. *J Alzheimers Dis* 20:1201–1213
- Hoyer D, Hannon JP, Martin GR (2002) Molecular, pharmacological and functional diversity of 5-HT receptors. *Pharmacol Biochem Behav* 71:533–554
- Huang Y, Zheng MQ, Gerdes JM (2010) Development of effective PET and SPECT imaging agents for the serotonin transporter: has a twenty-year journey reached its destination? *Curr Top Med Chem* 10:1499–1526
- Jack CR Jr, Knopman DS, Jagust WJ, Shaw LM, Aisen PS, Weiner MW, Petersen RC, Trojanowski JQ (2010) Hypothetical model of dynamic biomarkers of the Alzheimer's pathological cascade. *Lancet Neurol* 9:119–128
- Jones T, Rabiner EA (2012) The development, past achievements, and future directions of brain PET. *J Cereb Blood Flow Metab* 32:1426–1454
- Jovanovic H, Lundberg J, Karlsson P, Cerin A, Saijo T, Varrone A, Halldin C, Nordstrom AL (2008) Sex differences in the serotonin 1A receptor and serotonin transporter binding in the human brain measured by PET. *Neuroimage* 39:1408–1419
- Kepe V, Barrio JR, Huang SC, Ercoli L, Siddarth P, Shoghi-Jadid K, Cole GM, Satyamurthy N, Cummings JL, Small GW, Phelps ME (2006) Serotonin 1A receptors in the living brain of Alzheimer's disease patients. *Proc Natl Acad Sci U S A* 103:702–707
- Kim JS, Ichise M, Sangare J, Innis RB (2006) PET imaging of serotonin transporters with [¹¹C]DASB: test-retest reproducibility using a multilinear reference tissue parametric imaging method. *J Nucl Med* 47:208–214
- King MV, Marsden CA, Fone KC (2008) A role for the 5-HT_{1A}), 5-HT₄ and 5-HT₆ receptors in learning and memory. *Trends Pharmacol Sci* 29:482–492
- Kristiansen H, Elfving B, Plenge P, Pinborg LH, Gillings N, Knudsen GM (2005) Binding characteristics of the 5-HT_{2A} receptor antagonists altanserin and MDL 100907. *Synapse* 58:249–257
- Lai MK, Tsang SW, Francis PT, Esiri MM, Hope T, Lai OF, Spence I, Chen CP (2003a) [³H]-GR113808 binding to serotonin 5-HT₄ receptors in the postmortem neocortex of Alzheimer disease: a clinicopathological study. *J Neural Transm* 110:779–788
- Lai MK, Tsang SW, Francis PT, Esiri MM, Keene J, Hope T, Chen CP (2003b) Reduced serotonin 5-HT_{1A} receptor binding in the temporal cortex correlates with aggressive behavior in Alzheimer disease. *Brain Res* 974:82–87

- Lai MK, Tsang SW, Alder JT, Keene J, Hope T, Esiri MM, Francis PT, Chen CP (2005) Loss of serotonin 5-HT_{2A} receptors in the postmortem temporal cortex correlates with rate of cognitive decline in Alzheimer's disease. *Psychopharmacology (Berl)* 179:673–677
- Lamirault L, Simon H (2001) Enhancement of place and object recognition memory in young adult and old rats by RS 67333, a partial agonist of 5-HT₄ receptors. *Neuropharmacology* 41:844–853
- Lee HM, Roth BL (2012) Hallucinogen actions on human brain revealed. *Proc Natl Acad Sci U S A* 109:1820–1821
- Lelong V, Dauphin F, Boulouard M (2001) RS 67333 and D-cycloserine accelerate learning acquisition in the rat. *Neuropharmacology* 41:517–522
- Leyssen JE (2004) 5-HT₂ receptors. *Curr Drug Targets CNS Neurol Disord* 3:11–26
- Lorke DE, Lu G, Cho E, Yew DT (2006) Serotonin 5-HT_{2A} and 5-HT₆ receptors in the prefrontal cortex of Alzheimer and normal aging patients. *BMC Neurosci* 7:36
- Lundberg J, Odano I, Olsson H, Halldin C, Farde L (2005) Quantification of 11C-MADAM binding to the serotonin transporter in the human brain. *J Nucl Med* 46:1505–1515
- Lundberg J, Halldin C, Farde L (2006) Measurement of serotonin transporter binding with PET and [11C]MADAM: a test-retest reproducibility study. *Synapse* 60:256–263
- Lundberg J, Christophersen JS, Petersen KB, Loft H, Halldin C, Farde L (2007) PET measurement of serotonin transporter occupancy: a comparison of escitalopram and citalopram. *Int J Neuropsychopharmacol* 10:777–785
- Lyketsos CG, Lopez O, Jones B, Fitzpatrick AL, Breitner J, DeKosky S (2002) Prevalence of neuropsychiatric symptoms in dementia and mild cognitive impairment: results from the cardiovascular health study. *JAMA* 288:1475–1483
- Lyon RA, Titeler M, Frost JJ, Whitehouse PJ, Wong DF, Wagner HN Jr, Dannals RF, Links JM, Kuhar MJ (1986) 3H-3-N-methylspiperone labels D₂ dopamine receptors in basal ganglia and S₂ serotonin receptors in cerebral cortex. *J Neurosci* 6:2941–2949
- Madsen K, Erritzoe D, Mortensen EL, Gade A, Madsen J, Baare W, Knudsen GM, Hasselbalch SG (2011a) Cognitive function is related to fronto-striatal serotonin transporter levels – a brain PET study in young healthy subjects. *Psychopharmacology (Berl)* 213:573–581
- Madsen K, Haahr MT, Marner L, Keller SH, Baare WF, Svarer C, Hasselbalch SG, Knudsen GM (2011b) Age and sex effects on 5-HT₄ receptors in the human brain: a [(11)C]SB207145 PET study. *J Cereb Blood Flow Metab* 31:1475–1481
- Madsen K, Marner L, Haahr M, Gillings N, Knudsen GM (2011c) Mass dose effects and in vivo affinity in brain PET receptor studies – a study of cerebral 5-HT₄ receptor binding with [(11)C]SB207145. *Nucl Med Biol* 38:1085–1091
- Madsen K, Neumann WJ, Holst K, Marner L, Haahr MT, Lehel S, Knudsen GM, Hasselbalch SG (2011d) Cerebral serotonin 4 receptors and amyloid-beta in early Alzheimer's disease. *J Alzheimers Dis* 26:457–466
- Maher-Edwards G, Zvartau-Hind M, Hunter AJ, Gold M, Hopton G, Jacobs G, Davy M, Williams P (2010) Double-blind, controlled phase II study of a 5-HT₆ receptor antagonist, SB-742457, in Alzheimer's disease. *Curr Alzheimer Res* 7:374–385
- Marchetti E, Dumuis A, Bockaert J, Soumireu-Mourat B, Roman FS (2000) Differential modulation of the 5-HT₄ receptor agonists and antagonist on rat learning and memory. *Neuropharmacology* 39:2017–2027
- Marchetti-Gauthier E, Roman FS, Dumuis A, Bockaert J, Soumireu-Mourat B (1997) BIMU1 increases associative memory in rats by activating 5-HT₄ receptors. *Neuropharmacology* 36:697–706
- Marner L, Gillings N, Comley RA, Baare WF, Rabiner EA, Wilson AA, Houle S, Hasselbalch SG, Svarer C, Gunn RN, Laruelle M, Knudsen GM (2009) Kinetic modeling of 11C-SB207145 binding to 5-HT₄ receptors in the human brain in vivo. *J Nucl Med* 50:900–908
- Marner L, Gillings N, Madsen K, Erritzoe D, Baare WF, Svarer C, Hasselbalch SG, Knudsen GM (2010) Brain imaging of serotonin 4 receptors in humans with [11C]SB207145-PET. *Neuroimage* 50:855–861
- Marner L, Knudsen GM, Madsen K, Holm S, Baare W, Hasselbalch SG (2011) The reduction of baseline serotonin 2A receptors in mild cognitive impairment is stable at two-year follow-up. *J Alzheimers Dis* 23:453–459

- Marner L, Frokjaer VG, Kalbitzer J, Lehel S, Madsen K, Baare WF, Knudsen GM, Hasselbalch SG (2012) Loss of serotonin 2A receptors exceeds loss of serotonergic projections in early Alzheimer's disease: a combined [^{11}C]DASB and [^{18}F]altanserin-PET study. *Neurobiol Aging* 33:479–487
- Matuskey D, Pittman B, Planeta-Wilson B, Walderhaug E, Henry S, Gallezot JD, Nabulsi N, Ding YS, Bhagwagar Z, Malison R, Carson RE, Neumeister A (2012) Age effects on serotonin receptor 1B as assessed by PET. *J Nucl Med* 53:1411–1414
- Meltzer CC, Price JC, Mathis CA, Greer PJ, Cantwell MN, Houck PR, Mulsant BH, Ben-Eliezer D, Lopresti B, Dekosky ST, Reynolds CF III (1999) PET imaging of serotonin type 2A receptors in late-life neuropsychiatric disorders. *Am J Psychiatry* 156:1871–1878
- Meyer JH, Wilson AA, Sagrati S, Hussey D, Carella A, Potter WZ, Ginovart N, Spencer EP, Cheok A, Houle S (2004) Serotonin transporter occupancy of five selective serotonin reuptake inhibitors at different doses: an [^{11}C]DASB positron emission tomography study. *Am J Psychiatry* 161:826–835
- Milak MS, Severance AJ, Ogden RT, Prabhakaran J, Kumar JS, Majo VJ, Mann JJ, Parsey RV (2008) Modeling considerations for ^{11}C -CUMI-101, an agonist radiotracer for imaging serotonin 1A receptor in vivo with PET. *J Nucl Med* 49:587–596
- Nelson DL (2004) 5-HT₅ receptors. *Curr Drug Targets CNS Neurol Disord* 3:53–58
- Newberg AB, Plossl K, Mozley PD, Stubbs JB, Wintering N, Udeshi M, Alavi A, Kauppinen T, Kung HF (2004) Biodistribution and imaging with (123)I-ADAM: a serotonin transporter imaging agent. *J Nucl Med* 45:834–841
- Ouchi Y, Yoshikawa E, Futatsubashi M, Yagi S, Ueki T, Nakamura K (2009) Altered brain serotonin transporter and associated glucose metabolism in Alzheimer disease. *J Nucl Med* 50:1260–1266
- Parker RM, Barnes JM, Ge J, Barber PC, Barnes NM (1996) Autoradiographic distribution of [^3H]-(*S*)-zacopride-labelled 5-HT₃ receptors in human brain. *J Neurol Sci* 144:119–127
- Parker CA, Gunn RN, Rabiner EA, Slifstein M, Comley R, Salinas C, Johnson CN, Jakobsen S, Houle S, Laruelle M, Cunningham VJ, Martarello L (2012) Radiosynthesis and characterization of ^{11}C -GSK215083 as a PET radioligand for the 5-HT₆ receptor. *J Nucl Med* 53:295–303
- Paterson LM, Kornum BR, Nutt DJ, Pike VW, Knudsen GM (2013) 5-HT radioligands for human brain imaging with PET and SPECT. *Med Res Rev* 33:54–111
- Pinborg LH, Adams KH, Svarer C, Holm S, Hasselbalch SG, Haugbol S, Madsen J, Knudsen GM (2003) Quantification of 5-HT_{2A} receptors in the human brain using [^{18}F]altanserin-PET and the bolus/infusion approach. *J Cereb Blood Flow Metab* 23:985–996
- Pinborg LH, Arfan H, Haugbol S, Kyvik KO, Hjelmberg JV, Svarer C, Frokjaer VG, Paulson OB, Holm S, Knudsen GM (2008) The 5-HT_{2A} receptor binding pattern in the human brain is strongly genetically determined. *Neuroimage* 40:1175–1180
- Pinborg LH, Feng L, Haahr ME, Gillings N, Dyssegaard A, Madsen J, Svarer C, Yndgaard S, Kjaer TW, Parsey RV, Hansen HD, Ettrup A, Paulson OB, Knudsen GM (2012) No change in [(1)(1)C]CUMI-101 binding to 5-HT(1A) receptors after intravenous citalopram in human. *Synapse* 66:880–884
- Ridler K, Plisson C, Rabiner EA, Gunn RN, Easwaramoorthy B, bi-Dargham A, Laruelle M, Slifstein M (2011) Characterization of in vivo pharmacological properties and sensitivity to endogenous serotonin of [^{11}C]P943: a positron emission tomography study in *Papio anubis*. *Synapse* 65:1119–1127
- Ryu YH, Liow JS, Zoghbi S, Fujita M, Collins J, Tipre D, Sangare J, Hong J, Pike VW, Innis RB (2007) Disulfiram inhibits defluorination of (18)F-FCWAY, reduces bone radioactivity, and enhances visualization of radioligand binding to serotonin 5-HT_{1A} receptors in human brain. *J Nucl Med* 48:1154–1161
- Savli M, Bauer A, Mitterhauser M, Ding YS, Hahn A, Kroll T, Neumeister A, Haeusler D, Ungersboeck J, Henry S, Isfahani SA, Rattay F, Wadsak W, Kasper S, Lanzenberger R (2012) Normative database of the serotonergic system in healthy subjects using multi-tracer PET. *Neuroimage* 63:447–459

- Schmitt JA, Wingen M, Ramaekers JG, Evers EA, Riedel WJ (2006) Serotonin and human cognitive performance. *Curr Pharm Des* 12:2473–2486
- Szabo Z, Kao PF, Scheffel U, Suehiro M, Mathews WB, Ravert HT, Musachio JL, Marengo S, Kim SE, Ricaurte GA (1995) Positron emission tomography imaging of serotonin transporters in the human brain using [¹¹C](+)-McN5652. *Synapse* 20:37–43
- Talbot PS, Slifstein M, Hwang DR, Huang Y, Scher E, bi-Dargham A, Laruelle M (2012) Extended characterisation of the serotonin 2A (5-HT_{2A}) receptor-selective PET radiotracer 11C-MDL100907 in humans: quantitative analysis, test-retest reproducibility, and vulnerability to endogenous 5-HT tone. *Neuroimage* 59:271–285
- Tejani-Butt SM, Yang J, Pawlyk AC (1995) Altered serotonin transporter sites in Alzheimer's disease raphe and hippocampus. *Neuroreport* 6:1207–1210
- Terry AV Jr, Buccafusco JJ, Jackson WJ, Prendergast MA, Fontana DJ, Wong EH, Bonhaus DW, Weller P, Eglen RM (1998) Enhanced delayed matching performance in younger and older macaques administered the 5-HT₄ receptor agonist, RS 17017. *Psychopharmacology (Berl)* 135:407–415
- Tfelt-Hansen P (2012) Clinical pharmacology of current and future drugs for the acute treatment of migraine: a review and an update. *Curr Clin Pharmacol* 7:66–72
- Thomas AJ, Hendriksen M, Piggott M, Ferrier IN, Perry E, Ince P, O'Brien JT (2006) A study of the serotonin transporter in the prefrontal cortex in late-life depression and Alzheimer's disease with and without depression. *Neuropathol Appl Neurobiol* 32:296–303
- Truchot L, Costes SN, Zimmer L, Laurent B, Le BD, Thomas-Anterion C, Croisile B, Mercier B, Hermier M, Vighetto A, Krolak-Salmon P (2007) Up-regulation of hippocampal serotonin metabolism in mild cognitive impairment. *Neurology* 69:1012–1017
- Tsang SW, Lai MK, Francis PT, Wong PT, Spence I, Esiri MM, Keene J, Hope T, Chen CP (2003) Serotonin transporters are preserved in the neocortex of anxious Alzheimer's disease patients. *Neuroreport* 14:1297–1300
- Varnas K, Nyberg S, Halldin C, Varrone A, Takano A, Karlsson P, Andersson J, McCarthy D, Smith M, Pierson ME, Soderstrom J, Farde L (2011) Quantitative analysis of [¹¹C]AZ10419369 binding to 5-HT_{1B} receptors in human brain. *J Cereb Blood Flow Metab* 31:113–123
- Versijpt J, Van Laere KJ, Dumont F, Decoo D, Vandecapelle M, Santens P, Goethals I, Audenaert K, Slegers G, Dierckx RA, Korf J (2003) Imaging of the 5-HT_{2A} system: age-, gender-, and Alzheimer's disease-related findings. *Neurobiol Aging* 24:553–561
- Volk B, Nagy BJ, Vas S, Kostyalik D, Simig G, Bagdy G (2010) Medicinal chemistry of 5-HT_{5A} receptor ligands: a receptor subtype with unique therapeutical potential. *Curr Top Med Chem* 10:554–578
- Wilson AA, Houle S (1999) Radiosynthesis of carbon-11 labelled N-methyl-2-(arylthio)benzylamines; potential radiotracers for the serotonin reuptake receptor. *J Labelled Compd Radiopharm* 42:1277–1288
- Wong DF, Wagner HN Jr, Dannals RF, Links JM, Frost JJ, Ravert HT, Wilson AA, Rosenbaum AE, Gjedde A, Douglass KH (1984) Effects of age on dopamine and serotonin receptors measured by positron tomography in the living human brain. *Science* 226:1393–1396
- Woolley ML, Marsden CA, Fone KC (2004) 5-HT₆ receptors. *Curr Drug Targets CNS Neurol Disord* 3:59–79
- Xu Y, Yan J, Zhou P, Li J, Gao H, Xia Y, Wang Q (2012) Neurotransmitter receptors and cognitive dysfunction in Alzheimer's disease and Parkinson's disease. *Prog Neurobiol* 97:1–13

Serotonin Synthesis Studied with Positron Emission Tomography (PET)

24

Per Hartvig Honoré and Pinelopi Lundquist

Contents

24.1	Introduction	688
24.1.1	Synthesis of Serotonin	688
24.1.2	The Serotonin System	689
24.1.3	Methods to Study Biosynthesis	692
24.2	Modelling in PET	693
24.2.1	Models	693
24.2.2	Graphical Analysis	693
24.3	PET Imaging of 5HT Synthesis	694
24.4	Perturbation Studies Using 5HT and AMT	695
24.4.1	Comparison of the Two Substrates in 5HT Biosynthesis	696
24.5	[¹¹ C]HTP Target Specificity and Brain Metabolites	697
24.5.1	Graphical Strategies for [¹¹ C]5HTP Data Analysis	700
24.6	Applications of Two Tracers to Indicate Serotonin Synthesis	703
24.6.1	Clinical Applications of (11C)-5-Hydroxytryptophan (5HTP)	703
24.6.2	Clinical Applications of (¹¹ C)-Alpha-methyl-tryptophan (AMT)	704
	References	705

Abstract

Positron emission tomography (PET) has the potential to study the biosynthesis and release of serotonin (5HT) at brain serotonergic neurons. PET requires probe compounds with specific attributes to enable imaging and quantification of biological processes. This section focuses on probes to measure serooinin synthesis rate. Knowledge of altered 5HT synthesis and release in disease states may

P.H. Honoré (✉)

Department of Drug Design and Pharmacology, Faculty of Health and Medical Sciences,
University of Copenhagen, Copenhagen, DK 2100, Denmark
e-mail: peh@sund.ku.dk

P. Lundquist

Department of Pharmacy, Uppsala University, Uppsala 751 85, Sweden

National Board of Health and Welfare, Stockholm 106 30, Sweden

furnish basis for effective pharmacotherapy that may improve the care of psychiatric and neurological disease.

Validation of PET measurements of the two PET tracers using perturbation showed that 5-hydroxy-L-(beta-¹¹C tryptophan) (5HTP) quantifies the activity of amino acid decarboxylase in the conversion to 5HT. On the other hand, alpha-methyl-tryptophan (AMT) measures the conversion to the corresponding 5-hydroxytryptophan analogue. The irreversible binding of the PET probe 5HTP in the monkey brain was lower in the presence of NSD1015 which was used to inhibit the decarboxylation step in 5HT synthesis. 5HTP seems thus to have potential for tracking changes in the activity of the biosynthesis enzyme. In contrast, the accumulation of 5HTP was unaffected by clorgyline used to inhibit the metabolism of the probe in the brain. This indicates that on a PET timescale, elimination of the main metabolite from the brain is negligible and would not alter calculation of 5HTP transfer to 5HT. The extent and distribution of irreversible binding of a substrate for the first enzyme in 5HT formation alpha-methyltryptophan AMT were different from those of 5HTP, suggesting that the two PET probes provide estimates related to the enzyme activity of different steps in the 5HT synthesis pathway.

Applications of the two tracers HTP and AMT are reviewed. Up to now, 5HTP has mainly been used for the detection, staging and treatment evaluations of neuroendocrine tumours. Though, a few studies using 5HT have been conducted on CNS disorders. AMT-PET studies have mainly been confined to brain diseases causing various degree of neurodegeneration.

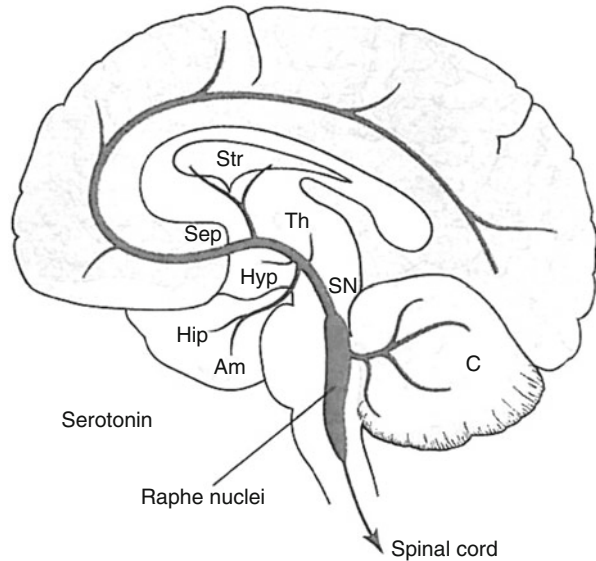
24.1 Introduction

24.1.1 Synthesis of Serotonin

Serotonin (5-hydroxytryptamine, 5HT) is a platelet-stored vasoconstrictor that also acts as a transmitter in the central nervous system (CNS) to modulate a wide spectrum of behaviours (Jacobs and Azmitia 1992; Meltzer 1990; Weiger 1997; Vogt 1982). The importance of understanding different components of the 5HT system relevant to physiological and disease states has been recognised for ~50 years (Gaddum 1953; Marshall et al. 1960; Pletscher et al. 1955). However, the complexity of the 5HT system has hampered attempts to achieve this understanding. At least 14 different receptors that respond to 5HT as well as multiple enzymes and proteins that influence its metabolism and release have been identified through molecular cloning of 5HT-related genes (Gingrich and Hen 2001; Murphy et al. 1999). Serotonergic neurotransmission in the brain is controlled by negative 5HT receptor-mediated feedback mechanisms (Stenfors and Ross 2004) and is influenced by other neurotransmitters and peptides (Valentino and Commons 2005).

As the concentration of brain 5HT increases, for example, following administration of the precursors, tryptophan or 5-hydroxytryptophan (5HTP), the rate of discharge of 5HT neurons shows a corresponding decrease (Aghajanian 1972; Trulson

Fig. 24.1 Summary diagram of primate serotonergic system. Main nuclei are indicated by initial letters and fibre pathways are shaded. *Am* amygdaloid nucleus, *C* cerebellum, *Hip* hippocampus, *Hyp* hypothalamus, *Sep* septum, *SN* substantia nigra, *Str* striatum, *Tha* thalamus (Jacobs and Azmitia 1992)



and Jacobs 1976). It is presumed that this decrease is a homeostatic response that acts to compensate for increases in synaptic concentrations of 5HT. In other words, it appears as if 5HT synthesis in some way is coupled to 5HT release and can be adjusted in order to match the extent of transmitter release and loss. Consequently, both mechanisms (biosynthesis and release) should be recognised separately when the activity of the 5HT system is assessed as they can change in opposite directions.

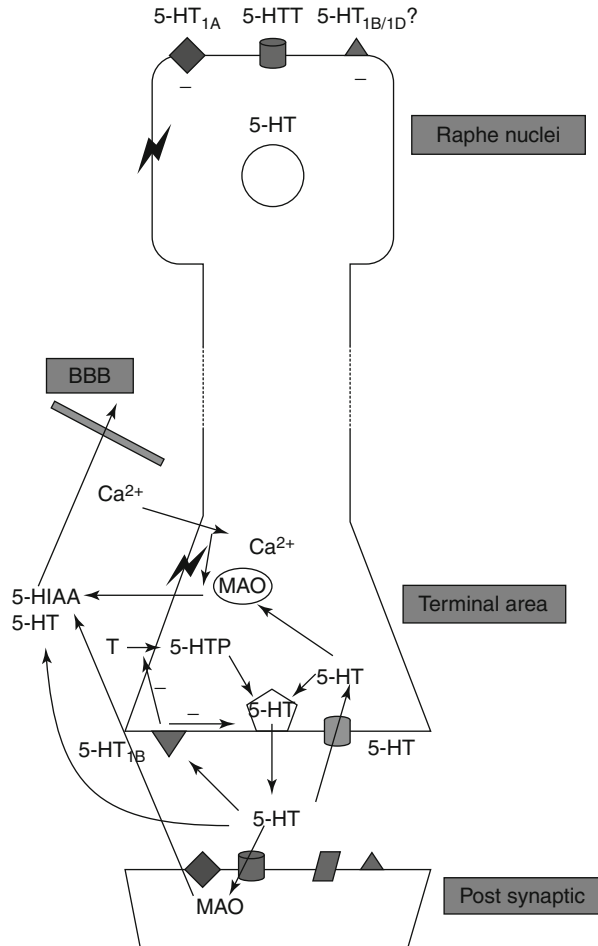
Since little of the 5HT found in brain originates in peripheral tissues, it is assumed that brain 5HT synthesis is equivalent to the process of renewal of 5HT in brain (Neckers 1982). Peripheral markers, usually measured in the blood or CSF, for assessing central serotonergic activity are sometimes used. However, these measures may well differ from those corresponding parameters in the brain, both under healthy conditions and in the presence of disease. Direct measurement of the activity of serotonergic neurons within the brain is much more complicated.

The feasibility to study the mechanisms of cerebral serotonin synthesis was assessed by administering endogenous and exogenous compounds as radiolabelled probes. The probes have been studied using positron emission tomography (PET). This chapter focuses on the evaluation of PET tracers for quantification of 5HT biosynthesis.

24.1.2 The Serotonin System

The cells that produce 5HT are located in the dorsal raphe nucleus, which extensively innervates neocortical regions (Fig. 24.1).

Fig. 24.2 Schematic illustration of factors that determine 5HT concentration in the extracellular space (Stenfors and Ross 2004)



24.1.2.1 Release and Extracellular Concentrations

Exocytotic release of 5HT from the storage vesicles upon nerve firing is regulated by inhibitory $5HT_{1A}$ (somatodendritic) and $5HT_{1B}$ (located on nerve terminals) autoreceptors. It is possible that $5HT_{1B}$ and/or $5HT_{1D}$ receptors in the midbrain raphe nuclei also contribute to the regulation of the rate of nerve firing (Stenfors and Ross 2004).

Based on the turnover rate and the measured extracellular concentration of 5HT in the rat striatum (Kalen et al. 1988), very little of the released 5HT is present in the extracellular space. The main factors that regulate the 5HT concentration in the synaptic cleft at the serotonergic nerve terminals and thereby also the concentrations of extracellular 5HT are shown in Fig. 24.2.

Most of the released 5HT is transported back into the nerve terminals by transporter proteins in the cell membrane. This 5HT transporter is the target for the

widely prescribed drug class of SSRIs that increase 5HT neurotransmission but decrease the activity of the 5HT neuron itself (Fuller 1994; White et al. 2005). Both effects occur because the increased concentration of 5HT in the synapse is increased by the uptake inhibition, resulting in increased activation of postsynaptic receptors on target neurons (leading to various functional changes) and increased activation of presynaptic autoreceptors (which leads to decreased 5HT synthesis and firing of the 5HT neuron itself, presumably also to decreased 5HT release).

The 5HT molecules, which have been transported back into the neuron, are either stored in vesicles or captured by mitochondrial monoamine oxidase (MAO) and deaminated to 5-hydroxyindoleacetic acid (5HIAA). This metabolite is not stored in the neurons but passes to the extracellular space and leaves the brain via an active acid transport mechanism.

5HT and 5HIAA in the extracellular space originate mainly from serotonergic nerves (Kalen et al. 1988; Sharp et al. 1989; Sharp and Foster 1989). Changes in the extracellular 5HT concentrations are therefore regarded as reflecting changes in 5HT release. The effect of 5HT-releasing drugs, such as fenfluramine (which increases both 5HT release and extracellular 5HT concentrations), is assessed as a balanced effect since the compounds increase extracellular 5HT concentrations while resulting in an adaptive decrease in 5HT release.

24.1.2.2 Biosynthesis

5HT is formed in a two-step reaction starting with tryptophan being taken up in neurons by an amino acid carrier-mediated transport mechanism (Pardridge 1998). The barrier across cell membranes, including the BBB, expresses the sodium-independent L system transporter (Pardridge and Oldendorf 1977).

The amino acid is then hydroxylated into 5-hydroxytryptophan (5HTP) by the action of tryptophan hydroxylase-2, expressed predominantly in serotonergic neurons of the raphe nuclei (Walther et al. 2003; Zhang et al. 2004). The overall tryptophan concentration in the human brain of 30 μM (Fernström and Wurtman 1971; Young and Gauthier 1981; Young et al. 1977) is about equal to the half-saturation concentrations (K_m) for the enzyme (Friedman et al. 1972).

Finally, 5HTP is decarboxylated into 5HT by aromatic L-amino acid decarboxylase (AADC). AADC is mainly localised in 5HT- and catecholamine-containing neurons in the CNS (Hokfelt et al. 1973). The recombinant human AADC also catalyses the decarboxylation of L-DOPA to dopamine (Sumi et al. 1990). The K_m for the enzyme is 5–270 μM (Ota et al. 1990; Zhu and Juorio 1995) and is much higher than the overall 5HTP concentration in the monkey brain of 3–30 nM (Brown et al. 1979).

AADC activity is present in brain extracts in far greater amounts than tryptophan hydroxylase (Ichiyama et al. 1968), and for this reason, the hydroxylation of tryptophan rather than the decarboxylation of 5HTP is presumed to be the rate-limiting step in 5HT formation. The fact that 5HTP is found only in trace amounts in brain tissue (Tappaz and Pujol 1980) indicates that it is decarboxylated almost as rapidly as it is formed and also suggests that the hydroxylase step is rate limiting in 5HT formation.

24.1.3 Methods to Study Biosynthesis

There are *in vitro* models of the 5HT system that allows measurement of 5HT synthesis or enzyme activities. These models use, e.g., homogenates, tissue slices or synaptosomes. *In vivo* methods are preferable for quantitative measurements as release and biosynthesis take place at multiple sites within the CNS and also seem to be regulated in a complex manner.

One quantitative *in vivo* method that has been used for studying both neurotransmitter release and biosynthesis is PET.

24.1.3.1 Methodological Considerations

The design of a successful imaging probe is critical and can be a bottleneck (Laruelle et al. 2003). Several aspects need to be considered before performing a PET experiment in order to obtain quantitative measurements in the brain.

From the viewpoint of radiochemistry, the half-life of the positron-emitting isotope must be chosen to match the timescale of the process being probed. A rapid tracer synthesis by the chemists must also be feasible, due to the short half-lives of most positron-emitting nuclides. Typically one molecule out of 1,700–34,000 is made radioactive in the labelling of a probe with [¹¹C]. In most applications, the tracer dose (i.e. sum of labelled and unlabelled molecules) introduced to the system is assumed to be negligible so that it does not affect or perturb the system by changing endogenous biomolecule concentrations. It is important that the candidate probe can be radiolabelled with as high amount of radioactivity per amount of probe substance (specific radioactivity) as possible. A high specific radioactivity means that a low mass of the probe can be administered and can still provide a sufficient strong radioactivity signal.

From a pharmacokinetic perspective, the labelled probe should cross the BBB but its metabolism should not result in the formation of radiolabelled compounds that enter the brain. Otherwise, the background signal from accumulating metabolites may interfere with the desired signal from the parent molecule. To determine the time-dependent amount of intact tracer available for brain uptake, blood samples can be drawn during the PET scan. These samples are typically analysed using liquid chromatography allowing the radioactivity from the parent compound to be separated from metabolites. The ratio of parent tracer radioactivity to total plasma radioactivity as a function of time reflects the amount of intact probe available for brain uptake which is important information for further quantification. Metabolism within the brain can be measured in samples of excised brain tissue or be assessed *in vivo* by studying the impact of pharmacological challenges.

The ratio of target to nontarget localisation of the radiotracer within tissue is critical. The higher the ratio, the more likely it is that the signal can be used to measure changes in receptors or transporters available caused by disease or drug treatment. Non-specific binding is one crucial factor that affects the target to nontarget ratios. Usually, radioactivity in a brain region devoid of target receptors is used as an estimate of non-specific binding. The ideal reference region should have similar free and non-specific binding properties as brain regions with specific binding.

These properties are tracer dependent and will vary depending on the characteristics of the macromolecules in the brain that non-specifically bind the radioligand.

Finally, the affinity of a radiotracer must represent a compromise between the need to acquire a high signal-to-noise ratios and the need to finish the measurements (exclude) in a reasonable period of time (Laruelle et al. 2003).

24.2 Modelling in PET

PET tracer kinetic data could be evaluated by techniques that broadly can be divided into model-driven methods and data-driven methods (Gunn et al. 2002). The clear distinction is that data-driven methods such as graphical analysis require no a priori decision about the most appropriate model structure. Instead, this information is obtained directly from the kinetic data.

24.2.1 Models

Because of the statistical limits of the data, and because PET measures only the sum of the radioactivity across all compartments, the models for data analysis must be simple (Koeppel 2002). Most PET radioligands can support models with two to maximally six parameters under the best of circumstances.

Well-established models in PET include those for quantification of blood flow (Kety and Schmidt 1948), cerebral metabolic rate of glucose (Sokoloff et al. 1977) and neuroreceptor ligand binding (Mintun et al. 1984). Those are plasma input models which in PET often are considered related as a gold standard (Gunn et al. 2001). Further developments have created a series of reference tissue models that avoid the need for blood sampling (Blomqvist et al. 1989; Cunningham et al. 1991; Hume et al. 1992; Lammertsma et al. 1996; Lammertsma and Hume 1996) (Fig. 24.3).

24.2.2 Graphical Analysis

Graphical analysis (Gjedde 1982; Logan et al. 1990, 1996; Patlak and Blasberg 1985; Patlak et al. 1983) is a data-driven method that derives macro-system parameters from a less constrained description of the tracer kinetics. One graphical approach used with irreversible radiotracers is called a Patlak plot. The method uses a transformation of the data such that a linear regression of the transformed data yields the parameter of interest. The linear fitting procedure provides excellent stability against the noise from the dynamic PET measurements (Koeppel 2002). Visual examination of a Patlak plot provides an indication of whether the irreversibility assumption is valid. The Patlak approach is valid for an arbitrary number of compartments for both plasma and reference tissue input models (Patalak and Blasberg 1985; Patlak et al. 1983). Graphical analysis is attractive due to its simplicity but requires determination of the moment when the plot becomes linear; it does not give

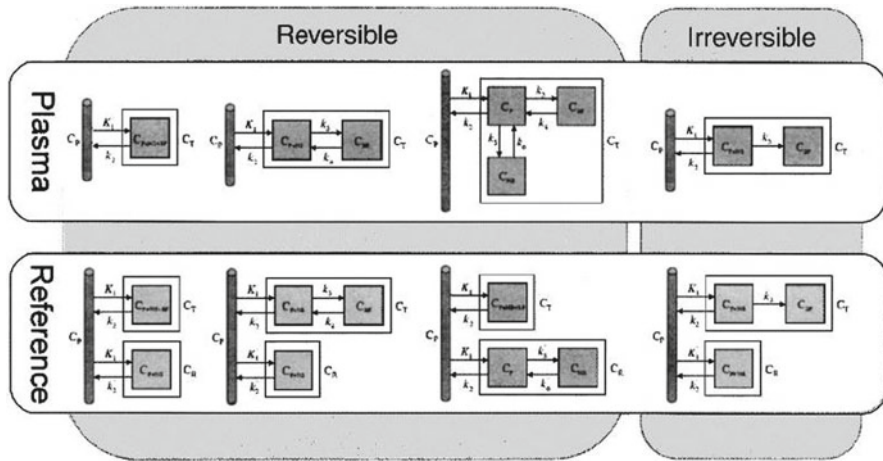


Fig. 24.3 Compartment models commonly used to quantify PET radiotracers. These include models for tracers that exhibit reversible and irreversible kinetics and models that use either a plasma or reference tissue input function (Gunn et al. 2002)

information about the underlying compartment structure and may be biased by statistical noise (Slifstein and Laruelle 2000).

Graphical parameters in the analysis of 5-(11C)HTP data were derived by Patlak analysis (Patlak and Blasberg 1985; Patlak et al. 1983). This was accomplished by performing linear regression on the tissue concentration divided by the model input concentration as a function of the integral of the model input concentration divided by the model input concentration. This Patlak plot becomes linear over time with a slope that yields an estimate of the net rate of radiotracer accumulation in an irreversible compartment (Lundquist et al. 2006, 2007).

Similar to the kinetic modelling, the radioligand binding in the brain was described by fractional rate constants, however, now lumped in macro-parameter estimates obtained from the Patlak slopes. Models comprising input from plasma (slope K_{pPat}) and cerebellum tissue, without (slope K_{rPat}) or with (slope K_{cPat}) irreversible binding, were considered.

24.3 PET Imaging of 5HT Synthesis

Two radiolabelled compounds have been used for probing the first and second enzymatic steps in the biosynthesis of 5HT.

The studies that were carried out targeting the first enzyme, tryptophan hydroxylase, used [¹¹C]AMT, a radiolabelled methyl analogue of tryptophan (Chandana et al. 2005; Chugani et al. 1998a; Fedi et al. 2003; Juhasz et al. 2003; Kagawa et al. 2005; Muzik et al. 1997; Natsume et al. 2003; Nishikawa et al. 2005). Only partial conversion of this probe to α -methylserotonin in the brain was demonstrated (Diksic et al. 1990; Gharib et al. 1999; Shoaf et al. 2000).

The second enzyme, AADC, has also been employed as probe target. The tracer used was the radiolabelled substrate 5-hydroxytryptophan, [^{11}C]5HTP (Agren and Reibring 1994; Agren et al. 1993; Hagberg et al. 2002; Reibring et al. 1992). The time-dependent accumulation of radioactivity in the basal ganglia using this tracer was mainly a consequence of the trapping of decarboxylated tracer products, thus providing an *in vivo* index of the activity of the decarboxylating enzyme (Lindner et al. 1997). The ubiquitous distribution of AADC results in that the enzyme activity measurements are not restricted to 5HT-producing cells.

24.4 Perturbation Studies Using 5HT and AMT

The data in papers by Lundquist et al. (2006) and Lundquist et al. (2007) were analysed by compartment and graphical analysis using in-house-developed software implemented in MATLAB 6.5 (The MathWorks Inc., Natick, MA, USA). In this analysis, absolute values of radioactivity plasma, blood and tissue concentrations were used (nCi/cc).

A few operations were performed to extract the plasma and blood data required for modelling. The initial continuous whole blood withdrawal (on-line detection in the first 2–3 min) was corrected for detector dead time and background radioactivity. The density of blood and plasma was fixed to 1.03 g/cc to convert the radioactivity of the manual plasma and blood samples measured in the γ -counter (Bq/g tissue) to the same units as camera data. A full plasma curve (only blood radioactivity measured at early time points) was generated from the blood curve using the ratio of plasma to whole blood concentrations of the manual samples. These arterial plasma concentrations were modelled after correction for the individual estimates of tracer metabolism (ratio of tracer to total radioactivity concentrations) obtained by metabolite analysis.

The total brain radioactivity concentrations in the ROIs were corrected for a 3–5 % blood-borne radioactivity. The midpoint of each PET (time frame) was used as the time of observation. Data from each individual was modelled and the parameters estimated were presented as means (\pm SD).

The radioligand binding in the brain was parameterised in terms of fractional rate constants. Models comprising one or two compartments in the brain were considered. Parameters were derived by nonlinear regression using the Marquardt-Levenberg least-square minimisation procedure.

Graphical parameters in the analysis of 5HTP data were derived by Patlak analysis (Patlak and Blasberg 1985; Patlak et al. 1983). This was accomplished by performing linear regression on the tissue concentration divided by the model input concentration as a function of the integral of the model input concentration divided by the model input concentration. This Patlak plot becomes linear over time with a slope that yields an estimate of the net rate of radiotracer accumulation in an irreversible compartment (Lundquist et al. 2006, 2007).

Similar to the kinetic modelling, the radioligand binding in the brain was described by fractional rate constants, however, now lumped in macro-parameter

Fig. 24.4 Chemical structure of (^{11}C)-5-hydroxytryptophan (5HTP). The asterisk (*) indicates the position of the ^{11}C label

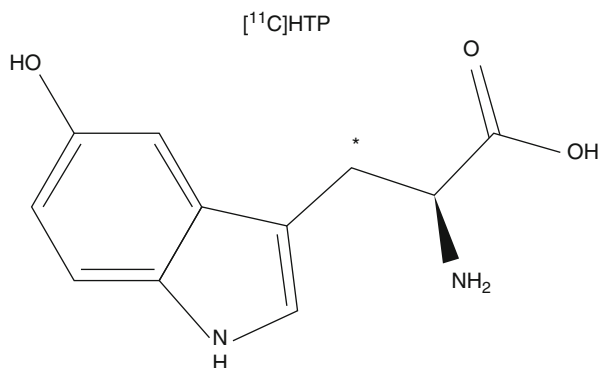
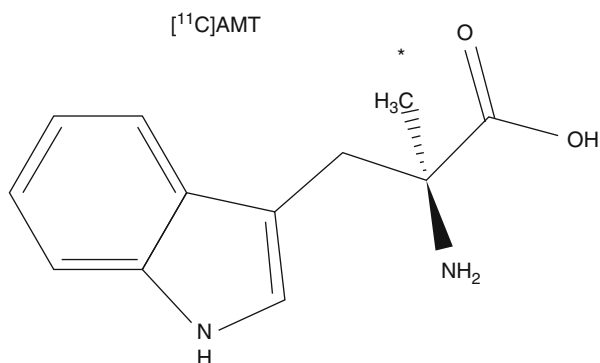


Fig. 24.5 Chemical structure of (^{11}C)-alpha-methyl-tryptophan (AMT). The asterisk (*) indicates the position of the ^{11}C label



estimates obtained from the Patlak slopes. Models comprising input from plasma (slope K_{pPat}) and cerebellum tissue, without (slope K_{rPat}) or with (slope K_{cPat}) irreversible binding, were considered.

24.4.1 Comparison of the Two Substrates in 5HT Biosynthesis

Although none of the tracers $[^{11}\text{C}]\text{AMT}$ and $[^{11}\text{C}]\text{5HTP}$ can be used to measure absolute 5HT synthesis rates, their net accumulation rate constants (K_{acc}) have been suggested as indexes of 5HT synthesis (Chugani and Muzik 2000; Hagberg et al. 2002). It has also been suggested that K_{acc} values for these tracers are correlated (Hagberg et al. 2002; Leyton et al. 2005) (Figs. 24.4 and 24.5).

Modelling of data taking peripheral tracer metabolism into account showed that transfer influx of the tracers into the brain was similar or higher for $[^{11}\text{C}]\text{5HTP}$ (in the striatum and thalamus) when comparing $[^{11}\text{C}]\text{AMT}$ and $[^{11}\text{C}]\text{5HTP}$ tracers targeting the first and second enzymatic steps in 5HT synthesis. The rank order of K_{acc} measured with $[^{11}\text{C}]\text{5HTP}$ PET was in agreement with previous post-mortem regional 5HTP accumulation rates in the Rhesus monkey brain (Brown et al. 1979), namely,

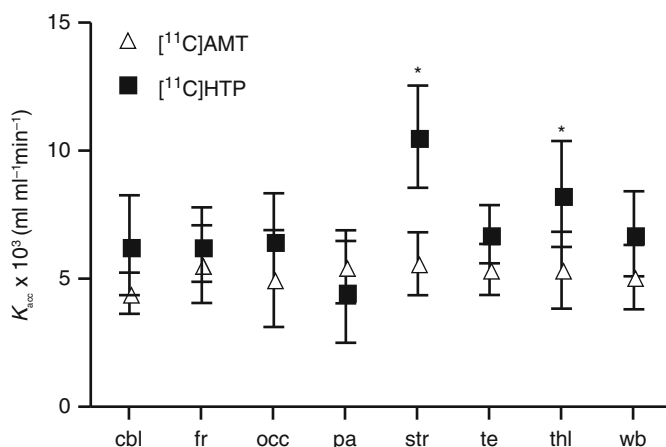


Fig. 24.6 Estimates of the net accumulation rate constant (average \pm SE) for [¹¹C]AMT and [¹¹C]5HTP in the monkey brain

highest in the striatum, intermediate in the thalamus and lowest in cortical areas (Fig. 24.6). While there were no substantial differences in K_{acc} for [¹¹C]AMT among the outlined brain regions, this was consistent with the results of earlier PET studies in Rhesus monkeys (Shoaf et al. 2000). The compartmental analysis results of K_{acc} were quite similar to or somewhat lower than the graphically obtained estimates. Thus, in contrast to two previous reports (Hagberg et al. 2002; Leyton et al. 2005), K_{acc} of [¹¹C]5HTP and [¹¹C]AMT were not seen to be well correlated (Shoaf et al. 2000).

It seems reasonable that these measures should be different as the tracers target different enzymes that differ in their enzyme activity in the brain (Ichiyama et al. 1968). In rats, pharmacological inhibition of AADC by NSD1015 decreased the trapping rate constant of [¹¹C]5HTP (Lindner et al. 1997). In recent autoradiographic studies, pharmacological inhibition of the tryptophan hydroxylase with *p*-chlorophenylalanine or AGN-2979 decreased the unidirectional trapping of [¹⁴C]AMT (Hasegawa et al. 2005; Tohyama et al. 2002). This suggests that K_{acc} of [¹¹C]AMT gives a reasonable estimation of the activity of tryptophan hydroxylase, while K_{acc} of [¹¹C]5HTP is providing an *in vivo* index of the activity of the decarboxylating enzyme AADC.

24.5 [¹¹C]HTP Target Specificity and Brain Metabolites

The conversion of 5HTP to 5HT was inhibited *in vivo* to investigate whether the suggested compartment model for [¹¹C]5HTP (Hagberg et al. 2002) was capable of demonstrating changes in the parameter or combination of parameters that are interpreted as reflecting AADC activity.

As [¹¹C]5HTP is also subject to decarboxylation by AADC in the periphery, inhibition of the enzyme using NSD1015 increased the radioactivity concentrations of

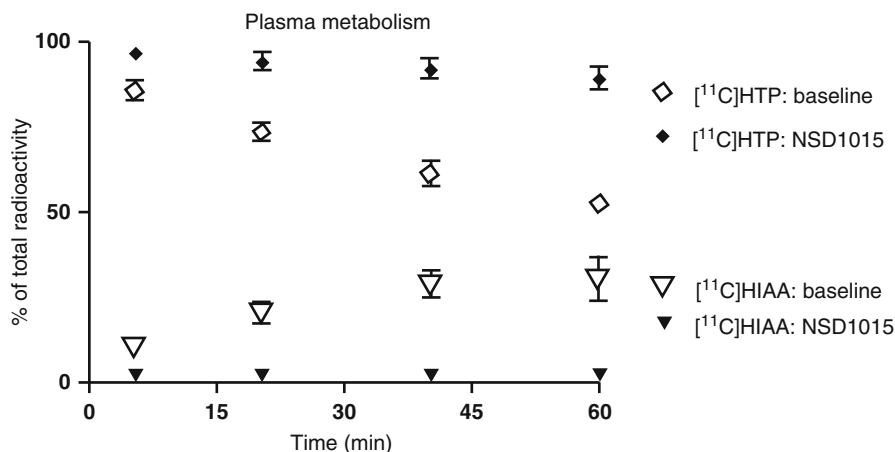


Fig. 24.7 Contribution of (^{11}C)5HTP and the metabolite (^{11}C)5HIAA to the total radioactivity concentrations in plasma before and after administration of NSD1015

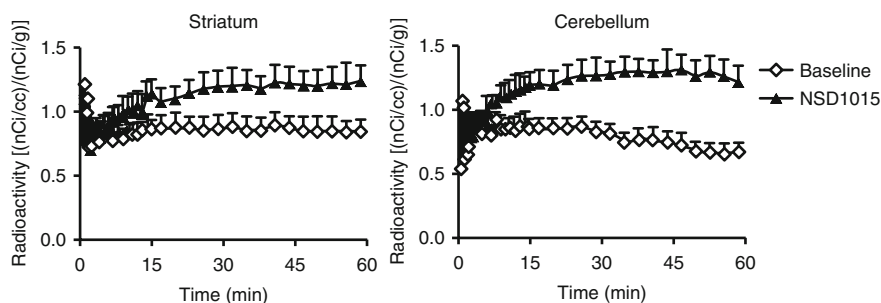


Fig. 24.8 Radioactivity concentrations (average \pm SE) in the striatum and cerebellum after bolus administration of (^{11}C)5HTP to monkeys before and after treatment with NSD1015

the fraction corresponding to $[^{11}\text{C}]\text{HTP}$ in plasma (Fig. 24.7). The uptake of $[^{11}\text{C}]\text{5HTP}$ -derived radioactivity after NSD1015 was also increased in all outlined brain regions, probably because of the increased availability of $[^{11}\text{C}]\text{HTP}$ to the brain.

After AADC inhibition using NSD1015, the parameters that are interpreted as reflecting AADC activity decreased in the striatum compared to baseline (Fig. 24.8). All the investigated brain regions were affected but only the decrease in the striatum was statistically significant. This could be due to the small sample size in this study, the degree of AADC inhibition achieved in brain tissue with NSD1015 10 mg/kg or the fact that the AADC activity in extra-striatal regions is low (Brown et al. 1979). The signal provided by $[^{11}\text{C}]\text{5HTP}$ PET might be difficult to use for monitoring changes in the enzyme system in other regions than the striatum. However, signal changes may be better measured in the human brain as the K_{acc} values in healthy volunteers are higher than the values obtained in the current monkey study (Hagberg et al. 2002).

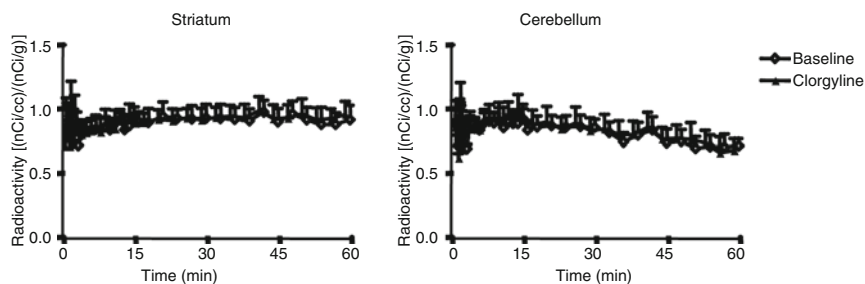


Fig. 24.9 Radioactivity concentrations (average \pm SE) in the monkey brain and cerebellum after bolus administration of [^{11}C]5HTP before and after administration of clorgyline to inhibit MAO

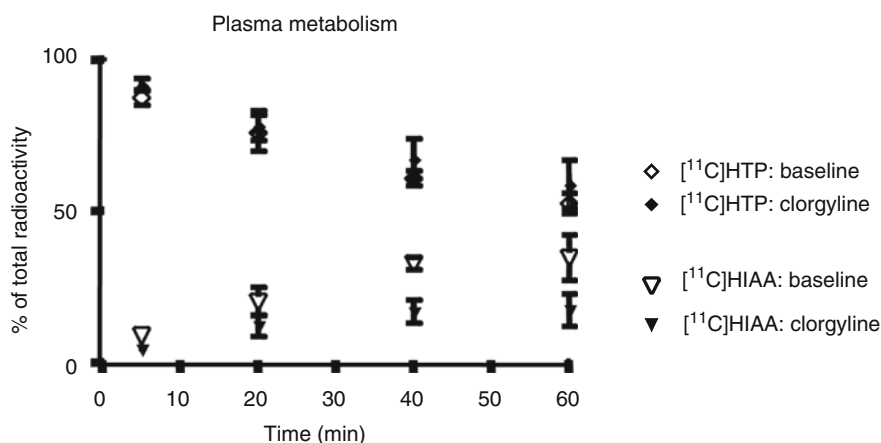


Fig. 24.10 Contribution of (^{11}C)5HTP and the metabolite (^{11}C)5HIAA to the total radioactivity concentrations in plasma before and after administration of clorgyline

Verification that no loss of [^{11}C]5HTP-derived radioactivity occurred during the PET study was undertaken by using clorgyline, an irreversible antagonist of MAO. Pretreatment of monkeys with clorgyline did not change the brain uptake of [^{11}C]5HTP-derived radioactivity (Fig. 24.9). This is in agreement with a previous study in rats where pretreatment with clorgyline altered the metabolism in favour of 5HT formation but did not change the uptake of [^{11}C]5HTP-derived radioactivity (Lindner et al. 1997). In healthy volunteers, an attempt to account for loss of labelled 5HIAA by introducing additional model rate constants did not improve the fit of the model (Hagberg et al. 2002).

The accumulation rate constant was not altered after clorgyline treatment (Fig. 24.10). This suggests that the amount of decarboxylated tracer metabolites eliminated from the brain is negligible and would not greatly prejudice estimation of AADC enzyme activity in the duration of the PET study.

24.5.1 Graphical Strategies for [¹¹C]5HTP Data Analysis

The Patlak analysis using plasma as input yielded similar estimates of the net accumulation rate constant to those obtained with the compartmental analysis but with less variability in the frontal, occipital and temporal cortices. As previously mentioned, using plasma as input is considered as gold standard, and therefore, a comparison with graphical analysis of two reference tissue models has also been tried (Lundquist et al. 2006).

The estimates from the reference tissue Patlak plots showed high variability in all outlined brain regions (Table 24.1, (Fig. 24.11)). Using the modified reference tissue input for Patlak analysis, the variability in the average macro-system parameter was lower and negative slopes, or slopes close to zero, were avoided.

The new approach requires an estimate of the trapping rate constant in the chosen reference region (l_3). If not measured previously, l_3 can be obtained from the literature. Alternatively, it has to be estimated by compartment modelling using the plasma input function.

A decrease in striatal K_{cPat} was seen after premedication with NSD1015 just as for the plasma input Patlak analysis (Table 24.1). It should be noted that the numerator in the expression for the irreversible uptake rate constant varies with the macro-system parameter used. Assuming a two-tissue compartment model with irreversible trapping in the second compartment, the different Patlak slopes of the reference tissue versions will be as follows:

Plasma input	$K_{\text{pPat}} = K_1 k_3 / (k_2 + k_3)$
Reference tissue input	$K_{\text{rPat}} = k_2 k_3 / (k_2 + k_3)$
Corrected reference tissue input	$K_{\text{cPat}} = ((k_2 + R l_3) k_3) / (k_2 + k_3)$ where $R = K_1 / l_1 = k_2 / l_2$

Finally, in studies using drug challenges, it could be argued if to use the baseline trapping value or the one after treatment.

24.6 Applications of Two Tracers to Indicate Serotonin Synthesis

The two tracers used to indicate serotonin synthesis rate, AMT and 5HTP have both advantages and disadvantages (Visser et al. 2011; Lundquist et al. 2007). AMT may enter the kynurenine pathway under inflammatory conditions, providing a false signal (Visser et al. 2011). Neuroinflammation occurs in many brain disorders and is a component of neurodegeneration occurring in PD, AD, depression and many other brain diseases. AMT has been used in several clinical studies particularly in epilepsy but also to give insight into depression and the action of antidepressants. The trapping of 5HTP may represent the last step in the serotonin synthesis. The two tracers are differently affected by tryptophan depletion and mood changes and their kinetics is influenced by different enzymatic processes (Visser et al. 2011).

Fig. 24.11 Patlak plots of (11C)5HTP data for the striatum using input data from plasma (a), cerebellum (b) and cerebellum tissue corrected for tracer trapping (c)

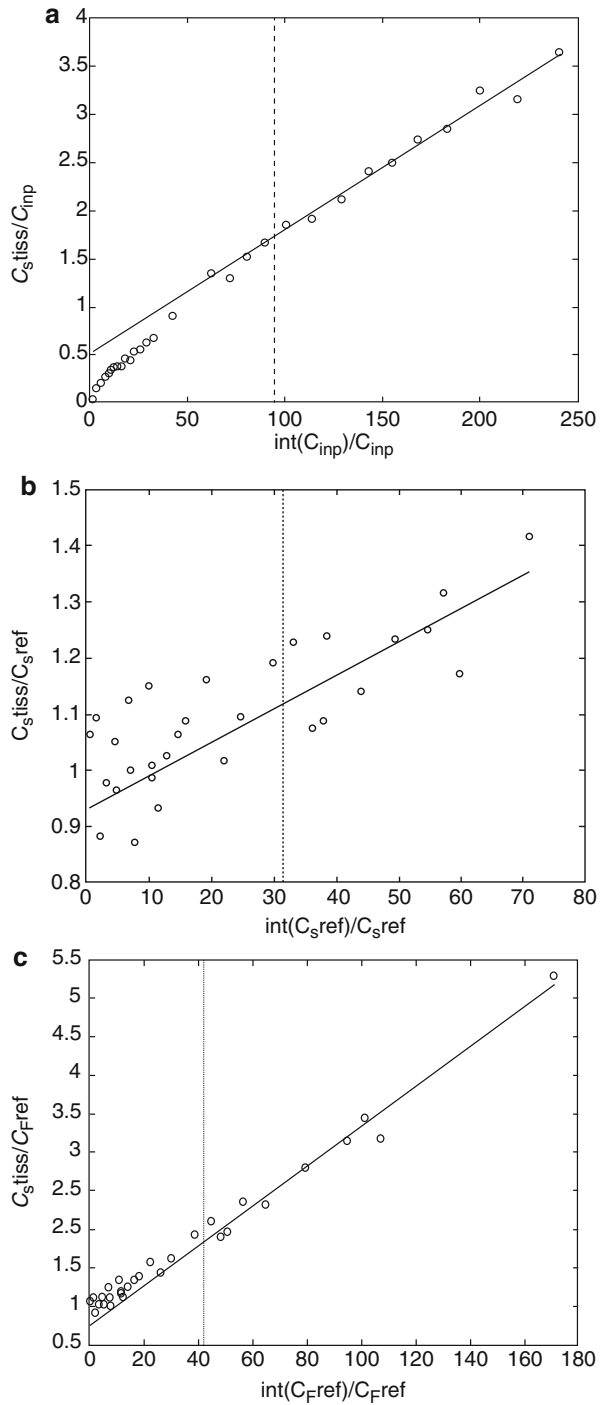


Table 24.1 Estimates of the net accumulation rate constant (Patlak slope) 30–60 min in the monkey after administration of (11C)5HTP at baseline and after NSD1015 and clorgyline treatment

Parameter	Condition	Brain region					
		Cerebellum	Frontal ctx	Occipital ctx	Striatum	Thalamus	
$K_{\text{pat}} \times 10^3$ (ml · ml ⁻¹ · min ⁻¹)	Baseline	6.2 (1.5)	5.4 (1.2)	5.4 (1.8)	9.2 (1.9)	5.6 (1.2)	6.7 (2.5)
	NSD1015	5.8 (-4.0; 1.7)	5.6 (-3.3; 2.4)	5.2 (-4.0; 1.7)	6.3 (-6.7; -1.0)	4.9 (-4.0; 1.7)	6.7 (-4.3; 1.4)
	Clorgyline	5.6 (-3.2; 1.3)	5.8 (-2.0; 2.5)	5.8 (-2.1; 2.3)	10.5 (-0.8; 3.7)	7.0 (-0.7; 3.8)	7.1 (-3.2; 1.3)
$K_{\text{pat}} \times 10^3$ (min ⁻¹)	Baseline	1.4 (2.2)	1.4 (2.2)	0.4 (2.2)	6.0 (3.0)	1.6 (3.2)	2.3 (3.3)
	NSD1015	2.9 (-2.9; 5.9)	2.9 (-2.9; 5.9)	0.5 (-3.7; 5.1)	2.9 (-7.9; 0.9)	2.0 (-4.1; 4.6)	3.9 (-3.4; 5.4)
	Clorgyline	3.3 (-3.8; 10.3)	3.3 (-3.8; 10.3)	3.0 (-3.8; 10.2)	9.2 (-1.6; 12.5)	5.5 (-1.1; 13.0)	4.7 (-5.4; 8.6)
$K_{\text{cPat}} \times 10^3$ (min ⁻¹)	Baseline	15.9 (1.6)	15.9 (1.6)	16.4 (2.7)	25.1 (2.3)	15.3 (3.3)	18.7 (3.9)
	NSD1015	16.7 (-4.3; 5.7)	16.7 (-4.3; 5.7)	16.2 (-6.0; 3.9)	18.6 (-11.6; -1.6)	15.7 (-4.3; 5.7)	18.9 (-5.9; 4.1)
	Clorgyline	18.2 (-5.3; 10.0)	18.2 (-5.3; 10.0)	19.5 (-5.1; 10.1)	28.6 (-3.0; 12.2)	20.3 (-0.6; 14.6)	20.5 (-7.0; 8.2)

24.6.1 Clinical Applications of (11C)-5-Hydroxytryptophan (5HTP)

5HTP is prepared by an enzymatic process by a nucleophile attack on the phenyl ring of L-alanine (Bjurling et al. 1989). 5HTP showed that brain radioactivity uptake in the whole brain of depressed patients was significantly lower as compared to healthy controls (Agren et al. 1991). This finding supported a compromised blood-brain transport of transmitters in depression. In a subsequent report, it was concluded that the utilisation rate of 5HTP was significantly higher in depressed patients in the striatum and areas of anterior frontal cortex of depressed patients (Agren et al. 1993). The higher utilisation rate was interpreted as local increased synthesis rate in the diseased brain and lends support that initiation of antidepressant treatment will further increase serotonin function in these areas giving symptoms of exaggeration after the onset of drug treatment.

Cardinal mood symptoms in premenstrual disorders were investigated in parallel with 5HTP positron emission tomography (Eriksson et al. 2006). Symptoms such as irritability and depressed mood were inversely correlated with cerebral 5HTP uptake. Variables associated with positive symptoms mood variables showed positive association, whereas no or little relation was found of 5HTP uptake to physical symptoms.

5HTP was also shown to have value in diagnosis, prognosis and the evaluation of therapy response of neuroendocrine tumours. These tumours may form serotonin at high rates. Detection of small tumours has become possible in the gastrointestinal tract which showed a close correlation of 5HTP utilisation and urine 5-hydroxyindoleacetic acid (5HIAA) excretion providing support for PET with 5HTP also to monitor therapy effectiveness (Orlefors et al. 1998). A further higher contrast of the signal to surrounding tissue was achieved by pretreatment of patients with carbidopa, a decarboxylase inhibitor which decreased the urinary radioactivity excretion of 5HTP sixfold while tumour radioactivity increased three times (Neels et al. 2009; Eriksson et al. 2000). 5HTP PET has been shown capable of detecting small metastatic lesions in surrounding tissue at an early stage, e.g. in the case of midgut carcinoids and prostatic carcinoma (Kälkner et al. 1997). 5HTP was explored as a universal tracer to detect foregut carcinoids extending investigation to the thorax and abdomen (Eriksson et al. 2000). Using this technique, it became possible to visualise small lesions in the pancreas and thorax which could not be detected with any other imaging method. 5HTP also detects more lesions in the liver and lymph nodes can be used to monitor treatment effects (Eriksson et al. 2000). As a conclusion, 5HTP PET is now established as the most valuable tool in the detection of neuroendocrine tumours.

24.6.2 Clinical Applications of (¹¹C)-Alpha-methyl-tryptophan (AMT)

AMT is synthesised by a stereoselective ¹¹C-methylation in a series of chemical reactions. The first synthesis reports appeared already in the late 1980s, but it took more than a decade to achieve clinical use of the new tracer (Chakraborty et al. 1996).

The first reports on epilepsy patients showed an interictal increase of AMT uptake in cortical epileptic foci (Chugani et al. 1998b) but also in cortical development malformations. The significance of increased AMT uptake may be increased activity of the inflammatory kynurenine pathway of tryptophan metabolism in the lesions which would correspond to histopathology findings (Chugani et al. 2008b). PET using AMT is considered less sensitive but more selective than FDG PET, possibly due to the increased kynurenic acid metabolism (Juhász et al. 2003).

The increased uptake in epilepsy was diffuse (Natsume et al. 2008). In fact, radioactivity uptake of AMT over time evaluated using the Patlak method did not show any time period of a linear increase, and slopes were not significantly different from zero which is consistent with a minimal rate of conversion (Gjedde 1982). The calculated accumulated rate showed a uniform pattern in the normal brain (Lundquist et al. 2007). A sex difference of AMT trapping was seen in patients with irritable bowel syndrome (Nakai et al. 2003) with higher synthesis rate in females. The finding was suggested to be related to a pathological visceral pain processing in the patients as compared to controls. Females may have lower plasma tryptophan concentrations (Young et al. 1999) which if not compensated for will contribute to falsely calculated values. Calculation of AMT synthesis rate is complicated and may include plasma concentration measurements of the tracer.

Different patterns of AMT synthesis changes in limbic and paralimbic cortices were observed in males and females suffering from major depression. In females, significant decreases in trapping as measured bilaterally in anterior cingulate cortex, while in males a decrease only in left anterior cingulate cortex was detected. The decrease in left mesial temporal cortex was similar in both sexes (Rosa-Neto et al. 2004). A lower AMT trapping in orbital and ventrolateral prefrontal cortex correlated negatively with suicide intent, indicating a lower threshold for suicidal behaviour with low serotonin synthesis rate (Leyton et al. 2006). AMT was also able to detect an increase on 5HT synthesis in the prefrontal cortex after addition of pindolol (a non-selective 5HT_{1A} receptor antagonist) to citalopram therapy as compared to citalopram alone in treatment of depression (Berney et al. 2008).

AMT trapping in the anterior cingulate cortex also correlated to experienced emotions. Consequently, lower AMT trapping evident in cortico-striatal areas was evident in borderline personality disorder and is possibly linked to impulsive behaviours of the patients (Leyton et al. 2001).

AMT has further been used in other affective disorders as obsessive-compulsive disorders (OCD) and Tourette's syndrome. OCD patients exhibited significantly higher AMT trapping in the right hippocampus and left temporal gyrus, and no brain regions showed lower trapping than controls. The higher striatal and temporal lobe activities in OCD, as seen with AMT, suggest a role of serotonin in the disease as well as in Tourette's syndrome.

Finally, AMT has also been used to supplement brain tumour diagnosis (Juhász et al. 2006). Primary and residual gliomas and glioneuronal tumours showed increased AMT uptake, suggesting an increased tryptophan turnover. In low-grade tumours, the contribution of the kynurenine pathway due to its regulation of tumour cell growth mechanism must be considered.

In conclusion, both tracers 5HTP and AMT are involved in the serotonergic machinery and may be used for diagnosis, prognosis and treatment follow-up of many diseases. In neuroendocrine tumours, 5HTP PET might even be a better modality than other imaging methods. The two tracers are indicating activity involved in the process of converting tryptophan to serotonin. AMT is a marker of hydroxylase, whereas 5HTP monitors the decarboxylase activity. The two tracers cannot be interchanged and it is not mandatory that results from one tracer coincide with results from the other. Therefore, they may be used in a complementary way.

References

- Aghajanian GK (1972) Chemical-feedback regulation of serotonin-containing neurons in brain. *Ann N Y Acad Sci* 193:86–94
- Agren H, Reibring L (1994) PET studies of presynaptic monoamine metabolism in depressed patients and healthy volunteers. *Pharmacopsychiatry* 27:2–6
- Agren H, Reibring L, Hartvig P, Tedroff J, Bjurling P, Hornfeldt K, Andersson Y, Lundqvist H, Langstrom B (1991) Low brain uptake of L-[11C]5-hydroxytryptophan in major depression: a positron emission tomography study on patients and healthy volunteers. *Acta Psychiatr Scand* 83:449–455
- Agren H, Reibring L, Hartvig P, Tedroff J, Bjurling P, Lundqvist H, Laengstrom B (1993) Monoamine metabolism in human prefrontal cortex and basal ganglia. PET studies using and [beta-11C]L-5-hydroxytryptophan and [beta-11C]L-DOPA in healthy volunteers and patients with unipolar major depression. *Depression* 1:71–81
- Berney A, Nishikawa M, Benkelfat C, Debonnel G, Gobbi G, Diksiz M (2008) An index of 5-HT synthesis changes during early antidepressant treatment: alpha-(11C)methyl-L-tryptophan PET study. *Neurochem Int* 52:701–708
- Bjurling P, Watanabe Y, Tokushige M, Oda T, Långström B (1989) Synthesis of β -II-L-tryptophan and 5-hydroxy-L-tryptophan using a multi-enzymatic reaction route. *J Chem Soc Perkin Trans 1*:1331–1334
- Blomqvist G, Pauli S, Farde L, Ericksson L, Persson A, Halldin C (1989) Dynamic models of reversible ligand binding. In: Beckers CGA, Bol A (eds) *Clinical research and clinical diagnosis*. Kluwer Academic Publishers, Dordrecht, pp 35–44
- Brown RM, Crane AM, Goldman PS (1979) Regional distribution of monoamines in the cerebral cortex and subcortical structures of the rhesus monkey: concentrations and in vivo synthesis rates. *Brain Res* 168:133–150
- Chakraborty PK, Mangner TJ, Chugani DC, Muzik O, Chugani HT (1996) A high-yield and simplified procedure for the synthesis of alpha-[11C]methyl-L-tryptophan. *Nucl Med Biol* 23:1005–1008
- Chandana SR, Behen ME, Juhasz C, Muzik O, Rothermel RD, Mangner TJ, Chakraborty PK, Chugani HT, Chugani DC (2005) Significance of abnormalities in developmental trajectory and asymmetry of cortical serotonin synthesis in autism. *Int J Dev Neurosci* 23:171–182
- Chugani DC, Muzik O (2000) Alpha-[C-11]methyl-L-tryptophan PET maps brain serotonin synthesis and kynurenine pathway metabolism. *J Cereb Blood Flow Metab* 20:2–9
- Chugani DC, Muzik O, Chakraborty P, Mangner T, Chugani HT (1998a) Human brain serotonin synthesis capacity measured in vivo with alpha-[C-11]methyl-L-tryptophan. *Synapse* 28:33–43
- Chugani DC, Chugani HT, Muzik O, Shah JR, Canady A, Magner TJ, Chakraborty PK (1998b) Imaging epileptogenic tubers in children with tuberous sclerosis complex using alpha-(11C) methyl-L-tryptophan positron emission tomography. *Ann Neurol* 44:858–866
- Chugani HT, Juhász C, Chugani DC, Lawrenson L, Muzik O, Chakraborty PK, Sood S (2008) Increased striatal serotonin synthesis following cortical resection in children with intractable epilepsy. *Epilepsy Res* 78:124–130

- Cunningham VJ, Hume SP, Price GR, Ahier RG, Cremer JE, Jones AK (1991) Compartmental analysis of diprenorphine binding to opiate receptors in the rat in vivo and its comparison with equilibrium data in vitro. *J Cereb Blood Flow Metab* 11:1–9
- Diksic M, Nagahiro S, Sourkes TL, Yamamoto YL (1990) A new method to measure brain serotonin synthesis in vivo. I. Theory and basic data for a biological model. *J Cereb Blood Flow Metab* 10:1–12
- Eriksson B, Bergström ÖH, Sundin A, Öberg K, Långström B (2000) Use of PET in neuroendocrine tumors. In vivo applications and in vitro studies. *Q J Nucl Med* 44:68–75
- Eriksson O, Wall A, Marteinsdottir I, Ågren H, Hartvig P, Blomquist G, Långström B (2006) Mood changes correlate to changes in brain serotonin precursor trapping in women with premenstrual dysphoria. *Psychiatry Res* 146:107–116
- Fedi M, Reutens DC, Andermann F, Okazawa H, Boling W, White C, Dubeau F, Nakai A, Gross DW, Andermann E, Diksic M (2003) Alpha-(11C) methyl-L-tryptophan PET identifies the epileptogenic tuber and correlates with interictal spike frequency. *Epilepsy Res* 52:203–213
- Fernström JD, Wurtman RJ (1971) Brain serotonin content: physiological dependence on plasma tryptophan levels. *Science* 173:149–152
- Friedman PA, Kappelman AH, Kaufman S (1972) Partial purification and characterization of tryptophan hydroxylase from rabbit hindbrain. *J Biol Chem* 247:4165–4173
- Fuller RW (1994) Uptake inhibitors increase extracellular serotonin concentration measured by brain microdialysis. *Life Sci* 55:163–167
- Gaddum JH (1953) Antagonism between lysergic acid diethylamide and 5-hydroxytryptamine. *J Physiol* 121:15P
- Gharib A, Balende C, Sarda N, Weissmann D, Plenevaux A, Luxen A, Bobillier P, Pujol JF (1999) Biochemical and autoradiographic measurements of brain serotonin synthesis rate in the freely moving rat: a reexamination of the alpha-methyl-L-tryptophan method. *J Neurochem* 72:2593–2600
- Gingrich JA, Hen R (2001) Dissecting the role of the serotonin system in neuropsychiatric disorders using knockout mice. *Psychopharmacology (Berl)* 155:1
- Gjedde A (1982) Calculation of cerebral glucose phosphorylation from brain uptake of glucose analogs in vivo: a re-examination. *Brain Res Rev* 257:237–274
- Gunn RN, Gunn SR, Cunningham VJ (2001) Positron emission tomography compartmental models. *J Cereb Blood Flow Metab* 21:635–652
- Gunn RN, Gunn SR, Turkheimer FE, Aston JA, Cunningham VJ (2002) Positron emission tomography compartmental models: a basis pursuit strategy for kinetic modeling. *J Cereb Blood Flow Metab* 22:1425–1439
- Hagberg GE, Torstenson R, Marteinsdottir I, Fredrikson M, Langstrom B, Blomqvist G (2002) Kinetic compartment modeling of [11C]-5-hydroxy-L-tryptophan for positron emission tomography assessment of serotonin synthesis in human brain. *J Cereb Blood Flow Metab* 22:1352–1366
- Hasegawa S, Kanemaru K, Gittos M, Diksic M (2005) The tryptophan hydroxylase activation inhibitor, AGN-2979, decreases regional 5-HT synthesis in the rat brain measured with alpha-[14C]methyl-L-tryptophan: an autoradiographic study. *Brain Res Bull* 67:248–255
- Hokfelt T, Fuxe K, Goldstein M (1973) Immunohistochemical localization of aromatic L-amino acid decarboxylase (DOPA decarboxylase) in central dopamine and 5-hydroxytryptamine nerve cell bodies of the rat. *Brain Res* 53:175–180
- Hume SP, Myers R, Bloomfield PM, Opacka-Juffry J, Cremer JE, Ahier RG, Luthra SK, Brooks DJ, Lammertsma AA (1992) Quantitation of carbon-11-labeled raclopride in rat striatum using positron emission tomography. *Synapse* 12:47–54
- Ichiyama A, Nakamura S, Nishizuka Y, Hayaishi O (1968) Tryptophan-5-hydroxylase in mammalian brain. *Adv Pharmacol* 6:5–17
- Jacobs BL, Azmitia EC (1992) Structure and function of the brain serotonin system. *Physiol Rev* 72:165–229
- Juhász C, Chugani DC, Muzik O, Shah A, Asano E, Mangner TJ, Chakraborty PK, Sood S, Chugani HT (2003) Alpha-methyl-L-tryptophan PET detects epileptogenic cortex in children with intractable epilepsy. *J Cereb Blood Flow Metab* 60:960–968

- Juhász C, Chugani DC, Muzik O, Wu D, Sloan AE, Barger G, Watson C, Shah AK, Sood S, Ergun EL, Mangner TJ, Chakraborty PK, Kupsky WJ, Chugani HT (2006) In vivo uptake and metabolism of alpha-(11)methyl-L-tryptophan in human brain tumors. *J Cereb Blood Flow Metab* 26:345–357
- Kagawa K, Chugani DC, Asano E, Juhász C, Muzik O, Shah A, Shah J, Sood S, Kupsky WJ, Mangner TJ, Chakraborty PK, Chugani HT (2005) Epilepsy surgery outcome in children with tuberous sclerosis complex evaluated with alpha-[11C]methyl-L-tryptophan positron emission tomography (PET). *J Child Neurol* 20:429–438
- Kalen P, Strecker RE, Rosengren E, Bjorklund A (1988) Endogenous release of neuronal serotonin and 5-hydroxyindoleacetic acid in the caudate-putamen of the rat as revealed by intracerebral dialysis coupled to high-performance liquid chromatography with fluorimetric detection. *J Neurochem* 51:1422–1435
- Kälkner KM, Ginman C, Nilsson S, Bergström M, Antoni G, Ahlström H, Långström B (1997) Positron emission tomography (PET) with 11C-5-hydroxytryptophan (5-HTP) in patients with metastatic hormone refractory prostatic adenocarcinoma. *Nucl Med Biol* 24: 319–325
- Kety SS, Schmidt CF (1948) The nitrous oxide method for the quantitative determination of cerebral blood flow in man: theory, procedure and normal values. *J Clin Invest* 27:476–483
- Koepp RA (2002) Data analysis and image processing. In: Wahl RL (ed) *Principles and practice of positron emission tomography*. Lippincott Williams & Wilkins, Philadelphia, pp 69–105
- Lammertsma AA, Hume SP (1996) Simplified reference tissue model for PET receptor studies. *Neuroimage* 4:153–158
- Lammertsma AA, Bench CJ, Hume SP, Osman S, Gunn K, Brooks DJ, Frackowiak RS (1996) Comparison of methods for analysis of clinical [11C]raclopride studies. *J Cereb Blood Flow Metab* 16:42–52
- Laruelle M, Slifstein M, Huang Y (2003) Relationships between radiotracer properties and image quality in molecular imaging of the brain with positron emission tomography. *Mol Imaging Biol* 5:363–375
- Leyton M, Okazawa H, Diksic M, Paris J, Rosa P, Mzengeza S, Young SN, Blier P, Benkelfat C (2001) Brain regional alpha-(11)methyl-L-tryptophan trapping in impulsive subjects with borderline personality disorder. *Am J Psychiatry* 158:775–782
- Leyton M, Diksic M, Benkelfat C (2005) Alpha-(11C)methyl-L-tryptophan trapping correlates with post-mortem tissue serotonin content and [11C]5-hydroxytryptophan accumulation. *Int J Neuropsychopharmacol* 8:633–634
- Leyton M, Paquette V, Gravel P, Rosa-Neto P, Weston F, Diksic M, Benkelfat C (2006) Alpha-(11C)methyl-L-tryptophan trapping in the orbital and ventral medial prefrontal cortex of suicide attempters. *Eur Neuropsychopharmacol* 16:220–223
- Lindner KJ, Hartvig P, Bjurling P, Fasth KJ, Westerberg G, Langstrom B (1997) Determination of 5-hydroxy-L-[beta-11C]tryptophan and its in vivo-formed radiolabeled metabolites in brain tissue using high performance liquid chromatography: a study supporting radiotracer kinetics obtained with positron emission tomography. *Nucl Med Biol* 24:733–738
- Logan J, Fowler JS, Volkow ND, Wolf AP, Dewey SL, Schlyer DJ, MacGregor RR, Hitzemann R, Bendriem B, Gatley SJ et al (1990) Graphical analysis of reversible radioligand binding from time-activity measurements applied to [N-11C-methyl]-(-)-cocaine PET studies in human subjects. *J Cereb Blood Flow Metab* 10:740–747
- Logan J, Fowler JS, Volkow ND, Wang GJ, Ding YS, Alexoff DL (1996) Distribution volume ratios without blood sampling from graphical analysis of PET data. *J Cereb Blood Flow Metab* 16:834–840
- Lundquist P, Blomquist G, Hartvig P, Hagberg GE, Torstenson R, Hammarlund-Udenaes M, Långström B (2006) Validation studies on the 5-hydroxy-L-[beta-11C]-tryptophan/PET method for probing the decarboxylase step in serotonin synthesis. *Synapse* 59(8):521–531
- Lundquist P, Hartvig P, Blomquist G, Hammarlund-Udenaes M, Långström B (2007) 5-Hydroxy-L-[beta-11C]tryptophan versus alpha-[11C]methyl-L-tryptophan for PET imaging of serotonin synthesis capacity in the rhesus monkey brain. *J Cereb Blood Flow Metab* 27:821–830

- Marshall EF, Stirling GS, Tait AC, Todrick A (1960) The effect of iproniazid and imipramine on the blood platelet 5-hydroxytryptamine level in man. *Br J Pharmacol Chemother* 15:35–41
- Meltzer HY (1990) Role of serotonin in depression. *Ann N Y Acad Sci* 600:448–500
- Mintun MA, Raichle ME, Kilbourn MR, Wooten GF, Welch MJ (1984) A quantitative model for the in vivo assessment of drug binding sites with positron emission tomography. *Ann Neurol* 15:217–227
- Murphy DL, Wichems C, Li Q, Heils A (1999) Molecular manipulations as tools for enhancing our understanding of 5-HT neurotransmission. *Trends Pharmacol Sci* 20:246–252
- Muzik O, Chugani DC, Chakraborty P, Mangner T, Chugani HT (1997) Analysis of [^{11}C]alpha-methyl-tryptophan kinetics for the estimation of serotonin synthesis rate in vivo. *J Cereb Blood Flow Metab* 17:659–669
- Nakai A, Kumakura Y, Boivin M, Rosa P, Diksic M, D Souza D, Kersey K (2003) Sex difference of brain serotonin synthesis in patients with irritable bowel syndrome using alpha-(^{11}C)methyl-L-tryptophan, positron emission tomography and statistical parametric mapping. *Can J Gastroenterol* 17:191–196
- Natsume J, Kumakura Y, Bernasconi N, Soucy JP, Nakai A, Rosa P, Fedi M, Dubeau F, Andermann F, Lisbona R, Bernasconi A, Diksic M (2003) Alpha-[^{11}C]methyl-L-tryptophan and glucose metabolism in patients with temporal lobe epilepsy. *Neurology* 60:756–761
- Natsume J, Bernasconi N, Aghakhani Y, Kumakura Y, Nishikawa M, Fedi M, Soualmi L, Dubeau F, Andermann F, Bernasconi A, Diksiz M (2008) Alpha-[^{11}C]methyl-L-tryptophan uptake in neuroendocrine nodular heterotopia and epilepsy. *Epilepsia* 49:826–831
- Neckers LM (1982) Serotonin turnover and regulation. In: Osborne NN (ed) *Biology of serotonergic transmission*. John Wiley & Sons Ltd., New York, pp 139–158
- Neels OC, Koopmans KP, Jager PL, Vercauteren L, van Waarde A, Doorduyn J, Timmer-Boscha H, Brouwers AH, de Vries EG, Dierckx RA, Kerma IP, Elsinga PH (2009) Manipulation of (^{11}C)-5-hydroxytryptophan and 6(^{18}F)-fluoro-3,4-dihydroxyphenylalanine accumulation in neuroendocrine tumor cells. *Cancer Res* 69:7183–7190
- Nishikawa M, Kumakura Y, Young SN, Fiset P, Vogelzangs N, Leyton M, Benkelfat C, Diksic M (2005) Increasing blood oxygen increases an index of 5-HT synthesis in human brain as measured using alpha-[(^{11}C)]methyl-L-tryptophan and positron emission tomography. *Neurochem Int* 47:556–564
- Orlefors H, Sundin A, Ahlström H, Bjurling P, Bergström M, Lilja A, Långström B, Oberg K, Eriksson B (1998) Positron emission tomography with 5-hydroxytryptophan in neuroendocrine tumors. *J Clin Oncol* 16:2534–2541
- Ota M, Naoi M, Hamanaka T, Nagatsu T (1990) Inhibition of human aromatic L-amino acid decarboxylase by cooked food-derived 3-amino-1-methyl-H-pyridol (4,3-b)indole (Trp-P-2) and other heterocyclic amines. *Neurosci Lett* 116:372–378
- Pardridge WM (1998) Blood-brain barrier carrier-mediated transport and brain metabolism of amino acids. *Neurochem Res* 23:635–644
- Pardridge WM, Oldendorf WH (1977) Transport of metabolic substrates through the blood-brain barrier. *J Neurochem* 28:5–12
- Patlak CS, Blasberg RG (1985) Graphical evaluation of blood-to-brain transfer constants from multiple – time uptake data. Generalizations. *J Cereb Blood Flow Metab* 5:584–590
- Patlak CS, Blasberg RG, Fenstermacher JD (1983) Graphical evaluation of blood-to-brain transfer constants from multiple-time uptake data. *J Cereb Blood Flow Metab* 3:1–7
- Pletscher A, Shore PA, Brodie BB (1955) Serotonin release as a possible mechanism of reserpine action. *Science* 122:374–375
- Reibring L, Agren H, Hartvig P, Tedroff J, Lundqvist H, Bjurling P, Kihlberg T, Langstrom B (1992) Uptake and utilization of [^{11}C]5-hydroxytryptophan in human brain studied by positron emission tomography. *Psychiatry Res* 45:215–225
- Rosa-Neto P, Diksic M, Okazawa H, Leyton M, Mzengeza S, Nakai A, Debonnel G, Blier BC (2004) Measurement of brain regional alpha-(^{11}C)methyl-L-tryptophan trapping as a measure of serotonin synthesis in medication-free patients with major depression. *Arch Gen Psychiatry* 61:556–563

- Sharp T, Foster GA (1989) In vivo measurement using microdialysis of the release and metabolism of 5-hydroxytryptamine in raphe neurones grafted to the rat hippocampus. *J Neurochem* 53:303–306
- Sharp T, Bramwell SR, Clark D, Grahame-Smith DG (1989) In vivo measurement of extracellular 5-hydroxytryptamine in hippocampus of the anaesthetized rat using microdialysis: changes in relation to 5-hydroxytryptaminergic neuronal activity. *J Neurochem* 53:234–240
- Shoaf SE, Carson RE, Hommer D, Williams WA, Higley JD, Schmall B, Herscovitch P, Eckelman WC, Linnoila M (2000) The suitability of [¹¹C]-alpha-methyl-L-tryptophan as a tracer for serotonin synthesis: studies with dual administration of [¹¹C] and [¹⁴C] labeled tracer. *J Cereb Blood Flow Metab* 20:244–252
- Slifstein M, Laruelle M (2000) Effects of statistical noise on graphic analysis of PET neuroreceptor studies. *J Nucl Med* 41:2083–2088
- Sokoloff L, Reivich M, Kennedy C, Des Rosiers MH, Patlak CS, Pettigrew KD, Sakurada O, Shinohara M (1977) The [¹⁴C]deoxyglucose method for the measurement of local cerebral glucose utilization: theory, procedure, and normal values in the conscious and anesthetized albino rat. *J Neurochem* 28:897–916
- Stenfors C, Ross SB (2004) Changes in extracellular 5-HIAA concentrations as measured by in vivo microdialysis technique in relation to changes in 5-HT release. *Psychopharmacology (Berl)* 172:119–128
- Sumi C, Ichinose H, Nagatsu T (1990) Characterization of recombinant human aromatic L-amino acid decarboxylase expressed in COS cells. *J Neurochem* 55:1075–1078
- Tappaz ML, Pujol JF (1980) Estimation of the rate of tryptophan hydroxylation in vivo: a sensitive microassay in discrete rat brain nuclei. *J Neurochem* 34:933–940
- Tohyama Y, Takahashi S, Merid MF, Watanabe A, Diksic M (2002) The inhibition of tryptophan hydroxylase, not protein synthesis, reduces the brain trapping of alpha-methyl-L-tryptophan: an autoradiographic study. *Neurochem Int* 40:603–610
- Trulsson ME, Jacobs BL (1976) Dose-response relationships between systemically administered L-tryptophan or L-5-hydroxytryptophan and raphe unit activity in the rat. *Neuropharmacology* 15:339–344
- Valentino RJ, Commons KG (2005) Peptides that fine-tune the serotonin system. *Neuropeptides* 39:1–8
- Visser AK, van Waarde A, Willemsen AT, Bosker FJ, Luiten PG, den Boer JA, Kema IP, Dierrckx RA (2011) Measuring serotonin synthesis: from conventional methods to PET tracers and their (pre)clinical implications. *Eur J Nucl Med Mol Imaging* 38(3):576–591
- Vogt M (1982) Some functional aspects of central serotonergic neurones. In: Osborne NN (ed) *Biology of serotonergic transmission*. John Wiley & Sons Ltd., New York, pp 299–315
- Walther DJ, Peter JU, Bashammakh S, Hortnagl H, Voits M, Fink H, Bader M (2003) Synthesis of serotonin by a second tryptophan hydroxylase isoform. *Science* 299:76
- Weiger WA (1997) Serotonergic modulation of behaviour: a phylogenetic overview. *Biol Rev Camb Philos Soc* 72:61–95
- White KJ, Walline CC, Barker EL (2005) Serotonin transporters: implications for antidepressant drug development. *Aaps J* 7:E421–E433
- Young SN, Gauthier S (1981) Effect of tryptophan administration on tryptophan, 5-hydroxyindoleacetic acid and indoleacetic acid in human lumbar and cisternal cerebrospinal fluid. *J Neurol Neurosurg Psychiatry* 44:323–328
- Young SN, Tsang D, Lai S, Sourkes TL (1977) Changes in tryptophan content of excised human cerebral cortex. *J Neurochem* 28:439–449
- Young SN, Leyton M, Benkelfat C (1999) PET studies of serotonin synthesis in human brain. *Adv Exp Med Biol* 467:11–18
- Zhang X, Beaulieu JM, Sotnikova TD, Gainetdinov RR, Caron MG (2004) Tryptophan hydroxylase-2 controls brain serotonin synthesis. *Science* 305:217
- Zhu MY, Juorio AV (1995) Aromatic L-amino acid decarboxylase: biological characterization and functional role. *Gen Pharmacol* 26:681–696

Monoamine Oxidase A and Serotonin Transporter Imaging with Positron Emission Tomography

25

Jeffrey H. Meyer

Contents

25.1	Why Image Indices of Monoamine Oxidase A Density?.....	712
25.1.1	Radioligands Available for Neuroimaging Monoamine Oxidase A	713
25.1.2	Major Depressive Disorder	714
25.1.3	Early Postpartum.....	716
25.1.4	Cigarette Smoking.....	718
25.1.5	Aggression	719
25.2	Why Image Indices of Serotonin Transporter Density?.....	721
25.2.1	Radioligands Available for Imaging Serotonin Transporters.....	722
25.2.2	Developing New Antidepressants with Serotonin Transporter Neuroimaging	723
25.2.3	Major Depressive Disorder	726
25.2.4	Ecstasy Abuse and Serotonin Transporter Imaging	728
25.2.5	Obsessive-Compulsive Disorder.....	729
25.2.6	Season and Serotonin Transporter Imaging.....	730
	Conclusions.....	730
	References.....	732

Abstract

Serotonin has a major role in neural circuits of mood regulation, substance abuse, and neurodevelopment (Azmitia, *Neuropsychopharmacology* 21:1S–45S, 1999). Although they differ in cellular and anatomical location, the two brain proteins most strongly implicated in influencing serotonin levels are monoamine oxidase A and the serotonin transporter (Blier and De Montigny, *J Neurosci* 3:1270–1278, 1983; Bel and Artigas, *Eur J Pharmacol* 229:101–103, 1992; Synapse 15:243–245, 1993; Naunyn Schmiedebergs *Arch Pharmacol* 351:475–482, 1995; Dreshfield et al., *Neurochem Res* 21:557–562, 1996; Moret and Briley, *Eur J Pharmacol* 295:189–197, 1996; Mathews et al., *Soc Neurosci* 30:624, 2000;

J.H. Meyer

Department of Psychiatry, Center for Addiction and Mental Health, University of Toronto,
250 College Street, Toronto, ON M5T 1R8, Canada
e-mail: jeff.meyer@camhpet.ca

Youdim et al., *Nat Rev Neurosci* 7:295–309, 2006). Coincidentally, there have been major advances in positron emission tomography (PET) radioligand development for these two targets over the past decade, and the application of these advances has greatly increased our knowledge about fundamental processes in many important, impactful conditions including major depressive disorder, early postpartum, cigarette smoking, aggressive behavior, antidepressant development, ecstasy abuse, obsessive-compulsive disorder, and seasonal affective disorder as reviewed in this chapter.

25.1 Why Image Indices of Monoamine Oxidase A Density?

Monoamine oxidase A (MAO-A) is an enzyme that metabolizes three major monoamines (serotonin, norepinephrine, dopamine) in the brain and has a role in creating oxidative stress and predisposition to apoptosis (Youdim et al. 2006). In contrast to MAO-A, monoamine oxidase B (MAO-B) metabolizes primarily dopamine. Monoamine levels influence mood (Freis 1954; Ruhe et al. 2007), and oxidative stress and apoptosis influence brain development (Bortolato et al. 2008) and neurodegenerative mechanisms. Hence, MAO-A is a logical target for investigations in mood disorders, neuronal damage, substance abuse (during which markers of dysregulated monoamine levels occur; Stockmeier 2003; Meyer 2008), and aggression for which abnormal neurodevelopment is implicated (Buckholtz and Meyer-Lindenberg 2008). Illnesses and conditions for which dysregulation of monoamine levels is implicated include major depressive disorder, substance abuse, neurodegenerative diseases, and aggression (Fowler et al. 1996; Youdim et al. 2006; Meyer et al. 2006; Bacher et al. 2011). MAO-A is predominantly located on outer mitochondria membranes in neurons (as well as glia) and has a high density in brain regions that influence mood (Saura et al. 1992) although the cellular distribution varies by region (Saura et al. 1992, 1996; Finberg 2012). MAO-A density is highest in brain stem (within the locus coeruleus); moderately high in the cortex, hippocampus, and striatum; lower in cerebellar cortex; and minimal in white matter tissue (Saura et al. 1992, 1996).

Early investigations measured MAO density and activity in platelets, which do not reflect brain MAO-A. Platelet MAO only reflects MAO-B activity because metabolism of MAO substrates tryptamine, tyramine, and benzylamine can be inhibited to near 100 % by moderate doses of the MAO-B inhibitor selegiline, but metabolism of these substrates in platelets is insensitive to MAO-A inhibitors such as moclobemide and clorgyline (Donnelly and Murphy 1977; Murphy et al. 1979; Wiesel et al. 1985; Lensch et al. 1987).

The density of MAO-A correlates highly with the level of its metabolic activity (Nelson et al. 1979; Saura et al. 1992); hence, neuroimaging of measures of MAO-A binding can be interpreted as having functional implications (Saura et al. 1992). This approach represents an optimal practical method for applying neuroimaging towards a strongly functional index of MAO-A activity. Another approach would be to measure a radiotracer which is metabolized by MAO-A, but this is extremely

difficult because the potential brain radiotracer would require kinetics in which the dominant, separable, and measurable effect is its metabolism by MAO-A, rather than its crossing of the blood-brain barrier. In addition, most radiotracers that assess metabolism accumulate as a product in the brain which can be a disadvantageous strategy in radiotracer development because such radiotracers are less likely to exhibit reversible time-activity curves and irreversible time-activity curves are usually subject to bias from blood flow. Hence, the most optimal, practical neuroimaging approach towards quantitating MAO-A function with PET or SPECT is the use of radioligands that bind to MAO-A as reversible inhibitors.

25.1.1 Radioligands Available for Neuroimaging Monoamine Oxidase A

There are three PET radiotracers that have been applied for measurement of available monoamine oxidase A in human study (see Table 25.1). The first radiotracer developed, [^{11}C]clorgyline, demonstrated adequate brain penetration and selectivity, but did not have reversible time-activity curves (Fowler et al. 1987). Clorgyline is a mechanism-based MAO-A inhibitor which irreversibly binds to MAO-A, while in the enzyme-substrate complex and thus when [^{11}C]clorgyline is administered, the enzyme becomes irreversibly labeled. A deuterium-substituted version of [^{11}C]clorgyline was developed to verify that the PET image results from cleavage of the C–H or C–D bond on the propargyl group and to facilitate the separation of radiotracer delivery from radioligand binding to the enzyme. While deuterium substitution did reduce the binding rate verifying MAO-A binding as predicted, it also revealed high white matter binding with reduced signal-to-noise ratio (Fowler et al. 1996). More recently, [^{11}C]befloxatone and [^{11}C]harmine were developed. [^{11}C]Befloxatone shows promising radiotracer qualities of selectivity and reversibility and has been modeled in baboons (Curet et al. 1998; Dolle et al. 2003; Bottlaender et al. 2010). Unfortunately, it has not been modeled in humans, test-retest reliability

Table 25.1 Comparison of PET radiotracers for monoamine oxidase A

	[^{11}C]Clorgyline	[^{11}C]Harmine	[^{11}C]Befloxatone
Selectivity	Excellent (Fowler et al. 1987)	Excellent (Bergstrom et al. 1997b)	Excellent (Dolle et al. 2003)
Reversibility	Not reversible (Fowler et al. 1987)	Highly reversible (Ginovart et al. 2006)	Highly reversible (Bottlaender et al. 2010)
Modeling	2-tissue compartment (Fowler et al. 1987)	2-tissue compartment (human) (Ginovart et al. 2006)	2-tissue compartment (baboon) (Bottlaender et al. 2010)
Reliability	Very good (Fowler et al. 1996)	Excellent (Sacher et al. 2012)	Not reported
Metabolites crossing the blood-brain barrier?	Unlikely	No brain penetrant metabolites (Wilson et al. 2003)	Unlikely

in humans is not known, and there may be some proprietary issues limiting its widespread use.

[¹¹C]Harmine demonstrates the properties of an excellent PET radiotracer for an index of available MAO-A density in humans. [¹¹C]Harmine has high affinity for the MAO-A enzyme ($K_i=2$ nM) with high brain uptake in humans and is selective for MAO-A (Bergstrom et al. 1997b; Ginovart et al. 2006; Meyer et al. 2006). The affinity of [¹¹C]harmine is three orders of magnitude higher for MAO-A than MAO-B (Bergstrom et al. 1997a). Displacement studies in baboons using MAO-A selective inhibitors show complete displacement of [¹¹C]harmine in regions with high density of MAO-A (Bergstrom et al. 1997a). The uptake is specific to the parent compound as metabolites of harmine are polar and do not cross the blood-brain barrier (Tweedie and Burke 1987). The uptake of [¹¹C]harmine is highest in brain regions with greater MAO-A density such as the cortex and lowest in regions with low MAO-A density such as white matter (Bergstrom et al. 1997c). The MAO-A V_T (MAO-A distribution volume) is primarily an index of specifically bound [¹¹C]harmine at equilibrium since 80–85 % represents specific binding and the levels of free and nonspecific binding are similar among different people (Ginovart et al. 2006; Sacher et al. 2011). The modeling of this compound in humans best fits a two-tissue-compartment model, and negligible bias is found when the Logan model is applied (Ginovart et al. 2006).

25.1.2 Major Depressive Disorder

The in vivo aspect of neuroimaging offers the ability to readily sample medication-free subjects and to selectively choose early-onset major depressive disorder (MDD) which is the most common form (WHO 2008). Late-onset MDD is often attributable to neurodegenerative diseases such as Parkinson's disease and Alzheimer's disease (Krishnan 2002), which would be expected to have very different pathologies from early-onset MDD. Since postmortem studies often preferentially sample older subjects, sometimes they are not targeted towards early-onset MDD. The first three postmortem studies of MAO-A levels and activity had not selectively targeted early-onset MDD, and the early perspective of the field was that there was no abnormality of MAO-A level or activity in MDD (Mann and Stanley 1984; Sherif et al. 1991; Ordway et al. 1999).

In 2006, MAO-A V_S , an index of MAO-A density, was measured using [¹¹C]harmine PET in medication-free major depressive episodes secondary to early-onset MDD (Meyer et al. 2006). Subjects with major depression (MDE) were drug-free for at least 5 months, and most were antidepressant naive. All MDE subjects and controls were otherwise healthy. The MAO-A V_S was highly significantly elevated ($p<0.001$ each region, average magnitude 34 % (or two standard deviations)) during MDE (see Fig. 25.1). This was the first definitive study of MAO-A binding in MDE from early-onset MDD: The samples excluded comorbidity, thereby focusing on the differences between this common, early-onset type of MDD and health. The effect size was large, and the radiotracer has outstanding qualities for

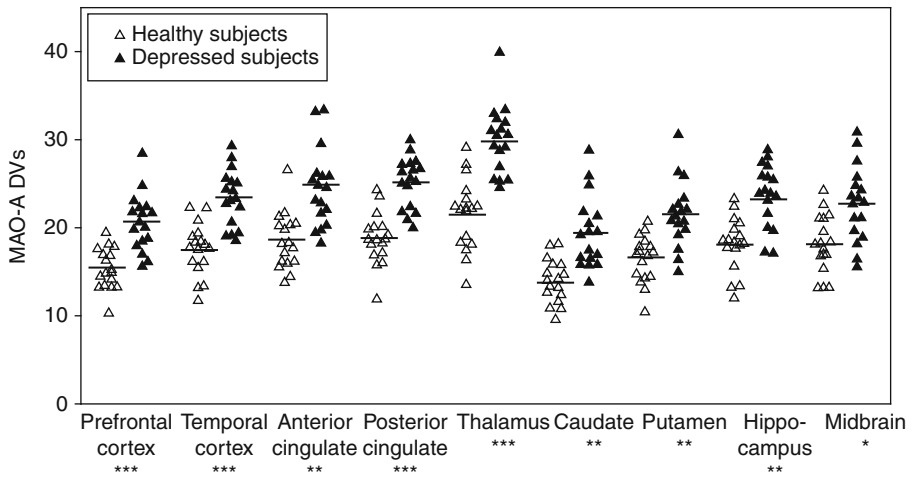


Fig. 25.1 Comparison of MAO-A DVs between depressed and healthy subjects. On average, MAO-A DVs was elevated by 34 %, or two standard deviations, in depressed individuals. Differences between groups were highly significant in each region: * $p=0.001$, ** $p=1:1.0001$, *** $p<0.00001$ (Reprinted from Meyer et al. (2006))

measuring MAO-A binding. In 2008, Barton et al. (2008) reported a consistent finding of elevated brain serotonin turnover in unmedicated depressed patients. In 2009, the finding of greater MAO-A binding in MDE was replicated with [^{11}C]harmine PET, and in 2011 the finding was replicated in antidepressant-free MDE subjects in postmortem study of orbitofrontal cortex applying Western blot (Johnson et al. 2011; Meyer et al. 2009).

Greater MAO-A binding in affect-modulating regions has important implications for understanding the pathophysiology of MDD. A key long-standing theory of MDD is that monoamines were low, but no clear mechanism of monoamine loss had been previously identified, and this finding represents the clearest mechanism to support this theory (Meyer et al. 2006). In addition, since MAO-A has multiple functions, metabolizing serotonin, norepinephrine, and dopamine, oxidizing, and facilitating apoptosis (Youdim et al. 2006), it suggests that new antidepressants should optimally target these additional functions rather than solely raise extracellular serotonin. Such approaches have notable potential to address the issue that at least 40 % of MDE does not respond to the common first-line treatment of selective serotonin reuptake inhibitors (Trivedi et al. 2006).

Investigations of MAO-A V_T , or monoamine oxidase distribution volume, were subsequently extended into different states of MDD, an approach which is readily feasible with positron emission tomography. While it might be expected that MAO-A levels would normalize with euthymic mood, the recovered state of MDD is also a state of high risk for another MDE. The risk for a recurrent MDE over 2 years is 20–50 % depending upon treatment conditions (Frank et al. 1990; Fava et al. 2004). Elevated MAO-A V_T may be considered an index of a monoamine

lowering process, and in the 1950s during treatment with reserpine-based antihypertensives, it was discovered that chronic monoamine lowering is associated with subsequent onset of MDEs which typically occurred 2 weeks to 4 months later (Freis 1954). In recovered MDD, MAO-A V_T was significantly elevated in prefrontal cortex, anterior cingulate cortex, striatum, hippocampus, thalamus, and midbrain in a sample of 18 medication-free recovered MDD subjects compared to 28 healthy controls (Meyer et al. 2009). Recovered MDD subjects who had recurrence of their MDE in the subsequent 6 months had the highest levels of MAO-A binding in the prefrontal and anterior cingulate cortex at the time of scanning (Meyer et al. 2009). The prefrontal cortex and anterior cingulate cortex were of particular interest because these regions (and/or subregions of these structures) are activated in mood induction studies (Liotti et al. 2002) and during cognitive functions like pessimistic perspective that generate sad mood (Sharot et al. 2007; Tom et al. 2007). To address the possibility that other factors related to risk of recurrence did not contribute to the finding, subjects were medication-free for at least a year, had no cognitive behavioral therapy within 3 years, were currently asymptomatic, and had no comorbid medical, psychiatric, or substance abuse illnesses. Given the link between elevated MAO-A binding in prefrontal and anterior cingulate cortex and subsequent MDE, this argues that new interventions are needed to decrease MAO-A levels in these brain regions even beyond the duration of a therapeutic intervention so as to prevent recurrence.

25.1.3 Early Postpartum

Early postpartum is a time of greater risk for three types of mood disturbance (O'Hara and Swain 1996). The first is the common, postpartum blues, present in up to 75 % of women involving mild sadness and can be accompanied by some trouble sleeping, irritability, desire for isolation, and difficulty concentrating (O'Hara and Swain 1996). It is considered within the healthy range of experience, typically starting on day 4 postpartum and finishing within the first week. The second is postpartum depression, which is a MDE that occurs within the first 4 weeks after giving birth, although some definitions include onset within the first 3 months after giving birth (O'Hara and Swain 1996; American Psychiatric Association 1994). MDE in postpartum is the most common complication of childbearing with a 13 % prevalence over the first 3 months (O'Hara and Swain 1996). The third is a rare, serious condition of postpartum psychosis (which may be accompanied by a MDE) occurring in 0.2 % of deliveries.

In contrast to postmortem investigations, MAO-A neuroimaging is well suited to postpartum study, even though it is challenging for subjects to organize their time to come for an imaging scan. While several studies reported an inverse relationship between decline in estrogen and rise in MAO-A levels, mRNA, and activity (Luine et al. 1975; Ma et al. 1993, 1995; Holschneider et al. 1998), prior to 2010, MAO-A binding, mRNA, or activity had never been studied in any species in early postpartum. Given that estrogen levels are more than 100-fold over the first several days in

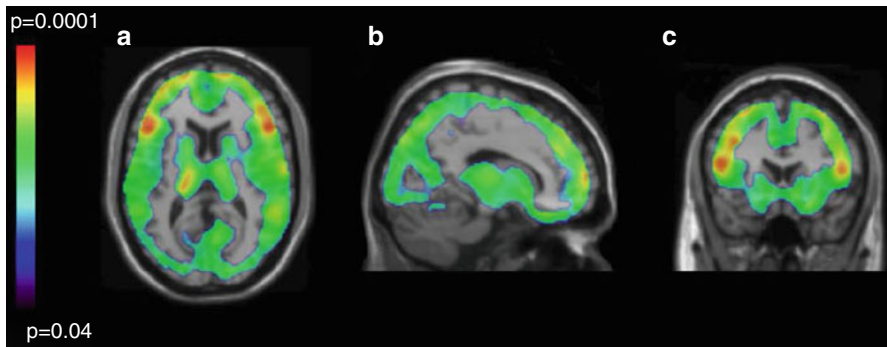


Fig. 25.2 Regional distribution of p -values reflecting elevated MAO-A binding in immediate postpartum period. Parametric maps of elevated monoamine oxidase A binding in the postpartum group versus the control group. Maps are superimposed on a T1-weighted magnetic resonance image that is normalized to the T1-weighted template (SPM2; Department of Cognitive Neurology, Wellcome Trust Centre for Neuroimaging, London, UK). (a) Transverse. (b) Sagittal. (c) Coronal. Individual voxel threshold was set at $p < 0.05$; 86 412 voxels comprised a single cluster, which had a cluster-corrected significance of $p = 0.03$. Mean regional difference was 43 % (Reprinted from Sacher et al. (2010))

humans (O'Hara et al. 1991), a [^{11}C]harmine PET study measured MAO-A binding during early postpartum (days 4–6) (Sacher et al. 2010). A highly significant elevation of MAO-A binding was found, which was, on average, 43 % greater across the brain regions assayed (prefrontal cortex, anterior cingulate cortex, striatum, thalamus, hippocampus, midbrain) as compared to women not recently pregnant (Sacher et al. 2010). A voxel-based analysis demonstrated that the elevation in MAO-A binding was present throughout the gray matter of the brain (see Fig. 25.2) (Sacher et al. 2010).

This study has several major important implications. The first is that this provides a new neurobiological explanation for postpartum blues, involving a rapid decline in estrogen, followed by a rapid rise in MAO-A levels in affect-modulating structures in the brain, with subsequent sad mood and symptoms of postpartum blues (Sacher et al. 2010). The second is that since elevated MAO-A V_T is associated with both MDE and subsequent onset of MDE, elevated MAO-A V_T in early postpartum provides a mechanistic explanation for the high risk of MDE in early postpartum. The third is that there may be an opportunity to develop strategies to prevent postpartum depression, based upon these neurobiological models. Greater severity of postpartum blues, which typically occurs before postpartum depression, is associated with greater risk for postpartum depression (PPD) (O'Hara et al. 1991). Thus, reducing the intensity of postpartum blues might reduce the risk for PPD, and this may be done by specifically targeting the pathway of estrogen decline, rise in MAO-A levels, and excessive metabolism of monoamines. For example, it is possible that amino acid supplementation with monoamine precursors might compensate for monoamine loss and reduce severity of postpartum blues.

25.1.4 Cigarette Smoking

Most biological descriptions of early cigarette withdrawal focus upon abnormal modulation by nicotine of dopamine-releasing neurons projecting from the ventral tegmental area to ventral striatum (Laviolette and Van der Kooy 2004; Brody et al. 2006; Cosgrove et al. 2009). This model has been successful in clinical applications since therapeutics targeting this pathway, when combined with therapy, achieve 6-month abstinence rates of up to 40 % (Law and Tang 1995; Piper et al. 2009). However, there are other central nervous system targets affected by cigarette smoke that may be important in the mechanism of cigarette withdrawal, and several substances in cigarette smoking have been reported to binding with moderate affinity to monoamine oxidase A (MAO-A) (Hauptmann and Shih 2001; Herraiz and Chaparro 2005). Harman is the chemical in cigarette smoke that has the highest affinity for MAO-A (Hauptmann and Shih 2001; Herraiz and Chaparro 2005).

The first PET study of MAO-A binding applying [^{11}C]clorgyline reported reduced available MAO-A binding in those who smoke cigarettes in the active smoking state (Fowler et al. 1996). This finding was confirmed in a recent PET study with the tracer [^{11}C]befloxatone (Leroy et al. 2009). Given that the plasma half-life of the key MAO-A binding substances found in cigarette smoke (harman and norharman) is only an hour (Rommelspacher et al. 2002), there was reason to specifically assess MAO-A V_T during both active smoking and withdrawal conditions. When MAO-A V_T was assessed in both conditions, it was discovered that prefrontal and anterior cingulate cortex MAO-A V_T (as well the other brain regions assessed) rose during withdrawal in those who smoke heavily, that is, more than one pack of cigarettes per day, but not in those who smoke more moderately at less than one pack per day (see Fig. 25.3) (Bacher et al. 2011) and that during withdrawal from heavy smoking, MAO-A V_T was greater than in health in all regions assessed (see Fig. 25.4) (Bacher et al. 2011).

The elevation in MAO-A V_T has important implications for the problem of sad mood in people who smoke cigarettes. There is a very high comorbidity between cigarette smoking and major depressive disorder with 50 % of people with MDD also smoking cigarettes, and the pattern is such that cigarette smoking predisposes to MDD and vice versa (Anda et al. 1990; Breslau et al. 1998). It is the heavy cigarette smoking group who are at much greater risk for MDD (Pratt and Brody 2010), and this group had a 25 % elevated MAO-A V_T in the prefrontal and anterior cingulate cortex during withdrawal as compared to healthy controls, arguing for a process of elevated MAO-A level during withdrawal as a mechanism to create risk for MDD (Bacher et al. 2011). Hence, repeated exposure of elevated MAO-A level, in the prefrontal and anterior cingulate cortex, a mechanism associated with onset and maintenance of MDE state, occurring after a short period of 8-h withdrawal could explain the predisposition to MDE in people who smoke cigarettes heavily.

A second problem with mood in people who smoke cigarettes is the depressed mood of acute withdrawal (Carey et al. 1993; Kenford et al. 2002). In the imaging study of MAO-A during cigarette withdrawal, in those who smoked heavily, the magnitude of rise in MAO-A V_T in prefrontal and anterior cingulate cortex during

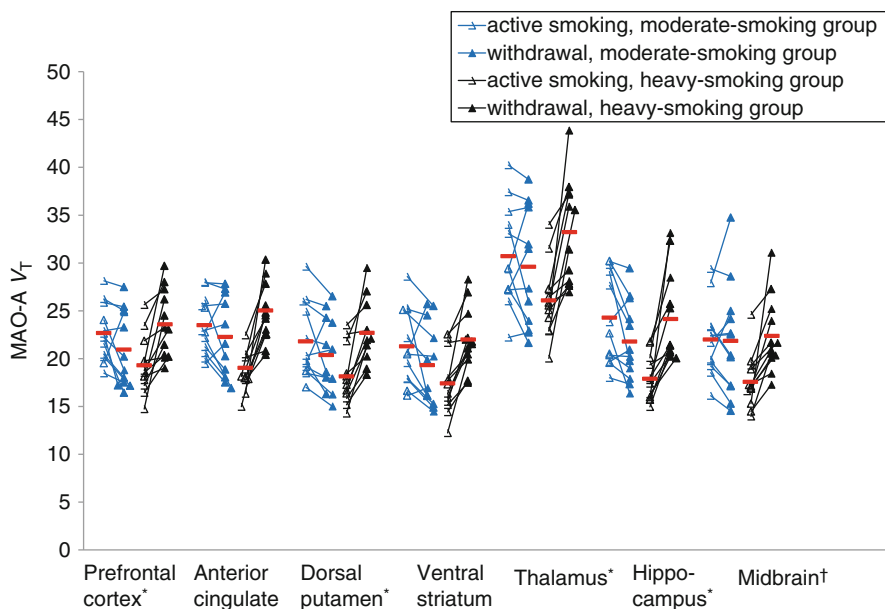


Fig. 25.3 Monoamine Oxidase-A binding in cigarette smoking subjects during active smoking and withdrawal. Repeated measures MANOVA found a highly significant effect between smoking severity and change in MAO-A V_T in the prefrontal cortex and anterior cingulate cortex regions ($F_{1,22}=25.58$, $p<0.001$). Repeated measures MANOVA also found a significant effect between smoking severity and change in MAO-A V_T for all the regions assayed ($F_{1,22}=28.24$, $p<0.001$). The effect was confirmed in each region with a repeated measures ANOVA (interaction between smoking severity and change in MAO-A V_T , repeated measures ANOVA, $F_{1,22}=11.16$ to 28.87 , $p=0.003$ to $p<0.001$), * $p<0.001$, † $p=0.003$ (Reprinted from Bacher et al. (2011))

withdrawal was significantly correlated with the shift in visual analogue scales towards depressed mood (Bacher et al. 2011). This rise in MAO-A V_T also correlated with the decline in harman in those who smoke heavily. These results suggest that rapid removal of harman from occupying MAO-A sites leaves a high level of available MAO-A for metabolizing monoamines in prefrontal and anterior cingulate cortex resulting in depressed mood. This argues for testing of MAO-A inhibitor treatments in people who experience sad mood during early cigarette withdrawal as a strategy to assist in quitting, an important issue since 50 % of people tend to relapse in the first few days of trying to quit cigarette smoking (Law and Tang 1995; Garvey et al. 1992).

25.1.5 Aggression

Aggression has major social costs since 50 % of prisoners have problems with aggression (Fazel and Danesh 2002). Substantial evidence has accumulated to suggest that inherited levels of MAO-A may also have influence upon neurodevelopment and lead to impulsive behavior: MAO-A knockout (KO) and wild-type mice

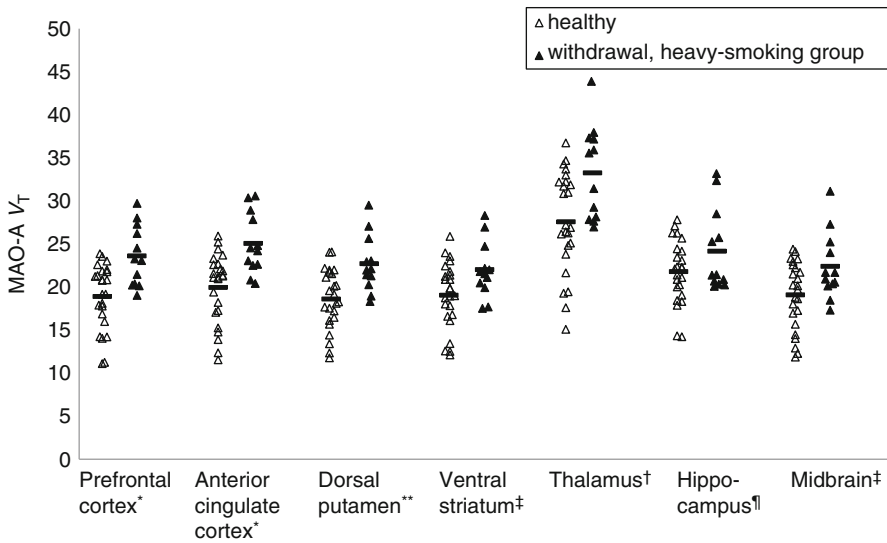


Fig. 25.4 Greater MAO-A binding during acute cigarette withdrawal in heavy-smoking group compared with healthy subjects. MAO-A V_T was significantly greater in the prefrontal and anterior cingulate cortex in the withdrawal state of those in the heavy-smoking subgroup as compared to healthy controls (MANOVA, $F_{2,33}=6.72$, $p=0.004$). Most other individual regions were also significantly different (independent t -test) (Reprinted from Bacher et al. (2011)). * $p \leq 0.001$, ** $p \leq 0.005$, † $p \leq 0.01$, ‡ $p \leq 0.1$, ¶ $p \leq 0.05$

given MAO-A inhibitors during development demonstrate elevated brain serotonin during development, which disrupts the organization of somatosensory thalamocortical afferents and abnormalities in the somatosensory cortex barrel fields (Cases et al. 1996; Vitalis et al. 1998; Mejia et al. 2002). It has been proposed that impulsive aggression observed in MAO-A KO mice and mice given MAO-A inhibitors during development is consequent to impairment in organizing sensory input secondary to these abnormalities (Bortolato et al. 2008). Men who are deficient in MAO-A, consequent to an X chromosome mutation that impairs function of the MAO-A gene, demonstrate frequent aggressive behavior (Brunner et al. 1993). Consistent with this, people with a genotype associated with low levels of MAO-A in an in vitro assay have been associated with greater risk of developing antisocial behavior (Caspi et al. 2002; Kim-Cohen et al. 2006).

Two PET imaging studies of MAO-A in relation to aggressive personality traits show consistent results. The first, an [^{11}C]clorgyline PET study, reported a correlation between reduced MAO-A binding in prefrontal cortex and subregions of the prefrontal cortex such as the orbitofrontal cortex, with self-reported aggression in healthy men (Alia-Klein et al. 2008). The second study, which applied [^{11}C]harmine positron emission tomography with the Revised NEO Personality Inventory, found that prefrontal cortex and subregions of the prefrontal cortex (such as the orbitofrontal cortex) correlated strongly with personality facets angry hostility negatively ($r=-0.515$, $p=0.001$) and deliberation facets positively ($r=0.514$, $p=0.001$)

(Soliman et al. 2011). In a 2-factor regression model, these facets explained 38 % of variance in prefrontal cortex MAO-A binding. In both studies, the MAO-A binding measures among different regions were intercorrelated so the correlations of MAO-A binding with aggression-related measures were also present in all brain regions sampled which included both cortical and subcortical regions.

Currently, this neuroimaging direction is still progressing towards creating impactful information for society. Ideally, future studies should investigate MAO-A binding in samples with pathological levels of aggression. Should it be that reduced MAO-A binding is related to pathological aggression, a longer-term strategy could be to identify whether harmful environmental influences predispose to this low-MAO-A-level phenotype in prefrontal cortex so as to develop novel prevention strategies against harmful neurodevelopment.

25.2 Why Image Indices of Serotonin Transporter Density?

The serotonin transporter (5-HTT) is a 630-amino-acid-long receptor with 12 transmembrane domains (Lesch et al. 1993a, b) and is mainly found in soma, dendrites, and terminals of serotonin-releasing neurons (Zhou et al. 1998; Tao-Cheng and Zhou 1999). Most 5-HTT are located on plasma cell membranes, mainly perisynaptically or along axons (Zhou et al. 1998; Tao-Cheng and Zhou 1999). In human brain, there is wide variation in regional 5-HTT density: superior and inferior raphe nuclei > hypothalamus > thalamus (depending upon nucleus) \approx amygdala > putamen > caudate \approx hippocampus > insular cortex > prefrontal cortex > white matter > cerebellar cortex (except vermis) (Cortes et al. 1988; Laruelle et al. 1988; Kish et al. 2005). The serotonin transporter is coupled to sodium, chlorine, and potassium transport (Blakely et al. 1997), but the physiological role of greatest interest of 5-HTT in the brain is its influence upon extracellular serotonin levels. Antidepressants which bind to the serotonin transporter raise extracellular serotonin, and 5-HTT knockout mice have elevated extracellular serotonin, confirming the role of the serotonin transporter in modulating extracellular serotonin levels in vivo (Blier and De Montigny 1983; Bel and Artigas 1992, 1993, 1995; Dreshfield et al. 1996; Moret and Briley 1996; Mathews et al. 2000).

Neuroimaging studies of the 5-HTT offer the opportunity to measure an index of total 5-HTT density, the 5-HTT BP_{ND}. This marker is useful for determining therapeutic occupancy of antidepressants as well as several different models of 5-HTT dysregulation in disease. Most disease investigations focus upon potential mechanisms for lowering brain serotonin, and there are at least four models to explain how 5-HTT BP_{ND} could be altered in a disease that lowers brain monoamines (Meyer 2007). The first model is a lesion model in which the density of serotonin-releasing neurons is reduced and reductions in 5-HTT BP_{ND} occur. The second model is a secondary change in transporter binding consequent to serotonin lowering via a different process. However, available evidence suggests that the different monoamine transporters do not regulate in the same fashion after chronic depletion of their endogenous monoamine. Acute reductions in serotonin lead to reductions in 5-HTT

mRNA (Yu et al. 1995), but long-term reductions or elevations in serotonin typically show no effect upon regional 5-HTT density (Graham et al. 1987; Dewar et al. 1992; Benmansour et al. 1999). The third model is increased clearance of extracellular monoamine via greater serotonin transporter density. In the third model, greater total available 5-HTT BP_{ND} is interpreted as representative of greater functional 5-HTT density. The fourth model is endogenous displacement and is dependent upon the properties of the radioligand: Endogenous displacement is the property of a few radioligands to express different binding after short-term manipulations of their endogenous neurotransmitter (Paterson et al. 2010). Available evidence suggests that this fourth model is unlikely to be relevant in humans with [^{11}C] DASB (Talbot et al. 2005; Praschak-Rieder et al. 2005), but the issue has not been investigated for other radioligands. Abnormalities in 5-HTT BP_{ND} may be discussed in the context of these models.

25.2.1 Radioligands Available for Imaging Serotonin Transporters

There are at least six different radiotracer imaging protocols for imaging serotonin transporters, and the quality of technique varies widely. Originally, the only two radiotracer techniques were 2-beta-carbomethoxy-3-beta-(4-iodophenyl)-tropane (β -CIT) single-photon emission tomography (SPECT) and [^{11}C](+)McN5652 PET, but both of these methods have significant limitations for quantitation (Kuikka et al. 1993). β -CIT has almost equal affinity for the dopamine transporter as compared to the serotonin transporter (Laruelle et al. 1994). As dopamine transporter density is high in the substantia nigra (Ciliax et al. 1999), the relative contributions of dopamine and serotonin transporter binding to the measure of specific binding cannot be separated in the midbrain, the location where this radiotracer technique is applied. The other early radiotracer, [^{11}C](+)McN5652, has a low ratio of specific binding relative to free and nonspecific binding, which, in combination with modest reversibility, makes valid and reliable quantitation difficult in regions other than the thalamus and impossible in human cortex (Kent et al. 2002; Buck et al. 2000).

The radiotracer [^{11}C]DASB (3-amino-4-(2-dimethylaminomethylphenyl)sulfanyl)-benzotrile) was a major advance as a result of its selectivity, reversibility, greater specific binding, and reliability (Wilson et al. 2000, 2002; Ginovart et al. 2001; Meyer et al. 2001, 2004a, b; Praschak-Rieder et al. 2005). This radiotracer was three orders of magnitude more selective for the 5-HTT over other monoamine transporters and highly selective for the 5-HTT in comparison to a number of other targets screened (Wilson et al. 2000, 2002). Selectivity was also demonstrated when 94 % of the specific binding was displaceable by 5-HTT binding medications in animal models (Wilson et al. 2000, 2002). [^{11}C]DASB has very good brain uptake in humans (Ginovart et al. 2001). In humans, its ratio of specific binding relative to free and nonspecific is good, and its free and non-specific binding has low between-subject variability (Ginovart et al. 2001; Ichise et al. 2003). Multiple brain regions may be assessed (Wilson et al. 2000, 2002; Ginovart et al. 2001; Meyer et al. 2001, 2004a;

Praschak-Rieder et al. 2005), and reliability of regional 5-HTT BP_{ND} measures is very good (Meyer et al. 2001, 2004a; Praschak-Rieder et al. 2005). The 5-HTT BP_{ND} measures are low in cortex, but with standardized region-of-interest methods, very good reliability of 5-HTT BP_{ND} in human cortex is achievable (Meyer et al. 2001, 2004a; Praschak-Rieder et al. 2005). Thus, the discovery of [¹¹C]DASB PET imaging created a new opportunity for validly quantifying 5-HTT binding in humans.

Subsequent to the development of [¹¹C]DASB, several new similarly structured radiotracers were created for imaging techniques of [¹²³I]ADAM SPECT, [¹¹C]MADAM PET, and [¹¹C]HOMADAM PET (see Table 25.2 for a comparison). [¹²³I]ADAM SPECT is superior to β-CIT SPECT; however, [¹²³I]ADAM SPECT is not as useful a technique as the other methods because of its limited specific binding to free and nonspecific binding signal and lack of formal modeling development. [¹¹C]MADAM PET approaches the quality of [¹¹C]DASB PET, but [¹¹C]MADAM has substantially less brain uptake which would be expected to increase the variability of the measurement, especially in regions of lower 5-HTT density (Lundberg et al. 2006). However, it is clear that [¹¹C]MADAM is superior to [¹¹C](+)McN5652 in terms of the reversibility of time-activity curves and specific binding signal relative to free and nonspecific binding signal. [¹¹C]HOMADAM PET shows some advantage over [¹¹C]DASB PET (and the other radiotracers) in that it has a more reversible time-activity curve and a somewhat greater specific binding to free and nonspecific binding signal (Ginovart et al. 2001; Nye et al. 2008), but there are still key areas of development for [¹¹C]HOMADAM PET, including a reliability assessment of binding measures and assessment of its sensitivity to endogenous serotonin. Initial attempts have been made to apply a ¹⁸F-labeled derivative of McN5652 in humans (Hesse et al. 2012), but data on test-retest reliability and sensitivity to endogenous 5-HT are still lacking.

25.2.2 Developing New Antidepressants with Serotonin Transporter Neuroimaging

In two seminal studies published in 2001 and 2004 applying [¹¹C]DASB PET, it was demonstrated across five different selective serotonin reuptake inhibitors (SSRIs) that after 4 weeks of treatment, for doses which clinically distinguish from placebo, an 80 % occupancy occurs in most brain regions (Meyer et al. 2001, 2004b) (see Fig. 25.5 and 25.6). These SSRIs are defined as such by the property of having at least two orders of magnitude preferential affinity for the serotonin transporter over other target sites. Within the datasets, there was increasing occupancy with increasing dose (and plasma level), with plateauing at the higher doses and higher plasma levels. The dose occupancy relationships consistently demonstrated that the threshold of reaching 80 % occupancy was important. Even though these SSRIs have a 100-fold range in affinity for the serotonin transporter, an 80 % striatal 5-HTT occupancy occurs at minimum clinical dose, thereby demonstrating an additional, important predictive value of the 5-HTT occupancy data in relation to clinical trial development.

Table 25.2 Comparison of PET radiotracers for the serotonin transporter

	[¹²³ I]β-CIT SPECT	[¹¹ C]McN5652 PET	[¹¹ C]DASB PET	[¹²³ I]ADAM SPECT	[¹¹ C]MADAM PET	[¹¹ C] HOMADAM PET
Selectivity	Nonselective—near 1:1 affinity for 5-HTT to DAT (Laruelle et al. 1994; Carroll et al. 1995)	Likely selective 10:1 to 100:1 affinity for 5-HTT over NET (Shank et al. 1988; Kung et al. 1999)	Highly selective 1,000:1 affinity for 5-HTT over NET or DAT; negligible affinity for many other targets (Wilson et al. 2000, 2002)	Highly selective 1,000:1 affinity for 5-HTT over NET or DAT (Choi et al. 2000; Oya et al. 2000)	Highly selective (Hallidin et al. 2005; Chalou et al. 2003)	Highly selective (Jarkas et al. 2005)
Displaceability of specific binding	Incomplete (Pirker et al. 1995; Tauscher et al. 1999)	In most reports (Kent et al. 2002; Parsey et al. 2000; Suhara et al. 2003)	Highly displaceable (Meyer et al. 2001, 2004a, b; Wilson et al. 2000, 2002)	Highly displaceable (Choi et al. 2000; Oya et al. 2000; Erlandsson et al. 2005)	Highly displaceable (Hallidin et al. 2005; Chalou et al. 2003; Lundberg et al. 2007)	Highly displaceable (Jarkas et al. 2005)
Reversibility (in human imaging)	Good (Kuikka et al. 1993; Brucke et al. 1993)	Not adequate to adequate, depending upon region (Buck et al. 2000; Parsey et al. 2000; Ikoma et al. 2002)	Adequate in midbrain, good to very good in other regions (Ginovart et al. 2001; Ichise et al. 2003; Houle et al. 2000)	Adequate in midbrain (Erlandsson et al. 2005; Catafau et al. 2005)	Adequate in midbrain, good to very good in other regions	Very reversible in all regions (Nye et al. 2008)
Brain uptake	Adequate (Kuikka et al. 1993; Brucke et al. 1993)	Good (Parsey et al. 2000; Ikoma et al. 2002)	Very good (Ginovart et al. 2001; Ichise et al. 2003; Houle et al. 2000)	Adequate (Erlandsson et al. 2005; Catafau et al. 2005)	Good (Lundberg et al. 2006)	Very good (Nye et al. 2008)
Sensitivity to endogenous serotonin	Not known	Not known	Negligible (Talbot et al. 2005; Praschak-Rieder et al. 2005)	Not known	Not known	Not known

Specific binding to free and nonspecific binding ratio	Good	Not adequate in most regions; adequate in thalamus (Ikoma et al. 2002; Frankle et al. 2005)	Adequate to very good, depending upon region (Gimovart et al. 2001; Ichise et al. 2003)	Not adequate in most regions; adequate in midbrain (Erlandsson et al. 2005; Catafau et al. 2005)	Adequate to very good (Lundberg et al. 2005, 2006)	Adequate to very good (Nye et al. 2008)
Reliability of 5-HTT BP	Not measured	Modest (Kent et al. 2002)	Very good to excellent (Praschak-Rieder et al. 2005; Meyer et al. 2001)	Most regions reasonable (Catafau et al. 2005)	Good to very good (Lundberg et al. 2006)	Not yet reported
5-HTT BP measurable in multiple regions?	Brain stem only (Kuikka et al. 1993; Brucke et al. 1993)	Measurable in thalamus (Ikoma et al. 2002), not measurable in cortex (Parsey et al. 2000)	Yes (Gimovart et al. 2001; Ichise et al. 2003)	Measurable in midbrain; unclear for other regions (Erlandsson et al. 2005; Catafau et al. 2005)	Yes (Lundberg et al. 2006)	Yes (Nye et al. 2008)

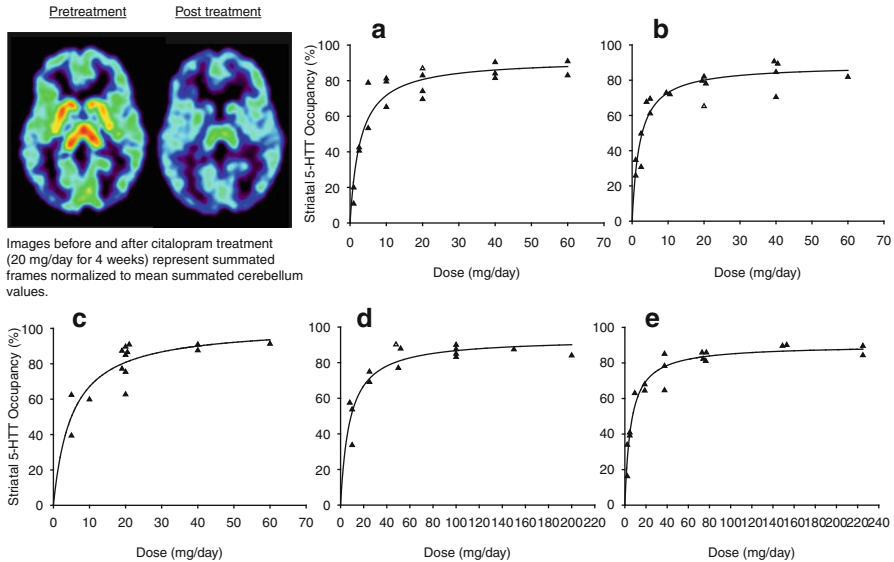


Fig. 25.5 Eighty percent threshold for selective serotonin reuptake inhibitor doses that distinguish from placebo. The data was fit using an equation of form $f(x) = a \times x / (b + x)$. Each fit was highly significant ($p < 0.0002$ for all). Scanning occurred before treatment after 4 weeks of the treating dose. Medication type and dosage that differentiate from placebo are listed as follows: (a) citalopram (20–40 mg); (b) fluoxetine (20 mg); (c) paroxetine (20 mg); (d) sertraline (50–100 mg); (e) venlafaxine XR (75 mg). Occupancy is the percent reduction in binding potential (BP_{ND}), i.e., occupancy = (baseline BP_{ND} – treatment BP_{ND}) / baseline BP_{ND} (Reprinted from Meyer et al. (2001, 2004a, b))

Furthermore, the added information from occupancy measurement is clear because the in vivo EC_{50} does not correlate with affinity (Meyer et al. 2004b). This association of 80 % occupancy with doses of SSRI that distinguish from placebo in clinical trial is consistently reported (Kent et al. 2002; Suhara et al. 2003). Hence, while affinity is an essential piece of information regarding an antidepressant, it cannot predict occupancy, even when plasma levels are known (Meyer et al. 2004b). Given the association between the clinically relevant dose and 5-HTT occupancy for SSRIs, it is now generally believed that an 80 % 5-HTT occupancy is a therapeutic threshold for new antidepressants. This technique is frequently applied during phase I trials to assess whether new antidepressants in development are adequately brain penetrant and to guide dosing selection for subsequent phase II clinical trials.

25.2.3 Major Depressive Disorder

Neuroimaging studies of 5-HTT enable the measurement of 5-HTT BP_{ND} in the midst of a MDE, as well as the ability to select more homogeneous subtypes of MDD like early-onset MDD (in contrast to the more heterogeneous late-onset MDD).

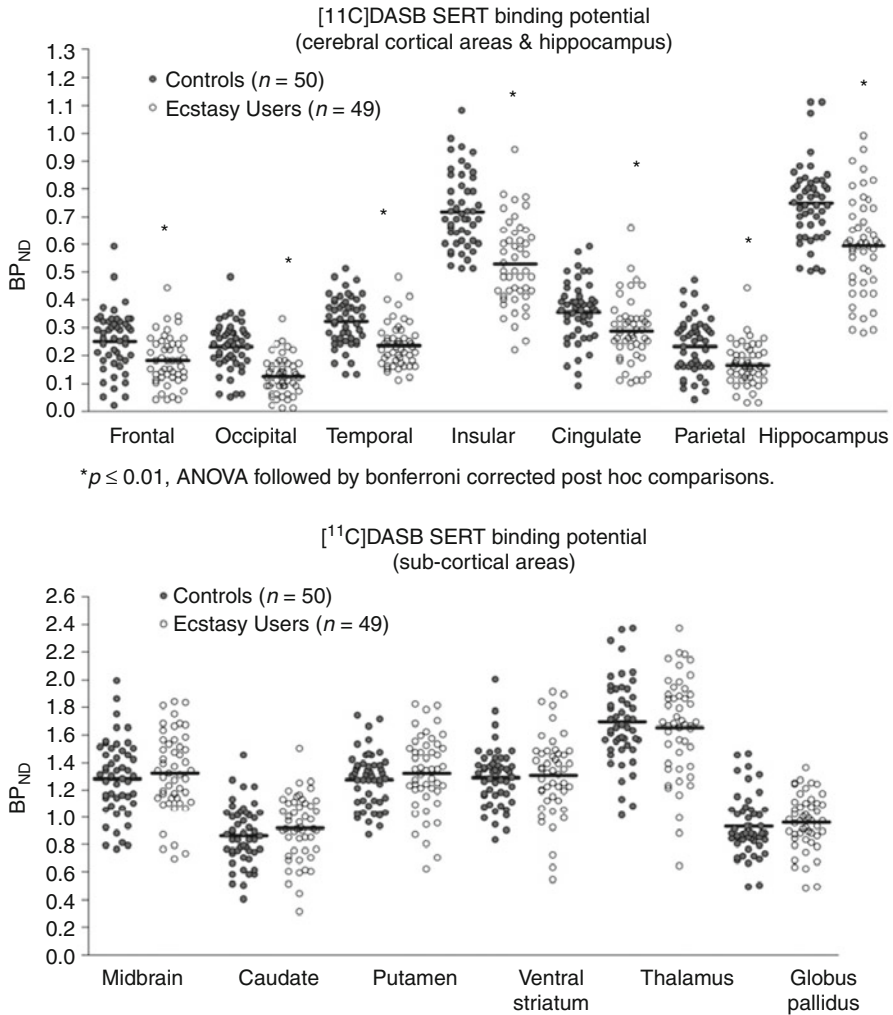


Fig. 25.6 Scattergram of [¹¹C]DASB BPND in control subjects and ecstasy users. Note group differences in cerebral cortical but not subcortical brain areas (Reprinted from Kish et al. (2010))

Sampling early-onset MDD is usually not feasible for postmortem studies of 5-HTT density due to challenges sampling subjects at older ages. The two postmortem investigations of 5-HTT density in subjects with recent symptoms of MDE evaluated 5-HTT density in the dorsal raphe and locus coeruleus, finding similar levels between MDD and healthy subjects (see review for more details, Stockmeier 2003).

Neuroimaging studies of 5-HTT binding in untreated MDD exemplify a wide range of sample sizes and quality of techniques. However, there are three studies that focus upon medication-free subjects, with minimum sample sizes of 15 in each group, apply a radioligand of [¹¹C]DASB level quality, and tend to focus upon

early-onset MDD. For a broader review of these studies, including smaller studies not meeting these criteria, the reader is referred to Meyer (2008). The first study was applied [^{11}C]DASB PET to a sample of 20 subjects with early-onset MDE and 20 healthy controls (Meyer et al. 2004a, b). Subjects were medication-free for at least 3 months, were age matched, had no comorbid axis I illnesses, were nonsmoking, and had early-onset MDD. There was no difference in 5-HTT BP_{ND} between MDE and healthy controls, but MDE subjects with severely pessimistic dysfunctional attitudes had significantly higher 5-HTT BP_{ND} (on average 21 %) compared to healthy controls in brain regions sampling serotonin nerve terminals (prefrontal cortex, anterior cingulate, thalamus, bilateral caudate, bilateral putamen). Consistent with the postmortem studies of MDE, there was no difference in midbrain 5-HTT BP_{ND} . Within the MDE group, greater 5-HTT BP_{ND} was strongly associated with more negativistic dysfunctional attitudes in the same brain regions. An interpretation of the relationship between the functional measure of dysfunctional attitudes and the measure of 5-HTT BP_{ND} is that greater regional 5-HTT levels could provide greater vulnerability to low extracellular 5-HT through excessive clearance of extracellular serotonin, leading to subsequent symptoms of extremely negativistic dysfunctional attitudes. There is particular utility in relating a functional symptom measure to 5-HTT binding because not all neuronal 5-HTT are not in a functional location (Zhou et al. 1998; Tao-Cheng and Zhou 1999), although total 5-HTT level correlates with extracellular 5-HT in knockout models in vivo (Mathews et al. 2004). The second study reported elevated 5-HTT binding in several brain regions (thalamus, striatum, insula) during MDE (Cannon et al. 2007), and the third study reports no difference in remitted MDD (Bhagwagar et al. 2007) (dysfunctional attitudes were not assessed in the latter two studies), demonstrating fairly consistent results across groups.

25.2.4 Ecstasy Abuse and Serotonin Transporter Imaging

Ecstasy (3,4-methylenedioxymethamphetamine, MDMA) is a substance that is frequently used in social contexts as it enhances emotional well-being, feelings of closeness, and desire to be sociable. Its mechanism, based upon the effects of serotonin transporter blockade and serotonin transporter knockout mice, is likely mainly mediated through binding to the serotonin transporter. Animal models suggest that exposure to MDMA is associated with widespread, persistent loss in serotonin transporter density, raising concern about the safety of exposure to this substance (Fig. 25.6).

PET imaging allows for assessment in regard to the effects of MDMA upon 5-HTT BP_{ND} in vivo including the regional distribution of this effect and its persistence at amounts typically self-administered by people. Neuroimaging results applying [^{11}C]DASB PET have been very consistent across sites with reductions in 5-HTT BP_{ND} in prefrontal, anterior cingulate, parietal, temporal, occipital cortex, insula, and hippocampus but no change in subcortical regions including the striatum, thalamus, and midbrain being typical (McCann et al. 2005, 2008; Kish et al. 2010; Erritzoe et al. 2011; Urban et al. 2012). All studies to date report reductions in 5-HTT BP_{ND} in cortical regions, and four out of five reports sparing of subcortical

structures (McCann et al. 2005, 2008; Kish et al. 2010; Erritzoe et al. 2011; Urban et al. 2012). The question of persistence of the reduction in 5-HTT BP_{ND} requires further investigations. McCann et al. (2008) reported no correlation between recency of use and 5-HTT BP_{ND} over the initial 7 months, and Selvaraj et al. (2009) reported no regional difference in 5-HTT BP_{ND} in people who had abstained on average for 2.7 years suggesting a normalization window in between these two time frames, which ideally should be followed longitudinally.

25.2.5 Obsessive-Compulsive Disorder

Obsessive-compulsive disorder (OCD) is a disabling illness characterized by repeated obsessions and/or compulsions that are distressing and impair function (First et al. 1995). OCD tends to be either relapsing/remitting or chronic (American Psychiatric Association 1994) affecting 2 % of adults (Robins et al. 1984; Weissman et al. 1994). Most likely time of onset is bimodally distributed with an early-onset group in childhood to teenaged years and a late-onset group occurring in the second to third decade. There have been virtually no postmortem investigations into this condition making neuroimaging studies an important source of information towards understanding potential neurochemical abnormalities in this illness.

There have been three investigations of serotonin transporter imaging in OCD applying a newer imaging method (all with [¹¹C]DASB PET), and although the individual results focused within each study vary, further scrutiny suggests some consistency (Reimold et al. 2007; Matsumoto et al. 2010; Hesse et al. 2011). Reimold et al. (2007) applied a voxel-based analysis and reported decreased 5-HTT BP_{ND} in the midbrain and thalamus in a sample of 9 subjects with OCD. In a sample of 10 subjects with OCD, Matsumoto et al. (2010) reported significantly decreased 5-HTT BP_{ND} within the orbitofrontal and insular cortex, and in a sample of 19 OCD subjects, divided by early ($n=6$) and late ($n=13$) onset, Hesse et al. (2011) reported decreased 5-HTT BP_{ND} in medial prefrontal cortex, hippocampus, caudate, putamen, thalamus, occipital cortex, and midbrain, which was primarily driven by reduced 5-HTT BP_{ND} in the late-onset OCD. What was reasonably consistent across the studies was a decrease in 5-HTT BP_{ND}, as Matsumoto noted reductions in 5-HTT BP ranging from 6.3 to 42 % across all regions studied. The data of Hesse et al. suggests that late-onset OCD is primarily responsible for the differences in 5-HTT BP_{ND} between OCD and health. It is plausible that the studies conducted to date may be underpowered to fully determine the regional extent of the reduction of 5-HTT BP_{ND} in late-onset OCD. The main reasons for being underpowered are that the voxel-based analyses tend to be less sensitive than region-of-interest-based analyses and the sample sizes may not be large enough to achieve results that are regionally consistent even though the direction of effect is consistent. In support of this perspective, the nonsignificant reductions in OCD across studies suggest a global reduction in 5-HTT BP_{ND}. Based upon the data from these studies, future serotonin transporter imaging investigations should consider larger sample sizes focused upon late-onset OCD.

25.2.6 Season and Serotonin Transporter Imaging

Seasonal affective disorder (SAD), that is, major depressive disorder with regular MDE in winter with full remissions in summer, is an important problem, especially in areas of the world at greater extremes of latitude: Prevalence rates of SAD are about 1 % at 40' latitude and 6 % at 60' latitude or greater (Magnusson 2000). The functions of mood, appetite, sleep, and energy which fluctuate with season also are influenced by the serotonin system, and some indicators of serotonin physiology fluctuate with season in humans (Praschak-Rieder et al. 2008).

Prior to serotonin transporter imaging across season, several markers of seasonal fluctuations in serotonin physiology had been reported. In a human postmortem study of serotonin concentrations in the hypothalamus, Carlsson et al. (1980) reported lower levels in late winter and higher levels in late summer. More recently, Lambert et al. (2002) reported seasonal variation in whole-brain serotonin turnover in vivo in humans. Investigations in rodents find that reduced light exposure is associated with greater 5-HTT density (Rovescalli et al. 1989), lower 5-HT release (Blier et al. 1989), and greater 5-HT clearance (Rovescalli et al. 1989) in the hypothalamus and suprachiasmatic nucleus (two regions with high 5-HT concentration and density).

The four largest studies of 5-HTT binding and season have very consistent results. The first study that applied [¹¹C]DASB PET, in 88 healthy, nonsmoking humans in Toronto, Canada, found greater 5-HTT binding in the fall/winter as compared to spring/summer in all the brain regions sampled (medial prefrontal cortex, anterior cingulate cortex, thalamus, striatum, and midbrain) (Praschak-Rieder et al. 2008). See Fig. 25.7. The next [¹¹C]DASB PET study of seasonality evaluated 54 subjects in Copenhagen, Denmark, and replicated the same seasonal variation in 5-HTT BP_{ND} (Kalbitzer et al. 2010). Ruhe et al. (2009) reported the same relationship between midbrain binding and season in a sample of 49 healthy and 49 depressed subjects applying [¹²³I]β-CIT SPECT. Buchert et al. (2006) reported the same seasonal finding in the midbrain but not in the thalamus in a sample of 39 subjects using [¹¹C]McN5652 PET. Thus, studies with large sample size located in more northern latitudes report greater 5-HTT BP_{ND} in the brain regions sampled in fall/winter compared to spring/summer.

Conclusions

Neuroimaging studies applying recently optimized radiotracers for MAO-A (Bergstrom et al. 1997a, b; Ginovart et al. 2006) and serotonin transporter (Ginovart et al. 2001; Wilson et al. 2000) have created new advances in our knowledge of the relationship of these proteins to mood disorder, aggression, substance abuse, anxiety, and antidepressant development.

Prior to 2006, MAO-A had been viewed as a target for treatment of mood disorders, but neuroimaging studies have led to a new view that elevations in MAO-A level, particularly in the prefrontal and anterior cingulate cortex, occur during major depressive episodes and during high-risk states for major depressive episodes in adults (Meyer et al. 2006, 2009; Sacher et al. 2010; Bacher et al. 2011).

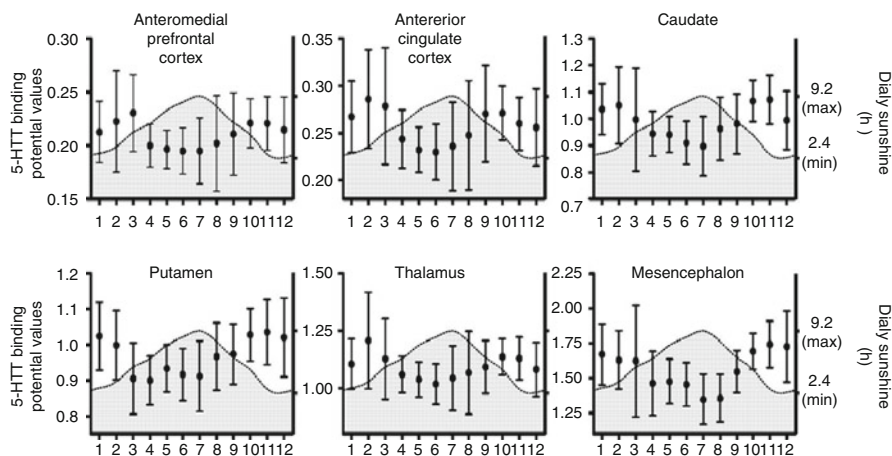


Fig. 25.7 Regional 5-HTT BPND versus month ($n=88$ healthy subjects). Reciprocal peaks and troughs of brain serotonin transporter binding and duration of sunshine in 88 healthy study participants. Serotonin transporter binding potential values were measured in six brain regions. Circles represent bimonthly moving average means. Error bars represent 95 % confidence intervals of the mean. The shaded areas represent the average duration of sunshine in Toronto, Ontario, Canada. Regional 5-HTT BPND was significantly greater in spring/summer than fall/winter by 10–16 %, $p<0.02$ for each region. Differences in peak to trough ranged from 22 to 42 % (Reprinted from Praschak-Rieder et al. (2008))

New advances in understanding substance abuse are also emerging: During active cigarette smoking, available MAO-A binding is lowered, whereas during acute withdrawal MAO-A binding is elevated (Fowler et al. 1996; Bacher et al. 2011). These findings suggest that changes in MAO-A availability in adulthood predispose to persistent alterations in mood state. Interestingly, the personality traits of aggression and reduced deliberation are associated with reduced MAO-A binding, particularly in the prefrontal cortex, and in the context of the relationship of MAO-A levels to these traits in other models, we suggest that this may reflect a marker of a neurodevelopmental influence predisposing to a personality characteristic (Alia-Klein et al. 2008; Soliman et al. 2011).

5-HTT imaging now has a major influence upon novel antidepressant development since an 80 % occupancy is predictive of a differential response versus placebo (Meyer et al. 2001; Wilson et al. 2000). 5-HTT imaging has verified that the effects of ecstasy upon reducing 5-HTT density in animal models and post-mortem humans apply in vivo (McCann et al. 2005, 2008; Kish et al. 2010; Erritzoe et al. 2011; Urban et al. 2012) and is suggesting that diffuse 5-HTT loss occurs in OCD (Meyer et al. 2001, 2004a, b). In contrast, greater 5-HTT BP_{ND} in untreated MDD and winter season suggests that a model of predisposition to serotonin loss may contribute towards a similar predisposition towards sad mood (Meyer et al. 2004a, b; Buchert et al. 2006; Bhagwagar et al. 2007; Cannon et al. 2007; Praschak-Rieder et al. 2008; Ruhe et al. 2009; Kalbitzer et al. 2010).

References

- Alia-Klein N, Goldstein RZ, Kriplani A et al (2008) Brain monoamine oxidase activity predicts trait aggression. *J Neurosci* 28:5099–5104
- American Psychiatric Association (1994) Diagnostic and statistical manual of mental disorders, 4th edn. American Psychiatric Association, Washington, DC
- Anda RF, Williamson DF, Escobedo LG et al (1990) Depression and the dynamics of smoking. A national perspective. *JAMA* 264:1541–1545
- Azmitia E (1999) Serotonin neurons, neuroplasticity, and homeostasis of neural tissue. *Neuropsychopharmacology* 21:1S–45S
- Bacher I, Houle S, Xu X et al (2011) Monoamine oxidase A binding in the prefrontal and anterior cingulate cortices during acute withdrawal from heavy cigarette smoking. *Arch Gen Psychiatry* 68:817–826
- Barton DA, Esler MD, Dawood T et al (2008) Elevated brain serotonin turnover in patients with depression: effect of genotype and therapy. *Arch Gen Psychiatry* 65:38–46
- Bel N, Artigas F (1992) Fluvoxamine preferentially increases extracellular 5-hydroxytryptamine in the raphe nuclei: an in vivo microdialysis study. *Eur J Pharmacol* 229:101–103
- Bel N, Artigas F (1993) Chronic treatment with fluvoxamine increases extracellular serotonin in frontal cortex but not in raphe nuclei. *Synapse* 15:243–245
- Bel N, Artigas F (1995) In vivo evidence for the reversible action of the monoamine oxidase inhibitor brofaromine on 5-hydroxytryptamine release in rat brain. *Naunyn Schmiedeberg Arch Pharmacol* 351:475–482
- Benmansour S, Cecchi M, Morilak D et al (1999) Effects of chronic antidepressant treatments on serotonin transporter function, density and mRNA level. *J Neurosci* 19:10494–10501
- Bergstrom M, Westerberg G, Kihlberg T et al (1997a) Synthesis of some 11C-labelled MAO-A inhibitors and their in vivo uptake kinetics in rhesus monkey brain. *Nucl Med Biol* 24:381–388
- Bergstrom M, Westerberg G, Langstrom B (1997b) 11C-harmine as a tracer for monoamine oxidase A (MAO-A): in vitro and in vivo studies. *Nucl Med Biol* 24:287–293
- Bergstrom M, Westerberg G, Nemeth G et al (1997c) MAO-A inhibition in brain after dosing with esuprone, moclobemide and placebo in healthy volunteers: in vivo studies with positron emission tomography. *Eur J Clin Pharmacol* 52:121–128
- Bhagwagar Z, Murthy N, Selvaraj S et al (2007) 5-HTT binding in recovered depressed patients and healthy volunteers: a positron emission tomography study with [11C]DASB. *Am J Psychiatry* 164:1858–1865
- Blakely R, Ramamoorthy S, Qian Y et al (1997) Regulation of antidepressant-sensitive serotonin transporters. In: Reith M (ed) *Neurotransmitter transporters: structure, function, and regulation*. Humana Press, Totowa NJ, pp 29–72
- Blier P, De Montigny C (1983) Electrophysiological investigations on the effect of repeated zimelidine administration on serotonergic neurotransmission in the rat. *J Neurosci* 3:1270–1278
- Blier P, Galzin AM, Langer SZ (1989) Diurnal variation in the function of serotonin terminals in the rat hypothalamus. *J Neurochem* 52:453–459
- Bortolato M, Chen K, Shih JC (2008) Monoamine oxidase inactivation: from pathophysiology to therapeutics. *Adv Drug Deliv Rev* 60:1527–1533
- Bottlaender M, Valette H, Delforge J et al (2010) In vivo quantification of monoamine oxidase A in baboon brain: a PET study using [11C]befloxatone and the multi-injection approach. *J Cereb Blood Flow Metab* 30:792–800
- Breslau N, Peterson EL, Schultz LR et al (1998) Major depression and stages of smoking. A longitudinal investigation. *Arch Gen Psychiatry* 55:161–166
- Brody AL, Mandelkern MA, London ED et al (2006) Cigarette smoking saturates brain alpha 4 beta 2 nicotinic acetylcholine receptors. *Arch Gen Psychiatry* 63:907–915
- Brucke T, Kornhuber J, Angelberger P et al (1993) SPECT imaging of dopamine and serotonin transporters with [123I]beta-CIT. Binding kinetics in the human brain. *J Neural Transm Gen Sect* 94:137–146

- Brunner HG, Nelen M, Breakefield XO et al (1993) Abnormal behavior associated with a point mutation in the structural gene for monoamine oxidase A. *Science* 262:578–580
- Buchert R, Schulze O, Wilke F et al (2006) Is correction for age necessary in SPECT or PET of the central serotonin transporter in young, healthy adults? *J Nucl Med* 47:38–42
- Buck A, Gucker PM, Schonbachler RD et al (2000) Evaluation of serotonergic transporters using PET and [¹¹C](+)-McN-5652: assessment of methods. *J Cereb Blood Flow Metab* 20:253–262
- Buckholtz JW, Meyer-Lindenberg A (2008) MAOA and the neurogenetic architecture of human aggression. *Trends Neurosci* 31:120–129
- Cannon DM, Ichise M, Rollis D et al (2007) Elevated serotonin transporter binding in major depressive disorder assessed using positron emission tomography and [¹¹C]DASB; comparison with bipolar disorder. *Biol Psychiatry* 62:870–877
- Carey MP, Kalra DL, Carey KB et al (1993) Stress and unaided smoking cessation: a prospective investigation. *J Consult Clin Psychol* 61:831–838
- Carlsson A, Svennerholm L, Winblad B (1980) Seasonal and circadian monoamine variations in human brains examined post mortem. *Acta Psychiatr Scand Suppl* 280:75–85
- Carroll FI, Kotian P, Dehghani A et al (1995) Cocaine and 3 beta-(4'-substituted phenyl)tropane-2 beta-carboxylic acid ester and amide analogues. New high-affinity and selective compounds for the dopamine transporter. *J Med Chem* 38:379–388
- Cases O, Vitalis T, Seif I et al (1996) Lack of barrels in the somatosensory cortex of monoamine oxidase A-deficient mice: role of a serotonin excess during the critical period. *Neuron* 16:297–307
- Caspi A, McClay J, Moffitt TE et al (2002) Role of genotype in the cycle of violence in maltreated children. *Science* 297:851–854
- Catafau AM, Perez V, Penengo MM et al (2005) SPECT of serotonin transporters using ¹²³I-ADAM: optimal imaging time after bolus injection and long-term test-retest in healthy volunteers. *J Nucl Med* 46:1301–1309
- Chalon S, Tarkiainen J, Garreau L et al (2003) Pharmacological characterization of N, N-dimethyl-2-(2-amino-4-methylphenyl thio)benzylamine as a ligand of the serotonin transporter with high affinity and selectivity. *J Pharmacol Exp Ther* 304:81–87
- Choi SR, Hou C, Oya S et al (2000) Selective in vitro and in vivo binding of [¹²⁵I]ADAM to serotonin transporters in rat brain. *Synapse* 38:403–412
- Ciliax BJ, Drash GW, Staley JK et al (1999) Immunocytochemical localization of the dopamine transporter in human brain. *J Comp Neurol* 409:38–56
- Cortes R, Soriano E, Pazos A et al (1988) Autoradiography of antidepressant binding sites in the human brain: localization using [³H]imipramine and [³H]Paroxetine. *Neuroscience* 27:473–496
- Cosgrove KP, Batis J, Bois F et al (2009) beta2-Nicotinic acetylcholine receptor availability during acute and prolonged abstinence from tobacco smoking. *Arch Gen Psychiatry* 66:666–676
- Curet O, Damoiseau-Ovens G, Sauvage C et al (1998) Preclinical profile of beffoxatone, a new reversible MAO-A inhibitor. *J Affect Disord* 51:287–303
- Dewar KM, Grondin L, Carli M et al (1992) [³H]paroxetine binding and serotonin content of rat cortical areas, hippocampus, neostriatum, ventral mesencephalic tegmentum, and midbrain raphe nuclei region following p-chlorophenylalanine and p-chloroamphetamine treatment. *J Neurochem* 58:250–257
- Dolle F, Valette H, Bramouille Y et al (2003) Synthesis and in vivo imaging properties of [¹¹C] beffoxatone: a novel highly potent positron emission tomography ligand for mono-amine oxidase-A. *Bioorg Med Chem Lett* 13:1771–1775
- Donnelly CH, Murphy DL (1977) Substrate- and inhibitor-related characteristics of human platelet monoamine oxidase. *Biochem Pharmacol* 26:853–858
- Dreshfield LJ, Wong DT, Perry KW et al (1996) Enhancement of fluoxetine-dependent increase of extracellular serotonin (5-HT) levels by (-)-pindolol, an antagonist at 5-HT_{1A} receptors. *Neurochem Res* 21:557–562
- Erlandsson K, Sivananthan T, Lui D et al (2005) Measuring SSRI occupancy of SERT using the novel tracer [¹²³I]ADAM: a SPECT validation study. *Eur J Nucl Med Mol Imaging* 32:1329–1336

- Erritzoe D, Frokjaer VG, Holst KK et al (2011) In vivo imaging of cerebral serotonin transporter and serotonin(2A) receptor binding in 3,4-methylenedioxymethamphetamine (MDMA or "ecstasy") and hallucinogen users. *Arch Gen Psychiatry* 68:562–576
- Fava GA, Ruini C, Rafanelli C et al (2004) Six-year outcome of cognitive behavior therapy for prevention of recurrent depression. *Am J Psychiatry* 161:1872–1876
- Fazel S, Danesh J (2002) Serious mental disorder in 23000 prisoners: a systematic review of 62 surveys. *Lancet* 359:545–550
- Finberg J (2012) Role of the organic cation transporter (OCT-3) and monoamine oxidase types A and B in the metabolism of dopamine derived from L-DOPA in rat striatum depleted of dopaminergic and serotonergic afferent inputs. Tenth International Catecholamine Symposium. Pacific Grove, 82
- First M, Spitzer R, Williams J et al (1995) Structured clinical interview for DSM-IV axis I disorders, patient edition (SCID-P), version 2. Biometrics Research, New York
- Fowler JS, MacGregor RR, Wolf AP et al (1987) Mapping human brain monoamine oxidase A and B with 11C-labeled suicide inactivators and PET. *Science* 235:481–485
- Fowler JS, Volkow ND, Wang GJ et al (1996) Brain monoamine oxidase A inhibition in cigarette smokers. *Proc Natl Acad Sci U S A* 93:14065–14069
- Frank E, Kupfer DJ, Perel JM et al (1990) Three-year outcomes for maintenance therapies in recurrent depression. *Arch Gen Psychiatry* 47:1093–1099
- Frankle WG, Lombardo I, New AS et al (2005) Brain serotonin transporter distribution in subjects with impulsive aggressivity: a positron emission study with [11C]McN 5652. *Am J Psychiatry* 162:915–923
- Freis ED (1954) Mental depression in hypertensive patients treated for long periods with large doses of reserpine. *N Engl J Med* 251:1006–1008
- Garvey AJ, Bliss RE, Hitchcock JL et al (1992) Predictors of smoking relapse among self-quitters: a report from the Normative Aging Study. *Addict Behav* 17:367–377
- Ginovart N, Wilson AA, Meyer JH et al (2001) Positron emission tomography quantification of [11C]-DASB binding to the human serotonin transporter: modeling strategies. *J Cereb Blood Flow Metab* 21:1342–1353
- Ginovart N, Meyer JH, Boovariwala A et al (2006) Positron emission tomography quantification of [11C]-harmine binding to monoamine oxidase-A in the human brain. *J Cereb Blood Flow Metab* 26:330–344
- Graham D, Tahraroui L, Langer SZ (1987) Effect of chronic treatment with selective monoamine oxidase inhibitors and specific 5-hydroxytryptamine uptake inhibitors on [3H]paroxetine binding to cerebral cortical membranes of the rat. *Neuropharmacology* 26:1087–1092
- Halldin C, Lundberg J, Sovago J et al (2005) [11C]MADAM, a new serotonin transporter radioligand characterized in the monkey brain by PET. *Synapse* 58:173–183
- Hauptmann N, Shih JC (2001) 2-Naphthylamine, a compound found in cigarette smoke, decreases both monoamine oxidase A and B catalytic activity. *Life Sci* 68:1231–1241
- Herraiz T, Chaparro C (2005) Human monoamine oxidase is inhibited by tobacco smoke: beta-carboline alkaloids act as potent and reversible inhibitors. *Biochem Biophys Res Commun* 326:378–386
- Hesse S, Stengler K, Regenthal R et al (2011) The serotonin transporter availability in untreated early-onset and late-onset patients with obsessive-compulsive disorder. *Int J Neuropsychopharmacol* 14:606–617
- Hesse S, Brust P, Mäding P et al (2012) Imaging of the brain serotonin transporters (SERT) with 18F-labelled fluoromethyl-McN5652 and PET in humans. *Eur J Nucl Med Mol Imaging* 39:1001–1011
- Holschneider DP, Kumazawa T, Chen K et al (1998) Tissue-specific effects of estrogen on monoamine oxidase A and B in the rat. *Life Sci* 63:155–160
- Houle S, Ginovart N, Hussey D et al (2000) Imaging the serotonin transporter with positron emission tomography: initial human studies with [11C]DAPP and [11C]DASB. *Eur J Nucl Med* 27:1719–1722
- Ichise M, Liow JS, Lu JQ et al (2003) Linearized reference tissue parametric imaging methods: application to [11C]DASB positron emission tomography studies of the serotonin transporter in human brain. *J Cereb Blood Flow Metab* 23:1096–1112

- Ikoma Y, Suhara T, Toyama H et al (2002) Quantitative analysis for estimating binding potential of the brain serotonin transporter with [¹¹C]McN5652. *J Cereb Blood Flow Metab* 22:490–501
- Jarkas N, Votaw JR, Voll RJ et al (2005) Carbon-11 HOMADAM: a novel PET radiotracer for imaging serotonin transporters. *Nucl Med Biol* 32:211–224
- Johnson S, Stockmeier CA, Meyer JH et al (2011) The reduction of R1, a novel repressor protein for monoamine oxidase a, in major depressive disorder. *Neuropsychopharmacology* 36:2139–2148
- Kalbitzer J, Erritzoe D, Holst KK et al (2010) Seasonal changes in brain serotonin transporter binding in short serotonin transporter linked polymorphic region-allele carriers but not in long-allele homozygotes. *Biol Psychiatry* 67:1033–1039
- Kenford SL, Smith SS, Wetter DW et al (2002) Predicting relapse back to smoking: contrasting affective and physical models of dependence. *J Consult Clin Psychol* 70:216–227
- Kent JM, Coplan JD, Lombardo I et al (2002) Occupancy of brain serotonin transporters during treatment with paroxetine in patients with social phobia: a positron emission tomography study with ¹¹C McN 5652. *Psychopharmacology (Berl)* 164:341–348
- Kim-Cohen J, Caspi A, Taylor A et al (2006) MAOA, maltreatment, and gene-environment interaction predicting children's mental health: new evidence and a meta-analysis. *Mol Psychiatry* 11:903–913
- Kish SJ, Furukawa Y, Chang LJ et al (2005) Regional distribution of serotonin transporter protein in postmortem human brain: is the cerebellum a SERT-free brain region? *Nucl Med Biol* 32:123–128
- Kish SJ, Lerch J, Furukawa Y et al (2010) Decreased cerebral cortical serotonin transporter binding in ecstasy users: a positron emission tomography/[¹¹C]DASB and structural brain imaging study. *Brain* 133:1779–1797
- Krishnan KR (2002) Biological risk factors in late life depression. *Biol Psychiatry* 52:185–192
- Kuikka JT, Bergstrom KA, Vanninen E et al (1993) Initial experience with single-photon emission tomography using iodine-123-labelled 2 beta-carbomethoxy-3 beta-(4-iodophenyl) tropane in human brain. *Eur J Nucl Med* 20:783–786
- Kung MP, Hou C, Oya S et al (1999) Characterization of [¹²³I]IDAM as a novel single-photon emission tomography tracer for serotonin transporters. *Eur J Nucl Med* 26:844–853
- Lambert GW, Reid C, Kaye DM et al (2002) Effect of sunlight and season on serotonin turnover in the brain. *Lancet* 360:1840–1842
- Laruelle M, Vanisberg M-A, Maloteaux J-M (1988) Regional and subcellular localization in human brain of [³H]paroxetine binding, a marker of serotonin uptake sites. *Biol Psychiatry* 24:299–309
- Laruelle M, Giddings SS, Zea-Ponce Y et al (1994) Methyl 3 beta-(4-[¹²⁵I]iodophenyl)tropane-2 beta-carboxylate in vitro binding to dopamine and serotonin transporters under “physiological” conditions. *J Neurochem* 62:978–986
- Laviolette SR, van der Kooy D (2004) The neurobiology of nicotine addiction: bridging the gap from molecules to behaviour. *Nat Rev Neurosci* 5:55–65
- Law M, Tang JL (1995) An analysis of the effectiveness of interventions intended to help people stop smoking. *Arch Intern Med* 155:1933–1941
- Lensch K, Fuchs G, Boning J et al (1987) A clinical study of the selective MAO-A-inhibitor moclobemide (Ro 11-1163): a comparison of 2 different dosages with particular reference to platelet MAO-activity and urinary MHPG-excretion. *Int Clin Psychopharmacol* 2:165–171
- Leroy C, Bragulat V, Berlin I et al (2009) Cerebral monoamine oxidase A inhibition in tobacco smokers confirmed with PET and [¹¹C]befloxatone. *J Clin Psychopharmacol* 29:86–88
- Lesch KP, Wolozin BL, Estler HC et al (1993a) Isolation of a cDNA encoding the human brain serotonin transporter. *J Neural Transm Gen Sect* 91:67–72
- Lesch KP, Wolozin BL, Murphy DL et al (1993b) Primary structure of the human platelet serotonin uptake site: identity with the brain serotonin transporter. *J Neurochem* 60:2319–2322
- Liotti M, Mayberg HS, McGinnis S et al (2002) Unmasking disease-specific cerebral blood flow abnormalities: mood challenge in patients with remitted unipolar depression. *Am J Psychiatry* 159:1830–1840

- Luine VN, Khychevskaya RI, McEwen BS (1975) Effect of gonadal steroids on activities of monoamine oxidase and choline acetylase in rat brain. *Brain Res* 86:293–306
- Lundberg J, Odano I, Olsson H et al (2005) Quantification of ¹¹C-MADAM binding to the serotonin transporter in the human brain. *J Nucl Med* 46:1505–1515
- Lundberg J, Halldin C, Farde L (2006) Measurement of serotonin transporter binding with PET and [¹¹C]MADAM: a test-retest reproducibility study. *Synapse* 60:256–263
- Lundberg J, Christophersen JS, Petersen KB et al (2007) PET measurement of serotonin transporter occupancy: a comparison of escitalopram and citalopram. *Int J Neuropsychopharmacol* 10:777–785
- Ma ZQ, Bondiolotti GP, Olasmaa M et al (1993) Estrogen modulation of catecholamine synthesis and monoamine oxidase A activity in the human neuroblastoma cell line SK-ER3. *J Steroid Biochem Mol Biol* 47:207–211
- Ma ZQ, Violani E, Villa F et al (1995) Estrogenic control of monoamine oxidase A activity in human neuroblastoma cells expressing physiological concentrations of estrogen receptor. *Eur J Pharmacol* 284:171–176
- Magnusson A (2000) An overview of epidemiological studies on seasonal affective disorder. *Acta Psychiatr Scand* 101:176–184
- Mann JJ, Stanley M (1984) Postmortem monoamine oxidase enzyme kinetics in the frontal cortex of suicide victims and controls. *Acta Psychiatr Scand* 69:135–139
- Mathews T, Fedele D, Unger E et al (2000) Effects of serotonin transporter inactivation on extracellular 5-HT levels, in vivo microdialysis recovery, and MDMA-induced release of serotonin and dopamine in mouse striatum. *Soc Neurosci* 30:624, Abstracts
- Mathews TA, Fedele DE, Coppelli FM et al (2004) Gene dose-dependent alterations in extraneuronal serotonin but not dopamine in mice with reduced serotonin transporter expression. *J Neurosci Methods* 140:169–181
- Matsumoto R, Ichise M, Ito H et al (2010) Reduced serotonin transporter binding in the insular cortex in patients with obsessive-compulsive disorder: a [¹¹C]DASB PET study. *Neuroimage* 49:121–126
- McCann UD, Szabo Z, Seckin E et al (2005) Quantitative PET studies of the serotonin transporter in MDMA users and controls using [¹¹C]McN5652 and [¹¹C]DASB. *Neuropsychopharmacology* 30:1741–1750
- McCann UD, Szabo Z, Vranesic M et al (2008) Positron emission tomographic studies of brain dopamine and serotonin transporters in abstinent (+/-)3,4-methylenedioxymethamphetamine (“ecstasy”) users: relationship to cognitive performance. *Psychopharmacology (Berl)* 200:439–450
- Mejia JM, Ervin FR, Baker GB et al (2002) Monoamine oxidase inhibition during brain development induces pathological aggressive behavior in mice. *Biol Psychiatry* 52:811–821
- Meyer JH (2007) Imaging the serotonin transporter during major depressive disorder and antidepressant treatment. *J Psychiatry Neurosci* 32:86–102
- Meyer JH (2008) Applying neuroimaging ligands to study major depressive disorder. *Semin Nucl Med* 38:287–304
- Meyer JH, Wilson AA, Ginovart N et al (2001) Occupancy of serotonin transporters by paroxetine and citalopram during treatment of depression: a [¹¹C]DASB PET imaging study. *Am J Psychiatry* 158:1843–1849
- Meyer JH, Houle S, Sagrati S et al (2004a) Brain serotonin transporter binding potential measured with carbon 11-labeled DASB positron emission tomography: effects of major depressive episodes and severity of dysfunctional attitudes. *Arch Gen Psychiatry* 61:1271–1279
- Meyer JH, Wilson AA, Sagrati S et al (2004b) Serotonin transporter occupancy of five selective serotonin reuptake inhibitors at different doses: an [¹¹C]DASB positron emission tomography study. *Am J Psychiatry* 161:826–835
- Meyer JH, Ginovart N, Boovariwala A et al (2006) Elevated monoamine oxidase A levels in the brain: an explanation for the monoamine imbalance of major depression. *Arch Gen Psychiatry* 63:1209–1216
- Meyer JH, Wilson AA, Sagrati S et al (2009) Brain monoamine oxidase A binding in major depressive disorder: relationship to selective serotonin reuptake inhibitor treatment, recovery, and recurrence. *Arch Gen Psychiatry* 66:1304–1312

- Moret C, Briley M (1996) Effects of acute and repeated administration of citalopram on extracellular levels of serotonin in rat brain. *Eur J Pharmacol* 295:189–197
- Murphy DL, Lipper S, Slater S et al (1979) Selectivity of clorgyline and pargyline as inhibitors of monoamine oxidases A and B in vivo in man. *Psychopharmacology (Berl)* 62:129–132
- Nelson DL, Herbet A, Glowinski J et al (1979) [³H]Harmaline as a specific ligand of MAO A–II. Measurement of the turnover rates of MAO A during ontogenesis in the rat brain. *J Neurochem* 32:1829–1836
- Nye JA, Votaw JR, Jarkas N et al (2008) Compartmental modeling of ¹¹C-HOMADAM binding to the serotonin transporter in the healthy human brain. *J Nucl Med* 49:2018–2025
- O'Hara MW, Swain A (1996) Rates and risk of postpartum depression – a meta analysis. *Int Rev Psychiatry* 8:37–54
- O'Hara MW, Schlechte JA, Lewis DA et al (1991) Prospective study of postpartum blues. Biologic and psychosocial factors. *Arch Gen Psychiatry* 48:801–806
- Ordway GA, Farley JT, Dilley GE et al (1999) Quantitative distribution of monoamine oxidase A in brainstem monoamine nuclei is normal in major depression. *Brain Res* 847:71–79
- Oya S, Choi SR, Hou C et al (2000) 2-((2-((dimethylamino)methyl)phenyl)thio)-5-iodophenylamine (ADAM): an improved serotonin transporter ligand. *Nucl Med Biol* 27:249–254
- Parsey RV, Kegeles LS, Hwang DR et al (2000) In vivo quantification of brain serotonin transporters in humans using [¹¹C]McN 5652. *J Nucl Med* 41:1465–1477
- Paterson LM, Tyacke RJ, Nutt DJ et al (2010) Measuring endogenous 5-HT release by emission tomography: promises and pitfalls. *J Cereb Blood Flow Metab* 30:1682–1706
- Piper ME, Smith SS, Schlam TR et al (2009) A randomized placebo-controlled clinical trial of 5 smoking cessation pharmacotherapies. *Arch Gen Psychiatry* 66:1253–1262
- Pirker W, Asenbaum S, Kasper S et al (1995) beta-CIT SPECT demonstrates blockade of 5HT-uptake sites by citalopram in the human brain in vivo. *J Neural Transm Gen Sect* 100:247–256
- Praschak-Rieder N, Wilson AA, Hussey D et al (2005) Effects of tryptophan depletion on the serotonin transporter in healthy humans. *Biol Psychiatry* 58:825–830
- Praschak-Rieder N, Willeit M, Wilson AA et al (2008) Seasonal variation in human brain serotonin transporter binding. *Arch Gen Psychiatry* 65:1072–1078
- Pratt L, Brody D (2010) Depression and smoking in the U.S. household population aged 20 and over, 2005–2008. *NCHS Data Brief* 34:1–8
- Reimold M, Smolka MN, Zimmer A et al (2007) Reduced availability of serotonin transporters in obsessive-compulsive disorder correlates with symptom severity – a [¹¹C]DASB PET study. *J Neural Transm* 114:1603–1609
- Robins LN, Helzer JE, Weissman MM et al (1984) Lifetime prevalence of specific psychiatric disorders in three sites. *Arch Gen Psychiatry* 41:949–958
- Rommelspacher H, Meier-Henco M, Smolka M et al (2002) The levels of norharman are high enough after smoking to affect monoamine oxidase B in platelets. *Eur J Pharmacol* 441:115–125
- Rovescalli AC, Brunello N, Riva M et al (1989) Effect of different photoperiod exposure on [³H] imipramine binding and serotonin uptake in the rat brain. *J Neurochem* 52:507–514
- Ruhe HG, Mason NS, Schene AH (2007) Mood is indirectly related to serotonin, norepinephrine and dopamine levels in humans: a meta-analysis of monoamine depletion studies. *Mol Psychiatry* 12:331–359
- Ruhe HG, Boij J, Reitsma JB et al (2009) Serotonin transporter binding with [¹²³I]beta-CIT SPECT in major depressive disorder versus controls: effect of season and gender. *Eur J Nucl Med Mol Imaging* 36:841–849
- Sacher J, Wilson A, Houle S et al (2010) Elevated brain monoamine oxidase A binding in early postpartum. *Arch Gen Psychiatry* 67:468–474
- Sacher J, Houle S, Parkes J et al (2011) Monoamine oxidase A inhibitor occupancy during treatment of major depressive episodes with moclobemide or St. John's wort: an [¹¹C]-harmine PET study. *J Psychiatry Neurosci* 36:375–382
- Sacher J, Rabiner EA, Clark M et al (2012) Dynamic, adaptive changes in MAO-A binding after alterations in substrate availability: an in vivo [¹¹C]-harmine positron emission tomography study. *J Cereb Blood Flow Metab* 32:443–446

- Saura J, Kettler R, Da Prada M et al (1992) Quantitative enzyme radioautography with 3H-Ro 41–1049 and 3H-Ro 19–6327 in vitro: localization and abundance of MAO-A and MAO-B in rat CNS, peripheral organs, and human brain. *J Neurosci* 12:1977–1999
- Saura J, Bleuel Z, Ulrich J et al (1996) Molecular neuroanatomy of human monoamine oxidases A and B revealed by quantitative enzyme radioautography and in situ hybridization histochemistry. *Neuroscience* 70:755–774
- Selvaraj S, Hoshi R, Bhagwagar Z et al (2009) Brain serotonin transporter binding in former users of MDMA ('ecstasy'). *Br J Psychiatry* 194:355–359
- Shank RP, Vaught JL, Pelley KA et al (1988) McN-5652: a highly potent inhibitor of serotonin uptake. *J Pharmacol Exp Ther* 247:1032–1038
- Sharot T, Riccardi AM, Raio CM et al (2007) Neural mechanisms mediating optimism bias. *Nature* 450:102–105
- Sherif F, Marcusson J, Orelund L (1991) Brain gamma-aminobutyrate transaminase and monoamine oxidase activities in suicide victims. *Eur Arch Psychiatry Clin Neurosci* 241:139–144
- Soliman A, Bagby RM, Wilson AA et al (2011) Relationship of monoamine oxidase A binding to adaptive and maladaptive personality traits. *Psychol Med* 41:1051–1060
- Stockmeier CA (2003) Involvement of serotonin in depression: evidence from postmortem and imaging studies of serotonin receptors and the serotonin transporter. *J Psychiatr Res* 37:357–373
- Suhara T, Takano A, Sudo Y et al (2003) High levels of serotonin transporter occupancy with low-dose clomipramine in comparative occupancy study with fluvoxamine using positron emission tomography. *Arch Gen Psychiatry* 60:386–391
- Talbot PS, Frankle WG, Hwang DR et al (2005) Effects of reduced endogenous 5-HT on the in vivo binding of the serotonin transporter radioligand 11C-DASB in healthy humans. *Synapse* 55:164–175
- Tao-Cheng JH, Zhou FC (1999) Differential polarization of serotonin transporters in axons versus soma-dendrites: an immunogold electron microscopy study. *Neuroscience* 94:821–830
- Tauscher J, Pirker W, de Zwaan M et al (1999) In vivo visualization of serotonin transporters in the human brain during fluoxetine treatment. *Eur Neuropsychopharmacol* 9:177–179
- Tom SM, Fox CR, Trepel C et al (2007) The neural basis of loss aversion in decision-making under risk. *Science* 315:515–518
- Trivedi MH, Rush AJ, Wisniewski SR et al (2006) Evaluation of outcomes with citalopram for depression using measurement-based care in STAR*D: implications for clinical practice. *Am J Psychiatry* 163:28–40
- Tweedie DJ, Burke MD (1987) Metabolism of the beta-carbolines, harmine and harmol, by liver microsomes from phenobarbitone- or 3-methylcholanthrene-treated mice. Identification and quantitation of two novel harmine metabolites. *Drug Metab Dispos* 15:74–81
- Urban NB, Girgis RR, Talbot PS et al (2012) Sustained recreational use of ecstasy is associated with altered pre and postsynaptic markers of serotonin transmission in neocortical areas: a PET study with [11C]DASB and [11C]MDL 100907. *Neuropsychopharmacology* 37:1465–1473
- Vitalis T, Cases O, Callebert J et al (1998) Effects of monoamine oxidase A inhibition on barrel formation in the mouse somatosensory cortex: determination of a sensitive developmental period. *J Comp Neurol* 393:169–184
- Weissman MM, Bland RC, Canino GJ et al (1994) The cross national epidemiology of obsessive compulsive disorder. The Cross National Collaborative Group. *J Clin Psychiatry* 55(Suppl):5–10
- Wiesel FA, Raaflaub J, Kettler R (1985) Pharmacokinetics of oral moclobemide in healthy human subjects and effects on MAO-activity in platelets and excretion of urine monoamine metabolites. *Eur J Clin Pharmacol* 28:89–95
- Wilson A, Schmidt M, Ginovart N et al (2000) Novel radiotracers for imaging the serotonin transporter by positron emission tomography: synthesis, radiosynthesis, in vitro and ex vivo evaluation of [11C]-labelled 2-(phenylthio) aralkylamines. *J Med Chem* 43:3103–3110

- Wilson AA, Ginovart N, Hussey D et al (2002) In vitro and in vivo characterisation of [11C]-DASB: a probe for in vivo measurements of the serotonin transporter by positron emission tomography. *Nucl Med Biol* 29:509–515
- Wilson A, Meyer J, Garcia A et al (2003) Determination of the arterial input function of the MAO-A inhibitor [11C] harmine in human subjects. *J Label Comp Radiopharm* 46:S367
- World Health Organization (2008) The global burden of disease: 2004 update. Department of Health Statistics and Informatics, Information Evidence and Research Cluster, WHO, Switzerland
- Youdim MB, Edmondson D, Tipton KF (2006) The therapeutic potential of monoamine oxidase inhibitors. *Nat Rev Neurosci* 7:295–309
- Yu A, Yang J, Pawlyk AC et al (1995) Acute depletion of serotonin down-regulates serotonin transporter mRNA in raphe neurons. *Brain Res* 688:209–212
- Zhou FC, Tao-Cheng JH, Segu L et al (1998) Serotonin transporters are located on the axons beyond the synaptic junctions: anatomical and functional evidence. *Brain Res* 805:241–254

Jun Toyohara, Muneyuki Sakata, and Kiichi Ishiwata

Contents

26.1	Introduction	744
26.2	Brain Imaging of Sigma Receptors	745
26.2.1	Post-mortem Studies	745
26.2.2	Radioligands for Imaging of Sigma Receptors	745
26.2.3	PET Imaging of the Sigma ₁ Receptors in the Human Brain	748
26.3	Sigma Receptors in CNS Diseases.....	755
26.3.1	Schizophrenia.....	755
26.3.2	Mood Disorders	756
26.3.3	Ischemia	757
26.3.4	Neurodegenerative Diseases	757
26.3.5	Drug Addiction and Alcoholism.....	757
	Conclusion	758
	References.....	758

Abstract

Sigma receptors are classified into sigma₁ and sigma₂ subtypes. Sigma₁ receptors are widely distributed in the central nervous system (CNS) and in peripheral tissues. Sigma₁ receptors play a role in a variety of human CNS diseases, including mood disorders, stroke, neurodegenerative disease, and drug addiction. Therefore, there is a great deal of interest in imaging of sigma₁ receptors in the living human brain. In contrast, sigma₂ receptors have also been the focus of tumour imaging studies. A number of radioligands have been developed for imaging of sigma₁ receptors in the human brain, and a few, including [¹¹C]SA4503, have been used in clinical studies. Sigma₁ receptors are distributed throughout the grey matter of the human brain. A widespread decrease in [¹¹C]SA4503 binding in patients with

J. Toyohara (✉) • M. Sakata • K. Ishiwata
 Research Team for Neuroimaging,
 Tokyo Metropolitan Institute of Gerontology,
 35-2 Sakaecho, Itabashi-ku, Tokyo 173-0015, Japan
 e-mail: toyohara@pet.tmig.or.jp

Alzheimer's disease and a significant decrease in binding on the more affected side of the anterior putamen in patients with Parkinson's disease have been reported. Receptor occupancy studies with [^{11}C]SA4503-PET have shown that some antidepressants and antipsychotics have an affinity for σ_1 receptors in the human brain in addition to their main targets.

Abbreviations

AChE	Acetylcholinesterase
AD	Alzheimer's disease
BD-1047	<i>N'</i> -[2-(3,4-dichlorophenyl)ethyl]- <i>N,N,N'</i> -trimethylethane-1,2-diamine
BDNF	Brain-derived neurotrophic factor
BMY14802 (BMS181100)	1-(4-fluorophenyl)-4-[4-(5-fluoropyrimidin-2-yl)piperazin-1-yl]butan-1-ol
BP_{ND}	Specific binding potential relative to non-displaceable binding
CNS	Central nervous system
CFT	(1 <i>R</i> ,2 <i>S</i> ,3 <i>S</i> ,5 <i>S</i>)-3-(4-fluorophenyl)-8-methyl-8-azabicyclo[3.2.1]octane-2-carboxylate
Cutamesine	SA4503 = 1-[2-(3,4-dimethoxyphenyl)ethyl]-4-(3-phenylpropyl)piperazine
DHEA	Dehydroepiandrosterone
Donepezil	(<i>RS</i>)-2-[(1-benzyl-4-piperidyl)methyl]-5,6-dimethoxy-2,3-dihydroinden-1-one
DTG	1,3-di(2-tolyl)guanidine
DuP734	2-[1-(cyclopropylmethyl)piperidin-4-yl]-1-(4-fluorophenyl)ethanonehydrobromide
EBP	Emopamil binding protein = sterol $\Delta 8 - \Delta 7$ isomerase
Eliprodil (SL82.0715)	1-(4-chlorophenyl)-2-[4-[(4-fluorophenyl)methyl]piperidin-1-yl]ethanol
ER	Endoplasmic reticulum
FDG	2-deoxy-2-fluoro- D -glucose
Fluspidine	1'-benzyl-3-(2-fluoroethyl)-3 <i>H</i> -spiro[isobenzofurane-1,4'-piperidine]
Fluvoxiamine	(<i>E</i>)-5-methoxy-1-[4-(trifluoromethyl)phenyl]pentan-1-one <i>O</i> -2-aminoethyl oxime
FM-SA4503	1-[2-(4-fluoromethoxy-3-methoxyphenyl)ethyl]-4-(3-phenylpropyl)piperazine
FPS	1-(3-fluoropropyl)-4-[(4-cyanophenoxy)methyl]piperidine
Haloperidol	4-[4-(4-chlorophenyl)-4-hydroxy-1-piperidyl]-1-(4-fluorophenyl)-butan-1-one

Ifenprodil	4-[2-(4-benzylpiperidin-1-yl)-1-hydroxypropyl]phenol
Igmesine (JO1,784)	(<i>E</i>)- <i>N</i> -(cyclopropylmethyl)- <i>N</i> -ethyl-3,6-diphenylhex-5-en-3-amine
LID	Levodopa-induced dyskinesia
mI-SA4503	1-[2-(3,4-dimethoxyphenyl)ethyl]-4-[3-(3-iodophenyl)propyl]piperazine
NE-100	4-[2-(dipropylamino)ethyl]-2-(2-phenylethoxy)anisole
Nemonapride (YM-09151-2)	<i>N</i> -(1-benzyl-2-methylpyrrolidin-3-yl)-5-chloro-2-methoxy-4-(methylamino)benzamide
NGF	Nerve growth factor
NMDA	<i>N</i> -methyl- <i>D</i> -aspartate
oI-SA4503	1-[2-(3,4-dimethoxyphenyl)ethyl]-4-[3-(2-iodophenyl)propyl]piperazine
Panamesine	(5 <i>S</i>)-5-[[4-(1,3-benzodioxol-5-yl)-4-hydroxypiperidin-1-yl]methyl]-3-(4-methoxyphenyl)-1,3-oxazolidin-2-one
Paroxetine	(3 <i>S</i> ,4 <i>R</i>)-3-[(2 <i>H</i> -1,3-benzodioxol-5-yloxy)methyl]-4-(4-fluorophenyl)piperidine
PD	Parkinson's disease
Pentazocine (EMD57445)	(2 <i>RS</i> ,6 <i>RS</i> ,11 <i>RS</i>)-6,11-dimethyl-3-(3-methylbut-2-en-1-yl)-1,2,3,4,5,6-hexahydro-2,6-methano-3-benzazocin-8-ol
PET	Positron emission tomography
PGRMC1	Progesterone receptor membrane component 1
Physostigmine	(3 <i>aR</i> ,8 <i>aS</i>)-1,3 <i>a</i> ,8-trimethyl-1 <i>H</i> ,2 <i>H</i> ,3 <i>H</i> ,3 <i>aH</i> ,8 <i>H</i> ,8 <i>aH</i> -pyrrolo [2,3- <i>b</i>] indol-5-yl <i>N</i> -methylcarbamate
PPBP	4-phenyl-1-(4-phenylbutyl)piperidine
3-PPP	(+)-3-(3-hydroxyphenyl)- <i>N</i> -(1-propyl)piperidine
Raclopride	3,5-dichloro- <i>N</i> -{[(2 <i>S</i>)-1-ethylpyrrolidin-2-yl]methyl}-2-hydroxy-6-methoxybenzamide
rCBF	Regional cerebral blood flow
Rimcazole (BW234U)	9-{3-[(3 <i>R</i> ,5 <i>S</i>)-3,5-dimethylpiperazin-1-yl]propyl}-9 <i>H</i> -carbazole
SFE	WLS1.002 = 1-(2-fluoroethyl)-4-[(4-cyanophenoxy)methyl]piperidine
SKF 10,047 (<i>N</i> -allylnormetazocine)	(2 <i>R</i> ,6 <i>R</i> ,11 <i>R</i>)-6,11-dimethyl-3-prop-2-en-1-yl-1,2,3,4,5,6-hexahydro-2,6-methano-3-benzazocin-8-ol

SPECT	Single-photon emission computed tomography
Spiperone	8-[4-(4-fluorophenyl)-4-oxo-butyl]-1-phenyl-1,3,8-triazaspiro[4.5]decan-4-one
SSRI	Selective serotonin reuptake inhibitor
SUV	Standardised uptake value
TAC	Time-activity curve
Tamoxifen	(<i>Z</i>)-2-[4-(1,2-diphenylbut-1-enyl)phenoxy]- <i>N,N</i> -dimethylethanamine
TPCNE	1(<i>trans</i> -iodopropen-2-yl)-4-[(4-cyanophenoxy)methyl]piperidine
Trifluorperazine	10-[3-(4-methylpiperazin-1-yl)propyl]-2-(trifluoromethyl)-10 <i>H</i> -phenothiazine
VAChT	Vesicular acetylcholine transporter
VT	Total volume of distribution

26.1 Introduction

Sigma receptors were initially categorised as a subtype of opioid receptors, because the effects of a prototypical opioid agonist, SKF10,047 (*N*-allylnormetazocine), were independent from those of other opioid receptor agonists (Martin et al. 1976). Later, it was determined that sigma receptors have unique binding sites that are different from those of other opioid receptors, and at least two subtypes (σ_1 and σ_2) were classified based on pharmacological criteria (Bowen et al. 1989). These subtypes display different tissue distributions and distinct physiological and pharmacological profiles in the central and peripheral nervous systems (Hashimoto and Ishiwata 2006). σ_1 receptors are widely distributed in the central nervous system (CNS) and in peripheral tissues (Hayashi and Su 2004). Peripherally, both subtypes are overexpressed in rapidly proliferating cells, such as those in various types of cancer, and the functional roles of the receptors, especially σ_2 , have also been the focus of tumour imaging studies (van Waarde et al. 2010). In the CNS, the σ_1 receptor may function as a modulator of signal transduction through glutamatergic transmitter systems mediated by the *N*-methyl-D-aspartate (NMDA) receptors. σ_1 agonists show anti-amnesic and neuroprotective effects (van Waarde et al. 2011) and for that reason they are attractive novel targets for the treatment of neuropsychiatric diseases (schizophrenia, depression and cognition) and neurodegenerative diseases like ischemic stroke and Alzheimer's disease.

The σ_1 receptor was successfully cloned and characterised as a protein of 233 amino acids with two transmembrane domains (Hanner et al. 1996). Although the σ_1 receptor is not homologous to any mammalian protein, it shows 30 % overlap with yeast $\Delta 8 - \Delta 7$ sterol isomerase, also known as emopamil-binding protein (EBP). In contrast, the σ_2 receptor has yet to be cloned.

σ_1 receptors have been shown to act as ligand-regulated molecular chaperones in the endoplasmic reticulum (ER) (Hayashi and Su 2007). Very recently, the putative σ_2 binding site was identified as progesterone receptor membrane component 1 (PGRMC1) (Xu et al. 2011). Similar to the σ_1 receptors, PGRMC1s were localised at the ER and mitochondria.

Endogenous ligands for the sigma₁ and sigma₂ receptors have not been fully identified, and those for the sigma₁ receptor were first proposed to be neurosteroids, including pregnenolone sulphate and progesterone (Su et al. 1988). Recently, the endogenous hallucinogenic trace amine *N,N*-dimethyltryptamine was found to be a potent endogenous ligand for the sigma₁ receptor (Fontanila et al. 2009).

In this chapter, investigations related to brain imaging of sigma₁ receptors and their role in neurology and psychiatric diseases are reviewed.

26.2 Brain Imaging of Sigma Receptors

26.2.1 Post-mortem Studies

Several post-mortem studies on the distribution and densities of sigma receptors in the human brain have been reported. Weissman et al. (1988) reported that the densities of sigma sites in the brain were highest in the cerebellum, nucleus accumbens and cerebral cortex, using a membrane binding assay with [³H]haloperidol in the presence of spiperone. The binding is moderate in the caudate nucleus and substantia nigra and low in the thalamic and pontine nuclei. Autoradiographic measurements using [³H]DTG showed slightly different results, i.e. high prevalence in the substantia nigra pars compacta and cerebellum with moderate prevalence in the hippocampal dentate granular cells, striatum and the pineal and pituitary glands (Jansen et al. 1991). In the neocortex, binding was high in the laminae II-IVA and low in the narrow band (5 % layer) of midzone. Subtype-selective regional distribution in the brain has been reported in non-human primates but not in humans. Mash and Zabetian (1992) quantified the binding of [³H]3-PPP (sigma₁ K_i =5.1 nM, sigma₂/sigma₁=87; Walker et al. 1990) within 36 brain regions in Rhesus macaque monkeys (*Macaca mulatta*) and demonstrated marked enrichment of sigma binding sites over the paralimbic belt cortices, medial and central nuclei of the amygdala and hippocampal formation. Moderate sigma receptor densities were observed in the caudate and putamen.

Several studies reported on the effects of age on sigma receptor expression. Kornhuber et al. (1996) reported an 8.5 % decrease per decade in [³H](+)-pentazocine (sigma₁ K_i =2.0 nM, sigma₂/sigma₁=228; Walker et al. 1990) in the frontal cortex. Moreover, altered densities of sigma receptors were observed in patients with schizophrenia and AD (see also Sects. 26.3.1 and 3.4).

Most post-mortem examinations of the human brain reported to date measured both sigma₁ and sigma₂ binding sites using non-selective radioligands. One exception is a previous study of aging effects, which used the sigma₁ selective ligand [³H](+)-pentazocine (Kornhuber et al. 1996).

26.2.2 Radioligands for Imaging of Sigma Receptors

Since the early 1990s, different classes of compounds, such as benzomorphans, phenyl piperidines, *N,N*-disubstituted pyrrolidinyethylamines and *N,N'*-disubstituted piperazines, have been evaluated as radioligands for use in the

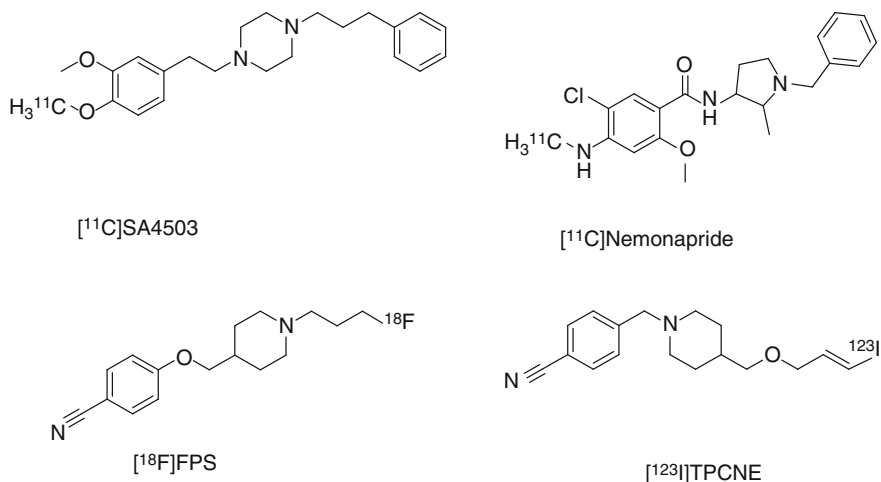


Fig. 26.1 Chemical structures of clinically used sigma ligands for brain imaging

imaging of sigma receptors by positron emission tomography (PET) and single-photon emission computed tomography (SPECT). A comprehensive overview of the development of radioligands for the different sigma receptor subtypes has been presented in a number of recent reviews (Hashimoto and Ishiwata 2006; Mach and Wheeler 2009). The chemical structures of radioligands used clinically for brain imaging of sigma receptors are summarised in Fig. 26.1.

The first radioligand used for imaging sigma₁ receptors in the CNS was [¹¹C]SA4503 (Fig. 26.1), which was developed by Ishiwata and co-workers (2001). SA4503 has high and selective affinity for the sigma₁ receptor (sigma₁ IC₅₀ = 17.4 nM, sigma₂/sigma₁ = 103) but low affinity for 36 neuroreceptors, ion channels and second messenger systems (Matsuno et al. 1996; Matsuno and Mita 1998). Later, three groups reinvestigated the binding properties of SA4503 and reported slightly different affinities and selectivities: sigma₁ K_i = 4.0–4.6 nM, sigma₂/sigma₁ = 13.3–55.0 (Lever et al. 2006; Shiba et al. 2006; Hirata et al. 2006). Density (B_{max}) of the sigma receptor was estimated to be 30–600 fmol/mg protein (approximately 3–60 nM) in the human brain (Weissman et al. 1988; Kornhuber et al. 1996; Jansen et al. 1993). Theoretically, radioligands with nanomolar affinity (0.3–6 nM) will be suitable for sigma receptor imaging. From this viewpoint, SA4503 has a suitable range of affinity for quantitative in vivo imaging. In human studies, the use of [¹¹C]SA4503-PET allowed successful visualisation of the sigma₁ receptor in the brain as described in Sect. 26.2.3.1, but the affinity of [¹¹C]SA4503 was slightly high (i.e. the rate of dissociation of the ligand somewhat low) for measurement of the sigma₁ receptor on the time scale of the PET scan using a ¹¹C-labelled tracer with a short half-life (20.4 min) (Sakata et al. 2008).

The second PET ligand that was applied in human studies was [¹⁸F]FPS, which was developed by Waterhouse and co-workers (Collier et al. 1996). [¹⁸F]FPS was not cleared fast enough from the CNS to reach transient equilibrium by 4 h after

administration in healthy volunteers due to its high affinity for the sigma₁ receptor ($K_d=0.5$ nM) (Waterhouse et al. 2004; Zhao et al. 2005). In an effort to improve the CNS clearance for in vivo PET studies, Zhao et al. (2005) synthesised and evaluated [¹⁸F]SFE (previously designated as [¹⁸F]WLS1.002), a fluoroethyl derivative of [¹⁸F]FPS that exhibits a lower affinity for sigma₁ receptors ($K_d=5$ nM). A preclinical study showed that [¹⁸F]SFE exhibits very similar regional brain distribution and specific binding in the rodent brain compared to [¹⁸F]FPS. As expected from its lower affinity, [¹⁸F]SFE is cleared much faster from the brain than [¹⁸F]FPS (Waterhouse et al. 2006a). Preclinical toxicity and dosimetry studies of [¹⁸F]SFE suggested that [¹⁸F]SFE will be safe for use in human PET studies (Waterhouse et al. 2006b). However, no further clinical imaging studies have been reported to date.

Carbon-11-labelled nemonapride, which was originally developed as a dopamine D₂-like receptor radioligand (Hatano et al. 1989; Hatazawa et al. 1991), binds not only to D₂-like receptors in the striatum but also to sigma receptors in other regions, such as the cerebral cortex and cerebellum (Ishiwata and Senda 1999), as has rather high affinities for both receptors. Nimura et al. (2004) applied [¹¹C]nemonapride to imaging of sigma receptors in the cerebellum of patients suffering from levodopa-induced dyskinesia (LID), a brain area devoid of D₂-like receptors.

More recently, two sigma₁ receptor ligands with novel structures have been reported. Although these compounds showed promising properties for in vivo sigma₁ receptor imaging, no clinical studies have been conducted to date. Maestrup and co-workers developed an innovative compound class of spirocyclic piperidines (Maestrup et al. 2009a, b). They found that a fluoroethyl derivative, [¹⁸F]fluspidine, had the best properties among the homologous fluoroalkyl-substituted spirocyclic sigma₁ radiotracers (Maisonial et al. 2012). [¹⁸F]Fluspidine demonstrated favourable target affinity and specificity (sigma₁ $K_i=0.59$ nM, sigma₂/sigma₁=1,330) as well as metabolic stability both in vitro and in animal experiments (Fischer et al. 2011). Moussa and co-workers developed a series of *N*-(2-benzofuranylmethyl)-*N'*-(alkoxybenzyl)piperazines as selective sigma₁ receptor ligands. They found high affinity sigma₁ selective ligands, such as the 4-[¹¹C]methoxy (sigma₁ $K_i=2.7$ nM, sigma₂/sigma₁=38) and 4-(2-[¹⁸F]fluoroethoxy) derivatives (sigma₁ $K_i=2.6$, sigma₂/sigma₁=187) (Moussa et al. 2010; 2011). These compounds showed good brain uptake and specific binding to sigma₁ receptors in the *Papio hamadryas* (baboon) brain. However, these compounds showed irreversible binding profiles during the scan periods because of their high affinities.

The sigma₁ receptor-selective ligand [¹²³I]TPCNE ($K_i=0.67$ nM, sigma₂/sigma₁=58) was used in a human SPECT study (Waterhouse et al. 1997; Stone et al. 2006). High brain uptake was reduced by haloperidol pretreatment, suggesting the specific binding of [¹²³I]TPCNE to sigma₁ receptors. However, the time-activity data were best described by an irreversible model. Thus, no further studies for this ligand have been conducted. Radioiodinated analogues of SA4503 were also prepared for SPECT, i.e. *o*I-SA4503 and *m*I-SA4503 (designated as *o*-BON and *m*-BON, respectively) (Hirata et al. 2006). The affinity and selectivity of *m*I-SA4503 for the sigma₁ receptor (sigma₁ $K_i=8.9$ nM, sigma₂/sigma₁=6.1) were approximately half those of

SA4503. Although Hirata et al. (2008) used these compounds in a tumour study on rodents, no clinical studies have been conducted to date.

A review of the clinical trials for a few sigma₁ receptor radioligands showed that ligands with affinities (K_i) for the sigma₁ receptor of 5–10 nM may be preferable for human studies and that [¹⁸F]FM-SA4503 may be more suitable than [¹¹C]SA4503 (Kawamura et al. 2007). However, many sigma receptor ligands have affinity for the vesicular acetylcholine transporter (VACHT) (Efange 2000) and the EBP (Berardi et al. 2001). SA4503 was reported to show affinities for VACHT (K_i = 50 nM, Shiba et al. 2006) and EBP (K_i = 1.7 nM, Berardi et al. 2001), but [¹¹C]SA4503 did not seem to bind to VACHT in the rat brain in vivo (Ishiwata et al. 2006a). Recently, Toyohara et al. (2012) confirmed that the brain uptake of [¹¹C]SA4503 in mice was not blocked by high affinity EBP blockers tamoxifen (EBP K_i = 2.8 nM, sigma₁/EBP = 12) and trifluoperazine (EBP K_i = 3.9 nM, sigma₁/EBP = 52). The newly developed compound [¹⁸F]fluspidine showed weak affinity for VACHT (K_i = 1,400 nM) and EBP (K_i = 211 nM). Selectivity toward these binding sites should be taken into consideration when designing new selective ligands, although the relationship between the sigma receptor and EBP has not been clearly elucidated.

26.2.3 PET Imaging of the Sigma₁ Receptors in the Human Brain

Three radioligands, [¹¹C]SA4503 (Ishii et al. 2001; Sakata et al. 2007), [¹⁸F]FPS (Waterhouse et al. 2004) and [¹²³I]TPCNE (Stone et al. 2006), were used for in vivo investigations of the density of the sigma₁ receptor in the human brain by PET or SPECT; however, [¹⁸F]FPS and [¹²³I]TPCNE showed irreversible binding profiles during the scan periods because of their high affinities. No further clinical studies were conducted. At present, clinical studies on sigma₁ receptor imaging in living human brains are limited to [¹¹C]SA4503 (Toyohara et al. 2009).

26.2.3.1 Healthy Subjects

[¹¹C]SA4503 was distributed in all grey matter regions in the human brain (Fig. 26.2). The distribution patterns did not differ between the early and late phases and were similar to those of regional cerebral blood flow (rCBF). The regional tissue time-activity curves (TACs) of [¹¹C]SA4503 in the brain showed a gradual increase in radioactivity over 30 min and then reached a plateau, whereas the radioactivity in plasma decreased very rapidly (Fig. 26.3). These findings suggest that the regional distributions of [¹¹C]SA4503 could depend on the blood flow or permeability rather than receptor density because of its slow dissociation kinetics.

Preclinical studies confirmed age-dependent increases in sigma₁ receptors in the brains of non-human primates (Kawamura et al. 2003). These results contrast strikingly with the age-dependent decreases in several other receptors in the primate brain. For investigation of the neuroprotective functions of sigma₁ receptors, a PET study with [¹¹C]SA4503 for evaluation of the aging process in the human brain would be of great interest.

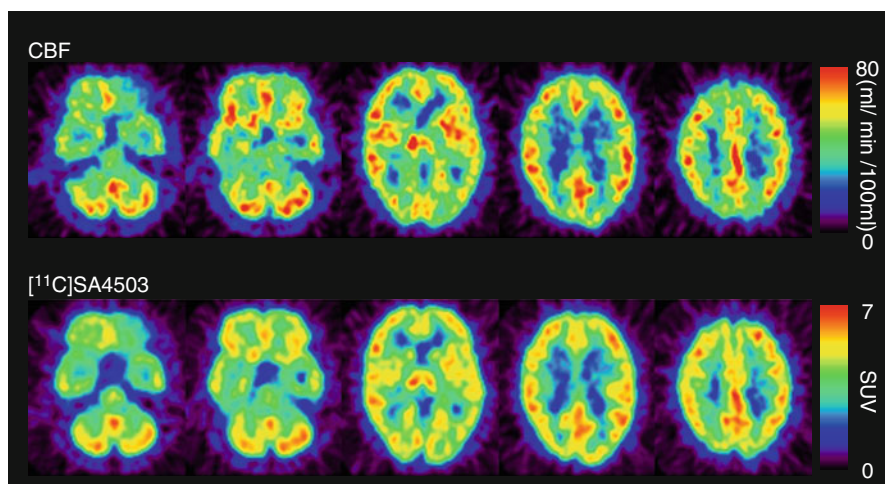
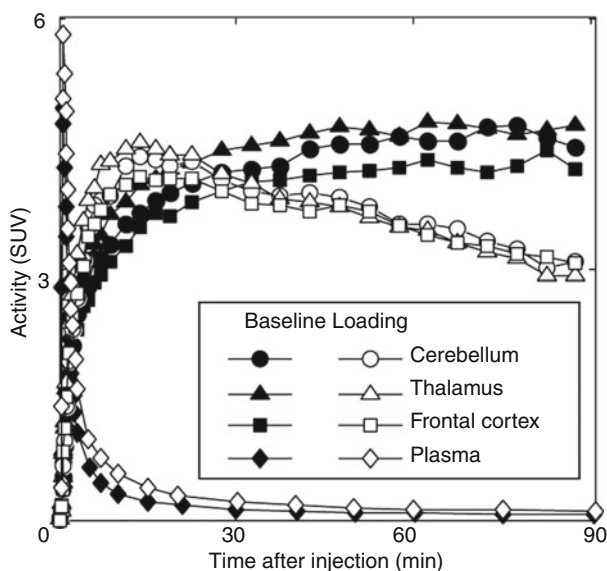


Fig. 26.2 rCBF and sigma₁ receptors in the brain of a healthy human subject. rCBF (*upper*): rCBF was measured using PET and [¹⁵O]H₂O, and calculated as ml/min/100 ml tissue. [¹¹C]SA4503 (*lower*): Static images were acquired 40–60 min after injection of [¹¹C]SA4503 and expressed as standardised uptake value (SUV: regional activity divided by administered dose per body weight)

Fig. 26.3 TACs in the healthy human brain and plasma after intravenous injection of [¹¹C]SA4503 under baseline and haloperidol-loading (3 mg) conditions. Decay-corrected radioactivity was expressed as SUV. Haloperidol was administered orally 18 h before injection of [¹¹C]SA4503



26.2.3.2 Kinetic Analysis

In the traditional PET pharmacokinetics analysis for neuroreceptor radioligands, the ratio of k_3 (association constant rate between the free plus non-specifically and specifically bound compartments) over k_4 (dissociation constant rate between the free

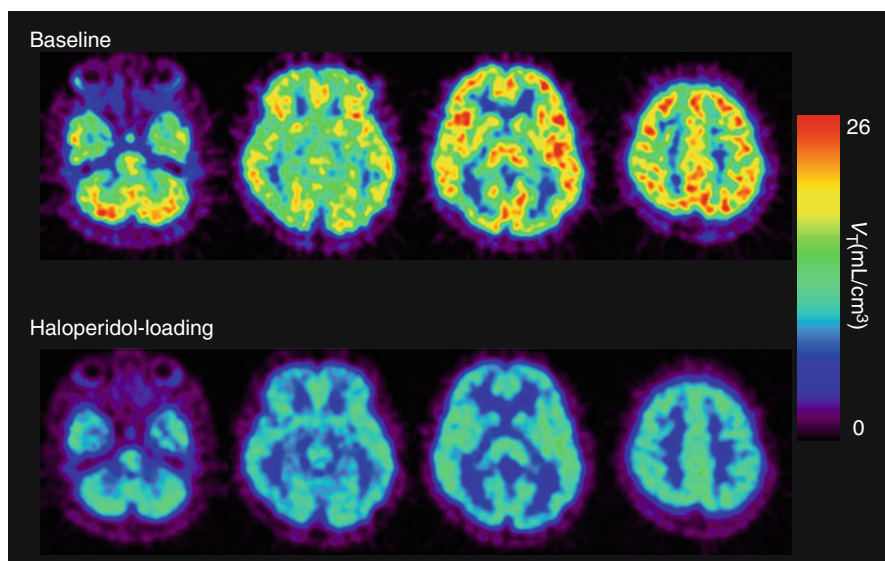


Fig. 26.4 V_T images of [^{11}C]SA4503 in the human brain under baseline (*upper*) and haloperidol-loading conditions (*lower*). The binding of [^{11}C]SA4503 was considerably reduced after oral administration of haloperidol (3 mg, 18 h prior to the PET scan)

plus non-specifically and specifically bound compartments) in a two-tissue compartmental model (Mintun et al. 1984) is often used as the binding potential, which is currently defined as the specific binding potential relative to non-displaceable binding (BP_{ND}) (Innis et al. 2007). As σ_1 receptors are distributed throughout all brain regions, no suitable reference region with negligible specific binding is available. Therefore, in the kinetic analysis of [^{11}C]SA4503, arterial blood sampling measurements corrected by metabolite analysis are essential for obtaining the input function. In general, however, the variability of BP_{ND} estimated from direct compartmental analysis without any constraints is clearly larger than that with indirect methods, such as a reference tissue model analysis (Vilkman et al. 2000). In the case of [^{11}C]SA4503, slow kinetics due to its slightly higher affinity (Fig. 26.3) increased the variability of BP_{ND} in the time scale of the PET scan using a ^{11}C -labelled tracer with a short half-life (20.4 min). An alternative parameter for the evaluation of [^{11}C]SA4503 binding is the total volume of distribution (V_T) estimated by the linear graphical method (Logan et al. 1990), although V_T includes both specific and non-specific binding (Kimura et al. 2007). The estimation of V_T ($K_1/k_2 \times (1 + k_3/k_4)$) in compartmental analysis tends to be more stable than that of BP_{ND} . Figure 26.4 shows representative V_T images of [^{11}C]SA4503 in a healthy brain. The binding of [^{11}C]SA4503 was high in the cerebellar cortex, moderate in the temporal and parietal cortices and low in the caudate and putamen (Sakata et al. 2007). These distribution patterns resemble the distribution patterns of radioligand binding in primate brains, where σ_1 receptors were noticed to be widely distributed with regionally

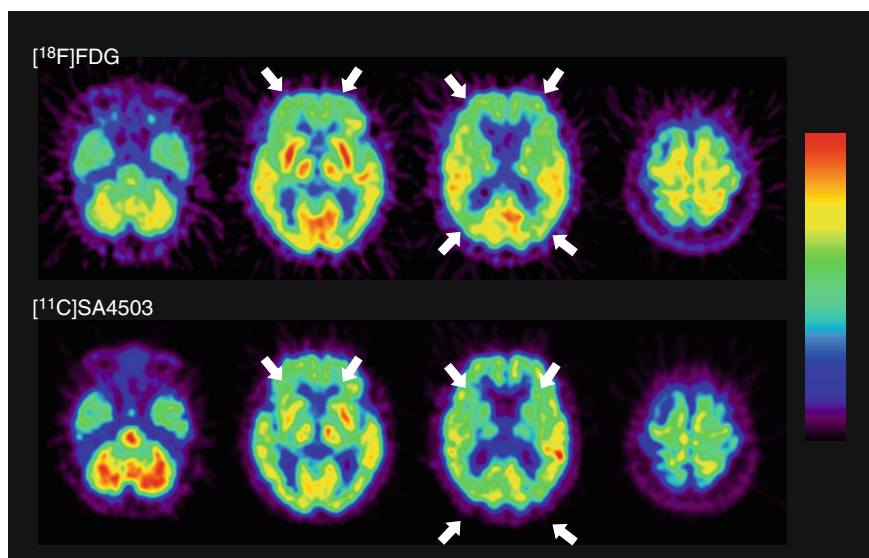


Fig. 26.5 Glucose metabolism and densities of sigma₁ receptors in the brain of a patient with AD. Glucose metabolism (*upper*): static image acquired 45–51 min after injection of [¹⁸F]FDG. Sigma₁ receptors (*lower*): V_T derived from Logan graphical analysis of a 90-min dynamic scan of [¹¹C]SA4503. In this patient, uptake of [¹⁸F]FDG was primarily decreased in the frontal and parietal cortex (*arrow*), and the distribution of [¹¹C]SA4503 was consistent with this reduction (*arrow*)

different densities, using an in vitro binding assay and autoradiography (Weissman et al. 1988; Shibuya et al. 1992; Mash and Zabetian 1992).

An interaction between sigma₁ receptors and steroids has been established (Collier et al. 2007; Su et al. 1988). Currently, no information is available regarding the relationship between plasma hormone levels and [¹¹C]SA4503 binding in the living human brain. If the binding of [¹¹C]SA4503 is sensitive to competition by endogenous steroids, intra-subject variability in BP_{ND} of [¹¹C]SA4503 in women during the menstrual cycle and inter-subject variability in aged subjects, including post-menopausal subjects, may be found. Therefore, plasma steroid levels should be taken into account in PET studies of patients and healthy volunteers.

26.2.3.3 CNS Disease

Mishina et al. (2008) performed [¹¹C]SA4503-PET in AD patients in the early stages of the disease. Figure 26.5 shows representative [¹¹C]SA4503 images compared with those for glucose metabolism evaluated with [¹⁸F]FDG-PET. Although the results may have been influenced by atrophy or changes in regional blood flow, a widespread decrease in [¹¹C]SA4503 binding in the brain was found; BP_{ND} for [¹¹C]SA4503 was significantly lower in the cerebellum, thalamus and frontal, temporal and occipital cortices of AD patients than in those of healthy subjects. In other regions of the AD brain, BP_{ND} tended to be reduced. However, the data from these PET studies should be taken interpreted with caution because donepezil taken by

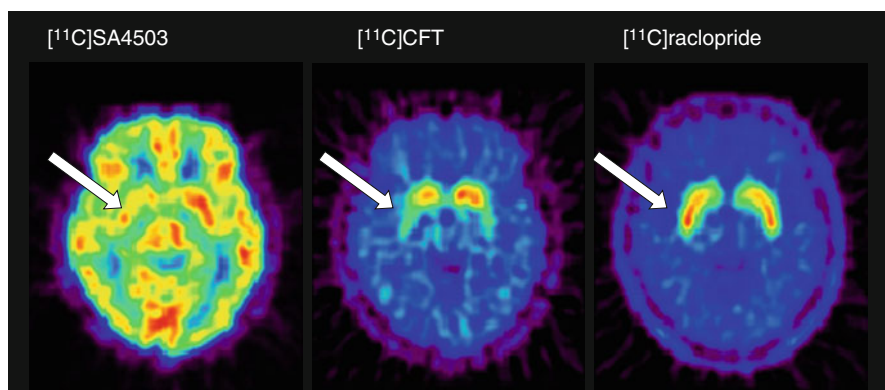


Fig. 26.6 Sigma_1 receptors, dopamine transporters and dopamine D_2 receptors in the brain of a patient with PD. [^{11}C]SA4503 (left): V_T derived from the Logan graphical analysis of a 90-min dynamic scan; [^{11}C]CFT (middle) and [^{11}C]raclopride (right): static image acquired 75–90 min and 40–55 min, respectively, after injection of the radiotracers. V_T of [^{11}C]SA4503 was smaller in the right anterior putamen (arrow). The uptake of [^{11}C]CFT was reduced in the anterior putamen, especially on the right (arrow). The uptake of [^{11}C]raclopride was preserved in the striatum and was larger in the right anterior putamen (arrow) than in the left

some subjects shows a potent sigma_1 receptor agonist activity (see Sects. 26.2.3.4 and 26.3.4).

Parkinson's disease (PD) is also a progressive degenerative disorder of the CNS, characterised clinically by resting tremors, sluggish movements, cogwheel rigidity and postural instability. These symptoms are mainly caused by insufficient dopamine synthesis and death of dopaminergic neurons in the substantia nigra. Some studies have suggested that sigma_1 receptors are involved in modulating the synthesis and release of dopamine (Chaki et al. 1998). Using [^{11}C]SA4503-PET, Mishina et al. (2005) investigated whether sigma_1 receptors were involved in the damage to the dopaminergic system in patients with PD, who showed low densities of dopamine transporters and normal or high densities of dopamine D_2 receptors in the putamen using [^{11}C]CFT and [^{11}C]raclopride, respectively. Although the differences in BP_{ND} of [^{11}C]SA4503 between normal and PD patients were not clear because of a large inter-subject variability, BP_{ND} in PD patients was significantly lower on the more affected side of the anterior putamen than on the less affected side (Fig. 26.6).

LID in patients with PD mimics acute dystonic reactions induced by antipsychotic drugs, possibly mediated by sigma receptors. A PET study using [^{11}C]nemonapride showed a strong positive correlation between [^{11}C]nemonapride binding and the preoperative LID severity score when the patients were receiving medication (Nimura et al. 2004).

26.2.3.4 Measurement of Sigma_1 Receptor Occupancy in the Human Brain

While the physiological and pathophysiological roles of sigma receptors remain under investigation, a number of neuropsychiatric drugs are known to have moderate to high affinities for sigma receptors. Moreover, sigma_1 receptor ligands

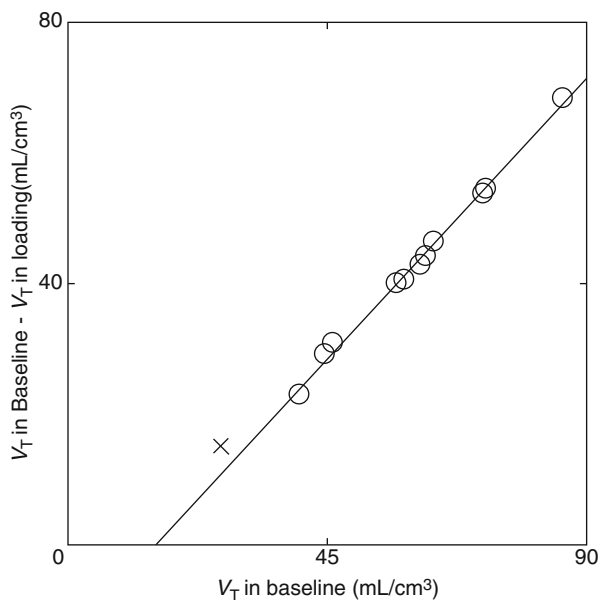


Fig. 26.7 Typical Lassen plot analysis applied to a haloperidol-loading study. In this plot, the x -axis is V_T under baseline conditions and the y -axis is the difference between V_T under loading and baseline conditions. The circles represent data from the grey matter regions (cerebral cortices, basal ganglia and cerebellar cortex) and the crosses represent data from the white matter region (centrum semi-ovale). The clear linear relationship suggests homogeneous non-specific binding across the grey matter regions investigated, and the x -intercept and gradient of the regression line ($y = 0.96(x - 15.1)$) represent the volume of free plus non-specifically bound radioligand (V_{ND}) and the receptor occupancy by non-radioactive haloperidol, respectively. Moreover, the absence of data near the x -axis indicates that no regions, including the white matter, are available as a true reference region devoid of specific binding, and that most [¹¹C]SA4503 binding under baseline conditions is specific

represent a new class of therapeutic agents for neuropsychiatric disorders (Hashimoto and Ishiwata 2006; Ishikawa and Hashimoto 2010). Therefore, levels of sigma receptor occupancy of therapeutic drugs in the living human brain are of great interest. In a feasibility study, Ishiwata et al. (2006b) measured sigma₁ receptor and dopamine D₂ receptor occupancy by haloperidol in the human brain by PET using [¹¹C]SA4503 and [¹¹C]raclopride, respectively. Sigma₁ receptor occupancy was approximately 80 % after oral administration of 3 mg haloperidol, whereas dopamine D₂ receptor occupancy was approximately 60 %.

With respect to studies involving drugs with good potential for high receptor occupancy, a graphical analysis using a Lassen plot (Lassen et al. 1995; Cunningham et al. 2010) may be applicable for the evaluation of specific binding of the radioligand and receptor occupancy by the therapeutic drug, thus providing more stable estimates. The Lassen plot is based on regional changes in V_T between baseline and drug-loaded conditions. The assumptions for the analysis are that non-specific binding is homogeneous, occupancy is the same in all regions of a regression line and there is a steady state of occupancy for the duration of the scan. A typical Lassen plot for haloperidol-loading study is shown in Fig. 26.7,

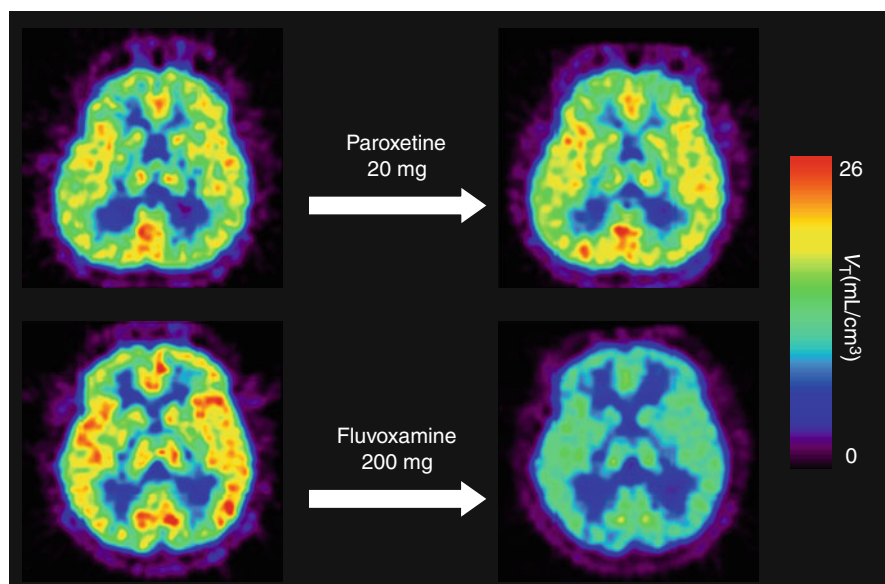


Fig. 26.8 V_T images of [^{11}C]SA4503-PET before and after a single oral administration of an SSRI. The upper pair represents V_T images at baseline (*left*) and at paroxetine (20 mg) loading (*right*) in the same subject. The lower pair shows V_T images at baseline (*left*) and fluvoxamine (200 mg) loading (*right*) in another subject

and the parametric V_T images of [^{11}C]SA4503 for baseline and loading conditions (Fig. 26.4) show that the binding of [^{11}C]SA4503 was globally decreased by haloperidol loading.

Ishikawa et al. (2007) measured σ_1 receptor occupancy by two therapeutic drugs using [^{11}C]SA4503-PET. Selective serotonin reuptake inhibitor (SSRI) is the treatment of choice for many disorders, including major depressive disorder, dysthymia, obsessive–compulsive disorder, and obsessive–compulsive spectrum disorders. Fluvoxamine has moderate affinity ($K_i=36$ nM) for σ_1 receptors in addition to the main affinity for serotonin reuptake sites (Narita et al. 1996). A single administration of therapeutic doses of fluvoxamine (50–200 mg) decreased [^{11}C]SA4503 binding in the human brain in a dose-dependent manner, whereas that of paroxetine (20 mg), another SSRI with very low affinity for σ_1 receptors ($K_i=1,893$ nM), did not (Fig. 26.8). A similar occupancy study of an antipsychotic drug was also preliminarily described (van Waarde et al. 2011). The second example evaluated was donepezil. This drug has high affinity for σ receptors ($\text{IC}_{50}=14$ nM measured with [^3H]DTG) (Kato et al. 1999). Figure 26.9 shows that a single administration of donepezil (5 or 10 mg) decreased [^{11}C]SA4503 binding in the human brain in a dose-dependent manner (Ishikawa et al. 2009). The levels of σ_1 receptor occupancy by fluvoxamine and donepezil were approximately 60 and 75 %, respectively. These findings suggest that σ_1 receptors may be involved in the mechanism of action of fluvoxamine and donepezil.

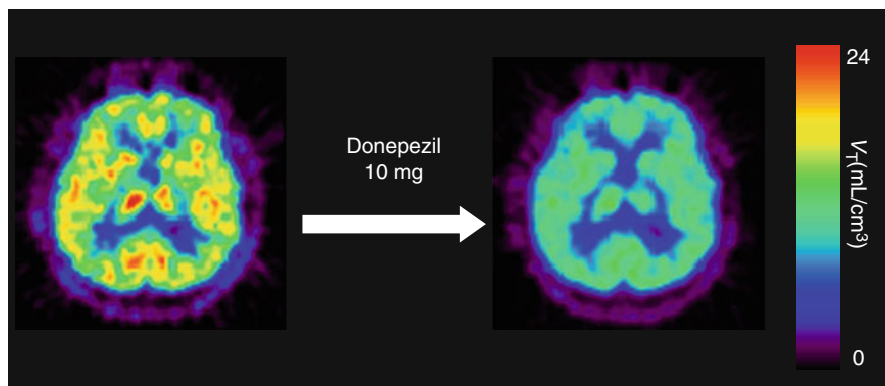


Fig. 26.9 Representative V_T images of [¹¹C]SA4503-PET before and after a single oral administration of donepezil (10 mg) in a healthy subject. *Left* image at baseline, *right* image after donepezil (10 mg) loading

26.3 Sigma Receptors in CNS Diseases

Since the prototypic sigma₁ receptor ligand SKF10,047 (sigma₁ K_i =44.8 nM, sigma₂/sigma₁=95.1; Walker et al. 1990) was found in the 1980s to exhibit psychotomimetic actions, the antipsychotic potential of sigma₁ receptor ligands has been examined extensively. During the 1990s, sigma₁ receptor ligands were synthesised mostly to develop new drugs for the treatment of schizophrenia. However, after cloning of the sigma₁ receptor gene, molecular biological characterisation indicated relationships between sigma₁ receptors and a variety of human diseases, including mood disorders, stroke, neurodegenerative diseases and drug addiction.

26.3.1 Schizophrenia

Five sigma₁ receptor ligands, panamesine (EMD57445), eliprodil (SL82.0715), rimcazole (BW234U), BMY14802 (BMS181100) and DuP734, were introduced into clinical trials for treatment of schizophrenia (Hayashi and Su 2004). The findings of these clinical trials suggest that sigma₁ receptor ligands may not possess potent antipsychotic actions against the positive symptoms of schizophrenia, but may be useful for ameliorating certain negative symptoms (Hayashi and Su 2004). Recently, it was reported that fluvoxamine, an SSRI possessing potent sigma₁ receptor agonistic activity, improves negative symptoms and cognitive deficits of schizophrenic patients undergoing antipsychotic treatment (Iyo et al. 2008; Niitsu et al. 2010).

Using [³H]haloperidol (sigma₁ K_i =0.3 nM, sigma₂/sigma₁=120; Walker et al 1990) in the presence of spiperone to block binding to dopamine D₂ receptors, Weissman et al. (1991) first reported reductions in the density of sigma binding sites in schizophrenic patients on antipsychotic medication; these reductions were most

prominent in the temporal cerebral cortex followed by the parietal cortex. Shibuya et al. (1992) measured sigma receptor binding with [^3H]DTG ($\sigma_1 K_i = 11.9$ nM, $\sigma_2/\sigma_1 = 3.2$; Walker et al. 1990) in 17 areas of the cerebral cortex and found no significant differences between schizophrenic patients and controls, with exception of the superior parietal cortex in which the binding was significantly increased in the schizophrenic group. In addition, no significant differences were observed between off-drug and on-drug schizophrenic patients in any brain areas. Helmeste et al. (1996) reported no differences in the binding of [^3H]nemonapride (previously designated as [^3H]YM-09151-2: $\sigma_1 K_i = 8.4$ nM, $\sigma_2/\sigma_1 = 1.1$; Ujike et al. 1996) in the presence of spiperone in the frontal cortex and cerebellum; however, they observed a decrease in the caudate nucleus. The discrepancies between these results may have been due to differences in schizophrenia types, medication period, quantification methods (receptor binding assay or autoradiography) and radioligands used.

Three out of four case-control association studies failed to find significant associations between alleles of the σ_1 receptor gene [G-241T/C-240T and Gln2Pro (A61C)] and schizophrenia (Uchida et al. 2003).

26.3.2 Mood Disorders

Recent animal and human studies demonstrated a tight link between σ_1 receptors and higher-order brain functions, such as mood and cognition (Hayashi and Su 2004; Fishback et al. 2010). It is noteworthy that some clinically used antidepressants, such as fluvoxamine ($\sigma_1 K_i = 36$ nM), possess affinities for σ_1 receptors within the nanomolar concentration range (Narita et al. 1996).

Brain-derived neurotrophic factor (BDNF) plays a critical role in the pathophysiology and in the activity of therapeutic agents in patients with mood disorders (Hashimoto et al. 2004). Furthermore, altered expression of BDNF is considered to be a mechanism of action of antidepressant drugs and mood stabilisers (Hashimoto et al. 2004). Interestingly, cutamesine (SA4503), a selective σ_1 receptor agonist, was also shown to increase BDNF in the hippocampus of rats (Kikuchi-Utsumi and Nakai 2008). Very recently, Fujimoto et al. (2012) found that cutamesine potentiates the post-translational processing of neurotrophins; in contrast, clinically used antidepressants promote the transcriptional upregulation of BDNF.

The σ_1 receptor contains binding sites for neurosteroids. It was reported that serum dehydroepiandrosterone (DHEA) and DHEA-sulphate levels are altered in patients with depression (Takebayashi et al. 1998). Administration of DHEA is associated with the improvement of symptoms in cases of major depression or dysthymia (van Broekhoven and Verks 2003).

Igmesine (JO1,784) is the first σ_1 receptor agonist introduced into clinical trials for treatment of depression. The clinical trial moved into Phase III; however, the antidepressant effect failed to be confirmed in a large-sample study (Hayashi et al. 2011). Recently, cutamesine has been introduced into Phase II clinical trials for treatment of depression (Urfer et al. 2009).

26.3.3 Ischemia

There is substantial experimental evidence that sigma receptors play a role in the modulation of ischemic neuronal injury (Maurice and Lockhart 1997; O'Neill et al. 1995). *In vitro* studies demonstrated that sigma₁ agonists exert potent protective effects in a variety of cell types, such as primary cerebral neurons (Yang et al. 2007), retinal ganglion cells (Ha et al. 2011) and lens cells (Wang and Duncan 2006). Similarly, sigma₁ agonists were reported to show robust neuroprotective effects in animal studies. 4-Phenyl-1-(4-phenylbutyl)piperidine (PPBP) prevented early brain injury in rat (Takahashi et al. 1996) and cat (Takahashi et al. 1995) models of transient focal ischemic stroke, suggesting that sigma receptors play an important role in the mechanism of acute injury after transient focal ischemia. Cutamesine has been introduced into Phase II clinical trials for treatment of post-stroke neurological disturbances (Urfer et al. 2009).

26.3.4 Neurodegenerative Diseases

[³H]DTG binding was measured in seven hippocampal regions in the brains of Alzheimer's disease (AD) patients by autoradiography; an average reduction of 26 % was found, which correlated with an average 29 % pyramidal cell loss in the same region (Jansen et al. 1993). One study suggested that haplotype TT-241-240P2 of the sigma₁ receptor gene, which could lead to a reduction of sigma₁ receptor transcription, may be a protective factor against AD (Uchida et al. 2005). However, another study failed to replicate this finding (Maruszak et al. 2007).

Donepezil, an acetylcholinesterase (AChE) inhibitor, is the most widely prescribed drug so far for AD. Donepezil was found to be protective against amyloid β_{25-35} peptide-induced neurotoxicity in mice (Meunier et al. 2006). This effect of donepezil was antagonised by the sigma₁ receptor antagonist BD-1047. *In vitro* studies demonstrated that donepezil, but not the AChE inhibitor physostigmine (also known as eserine), significantly potentiated nerve growth factor (NGF)-induced neurite outgrowth in PC12 cells in a concentration-dependent manner and that the effect of donepezil could be antagonised by NE-100 (Ishima et al. 2008). Furthermore, donepezil, but not physostigmine, significantly improved phencyclidine-induced cognitive impairments in mice, and the effect of donepezil could be antagonised by co-administration of NE-100 (Kunitachi et al. 2009). In summary, it is likely that sigma₁ receptors are involved in the mechanism of the neuroprotective pharmacological action of donepezil.

26.3.5 Drug Addiction and Alcoholism

Numerous animal studies have demonstrated a relationship between cocaine dependence and sigma₁ receptors (Robson et al 2012). Many of these studies suggested the potential of sigma₁ antagonists to ameliorate cocaine intoxication, dependence

and craving, although these effects have not been tested in clinical studies. Cocaine at clinically relevant concentrations can interact with σ_1 receptors and upregulate σ_1 receptors in animals (Liu and Matsumoto 2008).

Despite the fact that substantial preclinical studies demonstrated roles of σ receptors in drug abuse, only two clinical studies have been published to date in this regard, both of which were gene-association studies. The association of the σ_1 receptor polymorphism GC-241-240TT or A61C (Gln2Pro) with methamphetamine dependence was examined in a Japanese cohort study of 143 methamphetamine abusers and 181 control subjects (Inada et al. 2004). This study indicated no significant association between σ_1 receptor polymorphisms and methamphetamine abuse, although the frequency of the CC genotype of A61C tended to be higher in methamphetamine abusers who had experienced spontaneous relapse of methamphetamine psychosis. One gene-association study indicated a link between σ_1 receptor polymorphisms and alcoholism (Miyatake et al. 2004). The distribution of σ_1 receptor gene polymorphisms was analysed in 307 alcoholic and 302 control subjects. The frequencies of the A-485 allele and the TT-241-240/Pro2 haplotype in the 5'-upstream region, which lower transcriptional activity of the σ_1 receptor gene, were significantly higher in control subjects compared with alcoholic subjects. These results suggest that the A-485 allele or TT-241-240/Pro2 haplotype lowers the expression of σ_1 receptors and may be a possible protective factor against alcoholism.

Conclusion

σ_1 receptors are implicated in the pathophysiology of some neurological and neuropsychiatric disorders. A number of radioligands have been developed and evaluated for imaging of σ_1 receptors in the CNS by PET and SPECT. [^{11}C]SA4503 was used to generate new findings regarding brain functions in patients with AD and PD. Moreover, [^{11}C]SA4503-PET demonstrated that some therapeutic drugs for neurological and neuropsychiatric disorders have considerable affinity for σ_1 receptors in the human brain. σ_1 receptor imaging could be useful for pathophysiological studies of the human brain and help in the discovery and validation of potential therapeutic drugs for several CNS disorders. However, clinical σ_1 receptor imaging is only just beginning to be explored. In view of the recent progress in σ_1 receptor research and accumulating evidence of the therapeutic potentials of σ_1 ligands, introduction of new tracers and further clinical studies should be encouraged.

References

- Berardi F, Ferorelli S, Colabufo NA et al (2001) A multireceptorial binding reinvestigation on an extended class of σ ligands: N-[ω -(indan-1-yl and tetralin-1-yl)alkyl] derivatives of 3,3-dimethylpiperidine reveal high affinities toward σ_1 and EBP sites. *Bioorg Med Chem* 9:1325–1335
- Bowen WD, Hellewell SB, McGarry KA (1989) Evidence for a multi-site model of the rat brain σ receptor. *Eur J Pharmacol* 163:309–318

- Chaki S, Okuyama S, Ogawa S et al (1998) Regulation of NMDA-induced [³H]dopamine release from rat hippocampal slices through sigma-1 binding sites. *Neurochem Int* 33:29–34
- Collier TL, O'Brien JC, Waterhouse RN (1996) Synthesis of [¹⁸F]-1-(3-fluoropropyl)-4-(4-cyanophenoxyethyl)piperidine: a potential sigma-1 receptor radioligands for PET. *J Label Compd Radiopharm* 38:785–794
- Collier TL, Waterhouse RN, Kassiou M (2007) Imaging sigma receptors: applications in drug development. *Curr Pharm Des* 13:51–72
- Cunningham VJ, Rabiner EA, Slifstein M et al (2010) Measuring drug occupancy in the absence of a reference region: the Lassen plot re-visited. *J Cereb Blood Flow Metab* 30:46–50
- Efange SMN (2000) In vivo imaging of the vesicular acetylcholine transporter and the vesicular monoamine transporter. *FASEB J* 14:2401–2413
- Fischer S, Wiese C, Maestrup EG et al (2011) Molecular imaging of σ receptors: synthesis and evaluation of the potent σ_1 selective radioligand [¹⁸F]fluspidine. *Eur J Nucl Med Mol Imaging* 38:540–551
- Fishback JA, Robson MJ, Xu YT et al (2010) Sigma receptors: potential targets for a new class of antidepressant drug. *Pharmacol Ther* 127(3):271–282
- Fontanila D, Johannessen M, Hajipour AR et al (2009) The hallucinogen N, N-dimethyltryptamine (DMT) is an endogenous sigma1 receptor regulator. *Science* 323:934–937
- Fujimoto M, Hayashi T, Urfer R et al (2012) Sigma-1 receptor chaperones regulate the secretion of brain-derived neurotrophic factor. *Synapse*. doi:10.1002/syn.21549
- Ha Y, Dun Y, Thanagaraju M et al (2011) Sigma receptor 1 modulates endoplasmic reticulum stress in retinal neurons. *Invest Ophthalmol Vis Sci* 52:527–540
- Hanner M, Moebius FF, Flandorfer A et al (1996) Purification, molecular cloning, and expression of the mammalian sigma1-binding site. *Proc Natl Acad Sci U S A* 93:8072–8077
- Hashimoto K, Ishiwata K (2006) Sigma receptor ligands: possible application as therapeutic drugs and as radiopharmaceuticals. *Curr Pharm Des* 12:3857–3876
- Hashimoto K, Shimizu E, Iyo M (2004) Critical role of brain-derived neurotrophic factor in mood disorders. *Brain Res Brain Res Rev* 45:104–114
- Hatano K, Ishiwata K, Kawashima K et al (1989) D₂-dopamine receptor specific brain uptake of carbon-11-labeled YM-09151-2. *J Nucl Med* 30:515–522
- Hatazawa J, Hatano K, Ishiwata K et al (1991) Measurement of D₂ dopamine receptor-specific carbon-11-YM-09151-2 binding in the canine brain by PET: importance of partial volume correction. *J Nucl Med* 32:713–718
- Hayashi T, Su TP (2004) Sigma-1 receptor ligands: potential in the treatment of neuropsychiatric disorders. *CNS Drugs* 18:269–284
- Hayashi T, Su TP (2007) Sigma-1 receptor chaperones at the ER-mitochondrion interface regulate Ca²⁺ signaling and cell survival. *Cell* 131:596–610
- Hayashi T, Tsai S-Y, Mori T et al (2011) Targeting ligand-operated chaperone sigma-1 receptors in the treatment of neuropsychiatric disorders. *Expert Opin Ther Targets* 15:557–577
- Helmeste DM, Tang SW, Bunney WE Jr et al (1996) Decrease in sigma but no increase in striatal dopamine D₄ sites in schizophrenic brains. *Eur J Pharmacol* 314(Supp):R3–R5
- Hirata M, Mori T, Soga S et al (2006) Synthesis and in vitro evaluation of iodinated derivatives of piperazine as a new ligand for sigma receptor imaging by single photon emission computed tomography. *Chem Pharm Bull* 54:407–475
- Hirata M, Mori T, Umeda T et al (2008) Evaluation of radioiodinated 1-[2-(3,4-Dimethoxyphenyl)ethyl]-4-(2-iodophenylpropyl)piperazine as a tumor diagnostic agent with functional sigma receptor imaging by single photon emission computed tomography. *Biol Pharm Bull* 31:879–883
- Inada T, Iijima Y, Uchida N et al (2004) No association found between the type 1 sigma receptor gene polymorphisms and methamphetamine abuse in the Japanese population: a collaborative study by the Japanese Genetics Initiative for Drug Abuse. *Ann N Y Acad Sci* 1025:27–33
- Innis RB, Cunningham VJ, Delforge J et al (2007) Consensus nomenclature for in vivo imaging of reversibly binding radioligands. *J Cereb Blood Flow Metab* 27:1533–1539
- Ishii K, Ishiwata K, Kimura Y et al (2001) Mapping of sigma₁ receptors in living human brain. *Neuroimage* 13(Supp):S984

- Ishikawa M, Hashimoto K (2010) The role of sigma-1 receptors in the pathophysiology of neuropsychiatric diseases. *J Recept Ligand Channel Res* 3:25–36
- Ishikawa M, Ishiwata K, Ishii K et al (2007) High occupancy of sigma-1 receptors in the human brain after single oral administration of fluvoxamine: a positron emission tomography study using [¹¹C]SA4503. *Biol Psychiatry* 62:878–883
- Ishikawa M, Sakata M, Ishii K et al (2009) High occupancy of sigma₁ receptors in the human brain after single oral administration of donepezil: a positron emission tomography study using [¹¹C]SA4503. *Int J Neuropsychopharmacol* 12:1127–1131
- Ishima T, Nishimura T, Iyo M et al (2008) Potentiation of nerve growth factor-induced neurite outgrowth in PC12 cells by donepezil: role of sigma-1 receptors and IP₃ receptors. *Prog Neuropsychopharmacol Biol Psychiatry* 32:1656–1659
- Ishiwata K, Senda M (1999) In vivo binding of [¹¹C]nemonapride to sigma receptors in the cortex and cerebellum. *Nucl Med Biol* 26:627–631
- Ishiwata K, Kawamura K, Yajima K et al (2006a) Evaluation of (+)-p-[¹¹C]methylvesamicol for mapping sigma₁ receptors: a comparison with [¹¹C]SA4503. *Nucl Med Biol* 33:543–548
- Ishiwata K, Oda K, Sakata M et al (2006b) A feasibility study of [¹¹C]SA4503-PET for evaluating sigma₁ receptor occupancy by neuroleptics: the binding of haloperidol to sigma₁ and dopamine D₂-like receptors. *Ann Nucl Med* 20:569–573
- Iyo M, Shirayama Y, Watanabe H et al (2008) Fluvoxamine as a sigma-1 receptor agonist improved cognitive impairments in a patient with schizophrenia. *Prog Neuropsychopharmacol Biol Psychiatry* 15:1072–1073
- Jansen KL, Faull RL, Dragunow M et al (1991) Autoradiographic distribution of sigma receptors in human neocortex, hippocampus, basal ganglia, cerebellum, pineal and pituitary glands. *Brain Res* 559:17–27
- Jansen KL, Faull RL, Storey P et al (1993) Loss of sigma binding sites in the CA1 area of the anterior hippocampus in Alzheimer's disease correlates with CA1 pyramidal cell loss. *Brain Res* 623:299–302
- Kato K, Hayako H, Ishihara Y et al (1999) TAK-147, an acetylcholinesterase inhibitor, increases choline acetyltransferase activity in cultured rat septal cholinergic neurons. *Neurosci Lett* 260:5–8
- Kawamura K, Kimura Y, Tsukada H et al (2003) An increase of sigma receptors in the aged monkey brain. *Neurobiol Aging* 24:745–752
- Kawamura K, Tsukada H, Shiba K et al (2007) Synthesis and evaluation of fluorine-18-labeled SA4503 as a selective sigma₁ receptor ligand for positron emission tomography. *Nucl Med Biol* 34:571–577
- Kikuchi-Utsumi K, Nakai T (2008) Chronic treatment with a selective ligand for the sigma-1 receptor chaperone, SA4503, up-regulates BDNF protein levels in the rat hippocampus. *Neurosci Lett* 440:19–22
- Kimura Y, Naganawa M, Sakata M et al (2007) Distribution volume as an alternative to the binding potential for sigma₁ receptor imaging. *Ann Nucl Med* 21:533–535
- Kornhuber J, Schoppmeyer K, Bendig C et al (1996) Characterization of [³H]pentazocine binding sites in post-mortem human frontal cortex. *J Neural Transm* 103:45–53
- Kunitachi S, Fujita Y, Ishima T et al (2009) Phencyclidine-induced cognitive deficits in mice are ameliorated by subsequent subchronic administration of donepezil: role of sigma-1 receptors. *Brain Res* 71279:189–196
- Lassen NA, Bartenstein PA, Lammertsma AA et al (1995) Benzodiazepine receptor quantification in vivo in humans using [¹¹C]flumazenil and PET: application of the steady-state principle. *J Cereb Blood Flow Metab* 10:740–747
- Lever JR, Gustafson JL, Xu R et al (2006) Sigma₁ and sigma₂ receptor binding affinity and selectivity of SA4503 and fluoroethyl SA4503. *Synapse* 59:350–358
- Liu Y, Matsumoto RR (2008) Alterations in FOS-related antigen 2 and σ₁ receptor gene and protein expression are associated with the development of cocaine-induced behavioral sensitization: time course and regional distribution studies. *J Pharmacol Exp Ther* 327:187–195
- Logan J, Fowler JS, Volkow ND et al (1990) Graphical analysis of reversible radioligand binding from time-activity measurements applied to [N-¹¹C-methyl]-(-)-cocaine PET studies in human subjects. *J Cereb Blood Flow Metab* 10:740–747

- Mach RH, Wheeler KT (2009) Development of molecular probes for imaging sigma-2 receptors in vitro and in vivo. *Cent Nerv Syst Agents Med Chem* 9:230–245
- Maestrup EG, Fischer S, Wiese C et al (2009a) Evaluation of spirocyclic 3-(3-fluoropropyl)-2-benzofurans as σ_1 receptor ligands for neuroimaging with positron emission tomography. *J Med Chem* 52:6062–6072
- Maestrup EG, Wiese C, Schepmann D et al (2009b) Synthesis of spirocyclic σ_1 receptor ligands as potential PET radiotracers, structure-activity relationships and in vitro metabolic stability. *Bioorg Med Chem* 17:3630–3641
- Maisonial A, Maestrup EG, Wiese C et al (2012) Synthesis, radiofluorination and pharmacological evaluation of a fluoromethyl spirocyclic PET tracer for central σ_1 receptors and comparison with fluoroalkyl homologs. *Bioorg Med Chem* 20:257–269
- Martin WR, Eades CG, Thompson JA et al (1976) The effects of morphine- and nalorphine- like drugs in the nondependent and morphine-dependent chronic spinal dog. *J Pharmacol Exp Ther* 197:517–532
- Maruszak A, Safranow K, Gacia M et al (2007) Sigma receptor type 1 gene variation in a group of Polish patients with Alzheimer's disease and mild cognitive impairment. *Dement Geriatr Cogn Disord* 23:432–438
- Mash DC, Zabetian CP (1992) Sigma receptors are associated with cortical limbic areas in the primate brain. *Synapse* 12:195–205
- Matsuno K, Mita S (1998) SA4503: a novel sigma₁ receptor agonist. *CNS Drug Rev* 4:1–24
- Matsuno K, Nakazawa M, Okamoto K et al (1996) Binding properties of SA4503, a novel and selective sigma 1 receptor agonist. *Eur J Pharmacol* 306:271–279
- Maurice T, Lockhart BP (1997) Neuroprotective and anti-amnesic potentials of sigma (σ) receptor ligands. *Prog Neuropsychopharmacol Biol Psychiatry* 21:69–102
- Meunier J, Ieni J, Maurice T (2006) The anti-amnesic and neuroprotective effects of donepezil against amyloid β_{25-35} peptide-induced toxicity in mice involve an interaction with the σ_1 receptor. *Br J Pharmacol* 149:998–1012
- Mintun MA, Raichle ME, Kilbourn MR et al (1984) A quantitative model for the in vivo assessment of drug binding sites with positron emission tomography. *Ann Neurol* 15:217–227
- Mishina M, Ishiwata K, Ishii K et al (2005) Function of sigma₁ receptors in Parkinson's disease. *Acta Neurol Scand* 112:103–107
- Mishina M, Ohyama M, Ishii K et al (2008) Low density of sigma₁ receptors in early Alzheimer's disease. *Ann Nucl Med* 22:151–156
- Miyatake R, Furukawa A, Matsushita S et al (2004) Functional polymorphisms in the sigma₁ receptor gene associated with alcoholism. *Biol Psychiatry* 55:85–90
- Moussa IA, Banister SD, Beinart C et al (2010) Design, synthesis, and structure–affinity relationships of regioisomeric N-benzyl alkyl ether piperazine derivatives as σ -1 receptor ligands. *J Med Chem* 53:6228–6239
- Moussa IA, Banister SD, Giboureau N et al (2011) Synthesis and in vivo evaluation of [¹⁸F]N-(2-benzofuranylmethyl)-N'-[4-(2-fluoroethoxy)benzyl]piperazine, a novel σ_1 receptor PET imaging agent. *Bioorg Med Chem* 21:6820–6823
- Narita N, Hashimoto K, Tomitaka S et al (1996) Interactions of selective serotonin reuptake inhibitors with subtypes of σ receptors in rat brain. *Eur J Pharmacol* 307:117–119
- Niitsu T, Shirayama Y, Fujisaki M (2010) Fluvoxamine improved cognitive impairments in a patient with schizophrenia. *Prog Neuropsychopharmacol Biol Psychiatry* 34:1345–1346
- Nimura T, Ando T, Yamaguchi K et al (2004) The role of σ -receptors in levodopa-induced dyskinesia in patients with advanced Parkinson disease: a positron emission tomography study. *J Neurosurg* 100:606–610
- O'Neill M, Caldwell M, Earley B et al (1995) The sigma receptor ligand JO1784 (igmesine hydrochloride) is neuroprotective in the gerbil model of global cerebral ischemia. *Eur J Pharmacol* 283:217–225
- Robson MJ, Noorbakhsh B, Seminerio MJ et al (2012) Sigma-1 receptors: potential targets for the treatment of substance abuse. *Curr Pharm Des* 18:902–919
- Sakata M, Kimura Y, Naganawa M et al (2007) Mapping of human cerebral sigma₁ receptors using positron emission tomography and [¹¹C]SA4503. *Neuroimage* 35:1–8

- Sakata M, Kimura Y, Naganawa M et al (2008) Shortened protocol in practical [¹¹C]SA4503-PET studies for sigma₁ receptor quantification. *Ann Nucl Med* 22:143–146
- Shiba K, Ogawa K, Ishiwata K et al (2006) Synthesis and binding affinities of methyl vesamicol analogs for the acetylcholine transporter and sigma receptor. *Bioorg Med Chem* 14:2620–2626
- Shibuya H, Mori H, Toru M (1992) Sigma receptors in schizophrenic cerebral cortices. *Neurochem Res* 17:983–990
- Stone JM, Arstad E, Erlandsson K et al (2006) [¹²³I]TPCNE – a novel SPET tracer for the sigma-1 receptor: first human studies and in vivo haloperidol challenge. *Synapse* 60:109–117
- Su TP, London ED, Jaffe JH (1988) Steroid binding at sigma receptors suggests a link between endocrine, nervous, and immune systems. *Science* 240:219–221
- Takahashi H, Kirsch JR, Hashimoto K et al (1995) PPBP [4-phenyl-1-(4-phenylbutyl)piperidine], a potent sigma-receptor ligand, decreases brain injury after transient focal ischemia in cats. *Stroke* 26:1676–1682
- Takahashi H, Kirsch JR, Hashimoto K et al (1996) PPBP [4-phenyl-1-(4-phenylbutyl)piperidine] decreases brain injury after transient focal ischemia in rats. *Stroke* 27:2120–2123
- Takebayashi M, Kagaya A, Uchitomi Y et al (1998) Plasma dehydroepiandrosterone sulfate in unipolar major depression. Short communication. *J Neural Transm* 105:537–542
- Toyohara J, Sakata M, Ishiwata K (2009) Imaging of sigma₁ receptors in the human brain using PET and [¹¹C]SA4503. *Cent Nerv Syst Agents Med Chem* 9:190–196
- Toyohara K, Sakata M, Ishiwata K (2012) Re-evaluation of in vivo selectivity of [¹¹C]SA4503 to sigma₁ receptors in the brain: contributions of emopamil binding protein. *Nucl Med Biol* 39:1049–1052
- Uchida N, Ujike H, Nakata K et al (2003) No association between the sigma receptor type 1 gene and schizophrenia: results of analysis and meta-analysis of case-control studies. *BMC Psychiatry* 3:13
- Uchida N, Ujike H, Tanaka Y et al (2005) A variant of sigma receptor type-1 gene is a protective factor for Alzheimer disease. *Am J Geriatr Psychiatry* 13:1062–1066
- Ujike H, Akiyama K, Kuroda S (1996) [³H]YM-09151-2 (nemonapride), a potent radioligand for both sigma 1 and sigma 2 receptor subtypes. *Neuroreport* 7:1057–1061
- Urfer R, Takao K, Sato W et al (2009) SA4503 is a potent and selective sigma-1 receptor agonist in clinical development for depression and stroke. *Soc Neurosci Abstr* 496:3
- van Broekhoven F, Verks RJ (2003) Neurosteroids in depression: a review. *Psychopharmacology (Berl)* 165:97–100
- van Waarde A, Rybczynska AA, Ramakrishnan N et al (2010) Sigma receptors in oncology: therapeutic and diagnostic applications of sigma ligands. *Curr Pharm Des* 16:3519–3537
- van Waarde A, Ramakrishnan NK, Rybczynska AA et al (2011) The cholinergic system, sigma-1 receptors and cognition. *Behav Brain Res* 221:543–554
- Vilkman H, Kajander J, Nagren K et al (2000) Measurement of extrastriatal D₂-like receptor binding with [¹¹C]FLB 457 – a test-retest analysis. *Eur J Nucl Med* 27:1666–1673
- Walker JM, Bowen WD, Walker FO et al (1990) Sigma receptors: biology and function. *Pharmacol Rev* 42:355–402
- Wang L, Duncan G (2006) Silencing of sigma-1 receptor induces cell death in human lens cells. *Exp Cell Res* 312:1439–1446
- Waterhouse RN, Mardon K, Giles KM et al (1997) Halogenated 4-(phenoxy)methylpiperidines as potential radiolabeled probes for sigma-1 receptors: in vivo evaluation of [¹²³I]-1-(iodopropen-2-yl)-4-[(4-cyanophenoxy)methyl]piperidine. *J Med Chem* 40:1657–1667
- Waterhouse RN, Nobler MS, Zhou Y et al (2004) First evaluation of the sigma-1 receptor radioligand [¹⁸F]1-3-fluoropropyl-4-((4-cyanophenoxy)-methyl)piperidine ([¹⁸F]FPS) in humans. *Neuroimage* 22(Supp 2):T29–T30
- Waterhouse RN, Chang RC, Zhao J et al (2006a) In vivo evaluation in rats of [¹⁸F]1-(2-fluoroethyl)-4-[(4-cyanophenoxy)methyl]piperidine as a potential radiotracer for PET assessment of CNS sigma-1 receptors. *Nucl Med Biol* 33:211–215

- Waterhouse RN, Zhao J, Stabin MG et al (2006b) Preclinical acute toxicity studies and dosimetry estimates of the novel sigma-1 receptor radiotracer, [¹⁸F]SFE. *Mol Imaging Biol* 8:284–291
- Weissman AD, Su TP, Hedreen JC et al (1988) Sigma receptors in post-mortem human brains. *J Pharmacol Exp Ther* 247:29–33
- Weissman AD, Casanova MF, Kleinman JE et al (1991) Selective loss of cerebral cortical sigma, but not PCP binding sites in schizophrenia. *Biol Psychiatry* 29:41–54
- Xu J, Zeng C, Chu W et al (2011) Identification of the PGRMC1 protein complex as the putative sigma-2 receptor binding. *Nat Commun* 2:380
- Yang S, Bhardwaj A, Cheng J et al (2007) Sigma receptor agonists provide neuroprotection in vitro by preserving bcl-2. *Anesth Analg* 104:1179–1184
- Zhao J, Chang R, Carambot P et al (2005) Radiosynthesis and in vivo study of [¹⁸F]1-(2-fluoroethyl)-4-[(cyanophenoxy)methyl]piperidine: a promising new sigma-1 receptor ligand. *J Label Compd Radiopharm* 48:547–555

Michael R. Kilbourn

Contents

27.1	Introduction	767
27.2	Biology and Pharmacology of the Vesicular Monoamine Transporter Type 2	768
27.2.1	Molecular Biology of the VMAT2.....	768
27.2.2	Localization of the VMAT2 in Mammalian Brain.....	768
27.2.3	VMAT2 Substrates and Inhibitors	769
27.3	VMAT2 Radioligands for Autoradiography	771
27.3.1	[³ H]Tetrabenazine ([³ H]TBZ).....	771
27.3.2	α-[³ H]Dihydrotetrabenazine ([³ H]DTBZ).....	771
27.3.3	(+/-)-[³ H]Methoxytetrabenazine ([³ H]MTBZ).....	771
27.3.4	[³ H]/[¹²⁵ I]Reserpine	772
27.3.5	[¹²⁵ I]Iodovinyltetrabenazine	772
27.3.6	Ketanserin Derivatives	772
27.4	VMAT2 Radioligands for Positron Emission Tomography (PET) Imaging Studies	772
27.4.1	[¹¹ C]Tetrabenazine ([¹¹ C]TBZ).....	773
27.4.2	(+/-)-α-[¹¹ C]Dihydrotetrabenazine ([¹¹ C]DTBZ)	773
27.4.3	(+)-α-[¹¹ C]Dihydrotetrabenazine ((+)-α-[¹¹ C]DTBZ).....	774
27.4.4	[¹¹ C]Methoxytetrabenazine ([¹¹ C]MTBZ).....	774
27.4.5	Fluorine-18-Labeled Dihydrotetrabenazines	774
27.5	Evaluation of VMAT2 Imaging Radioligands in Animals.....	776
27.5.1	Mouse Brain VMAT2 Studies.....	776
27.5.2	Rat Brain VMAT2 Studies	776
27.5.3	VMAT2 Radioligand Studies in Nonhuman Primates	777
27.6	Applications of VMAT2 Radioligands in Human Imaging Studies.....	778
27.6.1	Pharmacokinetic Studies of VMAT2 Radioligands in Normal Brain.....	779
27.6.2	Aging.....	781
27.6.3	Parkinson's Disease.....	781
27.6.4	Non-Parkinson Movement Disorders.....	782
27.6.5	Huntington's Disease	782
27.6.6	Dementia.....	782

M.R. Kilbourn

Division of Nuclear Medicine, Department of Radiology,
University of Michigan Medical School, Ann Arbor, MI 48109, USA
e-mail: mkilbour@med.umich.edu

27.6.7	Psychiatric Disease	783
27.6.8	Drug Abuse	783
	Conclusions	784
	References	784

Abstract

The vesicular monoamine transporter type 2 (VMAT2) is a protein specifically located in the membrane of neurotransmitter storage vesicles of monoaminergic neurons (dopamine, serotonin, norepinephrine, and histamine). The noninvasive *in vivo* imaging of this transporter has been utilized as a marker of the changes in monoaminergic innervation in human neurological diseases. Development of suitably radiolabeled compounds for *in vivo* imaging using positron emission tomography (PET) produced optimized carbon-11 ((+)- α -[^{11}C]dihydratetrabenazine, DTBZ) and fluorine-18 (9-(3-[^{18}F]fluoropropyl)-dihydratetrabenazine, AV-133) radioligands. Applications of VMAT2 radioligand imaging in numerous neurodegenerative diseases (e.g., Parkinson's and related movement disorders, dementia with Lewy bodies) and psychiatric diseases (e.g., schizophrenia) and drug abuse have demonstrated that *in vivo* imaging of the VMAT2 provides a powerful tool to examine the progress and extent of changes of monoaminergic innervation in human disease conditions.

Abbreviations

AD	Alzheimer's disease
AMPT	Alpha-methyl-para-tyrosine
AV-133	9-(3-fluoropropyl)-10-methoxy-3-(2-methylpropyl)-1,3,4,6,7,11b-hexahydrobenzo[<i>a</i>]quinolizin-2-ol
DOPA	3,4-dihydroxyphenylalanine
DTBZ	Dihydratetrabenazine: 9,10-dimethoxy-3-(2-methylpropyl)-1,3,4,6,7,11b-hexahydrobenzo[<i>a</i>]quinolizin-2-ol
fluoroDOPA	6-fluoro-3,4-dihydroxyphenylalanine
MDMA	3,4-methylenedioxy-N-methylamphetamine
MPTP	1-methyl-4-phenyl-2,3,5,6-tetrahydropyridine
MPP+	1-methyl-4-phenylpyridinium
MTBZ	Methoxytetrabenazine
NMR	Nuclear magnetic resonance
HD	Huntington's disease
LBD	Lewy body disease
MSA	Multiple system atrophy
OPCA	Olivopontocerebellar atrophy
PD	Parkinson's disease
PDD	Parkinson's disease with dementia
PET	Positron emission tomography

PSP	Progressive supranuclear palsy
SPECT	Single photon emission computed tomography
TBZ	Tetrabenazine: 3-isobutyl-9,10-dimethoxy-1,3,4,6,7,11b-hexahydro-pyrido[2,1- <i>a</i>]isoquinolin-2-one
VMAT	Vesicular monoamine transporter
VACHT	Vesicular acetylcholine transporter
VGLUT	Vesicular glutamate transporter
VGAT	Vesicular GABA transporter

27.1 Introduction

A somewhat simplified but classical view of neurotransmission involves the biosynthesis of neurotransmitters, packaging of the neurotransmitter molecules within synaptic vesicles, release of the neurotransmitters into the synapse through exocytosis through the neuronal membrane, and binding of the neurotransmitter to postsynaptic receptors; termination of the signal is accomplished by transporter-mediated reuptake of neurotransmitter back across the neuronal membrane into the cytosol and/or intra-synaptic catabolism of the neurotransmitter. The recovered neurotransmitter can then be metabolically degraded or repackaged into vesicles for future release. All of these processes have been targeted for *in vivo* radioligand design (Zimmer and Luxen 2012): in the dopaminergic system, for example, this has produced useful radiotracers for neurotransmitter synthesis, vesicular storage, postsynaptic receptor binding, presynaptic reuptake, and catabolism (Brooks and Pavese 2011).

As a critical part of this process of neurotransmission, the vesicular neurotransmitter transporters are synaptic vesicle-specific proteins that actively transport newly synthesized or recovered neurotransmitter molecules across the vesicle lipid bilayer and into the lumen. Such specific transporters are found for the monoamines (VMAT, the vesicular monoamine transporters types 1 and 2), acetylcholine (VACHT, the vesicular acetylcholine transporter), inhibitory amino acids (VGAT, the vesicular GABA transporter), and the excitatory amino acids (VGLUT, the vesicular glutamate transporters) (Eiden et al. 2004; Gasnier 2004; Omote et al. 2011). As the vesicular transporters are quite specifically located only within the vesicle membranes of neurons and except for the VMAT2 (which is found in all monoaminergic neurons including those using norepinephrine, dopamine, serotonin, and histamine) are specific for one type of neuron (i.e., VACHT for cholinergic neurons), they have made a logical choice for development of radioligands with the potential for marking the changes in numbers of specific neuronal populations in the healthy and diseased human brain. As such, these vesicular transporter targets complement the more extensive efforts in radioligand development for the neuronal membrane neurotransmitter transporters (Brooks and Pavese 2011), a structurally unrelated family of proteins responsible for the reuptake of intra-synaptic neurotransmitters across the synaptic membrane and into the cytosol.

Although there are vesicular transporters for all of the different neurotransmitters, in practice only two of these (VMAT2 and VACHT) have been successfully targeted in

the development of *in vivo* radioligands for human studies. In contrast to VMAT2 radiotracer development (described in following sections), a much wider variety of compounds have been radiolabeled as prospective *in vivo* imaging agents for the VACht, but only two (one for single photon emission computed tomography (SPECT), one for positron emission tomography (PET)) have reached the stage of achieving approvals for human studies (Kuhl et al. 1994; Petrou et al. 2012). At present there are limited opportunities for development of *in vivo* radioligands for the VGAT and VGLUT transporter due to the paucity of structures known to be high-affinity inhibitors that can serve as templates for radiotracer design (Thompson et al. 2005).

27.2 Biology and Pharmacology of the Vesicular Monoamine Transporter Type 2

27.2.1 Molecular Biology of the VMAT2

The VMAT2 (SLC18A1) is part of the family of amine transporters (Eiden et al. 2004) and transports single positively charged amine substrates into vesicles with a concomitant extrusion of two protons. The protons are accumulated within vesicles by the action of a separate membrane-bound ATPase. Most models of VMAT2 describe a 12 transmembrane domain configuration with both the amino and carboxyl terminal ends within the cytoplasm and a large intracellular loop between transmembrane domains I and II (Wimalasena 2010). The VMAT2 is the form located in the neurons of the brain, although it is also expressed in nerves and exocrine cells of a variety of peripheral organs; the structurally related VMAT1 (SLC18A2, with 40 % sequence homology) is peripherally located with highest concentrations in the adrenals. With rare exceptions, the functionality of a monoaminergic neuron is determined by the combination of VMAT2 with the neurotransmitter-specific biosynthetic enzymes and corresponding neuronal membrane reuptake transporter (e.g., dopaminergic neurons have tyrosine hydroxylase, DOPA decarboxylase, and the dopamine transporter (DAT)). Homozygous knockout of the VMAT2 is lethal in mice, but heterozygous knockouts appear normal with reduced filling of neuronal vesicles (Miller et al. 2001).

27.2.2 Localization of the VMAT2 in Mammalian Brain

In vitro studies with the radiolabeled VMAT2 ligand [³H]dihydrotrabenazine (DTBZ, originally termed TBZOH) in rodent and human brain tissues have demonstrated the concentration of the transporter in brain regions rich in monoaminergic neuronal synapses, with the highest concentrations in the basal ganglia, intermediate in such cell bodies as the substantia nigra, and low in the cortex (Scherman et al. 1988) (Table 27.1). In the striatum, radioligand binding is predominantly (>95 %) to dopaminergic terminals; in other brain regions binding is likely due to a mixture of dopaminergic, serotonergic, and adrenergic innervation. The high concentration of

Table 27.1 Regional in vitro and in vivo binding data for VMAT2 radioligands in mouse, rat, and human brains

Mouse	fmol/mg protein^a	[¹¹C]TBZ % inj dose/g^b
Striatum	1,345	4.96
Thalamus	111	2.06
Hippocampus	141	2.01
Hypothalamus	411	2.96
Pons-medulla	167	1.96
Cortex (frontal)	115	1.91
Cerebellum	56	1.76
Rat	fmol/mg protein^c	[¹¹C]DTBZ DV_{total}^d
Striatum	1,199	7.35
Thalamus	111–669	2.80
Hippocampus	124	2.51
Hypothalamic nuclei	838	5.13
Pons-medulla	–	–
Cortex (frontal)	103	2.18
Cerebellum	60	2.07
Human	fmol/mg protein^a	[¹¹C]DTBZ DV_{total}^e
Caudate	742	12.5
Putamen	766	11.7
Hypothalamus	245	–
Hippocampus	83	–
Thalamus	–	4.75
Cortex (frontal)	57	4.16
Cerebellum	–	4.06

DV_{total} total distribution volume

^aSpecific in vitro [³H]DTBZ binding from Scherman et al. (1988)

^bEx vivo data from DaSilva and Kilbourn (1992)

^cSpecific in vitro [³H]MTBZ binding from Vander Borgh et al. (1995c)

^dEx vivo data from Kilbourn and Sherman (1997)

^eIn vivo PET data from Koeppe et al. (1996)

VMAT2 in the basal ganglia has also been demonstrated using immunochemical techniques and a specific hVMAT2 antibody (Tong et al. 2011). Both radioligand binding and immunochemical staining techniques have demonstrated the significant loss of VMAT2 in the basal ganglia in neurodegenerative diseases such as Parkinson's disease (Miller et al. 1998; Scherman et al. 1989). The extremely low levels of VMAT2 in regions such as the occipital cortex or cerebellar cortex has proven advantageous for in vivo imaging, as these regions can then be used to estimate nonspecific distribution of radioligands for pharmacokinetic modeling purposes.

27.2.3 VMAT2 Substrates and Inhibitors

The VMAT2, being a transporter of multiple neurotransmitters (DA, NE, 5HT, histamine), has a fairly unspecific substrate specificity that extends to many biogenic

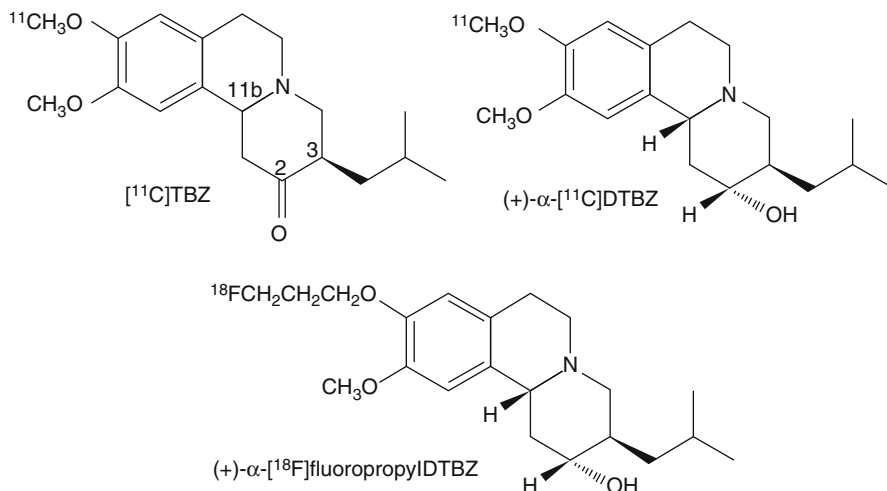


Fig. 27.1 Structures of tetraabenazine and PET radiopharmaceuticals currently in use in human PET studies of the VMAT2 in the human brain

amines, drugs of abuse (e.g., amphetamines), and neurotoxins (e.g., 1-methyl-4-phenylpyridinium, MPP+). The *in vitro* affinities of the transported molecules (endogenous neurotransmitters and amphetamines) for the [³H]DTBZ binding site are however quite low (>100 μmol). Compounds known to be antagonists for the receptors and neuronal membrane transporters for the monoamines are ineffective inhibitors of either VMAT2 transport function or high-affinity radioligand binding to the VMAT2 (Gonzalez et al. 1994; Wimalasena 2010).

When development of *in vivo* VMAT2 radioligands was begun, the list of known high-affinity ligands (agonist or antagonist) for the VMAT2 was limited to reserpine, tetraabenazine, and ketanserin. Reserpine, a complex alkaloid, has an extremely high affinity for VMAT2 ($K_D=0.3$ nM) but is essentially an irreversible inhibitor, with a protracted effect on brain VMAT2 (Naudon et al. 1995). Ketanserin has a moderate affinity for the VMAT2 ($K_D=45$ nM) but also high affinity for serotonin receptors, making it a less than optimal target for development of ligands with potential as *in vivo* imaging agents; attempts at modification of the ketanserin structure failed to yield higher affinity or more specific ligands (Darchen et al. 1988). Most recently, a series of compounds derived from lobelane and with moderate inhibitory activity towards the VMAT2 have been described (Zheng et al. 2005), but have yet been the target of radiotracer design.

Tetraabenazine (TBZ: 3-isobutyl-9,10-dimethoxy-1,3,4,6,7,11b-hexahydro-pyrido[2,1-a]isoquinolin-2-one, Fig. 27.1) is one of a series of compounds initially developed by Hoffman-LaRoche (Quinn et al. 1959); of a set of compounds with different alkyl substituents at the 3-position, it was selected for further development and eventually reached clinical use. For several decades following its clinical introduction, there had been little further examination of the structure-affinity relationships of these

benzoisoquinolines for the VMAT2. It has only been more recently, and largely prompted by the interest in developing optimal radioligands for imaging, that a much larger set of derivatives of tetrabenazine have been synthesized and evaluated in vitro and in vivo. This includes DTBZ derivatives with 2-alkyl substituents (Lee et al. 1996), altered 3-alkyl groups (Zheng et al. 2011), and substitutions of longer alkyl or fluoroalkyl chains for the 9-*O*-methyl substituent (Goswami et al. 2006; Hostetler et al. 2007). Most importantly, however, and prompted entirely by the desire to optimize in vivo performance (see Sect. 27.4.3) was the resolution of dihydrotetrabenazine into active and inactive stereoisomers (Kilbourn et al. 1997), followed later by the synthesis and identification of all eight potential stereoisomers of DTBZ (Tridgett et al. 2012; Yao et al. 2011). Fortuitously, the isomer selected for the current generation of VMAT2 imaging agents turned out to be that with the highest affinity ($K_D=1$ nM) for VMAT2.

27.3 VMAT2 Radioligands for Autoradiography

27.3.1 [³H]Tetrabenazine ([³H]TBZ)

Tritiated tetrabenazine was only recently reported by Rhee et al. (2011), using the catalytic hydrogenation of a suitably constructed alkene precursor (1,3,4,6,7,11b-hexahydro-3-(2-methyl-2-propenyl)-9,10-dimethoxy-2-oxo-2*H*-benzo[*a*]quinolizine) that upon reduction with tritium gas gave the doubly tritiated tetrabenazine with a specific activity of 1,850 GBq/mmol.

27.3.2 α -[³H]Dihydrotetrabenazine ([³H]DTBZ)

Most of the in vitro work using tritiated VMAT2 ligands has been performed with tritiated forms of α -dihydrotetrabenazine (termed TBZOH or DTBZ: 9,10-dimethoxy-3-(2-methylpropyl)-1,3,4,6,7,11b-hexahydrobenzo[*a*]quinolizine-2-ol, Fig. 27.1). This radioligand was first reported in 1981 (Scherman et al. 1981) and was prepared by the sodium borotritide reduction of the 2-ketone group of racemic tetrabenazine. The radioligand was thus obtained as a mixture of the α - and β -isomers resulting from a non-stereospecific reduction of the ketone. Although not clearly identified at the time, chromatographic isolation of a single isomer likely gave the α -(+/-)-[³H]dihydrotetrabenazine, in a specific activity of 185–555 GBq/mmol. More recently, the synthesis of the single isomer (+)- α -[³H]DTBZ was accomplished by *O*-methylation of (+)- α -9-*O*-desmethylDTBZ using [³H]methyl iodide, with a specific activity of 2,923 GBq/mmol (Kilbourn et al. 1997).

27.3.3 (+/-)-[³H]Methoxytetrabenazine ([³H]MTBZ)

In an attempt to prepare a radioligand with better radiochemical stability, the derivative 2-*O*-methyl-dihydrotetrabenazine was prepared in tritiated form (Vander Borgh

et al. 1995c). Alkylation of (+/-)- α -dihydrotrabenzazine with tritiated methyl iodide yielded the radioligand termed (+/-)- α -[^3H]methoxytrabenzazine ([^3H]MTBZ) in a specific activity of 3,034 GBq/mmol. This tritiated molecule was considerably more stable and showed less radiolytic decomposition upon storage as compared to tritiated dihydrotrabenzazine.

27.3.4 [^3H]/[^{125}I]Reserpine

Tritiated reserpine (292 Gbq/mmol) has been synthesized from [2,6- ^3H]3,4,5-trimethoxybenzoic acid and used for ex vivo autoradiography in rat brain. A radioiodinated reserpine derivative, 18-*O*-[3-(3-[^{125}I]iodo-4-azidophenyl)-propionyl]methyl reserpate, has been used for photoaffinity labeling experiments with the VMAT2 (Sievert et al. 2007).

27.3.5 [^{125}I]Iodovinyltrabenzazine

A radioiodinated derivative of trabenzazine suitable for in vitro autoradiography was reported by Kung and coworkers (Kung et al. 1994). This was a dihydrotrabenzazine derivative with an iodovinyl substituent at the 2-position. The radioligand was prepared in very high specific activities (81,400 GBq/mmol) by an iododestannylation reaction and obtained as a mixture of two isomers, only one of which showed high-affinity binding to the VMAT2 ($K_d=0.22$ nM). The absolute stereochemistry of the radioiodinated ligand was not determined at that time, but based on the knowledge that has since been gained through the synthesis and characterization of all eight of the isomers of dihydrotrabenzazine, it is likely the higher-affinity compound had the 3*R*,11*bR* configuration but with the absolute configuration at the 2-position more difficult to predict as both 2*R* and 2*S* isomers of 2-substituted DTBZ derivatives have good binding affinities (Lee et al. 1996).

27.3.6 Ketanserin Derivatives

Although ketanserin is a nonspecific ligand for the VMAT2, it does have a high affinity for the transporter, and with appropriate pharmacological blocking of its other binding sites (e.g., serotonin receptors), two radioiodinated derivatives, 7-amino-8-[^{125}I]iodoketanserin and 7-azido-8-[^{125}I]iodoketanserin, have been used for in vitro autoradiography and photoaffinity labeling experiments (Darchen et al. 1989).

27.4 VMAT2 Radioligands for Positron Emission Tomography (PET) Imaging Studies

The development of VMAT2 radioligands for positron emission tomography (PET) began with trabenzazine as the initial target compound. The choice was mostly practical. The molecule has two phenolic methoxy groups quite suitable for radiolabeling

using carbon-11 methyl iodide, and the resultant radioligand would be unchanged from a well-known and characterized drug that had been in human use for decades; this averted any worries about toxicology, and the pharmacology of the drug was very well known. Interestingly, as will become evident in the following sections, the quest for optimal in vivo radioligand structures derived from tetrabenazine led to the synthesis of quite a number of derivatives, providing insights into the structure-activity relationships of the benzoisoquinolines and the identification of the absolute structures of the stereoisomers, which had never been done for this clinical drug.

27.4.1 [^{11}C]Tetrabenazine ([^{11}C]TBZ)

The labeling of tetrabenazine simply required removal of one of the *O*-methyl groups and replacement with the carbon-11 ($t_{1/2}=20$ min)-labeled methyl group (DaSilva and Kilbourn 1992; DaSilva et al. 1993b). Although simple in concept, the cleavage of the phenolic methoxy group using reagents such as boron tribromide proved to be a difficult reaction and led to complex mixtures of the mono- and bis-demethylated products. Careful chromatography yielded a single pure product assigned as the 9-*O*-desmethyltetrabenazine, with the assignment (9 vs. 10) based on proton and carbon-13 NMR spectroscopy; that assignment was later proved correct through a synthesis of the 9-*O*-desmethyltetrabenazine by an independent and unambiguous route. The reaction of the free phenolic compound with [^{11}C]methyl iodide under basic conditions then yielded the desired [^{11}C]tetrabenazine, in modest yields and specific activities (74,000–92,500 GBq/mmol) (DaSilva et al. 1993b). At the time of preparation, this radioligand was obtained as an unknown and uncharacterized mixture of stereoisomers; based on the data obtained in more recent studies (see below), the starting material and the final radiochemical product were both likely racemic mixtures of 3*R*,11*B**R* and 3*S*,11*B**S*-tetrabenazine.

27.4.2 (+/–)- α -[^{11}C]Dihydrotetrabenazine ([^{11}C]DTBZ)

[^{11}C]Tetrabenazine was used for initial VMAT2 imaging studies, but consideration of its metabolic fate in the human body led to the rapid realization that what was really desired was the molecule termed dihydrotetrabenazine; this is the product of the first step in the metabolism of TBZ and is the predominant chemical species in the bloodstream after administration of the drug to rats or humans (Mehvar et al. 1987). Interestingly, this metabolite (termed TBZOH or DTBZ) had been used for years for in vitro studies of the VMAT2 (Scherman et al. 1988). The reduction of the ketone of TBZ by in vivo metabolism, or by chemical means in the laboratory, produces two isomers termed α - and β -DTBZ; the desired higher-affinity isomer was the α stereoisomer but with absolute stereochemistry unknown. The required precursor for radiolabeling was now the 9-desmethyl-2-hydroxy derivative with the hydroxyl in the α configuration, prepared in two steps from TBZ by reduction of the ketone followed by demethylation (Jewett et al. 1997). Alkylation with [^{11}C]methyl iodide produced (+/–)- α -[^{11}C]DTBZ in moderate yields and useful specific activities (>59,200 GBq/mmol) but still as an undefined and likely racemic mixture of stereoisomers.

27.4.3 (+)- α -[^{11}C]Dihydrotrabenzazine ((+)- α -[^{11}C]DTBZ)

As the last step in the optimization of a specific VMAT2 radioligand, the stereoisomers of α -DTBZ were separated using preparative chiral HPLC (Kilbourn et al. 1995b, 1997). There were found to be only two isomers which rotated polarized light in opposite directions, assigned as the (+)- and (–)-isomers. Crystals of the (–)-DTBZ isomer were successfully grown for X-ray structural analysis, and the absolute stereochemistry of these isomers finally assigned: (2*R*,3*R*,11*bR*) for the (+)-isomer and (2*S*,3*S*,11*bS*) for the (–)-isomer (Kilbourn et al. 1997). In vitro binding assays showed that these two isomers had drastically different binding affinities, with only the (+)-isomer showing high-affinity binding (1 nM) and a very low affinity (4,000 nM) for the (–)-isomer. More recently, efforts have been successful at the synthesis and identification of all eight of the possible stereoisomers of dihydrotrabenzazine (Tridgett et al. 2012; Yao et al. 2011). Subsequent syntheses of all of the isomers and determination of the in vitro binding affinities have shown that the isomer with the 2*R*,3*R*,11*bR* absolute stereochemistry is the highest-affinity DTBZ ligand for the VMAT2 (Yao et al. 2010).

The synthesis of (+)- α -[^{11}C]DTBZ then required the preparation of the single resolved isomer of the 9-*O*-desmethylDTBZ, which was first accomplished by a low-yield sequence of reduction of TBZ, chiral column resolution of DTBZ isomers, and a modified demethylation reaction condition (sodium hydride/*N*-methylaniline/hexamethylphosphoramide) (Kilbourn et al. 1997). More recently, improved synthetic routes to TBZ, (+)- α DTBZ, and (+)- α -9-desmethylDTBZ have been published (Boldt et al. 2008; Paek et al. 2010; Rishel et al. 2009a; Yu et al. 2010), making the synthesis of the precursor to the desired radioligand much more practical. Alkylation of the desmethyl precursor with [^{11}C]methyl iodide yields the currently routinely used radioligand, (+)- α [^{11}C]DTBZ, in high average specific activities (370,000 GBq/mmol) and a defined 2*R*,3*R*,11*bR* absolute stereochemistry.

27.4.4 [^{11}C]Methoxytrabenzazine ([^{11}C]MTBZ)

In an attempt to alter and perhaps improve the metabolic disposition of VMAT2 radioligands, a new derivative with a [^{11}C]methoxy substituent at the 2-position was synthesized (DaSilva et al. 1993c). Prepared by reaction of (+/–)-DTBZ with [^{11}C]methyl iodide under strong basic conditions, the radioligand 2-*O*-methoxydihydrotrabenzazine (MTBZ) was successfully introduced into human studies (Vander Borghet et al. 1995b). However, the radiochemical synthesis proved more difficult than the alkylation of the phenol (as for DTBZ), and with the development of (+)- α [^{11}C]DTBZ, MTBZ was not extensively studied although it is excellent as an in vitro ligand when prepared in tritiated form.

27.4.5 Fluorine-18-Labeled Dihydrotrabenzazines

The carbon-11-labeled ligands and in particular (+)- α -[^{11}C]DTBZ have now been used in a wide variety of clinical studies of neurological and psychiatric diseases.

The application of VMAT2 imaging to clinical care, however, was likely to require the availability of radioligands labeled with longer half-life radionuclides. Fortunately, development of fluorine-18 ($t_{1/2}=109.6$ min)-labeled VMAT2 radioligands was able to build on and extend the chemistry and pharmacology developed in the carbon-11 series.

The substitution of the 9-methoxy group of DTBZ with [^{18}F]fluoroalkoxy groups resulted in the successful synthesis of 9-*O*-[^{18}F]fluoromethyl-, 9-*O*-(2-[^{18}F]fluoroethyl)- and 9-*O*-(3-[^{18}F]fluoropropyl)DTBZ (Goswami et al. 2006; Hostetler et al. 2007; Kung et al. 2007). The [^{18}F]fluoromethyl derivative ($K_i=0.87$ nM for rat VMAT2) was prepared by *O*-alkylation of (+)- α -9-*O*-desmethylDTBZ with [^{18}F]FCH₂Br under basic conditions (Hostetler et al. 2007). The [^{18}F]fluoroethyl ($K_i=0.76$ nM) and [^{18}F]fluoropropyl ($K_i=0.56$ nM) derivatives were first prepared in racemic form by [^{18}F]fluoride ion displacement of the corresponding mesylates (Fig. 27.1) in specific activities >74,000 GBq/mmol. Subsequently, a stereospecific synthesis of (+)- α -9-*O*-(3-[^{18}F]fluoropropyl)DTBZ (also termed [^{18}F]AV-133: (2*R*,3*R*,11*B**R*)-9-(3-[^{18}F]fluoropropoxy)-10-methoxy-3-(2-methylpropyl)-1,3,4,6,7,11b-hexahydro-2*H*-benzo[*a*]quinolizin-2-ol) from the corresponding chirally resolved mesylate was developed, yielding the very high-affinity ($K_i=0.1$ nM) single isomer, with specific activities of 55,000–74,000 GBq/mmol. As was expected, the (–)- α -(3-fluoropropyl)DTBZ isomer showed negligible affinity for VMAT2 (>3,000 nM). Recently, in an attempt to improve on the in vivo defluorination of [^{18}F]fluoroethylDTBZ, the radioligand was synthesized using tetradeuterated [^{18}F]fluoroethyl bromide; the deuterated ligand showed regional brain pharmacokinetics similar to [^{11}C]DTBZ with slightly higher total uptake and higher striatal binding potentials (Varone et al. 2012).

In the pursuit of improved properties for in vivo imaging, Kung and coworkers have explored several other derivatives of TBZ derivatives. Replacement of the 2-hydroxyl group of DTBZ with a 2-fluoropropylamino group yielded a derivative with an in vitro affinity of 7 nM (as racemate) (Zhu et al. 2009). Substitution of the 2-hydroxyl function of 2-[^{18}F]fluoropropyl-(+)-DTBZ with an epoxide ring provided a derivative with an excellent in vitro affinity (0.08 ± 0.01 nM) (Kung et al. 2008).

A completely different approach to fluorine-18-labeled DTBZ molecules was reported in a series of patents (Amarasinghe et al. 2009; Kankanamalage et al. 2009; Rishel et al. 2009b). A very large number of fluoro-substituted (+)- α -DTBZ derivatives are claimed in this series of patents, but in vitro biological information is only available for a few of the compounds claimed. The 2-fluoroethyl-substituted DTBZ derivative shows reasonable affinity ($K_i=19$ nM), consistent with the earlier demonstration of bulk tolerance of reasonably small 2-alkyl substituents (Lee et al. 1996). Similarly, the 2-fluoroethoxy ether derivative has a good in vitro binding affinity of 3.2 nM, not significantly different than that previously obtained for the slightly smaller methyl ether derivative (3.9 nM; Vander Borgh et al. 1995c).

Of the numerous fluorine-18 radiotracers that have been prepared, only the 9-(3-[^{18}F]fluoropropyl)-dihydrotrabenazine has been reported to be used in human imaging studies.

27.5 Evaluation of VMAT2 Imaging Radioligands in Animals

The evaluation of VMAT2 radioligands for pharmacological specificity, kinetics, sensitivity to endogenous neurotransmitters, propensity for up- or downregulation, and changes in models of human disease has been extensively pursued in both small and large animal models.

27.5.1 Mouse Brain VMAT2 Studies

The mouse was utilized for the initial evaluation of [^{11}C]TBZ, where it was demonstrated that the (a) radioligand localized in regions of the brain containing high concentrations of the VMAT2 (b) localization was likely not specific only to dopaminergic neurons but, as expected, also due to noradrenergic and serotonergic innervation (Table 27.1), and (c) binding could be blocked by pharmacological doses of TBZ but not drugs that bound to the neuronal membrane dopamine transporter (DaSilva and Kilbourn 1992). These simple initial studies also demonstrated the reversibility of [^{11}C]TBZ binding in the rodent brain.

Subsequent studies of VMAT2 radioligand binding in the mouse brain demonstrated that both simple measurement of tissue ratios between high (striatum) and low (cerebellum) regions of the mouse brain, and more quantitative methods using PET imaging, could be used to show decreases of VMAT2 binding sites after MPTP (1-methyl-4-phenyl-1,2,3,4-tetrahydropyridine) lesioning (Chao et al. 2012; Kilbourn et al. 2000). The utility of *in vivo* radioligand binding methods to demonstrate increases of VMAT2 binding was accomplished through studies of genetic mutants, known from *in vitro* studies to overexpress the VMAT2 in the brain (Kilbourn et al. 1995a).

27.5.2 Rat Brain VMAT2 Studies

A larger number of studies of *in vivo* VMAT2 radioligands have been conducted in rats. These have utilized a variety of techniques, including (a) *ex vivo* measurements of tissue distributions following bolus injections, (b) *ex vivo* autoradiography of rat brain slices (Tsao et al. 2010), (c) *ex vivo* determination of regional brain distributions after equilibrium infusions (Kilbourn and Sherman 1997), and (d) *in vivo* PET imaging studies including dynamic multi-tracer approaches (Kilbourn et al. 2007; Sossi et al. 2009), in attempts to characterize the distribution, pharmacology, and sensitivity of the VMAT2 radioligand methods.

As with the studies in mice, determinations of regional brain distributions of VMAT2 radioligands in rats show excellent correlations with the published *in vitro* distribution of VMAT2 binding sites (Table 27.1). Use of both the active and inactive isomers of [^{11}C]DTBZ has shown that uptake and retention of VMAT2 radioligands in regions of the rat brain such as the cerebellum and the occipital cortex represent essentially negligible concentrations of the VMAT2 (Kilbourn and

Sherman 1997) and thus are reasonable regions for estimations of nonspecific distributions of these radiotracers.

The sensitivity of measures of VMAT2 radioligand binding to regulation by chronic drug use has been examined using both *in vitro* and *in vivo* rat studies, with decidedly mixed results. Numerous studies have demonstrated that chronic administration of such drugs as L-DOPA/benserazide, apomorphine, tetrabenazine, pramipexole, paroxetine, amphetamine, or cocaine did not alter *in vitro* levels of VMAT2 radioligand binding, nor was *in vivo* DTBZ binding altered by repeated administration of L-DOPA, deprenyl, or tetrabenazine (Kemmerer et al. 2003; Kilbourn et al. 1996; Schwartz et al. 2006; Vander Borgh et al. 1995a; Vilpoux et al. 2000; Wilson and Kish 1996). These results supported the hypothesis that VMAT2 was a less regulated site than, for example, the neuronal membrane dopamine transporter, for which changes could be seen following such drug treatments (Vander Borgh et al. 1995a). In contrast, several other studies have reported increases or decreases of VMAT2 radioligand binding after administration of some of the same or related drug substances (Frey et al. 1997; Schwartz et al. 2006; Sossi et al. 2010); for methamphetamine, reductions of VMAT2 binding are observed after neurotoxic but not lower behaviorally effective doses (Frey et al. 1997). A few studies in rats have supported a sensitivity of VMAT2 radioligand binding *in vivo* to alterations of endogenous dopamine levels following administration of drugs which directly decrease endogenous dopamine levels (α -methyl-p-tyrosine, AMPT) (Kilbourn et al. 2008, 2010; Tong et al. 2008) or indirectly raise dopamine levels (pramipexole) (Sossi et al. 2010). Those studies have indicated that alterations of vesicular dopamine concentrations may in fact result in changes of *in vivo* VMAT2 radioligand binding, and the increases of VMAT2 radioligand binding can be reversed by replenishment of vesicular dopamine levels using exogenous L-DOPA (Kilbourn et al. 2010). It should be noted that modest changes of *in vivo* radioligand binding (36 % increase) require significant depletion of endogenous dopamine concentrations (>75 %) in the rat brain.

27.5.3 VMAT2 Radioligand Studies in Nonhuman Primates

In the normal monkey brain, VMAT2 radioligands show high *in vivo* binding in the striatal regions, with lower levels of radioactivity retention in the thalamus, hypothalamus, and midbrain cell bodies (raphe nucleus, locus ceruleus, substantia nigra) (DaSilva et al. 1993a; Kilbourn et al. 2007) and negligible in cortex and cerebellum. The binding is stereospecific with low and uniform brain distribution of the corresponding inactive stereoisomers (Kilbourn et al, unpublished data). A comprehensive study of the *in vitro* distribution of VMAT2 radioligand binding site in the nonhuman primate brain is still missing from the literature, but specific binding in the caudate and putamen has been demonstrated using *in vitro* autoradiography (Chen et al. 2008; Tian et al. 2012), and the *in vivo* distribution of binding would be consistent with the expected distribution of the dopaminergic, noradrenergic, and serotonergic systems as seen in rodents and human brain (Table 27.1).

An early study of [^{11}C]tetrabenazine in a monkey with a unilateral MPTP-injected monkey demonstrated the complete loss of *in vivo* radioligand binding in that severe example of dopaminergic neuronal degeneration (DaSilva et al. 1993a). Subsequent studies have used improved imaging instrumentation, the better radioligand (+)- α -[^{11}C]DTBZ, large numbers of monkeys, and multi-tracer studies to better characterize the MPTP-induced loss of *in vivo* VMAT2 binding sites in this animal model of Parkinson's disease. Using a multi-tracer approach ((+)-[^{11}C]DTBZ, [^{11}C]methylphenidate (for the neuronal membrane dopamine transporter, DAT) and [^{18}F]fluoroDOPA), Doudet and coworkers (2006) demonstrated an age-related decrease of VMAT2 radioligand binding in a small cohort of monkeys and that the measures of losses of DTBZ binding were the most sensitive of the three radiotracer methods for detecting striatal changes in asymptomatic, mild unilateral MPTP intoxication. Similar results were obtained in a study using [^{11}C]DTBZ (for VMAT2) and [^{11}C]WIN 35,428 (for DAT) in asymptomatic MPTP-treated monkeys, where significant (50 %) losses of VMAT2 radioligand binding preceded changes in the DAT (Chen et al. 2008). In a monkey model of progressive Parkinsonism induced by repeated MPTP administration spread over several months, losses of DTBZ binding to the VMAT2 were detectable earlier at the less affected stages and then also in monkeys that showed behavioral recovery, than with fluoroDOPA (Blesa et al. 2010). Consistently, unilateral administration of MPTP results in significant decreases in [^{11}C]DTBZ binding (as well as other dopaminergic markers such as DAT radioligands and 6-[^{18}F]fluoroDOPA) and the extent of the decreases agree with postmortem autoradiographic studies of monkey brains after MPTP lesioning (Tian et al. 2012).

In a single study, Fantegrossi et al. (2004) examined the potential changes of *in vivo* [^{11}C]DTBZ binding in a primate model of self-administration of methylenedioxymethamphetamine (MDMA) and found no evidence of dopaminergic degeneration in the striatum. In contrast, a postmortem study of amphetamine-treated baboons showed evidence of neuronal toxicity in the form of reduced binding of [^3H]DTBZ to the VMAT2 (and also reduced radioligand binding to the DAT) (Ricuarte et al. 2005).

27.6 Applications of VMAT2 Radioligands in Human Imaging Studies

The initial human studies of the VMAT2 using *in vivo* imaging with PET began in 1993 using [^{11}C]tetrabenazine (Kilbourn et al. 1993); the first studies using the fluorine-18-labeled derivative 9-(3-[^{18}F]fluoropropyl)- α -(+)-dihydro-tetrabenazine ([^{18}F]AV-133) were reported in 2008 (Frey et al. 2008). The majority of studies using VMAT2 in normals and patient groups have utilized [^{11}C]dihydro-tetrabenazine (DTBZ), the second generation improved carbon-11-labeled radiotracer, and a relatively few studies using the fluorine-18 radioligand [^{18}F]AV-133 have recently appeared in the literature. Examples of data from some representative studies examining VMAT2 radioligand binding in multiple neurodegenerative diseases are

Table 27.2 In vivo binding estimates for (+)- α -[^{11}C]DTBZ and [^{18}F]AV-133 ((+)- α -(3-[^{18}F]fluoropropyl)DTBZ) in healthy controls (HC), Parkinson's disease (PD), dementia with Lewy bodies (DLB), and Alzheimer's disease (AD)

Ligand	Disease	Region	BP (binding potential) Mean (SD)
(+)-[^{11}C]DTBZ ^a	HC	Caudate nucleus	1.69 (0.23)
		Anterior putamen	2.00 (0.25)
		Posterior putamen	1.91 (0.25)
	PD	Caudate nucleus	0.93 (0.26)
		Anterior putamen	0.65 (0.21)
		Posterior putamen	0.43 (0.15)
	DLB	Caudate nucleus	0.87 (0.30)
		Anterior putamen	0.71 (0.21)
		Posterior putamen	0.57 (0.22)
	AD	Caudate nucleus	1.74 (0.35)
		Anterior putamen	2.06 (0.41)
		Posterior putamen	1.92 (0.42)
[^{18}F]AV-133 ^{b,c}	HC	Caudate nucleus	2.53 (0.3)
		Anterior putamen	2.56 (0.3)
		Posterior putamen	2.53 (0.3)
	PD	Caudate nucleus	1.20 (0.5)
		Anterior putamen	0.66 (0.3)
		Posterior putamen	0.30 (0.2)
	DLB	Caudate nucleus	1.24 (0.6)
		Anterior putamen	0.90 (0.5)
		Posterior putamen	0.62 (0.5)
	AD	Caudate nucleus	2.83 (0.9)
		Anterior putamen	3.01 (0.9)
		Posterior putamen	2.87 (0.9)

^aData from Koeppe et al. (2008)^bData from Okamura et al. (2010)^cAV-133 is 9-(3-[^{18}F]fluoropropyl)-dihydrotrabenazine

shown in Table 27.2; these and additional studies in neurology, psychiatry, and drug abuse are discussed in the following sections.

27.6.1 Pharmacokinetic Studies of VMAT2 Radioligands in Normal Brain

The in vivo regional distribution of VMAT2 binding (Table 27.2) and pharmacokinetics of (+)- α -[^{11}C]DTBZ in the normal human brain have now been thoroughly studied. Initial evaluation of radioligand binding was done using bolus radiotracer injections, arterial blood sampling and determination of metabolite-corrected blood curves, and compartmental modeling to obtain estimates of binding potentials for [^{11}C]DTBZ in multiple regions of the human brain (Koeppe et al. 1996). (+)- α -[^{11}C]DTBZ is a reversibly binding radioligand also well suited for use in equilibrium

infusion applications (Koepp et al. 1997). Subsequent studies using injections of both the active and inactive stereoisomers, each in carbon-11-labeled form, provided direct evidence of very low binding of the radioligand in nontarget regions such as the cerebellum and the occipital cortex (Koepp et al. 1999), consistent with studies of immunoreactivity for VMAT2 (Tong et al. 2011) and in vitro autoradiographic studies (Scherman et al. 1988). The reproducibility of binding measures using [¹¹C]DTBZ in humans has been examined and found reliable, provided care is exercised in selecting appropriate reference regions (Chan et al. 1999).

The in vivo pharmacokinetics of the fluorine-18-labeled radiotracer ([¹⁸F] AV-133) have similarly been evaluated using a variety of analysis methods (Frey et al. 2008; Lin et al. 2011; Okamura et al. 2010). The longer half-life of this radiotracer permits a proposed use of delayed single-frame imaging protocols to estimate standard uptake value ratios as reasonable estimates of the specific binding of the radioligand (Lin et al. 2011). Kinetic analyses of the fluorine-18-labeled radioligand (Okamura et al. 2010) have provided estimates of specific binding (binding potentials, BP) that are very similar to those obtained with [¹¹C]DTBZ.

A part of the rationale for development of VMAT2 radioligands was the hypothesis that the vesicular transporter would be resistant (or less so) to regulation of total numbers (B_{\max}) in response to pharmacological treatments, a hypothesis largely but not entirely supported by studies in animals (see Sect. 27.5.2). Studies intended to perturb brain biochemistry are, of course, much harder to perform in living human subjects. The administration of amphetamine could lead to depletion of vesicular dopamine levels due to stimulant-induced release, but a low acute dose of amphetamine in human subjects was found to produce only a small (5 %) decrease in radioligand binding to the VMAT2 (Boileau et al. 2010); whether the dose of amphetamine administered was adequate to reduce vesicular dopamine levels to an extent sufficient to subsequently reduce competition for radioligand binding remains an open question. It should be noted that in animals, demonstration of such an effect of amphetamine required extensive depletion of tissue dopamine concentrations. The clinical equivalent of depletion of synaptic vesicle dopamine is the condition known as DOPA-responsive dystonia: the observation that in vivo binding of [¹¹C]DTBZ is increased in those subjects (De la Fuente-Fernandez et al. 2003a) was an indication that vesicular dopamine may compete for VMAT2 binding of radioligands. However, in both these patients and in studies of dopamine-depleted rat brains, extensive or complete neurotransmitter depletion was accomplished, and the sensitivity of VMAT2 radioligand binding to smaller changes in dopamine levels remains to be fully determined. The potential effects of increased endogenous dopamine levels affecting human [¹¹C]DTBZ studies has been examined through acute administration of L-DOPA to subjects with advanced Parkinson's disease (De la Fuente-Fernandez et al. 2009), where significant decreases in radioligand binding in caudate and putamen were proposed to be due to the increases in vesicular dopamine. Taken together, the animal and human studies involving manipulations of endogenous dopamine levels suggest that care should be taken to account for use of L-DOPA, or other dopamine-modifying drugs, when performing studies with VMAT2 radioligands.

27.6.2 Aging

As numerous of the potential applications of VMAT2 imaging involve neurodegenerative disease occurring in elderly populations (e.g., PD, AD), an understanding of the possible age-related decline in radioligand binding is a necessity, and this has been examined with inconsistent results; studies have shown both no decline of VMAT2 radioligand binding with age (Troiano et al. 2010) as well as a small but steady decrease (0.5–0.77 %/year: Frey et al. 1996; Bohnen et al. 2006). The potential of age-related effects on radioligand binding remains in question, and for that reason well-designed studies of VMAT2 changes in disease require the inclusion of age-matched control subjects.

27.6.3 Parkinson's Disease

By far, the single largest application of VMAT2 radioligand imaging has been in Parkinson's disease, with more than a dozen published studies involving over 450 patients total. Overall the studies have been quite consistent, showing losses of VMAT2 radioligand binding in the basal ganglia in PD with observations of a gradient (losses in posterior putamen before the caudate nucleus and ventral striatum/nucleus accumbens), often a unilateral initiation and development of more severe losses, a correlation with some but not all clinical signs, significant losses of radioligand binding in the presymptomatic phase, and essentially complete loss of binding sites throughout the basal ganglia in severe disease (Adams et al. 2005; Bohnen et al. 2006; Chou et al. 2011; De La Fuente-Fernandez et al. 2003b, 2009, 2011; Frey et al. 1996; Kumar et al. 2003; Lee et al. 2000, 2004; Lin et al. 2011; Martin et al. 2008; Nandhagopal et al. 2011; Okamura et al. 2010; Troiano et al. 2010).

Several studies have examined particular subsets of patients to probe different aspects of the disease. Martin et al. (2008) examined VMAT2 binding in a cohort of early, untreated PD patients and demonstrated that even in these subjects there was a significant loss (>50 %) of VMAT2 binding sites particularly in the putamen; a significant loss of DTBZ binding in the clinically unaffected side of PD patients has also been reported (Bohnen et al. 2006). In studies of unilateral Parkinsonism, the greater decrease of DTBZ binding on the more clinically affected side correlated with responsiveness to L-DOPA treatment (Kumar et al. 2003). A study of both the VMAT2 and the DAT in controls vs. Parkinson's disease with dyskinesias showed no significant differences of DTBZ binding between groups, but a difference in the ratio of dopamine transporter (DAT) to VMAT2 radioligand binding in the putamen, with ratios being significantly lower in the group having dyskinesias. The comparison of VMAT2 radioligand binding measurements with matched studies of the dopamine neuronal membrane transporter (DAT) and 6-[¹⁸F]fluoroDOPA uptake in a large cohort of Parkinson's disease patients (De La Fuente-Fernandez et al. 2011) provided evidence that younger-onset subjects had better compensatory mechanisms operating to maintain the biochemical balance of the dopaminergic system as compared to late-onset PD patients. A longitudinal multi-tracer study of PD patients

provided evidence for compensatory upregulation of the DAT radioligand binding and 6- ^{18}F fluoroDOPA uptake in earlier stages of the disease but that compensatory mechanisms decline with advanced neuronal losses as shown by extensive losses of ^{11}C DTBZ binding (Nandhagopal et al. 2011). The numerous studies that have now compared multiple presynaptic radiotracers have clearly demonstrated differential rates and extents of losses between the measures of the VMAT2, the DAT, and dopamine synthesis (^{18}F fluoroDOPA uptake), with some study authors suggesting that in vivo measures of the VMAT2 binding may be the least regulated by compensatory changes (Lee et al. 2000).

27.6.4 Non-Parkinson Movement Disorders

Losses of in vivo VMAT2 radioligand binding have been observed in studies of less common neurodegenerative movement disorders (progressive supranuclear palsy (PSP), multiple system atrophy (MSA), and olivopontocerebellar atrophy (OPCA)) that share traits with idiopathic parkinsonism but express additional clinical symptoms. Involvement of the basal ganglia is generally observed, but the pattern of VMAT2 radioligand binding changes are different: for example, whereas in idiopathic Parkinson's disease losses are earlier and more predominant in the posterior putamen, in PSP there was observed a more uniform involvement of both the caudate and the putamen (Raffel et al. 2006). Similarly, VMAT2 radioligand binding is altered in MSA, OPCA, and other degenerative diseases involving monoaminergic nerve terminals of the basal ganglia (Gilman et al. 1996, 2003).

27.6.5 Huntington's Disease

Huntington's disease (HD) is characterized by significant neuronal loss and atrophy in the caudate nucleus and putamen. A single study of ^{11}C DTBZ binding in HD subjects showed reductions in total radioligand binding in caudate nucleus and anterior and posterior putamen, with losses most prominent in the posterior putamen (Bohnen et al. 2000). Within the study group, individuals with the akinetic-rigid phenotype (ADr) showed more significant losses of total radioligand binding than the subgroup with the chorea phenotype (HDc).

27.6.6 Dementia

The underlying biochemical changes in different clinical manifestations of dementia (Alzheimer's disease (AD), Parkinson's disease with dementia (PDD), and Lewy body disease (LBD)) do not uniformly involve the same degenerative pathways. In Alzheimer's disease the striatal monoaminergic innervation is generally intact and no losses of in vivo VMAT2 radioligand binding reported (Gilman et al. 2004; Koeppe et al. 2008). In contrast, the basal ganglia is significantly affected in

dementia with Lewy bodies, with losses of radioligand binding clearly evident throughout the caudate nucleus and putamen; use of imaging techniques to clearly identify LBD vs. AD patients (Koeppel et al. 2008; Villemagne et al. 2011, 2012) has clinical impact, as LBD patients are subject to adverse reactions from dopaminergic treatments that might otherwise be useful for treatment of hallucinations or behavioral disturbances in AD patients. Finally, Parkinson's disease with dementia patients show the expected significant losses of striatal VMAT2 radioligand binding (Koeppel et al. 2008); the dementia is proposed to be associated with concurrent changes in the cholinergic system, which can sometimes be demonstrated by separate imaging studies with radiotracers for that neurotransmitter system (Bohnen and Albin 2011; Bohnen and Frey 2007). The combination of [^{11}C]DTBZ imaging studies with PET imaging of amyloid deposits using such radioligands as [^{11}C]PIB provides a method for classifications of dementia subjects which may not always agree with consensus clinical evaluations (Burke et al. 2011).

27.6.7 Psychiatric Disease

A few studies have been completed looking at VMAT2 radioligand binding in schizophrenia and bipolar disorder type I. In schizophrenia, no differences in striatal or thalamic binding of VMAT2 radioligands was observed, but small increases in binding in the ventral brainstem of schizophrenics were observed relative to controls (Taylor et al. 2000; Zubietta et al. 2001). The importance of that observation is difficult to ascribe to any single neurotransmitter system, as that portion of the brain has cell bodies and projections for both serotonergic and dopaminergic neurons. For the bipolar disorder type I group, increases of VMAT2 binding in the thalamus relative to controls can at least be proposed not to be due to changes in dopaminergic innervation, which is very low in that brain region, but to changes in the serotonergic and noradrenergic innervation (Zubietta et al. 2000).

The *in vivo* binding of VMAT2 radioligands has also been examined in Tourette's syndrome, with inconsistent results have been obtained, and the discrepant observations of both no changes (Albin et al. 2009) and increased [^{11}C]DTBZ binding (Albin et al. 2003) attributed to the heterogeneity of Tourette's syndrome patient populations.

27.6.8 Drug Abuse

As many drugs which are abused are known to interact with the monoaminergic systems of the brain (e.g., amphetamine, methamphetamine, cocaine), the effects of such drug use on the *in vivo* binding of VMAT2 radioligands to monoaminergic terminals have been examined, with particular interest in the potential neurotoxic effects on monoaminergic terminals. A postmortem study of chronic cocaine users demonstrated a modest (-17 to -22%) decrease in VMAT2 radioligand binding (Wilson et al. 1996a, b), a result different from that found by the same research group in a rat

model (Wilson and Kish 1996). In a study of recently abstinent cocaine users, reduced VMAT2 binding was shown in several striatal regions, suggesting either a compensatory downregulation of VMAT2 storage systems after drug use or a loss of dopaminergic terminals (Narendran et al. 2012); which of these is occurring and the clinical impact need further study. The effects of methamphetamine on striatal VMAT2 radioligand binding has been examined both in vitro and in vivo with conflicting results. In active methamphetamine users, postmortem in vitro studies showed no changes in striatal VMAT2 binding, suggesting little if any toxicity of chronic methamphetamine use to dopaminergic terminals (Wilson et al. 1996a, b). Studies of in vivo radioligand binding in abstinent methamphetamine users have shown small decreases in striatal binding of both VMAT2 (−10 %) and DAT (−15 %) radioligands (Johanson et al. 2006), a finding consistent with observations of striatal neuronal toxicity for methamphetamine in animals (Frey et al. 1997) but possibly not severe enough to produce clinical symptoms. In contrast, studies of recently abstinent methamphetamine users demonstrated an unexpected increase in VMAT2 radioligand binding (Boileau et al. 2008). This latter finding was proposed to possibly reflect sensitivity of the radioligand method to endogenous levels of dopamine in the vesicles, which might be significantly altered in the chronic drug users. The effects of drugs of abuse such as the amphetamines are thus poorly understood as to their potential neurotoxicity.

Conclusions

In contrast to the development of radiopharmaceuticals for in vivo PET imaging of most other biochemical targets, where multiple competing radioligands have been synthesized and advanced through to human studies (e.g., dopamine receptors, amyloid imaging), the development of an in vivo imaging radiotracer for the VMAT2 has been focused on derivatives of a single basic structure, that of tetrabenazine. The currently available radiotracers, (+)- α -[¹¹C]DTBZ and [¹⁸F]AV-133, present very favorable characteristics: good brain permeability, reversible kinetics, lack of interfering metabolites, well-known pharmacology, acceptable radiation dosimetry, and simple radiochemical preparation. In vivo human imaging of the vesicular monoamine transporter 2 (VMAT2) has now been pursued for two decades, and it can be expected that VMAT2 radiotracer studies will continue to be useful in studies of diseases involving changes of monoaminergic neuronal densities in the brain.

Acknowledgements The author would like to acknowledge the efforts of a large number of individuals at the University of Michigan and University of Pennsylvania who participated in the development of VMAT2 radioligands for human PET studies and in particular the advice, support, encouragement, and cooperation of Drs. Kirk Frey, Robert Koeppe, David Kuhl, and Hank Kung. This work was supported by a grant from the National Institutes of Health NS-15655.

References

- Adams JR, van Netten H, Schulzer M et al (2005) PET in LRRK2 mutations: comparison to sporadic Parkinson's disease and evidence for presymptomatic compensation. *Brain* 128:2777–2785

- Albin RA, Koeppe RA, Bohnen NI et al (2003) Increased ventral striatal monoaminergic innervation in Tourette syndrome. *Neurology* 61:310–315
- Albin RL, Koeppe RA, Wernette K et al (2009) Striatal [¹¹C]dihydrotrabenzazine and [¹¹C]methylphenidate binding in Tourette syndrome. *Neurology* 72:1390–1396
- Amarasinghe K, Rishel M, Dinn, S et al (2009) Fluorinated dihydrotrabenzazine ether imaging agents and probes. World Patent WO 2009/05520 A2
- Blesa J, Juri C, Collantes M et al (2010) Progression of dopaminergic depletion in a model of MPTP-induced Parkinsonism in non-human primates. An ¹⁸F-DOPA and ¹¹C-DTBZ study. *Neurobiol Dis* 38:456–463
- Bohnen NI, Albin RL (2011) The cholinergic system and Parkinson's disease. *Behav Brain Res* 221:564–573
- Bohnen NI, Frey KA (2007) Imaging of cholinergic and monoaminergic neurochemical changes in neurodegenerative disorders. *Mol Imaging Biol* 9:243–257
- Bohnen NI, Koeppe RA, Mayer P et al (2000) Decreased striatal monoaminergic terminals in Huntington's disease. *Neurology* 54:1753–1759
- Bohnen NI, Albin RL, Koeppe RA et al (2006) Positron emission tomography of monoaminergic vesicular binding in aging and Parkinson's disease. *J Cereb Blood Flow Metab* 26:1198–1212
- Boileau I, Rusjan P, Houle S et al (2008) Increased vesicular monoamine transporter binding during early abstinence in human methamphetamine users: is VMAT2 a stable dopamine neuron marker? *J Neurosci* 28:9850–9856
- Boileau I, Houle S, Rusjan PM et al (2010) Influence of a low dose of amphetamine on vesicular monoamine transporter binding: a PET (+)[¹¹C]DTBZ study in humans. *Synapse* 64:417–420
- Boldt KG, Brine GA, Rehder K (2008) Synthesis of (+)-9-O-desmethyl-dihydrotrabenzazine, precursor for the high affinity VMAT2 imaging PET radioligand [¹¹C]-(+)-dihydrotrabenzazine. *Org Prep Proc Int* 40:379–384
- Brooks DJ, Pavese N (2011) Imaging biomarkers in Parkinson's disease. *Prog Neurobiol* 95:614–628
- Burke JF, Albin RL, Koeppe RA et al (2011) Assessment of mild dementia with amyloid and dopamine terminal positron emission tomography. *Brain* 134:1647–1657
- Chan GLY, Holden JE, Stoessl AJ et al (1999) Reproducibility studies with ¹¹C-DTBZ, a monoamine vesicular transporter inhibitor, in healthy human subjects. *J Nucl Med* 40:283–289
- Chao K-T, Tsao H-H, Weng Y-H et al (2012) Quantitative analysis of binding sites for 9-fluoropropyl-(+)-dihydrotrabenzazine ([¹⁸F]AV-133) in a MPTP-lesioned PD mouse model. *Synapse* 66:823–831
- Chen MK, Kuwabara H, Zhou Y et al (2008) VMAT2 and dopamine neuron loss in a primate model of Parkinson's disease. *J Neurochem* 105:78–90
- Chou KL, Koeppe RA, Bohnen NI (2011) Rhinorrhea: a common nondopaminergic feature of Parkinson's disease. *Mov Dis* 26:320–323
- Darchen F, Scherman D, Laduron PM et al (1988) Ketanserin binds to the monoamine transporter of chromaffin granules and of synaptic vesicles. *Mol Pharmacol* 33:672–677
- Darchen F, Masuo Y, Vial M et al (1989) Quantitative autoradiography of the rat brain vesicular monoamine transporter using the binding of [³H]dihydrotrabenzazine and 7-amino-8-[¹²⁵I]iodoketanserin. *Neuroscience* 33:4341–4349
- DaSilva JN, Kilbourn MR (1992) In vivo binding of [¹¹C]trabenzazine to vesicular monoamine transporters in mouse brain. *Life Sci* 51:593–600
- DaSilva JN, Kilbourn MR, Domino EF (1993a) In vivo imaging of monoaminergic nerve terminals in normal and MPTP-lesioned primate brain using positron emission tomography (PET) and [¹¹C]trabenzazine. *Synapse* 14:128–131
- DaSilva JN, Kilbourn MR, Mangner TJ (1993b) Synthesis of [¹¹C]trabenzazine, a vesicular monoamine uptake inhibitor, for PET imaging studies. *Appl Radiat Isot* 44:673–676
- DaSilva JN, Kilbourn MR, Mangner TJ (1993c) Synthesis of a [¹¹C]methoxy derivative of α -dihydrotrabenzazine: a radioligand for studying the vesicular monoamine transporter. *Appl Radiat Isot* 44:1487–1489
- De la Fuente-Fernandez R, Furtado S, Guttman M et al (2003a) VMAT2 binding is elevated in Dopa-responsive dystonia: visualizing empty vesicles by PET. *Synapse* 49:20–28

- De la Fuente-Fernandez R, Lim AS, Sossi V et al (2003b) Age and severity of nigrostriatal damage at onset of Parkinson's disease. *Synapse* 47:152–158
- De la Fuente-Fernandez R, Sossi V, McCormick S et al (2009) Visualizing vesicular dopamine dynamics in Parkinson's disease. *Synapse* 63:713–716
- De la Fuente-Fernandez R, Schulzer M, Kuramoto L et al (2011) Age-specific progression of nigrostriatal dysfunction in Parkinson's disease. *Ann Neurol* 69:803–810
- Doudet DJ, Rosa-Neto P, Munk OL et al (2006) Effect of age on markers for monoaminergic neurons of normal and MPTP-lesioned rhesus monkeys: a multitracer PET study. *Neuroimage* 30:26–35
- Eiden LE, Schafer MK-H, Weihe E et al (2004) The vesicular amine transporter family (SLC18): amine/proton antiporters required for vesicular accumulation and regulated exocytotic secretion of monoamines and acetylcholine. *Pflugers Arch* 447:636–640
- Fantegrossi WE, Woolverton WL, Kilbourn M et al (2004) Behavioral and neurochemical consequences of long-term intravenous self-administration of MDMA and its enantiomers by rhesus monkeys. *Neuropsychopharmacology* 29:1270–1281
- Frey KA, Koeppe RA, Kilbourn MR et al (1996) Presynaptic monoamine vesicles in Parkinson's disease and normal aging. *Ann Neurol* 40:873–884
- Frey K, Kilbourn M, Robinson T (1997) Reduced striatal vesicular monoamine transporters after neurotoxic but not after behaviorally-sensitizing doses of methamphetamine. *Eur J Pharmacol* 334:273–279
- Frey KA, Koeppe RA, Kilbourn MR et al (2008) Imaging VMAT2 in Parkinson's disease with [F-18]AV-133. *J Nucl Med* 49:5P
- Gasnier B (2004) The SLC32 transporter, a key protein for the synaptic release of inhibitory amino acids. *Pflugers Arch* 447:756–759
- Gilman S, Frey KA, Koeppe RA et al (1996) Decreased striatal monoaminergic terminals in olivopontocerebellar atrophy and multiple system atrophy demonstrated with positron emission tomography. *Ann Neurol* 40:885–892
- Gilman S, Koeppe RA, Chervin RD et al (2003) REM sleep behavior disorder is related to striatal monoaminergic deficit in MSA. *Neurology* 61:29–34
- Gilman S, Koeppe RA, Little R et al (2004) Striatal monoamine terminals in Lewy body dementia and Alzheimer's disease. *Ann Neurol* 55:774–780
- Gonzalez AM, Walther D, Pazos A et al (1994) Synaptic vesicular monoamine transporter expression: distribution and pharmacologic profile. *Mol Brain Res* 22:219–226
- Goswami R, Kung M-P, Ponde D et al (2006) Fluoroalkyl derivatives of dihydrotetrabenazine as PET imaging agents targeting vesicular monoamine transporters. *Nucl Med Biol* 33:685–694
- Hostetler ED, Patel S, Guenther I et al (2007) Characterization of a novel F-18 labeled radioligand for VMAT2. *J Label Compd Radiopharm* 50:S330
- Johanson C-E, Frey KA, Lundahl LH et al (2006) Cognitive function and nigrostriatal markers in abstinent methamphetamine abusers. *Psychopharmacology (Berl)* 185:327–338
- Jewett DM, Kilbourn MR, Lee LC (1997) A simple synthesis of [¹¹C]dihydrotetrabenazine. *Nucl Med Biol* 24:197–199
- Kankanamalage K, Amarasinghe D, Rishel M et al (2009) Fluorinated dihydrotetrabenazine ether imaging agents and probes. US Patent 2009/0110636 A1
- Kemmerer ES, Desmond TJ, Albin RL et al (2003) Treatment effects on nigrostriatal projection integrity in partial 6-OHDA lesions: comparison of L-DOPA and pramipexole. *Exp Neurol* 183:81–86
- Kilbourn M, Sherman P (1997) In vivo binding of (+)- α -[³H]dihydrotetrabenazine to the vesicular monoamine transporter of rat brain: bolus vs. equilibrium studies. *Eur J Pharmacol* 331:161–168
- Kilbourn MR, DaSilva JN, Frey KA et al (1993) In vivo imaging of vesicular monoamine transporters in human brain using [¹¹C]tetrabenazine and positron emission tomography. *J Neurochem* 60:2315–2318

- Kilbourn MR, Sherman PS, Abbott LC (1995a) Mutant mouse strains as models for in vivo radiotracer evaluations: [^{11}C]methoxytetraabenazines ([^{11}C]MTBZ) in tottering mice. *Nucl Med Biol* 22:565–567
- Kilbourn MR, Lee L, Vander Borgh T et al (1995b) Binding of α -dihydrotetraabenazine to the vesicular monoamine transporter is stereospecific. *Eur J Pharmacol* 278:249–252
- Kilbourn MR, Frey KA, Vander Borgh T et al (1996) Effects of dopaminergic drug treatments on in vivo radioligand binding to brain vesicular monoamine transporters. *Nucl Med Biol* 23:467–471
- Kilbourn MR, Lee LC, Jewett DM et al (1997) The absolute configuration of (+)- α -dihydrotetraabenazine, an active metabolite of tetraabenazine. *Chirality* 9:59–62
- Kilbourn MR, Kuszpit K, Sherman P et al (2000) Rapid and differential losses of in vivo dopamine transporter (DAT) and vesicular monoamine transporter (VMAT2) radioligand binding in MPTP-treated mice. *Synapse* 35:250–255
- Kilbourn MR, Hockley B, Lee L et al (2007) Pharmacokinetics of [^{18}F]fluoroalkyl derivatives of dihydrotetraabenazine (DTBZ) in rat and monkey brain. *Nucl Med Biol* 34:233–237
- Kilbourn MR, Butch ER, Desmond T et al (2008) Dopamine depletion increases in vivo [^{11}C]DTBZ binding in awake rat brain. *Neuroimage* 41(Suppl 2):T54
- Kilbourn MR, Butch ER, Desmond T et al (2010) Dopamine depletion increases in vivo [^{11}C]dihydrotetraabenazine ([^{11}C]DTBZ) binding in rat striatum. *Nucl Med Biol* 37:3–8
- Koeppel RA, Frey KA, Vander Borgh TM et al (1996) Kinetic evaluation of [^{11}C]dihydrotetraabenazine by dynamic PET: measurement of the vesicular monoamine transporter. *J Cereb Blood Flow Metab* 16:1288–1299
- Koeppel RA, Frey KA, Kume A et al (1997) Equilibrium versus compartmental analysis for assessment of the vesicular monoamine transporter using (+)- α -[^{11}C]dihydrotetraabenazine (DTBZ) and PET. *J Cereb Blood Flow Metab* 17:919–931
- Koeppel RA, Frey KA, Kuhl DE et al (1999) Assessment of extrastriatal vesicular monoamine transporter binding site density using stereoisomers of [^{11}C]dihydrotetraabenazine. *J Cereb Blood Flow Metab* 19:1376–1384
- Koeppel RA, Gilman S, Junck L et al (2008) Differentiating Alzheimer's disease from dementia with Lewy bodies and Parkinson's disease with (+)-[^{11}C]dihydrotetraabenazine positron emission tomography. *Alzheimers Dement* 4:S67–S76
- Kumar A, Mann S, Sossi V et al (2003) [^{11}C]DTBZ-PET correlates of levodopa responses in asymmetric Parkinson's disease. *Brain* 126:2648–2655
- Kuhl DE, Koeppel RA, Fessler JA et al (1994) In vivo mapping of cholinergic neurons in the human brain using SPECT and IBVM. *J Nucl Med* 35:405–410
- Kung M-P, Canney DJ, Frederick D et al (1994) Binding of [^{125}I]iodovinyltetraabenazine to CNS vesicular monoamine transport sites. *Synapse* 18:225–232
- Kung M-P, Hou C, Goswami R et al (2007) Characterization of optically resolved 9-fluoropropyl-dihydrotetraabenazine as a potential PET imaging agent targeting vesicular monoamine transporters. *Nucl Med Biol* 34:239–246
- Kung M-P, Lieberman BP, Zhuang Z-P et al (2008) In vivo imaging of vesicular monoamine transporter 2 in pancreas using an [^{18}F] epoxide derivative of tetraabenazine. *Nucl Med Biol* 35:825–837
- Lee CS, Samii A, Sossi V et al (2000) In vivo positron emission tomographic evidence for compensatory changes in synaptic dopaminergic nerve terminals in Parkinson's disease. *Ann Neurol* 47:493–503
- Lee CS, Schulzer M, de la Fuente-Fernandez R et al (2004) Lack of regional selectivity during the progression of Parkinson disease. *Arch Neurol* 61:1920–1925
- Lee LC, Vander Borgh T, Sherman PS, Frey KA, Kilbourn MR (1996) In vitro and in vivo studies of benzoisoquinoline ligands for the brain synaptic vesicle monoamine transporter. *J Med Chem* 39:191–196
- Lin K-J, Lin W-Y, Hsieh C-J et al (2011) Optimal scanning time window for [^{18}F -FP-(+)-DTBZ (^{18}F -AV-133)] summed uptake measurements. *Nucl Med Biol* 38:1149–1155

- Martin W, Wieler M, Stoessl AJ et al (2008) Dihydrotetraabenazine positron emission tomography imaging in early, untreated Parkinson's disease. *Ann Neurol* 63:388–394
- Mehvar R, Jamali F, Watson MWB et al (1987) Pharmacokinetics of tetraabenazine and its major metabolite in man and rat. *Drug Metab Dispos* 12:250–255
- Miller GW, Erickson JD, Perez JT et al (1998) Immunochemical analysis of vesicular monoamine transporter (VMAT2) protein in Parkinson's disease. *Exp Neurol* 156:138–148
- Miller GW, Wang YM, Gainetdinov RR et al (2001) Dopamine transporter and vesicular monoamine transporter knockout mice: implications for Parkinson's disease. *Methods Mol Med* 62:179–190
- Nandhagopal R, Kuramoto L, Schulzer M et al (2011) Longitudinal evolution of compensatory changes in striatal dopamine processing in Parkinson's disease. *Brain* 134:3290–3298
- Naudon L, Leroux-Nicollet I, Raisman-Vozari R et al (1995) Time course of modifications elicited by reserpine on the density and mRNA synthesis of the vesicular monoamine transporter, and on the density of the membrane dopamine uptake complex. *Synapse* 21:29–36
- Narendran R, Lopresti BJ, Martinez D et al (2012) In vivo evidence for low striatal vesicular monoamine transporter 2 (VMAT2) availability in cocaine abusers. *Am J Psychiatry* 169:55–63
- Okamura N, Villemagne VL, Drago J et al (2010) In vivo measurement of vesicular monoamine transporter type 2 density in Parkinson disease with (18)F-AV-133. *J Nucl Med* 51:223–228
- Omote H, Miyaji T, Juge N et al (2011) Vesicular neurotransmitter transporter: bioenergetics and regulation of glutamate transport. *Biochemistry* 50:5558–5565
- Quinn GP, Shore PA, Brodie BB (1959) Biochemical and pharmacological studies of RO 1–9568 (Tetraabenazine), a non-indole tranquilizing agent with reserpine-like effects. *J Pharmacol Exp Ther* 127:103–109
- Paek S-M, Kim N-J, Shin D et al (2010) A concise total synthesis of (+)-tetraabenazine and (+)- α -dihydrotetraabenazine. *Chem Eur J* 16:4623–4628
- Petrou M, Koeppel R, Scott P et al (2012) PET imaging of the vesicular acetylcholine transporter. *J Nucl Med* 53:290
- Raffel DM, Koeppel RA, Little R et al (2006) PET measurement of cardiac and nigrostriatal denervation in Parkinsonian syndromes. *J Nucl Med* 47:1769–1777
- Rhee S-W, Ryan KJ, Tanga MJ (2011) Synthesis of ^3H -labeled tetraabenazine. *J Label Compd Radiopharm* 54:367–370
- Ricuarte GA, Mechan AO, Yuan J et al (2005) Amphetamine treatment similar to that used in the treatment of adult attention-deficit/hyperactivity disorder damages dopaminergic nerve endings in striatum of adult nonhuman primates. *J Pharmacol Exp Ther* 315:91–98
- Rishel MJ, Amarasinghe KKD, Dinn SR et al (2009a) Asymmetric synthesis of tetraabenazine and dihydrotetraabenazine. *J Org Chem* 74:4001–4004
- Rishel MJ, Johnson BF, Kankanamalage K et al (2009b) Alpha-fluoroalkyl dihydrotetraabenazine imaging agents and probes. US Patent 2009/0142276 A1
- Scherman D, Jaudon P, Henry JP (1981) Binding of a tetraabenazine derivative to the monoamine transporter of the chromaffin granule membrane. *C R Seances Acad Sci III* 293:221–224
- Scherman D, Raisman R, Ploska A et al (1988) [^3H]Dihydrotetraabenazine, a new in vitro monoaminergic probe for human brain. *J Neurochem* 50:1131–1136
- Scherman D, Desnos C, Darchen F et al (1989) Striatal dopamine deficiency in Parkinson's disease: role of aging. *Ann Neurol* 26:551–557
- Schwartz K, Nachman R, Yossifoff M et al (2006) Cocaine, but not amphetamine, short term treatment elevates the density of rat brain vesicular monoamine transporter 2. *J Neural Transm* 114:427–430
- Sievert MK, Hajipour AR, Ruoho AE (2007) Specific derivatization of the vesicular monoamine transporter with novel carrier-free radioiodinated reserpine and tetraabenazine photoaffinity labels. *Anal Biochem* 367:68–78
- Sossi V, Dinelle K, Topping GJ (2009) Dopamine transporter relation to levodopa-derived synaptic dopamine in a rat model of Parkinson's: an in vivo imaging study. *J Neurochem* 109:85–92

- Sossi V, Dinelle K, Schulzer M (2010) Levodopa and pramipexole effects on presynaptic dopamine PET markers and estimated dopamine release. *Eur J Nucl Med Mol Imaging* 37:2364–2370
- Taylor SF, Koeppe RA, Tandon R et al (2000) In vivo measurement of the vesicular monoamine transporter in schizophrenia. *Neuropsychopharmacology* 23:667–675
- Thompson CM, Davis E, Carrigan CN et al (2005) Inhibitor of the glutamate vesicular transporter (VGLUT). *Curr Med Chem* 12:2041–2056
- Tian L, Karimi M, Loftin SK et al (2012) No differential regulation of dopamine transporter (DAT) and vesicular monoamine transporter 2 (VMAT2) binding in a primate model of Parkinson's disease. *PLoS one* 7(2):e31439
- Tong J, Wilson AA, Boileau I et al (2008) Dopamine modulating drugs influence striatal (+)-[¹¹C]DTBZ binding in rats: VMAT2 binding is sensitive to changes in vesicular dopamine concentration. *Synapse* 62:873–876
- Tong J, Boileau I, Furakawa Y et al (2011) Distribution of vesicular monoamine transporter 2 protein in human brain; implications for brain imaging studies. *J Cereb Blood Flow Metab* 31:2065–2075
- Tridgett R, Turtle R, Johnston G (2012) Dihydropyridazines and pharmaceutical compositions containing them. US Patent 2008/0108645 A1
- Troiano AR, Schulzer M, De La Fuente-Fernandez R et al (2010) Dopamine transporter PET in normal aging: dopamine transporter decline and its possible role in preservation of motor function. *Synapse* 64:146–151
- Tsao H-H, Lin K-J, Juang J-H et al (2010) Binding characteristics of 9-fluoropropyl-(+)-dihydro-tetabenazine (AV-133) to the vesicular transporter type 2 in rats. *Nucl Med Biol* 37:413–419
- Vander Borght TM, Kilbourn MR, Desmond TJ et al (1995a) The vesicular monoamine transporter is not regulated by dopaminergic drug treatments. *Eur J Pharmacol* 294:577–583
- Vander Borght TM, Kilbourn MR, Koeppe RA et al (1995b) In vivo imaging of the brain vesicular monoamine transporter. *J Nucl Med* 36:2252–2260
- Vander Borght TM, Sima AAF, Kilbourn MR et al (1995c) [³H]Methoxytetabenazine: a high specific activity ligand for estimating monoaminergic neuronal integrity. *Neuroscience* 68:955–962
- Varone A, Jahan M, Toth M et al (2012) PET imaging of VMAT2 with the novel radioligand [¹⁸F]FE-DTBZ-d4 in non human primates: comparison with [¹¹C]DTBZ and [¹⁸F]FE-DTBZ. *J Cereb Blood Flow Metab* 32(suppl 1):S113–S114
- Villemagne VL, Okamura N, Pejoska S et al (2011) In vivo assessment of vesicular monoamine transporter type 2 in dementia with lewy bodies and Alzheimer disease. *Arch Neurol* 68:905–912
- Villemagne VL, Okamura N, Pejoska S et al (2012) Differential diagnosis in Alzheimer's disease and dementia with Lewy bodies via VMAT2 and amyloid imaging. *Neurodegener Dis* 10:161–165
- Vilpoux C, Leroux-Nicollet I, Naudon L et al (2000) Reserpine or chronic paroxetine treatments do not modify the vesicular monoamine transporter 2 expression in serotonin-containing regions of the rat brain. *Neuropharmacology* 39:1075–1082
- Wilson JM, Kish SJ (1996) The vesicular monoamine transporter, in contrast to the dopamine transporter, is not altered by chronic cocaine self-administration in the rat. *J Neurosci* 16:3507–3510
- Wilson JM, Kalasinsky KS, Levey AI et al (1996a) Striatal dopamine nerve terminal markers in human, chronic methamphetamine users. *Nat Med* 2:699–703
- Wilson JM, Levey AI, Bergeron C et al (1996b) Striatal dopamine, dopamine transporter, and vesicular monoamine transporter in chronic cocaine users. *Ann Neurol* 40:428–439
- Wimalasena K (2010) Vesicular monoamine transporters: structure-function, pharmacology, and medicinal chemistry. *Med Res Rev* 31:483–519
- Yao Z, Wei X, Wu X et al (2011) Preparation and evaluation of tetabenazine enantiomers and all eight stereoisomers of dihydropyridazines as VMAT2 inhibitors. *Eur J Med Chem* 46:1841–1848

- Yu Q, Luo W, Deschamps J, Holloway HW et al (2010) Preparation and characterization of tetra-benzazine enantiomers against vesicular monoamine transporter 2. *ACS Med Chem Lett* 1:105–109
- Zheng G, Dwoskin LP, Deaciuc AG et al (2005) Lobelane analogues as novel ligands for the vesicular monoamine transporter-2. *Bioorg Med Chem* 13:3899–3909
- Zheng P, Lieberman BP, Choi SR et al (2011) Synthesis and biological evaluation of 3-alkyl-dihydro-tetra-benzazine derivatives as vesicular monoamine transporter-2 (VMAT2) ligands. *Bioorg Med Chem Lett* 21:3435–3438
- Zhu L, Liu J, Kung HF (2009) Synthesis and evaluation of 2-amino-dihydro-tetra-benzazine derivatives as probes for imaging vesicular monoamine transporter-2. *Bioorg Med Chem Lett* 19:5026–5028
- Zimmer L, Luxen A (2012) PET radiotracers for molecular imaging in the brain: past, present and future. *Neuroimage* 61:363–370
- Zubieta J-K, Huguleit P, Ohl LE et al (2000) High vesicular monoamine transporter binding in asymptomatic bipolar I disorder: sex differences and cognitive correlates. *Am J Psychiatry* 157:1619–1628
- Zubieta J-K, Taylor SF, Huguleit P et al (2001) Vesicular monoamine transporter concentrations in bipolar disorder type I, schizophrenia, and healthy subjects. *Biol Psychiatry* 49:110–116

The Editors

Prof. Dr. Rudi A.J.O. Dierckx

Board-certified in Neuropsychiatry and Nuclear Medicine

Affiliations:

Nuclear Medicine and Molecular Imaging, University Medical Center Groningen, University of Groningen. Hanzeplein 1, 9713GZ Groningen, Netherlands. E-mail: r.a.dierckx@umcg.nl

Nuclear Medicine, University Hospital Gent, University of Gent, De Pintelaan 185, 9000 Gent, Belgium

Research fields:

Broad interest in nuclear medicine, focus on neuroscience and oncology

- SPECT/conventional nuclear medicine
- PET: research and clinical applications
- Development of novel radiotracers
- Rodent models of human disease
- Medical physics
- Quality, ethics, and economics

Prof. Dr. Andreas Otte

Board-certified in Nuclear Medicine

Affiliation:

Biomedical Engineering, Faculty of Electrical Engineering and Information Technology, University of Applied Sciences Offenburg, Badstr. 24, D-77652 Offenburg, Germany, E-mail: andreas.otte@hs-offenburg.de

Research fields:

Focus on neurosciences and functional biomedical imaging

- Research in neurosciences includes functional neuroimaging of various indications (e.g., traumatic brain injury, whiplash syndrome, Alzheimer's disease). In addition, there is a special focus on deep brain stimulation.
- Research in biomedical imaging ranges from opening new applications to optimizing image reconstruction. This comprises, e.g., sonography, statistical parametric mapping, nuclear medicine, or radiological imaging instruments (SPECT, PET; PET/CT, MR/PET; DSA, CT, MRT).

Dr. Erik F.J. de Vries

Radiochemist

Affiliation:

Nuclear Medicine and Molecular Imaging, University Medical Center Groningen, University of Groningen. Hanzeplein 1, 9713GZ Groningen, Netherlands. E-mail: e.f.j.de.vries@umcg.nl

Research fields:

Focus on the development and application of radiopharmaceuticals for PET imaging of inflammation and hormone receptors

- Monitoring of immune cell activation and migration
- Inflammation and related events in psychiatric and neurodegenerative disorders
- Visualization of the gut-immune-brain interaction
- Treatment-induced immune response in tumors
- Steroid hormone receptor expression in tumors and the brain

Dr. Aren van Waarde

Biologist

Affiliation:

Nuclear Medicine and Molecular Imaging, University Medical Center Groningen, University of Groningen. Hanzeplein 1, 9713GZ Groningen, Netherlands. E-mail: a.van.waarde@umcg.nl

Research fields:

Focus on small animal imaging

- Development of techniques for quantification of neuroreceptors in the living brain (adenosine A1 and A2A receptors, beta-adrenoceptors, serotonin-1A and 2A receptors, sigma-1 receptor)
- Development of targeted imaging probes for early in vivo diagnosis of cancer and evaluation of tumor response to therapy (ABC transporter substrates, matrix metalloproteinase inhibitors, sigma receptor ligands)

Guest Editor

Prof. Dr. Paul G.M. Luiten

Neurobiologist

Affiliation:

Department of Molecular Neurobiology, Faculty of Mathematics and Natural Sciences, Nijenborgh 7, 9747 AG Groningen, and Department of Biological Psychiatry, University Medical Center Groningen, University of Groningen, Hanzeplein 1, 9713 GZ Groningen, Netherlands. E-mail: p.g.m.luiten@rug.nl

Research fields:

- Biomedical study of molecular mechanisms of neuronal and cerebrovascular degeneration in particular after stroke, Alzheimer's disease and aging, and associated depression. Particular focus on glutamate signaling, neuronal overstimulation, and calcium homeostasis. Study approaches in cell culture, animal models, and postmortem human brain material
- Development and testing of neuroprotective drugs and noninvasive "medical food" application to combat breakdown of nervous tissue in stroke and Alzheimer's disease and associated depression

Reviewers

- Alia-Klein, Nelly (Neuropsychology, Brookhaven National Laboratory, Upton, NY, USA)
- Al-Shammari, Suhail (Neurology, Faculty of Medicine, Kuwait University, Kuwait)
- Årstad, Erik (Institute of Nuclear Medicine, University College London, London, UK)
- Baron, Jean-Claude (Clinical Neurosciences, Addenbrooke's Hospital, Cambridge, UK)
- Biegon, Anat (Neurology, Stony Brook University Sch. Medicine, Stony Brook, NY, USA)
- Bourdet, David L (Drug Metabolism, Theravance Inc., San Francisco, CA, USA)
- Casteels, Cindy (Nuclear Medicine and Molecular Imaging, KU Leuven, Leuven, Belgium)
- DeLorenzo, Christine (Psychiatry, Columbia University, New York, NY, USA)
- Diksic, Mirko (Neurology and Neurosurgery, McGill University, Montreal, Canada)
- Ebmeier, Klaus (University Department, Warneford Hospital, Oxford, UK)
- Eckelman, William C. (Molecular Tracer LLC, Bethesda, MD, USA)
- Elsinga, Philip H (Nuclear Medicine and Molecular Imaging, UMC Groningen, Netherlands)
- Fleisher, Adam S (Neurosciences, University of California, San Diego, CA, USA)
- Flood, Dorothy G (EnVivo Pharmaceuticals, Watertown, MA, USA)
- Forsback, Sarita (Radiopharmaceutical Chemistry, Turku PET Centre, Turku, Finland)
- Hayashi, Takuya (Riken Center for Molecular Imaging Science, Kobe, Japan)
- Hesse, Swen (Nuclear Medicine, University of Leipzig, Leipzig, Germany)
- Hirano, Shigeki (Neurology, Chiba University Graduate School of Medicine, Chiba, Japan)
- Ishiwata, Kiichi (Positron Med Ctr, Tokyo Metropolitan Institute of Gerontology, Japan)
- Jaaro-Peled, Hanna (Molecular Psychiatry, John Hopkins University, Baltimore, MD, USA)

- Jahan, Mahabuba (Clinical Neuroscience, Karolinska Institute, Stockholm, Sweden)
Jučaitė, Aurelija (Astra Zeneca Global Clinical Development, Södertälje, Sweden)
Kiesewetter, Dale O. (Lab. Molecular Imaging and Nanomedicine, Bethesda, MD, USA)
Kimura, Yasuyuki (National Institute of Radiological Sciences, Chiba, Japan)
Kung, Mei-Ping (Mol. Imaging Center, Chang Gung Memorial Hospital, Taoyuan, Taiwan)
Lambert, Gavin W (Human Neurotransmitter Lab, Baker Institute, Melbourne, Australia)
Luiten, Paul (Molecular Neurobiology, University of Groningen, Groningen, Netherlands)
Lothe, Amélie (Lyon Neuroscience Research Center, Université de Lyon, Lyon, France)
Lundberg, Johan (Clinical Neuroscience, Karolinska Institute, Stockholm, Sweden)
Maier, Donna (Sanford-Burnham Medical Research Institute, La Jolla, CA, USA)
Matuskey, David (Psychiatry, Yale University School of Medicine, New Haven, CT, USA)
Melcangi, Roberto C (Neuroendocrinology, University of Milan, Milan, Italy)
Mizrahi, Romina (PET Centre, CAMH, University of Toronto, Toronto, Canada)
Mukherjee, Jogesh (Radiological Sciences, University of California, Irvine, CA, USA)
Nyakas, Csaba J (Sport Sciences, Semmelweis University, Budapest, Hungary)
Ogasawara, Kunioki (Neurosurgery, Iwate Medical University, Morioka, Japan)
Ota, M (National Institute of Neuroscience, Center Neurology and Psychiatry, Tokyo, Japan)
Ouchi, Yasuomi (Brain Imaging Research Lab, Hamamatsu University, Hamamatsu, Japan)
Parker, Christine (Clinical Imaging Centre, Glaxo Smith Kline, London, UK)
Paulson, Olaf B (Neurobiology Research Unit, Rigshospitalet, Copenhagen, Denmark)
Pontecorvo, Michael J (Avid Radiopharmaceuticals, Philadelphia, PA, USA)
Ramakrishnan, Nisha K. (Nuclear Medicine and Molecular Imaging, UMC Groningen, NL)
Scherfler, Christoph (Neurology, Innsbruck Medical University, Innsbruck, Austria)
Schou, Magnus (AstraZeneca Translational Sciences Centre, Stockholm, Sweden)
Sesay, Musa-Behahid (Service de Neuroradiologie, Hôpital Pellegrin, Bordeaux, France)
Skinbjerg, Mette (Psychiatry, Columbia University, New York, NY, USA)
Sobrio, Franck (Cyceron, Caen, France)
Suhara, Tetsuya (Mol. Imaging, National Institute of Radiological Sciences, Chiba, Japan)
Sultzer, David (Psychiatry, David Geffen School of Medicine, UCLA, Los Angeles, USA)
Varnäs, Katarina (Clinical Neuroscience, Karolinska Institute, Stockholm, Sweden)

Visser, Anniek KD (Nuclear Medicine and Molecular Imaging, UMC Groningen, NL)

Wadsak, Wolfgang (Nuclear Medicine, Medical University of Vienna, Vienna, Austria)

Wang, Yuchuan (Radiology, John Hopkins School of Medicine, Baltimore, MD, USA)

Yuh, William (Radiology, Ohio State University Medical Center, Columbus, OH, USA)

Zavitsanou, Katerina (Australian Nuclear Science and Technology Organisation, Sydney)

Zanotti-Fregonara, Paolo (Molecular Imaging Branch, NIMH, NIH, Bethesda, MD, USA)

Zhang, Ming-Rong (National Institute of Radiological Sciences, Chiba, Japan)

Zhou, Xingqin (Jiangsu Institute of Nuclear Medicine, Jiangsu, China)

Anthology of Apologies

While the authors' expert contributions lead to book chapters, it is the task of editors to determine the contents of a book and to orchestrate its realization. As all parties volunteer for the sake of science, timely publication according to schedule depends on the efforts of many human beings, intending to do their best but often delayed by daily realities.

Such realities may complicate the life of an editor. Clear deadlines can be neglected and even repeated reminders do not always lead to the expected results. In the (unlikely) case that one receives a speedy reply, the returning message contains a plethora of apologies. We recognize these reflections of our daily struggles to comply and respect the authors for their efforts. Some responses made us smile; we hope this will also be the case with the reader. Six examples from e-mail correspondence concerning the Neurobiology volume are listed below:

1. "I will try to revise my manuscript as much as possible according to the reviewers' comments. However, since these criticisms seem more severe than those I received when I submitted the original research papers, revision will take much time."
2. "Intended to finish my manuscript last week but we had a malfunctioning sprinkler at the first floor of our building on Sunday. Thus, the GMP labs on that floor and the clinical labs on ground level were flooded. A huge amount of cleaning and repair work must be done."
3. "Apologies for the delay. It has been quite chaotic lately... Our city lost power for two weeks, and I have become sick. I will try to get back to the writing mode soon again."
4. "I must inform you, that I need more time for compilation of the book chapter. As I'm now on a 61 page, single-spaced, text file I would also like to inquire if there are any size limits."
5. "Sorry for the delay in answering you – was away at a conference last week. I'm still in process of finishing the chapter. Originally I had hoped to finish before August but I adopted my third child in July which took me off my schedule. Plan to be a fair bit earlier than December 31."
6. "Problem is that little has been published on the subject matter of my proposed review. Thus, completion of a manuscript is time-consuming."

Index

A

A_{2A} adenosine receptor (A_{2A}AR) ligands
[¹¹C]TMSX, 192–193
dopamine D2 and, 193
EPICA, 193
EPISA, 193
theophylline infusion, 193

A_{2A}AR ligands. *See* A_{2A} adenosine receptor (A_{2A}AR) ligands

AADC. *See* Aromatic L-amino acid decarboxylase (AADC)

A₁ adenosine receptor (A₁AR) ligands
age-related changes, 190
caffeine, *in vitro* inhibitory concentration, 189–190
cerebellar cortex, 189
[¹¹C]MPDX, 191–192
epilepsy, MRI and [¹⁸F]CPFPX PET, 191
[¹⁸F]CPFPX administration, 187–188
metabolites, pathways, 187–188
PET tracers, 184
P-gp blocker cyclosporine A, 192
plasma time-activity curves, 192
test-retest evaluation, 189
unlabeled CPFPX, 189

A₃ adenosine receptor (A₃AR) ligands, 194

AAI. *See* Aminoalkylindoles (AAI)

A₁AR ligands. *See* A₁ adenosine receptor (A₁AR) ligands

A₃AR ligands. *See* A₃ adenosine receptor (A₃AR) ligands

A_{2B} adenosine receptor (A_{2B}AR) ligands, 194

ABC. *See* ATP-binding cassette (ABC)

AD. *See* Alzheimer's disease (AD)

Addiction and psychiatric disorders
nicotine effects
chronic treatment, 493
CMRglc, 493
dopamine, 494
schizophrenia and depression, 495

Adenosine receptors

A_{2A} ligands, 192–193

A₁AR and A_{2A}AR antagonists, 184

BBB, 184, 192, 194

A_{2B} ligands, 194

G-protein coupled receptors, 182

ligand-receptor interaction, 184

A₁ ligands, 184–192

A₃ ligands, 194

lipophilicity, 184

neurostimulant caffeine, 182

neurotransmitters, 182

nitrogen polyheterocyclic A_{2A}AR ligands, 184

non-xanthine monocyclic, 184

nucleoside composition, 182

nucleoside transporters, 182

PET ligands selection, 184–187

radiopharmaceuticals, 183

radiotracers, 183–184

xanthines, 184

Aging, NET, 575–576

Alcohol dependence, NET, 573–574

ALS. *See* Amyotrophic lateral sclerosis (ALS)

Alzheimer's disease (AD)

Aβ plaque-bearing mice, 32

advantages, (micro)PET, 33–34

aetiology and symptomatology, 21
amyloid

11C-PIB retention, 203–205

mild cognitive impairment (MCI), 205

amyloid-β infusion rodent models, 26–27

asymptomatic, 202

brain amyloidosis, 33, 34

bred models

ageing rodents, 24–25

pharmacological, chemical and

lesion-induced rodent, 25–26

deposition, amyloid, 206

and ECS, 262, 294

- Alzheimer's disease (AD) (*cont.*)
 familial AD (FAD) brains, 203
 [¹⁸F]cyclofoxy, 611
 histamine receptors, 347
 5-HT system
 description, 676
 5-HT_{1A} receptor, 677
 5-HT_{2A} receptor, 677–678
 5-HT₄ receptor, 678–679
 5-HT₆ receptor, 679
 postmortem and clinical studies, 676
 SERT binding, 679–680
in vivo binding estimation, 779
 molecular imaging, 200
 monoaminergic innervation, 782
 nAChR, 488–489
 NFT distribution, 200
 NFT formation, 28–29
 PDAPP, 27–28
 PET Aβ tracers studies, 202
 P-gp stimulators, 639
 polymorphisms, 628
 prodromal, 202, 206
 treatment, 783
 TSPO imaging, 656–658
 validation, animal models
 BPSD-related symptoms, 22–23
 cognitive symptoms, 21–22
 neurochemical alterations, 23–24
 pathological alterations, 23
- Aminoalkylindoles (AAI), 271–272
- Amyloid-β (Aβ) infusion rodent models, AD
 caveats, 27
 CNS, 26
 processing pathways, APP, 26, 27
- Amyloid PET tracers. *See* Positron emission
 tomography (PET)
- Amyloid precursor protein (APP)
 APP derived molecules, 23
 and Aβ peptides, 26, 27
 definition, 28
 development, 27–28
 mutant and tau, 28–29
- Amyotrophic lateral sclerosis (ALS)
 and ECS, 262
 motor neurone disease, 659
- AN. *See* Anorexia nervosa (AN)
- Androgen receptor (AR)
 PET, 392–394
 SPECT, 394
- Androgens, 382–383
- Animal models, brain research
 human brain disease, 5–9
 neurological disorders (*see* Neurological
 disorders, animal models)
 psychiatric disorders (*see* Psychiatric
 disorders, animal models)
- Anorexia nervosa (AN)
 histamine receptors, 349–350
 serotonin 1A receptor, 155
- Antidepressants, 273, 276
- Antihistamines
 administration, 334, 351
 classification, 351–352
 sedative effects, 334
- Anxiety disorders
 and ECS, 259
 estrogens, 380
 HD, 467
 PTSD, 573
- APP. *See* Amyloid precursor protein (APP)
- AR. *See* Androgen receptor (AR)
- Aromatic L-amino acid decarboxylase
 (AADC)
 enzyme activity, 695
 and 5HTP, 691
 inhibition, NSD1015, 698
 recombinant human, 691
- Atherosclerosis, 262–263
- Atomoxetine (ATX)
 depression and ADHD
 blocking effect, 569
 development, 568
 inhibitory effect, 570
 treatment, 578
 humans and nonhuman primates, 566–568
 NET and SERT, 570
- ATP-binding cassette (ABC)
 ABCB1 gene, 628
 and AD, 628
 animal and human tissues, 628–629
 and BBB, 626
 binding, P-gp, 629–630
 and brain disorders, 627–628
 and ETB, 640
 MDR, 626
 and MRP, 626–627
 and PET (*see* Positron emission
 tomography (PET))
 P-glycoprotein transport activity, 641, 643
 sexual hormones, 640
 signaling pathways and key transcription
 factors, 641, 642
 substrate radiotracer, 641
 VEGF, 640
- Attention-deficit hyperactivity disorder
 (ADHD)
 ATX (*see* Atomoxetine (ATX))
 MPH effects, humans, 570–572
 pharmacologic treatments, 566
- ATX. *See* Atomoxetine (ATX)
- Autoradiography
 ex vivo, 418
 [¹⁸F]FPIT binding, 421

- α -[^3H]dihydrotrabenazine
 ([^3H]DTBZ), 771
 [^3H]/[^{125}I]reserpine, 772
 (+/-)-[^3H]methoxytrabenazine ([^3H]
 MTBZ), 771–772
 [^3H]trabenazine ([^3H]TBZ), 771
 human and monkey brain slices, 420
in vitro, 418
 [^{125}I]iodovinyltrabenazine, 772
 ketanserin derivatives, 772
- B**
- BAT. *See* Brown adipose tissue (BAT)
 BBB. *See* Blood–brain barrier (BBB)
 BCRP. *See* Breast cancer resistance protein
 (BCRP)
 Behavioural and psychological signs and
 symptoms of dementia (BPSD)
 cognitive deterioration, 21
 symptoms, 22–23
 Beta amyloid (A β) plaques, 200
 Blood–brain barrier (BBB)
 ABC (*see* ATP-binding cassette (ABC))
 P-gp, 192
 BPSD. *See* Behavioural and psychological
 signs and symptoms of dementia
 (BPSD)
 Brain derived neurotrophic factor (BDNF)
 polymorphisms (Val66Met),
 154–156
 Brain disease
 human, 5–9
 imaging, rodent models (*see* Imaging,
 rodent models)
 Brain disorders
 androgens, 382–383
 corticosteroids, 383
 estrogens, 380–381
 progestins, 381–382
 SHR
 functional domains, 384
 genomic pathway, 384, 385
 GR, 386
 MR, 386
 polymorphisms, 385
 Brain energy metabolism
 applications, FDG-PET
 and coregistered MRI, 97, 98
 decline, cerebral metabolic rate, 96, 97
 differential diagnosis, 97–98
 changes, local brain, 88
 consumption, glucose (*see* Glucose
 consumption, brain)
 glucose, 86–87
 glycolysis and oxidative
 phosphorylation, 88
 neuronal activity coupling, metabolism
 and flow, 95, 96
 rCMRGI (*see* Regional cerebral metabolic
 rate for glucose (rCMRGI))
 whole-organ studies, 87
 Brain imaging, sigma receptors
 post-mortem studies, 745
 radioligands, 745–748
 Brain NET system
 analysis, [^{11}C]MRB, 576, 577
 density, 562
 disadvantages, 562
 distribution, 562–563
 [^{18}F]F-MeNER-D2, 577
 ligands, PET imaging, 563
 lower contrast, NET-poor and-rich
 regions, 563, 576–577
 MRTM2, 577
 rhesus monkeys, 577
 Brain perfusion SPECT
 acetazolamide (vasodilatory), 139–140
 camera requirements and image
 acquisition, 135–136
 changes, posterior cingulate
 hypoperfusion, 127, 130
 DLB, DaTSCAN imaging, 127, 131
 focal hyperperfusion, 129, 138
 image reconstruction and
 post-processing
 attenuation correction, software
 methods, 141
 computer-assisted diagnosis,
 141–143
 filtering, 140
 fusion, anatomic imaging, 143
 slicing planes, 141
 indications, 126–129
 interpretation and reporting, 143–144
 $^{99\text{m}}\text{Tc}$ -HMPAO brain, 127, 130
 neuroactivation, 140
 patient preparation, 134–135
 radiopharmaceuticals
 (*see* Radiopharmaceuticals)
 seizure imaging, 137–138
 Breast cancer resistance protein (BCRP)
 [^{11}C]elacridar, 634
 and P-gp, 634, 635
 Brown adipose tissue (BAT), 574–576
- C**
- cAMP. *See* Cyclic adenosine monophosphate
 (cAMP)
 Cannabinoid-1 (CB $_1$) receptor
 PET (*see* Positron emission
 tomography (PET))
 presynaptic, 253

- Cannabinoid receptors
 CB₂ imaging (*see* Cannabinoid subtype 2 (CB₂) imaging)
 CB₁ radioligands
 and AAI, 271–272
 human (*see* Human PET imaging, CB₁ radioligands)
 PET imaging (*see* Positron emission tomography (PET))
 rimonabant, 267–271
 structure, (–)-5′-[¹⁸F]-Δ⁸-THC, 267
- Cannabinoid subtype 2 (CB₂) imaging
 AD and HD, 294
 animals, 298–299
 effects, 295
 human, 299
in vivo and dynamic monitoring,
 MS, 299–300
 immune system, 294
 neuroinflammatory disorders, 294
 peripheral immune system, 253
 and pharmacokinetic modeling, 299
 and radioligand development
 BBB permeability, 295, 297
 [¹¹C]NE40, 298
 early stage, 295
 nanomolar affinity, 295
 2-oxoquinoline derivatives, 298
 physical-chemical properties, 297–298
 properties, 295–297
 TBI, 294–295
- Carfentanil (CFN)
 amygdala and hypothalamus, 596
 [¹¹C]DPN, 594
 somnolence and sedation, 593
- Carotid Occlusion Surgery Study (COSS),
 214–215
- Catechol-O-methyltransferase (COMT),
 163–165
- CBF. *See* Cerebral blood flow (CBF)
- CB₂ imaging. *See* Cannabinoid subtype 2 (CB₂) imaging
- [¹¹C]Elacridar
 BCRP, 634
 structure, 634
- Central dopamine system, humans
 dopamine D₂-like receptors
 D_{2/3} imaging, 237–240
 D₄ imaging, 240
 D₁ receptors, 236–237
 presynaptic dopamine system
 DAT, 234–236
 D₁ receptors, 236–237
 [¹⁸F]FDOPA and [¹⁸F]FMT, 231–233
 VMAT-2, 233–234
- Central nervous system (CNS)
 Aβ infusion animal models, 26
 diseases
 drug addiction and alcoholism,
 757–758
 ischemia, 757
 mood disorders, 756
 neurodegenerative diseases, 757
 schizophrenia, 755–756
- histamine receptors
 anti-allergy drugs, 334
 cAMP regulation, H₃ and H₄ receptors,
 335
d-chlorpheniramine administration,
 334, 336
 histaminergic signalling, [¹⁸F]FDG
 PET, 334, 337
 H₂R, 365
 H₁R inhibition, 334
 rCBF measurements, 334, 335
 sedative effects, antihistamines, 334
 thioperamide, H₃R, 336–337
- radiotracers
 BBB, 414
 high affinity and selectivity, 413–414
in vivo stability, 415
 radiosynthesis, 415
 target sites concentration, 414
 serotonin system, 151
 structural anomalies, 10–11
- Central-type benzodiazepine receptors (cBZR)
 chronic hemodynamic compromise and
 stroke risk
 COSS, 214–215
 disabling stroke, 214–215
 evaluation, hemodynamic status, 215
 extracranial-to-intracranial (EC-IC)
 bypass surgery, 214–215
 ICA, 214
 MCA, 214
 OEF, 214–215
 vascular reconstruction surgery,
 214–215
- ¹¹C labeled flumazenil (FMZ), 216–217
 cognitive impairment, 222–225
 FMZ binding, 216–217
 oxygen metabolism, 218–219
 pathophysiology
 BZR index, 220
 and chronic hemodynamic cerebral
 ischemia, 217–218

- neuronal damage and low-flow infarction, 218–219
- selective cortical neuronal damage and misery perfusion, 219–221
- stereotactic extraction estimation (SEE) method, 220
- three-dimensional stereotactic surface projection (3D-SSP) technique, 219–220
- selective neuronal damage, 215–216
- silent cortical neuronal damage, asymptomatic patients, 222
- Cerebral blood flow (CBF) measurements
 - activation studies, 119
 - kinetic modeling
 - Fick principle, 109
 - Kety–Schmidt assumption, 109
 - model parameter estimation, 110
 - [¹⁵O]H₂O, 111
 - single-tissue compartment, 108, 109
 - neo-formed vessels, 120
- PET, [¹⁵O]H₂O
 - brain PET data generation, 107–108
 - cerebral ischemia (*see* Cerebral ischemia, CBF PET)
 - interruption, brain–blood supply, 105
 - radiochemistry, 106–107
- Cerebral glucose metabolism
 - brain energy metabolism (*see* Brain energy metabolism)
 - energy requirements, brain tissue, 86
- Cerebral ischemia, CBF PET
 - “diaschisis”, 115
 - ischemic penumbra, 115
 - perfusion imaging, preclinical stroke research
 - iNO, penumbral blood flow, 117, 118
 - multimodal PET-MRI, Leipzig sheep stroke model, 117, 118
 - occlusion types, sheep, 115, 116
 - parametric map [¹⁵O]H₂O, 116
 - serial [¹⁵O]H₂O PET scans, iNO, 117
- Cerebral metabolic rate for glucose (CMRglc), 493
- CFN. *See* Carfentanil (CFN)
- CFS. *See* Chronic fatigue syndrome (CFS)
- Chronic fatigue syndrome (CFS)
 - fatigue scores, 460
 - heterogeneous disorder, 459
 - radioligand assay, 460
 - thresholds, 461
- Cigarette smoking, 718–719
- Cirrhosis, 263
- [¹¹C]Laniquidar
 - factors, 636
 - structure, 636
- [¹¹C]Loperamide
 - P-gp inhibitor, 633
 - pretreatment, 633
 - structures, 633
- (+)-*N*-[¹¹C]methyl-3-piperidyl benzilate ([¹¹C](+)-MPB)
 - [¹¹C]alkyl chain lengths, 451, 453
- CFS, 459–461
- [¹¹C]4-MPB
 - labeled compound, 448
 - Macaca mulatta, 448
 - monkey brain, 448–L489
 - muscarinic receptor ligand, 448
 - Patlak plot analysis, 450
 - ROI, 448
 - TAC, 449–450
 - dose-dependent effects, Aricept, 451, 453
 - in vitro* assay, 451, 452
 - microdialysis method, 450
 - synaptic neurotransmitters, 451
- CMRglc. *See* Cerebral metabolic rate for glucose (CMRglc)
- CNS. *See* Central nervous system (CNS)
- Cocaine, 606–607
- Computed tomography (CT)
 - CBF measurements, 113–114
 - and contrast-enhanced MR, 111
- COMT. *See* Catechol-O-methyltransferase (COMT)
- Contrast recovery coefficient (CRC)
 - calculation, 52
 - curves, capillary diameters, 53, 54
- Corticosteroids, 383
- COSS. *See* Carotid Occlusion Surgery Study (COSS)
- CRC. *See* Contrast recovery coefficient (CRC)
- CT. *See* Computed tomography (CT)
- [¹¹C]Tariquidar
 - advantages, 635
 - BBB, 635
 - structure, 635
- [¹¹C]Verapamil
 - and [¹¹C]dLop, 638–639
 - distribution volume, 632
 - (*R*)-enantiomer, 631
 - metabolite, 637–638
 - neurological diseases, 636–637
 - structure, 631

- Cyclic adenosine monophosphate (cAMP), 335
- Cyclofoxy
bolus injection and constant infusion, 593
chemical structures, 592
kinetic analysis, 592
rat brain, *in vivo* injection, 591–592
- Cytisine, 478
- D**
- DAT. *See* Dopamine transporter (DAT)
- DBS. *See* Deep brain stimulation (DBS)
- Deep brain stimulation (DBS)
bipolar HFS and PDS, 59
definition, 54–55
rCBF decrease, ipsilateral and contralateral hippocampus, 57, 58
 μ SPECT imaging and analysis, 56–57
stimulation, 56
subtraction analysis, rats, 57–59
- Delayed matching to sample (DMS)
task, 456
- Dementia with Lewy bodies (DLB),
127, 130, 143, 200, 207
- Depression and ADHD
ATX occupancy (*see* Atomoxetine (ATX))
[^{11}C]AFM, 569–570
NET and SERT, 569
noradrenergic action, 569
treatment, 568–569
- Diagnostic and statistical manual of
mental disorders 4th edition
(DSM-IVTR), 10
- “Diaschisis”, 115
- Diazabicyclononane, 484, 486–487
- Dihydrotrabenazine (DTBZ)
2-alkyl substituents, 771
binding, 781
bloodstream, 773
chiral column resolution, 774
demethylation, 773
2-fluoropropylamino group, 775
 α - and β -isomer, 771
2*R* and 2*S* isomers, 772
VMAT2 radioligands, mouse, rat and
human brains, 768, 769
X-ray structural analysis, 774
- Diprenorphine (DPN)
[^{11}C]DPN and [^{11}C]CFN, 594
[^3H]DPN binding, 594
radiofluorinated analog, 595
rat brain and human frontal cortex, 594
- Dissociative anesthetics
[^{11}C]ketamine, 524
development, 548–549
memantine, 524–525
MK-801
Alzheimer’s diseases, 522
chemical structure, 522
[^{11}C]MKC autoradiography, rat brain,
522–523
identification, 521
preparation [^{18}F]fluoromethyl analog,
521
rCBF, 523–524
synthesis, [^{11}C]cyanation, 522
- PCP and TCP
chemical structure, 518–519
[^{11}C]-radiotracers, 519
[^{18}F]fluoroethyl analog, 519
fluorocyclohexyl analog, 519
NMDARs actions, 518
regional cerebral distribution, 519–520
rhesus monkey brain, 520–521
- DLB. *See* Dementia with Lewy bodies (DLB)
- DMS task. *See* Delayed matching to sample
(DMS) task
- Dopamine $\text{D}_{2/3}$ receptor imaging
agonist radioligands, 239
autoreceptors, 240
benzamide [^{11}C]raclopride, 238–239
dexamphetamine administration, 240
extrastriatal distribution, brain-dedicated
SPECT systems, 238
human brain, 237
intracellular compartment, 240
PET radioligands, 239
ultrahigh-affinity SPECT radioligand, 238
- Dopamine D_4 receptor imaging, 240
- Dopamine D_1 receptors, 236–237
- Dopamine $\text{D}_{2/3}$ receptors, 159–162
- Dopamine transporter (DAT), 162, 234–236
- DPN. *See* Diprenorphine (DPN)
- Drug addiction
and ECS, 258
opioid receptors
alcohol dependence, 607–608
borderline personality, 603
cocaine dependence, 606–607
eating disorders, 609
epilepsy, 609–610
lung tumors, 612
MDD, 602
neurodegenerative diseases, 611–612
nicotine dependence, 608–609

- opioid dependence, 607
 - pain, 603–605
 - PTSD, 603
 - treatment, 605–606
- Drug-induced schizophrenia models
- development, animal model, 16
 - hallucinogen, 17
 - psychostimulant, 16–17
- Drug testing, μ PET
- exemplified, schizophrenia, 76–77
 - study design, 77, 78
 - SUV (*see* Standard uptake value (SUV))
 - VOI-based approach, 76
- DSM-IVTR. *See* Diagnostic and statistical manual of mental disorders 4th edition (DSM-IVTR)
- DTBZ. *See* Dihydrotrabenazine (DTBZ)
- ## E
- Eating disorders
- CB₁ receptors, 292
 - and ECS, 257–258
 - histamine receptors, 333
- ECS. *See* Endocannabinoid system (ECS)
- Endocannabinoid system (ECS)
- and AD, 262
 - and ALS, 262
 - anandamide, 252, 253
 - anxiety disorders, 259
 - 2-arachidonoylglycerol (2-AG), 252, 253
 - atherosclerosis, 262–263
 - binding site density, 264, 265
 - CB₁ and CB₂ receptors (*see* Cannabinoid receptors)
 - cellular functions, 254
 - cirrhosis, 263
 - degradation and reuptake process, 254
 - drug addiction, 258
 - Δ^9 -tetrahydrocannabinol (Δ^9 -THC)
 - effect, 252, 253
 - eating disorders, 257–258
 - epilepsy, 261–262
 - and FAAH (*see* Fatty acid amide hydrolase (FAAH) imaging)
 - and GPCRs, 252
 - and HD, 261
 - heteromerization, 254
 - illegal drugs, 251
 - lipids, 253
 - lipophilicity, 254
 - mood disorders, 259
 - multiple sclerosis (MS), 259–260
 - pain, 260
 - and PD, 260–261
 - pharmacology, 256–257
 - physiology, 255–256
 - psychoactive component, 251–252
 - radioligand
 - binding affinity, 264–265
 - molecular descriptors, CNS, 265–266
 - requirements, PET, 263–264
 - research, PET and SPECT performance, 263
 - schizophrenia, 258–259
 - signaling, 254
 - stroke, 262
- Endothelin receptor type B (ETB), 640
- Epibatidine
- binding potential, 479
 - brain uptake, 481
 - heteromeric nAChRs, 479
 - N*-methyl- and *N*-ethyl-derivatives, flubatine, 481
 - radiotracer, 480
 - toxicology and radiation dosimetry, 480
- EPICA. *See* Estimated plasma time-activity curve by independent component analysis (EPICA)
- ER. *See* Estrogen receptor (ER)
- Estimated plasma time-activity curve by independent component analysis (EPICA), 193
- Estrogen receptor (ER)
- PET, 387–389
 - SPECT, 389–390
 - western blotting and in situ hybridization, 387
- Estrogens, 380–381
- ETB. *See* Endothelin receptor type B (ETB)
- ^{99m}Tc-Ethyl cysteinate dimer (ECD)
- and ^{99m}Tc-HMPAO (*see* ^{99m}Tc-Hexamethylpropylene amine oxime (HMPAO))
 - SPECT images, focal hyperperfusion, 138
- ## F
- FAAH. *See* Fatty acid amide hydrolase (FAAH) imaging
- Fatty acid amide hydrolase (FAAH) imaging
- [¹¹C]MK-3168, 302
 - degradation and reuptake process, 254
 - [¹⁸F]PF-9811, 301–302
 - periphery and CNS, 300
 - radiolabeled analogs, AEA and URB597, 300–301
 - radioligands, 300

- FDG. *See* F18-labelled deoxyglucose (FDG)
- ¹⁸F-(E)-3-((6-Fluoropyridin-2-yl)ethyl) cyclohex-2-enone *O*-methyl oxime ([¹⁸F]FPECMO), 432
- [¹⁸F]FDOPA and [¹⁸F]FMT
- AADC enzyme, 231–233
 - Parkinson's disease (PD) and dementia, 233
 - PET systems, performance characteristics, 233
 - presynaptic dopamine neurons, 231
 - radiotracer, 231
 - striatal dopaminergic synapse, 231–232
 - tyrosine derivative, 231
- ¹⁸F-fluoro-deoxyglucose (¹⁸F-FDG), 206
- 4-[¹⁸F]Fluoro-*N*-[4-[6-(isopropylamino)pyrimidin-4-yl]-1,3-thiazol-2-yl]-*N*-methylbenzamide ([¹⁸F]FITM), 421–422
- Fick principle, 105, 108, 109
- F18-labelled deoxyglucose (FDG)
- FDG-PET (*see* Brain energy metabolism)
 - glucose metabolism, 88
 - LC, 90
 - metabolic rate, 90
 - tissue, 89–90
- G**
- Genetic polymorphisms, neuroreceptor imaging
- COMT, 163–165
 - dopamine
 - dopamine D_{2/3} receptors, 159–162, 164
 - effects, 160
 - SLC6A3 dopamine transporter gene, 161
 - transporter function measurement, 162–163
 - GWAS, 150–151
 - 18-kD translocator protein, 166–167
 - monoamine oxidase A, 165–166
 - serotonin (*see* Serotonin)
 - VBM, 151
- Genetic schizophrenia models
- inbred and selectively bred rodent strains, 18–19
 - modified, 19–20
- Genome-wide association studies (GWAS), 150–151
- Glucocorticoid receptor (GR)
- adrenalectomized and shamoperated rats, 396
 - cortisol, 386
 - imaging tracer, 394–395
- Glucose consumption, brain
- FDG images, 91–93
 - PET scans and mean global metabolic rate, 91, 93
 - stages II–IV sleep, 94
- Glutamate receptors
- iGluRs, 411
 - intracellular secondary messenger systems, 411
 - neuronal and glial cells, 412
 - types, 411–412
- Glycine-binding site antagonists
- B_{max}/K_d value, rat brain, 534
 - cyclic amino acids
 - 7-chloro-5-iodokynurenic acid, 531–532
 - [¹¹C]3MPICA, 532
 - GV150526A, 532
 - structure, 533
 - warfarin treatment, 532–533
 - 4-hydroxyquinolones
 - carboxylic acids, 534
 - [¹¹C]L-703,717, 535–537
 - in vitro* binding, [¹¹C]22 and [¹¹C]23, 538–539
 - 3-methoxy-MDL-104,653, 537–538
 - nonradioactive L-703,717, 535
 - regioselective methylation, 534
 - structure, 534, 535
 - synthesis, 534
 - warfarin, 535
 - hypofunction, NMDARs, 531
 - NMDA ion-channel activation, 531
 - PAMQX, 534
 - structure, 531, 532
- Glycine transporters (GlyT1)
- carbon-11/fluorine-18, 323
 - glycinergic neurones, 322
 - hypofunction, 322
 - inhibitory neurotransmitter, 321
 - PET, 322–324
 - radiopharmaceutical development, 328
 - schizophrenia, 328
 - tracer development
 - [¹¹C]ALX5407, 324
 - [¹¹C]GSK931145, 324, 326
 - [¹¹C]labeled CHIBA and SA compounds, 327–328
 - [¹¹C]-*N*-methyl-SSR504734, 327
 - [¹¹C]Ro5013853, 326–327
 - [¹⁸F]MK-6577, 326
- Glycolysis, 88
- GlyT1. *See* Glycine transporters (GlyT1)
- G protein-coupled receptors (GPCR), 252
- GR. *See* Glucocorticoid receptor (GR)
- GTS-21, 484
- GWAS. *See* Genome-wide association studies (GWAS)

H

- Hallucinogen models, 17
- HD. *See* Huntington's disease (HD)
- ^{99m}Tc-Hexamethyl propylene amine oxime (HMPAO)
- brain tissue, 134
 - interchangeable technetium-labeled compounds, 132, 133
- HFS. *See* High-frequency stimulation (HFS)
- High-frequency stimulation (HFS), 56, 59
- Histamine receptors imaging
- CNS (*see* Central nervous system (CNS))
 - drugs effect, 365
 - H₁ receptor (*see* H₁ receptor)
 - H₂ receptor, 352–353
 - H₃ receptor (*see* H₃ receptor)
 - H₄ receptor, 364, 365
 - neurotransmission and regulation, 332, 364
 - radiosynthesis, 364
- H₁ receptor
- AD, 347–348
 - age-correlated, 342, 344
 - AN, 349–350
 - baboon brain, 340, 342
 - blockade, 343, 345
 - carbon-11-labelled ligands, 1980s, 338
 - [¹¹C]doxepin, 338, 339
 - characteristics, 345
 - circadian rhythm, 350–351
 - [¹¹C]pyrilamine metabolism, 338–340
 - density and activity, 342–343
 - depressive disorder, 348–349
 - differences, 342
 - expression, 347
 - healthy human brain, 340, 343
 - Logan graphical analysis, 347
 - mapping, 340–342, 344
 - metabolite analysis, 342
 - N*-[¹¹C]methylation, 338
 - neural network, 345
 - neurological and neuropsychiatric disorders, 364
 - optimal compartmental model, 347
 - PET performance, dog brain, 340, 341
 - radiolabelled metabolites measurement, 347
 - schizophrenia, 349
 - side effects, antihistamines, 351–352
 - signalling, 345
 - uptake patterns, 345–346
- H₂ receptor, 352–353
- H₃ receptor
- [¹¹C]GSK189254, humans, 355–359
 - [¹⁸F]fluoroproxyfan, 354
 - [¹⁸F]FUB 272, 353
 - neuronal SPECT, 363
 - non-imidazole, pharmaceuticals, 354–355
 - PET imaging, rats, 362–363
 - radiosynthesis, 353–354
 - rhesus monkey brain, 359–361, 365
 - S*-[¹¹C]methylation, 353
 - tritiated and radioiodinated compounds, 353
- H₄ receptor, 364, 365
- Human brain disease, animal modelling
- aetiological and predictive validity, 8
 - Alzheimer's disease (AD), 5
 - face and construct validity, 7–8
 - generalisation and extrapolation, 9
 - homology, analogy and isomorphism, 8–9
 - neuroscience research, 5, 6
 - prefrontal cortex, 7
 - psychiatric, 6
- Human imaging studies, VMAT2
- aging, 781
 - dementia, 782–783
 - description, 778
 - drug abuse, 783–784
 - Huntington's disease (HD), 782
 - in vivo* binding estimation, 779
 - non-Parkinson movement disorders, 782
 - PD, 781–782
 - pharmacokinetic studies, 779–780
 - psychiatric disease, 783
- Human PET imaging, CB₁ radioligands
- [¹¹C]MePPEP and [¹⁸F]FMPEP-d₂
 - data analysis, 277–278
 - monkey brain, 277, 278
 - radioactivity, brain, 278–279
 - radiosynthesis, 277
 - structure, 273
 - [¹¹C]OMAR ([¹¹C]JHU75528)
 - baboon brain HRRRT, 273–275
 - BP values, 273
 - CB₁ antagonist blocker AVE1625, 274
 - cerebral transaxial images, 273–274
 - lipophilicity, 272–273
 - pharmacological evaluation, 273
 - physical-chemical and *in vivo* imaging, 273, 274
 - radiosynthesis, 273
 - structure, 272, 273
 - [¹⁸F]MK-9470
 - methoxy analog, 277
 - rimonabant and non-rimonabant analogs, 275–276
 - treatment, MK-3640/placebo, 276–277
- Huntington's disease (HD)
- caudate and putamen, 611
 - and ECS, 261, 285
 - and microglial activation, 660–661

IICA. *See* Internal carotid artery (ICA)

Ifenprodil-binding site

compounds, 539

derivatives

1-(arylalkynyl)-4-benzylpiperidine,
542–543

and bis(phenylalkyl)-amines, 540, 541

[¹¹C] EMD-95885, 543[¹¹C]26 location, 540–542[¹⁸F]35 and [¹⁸F] RGH-896, 544[¹²⁵I]33 and [¹²⁵I]34, 544, 545

NR1A/2B receptors, 543–544

non-ifenprodil-related NR2B antagonists

[¹¹C]36 and [¹¹C]37, 546[¹⁸F]*trans*-39 and [¹⁸F]*cis*-39, 546–548

Ro-647312, 545–546

NR2B expression, 539, 550

structure, 539–540

iGluRs. *See* Ionotropic glutamate receptors

(iGluRs)

¹²³I-isopropylidoamphetamine (¹²³I-IMP), 132

Imaging, rodent models

AD, 32–34

drug development research, 29

schizophrenia

dopamine content, 32

neurological and psychiatric

disorders, 30, 31

PET marker [¹¹C]-PK11195, 30

Internal carotid artery (ICA), 214

Ionotropic glutamate receptors (iGluRs),

411, 412

Ischemic penumbra, 115

K

Kety–Schmidt method, 91

LLC. *See* Lumped constant (LC)

Lesion-induced schizophrenia models, 17–18

Lumped constant (LC), 89, 90

Lung tumors, opioid receptor expression, 612

MmAChR. *See* Muscarinic acetylcholine
receptors (mAChR)MAGL. *See* Monoacylglycerol lipase (MAGL)

Magnetic resonance (MR) methods

CBF estimation, 114

and comparative PET, 117

and CT, 111

Major depressive disorder (MDD)

affect-modulating regions, 715

density, MAO-A, 714

5-HTT binding, 727

MAO-A DV comparison, 714, 715

MAO-A V_T, 715

neuroimaging, 714

μOR binding, 602

postmortem studies, 727

prefrontal cortex, 716

studies, neuroimaging, 726

MAO-A. *See* Monoamine oxidase

A (MAO-A)

MDD. *See* Major depressive

disorder (MDD)

MDR. *See* Multidrug resistance (MDR)

MeNTI, 595

Metabotropic glutamate receptors (mGluRs)

drugs, 436

ligands, 435

neurotransmission, 435

psychiatric and neurologic diseases, 435

structure, GluR2/3 ligands, 434

Metabotropic glutamate receptor subtype 1

(mGluR1)

¹¹C-label

carbon-11 radioligands, 416

[¹¹C]MMTP, 418[¹¹C]YM-202074, 416, 418

shake-flask method, 419

[¹⁸F]EFMC, 422[¹⁸F]FITM, 421–422¹⁸F-labeled triazole analogues, 419–421

Metabotropic glutamate receptor subtype 5

(mGluR5)

ABP688, 430–433

MPEP (*see* 6-Methyl-2-(phenylethynyl)-

pyridine (MPEP))

MTEP, 427–430

Methoxytetraabenazine (MTBZ)

alkylation, phenol, 774

metabolic disposition, 774

tritiated form, 771–772

Methylphenidate hydrochloride (MPH)

effects

animal and human data, 571

[¹¹C]MRB injection, 571

and NET densities, 571–572

pharmacological, 570–571

treatment, ADHD, 571

6-Methyl-2-(phenylethynyl)-pyridine

(MPEP)

brain areas, 424

gray matter regions, 427

human and rat brain tissues, 425

- lipophilicity, 426
- radio-chemical yields, 426
- radiosynthesis, 424–425
- saturation assays, 426
- structure, 423–424
- 3-(6-Methyl-pyridin-2-ylethynyl)-cyclohex-2-enonemethyl-oxime (ABP688)
 - cyclohexanone moiety, 430
 - description, 430, 431
 - [¹⁸F]FDEGPECO, 432–433
 - [¹⁸F]FE-DABP688, 431–432
 - [¹⁸F]FPCEMO, 432
 - radioactivity concentrations, 431, 432
- 3-[(2-Methyl-1,3-thiazol-4-yl)ethynyl]pyridine (MTEP)
 - carbon-11-and fluorine-18-labeled PET radioligands, 427
 - [¹⁸F]F-MTEB, 428
 - [¹⁸F]SP203, 429–430
 - radiosynthetic routes, 427, 428
 - structural modification, 427
- mGluR1. *See* Metabotropic glutamate receptor subtype 1 (mGluR1)
- mGluR5. *See* Metabotropic glutamate receptor subtype 5 (mGluR5)
- mGluRs. *See* Metabotropic glutamate receptors (mGluRs)
- Microglial activation and stroke, 662–663
- Micro-positron emission tomography (μPET)
 - drug testing (*see* Drug testing, μPET)
 - evaluation, quantification methods, 73–74
 - [¹⁸F]FDG uptake, brain
 - anesthesia, 73
 - experimental protocol, fasting experiment, 67, 68
 - glucose levels, 67
 - injection route, 73
 - pre-scan glucose levels, fasting durations, 68, 69
 - quantification methods, 68, 69
 - serum corticosterone levels, rats, 70
 - Sprague–Dawley rats, 70
 - variables, cerebral uptake, 71
 - whole brain, fasting groups, 70
 - whole brain uptake values, 71, 72
 - isotopes, 65
 - preclinical protocol optimization, 75–76
- Micro-single photon emission computed tomography (μSPECT)
 - application, neuromodulation (*see* Neuromodulation, μSPECT)
 - contrast to noise
 - CRC curves, capillary diameters, 53, 54
 - custom-made contrast phantom, 52, 53
 - multipinhole collimators, 49
 - vs. μPET, 48
 - resolution, 51–52
 - U-SPECT-II, X-SPECT and NanoSPECT, 50, 51
- Middle cerebral artery (MCA). *See also* Central-type benzodiazepine receptors (cBZR)
 - chronic stage, occlusive disease, 214
 - distribution, arterial disease, 221
 - occlusions, 115, 116
- Mineralocorticoid receptor (MR), 396, 397
- Molecular imaging. *See* Positron emission tomography (PET); Single-photon emission computed tomography (SPECT)
- Monoacylglycerol lipase (MAGL), 254
- Monoamine oxidase A (MAO-A)
 - aggression, 719–721
 - antidepressants (*see* Antidepressants)
 - cigarette smoking, 718–719
 - definition, 165–166
 - density, 712–713
 - early postpartum, 716–717
 - 5-HTT density, 721–722
 - MDD (*see* Major depressive disorder (MDD))
 - neuroimaging, radioligands, 713–714
 - radioligands, 722–723
 - and SAD, 730, 731
- Mood disorders
 - ECS, 259
 - MAO-A, 712
- Motor neurone disease and frontotemporal dementia, 658–659
- MPH effects. *See* Methylphenidate hydrochloride (MPH) effects
- MR. *See* Mineralocorticoid receptor (MR)
- MR methods. *See* Magnetic resonance (MR) methods
- MRP. *See* Multidrug resistance-associated proteins (MRP)
- MS. *See* Multiple sclerosis (MS)
- MTBZ. *See* Methoxytetraabenazine (MTBZ)
- Multidrug resistance (MDR)
 - development, 626
 - and MRP transporters, 626
- Multidrug resistance-associated proteins (MRP)
 - MDR transporters, 626
 - P-gp ligand activity, 639
- Multiple sclerosis (MS)
 - ECS, 259–260
 - measurement, inflammation, 661–662

- Multiplexing, 51
- Muscarinic acetylcholine receptors (mAChR)
- Alzheimer disease, 446, 456
 - anesthetic effects, 447
 - brainstem cholinergic system, 457
 - [¹¹C](+)-3-MPB (*see* (+)-*N*-[¹¹C]methyl-3-piperidyl benzilate ([¹¹C](+)-3-MPB))
 - DMS task, 456
 - logan reference tissue method, 456
 - OAB, 459
 - PET, 446
 - scopolamine, 456
 - T-DMS task test, 456–457
- Myocardial opioid receptors, 600
- N**
- nAChRs. *See* Nicotinic acetylcholine receptors (nAChRs)
- NET. *See* Norepinephrine transporter (NET)
- Neuroactivation, brain perfusion SPECT, 140
- Neurodegenerative diseases
- AD, 488–489
 - description, 488
 - HD and AD, 611
 - Parkinson's disease, 489–491
 - PD, 611–612
- Neurofibrillary tangle (NFT)
- intracellular, 21
 - lack of formation, 28
 - pathology, 29
- Neurological disorders, animal models
- AD (*see* Alzheimer's disease (AD))
 - approaches, modelling, 21
- Neuromodulation, μ SPECT
- DBS (*see* Deep brain stimulation (DBS))
 - rTMS, 55
 - TMS (*see* Transcranial magnetic stimulation (TMS))
- NFT. *See* Neurofibrillary tangle (NFT)
- Nicotinic acetylcholine receptors (nAChRs)
- addiction and psychiatric disorders, 493–495
 - autoradiography, 469
 - cerebral cortex, 497
 - [¹¹C]-SIB-1553A, 484
 - incubation medium, 497
 - levels, 496
 - membrane homogenates, 468
 - molecular imaging, 496
 - neurodegenerative diseases, 488–491
 - neuronal, 468
 - nicotinic receptors, 496–497
 - pentameric ligand-gated ion channels, 467
 - PET and SPECT technology, 470–472
 - physostigmine, 496
 - radioligands (*see* Radioligands)
 - stroke and neuroinflammation, 491–492
 - α and β subunits, 467
 - supernormal, 497
 - tobacco plant, 466
 - traumatic brain injury, 492–493
- N*-methyl-D-aspartate receptors (NMDARs), 322–323. *See also* Radioligands
- Nondiffusible CBF tracers, 111
- Noninvasive nuclear imaging techniques, 322
- Norepinephrine transporter (NET)
- abnormalities, 578
 - applications, 577
 - brain (*see* Brain NET system)
 - data, PET and MRI, 578–579
 - design and biological evaluation, 562
 - pathophysiology and treatment, 577–578
 - and SERT, 569
 - therapeutic effect, MPH, 578
 - translational PET imaging (*see* Translational PET imaging, NET)
- N*-[1-(2-Thienyl)cyclohexyl]-3,4-piperidine (TCP), 518–520
- Nuclear medicine methods, CBF measurements, 112–113
- O**
- OAB. *See* Overactive bladder (OAB)
- Obesity, 575
- Obsessive-compulsive disorder (OCD), 729
- OCD. *See* Obsessive-compulsive disorder (OCD)
- OEF. *See* Oxygen extraction fraction (OEF)
- Opioid receptor-like 1 (ORL1), 591
- Opioid receptors
- affective responses, 597–598
 - analgesic and recreational drug, 586
 - antagonist radioligands, 590
 - bound tracer, 588
 - carboxylic acid, 588
 - [¹¹C]BPN, 589
 - ¹¹C-CFN-PET, 596
 - CFN, 593–594
 - [¹¹C]GR103545, 590
 - characterization, 587
 - [¹¹C]MeNTI, 589
 - cyclofoxy, 591–593
 - cyclopropylmethyl group, 589

- DPN, 594–595
drug addicts (*see* Drug addiction)
 β -endorphin binds, 587
[¹⁸F]cyclofoxy, 596
¹⁸F-FE-PEO, 589
fluorinated analogs, 590
GR103545, 595–596
[³H]naloxone, 588
MeNTI, 595
myocardial opioid receptors, 600
neuroimaging, 596
nociceptin/orphanin, 591
ORL1, 591
pain, healthy volunteers
 capsaicin, 598
 [¹¹C]DPN binding, 603, 604
 dopaminergic neurotransmission, 599
 expression, 598
 neurotransmission, 606
 opioid receptor-mediated
 antinociceptive responses, 599
 opioid system, 604
 pain-induced alterations, 599
 placebo and nocebo effects, 599
 sensitivity and placebo treatment, 599
personality traits, 597
PET probes, 587, 588
radiofluorinated δ OR antagonist, 590
receptor occupancy
 buprenorphine, 601
 [¹¹C]CFN-PET, 602
 [¹¹C]DPN binding, 601
 nalmefene, 600
 naloxone, 602
 pharmacological effects, 600
 vestibular processing, 600
ORL1. *See* Opioid receptor-like 1 (ORL1)
Overactive bladder (OAB), 447, 459
Oxidative phosphorylation, 88
Oxygen extraction fraction (OEF), 214
Oxygen-15 water PET. *See* Cerebral Blood Flow (CBF) measurements
- P**
Parkinson's disease (PD)
 CB₁ receptors, 260–261, 284–286
 and dementia, 233
 and neurodegenerative diseases, 489–490
 striatum and thalamus, 611
 and TSPO imaging, 659–660
PBR. *See* Peripheral benzodiazepine receptor (PBR)
- PCP. *See* Phencyclidine (PCP)-binding site, radioligands
PD. *See* Parkinson's disease (PD)
PDAPP. *See* Promoter-driven APP (PDAPP)
PDS. *See* Poisson distributed stimulation (PDS)
Perfusion imaging methods
 CT, 113–114
 MR, 114
 nuclear medicine, 112–113
Peripheral benzodiazepine receptor (PBR), 166
Permanent MCA occlusion (pMCAO)
 Leipzig sheep stroke model, 117
 occlusion types, experimental, 115, 116
Perturbation studies, 5HT and AMT
 macro-parameter estimation, 695–696
 MATLAB 6.5, 695
 radioactivity concentrations, 695
 substrates, 5HT biosynthesis, 696–697
PET. *See* Positron emission tomography (PET)
 μ PET. *See* Micro-positron emission tomography (μ PET)
P-gp inhibitors
 [¹¹C]elacridar, 634
 [¹¹C]laniquidar, 636
 [¹¹C]tariquidar, 635
 ¹⁸F-labeled compounds, 639
 neurodegenerative diseases, 639
 substrates
 [¹¹C]loperamide, 632–633
 [¹¹C]verapamil, 631–632
Phencyclidine (PCP)-binding site, radioligands
 BIII277CL, 530–531
 diarylguanidine derivatives
 blocking effect, anesthesia, 528
 chemical structure, 525, 526
 CNS 5161, 526, 528–529
 compounds, 525
 ¹⁸F-labeled S-fluoroalkyl, 529
 [¹²³I]CNS 1261 and [¹²⁵I]CNS 1261, 525–528
 neurotransmitter receptors, 525
 NMDARs affinity, 528
 structure, open channel blockers, 518
 synthesis and evaluation, 526, 528
 dissociative anesthetic derivatives (*see* Dissociative anesthetics)
 6,11-ethanobenzo[b]quinolizinium, 529
 NPS 1506, 531
 open channel blocker, 529
 radiosynthesis, [¹⁸F]9 and [¹⁸F]10, 529–530
 and TCP (*see* Dissociative anesthetics)

- (D)-7-iodo-*N*-(1-phosphonoethyl)-5-aminomethylquinoxaline-2,3-dione (PAMQX), 534
- pMCAO. *See* Permanent MCA occlusion (pMCAO)
- Poisson distributed stimulation (PDS), 56, 57, 59
- Positron emission tomography (PET)
- advantages and disadvantages, 291–292
 - agonist radiotracer, 293–294
 - 16 α -[¹⁸F]fluoro-17 β -estradiol ([¹⁸F]FES), 387
 - amyloid deposition
 - healthy elderly, 207
 - longitudinal changes, 206
 - amyotrophic lateral sclerosis (ALS), 200
 - anesthetics, 447
 - AR, 392–394
 - baseline transporter, 323
 - beta amyloid (A β)
 - cortical deposition, 200
 - oligomers, 201
 - soluble amyloid precursor protein (s-APP), 200–201
 - binding potential, marker [¹¹C]-PK11195, 30
 - brain concentration, 252, 280–281
 - carbon-11, 323
 - CBF measurements
 - perfusion imaging methods, 112–114
 - principles, 111
 - (+)- α -[¹¹C]dihydrotrabenazine
 - (+)- α -[¹¹C]DTBZ), 774
 - (+/-)- α -[¹¹C]dihydrotrabenazine ([¹¹C]DTBZ), 773
 - cerebral distribution, 446
 - cerebral glucose metabolism, correlation, 206–207
 - clinical scanners, 470
 - [¹¹C]MePPEP and [¹⁸F]FMPEP-d₂
 - alcohol users, 290
 - genetic and pharmacologic rodent model, 287
 - limitation, 288–289
 - radioactivity, human brain, 287–288
 - SPM analysis, chronic cannabis smokers, 289–290
 - [¹¹C]methoxytrabenazine ([¹¹C]MTBZ), 774
 - CNS radiotracers (*see* Central nervous system (CNS))
 - [¹¹C]OMAR, 282–283
 - compartment and mathematical modeling, 279–280
 - [¹¹C]trabenazine ([¹¹C]TBZ), 773
 - [¹¹C]verapamil, 636–637
 - description, 630, 772–773
 - development and evaluation, 290–291
 - differences, 281–282
 - ECS (*see* Endocannabinoid system (ECS))
 - ER, 387–389
 - excretion phase, 281
 - fluorine-18 and carbon-11, 413
 - fluorine-18-labeled dihydrotrabenazines, 774–775
 - [¹⁸F]MK-9470
 - anorexia nervosa patients, 286
 - brain uptake measures, 283, 284, 287
 - episodic migraine, women, 286–287
 - HD, 285
 - hippocampal sclerosis, 286
 - male rats, 284
 - metabolites, 284
 - monkeys and humans, 283
 - nicotine impact, 284
 - PD, 284–286
 - radioligand's characterization, 283, 284
 - reductions, 285–286
 - sex-dependent differences, 285
 - 2-tissue compartment modeling, 283–284
 - gamma photons, 470
 - glutamate receptors (*see* Glutamate receptors)
 - healthy subjects, 748, 749
 - 5HT
 - AADC, 695
 - graphical analysis, 693–694
 - α -methylserotonin, 694
 - models, 693
 - radiolabelled compounds, 694
 - 5-HT₄, measurements, 674
 - 5-HT target, 670–671
 - in vivo* properties, 291, 292
 - imaging, amyloid
 - AD and MCI (*see* Alzheimer's disease (AD))
 - frontotemporal dementia (FTLD), 207
 - imaging data, 448
 - kinetic analysis, 749–751
 - location, 280
 - measurements, 279
 - metabolite-corrected arterial input function, 324
 - mGluR, 23–24
 - mGluR1 (*see* Metabotropic glutamate receptor subtype 1 (mGluR1))
 - mGluR5 (*see* Metabotropic glutamate receptor subtype 5 (mGluR5))

- microdialysis and behavioral cognition task, 455
- molecular brain imaging, 471
- molecular imaging
- amyloid PET imaging, 201
 - ¹⁸F-flutemetamol, 202
 - preclinical stage detection, 202
- multiple tracer, 471
- NFTs, 200
- non-CNS applications, 294
- noninvasive imaging technology, 412
- noninvasive nuclear imaging
- techniques, 322
- PET tracers, amyloid
- amyloid dyes, 202
 - chemical structures and, 202, 203
 - multiple binding sites, 202–203
 - tau proteins binding, 202
- P-gp inhibitors (*see* P-gp inhibitors)
- pharmacokinetic modeling, 279, 280
- PR, 390–392
- radioligand, 674
- radiotracers, 322
- serotonergic system, AD, 676–680
- serum autoantibody, 460
- sigma₁, measurement
- fluvoxamine, 754
 - Lassen plot analysis, 753
 - physiological and pathophysiological roles, 752
 - receptor occupancy, 753
 - V_T images, 754, 755
- slow pharmacokinetics, 293
- and SPECT, 629, 670
- “synaptic barrier”, 280
- TAU PET imaging, 207–208
- tissue modeling methods, 280
- tracer doses, 280
- TSPO (*see* Translocator protein (TSPO) expression)
- Posttraumatic stress disorder (PTSD), 573, 603
- Progesterone receptor (PR)
- PET, 390–392
 - SPECT, 392
- Progestins, 381–382
- Promoter-driven APP (PDAPP), 27–28
- Psychiatric disorders, animal models
- behavioural approach, 11
 - DSM-IVTR, 10
 - endophenotype, 10–11
 - genetic models, 12
 - pharmacological models, 11
 - schizophrenia (*see* Schizophrenia, animal models)
- Psychosis, 663
- Psychostimulant models, 16–17
- PTSD. *See* Posttraumatic stress disorder (PTSD)
- ## R
- Radioligands
- cerebral binding, 472–488
 - cytisine, 478
 - development, NMDARs
 - activation, 516
 - classifications, 517
 - description, 549–551
 - excitatory neurotransmission, 515
 - glycine and D-serine (*see* Glycine-binding site antagonists)
 - hypofunction, 515
 - ifenprodil-binding site (*see* Ifenprodil-binding site)
 - interpretation, 551
 - ischemic rats, 549
 - ligand-gated ion channels, 548
 - overactivation, 515
 - PET and SPECT, 517
 - structure and location, 516–517
 - structure, open channel blockers, 518
 - and TCP derivatives, 518 - diazabicyclononane, 484, 486–487
 - epibatidine (*see* Epibatidine)
 - GTS-21, 484
 - 5-HT system
 - 5-HT_{1A} receptor, 671
 - 5-HT_{2A} receptor, 672–673
 - 5-HT_{2B} and 5-HT_{2C} receptor, 673
 - 5-HT_{1B} receptor, 672
 - 5-HT₃ receptor, 673
 - 5-HT₄ receptor, 673–674
 - 5-HT₅ receptor, 674
 - 5-HT₆ receptor, 674
 - 5-HT₇ receptor, 675
 - SERT, 675–676
- [¹²⁵I]I-TSA, 487
- nicotine, 478
- non-epibatidine-and-non-A-85380, 483
- 3-pyridyl ethers, 481–483
- quinuclidine-based ligands, 484
- R-[¹¹C]MeQAA, 487
- sigma receptors
- carbon-11-labelled nemonapride, 747
 - chemical structures, 746
 - description, 745–746
 - PET ligand, 746
 - receptor-selective ligand, 747

- Radioligands (*cont.*)
 toxicity and dosimetry, 747
 VAcHT, 748
 steric and electronic requirements, site,
 484–486
- Radiopharmaceuticals
 estimation, rCBF, 131
 HMPAO and ECD, 132–134
¹²³I-isopropylidoamphetamine
 (¹²³I-IMP), 132
 133-Xenon (¹³³Xe), 132
- rCBF. *See* Regional cerebral blood flow
 (rCBF)
- rCMRGI. *See* Regional cerebral metabolic
 rate for glucose (rCMRGI)
- Regional cerebral blood flow (rCBF)
 and BBB function, 347
 brain perfusion SPECT, 126
 estimation, 131
 human experiments, 63
 induction, low-frequency (1 Hz)
 stimulation, 62–64
 interventional SPECT, 136
 measurements, 334
 quantification, 132
 repetitive TMS, rats, 62
- Regional cerebral metabolic rate for glucose
 (rCMRGI)
 avoidance, conversion factor, 91
 calculation, 89, 90
¹⁸FDG, 88
- Regions of interest (ROI), 448, 451
- Repetitive transcranial magnetic
 stimulation (rTMS)
 definition, 55
 position, 62
- Rimonabant
 analogs, 269–271
 development, 267–268
 human, 269, 271
 lipophilicity, 271
 PET/SPECT imaging, 269–270
 structure, 268
- ROI. *See* Regions of interest (ROI)
- rTMS. *See* Repetitive transcranial magnetic
 stimulation (rTMS)
- S**
- SAD. *See* Seasonal affective disorder (SAD)
- Scanning focus method (SFM), 50
- Schizophrenia
 animal models
 aetiology and symptomatology, 12–13
 cognitive endophenotypes, 14
 drug-induced (*see* Drug-induced
 schizophrenia models)
 electrophysiological endophenotypes,
 13–14
 genetic, 18–20
 imaging (*see* Imaging, rodent models)
 lesion-induced, 17–18
 locomotor activity, 14
 negative symptoms, 15
 neurodevelopmental, 15–16
 sensory discrimination, 14–15
 and autism, 12
 ECS, 258–259
 [³H]haloperidol, 12
 histamine receptors, 349
- Seasonal affective disorder (SAD), 730, 731
- Serotonin
 1A receptor, 155–158
 2A receptor polymorphisms, 154, 158
 binding, transporter, 156
 brain derived neurotrophic factor (BDNF)
 polymorphisms (Val66Met),
 154–156
 5-HTTLPR effects, 152–154, 156
 presynaptic serotonin transporter
 (5-HTT), 151
 4 receptor, 157, 158
 transporter gene linked polymorphic region
 (5-HTTLPR), 152
 tryptophan hydroxylase (TPH), 151
- Serotonin (5-hydroxytryptamine (5HT))
 AD, PET imaging, 676–680
 AD symptomatology, 680–681
 (¹¹C)-alpha-methyl-tryptophan (AMT),
 704–705
 biosynthesis
 nontarget localisation, 692
 pharmacokinetics, 692
 quantitative measurements, 692
 radioactivity, 692
 radiotracer, 693
 [¹¹C]HTP target specificity and brain
 metabolites
 AADC inhibition, 698
 accumulation rate constant, 699
 baseline trapping value, 703
 conversion, 697
 net accumulation rate constant, 700, 701
 Patlak plots, 700, 702
 radioactivity concentrations, 698, 699
 reference tissue models, 700
 description, 670
 homeostatic response, 689
 (11C)-5-hydroxytryptophan (5HTP),
 703–704

- molecular cloning, PET, 688
 peripheral tissues, 689
 perturbation studies (*see* Perturbation studies, 5HT and AMT)
 PET (*see* Positron emission tomography (PET))
 platelet-stored vasoconstrictor, 688
 radioligands, *in vivo* brain imaging, 671–676
 SPECT and PET, 670–671
 system
 biosynthesis, 691
 primate serotonergic system, 689
 release and extracellular concentrations, 690–691
- Serotonin transporter (5-HTT)
 antidepressants (*see* Antidepressants)
 density, 721–722
 depressive disorder, 726–728
 ecstasy abuse, 728–729
 OCD, 729
 radioligands, transporters, 722–723
- Serotonin transporter (SERT)
 binding, AD, 679–680
 radioligands, *in vivo* brain imaging, 675–676
- Serotonin transporter gene linked polymorphic region (5-HTTLPR), 152
- SERT. *See* Serotonin transporter (SERT)
- SFM. *See* Scanning focus method (SFM)
- SHR. *See* Steroid hormone receptors (SHR)
- Sigma receptors
 binding sites, 744
 brain imaging (*see* Brain imaging, sigma receptors)
 categorization, 744
 CNS diseases, 755–758
 Sigma₁ (*see* Sigma₁ receptors)
- Sigma₂ receptors
 classification, 744
 CNS, 744
 PET imaging, human brain, 748–755
 radioligand, 746
 radiotracers, 747
 receptor-selective ligand, 747
 transmembrane domains, 744
- Sigma₃ receptors
 binding sites, 745
 EBP, 744
- Single-photon emission computed tomography (SPECT)
 and animal PET, 470–472
 AR, 394
 brain perfusion (*see* Brain perfusion SPECT)
 ER, 389–390
 5-HT target, 670–671
 human brain, 670
 PR, 392
 SPECT. *See* Single-photon emission computed tomography (SPECT)
 μSPECT. *See* Micro-single photon emission computed tomography (μSPECT)
 Split-dose technique, 137, 139
 SPM. *See* Statistical parametric mapping (SPM)
- Standard uptake value (SUV)
 cerebellum, 205
 effects, LY404039, 78–80
 effects, memantine/ketamine, 77–79
- Statistical parametric mapping (SPM)
 analysis, 289
 SPM8, 62
 and VOI-based, 60
- Steroid hormone receptors (SHR)
 AR, 392–394
 brain
 ex-vivo brain autoradiography, 397
 [¹⁸F]FES, 399
 [¹²⁵I]MIE₂, 397–398
 metastasized breast cancer, 399
 CNS, 379, 383
 corticoid imaging
 GR, 394–397
 MR, 397
 disorders, brain (*see* Brain disorders)
 messenger molecules, 379
 neurological and psychiatric disorders, 400
 neurosteroidogenesis, 379, 380
- Stress hyperglycemia, 70
- Stroke
 ECS, 262
 rTMS, 55
- Stroke and neuroinflammation, 491–492
- SUV. *See* Standard uptake value (SUV)
- SzGene database, 19
- T**
- TAC. *See* Time-activity curves (TAC)
- TAU PET imaging, 207–208
- TBI. *See* Traumatic brain injury (TBI)
- TBZ. *See* Tetrabenazine (TBZ)
- T-DMS task. *See* Titration version of delayed matching to sample (T-DMS) task
- Tetrabenazine (TBZ)
 catalytic hydrogenation, 771
 labeling, 773
 reduction, ketone, 773

Time-activity curves (TAC), 451, 454
 Titration version of delayed matching to sample (T-DMS) task, 456–458
 TMS. *See* Transcranial magnetic stimulation (TMS)
 Transcranial magnetic stimulation (TMS)
 experimental procedures, 60
 multimodality imaging, electrical field calculations
 changes, rCBF, 62–64
 position, figure-of-eight coil and rat, 61
 SPM analysis, 62
 T-map, 62
 VOI and SPM, 60
 Translational PET imaging, NET
 ADHD (*see* Attention-deficit hyperactivity disorder (ADHD))
 aging, 575–576
 alcohol dependence, 573–574
 brain, 576–577
 (S,S)-[¹¹C]MRB, 563–564
 cocaine inhibition
 abstinence effects, 565–566
 [¹¹C]MRB and HRRT, 564–565
 effects, 564
 MRI, 564
 disorders, 563
 obesity and brown adipose tissue, 574–575
 PTSD, 573
 Translocator protein (TSPO) expression
 frontotemporal dementia and motor neurone disease, 658–659
 HD and microglial activation, 660–661
 imaging, AD, 656–658
 inflammation measurement, MS, 661–662
 microglia, 654
 and Parkinson's disease (PD), 659–660
 PET, 655–656
 psychosis, 663
 stroke and microglial activation, 662–663
 TBI, 662
 Traumatic brain injury (TBI), 294–295, 492–493, 662
 Triallelic 5-HTTLPR, 153
 TSPO expression. *See* Translocator protein (TSPO) expression

V

VACHT. *See* Vesicular acetylcholine transporter (VACHT)
 Vascular endothelial growth factor (VEGF), 640, 643
 VBM. *See* Voxel-based morphometry (VBM)
 VEGF. *See* Vascular endothelial growth factor (VEGF)
 Vesicular acetylcholine transporter (VACHT), 767–768
 Vesicular monoamine transporter type 2 (VMAT-2)
 animals
 mouse brain, 776
 nonhuman primates, 777–778
 rat brain, 776–777
 autoradiography (*see* Autoradiography)
 human, 778–784
 imaging, 233–234
 localization, mammalian brain, 768–769
 molecular biology, 768
 PET (*see* Positron emission tomography (PET))
 radiotracer development, 768
 substrates and inhibitors, 769–771 and VACHT, 767–768
 vesicular transporters, 767
 VMAT-2. *See* Vesicular monoamine transporter type 2 (VMAT-2)
 VOIs. *See* Volumes of interest (VOIs)
 Volumes of interest (VOIs)
 calculation, 62
 capillary and background, 52
 molecular imaging, PET in rat, 76 and SPM, 60
 VOI-map electric field strength, 63
 Voxel-based morphometry (VBM), 151

W

WCST. *See* The Wisconsin Card Sorting Test (WCST)
 The Wisconsin Card Sorting Test (WCST), 223

X

133-Xenon (¹³³Xe), 132